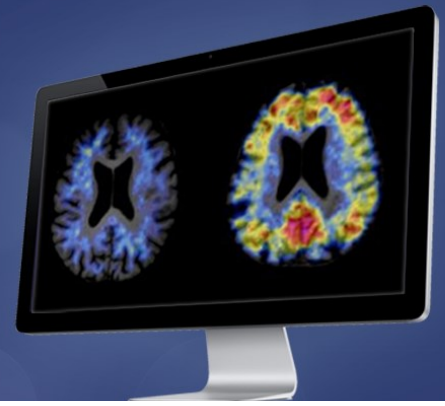


14th Human Amyloid Imaging

January 15-17, 2020
Miami, Florida



Co-organizers:

Keith A. Johnson, MD • William J. Jagust, MD • William E. Klunk, MD, PhD • Chester A. Mathis, PhD • Maria Carrillo, PhD

Conference Program and Abstracts

hai.worldeventsforum.com

TABLE OF CONTENTS

TABLE OF CONTENTS.....	2
PRESENTER INDEX.....	17
POSTER INDEX (by poster board number).....	20
POSTER INDEX (by presenter's last name).....	29
HAI 2020 PROGRAM.....	37
HAI 2020 ABSTRACTS.....	40
Wednesday, January 15, 2020 - 9:45 - 10:30am.....	40
P1A: POSTER SESSION 1A.....	40
<i>Badano, Aldo.....</i>	<i>43</i>
P1: Label-free x-ray method for estimating brain amyloid load.....	43
<i>Aldo Badano¹, Eshan Dahal¹, Bahaa Ghamraoui¹.....</i>	<i>43</i>
Bethausser, Tobey.....	44
P2: Examining regional MK-6240 patterns and associations with amyloid and cognitive decline.....	44
<i>Tobey Bethausser¹, Karly Cody¹, Rebecca Kosciak¹, Erin Jonaitis¹, Claire Erickson¹, Alexander Converse¹, Dhanabalan Murali¹, Todd Barnhart¹, Charles Stone¹, Kimberly Mueller¹, Lindsay Clark¹, Sanjay Asthana¹, Bradley Christian¹, Sterling Johnson¹.....</i>	<i>44</i>
Bharthur Sanjay, Apoorva.....	47
P3: Transcriptomic profiling of brain amyloidosis using peripheral blood-based gene expression.....	47
<i>Apoorva Bharthur Sanjay¹, Diana Svaldi¹, Liana Apostolova¹.....</i>	<i>47</i>
Bischof, Gerard.....	50
P4: A pons cluster detected by a data-driven approach may serve as a favorable reference region for 18F-PI-2620 Tau PET analysis.....	50
<i>Gerard Bischof¹, Thilo van Eimeren^{1,3,4}, Norman Koglin⁵, Andre Müller⁵, Santiago Bullich⁵, Audrey Perrotin⁵, Andrew Stephens⁵, Alexander Drzezga^{1,4}.....</i>	<i>50</i>
Bullich, Santiago.....	51
P5: Early detection of amyloid load using 18F-Florbetaben PET.....	51
<i>Santiago Bullich^{1,2}, Núria Roé-Vellyé^{1,2}, Marta Marquíe^{2,3,4,5}, Victor L. Villemagne⁶, Ángela Sanabria^{3,4,5}, Juan Pablo Tartari^{3,5}, Oscar Sotolongo^{3,5}, Vincent Doré⁶, Norman Koglin^{1,2}, Andre Müller^{1,2}, Audrey Perrotin^{1,2}, Susan De Santi⁷, Lluís Tárraga^{2,3,4,5}, Andrew W. Stephens^{1,2}, Christopher C. Rowe⁶, John P. Seibyl⁸, Mercè Boada^{2,3,4,5}.....</i>	<i>51</i>
Cassady, Kaitlin.....	52
P6: Age-related neural dedifferentiation of episodic memory networks is related to beta-amyloid and tau pathology in normal aging.....	52
<i>Kaitlin Cassady¹, Jenna Adams¹, Anne Maass², Theresa Harrison¹, Suzanne Baker³, William Jagust^{1,3}.....</i>	<i>52</i>
Coomans, Emma M.....	54

P7: Tau pathology and synaptic loss are closely associated in Alzheimer's disease in vivo: a combined [18F]flortaucipir and [11C]UCB-J PET study.....	54
<i>Emma M Coomans¹, Sander CJ Verfaillie¹, Emma E Wolters^{1,2}, Hayel Tuncel¹, Sandeep SV Golla¹, Rik Ossenkoppele^{2,3}, Wiep Scheper^{2,4,5}, Patrick Schober⁶, Steven P Sweeney⁷, J Michael Ryan⁷, Robert C Schuit¹, Albert D Windhorst¹, Philip Scheltens², Ronald Boellaard¹, Bart NM van Berckel¹.....</i>	<i>54</i>
Coomans, Emma.....	58
P8: Longitudinal dynamic [18F]flortaucipir PET reveals increased early stage tau pathology in individuals with subjective cognitive decline.....	58
<i>Emma Coomans¹, Denise Visser¹, Rik Ossenkoppele^{2,3}, Sander CJ Verfaillie¹, Tessa Timmers^{1,2}, Emma E Wolters^{1,2}, Hayel Tuncel¹, Mark E Schmidt⁴, Ronald Boellaard¹, Albert D Windhorst¹, Philip Scheltens², Wiesje M van der Flier^{2,5}, Bart NM van Berckel¹.....</i>	<i>58</i>
DiFilippo, Alexandra.....	61
P9: Preliminary evaluation of synaptic vesicle protein SV2A imaging with [11C]UCB-J across the cognitive spectrum.....	61
<i>Alexandra DiFilippo^{1,2}, Dhanabalan Murali^{1,2}, Grace McKinney¹, Nancy Davenport¹, Todd Barnhart¹, Jonathan Engle¹, Tobey Bethausser¹, Sterling Johnson¹, Barbara Bendlin¹, Bradley Christian^{1,2}.....</i>	<i>61</i>
Flores, Shaney.....	62
P10: Quantifying off-target skull binding in [18F]Flortaucipir PET studies.....	62
<i>Shaney Flores¹, Brian Gordon^{1,2}, Yi Su⁴, Jon Christensen¹, Aylin Dincer¹, Adedamola Adedokun¹, Russ Hornbeck¹, John Morris^{2,3}, Tammie Benzinger^{1,2}.....</i>	<i>62</i>
Foster, Chris.....	65
P11: Influence of iron and beta-amyloid deposition on entorhinal cortex and hippocampal subfield volumes in the aging brain.....	65
<i>Chris Foster¹, Kristen Kennedy¹, Karen Rodrigue¹.....</i>	<i>65</i>
Lange, Catharina.....	66
P12: Voxel-wise relationships between white matter hyperintensities (WMH) and multimodal neuroimaging biomarkers of Alzheimer's disease ...	66
<i>Malo Gaubert¹, Catharina Lange^{1,2}, Antoine Garnier-Crussard^{3,4}, Salma Bougacha³, Julie Gonneaud³, Robin de Flores³, Clémence Tomadesso³, Florence Mézenge³, Brigitte Landeau³, Vincent de La Sayette^{5,6}, Gaël Chételat³, Miranka Wirth¹.....</i>	<i>66</i>
Gordon, Brian.....	68
P13: Beta-amyloid deposition and its association with metabolism.....	68
<i>Brian Gordon¹, Manu Goyal¹, Lars Couture¹, Shaney Flores¹, John Morris¹, Marc Raichle¹, Tammie Benzinger¹, Andrei Vlassenko¹.....</i>	<i>68</i>
Goubran, Maged.....	70

P14: Amyloid binding is associated with markers of white matter microstructure in patients with significant white matter disease.....	70
<i>Maged Goubran¹, Miracle Ozzoude¹, Sabrina Adamo¹, Katherine Zukotynski², Christian Bocti⁴, Michael Borrie³, Howard Chertkow³, Richard Frayne⁶, Fuqiang Gao¹, Robin Hsiung⁷, Alex Kiss¹, Robert Jr. Laforce⁸, Michael D. Noseworthy², Frank S. Prato³, Joel Ramirez¹, Jim D. Sahlas², Christopher Scott¹, Eric E. Smith⁹, Vesna Sossi⁷, Stephen Strother¹², Richard Swartz¹, Jean-Claude Tardif¹, Alex Thiel¹⁰, Jean-Paul Soucy¹⁰, Sandra E. Black¹</i>	
Gunter, Jeffrey	73
P15: CSF dynamics explains discrepant PET-CSF AD biomarkers	73
<i>Jeffrey Gunter¹, Matthew Senjem¹, Petrice Cogswell¹, Christopher Schwarz¹, Val Lowe¹, Kejal Kantarci¹, Prashanthi Vemuri¹, Benjamin Elder⁴, Hugo Botha², Jonathan Graff-Radford², David Jones², Michelle Mielke², Neill Graff-Radford³, David Knopman², Ronald Petersen², Clifford Jack, Jr.¹</i>	
Singh, Vikas	76
P16: Predicting future amyloid spread with machine learning using longitudinal [C11]PiB-PET in preclinical Alzheimer's disease	76
<i>Wei Hao¹, Nicholas Vogt¹, Zihang Meng¹, Seong Jae Hwang², Rebecca Kosciak¹, Tobey Betthausen¹, Bradley Christian¹, Sterling Johnson¹, Barbara Bendlin¹, Vikas Singh¹</i>	
Heeman, Fiona	80
P17: [11C]PiB amyloid quantification and choice of reference region	80
<i>Fiona Heeman¹, Janine Hendriks¹, Bart N.M. van Berckel¹, Isadora Lopes Alves¹, Adriaan Lammertsma¹, Maqsood Yaqub¹</i>	
Hwang, Seong Jae	82
P18: Retrospective prediction of amyloid accumulation trajectories in a risk-enriched Alzheimer's disease cohort with sequential neural network.....	82
<i>Seong Jae Hwang¹, Rebecca Kosciak^{2,3}, Tobey Betthausen^{2,5}, Zirui Tao², Won Hwa Kim⁴, Sterling Johnson^{2,3,5,6}, Vikas Singh²</i>	
Jones, David.....	85
P19: Data-driven biological pattern scoring of Flortaucipir scans outperforms ROIs	85
<i>David Jones¹, Jonathan Graff-Radford¹, Hugo Botha¹, Matthew Senjem¹, Heather Wiste¹, Keith Josephs¹, Jennifer Whitwell¹, Kejal Kantarci¹, Bradley Boeve¹, Ronald Petersen¹, David Knopman¹, Val Lowe¹, Clifford Jack¹ ...</i>	
Hahn, Alice	88
P20: Hippocampal volume mediates the relationship between amyloidosis and amyloid-sensitive cognitive composite in preclinical AD	88
<i>Young Ju Kim^{1,2}, Alice Hahn^{1,2}, Soo Jong Kim^{1,2}, Si Eun Kim⁷, Juhee Chin^{1,2,4}, Sang Won Seo^{1,2,4,5,6}</i>	
Klein, Gregory.....	89
P21: Concordance of visual and quantitative assessments of baseline amyloid scans in the GRADUATE gantenerumab studies	89
<i>Gregory Klein¹, Paul Delmar², Nicola Voyle³, Jacob Hesterman⁴, Ryan Petrulli⁴, Heather Ovens⁴, Monika Baudler², Paulo Fontoura², Rachele Doody², Geoffrey A. Kerchner²</i>	
Kohli, Akshay	90
P22: Regional amyloid burden is associated with higher quantitative T1 in discrete hippocampal sub-regions	90
<i>Akshay Kohli¹, Kao Lee Yang¹, Nicholas M Vogt¹, Sanjay Asthana^{1,3}, Tobey J Betthausen¹, Andrew L. Alexander^{1,3}, Bradley T Christian¹, Sterling C Johnson, Steven R Kecskemeti, Barbara B Bendlin</i>	
Kothapalli, Satya	93
P23: Genetically informed quantitative Gradient Recalled Echo MRI reveals brain tissue in hippocampal subfields void of neurons in mild Alzheimer's disease	93
<i>Satya Kothapalli¹, Tammie Benzinger^{1,2}, Andrew Aschenbrenner^{2,3}, Manu Goyal^{1,3}, Anne M Fagan^{2,3,4}, Marcus Raichle^{1,3,4}, John Morris^{2,3}, Dmitriy Yablonskiy^{1,2,4}</i>	
Landau, Susan	94
P24: Validation of highly sensitive and specific florbetaben positivity thresholds using ADNI participants and young controls	94
<i>Susan Landau¹, Deniz Korman¹, Santiago Bullich², Susan De Santi², Andrew Stephens², Robert Koeppe^{1,3}, William Jagust¹</i>	
Lao, Patrick	97
P25: Additive contribution of white matter hyperintensity to amyloid and neurodegeneration on cognitive decline in a diverse, community-based cohort of older adults.....	97
<i>Patrick Lao¹, Anthony Chesebro¹, Juliet Colon¹, Kay Igwe¹, Yian Gu¹, Nicole Schupf¹, Jennifer Manly¹, Yaakov Stern¹, Richard Mayeux¹, Adam Brickman¹</i>	
Lao, Patrick	98
P26: White matter hyperintensities are related to tau burden in late-Braak stage regions.....	98
<i>Patrick Lao¹, Krystal Laing¹, Kay Igwe¹, Anthony Chesebro¹, William Kreisl¹, Herman Moreno², Jose Luchsinger¹, Adam Brickman¹</i>	
Laymon, Charles	100
P27: Probability template method for analysis of Down Syndrome amyloid PET	100
<i>Charles Laymon¹, Davneet Minhas¹, Jeffrey James¹, Bradley Christian², Ann Cohen¹, William Klunk¹, Dana Tudorascu¹, Sarah Royse¹, Shahid Zaman³, Benjamin Handen¹</i>	
Lemoine, Laetitia.....	102
P28: Visualizing brain astrocytes - characterization of 3H-BU99008 in human AD brain tissue.....	102
<i>Laetitia Lemoine¹, Mona-Lisa Malarte¹, Niina Koistinen¹, Agneta Nordberg^{1,2}</i>	

Levitis, Elizabeth	103
P29: Application of an epidemic spreading model to characterize amyloid beta accumulation in autosomal dominant Alzheimer's disease mutation carriers...	103
<i>Elizabeth Levitis¹, Jacob W Vogel¹, Gregory Kiar¹, Thomas Funck¹, Yasser Iturria-Medina¹, Alan C Evans¹.....</i>	
Lois, Cristina	106
P30: Phantom-based harmonization of PET image reconstruction parameters between the Siemens ECAT HR+ PET and the GE Discovery MI PET/CT scanners	106
<i>Cristina Lois¹, Kira Grogg¹, Georges El Fakri¹, Keith Johnson¹, Julie Price¹.....</i>	
Martersteck, Adam	108
P31: Age prediction and amyloid deposition in SuperAgers	108
<i>Adam Martersteck^{1,2}, Pierre Besson^{2,3}, Jaiashre Sridhar¹, Beth Makowski-Woidan¹, Todd Parrish², Aggelos Katsaggelos⁴, M.-Marsel Mesulam^{1,3}, Kathleen Bandt³, Emily Rogalski^{1,6}.....</i>	
Mayblyum, Danielle	109
P32: PiB tracer delivery decreases overtime in preclinical AD – impact for amyloid pathology measurement	109
<i>Danielle Mayblyum¹, J. Alex Becker¹, Aaron Schultz¹, Michelle Farrell¹, Heidi Jacobs¹, Zoe Rubinstein¹, Justin Sanchez¹, Emma Thibault¹, Reisa Sperling^{1,2}, Julie Price¹, Keith Johnson^{1,2}, Bernard Hanseeuw^{1,3}.....</i>	
Tudorascu, Dana	111
P33: MRI and PET data harmonization in a two-site Down syndrome study	111
<i>Davneet Minhas¹, Zixi Yang¹, John Muschelli², Charles Laymon¹, Matthew Zammit³, Paul Ellison³, Sterling Johnson³, Chester Mathis¹, Ciprian Crainiceanu², William Klunk¹, Benjamin Handen¹, Bradley Christian³, Ann Cohen¹, Dana Tudorascu¹.....</i>	
Minhas, Davneet	115
P34: Sex-specific differences in [18F]AV-1451 off-target retention	115
<i>Davneet Minhas¹, Zheming Yu¹, Charles Laymon¹, Brian Lopresti¹, Beth Snitz², Dana Tudorascu³, Howard Aizenstein⁴, Oscar Lopez², Chester Mathis¹, William Klunk⁴, Ann Cohen⁴.....</i>	
Moore, Annah	117
P35: Polygenic risk for Cerebrospinal Fluid (CSF) amyloid predicts brain amyloid in clinically normal older adults	117
<i>Annah Moore^{1,2,3}, Logan Dumitrescu^{1,2}, Aaron Schultz⁴, Neha Raghavan^{5,6,7}, Keith Johnson⁴, Richard Mayeux^{5,6,7}, Reisa Sperling⁴, Timothy Hohman^{1,2}, Elizabeth Mormino⁸.....</i>	
O'Dell, Ryan	120
P36: Association between cerebral amyloid accumulation and synaptic density in Alzheimer's disease: a multitracer PET study	120
<i>Ryan O'Dell^{1,2}, Adam Mecca^{1,2}, Ming-Kai Chen³, Tyler Godek^{1,2}, Joanna Harris^{1,2}, Hugh Bartlett^{1,2}, Emmie Banks^{1,2}, Victoria Kominek^{1,2}, Wenzhen Zhao^{1,2}, Mika Naganawa³, Takuya Toyonaga³, Yihuan Lu³, Nabeel Nabulsi³, Brent Vander Wyk⁴, Pradeep Varma³, Amy Arnsten⁵, Yiyun Huang³, Richard Carson³, Christopher van Dyck^{1,2,5,6}.....</i>	
Ottoy, Julie	121
P37: A clinically applicable proxy for gold standard quantification of amyloid-beta in Alzheimer's disease: Bolus plus constant infusion 18F-AV45 PET	121
<i>Julie Ottoy¹, Min Su Kang^{2,4}, Jeroen Verhaeghe¹, Sigrid Stroobants³, Reda Bouhachi⁴, Chris Hsiao⁴, Jenna Stevenson², Nesrine Rahmouni², Daniel Chartrand⁴, Gassan Massarweh⁴, Jean-Paul Soucy⁴, Serge Gauthier^{1,2}, Pedro Rosa-Neto^{2,4}, Steven Staelens¹.....</i>	
Manber, Richard	124
P38: Amyloid PET variability due to variation in MRI protocol and anatomical segmentation	124
<i>Alessandro Palombit¹, Richard Manber¹, Richard Joules¹, Robin Wolz¹.....</i>	
Manber, Richard	126
P39: The impact of automatic Tau PET processing on uptake variability and power analysis in AD	126
<i>Alessandro Palombit¹, Richard Manber¹, Richard Joules¹, Robin Wolz¹.....</i>	
Rabiner, Eugenii	127
P40: MIND MAPS: Assessment of the mitochondrial - endoplasmic reticulum - synaptic axis in neurodegeneration by [18F]BCPP-EF, [11C]SA4503 and [11C]UCB-J PET imaging	127
<i>Eugenii Rabiner^{1,2}, Ayla Mansur^{1,3}, Ashwin Venkataraman^{3,4}, Geraint Price³, Heather Wilson², Gennaro Pagano², Mica Clarke⁵, Yvonne Lewis¹, Paul M. Matthews^{3,4}, James B. Rowe⁶, David Brooks⁷, Lefkos Middleton³, Marios Politis², Jonathan D. Rohrer⁵, Robert Comley⁸, Karleyton C. Evans⁹, Laurent Martarello⁹, Laigao Chen¹⁰, Adam J. Schwarz¹¹, Karl Schmidt¹², Hideo Tsukada¹³, Jan Passchier¹, Roger N. Gunn^{1,3}, MIND MAPS Consortium¹.....</i>	
Rahmouni, Nesrine	131
P41: Associations between Neurogranin and imaging biomarkers of Alzheimer's disease	131
<i>Nesrine Rahmouni^{1,2}, Andrea Benedet^{1,2}, Ashton Nicholas^{4,5,6,7}, Cécile Tissot^{1,2}, Tharick A. Pascoal^{1,2}, Hlin Kvartsberg⁸, Mira Chamoun^{1,2}, Min Su Kang^{1,2}, Firoza Lussier^{1,2}, Joseph Therriault^{1,2}, Jenna Stevenson^{1,2}, Melissa Savard^{1,2}, Sulantha Mathotaarachchi^{1,2}, Emilie Thomas^{1,2}, Serge Gauthier^{1,3}, Henrik Zetterberg^{4,8,9,10}, Kaj Blennow^{4,8}, Pedro Rosa-Neto^{1,2}.....</i>	
Riphagen, Joost	133
P42: Linking APOE ε4, blood-brain barrier dysfunction and inflammation to Alzheimer's pathology	133
<i>Joost Riphagen^{1,5}, Inez Ramakers¹, Whitney Freeze¹, Linda Pagen¹, Bernard Hanseeuw^{2,4}, Marcel Verbeek³, Frans Verhey¹, Heidi Jacobs^{1,2,5}.....</i>	
Rubinstein, Zoe	136
P43: Heterogeneity of tau PET signal in the sub-nuclei of the amygdala	136

<i>Zoe B Rubinstein¹, Heidi IL Jacobs¹, Jean Augustinack¹, Michael Properzi¹, J Alex Becker¹, Danielle Mayblyum¹, Emma Thibault¹, Justin Sanchez¹, Aaron Schultz¹, Bernard Hanseeuw^{1,2}, Teresa Gomez-Isla¹, Cristina Lois-Gomez¹, Julie Price¹, Reisa Sperling^{1,3}, Keith A Johnson^{1,3}</i>	<i>Benedet^{1,2,3}, Emilie Thomas^{1,2,3}, Pedro Rosa-Neto^{1,2,3}, Serge Gauthier^{1,3}</i>
Scott, David	140
P44: MCI patients demonstrate reliably increasing 18F-AV1451 PET uptake across three exams	140
<i>David Scott¹, Katarzyna Adamczuk¹, Beth Gorman², Maureen Runkle², Joyce Suhy¹</i>	<i>140</i>
Seibyl, John	141
P45: Development of a qualitative read method for characterizing the presence and extent of brain tau deposition using [18F]MK-6240 PET imaging	141
<i>John Seibyl¹, Cristian Salinas², Raj Rajagovindan², R. Matthew Hutchison², John Beaver², Laurent Martarello²</i>	<i>141</i>
Solingapuram sai, Kiran kumar	142
P46: PET imaging of [11C]MPC-6827, a microtubule-based PET tracer in murine models of Alzheimer's disease	142
<i>Kiran Kumar Solingapuram Sai¹, Shannon Macauley¹, Christopher Whitlow¹, Akiva Mintz², Suzanne Craft¹</i>	<i>142</i>
Soucy, Jean-Paul	143
P47: Quantifying the relationship between the brain distributions of tau and local atrophy to inter-regional connectivity based on individual human data	143
<i>Jean-Paul Soucy^{1,2}, Fatameh Mohammadi², Pedro Rosa-Neto¹, Tharick Pascoal¹, Melissa Savard¹, Min Su Peter Kang¹, Joseph Therriault¹, Habib Benali²</i>	<i>143</i>
Stevenson, Jenna	144
P48: Monitoring disease pathophysiology using multiparametric PET acquisitions: The McGill TRIAD Cohort	144
<i>Jenna Stevenson^{1,2}, Mira Chamoun^{1,2}, Tharick A. Pascoal^{1,2}, Andrea Benedet^{1,2}, Min Su Kang^{1,2}, Sulantha Mathotaarachchi^{1,2}, Joseph Therriault^{1,2}, Emilie Thomas^{1,2}, Melissa Savard^{1,2}, Cecile Tissot^{1,2}, Firoza Lussier^{1,2}, Tasha Vinet-Celluci^{1,2}, Nesrine Rahmouni^{1,2}, Guylaine Gagné^{1,2}, Meong Joung^{1,2}, Sarah Sbeiti^{1,2}, Monica Shin^{1,2}, Paolo Vitali^{1,2}, Serge Gauthier^{1,3}, Pedro Rosa-Neto^{1,2}</i>	<i>144</i>
Tissot, Cécile	145
P49: Interaction between amyloid and neuroinflammation on apathy along the Alzheimer's disease spectrum	145
<i>Cécile Tissot^{1,2,3}, Min Su Kang^{1,2}, Andrea Benedet^{1,2,3}, Nesrine Rahmouni^{1,2}, Tharick A. Pascoal^{1,2}, Mira Chamoun^{1,2,3}, Joseph Therriault^{1,2,3}, Firoza Lussier^{1,2,3}, Melissa Savard^{1,2}, Sulantha Mathotaarachchi^{1,2,3}, Emilie Thomas^{1,2}, Serge Gauthier^{1,2,3}, Pedro Rosa-Neto^{1,2,3}</i>	<i>145</i>
Tissot, Cécile	147
P50: Neuropsychiatric symptoms in cognitively impaired individuals are correlated with tau deposition	147
<i>Cécile Tissot^{1,2,3}, Joseph Therriault^{1,2,3}, Tharick A. Pascoal^{1,2,3}, Mira Chamoun^{1,2}, Firoza Lussier^{1,2,3}, Melissa Savard^{1,2}, Sulantha Mathotaarachchi^{1,2}, Andrea</i>	<i>Benedet^{1,2,3}, Emilie Thomas^{1,2,3}, Pedro Rosa-Neto^{1,2,3}, Serge Gauthier^{1,3}</i>
<i>147</i>	147
Wang, Yi-Ting	149
P51: Association between [18F]NAV4694 PET amyloid-β measures and fluid biomarkers across the spectrum of Alzheimer's disease	149
<i>Yi-Ting Wang^{1,2}, Tharick Pascoal^{1,2}, Joseph Therriault^{1,2}, Andréa Benedet^{1,2}, Firoza Lussier^{1,2}, Melissa Savard^{1,2}, Min Su Kang^{1,2}, Cecile Tissot^{1,2}, Serge Gauthier^{1,2}, Pedro Rosa-Neto^{1,2}</i>	<i>149</i>
Webb, Christina	153
P52: PET beta-amyloid deposition in healthy older adults is associated with decreased lure discrimination on a spatial mnemonic similarity task	153
<i>Christina Webb¹, Chris Foster¹, Marci Horn¹, Kristen Kennedy¹, Karen Rodrigue¹</i>	<i>153</i>
Ances, Beau	154
P53: Socioeconomic status mediates racial differences seen using the A-T(N) Framework	154
<i>Julie Wisch¹, Darrell Hudson¹, Dean Coble¹, Chengjie Xiong¹, Ganesh Babula¹, Brian Gordon¹, Shaney Flores¹, Aylin Dincer¹, Tammie Benzinger¹, John Morris¹, Beau Ances¹</i>	<i>154</i>
Wolters, Emma	157
P54: Tau pathology and relative cerebral blood flow are independently associated with cognition in Alzheimer's disease	157
<i>Emma Wolters^{1,2}, Denise Visser¹, Sander Verfaillie¹, Emma Coomans¹, Tessa Timmers^{1,2}, Hayel Tuncel¹, Ronald Boellaard¹, Albert Windhorst¹, Philip Scheltens², Wiesje van der Flier van der Flier^{2,4}, Rik Ossenkoppele^{2,3}, Bart van Berckel¹</i>	<i>157</i>
Zammit, Matt	160
P55: Amyloid Load trajectories and chronicity reveal groups of early amyloid accumulators in Down syndrome	160
<i>Matt Zammit¹, Rebecca Kosciak¹, Charles Laymon², Tobey Betthausen¹, Dana Tudorascu², Ann Cohen², Davneet Minhas², Sterling Johnson¹, Shahid Zaman³, Chester Mathis², William Klunk², Benjamin Handen², Bradley Christian¹</i>	<i>160</i>
Ziontz, Jacob	163
P56: Hippocampal-retrosplenial cortex connectivity predicts tau accumulation in cognitively normal older adults	163
<i>Jacob Ziontz¹, Jenna Adams¹, Suzanne Baker², William Jagust^{1,2}</i>	<i>163</i>
Wednesday, January 15, 2020 - 1:45 - 3:15pm	165
SESSION 1: TECHNICAL I	165
Baker, Suzanne	166
Evaluation of 18F-JNJ-067 as a tau tracer	166
<i>Suzanne Baker¹, Karine Provost², Wesley Thomas³, AJ Whitman³, Mustafa Janabi¹, Mark Schmidt⁴, Maarten Timmers⁴, Hartmuth Kolb⁵, Gil Rabinovici², William Jagust^{1,3}</i>	<i>166</i>
Lopresti, Brian	170

A direct comparison of tau imaging agents [F-18]AV-1451 AND [F-18]MK-6240 in human subjects	170	Gong, Kuang	194
<i>Brian Lopresti¹, Davneet Minhas¹, Alexandra Gogola¹, Charles Laymon¹, Ann Cohen², N. Scott Mason¹, Chester Mathis¹, William Klunk².....</i>	<i>170</i>	Correction of partial volume effects for tau PET imaging using the kernel method.....	194
Ossenkoppele, Rik.....	172	<i>Kuang Gong¹, Paul Han¹, Jianan Cui¹, Nicolas Guehl¹, Keith Johnson¹, Quanzheng Li¹, Georges El Fakhri¹.....</i>	<i>194</i>
A multi-center comparison of [18F]flortaucipir, [18F]RO948 and [18F]MK6240 tau-PET tracers to detect optimal target ROIs for differential diagnosis	172	Thursday, January 16, 2020 - 8:30 - 10:00am	197
<i>Antoine Leuzy¹, Rik Ossenkoppele^{1,2}, Ruben Smith^{1,3}, Philip Insel¹, Niklas Mattsson^{1,3,4}, Tharick Pascoal⁵, Andréa Benedet^{5,6}, Hannah Cho⁷, Chul H. Lyoo⁷, Renaud La Joie⁸, Gil Rabinovici⁸, Pedro Rosa-Neto^{5,9,10}, Oskar Hansson^{1,11}.....</i>	<i>172</i>	SESSION 3: NEUROPATHOLOGY I.....	197
Sanchez, Justin	176	Lowe, Val.....	198
Capturing extra-cerebral MK-6240 signal with surface projections.....	176	Flortaucipir PET often shows uptake greater in regions outside of the medial temporal lobe than in entorhinal cortex in low Braak tangle stage participants.....	198
<i>Justin Sanchez¹, Alex Becker¹, Zoe Rubinstein¹, Danielle Mayblyum¹, Emma Thibault¹, Julie Price¹, Keith Johnson^{1,2}.....</i>	<i>176</i>	<i>Val Lowe¹, Emily Lundt¹, Christopher Schwarz¹, Hugo Botha¹, Prashanthi Vemuri¹, Jeffrey Gunter¹, Ronald Petersen¹, Clifford Jack¹, Paul Min¹, Scott Przybelski¹, Matthew Senjem¹, Kejal Kantarci¹, Bradley Boeve¹, David Jones¹, Robert Reichard¹, Jessica Tranovich², Sydney Labuzan², Fadi Hanna Al-Shaikh², David Knopman¹, Dennis Dickson², Melissa Murray².....</i>	<i>198</i>
Evans, Alan	180	Whitwell, Jennifer	199
KEYNOTE LECTURE 1	180	Brain volume and [18F]flortaucipir PET analysis of progressive supranuclear palsy clinical variants....	199
Pathology progression modelling in Alzheimer's disease	180	<i>Jennifer Whitwell¹, Nirubol Tosakulwong¹, Hugo Botha¹, Farwa Ali¹, Heather Clark¹, Joseph Duffy¹, Rene Utianski¹, Chase Stevens¹, Stephen Weigand¹, Christopher Schwarz¹, Matthew Senjem¹, Clifford Jack¹, Val Lowe¹, J. Eric Ahlskog¹, Dennis Dickson², Keith Josephs¹.....</i>	<i>199</i>
<i>Alan Evans.....</i>	<i>180</i>	Agüero, Cinthya	201
Wednesday, January 15, 2020 - 4:45 - 6:30pm.....	181	Comparison of autoradiographic binding profiles of Flortaucipir, MK-6240 and PI-2620 in human postmortem tissue samples across the spectrum of neurodegenerative diseases	201
SESSION 2: TECHNICAL II	181	<i>Cinthya Agüero^{1,2}, Maeva Dhaynaut^{3,4}, Marta Marquie^{1,2}, Ana C Amaral^{1,2}, Ramesh Neelamegam^{3,4}, Sung-Hyun Moon^{3,4}, Patrick M. Dooley^{1,2,3}, Dominique Denbow^{1,2}, Georges El Fakhri^{3,4}, Matthew P Frosch⁵, Marc Normandin^{3,4}, Teresa Gómez-Isla^{1,2}.....</i>	<i>201</i>
Zammit, Matt.....	182	Ikonovic, Milos.....	202
Amyloid Load predicts elevated tau deposition in Down syndrome	182	Biochemical correlates of tau and amyloid PET imaging in four autopsy brains	202
<i>Matt Zammit¹, Charles Laymon², Dana Tudorascu², Ann Cohen², Davneet Minhas², Shahid Zaman³, Beau Ances⁴, Chester Mathis², William Klunk², Benjamin Handen², Bradley Christian¹.....</i>	<i>182</i>	<i>Milos Ikonovic¹, Eric Abrahamson¹, Julia Kofler¹, William Paljug¹, Carl Becker¹, Chester Mathis¹, Oscar Lopez¹, William Klunk¹.....</i>	<i>202</i>
Gunn, Roger N.....	184	Schneider, Julie.....	203
TauIQ demonstrates increased power for cross-sectional and longitudinal analysis of Tau tracers as evidenced by [18F]Flortaucipir and [18F]GTP1....	184	KEYNOTE LECTURE 2.....	203
<i>Alex Whittington¹, Jacob Hesterman¹, Sandra Sanabria², Paul Manser², Robby Weimer², John Seibyl¹, Roger N. Gunn^{1,3}.....</i>	<i>184</i>	Amyloid and tau: one of multiple pathways to tissue injury, degeneration, and Alzheimer's dementia ...	203
Vogel, Jacob.....	186	<i>Julie Schneider.....</i>	<i>203</i>
Spatiotemporal imaging phenotypes of tau pathology in Alzheimer's disease	186	Thursday, January 16, 2020 - 10:45 - 11:30am	204
<i>Jacob Vogel¹, Alexandra Young², Neil Oxtoby², Ruben Smith^{3,4}, Rik Ossenkoppele^{3,5}, Olof Strandberg³, Leon Aksman², Renaud La Joie⁶, Michel Grothe⁷, Chul Hyounng Lyoo⁸, Gil Rabinovici⁶, Daniel Alexander², Alan Evans¹, Oskar Hansson^{3,4}.....</i>	<i>186</i>	P2A: POSTER SESSION 2A	204
Luckett, Patrick.....	190	Utianski, Rene	207
Predicting structural, metabolic and pathologic disease progression in autosomal dominant Alzheimer's disease with machine learning.....	190	P60: Longitudinal flortaucipir ([18F]AV-1451) PET uptake in Semantic Dementia	207
<i>Patrick Luckett¹, Austin McCullough¹, Randall J. Bateman¹, Tammie Benzinger¹, Eric McDade¹, Beau Ances¹.....</i>	<i>190</i>	<i>Rene Utianski¹, Jennifer Whitwell¹, Peter Martin¹, Hugo Botha¹, Christopher Schwarz¹, Joseph Duffy¹, Heather Clark¹, Anthony Spychalla¹, Matthew Senjem¹, Ronald</i>	

<i>Petersen¹, David Knopman¹, Cliff Jack, Jr.¹, Val Lowe¹, Keith Josephs¹.....</i>	207
Hanseeuw, Bernard	211
P61: Defining a Centiloid scale threshold predicting long-term progression to dementia in patients attending the memory clinic: An F18-Flutemetamol amyloid-PET study	211
<i>Bernard Hanseeuw^{1,2}, Vincent Malotaux¹, Laurence Dricot¹, Lisa Quenon¹, Jiri Cerman³, Christopher Buckley⁴, Gill Farrar⁴, Adrian Ivanoiu¹, Renaud Lhomme¹</i>	211
Cogswell, Petrice	214
P62: Correlation of QSM signal with Alzheimer's Disease biomarkers	214
<i>Petrice Cogswell¹, Heather Wiste¹, Matthew Senjem¹, Terry Therneau¹, Val Lowe¹, David Knopman¹, Hugo Botha¹, Jonathan Graff-Radford¹, David Jones¹, Kejal Kantarci¹, Prashanthi Vemuri¹, Tanis Ferman¹, Bradley Boeve¹, Michelle Mielke¹, Christopher Schwarz¹, Jeffrey Gunter¹, Ronald Petersen¹, Clifford Jack¹</i>	214
Vokali, Efthymia	218
P63: Developing a novel alpha-synuclein (a-syn) positron emission tomography (PET) tracer for the diagnosis of Parkinson's disease (PD) and other a-synucleinopathies	218
<i>Efthymia Vokali¹, Jerome Molette¹, Elpida Tsika¹, Myriam Ravache¹, Patrick Rodriguez¹, Tanja Jürgens¹, Antonio Melo dos Santos¹, Christine Sandiego², David Russell^{2,3}, Roger Gunn², Vincent Darmency¹, Kasia Piorkowska¹, Sonia Poli¹, Heiko Kroth¹, Francesca Capotosti¹, Valérie Hliva¹, Olivier Sol¹, Kenneth Marek³, Jan Stöhr¹, David Lowe¹, Andrea Pfeifer¹, Marie Kosco-Vilbois¹</i>	218
Klein, Julia	219
P64: Evaluating the relationships among odor identification, tau pathology and neuroinflammation in Alzheimer's disease	219
<i>Julia Klein^{1,3}, Jack Yan², Aubrey Johnson¹, Zeljko Tomljanovic¹, James Zou¹, Krista Polly¹, Lawrence Honig¹, Adam Brickman¹, Yaakov Stern¹, Seonjoo Lee², William C. Kreis¹</i>	219
McDade, Eric	220
P65: Elevated soluble phosphorylated tau is a marker of early amyloid PiB PET abnormalities and accumulation	220
<i>McDade¹, Yan Li¹, Nelly Joseph-Mathurin¹, Tammie Benzinger¹, Anne Fagan¹, Chengjie Xiong¹, Nicolas Barthélemy¹, Randall Bateman¹</i>	220
Meyer, Pierre-Francois	222
P66: Cerebrospinal fluid and PET measures of tau pathology may indicate different stages of AD pathological progression	222
<i>Pierre-Francois Meyer^{1,2,3}, Alexa Pichet Binette^{1,2,3}, Julie Gonneaud^{1,2}, John Breitner^{1,2,3}, Sylvia Villeneuve^{1,2,3,4}</i>	222
Lee, Jin San	225
P67: Distinct effects of APOE ε2 on Aβ in Alzheimer- and vascular-type cognitive impairment	225
<i>Jin San Lee¹, Hyejoo Lee², Seongbeom Park², Yeongsim Choe², Yu Hyun Park², Bo Kyoung Cheon², Alice Hahn², Rik Ossenkoppele³, Hee Jin Kim², Seonwoo Kim², Heejin Yoo², Hyemin Jang², Soo Hyun Cho⁴, Seung Joo Kim⁵, Jun Pyo Kim², Young Hee Jung⁶, Key-Chung Park¹, Charles DeCarli⁷, Michael Weiner⁸, Gyihaeon Yun¹, Duk L. Na², Sang Won Seo²</i>	225
Gatchel, Jennifer	226
P68: Association of tau tangle burden with depressive symptoms in community dwelling older adults: a longitudinal study	226
<i>Jennifer Gatchel^{1,2,4}, Gad A. Marshall^{1,3,4}, Hyun-Sik Yang^{1,3,4}, Nancy J. Donovan^{1,3,4}, Rachel F. Buckley^{1,3,7}, Michael Properzi^{1,4}, Yakeel T. Quiroz^{1,4}, Jennifer S. Rabin⁸, Patrizia Vannini^{1,3,4}, Rebecca E. Amariglio^{1,3,4}, Jasmeer Chhatwal^{1,3,4}, Dorene M. Rentz^{1,3,4}, Deborah Blacker^{1,4,6}, Reisa A. Sperling^{1,3,4}, Keith A. Johnson^{1,3,4}, Bernard J. Hanseeuw^{1,3,4}</i>	226
Ewers, Michael	229
P69: Higher microglia biomarker levels are associated with slower rates of amyloid-beta accumulation in humans and in a transgenic mouse model of amyloid-beta	229
<i>Michael Ewers¹, Matthias Brendel², Marc Suarez-Calvet³, Gloria Biechele², Christian Sacher², Tanja Blume², Christian Haass⁴, Nicolai Franzmeier¹</i>	229
Collins, Jessica	232
P70: Individual variability in the cortical distribution of elevated 18F-AV1451 and 11C-PIB in a heterogeneous sample of AD patients	232
<i>Jessica Collins¹, Ryan Eckbo¹, Scott McGinnis², Brad Dickerson¹</i>	232
Collij, Lyduine	233
P71: Quantitative regional amyloid burden and white matter changes in preclinical Alzheimer's disease	233
<i>Lyduine Collij¹, Herwin Top¹, Kristine Stickney², Silvia Ingala¹, Jori Tomassen³, Isadora Lopes Alves¹, Maqsood Yaqub¹, Alle Meije Wink¹, Dennis Van 't Ent², Philip Scheltens³, Bart N.M. Van Berckel¹, Pieter Jelle Visser³, Frederik Barkhof^{1,4}, Anouk Den Braber^{2,3}, On behalf of the AMYPAD consortium⁵</i>	233
Schaefferbeke, Jolien	235
P72: Effect of genetic risk, brain amyloid and hippocampal volume on normal variation in episodic memory performance in middle-aged and older adults	235
<i>Jolien Schaefferbeke^{1,2}, Silvy Gabel^{1,2}, Katarzyna Adamczuk^{1,2,5}, Koen Van Laere³, Patrick Dupont^{1,2}, Rik Vandenberghe^{1,2,4}</i>	235
Clarke, Mica	236
P73: Imaging synaptic and mitochondrial function in frontotemporal dementia using [11C]UCB-J, [18F]BCPP-EF and [11C]SA4503 PET	236
<i>Mica Clarke¹, Ayla Mansur^{2,3}, Jan Passchier³, Yvonne Lewis³, Karleyton Evans⁴, Laigao Chen⁵, Adam Schwarz⁶, Akihiro Takano⁷, Roger Gunn^{2,3}, David Cash¹, Eugenii Rabiner^{3,8}, Jonathan Rohrer¹</i>	236
Kim, Min-Jeong	238
P74: First-in-human evaluations of [11C]PS13 for imaging COX-1 and [11C]MC1 for imaging COX-2	238

<i>Min-Jeong Kim¹, Fernanda Juarez Anaya¹, Jae-Hoon Lee¹, Jinsoo Hong¹, William Miller¹, Sanjay Telu¹, Cheryl Morse¹, Prachi Singh¹, Michelle Cortes-Salva¹, Katharine Henry¹, Yanira Ruiz-Perdomo², Jose Montero Santamaria¹, Jieih-San Liow¹, Sami Zoghbi¹, Masahiro Fujita¹, James Katz², Victor Pike¹, Robert Innis¹.....</i>	238
Pascual, Belen.....	239
P75: [11C]MK-6884 PET tracer for M4 muscarinic cholinergic receptors in Alzheimer's disease: Comparison with [18F]FDG PET	239
<i>Belen Pascual¹, Paolo Zanotti-Fregonara¹, Meixiang Yu¹, Quentin Funk¹, Victoria Arbones¹, Yuchuan Wang², Wenping Li², Amy Cheng², Matt Anderson², Eric D Hostetler², Anthony S Basile², Joseph C Masdeu¹.....</i>	239
Villemagne, Victor	240
P76: Assessing Aβ, tau, and reactive astrocytosis in aging and AD.....	240
<i>Victor Villemagne^{1,7}, Ryuichi Harada^{2,3}, Vincent Doré^{1,4}, Shozo Furumoto², Rachel Mulligan¹, Yukitsuka Kudo³, Natasha Krishnadas¹, Kun Huang¹, Kazuhiko Yanai², Christopher Rowe^{1,6,7}, Nobuyuki Okamura^{2,5}.....</i>	240
Hahn, Alice	243
P77: A sensitive composite model to determine subtle cognitive differences in preclinical Alzheimer's disease	243
<i>Alice Hahn^{1,2}, Young Ju Kim^{1,2}, Hee Jin Kim^{1,2}, Hyemin Jang^{1,2}, Soo Jong Kim^{1,2}, Duk L Na^{1,2,3}, Juhee Chin^{1,2,4}, Sang Won Seo^{1,2,4,5,6,7}.....</i>	243
Gomperts, Stephen	244
P78: Amyloid deposition affects the topography of cortical thinning in Lewy Body Disease	244
<i>Rong Ye¹, Alexandra Touroutoglou¹, Michael Brickhouse¹, Samantha Katz^{1,2}, John Growdon¹, Keith Johnson², Bradford Dickerson¹, Stephen Gomperts¹.....</i>	244
Luckett, Emma	245
P79: Longitudinal change in amyloid load over a 5-year period in cognitively healthy APOE4 carriers versus non-carriers: Effect of reference region.....	245
<i>Emma Luckett^{1,2}, Katarzyna Adamczuk^{1,2,5}, Jolien Schaefferbeke^{1,2}, Silvy Gabel^{1,2}, Koen Van Laere³, Patrick Dupont¹, Rik Vandenberghe^{1,2,4}.....</i>	245
Buckley, Rachel	246
P80: Sex differences in the rates of cognitive decline associated with temporal lobe FTP-PET signal: findings from the Harvard Aging Brain Study	246
<i>Rachel Buckley^{1,2,3}, Michael Properzi¹, Aaron Schultz¹, Heidi Jacobs¹, Dylan Kirn¹, Dorene Rentz^{1,2}, Bernard Hanseuw^{1,4}, Keith Johnson¹, Reisa Sperling^{1,2}.....</i>	246
Pichet Binette, Alexa.....	248
P81: Amyloid and tau PET burden are associated with white matter bundle abnormalities in asymptomatic individuals at risk of Alzheimer's disease	248
<i>Alexa Pichet Binette¹, Guillaume Theaud², Julie Gonneaud¹, Judes Poirier¹, Maxime Descoteaux², Sylvia Villeneuve¹.....</i>	248
Salvadó, Gemma	251
P82: NeuroToolkit CSF biomarkers track the progression of Alzheimer's disease at very early stages and show that inflammatory markers modulate cerebral amyloid accumulation.....	251
<i>Gemma Salvadó^{1,2,3}, José Luis Molinuevo^{1,2,3,4}, Marta Milà-Alomà^{1,2,4}, Kaj Blennow^{5,6}, Henrik Zetterberg^{5,6,7,8}, Grégory Operto^{1,2,3,4}, Carles Falcón^{1,2,9}, Richard Batrla¹⁰, Mark Battle¹¹, Christopher Buckley¹¹, Gill Farrar¹¹, Carolina Minguillon^{1,2,4}, Karine Fauria^{1,2,4}, Gonzalo Sánchez-Benavides^{1,2,4}, Marc Suárez-Calvet^{1,2,4}, Juan Domingo Gispert^{1,2,3,9}, on behalf of the ALFA study¹.....</i>	251
Salvadó, Gemma.....	254
P83: T1rho MRI measurement of amyloid plaque burden in cognitively unimpaired individuals: preliminary results in the ALFA+ cohort	254
<i>Carles Falcón^{1,2,3}, Paula Montesinos⁴, Oriol Grau-Rivera^{1,3,5}, Marc Suárez-Calvet^{1,3,5}, Albert Puig-Pi Joan^{6,7}, Diego Cascales^{1,6}, Irene Navalpotro-Gomez^{1,6}, Aida Fernández-Lebrero^{1,6}, Raquel Sánchez-Valle^{8,9}, Ellen Gelpi^{9,10}, Coral Sanfeliu^{11,12}, Santiago Rojas¹³, Andrés Perissinotti^{9,14}, Aida Niñerola-Baizán^{2,14}, Gemma Salvadó^{1,3,15}, Carolina Minguillon^{1,3,5}, Karine Fauria^{1,3,5}, José Luis Molinuevo^{1,3,5,15}, Javier Sánchez-González⁴, Juan Domingo Gispert^{1,2,3,15}, on behalf of the ALFA study¹.....</i>	254
Salvadó, Gemma.....	257
P84: Preliminary quantitative results of the AMYPAD prognostic and natural history study....	257
<i>Juan Domingo Gispert^{1,2,3,4}, Isadora Lopes-Alves⁵, Katherine Gray⁶, Christopher Buckley⁷, Lyduine Collig⁵, Fiona Heeman⁵, Gemma Salvadó^{1,2,3}, Phillip Scheltens⁵, Giovanni Frisoni⁸, Craig W Ritchie⁹, Bruno Vellas¹⁰, Andrew W Stephens¹¹, Lisa Ford¹², José Luis Molinuevo^{1,2,3,13}, Gill Farrar⁷, Frederik Barkhof^{6,14}, on behalf of the AMYPAD Consortium¹⁵.....</i>	257
Edwards, Lauren	260
P85: Sex differences in regional tau deposition in cognitively impaired patients with Alzheimer's disease	260
<i>Lauren Edwards¹, Renaud La Joie¹, Leonardo Iaccarino¹, Minseon Kim¹, Suzanne Baker², Kaitlin Casaletto¹, Bruce Miller¹, William Jagust^{2,3}, Gil Rabinovici^{1,2,3}.....</i>	260
Sala, Arianna	262
P86: Cross-sectional and longitudinal non-dichotomized CSF/PET Aβ data support existence of "CSF+ first" vs. "PET+ first" pathways of Aβ biomarkers changes	262
<i>Arianna Sala^{1,2,3}, Agneta Nordberg^{1,4}, Elena Rodriguez-Vieitez¹.....</i>	262
Yoon, Bora.....	263
P87: Personality and amyloid accumulation in cognitively normal aging	263
<i>Bora Yoon¹, Suzanne Baker², Deniz Korman², Victoria Tennant³, Theresa Harrison³, William Jagust^{2,3}.....</i>	263
Seo, Sang Won	264
P88: Head-to-head comparison of F-Florbetaben and F-Flutemetamol uptakes in the cortex, striatum and white matter.....	264
<i>Sang Won Seo¹, Soo Hyun Cho², Seung Hwan Moon, Yeong Sim Choe, Duk L. Na</i>	264

Winer, Joseph	265
P89: Sleep impairment predicts longitudinal accumulation of β-amyloid	265
<i>Joseph Winer¹, Bryce Mander², William Jagust^{3,4}, Matthew Walker^{1,3}.....</i>	
Stephens, Andrew	268
P90: PI-2620 Tau PET is associated with amyloid-beta levels in scans from subjects of the elenbecestat MissionAD program	268
<i>Andrew Stephens¹, Santiago Bullich¹, Andre Mueller¹, Mathias Berndt¹, Susan De Santi², David Scott³, Kate Adamczuk³, Joyce Suhy³, June Kaplow⁴, Monique Giroux⁴, Stephen Krause⁴, Julia Chang⁴, Bruce Albalá⁴.....</i>	
Kim, Jaeho	270
P91: Prevalence of amyloid PET positivity in cognitively normal the East Asian populations	270
<i>Jaeho Kim^{1,2,3}, Sang-Hyuk Jung^{7,8}, Duk L Na^{1,2,3,4,6}, Hee Jin Kim^{1,2,3}, Hong-Hee Won⁷, Sang Won Seo^{1,2,3,5,6}.....</i>	
den Braber, Anouk	273
P92: Amyloid deposition disrupts functional connectivity and graph properties within the default mode network	273
<i>Silvia Ingala¹, Alle Meije Wink¹, Naomi Prent², Dennis van 't Ent³, Jori Tomassen², Mara ten Kate^{1,2}, Ellen Konijnenberg², Lyduine E Collij¹, Maqsood M. Yaqub¹, Philip Scheltens², Eco JC de Goes³, Charlotte E Teunissen⁴, Frederik Barkhof^{1,5}, Bart NM van Berckel¹, Pieter Jelle Visser², Anouk den Braber^{2,3}.....</i>	
Edison, Paul	276
P93: Neuroinflammation in Alzheimer's disease patients and correlates with amyloid and tau deposition	276
<i>Paul Edison¹, Fangda Leng¹, Melanie Dani¹, David Brooks².....</i>	
Nordberg, Agneta	277
P94: Development of new alpha7 nicotinic receptor ASEM analogs for PET imaging	277
<i>Agneta Nordberg^{1,2}, Laetitia Lemoine¹, Sathya Mohan¹, Guanglin Kuang⁴, Sangram Nag³, Zhisheng Jia³, Patricia Miranda Azpiaz³, Prodip Datta³, Ryosuke Arakawa³, Katarina Varnäs³, Hans Ågren⁴, Bengt Långström⁵, Christer Halldin³.....</i>	
Whitwell, Jennifer	278
P95: Biological underpinnings of typical and atypical Alzheimer's dementia phenotypes	278
<i>Jennifer Whitwell¹, Nirubol Tosakulwong¹, Jonathan Graff-Radford¹, Stephen Weigand¹, Christopher Schwarz¹, Matthew Senjem¹, Nilufer Ertekin-Taner², David Jones¹, Bradley Boeve¹, David Knopman¹, Clifford Jack¹, Ronald Petersen¹, Val Lowe¹, Keith Josephs¹.....</i>	
Mielke, Michelle	280
P96: Use of the plasma amyloid-beta 42/40 ratio for predicting amyloid PET in a community-based population	280
<i>Michelle Mielke¹, Alicia Algeciras-Schimmich¹, Michelle Campbell¹, Jeremy Syrjanen¹, David Knopman¹, Clifford Jack Jr.¹, Ronald Peterson¹.....</i>	
Tudorascu, Dana	281
P97: Associations between longitudinal cognitive measures and cross-sectional tau in adults with Down syndrome	281
<i>Dana Tudorascu¹, Diane Comer¹, Matthew Zammit², Charles Laymon¹, Davneet Minhas¹, Paul Ellison², Shahid Zaman³, Beau Ances⁴, Sterling Johnson², Chester Mathis¹, William Klunk¹, Bradley Christian², Benjamin Handen¹, Sigan Hartley², Ann Cohen¹.....</i>	
Zukotynski, Katherine	284
P98: Associations of amyloid deposition and FDG uptake in aging and cognitively impaired elders with and without moderate to severe periventricular white matter hyperintensities	284
<i>Katherine Zukotynski^{1,2}, Vincent Gaudet⁵, Phillip Kuo³, Sabrina Adamo⁴, Maged Goubran⁴, Christopher Scott⁴, Christian Bocti⁶, Michael Borrie⁷, Howard Chertkow⁸, Richard Frayne⁹, Robin Hsiung¹⁰, Robert Jr. Laforce¹¹, Michael Noseworthy¹, Frank Prato⁷, Demetrios Sahlas¹, Eric Smith⁹, Vesna Sossi¹⁰, Alexander Thiel⁸, Jean-Paul Soucy¹², Jean-Claude Tardif³, Sandra Black^{2,4}.....</i>	
Farrell, Michelle	285
P99: Early declines in learning and executive function associated with accumulating Aβ not tau in low PIB adults	285
<i>Michelle Farrell¹, Kathryn Papp^{1,2}, Rachel Buckley^{1,2,3,4}, Heidi Jacobs^{1,5}, Aaron Schultz¹, Michael Properzi¹, Bernard Hanseeuw^{1,6}, Dorene M. Rentz^{1,2}, Keith Johnson^{1,2}, Reisa Sperling^{1,2}.....</i>	
Adams, Jenna	288
P100: Entorhinal tau pathology is associated with medial temporal lobe hyperactivity in aging	288
<i>Jenna Adams¹, Anne Maass^{1,2}, David Berron^{2,3,4}, Theresa Harrison¹, Suzanne Baker⁵, Wesley Thomas⁵, Morgan Stanfill¹, William Jagust^{1,5}.....</i>	
Maltais, Daniela	292
P101: Clinicopathological confirmation of 123I-FP-CIT SPECT (ioflupane) quantification methods in a spectrum of neurodegenerative syndromes and associated pathologies	292
<i>Daniela Maltais¹, Lennon Jordan¹, Toji Miyagawa¹, Timothy Lesnick¹, Scott Przybelski¹, Hoon-Ki Min¹, Dennis Dickson², Melissa Murray², Kejal Kantarci¹, Bradley Boeve¹, Val Lowe¹.....</i>	
Thibault, Emma	293
P102: Preliminary results: PiB and MK6240 regional PET measures associated with digitized clock drawing performance	293
<i>Danielle Mayblyum¹, Emma Thibault¹, Kirsten Moody¹, Michelle Farrell¹, Shu Jiang¹, Heidi IL Jacobs¹, Zoe Rubinstein¹, Justin Sanchez¹, Samantha Katz¹, Reisa Sperling^{1,2}, Kathryn Papp^{1,2}, Dorene Rentz^{1,2}, Keith Johnson^{1,2}.....</i>	
Scott, Matthew	296
P103: White matter disruption is an early and progressive feature of pre-symptomatic Dutch-type hereditary cerebral amyloid angiopathy	296
<i>Matthew Scott¹, Aaron Schultz¹, Hamid Sohrabi^{2,3}, Samantha Gardener², Kevin Taddei², Randall Bateman⁴,</i>	

<i>Tammie Benzinger⁴, Keith Johnson¹, Reisa Sperling¹, Ralph Martins^{2,3}, Steven Greenberg¹, Jasmeer Chhatwal¹, DIAN Investigators⁴</i>	296
Royse, Sarah	300
P104: Increased risk of Alzheimer's disease in alcohol use disorder is not mediated by amyloid-beta in a middle-aged cross-sectional cohort	300
<i>Sarah Royse¹, Michael Himes², Davneet Minhas¹, Brian Lopresti¹, Margaret Flanigan², Rajesh Narendran²</i>	300
Cody, Karly	302
P105: Longitudinal associations between lifestyle risk, β-amyloid, and cognition in late-midlife	302
<i>Karly Cody¹, Rebecca Kosci², Alex Birdsill¹, Sara Berman¹, Claire Erickson¹, Nathaniel Chin¹, Lindsay Clark^{1,2}, Brad Christian^{1,3}, Tobey Betthausen^{1,2}, Sterling Johnson^{1,2}</i>	302
Martersteck, Adam	306
P106: Exploring relationships between tau burden and naming in the aphasic variant of Alzheimer's disease	306
<i>Adam Martersteck^{1,2}, Jaiashre Sridhar¹, Christina Coventry¹, Fatima Eldes¹, Jessica Wood¹, Iktae Kim¹, M.-Marsel Mesulam^{1,3}, Emily Rogalski^{1,4}</i>	306
Groh, Jenna	308
P107: Data-driven approach to characterization of tau accumulation in Braak staging groups	308
<i>Jenna Groh¹, Diana O. Svaldi¹, Edwin Stage¹, Apoorva Sanjay¹, Shannon Risacher¹, Andrew Saykin¹, Liana G. Apostolova¹</i>	308
Oh, Hwamee	311
P108: Associations between Alzheimer's disease biomarkers and cognition among cognitively normal older adults	311
<i>Hwamee Oh^{1,2,3}, Stephen Correia^{1,2,3}, Stephen Salloway^{1,2,3}</i>	311
Terada, Tatsuhiko	312
P109: In vivo association of mitochondrial dysfunction with tau pathology in early Alzheimer's disease	312
<i>Tatsuhiko Terada^{1,2,3}, Joseph Therriault¹, Peter Kang Min Su¹, Melissa Savard¹, Yasuomi Ouchi², Pedro Rosa-Neto¹</i>	312
Tennant, Victoria	313
P110: Using famous faces to investigate the neural systems involved in name retrieval	313
<i>Victoria Tennant^{1,2}, William Jagust^{1,2}, Renaud La Joie³, Jenna Adams¹, Joseph Winer⁴</i>	313
Moore, Elizabeth	315
P111: Cerebrospinal fluid matrix metalloproteinases are associated with compromised white matter microstructure among older adults: the Vanderbilt Memory & Aging Project	315
<i>Elizabeth Moore¹, Kimberly Pechman¹, Lealani Mae Acosta¹, Susan Bell^{1,2}, Adam Anderson³, Bennett Landman³, Kaj Blennow⁴, Henrik Zetterberg^{4,5}, Katherine Gifford¹, Timothy Hohman¹, Angela Jefferson^{1,2}</i>	315
McGinnis, Scott	316
P112: A clinically-relevant scheme for qualitatively rating tau PET, amyloid PET, and MRI in neurodegenerative cognitive presentations	316
<i>Scott McGinnis^{1,2,3,4}, Jessica Collins^{1,4}, Ryan Eckbo^{1,4}, Michael Brickhouse^{1,4}, Brad Dickerson^{1,2,4}</i>	316
Lussier, Firoza	317
P113: Mild behavioral impairment is associated with tau pathology in cognitively impaired elderly individuals	317
<i>Firoza Lussier^{1,2}, Tharick A. Pascoal^{1,2}, Joseph Therriault^{1,2}, Cécile Tissot^{1,2}, Mélissa Savard^{1,2}, Andrea Lessa Benedet^{1,2}, Sulantha Mathotaarachchi^{1,2}, Jenna Stevenson², Zahinoor Ismail⁴, Pedro Rosa-Neto^{1,2}, Serge Gauthier³</i>	317
Lussier, Firoza	319
P114: Modeling the trajectory of tau deposition in autosomal-dominant Alzheimer's disease using the high-affinity tau tracer [18F]MK6240	319
<i>Firoza Lussier^{1,2}, Joseph Therriault^{1,2}, Tharick A. Pascoal^{1,2}, Mélissa Savard^{1,2}, Sulantha Mathotaarachchi^{1,2}, Laura Robb², Jenna Stevenson², Serge Gauthier³, Pedro Rosa-Neto^{1,2}</i>	319
Thursday, January 16, 2020 - 11:30am - 1:00pm ...321	
SESSION 4: NEUROPATHOLOGY II	321
Smith, Ruben	322
Derivation and potential utility of an Aβ-PET based pathology accumulation index for estimation of brain Aβ load	322
<i>Antoine Leuzy¹, Johan Lilja^{1,2,3}, Christopher J. Buckley⁴, Rik Ossenkoppele^{1,5}, Mark Battle⁴, Gill Farrar⁴, Dietmar R. Thal^{6,7}, Shorena Janelidze¹, Erik Stomrud^{1,8}, Olof Strandberg¹, Ruben Smith^{1,9}, Oskar Hansson^{1,8}</i>	322
Zeng, Zhizhen	326
In vitro study of the evidence of tauopathy in Parkinson's disease (PD) brains using a tau PET tracer, [3H]MK-6240, by autoradiography	326
<i>Zhizhen Zeng¹, Stacey O'Malley¹, Patricia Dockery¹, Mallory Stenslik¹, Wenping Li¹, Eric Hostetler¹</i>	326
Malarte, Mona-Lisa	327
In vitro characterization of second-generation tau pet tracers in human autopsy brain tissue	327
<i>Mona-Lisa Malarte¹, Agneta Nordberg^{1,2}, Laetitia Lemoine¹</i>	327
Moloney, Christina M.	328
Neurofibrillary tangle maturity: A comprehensive review	328
<i>Christina M. Moloney¹, Val J. Lowe², Melissa E. Murray¹</i>	328
Thursday, January 16, 2020 - 2:30 - 4:00pm	329
SESSION 5: CLINICAL I	329
Risacher, Shannon	330
History of head injury is associated with greater tau deposition on [18F]Flortaucipir PET in MCI and AD patients	330

<i>Shannon Risacher¹, John West¹, Rachael Deardorff¹, Sujuan Gao¹, Liana Apostolova¹, Andrew Saykin¹.....</i>	330
Mecca, Adam.....	332
In vivo measurement of widespread synaptic loss in early Alzheimer's disease with SV2A PET	332
<i>Adam Mecca¹, Ming-Kai Chen¹, Ryan O'Dell¹, Mika Naganawa¹, Tyler Godek¹, Joanna Harris¹, Hugh Bartlett¹, Wenzhen Zhao¹, Nabeel Nabulsi¹, Brent Vander Wyk¹, Pradeep Varma¹, Amy Arnsten¹, Yiyun Huang¹, Richard Carson¹, Christopher van Dyck¹.....</i>	332
Rowe, Christopher C.....	335
Amyloid PET is more than just positive or negative: Aβ-amyloid level impacts risk of clinical progression in non-demented individuals.....	335
<i>Laura M van der Kall¹, Thanh Truong¹, Samantha Burnham², Vincent Doré^{1,2}, Rachel Mulligan¹, Svetlana Bozinovsk¹, Pierrick Bourgeat³, Regan Tyrrell¹, Jürgen Fripp³, Colin L Masters⁴, Victor L Villemagne^{1,6}, Christopher C Rowe^{1,5,6}.....</i>	335
Brendel, Matthias	336
18F-PI2620 tau-PET in Progressive Supranuclear Palsy – A multi-center evaluation.....	336
<i>Matthias Brendel¹, Henryk Barthel², Thilo van Eimeren^{3,4,5,6}, Ken Marek^{7,8}, Leonie Beyer¹, Mengmeng Song¹, Carla Palleis⁹, Gesine Respondek^{6,10}, Julia Sauerbeck¹, Christian Zach¹, Jochen Hammes⁴, Michael Barbe⁵, Özgür Onur⁵, Frank Jessen^{6,11,12}, Dorothee Saur¹³, Matthias L. Schroeter^{14,15,16}, Jost-Julian Rumpf¹³, Michael Rullmann², Andreas Schildan², Marianne Patt², Bernd Neumaier^{3,4}, Oliver Barret^{7,8}, Jennifer Madonia^{7,8}, David S. Russel^{7,8}, Andrew Stephens¹⁷, Sigrun Roeber¹⁸, Jochen Herms^{6,18}, Kai Bötzel⁹, Johannes Levin^{6,9}, Joseph Classen¹³, Guenter Hoeglenger^{6,10,19}, Peter Bartenstein^{1,20}, Victor Villemagne^{21,22,23}, Alexander Drzezga^{4,6}, John Seibyl^{7,8}, Osama Sabri².....</i>	336
Thursday, January 16, 2020 - 4:45 - 6:00pm.....	338
SESSION 6: CLINICAL II	338
Landau, Susan	339
Tau-PET associations with amyloid positivity and cognitive impairment.....	339
<i>Susan Landau¹, Deniz Korman¹, Robert Koeppe², William Jagust¹.....</i>	339
Jacobs, Heidi.....	341
Locus coeruleus integrity tracks with initial Alzheimer's disease-related pathology and cognitive decline	341
<i>Heidi Jacobs^{1,2}, John Alex Becker¹, Kenneth Kwong¹, Fred D'Oleire Uquillas¹, Kathryn Papp^{1,3}, Michael Properzi¹, Reisa Sperling^{1,3}, Keith Johnson¹.....</i>	341
Berron, David.....	344
Area 35 is the earliest subregion in the medial temporal lobe affected by tau pathology.....	344
<i>David Berron¹, Olof Strandberg¹, Jacob Vogel³, Philip Insel¹, Erik Stomrud^{1,2}, Niklas Mattsson^{1,4,5}, Ruben Smith¹, Oskar Hansson^{1,2}.....</i>	344
Friday, January 17, 2020 - 8:30am - 9:15am.....	346
SESSION 7A: TAU I.....	346
Leuzy, Antoine	347
The implications of different approaches to define AT(N) in Alzheimer's disease.....	347
<i>Antoine Leuzy¹, Niklas Mattsson^{1,2,3}, Shorena Janelidze¹, Sebastian Palmqvist^{1,2}, Erik Stomrud^{1,4}, Olof Strandberg¹, Ruben Smith^{1,2}, Oskar Hansson^{1,4}.....</i>	347
Dore, Vincent	350
Towards a CenTauR cortical mask	350
<i>Vincent Dore^{1,2}, Christppher Rowe², Pierrick Bourgeat¹, Samantha Burnham¹, Kun Huang², Natasha Kirshnadas², Colin Masters³, Jurgen Fripp¹, Victor Villemagne².....</i>	350
Schwarz, Christopher	352
Tau positivity: comparing flortaucipir meta-ROI vs. maximum of regional Z-scores.....	352
<i>Christopher Schwarz¹, Terry Therneau¹, Scott Przybelski¹, Heather Wiste¹, Jeffrey Gunter¹, Matthew Senjem¹, Val Lowe¹, Kejal Kantarci¹, Ronald Petersen¹, David Knopman¹, Clifford Jack¹.....</i>	352
Friday, January 17, 2020 - 9:15 - 10:00am.....	355
P3A: POSTER SESSION 3A	355
Ances, Beau	359
P120: Depression is predicted by tau imaging biomarker among cognitively normal adults.....	359
<i>Ganesh Babulal¹, Catherine Roe¹, Sarah Stout¹, Ganesh Rajasekar¹, Julie Wisch¹, Tammie Benzinger¹, John Morris¹, Beau Ances¹.....</i>	359
Bilgel, Murat	360
P121: Local associations between tau and neurodegeneration among non-demented older adults	360
<i>Murat Bilgel¹, Dean Wong², Susan Resnick¹.....</i>	360
Brendel, Matthias.....	363
P122: Perfusion-phase 18F-PI-2620 tau-PET imaging as a surrogate marker of neuronal injury.....	363
<i>Matthias Brendel¹, Leonie Beyer¹, Alexander Nitschmann¹, Henryk Barthel², Thilo van Eimeren^{3,4,5,6}, Ken Marek^{7,8}, Mengmeng Song¹, Carla Palleis⁹, Gesine Respondek^{6,10}, Julia Sauerbeck¹, Jochen Hammes⁴, Michael Barbe⁵, Özgür Onur⁵, Frank Jessen^{6,11,12}, Dorothee Saur¹³, Matthias L. Schroeter^{14,15,16}, Jost-Julian Rumpf¹³, Michael Rullmann², Andreas Schildan², Marianne Patt², Bernd Neumaier^{3,4}, Oliver Barret^{7,8}, Jennifer Madonia^{7,8}, David S. Russel^{7,8}, Andrew Stephens¹⁷, Sigrun Roeber¹⁸, Jochen Herms^{6,18}, Kai Bötzel⁹, Johannes Levin^{6,9}, Joseph Classen¹³, Guenter Hoeglenger^{6,10,19}, Peter Bartenstein^{1,20}, Victor Villemagne^{21,22,23}, Alexander Drzezga^{4,6}, John Seibyl^{7,8}, Osama Sabri².....</i>	363
Brendel, Matthias.....	365
P123: Binding characteristics of 18F-PI-2620 differentiate the clinically predicted tau isoform in suspected 3/4-repeat and 4-repeat tauopathies.....	365
<i>Matthias Brendel¹, Mengmeng Song¹, Leonie Beyer¹, Henryk Barthel², Thilo van Eimeren^{3,4,5,6}, Ken Marek^{7,8}, Carla Palleis⁹, Lena Kaiser¹, Gesine Respondek^{6,10}, Julia Sauerbeck¹, Jochen Hammes⁴, Michael Barbe⁵, Özgür Onur⁵, Frank Jessen^{6,11,12}, Dorothee Saur¹³, Matthias L. Schroeter^{14,15,16}, Jost-Julian Rumpf¹³, Michael Rullmann², Andreas Schildan², Marianne Patt², Bernd Neumaier^{3,4}, Oliver Barret^{7,8}, Jennifer Madonia^{7,8}, David S. Russel^{7,8}, Andrew Stephens¹⁷, Sigrun Roeber¹⁸, Jochen Herms^{6,18}, Kai</i>	

<i>Bötzel</i> ⁹ , <i>Johannes Levin</i> ^{6,9} , <i>Joseph Classen</i> ¹³ , <i>Guenter Hoeglinger</i> ^{6,10,19} , <i>Peter Bartenstein</i> ^{1,20} , <i>Victor Villemagne</i> ^{21,22,23} , <i>Alexander Drzezga</i> ^{4,6} , <i>John Seibyl</i> ^{7,8} , <i>Osama Sabri</i> ²	365
Brendel, Matthias	367
P124: 18F-PI2620 tau-PET for assessment of heterogeneous neuropathology in corticobasal syndrome	367
<i>Matthias Brendel</i> ¹ , <i>Carla Palleis</i> ² , <i>Catharina Prix</i> ² , <i>Mona Gehmeyr</i> ² , <i>Kai Bötzel</i> ² , <i>Adrian Danek</i> ² , <i>Matthias Höllerhage</i> ³ , <i>Julia Sauerbeck</i> ¹ , <i>Leonie Beyer</i> ¹ , <i>Alexander Nitschmann</i> ¹ , <i>Mengmeng Song</i> ¹ , <i>Andrew Stephens</i> ⁴ , <i>Henryk Barthel</i> ⁵ , <i>Marianne Patt</i> ⁵ , <i>Osama Sabri</i> ⁵ , <i>Alexander Drzezga</i> ^{6,7} , <i>Thilo van Eimeren</i> ^{6,7,8,9} , <i>Victor Villemagne</i> ^{10,11,12} , <i>Peter Bartenstein</i> ^{1,13} , <i>Robert Perneczky</i> ^{7,14,15,16} , <i>Christian Haass</i> ^{7,13,17} , <i>Johannes Levin</i> ^{2,7} , <i>Guenter Hoeglinger</i> ^{3,7,18}	367
Bullich Roig, Santiago	369
P125: Optimal reference region for the quantification of tau load in the brain using 18F-PI-2620 PET	369
<i>Santiago Bullich</i> ¹ , <i>Andre Müller</i> ¹ , <i>Núria Roè-Vellvé</i> ¹ , <i>Aleksandar Jovalekic</i> ¹ , <i>Audrey Perrotin</i> ¹ , <i>Susan De Santi</i> ² , <i>Norman Koglin</i> ¹ , <i>Andrew W. Stephens</i> ¹	369
Chen, Charles	370
P126: Quantifying tau PET imaging reliably in the presence of off-target binding	370
<i>Charles Chen</i> ¹ , <i>Brian Gordon</i> ¹ , <i>Austin McCullough</i> ¹ , <i>Aiad Zaza</i> ¹ , <i>Christopher Mejias</i> ¹ , <i>Aylin Dincer</i> ¹ , <i>Shaney Flores</i> ¹ , <i>Sarah Keefe</i> ¹ , <i>Angela Paulick</i> ¹ , <i>Kelley Jackson</i> ¹ , <i>Deborah Koudelis</i> ¹ , <i>Yi Su</i> ² , <i>John Morris</i> ¹ , <i>Tammie Benzinger</i> ¹	370
Chiotis, Konstantinos	372
P127: [18F]THK5317 imaging as a predictive tool of prospective cognitive decline in prodromal and dementia-stage Alzheimer's disease	372
<i>Konstantinos Chiotis</i> ^{1,2} , <i>Irina Savitcheva</i> ³ , <i>Konstantinos Poulakis</i> ⁴ , <i>Laure Saint-Aubert</i> ^{1,5} , <i>Anders Wall</i> ^{6,7} , <i>Gunnar Antoni</i> ⁷ , <i>Agneta Nordberg</i> ^{1,8}	372
Cohen, Ann	374
P128: Comparison of quantitative cutoff methods for [18F]AV-1451	374
<i>Davneet Minhas</i> ¹ , <i>Charles Laymon</i> ¹ , <i>Brian Lopresti</i> ¹ , <i>Beth Snitz</i> ² , <i>Dana Tudorascu</i> ³ , <i>Howard Aizenstein</i> ⁴ , <i>Oscar Lopez</i> ² , <i>Chester Mathis</i> ¹ , <i>William Klunk</i> ⁴ , <i>Ann Cohen</i> ⁴	374
Fernandez Arias, Jaime	375
P129: Pilot study on the relationship between 18F-MK-6240 and VBM in early and late stages of AD	375
<i>Jaime Fernandez Arias</i> ^{1,4} , <i>Tharick Pascoal</i> ^{1,4} , <i>Andrea Benedet</i> ^{1,4} , <i>Joseph Thierrault</i> ^{1,4} , <i>Min Su Kang</i> ^{1,3,4} , <i>Melissa Savard</i> ^{1,4} , <i>Julie Ottoy</i> ² , <i>Sulantha Mathotaarachchi</i> ¹ , <i>Firoza Lussier</i> ^{1,4} , <i>Cécile Tissot</i> ^{1,4} , <i>Emilie Thomas</i> ¹ , <i>Jenna Stevenson</i> ^{1,4} , <i>Nesrine Rahmouni</i> ^{1,4} , <i>Tina Wang</i> ^{1,4} , <i>Gassan Massarweh</i> ³ , <i>Jean-Paul Soucy</i> ³ , <i>Serge Gauthier</i> ^{1,3,4} , <i>Pedro Rosa-Neto</i> ^{1,3,4}	375
Franzmeier, Nicolai	377
P130: Functional connectivity brain architecture predicts the rate of tau accumulation in Alzheimer's disease	377
<i>Nicolai Franzmeier</i> ¹ , <i>Julia Neitzel</i> ¹ , <i>Anna Rubinski</i> ¹ , <i>Ruben Smith</i> ^{2,3} , <i>Olof Strandberg</i> ³ , <i>Rik Ossenkoppele</i> ^{3,4} , <i>Oskar Hansson</i> ^{3,5} , <i>Michael Ewers</i> ¹	377
Groot, Colin	381
P131: How innocent is PART?: Mesial temporal tau is associated with worse cognitive performance in Aβ-negative cognitively normal individuals	381
<i>Colin Groot</i>	381
Guo, Tengfei	384
P132: CSF P-tau detects cerebral tau accumulation earlier than tau PET in amyloid positive elderly adults	384
<i>Tengfei Guo</i> ^{1,2} , <i>William Jagust</i> ^{1,2} , <i>Susan Landau</i> ^{1,2}	384
Hanseeuw, Bernard	388
P133: Amyloid, tau, and atrophy in preclinical Alzheimer's disease: A longitudinal study	388
<i>Bernard Hanseeuw</i> ^{1,2} , <i>Heidi Jacobs</i> ¹ , <i>Aaron Schultz</i> ¹ , <i>Rachel Buckley</i> ¹ , <i>Michael Properzi</i> ¹ , <i>Michelle Farrell</i> ¹ , <i>Matthew Scott</i> ¹ , <i>Olivia Hampton</i> ¹ , <i>Justin Sanchez</i> ¹ , <i>Reisa Sperling</i> ¹ , <i>Keith Johnson</i> ¹	388
Hansson, Oskar	391
P134: Increased levels and phosphorylation of soluble tau proteins occur earlier than changes in Tau PET in Alzheimer's disease	391
<i>Oskar Hansson</i> ¹ , <i>Emelie Andersson</i> ¹ , <i>Shorena Janelidze</i> ¹ , <i>Rik Ossenkoppele</i> ¹ , <i>Philip Insel</i> ¹ , <i>Olof Strandberg</i> ¹ , <i>Henrik Zetterberg</i> ² , <i>Kaj Blennow</i> ² , <i>Xiyun Chai</i> ³ , <i>Jeffrey Dage</i> ³ , <i>Erik Stomrud</i> ¹ , <i>Ruben Smith</i> ¹ , <i>Sebastian Palmqvist</i> ¹ , <i>Niklas Mattsson</i> ¹	391
Harada, Ryuichi	392
P135: Preclinical characterization of [18F]THK-5562, a novel tau PET tracer with little off-target binding	392
<i>Ryuichi Harada</i> ^{1,2} , <i>Pradith Lersdirisuk</i> ³ , <i>Du Yiqing</i> ¹ , <i>Michinori Ezura</i> ⁴ , <i>Yuki Shimizu</i> ³ , <i>Takahiro Morito</i> ¹ , <i>Hiroyuki Arai</i> ¹ , <i>Kazuhiko Yanai</i> ¹ , <i>Yukitsuka Kudo</i> ² , <i>Shozo Furumoto</i> ³ , <i>Nobuyuki Okamura</i> ^{2,3,5}	392
Hsiao, Ing-Tsung	393
P136: Comparison of tau PET imaging using 18F-APN-1607 and 18F-THK5351 in Alzheimer's disease patients and normal controls	393
<i>Ing-Tsung Hsiao</i> ^{1,2} , <i>Kun-Ju Lin</i> ^{1,2} , <i>Chin-Chang Huang</i> ³ , <i>Kuo-Lun Huang</i> ³	393
Iaccarino, Leonardo	395
P137: In vivo amyloid-PET and tau-PET evidence in early-onset Alzheimer's Disease: taking the LEADS	395
<i>Leonardo Iaccarino</i> ¹ , <i>Renaud La Joie</i> ¹ , <i>Orit Lesman-Segev</i> ¹ , <i>David Soleimani-Meigooni</i> ¹ , <i>Karine Provost</i> ¹ , <i>Jessica A. Collins</i> ² , <i>Paul S. Aisen</i> ³ , <i>Bret J. Borowski</i> ⁴ , <i>Ani Eloyan</i> ⁵ , <i>Anne M. Fagan</i> ⁶ , <i>Tatiana M. Foroud</i> ⁷ , <i>Constantine Gatsonis</i> ⁸ , <i>Clifford R. Jack Jr.</i> ⁴ , <i>Joel H. Kramer</i> ⁹ , <i>Andrew J. Saykin</i> ⁷ , <i>Arthur W. Toga</i> ¹¹ , <i>Prashanti Vemuri</i> ⁴ , <i>Gregory S. Day</i> ¹² , <i>Neill R. Graff-Radford</i> ¹³ , <i>Lawrence S. Honig</i> ¹⁴ , <i>David T. Jones</i> ⁴ , <i>Joseph C. Masdeu</i> ¹⁵ , <i>Mario Mendez</i> ¹⁶ , <i>Chiadi U. Onyike</i> ¹⁷ , <i>Emily J. Rogalski</i> ¹⁸ , <i>Stephen Salloway</i> ¹⁹ , <i>David A. Wolk</i> ²⁰ , <i>Thomas S. Wingo</i> ²¹ , <i>Robert Koeppe</i> ¹⁰ , <i>Brad C. Dickerson</i> ²² , <i>Liana G. Apostolova</i> ²⁴ , <i>Maria C. Carrillo</i> ²³ , <i>Gil D. Rabinovici</i> ¹	395

Iaccarino, Leonardo	399
P138: Multimodal in vivo investigation of amyloid and tau biomarkers associations with cerebrospinal fluid NFL and YKL40 levels	399
<i>Leonardo Iaccarino¹, Renaud La Joie¹, Lauren Edwards¹, Orit Lesman-Segev¹, Amelia Strom¹, Julie Pham¹, Kiran Chaudhary¹, Laura Fenton², Gina Jerome³, Mustafa Janabi⁴, Suzanne Baker⁴, Bruce Miller¹, William Jagust^{2,4}, Anne Fagan³, Gil Rabinovici^{1,2,4,5}</i>	
Kang, Min Su	403
P139: Activated microglia and amyloid load potentiate tau deposition leading to cognitive dysfunction in Alzheimer's disease	403
<i>Min Su Kang^{1,3,4}, Julie Ottoy², Melissa Savard^{1,4}, Tharick Pascoal^{1,4}, Sulantha Mathotaarachchi¹, Andréa Benedet^{1,4}, Mira Chamoun^{1,4}, Joseph Therriault^{1,4}, Firoza Lussier^{1,4}, Cécile Tissot^{1,4}, Emilie Thomas¹, Jenna Stevenson^{1,4}, Nesrine Rahmouni^{1,4}, Jaime Arias^{1,4}, Tina Wang^{1,4}, Gassan Massarweh³, Jean-Paul Soucy³, Serge Gauthier^{1,3,4}, Pedro Rosa-Neto^{1,3,4}</i>	
Kang, Min Su	404
P140: Tauopathy in females is more vulnerable to amyloid or neuroinflammation in Alzheimer's disease	404
<i>Min Su Kang^{1,3}, Julie Ottoy², Mira Chamoun¹, Sulantha Mathotaarachchi¹, Melissa Savard¹, Andréa Benedet¹, Tharick Pascoal¹, Joseph Therriault¹, Firoza Lussier¹, Cécile Tissot¹, Emilie Thomas¹, Jenna Stevenson¹, Nesrine Rahmouni¹, Jaime Fernandez-Arias¹, Tina Wang¹, Gassan Massarweh³, Jean-Paul Soucy³, Serge Gauthier¹, Pedro Rosa-Neto¹</i>	
Kim, Jaeho	406
P141: Prediction of brain tau accumulation in amyloid positive cognitive impairment patients using multimodal biomarkers with machine learning approach	406
<i>Jaeho Kim^{1,2,3}, Seongbeom Park¹, Yuhyun Park^{1,5}, Sung Hoon Kang^{1,2,3}, Soo Jong Kim¹, Hyemin Jang^{1,2,3}, Hee Jin Kim^{1,2,3}, Duk L. Na^{1,2,3,4,6}, Hyejoo Lee^{1,2,3}, Sang Won Seo^{1,2,3,5,6}</i>	
Klein, Gregory	408
P142: Comparison of longitudinal change metrics for 18F-RO948 PET among cognitively unimpaired and patients with MCI or AD dementia in the BioFINDER2 study	408
<i>Gregory Klein¹, Sandra Sanabria⁴, Antoine Leuzy², Edilio Borroni¹, Niklas Mattsson², Sebastian Palmqvist^{2,3}, Erik Stomrud^{2,3}, Ruben Smith^{2,3}, Oskar Hansson^{2,3}</i>	
Mormino, Elizabeth	410
P143: Validation of clinical protocols for clinicians analyzing 18F-PI-2620 tau PET/MRI images	410
<i>Mary Ellen Koran¹, Sara Shams¹, Patrick Adams¹, Emily Cazevedo¹, Tyler N. Toueg¹, Nicole Corso¹, Madison Hunt¹, Jessa Castillo¹, Jacob Hall¹, Sharon Sha¹, Carolyn Fredericks¹, Michael Greicius¹, Anthony Wagner¹, Greg Zaharchuk¹, Guido Davidzon¹, Frederick Chin¹, Elizabeth Mormino¹</i>	
Benedet, Andrea	412
P144: Cerebrospinal fluid tau phosphorylated at amino acid 181 or 231: a biomarker comparison in the detection of neurofibrillary tangle pathology in the Alzheimer's disease spectrum	412
<i>Andrea Benedet¹, Nicholas Ashton^{2,3,4,5}, Tharick Pascoal¹, Erik Stoops⁶, Cindy Francois⁶, Eugeen Vanmechelen⁶, Thomas Karikari², Sulantha Mathotaarachchi¹, Melissa Savard¹, Joseph Therriault¹, Mira Chamoun¹, Henrik Zetterberg^{2,7,8,9}, Kaj Blennow^{2,7}, Pedro Rosa-Neto^{1,10,11}</i>	
Leuzy, Antoine	415
P145: Diagnostic performance of [18F]RO948 tau positron emission tomography in the differentiation of AD from other neurodegenerative disorders	415
<i>Antoine Leuzy¹, Ruben Smith^{1,2}, Rik Ossenkoppele^{1,3}, Alexander Santillo¹, Edilio Borroni⁴, Gregory Klein⁴, Tomas Olsson⁵, Jonas Jögi⁶, Sebastian Palmqvist^{1,2}, Niklas Mattsson^{1,2,7}, Olof Strandberg¹, Erik Stomrud^{1,8}, Oskar Hansson^{1,8}</i>	
Leuzy, Antoine	418
P146: Longitudinal changes in tau pathology measured by [18F]RO948 tau-PET are associated with elevated CSF P-tau: preliminary findings from the Swedish BioFINDER-2 study	418
<i>Antoine Leuzy¹, Gregory Klein², Rik Ossenkoppele^{1,3}, Niklas Mattsson^{1,4,5}, Shorena Janelidze¹, Sebastian Palmqvist^{1,4}, Olof Strandberg¹, Preciosa Coloma², Edilio Borroni², Erik Stomrud^{1,6}, Ruben Smith^{1,4}, Oskar Hansson^{1,6}</i>	
Lin, Kun-Ju	420
P147: A comparison of ischemic stroke-induced changes on 18F-APN-1607 (18F-PMPBB3) and 18F-THK-5351 uptake patterns	420
<i>Kun-Ju Lin^{1,3}, Ing-Tsung Hsiao^{1,3}, Kuo-Lun Huang², Chin-Chang Huang²</i>	
Manser, Paul	421
P148: Longitudinal change in [18F]GTP1 SUVR over 18 months depends on baseline SUVR intensity and spatial distribution and shows trends with cognitive decline	421
<i>Paul Manser¹, Sandra Sanabria Bohorquez¹, Edmond Teng¹, Suzanne Baker¹, Balazs Toth¹, Jan Marik¹, Robby Weimer¹</i>	
Margolin, Richard	423
P149: 18F-APN-1607: a promising PET tracer for multiple tauopathies	423
<i>Richard Margolin^{1,2}, Kun-ju Lin^{1,3,4}, Paul Tempest¹, Poe-Jou Chen¹, Kenneth Marek⁵, David Russell⁵, Christine Sandiego⁵, Chin-Chang Huang^{4,6}, Ing-Tsung Hsiao^{3,4}, Gilles Tamagnan⁷, David Alagille⁷, Yihui Guan⁸, Jiaying Lu⁸, Chuantao Zuo⁸, Makoto Higuchi⁹, Ming-Kuei Jang¹</i>	
Mecca, Adam	425
P150: Entorhinal cortical tau accumulation is inversely associated with hippocampal synaptic density in older individuals with normal cognition and early Alzheimer's disease	425
<i>Adam Mecca¹, Ming-Kai Chen¹, Mika Naganawa¹, Takuya Toyonaga¹, Tyler Godek¹, Joanna Harris¹, Hugh Bartlett¹, Wenzhen Zhao¹, Jean-Dominique Gallezot¹, Nabeel</i>	

<i>Nabulsi¹, Yiyun Huang¹, Amy Arnsten¹, Richard Carson¹, Christopher van Dyck¹</i>	425
Min, Hoon-Ki	427
P151: Mental and physical activity during the uptake period affects off-target binding in extra- and within-brain Tau PET (18F-FTP)	427
<i>Hoon-Ki (Paul) Min¹, Christopher Apgar¹, Nancy Scott¹, Haakon Hol¹, Emily Lundt¹, Sabrina Albertson¹, Christopher Schwarz¹, Hugo Botha¹, Prashanthi Vemuri¹, Jeffrey Gunter¹, Ronald Petersen¹, Clifford Jack¹, Val Lowe¹</i>	427
Nakano, Yoshikazu	430
P152: In vivo uptake of 18F-PM-PBB3 (18F-APN-1607) in patients with corticobasal syndrome	430
<i>Yoshikazu Nakano¹, Hitoshi Shimada¹, Kenji Tagai¹, Kiwamu Matsuoka¹, Manabu Kubota¹, Keisuke Takahata¹, Yuhei Takado¹, Hitoshi Shinotoh^{1,2}, Yasuharu Yamamoto¹, Yasunori Sano¹, Chie Seki¹, Shigeki Hirano^{1,3}, Maiko Ono¹, Paul Tempest⁴, Ming-Kuei Jang⁴, Naruhiko Sahara¹, Kazunori Kawamura¹, Ming-Rong Zhang¹, Satoshi Kuwabara³, Makoto Higuchi¹</i>	430
Ossenkoppele, Rik	431
P153: Factors predicting tau PET status in cognitively unimpaired and impaired individuals .	431
<i>Rik Ossenkoppele¹, Antoine Leuzyl¹, Hannah Cho³, Renaud La Joie², Olof Strandberg¹, Niklas Mattsson¹, Sebastian Palmqvist¹, Chul Lyoo³, Gil Rabinovici², Ruben Smith¹, Oskar Hansson¹</i>	431
Ozlen, Hazel	433
P154: Widespread amyloid is necessary to detect tau-PET signal beyond the entorhinal cortex and cognitive decline	433
<i>Hazel Ozlen^{1,2}, Alexa Pichet Binette^{1,2,4}, Theresa Köbe^{1,2}, Pierre-Francois Meyer^{1,2,4}, Sylvia Villeneuve^{1,2,3,4}</i>	433
Provost, Karine	436
P155: Using 18F-Flortaucipir visual assessment to define T-status in the AT(N) framework: evaluation of intra- and inter-rater reliability	436
<i>Karine Provost¹, Leonardo Iaccarino¹, David Soleimani-Meigooni¹, Orit Lesman-Segev¹, Renaud La Joie¹, Lauren Edwards¹, Amelia Strom¹, Julie Pham¹, Taylor Mellinger¹, Mustafa Janabi², Suzanne Baker², William Jagust^{2,3}, Gil D. Rabinovici^{1,2,3,4}</i>	436
Provost, Karine	440
P156: Defining T-status in the AT(N) framework: comparison of 18F-Flortaucipir visual assessment, SUVR quantification and CSF pTau	440
<i>Karine Provost¹, Leonardo Iaccarino¹, David Soleimani-Meigooni¹, Orit Lesman-Segev¹, Renaud La Joie¹, Niklas Mattsson², Oskar Hansson², Udo Eichenlaub³, Lauren Edwards¹, Amelia Strom¹, Julie Pham¹, Taylor Mellinger¹, Mustafa Janabi⁴, Suzanne Baker⁴, William Jagust^{4,5}, Gil Rabinovici^{1,4,5,6}</i>	440
Quiroz, Yakeel T.	443
P157: Plasma neurofilament light is associated with regional tau tangle burden in autosomal dominant Alzheimer's disease: findings from the COLBOS Project	443
<i>Yakeel T. Quiroz¹, Henrik Zetterberg², Eric Reiman³, Justin Sanchez¹, Edmarie Guzman-Velez¹, Josh Fox-Fuller¹, Joseph Arboleda-Velasquez⁵, Ana Baena⁴, Jennifer Gatchel¹, Reisa Sperling⁶, Keith Johnson¹, Kaj Blennow², Francisco Lopera⁴</i>	443
Salinas, Cristian	444
P158: Application of tau PET as a biomarker of Alzheimer's disease in therapeutic trials: A pharmaceutical industry perspective	444
<i>Cristian Salinas¹, Talakad Lohith², Qi Guo³, Dustin Wooten³, Thom Tulip⁴, Sulantha Sanjeeva⁴, Robert Comley³, Cyrille Sur², Eric Hostetter², John Beaver¹, Laurent Martarello¹</i>	444
Sanabria Bohorquez, Sandra	446
P159: Measuring increases of tau pathology in Alzheimer's disease using [18F]GTP1 (Genentech tau probe 1) PET imaging	446
<i>Sandra Sanabria Bohorquez¹, Suzanne Baker^{1,2}, Paul Manser¹, Balazs Toth¹, Edmond Teng¹, Jan Marik¹, Robby Weimer¹</i>	446
Sanchez, Justin	449
P160: Evaluation of tau PET staging in the A4/LEARN study	449
<i>Justin Sanchez¹, Alex Becker¹, Heidi Jacobs^{1,3}, Bernard Hanseeuw^{1,4}, Danielle Mayblyum¹, Zoe Rubinstein¹, Emma Thibault¹, Aaron Schultz¹, Sudha Seshadri^{5,6}, Yakeel Quiroz¹, Dorene Rentz^{1,2}, Julie Price¹, Reisa Sperling^{1,2}, Keith Johnson^{1,2}, on behalf of the A4 Study Team²</i>	449
Schmidt, Mark	453
P161: Clinical evaluation of [18F]-JNJ-64326067, a candidate PET tracer for the detection of tau pathology in Alzheimer's disease	453
<i>Mark Schmidt¹, Luc Janssens¹, Diederik Moechars¹, Frederik Rombouts¹, Maarten Timmers¹, Olivier Barret², Christian Constantinescu², Jennifer Madonia², David Russell², Christine Sandiego², Hartmuth Kolb³</i>	453
Schultz, Stephanie	454
P162: Association between cerebrospinal fluid neurofilament light chain and markers of neurofibrillary pathophysiology: findings from the Knight Alzheimer Disease Research Center	454
<i>Stephanie Schultz¹, Suzanne Schindler¹, Charlie Chen¹, Courtney Sutphen¹, John Morris¹, Anne Fagan¹, Brian Gordon¹, Tammie Benzinger¹</i>	454
Shimada, Hitoshi	457
P163: 18F-PM-PBB3 (18F-APN-1607) uptake associates with plasma NFL level and motor disability in patients with progressive supranuclear palsy	457
<i>Hitoshi Shimada¹, Kenji Tagai¹, Harutsugu Tatebe², Kiwamu Matsuoka¹, Manabu Kubota¹, Keisuke Takahata¹, Yuhei Takado¹, Hitoshi Shinotoh^{1,4}, Yasuharu Yamamoto¹, Yasunori Sano¹, Chie Seki¹, Yoshikazu Nakano¹, Maiko Ono¹, Shigeki Hirano⁴, Paul Tempest⁵, Ming-Kuei Jang⁵, Naruhiko Sahara¹, Kazunori Kawamura¹, Ming-Rong Zhang¹, Takahiko Tokuda², Makoto Higuchi¹</i>	457
Smith, Ruben	458
P164: The rate of accumulation of tau aggregates is higher in females and younger individuals	458

<i>Ruben Smith</i> ^{1,2} , <i>Niklas Mattsson</i> ^{1,2,3} , <i>Michael Pontecorvo</i> ⁴ , <i>Michael Devous</i> ⁴ , <i>Olof Strandberg</i> ¹ , <i>Rik Ossenkoppele</i> ^{1,5} , <i>Oskar Hansson</i> ^{1,6}	458
Svaldi, Diana	462
P165: Resting state functional connectivity associations with F18-Florbetapir PET versus F18-Flortaucipir PET	462
<i>Diana Svaldi</i> ¹ , <i>Joaquin Goñi</i> ² , <i>Edwin Stage</i> ¹ , <i>Kausar Abbas</i> ² , <i>Mario Dzemidzic</i> ¹ , <i>John West</i> ¹ , <i>Shannon Risacher</i> ¹ , <i>Andrew Saykin</i> ¹ , <i>Liana Apostolova</i> ¹	462
Therneau, Terry	466
P166: Tau positivity: Comparing flortaucipir meta-ROI vs maximal single region	466
<i>Terry Therneau</i> ¹ , <i>Christopher Schwarz</i> ¹ , <i>Heather Wiste</i> ¹ , <i>Jeffrey Gunter</i> ¹ , <i>Matthew Senjem</i> ¹ , <i>Val Lowe</i> ¹ , <i>Kejal Kantarci</i> ¹ , <i>Ronald Petersen</i> ¹ , <i>David Knopman</i> ¹ , <i>Michelle Mielke</i> ¹ , <i>David Jones</i> ¹ , <i>Clifford Jack</i> ¹	466
Therriault, Joseph	469
P167: Intrinsic connectivity of the human brain provides scaffold for tau aggregation in Alzheimer's disease	469
<i>Joseph Therriault</i> ¹ , <i>Tharick Pascoal</i> ¹ , <i>Melissa Savard</i> ¹ , <i>Sulantha Mathotaarachchi</i> ¹ , <i>Andrea Benedet</i> ¹ , <i>Mira Chamoun</i> ¹ , <i>Serge Gauthier</i> ¹ , <i>Paramita Saha-Chaudhuri</i> ¹ , <i>Gassan Massarweh</i> ¹ , <i>Pedro Rosa-Neto</i> ¹	469
Toth, Balasz	473
P168: Changes in volumetric MRI measures at 12 months significantly correlate with baseline [18F]GTP1 SUVR, but not [18F]GTP1 change	473
<i>Balasz Toth</i> ¹ , <i>Sandra Sanabria Bohorquez</i> ¹ , <i>Paul Manser</i> ¹ , <i>Suzanne Baker</i> ¹ , <i>Edmond Teng</i> ¹ , <i>Jan Marik</i> ¹ , <i>Robby Weimer</i> ¹	473
Toueg, Tyler	475
P169: Elevated medial temporal lobe Tau PET with 18F-PI2620 in normal controls with "borderline" neuropsychological testing profiles	475
<i>Tyler Toueg</i> ¹ , <i>Gayle Deutsch</i> ¹ , <i>Jessa Castillo</i> ² , <i>Madison Hunt</i> ³ , <i>Nicole Corso</i> ³ , <i>Alexandra Trelle</i> ³ , <i>Marc Harrison</i> ³ , <i>Carmen Azevedo</i> ² , <i>Bin Shen</i> ² , <i>David Anders</i> ² , <i>Jacob Hall</i> ¹ , <i>Carolyn Fredericks</i> ⁴ , <i>Sharon Sha</i> ¹ , <i>Guido Davidzon</i> ² , <i>Frederick Chin</i> ² , <i>Mehdi Khalighi</i> ² , <i>Anthony Wagner</i> ³ , <i>Elizabeth Mormino</i> ¹	475
Trelle, Alexandra	476
P170: Hippocampal tau accumulation predicts individual differences in episodic memory in cognitively normal older adults	476
<i>Alexandra N. Trelle</i> ¹ , <i>Tyler N. Toueg</i> ¹ , <i>Jessa B. Castillo</i> ¹ , <i>Divya Channappa</i> ¹ , <i>Nicole Corso</i> ¹ , <i>Madison Hunt</i> ¹ , <i>Manasi Jayakumar</i> ³ , <i>Ayesha Nadiadwala</i> ² , <i>Wanjia Guo</i> ⁴ , <i>Carmen Azevedo</i> ¹ , <i>Bin Shin</i> ¹ , <i>Guido A. Davidson</i> ¹ , <i>Gayle Deutsch</i> ¹ , <i>Jacob N. Hall</i> ¹ , <i>Sharon J. Sha</i> ¹ , <i>Carolyn Fredericks</i> ⁵ , <i>Geoffrey Kerchner</i> ¹ , <i>Valerie Carr</i> ⁶ , <i>Frederick Chin</i> ¹ , <i>Anthony D. Wagner</i> ¹ , <i>Elizabeth C. Mormino</i> ¹	476
Unschuld, Paul	477
P171: Temporo-limbic tau burden, as measured by 18F-AV1451, is a correlate of hippocampal volume loss over time	477
<i>Jannis Fischer</i> ¹ , <i>Max Ahnen</i> ¹ , <i>Günther Dissertori</i> ¹ , <i>Werner Luster</i> ¹ , <i>Bruno Weber</i> ² , <i>Alfred Buck</i> ² , <i>Sonja Kagerer</i> ^{3,4} , <i>Anton Gietl</i> ^{3,4} , <i>Christoph Hock</i> ³ , <i>Paul Unschuld</i> ^{3,4}	477
Ances, Beau	479
P172: Temporal evaluation for maximum CSF pTau181 – [18F]Flortaucipir concordance	479
<i>Julie Wisch</i> ¹ , <i>Brian Gordon</i> ¹ , <i>Suzanne Schindler</i> ¹ , <i>Shaney Flores</i> ¹ , <i>Aylin Dincer</i> ¹ , <i>Anne Fagan</i> ¹ , <i>Tammie Benzinger</i> ¹ , <i>John Morris</i> ¹ , <i>Beau Ances</i> ¹	479
Wolters, Emma	481
P173: [18F]flortaucipir PET is more closely associated with disease severity than CSF p-tau in Alzheimer's disease	481
<i>Emma Wolters</i> ^{1,2} , <i>Rik Ossenkoppele</i> ^{2,3} , <i>Sander Verfaillie</i> ¹ , <i>Emma Coomans</i> ¹ , <i>Tessa Timmers</i> ^{1,2} , <i>Denise Visser</i> ¹ , <i>Hayel Tuncel</i> ¹ , <i>Sandeep Golla</i> ¹ , <i>Albert Windhorst</i> ¹ , <i>Ronald Boellaard</i> ¹ , <i>Wiesje van der Flier</i> ^{2,4} , <i>Charlotte Teunissen</i> ⁵ , <i>Philip Scheltens</i> ² , <i>Bart van Berckel</i> ¹	481
Ziontz, Jacob	485
P174: Associations of tau pathology and functional connectivity with retrospective cognitive change among cognitively normal older adults	485
<i>Andrea Shafer</i> ¹ , <i>Murat Bilgel</i> ¹ , <i>Jacob Ziontz</i> ^{1,2} , <i>Dean Wong</i> ³ , <i>Susan Resnick</i> ¹	485
Friday, January 17, 2020 - 10:00 - 11:00am	487
SESSION 7B: TAU II	487
Johnson, Keith	488
Critical threshold of elevated amyloid associated with rapid tau accumulation: a ca-tau-strope in the making	488
<i>Keith Johnson</i> ¹ , <i>Heidi Jacobs</i> ¹ , <i>Bernard Hanseeuw</i> ^{1,2} , <i>Justin Sanchez</i> ¹ , <i>John Alex Becker</i> ¹ , <i>Aaron Schultz</i> ¹ , <i>Kathryn Papp</i> ^{1,3} , <i>Julie Price</i> ¹ , <i>Dorene Rentz</i> ^{1,3} , <i>Reisa Sperling</i> ^{1,3}	488
Devous, Michael	492
The meaning of tau positivity with respect to clinical progression	492
<i>Michael Devous</i> ¹ , <i>Adam Fleisher</i> ¹ , <i>Michael Pontecorvo</i> ¹ , <i>Ming Lu</i> ¹ , <i>Vikas Kotari</i> ¹ , <i>Nicholas Galante</i> ¹ , <i>Sudeepti Southekal</i> ¹ , <i>Anupa Arora</i> ¹ , <i>Mark Mintun</i> ¹	492
Knopman, David	496
Longitudinal tau PET changes in cognitively unimpaired persons with different β-amyloid levels	496
<i>David Knopman</i> ¹ , <i>Emily Lundt</i> ¹ , <i>Terry Therneau</i> ¹ , <i>Michelle Mielke</i> ¹ , <i>Val Lowe</i> ¹ , <i>Sabrina Albertson</i> ¹ , <i>David Jones</i> ¹ , <i>Jon Graff-Radford</i> ¹ , <i>Ronald Petersen</i> ¹ , <i>Cliff Jack</i> ¹	496
Pontecorvo, Michael	497
Defining a tau positive Flortaucipir PET signal relative to AD neuropathology	497
<i>Michael Pontecorvo</i> ¹ , <i>Adam Fleisher</i> ¹ , <i>Michael Devous</i> ¹ , <i>Ming Lu</i> ¹ , <i>Vikas Kotari</i> ¹ , <i>Nicholas Galante</i> ¹ , <i>Edwin Lu</i> ¹ , <i>Sudeepti Southekal</i> ¹ , <i>Mark Mintun</i> ¹	497
KEYNOTE LECTURE 3	500
Tsai, Li-Huei	500

Leveraging brain rhythms as a therapeutic intervention for Alzheimer's disease.....	500
<i>Li-Huei Tsai.....</i>	<i>500</i>
Friday, January 17, 2020 - 2:00 - 3:15pm.....	501
SESSION 8: Clinical III.....	501
<i>Strom, Amelia.....</i>	502
Glucose metabolism reflects local atrophy and tau pathology at symptomatic stages of Alzheimer's disease.....	502
<i>Amelia Strom¹, Leonardo Iaccarino¹, Lauren Edwards¹, Orit Lesman Segev¹, David Soleimani-Meigooni¹, William Jagust^{2,3}, Bruce Miller¹, Gil D. Rabinovici^{1,3}, Renaud La Joie¹.....</i>	<i>502</i>
<i>Yang, Hyun-Sik.....</i>	506
Plasma FLT1 predicts amyloid-β related cognitive decline in cognitively normal older adults.....	506
<i>Hyun-Sik Yang¹, Becky Carlyle^{1,3}, Bianca Trombetta¹, Can Zhang^{1,3}, Aaron Schultz^{1,3}, Jeremy Pruzin^{1,2,3}, Colleen Fitzpatrick¹, Dylan Kirn^{1,2}, Dorene Rentz^{1,2,3}, Rudolph Tanzi^{1,3}, Keith Johnson^{1,2,3}, Reisa Sperling^{1,2,3}, Steven Arnold^{1,3}, Jasmeer Chhatwal^{1,3}.....</i>	<i>506</i>
<i>Lopes Alves, Isadora.....</i>	508
Reducing sample sizes to detect longitudinal amyloid accumulation.....	508
<i>Isadora Lopes Alves¹, Lyduine Collijl¹, Fiona Heeman¹, José Luis Molinuevo², Mark Schmidt³, Adriaan Lammertsma¹, Frederik Barkhof^{1,4}, Juan Domingo Gispert², On behalf of the AMYPAD Consortium⁵.....</i>	<i>508</i>
Friday, January 17, 2020 - 4:15 - 5:45pm.....	510
SESSION 9: PLASMA.....	510
<i>Hansson, Oskar.....</i>	511
Plasma P-tau181 as a marker of tau pathology in Alzheimer's disease: relationship to Tau PET, differential diagnosis, neuropathology and longitudinal progression.....	511
<i>Oskar Hansson¹, Shorena Janelidze¹, Niklas Mattsson¹, Sebastian Palmqvist¹, Ruben Smith¹, Thomas Beach², Geidy Serrano², Xiyun Chai³, Nicholas Proctor³, Henrik Zetterberg⁴, Kaj Blennow⁴, Eric Reiman⁵, Jeffrey Dage³.....</i>	<i>511</i>
<i>Chhatwal, Jasmeer.....</i>	514
Plasma levels of an N-terminal tau fragment are highly associated with future cognitive decline and neurodegeneration in clinically normal elderly: findings from the Harvard Aging Brain Study.....	514
<i>Jasmeer Chhatwal^{1,2,3}, Aaron Schultz^{1,3}, Yifan Dang², Beth Ostaszewski², Lei Liu², Hyun-Sik Yang^{1,2,3}, Keith Johnson^{1,2,3}, Reisa Sperling^{1,2,3}, Dennis Selkoe^{2,3}.....</i>	<i>514</i>
<i>Meyer, Pierre-Francois.....</i>	517
Plasma biomarkers associate with amyloid and tau PET binding in cognitively unimpaired older adults with a parental history of AD.....	517
<i>Pierre-Francois Meyer^{1,2,4}, Nicholas Ashton⁵, Thomas Karikari⁵, Theresa Köbe¹, Julie Gonneaud¹, Alexa Pichet Binette^{1,2,4}, Hazal Ozlen¹, Anne Labonté¹, Josef Pannee⁵, Joel Simrén⁵, Anne Labonté¹, Pedro Rosa-Neto^{1,2,3,4}, John Breitner^{1,2,4}, Judes Poirier^{1,2}, Henrik Zetterberg^{5,6}, Kaj Blennow⁵, Sylvia Villeneuve^{1,2,3,4}.....</i>	<i>517</i>
<i>Pascoal, Tharick.....</i>	521
High-performance plasma phospho-tau181 biomarker for Alzheimer's disease.....	521
<i>Tharick Pascoal², Thomas Karikari¹, Nicholas Ashton¹, Andréa Benedet², Melissa Savard², Min Su Kang², Joseph Therriault², Michael Schöll¹, Gassan Massarweh², Jean-Paul Soucy², Serge Gauthier², Henrik Zetterberg¹, Pedro Rosa-Neto², Kaj Blennow¹.....</i>	<i>521</i>

PRESENTER INDEX

Presenter	Page Number
Adams, Jenna	288
Aguero, Cinthya	201
Ances, Beau	154, 359, 479
Badano, Aldo	43
Baker, Suzanne	166
Benedet, Andrea	412
Berron, David	344
Betthausen, Tobey	44
Bharthur Sanjay, Apoorva	47
Bilgel, Murat	360
Bischof, Gerard	50
Brendel, Matthias	336, 363, 365, 367
Buckley, Rachel	246
Bullich Roig, Santiago	369
Bullich, Santiago	51
Cassady, Kaitlin	52
Chen, Charles	370
Chhatwal, Jasmeer	514
Chiotis, Konstantinos	372
Clarke, Mica	236
Cody, Karly	302
Cogswell, Petrice	214
Cohen, Ann	374
Collij, Lyduine	233
Collins, Jessica	232
Coomans, Emma	54, 58
den Braber, Anouk	273
Devous, Michael	492
DiFilippo, Alexandra	61
Dore, Vincent	350

Presenter	Page Number
Edison, Paul	276
Edwards, Lauren	260
Evans, Alan	180
Ewers, Michael	229
Farrell, Michelle	285
Fernandez Arias, Jaime	375
Flores, Shaney	62
Foster, Chris	65
Franzmeier, Nicolai	377
Gatchel, Jennifer	226
Gomperts, Stephen	244
Gong, Kuang	194
Gordon, Brian	68
Goubran, Maged	70
Groh, Jenna	308
Groot, Colin	381
Gunn, Roger N.	184
Gunter, Jeffrey	73
Guo, Tengfei	384
Hahn, Alice	88, 243
Hahn, Alice	243
Hanseeuw, Bernard	211, 388
Hansson, Oskar	391, 511
Hansson, Oskar	511
Harada, Ryuichi	392
Heeman, Fiona	80
Hsiao, Ing-Tsung	393
Hwang, Seong Jae	82
Iaccarino, Leonardo	395, 399
Ikonomovic, Milos	202

Presenter	Page Number
Jacobs, Heidi	341
Johnson, Keith	488
Jones, David	85
Kang, Min Su	403, 404
Kim, Jaeho	270, 406
Kim, Min-Jeong	238
Klein, Gregory	89, 408
Klein, Julia	219
Knopman, David	496
Kohli, Akshay	90
Kothapalli, Satya	93
Landau, Susan	94, 339
Lange, Catharina	66
Lao, Patrick	97, 98
Laymon, Charles	100
Lee, Jin San	225
Lemoine, Laetitia	102
Leuzy, Antoine	347, 415, 418
Levitis, Elizabeth	103
Lin, Kun-Ju	420
Lois, Cristina	106
Lopes Alves, Isadora	508
Lopresti, Brian	170
Lowe, Val	198
Luckett, Emma	245
Luckett, Patrick	190
Lussier, Firoza	317, 319
Malarte, Mona-Lisa	327
Maltais, Daniela	292
Manber, Richard	124,126
Manser, Paul	421
Margolin, Richard	423
Martersteck, Adam	108, 306

Presenter	Page Number
Mayblyum, Danielle	109
McDade, Eric	220
McGinnis, Scott	316
Mecca, Adam	332, 425
Meyer, Pierre-Francois	222, 517
Mielke, Michelle	280
Min, Hoon-Ki	427
Minhas, Davneet	115
Moloney, Christina M.	328
Moore, Annah	117
Moore, Elizabeth	315
Mormino, Elizabeth	410
Nakano, Yoshikazu	430
Nordberg, Agneta	277
O'Dell, Ryan	120
Oh, Hwamee	311
Ossenkoppele, Rik	172, 431
Ottoy, Julie	121
Ozlen, Hazal	433
Pascoal, Tharick	521
Pascual, Belen	239
Pichet Binette, Alexa	248
Pontecorvo, Michael	497
Provost, Karine	436, 440
Quiroz, Yakeel T.	443
Rabiner, Eugenii	127
Rahmouni, Nesrine	131
Riphagen, Joost	133
Risacher, Shannon	330
Rowe, Christopher C	335
Royse, Sarah	300
Rubinstein, Zoe	136
Sala, Arianna	262

Presenter	Page Number
Salinas, Cristian	444
Salvadó, Gemma	251, 254, 257
Sanabria Bohorquez, Sandra	446
Sanchez, Justin	176, 449
Sanchez, Justin	449
Schaefferbeke, Jolien	235
Schmidt, Mark	453
Schneider, Julie	203
Schultz, Stephanie	454
Schwarz, Christopher	352
Scott, David	140
Scott, Matthew	296
Seibyl, John	141
Seo, Sang Won	264
Shimada, Hitoshi	457
Singh, Vikas	76
Smith, Ruben	322, 458
Smith, Ruben	458
Solingapuram sai, Kiran kumar	142
Soucy, Jean-Paul	143
Stephens, Andrew	268
Stevenson, Jenna	144
Strom, Amelia	502
Svaldi, Diana	462
Tennant, Victoria	313
Terada, Tatsuhiro	312

Presenter	Page Number
Therneau, Terry	466
Therriault, Joseph	469
Thibault, Emma	293
Tissot, Cécile	145, 147
Toth, Balasz	473
Toueg, Tyler	475
Trelle, Alexandra	476
Tsai, Li-Huei	500
Tudorascu, Dana	111, 281
Unschuld, Paul.	477
Utianski, Rene	207
Villemagne, Victor	240
Vogel, Jacob	186
Vokali, Efthymia	218
Wang, Yi-Ting	149
Webb, Christina	153
Whitwell, Jennifer	199, 278
Winer, Joseph	265
Wolters, Emma	157
Yang, Hyun-Sik	506
Yoon, Bora	263
Zammit, Matt	160, 182
Zeng, Zhizhen	326
Ziontz, Jacob	163, 485
Zukotynski, Katherine	284

POSTER INDEX *(by poster board number)*

Board #	Poster Title	Authors	Presenter
01	Label-free x-ray method for estimating brain amyloid load	Badano Dahal Ghammraoui	Badano, Aldo
02	Examining regional MK-6240 patterns and associations with amyloid and cognitive decline	Betthausen Cody Kosciak Jonaitis Erickson Converse Murali Barnhart Stone Mueller Clark Asthana Christian Johnson	Betthausen, Tobey
03	Transcriptomic profiling of brain amyloidosis using peripheral blood-based gene expression	Bharthur Sanjay Svaldi Apostolova	Bharthur Sanjay, Apoorva
04	A pons cluster detected by a data-driven approach may serve as a favorable reference region for 18F-PI-2620 Tau PET analysis	Bischof van Eimeren Koglin Müller Bullich Perrotin Stephens Drzezga	Bischof, Gerard
05	Early detection of amyloid load using 18F-Florbetaben PET	Bullich Roé-Vellvé Marquié Villemagne Sanabria Tartari Sotolongo Doré Koglin Müller Perrotin De Santi Tárraga Stephens Rowe Seibyl Boada	Bullich, Santiago
06	Age-related neural dedifferentiation of episodic memory networks is related to beta-amyloid and tau pathology in normal aging	Cassady Adams Maass Harrison Baker Jagust	Cassady, Kaitlin
07	Tau pathology and synaptic loss are closely associated in Alzheimer's disease in vivo: a combined [18F]flortaucipir and [11C]UCB-J PET study	Coomans Verfaillie Wolters Tuncel Golla Ossenkoppele Scheper Schober Sweeney Ryan Schuit Windhorst Scheltens Boellaard van Berckel	Coomans, Emma
08	Longitudinal dynamic [18F]flortaucipir PET reveals increased early stage tau pathology in individuals with subjective cognitive decline	Coomans Visser Ossenkoppele Verfaillie Timmers Wolters Tuncel Schmidt Boellaard Windhorst Scheltens van der Flier van Berckel	Coomans, Emma
09	Preliminary evaluation of synaptic vesicle protein SV2A imaging with [11C]UCB-J across the cognitive spectrum	DiFilippo Murali McKinney Davenport Barnhart Engle Betthausen Johnson Bendlin Christian	DiFilippo, Alexandra
10	Quantifying off-target skull binding in [18F]Flortaucipir PET studies	Flores Gordon Su Christensen Dincer Adedokun Hornbeck Morris Benzinger	Flores, Shaney
11	Influence of iron and beta-amyloid deposition on entorhinal cortex and hippocampal subfield volumes in the aging brain	Foster Kennedy Rodrigue	Foster, Chris
12	Voxel-wise relationships between white matter hyperintensities (WMH) and multimodal neuroimaging biomarkers of Alzheimer's disease	Gaubert Lange Garnier-Crussard Bougacha Gonneaud de Flores Tomadesso Mézenge Landeau de La Sayette Chételat Wirth	Lange, Catharina
13	Beta-amyloid deposition and its association with metabolism	Gordon Goyal Couture Flores Morris Raichle Benzinger Vlassenko	Gordon, Brian
14	Amyloid binding is associated with markers of white matter microstructure in patients with significant white matter disease	Goubran Ozzoude Adamo Zukotynski Bocti Borrie Chertkow Frayne Gao Hsiung Kiss Laforce Noseworthy Prato Ramirez Sahlas Scott Smith Sossi Strother Swartz Tardif Thiel Soucy Black	Goubran, Maged
15	CSF dynamics explains discrepant PET-CSF AD biomarkers	Gunter Senjem Cogswell Schwarz Lowe Kantarci Vemuri Elder Botha Graff-Radford Jones Mielke Graff-Radford Knopman Petersen Jack, Jr.	Gunter, Jeffrey
16	Predicting future amyloid spread with machine learning using longitudinal [C11]PiB-PET in preclinical Alzheimer's disease	Hao Vogt Meng Hwang Kosciak Betthausen Christian Johnson Bendlin Singh	Singh, Vikas
17	[11C]PiB amyloid quantification and choice of reference region	Heeman Hendriks van Berckel Lopes Alves Lammertsma Yaqub	Heeman, Fiona
18	Retrospective prediction of amyloid accumulation trajectories in a risk-enriched Alzheimer's disease cohort with sequential neural network	Hwang Kosciak Betthausen Tao Kim Johnson Singh	Hwang, Seong Jae
19	Data-driven biological pattern scoring of Flortaucipir scans outperforms ROIs	Jones Graff-Radford Botha Senjem Wiste Josephs Whitwell Kantarci Boeve Petersen Knopman Lowe Jack	Jones, David
20	Hippocampal volume mediates the relationship between amyloidosis and amyloid-sensitive cognitive composite in preclinical AD	Kim Hahn Kim Kim Chin Seo	Hahn, Alice

Board #	Poster Title	Authors	Presenter
21	Concordance of visual and quantitative assessments of baseline amyloid scans in the GRADUATE gantenerumab studies	Klein Delmar Voyle Hesterman Petrulli Ovens Baudler Fontoura Doody Kerchner	Klein, Gregory
22	Regional amyloid burden is associated with higher quantitative T1 in discrete hippocampal sub-regions	Kohli Yang Vogt Asthana Betthausen Alexander Christian Johnson Kecskemeti Bendlin	Kohli, Akshay
23	Genetically informed quantitative Gradient Recalled Echo MRI reveals brain tissue in hippocampal subfields void of neurons in mild Alzheimer's disease	Kothapalli Benzinger Aschenbrenner Goyal Fagan Raichle Morris Yablonskiy	Kothapalli, Satya V.V.N.
24	Validation of highly sensitive and specific florbetaben positivity thresholds using ADNI participants and young controls	Landau Korman Bullich De Santi Stephens Koeppe Jagust	Landau, Susan
25	Additive contribution of white matter hyperintensity to amyloid and neurodegeneration on cognitive decline in a diverse, community-based cohort of older adults	Lao Chesebro Colon Igwe Gu Schupf Manly Stern Mayeux Brickman	Lao, Patrick
26	White matter hyperintensities are related to tau burden in late-Braak stage regions	Lao Laing Igwe Chesebro Kreis Moreno Luchsinger Brickman	Lao, Patrick
27	Probability template method for analysis of Down Syndrome amyloid PET	Laymon Minhas James Christian Cohen Klunk Tudorascu Royse Zaman Handen	Laymon, Charles
28	Visualizing brain astrocytes - characterization of 3H-BU99008 in human AD brain tissue	Lemoine Malarte Koistinen Nordberg	Lemoine, Laetitia
29	Application of an epidemic spreading model to characterize amyloid beta accumulation in autosomal dominant Alzheimer's disease mutation carriers	Levitis Vogel Kiar Funck Iturria-Medina Evans	Levitis, Elizabeth
30	Phantom-based harmonization of PET image reconstruction parameters between the Siemens ECAT HR+ PET and the GE Discovery MI PET/CT scanners	Lois Grogg El Fakri Johnson Price	Lois, Cristina
31	Age prediction and amyloid deposition in SuperAgers	Martersteck Besson Sridhar Makowski-Woidan Parrish Katsaggelos Mesulam Bandt Rogalski	Martersteck, Adam
32	PiB tracer delivery decreases overtime in preclinical AD – impact for amyloid pathology measurement	Mayblyum Becker Schultz Farrell Jacobs Rubinstein Sanchez Thibault Sperling Price Johnson Hanseeuw	Mayblyum, Danielle
33	MRI and PET data harmonization in a two-site Down syndrome study	Minhas Yang Muschelli Laymon Zammit Ellison Johnson Mathis Crainiceanu Klunk Handen Christian Cohen Tudorascu	Tudorascu, Dana
34	Sex-specific differences in [18F]AV-1451 off-target retention	Minhas Yu Laymon Lopresti Snitz Tudorascu Aizenstein Lopez Mathis Klunk Cohen	Minhas, Davneet
35	Polygenic risk for Cerebrospinal Fluid (CSF) amyloid predicts brain amyloid in clinically normal older adults	Moore Dumitrescu Schultz Raghavan Johnson Mayeux Sperling Hohman Mormino	Moore, Annah
36	Association between cerebral amyloid accumulation and synaptic density in Alzheimer's disease: A multitracers PET study	O'Dell Mecca Chen Godek Harris Bartlett Banks Kominek Zhao Naganawa Toyonaga Lu Nabulsi Vander Wyk Varma Arnsten Huang Carson van Dyck	O'Dell, Ryan
37	A clinically applicable proxy for gold standard quantification of amyloid-beta in Alzheimer's disease: Bolus plus constant infusion 18F-AV45 PET	Ottoy Kang Verhaeghe Stroobants Bouhachi Hsiao Stevenson Rahmouni Chartrand Massarweh Soucy Gauthier Rosa-Neto Staelens	Ottoy, Julie
38	Amyloid PET variability due to variation in MRI protocol and anatomical segmentation	Palombit Manber Joules Wolz	Manber, Richard
39	The impact of automatic Tau PET processing on uptake variability and power analysis in AD	Palombit Manber Joules Wolz	Manber, Richard
40	MIND MAPS: Assessment of the mitochondrial - endoplasmic reticulum - synaptic axis in neurodegeneration by [18F]BCPP-EF, [11C]SA4503 and [11C]UCB-J PET imaging	Rabiner Mansur Venkataraman Price Wilson Pagano Clarke Lewis Matthews Rowe Brooks Middleton Politis Rohrer Comley Evans Martarello Chen Schwarz Schmidt Tsukada Passchier Gunn Consortium	Rabiner, Eugenio
41	Associations between Neurogranin and imaging biomarkers of Alzheimer's disease	Rahmouni Benedet Nicholas Tissot Pascoal Kvartberg Chamoun Kang Lussier Therriault Stevenson Savard Mathotaarachchi Thomas Gauthier Zetterberg Blennow Rosa-Neto	Rahmouni, Nesrine
42	Linking APOE ε4, blood-brain barrier dysfunction and inflammation to Alzheimer's pathology	Riphagen Ramakers Freeze Pagen Hanseeuw Verbeek Verhey Jacobs	Riphagen, Joost

Board #	Poster Title	Authors	Presenter
43	Heterogeneity of tau PET signal in the sub-nuclei of the amygdala	Rubinstein Jacobs Augustinack Properzi Becker Mayblyum Thibault Sanchez Schultz Hanseeuw Gomez-Isla Lois-Gomez Price Sperling Johnson	Rubinstein, Zoe
44	MCI patients demonstrate reliably increasing 18F-AV1451 PET uptake across three exams	Scott Adamczuk Gorman Runkle Suh	Scott, David
45	Development of a qualitative read method for characterizing the presence and extent of brain tau deposition using [18F]MK-6240 PET imaging	Seibyl Salinas Rajagovindan Hutchison Beaver Martarello	Seibyl, John
46	PET imaging of [11C]MPC-6827, a microtubule-based PET tracer in murine models of AD	Solingapuram sai Macauley Whitlow Mintz Craft	Solingapuram Sai, Kiran Kumar
47	Quantifying the relationship between the brain distributions of tau and local atrophy to inter-regional connectivity based on individual human data	Soucy Mohammadi Rosa-Neto Pascoal Savard Kang Therriault Benali	Soucy, Jean-Paul
48	Monitoring disease pathophysiology using multiparametric PET acquisitions: The McGill TRIAD Cohort	Stevenson Chamoun Pascoal Benedet Kang Mathotaarachchi Therriault Thomas Savard Tissot Lussier Vinet-Celluci Rahmouni Gagné Joung Sbeiti Shin Vitali Gauthier Rosa-Neto	Stevenson, Jenna
49	Interaction between amyloid and neuroinflammation on apathy along the Alzheimer's disease spectrum	Tissot Kang Benedet Rahmouni Pascoal Chamoun Therriault Lussier Savard Mathotaarachchi Thomas Gauthier Rosa-Neto	Tissot, Cécile
50	Neuropsychiatric symptoms in cognitively impaired individuals are correlated with tau deposition	Tissot Therriault Pascoal Chamoun Lussier Savard Mathotaarachchi Benedet Thomas Rosa-Neto Gauthier	Tissot, Cécile
51	Association between [18F]NAV4694 PET amyloid- β measures and fluid biomarkers across the spectrum of Alzheimer's disease	Wang Pascoal Therriault Benedet Lussier Savard Kang Tissot Gauthier Rosa-Neto	Wang, Yi-Ting
52	PET beta-amyloid deposition in healthy older adults is associated with decreased lure discrimination on a spatial mnemonic similarity task	Webb Foster Horn Kennedy Rodrigue	Webb, Christina
53	Socioeconomic status mediates racial differences seen using the A-T(N) Framework	Wisch Hudson Coble Xiong Babulal Gordon Flores Dincer Benzinger Morris Ances	Ances, Beau
54	Tau pathology and relative cerebral blood flow are independently associated with cognition in Alzheimer's disease	Wolters Visser Verfaillie Coomans Timmers Tuncel Boellaard Windhorst Scheltens van der Flier Ossenkoppele van Berckel	Wolters, Emma
55	Amyloid Load trajectories and chronicity reveal groups of early amyloid accumulators in Down syndrome	Zammit Kosciak Laymon Betthausen Tudorasu Cohen Minhas Johnson Zaman Mathis Klunk Handen Christian	Zammit, Matt
56	Hippocampal-retrosplenial cortex connectivity predicts tau accumulation in cognitively normal older adults	Ziontz Adams Baker Jagust	Ziontz, Jacob
60	Longitudinal flortaucipir ([18F]AV-1451) PET uptake in Semantic Dementia	Utianski Whitwell Martin Botha Schwarz Duffy Clark Spychalla Senjem Petersen Knopman Jack, Jr. Lowe Josephs	Utianski, Rene
61	Defining a Centiloid scale threshold predicting long-term progression to dementia in patients attending the Memory Clinic: An F18-Flutemetamol amyloid-PET study	Hanseeuw Malotau Dricot Quenon Cerman Buckley Farrar Ivanoiu Lhommel	Hanseeuw, Bernard
62	Correlation of QSM signal with Alzheimer's Disease biomarkers	Cogswell Wiste Senjem Therneau Lowe Knopman Botha Graff-Radford Jones Kantarci Vemuri Ferman Boeve Mielke Schwarz Gunter Petersen Jack	Cogswell, Petrice
63	Developing a novel alpha-synuclein (a-syn) positron emission tomography (PET) tracer for the diagnosis of Parkinson's disease (PD) and other a-synucleinopathies	Vokali Molette Tsika Ravache Rodriguez Jürgens Melo dos Santos Sandiego Russell Gunn Darmency Piorowska Poli Kroth Capotosti Hliva Sol Marek Stöhr Lowe Pfeifer Kosco-Vilbois	Vokali, Efthymia
64	Evaluating the relationships among odor identification, tau pathology and neuroinflammation in Alzheimer's disease	Klein Yan Johnson Tomljanovic Zou Polly Honig Brickman Stern Lee Kreis	Klein, Julia
65	Elevated soluble phosphorylated tau is a marker of early amyloid PiB PET abnormalities and accumulation	McDade Li Joseph-Mathurin Benzinger Fagan Xiong Barthélemy Bateman	McDade, Eric

Board #	Poster Title	Authors	Presenter
66	Cerebrospinal fluid and PET measures of tau pathology may indicate different stages of AD pathological progression	Meyer Pichet Binette Gonneaud Breitner Villeneuve	Meyer, Pierre-Francois
67	Distinct effects of APOE ϵ 2 on A β in Alzheimer- and vascular-type cognitive impairment	Lee Lee Park Choe Park Cheon Hahn Ossenkuppele Kim Kim Yoo Jang Cho Kim Kim Jung Park DeCarli Weiner Yun Na Seo	Lee, Jin San
68	Association of tau tangle burden with depressive symptoms in community dwelling older adults: a longitudinal study	Gatchel Marshall Yang Donovan Buckley Properzi Quiroz Rabin Vannini Amariglio Chhatwal Rentz Blacker Sperling Johnson Hanseeuw	Gatchel, Jennifer
69	Higher microglia biomarker levels are associated with slower rates of amyloid-beta accumulation in humans and in a transgenic mouse model of amyloid-beta	Ewers Brendel Suarez-Calvet Biechele Sacher Blume Haass Franzmeier	Ewers, Michael
70	Individual variability in the cortical distribution of elevated 18F-AV1451 and 11C-PIB in a heterogeneous sample of AD patients	Collins Eckbo McGinnis Dickerson	Collins, Jessica
71	Quantitative regional amyloid burden and white matter changes in preclinical AD	Collij Top Stickney Ingala Tomassen Lopes Alves Yaqub Wink Van 't Ent Scheltens Van Berckel Visser Barkhof Den Braber AMYPAD consortium	Collij, Lyduine
72	Effect of genetic risk, brain amyloid and hippocampal volume on normal variation in episodic memory performance in middle-aged and older adults	Schaevebeke Gabel Adamczuk Van Laere Dupont Vandenberghe	Schaevebeke, Jolien
73	Imaging synaptic and mitochondrial function in frontotemporal dementia using [11C]UCB-J, [18F]BCPP-EF and [11C]SA4503 PET	Clarke Mansur Passchier Lewis Evans Chen Schwarz Takano Gunn Cash Rabiner Rohrer	Clarke, Mica
74	First-in-human evaluations of [11C]PS13 for imaging COX-1 and [11C]MC1 for imaging COX-2	Kim Juarez Anaya Lee Hong Miller Telu Morse Singh Cortes-Salva Henry Ruiz-Perdomo Montero Santamaria Liow Zoghbi Fujita Katz Pike Innis	Kim, Min-Jeong
75	[11C]MK-6884 PET tracer for M4 muscarinic cholinergic receptors in AD: Comparison with [18F]FDG PET	Pascual Zanotti-Fregonara Yu Funk Arbones Wang Li Cheng Anderson Hostetler Basile Masdeu	Pascual, Belen
76	Assessing A β , tau, and reactive astrocytosis in aging and AD	Villemagne Harada Doré Furumoto Mulligan Kudo Krishnadas Huang Yanai Rowe Okamura	Villemagne, Victor
77	A sensitive composite model to determine subtle cognitive differences in preclinical Alzheimer's disease	Hahn Kim Kim Jang Kim Na Chin Seo	Hahn, Alice
78	Amyloid deposition affects the topography of cortical thinning in Lewy Body Disease	Ye Touroutoglou Brickhouse Katz Growdon Johnson Dickerson Gomperts	Gomperts, Stephen
79	Longitudinal change in amyloid load over a 5-year period in cognitively healthy APOE4 carriers versus non-carriers: effect of reference region	Luckett Adamczuk Schaevebeke Gabel Van Laere Dupont Vandenberghe	Luckett, Emma
80	Sex differences in the rates of cognitive decline associated with temporal lobe FTP-PET signal: findings from the Harvard Aging Brain Study	Buckley Properzi Schultz Jacobs Kirn Rentz Hanseeuw Johnson Sperling	Buckley, Rachel
81	Amyloid and tau PET burden are associated with white matter bundle abnormalities in asymptomatic individuals at risk of AD	Pichet Binette Theaud Gonneaud Poirier Descoteaux Villeneuve	Pichet Binette, Alexa
82	NeuroToolkit CSF biomarkers track the progression of AD at very early stages and show that inflammatory markers modulate cerebral amyloid accumulation	Salvadó Molinuevo Milà-Alomà Blennow Zetterberg Operto Falcón Batrla Battle Buckley Farrar Minguillon Fauria Sánchez-Benavides Suárez-Calvet Gispert the ALFA study	Salvadó, Gemma
83	T1rho MRI measurement of amyloid plaque burden in cognitively unimpaired individuals: preliminary results in the ALFA+ cohort	Falcón Montesinos Grau-Rivera Suárez-Calvet Puig-Pijoan Cascales Navalpotro-Gomez Fernández-Lebrero Sánchez-Valle Gelpi Sanfeliu Rojas Perissinotti Niñerola-Baizán Salvadó Minguillon Fauria Molinuevo Sánchez-González Gispert the ALFA study	Salvadó, Gemma
84	Preliminary quantitative results of the AMYPAD prognostic and natural history study	Gispert Lopes-Alves Gray Buckley Collij Heeman Salvadó Scheltens Frisoni Ritchie Vellas Stephens Ford Molinuevo Farrar Barkhof the AMYPAD Consortium	Salvadó, Gemma

Board #	Poster Title	Authors	Presenter
85	Sex differences in regional tau deposition in cognitively impaired patients with Alzheimer's disease	Edwards La Joie Iaccarino Kim Baker Casaletto Miller Jagust Rabinovici	Edwards, Lauren
86	Cross-sectional and longitudinal non-dichotomized CSF/PET A β data support existence of "CSF+ first" vs. "PET+ first" pathways of A β biomarkers changes	Sala Nordberg Rodriguez-Vieitez	Sala, Arianna
87	Personality and amyloid accumulation in cognitively normal aging	Yoon Baker Korman Tennant Harrison Jagust	Yoon, Bora
88	Head-to-head comparison of F-Florbetaben and F-Flutemetamol uptakes in the cortex, striatum and white matter	Seo Cho Moon Choe Na	Seo, Sang Won
89	Sleep impairment predicts longitudinal accumulation of β -amyloid	Winer Mander Jagust Walker	Winer, Joseph
90	PI-2620 Tau PET is associated with amyloid-beta levels in scans from subjects of the elenbecestat MissionAD program	Stephens Bullich Mueller Berndt De Santi Scott Adamczuk Suhy Kaplow Giroux Krause Chang Albala	Stephens, Andrew
91	Prevalence of amyloid PET positivity in cognitively normal the East Asian populations	Kim Jung Na Kim Won Seo	Kim, Jaeho
92	Amyloid deposition disrupts functional connectivity and graph properties within the default mode network	Ingala Wink Prent van 't Ent Tomassen ten Kate Konijnenberg Collij Yaqub Scheltens de Goes Teunissen Barkhof van Berckel Visser den Braber	den Braber, Anouk
93	Neuroinflammation in AD patients and correlates with amyloid and tau deposition	Edison Leng Dani Brooks	Edison, Paul
94	Development of new alpha7 nicotinic receptor ASEM analogs for PET imaging	Nordberg Lemoine Mohan Kuang Nag Jia Miranda Azpiazu Datta Arakawa Varnäs Ågren Långström Halldin	Nordberg, Agneta
95	Biological underpinnings of typical and atypical Alzheimer's dementia phenotypes	Whitwell Tosakulwong Graff-Radford Weigand Schwarz Senjem Ertekin-Taner Jones Boeve Knopman Jack Petersen Lowe Josephs	Whitwell, Jennifer
96	Use of the plasma amyloid-beta 42/40 ratio for predicting amyloid PET in a community-based population	Mielke Algeciras-Schimmich Campbell Syrjanen Knopman Jack Jr. Peterson	Mielke, Michelle
97	Associations between longitudinal cognitive measures and cross-sectional tau in adults with Down syndrome	Tudorascu Comer Zammit Laymon Minhas Ellison Zaman Ances Johnson Mathis Klunk Christian Handen Hartley Cohen	Tudorascu, Dana
98	Associations of amyloid deposition and FDG uptake in aging and cognitively impaired elders with and without moderate to severe periventricular white matter hyperintensities	Zukotynski Gaudet Kuo Adamo Goubran Scott Bocti Borrie Chertkow Frayne Hsiung Laforce Noseworthy Prato Sahlas Smith Sossi Thiel Soucy Tardif Black	Zukotynski, Katherine
99	Early declines in learning and executive function associated with accumulating A β not tau in low PIB adults	Farrell Papp Buckley Jacobs Schultz Properzi Hanseeuw Rentz Johnson Sperling	Farrell, Michelle
100	Entorhinal tau pathology is associated with medial temporal lobe hyperactivity in aging	Adams Maass Berron Harrison Baker Thomas Stanfill Jagust	Adams, Jenna
101	Clinicopathological confirmation of 123I-FP-CIT SPECT (ioflupane) quantification methods in a spectrum of neurodegenerative syndromes and associated pathologies	Maltais Jordan Miyagawa Lesnick Przybelski Min Dickson Murray Kantarci Boeve Lowe	Maltais, Daniela
102	Preliminary results: PiB and MK6240 regional PET measures associated with digitized clock drawing performance	Mayblyum Thibault Moody Farrell Jiang Jacobs Rubinstein Sanchez Katz Sperling Papp Rentz Johnson	Thibault, Emma
103	White matter disruption is an early and progressive feature of pre-symptomatic Dutch-type hereditary cerebral amyloid angiopathy	Scott Schultz Sohrabi Gardener Taddei Bateman Benzinger Johnson Sperling Martins Greenberg Chhatwal Investigators	Scott, Matthew
104	Increased risk of AD in alcohol use disorder is not mediated by amyloid-beta in a middle-aged cross-sectional cohort	Royse Himes Minhas Lopresti Flanigan Narendran	Royse, Sarah
105	Longitudinal associations between lifestyle risk, β -amyloid, and cognition in late-midlife	Cody Kosciak Birdsill Berman Erickson Chin Clark Christian Betthausen Johnson	Cody, Karly
106	Exploring relationships between tau burden and naming in the aphasic variant of AD	Martersteck Sridhar Coventry Eldes Wood Kim Mesulam Rogalski	Martersteck, Adam
107	Data-driven approach to characterization of tau accumulation in Braak staging groups	Groh Svaldi Stage Sanjay Risacher Saykin Apostolova	Groh, Jenna

Board #	Poster Title	Authors	Presenter
108	Associations between AD biomarkers and cognition among cognitively normal older adults	Oh Correia Salloway	Oh, Hwamee
109	In vivo association of mitochondrial dysfunction with tau pathology in early AD	Terada Therriault Min Su Savard Ouchi Rosa-Neto	Terada, Tatsuhiro
110	Using famous faces to investigate the neural systems involved in name retrieval	Tennant Jagust La Joie Adams Winer	Tennant, Victoria
111	Cerebrospinal fluid matrix metalloproteinases are associated with compromised white matter microstructure among older adults: the Vanderbilt memory & aging project	Moore Pechman Acosta Bell Anderson Landman Blennow Zetterberg Gifford Hohman Jefferson	Moore, Elizabeth
112	A clinically-relevant scheme for qualitatively rating tau PET, amyloid PET, and MRI in neurodegenerative cognitive presentations	McGinnis Collins Eckbo Brickhouse Dickerson	McGinnis, Scott
113	Mild behavioral impairment is associated with tau pathology in cognitively impaired elderly individuals	Lussier Pascoal Therriault Tissot Savard Benedet Mathotaarachchi Stevenson Ismail Rosa-Neto Gauthier	Lussier, Firoza
114	Modeling the trajectory of tau deposition in autosomal-dominant AD using the high-affinity tau tracer [18F]MK6240	Lussier Therriault Pascoal Savard Mathotaarachchi Robb Stevenson Gauthier Rosa-Neto	Lussier, Firoza
120	Depression is predicted by tau imaging biomarker among cognitively normal adults	Babulal Roe Stout Rajasekar Wisch Benzinger Morris Ances	Ances, Beau
121	Local associations between tau and neurodegeneration among non-demented older adults	Bilgel Wong Resnick	Bilgel, Murat
122	Perfusion-phase 18F-PI-2620 tau-PET imaging as a surrogate marker of neuronal injury	Brendel Beyer Nitschmann Barthel van Eimeren Marek Song Palleis Respondek Sauerbeck Hammes Barbe Onur Jessen Saur Schroeter Rumpf Rullmann Schildan Patt Neumaier Barret Madonia Russel Stephens Roeber Herms Bötzel Levin Classen Hoeglenger Bartenstein Villemagne Drzezga Seibyl Sabri	Brendel, Matthias
123	Binding characteristics of 18F-PI-2620 differentiate the clinically predicted tau isoform in suspected 3/4-repeat and 4-repeat tauopathies	Brendel Song Beyer Barthel van Eimeren Marek Palleis Kaiser Respondek Sauerbeck Hammes Barbe Onur Jessen Saur Schroeter Rumpf Rullmann Schildan Patt Neumaier Barret Madonia Russel Stephens Roeber Herms Bötzel Levin Classen Hoeglenger Bartenstein Villemagne Drzezga Seibyl Sabri	Brendel, Matthias
124	18F-PI2620 tau-PET for assessment of heterogeneous neuropathology in corticobasal syndrome	Brendel Palleis Prix Gehmeyr Bötzel Danek Höllerhage Sauerbeck Beyer Nitschmann Song Stephens Barthel Patt Sabri Drzezga van Eimeren Villemagne Bartenstein Perneczky Haass Levin Hoeglenger	Brendel, Matthias
125	Optimal reference region for the quantification of tau load in the brain using 18F-PI-2620 PET	Bullich Müller Roé-Vellvé Jovalekic Perrotin De Santi Koglin Stephens	Bullich Roig, Santiago
126	Quantifying tau PET imaging reliably in the presence of off-target binding	Chen Gordon McCullough Zaza Mejias Dincer Flores Keefe Paulick Jackson Koudelis Su Morris Benzinger	Chen, Charles
127	[18F]THK5317 imaging as a predictive tool of prospective cognitive decline in prodromal and dementia-stage AD	Chiotis Savitcheva Poulakis Saint-Aubert Wall Antoni Nordberg	Chiotis, Konstantinos
128	Comparison of quantitative cutoff methods for [18F]AV-1451	Minhas Laymon Lopresti Snitz Tudorascu Aizenstein Lopez Mathis Klunk Cohen	Cohen, Ann
129	Pilot study on the relationship between 18F-MK-6240 and VBM in early and late stages of AD	Fernandez Arias Pascoal Benedet Thierrault Su Kang Savard Ottoy Mathotaarachchi Lussier Tissot Thomas Stevenson Rahmouni Wang Massarweh Soucy Gauthier Rosa-Neto	Fernandez Arias, Jaime
130	Functional connectivity brain architecture predicts the rate of tau accumulation in AD	Franzmeier Neitzel Rubinski Smith Strandberg Ossenkoppele Hansson Ewers	Franzmeier, Nicolai
131	How innocent is PART?: mesial temporal tau is associated with worse cognitive performance in A β -negative cognitively normal individuals	Groot	Groot, Colin
132	CSF P-tau detects cerebral tau accumulation earlier than tau PET in amyloid positive elderly adults	Guo Jagust Landau	Guo, Tengfei

Board #	Poster Title	Authors	Presenter
133	Amyloid, tau, and atrophy in preclinical AD: a longitudinal study	Hanseeuw Jacobs Schultz Buckley Properzi Farrell Scott Hampton Sanchez Sperling Johnson	Hanseeuw, Bernard
134	Increased levels and phosphorylation of soluble tau proteins occur earlier than changes in tau PET in AD	Hansson Andersson Janelidze Ossenkoppele Insel Strandberg Zetterberg Blennow Chai Dage Stomrud Smith Palmqvist Mattsson	Hansson, Oskar
135	Preclinical characterization of [18F]THK-5562, a novel tau PET tracer with little off-target binding	Harada Lersdirisuk Yiqing Ezura Shimizu Morito Arai Yanai Kudo Furumoto Okamura	Harada, Ryuichi
136	Comparison of tau PET imaging using 18F-APN-1607 and 18F-THK5351 in Alzheimer's disease patients and normal controls	Hsiao Lin Huang Huang	Hsiao, Ing-Tsung
137	In vivo amyloid-PET and tau-PET evidence in early-onset AD: taking the LEADS	Iaccarino La Joie Lesman-Segev Soleimani-Meigooni Provost Collins Aisen Borowski Eloyan Fagan Foroud Gatsonis Jack Jr. Kramer Saykin Toga Vemuri Day Graff-Radford Honig Jones Masdeu Mendez Onyike Rogalski Salloway Wolk Wingo Koeppe Dickerson Apostolova Carrillo Rabinovici	Iaccarino, Leonardo
138	Multimodal in vivo investigation of amyloid and tau biomarkers associations with cerebrospinal fluid NfL and YKL40 levels	Iaccarino La Joie Edwards Lesman-Segev Strom Pham Chaudhary Fenton Jerome Janabi Baker Miller Jagust Fagan Rabinovici	Iaccarino, Leonardo
139	Activated microglia and amyloid load potentiate tau deposition leading to cognitive dysfunction in AD	Kang Ottoy Savard Pascoal Mathotaarachchi Benedet Chamoun Therriault Lussier Tissot Thomas Stevenson Rahmouni Arias Wang Massarweh Soucy Gauthier Rosa-Neto	Kang, Min Su
140	Tauopathy in females is more vulnerable to amyloid or neuroinflammation in AD	Kang Ottoy Chamoun Mathotaarachchi Savard Benedet Pascoal Therriault Lussier Tissot Thomas Stevenson Rahmouni Fernandez-Arias Wang Massarweh Soucy Gauthier Rosa-Neto	Kang, Min Su
141	Prediction of brain tau accumulation in amyloid positive cognitive impairment patients using multimodal biomarkers with machine learning approach	Kim Park Park Kang Kim Jang Kim Na Lee Seo	Kim, Jaeho
142	Comparison of longitudinal change metrics for 18F-RO948 PET among cognitively unimpaired and patients with MCI or AD dementia in the BioFINDER2 study	Klein Sanabria Leuzy Borroni Mattsson Palmqvist Stomrud Smith Hansson	Klein, Gregory
143	Validation of clinical protocols for clinicians analyzing 18F-PI-2620 tau PET/MRI images	Koran Shams Adams Cazevedo Toueg Corso Hunt Castillo Hall Sha Fredericks Greicius Wagner Zaharchuk Davidzon Chin Mormino	Mormino, Elizabeth
144	Cerebrospinal fluid tau phosphorylated at amino acid 181 or 231: a biomarker comparison in the detection of neurofibrillary tangle pathology in the AD spectrum	Benedet J. Ashton A. Pascoal Stoops Francois Vanmechelen K. Karikari Mathotaarachchi Savard Therriault Chamoun Zetterberg Blennow Rosa-Neto	Benedet, Andrea
145	Diagnostic performance of [18F]RO948 tau positron emission tomography in the differentiation of AD from other neurodegenerative disorders	Leuzy Smith Ossenkoppele Santillo Borroni Klein Olsson Jögi Palmqvist Mattsson Strandberg Stomrud Hansson	Leuzy, Antoine
146	Longitudinal changes in tau pathology measured by [18F]RO948 tau-PET are associated with elevated CSF P-tau: preliminary findings from the Swedish BioFINDER-2 study	Leuzy Klein Ossenkoppele Mattsson Janelidze Palmqvist Strandberg Coloma Borroni Stomrud Smith Hansson	Leuzy, Antoine
147	A comparison of ischemic stroke-induced changes on 18F-APN-1607 (18F-PMPBB3) and 18F-THK-5351 uptake patterns	Lin Hsiao Huang Huang	Lin, Kun-Ju
148	Longitudinal change in [18F]GTP1 SUVR over 18 months depends on baseline SUVR intensity and spatial distribution and shows trends with cognitive decline	Manser Sanabria Bohorquez Teng Baker Toth Marik Weimer	Manser, Paul
149	18F-APN-1607: a promising PET tracer for multiple tauopathies	Margolin Lin Tempest Chen Marek Russell Sandiego Huang Hsiao Tamagnan Alagille Guan Lu Zuo Higuchi Jang	Margolin, Richard
150	Entorhinal cortical tau accumulation is inversely associated with hippocampal synaptic density in older individuals with normal cognition and early AD	Mecca Chen Naganawa Toyonaga Godek Harris Bartlett Zhao Gallezot Nabulsi Huang Arnsten Carson van Dyck	Mecca, Adam

Board #	Poster Title	Authors	Presenter
151	Mental and physical activity during the uptake period affects off-target binding in extra- and within-brain Tau PET (18F-FTP)	Min Apgar Scott Hol Lundt Albertson Schwarz Botha Vemuri Gunter Petersen Jack Lowe	Min, Hoon-Ki
152	In vivo uptake of 18F-PM-PBB3 (18F-APN-1607) in patients with corticobasal syndrome	Nakano Shimada Tagai Matsuoka Kubota Takahata Takado Shinotoh Yamamoto Sano Seki Hirano Ono Tempest Jang Sahara Kawamura Zhang Kuwabara Higuchi	Nakano, Yoshikazu
153	Factors predicting tau PET status in cognitively unimpaired and impaired individuals	Ossenkoppele Leuzy Cho La Joie Strandberg Mattsson Palmqvist Lyoo Rabinovici Smith Hansson	Ossenkoppele, Rik
154	Widespread amyloid is necessary to detect tau-PET signal beyond the entorhinal cortex and cognitive decline	Ozlen Binette Köbe Meyer Villeneuve	Ozlen, Hazal
155	Using 18F-Flortaucipir visual assessment to define T-status in the AT(N) framework: evaluation of intra- and inter-rater reliability	Provost Iaccarino Soleimani-Meigooni Lesman-Segev La Joie Edwards Strom Pham Mellinger Janabi Baker Jagust Rabinovici	Provost, Karine
156	Defining T-status in the AT(N) framework: comparison of 18F-Flortaucipir visual assessment, SUVR quantification and CSF pTau	Provost Iaccarino Soleimani-Meigooni Lesman-Segev La Joie Mattsson Hansson Eichenlaub Edwards Strom Pham Mellinger Janabi Baker Jagust Rabinovici	Provost, Karine
157	Plasma neurofilament light is associated with regional tau tangle burden in autosomal dominant AD: findings from the COLBOS Project	Quiroz Zetterberg Reiman Sanchez Guzman-Velez Fox-Fuller Arboleda-Velasquez Baena Gatchel Sperling Johnson Blennow Lopera	Quiroz, Yakeel
158	Application of tau PET as a biomarker of AD in therapeutic trials: a pharmaceutical industry perspective	Salinas Lohith Guo Wooten Tulip Sanjeeva Comley Sur Hostetler Beaver Martarello	Salinas, Cristian
159	Measuring increases of tau pathology in AD using [18F]GTP1 (Genentech tau probe 1) PET imaging	Sanabria Bohorquez Baker Manser Toth Teng Marik Weimer	Sanabria Bohorquez, Sandra
160	Evaluation of tau PET staging in the A4/LEARN study	Sanchez Becker Jacobs Hanseeuw Mayblyum Rubinstein Thibault Schultz Seshadri Quiroz Rentz Price Sperling Johnson the A4 Study Team	Sanchez, Justin
161	Clinical evaluation of [18F]-JNJ-64326067, a candidate PET tracer for the detection of tau pathology in AD	Schmidt Janssens Moechars Rombouts Timmers Barret Constantinescu Madonia Russell Sandiego Kolb	Schmidt, Mark
162	Association between cerebrospinal fluid neurofilament light chain and markers of neurofibrillary pathophysiology: findings from the Knight Alzheimer Disease Research Center	Schultz Schindler Chen Sutphen Morris Fagan Gordon Benzinger	Schultz, Stephanie
163	18F-PM-PBB3 (18F-APN-1607) uptake associates with plasma NfL level and motor disability in patients with progressive supranuclear palsy	Shimada Tagai Tatebe Matsuoka Kubota Takahata Takado Shinotoh Yamamoto Sano Seki Nakano Ono Hirano Tempest Jang Sahara Kawamura Zhang Tokuda Higuchi	Shimada, Hitoshi
164	The rate of accumulation of tau aggregates is higher in females and younger individuals	Smith Mattsson Pontecorvo Devous Strandberg Ossenkoppele Hansson	Smith, Ruben
165	Resting state functional connectivity associations with F18-Florbetapir PET versus F18-Flortaucipir PET	Svaldi Goñi Stage Abbas Dziedzic West Risacher Saykin Apostolova	Svaldi, Diana
166	Tau positivity: Comparing flortaucipir meta-ROI vs maximal single region	Therneau Schwarz Wiste Gunter Senjem Lowe Kantarci Petersen Knopman Mielke Jones Jack	Therneau, Terry
167	Intrinsic connectivity of the human brain provides scaffold for tau aggregation in AD	Therriault Pascoal Savard Mathotaarachchi Benedet Chamoun Gauthier Saha-Chaudhuri Massarweh Rosa-Neto	Therriault, Joseph
168	Changes in volumetric MRI measures at 12 months significantly correlate with baseline [18F]GTP1 SUVR, but not [18F]GTP1 change	Toth Sanabria Bohorquez Manser Baker Teng Marik Weimer	Toth, Balasz
169	Elevated medial temporal lobe Tau PET with 18F-PI2620 in normal controls with "borderline" neuropsychological testing profiles	Toueg Deutsch Castillo Hunt Corso Trelle Harrison Azevedo Shen Anders Hall Fredericks Sha Davidzon Chin Khalighi Wagner Mormino	Toueg, Tyler
170	Hippocampal tau accumulation predicts individual differences in episodic memory in cognitively normal older adults	Trelle Toueg Castillo Channappa Corso Hunt Jayakumar Nadiadwala Guo Azevedo Shin Davidson Deutsch Hall Sha Fredericks Kerchner Carr Chin Wagner Mormino	Trelle, Alexandra

Board #	Poster Title	Authors	Presenter
171	Temporo-limbic tau burden, as measured by 18F-AV1451, is a correlate of hippocampal volume loss over time	Fischer Ahnen Dissertori Lustermann Weber Buck Kagerer Gietl Hock Unschuld	Unschuld, Paul
172	Temporal evaluation for maximum CSF pTau181 – [18F]Flortaucipir concordance	Wisch Gordon Schindler Flores Dincer Fagan Benzinger Morris Ances	Ances, Beau
173	[18F]flortaucipir PET is more closely associated with disease severity than CSF p-tau in AD	Wolters Ossenkoppele Verfaillie Coomans Timmers Visser Tuncel Golla Windhorst Boellaard van der Flier Teunissen Scheltens van Berckel	Wolters, Emma
174	Associations of tau pathology and functional connectivity with retrospective cognitive change among cognitively normal older adults	Shafer Bilgel Ziontz Wong Resnick	Ziontz, Jacob

POSTER INDEX *(by presenter's last name)*

Board #	Poster Title	Authors	Presenter
100	Entorhinal tau pathology is associated with medial temporal lobe hyperactivity in aging	Adams Maass Berron Harrison Baker Thomas Stanfill Jagust	Adams, Jenna
120	Depression is predicted by tau imaging biomarker among cognitively normal adults	Babulal Roe Stout Rajasekar Wisch Benzinger Morris Ances	Ances, Beau
53	Socioeconomic status mediates racial differences seen using the A-T(N) Framework	Wisch Hudson Coble Xiong Babulal Gordon Flores Dincer Benzinger Morris Ances	Ances, Beau
172	Temporal evaluation for maximum CSF pTau181 – [18F]Flortaucipir concordance	Wisch Gordon Schindler Flores Dincer Fagan Benzinger Morris Ances	Ances, Beau
01	Label-free x-ray method for estimating brain amyloid load	Badano Dahal Ghamraoui	Badano, Aldo
144	Cerebrospinal fluid tau phosphorylated at amino acid 181 or 231: a biomarker comparison in the detection of neurofibrillary tangle pathology in the AD spectrum	Benedet J. Ashton A. Pascoal Stoops Francois Vanmechelen K. Karikari Mathotaarachchi Savard Therriault Chamoun Zetterberg Blennow Rosa-Neto	Benedet, Andrea
02	Examining regional MK-6240 patterns and associations with amyloid and cognitive decline	Bethausen Cody Kosciak Jonaitis Erickson Converse Murali Barnhart Stone Mueller Clark Asthana Christian Johnson	Bethausen, Tobey
03	Transcriptomic profiling of brain amyloidosis using peripheral blood-based gene expression	Bharthur Sanjay Svaldi Apostolova	Bharthur Sanjay, Apoorva
121	Local associations between tau and neurodegeneration among non-demented older adults	Bilgel Wong Resnick	Bilgel, Murat
04	A pons cluster detected by a data-driven approach may serve as a favorable reference region for 18F-PI-2620 Tau PET analysis	Bischof van Eimeren Koglin Müller Bullich Perrotin Stephens Drzezga	Bischof, Gerard
122	Perfusion-phase 18F-PI-2620 tau-PET imaging as a surrogate marker of neuronal injury	Brendel Beyer Nitschmann Barthel van Eimeren Marek Song Palleis Respondek Sauerbeck Hammes Barbe Onur Jessen Saur Schroeter Rumpf Rullmann Schildan Patt Neumaier Barret Madonia Russel Stephens Roeber Herms Bötzel Levin Classen Hoeglenger Bartenstein Villemagne Drzezga Seibyl Sabri	Brendel, Matthias
123	Binding characteristics of 18F-PI-2620 differentiate the clinically predicted tau isoform in suspected 3/4-repeat and 4-repeat tauopathies	Brendel Song Beyer Barthel van Eimeren Marek Palleis Kaiser Respondek Sauerbeck Hammes Barbe Onur Jessen Saur Schroeter Rumpf Rullmann Schildan Patt Neumaier Barret Madonia Russel Stephens Roeber Herms Bötzel Levin Classen Hoeglenger Bartenstein Villemagne Drzezga Seibyl Sabri	Brendel, Matthias
124	18F-PI2620 tau-PET for assessment of heterogeneous neuropathology in corticobasal syndrome	Brendel Palleis Prix Gehmeyr Bötzel Danek Höllerhage Sauerbeck Beyer Nitschmann Song Stephens Barthel Patt Sabri Drzezga van Eimeren Villemagne Bartenstein Perneczky Haass Levin Hoeglenger	Brendel, Matthias
80	Sex differences in the rates of cognitive decline associated with temporal lobe FTP-PET signal: findings from the Harvard Aging Brain Study	Buckley Properzi Schultz Jacobs Kirn Rentz Hanseeuw Johnson Sperling	Buckley, Rachel
125	Optimal reference region for the quantification of tau load in the brain using 18F-PI-2620 PET	Bullich Müller Roé-Vellvé Jovalekic Perrotin De Santi Koglin Stephens	Bullich Roig, Santiago
05	Early detection of amyloid load using 18F-Florbetaben PET	Bullich Roé-Vellvé Marquié Villemagne Sanabria Tartari Sotolongo Doré Koglin Müller Perrotin De Santi Tárraga Stephens Rowe Seibyl Boada	Bullich, Santiago
06	Age-related neural dedifferentiation of episodic memory networks is related to beta-amyloid and tau pathology in normal aging	Cassady Adams Maass Harrison Baker Jagust	Cassady, Kaitlin
126	Quantifying tau PET imaging reliably in the presence of off-target binding	Chen Gordon McCullough Zaza Mejias Dincer Flores Keefe Paulick Jackson Koudelis Su Morris Benzinger	Chen, Charles
127	[18F]THK5317 imaging as a predictive tool of prospective cognitive decline in prodromal and dementia-stage AD	Chiotis Savitcheva Poulakis Saint-Aubert Wall Antoni Nordberg	Chiotis, Konstantinos

Board #	Poster Title	Authors	Presenter
73	Imaging synaptic and mitochondrial function in frontotemporal dementia using [11C]UCB-J, [18F]BCPP-EF and [11C]SA4503 PET	Clarke Mansur Passchier Lewis Evans Chen Schwarz Takano Gunn Cash Rabiner Rohrer	Clarke, Mica
105	Longitudinal associations between lifestyle risk, β -amyloid, and cognition in late-midlife	Cody Kosciak Birdsill Berman Erickson Chin Clark Christian Betthausen Johnson	Cody, Karly
62	Correlation of QSM signal with Alzheimer's Disease biomarkers	Cogswell Wiste Senjem Therneau Lowe Knopman Botha Graff-Radford Jones Kantarci Vemuri Ferman Boeve Mielke Schwarz Gunter Petersen Jack	Cogswell, Petrice
128	Comparison of quantitative cutoff methods for [18F]AV-1451	Minhas Laymon Lopresti Snitz Tudorasu Aizenstein Lopez Mathis Klunk Cohen	Cohen, Ann
71	Quantitative regional amyloid burden and white matter changes in preclinical AD	Collij Top Stickney Ingala Tomassen Lopes Alves Yaqub Wink Van 't Ent Scheltens Van Berckel Visser Barkhof Den Braber AMYPAD consortium	Collij, Lyduine
70	Individual variability in the cortical distribution of elevated 18F-AV1451 and 11C-PIB in a heterogeneous sample of AD patients	Collins Eckbo McGinnis Dickerson	Collins, Jessica
07	Tau pathology and synaptic loss are closely associated in Alzheimer's disease in vivo: a combined [18F]flortaucipir and [11C]UCB-J PET study	Coomans Verfaillie Wolters Tuncel Golla Ossenkoppele Scheper Schober Sweeney Ryan Schuit Windhorst Scheltens Boellaard van Berckel	Coomans, Emma
08	Longitudinal dynamic [18F]flortaucipir PET reveals increased early stage tau pathology in individuals with subjective cognitive decline	Coomans Visser Ossenkoppele Verfaillie Timmers Wolters Tuncel Schmidt Boellaard Windhorst Scheltens van der Flier van Berckel	Coomans, Emma
92	Amyloid deposition disrupts functional connectivity and graph properties within the default mode network	Ingala Wink Prent van 't Ent Tomassen ten Kate Konijnenberg Collij Yaqub Scheltens de Goes Teunissen Barkhof van Berckel Visser den Braber	den Braber, Anouk
09	Preliminary evaluation of synaptic vesicle protein SV2A imaging with [11C]UCB-J across the cognitive spectrum	DiFilippo Murali McKinney Davenport Barnhart Engle Betthausen Johnson Bendlin Christian	DiFilippo, Alexandra
93	Neuroinflammation in AD patients and correlates with amyloid and tau deposition	Edison Leng Dani Brooks	Edison, Paul
85	Sex differences in regional tau deposition in cognitively impaired patients with Alzheimer's disease	Edwards La Joie Iaccarino Kim Baker Casaletto Miller Jagust Rabinovici	Edwards, Lauren
69	Higher microglia biomarker levels are associated with slower rates of amyloid-beta accumulation in humans and in a transgenic mouse model of amyloid-beta	Ewers Brendel Suarez-Calvet Biechele Sacher Blume Haass Franzmeier	Ewers, Michael
99	Early declines in learning and executive function associated with accumulating A β not tau in low PIB adults	Farrell Papp Buckley Jacobs Schultz Properzi Hanseeuw Rentz Johnson Sperling	Farrell, Michelle
129	Pilot study on the relationship between 18F-MK-6240 and VBM in early and late stages of AD	Fernandez Arias Pascoal Benedet Thierriault Su Kang Savard Ottoy Mathotaarachchi Lussier Tissot Thomas Stevenson Rahmouni Wang Massarweh Soucy Gauthier Rosa-Neto	Fernandez Arias, Jaime
10	Quantifying off-target skull binding in [18F]Flortaucipir PET studies	Flores Gordon Su Christensen Dincer Adedokun Hornbeck Morris Benzinger	Flores, Shaney
11	Influence of iron and beta-amyloid deposition on entorhinal cortex and hippocampal subfield volumes in the aging brain	Foster Kennedy Rodrigue	Foster, Chris
130	Functional connectivity brain architecture predicts the rate of tau accumulation in AD	Franzmeier Neitzel Rubinski Smith Strandberg Ossenkoppele Hansson Ewers	Franzmeier, Nicolai
68	Association of tau tangle burden with depressive symptoms in community dwelling older adults: a longitudinal study	Gatchel Marshall Yang Donovan Buckley Properzi Quiroz Rabin Vannini Amariglio Chhatwal Rentz Blacker Sperling Johnson Hanseeuw	Gatchel, Jennifer
78	Amyloid deposition affects the topography of cortical thinning in Lewy Body Disease	Ye Touroutoglou Brickhouse Katz Growdon Johnson Dickerson Gomperts	Gomperts, Stephen
13	Beta-amyloid deposition and its association with metabolism	Gordon Goyal Couture Flores Morris Raichle Benzinger Vlassenko	Gordon, Brian
14	Amyloid binding is associated with markers of white matter microstructure in patients with significant white matter disease	Goubran Ozzoude Adamo Zukotynski Bocti Borrie Chertkow Frayne Gao Hsiung Kiss Laforce Noseworthy Prato Ramirez Sahlas Scott	Goubran, Maged

Board #	Poster Title	Authors	Presenter
		Smith Sossi Strother Swartz Tardif Thiel Soucy Black	
107	Data-driven approach to characterization of tau accumulation in Braak staging groups	Groh Svaldi Stage Sanjay Risacher Saykin Apostolova	Groh, Jenna
131	How innocent is PART?: mesial temporal tau is associated with worse cognitive performance in A β -negative cognitively normal individuals	Groot	Groot, Colin
15	CSF dynamics explains discrepant PET-CSF AD biomarkers	Gunter Senjem Cogswell Schwarz Lowe Kantarci Vemuri Elder Botha Graff-Radford Jones Mielke Graff-Radford Knopman Petersen Jack, Jr.	Gunter, Jeffrey
132	CSF P-tau detects cerebral tau accumulation earlier than tau PET in amyloid positive elderly adults	Guo Jagust Landau	Guo, Tengfei
20	Hippocampal volume mediates the relationship between amyloidosis and amyloid-sensitive cognitive composite in preclinical AD	Kim Hahn Kim Kim Chin Seo	Hahn, Alice
77	A sensitive composite model to determine subtle cognitive differences in preclinical Alzheimer's disease	Hahn Kim Kim Jang Kim Na Chin Seo	Hahn, Alice
61	Defining a Centiloid scale threshold predicting long-term progression to dementia in patients attending the Memory Clinic: an F18-Flutemetamol amyloid-PET study	Hanseeuw Malotau Dricot Quenon Cerman Buckley Farrar Ivanoiu Lhommel	Hanseeuw, Bernard
133	Amyloid, tau, and atrophy in preclinical AD: a longitudinal study	Hanseeuw Jacobs Schultz Buckley Properzi Farrell Scott Hampton Sanchez Sperling Johnson	Hanseeuw, Bernard
134	Increased levels and phosphorylation of soluble tau proteins occur earlier than changes in Tau PET in AD	Hansson Andersson Janelidze Ossenkoppele Insel Strandberg Zetterberg Blennow Chai Dage Stomrud Smith Palmqvist Mattsson	Hansson, Oskar
135	Preclinical characterization of [18F]THK-5562, a novel tau PET tracer with little off-target binding	Harada Lersdirisuk Yiqing Ezura Shimizu Morito Arai Yanai Kudo Furumoto Okamura	Harada, Ryuichi
17	[11C]PiB amyloid quantification and choice of reference region	Heeman Hendriks van Berckel Lopes Alves Lammertsma Yaqub	Heeman, Fiona
136	Comparison of tau PET imaging using 18F-APN-1607 and 18F-THK5351 in Alzheimer's disease patients and normal controls	Hsiao Lin Huang Huang	Hsiao, Ing-Tsung
18	Retrospective prediction of amyloid accumulation trajectories in a risk-enriched Alzheimer's disease cohort with sequential neural network	Hwang Kosciak Betthausen Tao Kim Johnson Singh	Hwang, Seong Jae
137	In vivo amyloid-PET and tau-PET evidence in early-onset AD: taking the LEADS	Iaccarino La Joie Lesman-Segev Soleimani-Meigooni Provost Collins Aisen Borowski Eloyan Fagan Foroud Gatsonis Jack Jr. Kramer Saykin Toga Vemuri Day Graff-Radford Honig Jones Masdeu Mendez Onyike Rogalski Salloway Wolk Wingo Koeppe Dickerson Apostolova Carrillo Rabinovici	Iaccarino, Leonardo
138	Multimodal in vivo investigation of amyloid and tau biomarkers associations with cerebrospinal fluid NfL and YKL40 levels	Iaccarino La Joie Edwards Lesman-Segev Strom Pham Chaudhary Fenton Jerome Janabi Baker Miller Jagust Fagan Rabinovici	Iaccarino, Leonardo
19	Data-driven biological pattern scoring of Flortaucipir scans outperforms ROIs	Jones Graff-Radford Botha Senjem Wiste Josephs Whitwell Kantarci Boeve Petersen Knopman Lowe Jack	Jones, David
139	Activated microglia and amyloid load potentiate tau deposition leading to cognitive dysfunction in AD	Kang Ottoy Savard Pascoal Mathotaarachchi Benedet Chamoun Therriault Lussier Tissot Thomas Stevenson Rahmouni Arias Wang Massarweh Soucy Gauthier Rosa-Neto	Kang, Min Su
140	Tauopathy in females is more vulnerable to amyloid or neuroinflammation in AD	Kang Ottoy Chamoun Mathotaarachchi Savard Benedet Pascoal Therriault Lussier Tissot Thomas Stevenson Rahmouni Fernandez-Arias Wang Massarweh Soucy Gauthier Rosa-Neto	Kang, Min Su
91	Prevalence of amyloid PET positivity in cognitively normal the East Asian populations	Kim Jung Na Kim Won Seo	Kim, Jaeho
141	Prediction of brain tau accumulation in amyloid positive cognitive impairment patients using multimodal biomarkers with machine learning approach	Kim Park Park Kang Kim Jang Kim Na Lee Seo	Kim, Jaeho

Board #	Poster Title	Authors	Presenter
74	First-in-human evaluations of [11C]PS13 for imaging COX-1 and [11C]MC1 for imaging COX-2	Kim Juarez Anaya Lee Hong Miller Telu Morse Singh Cortes-Salva Henry Ruiz-Perdomo Montero Santamaria Liow Zoghbi Fujita Katz Pike Innis	Kim, Min-Jeong
21	Concordance of visual and quantitative assessments of baseline amyloid scans in the GRADUATE gantenerumab studies	Klein Delmar Voyle Hesterman Petrulli Ovens Baudler Fontoura Doody Kerchner	Klein, Gregory
142	Comparison of longitudinal change metrics for 18F-RO948 PET among cognitively unimpaired and patients with MCI or AD dementia in the BioFINDER2 study	Klein Sanabria Leuzy Borroni Mattsson Palmqvist Stomrud Smith Hansson	Klein, Gregory
64	Evaluating the relationships among odor identification, tau pathology and neuroinflammation in Alzheimer's disease	Klein Yan Johnson Tomljanovic Zou Polly Honig Brickman Stern Lee Kreisler	Klein, Julia
22	Regional amyloid burden is associated with higher quantitative T1 in discrete hippocampal sub-regions	Kohli Yang Vogt Asthana Betthausen Alexander Christian Johnson Kecskemeti Bendlin	Kohli, Akshay
23	Genetically informed quantitative Gradient Recalled Echo MRI reveals brain tissue in hippocampal subfields void of neurons in mild Alzheimer's disease	Kothapalli Benzinger Aschenbrenner Goyal Fagan Raichle Morris Yablonskiy	Kothapalli, Satya V.V.N.
24	Validation of highly sensitive and specific florbetaben positivity thresholds using ADNI participants and young controls	Landau Korman Bullich De Santi Stephens Koeppel Jagust	Landau, Susan
12	Voxel-wise relationships between white matter hyperintensities (WMH) and multimodal neuroimaging biomarkers of Alzheimer's disease	Gaubert Lange Garnier-Crussard Bougacha Gonneaud de Flores Tomadesso Mézenge Landeau de La Sayette Chételat Wirth	Lange, Catharina
25	Additive contribution of white matter hyperintensity to amyloid and neurodegeneration on cognitive decline in a diverse, community-based cohort of older adults	Lao Chesebro Colon Igwe Gu Schupf Manly Stern Mayeux Brickman	Lao, Patrick
26	White matter hyperintensities are related to tau burden in late-Braak stage regions	Lao Laing Igwe Chesebro Kreisler Moreno Luchsinger Brickman	Lao, Patrick
27	Probability template method for analysis of Down Syndrome amyloid PET	Laymon Minhas James Christian Cohen Klunk Tudorascu Royse Zaman Handen	Laymon, Charles
67	Distinct effects of APOE ε2 on Aβ in Alzheimer- and vascular-type cognitive impairment	Lee Lee Park Choe Park Cheon Hahn Ossenkoppele Kim Kim Yoo Jang Cho Kim Kim Jung Park DeCarli Weiner Yun Na Seo	Lee, Jin San
28	Visualizing brain astrocytes - characterization of 3H-BU99008 in human AD brain tissue	Lemoine Malarte Koistinen Nordberg	Lemoine, Laetitia
145	Diagnostic performance of [18F]RO948 tau positron emission tomography in the differentiation of AD from other neurodegenerative disorders	Leuzy Smith Ossenkoppele Santillo Borroni Klein Olsson Jögi Palmqvist Mattsson Strandberg Stomrud Hansson	Leuzy, Antoine
146	Longitudinal changes in tau pathology measured by [18F]RO948 tau-PET are associated with elevated CSF P-tau: preliminary findings from the Swedish BioFINDER-2 study	Leuzy Klein Ossenkoppele Mattsson Janelidze Palmqvist Strandberg Coloma Borroni Stomrud Smith Hansson	Leuzy, Antoine
29	Application of an epidemic spreading model to characterize amyloid beta accumulation in autosomal dominant Alzheimer's disease mutation carriers	Levitis Vogel Kiar Funck Iturria-Medina Evans	Levitis, Elizabeth
147	A comparison of ischemic stroke-induced changes on 18F-APN-1607 (18F-PMPBB3) and 18F-THK-5351 uptake patterns	Lin Hsiao Huang Huang	Lin, Kun-Ju
30	Phantom-based harmonization of PET image reconstruction parameters between the Siemens ECAT HR+ PET and the GE Discovery MI PET/CT scanners	Lois Grogg El Fakri Johnson Price	Lois, Cristina
79	Longitudinal change in amyloid load over a 5-year period in cognitively healthy APOE4 carriers versus non-carriers: Effect of reference region	Luckett Adamczuk Schaevebeke Gabel Van Laere Dupont Vandenberghe	Luckett, Emma
113	Mild behavioral impairment is associated with tau pathology in cognitively impaired elderly individuals	Lussier Pascoal Therriault Tissot Savard Benedet Mathotaarachchi Stevenson Ismail Rosa-Neto Gauthier	Lussier, Firoza
114	Modeling the trajectory of tau deposition in autosomal-dominant AD using the high-affinity tau tracer [18F]MK6240	Lussier Therriault Pascoal Savard Mathotaarachchi Robb Stevenson Gauthier Rosa-Neto	Lussier, Firoza
101	Clinicopathological confirmation of 123I-FP-CIT SPECT (ioflupane) quantification methods in a	Maltais Jordan Miyagawa Lesnick Przybelski Min Dickson Murray Kantarci Boeve Lowe	Maltais, Daniela

Board #	Poster Title	Authors	Presenter
	spectrum of neurodegenerative syndromes and associated pathologies		
38	Amyloid PET variability due to variation in MRI protocol and anatomical segmentation	Palombit Manber Joules Wolz	Manber, Richard
39	The impact of automatic tau PET processing on uptake variability and power analysis in AD	Palombit Manber Joules Wolz	Manber, Richard
148	Longitudinal change in [18F]GTP1 SUVR over 18 months depends on baseline SUVR intensity and spatial distribution and shows trends with cognitive decline	Manser Sanabria Bohorquez Teng Baker Toth Marik Weimer	Manser, Paul
149	18F-APN-1607: a promising PET tracer for multiple tauopathies	Margolin Lin Tempest Chen Marek Russell Sandiego Huang Hsiao Tamagnan Alagille Guan Lu Zuo Higuchi Jang	Margolin, Richard
31	Age prediction and amyloid deposition in SuperAgers	Martersteck Besson Sridhar Makowski-Woidan Parrish Katsaggelos Mesulam Bandt Rogalski	Martersteck, Adam
106	Exploring relationships between tau burden and naming in the aphasic variant of AD	Martersteck Sridhar Coventry Eldes Wood Kim Mesulam Rogalski	Martersteck, Adam
32	PiB tracer delivery decreases overtime in preclinical AD – impact for amyloid pathology measurement	Mayblyum Becker Schultz Farrell Jacobs Rubinstein Sanchez Thibault Sperling Price Johnson Hanseeuw	Mayblyum, Danielle
65	Elevated soluble phosphorylated tau is a marker of early amyloid PiB PET abnormalities and accumulation	McDade Li Joseph-Mathurin Benzinger Fagan Xiong Barthélemy Bateman	McDade, Eric
112	A clinically-relevant scheme for qualitatively rating tau PET, amyloid PET, and MRI in neurodegenerative cognitive presentations	McGinnis Collins Eckbo Brickhouse Dickerson	McGinnis, Scott
150	Entorhinal cortical tau accumulation is inversely associated with hippocampal synaptic density in older individuals with normal cognition and early AD	Mecca Chen Naganawa Toyonaga Godek Harris Bartlett Zhao Gallezot Nabulsi Huang Arnsten Carson van Dyck	Mecca, Adam
66	Cerebrospinal fluid and PET measures of tau pathology may indicate different stages of AD pathological progression	Meyer Pichet Binette Gonneaud Breitner Villeneuve	Meyer, Pierre-Francois
96	Use of the plasma amyloid-beta 42/40 ratio for predicting amyloid PET in a community-based population	Mielke Algeciras-Schimmich Campbell Syrjanen Knopman Jack Jr. Peterson	Mielke, Michelle
151	Mental and physical activity during the uptake period affects off-target binding in extra- and within-brain Tau PET (18F-FTP)	Min Apgar Scott Hol Lundt Albertson Schwarz Botha Vemuri Gunter Petersen Jack Lowe	Min, Hoon-Ki
34	Sex-specific differences in [18F]AV-1451 off-target retention	Minhas Yu Laymon Lopresti Snitz Tudorascu Aizenstein Lopez Mathis Klunk Cohen	Minhas, Davneet
35	Polygenic risk for Cerebrospinal Fluid (CSF) amyloid predicts brain amyloid in clinically normal older adults	Moore Dumitrescu Schultz Raghavan Johnson Mayeux Sperling Hohman Mormino	Moore, Annah
111	Cerebrospinal fluid matrix metalloproteinases are associated with compromised white matter microstructure among older adults: the Vanderbilt memory & aging project	Moore Pechman Acosta Bell Anderson Landman Blennow Zetterberg Gifford Hohman Jefferson	Moore, Elizabeth
143	Validation of clinical protocols for clinicians analyzing 18F-PI-2620 tau PET/MRI images	Koran Shams Adams Cazevedo Toueg Corso Hunt Castillo Hall Sha Fredericks Greicius Wagner Zaharchuk Davidzon Chin Mormino	Mormino, Elizabeth
152	In vivo uptake of 18F-PM-PBB3 (18F-APN-1607) in patients with corticobasal syndrome	Nakano Shimada Tagai Matsuoka Kubota Takahata Takado Shinotoh Yamamoto Sano Seki Hirano Ono Tempest Jang Sahara Kawamura Zhang Kuwabara Higuchi	Nakano, Yoshikazu
94	Development of new alpha7 nicotinic receptor ASEM analogs for PET imaging	Nordberg Lemoine Mohan Kuang Nag Jia Miranda Azpiazu Datta Arakawa Varnäs Ågren Långström Halldin	Nordberg, Agneta
36	Association between cerebral amyloid accumulation and synaptic density in Alzheimer's disease: a multitracer PET study	O'Dell Mecca Chen Godek Harris Bartlett Banks Kominek Zhao Naganawa Toyonaga Lu Nabulsi Vander Wyk Varma Arnsten Huang Carson van Dyck	O'Dell, Ryan
108	Associations between AD biomarkers and cognition among cognitively normal older adults	Oh Correia Salloway	Oh, Hwamee
153	Factors predicting tau PET status in cognitively unimpaired and impaired individuals	Ossenkuppele Leuzy Cho La Joie Strandberg Matsson Palmqvist Lyoo Rabinovici Smith Hansson	Ossenkuppele, Rik

Board #	Poster Title	Authors	Presenter
37	A clinically applicable proxy for gold standard quantification of amyloid-beta in Alzheimer's disease: Bolus plus constant infusion 18F-AV45 PET	Ottoy Kang Verhaeghe Stroobants Bouhachi Hsiao Stevenson Rahmouni Chartrand Massarweh Soucy Gauthier Rosa-Neto Staelens	Ottoy, Julie
154	Widespread amyloid is necessary to detect tau-PET signal beyond the entorhinal cortex and cognitive decline	Ozlen Binette Köbe Meyer Villeneuve	Ozlen, Hazal
75	[11C]MK-6884 PET tracer for M4 muscarinic cholinergic receptors in AD: comparison with [18F]FDG PET	Pascual Zanotti-Fregonara Yu Funk Arbones Wang Li Cheng Anderson Hostetler Basile Masdeu	Pascual, Belen
81	Amyloid and tau PET burden are associated with white matter bundle abnormalities in asymptomatic individuals at risk of AD	Pichet Binette Theaud Gonneaud Poirier Descoteaux Villeneuve	Pichet Binette, Alexa
155	Using 18F-Flortaucipir visual assessment to define T-status in the AT(N) framework: evaluation of intra- and inter-rater reliability	Provost Iaccarino Soleimani-Meigooni Lesman-Segev La Joie Edwards Strom Pham Mellinger Janabi Baker Jagust Rabinovici	Provost, Karine
156	Defining T-status in the AT(N) framework: comparison of 18F-Flortaucipir visual assessment, SUVR quantification and CSF pTau	Provost Iaccarino Soleimani-Meigooni Lesman-Segev La Joie Mattsson Hansson Eichenlaub Edwards Strom Pham Mellinger Janabi Baker Jagust Rabinovici	Provost, Karine
157	Plasma neurofilament light is associated with regional tau tangle burden in autosomal dominant AD: findings from the COLBOS Project	Quiroz Zetterberg Reiman Sanchez Guzman-Velez Fox-Fuller Arboleda-Velasquez Baena Gatchel Sperling Johnson Blennow Lopera	Quiroz, Yakeel
40	MIND MAPS: assessment of the mitochondrial - endoplasmic reticulum - synaptic axis in neurodegeneration by [18F]BCPP-EF, [11C]SA4503 and [11C]UCB-J PET imaging	Rabiner Mansur Venkataraman Price Wilson Pagano Clarke Lewis Matthews Rowe Brooks Middleton Politis Rohrer Comley Evans Martarello Chen Schwarz Schmidt Tsukada Passchier Gunn Consortium	Rabiner, Eugenio
41	Associations between Neurogranin and imaging biomarkers of Alzheimer's disease	Rahmouni Benedet Nicholas Tissot Pascoal Kvaratsberg Chamoun Kang Lussier Theriault Stevenson Savard Mathotaarachchi Thomas Gauthier Zetterberg Blennow Rosa-Neto	Rahmouni, Nesrine
42	Linking APOE ε4, blood-brain barrier dysfunction and inflammation to Alzheimer's pathology	Riphagen Ramakers Freeze Pagen Hanseeuw Verbeek Verhey Jacobs	Riphagen, Joost
104	Increased risk of AD in alcohol use disorder is not mediated by amyloid-beta in a middle-aged cross-sectional cohort	Royse Himes Minhas Lopresti Flanigan Narendran	Royse, Sarah
43	Heterogeneity of tau PET signal in the sub-nuclei of the amygdala	Rubinstein Jacobs Augustinack Properzi Becker Mayblyum Thibault Sanchez Schultz Hanseeuw Gomez-Isla Lois-Gomez Price Sperling Johnson	Rubinstein, Zoe
86	Cross-sectional and longitudinal non-dichotomized CSF/PET Aβ data support existence of "CSF+ first" vs. "PET+ first" pathways of Aβ biomarkers changes	Sala Nordberg Rodriguez-Vieitez	Sala, Arianna
158	Application of tau PET as a biomarker of AD in therapeutic trials: a pharmaceutical industry perspective	Salinas Lohith Guo Wooten Tulip Sanjeewa Comley Sur Hostetler Beaver Martarello	Salinas, Cristian
82	NeuroToolkit CSF biomarkers track the progression of AD at very early stages and show that inflammatory markers modulate cerebral amyloid accumulation	Salvadó Molinuevo Milà-Alomà Blennow Zetterberg Operto Falcón Batrla Battle Buckley Farrar Minguillon Fauria Sánchez-Benavides Suárez-Calvet Gispert the ALFA study	Salvadó, Gemma
83	T1rho MRI measurement of amyloid plaque burden in cognitively unimpaired individuals: preliminary results in the ALFA+ cohort	Falcón Montesinos Grau-Rivera Suárez-Calvet Puig-Pijoan Cascales Navalpotro-Gomez Fernández-Lebrero Sánchez-Valle Gelpi Sanfeliu Rojas Perissinotti Niñerola-Baizán Salvadó Minguillon Fauria Molinuevo Sánchez-González Gispert the ALFA study	Salvadó, Gemma
84	Preliminary quantitative results of the AMYPAD prognostic and natural history study	Gispert Lopes-Alves Gray Buckley Collij Heeman Salvadó Scheltens Frisoni Ritchie Vellas Stephens Ford Molinuevo Farrar Barkhof the AMYPAD Consortium	Salvadó, Gemma
159	Measuring increases of tau pathology in AD using [18F]GTP1 (Genentech tau probe 1) PET imaging	Sanabria Bohorquez Baker Manser Toth Teng Marik Weimer	Sanabria Bohorquez, Sandra
160	Evaluation of tau PET staging in the A4/LEARN study	Sanchez Becker Jacobs Hanseeuw Mayblyum Rubinstein Thibault Schultz Seshadri Quiroz Rentz Price Sperling Johnson the A4 Study Team	Sanchez, Justin

Board #	Poster Title	Authors	Presenter
72	Effect of genetic risk, brain amyloid and hippocampal volume on normal variation in episodic memory performance in middle-aged and older adults	Schaefferbeke Gabel Adamczuk Van Laere Dupont Vandenberghe	Schaefferbeke, Jolien
161	Clinical evaluation of [18F]-JNJ-64326067, a candidate PET tracer for the detection of tau pathology in AD	Schmidt Janssens Moechars Rombouts Timmers Barret Constantinescu Madonia Russell Sandiego Kolb	Schmidt, Mark
162	Association between cerebrospinal fluid neurofilament light chain and markers of neurofibrillary pathophysiology: findings from the Knight Alzheimer Disease Research Center	Schultz Schindler Chen Sutphen Morris Fagan Gordon Benzinger	Schultz, Stephanie
44	MCI patients demonstrate reliably increasing 18F-AV1451 PET uptake across three exams	Scott Adamczuk Gorman Runkle Suhy	Scott, David
103	White matter disruption is an early and progressive feature of pre-symptomatic Dutch-type hereditary cerebral amyloid angiopathy	Scott Schultz Sohrobi Gardener Taddei Bateman Benzinger Johnson Sperling Martins Greenberg Chhatwal Investigators	Scott, Matthew
45	Development of a qualitative read method for characterizing the presence and extent of brain tau deposition using [18F]MK-6240 PET imaging	Seibyl Salinas Rajagovindan Hutchison Beaver Martarello	Seibyl, John
88	Head-to-head comparison of F-Florbetaben and F-Flutemetamol uptakes in the cortex, striatum and white matter	Seo Cho Moon Choe Na	Seo, Sang Won
163	18F-PM-PBB3 (18F-APN-1607) uptake associates with plasma NfL level and motor disability in patients with progressive supranuclear palsy	Shimada Tagai Tatebe Matsuoka Kubota Takahata Takado Shinotoh Yamamoto Sano Seki Nakano Ono Hirano Tempest Jang Sahara Kawamura Zhang Tokuda Higuchi	Shimada, Hitoshi
16	Predicting future amyloid spread with machine learning using longitudinal [C11]PiB-PET in preclinical Alzheimer's disease	Hao Vogt Meng Hwang Kosciak Betthausen Christian Johnson Bendlin Singh	Singh, Vikas
164	The rate of accumulation of tau aggregates is higher in females and younger individuals	Smith Mattsson Pontecorvo Devous Strandberg Ossenkoppele Hansson	Smith, Ruben
46	PET imaging of [11C]MPC-6827, a microtubule-based PET tracer in murine models of AD	Solingapuram sai Macauley Whitlow Mintz Craft	Solingapuram Sai, Kiran Kumar
47	Quantifying the relationship between the brain distributions of tau and local atrophy to inter-regional connectivity based on individual human data	Soucy Mohammadi Rosa-Neto Pascoal Savard Kang Therriault Benali	Soucy, Jean-Paul
90	PI-2620 Tau PET is associated with amyloid-beta levels in scans from subjects of the elenbecestat MissionAD program	Stephens Bullich Mueller Berndt De Santi Scott Adamczuk Suhy Kaplow Giroux Krause Chang Albala	Stephens, Andrew
48	Monitoring disease pathophysiology using multiparametric PET acquisitions: The McGill TRIAD Cohort	Stevenson Chamoun Pascoal Benedet Kang Mathotaarachchi Therriault Thomas Savard Tissot Lussier Vinet-Celluci Rahmouni Gagné Joung Sbeiti Shin Vitali Gauthier Rosa-Neto	Stevenson, Jenna
165	Resting state functional connectivity associations with F18-Florbetapir PET versus F18-Flortaucipir PET	Svaldi Goñi Stage Abbas Dziedzic West Risacher Saykin Apostolova	Svaldi, Diana
110	Using famous faces to investigate the neural systems involved in name retrieval	Tennant Jagust La Joie Adams Winer	Tennant, Victoria
109	In vivo association of mitochondrial dysfunction with tau pathology in early AD	Terada Therriault Min Su Savard Ouchi Rosa-Neto	Terada, Tatsuhiro
166	Tau positivity: Comparing flortaucipir meta-ROI vs maximal single region	Therneau Schwarz Wiste Gunter Senjem Lowe Kantarci Petersen Knopman Mielke Jones Jack	Therneau, Terry
167	Intrinsic connectivity of the human brain provides scaffold for tau aggregation in AD	Therriault Pascoal Savard Mathotaarachchi Benedet Chamoun Gauthier Saha-Chaudhuri Massarweh Rosa-Neto	Therriault, Joseph
102	Preliminary results: PiB and MK6240 regional PET measures associated with digitized clock drawing performance	Mayblyum Thibault Moody Farrell Jiang Jacobs Rubinstein Sanchez Katz Sperling Papp Rentz Johnson	Thibault, Emma
49	Interaction between amyloid and neuroinflammation on apathy along the Alzheimer's disease spectrum	Tissot Kang Benedet Rahmouni Pascoal Chamoun Therriault Lussier Savard Mathotaarachchi Thomas Gauthier Rosa-Neto	Tissot, Cécile
50	Neuropsychiatric symptoms in cognitively impaired individuals are correlated with tau deposition	Tissot Therriault Pascoal Chamoun Lussier Savard Mathotaarachchi Benedet Thomas Rosa-Neto Gauthier	Tissot, Cécile

Board #	Poster Title	Authors	Presenter
168	Changes in volumetric MRI measures at 12 months significantly correlate with baseline [18F]GTP1 SUVR, but not [18F]GTP1 change	Toth Sanabria Bohorquez Manser Baker Teng Marik Weimer	Toth, Balasz
169	Elevated medial temporal lobe Tau PET with 18F-PI2620 in normal controls with “borderline” neuropsychological testing profiles	Toueg Deutsch Castillo Hunt Corso Trelle Harrison Azevedo Shen Anders Hall Fredericks Sha Davidzon Chin Khalighi Wagner Mormino	Toueg, Tyler
170	Hippocampal tau accumulation predicts individual differences in episodic memory in cognitively normal older adults	Trelle Toueg Castillo Channappa Corso Hunt Jayakumar Nadiadwala Guo Azevedo Shin Davidson Deutsch Hall Sha Fredericks Kerchner Carr Chin Wagner Mormino	Trelle, Alexandra
33	MRI and PET data harmonization in a two-site Down syndrome study	Minhas Yang Muschelli Laymon Zammit Ellison Johnson Mathis Crainiceanu Klunk Handen Christian Cohen Tudorascu	Tudorascu, Dana
97	Associations between longitudinal cognitive measures and cross-sectional tau in adults with Down syndrome	Tudorascu Comer Zammit Laymon Minhas Ellison Zaman Ances Johnson Mathis Klunk Christian Handen Hartley Cohen	Tudorascu, Dana
171	Temporo-limbic tau burden, as measured by 18F-AV1451, is a correlate of hippocampal volume loss over time	Fischer Ahnen Dissertori Lustermann Weber Buck Kagerer Gietl Hock Unschuld	Unschuld, Paul
60	Longitudinal flortaucipir ([18F]AV-1451) PET uptake in Semantic Dementia	Utianski Whitwell Martin Botha Schwarz Duffy Clark Spychalla Senjem Petersen Knopman Jack, Jr. Lowe Josephs	Utianski, Rene
76	Assessing A β , tau, and reactive astrocytosis in aging and AD	Villemagne Harada Doré Furumoto Mulligan Kudo Krishnadas Huang Yanai Rowe Okamura	Villemagne, Victor
63	Developing a novel alpha-synuclein (a-syn) positron emission tomography (PET) tracer for the diagnosis of Parkinson’s disease (PD) and other a-synucleinopathies	Vokali Molette Tsika Ravache Rodriguez Jürgens Melo dos Santos Sandiego Russell Gunn Darmency Piorowska Poli Kroth Capotosti Hliva Sol Marek Stöhr Lowe Pfeifer Kosco-Vilbois	Vokali, Efthymia
51	Association between [18F]NAV4694 PET amyloid- β measures and fluid biomarkers across the spectrum of Alzheimer’s disease	Wang Pascoal Therriault Benedet Lussier Savard Kang Tissot Gauthier Rosa-Neto	Wang, Yi-Ting
52	PET beta-amyloid deposition in healthy older adults is associated with decreased lure discrimination on a spatial mnemonic similarity task	Webb Foster Horn Kennedy Rodrigue	Webb, Christina
95	Biological underpinnings of typical and atypical Alzheimer’s dementia phenotypes	Whitwell Tosakulwong Graff-Radford Weigand Schwarz Senjem Ertekin-Taner Jones Boeve Knopman Jack Petersen Lowe Josephs	Whitwell, Jennifer
89	Sleep impairment predicts longitudinal accumulation of β -amyloid	Winer Mander Jagust Walker	Winer, Joseph
54	Tau pathology and relative cerebral blood flow are independently associated with cognition in Alzheimer’s disease	Wolters Visser Verfaillie Coomans Timmers Tuncel Boellaard Windhorst Scheltens van der Flier Ossenkoppele van Berckel	Wolters, Emma
173	[18F]flortaucipir PET is more closely associated with disease severity than CSF p-tau in AD	Wolters Ossenkoppele Verfaillie Coomans Timmers Visser Tuncel Golla Windhorst Boellaard van der Flier Teunissen Scheltens van Berckel	Wolters, Emma
87	Personality and amyloid accumulation in cognitively normal aging	Yoon Baker Korman Tennant Harrison Jagust	Yoon, Bora
55	Amyloid Load trajectories and chronicity reveal groups of early amyloid accumulators in Down syndrome	Zammit Kosciak Laymon Betthausen Tudorascu Cohen Minhas Johnson Zaman Mathis Klunk Handen Christian	Zammit, Matt
56	Hippocampal-retrosplenial cortex connectivity predicts tau accumulation in cognitively normal older adults	Ziontz Adams Baker Jagust	Ziontz, Jacob
174	Associations of tau pathology and functional connectivity with retrospective cognitive change among cognitively normal older adults	Shafer Bilgel Ziontz Wong Resnick	Ziontz, Jacob
98	Associations of amyloid deposition and FDG uptake in aging and cognitively impaired elders with and without moderate to severe periventricular white matter hyperintensities	Zukotynski Gaudet Kuo Adamo Goubran Scott Bocti Borrie Chertkow Frayne Hsiung Laforce Noseworthy Prato Sahlas Smith Sossi Thiel Soucy Tardif Black	Zukotynski, Katherine

HAI 2020 PROGRAM

Wednesday, January 15, 2020

7:30 AM	Check-in and Breakfast	
8:15 AM	Introductions/Welcome Notes	Keith Johnson, MD, <i>Massachusetts General Hospital</i>
8:30 AM	DIDACTIC SESSION A: PET Technical/Methods	CHAIR: Chester Mathis, PhD, <i>University of Pittsburgh</i>
8:30 AM	Multi-site and longitudinal studies considerations	Robert Koeppe, PhD, <i>University of Michigan</i>
8:55 AM	Centiloids	Christopher Rowe, MD, <i>Austin Health</i>
9:20 AM	In silico and computational chemistry methods in the development of PET radiotracers for imaging alpha synuclein	Robert Mach, PhD, <i>University of Pennsylvania</i>
9:45 AM	POSTER SESSION 1A and Coffee Break	
10:30 AM	DIDACTIC SESSION B: Neuropathology	CHAIR: William Klunk, MD, <i>University of Pittsburgh</i>
10:30 AM	Basic neuropathology of Abeta, tau and a-syn	Julie Schneider, MD, <i>Rush University</i>
11:00 AM	Technical considerations for IHC, HC, biochemistry	Milos Ikonovic, MD, <i>University of Pittsburgh</i>
11:30 AM	Technical considerations for homogenate binding	Laetitia Lemoine, PhD, <i>Karolinska Institute</i>
12:00 PM	Maturity states of plaques and tangles	Melissa Murray, PhD, <i>Mayo Clinic</i>
12:30 PM	Lunch	
1:45 PM	SESSION 1: TECHNICAL I	CHAIRS: Brad Christian, PhD, <i>University of Wisconsin-Madison</i> Ansel Hillmer, PhD, <i>Yale University</i>
1:45 PM	Evaluation of 18F-JNJ-067 as a tau tracer	Suzanne Baker, PhD, <i>Lawrence Berkeley National Laboratory</i>
2:00 PM	A direct comparison of tau imaging agents [F-18]AV-1451 AND [F-18]MK-6240 in human subjects	Brian Lopresti, MS, <i>University of Pittsburgh</i>
2:15 PM	A multi-center comparison of [18F]flortaucipir, [18F]RO948 and [18F]MK6240 tau-PET tracers to detect optimal target ROIs for differential diagnosis	Rik Ossenkoppele, PhD, <i>VU University Medical Center</i>
2:30 PM	Capturing extra-cerebral MK-6240 signal with surface projections	Justin Sanchez, BA, <i>Massachusetts General Hospital</i>
2:45 PM	Discussion Session 1	
3:15 PM	Keynote Lecture	Alan Evans, PhD, <i>McGill University</i>
3:45 PM	Keynote Discussion	
4:00 PM	POSTER SESSION 1B and Coffee Break	
4:45 PM	SESSION 2: TECHNICAL II	CHAIRS: Julie Price, PhD, <i>Harvard Medical School</i> Suzanne Baker, PhD, <i>Lawrence Berkeley National Laboratory</i>
4:45 PM	Amyloid Load predicts elevated tau deposition in Down syndrome	Matt Zammit, MS, <i>University of Wisconsin</i>
5:00 PM	TauIQ demonstrates increased power for cross-sectional and longitudinal analysis of Tau tracers as evidenced by [18F]Flortaucipir and [18F]GTP1	Roger Gunn, PhD, <i>Invicro</i>
5:15 PM	Spatiotemporal imaging phenotypes of tau pathology in Alzheimer's disease	Jacob Vogel, PhD (cand.), <i>McGill University</i>
5:30 PM	Predicting structural, metabolic and pathologic disease progression in autosomal dominant Alzheimer's disease with machine learning	Patrick Lueckert, PhD, <i>Washington University in St. Louis</i>
5:45 PM	Correction of partial volume effects for tau PET imaging using the kernel method	Kuang Gong, PhD, <i>MGH/Harvard Medical School</i>
6:00 PM	Discussion Session 2	
6:30 PM	Welcome Reception	

Thursday, January 16, 2020

7:30 AM	Check-in and Breakfast	
8:30 AM	SESSION 3: NEUROPATHOLOGY I	CHAIRS: Laetitia Lemoine, PhD, <i>Karolinska Institute</i> Teresa Gomez-Isla, <i>Mass. General Hospital</i>
8:30 AM	Flortaucipir PET often shows uptake greater in regions outside of the medial temporal lobe than in entorhinal cortex in low Braak tangle stage participants	Val Lowe, MD, <i>Mayo Clinic</i>
8:45 AM	Brain volume and [18F]flortaucipir PET analysis of progressive supranuclear palsy clinical variants	Jennifer Whitwell, PhD, <i>Mayo Clinic</i>
9:00 AM	Comparison of autoradiographic binding profiles of Flortaucipir, MK-6240 and PI-2620 in human postmortem tissue samples across the spectrum of neurodegenerative diseases	Cinthya Agüero, MD, <i>Massachusetts General Hospital</i>
9:15 AM	Biochemical correlates of tau and amyloid PET imaging in four autopsy brains	Milos Ikonovic, MD, <i>University of Pittsburgh</i>
9:30 AM	Discussion Session 3	
10:00 AM	Keynote Lecture: Amyloid and tau: one of multiple pathways to tissue injury, degeneration, and Alzheimer's dementia	Julie Schneider, MD, MS, <i>Rush University</i>
10:30 AM	Keynote Discussion	
10:45 AM	POSTER SESSION 2A and Coffee Break	
11:30 AM	SESSION 4: NEUROPATHOLOGY II	CHAIRS: Melissa Murray, PhD, <i>Mayo Clinic</i> Julie Schneider, MD, MS, <i>Rush University</i>
11:30 AM	Derivation and potential utility of an Aβ-PET based path. accumulation index for estimation of brain Aβ load	Ruben Smith, MD, PhD, <i>Lund University</i>
11:45 AM	In vitro study of the evidence of tauopathy in PD brains using a tau PET tracer, [3H]MK-6240, by autoradiography	Zhizhen Zeng, MD, PhD, <i>Merck & Co. Inc.</i>
12:00 PM	In vitro characterization of second-generation tau PET tracers in human autopsy brain tissue	Mona-Lisa Malarte, PhD (cand.), <i>Karolinska Institute</i>
12:15 PM	Neurofibrillary tangle maturity: a comprehensive review	Christina Moloney, PhD, <i>Mayo Clinic</i>
12:30 PM	Discussion Session 4	
1:00-2:30	Lunch	
2:30 PM	SESSION 5: CLINICAL I	CHAIRS: Keith Johnson, MD, <i>Mass. General Hospital</i> Pedro Rosa-Neto, MD, PhD, <i>McGill University</i>
2:30 PM	History of head injury is associated with greater tau deposition on [18F]Flortaucipir PET in MCI and AD patients	Shannon Risacher, PhD, <i>Indiana University School of Medicine</i>
2:45 PM	In vivo measurement of widespread synaptic loss in early Alzheimer's disease with SV2A PET	Adam Mecca, MD, PhD, <i>Yale University</i>
3:00 PM	Amyloid PET is more than just positive or negative: Aβ-amyloid level impacts risk of clinical progression in non-demented individuals	Christopher Rowe, MD, <i>Austin Health</i>
3:15 PM	18F-PI2620 tau-PET in Progressive Supranuclear Palsy: a multi-center evaluation	Matthias Brendel, MD, <i>University Hospital of Munich</i>
3:30 PM	Discussion Session 5	
4:00 PM	POSTER SESSION 2B and Coffee Break	
4:45 PM	SESSION 6: CLINICAL II	CHAIRS: William Jagust, MD, <i>UC Berkeley</i> David Wolk, MD, <i>University of Pennsylvania</i>
4:45 PM	Tau-PET associations with amyloid positivity and cognitive impairment	Susan Landau, PhD, <i>University of California, Berkeley</i>
5:00 PM	Locus coeruleus integrity tracks with initial Alzheimer's disease-related pathology and cognitive decline	Heidi Jacobs, PhD, <i>Massachusetts General Hospital</i>
5:15 PM	Area 35 is the earliest subregion in the medial temporal lobe affected by tau pathology	David Berron, PhD, <i>Lund University</i>
5:30 PM	Discussion Session 6	
6:00 PM	Networking Reception	

Friday, January 17, 2020

7:30 AM	Check-in and Continental Breakfast	
8:30 AM	SESSION 7: TAU I	CHAIRS: Tobey Betthausser, PhD, <i>University of Wisconsin</i> Sylvia Villeneuve, PhD, <i>McGill University</i>
8:30 AM	The implications of different approaches to define AT(N) in Alzheimer's disease	Antoine Leuzy, PhD, <i>Lund University</i>
8:45 AM	Towards a CenTauR cortical mask	Vincent Dore, PhD, <i>CSIRO</i>
9:00 AM	Tau Positivity: Comparing Flortaucipir Meta-ROI vs. Maximum of Regional Z-Scores	Christopher Schwarz, MD, <i>Mayo Clinic</i>
9:15 AM	POSTER SESSION 3A and Coffee Break	
10:00 AM	SESSION 7: TAU II	CHAIRS: Clifford Jack, MD, <i>Mayo Clinic</i> Reisa Sperling, MD, <i>Brigham and Women's Hospital</i> Victor Villemagne, MD, <i>Austin Health</i>
10:00 AM	Critical threshold of elevated amyloid associated with rapid tau accumulation: a ca-tau-strophe in the making	Keith Johnson, MD, <i>Massachusetts General Hospital</i>
10:15 AM	The meaning of tau positivity with respect to clinical progression	Michael Devous, PhD, <i>Avid Pharmaceuticals</i>
10:30 AM	Longitudinal tau PET changes in cognitively unimpaired persons with different β -amyloid levels	David Knopman, MD, <i>Mayo Clinic</i>
10:45 AM	Defining a tau positive flortaucipir PET signal relative to AD neuropathology	Michael Pontecorvo, PhD, <i>Avid Pharmaceuticals</i>
11:00 AM	Discussion Session 7 (TAU I and TAU II)	
12:00 PM	Keynote Lecture: Leveraging brain rhythms as a therapeutic intervention for Alzheimer's disease	Li-Huei Tsai, PhD, <i>MIT</i>
12:30 PM	Keynote Discussion	
12:45 PM	Lunch	
2:00 PM	SESSION 8: CLINICAL III	CHAIRS: Elizabeth Mormino, PhD, <i>Stanford University</i> Susan Landau, PhD, <i>UC, Berkeley</i>
2:00 PM	Glucose metabolism reflects local atrophy and tau pathology at symptomatic stages of Alzheimer's disease	Amelia Strom, BS, <i>University of California San Francisco</i>
2:15 PM	Plasma FLT1 predicts amyloid- β related cognitive decline in cognitively normal older adults	Hyun-Sik Yang, MD, <i>Brigham and Women's Hospital</i>
2:30 PM	Reducing sample sizes to detect longitudinal amyloid accumulation	Isadora Lopes Alves, PhD, <i>VUmc</i>
2:45 PM	Discussion Session 8	
3:15 PM	POSTER SESSION 3B and Coffee Break	
4:00 PM	Awards Ceremony	
4:15 PM	SESSION 9: PLASMA	CHAIR: Gil Rabinovici, MD, <i>UCSF</i>
4:15 PM	Plasma P-tau181 as a marker of tau pathology in Alzheimer's disease: relationship to Tau PET, differential diagnosis, neuropathology and longitudinal progression	Oskar Hansson, PhD, <i>Lund University</i>
4:30 PM	Plasma levels of an N-terminal tau fragment are highly associated with future cognitive decline and neurodegeneration in clinically normal elderly: findings from the Harvard Aging Brain Study	Jasmeer Chhatwal, MD, <i>MGH/Harvard University</i>
4:45 PM	Plasma biomarkers associate with amyloid and tau PET binding in cognitively unimpaired older adults with a parental history of AD	Pierre-Francois Meyer, PhD, <i>McGill University</i>
5:00 PM	High-performance plasma phospho-tau181 biomarker for Alzheimer's disease	Tharick Pascoal, PhD, <i>McGill University</i>
5:15 PM	Discussion Session 9	
5:45 PM	Closing Notes	Keith Johnson, MD, <i>Massachusetts General Hospital</i>

HAI 2020 ABSTRACTS

Wednesday, January 15, 2020 - 9:45 - 10:30am

P1A: POSTER SESSION 1A

Board #	Poster Title	Authors	Presenter	Page
53	Socioeconomic status mediates racial differences seen using the A-T(N) Framework	Wisch Hudson Coble Xiong Babulal Gordon Flores Dincer Benzinger Morris Ances	Ances, Beau	154
01	Label-free x-ray method for estimating brain amyloid load	Badano Dahal Ghamraoui	Badano, Aldo	43
02	Examining regional MK-6240 patterns and associations with amyloid and cognitive decline	Bethhauser Cody Koscik Jonaitis Erickson Converse Murali Barnhart Stone Mueller Clark Asthana Christian Johnson	Bethhauser, Tobey	44
03	Transcriptomic profiling of brain amyloidosis using peripheral blood-based gene expression	Bharthur Sanjay Svaldi Apostolova	Bharthur Sanjay, Apoorva	47
04	A pons cluster detected by a data-driven approach may serve as a favorable reference region for 18F-PI-2620 Tau PET analysis	Bischof van Eimeren Koglin Müller Bullich Perrotin Stephens Drzezga	Bischof, Gerard	50
05	Early detection of amyloid load using 18F-Florbetaben PET	Bullich Roé-Vellvé Marquié Villemagne Sanabria Tartari Sotolongo Doré Koglin Müller Perrotin De Santi Tárraga Stephens Rowe Seibyl Boada	Bullich, Santiago	57
06	Age-related neural dedifferentiation of episodic memory networks is related to beta-amyloid and tau pathology in normal aging	Cassady Adams Maass Harrison Baker Jagust	Cassady, Kaitlin	52
07	Tau pathology and synaptic loss are closely associated in Alzheimer's disease in vivo: a combined [18F]flortaucipir and [11C]UCB-J PET study	Coomans Verfaillie Wolters Tuncel Golla Ossenkoppele Scheper Schober Sweeney Ryan Schuit Windhorst Scheltens Boellaard van Berckel	Coomans, Emma	54
08	Longitudinal dynamic [18F]flortaucipir PET reveals increased early stage tau pathology in individuals with subjective cognitive decline	Coomans Visser Ossenkoppele Verfaillie Timmers Wolters Tuncel Schmidt Boellaard Windhorst Scheltens van der Flier van Berckel	Coomans, Emma	58
09	Preliminary evaluation of synaptic vesicle protein SV2A imaging with [11C]UCB-J across the cognitive spectrum	DiFilippo Murali McKinney Davenport Barnhart Engle Bethhauser Johnson Bendlin Christian	DiFilippo, Alexandra	61
10	Quantifying off-target skull binding in [18F]Flortaucipir PET studies	Flores Gordon Su Christensen Dincer Adedokun Hornbeck Morris Benzinger	Flores, Shaney	62
11	Influence of iron and beta-amyloid deposition on entorhinal cortex and hippocampal subfield volumes in the aging brain	Foster Kennedy Rodrigue	Foster, Chris	65
13	Beta-amyloid deposition and its association with metabolism	Gordon Goyal Couture Flores Morris Raichle Benzinger Vlassenko	Gordon, Brian	68
14	Amyloid binding is associated with markers of white matter microstructure in patients with significant white matter disease	Goubran Ozzoude Adamo Zukotynski Bocti Borrie Chertkow Frayne Gao Hsiung Kiss Laforce Noseworthy Prato Ramirez Sahlas Scott Smith Sossi Strother Swartz Tardif Thiel Soucy Black	Goubran, Maged	70
15	CSF dynamics explains discrepant PET-CSF AD biomarkers	Gunter Senjem Cogswell Schwarz Lowe Kantarci Vemuri Elder Botha Graff-Radford Jones Mielke Graff-Radford Knopman Petersen Jack, Jr.	Gunter, Jeffrey	73
20	Hippocampal volume mediates the relationship between amyloidosis and amyloid-sensitive cognitive composite in preclinical AD	Kim Hahn Kim Kim Chin Seo	Hahn, Alice	88
17	[11C]PiB amyloid quantification and choice of reference region	Heeman Hendriks van Berckel Lopes Alves Lammertsma Yaqub	Heeman, Fiona	80

Board #	Poster Title	Authors	Presenter	Page
18	Retrospective prediction of amyloid accumulation trajectories in a risk-enriched Alzheimer's disease cohort with sequential neural network	Hwang Kosciak Betthausen Tao Kim Johnson Singh	Hwang, Seong Jae	82
19	Data-driven biological pattern scoring of Flortaucipir scans outperforms ROIs	Jones Graff-Radford Botha Senjem Wiste Josephs Whitwell Kantarci Boeve Petersen Knopman Lowe Jack	Jones, David	85
21	Concordance of visual and quantitative assessments of baseline amyloid scans in the GRADUATE gantenerumab studies	Klein Delmar Voyle Hesterman Petrulli Ovens Baudler Fontoura Doody Kerchner	Klein, Gregory	89
22	Regional amyloid burden is associated with higher quantitative T1 in discrete hippocampal sub-regions	Kohli Yang Vogt Asthana Betthausen Alexander Christian Johnson Kecskemeti Bendlin	Kohli, Akshay	90
23	Genetically informed quantitative Gradient Recalled Echo MRI reveals brain tissue in hippocampal subfields void of neurons in mild Alzheimer's disease	Kothapalli Benzinger Aschenbrenner Goyal Fagan Raichle Morris Yablonskiy	Kothapalli, Satya V.V.N.	93
24	Validation of highly sensitive and specific florbetaben positivity thresholds using ADNI participants and young controls	Landau Korman Bullich De Santi Stephens Koeppel Jagust	Landau, Susan	94
12	Voxel-wise relationships between white matter hyperintensities (WMH) and multimodal neuroimaging biomarkers of Alzheimer's disease	Gaubert Lange Garnier-Crussard Bougacha Gonneaud de Flores Tomadesso Mézenge Landeau de La Sayette Chételat Wirth	Lange, Catharina	66
25	Additive contribution of white matter hyperintensity to amyloid and neurodegeneration on cognitive decline in a diverse, community-based cohort of older adults	Lao Chesebro Colon Igwe Gu Schupf Manly Stern Mayeux Brickman	Lao, Patrick	97
26	White matter hyperintensities are related to tau burden in late-Braak stage regions	Lao Laing Igwe Chesebro Kreisl Moreno Luchsinger Brickman	Lao, Patrick	98
27	Probability template method for analysis of Down Syndrome amyloid PET	Laymon Minhas James Christian Cohen Klunk Tudorascu Royse Zaman Handen	Laymon, Charles	100
28	Visualizing brain astrocytes - characterization of 3H-BU99008 in human AD brain tissue	Lemoine Malarte Koistinen Nordberg	Lemoine, Laetitia	102
29	Application of an epidemic spreading model to characterize amyloid beta accumulation in autosomal dominant Alzheimer's disease mutation carriers	Levitis Vogel Kiar Funck Iturria-Medina Evans	Levitis, Elizabeth	103
30	Phantom-based harmonization of PET image reconstruction parameters between the Siemens ECAT HR+ PET and the GE Discovery MI PET/CT scanners	Lois Grogg El Fakri Johnson Price	Lois, Cristina	106
38	Amyloid PET variability due to variation in MRI protocol and anatomical segmentation	Palombit Manber Joules Wolz	Manber, Richard	124
39	The impact of automatic Tau PET processing on uptake variability and power analysis in AD	Palombit Manber Joules Wolz	Manber, Richard	126
31	Age prediction and amyloid deposition in SuperAgers	Martersteck Besson Sridhar Makowski-Woidan Parrish Katsaggelos Mesulam Bandt Rogalski	Martersteck, Adam	108
32	PiB tracer delivery decreases overtime in preclinical AD – impact for amyloid pathology measurement	Mayblyum Becker Schultz Farrell Jacobs Rubinstein Sanchez Thibault Sperling Price Johnson Hanseeuw	Mayblyum, Danielle	109
34	Sex-specific differences in [18F]AV-1451 off-target retention	Minhas Yu Laymon Lopresti Snitz Tudorascu Aizenstein Lopez Mathis Klunk Cohen	Minhas, Davneet	115
35	Polygenic risk for Cerebrospinal Fluid (CSF) amyloid predicts brain amyloid in clinically normal older adults	Moore Dumitrescu Schultz Raghavan Johnson Mayeux Sperling Hohman Mormino	Moore, Annah	117
36	Association between cerebral amyloid accumulation and synaptic density in Alzheimer's disease: a multitracer PET study	O'Dell Mecca Chen Godek Harris Bartlett Banks Kominek Zhao Naganawa Toyonaga Lu Nabulsi Vander Wyk Varma Arnsten Huang Carson van Dyck	O'Dell, Ryan	120
37	A clinically applicable proxy for gold standard quantification of amyloid-beta in Alzheimer's disease: Bolus plus constant infusion 18F-AV45 PET	Ottoy Kang Verhaeghe Stroobants Bouhachi Hsiao Stevenson Rahmouni Chartrand Massarweh Soucy Gauthier Rosa-Neto Staelens	Ottoy, Julie	121

Board #	Poster Title	Authors	Presenter	Page
40	MIND MAPS: assessment of the mitochondrial - endoplasmic reticulum - synaptic axis in neurodegeneration by [18F]BCPP-EF, [11C]SA4503 and [11C]UCB-J PET imaging	Rabiner Mansur Venkataraman Price Wilson Pagano Clarke Lewis Matthews Rowe Brooks Middleton Politis Rohrer Comley Evans Martarello Chen Schwarz Schmidt Tsukada Passchier Gunn Consortium	Rabiner, Eugenio	127
41	Associations between Neurogranin and imaging biomarkers of Alzheimer's disease	Rahmouni Benedet Nicholas Tissot Pascoal Kvaratsberg Chamoun Kang Lussier Therriault Stevenson Savard Mathotaarachchi Thomas Gauthier Zetterberg Blennow Rosa-Neto	Rahmouni, Nesrine	131
42	Linking APOE ε4, blood-brain barrier dysfunction and inflammation to Alzheimer's pathology	Riphagen Ramakers Freeze Pagen Hanseeuw Verbeek Verhey Jacobs	Riphagen, Joost	133
43	Heterogeneity of tau PET signal in the sub-nuclei of the amygdala	Rubinstein Jacobs Augustinack Properzi Becker Mayblyum Thibault Sanchez Schultz Hanseeuw Gomez-Isla Lois-Gomez Price Sperling Johnson	Rubinstein, Zoe	136
44	MCI patients demonstrate reliably increasing 18F-AV1451 PET uptake across three exams	Scott Adamczuk Gorman Runkle Suhy	Scott, David	140
45	Development of a qualitative read method for characterizing the presence and extent of brain tau deposition using [18F]MK-6240 PET imaging	Seibyl Salinas Rajagovindan Hutchison Beaver Martarello	Seibyl, John	141
16	Predicting future amyloid spread with machine learning using longitudinal [C11]PiB-PET in preclinical Alzheimer's disease	Hao Vogt Meng Hwang Koscik Betthausen Christian Johnson Bendlin Singh	Singh, Vikas	76
46	PET imaging of [11C]MPC-6827, a microtubule-based PET tracer in murine models of AD	Solingapuram sai Macauley Whitlow Mintz Craft	Solingapuram Sai, Kiran Kumar	142
47	Quantifying the relationship between the brain distributions of tau and local atrophy to inter-regional connectivity based on individual human data	Soucy Mohammadi Rosa-Neto Pascoal Savard Kang Therriault Benali	Soucy, Jean-Paul	143
48	Monitoring disease pathophysiology using multiparametric PET acquisitions: the McGill TRIAD Cohort	Stevenson Chamoun A. Pascoal Benedet Kang Mathotaarachchi Therriault Thomas Savard Tissot Lussier Vinet-Celluci Rahmouni Gagné Joung Sbeiti Shin Vitali Gauthier Rosa-Neto	Stevenson, Jenna	144
49	Interaction between amyloid and neuroinflammation on apathy along the Alzheimer's disease spectrum	Tissot Kang Benedet Rahmouni Pascoal Chamoun Therriault Lussier Savard Mathotaarachchi Thomas Gauthier Rosa-Neto	Tissot, Cécile	145
50	Neuropsychiatric symptoms in cognitively impaired individuals are correlated with tau deposition	Tissot Therriault Pascoal Chamoun Lussier Savard Mathotaarachchi Benedet Thomas Rosa-Neto Gauthier	Tissot, Cécile	147
33	MRI and PET data harmonization in a two-site Down syndrome study	Minhas Yang Muschelli Laymon Zammit Ellison Johnson Mathis Crainiceanu Klunk Handen Christian Cohen Tudorascu	Tudorascu, Dana	111
51	Association between [18F]NAV4694 PET amyloid-β measures and fluid biomarkers across the spectrum of Alzheimer's disease	Wang Pascoal Therriault Benedet Lussier Savard Kang Tissot Gauthier Rosa-Neto	Wang, Yi-Ting	149
52	PET beta-amyloid deposition in healthy older adults is associated with decreased lure discrimination on a spatial mnemonic similarity task	Webb Foster Horn Kennedy Rodrigue	Webb, Christina	153
54	Tau pathology and relative cerebral blood flow are independently associated with cognition in Alzheimer's disease	Wolters Visser Verfaillie Coomans Timmers Tuncel Boellaard Windhorst Scheltens van der Flier Ossenkoppele van Berckel	Wolters, Emma	157
55	Amyloid Load trajectories and chronicity reveal groups of early amyloid accumulators in Down syndrome	Zammit Koscik Laymon Betthausen Tudorascu Cohen Minhas Johnson Zaman Mathis Klunk Handen Christian	Zammit, Matt	160
56	Hippocampal-retrosplenial cortex connectivity predicts tau accumulation in cognitively normal older adults	Ziontz Adams Baker Jagust	Ziontz, Jacob	163

P1: Label-free x-ray method for estimating brain amyloid load

Aldo Badano¹, Eshan Dahal¹, Bahaa Ghammraoui¹

¹*FDA, Silver Spring, MD, US*

We describe a label-free method based on small-angle x-ray scattering (SAXS) for estimating brain amyloid load *in vivo* in small-animals and humans. Our method is based on recording and analyzing the coherently scattered x rays from amyloid plaques in a mouse or human head at angles smaller than 10° with x-ray energies above 30 keV. Using a fixed head *ex vivo*, we demonstrate the feasibility of estimating amyloid load in a mouse head with skull without using contrast agent. Using our proposed method, high-energy polychromatic x rays can be efficiently used in conjunction with a spectral detector in a pre-clinical setting to estimate amyloid load. Furthermore, using Monte Carlo techniques, we have investigated the feasibility of using a photon-counting strip detector and high-energy x-ray spectra from 30 to 60 keV to identify amyloid plaques in a human head phantom. Phantoms with and without amyloid plaques were simulated to assess the method and determine the radiation dose required to obtain acceptable statistical power. The result shows the potential of the proposed method for accurate *in-vivo* detection and quantification of amyloid plaques in the human brain with acceptable level of radiation dose.

Keywords: SAXS, x rays, amyloid load

P2: Examining regional MK-6240 patterns and associations with amyloid and cognitive decline

Tobey Betthausen¹, Karly Cody¹, Rebecca Kosciak¹, Erin Jonaitis¹, Claire Erickson¹, Alexander Converse¹, Dhanabalan Murali¹, Todd Barnhart¹, Charles Stone¹, Kimberly Mueller¹, Lindsay Clark¹, Sanjay Asthana¹, Bradley Christian¹, Sterling Johnson¹

¹*University of Wisconsin-Madison School of Medicine and Public Health, Madison, USA, Madison, WI, US*

Objectives: This work investigated MK-6240 timing parameters and inter-regional binding patterns (including extra-axial signal impact), in relation to amyloid burden and cognitive decline in a mostly unimpaired sample to identify potential composite regions for tau imaging.

Methods: Individuals (N=301, 67±8 years, 273 unimpaired, 13 MCI, 7 dementia, 8 under evaluation) from the Wisconsin Registry for Alzheimer's Prevention (WRAP) and Wisconsin ADRC underwent MK-6240 imaging. 70-90 and 90-110 minute SUVR windows were compared in a subset covering 70-110 minutes (n=236 scans). Inter-regional MK-6240 correlations inside and outside the brain were investigated along with associations with global PIB DVR in a subset with PIB imaging (n=286). Regional MK-6240 positivity thresholds were compared with z-scores determined from either PIB(-) or age<64. Linear mixed-effects models assessed associations between longitudinal cognitive decline (PACC-3), estimated PIB(+) duration, and MK-6240 binding in a WRAP subset, cognitively unimpaired at baseline (n=215).

Results: MK-6240 increased 3-5% in NFT-associated regions and 10-15% in extra-axial regions from 70-90 to 90-110 timeframes, respectively. Compared to PIB(-) cases, PIB(+) cases had higher MK-6240 SUVRs, higher inter-cerebral MK-6240 correlations and lower correlations between brain and extra-axial ROIs (Fig.1). Three regional groupings were observed for MK-6240 binding (medial temporal; temporal, parietal and frontal; visual cortex). MK-6240 positivity thresholds were consistent with PIB(-) or age<64 to establish z-scores. Regional MK-6240 z-scores indicated stepwise increases in regions associated with early to advanced Braak NFT stages for increasing levels of PIB (Fig.2). LME models showed significant three-way interactions between age, estimated PIB(+) duration at baseline PACC-3 and MK-6240 SUVR for all three MK-6240 composite regions wherein longer PIB(+) duration and higher MK-6240 were associated with faster rates of PACC-3 decline (Fig.3).

Conclusions: These findings suggest that a medial temporal composite ROI for MK-6240 minimizes extra-axial spill-in and is associated with early changes in amyloid and preclinical cognitive decline.

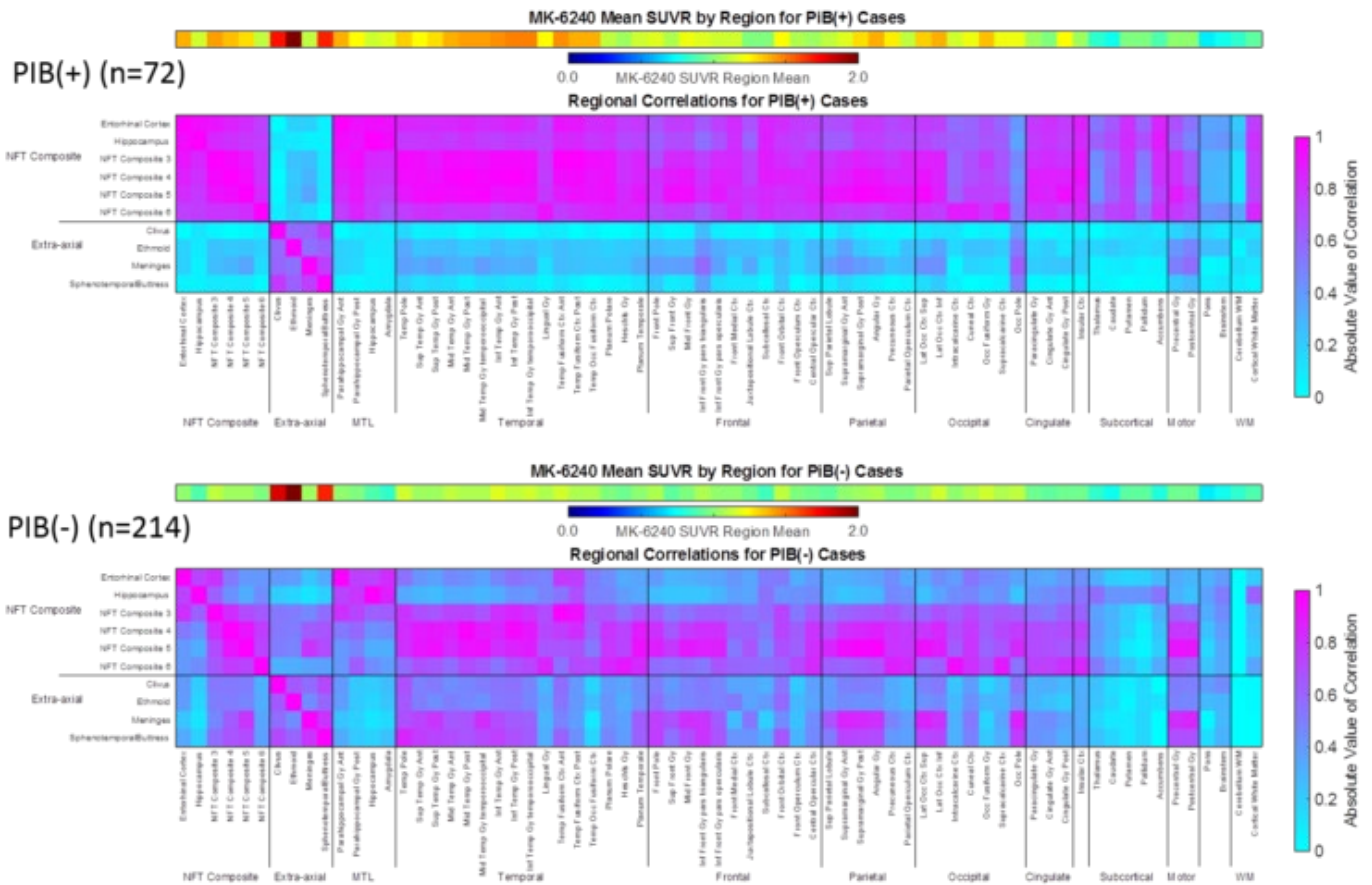


Figure 1: Inter-regional MK-6240 correlations (cyan-blue) for PIB(+) (top) and PIB(-) (bottom) participants with the average MK-6240 SUVR (rainbow) shown for each region above each correlation matrix. ROIs used for NFT composite regions were based on concordance with slice and region selection from Braak, et al, 2006. Compared to PIB(-) cases, PIB(+) cases had higher average MK-6240 SUVRs, higher MK-6240 interregional correlations in the brain and lower MK-6240 correlations between regions in the brain and extra-axial signal. Medial temporal regions including the entorhinal cortex, hippocampus, and amygdala were highly correlated with each other and showed low correlation with signal outside the brain for MK-6240 in both PIB(+) and PIB(-) cases.

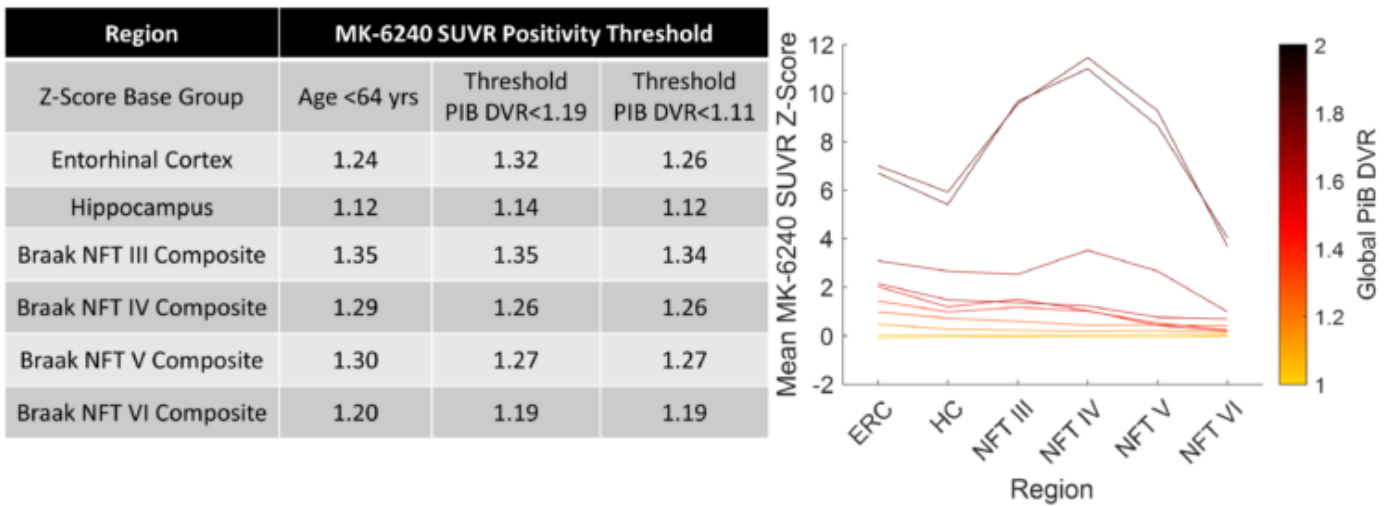


Figure 2. Left: Comparisons of regional MK-6240 positivity thresholds using the mean plus two standard deviations of MK-6240 SUVR for each region with z-scores established using younger participants, and PIB(-) participants using conservative and more liberal PIB(+) thresholds. Right: MK-6240 SUVR Z-scores using persons under age 64 were used to compare regional MK-6240 SUVR for varying levels of PIB DVR. The results indicated that those with lower PiB DVR values showed higher MK-6240 binding restricted primarily to early Braak NFT regions, whereas those with higher PiB DVR showed higher MK-6240 binding in all regions.

ERC = entorhinal cortex; HC = hippocampus; NFT = neurofibrillary tangle

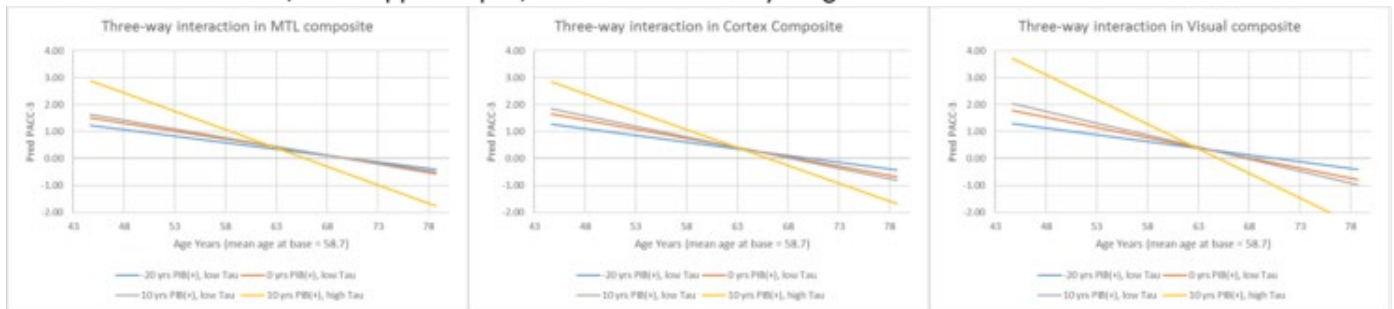


Figure 3: Linear mixed-effects models indicated significant 3-way interactions between age, PIB(+) duration at baseline PACC-3, and MK-6240 SUVR for each of the three composite MK-6240 regions tested (medial temporal $p_{3-way} = 0.0018$, neocortex $p_{3-way} = 0.0016$, visual cortex $p_{3-way} = <0.0001$). In all cases, longer duration of estimated PIB(+) at baseline PACC-3 with higher levels of MK-6240 binding had steeper rates of cognitive decline compared to those with lower levels of MK-6240. The plots above depict the three-way interaction between age, estimated duration of PIB(+) at baseline PACC-3, and MK-6240 z-scores for the average female participant. Values for estimated PIB(+) duration (-20, 0, 10 years) and regional MK-6240 z-scores (low tau = 0.5, high tau = 5.0) were selected based on combinations of values actually observed in the data (i.e. cases with high tau and low PIB(+) duration were not observed).

Estimated duration of PIB(+) was determined using group-based trajectory modeling. MK-6240 regional z-scores were established from participants under the age of 64 years at time of MK-6240. Cognition was assessed using a 3-test Preclinical Alzheimer's Cognitive Composite (PACC-3; mean - z-scored Rey Auditory Verbal Learning Test, Logical Memory Delayed Recall [WMS-R], and Digit Symbol Coding [WAIS-R]).

Model: $PACC-3 \sim Sex + WRAT-III \text{ reading score} + Practice + Age + Age \times \text{Estimated PIB(+) duration at baseline PACC-3} + Age \times \text{MK-6240 z-score} + \text{Estimated PIB(+) duration at baseline PACC-3} \times \text{MK-6240 z-score} + Age \times \text{Estimated PIB(+) duration at baseline PACC-3} \times \text{MK-6240 z-score} + \text{random slope} + \text{random intercept}$. Age was the time-varying predictor in the model.

Keywords: tau, preclinical, decline, amyloid, PET

P3: Transcriptomic profiling of brain amyloidosis using peripheral blood-based gene expression

Apoorva Bharthur Sanjay¹, Diana Svaldi¹, Liana Apostolova¹

¹Indiana University School of Medicine, Indianapolis, IN, US

Objective: In an effort towards pre-symptomatic risk assessment, precision medicine and biomarker development in AD, we evaluated the efficacy of characterizing and clustering peripheral blood transcriptomic data with respect to brain amyloidosis.

Methods: We identified 356 ADNI participants who had corresponding blood gene expression, Florbetapir SUVR, neurodegenerative and CSF measures (Table 1) (CN=120, EMCI=130, LMCI=72 and AD=34) from same visit. Between-group differential expression analyses yielded 864 genes from ~50,000 transcripts ($p < 0.001$). Pairwise Euclidean distance between genes was used to construct a gene-gene distance matrix followed by K-means clustering to identify clusters of genes with similar transcriptomic profile (Fig1). We used cluster-level gene enrichment analysis to identify the most relevant biological process associated with each cluster. Using principal component analysis, we assigned the first principal component as the “eigen-gene”. The eigen-genes were used to assess the association of the clusters to amyloid SUVR, hippocampus volume, entorhinal thickness, CSF Aβ and p-tau measures. The top driver genes that beat the eigen-gene association to amyloid SUVR were identified from each cluster. The transcripts identified through our analyses were validated in an external dataset (ImaGene) with overlapping data types for association to amyloid SUVR.

Results: We identified five clusters with distinct overrepresented biological processes highly relevant in AD pathogenesis. These were mitochondrial function, protein oligomerization, TGF β signaling, protein phosphorylation and MAPK activation. All five clusters were significantly associated with Florbetapir SUVR and CSF Aβ measures ($p < 0.05$) (Fig 2). The top driver genes showed similar correlation to amyloid SUVR in the ImaGene dataset.

DX	CN(n=120)	EMCI(n=130)	LMCI(n=72)	AD(n=34)	p-value
Age(Mean, std)	73.56 (6.1)	70.25 (7.1)	71.46 (6.9)	74.45 (9.5)	<0.001*
Gender(M/F)	56/64	67/63	38/34	18/16	0.8
Education(Mean, std)	16.58 (2.6)	16.08 (2.5)	16.97 (2.4)	15.32 (2.7)	0.006*
MMSE(Mean, std)	28.25 (2.1)	28.08 (1.9)	27.63 (2.5)	26.9 (3.1)	<0.01*
Amyloid SUVR(Mean, std)	1.11 (0.18)	1.17 (0.2)	1.28 (0.2)	1.4 (0.2)	<0.001*

Demographics table

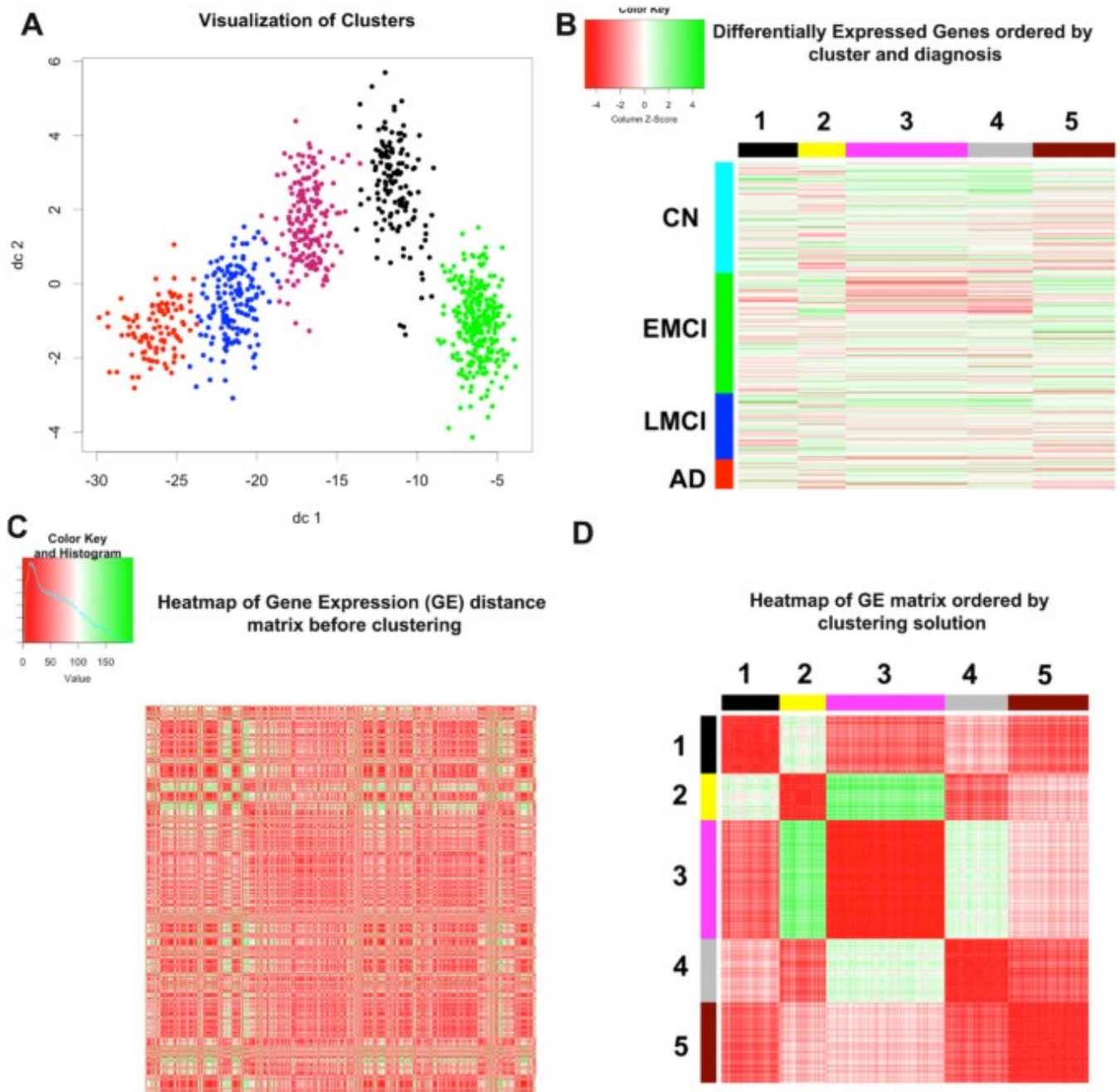
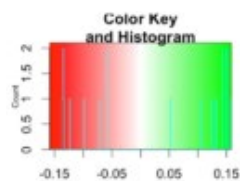


Fig1- Visualization of the k-means clustering (A) and raw gene expression data ordered by the clustering solution and diagnosis(B). Panel on the bottom shows heatmap of the gene-gene network before clustering (C) and structured distinct clusters of genes after clustering(D)



CLUSTER-TRAIT RELATIONSHIP

	MITOCHONDRIAL FUNCTION	PROTEIN OLIGOMERIZATION	TGF BETA SIGNALING	PROTEIN AUTO-PHOSPHORYLATION	MAPK ACTIVATION
HIPPOCAMPUS VOLUME	0.053	0.003	0.241	0.012	0.021
ENTORHINAL THICKNESS	0.169	0.076	0.282	0.07	0.163
AMYLOID SUVR	0.016	0.014	0.01	0.017	0.028
AGE	0.066	0.638	0.01	0.661	0.344
SEX	0.095	0.364	0.111	0.197	0.158
CSF ABETA	0.017	0.006	0.013	0.01	0.015
CSF TAU	0.195	0.287	0.025	0.285	0.348
CSF PTAU	0.015	0.077	0.004	0.025	0.057

FIG2-Visualization of the association of each cluster with relevant clinical traits and amyloidosis. Color intensity from green to red signifies strength of correlation (green positive and red negative) and values displayed are the p-values for the association. Association with amyloid SUVR is highlighted in blue box.

Conclusions: Using a data driven approach we found five AD-relevant clusters of peripheral blood RNA transcripts which were significantly correlated to amyloid burden. Systems level genetic signatures from blood show promise as non-invasive markers for AD pathology. Further investigations into the driver genes and their metabolic pathways are warranted.

Keywords: blood biomarkers, amyloid burden, genetic profiling, CSF measures

P4: A pons cluster detected by a data-driven approach may serve as a favorable reference region for 18F-PI-2620 Tau PET analysis

Gerard Bischof¹, Thilo van Eimeren^{1,3,4}, Norman Koglin⁵, Andre Müller⁵, Santiago Bullich⁵, Audrey Perrotin⁵, Andrew Stephens⁵, Alexander Drzezga^{1,4}

¹*Multimodal Neuroimaging Group, Department of Nuclear Medicine, University Hospital Cologne, Cologne, Germany*

²*Department of Neurology, University Hospital Cologne, Cologne, Germany*

³*Department of Neurology, University Hospital Cologne, Cologne, Germany*

⁴*German Center for Dementia Research (DZNE), Bonn, Germany*

⁵*Life Molecular Imaging GmbH, Berlin, Germany*

⁶*Molecular Organization of the Brain, Institute for Neuroscience and Medicine (INM-2), Jülich, Germany, Cologne, Germany*

One of the current challenges in static tau PET imaging is the establishment of a suitable reference region for count normalization and definition of thresholds for consistent identification of individuals with disease-related tau pathology. For the available tau-selective tracers, retention in certain sub-regions of cerebellum (e.g., superior cerebellar peduncles, dentate nuclei) in both healthy and disease populations has been reported, rendering the cerebellum as a suboptimal reference region. A hypothesis-free data-driven approach may allow to identify regions with negligible levels of target expression which may serve as a suitable reference region. Using proportional scaling for group comparison, regions consistently void of any specific tracer retention can be expected to exhibit relatively lower signal in target-positive patients as compared to controls. Here, we tested this approach in a cohort of AD patients (N=12) and amyloid-negative controls (N=10) who underwent ¹⁸F-PI-2620 imaging and MRI scanning. Dynamic frames from 45-75 minutes p.i., were summed and normalized to the individual MRI, skull-stripped and submitted to a statistical non-parametric mapping algorithm. A two-sample t-test using proportional scaling examined which regions of the brain elicited relatively lower signal in AD compared to controls with a FWE $p < .05$ cluster threshold. The identified clusters were located in thalamus, pons, cerebral white matter and brain stem. These regions were then tested as reference regions to examine differences in cortical uptake between healthy controls and AD patients. The whole mask, produced the highest effect size ($d = 2.6$), closely followed by the pons cluster ($d = 2.5$) compared to a cerebellar crus region ($d = 1.0$). Together, this data underscores the utility of a data-driven approach for identification of a suitable reference region and suggest that a specific pons cluster may show favorable properties as a reference region for static 18F-PI-2620 PET imaging data. Further cross-validation in clinically diverse samples may be justified.

Keywords: Tau PET, Reference Region, 18F-PI2620, static imaging

P5: Early detection of amyloid load using 18F-Florbetaben PET

Santiago Bullich^{1,2}, Núria Roé-Vellvé^{1,2}, Marta Marquié^{2,3,4,5}, Victor L. Villemagne⁶, Ángela Sanabria^{3,4,5}, Juan Pablo Tartari^{3,5}, Oscar Sotolongo^{3,5}, Vincent Doré⁶, Norman Koglin^{1,2}, Andre Müller^{1,2}, Audrey Perrotin^{1,2}, Susan De Santi⁷, Lluís Tàrraga^{2,3,4,5}, Andrew W. Stephens^{1,2}, Christopher C. Rowe⁶, John P. Seibyl⁸, Mercè Boada^{2,3,4,5}

¹Life Molecular Imaging GmbH, Berlin, Germany

²On behalf of the AMYPAD Consortium, Brussels, Belgium

³Fundació ACE Institut Català de Neurociències Aplicades, Alzheimer Treatment and Research Center - Universitat Internacional de Catalunya, Barcelona, Spain

⁴Centro de Investigación Biomédica en Red Enfermedades Neurodegenerativas (CIBERNED), Instituto de Salud Carlos III, Madrid, Spain

⁵On behalf of the FACEHBI study group, Barcelona, Spain

⁶Departments of Medicine and Molecular Imaging, University of Melbourne, Austin Health, Melbourne, Australia

⁷Life Molecular Imaging Inc, Boston, MA, US

⁸Invicro, New Haven, CT, US

Introduction: Pathology-proven ¹⁸F-Florbetaben (FBB) SUVR abnormality cutoffs have been developed to discriminate between Alzheimer's disease patients and elderly A β -negative non-demented controls (SUVR=1.48 (Sabri et al. 2015)). However, observational research studies or interventional therapeutic trials focus on the early stages of A β deposition. A lower A β amount and extent may limit the use of previously developed SUVR cutoffs. The objective of this study was to develop and validate a FBB SUVR abnormality cutoff to detect early A β deposition and to identify those subjects that will likely accumulate A β .

Methods: SUVR cutoff was derived from a sample of young healthy controls (YHC) (n=70, 27.6 \pm 5.1 y) as 2 standard deviation above the mean SUVR. Subsequently, the SUVR cutoff was tested in two longitudinal studies: (1) Individuals with subjective cognitive decline (SCD) (Fundació ACE Healthy Brain Initiative (FACEHBI) study) (n=166; 64.9 \pm 7.2 y (Rodríguez-Gómez et al. 2017) and (2) mild cognitively impaired (MCI) subjects (n=45, 72.69 \pm 6.54 y) (Ong et al. 2013). All subjects were quantified and SUVR derived using MRI-based regions of interest (reference region: cerebellar gray matter) (Bullich et al. 2017) and using the standard centiloid (CL) analysis (reference region: whole cerebellum (Klunk et al. 2015)).

Results: Mean SUVRs derived from YHC was 1.16 \pm 0.04 (SUVR_{cutoff}=1.25) (MRI-based ROIs) and 1.02 \pm 0.4 (SUVR_{cutoff}=1.09, CL_{cutoff}=12) (CL). Three regions in the SUVR continuum were defined as: A β -negative subjects (SUVR<1.25), early A β accumulation ("gray zone") (1.25-1.48) and established A β deposition (SUVR>1.48). In the test datasets, only subjects in the "gray zone" (2.8 \pm 3.3 %/year (SCD), 0.94 \pm 1.6 %/year (MCI)) or "established A β pathology" (4.4 \pm 3.5 %/year (SCD), 1.1 \pm 2.1 %/year (MCI)) accumulated amyloid in a statistically significant manner (p<0.05).

Conclusions: An SUVR range from 1.25 to 1.48 is optimal to detect early A β deposition and to identify subjects that are likely accumulating A β .

Keywords: florbetaben, amyloid, SUVR, cutoff

P6: Age-related neural dedifferentiation of episodic memory networks is related to beta-amyloid and tau pathology in normal aging

Kaitlin Cassady¹, Jenna Adams¹, Anne Maass², Theresa Harrison¹, Suzanne Baker³, William Jagust^{1,3}

¹Helen Wills Neuroscience Institute, UC Berkeley, Berkeley, CA, US

²German Center for Neurodegenerative Disease, Magdeburg, Germany

³Lawrence Berkeley National Laboratory, Berkeley, CA, US

Episodic memory loss is a hallmark cognitive dysfunction in normal aging and Alzheimer's disease (AD), which is associated with A β and tau accumulation. An important open question is how A β and tau accumulation lead to memory decline. One possibility is that the accumulation of these protein aggregates is associated with reduced differentiation of large-scale neural networks. Neural *dedifferentiation* reflects the finding that neural networks specialized for different cognitive functions become less selective or 'differentiated' (i.e., reduced within- and increased between-network connectivity). Dedifferentiation of functional networks has been consistently reported in the aging brain and has also been associated with impaired memory performance. In the present study, we investigated whether dedifferentiation in two distinct episodic memory networks, the anterior-temporal (AT) and posterior-medial (PM) networks is associated with the accumulation of A β and tau. The AT network is related to memory for objects, recognition, and semantics and links anterolateral entorhinal cortex (alEC) to ventral anterior temporal, lateral orbitofrontal and perirhinal cortex. The PM network is related to context, retrieval, and spatial cognition and links posteromedial entorhinal cortex (pmEC) to retrosplenial, posterior-cingulate, precuneus, and parahippocampal cortex. We used resting state fMRI to measure functional connectivity (FC) in the AT and PM networks in older (OA; N=87, 76 \pm 6 years, 55F) and younger adults (YA; N=55, 25 \pm 4 years, 29F), and PIB-PET to measure A β and FTP-PET to measure tau in OA. We found evidence for age-related dedifferentiation (i.e., reduced within- and increased between-network FC with older age) in these networks, with left alEC showing aberrant connectivity to retrosplenial cortex in OA compared to YA (Fig-1). This increased connectivity was associated with greater retrosplenial tau in A β -positive older adults ($r=.33$, $p=.04$; Fig-2). These findings show that AD pathology disrupts the normal AT network in aging by increasing cross-network connectivity between AT and PM network components.

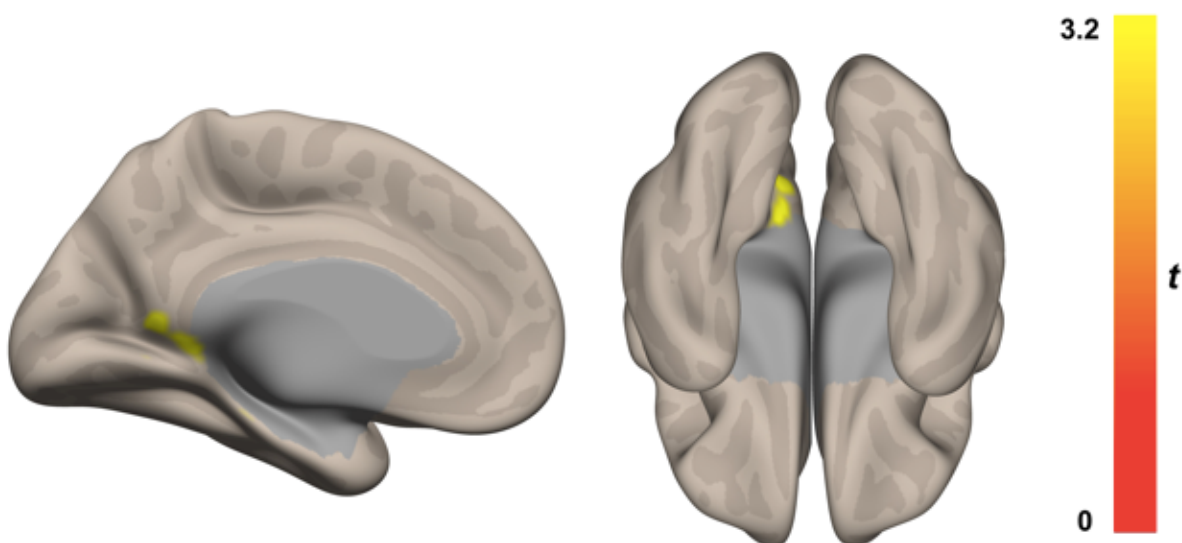


Figure 1. Age-related dedifferentiation of alEC/pmEC resting state networks. Older adults exhibit stronger FC between left alEC seed region and left retrosplenial cortex (a key region in pmEC network) compared to younger adults.

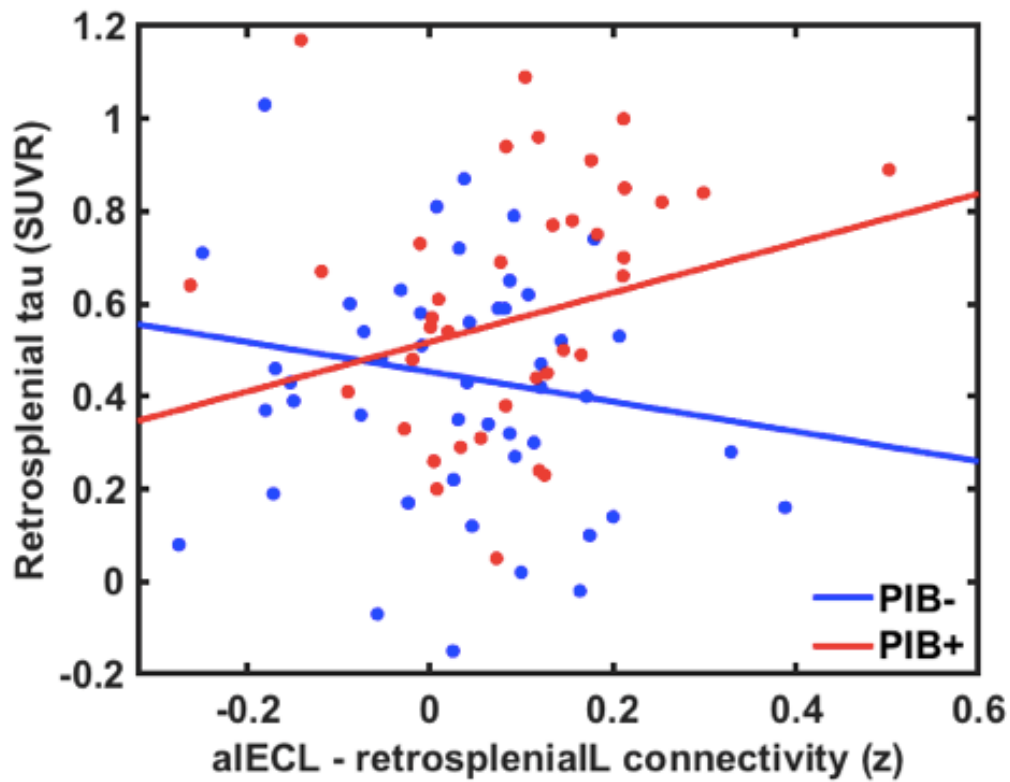


Figure 2. Stronger positive FC between left aIEC and left retrosplenial cortex is associated with more tau in retrosplenial cortex in amyloid-positive older adults (in red).

Keywords: aging, dedifferentiation, anterior-temporal (AT), posterior-medial (PM), tau

P7: Tau pathology and synaptic loss are closely associated in Alzheimer's disease in vivo: a combined [¹⁸F]flortaucipir and [¹¹C]UCB-J PET study

Emma M Coomans¹, Sander CJ Verfaillie¹, Emma E Wolters^{1,2}, Hayel Tuncel¹, Sandeep SV Golla¹, Rik Ossenkoppele^{2,3}, Wiep Scheper^{2,4,5}, Patrick Schober⁶, Steven P Sweeney⁷, J Michael Ryan⁷, Robert C Schuit¹, Albert D Windhorst¹, Philip Scheltens², Ronald Boellaard¹, Bart NM van Berckel¹

¹Department of Radiology & Nuclear Medicine, Amsterdam Neuroscience, Vrije Universiteit Amsterdam, Amsterdam University Medical Center, Amsterdam, The Netherlands

²Alzheimer Center Amsterdam, Department of Neurology, Amsterdam Neuroscience, Vrije Universiteit Amsterdam, Amsterdam University Medical Center, Amsterdam, The Netherlands

³Clinical Memory Research Unit, Lund University, Lund, Sweden

⁴Department of Clinical Genetics, Amsterdam Neuroscience, Vrije Universiteit Amsterdam, Amsterdam University Medical Center, Amsterdam, The Netherlands

⁵Center for Neurogenomics and Cognitive Research, Department of Functional Genomics, Faculty of Science, Vrije Universiteit, Amsterdam, The Netherlands

⁶Department of Anaesthesiology, Vrije Universiteit Amsterdam, Amsterdam University Medical Center, Amsterdam, The Netherlands

⁷Rodin Therapeutics, Boston, MA, US

Background: Synaptic loss, a pathological hallmark of Alzheimer's disease (AD), can be measured *in vivo* using the synaptic vesicle 2A (SV2A)-radiotracer [¹¹C]UCB-J. Indeed, reduced hippocampal SV2A-tracer binding in AD has previously been reported^{1,2}. It is currently unknown, however, to what extent synaptic loss is associated with tau pathology *in vivo*.

Methods: Seven amyloid-positive AD subjects (age 64.3±8.2; 3/7 female; MMSE 24.1±1.8) were included from the Amsterdam Dementia Cohort³. All subjects underwent 60-min dynamic [¹¹C]UCB-J PET with arterial sampling and 130-min dynamic [¹⁸F]flortaucipir PET. [¹¹C]UCB-J distribution volume ratio (DVR, plasma input-derived) was obtained using the centrum semi-ovale as reference region. Specific [¹⁸F]flortaucipir binding (BP_{ND}) was determined with receptor parametric mapping (reference region: cerebellar gray matter). We performed generalized estimating equation (GEE) and Spearman correlation to investigate associations between [¹¹C]UCB-J and [¹⁸F]flortaucipir across and within subjects in 12 bilateral a priori defined temporal, parietal, frontal and occipital region-of-interests (ROIs).

Results: Across subjects and ROIs, higher [¹⁸F]flortaucipir BP_{ND} was associated with lower [¹¹C]UCB-J DVR ($\beta=-0.35$, $p<0.001$) (**Fig1**). Within subjects 1, 2 and 4, who showed high tau levels, higher [¹⁸F]flortaucipir BP_{ND} was associated with lower [¹¹C]UCB-J DVR across ROIs; AD subject 3 showed a trend ($r=-0.57$, $p=0.004$; $r=-0.73$, $p<0.001$; $r=-0.46$, $p=0.02$ and $r=-0.39$, $p=0.06$ respectively) (**Fig2**). In contrast, within AD subjects 5, 6 and 7, who showed low tau levels, higher [¹⁸F]flortaucipir BP_{ND} was associated with higher [¹¹C]UCB-J DVR ($r=0.41$, $p=0.05$; $r=0.80$, $p<0.001$; $r=0.64$, $p=0.001$ respectively). [¹⁸F]flortaucipir and [¹¹C]UCB-J PET images are shown for two AD subjects (**Fig3**).

Conclusion: Across subjects, higher regional tau pathology was associated with synaptic loss. Within subjects, negative associations were observed when total tau levels were high, whereas positive associations were observed when total tau levels were low, possibly suggesting synaptic upregulation prior to the occurrence of synaptic loss in response to tau pathology.

Figure 1. Correlation between [¹⁸F]flortaucipir and [¹¹C]UCB-J across ROIs and AD subjects

Scatterplot showing the correlation between [¹⁸F]flortaucipir BP_{ND} (x-axis) and [¹¹C]UCB-J DVR (y-axis). Colours represent different AD subjects. Multiple ROIs per AD subject are shown. Across subjects and ROIs, GEE analyses, corrected for multiple ROIs per subject, showed a significant association between higher [¹⁸F]flortaucipir BP_{ND} and lower [¹¹C]UCB-J DVR, represented by the dashed black line.

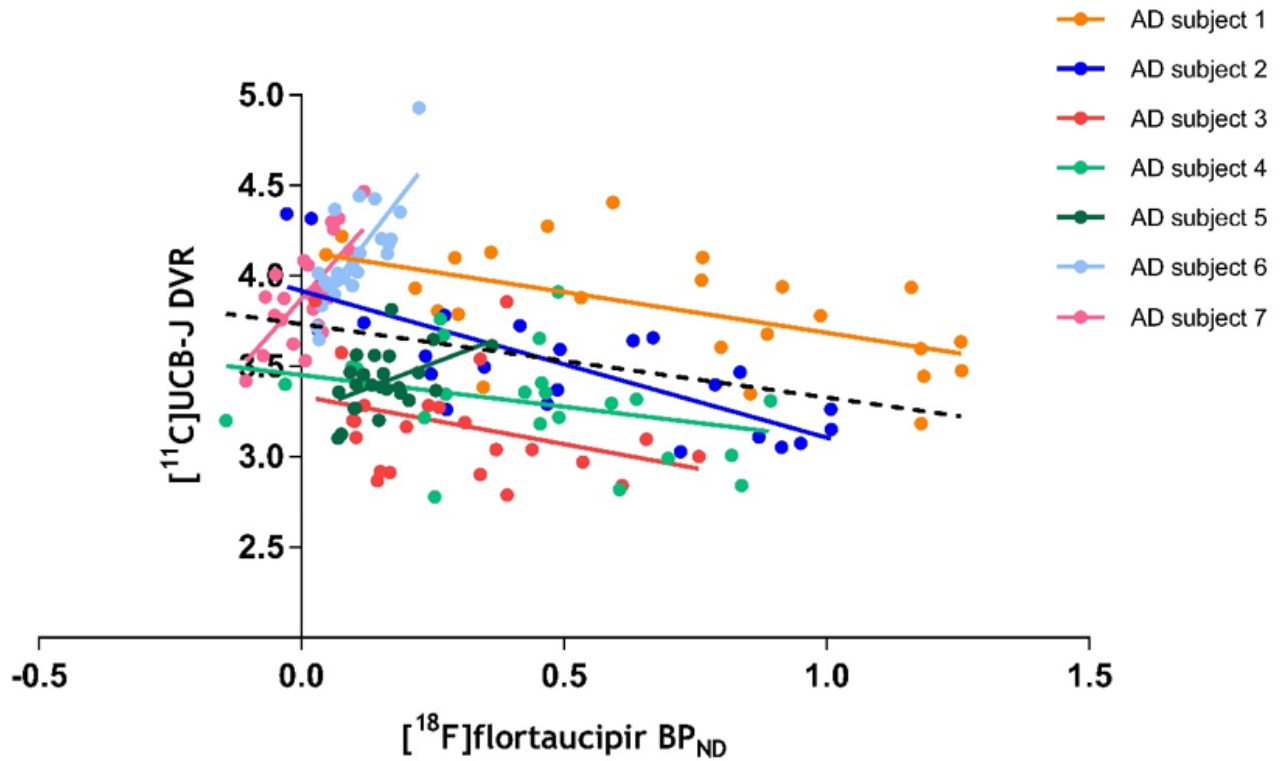


Figure 2. Correlation between [¹⁸F]flortaucipir and [¹¹C]UCB-J across ROIs per AD subject

Scatterplots showing the correlation between [¹⁸F]flortaucipir BP_{ND} (x-axis) and [¹¹C]UCB-J DVR (y-axis) per AD subject. AD subjects are ranked from high (AD subject 1) to low (AD subject 7) average volume-weighted tau load within the ROIs (range 0.01 to 0.78 (median: 0.34) [¹⁸F]flortaucipir BP_{ND}). Spearman correlation analyses revealed significant negative associations for AD subjects 1, 2 and 4; AD subject 3 showed a trend. Significant positive associations were observed for AD subjects 5, 6 and 7.

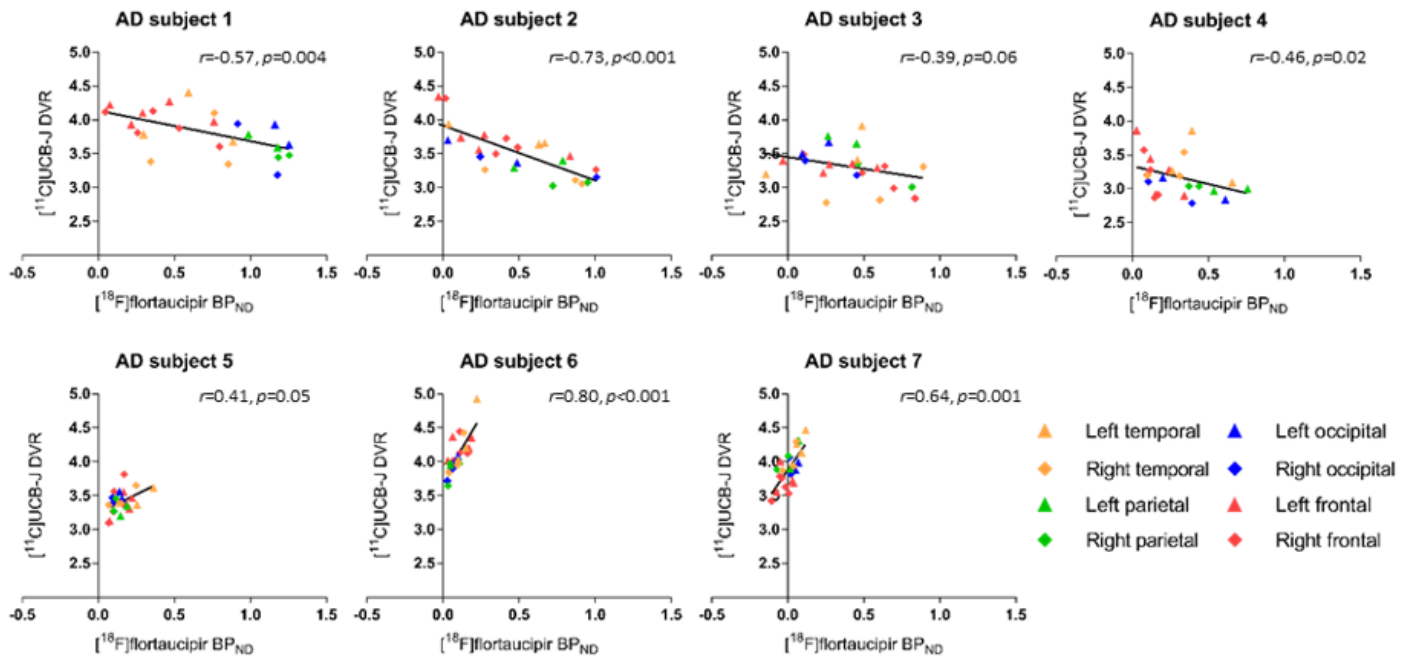
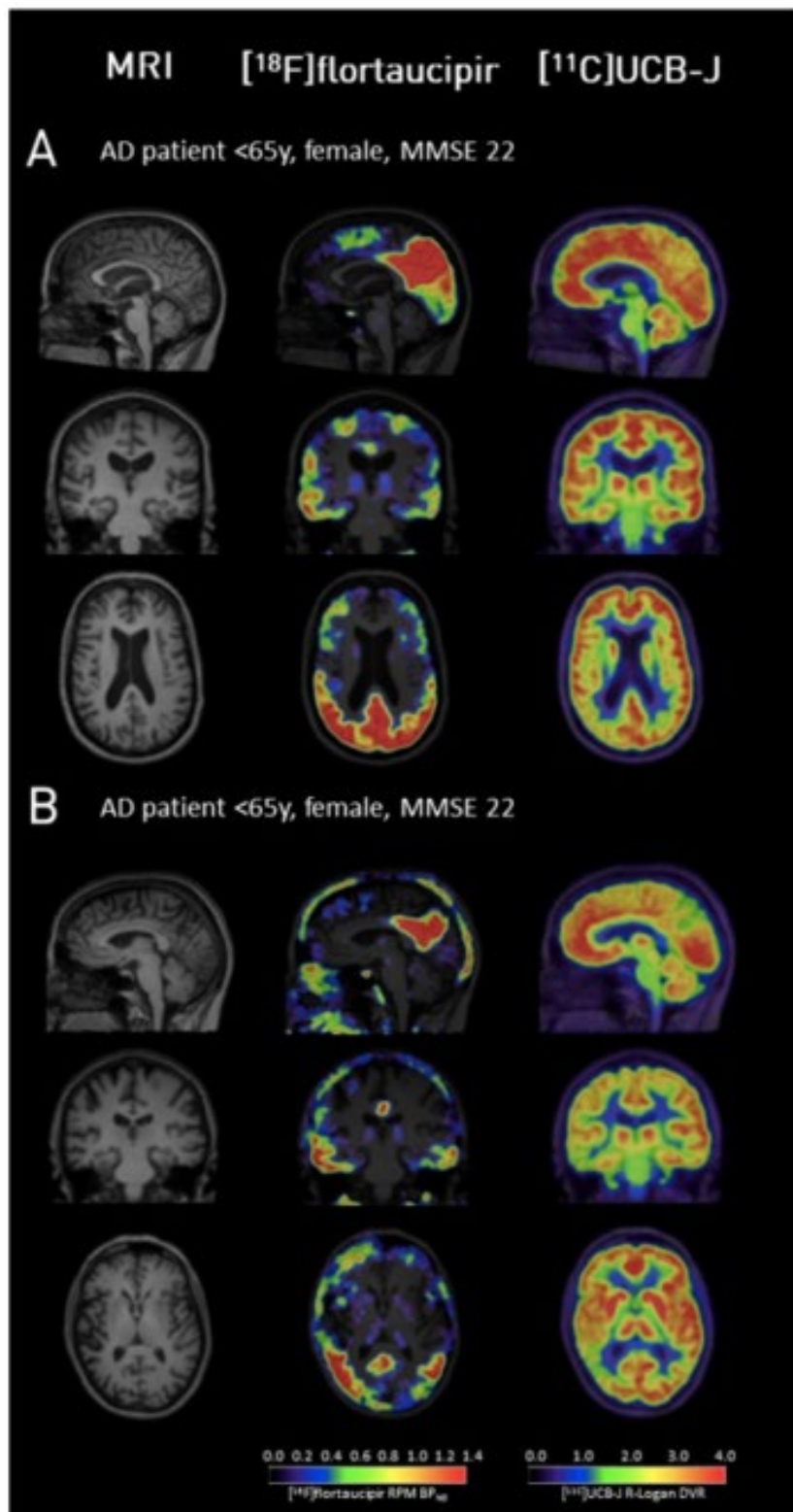


Figure 3. Regional distribution of [¹¹C]UCB-J and [¹⁸F]flortaucipir in two AD subjects.

Parametric [¹⁸F]flortaucipir and [¹¹C]UCB-J images for two AD subjects with high tau levels showing an inverse spatial association between tau pathology and synaptic integrity.



Keywords: Tau, SV2A, Synaptic Density, Neuroimaging, Alzheimer's disease

P8: Longitudinal dynamic [¹⁸F]flortaucipir PET reveals increased early stage tau pathology in individuals with subjective cognitive decline

Emma Coomans¹, Denise Visser¹, Rik Ossenkoppele^{2,3}, Sander CJ Verfaillie¹, Tessa Timmers^{1,2}, Emma E Wolters^{1,2}, Hayel Tuncel¹, Mark E Schmidt⁴, Ronald Boellaard¹, Albert D Windhorst¹, Philip Scheltens², Wiesje M van der Flier^{2,5}, Bart NM van Berckel¹

¹Department of Radiology & Nuclear Medicine, Amsterdam Neuroscience, Vrije Universiteit Amsterdam, Amsterdam University Medical Center, Amsterdam, The Netherlands

²Alzheimer Center Amsterdam, Department of Neurology, Amsterdam Neuroscience, Vrije Universiteit Amsterdam, Amsterdam University Medical Center, Amsterdam, The Netherlands

³Clinical Memory Research Unit, Lund University, Lund, Sweden

⁴Janssen Research & Development, Beerse, Belgium

⁵Department of Epidemiology and Biostatistics, Vrije Universiteit Amsterdam, Amsterdam University Medical Center, Amsterdam, The Netherlands

Background: Tau pathology is related to clinical progression in Alzheimer's disease (AD). Longitudinal tau imaging in preclinical AD may help to identify individuals at risk of progression. Dynamic scanning protocols allow for accurate quantitative measures of tracer retention over time. The aim of this study was to investigate whether individuals with subjective cognitive decline (SCD) show a change in tau pathology, measured using dynamic [¹⁸F]flortaucipir PET, over a time period of two years.

Methods: In an ongoing sub-study of the SCIENCE project, we included 31 SCD subjects (age 65±7, 45% female, MMSE 29±1, 26% [¹⁸F]florbetapir PET positive on visual read)(**Table 1**). All subjects underwent 90-minute dynamic [¹⁸F]florbetapir PET at baseline and 130-minute dynamic [¹⁸F]flortaucipir PET at baseline and 2.03±.01-year follow-up. [¹⁸F]flortaucipir binding potential (BP_{ND}) was determined using receptor parametric mapping (reference region: cerebellar gray matter) and extracted within three non-overlapping regions-of-interest reflecting early (medial temporal), intermediate (limbic) and late stage (neocortical) tau pathology. Repeated measures ANOVA, adjusted for age and sex, was used. To examine the interaction effect of amyloid-β, amyloid-β status was added to the model.

Results: A significant increase in medial temporal [¹⁸F]flortaucipir BP_{ND} was observed, $F(1,28)=5.001$, $p=0.033$, reflecting an average 2-year increase from 0.01 to 0.03 [¹⁸F]flortaucipir BP_{ND}(**Fig.1**). [¹⁸F]flortaucipir BP_{ND} in the limbic and neocortical regions did not significantly increase over time ($p>0.05$). Addition of amyloid status to the model revealed an interaction effect in the limbic and neocortical regions ($p\leq 0.02$), attributable to larger increases in [¹⁸F]flortaucipir BP_{ND} in amyloid-β positive individuals(**Fig.2**). Data collection is ongoing.

Conclusion: Over two years, quantitative imaging revealed an increase in tau pathology only in early stage tau pathology regions within SCD subjects. Individuals with higher amyloid-β load showed relatively higher levels and larger increases in intermediate and late stage tau pathology, supporting the hypothesis that amyloid-β facilitates the spread of tau.

Table 1. Demographics and [¹⁸F]flortaucipir BP_{ND} values

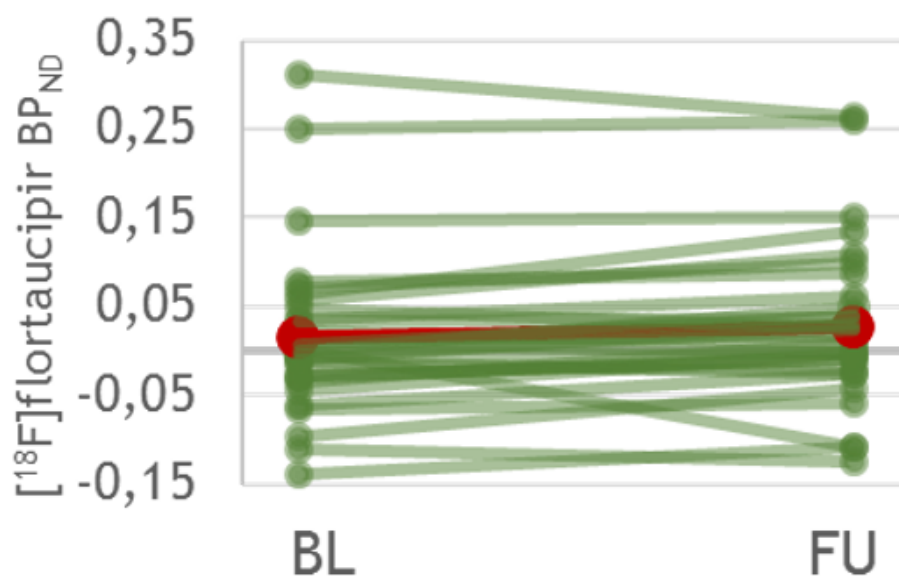
	Total sample (n=31)	Amyloid-β negative (n=23)	Amyloid-β positive (n=8)
Age, years	65 ± 7	65 ± 7	67 ± 7
Sex, % female	45.2%	47.8%	37.5%
MMSE	29 ± 1	29 ± 1	29 ± 2
Time lag BL vs. FU [¹⁸ F]flortaucipir PET, m	24 ± 2	24 ± 2	24 ± 2
Medial temporal [¹⁸F]flortaucipir BP_{ND}			
Baseline	0.01 ± 0.09	-0.01 ± 0.08	0.08 ± 0.11*
Follow-up	0.03 ± 0.09	0.00 ± 0.08	0.09 ± 0.09*
Limbic [¹⁸F]flortaucipir BP_{ND}			
Baseline	0.04 ± 0.06	0.02 ± 0.04	0.11 ± 0.07*
Follow-up	0.06 ± 0.08	0.03 ± 0.04	0.15 ± 0.10*
Neocortical [¹⁸F]flortaucipir BP_{ND}			
Baseline	0.00 ± 0.06	-0.02 ± 0.05	0.06 ± 0.07*
Follow-up	0.02 ± 0.08	-0.01 ± 0.05	0.10 ± 0.09*

Mean ± standard deviation (SD) are shown unless specified otherwise.

BP_{ND} = non-displaceable binding potential, BL = baseline, FU = follow-up.

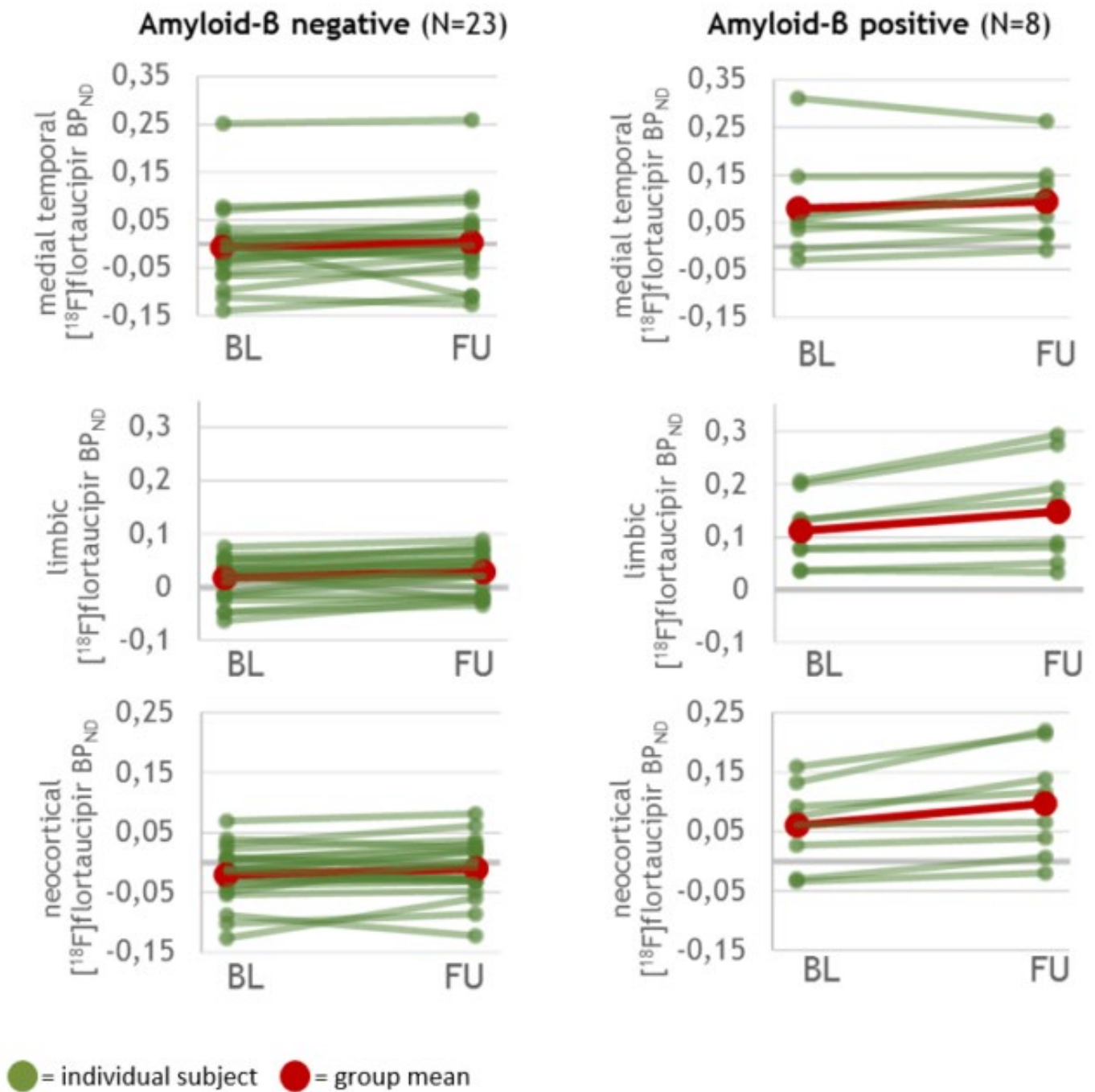
Independent Samples T tests were to assess differences between amyloid-β positive and negative individuals (*p<0.05).

Figure 1. Medial temporal [¹⁸F]flortaucipir BP_{ND} across the total sample at baseline and follow-up
 Repeated measures ANOVA revealed a significant increase in [¹⁸F]flortaucipir BP_{ND} across the total sample in the medial temporal region, $F(1,28)=5.001$, $p=0.033$.



● = individual subject ● = group mean

Figure 2. Medial temporal, limbic and neocortical [¹⁸F]flortaucipir BP_{ND} at baseline (BL) and follow-up (FU) for amyloid-β positive and negative individuals. When corrected for age and sex, addition of amyloid status (based on visual read of the baseline [¹⁸F]florbetapir PET scan) revealed an interaction effect of amyloid in the limbic and neocortical regions (both p<0.02), but not in the medial temporal regions (p>0.05).



Keywords: Tau, SCD, Neuroimaging, Longitudinal, Amyloid

P9: Preliminary evaluation of synaptic vesicle protein SV2A imaging with [11C]UCB-J across the cognitive spectrum

Alexandra DiFilippo^{1,2}, Dhanabalan Murali^{1,2}, Grace McKinney¹, Nancy Davenport¹, Todd Barnhart¹, Jonathan Engle¹, Tobey Betthausen¹, Sterling Johnson¹, Barbara Bendlin¹, Bradley Christian^{1,2}

¹University of Wisconsin-Madison School of Medicine and Public Health, Madison, WI, US

²University of Wisconsin-Madison Waisman Center, Madison, WI, US

Objectives: Synaptic pathology is integral for identifying many neurological and psychiatric disorders, although its identification is commonly performed post-mortem. [11C]UCB-J is a PET tracer targeting SV2A and serves as a proxy for in vivo analysis of synaptic density. As part of an ongoing investigation, we are studying synaptic loss across the clinical and pathological spectrum of AD to examine if regional synaptic loss can serve as a sensitive marker of neurodegeneration in the context of plaque and tangle accumulation and cognitive decline.

Methods: [11C]UCB-J dynamic PET imaging was conducted over 70 minutes in participants recruited from the UW ADRC. Amyloid (A) and tau (T) status was determined from [11C]PiB and [18F]MK6240 PET imaging. The participants included nine cognitively unimpaired (CU) A-/T-, one unimpaired A+/T+, one MCI (non-AD) A-/T-, and one non-AD dementia A-/T-. [11C]UCB-J binding was assessed using distribution volume ratios (DVR), calculated with Logan graphical analysis using the centrum semiovale as reference region. Region of interest analysis included the hippocampus and the entorhinal cortex as these regions have previously been identified as having lower [11C]UCB-J binding in the AD population.

Results: There was only small variation in [11C]UCB-J hippocampus DVR (1.95 ± 0.08) in the CU (A-/T-) participants. Relative to the CU (A-/T-) DVR, lower [11C]UCB-J DVRs were measured in the CU (A+/T+), MCI (A-/T-) and dementia (A-/T-) with DVR of 1.80, 1.56, 1.51 respectively. In the entorhinal cortex, reductions in DVR were only seen in the MCI and dementia participants (CU: 1.83 ± 0.11 vs. 1.49, 1.45 respectively).

Conclusions: This preliminary work reveals reductions in [11C]UCB-J in individuals across the spectrum of cognitive function. Ongoing, longitudinal studies with larger sample sizes will investigate associations between cognitive, amyloid, and tau status with [11C]UCB-J measured synaptic density.

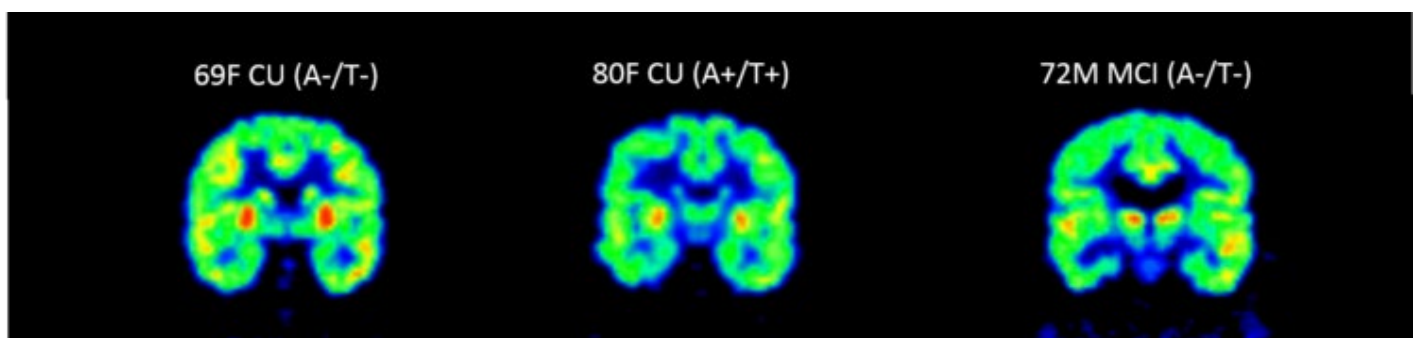


Figure 1: Comparison of parametric UCB-J DVR images in a cognitively unimpaired A-T- control with A+T+ and MCI subjects. UCB-J showed decreased binding in the hippocampus in all three non-control subjects and in the entorhinal cortex in the MCI and non-AD dementia subjects. These preliminary results suggest that UCB-J can be used to identify regions of decreased synaptic density in cognitively impaired subjects. Future work will involve correcting for atrophy.

Keywords: Alzheimer's disease, UCB-J, SV2A

P10: Quantifying off-target skull binding in [18F]Flortaucipir PET studies

Shaney Flores¹, Brian Gordon^{1,2}, Yi Su⁴, Jon Christensen¹, Aylin Dincer¹, Adedamola Adedokun¹, Russ Hornbeck¹, John Morris^{2,3}, Tammie Benzinger^{1,2}

¹*Department of Radiology, Washington University in St. Louis School of Medicine, St. Louis, MO, US*

²*Knight Alzheimer's Disease Research Center, , Washington University in St. Louis School of Medicine, St. Louis, MO, US*

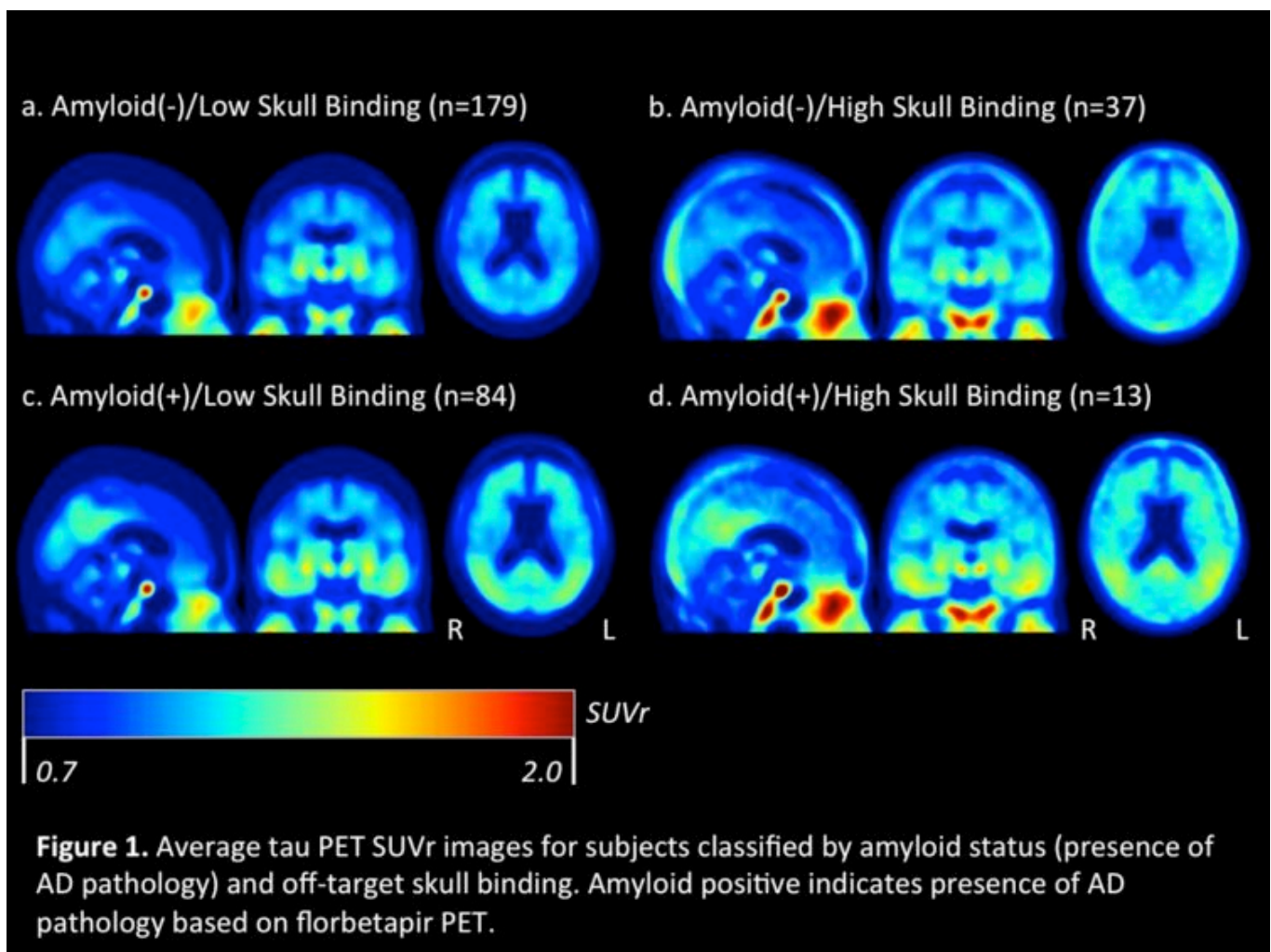
³*Department of Neurology, Washington University in St. Louis School of Medicine, St. Louis, MO, US*

⁴*Banner Alzheimer's Institute, Phoenix, AZ, US*

Background: Previous reports on tau PET using [¹⁸F]flortaucipir addressed off-target binding in the choroid plexus and basal ganglia while anecdotal reports of off-target skull binding have been minimally discussed. We evaluated off-target flortaucipir skull binding in a cohort of older adults classified as cognitively normal, mildly cognitively impaired, or with Alzheimer's disease (AD) dementia.

Methods: Head CT, flortaucipir (tau), florbetapir (amyloid) PET, and T1-weighted MR images were acquired for 313 participants. Standard uptake value ratios (SUVr) were calculated voxel-wise and for FreeSurfer defined regions of interest (ROI) using cerebellar grey as a reference. Subject specific CTs were used to define a skull ROI after removing non-skull related bone and tissue and then applied to the SUVr image to calculate the average SUVr for the skull. Individuals were classified as high and low skull binding using Gaussian mixture modeling. Flortaucipir skull binding was correlated with several brain regions, including off-target flortaucipir regions, and florbetapir skull binding.

Results: High tau PET skull binding was observed in 15.8% of the cohort with the greatest levels in occipital and temporal areas (see Figure 1).



Tau PET skull binding did not correlate with either caudate or choroid plexus, suggesting a unique off-target binding mechanism. Elevated skull binding was significantly related to higher inferior temporal flortaucipir SUVRs in amyloid- individuals ($t(214)=-2.83$, $p<.01$), and flortaucipir skull binding was positively correlated with a summary measure of tauopathy in amyloid- but not amyloid+ individuals (see Figure 2). This indicates a potential false positive reading for elevated tau pathology.

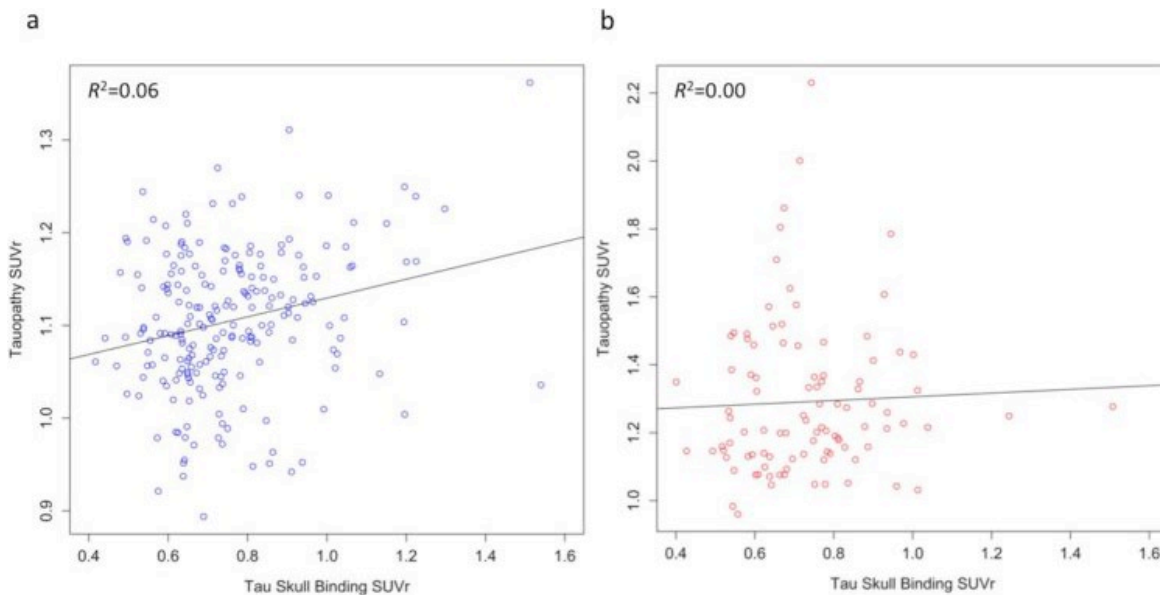


Figure 2. Correlation between tau PET skull binding with tauopathy summary SUVR measure for (a) amyloid negative and (b) amyloid positive individuals. After controlling for age, the relationship between tau PET skull binding and summary tau SUVR showed a partial correlation of $r=0.32$, $p<.001$ for amyloid negative, and $r=0.06$, $p=0.58$ for amyloid positive.

Skull binding was positively correlated between flortaucipir and florbetapir ($r=0.48$, $p<.001$; see Figure 3).

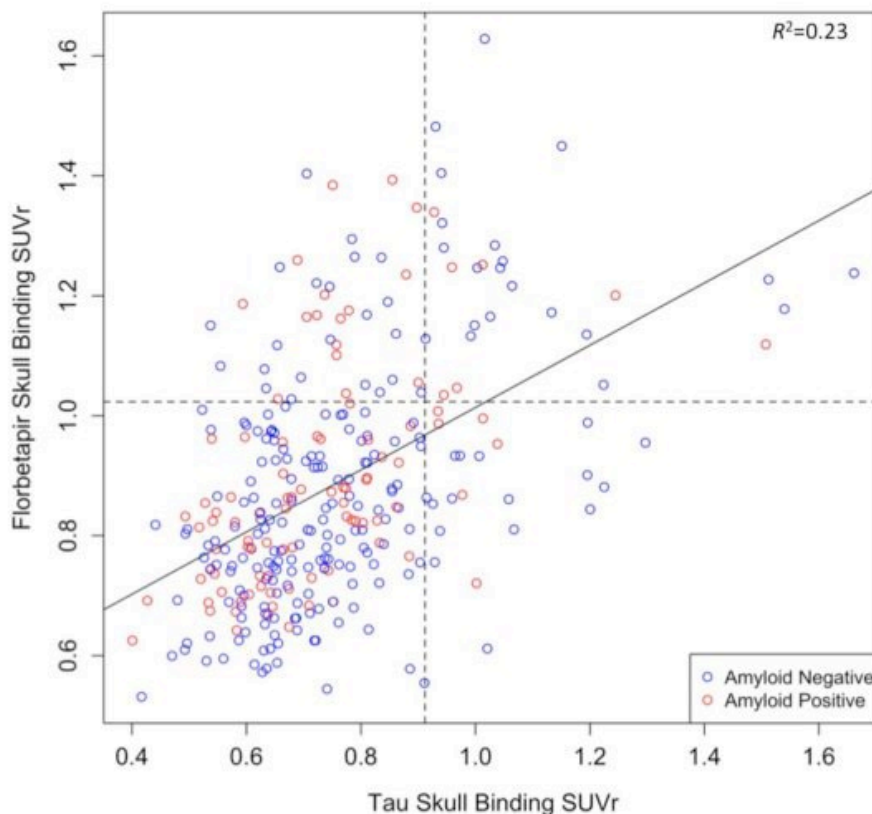


Figure 3. Relationship between florbetapir skull binding and tau skull binding. High skull binding was defined as $SUVr \geq 0.91$ for tau PET and $SUVr \geq 1.02$ for amyloid PET.

Discussion: Quantitative evidence confirms informal reports of off-target skull binding with flortaucipir. This skull binding is a unique source of off-target binding that can complicate analyses of tau PET images, particularly in regions proximal to the skull.

Keywords: flortaucipir, non-specific binding, off-target binding, skull

P11: Influence of iron and beta-amyloid deposition on entorhinal cortex and hippocampal subfield volumes in the aging brain

Chris Foster¹, Kristen Kennedy¹, Karen Rodrigue¹

¹*Center for Vital Longevity, School of Behavioral and Brain Science, The University of Texas at Dallas, Dallas, TX, US*

Age-related alterations to brain structure are regionally differential, even within the medial temporal structures, with overall hippocampus proper evidencing considerable vulnerability to even healthy aging, in contrast to entorhinal cortex, which evidences relative resilience to the normal aging process. However, in AD patients and individuals at increased risk for AD, the ERC becomes a focus of neuropathology, displaying sensitivity to amyloid and tau which begin to form early in disease pathogenesis. Non-heme iron also begins to accumulate in the brain early in the adult lifespan and in animal models, interacts with beta-amyloid, launching oxidative stress and a cascade of neurotoxic processes. Here we sought to investigate the independent and combined effects of beta-amyloid (via Flortetapir) and iron content (via susceptibility-weighted MRI) on aging of the hippocampal subfields (Dentate/CA3, CA1-2, subiculum) and ERC volumes in a sample of 71 cognitively normal older adults ($M_{\text{age}}=68.01$). We hypothesized that the combination of both elevated A β burden and greater iron content would be associated with smaller ERC volume, but not with HC subfield volumes in older adults. Mixed-effects models with MTL region as a within-subject factor and age, iron, and A β as between-subjects factors indicated a significant four-way interaction among age, iron, A β , and MTL region, $F(3,189) = 5.24$, $p = .002$. Post-hoc analyses revealed that the 3-way interaction was selective to the ERC, where a significant negative association between age and ERC volume was only present in individuals with both elevated iron and A β . Further, this effect was not present in individuals with elevated A β , but lower levels of iron. These findings highlight the importance of studying A β in the context of other, potentially synergistic age-related brain factors, such as iron accumulation, as well as highlighting the potential role for iron as an important contributor to the earliest, preclinical stages of pathological aging.

Keywords: beta-amyloid, iron, entorhinal cortex, preclinical AD, hippocampal subfields

P12: Voxel-wise relationships between white matter hyperintensities (WMH) and multimodal neuroimaging biomarkers of Alzheimer's disease

Malo Gaubert¹, Catharina Lange^{1,2}, Antoine Garnier-Crussard^{3,4}, Salma Bougacha³, Julie Gonneaud³, Robin de Flores³, Clémence Tomadesso³, Florence Mézenge³, Brigitte Landeau³, Vincent de La Sayette^{5,6}, Gaël Chételat³, Miranka Wirth¹

¹German Center for Neurodegenerative Diseases, Dresden, Germany

²Dep. of Nuclear Medicine, Charité - Universitätsmedizin Berlin, Corporate Member of Freie Universität Berlin, Humboldt-Universität zu Berlin, and Berlin Institute of Health, Berlin, Germany

³Inserm, Inserm UMR-S U1237, GIP Cyceron, Université de Caen-Normandie, Caen, France

⁴Lyon Institute for Elderly, Clinical and Research Memory Centre of Lyon, Hospices Civils de Lyon, Lyon I University, Lyon, France

⁵Normandie Univ, UNICAEN, PSL Recherche Universités, EPHE, INSERM, U1077, CHU de Caen, Neuropsychologie et Imagerie de la Mémoire Humaine, GIP Cyceron, Caen, France

⁶CHU de Caen, Service de Neurologie, Caen, France

Background: White matter hyperintensities (WMH), a marker of cerebrovascular disease, are associated with increased risk of cognitive impairment and Alzheimer's disease (AD). Findings across the AD continuum suggest that increased WMH load may be related to increased A β burden and neurodegeneration in regions affected in AD.

Objective: To investigate relationships between AD neuroimaging biomarkers and voxel-wise WMH distribution in older adults across the cognitive spectrum.

Methods: Participants (n=155) with normal cognition, subjective cognitive decline, mild cognitive impairment, and clinical AD were selected from the IMAP cohort with baseline scans of (1) FLAIR MRI, (2) AV45-PET, (3) FDG-PET, and (4) T1 MRI. FLAIR images were analyzed with the lesion-segmentation-tool (Schmidt, 2017) to generate template-space lesion probability maps. Other images (2-4) were processed using standard pipelines including construction of template-space PET-SUVr and GMV images. Mean AV45-SUVr, mean FDG-SUVr, and total GMV were extracted within AD signature templates (Besson et al., 2015). Exploratory voxel-wise analysis were conducted with each AD neuroimaging biomarker as a predictor of regional WMH (Graff-Radford et al., 2019).

Results: Greater A β deposition, reduced glucose metabolism, and reduced GMV in AD regions were associated with increased regional WMH across the entire cohort, adjusting for age, sex, and education. Topographic distributions of these AD biomarker associated WMH included the corpus callosum (splenium) for all imaging modalities and periventricular regions (posterior and anterior) for FDG-SUVr and GMV (Figure 1). When restricting our analysis to non-demented elderly (n=130), significant relationships were maintained for FDG-SUVr and GMV.

Conclusion: Our findings corroborate that regional WMH, including the posterior corpus callosum and periventricular regions, are associated with AD neuroimaging biomarkers of A β burden and/or atrophy and hypometabolism. These cross-sectional associations might reflect involvement of vascular damage in AD pathogenesis or, vice versa, contribution of AD pathology to white matter damage.

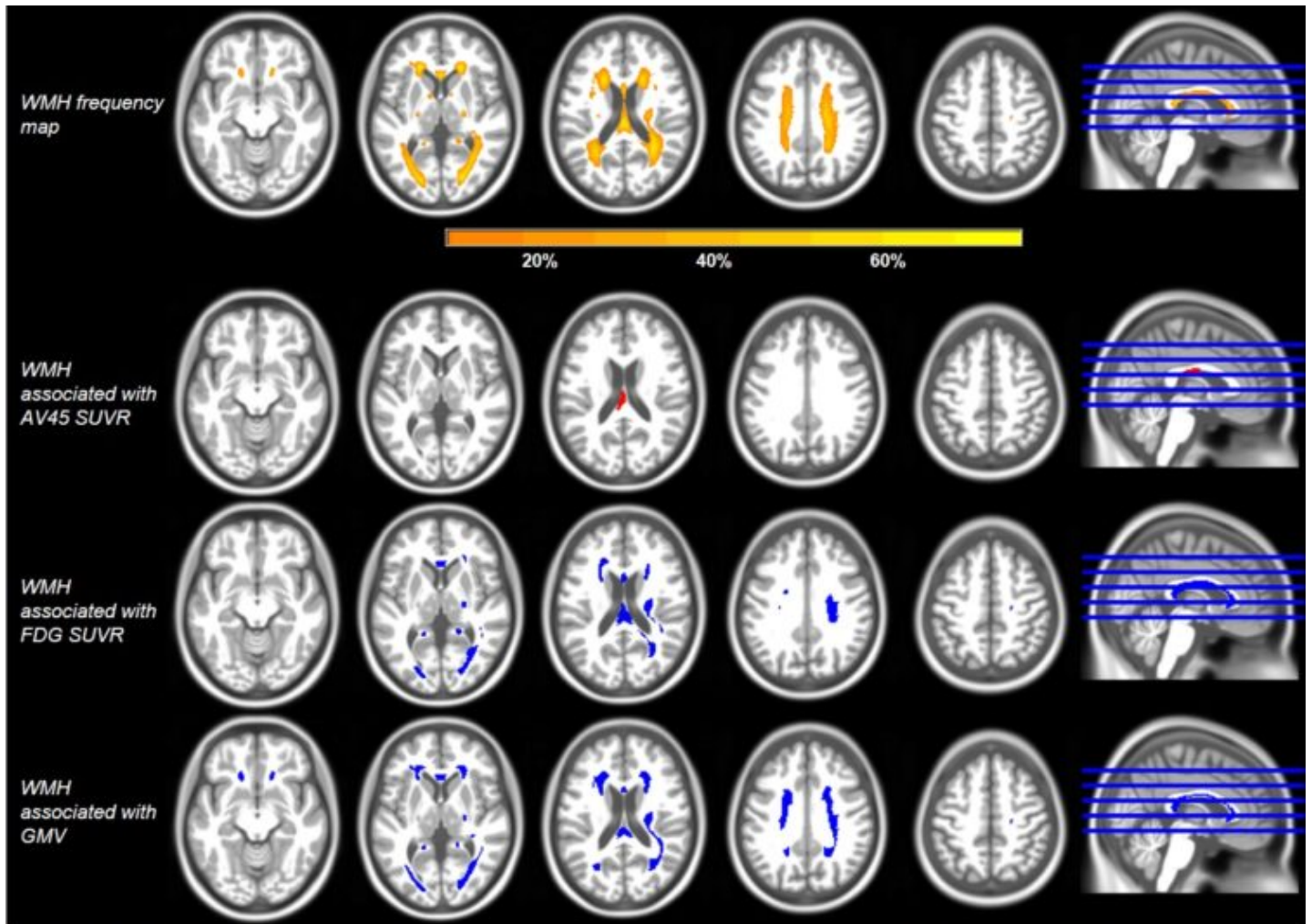


Figure 1: Results of the voxel-wise multiple regression analyses between AD neuroimaging biomarkers and white matter hyperintensities (WMH). The WMH frequency map thresholded at 10% was used as analysis mask (line 1). WMH associated with AV45 SUVR (line 2), FDG SUVR (line 3) and GMV (line 4) in AD signature templates are presented at p uncorrected at 0.005 (minimum cluster size = 200 voxels). The red cluster indicates a positive relationship, blue clusters indicate negative relationships.

Keywords: White matter hyperintensities, amyloid pathology, atrophy, hypometabolism

P13: Beta-amyloid deposition and its association with metabolism

Brian Gordon¹, Manu Goyal¹, Lars Couture¹, Shaney Flores¹, John Morris¹, Marc Raichle¹, Tammie Benzinger¹, Andrei Vlassenko¹

¹Washington University in St. Louis, St. Louis, MO, US

Introduction: The deposition of beta-amyloid (Ab) in the brain has a distinctive spatial pattern, with prominent areas of accrual in posterior parietal regions. Less attention has been paid to the interpretation of this spatial topography. Aerobic glycolysis (AG) refers to the non-oxidative use of glucose. Areas high in AG are very plastic, and often identified as cortical hubs in the brain. As Ab is tied to neuronal activity, understanding brain metabolism can provide insight into Ab accumulation.

Methods: 622 participants between the ages of 30-100 underwent 1024 PET scans with ¹¹C-PIB. PET data were processed using Freesurfer into ROIs. Regional SUVR values for each scan were quantile normalized to equalize the statistical distribution of values between scans while retaining the rank order of the regional values. The normalized regional data from all scans was analyzed then using multidimensional scaling. The resulting similarity matrix was reduced to two components using PCA. A map of AG was defined in a cohort of younger adults (20-40 years, Figure 1).

Results: PC1 represented the regional pattern and weights that explained the most variance in Ab across participants and is labeled the amyloid topography index (ATI). Older adults with a high ATI score (high Ab deposition) had spatial deposition patterns spatially remarkably similar to AG defined in younger adults. When examining ATI as a continuous measure, as levels increased, the spatial pattern of Ab deposition became more similar to that of AG in young adults. This same topographical relationship with Ab was not as strong for other markers of metabolism such as CMRGlc, CMRO₂, or CBF.

Conclusion: The current analyses indicate that the spatial deposition of Ab mirrors metabolic properties in the brain. In particular, there is a tight coupling between areas that develop Ab plaques and regions with neuronal activity tied to plasticity.

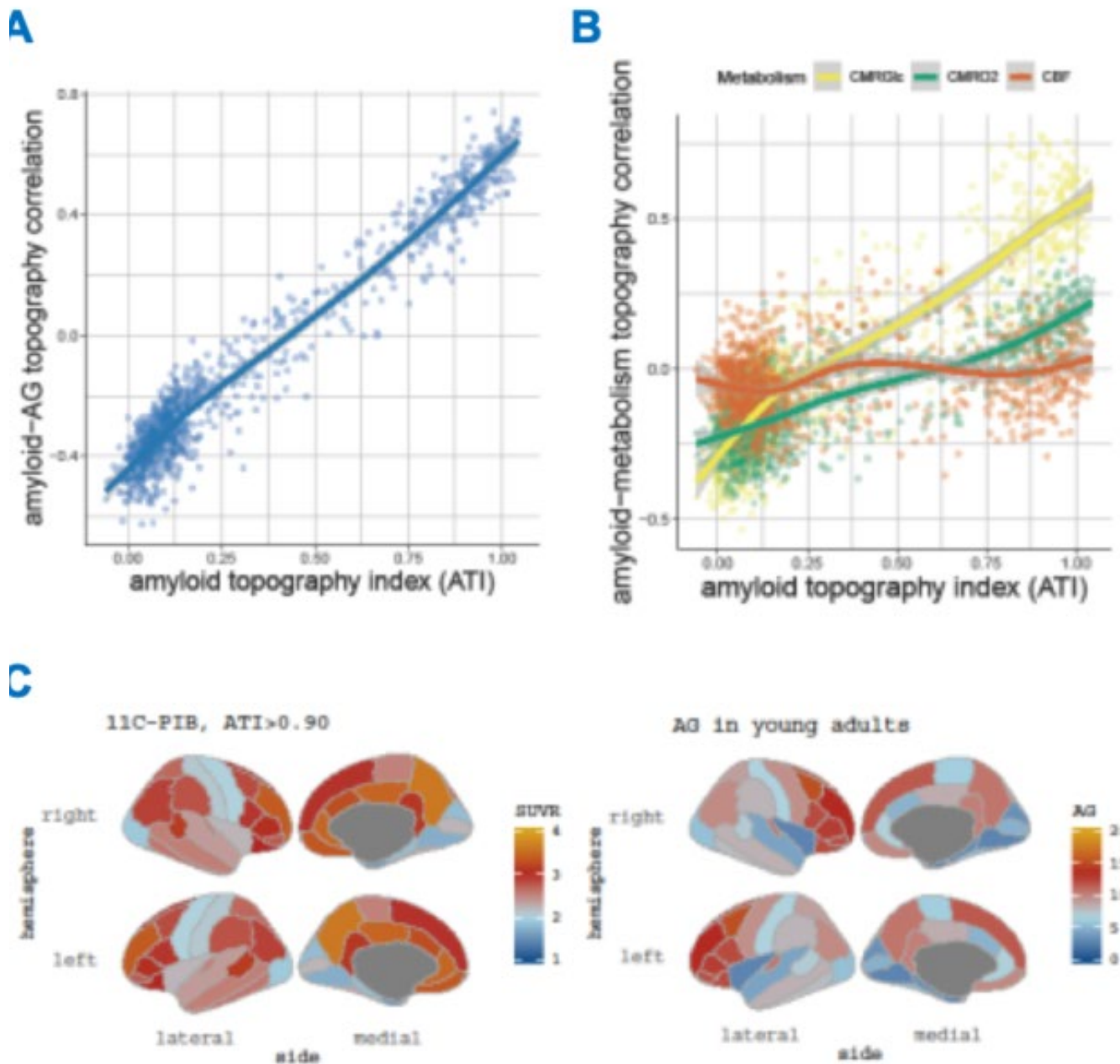


Figure 1. ATI versus AG. For each of the 11C-PIB scans, an ATI was calculated and a corresponding correlation between the A β topography and normal young adult AG topography was also calculated. The similarity between the A β and AG topography was then plotted as a function of ATI (**A**). This shows that ATI is very highly correlated with the amyloid-AG topographic correlation (R-squared = 0.95), suggesting that ATI might largely reflect the degree to which amyloid has deposited in high AG regions. (**B**) This high correlation is not an artifact of how AG or amyloid topography is calculated since a similar analysis using CMRGlC, CMRO2, or CBF maps does not produce as high correlations (R-squared = 0.83, 0.65, and 0.06, respectively). A β topography in very high ATI cases (ATI > 0.90) to AG topography in young adults shows them visually to be highly similar (**C**).

Keywords: amyloid, metabolism, PET, alzheimer, brain

P14: Amyloid binding is associated with markers of white matter microstructure in patients with significant white matter disease

Maged Goubran¹, Miracle Ozzoude¹, Sabrina Adamo¹, Katherine Zukotynski², Christian Bocti⁴, Michael Borrie³, Howard Chertkow⁵, Richard Frayne⁶, Fuqiang Gao¹, Robin Hsiung⁷, Alex Kiss¹, Robert Jr. Laforce⁸, Michael D. Noseworthy², Frank S. Prato³, Joel Ramirez¹, Jim D. Sahlas², Christopher Scott¹, Eric E. Smith⁹, Vesna Sossi⁷, Stephen Strother¹², Richard Swartz¹, Jean-Claude Tardif¹¹, Alex Thiel¹⁰, Jean-Paul Soucy¹⁰, Sandra E. Black¹

¹*Sunnybrook Research Institute, Toronto, ON, Canada*

²*McMaster University, Hamilton, ON, Canada*

³*Western University, London, ON, Canada*

⁴*Université de Sherbrooke, Sherbrooke, QC, Canada*

⁵*Jewish General Hospital, Montreal, QC, Canada*

⁶*University of Calgary, Calgary, AB, Canada*

⁷*University of British Columbia, Vancouver, BC, Canada*

⁸*Université Laval, Quebec City, QC, Canada*

⁹*Hotchkiss Brain Institute, Calgary, AB, Canada*

¹⁰*Montreal Neurological Institute, Montreal, QC, Canada*

¹¹*Montreal Heart Institute, Montreal, QC, Canada*

¹²*Rotman Research Institute, Toronto, ON, Canada*

Background: Cognitive impairment involves degeneration in the grey matter, but also white matter pathology, manifested as hyperintensities (WMH). WMH may be reflective of demyelination or vasogenic edema. Non-specific WM binding of 18F-Florbetapir is thought to depend on the myelination status of the white matter tracts. Our objective was to determine if amyloid deposition in WM is associated with DTI changes in a population with significant WMH.

Methods: 45 patients had baseline 3T MRI including DTI, 18F-Florbetapir PET/CT, and MMSE. A normal population with low WMH from ADNI was used as a control group. We segmented WMH and incorporated this in the *Freesurfer* pipeline. Standardized uptake value ratios (SUVr) normalized to the pons was used as a measure for amyloid load. Multiple linear regression and partial correlations were performed, adjusting for age, between PET, DTI metrics and WMH volumes. All tests were corrected for multiple comparisons using false discovery rate.

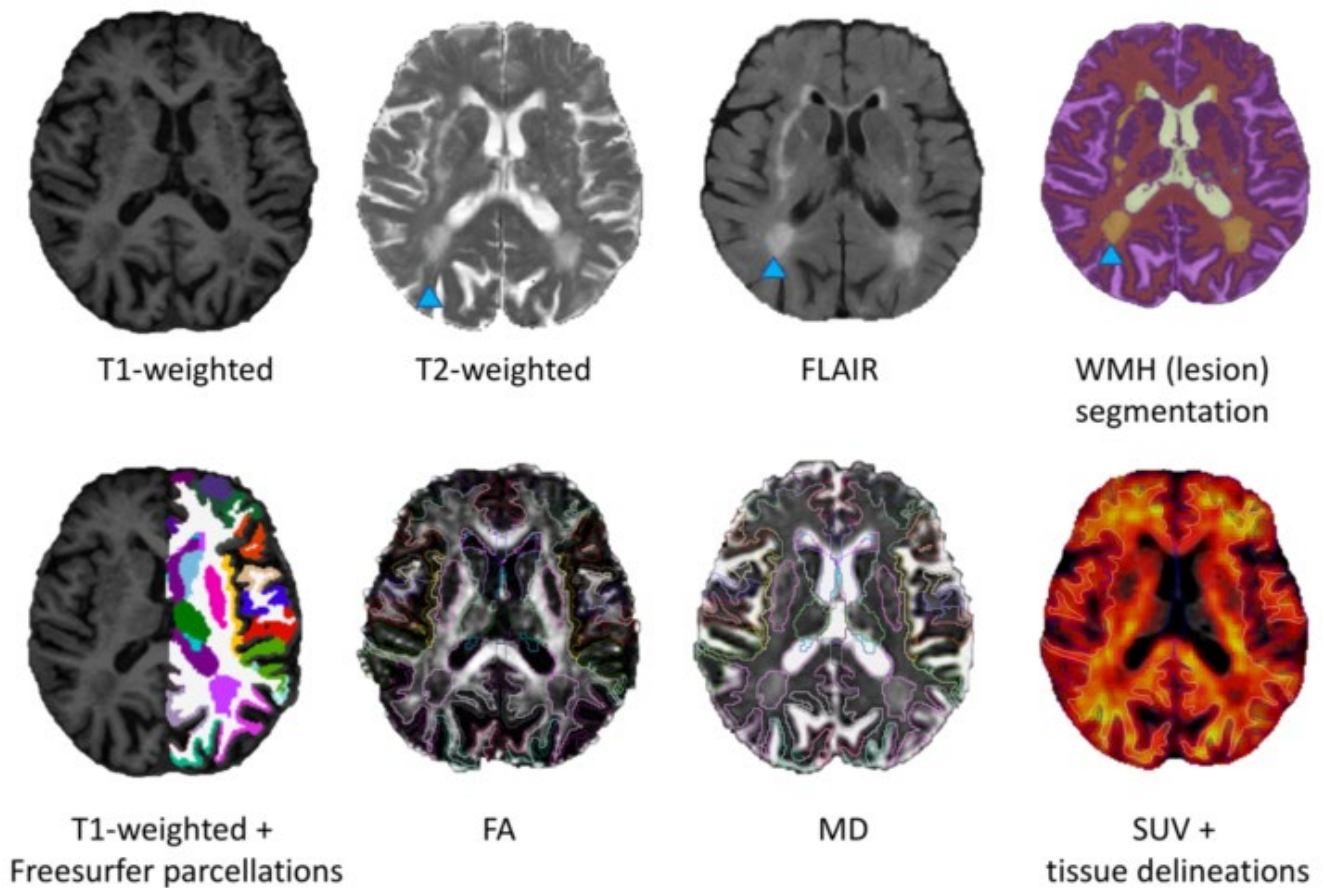


Figure 1. Top row: Segmentation of WMH. Bottom row: Freesurfer pipeline after incorporating the lesion segmentation.

Results: White matter amyloid load was correlated with FA ($r=0.39$) and inversely correlated with MD ($r=-0.35$) in patients with high WMH load but not in ADNI controls. Normal appearing white matter FA predicted WMH volumes ($B=-5.69e04$, $p < 0.001$). Normalized FA was decreased and MD increased for patients with high WMH volumes compared to controls ($p=2.3e-20$, $p=0.00013$). MMSE was negatively correlated with MD in the left medial temporal regions and SUVr in the left paracentral gyrus ($r > -0.40$).

Cerebral-White-Matter

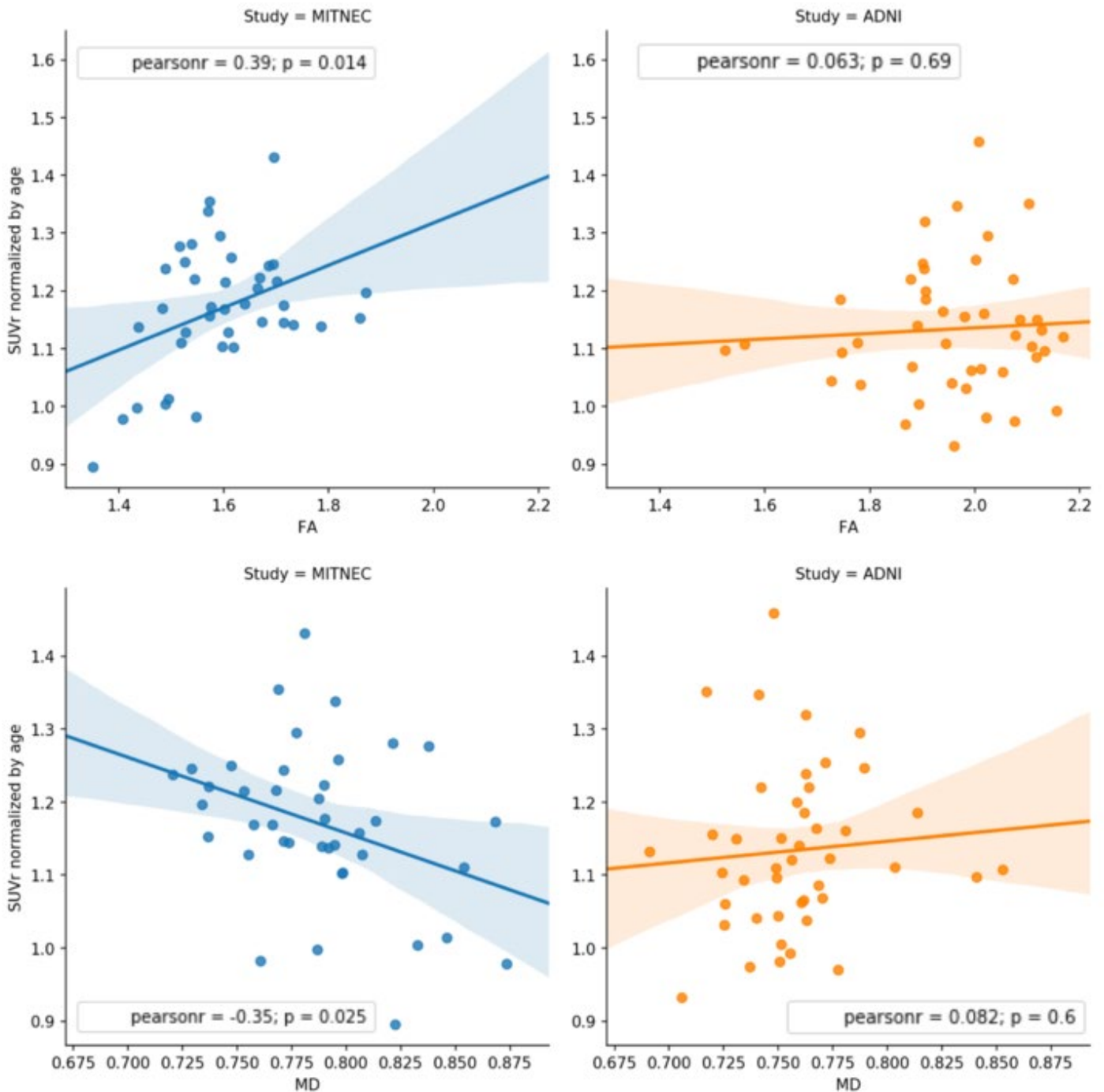


Figure 2. Partial correlations of AV-45 SUVR and DTI metrics, adjusting for age, in the white matter for both populations.

Conclusion: This work supports the hypothesis that non-specific WM amyloid binding may reflect microstructural integrity (myelination status) in patients with high WMH load. Future work will include analysis of free-water diffusion MRI.

Keywords: Amyloid PET, White matter disease, diffusion MRI, microstructure, non-specific binding

P15: CSF dynamics explains discrepant PET-CSF AD biomarkers

Jeffrey Gunter¹, Matthew Senjem¹, Petrice Cogswell¹, Christopher Schwarz¹, Val Lowe¹, Kejal Kantarci¹, Prashanthi Vemuri¹, Benjamin Elder⁴, Hugo Botha², Jonathan Graff-Radford², David Jones², Michelle Mielke², Neill Graff-Radford³, David Knopman², Ronald Petersen², Clifford Jack, Jr.¹

¹Department of Radiology, Mayo Clinic, Rochester, MN, US

²Department of Neurology, Mayo Clinic, Rochester, MN, US

³Department of Neurology, Mayo Clinic, Jacksonville, FL, US

⁴Department of Neurosurgery, Mayo Clinic, Rochester, MN, US

Objective: Discordance of CSF $a\beta_{42}$ and amyloid PET measures is commonly reported. CSF biomarkers are abnormally low in NPH populations, possibly due to dilution or impeded clearance. A common anatomic spatial pattern in shunt-responsive NPH including tight high convexity sulci in conjunction with ventriculomegaly and enlarged Sylvian fissures (Figure 1) is Disproportionately Enlarged Subarachnoid-space Hydrocephalus (DESH). DESH features may be detected on MRI using machine learning, generating a pattern matching score referred to as “computational DESH” or “CDESH”. The question we addressed was, do CSF and amyloid PET biomarkers differ and is discordance of amyloid PET and CSF $a\beta_{42}$, higher in persons with a positive CDESH match?

Methods: CDESH scores were calculated from T1-weighted MRI for individuals in the Mayo Clinic Study of Aging (MCSA) and ADNI-GO/2. CSF $a\beta_{42}$, pTau and tTau were assessed using Elecsys assays with amyloid PET SUVR from PiB in MCSA and florbetapir in ADNI. Two-sample Kolmogorov-Smirnov tests were used to evaluate whether distributions of CSF and PET biomarkers differed between CDESH positive and negative groups.

Results: The study included 843 (ADNI-2) and 829 (MCSA) participants. A CDESH pattern was found in 7.0% and 7.7% of participants, respectively. Within each study amyloid PET SUVR distributions were not different based on CDESH ($p=0.13$ and 0.70 respectively). Within each study, CSF $a\beta_{42}$, pTau and total tau differed based on CDESH, all p -values <0.01 (Figure 2). In amyloid PET negative participants CSF $a\beta_{42}$ distributions differed based on CDESH, but the ratios of CSF $a\beta_{42}$ to total tau did not (Figure 3).

Conclusions: Distributions of absolute CSF analyte concentrations differed systematically in participants with and without CDESH; amyloid PET and ratios of CSF markers did not. We conclude that CDESH is associated with lower absolute concentrations (possibly by dilution or disordered CSF dynamics), but using CSF ratios normalizes this phenomenon.

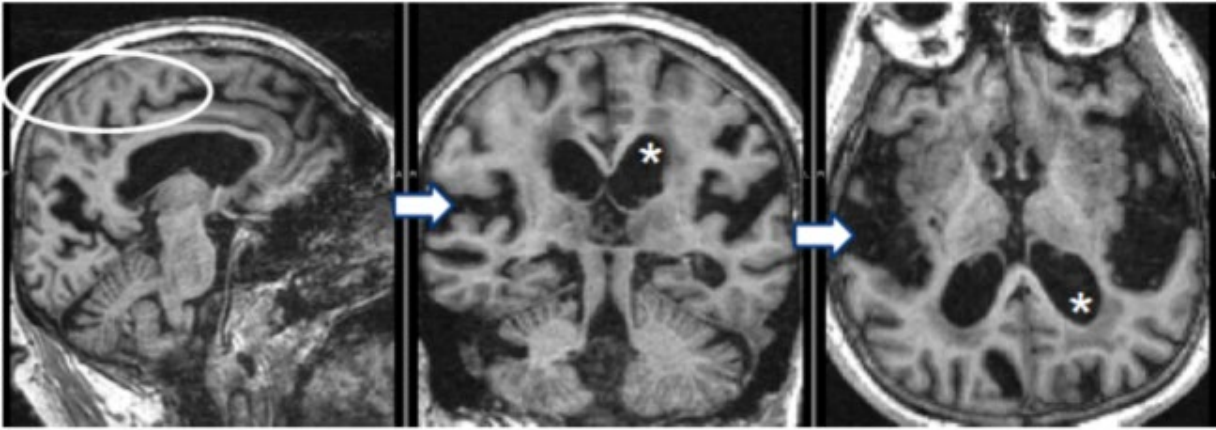


Figure 1: Regional (sulcal and ventricular) CSF volumes from probabilistic tissue segmentation are used as features in a support vector machine to generate the CDESH pattern matching score. Key elements the pattern include tight high convexity sulci (oval), ventriculomegaly (*), and enlarged Sylvian fissures (arrow).

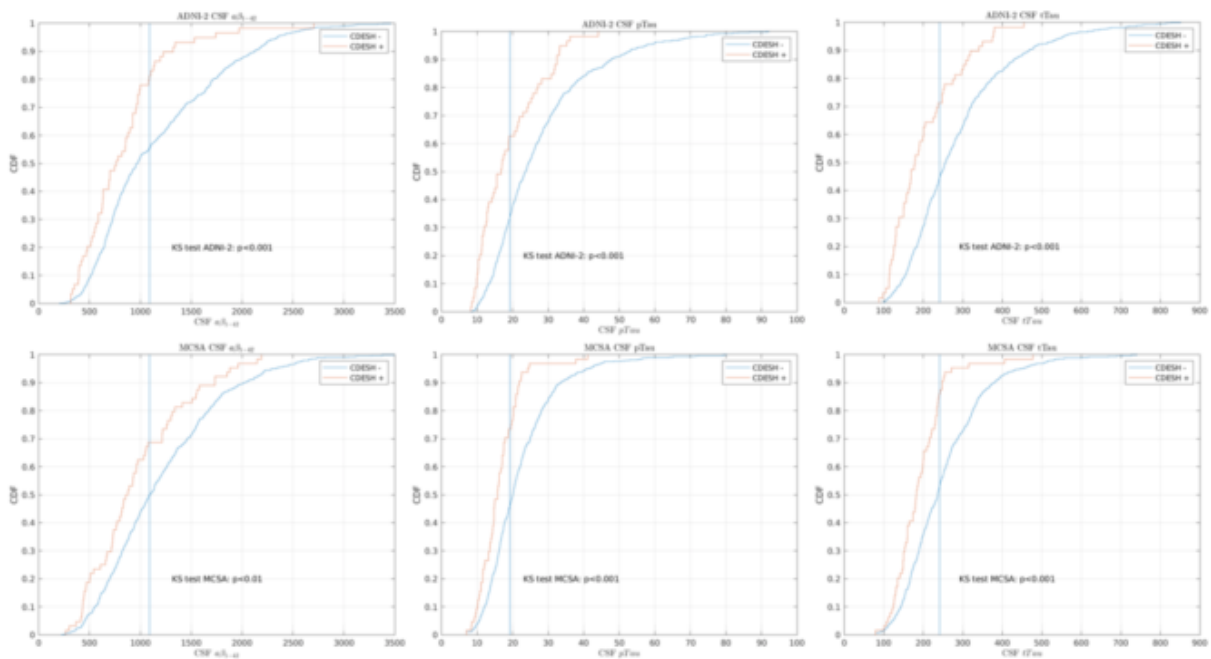


Figure 2: Cumulative distribution functions of CSF protein levels for CDESH pattern matching positive and negative groups are shown for ADNI-2 (top row) and MCSA (bottom row) participants agnostic of amyloid PET status. Two-sample Kolmogorov-Smirnov test (KS test) p-values are presented: small p-values indicating that the observed distributions are unlikely to have come from the same underlying parent distribution. In all cases the distributions of CSF biomarker levels for pattern matching participants are lower than for non-matching participants. Vertical lines are drawn at suggested cut-points for ADNI-2 data.

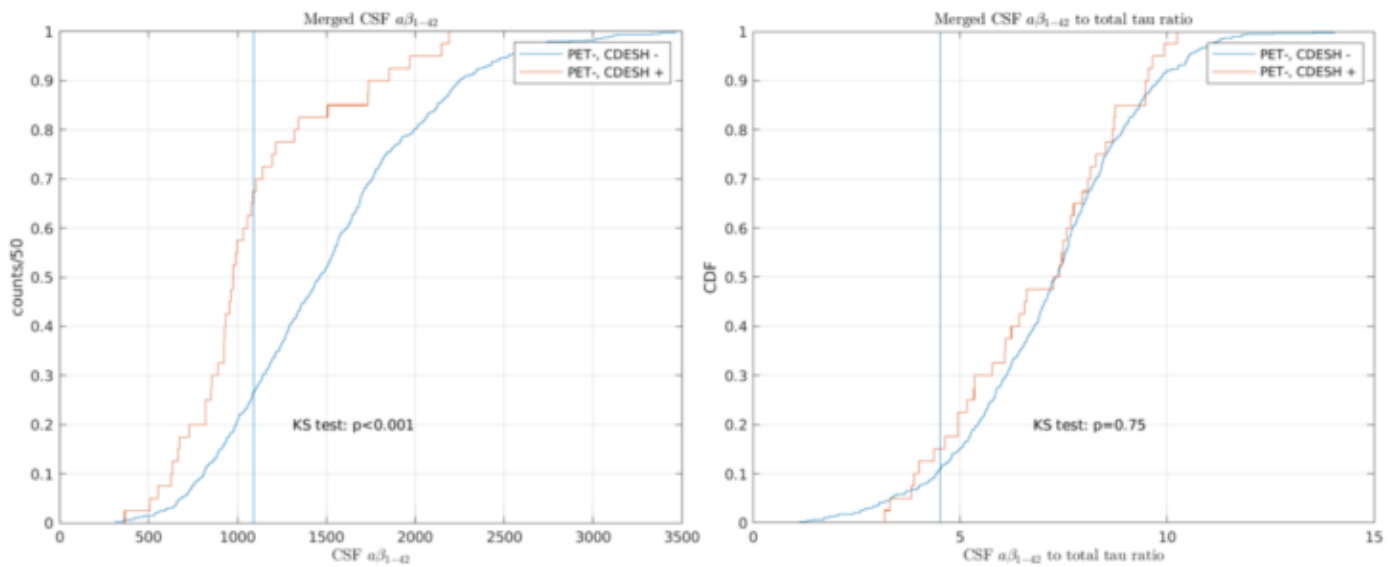


Figure 3: Cumulative distributions functions (CDFs) for CSF $a\beta_{42}$ (left) and CSF $a\beta_{42}$ to total tau ratios (right) for *amyloid PET negative* participants (fluorbetapir SUVR < 1.11; PiB SUVR < 1.42) are shown. The vertical line in the left plot is at the ADNI-recommended CSF $a\beta_{42}$ cut-point. The vertical line in the ratio plot is taken from the ratio of recommended cut-points for CSF $a\beta_{42}$ and total tau. Participants with CSF biomarker values lower than the cut-points are discordant (i.e. negative amyloid PET with abnormally low CSF $a\beta_{42}$ concentration). Data from ADNI-2 and MCSA were similar and have been pooled. Approximately 68% of amyloid PET negative, CDESH positive participants and 27% of amyloid PET negative, CDESH negative participants were discordant using only CSF $a\beta_{42}$ levels. Distributions of ratios for CDESH pattern matching positive and negative participants are not, however, different ($p=0.75$).

Keywords: amyloid PET, Alzheimer's disease, discordant biomarkers

P16: Predicting future amyloid spread with machine learning using longitudinal [C11]PiB-PET in preclinical Alzheimer's disease

Wei Hao¹, Nicholas Vogt¹, Zihang Meng¹, Seong Jae Hwang², Rebecca Kosciak¹, Tobey Betthausen¹, Bradley Christian¹, Sterling Johnson¹, Barbara Bendlin¹, Vikas Singh¹

¹*University of Wisconsin-Madison, Madison, WI, US*

²*University of Pittsburgh, Pittsburgh, PA, US*

Background: Predicting progression of Alzheimer's disease (AD) pathology may facilitate identifying individuals most likely to benefit from anti-amyloid therapy. We propose a machine learning model which predicts future amyloid burden based on baseline [C11]PiB-PET and T1-weighted MRI.

Method: Cognitively unimpaired participants from the Wisconsin Registry for Alzheimer's Prevention study (N=112, baseline age 67.6 ± 6.0 years) with at least three time points of PiB-PET and T1-weighted MRI were included. PiB DVR values were extracted from 8 bilateral regions in the PET images known to accumulate amyloid. T1-weighted images were processed using the Computational Anatomy Toolbox and 'graynet' to construct single-subject level brain connectivity. We designed a differential equation/diffusion model which uses both the individual-level MR derived connectivity networks and baseline PiB to predict the amyloid burden measured at future visits.

A training set was used to estimate the parameters of the model which characterizes amyloid propagation from time-1 to time-2, informed by the individual-level connectivity matrix, in order to accurately predict the PiB measurements at time-3. In experiments, 90% of subjects were used for training from time-1 to time-2 and the remaining served as the test set. A 10-fold cross-validation was performed.

Result: Fig. 3 shows the performance of our model on the test set compared to group differences derived from a linear estimate of the average group change between two time points. Our model yields more accurate predictions of PiB-PET measurements in 69.6% of time-2 samples and 81.3% of time-3 samples.

Conclusion: Our model captures propagation patterns using only the baseline scans from each subject (MR and PiB-PET) and performs much better than using the linear estimate of the average group change. Additional replication studies are planned.

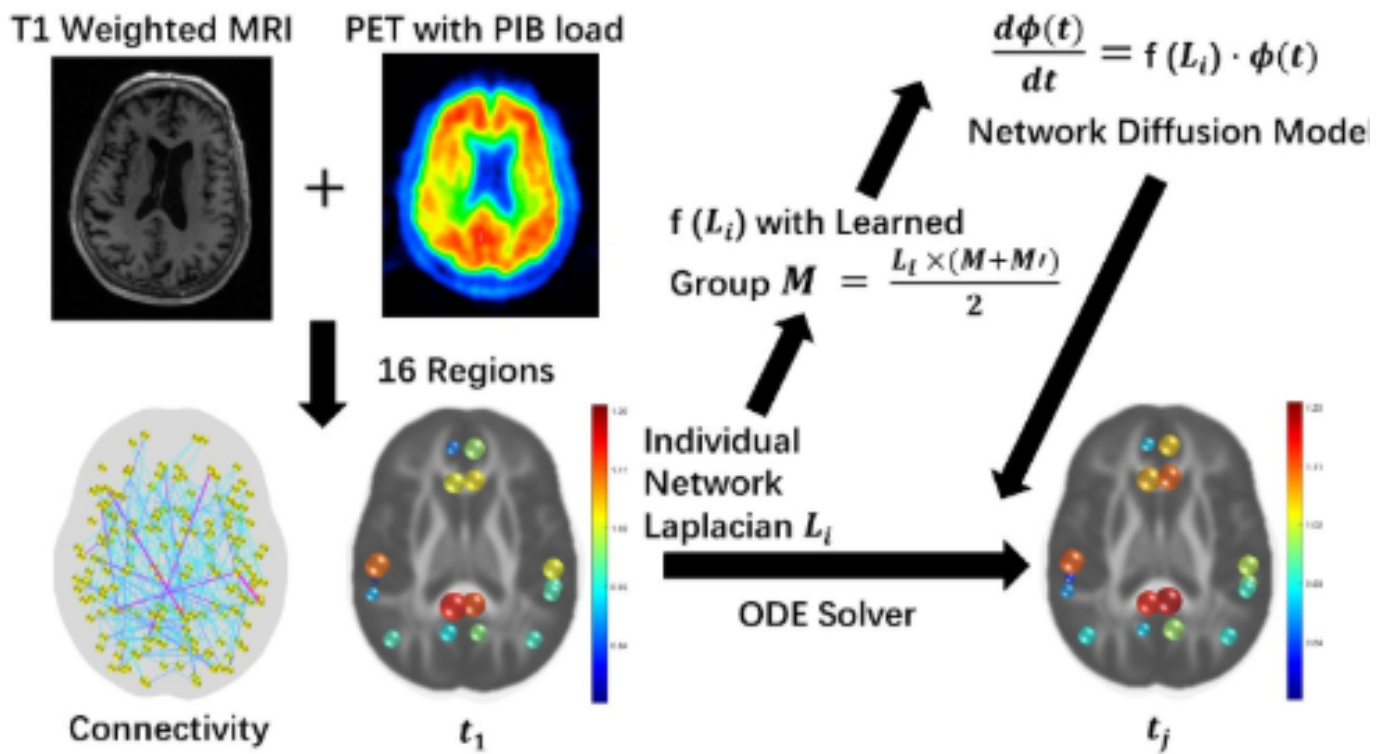


Fig 1. To learn the propagation pattern using the longitudinal scans as well as connectivity obtained from graynet based on our training dataset, our model learns a function with trainable parameters in the matrix M . The function maps the individual subject's connectivity Laplacians to a quantity that characterizes the diffusion process whose start and end points are given by the time-1, time-2 and time-3 PiB-PET image measurements of the pathology. The diffusion process is specified by the differential equation. In other words, instead of assuming that the differential equation between the start and end points is independent of the connectivity, our model learns how the connectivity and the baseline PiB-PET imaging data jointly predict future PiB-PET measurements at future time points.

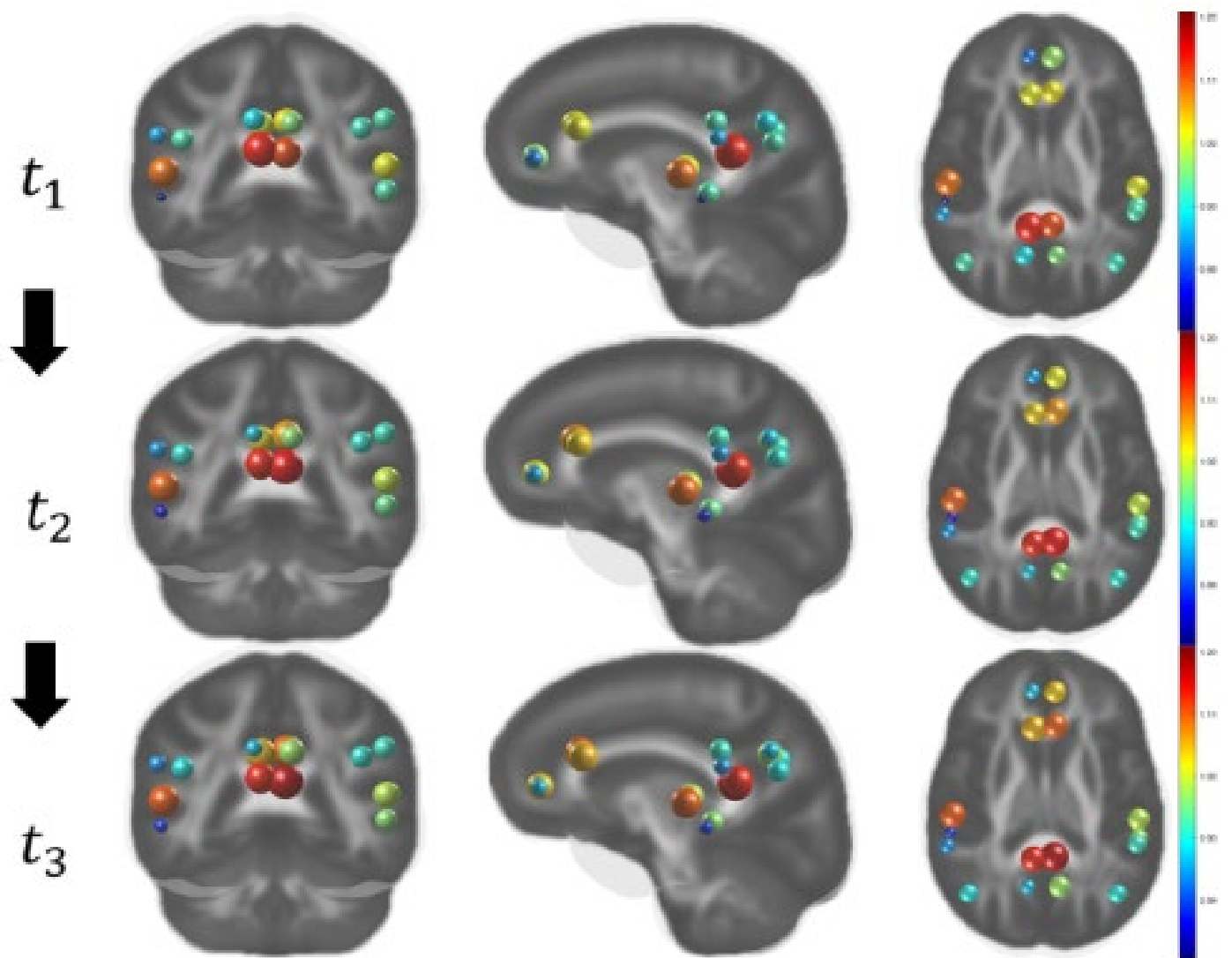


Fig 2. Amyloid propagation predicted by our model over time (time-1→ time-2→ time-3), conditioned on the baseline PIB data (acquired at time-1).

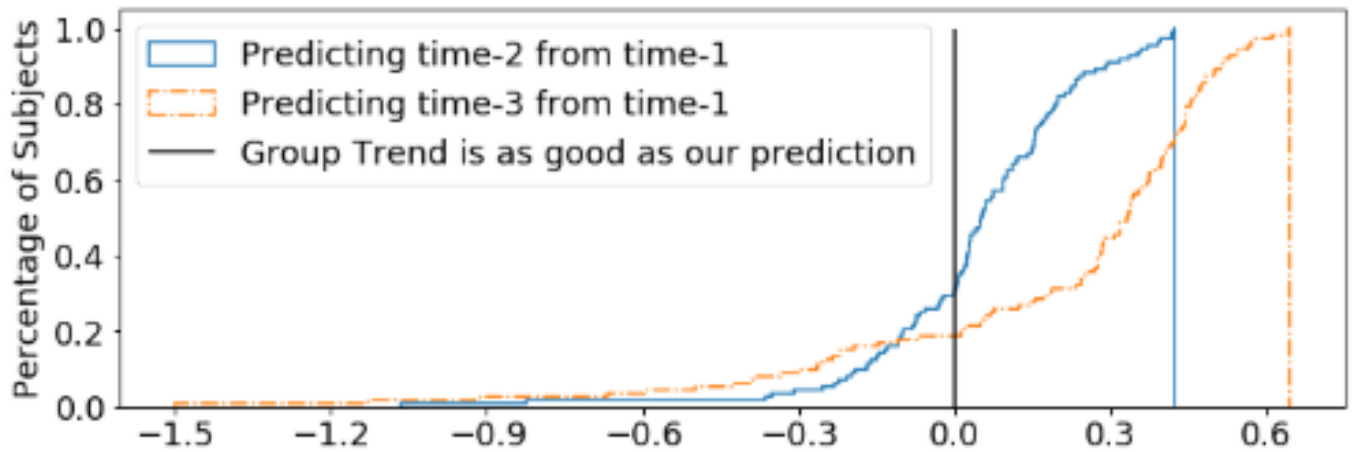


Fig 3. Relative performance compared to a linear estimate of the average group change. A point on the x-axis shows how much better (in percentage) the prediction from our method is (when compared to the ground truth time-2 and time-3 PiB-PET image scans) and the y-axis shows the frequency. We see that our model consistently makes better predictions compared to the linear estimate of the group trend where 69.6% of them are better than the group trend predictions when we predict time-2 measurements using baseline data. Since we compare our performance to a method which assumes that the global trend is linear, we notice that the margin of improvement is greater when estimating a farther away time point time-3, where our proposed model achieves better prediction in 81.3% of cases.

Keywords: Alzheimer's disease, Network diffusion, Differential equations, PiB PET image, MRI connectivity

P17: [¹¹C]PiB amyloid quantification and choice of reference region

Fiona Heeman¹, Janine Hendriks¹, Bart N.M. van Berckel¹, Isadora Lopes Alves¹, Adriaan Lammertsma¹, Maqsood Yaqub¹

¹Amsterdam UMC, Vrije Universiteit Amsterdam, Radiology and Nuclear Medicine, Amsterdam Neuroscience, Amsterdam, The Netherlands

Introduction: Reference tissue approaches for quantification of amyloid load in Alzheimer's disease (AD) using [¹¹C]PiB PET circumvent the need for arterial sampling. These approaches are less burdensome to the patient and better suited for large clinical trials. The generally accepted reference region (RR), cerebellar grey matter (CBGM), may be compromised in late disease stages,^a difficult to delineate and possibly suffer from truncation or lower statistics. This has resulted in the search for alternative RRs, but in general full validation of these RRs against dynamic scans using the CBGM, is mostly lacking^{b,c}. The purpose of the present study was to evaluate the use of alternative reference regions against dynamic scans using CBGM.

Methods: 43 subjects (17 AD, 13 MCI, 13 control) part of a single-centre test-retest^d (six with arterial sampling) or longitudinal study^e were included. Dynamic [¹¹C]PiB PET (90 minutes) and T1 MRI scans were co-registered and time-activity curves (TACs) were extracted for several regions, including five regularly used RR: CBGM, whole cerebellum, whole brainstem, brainstem white matter/pons and eroded subcortical white matter (ERWM). All RR TACs were fitted using a plasma (2T4k_V_b) model, reference Logan^f and the simplified reference tissue model^g, and SUV ratios were calculated. Next, relative test-retest variability, correlations and annual rates of change were calculated.

Results: Across reference tissue methods, whole cerebellum showed lowest test-retest variability (maximum 2.77%, Table 1). Quantitative measures for all methods and RR showed good correlations with those of the 2T4k_V_b derived DVR with CBGM ($r > 0.80$), but cerebellar RRs showed best slope. Furthermore, an inverted u-shape was consistently observed for rates of change computed with cerebellar RRs (Figure 1), similar to what has been observed before.^{h,i}

Conclusion: Across reference tissue approaches, the whole cerebellum is the region of choice for measuring amyloid using [¹¹C]PiB PET, in particular in a longitudinal setting.

Table 1. Relative test-retest variability across methods and reference regions

	2T4k_V _b (DVR)	RLogan (DVR)	SRTM (BP _{ND} +1)	SUV _{T40-60}	SUV _{T60-90}
Cerebellum GM	12.42 ± 14.47	2.77±2.34	2.94 ± 2.24	3.52±2.55	5.14 ± 4.57
Cerebellum whole	8.54 ± 5.85	1.41±1.10	2.04 ± 1.65	2.20±1.38	2.77 ± 3.19
Brainstem WM/ Pons	1.88 ± 2.18	2.44±1.81	3.31 ± 2.55	2.32±2.03	3.71 ± 3.00
Brainstem whole	2.18 ± 2.83	2.14±1.89	3.83± 3.95	2.24±1.92	3.13 ± 2.51
Eroded WM	7.50 ± 4.67	2.39±1.60	2.66 ± 1.57	3.66±2.29	3.94 ± 2.51

*values depicted as average (%) ±SD

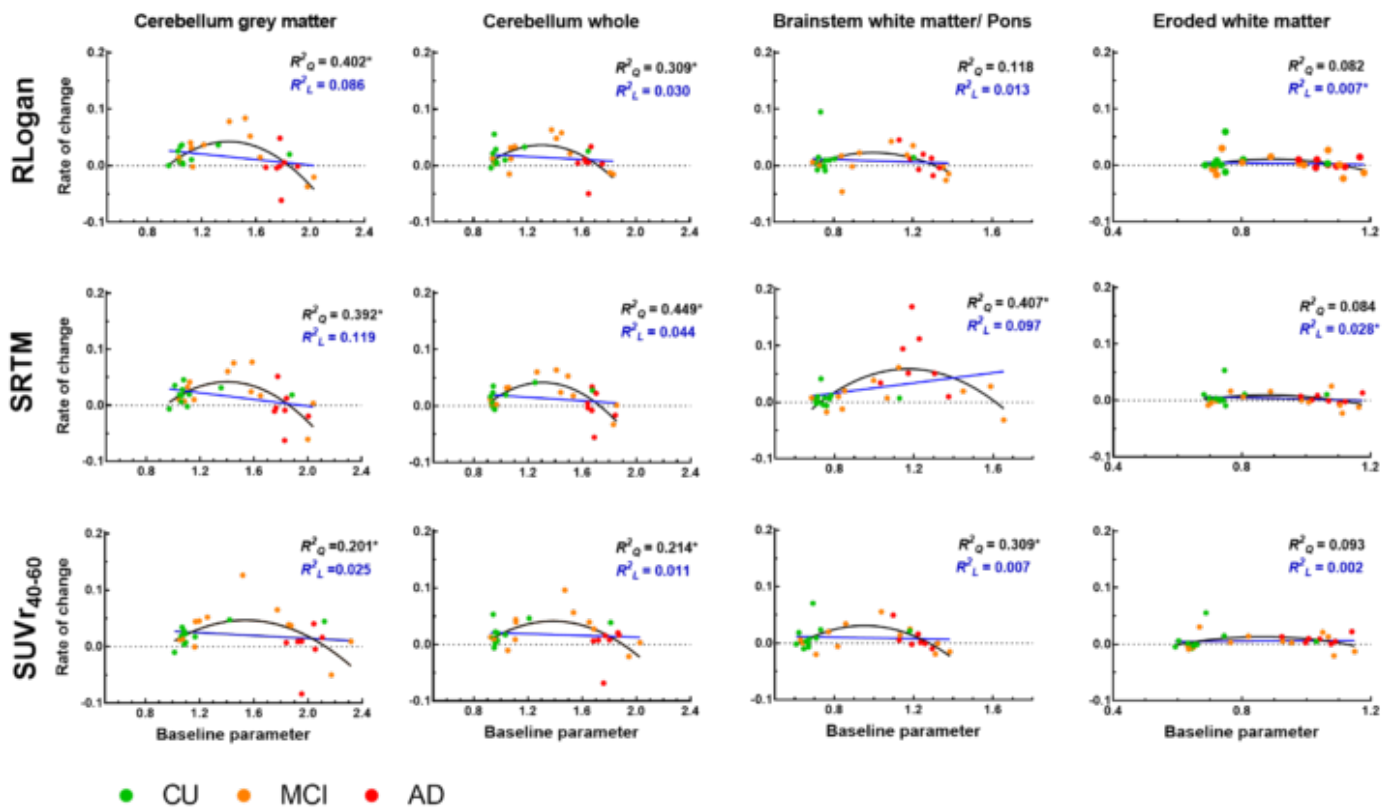


Figure 1. Annual rates of change across reference regions and methods
 The asterisk indicates the model that was preferred by both the AIC and F-test

Keywords: *[11C]PiB, reference region, amyloid quantification*

P18: Retrospective prediction of amyloid accumulation trajectories in a risk-enriched Alzheimer's disease cohort with sequential neural network

Seong Jae Hwang¹, Rebecca Kosciuk^{2,3}, Tobey Betthausen^{2,5}, Zirui Tao², Won Hwa Kim⁴, Sterling Johnson^{2,3,5,6}, Vikas Singh²

¹University of Pittsburgh, Pittsburgh, PA, US

²University of Wisconsin-Madison, Madison, WI, US

³The Wisconsin Alzheimer's Institute, Madison, WI, US

⁴University of Texas, Arlington, Arlington, TX, US

⁵Wisconsin Alzheimer's Disease Research Center, Madison, WI, US

⁶VA Geriatric Research, Education and Clinical Center (GRECC), Madison, WI, US

Background: Understanding the longitudinal pattern of amyloid accumulation is crucial for early detection/intervention in Alzheimer's disease (AD). The PiB+ Age (PA) when amyloid accumulation crosses a critical threshold is one of the earliest signs of AD progression. We developed a sequential neural network to extrapolate the PiB-PET amyloid trajectories retrospectively, estimate the subject- and region-wise PAs, and investigate their associations with APOE in a preclinical cohort.

Method: We measured the PiB-DVR in 8 AAL (left-right combined) regions of cognitively asymptomatic participants from the Wisconsin Registry for Alzheimer's Prevention (N=234) with at most four longitudinal [C11]PiB-PET scans (mean=3.42/s.d.=1.57 interval; mean=63.8/s.d.=6.7 age). We developed a sequential neural network called *CRow* which maps PiB-DVR trajectories to corresponding ages and predicts PiB-DVR trajectories beyond observed ages. We used all subjects to train *CRow* and retrospectively predict their PAs. Then, we computed the region-wise PiB-DVR thresholds based on the global PiB-DVR threshold of 1.2 from prior studies. The age when PiB-DVR reaches the region-wise PiB-DVR threshold was considered as the PA (minimum=45, Wisconsin Life Expectancy Table for PiB-subjects). For each region, we tested the difference of the PAs between APOE+ (ϵ 4-allele) and APOE- (no ϵ 4-allele) groups using the two-sample t-test.

Result: Fig. 1 shows the predicted trajectories (dotted) given the original trajectories (solid) of the PiB+ subjects in all 8 regions. Table 1 shows that all regions show significant differences in PAs between the APOE groups ($\alpha=0.05$ with Bonferroni correction). Fig. 2 shows the boxplots of PAs between APOE groups revealing less distinct PAs among the ROIs.

Conclusion: Early amyloid accumulation is one of the promising avenues for preclinical AD detection, and our results support this by demonstrating its association with APOE. Our model accurately extrapolates the PiB-DVR trajectories and estimates the PAs in AD-related regions.

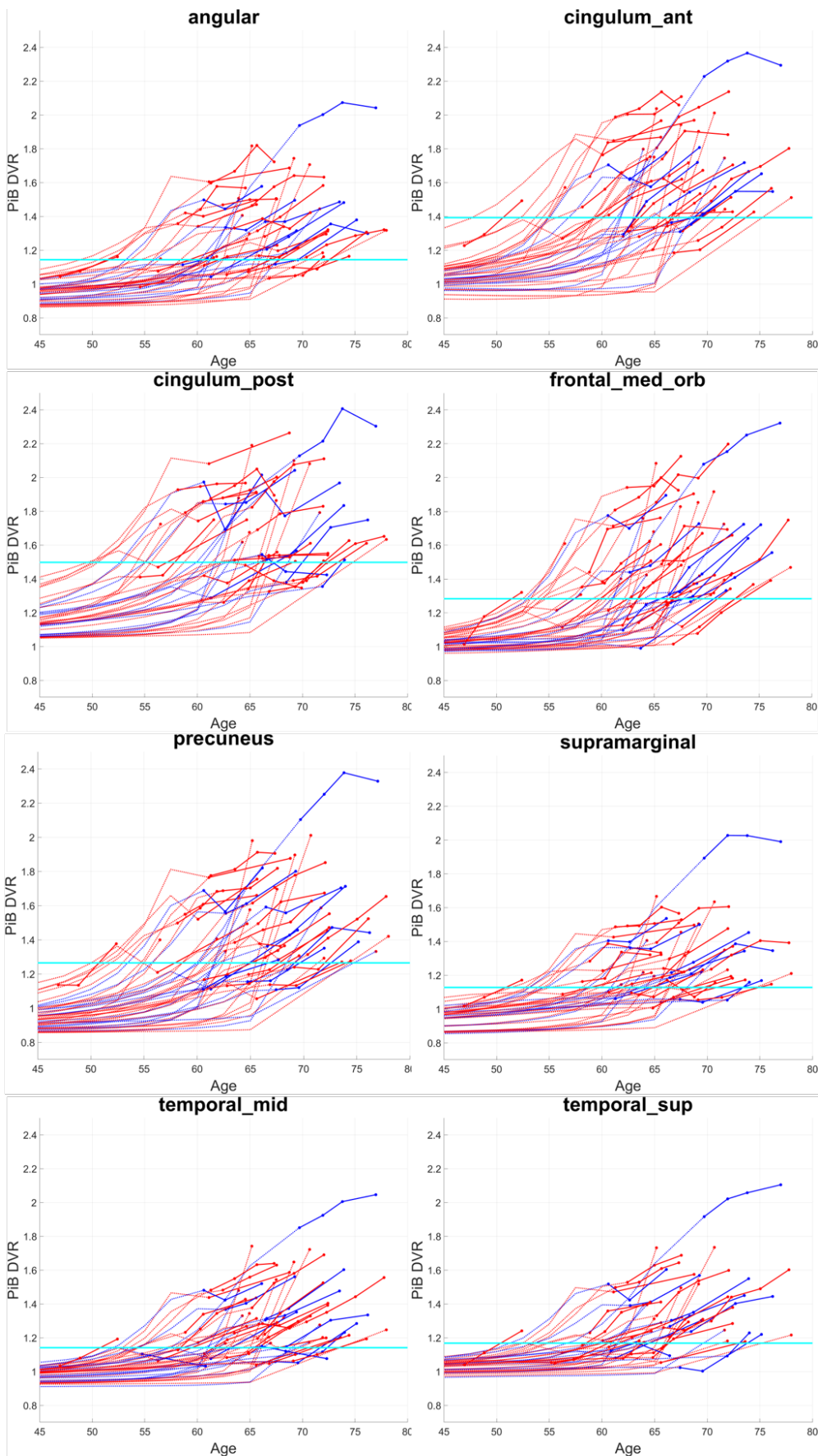


Fig 1: Retrospective PiB-DVR trajectory estimation. Straight lines: observed PiB-DVR trajectories. Dotted lines: Estimated PiB-DVR trajectories. Red lines: APOE+ subjects. Blue lines: APOE- subjects. Cyan lines: Region-wise PiB-DVR thresholds. Only showing the PiB+ subjects (i.e., those that cross the PiB-DVR thresholds) for visual clarity.

ROI	Mean PA (APOE+ / APOE-)	p-value
angular	76.5 / 81.7	*0.0001
cingulum_ant	76.4 / 82.2	*0.0001
cingulum_post	77.4 / 82.0	*0.0004
frontal_med_orb	76.1 / 81.6	*0.0001
precuneus	76.9 / 81.6	*0.0003
supramarginal	77.4 / 82.0	*0.0004
temporal_mid	77.4 / 81.1	*0.0061
temporal_sup	77.6 / 81.8	*0.0012

Table 1: Mean PiB+ Age and the group difference results in each ROI. * indicates statistical significance after the Bonferroni correction.

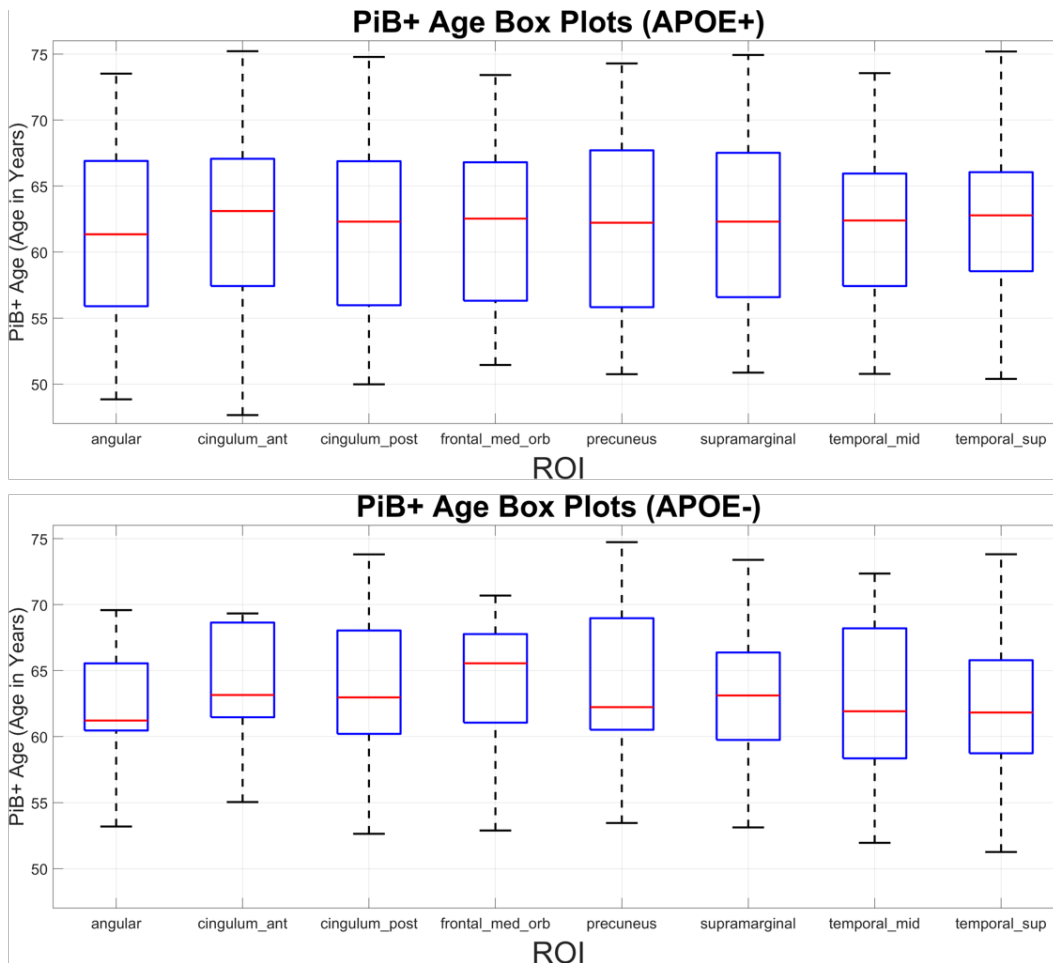


Fig. 2: Box plot of PAs of APOE+ and APOE-. For each ROI, the top and bottom bars are the max and min PAs of that ROI respectively. The box indicates the standard deviation from the mean which is the red line. While the mean PAs of the ROIs of APOE- (bottom) have noticeably different patterns (i.e., distinct mean PAs with relatively small standard deviations), the mean PAs of the ROIs of APOE+ (top) have less distinct patterns (i.e., mean PAs are similar with large standard deviations).

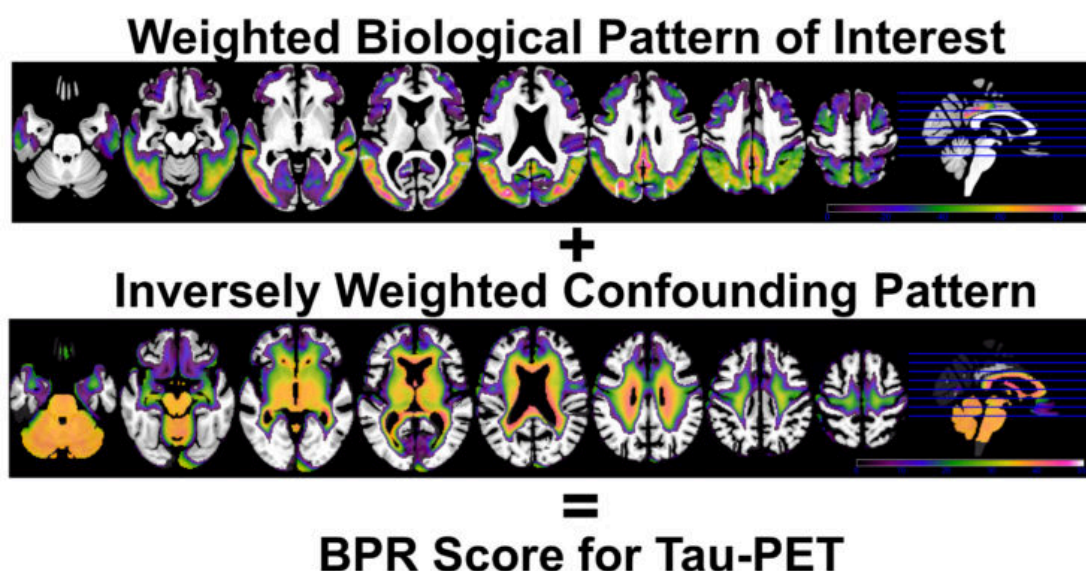
Keywords: Preclinical AD, Amyloid Imaging, Longitudinal Analysis, Machine Learning

P19: Data-driven biological pattern scoring of Flortaucipir scans outperforms ROIs

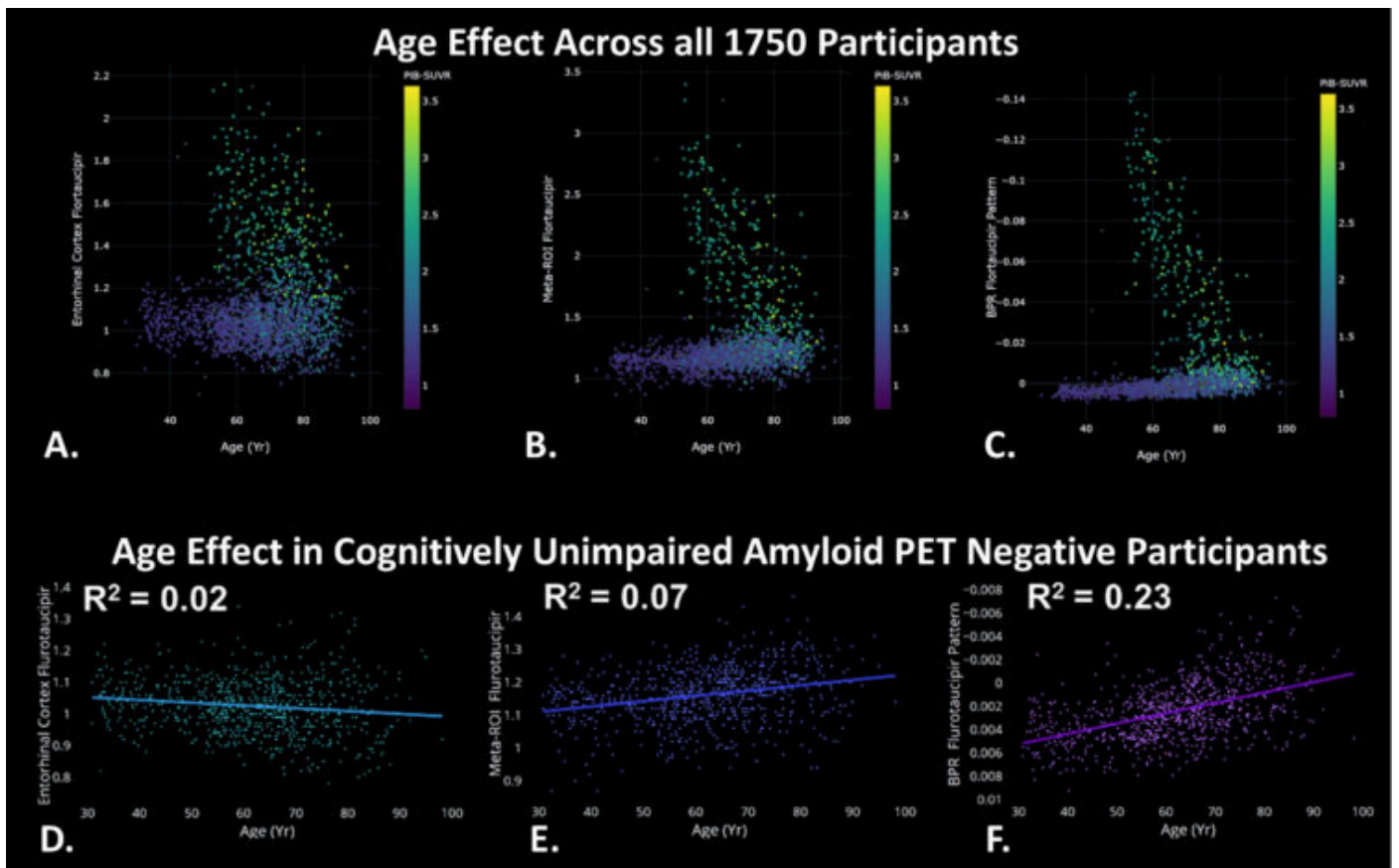
David Jones¹, Jonathan Graff-Radford¹, Hugo Botha¹, Matthew Senjem¹, Heather Wiste¹, Keith Josephs¹, Jennifer Whitwell¹, Kejal Kantarci¹, Bradley Boeve¹, Ronald Petersen¹, David Knopman¹, Val Lowe¹, Clifford Jack¹

¹Mayo Clinic, Rochester, MN, US

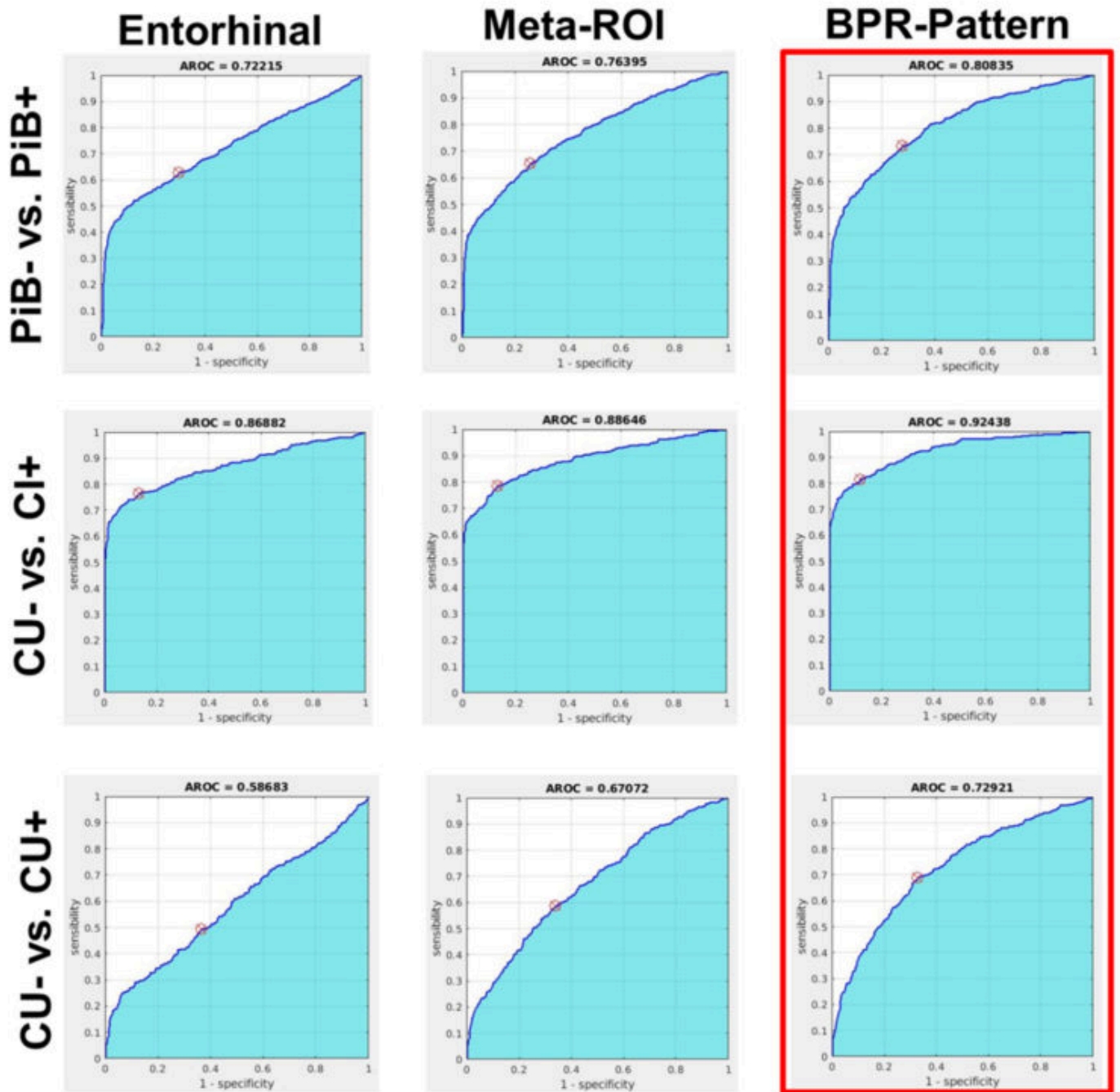
Background: Hypotheses about the location of biologically relevant tau-PET signal have driven the selection of ROIs based on Braak NFT staging. These ROIs may not capture the underlying biology of interest and are subject to off-target and partial volume confounds. ROI methods do not leverage global spatial information that can improve sensitivity. We propose to use a data driven method of identifying biologically relevant tau-PET signal, that is robust to these confounds, and compare its performance to ROIs.



Methods: Using data from N=1750 scans from the Mayo Clinic MCSA, ADRC, and NRG studies of normal aging and the spectrum of neurodegenerative diseases (e.g., AD, DLB, PCA, PPA, PSP, CBD, and FTD), we performed a data driven pattern analysis technique we developed called Between-subject-variance Projection and Reduction (BPR). BPR biological pattern-based scoring was then compared to entorhinal cortex (EC) and a temporal lobe meta-ROI (MR) performance.



Results: BPR identified a global flortaucipir pattern that accounted for 93% of the biological signal of interest in the cohort (Figure 1). Plots of flortaucipir signal versus age reveals superior group separation of high tau signal versus low signal using BPR (Figure 2 A, ERC; B, meta ROI; C, BPR). In cognitively unimpaired (CU) participants that are PiB negative (CU/PiB-), age is correlated with tau-PET signal most strongly using BPR scoring and not at all with EC-based scoring (Figure 2 D, ERC; E, meta-ROI; F, BPR). BPR based scoring showed superior AROC for discriminating PiB+ vs. PiB-, CU/PiB- vs. CI/PiB+, and CU/PiB- vs. CU/PiB+ (Figure 3).



Conclusions: BPR is designed to be robust to off target binding and partial volume confound while capturing non-focal biological patterns of tau-PET signal observed across the AD continuum. BPR scoring is superior to ROI scoring of tau-PET scans including in amyloid negative CU participants.

Keywords: Tau-PET, flortaucipir, ROI, Data, Pattern

P20: Hippocampal volume mediates the relationship between amyloidosis and amyloid-sensitive cognitive composite in preclinical AD

Young Ju Kim^{1,2}, Alice Hahn^{1,2}, Soo Jong Kim^{1,2}, Si Eun Kim⁷, Juhee Chin^{1,2,4}, Sang Won Seo^{1,2,4,5,6}

¹*Department of Neurology, Samsung Medical Center, Sungkyunkwan University School of Medicine, Seoul, Korea*

²*Neuroscience Center, Samsung Medical Center, Seoul, Korea*

³*Samsung Alzheimer Research Center, Samsung Medical Center, Seoul, Korea*

⁴*Center for Clinical Epidemiology, Samsung Medical Center, Seoul, Korea*

⁵*Department of Health Sciences and Technology, SAIHST, Sungkyunkwan University, Seoul, Korea*

⁶*Clinical Research Design and Evaluation, SAIHST, Sungkyunkwan University, Seoul, Korea*

⁷*Departments of Neurology, Inje University College of Medicine, Haeundae Paik Hospital, Busan, Korea*

Background: Amyloidosis and the neurodegenerative measures like cortical thickness (Cth) and hippocampal volume (HV) were found to be highly associated with cognitive function. Accordingly, it is essential to examine how these biomarkers are related to each other to impact on alterations of cognitive function in preclinical Alzheimer's disease (AD). Therefore, the present study aimed to investigate if the mediation effect of neurodegeneration exists between amyloidosis and cognitive function in cognitively normal (CN) elderly participants using the Preclinical Amyloid Sensitive Composite score (PASC).

Methods: The MRI scans, PET scans, and the cognitive test scores from the Seoul Neuropsychological Screening Battery-II of 373 CN elderly participants were used. First, we created the PASC by summing the z-scores of the Seoul Verbal Learning Test-delayed recall, the Rey Complex Figure Test-delayed recall, the Korean Color Word Stroop Test-color reading, the Controlled Oral Word Association Test-animal naming, and the Korean Mini-Mental State Examination with different weight on each test derived by principal component analysis. Then, we examined the mediation effects of Cth and HV on the relationship between amyloid positivity and the PASC.

Results: The results indicated that amyloid positivity was directly associated with the PASC. Moreover, amyloid positivity was found to be associated with HV, which was further related to the PASC. Furthermore, bootstrapping analyses were used to show that HV mediates the relationship between amyloid positivity and the PASC [95%CI (-0.301, -0.032), $p < .01$].

Conclusions: In the present study, we found that HV mediated the effect of amyloidosis on the PASC. Thus, the comprehensive relationship of HV and amyloidosis on cognitive function may be the key to early intervention of AD.

Keywords: preclinical Alzheimer's disease, cognitive composite, amyloid, neurodegeneration

P21: Concordance of visual and quantitative assessments of baseline amyloid scans in the GRADUATE gantenerumab studies

Gregory Klein¹, Paul Delmar², Nicola Voyle³, Jacob Hesterman⁴, Ryan Petrulli⁴, Heather Ovens⁴, Monika Baudler², Paulo Fontoura², Rachelle Doody², Geoffrey A. Kerchner²

¹Roche Pharma Research and Early Development, Basel, Switzerland

²Roche/Genentech Product Development, Neuroscience, Basel, Switzerland

³Roche Products Ltd, Welwyn Garden City, UK

⁴InviCRO, LLC., Boston, MA, US

Background: Gantenerumab is a fully human monoclonal antibody currently under evaluation in two Phase III trials (GRADUATE I/II [NCT03444870/ NCT03443973]) for the treatment of early Alzheimer's Disease. Eligible participants must show confirmation of beta-amyloid pathology via CSF or visual assessment of amyloid PET. This work compares visual with quantitative screening results.

Methods: Florbetaben and flutemetamol were scanned using 300 and 185 MBq respectively and a 20 min scan (4x5min) targeting 90min \pm 1min post-injection. Historical scans of florbetaben, florbetapir, and flutemetamol were also allowed. PET scans were acquired after the participant passed screening tests including NIA-AA criteria, MMSE \geq 22, CDR-GS of 0.5 or 1, and FCSRT inclusion criteria.

Visual reads were performed on the reconstructed, attenuation-corrected scans in PET subject space. Two independent reads were performed, and a third read was employed in case of disagreement.

Quantitative results were obtained using Freesurfer (v6.0). A cortical volume-weighted sum of the frontal, parietal, temporal and cingulate regions was used to compute a standard uptake value ratio with a whole-cerebellar reference region. SUVR's were translated into the centiloid scale, and a positivity threshold of 24 was used for all three amyloid tracers.

Results: GRADUATE enrollment is still ongoing. PET screening scans to date were evaluated for 976 participants (744 florbetaben, 62 florbetapir, 163 flutemetamol). Overall 70.3% of participants were positive via visual assessment, versus 81.3% quantitatively, resulting in an overall discordance rate of 11.8%. Rate of negative visual/positive centiloid was 11.4%, and for positive visual/negative centiloid was 0.4% ($p < 0.001$). Mean (SD) centiloid for the screened population was 68.8 (42.2). Mean centiloid for the visual-positive group was 5.1 centiloid units lower than for the centiloid-positive group.

Conclusions: Visual assessment of amyloid positivity is more conservative than quantitative assessment. This should be considered when designing clinical trials using amyloid as an enrichment criterion.

Table 1. Visual/Quantitative Discordance Rates. Overall discordance rate was 11.8%. Nearly all discordance was due to visual negative / quantitative positive reads (McNemar's p -value < 0.001)

N (%)	Centiloid Positive	Centiloid Negative
Visual positive	686 (70.3)	4 (0.4)
Visual negative	111 (11.4)	179 (18.3)

Keywords: amyloid, gantenerumab, positron emission tomography

P22: Regional amyloid burden is associated with higher quantitative T1 in discrete hippocampal sub-regions

Akshay Kohli¹, Kao Lee Yang¹, Nicholas M Vogt¹, Sanjay Asthana^{1,3}, Tobey J Betthausen¹, Andrew L. Alexander^{1,3}, Bradley T Christian¹, Sterling C Johnson, Steven R Keckskemeti, Barbara B Bendlin

¹*Wisconsin Alzheimer's Disease Research Center, University of Wisconsin School of Medicine and Public Health, Madison, WI, US*

²*Geriatric Research Education and Clinical Center, William S. Middleton Memorial Veterans Hospital, Madison, WI, US*

³*Department of Medical Physics, University of Wisconsin - Madison, Madison, WI, US*

Background: While neurodegeneration in Alzheimer's disease is well studied, conventional measures utilizing T₁-weighted MRI are often subject to bias field inhomogeneities and lower tissue contrast, limiting their reliability and reproducibility. In contrast, quantitative T₁ mapping provides a standardized metric of tissue relaxometry. MPnRAGE facilitates the generation of hundreds of T₁-weighted contrast images for the precise estimation of T₁. A previous study employing quantitative MRI linked cerebrospinal fluid A β levels to widespread alterations in R₁ (1/ T₁). Here we investigate the effect of regional A β burden (by [C-11]PiB-PET) on quantitative T₁. We hypothesized that T₁ would be higher in individuals with greater A β burden, and that affected regions would differ spatially based on regional [C-11]PiB distribution volume ratios (DVR).

Methods: 115 cognitively unimpaired participants (Table 1) underwent [C-11]PiB-PET and MPnRAGE MRI (to derive T₁). [C-11]PiB DVRs were calculated in 8 bilateral regions of interest (Table 2). T₁ maps were registered to a population template via ANTS, and smoothed using a 2mm gaussian kernel. Nine independent whole-brain voxelwise linear regressions were fit to examine relationships between each [C-11]PiB DVR ROI and T₁, controlling for age, sex, and *APOE4* positivity. Statistical maps were thresholded at p<0.001(uncorrected) with voxel extent>50.

Results: Higher A β in each ROI was associated with higher regional T₁ (Table 2). While several of the regional T₁ effects were similar across [C-11]PiB ROIs, A β in the anterior cingulate and medial orbitofrontal cortices was associated with higher T₁ in the right anterior hippocampus, whereas A β in the remaining—posterior—ROIs was associated with higher T₁ in the right posterior hippocampus (Figure 1). These results did not survive FWE-correction.

Conclusion: While A β accumulation appears to be broadly associated with altered T₁, anterior and posterior A β differentially effect the hippocampus. Higher T₁ signal may reflect changes to tissue content including myelin, iron, various macromolecules, and inflammation.

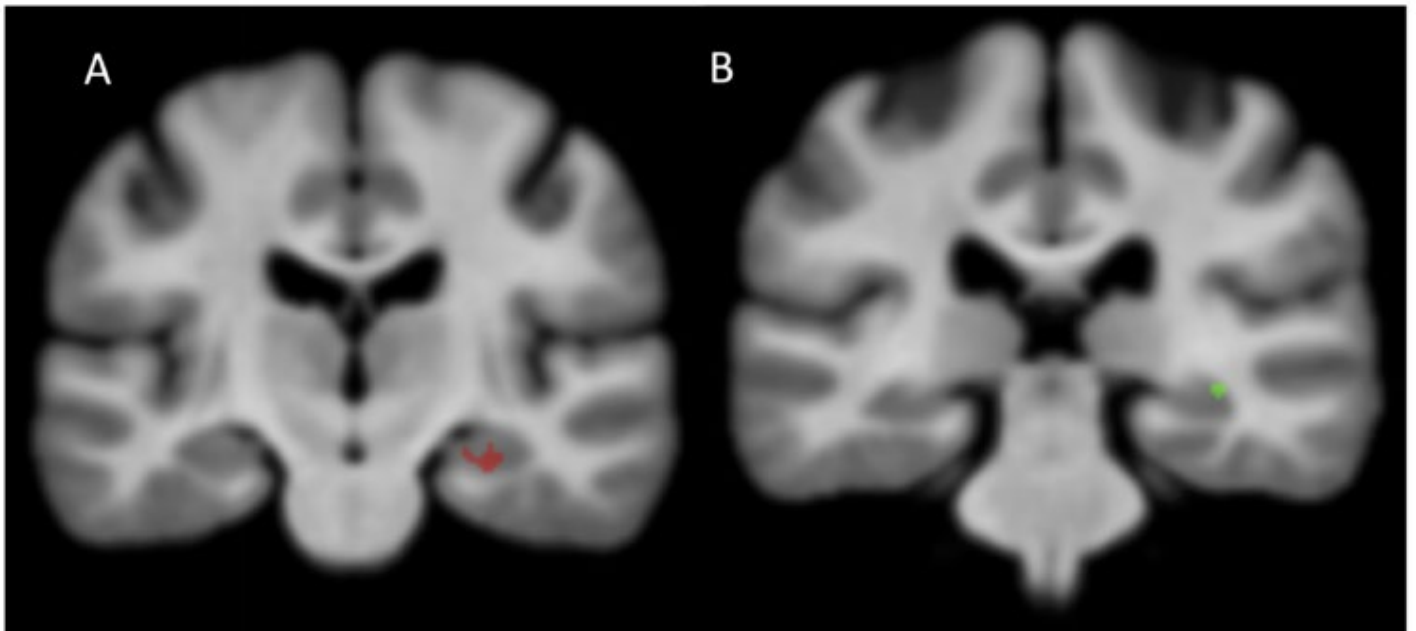


Figure 1: (A) Coronal section highlighting higher T_1 (green) as predicted by averaged [C-11]PiB DVR from 6 ROIs (posterior cingulate, angular gyrus, precuneus, supramarginal gyrus, middle and superior temporal cortices) overlaid onto an averaged population R_1 ($1/T_1$) map. (B) Coronal section highlighting higher T_1 (red) as predicted by average [C-11]PiB DVR from 2 ROIs (anterior cingulate and medial orbitofrontal cortices) overlaid onto an averaged population R_1 ($1/T_1$) map. Both models controlled for age, sex, and *APOE* carrier status.

Characteristic	Value
# of participants	115
Age, mean (SD), years	67.428 (6.174)
Sex	
Male	28
Female	87
<i>APOE4</i> carrier status, # positive / # negative	47 / 68
Time between MRI and PET, mean (range), years	0.056 (0 – 0.29)
[C-11]PiB status, # positive / # negative	28 / 87

Table 1: Participant demographics and characteristics. Participants with global [C-11]PiB DVR > 1.19 were classified as PiB positive.

PIB DVR ROI	Location	Cluster Size	Peak Voxel T-statistic	Peak Voxel P-value
Posterior Cingulate Cortex	R Anterior Cingulate	68	6.16	6.17E-09
	L Anterior Insula	63	4.72	3.54E-06
	R Calcarine Sulcus	109	4.44	1.08E-05
	R Dorsolateral PFC	66	4.38	1.35E-05
	R Posterior Hippocampus	55	4.33	1.66E-05
	L Posterior Cingulate	56	4.14	3.41E-05
Anterior Cingulate Cortex	R Anterior Cingulate	67	6.35	2.48E-09
	R Posterior Occipital	50	5.2	4.74E-07
	L Ventrolateral PFC	52	5.19	4.92E-07
	R Anterior Hippocampus	63	4.82	2.29E-06
Precuneus	R Anterior Cingulate	59	5.84	2.68E-08
	L Anterior Insula	56	5.79	3.38E-08
	R Posterior Hippocampus	125	5.01	1.04E-06
	R Calcarine Sulcus	82	4.53	7.63E-06
Supramarginal Gyrus	R Anterior Cingulate	52	5.61	7.66E-08
	R Calcarine Sulcus	97	4.78	2.70E-06
	R Posterior Hippocampus	72	4.6	5.72E-06
	L Posterior Insula	59	4.56	6.71E-06
Angular Gyrus	R Anterior Cingulate	63	5.94	1.69E-08
	R Calcarine Sulcus	77	4.61	5.43E-06
	R Posterior Occipital	54	4.52	7.68E-06
	R Precuneus	98	4.45	1.02E-05
	L Posterior Insula	65	4.43	1.35E-05
Middle Temporal Gyrus	R Anterior Cingulate	57	6.03	1.10E-08
	R Posterior Hippocampus	94	4.87	1.86E-06
	R Calcarine Sulcus	85	4.76	2.94E-06
	R Precuneus	68	4.41	1.19E-05
Superior Temporal Gyrus	R Posterior Hippocampus	90	4.71	3.65E-06
	L Posterior Insula	58	4.65	4.74E-06
	R Calcarine Sulcus	72	4.41	1.21E-05
	R Precuneus	52	4.07	4.42E-05
Medial Orbitofrontal Cortex	R Anterior Cingulate	60	6.44	1.59E-09
	R Anterior Hippocampus	158	4.69	3.93E-06
	R Precuneus	60	4.09	4.14E-05
Global	R Anterior Cingulate	65	6.29	3.33E-09
	R Posterior Hippocampus	67	4.51	8.06E-06
	R Calcarine Sulcus	88	4.47	9.54E-06
	R Precuneus	55	4.31	1.78E-05

Table 2: Brain regions in which there was an association between higher [C-11]PiB DVR and higher quantitative T₁. Statistical maps were thresholded at p<0.001 uncorrected with cluster size > 50 voxels. T-statistic (p<0.001 uncorrected) = 3.17. T-statistic (p<0.05 FWE-corrected) = 5.67.

Keywords: relaxometry, amyloid, quantitative T1, hippocampus, MRI

P23: Genetically informed quantitative Gradient Recalled Echo MRI reveals brain tissue in hippocampal subfields void of neurons in mild Alzheimer's disease

Satya Kothapalli¹, Tammie Benzinger^{1,2}, Andrew Aschenbrenner^{2,3}, Manu Goyal^{1,3}, Anne M Fagan^{2,3,4}, Marcus Raichle^{1,3,4}, John Morris^{2,3}, Dmitriy Yablonskiy^{1,2,4}

¹*Department of Radiology, Washington University, St. Louis, MO, US*

²*Knight Alzheimer's Disease Research Center, Washington University, St. Louis, MO, US*

³*Department of Neurology, Washington University, St. Louis, MO, US*

⁴*The Hope Center for Neurological Disorders, Washington University, St. Louis, MO, US*

Rationale: Brain tissue atrophy (volume loss) serves as an *in vivo* MRI biomarker of neuronal damage. However, postmortem histopathological studies show that neuronal loss in Alzheimer's disease (AD) significantly exceeds volumetric loss of tissue and that memory decline in AD does not start until neurons are lost. Hence, identifying neuronal loss *in vivo* before it can be measured by atrophy can be valuable for early diagnosis.

Methods: Here we use a recently developed genetically-informed quantitative-Gradient-Recalled-Echo (GI-qGRE) MRI (Wen, et al, PNAS-2018) for *in vivo* evaluation of neuronal damage caused by AD in the hippocampal subfields. Forty-seven participants were recruited from the Knight Alzheimer Disease Research Center, classified into three groups: (1) normal (CDR=0 and Amyloid status=negative) (n=26); (2) preclinical AD (CDR=0, Amyloid=positive) (n=12); and (3) very mild/mild AD dementia (CDR 0.5/1, Amyloid=positive) (n=9).

Results: GI-qGRE allowed identification of two tissue types: tissue void of neurons ("**dark matter**") and tissue with relatively preserved concentration of neurons ("**viable volume**"). In AD dementia, GI-qGRE detected a greater loss of neurons as compared with atrophy in all hippocampal subfields. In right subfields neuronal loss ranged between 35%-55% while volume loss ranged between 15%-20%. Also, our results exhibit asymmetry in hippocampal subfields - lower viable volume, and higher dark matter fraction in right hippocampal subfields compared with left in all groups. Consistently, viable volume was strongly correlated with cognitive performance on a battery of psychometric tests rather than the total volume. The strongest correlation occurred in the right hippocampus ($r=0.56$, $p<0.0001$ for neuron loss vs. $r=0.36$, $p<0.05$ for atrophy). Data also showed a positive association between brain tauopathy and dark matter fraction in right hippocampus ($r=0.7$; $p<0.0001$) as compared with association between brain tauopathy and atrophy ($r=-0.42$. $p<0.05$).

Conclusion: GI-qGRE identifies cognitively-associated neuronal loss in mild AD dementia greater than measured by atrophy.

Keywords: Quantitative-Gradient-Recalled-Echo method, Alzheimer's disease, Neuronal loss, Hippocampal subfields, Atrophy

P24: Validation of highly sensitive and specific florbetaben positivity thresholds using ADNI participants and young controls

Susan Landau¹, Deniz Korman¹, Santiago Bullich², Susan De Santi², Andrew Stephens², Robert Koeppe^{1,3}, William Jagust¹

¹University of California, Berkeley, Berkeley, CA, US

²Life Molecular Imaging, Boston, MA, US

³University of Michigan, Ann Arbor, MI, US

Objectives: Existing [18F] florbetaben-PET positivity thresholds have not been compared across samples using a uniform PET processing pipeline. We used several strategies to derive positivity thresholds, compare them across samples, and validate them with respect to tau PET in ADNI.

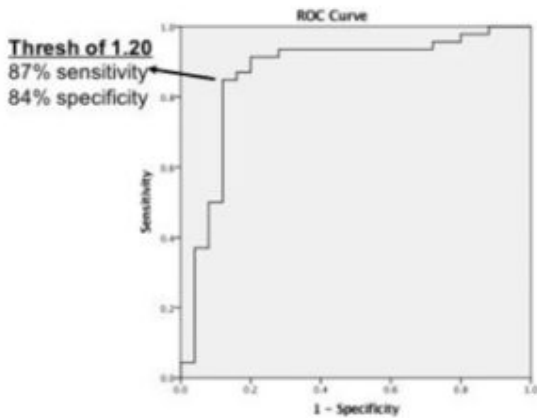
Methods: We carried out FreeSurfer-based quantification of cortical summary SUVRs using whole cerebellum normalization across several florbetaben samples: (1) 142 scans obtained in an FDA Phase II study rated as visually positive or negative (Barthel et al. Lancet Neurol 2011), (2) 71 FDA Phase III scans obtained in end-of-life patients and later evaluated with CERAD criteria at autopsy (Sabri et al. Alz & Dem 2015), (3) 189 ADNI3 participants, and (4) 62 young healthy (27.7+/-5.1yrs) controls (Seibyl et al. SocNuclMed 2015). We calculated thresholds in these samples using several strategies, and evaluated them by examining agreement across methods, associations with tau PET in ADNI, and conversion to centiloids.

Results: An ROC analysis of the autopsy sample resulted in a threshold of 1.20 (whole cerebellum normalization) or 39.2 centiloids (**Fig1A**), consistent with an ROC-based threshold calculated in the Phase II and III samples and linearly transformed to ADNI pipeline “units” (**Fig1B**). However, calculation of mean+2SD in 75 visually-negative ADNI scans, calculation of mean+2SD in young controls (**Fig2A**), and Gaussian Mixture Modelling of the ADNI florbetaben sample (**Fig2B**) all converged on a threshold of 1.08 (whole cerebellum normalization) or 20.2 centiloids. Categorization of ADNI florbetaben scans using the more sensitive (1.08) threshold accounted for 14% greater variance (**Fig3A**) in entorhinal tau-PET (flortaucipir) uptake among florbetaben+ individuals ($R^2=.42$), compared with the more specific (1.20) threshold ($R^2=.28$) (**Fig3B**).

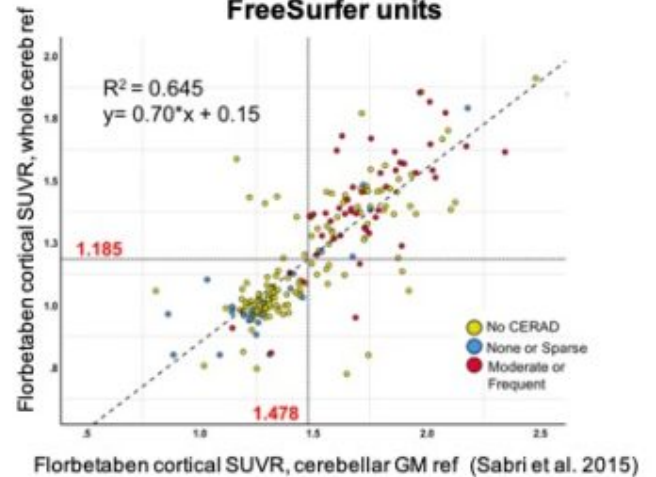
Conclusion: Using a uniform PET processing pipeline, we examined multiple threshold derivation strategies in several samples and converged on sensitive (1.08) and specific (1.20) thresholds. Selection between these thresholds is dependent on study-specific goals.

Figure 1

A ROC analysis of florbetaben scans in autopsy sample



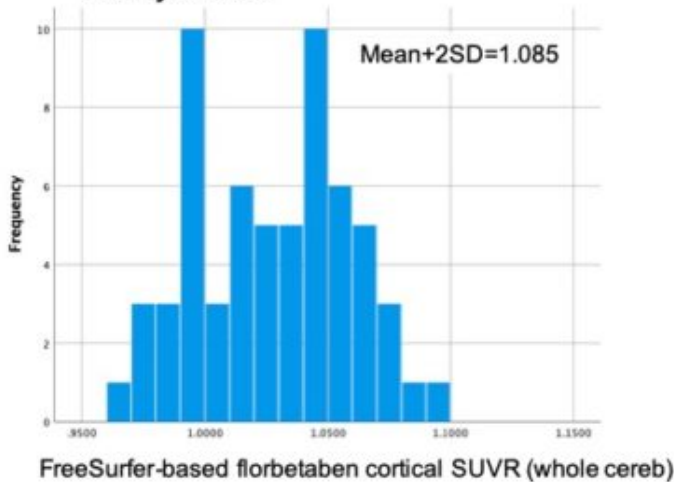
B Transformation of independently-derived ROC-based threshold to FreeSurfer units



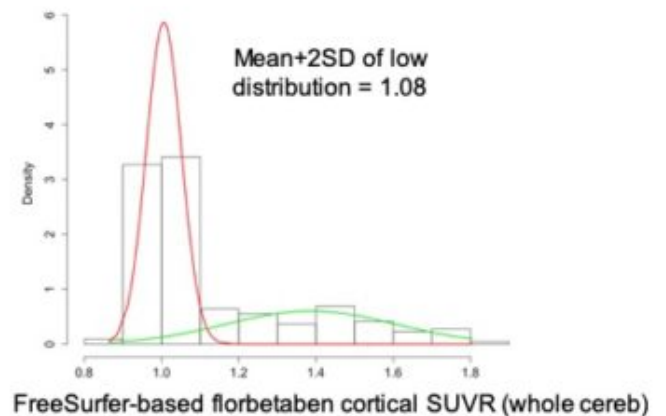
ROC analysis of florbetaben scans in 71 end-of-life patients with moderate/frequent plaques as standard of truth yielded a threshold of 1.20 using a FreeSurfer-based pipeline (whole cerebellum reference) (A). We also transformed an ROC-based threshold from the autopsy sample reported by Sabri et al. (2015) to FreeSurfer/whole cerebellum “units” using the association between the Phase II and III data analyzed using both methods, resulting in a FreeSurfer-based threshold of 1.19 (B).

Figure 2

A Florbetaben SUVR distribution in young healthy controls

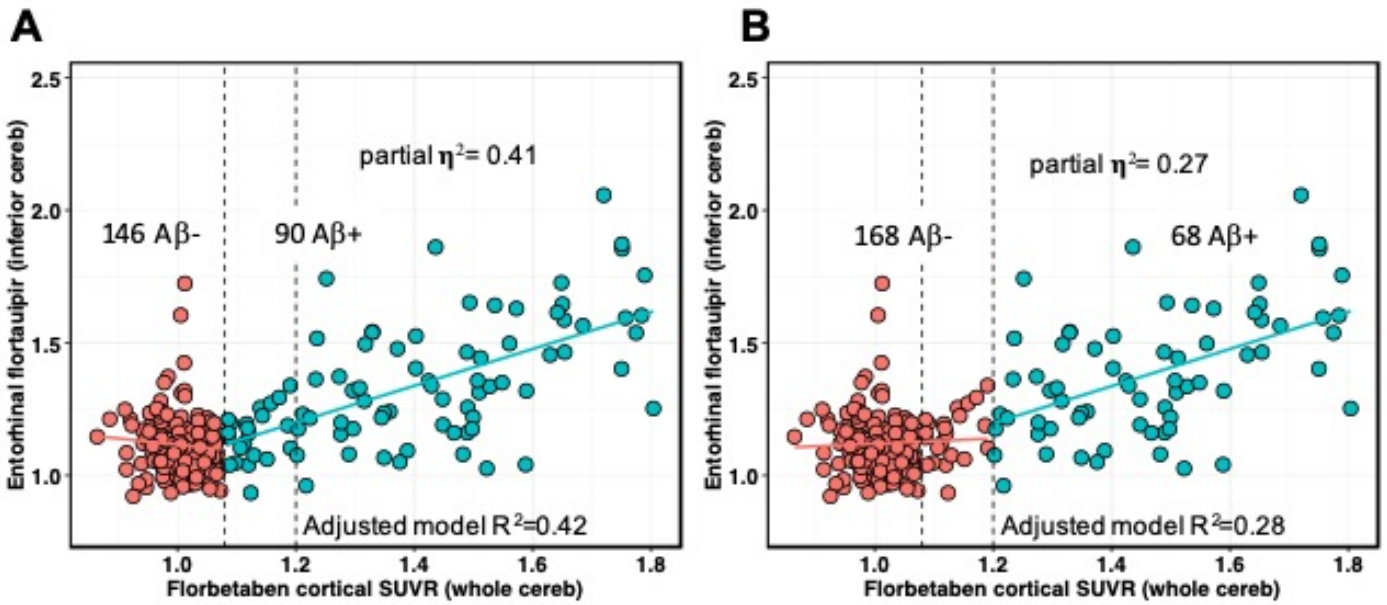


B Gaussian Mixture Modelling in baseline ADNI florbetaben scans



FreeSurfer-based analysis of florbetaben scans in 62 young controls resulted in a mean of 1.023+/-0.031 and a mean+2SD threshold of 1.085 (A). Gaussian Mixture Modelling in 189 baseline florbetaben scans resulted in a threshold of 1.08 based on the mean+2SD above the lower distribution (B).

Figure 3



We examined the association between continuous florbetaben among A β^+ individuals and contemporaneous entorhinal flortaucipir SUVRs in 236 ADNI participants (144 unimpaired, 92 impaired) using regression models that included age and sex. Use of the more sensitive threshold (left dotted line in both plots; 1.08) to determine positivity explained 15% more variance **(A)** than use of the more specific threshold (right dotted line in both plots; 1.20) **(B)**.

Keywords: amyloid positivity, florbetaben, centiloids, flortaucipir

P25: Additive contribution of white matter hyperintensity to amyloid and neurodegeneration on cognitive decline in a diverse, community-based cohort of older adults

Patrick Lao¹, Anthony Chesebro¹, Juliet Colon¹, Kay Igwe¹, Yian Gu¹, Nicole Schupf¹, Jennifer Manly¹, Yaakov Stern¹, Richard Mayeux¹, Adam Brickman¹

¹*Columbia University, New York, NY, US*

Introduction: The 2018 NIA-AA Alzheimer's disease (AD) research framework moves towards a multiple biomarker approach to explain AD development and progression more fully. An advantage of the research framework is the flexibility to incorporate various biomarkers into a full or partial amyloid-tau-neurodegeneration profile. The objective of this study was to determine the additive contribution of white matter hyperintensity (WMH) to amyloid and neurodegeneration on cognitive decline in a diverse, community-based cohort of older adults.

Methods: A subset of cognitively healthy participants (n=155; age=69-99yrs; 65% women, 30%/44%/26% Non-Hispanic White/Non-Hispanic Black/Hispanic) from the Washington Heights-Inwood Columbia Aging Project underwent baseline Florbetaben PET (amyloid SUVR), T1-weighted (cortical thickness) and T2-weighted FLAIR MRI (WMH volume), as well as subsequent neuropsychological assessments every 1.5 years (up to 6 visits). Mixed effects models tested changes of four cognitive domains (memory, language, executive function, visuospatial ability) over time and their associations with amyloid (model 1), amyloid and cortical thickness (model 2), and amyloid, cortical thickness, and WMH (model 3), all adjusted for demographics (age, sex, education, race/ethnicity). Model fit was assessed with negative log likelihood information criteria (IC).

Results: Higher baseline amyloid SUVR was associated with faster decline in language, memory, and visuospatial ability. Lower baseline cortical thickness was additionally associated with baseline language, executive function, and visuospatial ability. Higher baseline WMH volume was additionally associated with decline in executive function and visuospatial ability. Interestingly, while WMH volume was not directly associated with memory, it did improve the overall fit of the statistical model ($\Delta\text{IC}=19.7$, $p=5\text{E-}5$) by increasing the effect size of amyloid ($F_{\text{amyloid, model 2}}=18.4$; $F_{\text{amyloid, model 3}}=30.8$).

Conclusion: The contribution of WMH to amyloid and neurodegeneration improved the fit of longitudinal cognitive trajectories over time in memory, executive function, and visuospatial ability, supporting the inclusion of vascular biomarkers in models of cognitive decline in AD.

Keywords: White matter hyperintensity, Amyloid, Cortical Thickness, Longitudinal cognitive decline, Community-based cohort

P26: White matter hyperintensities are related to tau burden in late-Braak stage regions

Patrick Lao¹, Krystal Laing¹, Kay Igwe¹, Anthony Chesebro¹, William Kreisl¹, Herman Moreno², Jose Luchsinger¹, Adam Brickman¹

¹*Columbia University, New York, NY, US*

²*State University of New York Downstate, New York, NY, US*

Introduction: There is mounting mechanistic evidence in mouse models that hypoperfusion leads to the hyperphosphorylation and aggregation of tau. In humans, image-based biomarkers of small vessel cerebrovascular disease, including white matter hyperintensities (WMH), are associated with risk and progression of mild cognitive impairment (MCI) and Alzheimer's disease (AD)-type dementia. The objective of this study was to examine the magnitude and spatial extent of associations between WMH and tau burden, one of the neuropathological culprits of AD, in a cohort of community-dwelling Hispanic late middle-aged adults.

Methods: Participants (n=106; age=65±3yrs; 67% women; 100% Hispanic) underwent T2* FLAIR MRI for quantification of WMH volume, as well as MK-6240 PET and T1 MRI for quantification of MK-6240 standard uptake value ratio (SUVR; inferior cerebellar gray matter reference region; 90-110 min post-injection) in an ongoing study. Total WMH volume was quantitated in cubic centimeters, while MK-6240 SUVR was calculated on the voxel-level. Voxelwise analysis (SPM12) was used to determine the spatial pattern of MK-6240 SUVR associated with total WMH volume.

Results: Descriptively, a scatterplot between WMH volume and regional MK-6240 SUVR demonstrates that WMH are present in the absence of substantial tau burden, suggesting that WMH are not exclusively due to Wallerian-like degeneration related to AD. Voxel-wise, higher WMH volume was associated with higher MK-6240 SUVR in frontal and parietal regions (no family-wise error correction for multiple comparisons, p<0.01).

Conclusions: In a community-based cohort of late middle-aged Hispanics, there is evidence that tau burden in early-Braak stage regions, primarily associated with aging, is not related to WMH, but tau burden in late-Braak stage regions, primarily associated with AD, is related to WMH. These results provide evidence that WMH may have a direct role in AD development and progression.

MK-6240 SUVR associations with total WMH

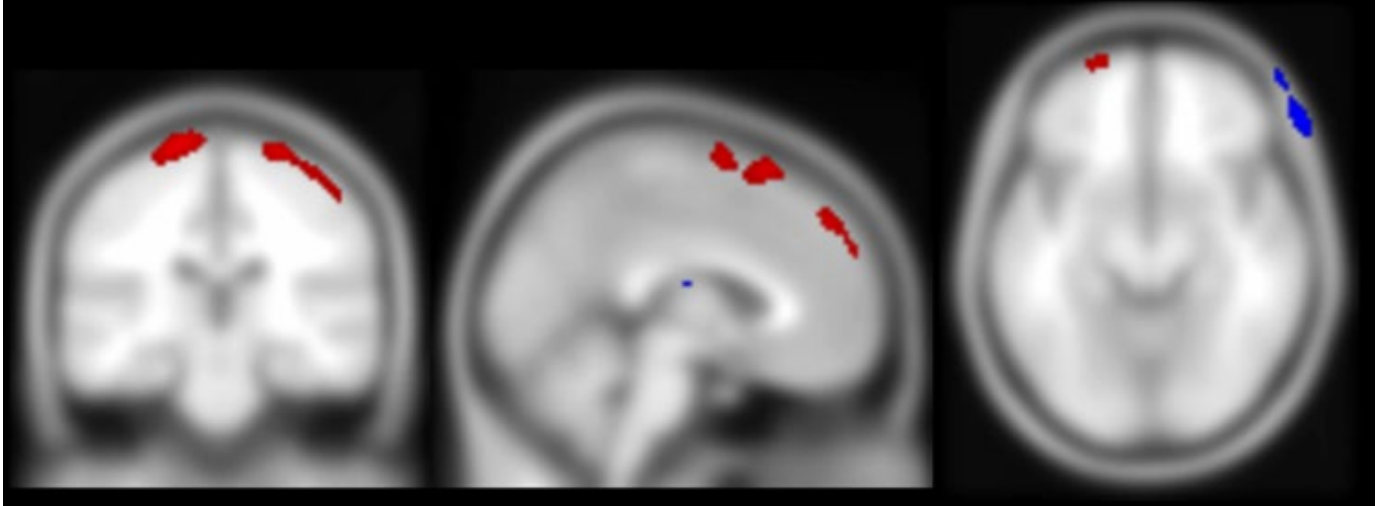


Figure 1. Clusters of significant positive (red) and negative (blue) associations between total WMH and voxelwise MK-6240 SUVR (no FWE correction, $p < 0.01$). Note that only negative associations were observed in the regions of potential off-target uptake.

Keywords: tau PET, MK6240, White matter hyperintensity, late middle-age, Hispanics

P27: Probability template method for analysis of Down Syndrome amyloid PET

Charles Laymon¹, Davneet Minhas¹, Jeffrey James¹, Bradley Christian², Ann Cohen¹, William Klunk¹, Dana Tudorascu¹, Sarah Royse¹, Shahid Zaman³, Benjamin Handen¹

¹University of Pittsburgh, Pittsburgh, PA, US

²University of Wisconsin, Madison, WI, US

³University of Cambridge, Cambridge, UK

Background: A component of the Alzheimer's Biomarkers Consortium-Down Syndrome (ABC-DS) is the study of amyloid deposition in Down syndrome (DS) using PET imaging. A standard method of PET analysis is to define regions-of-interest (ROIs) by parcellating the subject's T1-MR scan using FreeSurfer (FS). FreeSurfer, however, may not be ideal for DS subjects who exhibit variations in anatomy from FS-atlas priors and who are prone to motion during MR acquisition. In this work, we evaluated a Probability Template (PT) [Svarer et al, 2005] approach for improving parcellation results.

Method: MR and [¹¹C]PiB PET scans were acquired by the ABC-DS in 196 DS subjects. MR scans were first processed through the standard FS (version 5.3) pipeline, and parcellation results were rated (4-point scale, unusable-to-good). PT analysis began with selection of twelve templates, skull-stripped (SPM12) MR scans with good FS-based parcellations. Subject-specific PT-processing consisted of (1) skull-stripping the subject MR scan and (2) warping each template to the skull-stripped image (SPM8). The result was 12 versions of every FS region warped to the subject MR scan. For each FS region, the subject-specific PT-ROI was generated as the region of maximum overlap of corresponding template regions with volume equal to the average volume of the post-warp template regions. PT-ROIs for all subjects were rated and compared to FS-ratings. For subjects with acceptable FS- and PT-ratings, [¹¹C]PiB PET was sampled using ROIs from both methods and results were correlated.

Results: Twenty-one subjects had FS-based parcellations rated as unusable. Of these, 13 had acceptable PT parcellations. Correlation of PiB SUVR between the two methods was high (Figure 1).

Conclusion: While the PT-method cannot capture the cortical detail of FreeSurfer, it is frequently able to provide parcellations for cases in which FreeSurfer fails. The PT approach provides a useful alternative to FreeSurfer in the DS population.

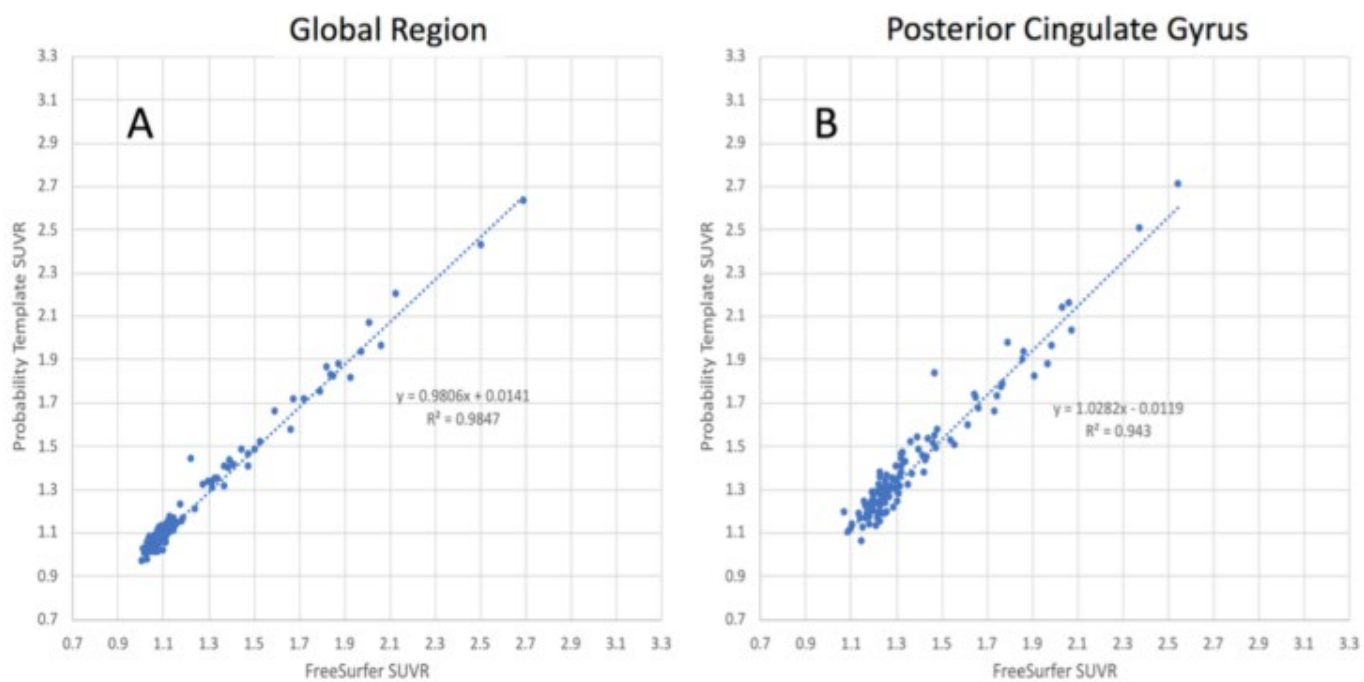


Figure 1. Correlation between PiB SUVR determined using the FreeSurfer pipeline and Probability Template pipeline for (A) a global composite region and (B) the posterior cingulate gyrus, the region with the worst correlation as measured by R^2 .

Keywords: PET, Image Analysis, MRI

P28: Visualizing brain astrocytes - characterization of 3H-BU99008 in human AD brain tissue

Laetitia Lemoine¹, Mona-Lisa Malarte¹, Niina Koistinen¹, Agneta Nordberg^{1,2}

¹*Center of Alzheimer Research, Department of Neurobiology, Care Sciences and Society, Karolinska Institutet, Stockholm, Sweden*

²*Theme Aging, Karolinska University Hospital, Stockholm, Stockholm, Sweden*

Background: Astrocytosis has been shown to be an early phenomenon in AD, and seems to be a promising therapeutic target in AD. However, there are few positron emission tomography (PET) tracers for investigating in vivo astrocyte activation available, therefore there is a growing interest in developing new astrocytic tracers. Presently, the only PET tracer used for the imaging of astrocyte reactivity in AD is 11C-deuterium-L-deprenyl (11C-DED). The aim of our study is to characterize BU99008, in the assessment of reactive astrocytes and neuroinflammation in AD, and to compare its characteristics with the DED.

Methods: In vitro characterization of 3H-BU99008 using competition, saturation binding assay as well as single concentration regional distribution binding assays was performed on AD and control brain tissues. Autoradiographies on large frozen hemisphere using 3H-BU99008 were performed and compared with 3H-DED.

Results: Saturation binding studies showed differences between AD (Bmax: 90fmol/mg; Kd: 2.2nM) and control (Bmax: 58fmol/mg; Kd: 0.65nM). Competition binding studies showed a similar IC50 in the nanomolar range for AD and control. Unlabeled deprenyl could not displace 3H-BU99008 when the reverse was possible. Single concentration regional binding distribution showed significantly higher binding in parietal cortex and cerebellum of AD in comparison to control. High binding was also observed in hippocampus and temporal cortex. Autoradiography on adjacent sections from AD cases shows similar regional distribution between 3H-BU99008 and 3H-DED but with different binding intensity.

Conclusions: To be able to detect astrocytosis early in AD, specific astrocyte biomarkers are needed. Our data shows that BU99008, proposed as novel astrocyte PET tracer, shows binding in CN and AD brain tissue in the nanomolar range, however with some difference in affinity with 3H-deprenyl. More characterization is needed to understand its binding properties and future use in comparison to existing astrocytic biomarkers.

Keywords: Deprenyl, astrocytes, BU99008, autoradiography, PET

P29: Application of an epidemic spreading model to characterize amyloid beta accumulation in autosomal dominant Alzheimer's disease mutation carriers

Elizabeth Levitis¹, Jacob W Vogel¹, Gregory Kiar¹, Thomas Funck¹, Yasser Iturria-Medina¹, Alan C Evans¹

¹*Montreal Neurological Institute, McGill University, Montreal, QC, Canada*

Previous work has shown that the pattern of amyloid beta (A β) deposition in individuals spanning the sporadic AD spectrum can be reproduced using an epidemic spreading model (ESM), which simulates the spread of A β as a diffusive process occurring across neuronal connections. We apply the ESM on subjects with autosomal dominant AD and evaluate the utility of the ESM for longitudinal evaluation and prediction.

Co-registered PiB PET scans from the Dominantly Inherited Alzheimer's Network dataset were used alongside Freesurfer-generated subject-specific DKT segmentations to quantify A β binding probabilities for 78 ROIs using a cerebellar or brainstem reference for 215 and 121 mutation carriers (MC) at baseline and follow-up, respectively. The ESM was first used to identify candidate seed regions and simulate the trajectory of A β spread across a template structural connectome. We then applied the ESM to learn the relationship between two initial timepoints for each subject and extrapolated this relationship to predict A β patterns of 53 MC who had subsequent visits (Fig 1). Categorizing subjects as accumulators or non-accumulators based on their mean rate of change in cortical A β binding allowed us to explore the relationship between model performance and A β spread.

The ESM reproduced baseline aggregated deposition patterns with an accuracy of 40% (Fig 2). The posterior cingulate and caudal anterior cingulate regions were found as the most likely seeds. Using parameters fit between the first two timepoints, the ESM learned the rate of A β change with an average accuracy of 24% for subjects consistently accumulating A β (Fig 3).

This work demonstrates that A β spread may be described in familial AD mutation carriers using a diffusion model. Efforts to predict out-of-sample regional patterns using the ESM are limited due in part to heterogeneous A β changes over the disease progression.

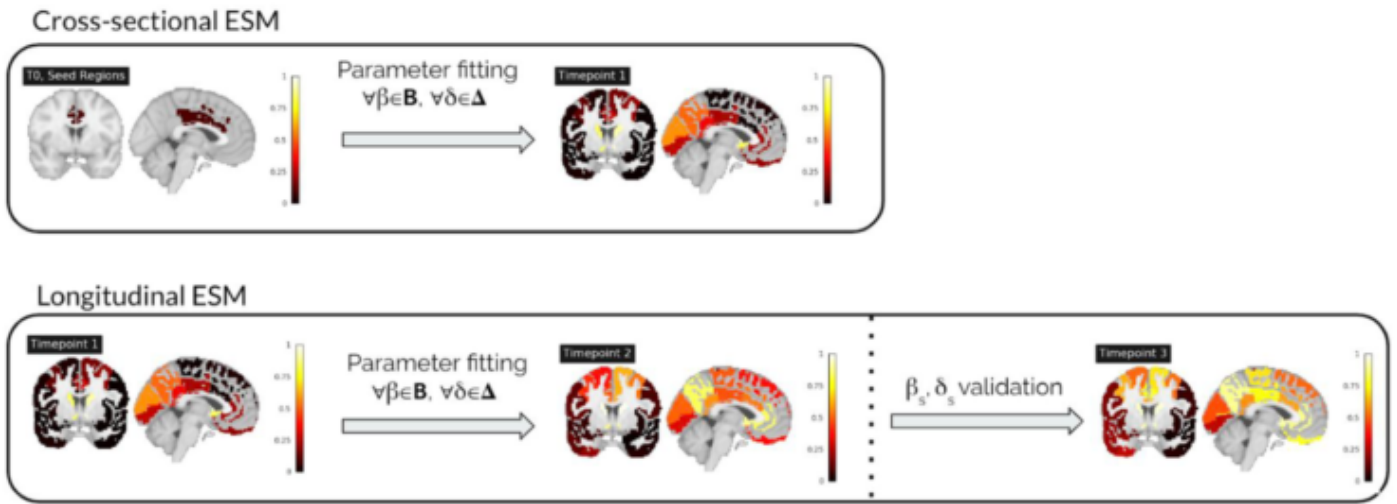


Fig 1. Top panel is a depiction of the original, cross-sectional ESM workflow. The bottom panel depicts the modifications made for the longitudinal ESM workflow. For each subject, parameters that best explain the change observed in the regional $A\beta$ pattern between timepoints 1 and 2 are selected, and these parameters are used to predict the regional $A\beta$ pattern at the 3rd timepoint using the 2nd timepoint as the initial pattern.

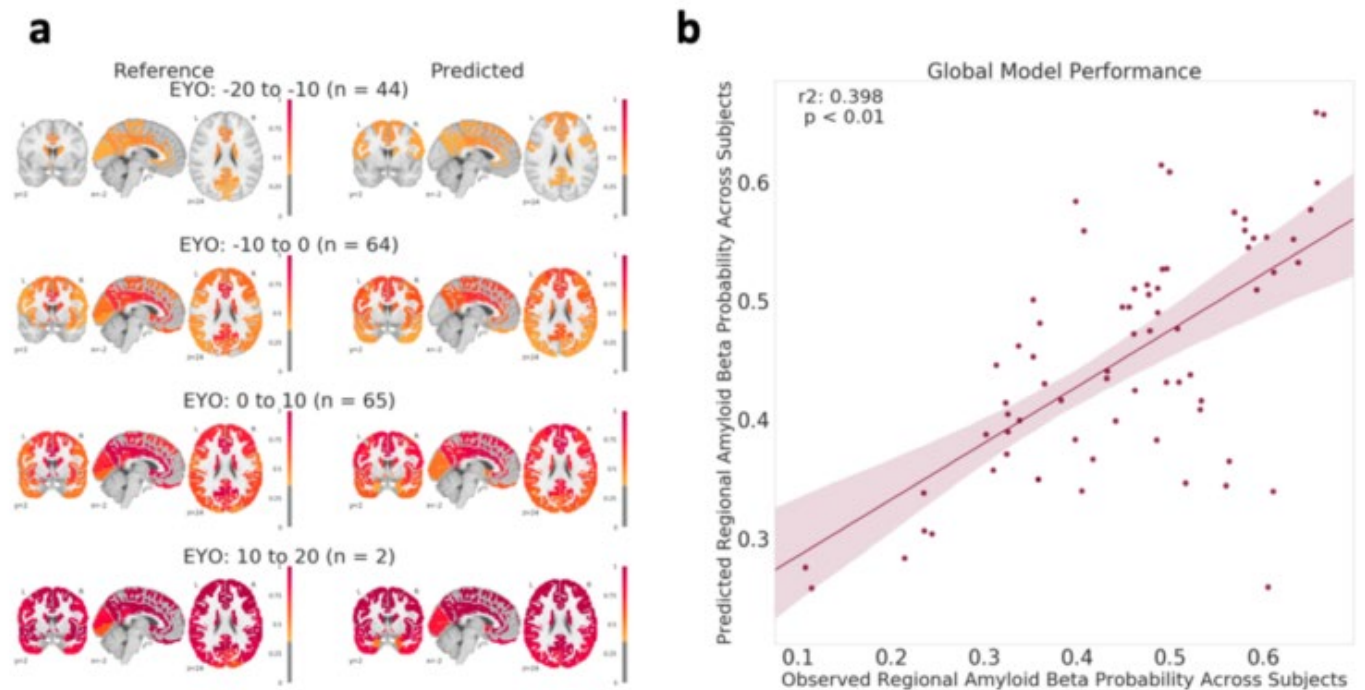


Fig 2. (a) Qualitative evaluation of model performance depicting the average observed regional probabilities (left) and the values predicted by the ESM (right). (b). Quantitative evaluation of model performance across all individuals, where each dot corresponds to an ROI.

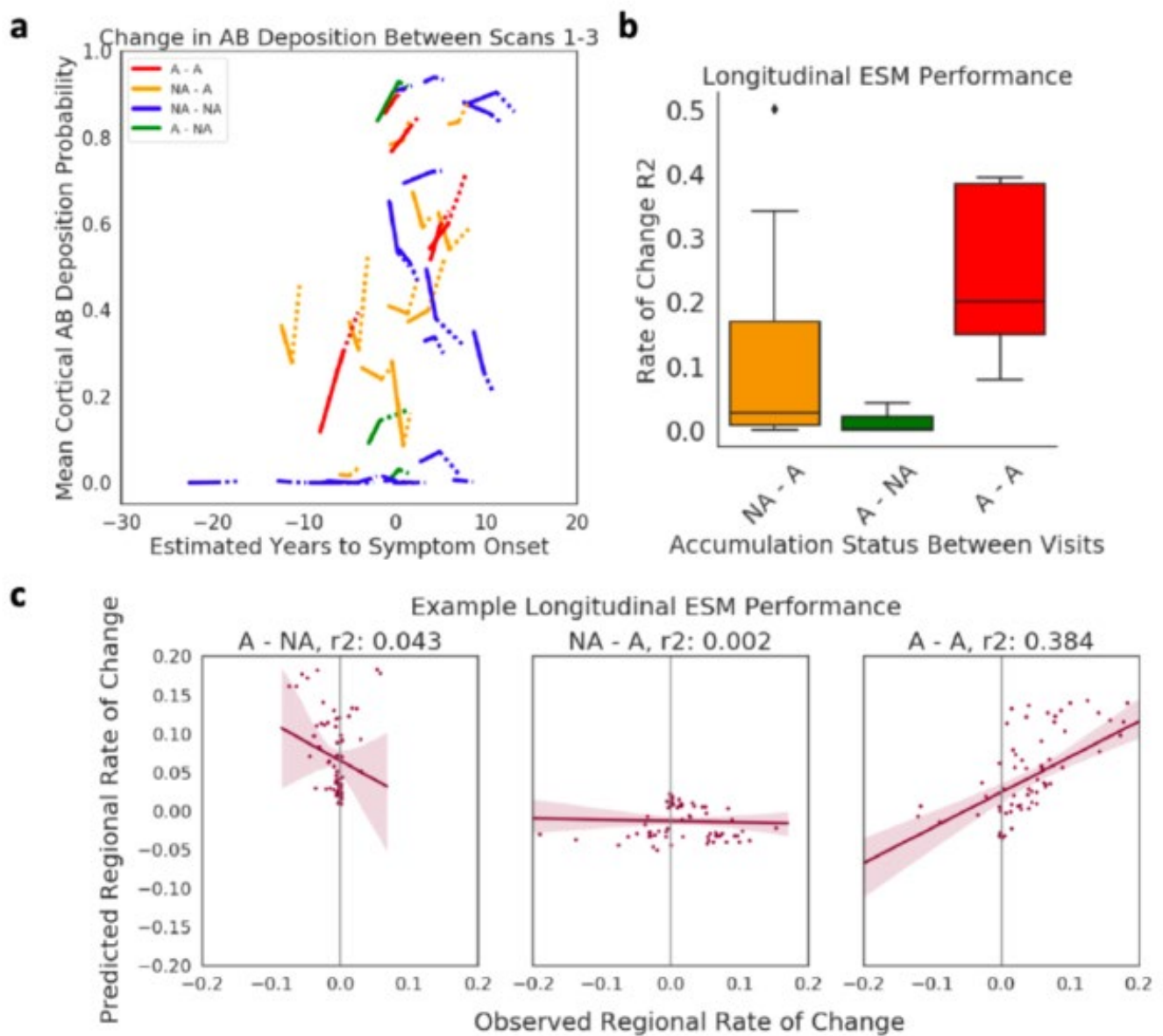


Fig 3. (a) Spaghetti plot depicting changes in $A\beta$ probabilities for mutation carriers who have three timepoints, with the second interval depicted using a dashed line. Subjects are color-coded based on whether they're consistently accumulating between both scans (A-A), consistently not accumulating (NA-NA), or alternating in accumulation status between scans (NA-A or A-NA) (b) Model accuracy for predicting within-subject regional rate of change across mutation carriers who are NA-A, A-A, or A-NA. (c) Predicted and observed values for one exemplar individual from each category in (b) is depicted, where each dot corresponds to an ROI.

Keywords: Alzheimer's disease, amyloid beta, computational modelling, DIAN

P30: Phantom-based harmonization of PET image reconstruction parameters between the Siemens ECAT HR+ PET and the GE Discovery MI PET/CT scanners

Cristina Lois¹, Kira Grogg¹, Georges El Fakri¹, Keith Johnson¹, Julie Price¹

¹Massachusetts General Hospital, Boston, MA, US

Background: Accuracy of PET quantification depends on detector hardware, image reconstruction and corrections. Systematic inter-scanner variability hampers the ability to compare and combine data from multiple scanners, and harmonization of imaging procedures is needed to maximize study power [1].

The Siemens ECAT HR+ PET scanner (HR+) has been of primary use by our group for 20 years. Recently, a GE Discovery MI (GE-DMI) PET/CT with increased sensitivity, PSF and TOF capability [2], was installed in our center.

Objective: To identify optimal reconstruction parameters that achieve the most comparable quantitative values between data acquired using the GE-DMI and the legacy HR+ data. The ultimate goal is to robustly combine data acquired in different individuals on these two scanners in our ongoing studies.

Methods: Jaszczak and Hoffman phantoms (total activity ~50MBq ¹⁸F-FDG) were imaged in both scanners. Our typical ¹⁸F-AV1451 protocol (6 5-min frames, OSEM (16 subsets 4 iterations (16s4i), 5mm filter) was applied for the HR+. For the GE-DMI, list-mode phantom data were rebinned into varying frame lengths (5, 2.5, 1.5, 1-min). Different reconstructions were evaluated: OSEM 34s2i and 16s4i, with and without PSF and TOF, and various filters. Regions-of-interest (ROI) were delineated in multiple phantom sections (spheres, vials, background for Jaszczak; cortical, subcortical for Hoffman). Quantitative ROI metrics were computed: contrast-to-noise ratio (CNR), signal-to-noise (SNR), contrast recovery (CR).

Results and Conclusions: The GE-DMI reconstructions evaluated in phantoms had large impact in image quality and quantification (Fig.1). GE-DMI data reconstructed with OSEM 34s2i (no PSF, no TOF), 1.5-min frames, 7 mm filter, presented an optimal balance of CNR, SNR, and CR (Fig.1) and were the most similar to the HR+ (Hoffman voxel-wise correlation, $r^2=0.98$, Fig.2). Evaluation of these results in a human tau PET data set is ongoing.

[1] Joshi et al. Neuroimage 2009, 46(1)

[2] Pan et al. Med Phys. 2019

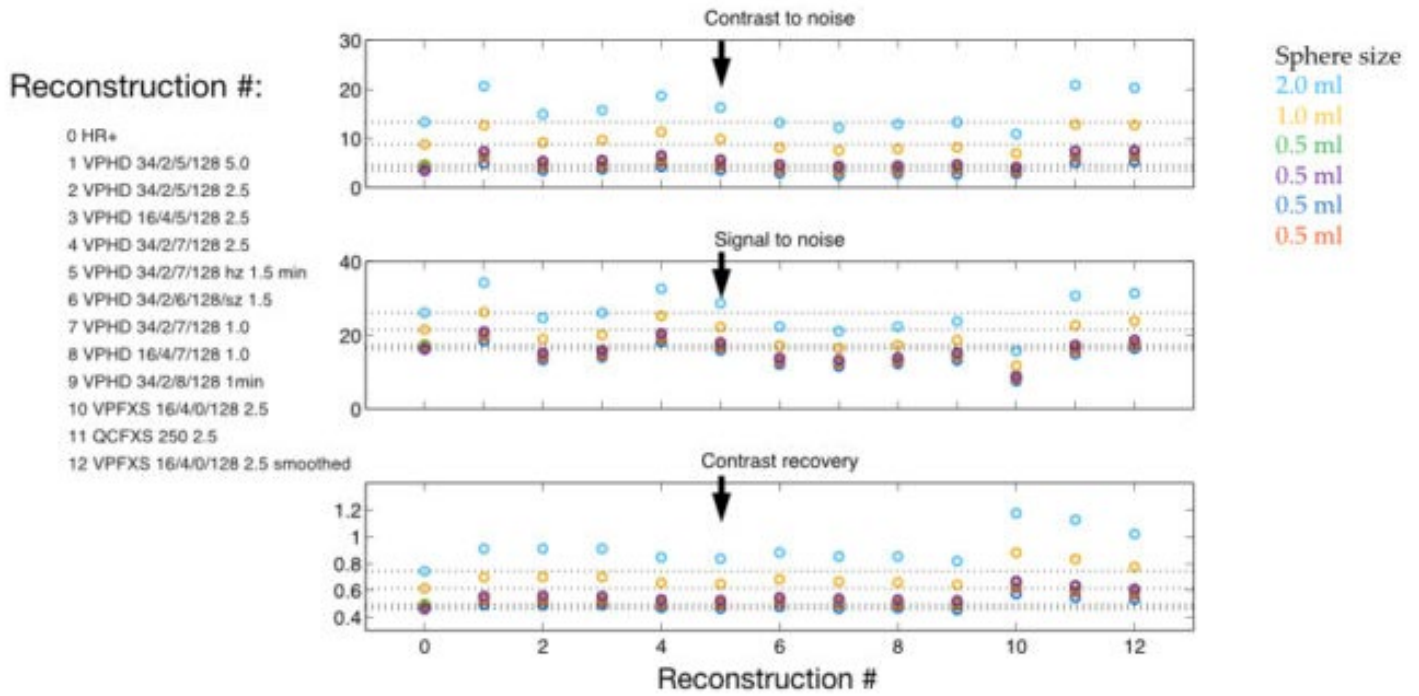


Figure 1. Visual and quantitative comparison of Jaszczak phantom scanned in HR+ and GE-DMI (several reconstructions). Arrow indicates the optimal reconstruction, with good balance of the quantitative metrics. Dotted lines show HR+ values.

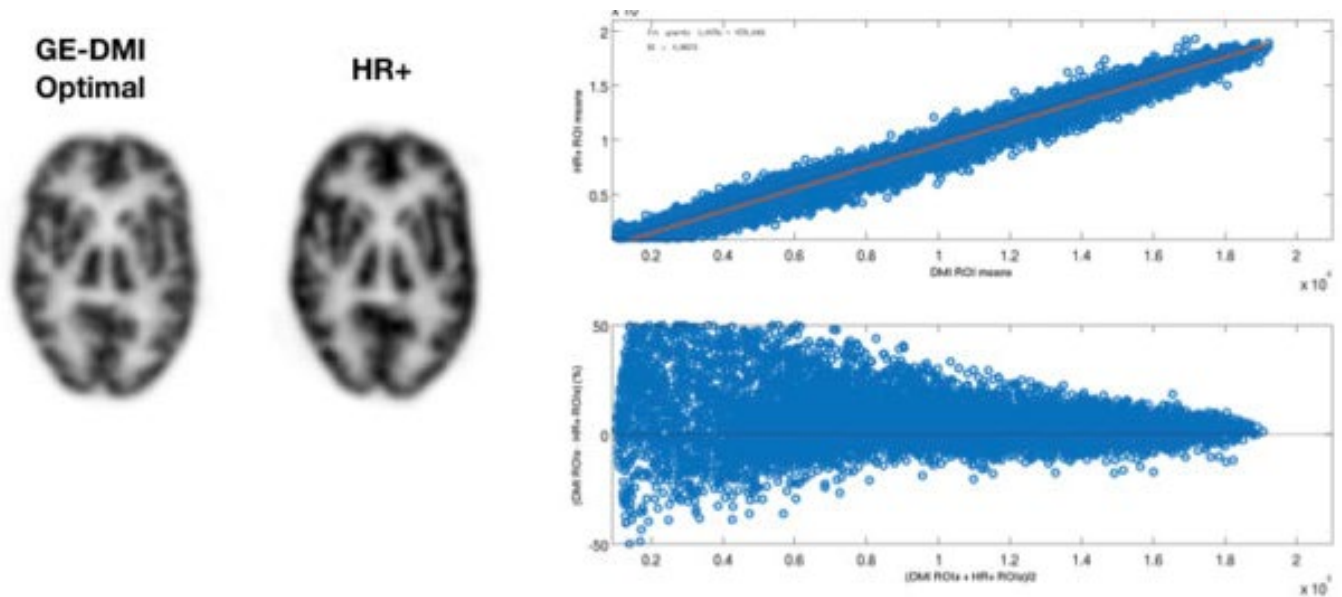


Figure 2. Visual and quantitative comparison of Hoffman phantom scanned in HR+ and GE-DMI (optimal GE-DMI reconstruction). Voxel-wise comparison of phantoms acquired in both scanners show high correlation.

Keywords: Harmonization, quantification, phantoms

P31: Age prediction and amyloid deposition in SuperAgers

Adam Martersteck^{1,2}, Pierre Besson^{2,3}, Jaiashre Sridhar¹, Beth Makowski-Woidan¹, Todd Parrish², Aggelos Katsaggelos⁴, M.-Marsel Mesulam^{1,5}, Kathleen Bandt³, Emily Rogalski^{1,6}

¹Mesulam Center for Cognitive Neurology and Alzheimer's Disease, Northwestern University Feinberg School of Medicine, Chicago, IL, US

²Department of Radiology, Northwestern University Feinberg School of Medicine, Chicago, IL, US

³Department of Neurological Surgery, Northwestern University Feinberg School of Medicine, Chicago, IL, US

⁴Department of Electrical & Computer Engineering, Northwestern University, Chicago, IL, US

⁵Department of Neurology, Northwestern University Feinberg School of Medicine, Chicago, IL, US

⁶Department of Psychiatry and Behavioral Sciences, Northwestern University Feinberg School of Medicine, Chicago, IL, US

Background: Machine learning techniques to predict biologic brain age versus chronologic brain age may be a potential biomarker for accelerated pathologic aging. Here, we use these same techniques to identify potential protective mechanisms of resilience and resistance to brain aging in SuperAgers. SuperAgers are over age 80 with episodic memory at least as good as that of average middle-age adults. SuperAgers have previously been shown to have higher cortical thickness than age-matched peers and resist cortical atrophy over time.

Objective: We examined whether SuperAgers resist amyloid accumulation using ¹⁸F-florbetapir PET and whether their predicted brain age is lower than their chronologic age using a deep learning framework.

Methods: We used a previously established graph convolutional neural network (gCNN), trained on 8,046 healthy individual's publicly available T₁-weighted images (age=6-89 years). The gCNN predicts age entirely based on the geometric shape of the brain. Briefly, it takes the x,y,z coordinates of four Freesurfer surfaces: pial and white, left and right hemispheres, 10,242 vertices each, affinely registered to MNI-space. Using 5-fold cross validation on 8,046 participants, the gCNN predicted age with Pearson's r=0.93 and average absolute error of 4.58 years. The model was implemented on MRI scans from 11 SuperAgers with florbetapir PET scans. Amyloid PET positivity was assessed with 6 bilateral Clark et al. 2011 cortical regions and full cerebellar reference region.

Results: gCNN predicted brain age from 11 SuperAgers was significantly lower than their chronologic age ($p < 0.0001$; mean difference 20.76 years \pm 8.65 [s.d.]). Only one of the 80+-year-old SuperAgers was amyloid positive (SUVR > 1.17).

Conclusions: SuperAgers show a mismatch between chronologic and biologic brain age, consistent with our previous reports. AD pathology is present in approximately 30% of cognitive healthy adults >65, but only <10% of SuperAgers. Both results suggest SuperAging may inform mechanisms of resistance to age-related changes.

Keywords: Deep learning, successful aging, amyloid

P32: PiB tracer delivery decreases overtime in preclinical AD – impact for amyloid pathology measurement

Danielle Mayblyum¹, J. Alex Becker¹, Aaron Schultz¹, Michelle Farrell¹, Heidi Jacobs¹, Zoe Rubinstein¹, Justin Sanchez¹, Emma Thibault¹, Reisa Sperling^{1,2}, Julie Price¹, Keith Johnson^{1,2}, Bernard Hanseeuw^{1,3}

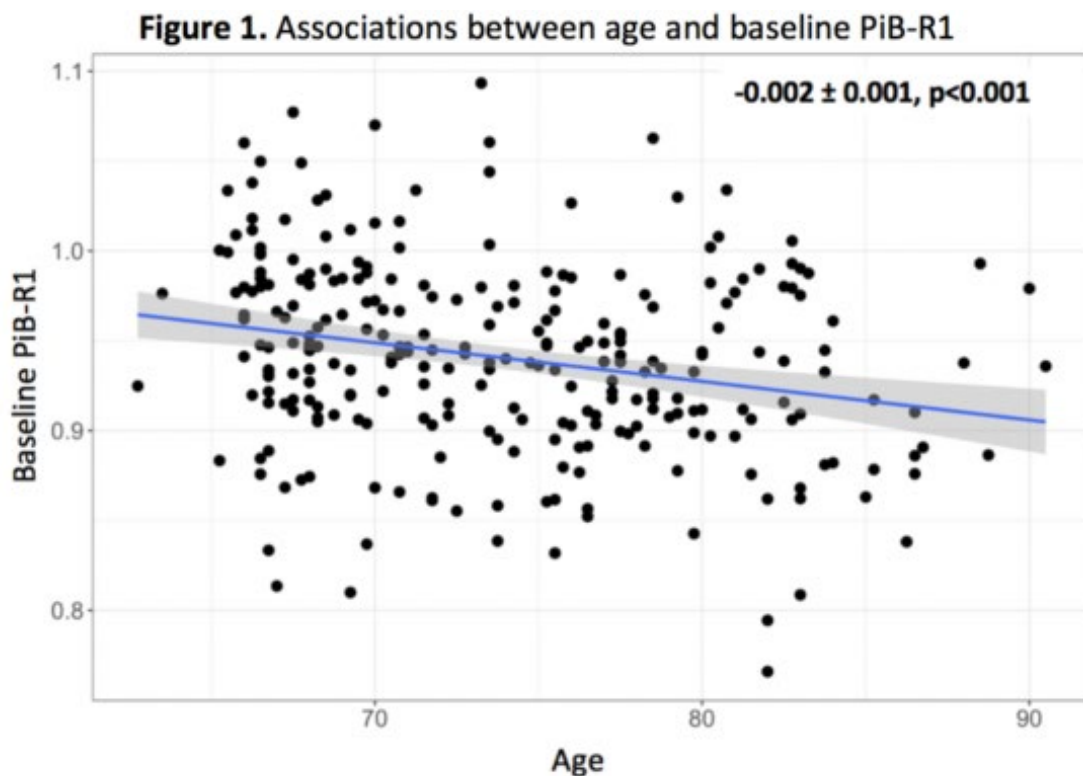
¹Massachusetts General Hospital, Boston, MA, US

²Brigham and Women Hospital, Boston, MA, US

³Cliniques Universitaires Saint-Luc, Brussels, Belgium

Background: PET measures of relative tracer delivery are potentially useful to predict Alzheimer's disease progression and/or to better estimate PET measures of A β pathology. Therefore, we aimed to characterize PiB-R1, a measure of tracer delivery derived from the PiB-PET full dynamic scan, in the longitudinal dataset available in the Harvard Aging Brain Study (HABS).

Methods: We analyzed baseline (N=269) and longitudinal (N=212, median follow-up: 4 years) dynamic PiB-data from clinically normal HABS participants. We calculated PiB-R1 and 40-60min PiB-DVR using SRTM2 in the same neocortical aggregate (FLR) with cerebellar gray reference. We explored associations between PiB-R1, demographics, and subsequent changes in the Preclinical Alzheimer's Cognitive Composite (PACC-5). We also evaluated cross-sectional and longitudinal associations between PiB-R1 and PiB-DVR.

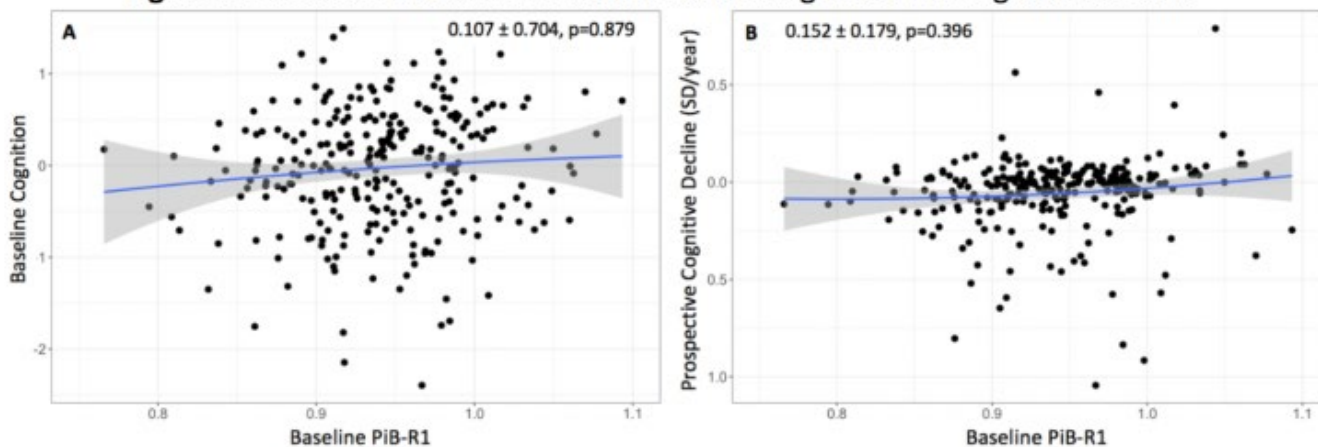


Legend: Baseline PiB-R1 is negatively associated with baseline age, adjusting for sex, education, and $\epsilon 4$ status.

Results: Baseline PiB-R1 was lower at older ages (Fig.1, $p<0.001$) and in males ($p=0.003$). Overall, it was not linearly associated with PiB-DVR ($p=0.412$), APOE e4 carriage ($p=0.162$), education years ($p=0.968$), baseline cognition (Fig.2A, $p=0.879$), or subsequent cognitive decline (Fig.2B, $p=0.396$). Of note, PiB-

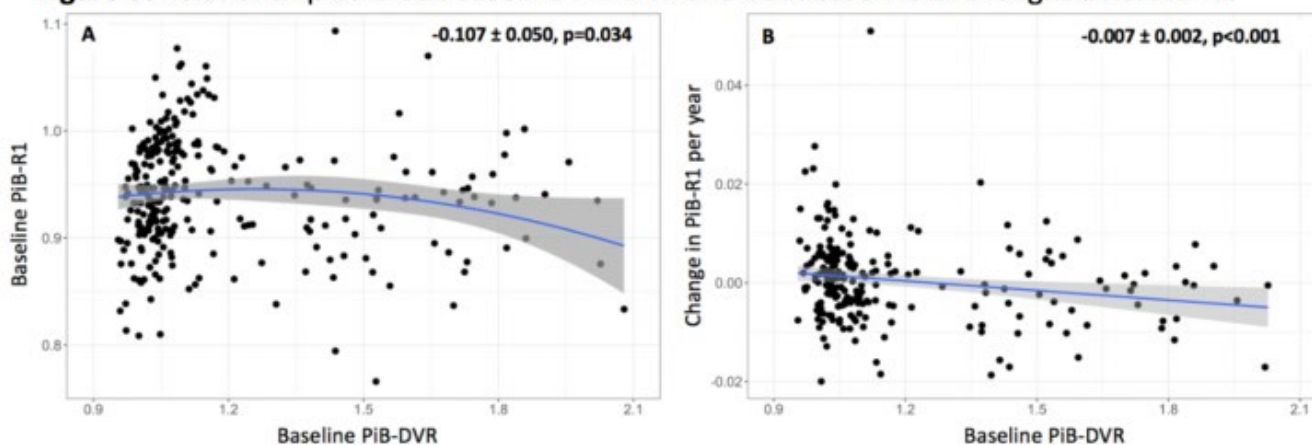
DVR had a quadratic association with PiB-R1 (Fig.3A, $p=0.034$), suggesting that PiB-R1 initially increased, and then decreased with increasing levels of PiB-DVR. Longitudinally, baseline PiB-DVR predicted subsequent decline in PiB-R1 (Fig.3B, $p=0.002$), adjusting for demographics. Results were similar when using Logan-DVR instead of SRTM2-DVR as both metrics were highly correlated ($R^2=0.96$).

Figure 2. PiB-R1 is not associated with baseline cognition and cognitive decline



Legend: Baseline PiB-R1 did not relate to baseline cognition (A) or predict subsequent cognitive decline (B) in the PACC5. All model values were adjusted for subject demographics.

Figure 3. Relationship between baseline PiB-DVR and both baseline and longitudinal PiB-R1



Legend: Baseline PiB-DVR shows an approximate quadratic relationship with baseline PiB-R1 (A) and predicts rate of decline of PiB-R1 (B). Models are adjusted for subject demographics.

Conclusion: PiB tracer delivery decreases with age in clinically normal adults, specifically in individuals with high- $A\beta$ burden. Overall, the association with $A\beta$ measures is weak although the relationships between $A\beta$ and tracer delivery at low retention levels deserve further attention. The PiB-R1 parameter is not associated with concurrent or subsequent cognition.

Keywords: R1, PiB, cognitive decline

P33: MRI and PET data harmonization in a two-site Down syndrome study

Davneet Minhas¹, Zixi Yang¹, John Muschelli², Charles Laymon¹, Matthew Zammit³, Paul Ellison³, Sterling Johnson³, Chester Mathis¹, Ciprian Crainiceanu², William Klunk¹, Benjamin Handen¹, Bradley Christian³, Ann Cohen¹, Dana Tudorascu¹

¹*University of Pittsburgh, Pittsburgh, PA, US*

²*Johns Hopkins University, Baltimore, MD, US*

³*University of Wisconsin-Madison, Madison, WI, US*

Introduction: Harmonization of MR data, structural segmentation, and MR-based PET SUVR quantification from multisite studies presents a challenging problem. In this study we used the RAVEL¹ method to normalize T1-MRI intensities collected at two sites in Down syndrome (DS) populations. Effects on cortical thickness and on MR-based quantification of [11C]PiB SUVR were evaluated.

Methods: MRI and [11C]PiB scans for forty participants (mean age: 39.13±6.60), age- and sex- matched from two sites were used. MR intensity histograms pre and post RAVEL processing were evaluated. FreeSurfer (v5.3.0) was used with and without RAVEL for MR parcellation, producing regional cortical thicknesses and PiB SUVRs. Neuroradiologists rated FreeSurfer parcellation accuracy before and after RAVEL. Effect sizes were computed for differences between PiB(+) and PiB(-) subjects within each method.

Results: Figure 1 shows per-scan histograms of MRI intensity classified by PiB global-SUVR status and site, with and without RAVEL. PiB SUVRs showed very good agreement between methods for both global and anteroventral striatum (AVS) regions (ICC's >0.99, not shown). Neuroradiological ratings of the hippocampus segmentation were higher after RAVEL (Figure 2). Differences in effect sizes ranged from 5% to 40% for cortical thickness (Table 1).

Discussion: RAVEL was effective at MRI intensity normalization in this population. As seen in Figure 1 individual intensity histograms were widely spread without RAVEL, while almost perfect overlap was observed with RAVEL. Neuroradiologist evaluations also demonstrated that RAVEL normalization improves segmentation. Harmonization using RAVEL had a much greater impact on cortical thickness measures than on PET SUVR measures. Large differences observed in effect sizes suggest that combining data from different sites/scanners should be properly addressed.

Figure 1: Individual intensity histograms with RAVEL and without RAVEL (raw) by PiB status and study site (x-axes shows probabilities).

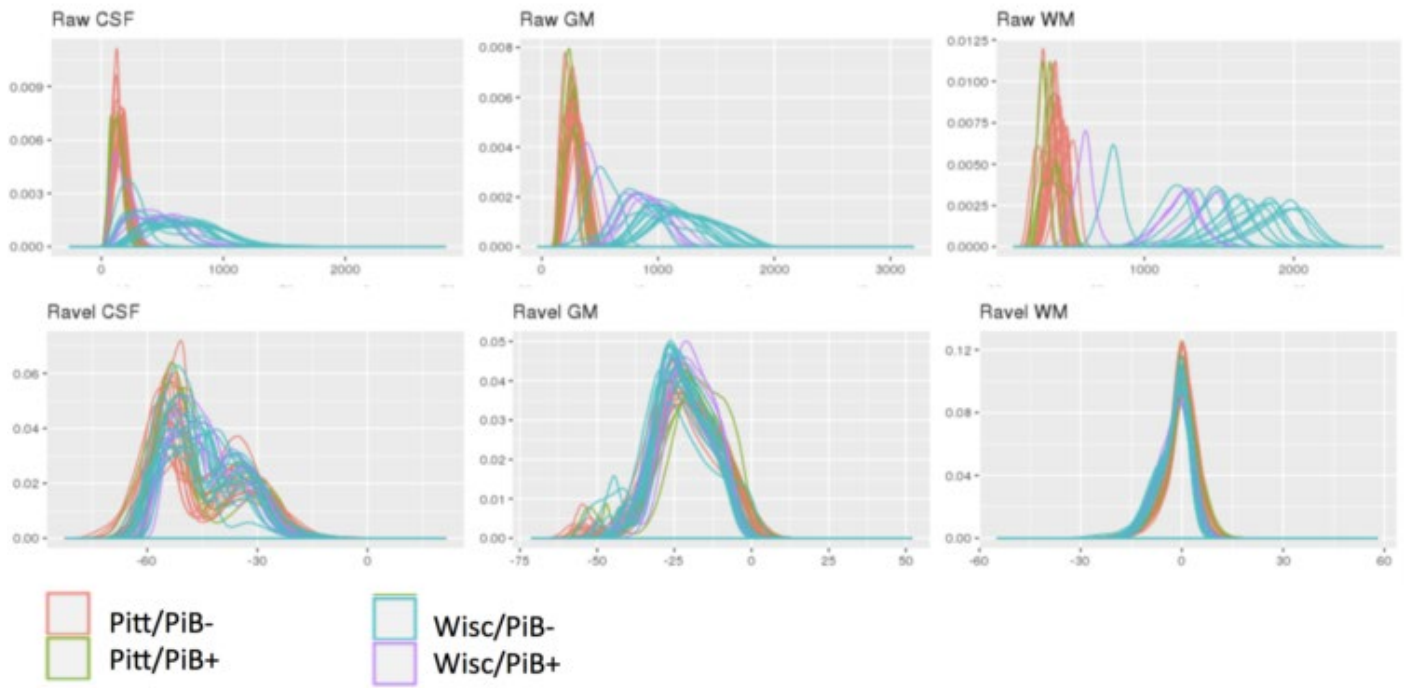


Figure 2: Neurological Ratings (Scale: 1=poor, 2=some errors, 3=good, 4=excellent).

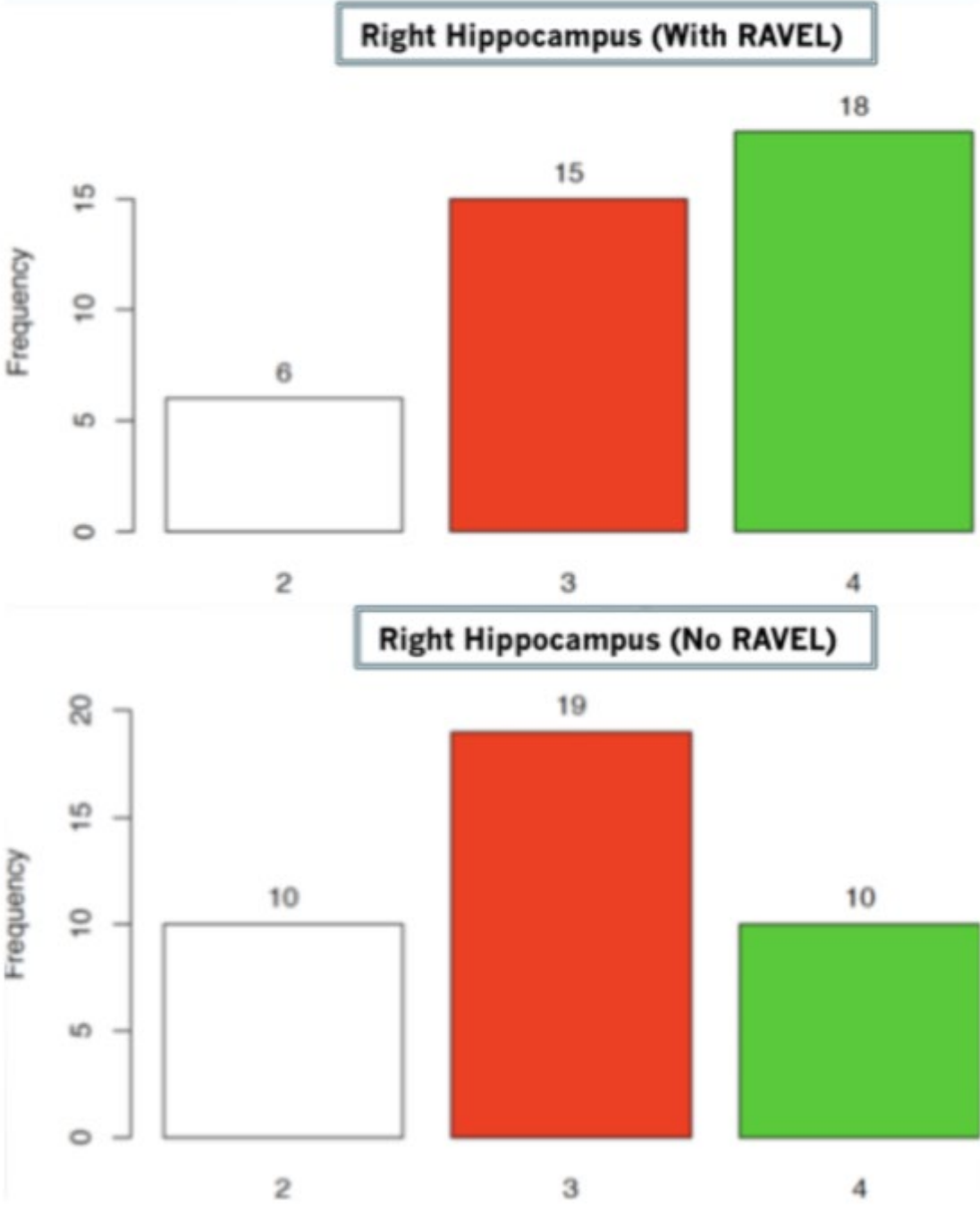


Table 1. Descriptive statistics and effect sizes.

Measure	Mean (SD)				Effect sizes	
Status	Negative		Positive			
	No RAVEL	RAVEL	No RAVEL	RAVEL	No RAVEL	RAVEL
SUVR						
	N=30	N=30	N=10	N=10		
Global	1.1 (0.07)	1.11 (0.07)	1.78 (0.4)	1.8 (0.39)	3.19	3.26
AVS	1.28 (0.18)	1.31 (0.19)	2.26 (0.37)	2.3 (0.38)	3.86	3.80
Cortical thickness						
Left Entorhinal	3.77 (0.4)	3.68 (0.39)	3.37 (0.44)	3.49 (0.42)	0.95	0.45
Right Entorhinal	3.93 (0.37)	3.94 (0.38)	3.55 (0.48)	3.55 (0.48)	0.91	0.90
Left Fusiform	2.82 (0.2)	2.87 (0.18)	2.65 (0.21)	2.71 (0.16)	0.81	0.90
Right Fusiform	2.95 (0.19)	2.94 (0.18)	2.78 (0.27)	2.82 (0.26)	0.77	0.53
Left Inferior Temporal	2.79 (0.27)	2.93 (0.2)	2.65 (0.22)	2.82 (0.14)	0.50	0.59
Right Inferior Temporal	2.86 (0.26)	2.92 (0.21)	2.75 (0.2)	2.82 (0.19)	0.41	0.47
Left Middle Temporal	2.86 (0.26)	3.09 (0.2)	2.75 (0.21)	2.94 (0.21)	0.43	0.71
Right Middle Temporal	2.8 (0.27)	3.01 (0.25)	2.7 (0.27)	2.86 (0.28)	0.37	0.58

Keywords: PET Harmonization, MRI, Down syndrome

P34: Sex-specific differences in [¹⁸F]AV-1451 off-target retention

Davneet Minhas¹, Zheming Yu¹, Charles Laymon¹, Brian Lopresti¹, Beth Snitz², Dana Tudorascu³, Howard Aizenstein⁴, Oscar Lopez², Chester Mathis¹, William Klunk⁴, Ann Cohen⁴

¹*Department of Radiology, University of Pittsburgh, Pittsburgh, PA, US*

²*Department of Neurology, University of Pittsburgh, Pittsburgh, PA, US*

³*Department of Medicine, University of Pittsburgh, Pittsburgh, PA, US*

⁴*Department of Psychiatry, University of Pittsburgh, Pittsburgh, PA, US*

Background: [¹⁸F]AV-1451 PET imaging has recently been used to evaluate sex-specific differences in early tau deposition. The objective of this work was to assess voxel-level differences in off-target [¹⁸F]AV-1451 retention, which may confound comparisons of tau deposition between sexes, in two independent cohorts.

Methods: For the UPitt cohort, [¹⁸F]AV-1451 PET and T1 MR images were acquired in 162 “non-demented” (CDR global: 0 or 0.5) Caucasian subjects (95F,67M;74±5y) at the University of Pittsburgh. For the ADNI cohort, fully processed [¹⁸F]AV-1451 PET SUVR and T1 MR images were downloaded from the ADNI database for 159 non-demented Caucasian subjects (83F,76M;76±8y). SUVR PET images for the UPitt cohort were created using FreeSurfer cerebellar gray matter (GM) as reference. Cohort-specific templates were created using the SPM12 DARTEL toolbox, and SUVR PET images were warped to respective cohort templates using subject-specific flow fields. Warped UPitt SUVR images were smoothed by 6mm; no additional smoothing was applied to warped ADNI SUVR images. Voxel-wise ANCOVAs of [¹⁸F]AV-1451 SUVR between sexes were performed using age, MMSE, education, and global amyloid status ([¹¹C]PiB for UPitt; [¹⁸F]AV45 for ADNI) covariates.

Results: Demographic data for the UPitt and ADNI cohorts are presented in Table 1. Significantly greater [¹⁸F]AV-1451 SUVR in females was observed in meningeal tissue on the frontal, parietal, occipital, and lateral temporal cortical surfaces in both cohorts (Figure 1). In the UPitt cohort, females also demonstrated significantly greater SUVR in meningeal tissue along the midline and anterior and posterior to the medial temporal cortex. Significantly greater retention in UPitt cohort males was observed in the basal ganglia.

Conclusion: These findings suggest sex comparisons of tau deposition using [¹⁸F]AV-1451 may be reflective of differences in off-target meningeal binding rather than actual tau deposition. Early detection of tau deposition in females may, in fact, be confounded by [¹⁸F]AV-1451 meningeal binding.

Table 1. Demographics

UPitt Cohort	Female	Male	<i>P</i> value*
	95	67	
Age, mean (SD), y	73.8 (4.7)	74.0 (4.7)	0.991
Education, mean (SD), y	14.6 (2.7)	15.2 (2.4)	0.162
MMSE, mean (SD)	28.3 (1.6)	28.3 (1.6)	0.731
Positive [¹¹ C]PiB status, No. (%)	20 (20)	16 (24)	0.670
Global [¹¹ C]PiB SUVR, mean (SD)	1.28 (0.33)	1.27 (0.27)	0.672
ADNI Cohort	Female	Male	<i>P</i> value*
	83	76	
Age, mean (SD), y	73.5 (7.9)	78.8 (7.5)	<0.001
Education, mean (SD), y	16.1 (2.3)	17.3 (2.5)	<0.001
MMSE, mean (SD)	29.1 (1.1)	28.6 (1.6)	0.025
Positive [¹⁸ F]AV45 status, No. (%)	34 (41)	29 (38)	0.718
Global [¹⁸ F]AV45 SUVR, mean (SD)	1.13 (0.17)	1.11 (0.18)	0.246

* *P* values were from a nonparametric Wilcoxon test for continuous variables or Chi-square test for categorical variables

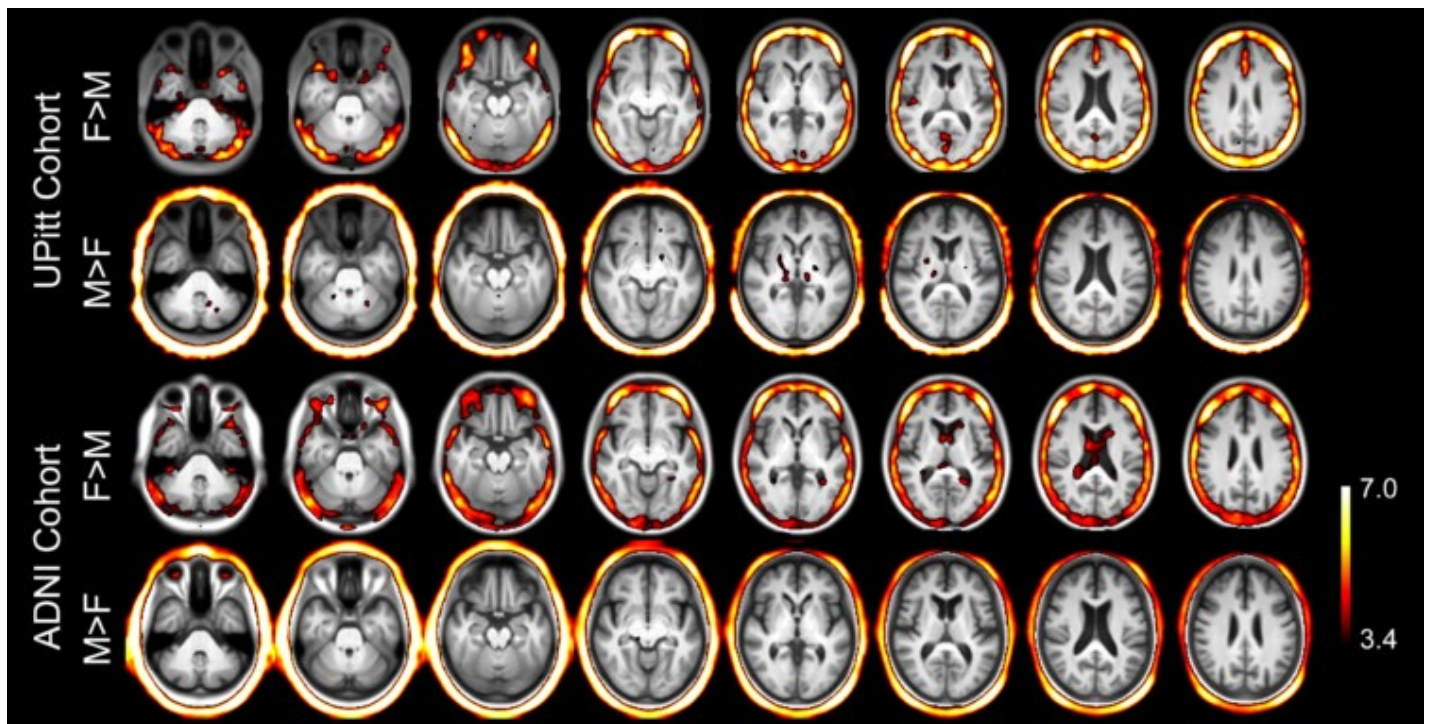


Figure 1. T-score maps of sex-related differences in [¹⁸F]AV-1451 SUVR overlaid on cohort-specific average MR images. A t-score of 3.4 corresponds to an uncorrected *p*-value of 0.0005 in both cohorts. T-scores of 5.4 and 4.9 correspond to FWE-corrected *p*-values of 0.05 for the UPitt cohort and ADNI cohort, respectively.

Keywords: AV1451, flortaucipir, tau, off-target, sex

P35: Polygenic risk for Cerebrospinal Fluid (CSF) amyloid predicts brain amyloid in clinically normal older adults

Annah Moore^{1,2,3}, Logan Dumitrescu^{1,2}, Aaron Schultz⁴, Neha Raghavan^{5,6,7}, Keith Johnson⁴, Richard Mayeux^{5,6,7}, Reisa Sperling⁴, Timothy Hohman^{1,2}, Elizabeth Mormino⁸

¹*Vanderbilt Memory and Alzheimer's Center, Vanderbilt University Medical Center, Nashville, TN, US*

²*Vanderbilt Genetics Institute, Vanderbilt University Medical Center, Nashville, TN, US*

³*Department of Pharmacology, Vanderbilt University Medical Center, Nashville, TN, US*

⁴*Department of Neurology, Massachusetts General Hospital, Nashville, TN, US*

⁵*Department of Neurology, Columbia University Medical Center and The New York Presbyterian Hospital, New York, NY, US*

⁶*The Taub Institute for Research on Alzheimer's Disease and The Aging Brain, Columbia University Medical Center and The New York Presbyterian Hospital, New York, NY, US*

⁷*The Institute for Genomic Medicine, Columbia University Medical Center and The New York Presbyterian Hospital, New York, NY, New York, NY, US*

⁸*Department of Neurology and Neurological Sciences, Stanford University School of Medicine, Palo Alto, CA, US*

Objective: Early detection may be key to the effective treatment of Alzheimer's Disease (AD), and polygenic risk scores (PRS) may increase sensitivity to detect preclinical disease among cognitively normal older individuals.

Methods: Two PRS were calculated using genome-wide association study (GWAS) summary statistics for (1) clinical AD diagnosis (PRS-ADdx; Jansen et al, 2019, n=455,258), and (2) cerebrospinal fluid (CSF) amyloid β_{42} (PRS-CSFA β_{42} ; Deming et. al, 2017, n=3,146). PRS derived from these GWAS studies were computed for an independent cohort of 2,988 Non-hispanic White, clinically normal older adults that were screened for the Anti-Amyloid Treatment in Asymptomatic Alzheimer's (A4) Study (age=71.4 \pm 4.8). All non-APOE SNPs (<1Mb) that were significant at the p=0.01 level in each parent GWAS study were included in the PRS calculation. Linear regression models assessed the association between PRS and continuous amyloid levels covarying for age, sex, education, APOE- $\epsilon 4$, and APOE- $\epsilon 2$. Age and sex interactions with PRS were also assessed.

Results: PRS-ADdx showed a significantly albeit low correlation with PRS-CSFA β_{42} (r=0.19). In separate models, both PRS were associated with amyloid (p-values<0.001, **Figure 1**). In a competitive model with both PRS as simultaneous predictors, both remained significantly associated with amyloid (p<0.001) and together explained an additional 0.7% of variance beyond covariates. Age interacted with the CSF A β_{42} PRS (p<0.001), whereby the association was only present in those 70 and older (p<0.0001, **Figure 2**). There was no age interaction for PRS-ADdx. There was no significant sex interaction with either score.

Discussion: Despite low correlation between CSF and clinical AD PRS, both scores independently are associated with amyloid deposition during preclinical phases of disease. Aggregate genetic risk scores across different endophenotypes of AD may aid in improving prediction models for amyloid deposition and help to identify the highest risk patients for developing brain amyloid pathology.

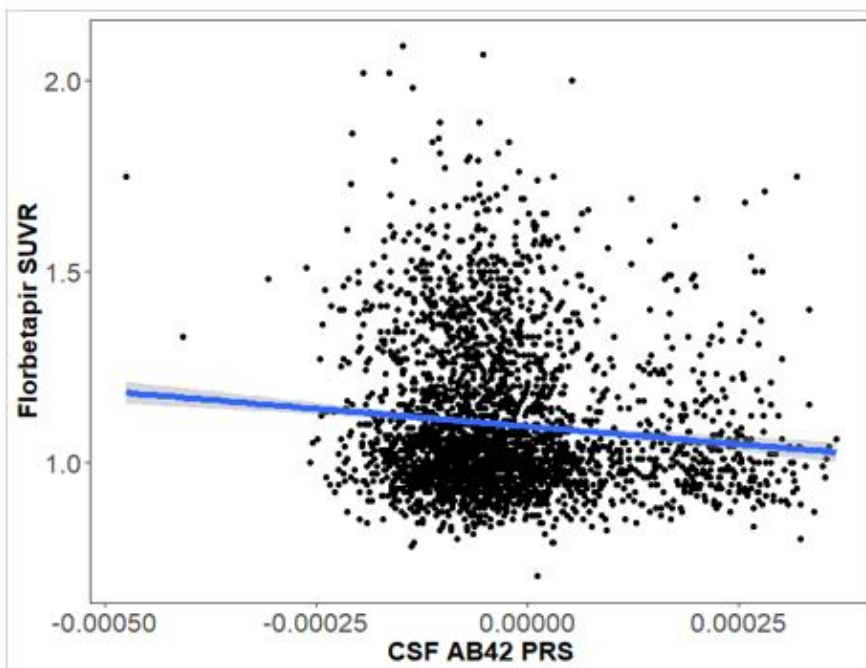


Figure 1A. PRS-CSFA β_{42} that excluded the *APOE* region was associated with florbetapir standardized uptake value ratio ([SUVR], $\beta = -1.1E2$, $p = 3.2E-4$). Note that the negative relationship reflects the scale of CSFA β_{42} (lower values are present in AD and are known to be inversely correlated with Amyloid PET measures).

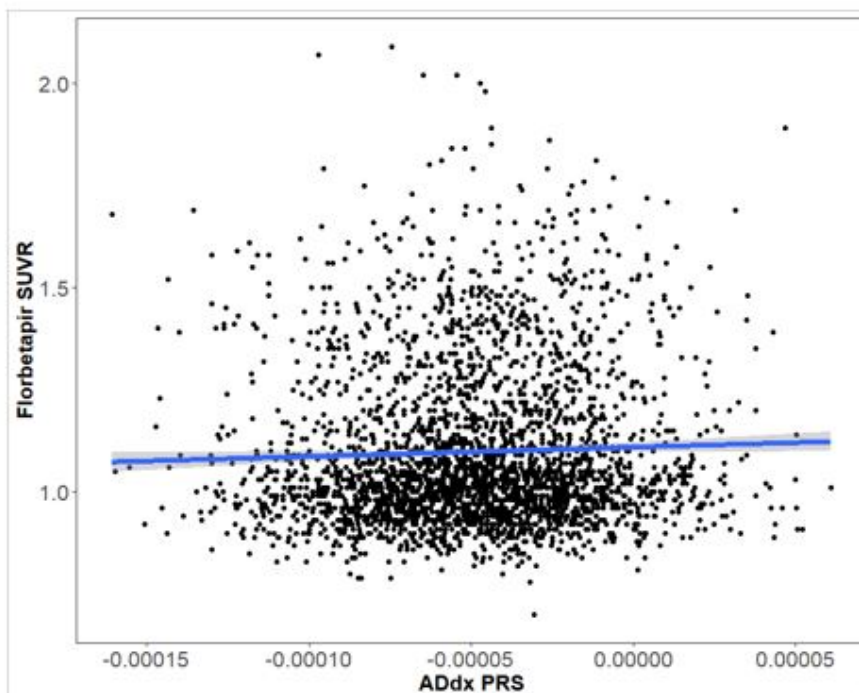


Figure 1B. PRS-ADdx that excluded the *APOE* region was associated with florbetapir standardized uptake value ratio ([SUVR], $\beta = 3.4E2$, $p = 5.9E-4$).

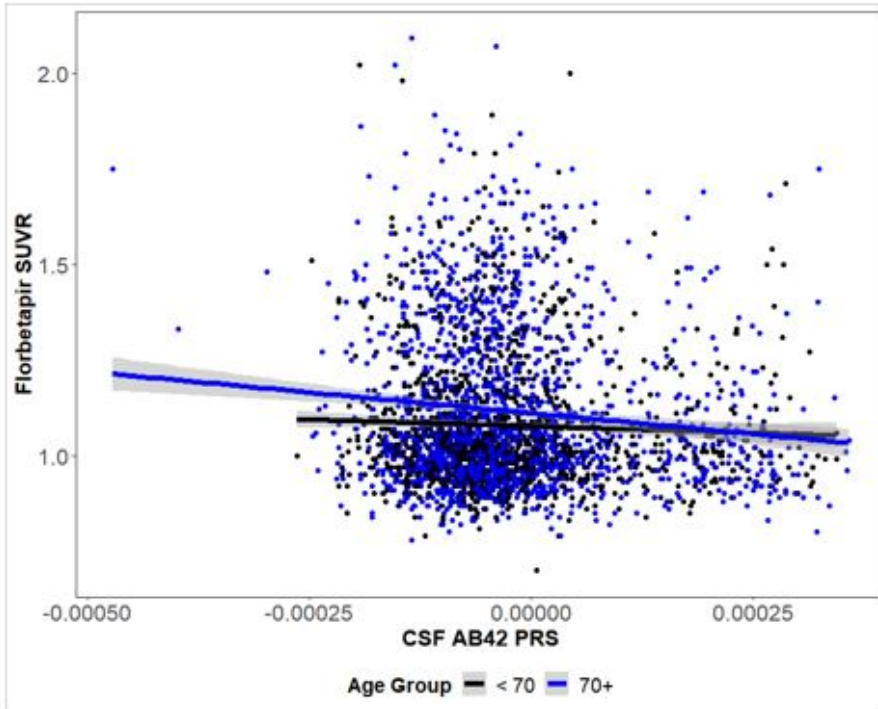


Figure 2. PRS-CSF β_{42} interacted with age, such that PRS for participants aged 70 and up was significantly associated with brain amyloid levels (PRS \times Age interaction: $p=6.5E-4$, PRS association with amyloid in: <70 $p=0.5$, 70+ $p=5.3E-5$).

Keywords: Polygenic Risk, Amyloid, Preclinical disease, Age interaction

P36: Association between cerebral amyloid accumulation and synaptic density in Alzheimer's disease: a multitracer PET study

Ryan O'Dell^{1,2}, Adam Mecca^{1,2}, Ming-Kai Chen³, Tyler Godek^{1,2}, Joanna Harris^{1,2}, Hugh Bartlett^{1,2}, Emmie Banks^{1,2}, Victoria Kominek^{1,2}, Wenzhen Zhao^{1,2}, Mika Naganawa³, Takuya Toyonaga³, Yihuan Lu³, Nabeel Nabulsi³, Brent Vander Wyk⁴, Pradeep Varma³, Amy Arnsten⁵, Yiyun Huang³, Richard Carson³, Christopher van Dyck^{1,2,5,6}

¹*Alzheimer's Disease Research Unit, Yale University School of Medicine, New Haven, CT, US*

²*Department of Psychiatry, Yale University School of Medicine, New Haven, CT, US*

³*Department of Radiology and Biomedical Imaging, Yale University School of Medicine, New Haven, CT, US*

⁴*Program on Aging, Yale University School of Medicine, New Haven, CT, US*

⁵*Department of Neuroscience, Yale University School of Medicine, New Haven, CT, US*

⁶*Department of Neurology, Yale University School of Medicine, New Haven, CT, US*

Introduction: Synaptic loss is an early pathology in Alzheimer's disease (AD) and the major structural correlate of cognitive impairment. Using [¹¹C]UCB-J –PET, we have recently demonstrated extensive synaptic loss in medial temporal and neocortical brain regions of participants with AD. In this study, we further investigate the association of global and local amyloid burden with synaptic density.

Methods: [¹¹C]UCB-J and [¹¹C]PiB binding were measured in 38 participants with AD and 20 cognitively normal participants aged 55-85 years. For [¹¹C]PiB analysis, parametric images of binding potential (BP_{ND}) were generated using SRTM2 with cerebellum as a reference region and converted to distribution volume ratios (DVR). For [¹¹C]UCB-J, BP_{ND} was first computed using SRTM2 with a shrunken centrum semiovale reference region and converted to DVR with a cerebellum reference region.

Results: The AD group showed significant reductions of synaptic density, most pronounced in medial temporal lobe, but also widespread across neocortical and subcortical regions. Among pooled participants, both higher global and local amyloid was associated with lower synaptic density in the majority of ROIs. In the AD group only, there were no significant associations between either global or local amyloid and synaptic density in any ROI.

Conclusions: Using [¹¹C]UCB-J PET, widespread reductions of synaptic density were observed in AD participants. Cortical regions associated with the least robust accumulation of fibrillar amyloid (medial temporal lobe) were associated with the most pronounced reductions in synaptic density. Significant negative associations between both global and local amyloid and synaptic density in the pooled sample were driven by group differences, and not significant within the AD group alone. Our findings are consistent with postmortem studies describing the patterns of fibrillar amyloid burden and synaptic loss in AD.

Funding Sources: P50-AG047270 (CHvD, MKC), K23-AG057784 (APM), R01-AG052560 (REC, CHV), R01-AG062276 (CHvD), Dana Foundation (MKC), R25-MH071584 (RSO), T32-MH019961 (RSO), and Thomas P. Detre Fellowship (RSO).

Keywords: Alzheimer's disease, amyloid, synaptic density

P37: A clinically applicable proxy for gold standard quantification of amyloid-beta in Alzheimer's disease: Bolus plus constant infusion 18F-AV45 PET

Julie Ottoy¹, Min Su Kang^{2,4}, Jeroen Verhaeghe¹, Sigrid Stroobants³, Reda Bouhachi⁴, Chris Hsiao⁴, Jenna Stevenson², Nesrine Rahmouni², Daniel Chartrand⁴, Gassan Massarweh⁴, Jean-Paul Soucy⁴, Serge Gauthier^{1,2}, Pedro Rosa-Neto^{2,4}, Steven Staelens¹

¹*Molecular Imaging Center Antwerp, University of Antwerp, Antwerp, Belgium*

²*Translational Neuroimaging Laboratory, The McGill University Research Centre for Studies in Aging, Montréal, QC, Canada*

³*Department of Nuclear Medicine, Antwerp University Hospital, Antwerp, Belgium*

⁴*Montreal Neurological Institute, Montréal, QC, Canada*

Introduction: The SUVR has been widely applied to quantify amyloid-beta (A β) in the clinic and anti-A β trials of Alzheimer's disease. However, it is prone to bias induced from reference region selection and blood flow alterations. Here, we report on a clinically feasible bolus-plus-constant-infusion (B/I) PET imaging technique to accurately quantify A β .

Methods: Five PSEN1 carriers (MMSE 26.4 \pm 3) underwent dynamic 90-min [¹⁸F]-AV45-PET on HRRT with continuous intravenous tracer infusion, and continuous and manual arterial sampling. Total volume of distribution based on B/I ($V_{T,B/I}$) was determined as the equilibrium ratio (50-70min) of tracer concentration in tissue (C_{PET}) to 3 unmetabolized arterial plasma samples (C_P). The $V_{T,B/I}$ was validated against the full pharmacokinetic 'gold standard' $V_{T,2TCM}$ and the graphical $V_{T,Logan}$ using individual metabolite-corrected plasma input functions. Additionally, distribution volume ratios (DVR) were determined as the V_T target-to-reference ratios (reference: cerebellar grey (CB), subcortical white matter (WM), or pons).

Results: The B/I method demonstrated true equilibrium conditions as both C_{PET} and C_P demonstrated low rate of tracer concentration change (e.g., $C_{parietal_lobe}$: 2.0 \pm 1.4%, C_{CB} : 3.1 \pm 3.4%, and C_P : 5.6 \pm 3.5%) (Fig.1). $V_{T,B/I}$ was similar to the full-kinetic $V_{T,2TCM}$ and $V_{T,Logan}$ (average difference over cortical lobes: 2.9 \pm 0.8 and 3.3 \pm 0.7%, respectively) (Fig.2).

$DVR_{B/I}$ normalized to the WM or pons was positively correlated to the full-kinetic V_T of cortical areas (e.g. pons: $R=0.7, P<0.001$). The WM- $DVR_{B/I}$ showed +6.2 \pm 1.3 and the pons- $DVR_{B/I}$ +6.9 \pm 1.2% difference compared to their DVR_{2TCM} . Cerebellar plaques were evident in two subjects with the same PSEN1 mutation (Fig.3), resulting in a negative correlation between $DVR_{B/I}$ and the full-kinetic V_T of all subjects.

Conclusion: A 20-min static scan in combination with 3 metabolite-corrected arterial samples is sufficient to reproduce the full-kinetic V_T . Considering a suitable reference region, the B/I method provides accurate quantification without the need for blood sampling. This method is promising for wide adaptation in clinical trials.

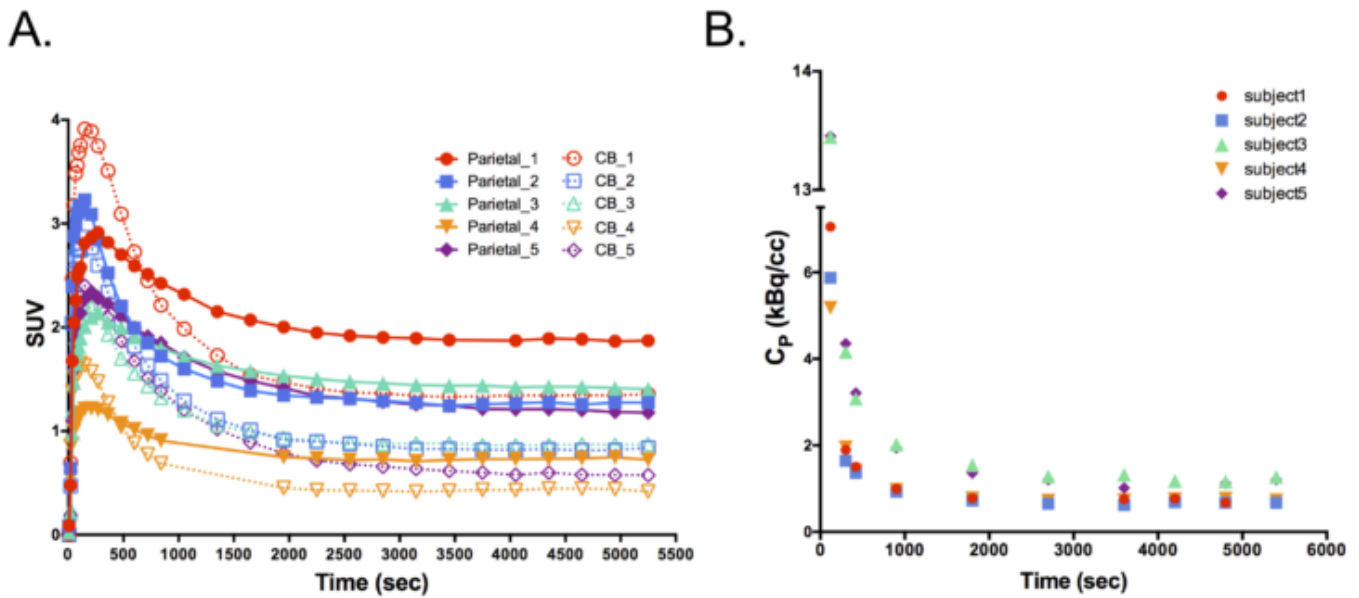


Figure 1. Regional time-activity curves of the parietal lobe and cerebellar gray matter (CB) (panel A), and metabolite-corrected plasma activity (C_p) (panel B) in five PSEN1 carriers.

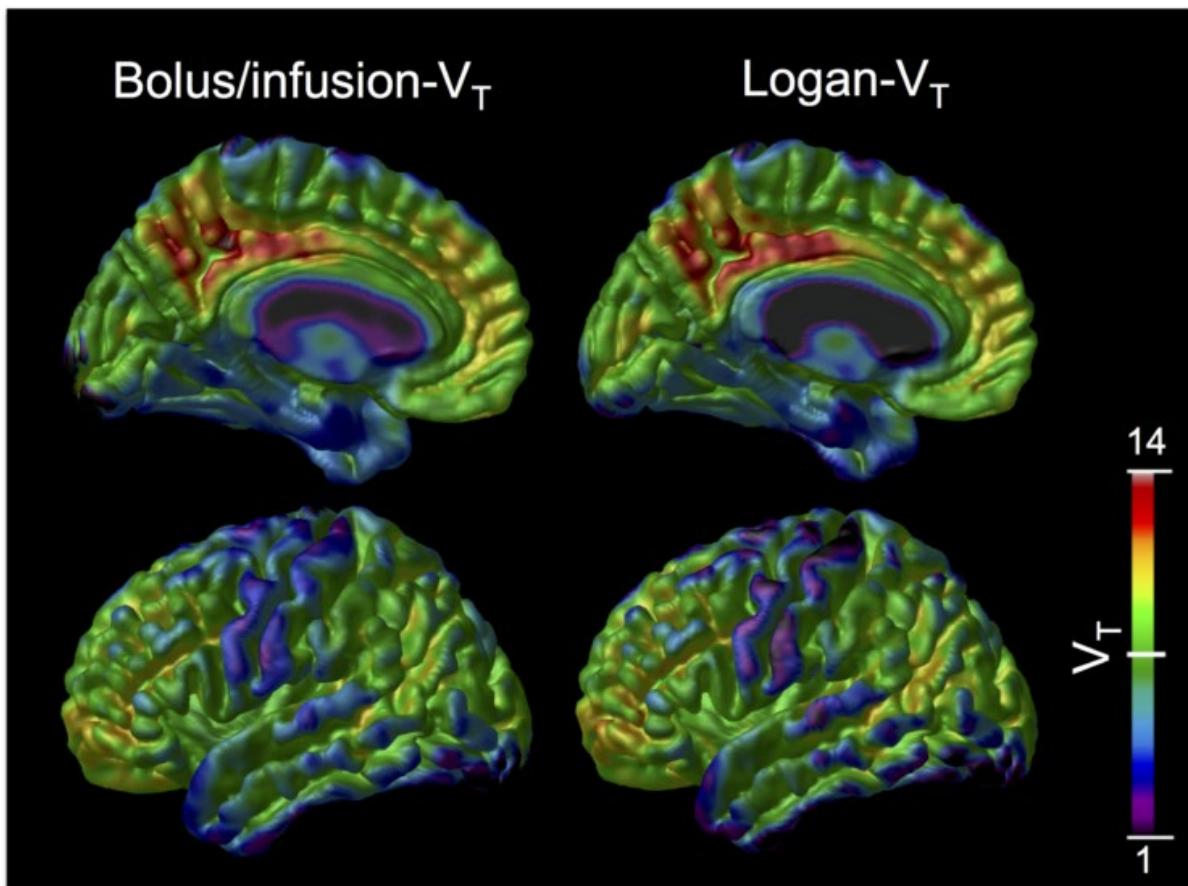


Figure 2. Voxel-wise representation of the $V_{T,Logan}$ (equilibrium start point $t^* = 50$ min) based on 90-min dynamic PET with continuous arterial sampling (right panel) and the $V_{T,B/I}$ based on the average C_{PET} divided by C_p in the 50-70 min interval (left panel). V_T patterns were overlaid on the MNI template. Figure displays one PSEN1 carrier with AD dementia clinical diagnosis.

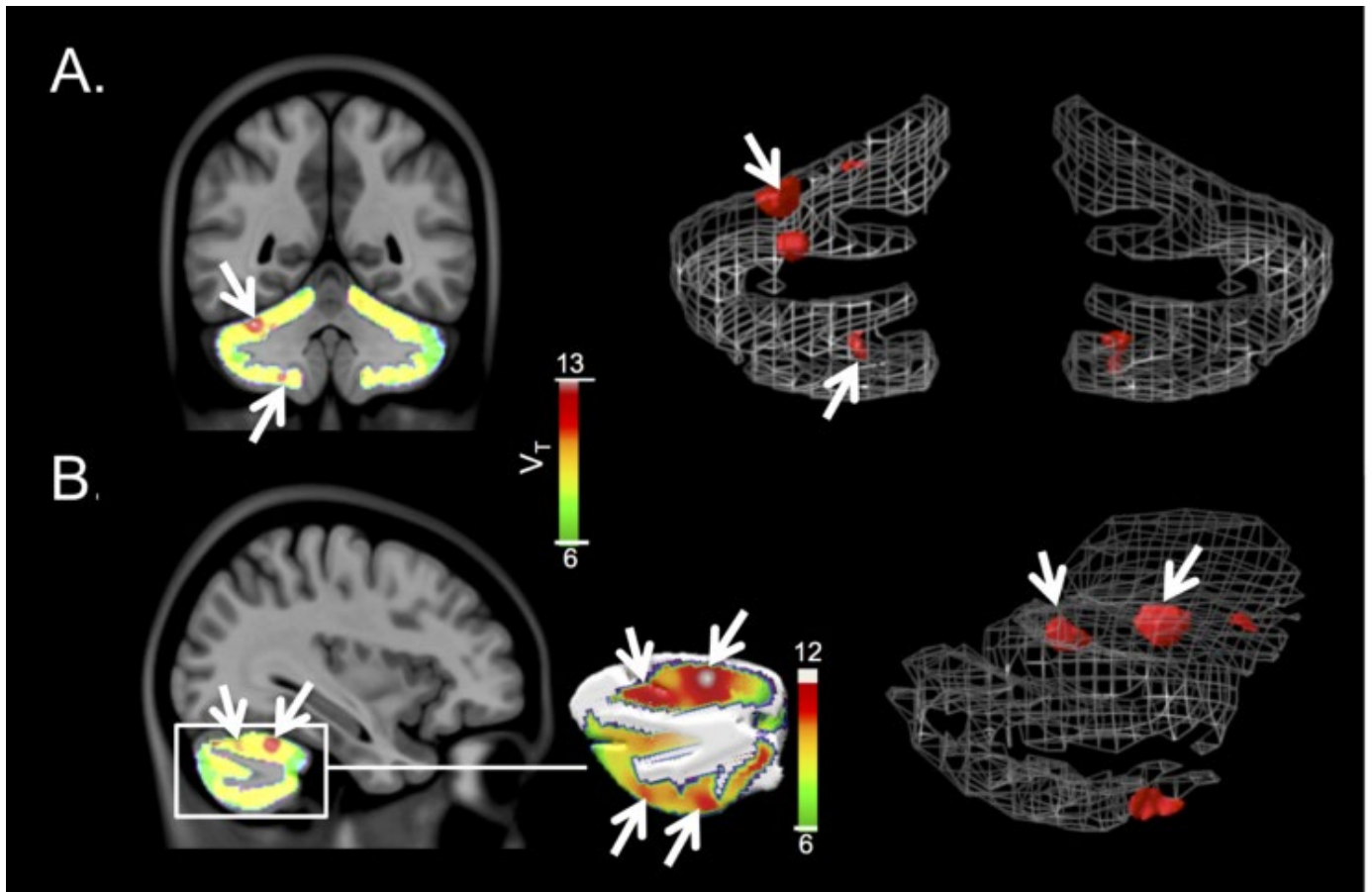


Figure 3. $[^{18}\text{F}]\text{-AV45}$ binding to $\text{A}\beta$ in the cerebellar grey matter (CB) of one PSEN1 carrier. Coronal section and 3D rendering (panel A), sagittal section and 3D rendering (panel B). The CB mask was eroded to exclude spill-over from the occipital lobe. Major plaques are indicated with white arrows and shown in 3D rendering.

Keywords: Flortbetapir, Positron emission tomography, Alzheimer's disease, constant infusion, equilibrium

P38: Amyloid PET variability due to variation in MRI protocol and anatomical segmentation

Alessandro Palombit¹, Richard Manber¹, Richard Joules¹, Robin Wolz¹

¹*IXICO plc., London, UK*

Background: Variability in MRI acquisition protocol (e.g. voxel-size, contrast parameters) cause anatomical segmentation differences, introducing additional sources of cross-sectional variance in regional amyloid beta PET (Ab-PET) SUVR.

Aims: To quantify the variability of Ab-PET attributable to brain segmentation differences arising from variation in MR acquisition protocol.

Methods: We employ two T1w-MRI datasets 1) single volunteer on different scanners (18 harmonised protocols; HZ) and 2) four subjects scanned with different acquisitions (eight non-harmonised protocols; NHZ).

Once bias field-corrected and skull-stripped, automatic whole brain parcellation was performed with LEAP and a subject-specific T1w template constructed with ANTs from skull-stripped T1w-MRI (see Figure 1).

Ab-PET images for 20 ADNI2 (<http://adni.loni.ucla.edu>) subjects, representative of the AD spectrum, were non-linearly warped to each subject-specific template.

Inter-segmentation Ab-PET variability was measured by the standard deviation of regional uptake across segmentations (within-subject and ROI) divided by the global average.

Intra-segmentation Ab-PET variability was quantified by the standard deviation of the uptake distribution within each ROI, averaged across segmentations and divided by the global within-ROI average.

Results: Ab-PET variability was not significantly different between harmonization levels (HZ vs NHZ datasets, Figure 2A; paired t-test, $p > 0.05$, Cohen's $d < 0.01$) with an inter-quartile range 1.6-5.3%, comparable to scan-rescan level (5-9%).

Intra-segmentation variability (uptake variability within-ROI) was an order of magnitude higher than any segmentation-related variability condition (Figure 2B; paired t-test, $p < 0.05$) with an inter-quartile range of 18.0-28.6%, significantly different between harmonization groups (HZ vs NHZ datasets, Figure 2A; paired t-test, $p > 0.05$) with however small effect size (Cohen's $d = 0.23$).

Conclusions: We found that the variability of regional Ab-PET introduced by MRI-related segmentation differences is within the physiological scan-rescan range and lower than the within-ROI variability suggesting the tolerability of using compliant MR data with minor impact in Ab-PET studies.

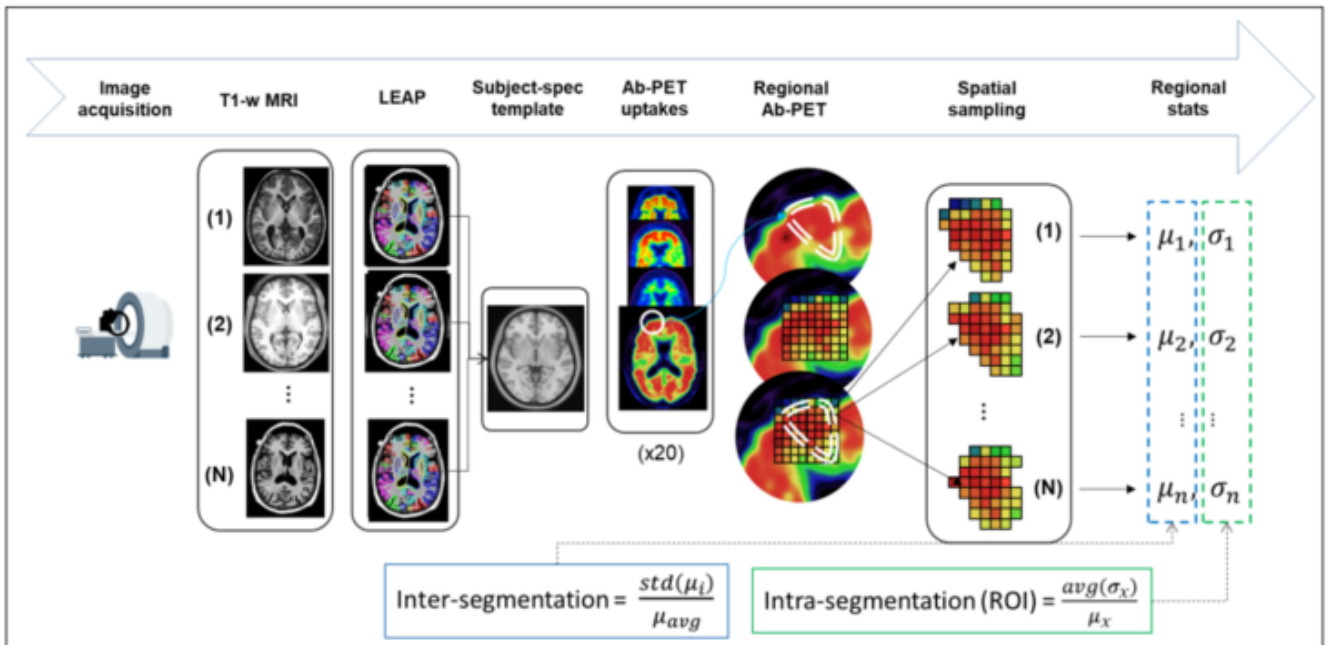


Figure 1. Methods workflow from MRI acquisition with multiple protocols (see dataset information) on left, subsequently segmented and used for template generation. Ab-PET patterns registered to each template are then regionally sampled and the normalised variability across segmentations (**inter-segmentation**) is finally calculated along with the average within-region uptake variability (**intra-segmentation** and region).

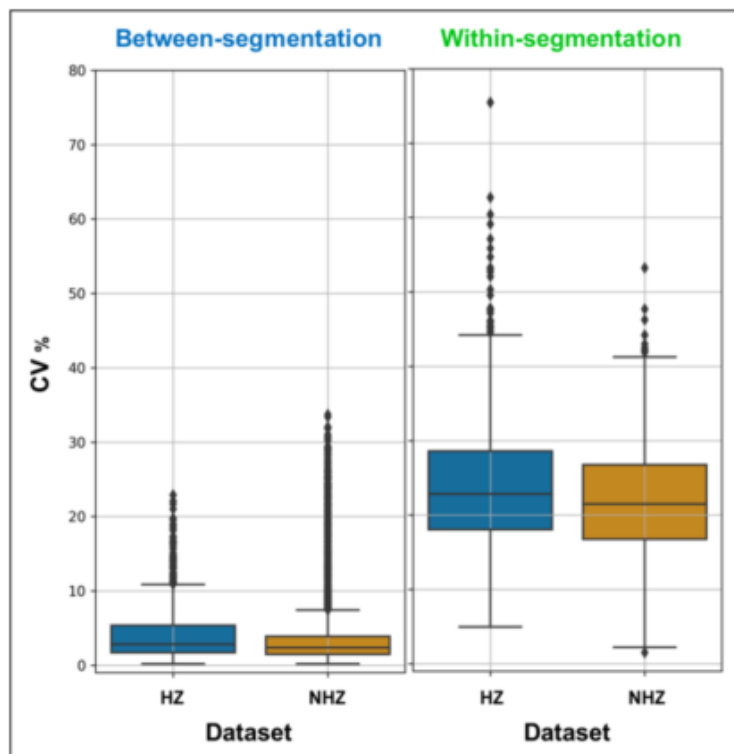


Figure 2. Distribution of ^{18}F -FLUT uptake variability in all regions (coefficient of variation, CV) respectively **left**) across segmentations (obtained from different MRI protocols); and **right**) within-segmentation (ROI). Distribution boxplots are separately reported for the harmonised (**HZ**) and non-harmonised (**NHZ**) protocol datasets.

Keywords: PET, MRI, Amyloid, Segmentation

P39: The impact of automatic Tau PET processing on uptake variability and power analysis in AD

Alessandro Palombit¹, [Richard Manber](#)¹, Richard Joules¹, Robin Wolz¹

¹*IXICO plc., London, UK*

Background: Tau protein-targeting Positron Emission Tomography (PET) based on [18F]-AV-1451 (Tau-PET) offer promises in Alzheimer's disease (AD) clinical trials but the role of registration on Tau-PET variability is unclear.

Aims: Explore the variability introduced by different image registration tools for Tau-PET pre-processing.

Methods: A total of 96 ADNI subjects (34 normal controls, 29 mild cognitively impaired, 33 AD) were randomly selected (<http://adni.loni.ucla.edu>) obtaining Tau-PET ([18F]-Flortaucipir) and T1w-MRI data along Tau-PET regional SUVR measures distributed from ADNI-core.

T1w-MRI data was anatomically segmented with LEAP and rigidly registered into native Tau-PET space, separately by means of IRTK or ANTs tools.

Regional Tau-PET SUVR measures, obtained using the cerebellum grey matter as reference region, were finally aggregated to merge LEAP regions into three Braak-like composites.

Results: Braak-SUVR estimates obtained with the two registration pipelines were highly correlated among them with determination coefficient $R^2=0.97$ and with ADNI-reported measures (respectively $R^2=0.89/0.85$ with IRTK or ANTs-based pipelines).

Paired-condition SUVR absolute difference was not correlated with the group-variable (Spearman's $r=-0.01, p>0.05$).

Relative SUVR difference within-region (ANTs – IRTK) was bound to the inter-quartile range -2.26 to 0.84% (75% of values differed less than 3.31% in absolute relative terms) with left-skewed distribution suggesting a possible ANTs-related underestimation over high-SUVR values.

Conclusions: Automatic Tau-PET processing requires accurate registration to anatomical-MRI for repeatable endpoint generation.

Here we found that the variability introduced by different registration schemes to be possibly under the typical scan-rescan variability providing alternative processing schemes that may have a significant impact on sample size estimation, and therefore on trial design.

Braak-SUVR measures in this test cohort (NC-AD) differed between registrations with Cohen's $d=-0.167$; -0.185 with IRTK and ANTs ($d=-0.255$ with ADNI as reference).

A power analysis based on these figures for example would require (5% significance, 80% power, paired-groups) 563 and 459 subjects respectively with IRTK and ANTs-registrations.

Keywords: PET, MRI, Tau, Power analysis, Braak

P40: MIND MAPS: Assessment of the mitochondrial - endoplasmic reticulum - synaptic axis in neurodegeneration by [18F]BCPP-EF, [11C]SA4503 and [11C]UCB-J PET imaging

Eugenii Rabiner^{1,2}, Ayla Mansur^{1,3}, Ashwin Venkataraman^{3,4}, Geraint Price³, Heather Wilson², Gennaro Pagano², Mica Clarke⁵, Yvonne Lewis¹, Paul M. Matthews^{3,4}, James B. Rowe⁶, David Brooks⁷, Lefkos Middleton³, Marios Politis², Jonathan D. Rohrer⁵, Robert Comley⁸, Karleyton C. Evans⁹, Laurent Martarello⁹, Laigao Chen¹⁰, Adam J. Schwarz¹¹, Karl Schmidt¹², Hideo Tsukada¹³, Jan Passchier¹, Roger N. Gunn^{1,3}, MIND MAPS Consortium¹

¹*Invicro, London, UK*

²*King's College London, London, UK*

³*Imperial College London, London, UK*

⁴*UKDRI @ Imperial College London, London, UK*

⁵*University College London, London, UK*

⁶*University of Cambridge, Cambridge, UK*

⁷*University of Newcastle, Newcastle, UK*

⁸*AbbVie, Deerfield, MA, US*

⁹*Biogen, Cambridge, MA, US*

¹⁰*Pfizer, Cambridge, MA, US*

¹¹*Takeda, Cambridge, MA, US*

¹²*Celgene, Summit, NJ, US*

¹³*Hamamatsu Photonics, Hamamatsu, Japan*

Background: A common feature of neurodegenerative disease is a failure of mitochondrial/endoplasmic reticulum (ER) function, contributing to the loss of synapses and ultimately neurons. Multimodal investigation of the mitochondria/ER/synaptic axis may enable the development of a mechanistic biomarker common to all neurodegenerative disease. Mitochondrial complex 1 (MC1), the sigma-1 receptor (S1R) and the synaptic vesicular glycoprotein 2A (SV2A) are attractive molecular markers for these processes. We used [18F]BCPP-EF, [11C]SA4503 and [11C]UCB-J PET in conjunction with a comprehensive MRI battery to determine MC1, S1R and SV2A status respectively, in the brains of healthy volunteers (HV, n=31), patients with Alzheimer's disease (AD, n=12), Parkinson's disease (PD, n=12) and fronto-temporal dementia (FTD, n=5) in the context of the MIND-MAPS programme.

Methods: Dynamic PET tissue, blood and metabolite data for the three radioligands, were acquired over 90 minutes for each subject (Fig 1). Analysis with an appropriate kinetic model, enabled the estimation of regional parameters (DVR-1, for [18F]BCPP-EF and [11C]UCB-J, V_T/f_p for [11C]SA4503). Group differences were assessed using One-Way ANOVA for the individual regions. Kendall's tau was used to assess the relationship between imaging parameters and subjects age and MMSE scores.

Results: Significant effect of age on MC1 and SV2A density were seen across multiple regions in HV. MMSE correlated significantly with MC1 density in the Thalamus, Cingulate and Caudate (Fig 2). Patients had significantly lower MC1 and SV2A density across multiple brain regions (10-36%, Fig 3), driven primarily by reductions in AD and FTD patients. SV2A and MC1 density in the patient group correlated significantly with the patient's MMSE score (Fig 2).

Conclusions: We have demonstrated significant reductions in mitochondrial and synaptic molecular markers, that correlate with global cognitive scores, in patients with neurodegeneration. Our results support the notion of a widespread mitochondrial and synaptic dysfunction in patients with neurodegenerative disease.

Figure 1 – Distribution of MC1, S1R and SV2A in a healthy brain

[¹⁸F]BCPP-EF [¹¹C]SA-4503 [¹¹C]UCB-J

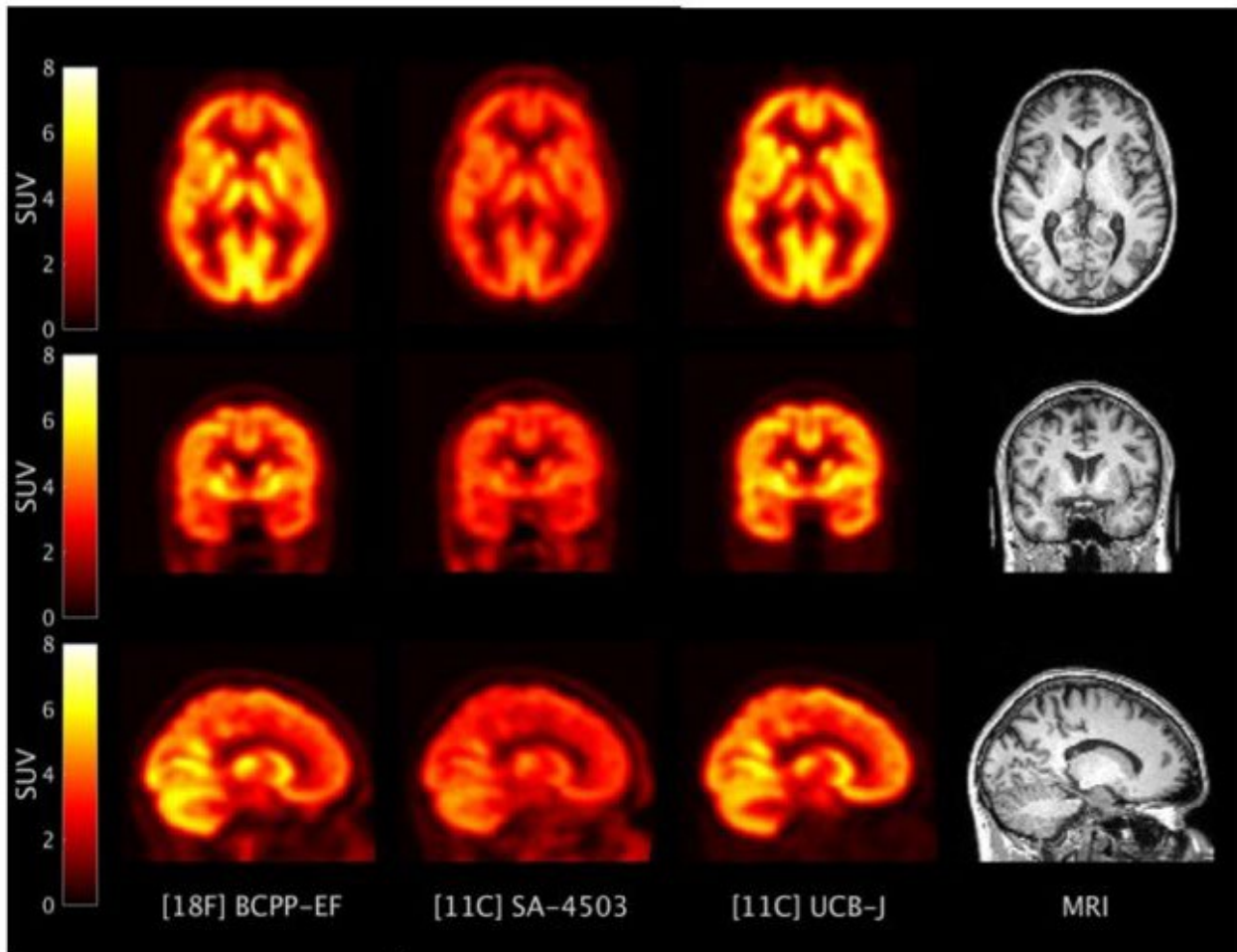


Figure 2 – Relationship between MC1 & SV2A density and MMSE

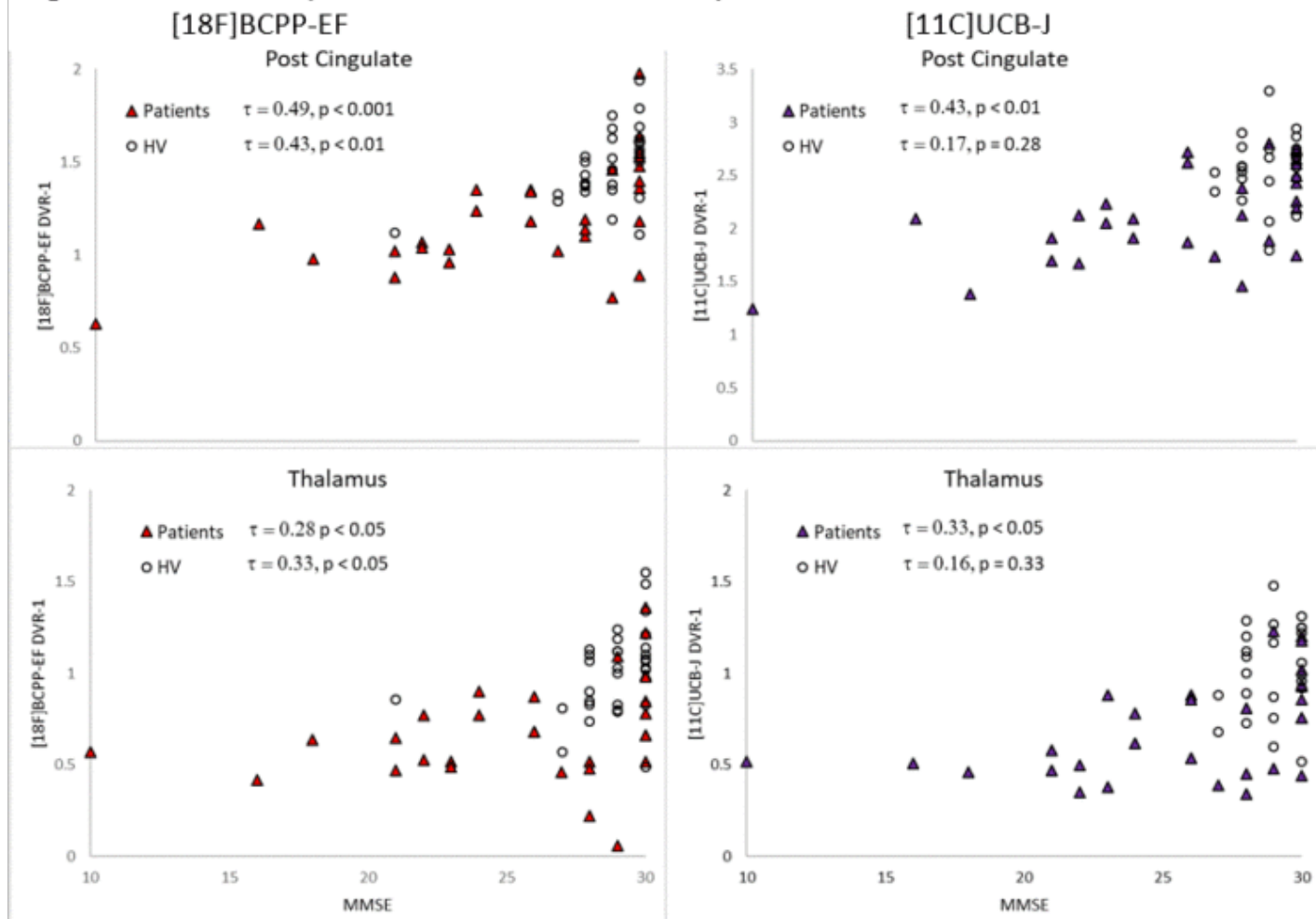
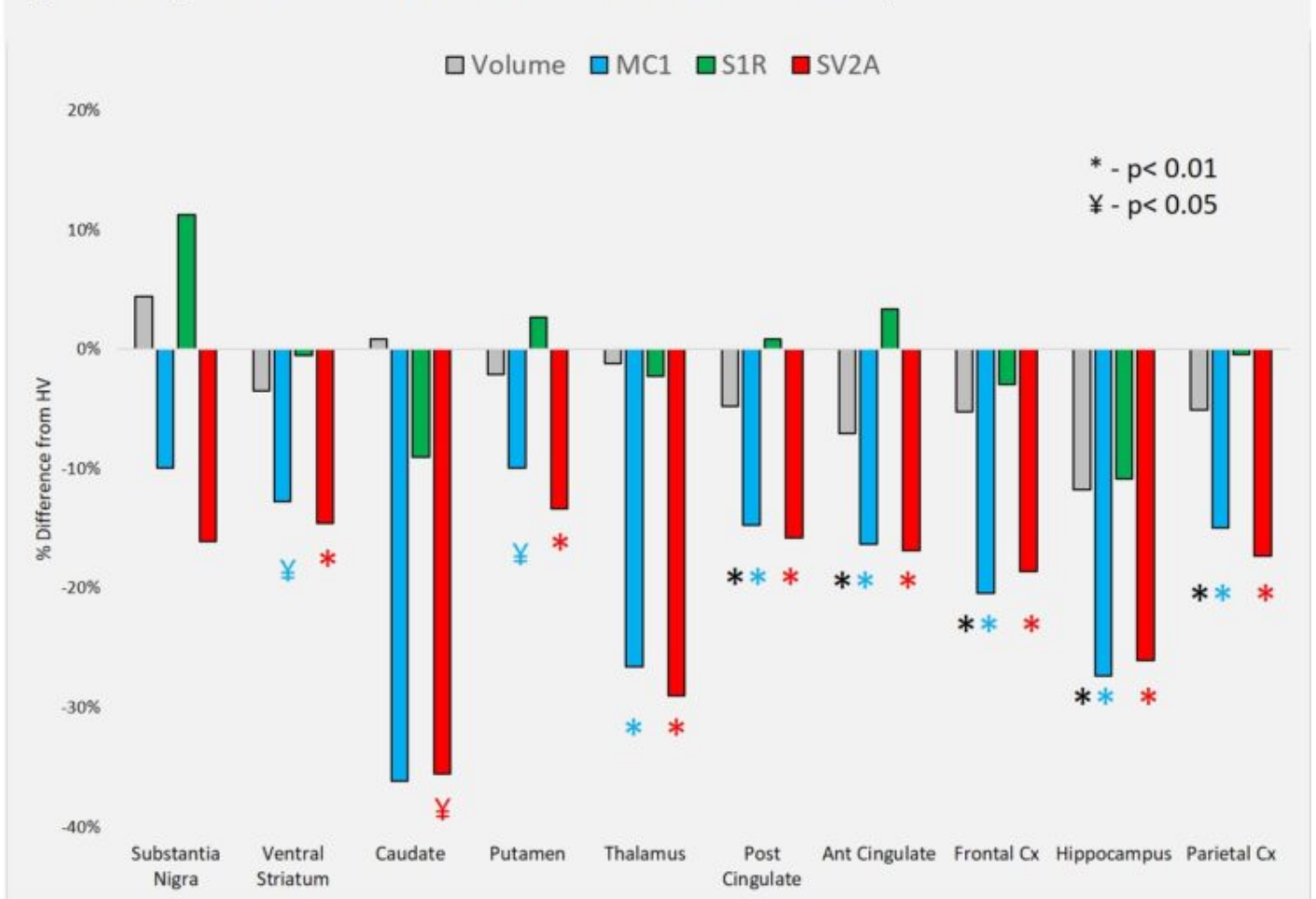


Figure 3 – Regional differences in volume and molecular marker density



Keywords: SV2A, Mitochondrial Complex 1, Sigma 1 receptor, Neurodegeneration, PET

P41: Associations between Neurogranin and imaging biomarkers of Alzheimer's disease

Nesrine Rahmouni^{1,2}, Andrea Benedet^{1,2}, Ashton Nicholas^{4,5,6,7}, Cécile Tissot^{1,2}, Tharick A. Pascoal^{1,2}, Hlin Kvartsberg⁸, Mira Chamoun^{1,2}, Min Su Kang^{1,2}, Firoza Lussier^{1,2}, Joseph Therriault^{1,2}, Jenna Stevenson^{1,2}, Melissa Savard^{1,2}, Sulantha Mathotaarachchi^{1,2}, Emilie Thomas^{1,2}, Serge Gauthier^{1,3}, Henrik Zetterberg^{4,8,9,10}, Kaj Blennow^{4,8}, Pedro Rosa-Neto^{1,2}

¹McGill University Research Center for Studies in Aging, Montreal, QC, Canada

²Translational Neuroimaging Laboratory-McGill University, Montreal, QC, Canada

³Douglas Hospital Research Center, Montreal, QC, Canada

⁴Department of Psychiatry and Neurochemistry, Institute of Neuroscience & Physiology, the Sahlgrenska Academy at the University of Gothenburg, Mölndal, Sweden

⁵Wallenberg Centre for Molecular and Translational Medicine, University of Gothenburg, Gothenburg, Sweden

⁶King's College London, Institute of Psychiatry, Psychology & Neuroscience, Maurice Wohl Clinical Neuroscience Institute, London, UK

⁷NIHR Biomedical Research Centre for Mental Health & Biomedical Research Unit for Dementia at South London & Maudsley NHS Foundation, London, UK

⁸Clinical Neurochemistry Laboratory, Sahlgrenska University Hospital, Mölndal, Sweden

⁹Department of Neurodegenerative Disease, UCL Institute of Neurology, Queen Square, London, UK

¹⁰UK Dementia Research Institute at UCL, London, UK

Introduction: Neurogranin, a postsynaptic protein, has recently been proposed as a biomarker of synaptic depletion and is known to be detected at elevated levels in cerebrospinal fluid (CSF) at early stages of Alzheimer's disease (AD). There is currently no published study showing a correlation between neurogranin levels in CSF and imaging biomarkers of AD *in vivo*.

Objective: To investigate whether neurogranin in CSF is correlated with brain accumulation of amyloid- β and tau across the AD spectrum.

Methods: The present study was conducted in a population of 111 individuals (17 young cognitively unimpaired individuals, 57 cognitively unimpaired, 25 mild cognitively impaired and 12 AD). CSF neurogranin was quantified using an in-house ELISA assay. Amyloid deposition was assessed with [¹⁸F]AZD4694 PET and accumulation of tau was assessed with [¹⁸F]MK6240 PET. [¹⁸F]AZD4694 and [¹⁸F]MK6240 standardized uptake value ratio (SUVRs) were calculated between 40 to 70 min and 90 to 110 min post-injection, respectively, using cerebellum grey matter as the reference region. A voxel-based regression model evaluated the relationship between the accumulation of neurogranin and the PET markers [¹⁸F]AZD4694 and [¹⁸F]MK6240.

Results: In the present study, positive correlations were found between levels of neurogranin in CSF and both accumulation of tau and amyloid deposition indexed by PET-imaging. The brain regions where this association was present were the temporal, occipital and parietal areas. These regions survived to corrections for multiple comparisons.

Conclusion: The associations between neurogranin and the hallmarks of AD pathophysiological process converge to brain regions vulnerable to synaptic depletion. These results support the claim that neurogranin is a biomarker for neurodegeneration in the spectrum of clinical presentations of AD.

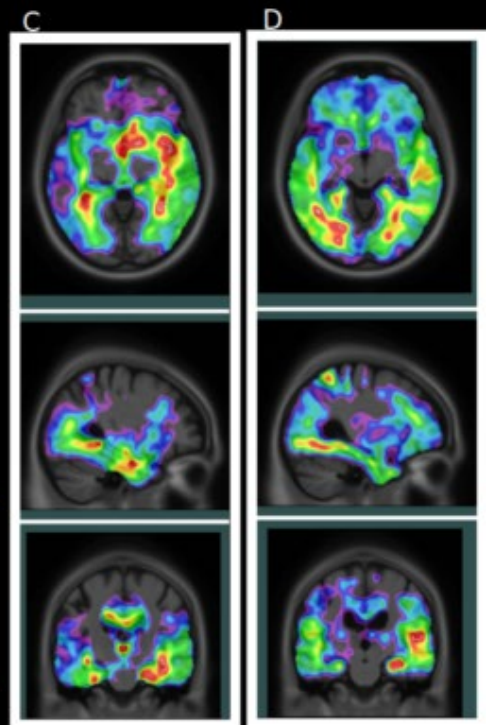
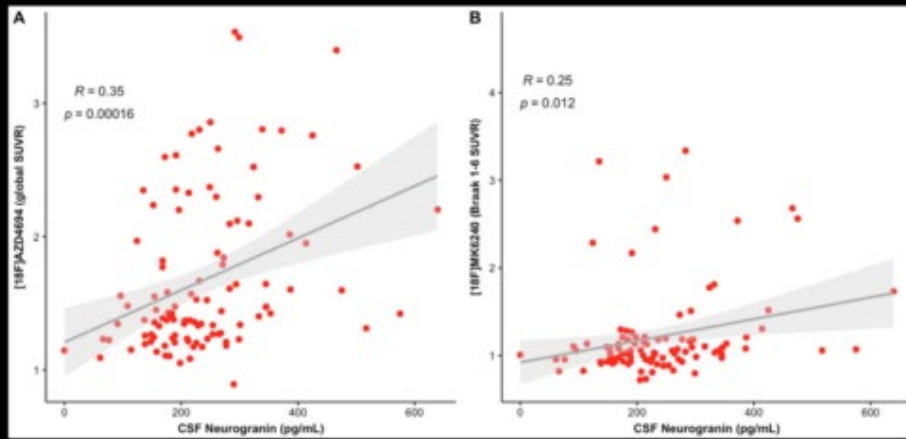


Figure 1: Neurogranin levels are significantly associated with tau accumulation and amyloid- β deposition in individuals.
A&B panels: Pearson's correlation, $p < 0.001$, correlating CSF neurogranin levels with respectively, the PET markers [¹⁸F]AZD4694 and [¹⁸F]MK6240.
C&D panels: A voxel-based regression model evaluated the relationship between the accumulation of neurogranin and, respectively, the PET markers [¹⁸F]AZD4694 and [¹⁸F]MK6240.

Keywords: neurogranin, synaptic depletion, in vivo biomarkers, cerebrospinal fluid

P42: Linking APOE ϵ 4, blood-brain barrier dysfunction and inflammation to Alzheimer's pathology

Joost Riphagen^{1,5}, Inez Ramakers¹, Whitney Freeze¹, Linda Pagen¹, Bernard Hanseeuw^{2,4}, Marcel Verbeek³, Frans Verhey¹, Heidi Jacobs^{1,2,5}

¹*Department of Psychiatry & Neuropsychology, Maastricht University, School for Mental Health & Neuroscience, Alzheimer Center Limburg, Maastricht, the Netherlands., Maastricht, The Netherlands*

²*Division of Nuclear Medicine and Molecular Imaging, Department of Radiology, Massachusetts General Hospital, Harvard Medical School, Boston, MA, US*

³*Department of Neurology, Donders Institute for Brain, Cognition and Behaviour, Department of Laboratory Medicine, Translational Metabolic Laboratory, Radboud University Medical Center, Nijmegen, The Netherlands*

⁴*Department of Neurology, Cliniques Universitaires Saint-Luc and Institute of Neurosciences, Université Catholique de Louvain, Brussels, Belgium*

⁵*Department of Radiology, Athinoula A. Martinos Center for Biomedical Imaging, Massachusetts General Hospital, Harvard Medical School, Charlestown, MA, US*

The APOE- ϵ 4 genotype is a risk factor for late-onset Alzheimer's disease (AD) as well as vascular pathology. Given the increased risk of blood-brain-barrier dysfunction and inflammation among APOE- ϵ 4 carriers, we aimed to examine whether blood-brain-barrier dysfunction and inflammation contribute to the relationship between APOE and Alzheimer's disease key pathologies, as measured in the cerebrospinal fluid (CSF). We applied bootstrapped regression (figure 2) and path analyses (figure 1) involving Q-albumin CSF/plasma ratio (a BBB/BSCFB function marker), interleukins (IL-1 β , IL6 and IL-12p70; inflammation markers) and CSF p-Tau181 and Amyloid- β 1-42 (AD pathology markers) of 97 participants (age 38-83 years) from a university memory clinic.

Our results showed that relationship between BBB dysfunction and AD pathology is modulated by IL-6 and these associations appear to be driven by the APOE- ϵ 4 genotype. This suggests that APOE- ϵ 4 related vascular factors are also part of the pathway to AD pathology, in synergy with an elevated immune response, and could become targets for trials focused on delaying AD.

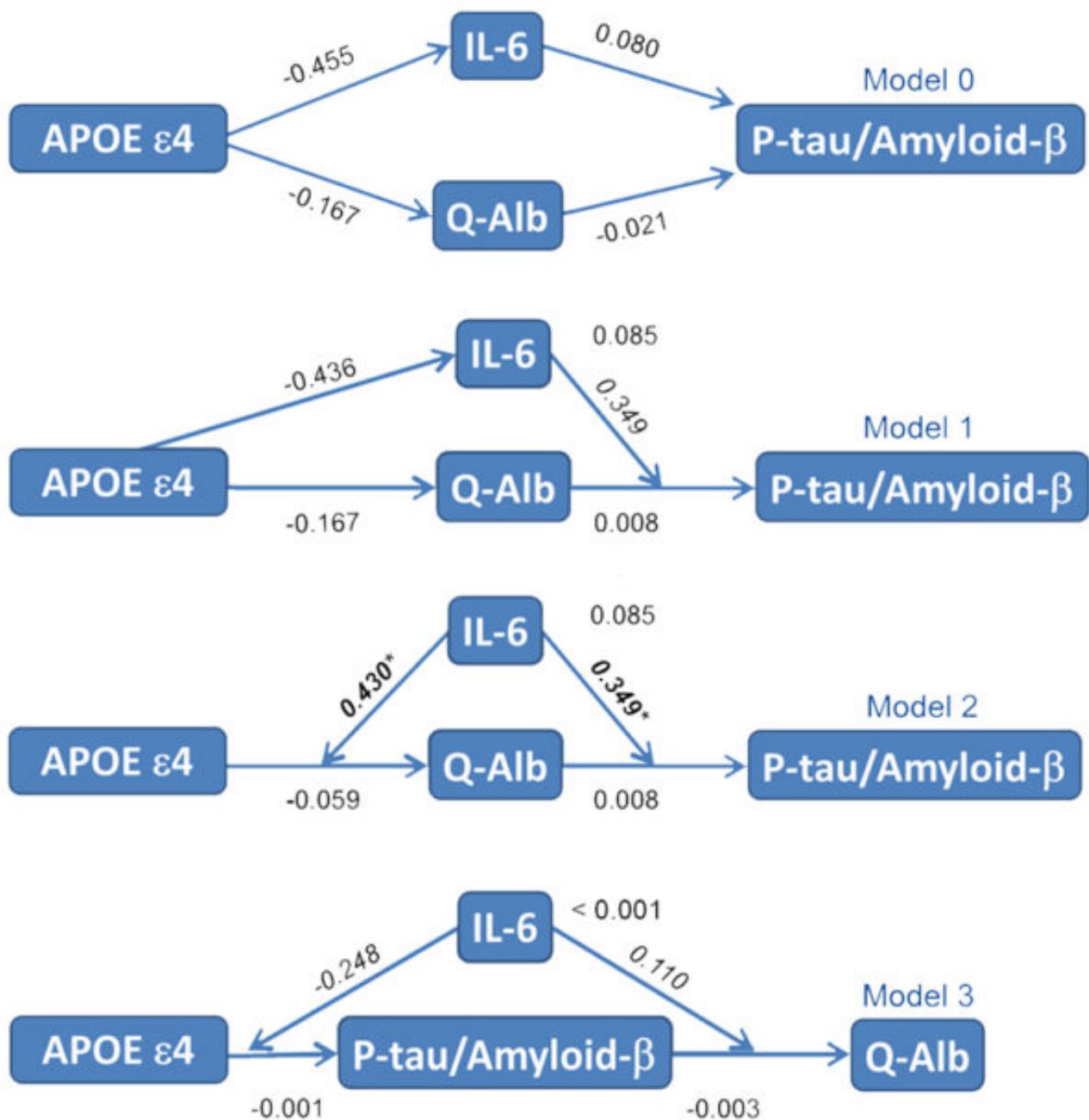


Figure 1 : Path analyses models describing the different examined relations

The interactions of model 2 were significant (Q-Alb~IL-6*APO-ε4 z=2.06, p=0.03; p-Tau/Aβ~Q-Alb*IL-6 z=2.31, p=0.02). This indicates that both BBB dysfunction and inflammation contribute to the relationship between APOE and AD pathology. Interaction estimates are marked in italic, significant associations are marked in bold*.

<i>P</i> -tau/amyloid- β		Q-Alb [95% CI]	Interleukin (IL) [95% CI]	Q-Alb*IL [95% CI]
IL-6	additive	B= -0.0007 [-4.05e-03 0.005]	B= 0.008 [-7.63e-03 0.037]	
	synergistic	B= -0.01 [-0.033 -0.006]**	B= -0.07 [-0.140 -0.01]**	B=0.014 [0.003 0.028] p= 0.002
IL-1b	additive	B= -0.0006 [-0.004 0.005]	B=0.027 [-0.005 0.072]	
	synergistic	B= -0.006 [-0.018 0.004]	B=-0.036 [-0.185 0.113]	B=-0.010 [-0.010 0.038]
IL12p70	additive	B= -0.005 [-0.004 0.004]	B= 0.041 [-0.014 0.061]	
	synergistic	B= -0.0025 [-9.20e-03 0.004]	B= -0.021 [-0.163 0.098]	B= 0.009 [-1.e-02 0.033]

<i>amyloid-β</i>		Q-Alb [95% CI]	Interleukin (IL) [95% CI]	Q-Alb*IL[95% CI]
IL-6	additive	B= 2.83 [-23.52 24.01]	B= 3.83 [-81.52 112.32]	
	synergistic	B= 67.86[9.33 131.95]	B= 291.43 [19.26 594.61]	B= -51.72 [-100.46 -7.64] p=0.037
IL-1b	additive	B= -3.45 [-22.23 25.11]	B= -31.21 [-201.03 216.42]	
	synergistic	B= 29.24[-23.39 89.15]	B= 237.36 [-387.78 934.94]	B= -48.53 [-167.31 49.76]
IL12p70	additive	B= 3.78 [-20.08 24.85]	B= -106.73 [-318.144 55.83]	
	synergistic	B= 1.77 [-29.02 30.22]	B= -170.25 [-693.18 439.69]	B=9.79 [-81.79 90.51]

<i>p</i> -tau		Q-Alb	Interleukin (IL)	Q-Alb*IL
IL-6	additive	B= -0.34 [-1.78 1.90]	B= 4.34 [-2.99 17.56]	
	synergistic	B= -7.34 [-14.79 -2.09]	B= -26.58 [-57.30 -4.45]	B= 5.46 [1.00 12.15] p=0.006
IL-1b	additive	B= -0.22 [-1.72 2.04]	B=6.19 [-7.04 23.61]	
	synergistic	B= -4.10 [-9.55 0.20]	B= -34.25[-101.91 13.76]	B= 7.30 [-0.78 19.85]
IL12p70	additive	B= -0.32 [-1.71 2.12]	B= 15.07 [-19.53 25.18]	
	synergistic	B= -1.63 [-5.25 0.90]	B= -28.46[-95.60 17.83]	B= 6.76 [-2.98 18.92]

Figure 2. synergistic associations of Q-Alb and interleukins on AD pathology

Notes: Significant regressions are denoted in bold taking into consideration of the 95% bootstrapped CI (10,000 draws).[†]

Keywords: APOE-e4, Amyloid, ptau, blood-brain barrier, Inflammation

P43: Heterogeneity of tau PET signal in the sub-nuclei of the amygdala

Zoe B Rubinstein¹, Heidi IL Jacobs¹, Jean Augustinack¹, Michael Properzi¹, J Alex Becker¹, Danielle Mayblyum¹, Emma Thibault¹, Justin Sanchez¹, Aaron Schultz¹, Bernard Hanseeuw^{1,2}, Teresa Gomez-Isla¹, Cristina Lois-Gomez¹, Julie Price¹, Reisa Sperling^{1,3}, Keith A Johnson^{1,3}

¹Massachusetts General Hospital, Boston, MA, US

²Cliniques Universitaires, Saint-Luc, Brussels, Belgium

³Brigham and Women Hospital, Boston, MA, US

Background: Neuropathology studies have shown heterogeneity of tau deposition across sub-nuclei of the amygdala, finding higher levels in the accessory basal nuclei and lower levels in the lateral nuclei. We sought to determine whether a similar pattern was detectable in vivo with tau PET.

Methods: Fifty-six adults (47 cognitively normal, 9 MCI-AD) received a 3T MRI, PiB and MK6240 PET acquisition on the GE Discovery MI PET/CT, and MMSE, GDS, and digital clock drawing test (see Table 1). We identified amygdala sub-nuclei with FreeSurfer 6.0 (Saygin and Kliemann et al. 2017, see Fig. 1), and sampled in 3 ROI, comparable to PET camera resolution: an aggregate Basal and Accessory basal (BasAcc), Lateral, and an aggregate of smaller nuclei including Central, Medial and Cortical (CMCA). We related ROI MK6240 SUVR (reference, cerebellar gray) to age, amyloid burden (PiB FLR), and MK6240 SUVR in whole amygdala, hippocampus, entorhinal cortex, and inferior temporal gyrus.

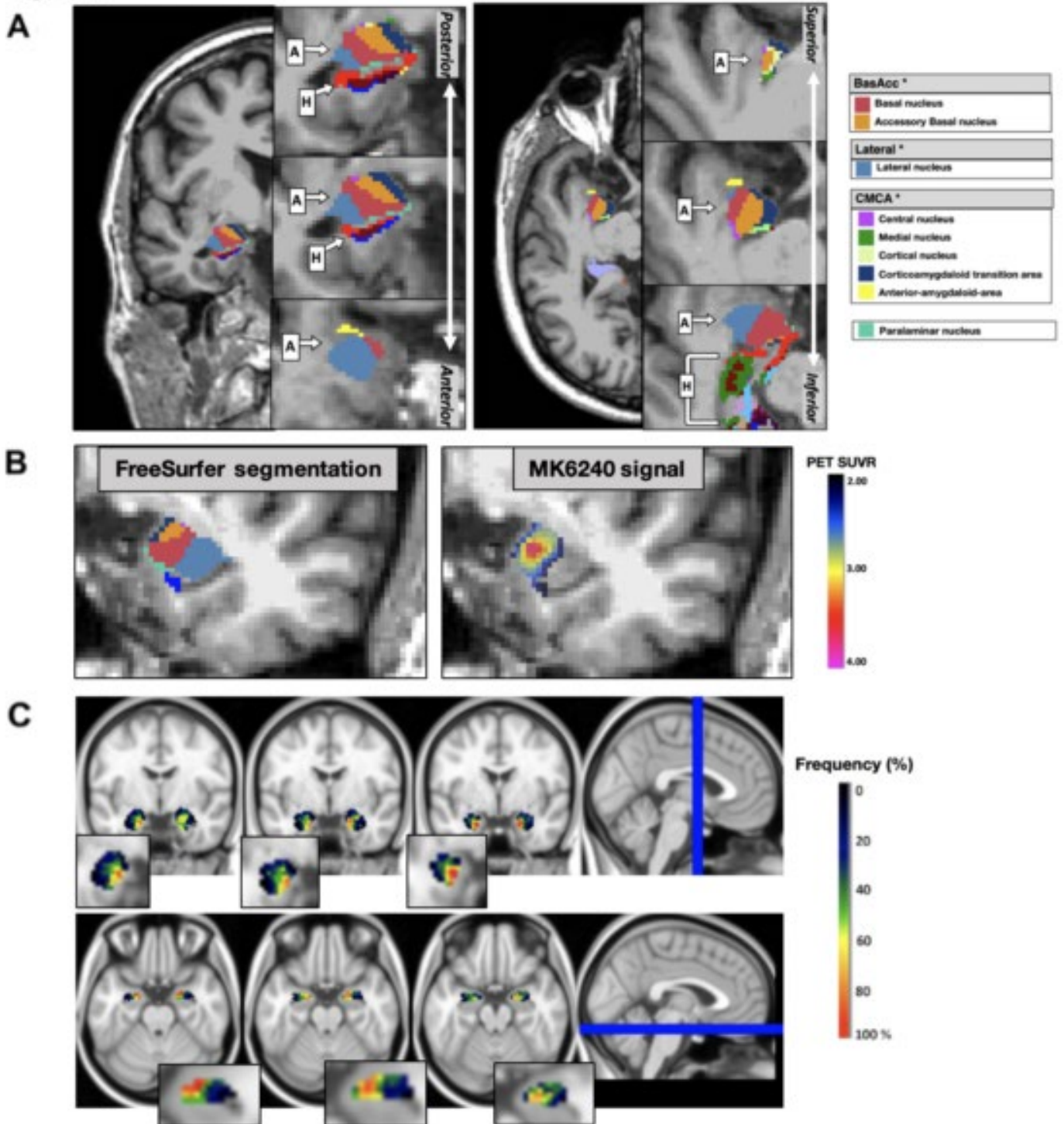
Results: In a sub-sample of people with the greatest MK6240 binding in the amygdala (N=14, 7 cognitively normal, 7 MCI-AD) the majority exhibited high signal (MK6240 SUVR > 1.5) in the medial portion of the amygdala (Figure 1C). In the full sample, we found no correlation between age and BasAcc ($r=-0.10$, $p=0.458$), CMCA ($r=-0.05$, $p=0.706$), or Lateral ($r=-0.04$, $p=0.781$). There was a relationship between neocortical PiB and amygdalar substructure tau (all $r>0.6$, $p<0.001$). Tau in the whole amygdala, hippocampus, entorhinal cortex, and inferior temporal also correlated with tau in the substructures (all $r>0.8$, $p<0.001$).

Conclusion: As AD tauopathy progresses to involve the amygdala, deposition is not uniformly distributed. Instead, specific substructures are selectively involved, particularly the basal and accessory basal nuclei. Considering the connectivity patterns of these substructures and their association with tauopathy, the heterogeneity of tau accumulation in the amygdala could relate to different cognitive phenotypes.

	Overall
N	56
Cognitively Impaired N (%)	9 (16.1%)
Age (years)	67.50 ± 10.20
Male N (%)	31 (55.4%)
High PiB N (%) *	24 (43.6%)
PiB FLR DVR	1.23 ± 0.27
MMSE Score	27.75 ± 3.29
Digital Clock Test Score	66.98 ± 30.00
GDS Score	5.67 ± 4.82
Whole Amygdala MK6240 SUVR	0.85 ± 0.62
Hippocampus MK6240 SUVR	0.83 ± 0.35
Entorhinal Cortex MK6240 SUVR	1.22 ± 0.69
Inferior Temporal MK6240 SUVR	1.30 ± 0.95
Volume of BasAcc (# of PET voxels)	351 ± 47
Volume of CMCA (# of PET voxels)	128 ± 21
Volume of Lateral (# of PET voxels)	331 ± 36

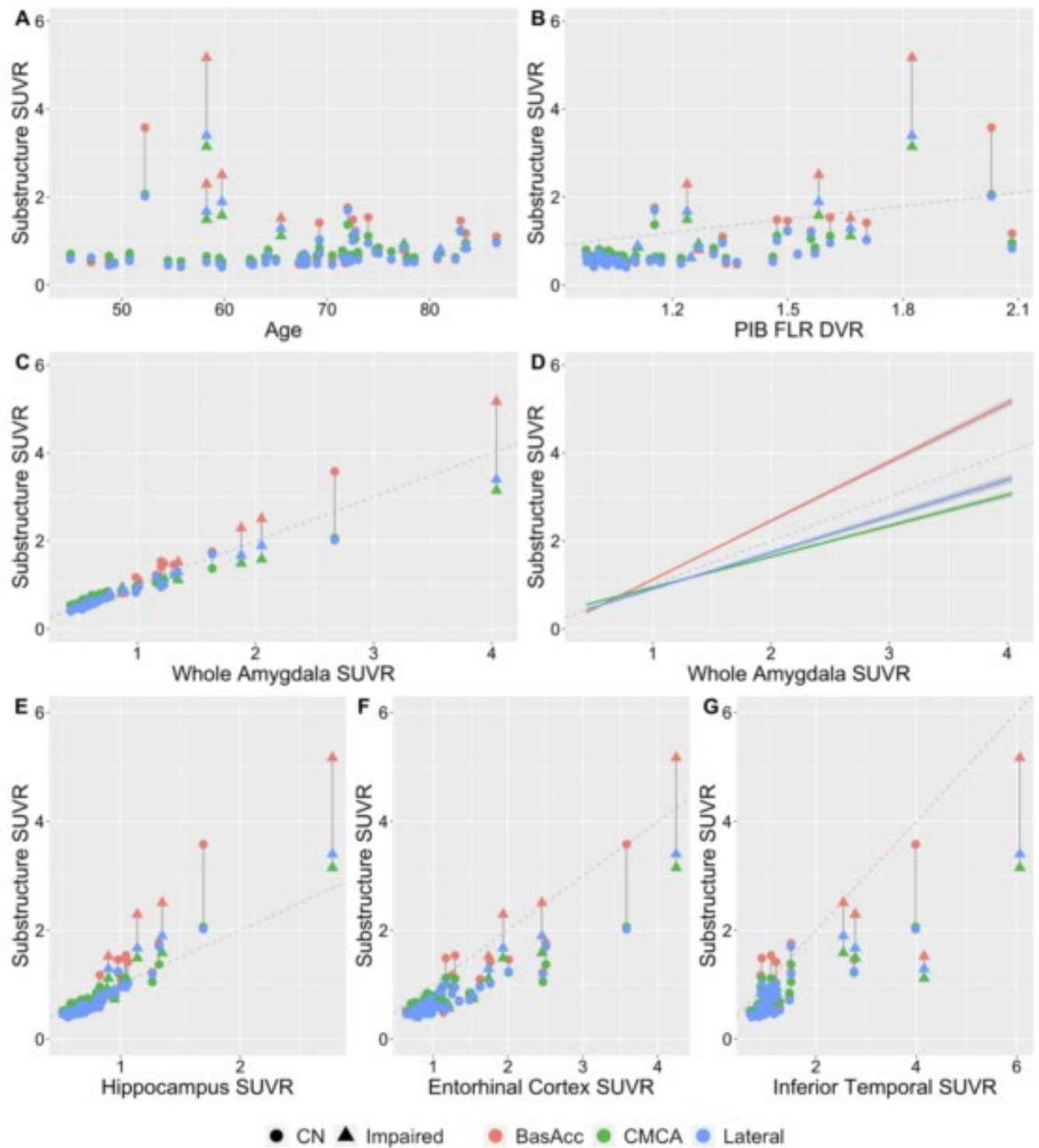
Table 1. Mean ± SD. *PiB FLR DVR ≥ 1.15. “BasAcc” is comprised of the basal and accessory basal nuclei; “CMCA” is comprised of the central nucleus, cortical nucleus, medial nucleus, corticoamygdaloid transition area, and anterior-amygdaloid-area; and “Lateral” is the lateral nucleus. Volumes of amygdala substructures are in PET voxels (1.17mm x 1.17mm x 2.8mm). All DVR and SUVR are computed in PET native space.

Figure 1



A) Sample case of the FreeSurfer segmentation of the amygdala in coronal and axial planes, respectively. Substructures used to sample MK6240 PET data are indicated with *. The paralaminar nucleus was not included in the analyses. Hippocampal subfields are also pictured, for reference: "A"=Amygdala, "H"=Hippocampus. **B)** Sample MR of 59-year-old individual with MCI and high amyloid burden (PiB FLR DVR = 1.58) with overlay of FreeSurfer segmentation and MK6240 PET, respectively. **C)** Frequency map in which voxel color indicates the percentage of individuals with high overall amygdala MK6240 signal (SUVR > 1.5, N=14). Thick blue line depicts orthogonal plane of slices.

Figure 2



Amygdala substructure MK6240 SUVR for each subject are plotted against **A) age, B) neocortical PiB, C) whole amygdala tau, E) hippocampal tau, F) entorhinal tau, and G) inferior temporal tau. D) depicts the linear regression for each substructure in relation to whole amygdala SUVR. Line of identity represented by dotted line in A-G.**

Keywords: amygdala, MK6240, FreeSurfer, PiB

P44: MCI patients demonstrate reliably increasing 18F-AV1451 PET uptake across three exams

David Scott¹, Katarzyna Adamczuk¹, Beth Gorman², Maureen Runkle², Joyce Suhy¹

¹*Bioclinica, Newark, CA, US*

²*Bioclinica, Philadelphia, PA, US*

Background: 18F-AV1451 PET allows in vivo visualization of tau pathology, the accumulation of which contributes to a neurodegenerative cascade toward Alzheimer's Disease. Interindividual differences in uptake patterns complicate the assessment of longitudinal trajectories, posing a challenge in utilizing tau PET signal as a clinical trial endpoint. From a biomarker perspective, a spatiotemporal distribution yielding reliably worsening (increasing) uptake presents the optimal trajectory against which a putative therapy could show some effect. We investigated whether reliably increasing signal could be detected in MCI patients with serial 18F-AV1451 PET exams.

Methods: We identified individuals with at least three 18F-AV1451 PET exams in the ADNI database (<http://adni.loni.ucla.edu>), yielding 120 analyzable exams over 21 normal subjects, 17 MCI and 2 AD patients (average between first and last exams 794 days \pm 122). Raw PET data was motion-corrected, summed, co-registered into MRI space, normalized into MNI template space, and smoothed to uniform resolution. Whole-brain SUVR maps were generated with an inferior cerebellar cortex reference region. Regional SUVR was extracted for AAL2 ROIs, and SUVR maps were entered into SPM voxelwise analysis. ROIs and voxels were classified as reliably increasing when uptake increased between visits 1 and 2 and visits 2 and 3.

Results and Conclusions: MCI patients demonstrated reliably increasing uptake in significantly more brain regions than normal subjects. MCI patients showed reliably increasing tau signal in the majority of ROIs ($t = 2.4$, two-tailed $p < 0.02$), with the most prominent effects seen in fusiform, lingual, parahippocampal gyri in addition to posterior cingulate, amygdala and inferior temporal lobe. A functionally-defined ROI in right parahippocampal gyrus yielded the most dramatic evidence of reliable increasing ($t = 3.6$, two-tailed $p = 0.001$). These results suggest a distributed spatial pattern where, left untreated, 18F-AV1451 uptake can be expected to continually accumulate over time.

Keywords: tau, PET, AV1451, MCI, longitudinal

P45: Development of a qualitative read method for characterizing the presence and extent of brain tau deposition using [18F]MK-6240 PET imaging

John Seibyl¹, Cristian Salinas², Raj Rajagovindan², R. Matthew Hutchison², John Beaver², Laurent Martarello²

¹*Institute for Neurodegenerative Disorders, New Haven, CT, US*

²*Biogen, Cambridge, MA, US*

Introduction: In vivo characterization of pathologic deposition of tau protein in human brain by PET imaging is a promising tool in drug development trials of Alzheimer's Disease and other tauopathies. [18F]MK-6240 is a radiotracer with high selectivity and subnanomolar affinity for neurofibrillary tangles that shows favorable off-target binding, brain penetration, and kinetics. The purpose of the present investigation was to develop a visual assessment method that provides a binary outcome (abnormal yes/no) for tau positivity, and further, to characterize changes in regional cortical tau uptake for use in longitudinal assessments.

Methods: Data from 218 subjects who underwent [18F]MK-6240 scans at 9 different sites was used to generate 60-90 min average static images for each participant. These were reviewed by an expert nuclear medicine physician blind to participants' diagnosis to identify common patterns of brain uptake. Based on this review, a visual read method was developed for field testing, adjustment, re-testing, and finalization.

Results: A three step read process was developed: 1) scan quality assessment, 2) interrogation of specified brain regions, 3) summary assessment. For Step 2, eight bilateral hippocampal and cortical regions are assessed as showing "no abnormal uptake", "<25% involvement", "25-75% involvement", or ">75% involvement" of the region. Step 3 entails application of three rules to render a characterization of "normal", "abnormal AD", or "abnormal not AD". Using this method, an independent read blinded to diagnosis had a sensitivity of 81% and specificity of 94% relative to the clinical diagnosis.

Conclusion: In this ongoing study using [18F]MK-6240 PET, a read algorithm was developed permitting both binary determination of the presence of abnormal brain tau and also the extent of cortical involvement. These cross-sectional results suggest the feasibility of a Braak-like visual PET characterization of progressive tau changes in AD. Further validation in longitudinal cohorts is pending

Keywords: tau, positron emission tomography, Alzheimer's disease, imaging biomarker

P46: PET imaging of [11C]MPC-6827, a microtubule-based PET tracer in murine models of Alzheimer's disease

Kiran Kumar Solingapuram Sai¹, Shannon Macauley¹, Christopher Whitlow¹, Akiva Mintz², Suzanne Craft¹

¹Wake Forest School of Medicine, Winston Salem, NC, US

²Columbia University Medical Center, New York, NY, US

Introduction: In healthy neurons, tau binds to microtubules (MTs) to regulate its stability. In Alzheimer's disease (AD) brain, tau is detached from MTs and phosphorylated at multiple sites. There is a critical need for early AD biomarkers that capture changes in neuronal integrity and stability, especially in the context of A β and tau pathology. MT PET imaging agent could be an ideal bridge between classical biomarkers and molecular imaging tools, providing a solid platform to image brain functions (early on) in AD. We have recently reported the radiochemical synthesis of the first brain-penetrating MT PET ligand, [11C]MPC-6827 and its *in vivo* PET imaging in normal mice. In this presentation, we report the *in vivo* evaluations of [11C]MPC-6827 in amyloid β (A β)-over expressing (APP-PS1, 5xFAD) and tau-over expressing (P301S) transgenic and wild-type AD mice.

Methods: Dynamic PET imaging was performed in both transgenic (TG) and wild-type (WT) (n=4/group); APP-PS1 at 3m, 18m and 22 months; 5xFAD (at 15 months) and P301S mice (at 8 months) by injecting 120 ± 20 μ Ci of [11C]MPC-6827. *Ex vivo* post-PET biodistribution studies were performed in both TG and WT APP/PS1 and 5xFAD mice (n=3/group).

Conclusions: [11C]MPC-6827 showed significant lower radioactive uptake in the transgenic APP-PS1, 5xFAD and P301S mice over their corresponding wild-type control mice. Post-PET biodistribution results in brain corroborated well with the microPET/CT analysis.

Next steps: We will correlate [11C]MPC-6827 uptake with tau pathologies and perform PET/CT imaging in NHP model of AD at our ADRC.

Therefore, [11C]MPC-6827 could serve as a potential early PET imaging biomarker of AD related diseases (ADRD).

Keywords: PET, Microtubule, novel biomarker, AD mice model, imaging

P47: Quantifying the relationship between the brain distributions of tau and local atrophy to inter-regional connectivity based on individual human data

Jean-Paul Soucy^{1,2}, Fatameh Mohammadi², Pedro Rosa-Neto¹, Tharick Pascoal¹, Melissa Savard¹, Min Su Peter Kang¹, Joseph Therriault¹, Habib Benali²

¹*McGill University, Montreal, QC, Canada*

²*PERFORM Centre - Concordia University, Montreal, QC, Canada*

Models of tau distribution in AD brains assume that progression proceeds through propagation along axons connecting specific regions. While this is a logical hypothesis, it has never been formally tested by demonstrating that connectivity between two regions results in correlation of tau SUVRs or cortical thickness across regions. We assessed this on human data from subjects of the ADNI cohort with AD.

We have included in this study 35 AD subjects from ADNI with 2 PET Tau studies (¹⁸F-florbetapir) at 2 different times, Ta and Tb, and a T₁ weighted MRI. Eighteen subjects turned out to be non-progressors (NP: no significant change between time 1 and 2 in hippocampal SUVRs values) while 17 subjects were progressors (P: significant change between time 1 and 2 in hippocampal SUVRs values). This criterion was considered to represent how far advanced the patients were in their disease. We also evaluated 19 age-matched controls to assess normal regional cortical thickness. Using FreeSurfer, the pre-processed T₁ images were segmented in 68 standard regions, for which SUVRs and cortical thickness values were extracted. No DTI-MRI being available, we used a standard connectivity map (Human Connectome Project). We used Moran's I statistics, which allow for determination of the impact of "spatial proximity" (here, connectivity) on the correlation between values of a parameter in different regions, to assess whether highly connected brain ROIs also show higher correlation of SUVRs/thickness than more weakly connected ones.

The p-values of Moran's I indices for NPs and Ps in both SUVRs and thickness at Ta and T2 were all <0,01. Hence, we conclude that there is a strong impact of structural connectivity on the correlation of both parameters across the whole brain. This confirms that indeed, *in vivo*, tau aggregates do diffuse in the brain as predicted by connectivity across regions.

Keywords: Tau, Atrophy, Progression, Model

P48: Monitoring disease pathophysiology using multiparametric PET acquisitions: The McGill TRIAD Cohort

Jenna Stevenson^{1,2}, Mira Chamoun^{1,2}, Tharick A. Pascoal^{1,2}, Andrea Benedet^{1,2}, Min Su Kang^{1,2}, Sulantha Mathotaarachchi^{1,2}, Joseph Therriault^{1,2}, Emilie Thomas^{1,2}, Melissa Savard^{1,2}, Cecile Tissot^{1,2}, Firoza Lussier^{1,2}, Tasha Vinet-Celluci^{1,2}, Nesrine Rahmouni^{1,2}, Guylaine Gagné^{1,2}, Meong Joung^{1,2}, Sarah Sbeiti^{1,2}, Monica Shin^{1,2}, Paolo Vitali^{1,2}, Serge Gauthier^{1,3}, Pedro Rosa-Neto^{1,2}

¹McGill University, Verdun, QC, Canada

²Translational Neuroimaging Laboratory, Montreal, QC, Canada

³Douglas Hospital Research Centre, Verdun, QC, Canada

Introduction: The Translational Biomarkers in Aging and Dementia (TRIAD) cohort aims at describing the biomarker trajectories and interactions between pathophysiological processes as drivers of dementia. As part of the McGill Research Centre for Studies in Aging, TRIAD focuses on advanced personalized and preclinical dementia diagnosis. TRIAD's main objectives include understanding the interactions between amyloid- β and tau and their role in the progression of brain atrophy and cognitive decline, as well as the role of neuroinflammation, epigenetics and synaptic depletion as mediators of cognitive decline.

Study Design: Inclusion into the TRIAD cohort begins with a telephone screening ensuring the participant's eligibility. Participants sign an ethically approved consent form where they agree to donate biofluids (blood, urine, saliva and cerebrospinal fluid) at the first on-site visit. The second visit consists of an extensive neuropsychological battery. During subsequent visits, participants undergo three PET scans and one MRI. The PET scans are dependent on their diagnosis and the project in which they are enrolled. TRIAD cohort uses a variety of tracers in their different projects to detect the presence of different protein accumulation in the brain. These tracers include [¹⁸F]MK6240, [¹⁸F]AV1451, [¹⁸F]PI2620 and [¹⁸F]RO948, [¹⁸F]AZD4694, [¹¹C]PBR or [¹⁸F]DPA, [¹⁸F]FEOBV [¹¹C]MRT and [¹¹C]UCB-J. TRIAD participants return for follow-up clinical and imaging visits 12 and 24 months after baseline with a retention rate of 70%.

Results: Since 2017, the TRIAD registry has recruited 1,285 people and has enrolled 576 participants. Enrolled in the TRIAD studies are individuals without cognitive impairment (n=345), with mild cognitive impairment (n=75), sporadic and autosomal-dominant Alzheimer's disease (n=90), atypical dementia (n=27) and individuals under evaluation (n=39).

Conclusion: TRIAD cohort presents a distinct opportunity to further understand the progression of Alzheimer's disease with resources ready to uphold the use of affordable biomarkers, capable of diagnosing and measuring disease progression.

Keywords: biomarkers, cohort, diagnosis

P49: Interaction between amyloid and neuroinflammation on apathy along the Alzheimer's disease spectrum

Cécile Tissot^{1,2,3}, Min Su Kang^{1,2}, Andrea Benedet^{1,2,3}, Nesrine Rahmouni^{1,2}, Tharick A. Pascoal^{1,2}, Mira Chamoun^{1,2,3}, Joseph Therriault^{1,2,3}, Firoza Lussier^{1,2,3}, Melissa Savard^{1,2}, Sulantha Mathotaarachchi^{1,2,3}, Emilie Thomas^{1,2}, Serge Gauthier^{1,2,3}, Pedro Rosa-Neto^{1,2,3}

¹McGill University, Montreal, QC, Canada

²Translational Neuroimaging Laboratory, Montreal, QC, Canada

³Douglas Hospital Research Center, Verdun, QC, Canada

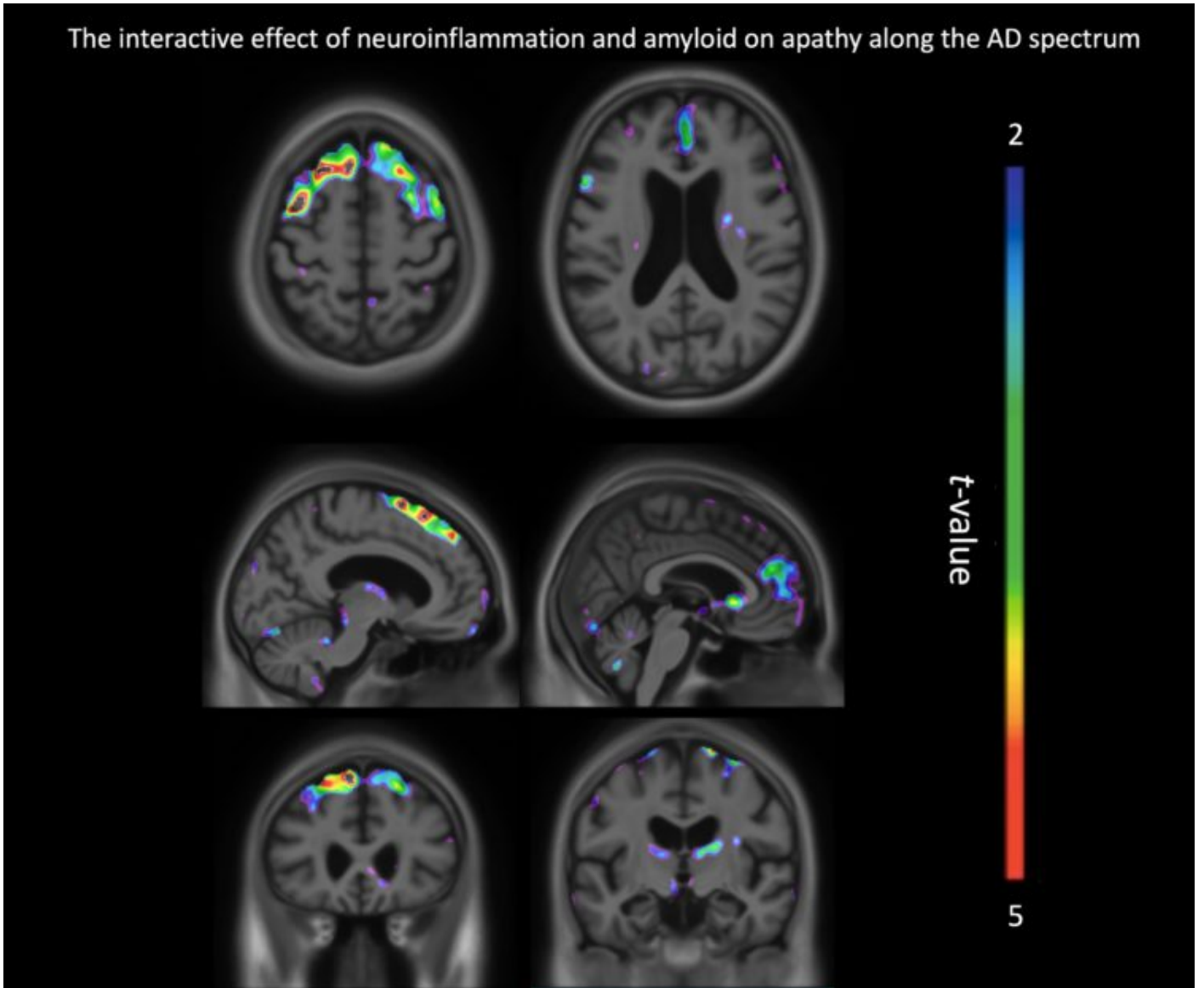
Introduction: The Apathy Inventory is a rating scale given to informants in order to assess levels of apathy globally. This neuropsychiatric symptom is the most common noncognitive symptom in Alzheimer's disease (AD), and it causes a great burden on diseased individuals and their caregivers. Even though it has been closely related to cerebrospinal fluid levels of neuroinflammation and amyloid, the interactive effect of pathologies is still unclear. Here we test the interaction between amyloid and neuroinflammation in the brain with apathy, along the AD spectrum.

Methods: We assessed 59 individuals (38 cognitively unimpaired, 15 mild-cognitive impairment, 6 AD) with [¹¹C]PBR28-neuroinflammation positron-emission tomography (PET) and [¹⁸F]AZD4694-amyloid PET. [¹¹C]PBR28 and [¹⁸F]AZD4694 uptake value ratios (SUVRs) used the cerebellum grey matter as the reference region and were calculated 0-90 min post-injection and 40-70 min post-injection respectively. A voxel-based regression model evaluated the relationship between the interaction of [¹⁸F]AZD4694 and [¹¹C]PBR28 with Apathy Inventory scores. The model's covariates were age, gender, education and diagnoses of the participants.

Results: We found a strong positive correlation between the interaction of [¹⁸F]AZD4694 and [¹¹C]PBR28 with apathy. The most impacted regions were the medialfrontal cortex, in the superior portion and prefrontal cortex, as well as the anterior nucleus of the thalamus.

Conclusion: These preliminary results show an interactive link between two pathophysiologicals of AD, amyloid and neuroinflammation, that potentiate apathy. The regions impacted are involved in behavioral regulation, such as the medialfrontal cortex. On the other hand, the results found in the thalamus might be indicators of a poorer connection between different brain regions, leading to an increase of apathetic symptom. This study corroborates with previous findings that amyloid and neuroinflammation are related to apathy. The limbic dysfunctions causing apathy might thus be due to the interactive effect of amyloid and neuroinflammation along the AD spectrum.

The interactive effect of neuroinflammation and amyloid on apathy along the AD spectrum



Keywords: apathy, neuroinflammation, amyloid, interaction

P50: Neuropsychiatric symptoms in cognitively impaired individuals are correlated with tau deposition

Cécile Tissot^{1,2,3}, Joseph Therriault^{1,2,3}, Tharick A. Pascoal^{1,2,3}, Mira Chamoun^{1,2}, Firoza Lussier^{1,2,3}, Melissa Savard^{1,2}, Sulantha Mathotaarachchi^{1,2}, Andrea Benedet^{1,2,3}, Emilie Thomas^{1,2,3}, Pedro Rosa-Neto^{1,2,3}, Serge Gauthier^{1,3}

¹McGill University, Montreal, QC, Canada

²Translational Neuroimaging Laboratory, Montreal, QC, Canada

³Douglas Hospital Research Center, Verdun, QC, Canada

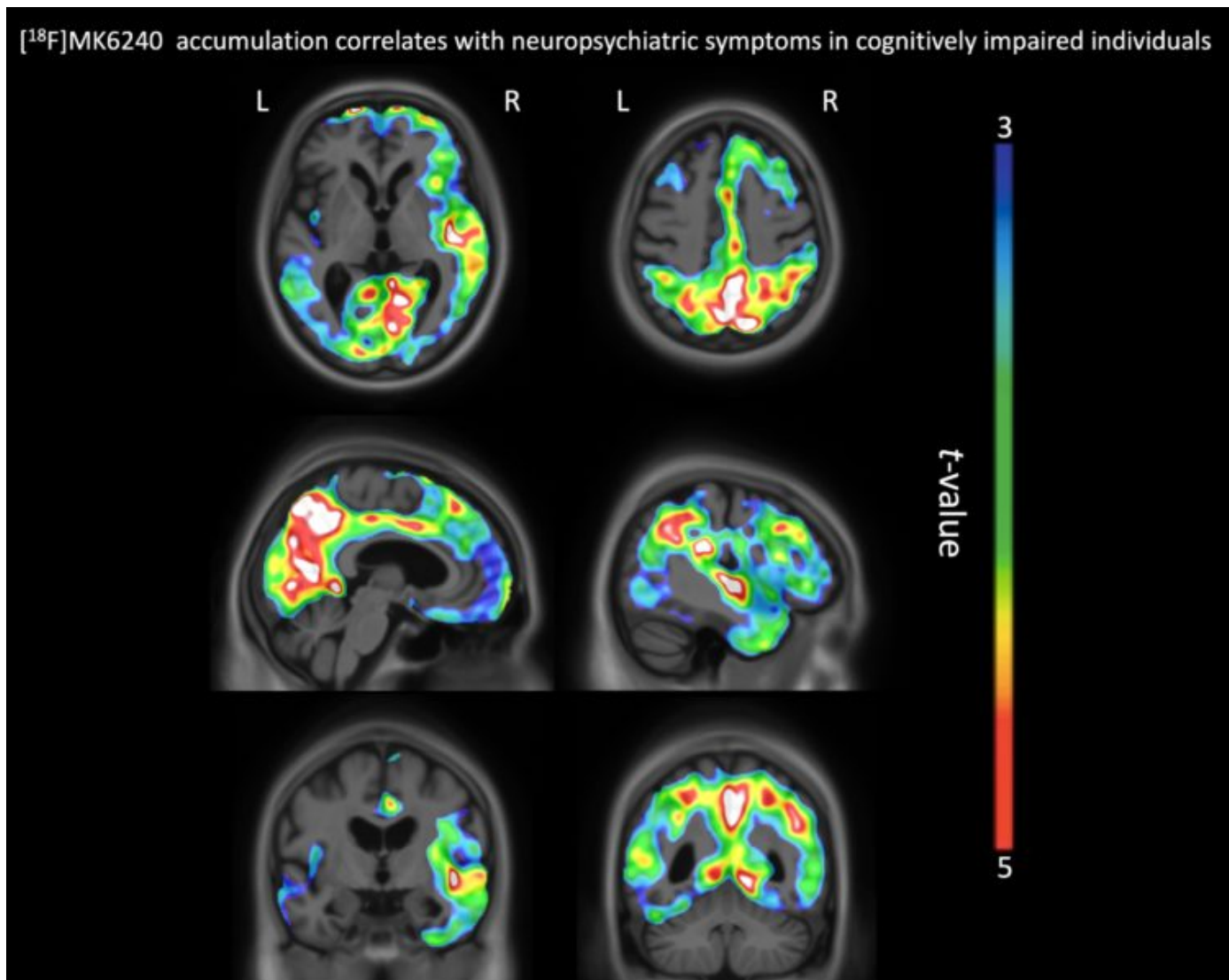
Introduction: Neuropsychiatric Inventory-Questionnaire (NPI-Q) is a survey addressed to informants to assess the participant's neuropsychiatric symptoms (NPS) and their impact on the participant and their informant. Although NPS have been closely related to the clinical progression to dementia in carriers of Alzheimer's disease (AD) pathophysiology, the relationship between NPS and brain amyloid, tau and neurodegeneration pathologies is still unclear. Here we test the relationship between tau aggregates in the brain and NPS in cognitively impaired (CI) individuals.

Methods: 61 CI individuals (MCI = 34, AD = 27) underwent positron emission tomography (PET) amyloid [¹⁸F]AZD4694 and tau [¹⁸F]MK-6240. [¹⁸F]AZD4694 and [¹⁸F]MK-6240 standardized uptake value ratios (SUVRs) used the cerebellum grey matter as the reference region and were calculated between 40-70 min and 90-110 min post-injection, respectively. Analyses with voxel-based morphometry (VBM) were also conducted. A voxel based regression model evaluated the relationship between the accumulation of a biomarker, using [¹⁸F]MK6240 or [¹⁸F]AZD4694 PET scans, VBM, and the NPI-Q scores. The model's covariates were age, gender and years of education. We corrected for amyloid deposition when analyzing [¹⁸F]MK6240, and for tau deposition when analyzing [¹⁸F]AZD4694.

Results: We found strong positive correlation between NPI-Q and [¹⁸F]MK6240. The most impacted regions were the precuneus, the hippocampal formation, and the frontal cortex. However, we did not find any correlation between NPI-Q and [¹⁸F]AZD4694 uptake nor VBM.

Conclusion: These preliminary results show a compelling correlation between NPS and regions related to behavioral disturbances, such as the frontal cortex, as well as the first regions impacted in AD, meaning the precuneus and hippocampus. This corroborates with the idea that tau is more closely related with cognitive and behavioral symptoms than other AD pathophysiology. This study demonstrates that NPS correlate with neurofibrillary tangles, it is thus important to assess them, with the help of a reliable informant.

[¹⁸F]MK6240 accumulation correlates with neuropsychiatric symptoms in cognitively impaired individuals



Keywords: neuropsychiatric symptoms, tau, Alzheimer's disease

P51: Association between [18F]NAV4694 PET amyloid- β measures and fluid biomarkers across the spectrum of Alzheimer's disease

Yi-Ting Wang^{1,2}, Tharick Pascoal^{1,2}, Joseph Therriault^{1,2}, Andr ea Benedet^{1,2}, Firoza Lussier^{1,2}, Melissa Savard^{1,2}, Min Su Kang^{1,2}, Cecile Tissot^{1,2}, Serge Gauthier^{1,2}, Pedro Rosa-Neto^{1,2}

¹Translational Neuroimaging Lab, Montreal, QC, Canada

²McGill Center for Studies in Aging, Montreal, QC, Canada

Background: [¹¹C]PiB and [¹⁸F]Florbetapir are by far the most well-studied amyloid PET radioligands. Standardised uptake value ratios (SUVRs) of both tracers are highly correlated with CSF A β biomarkers, and they showed similar classification accuracy and diagnostic agreement. Recently, intensive research focuses on plasma biomarkers due to its potential to be applied in routine clinical settings as a screening measure. [¹⁸F]NAV4694, a third generation A β PET radiotracer, has been validated to display imaging characteristics nearly identical to those of [¹¹C]PiB. In addition, the low white matter and high cortical binding support its utility in both research and clinical settings. However, the association between [¹⁸F]NAV4694 PET A β measures and AD fluid biomarkers has not yet been studied in living humans.

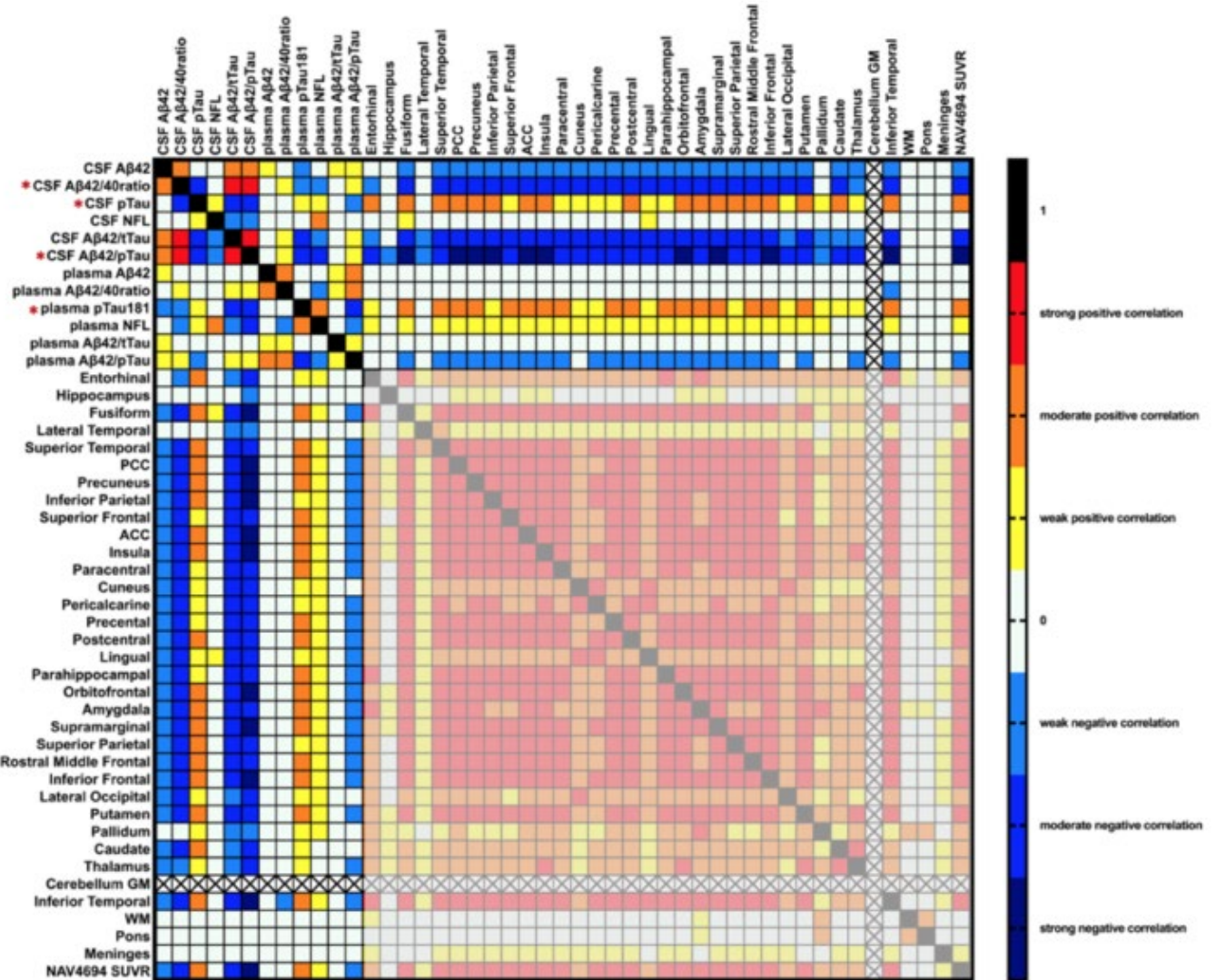
Objectives: (1) Validate the association between [¹⁸F]NAV4694 PET A β SUVR and CSF A β biomarkers
(2) Investigate the relationship between [¹⁸F]NAV4694 PET SUVR, CSF and plasma biomarkers

Methods: This was a cross-sectional study in 106 subjects with AD (n=10), MCI (n=22), cognitively normal controls (n=54) and young healthy controls (n=20) from the TRIAD cohort at McGill Centre for Studies in Aging, Canada. Associations were tested between [¹⁸F]NAV4694 PET SUVRs, CSF and plasma biomarkers.

Results: [¹⁸F]NAV4694 PET global SUVR showed strong correlation with CSF A β 42/pTau ratio (P<0.001, Pearson's $r=0.78$), and moderate correlation with CSF A β 42, CSF pTau and plasma pTau181 (P<0.001, Pearson's r : CSF A β 42=0.45, CSF pTau=0.58, plasma pTau181=0.6). [¹⁸F]NAV4694 PET A β measures demonstrated linear relationships with CSF A β 42, CSF A β 42/40, CSF pTau and plasma pTau181 level.

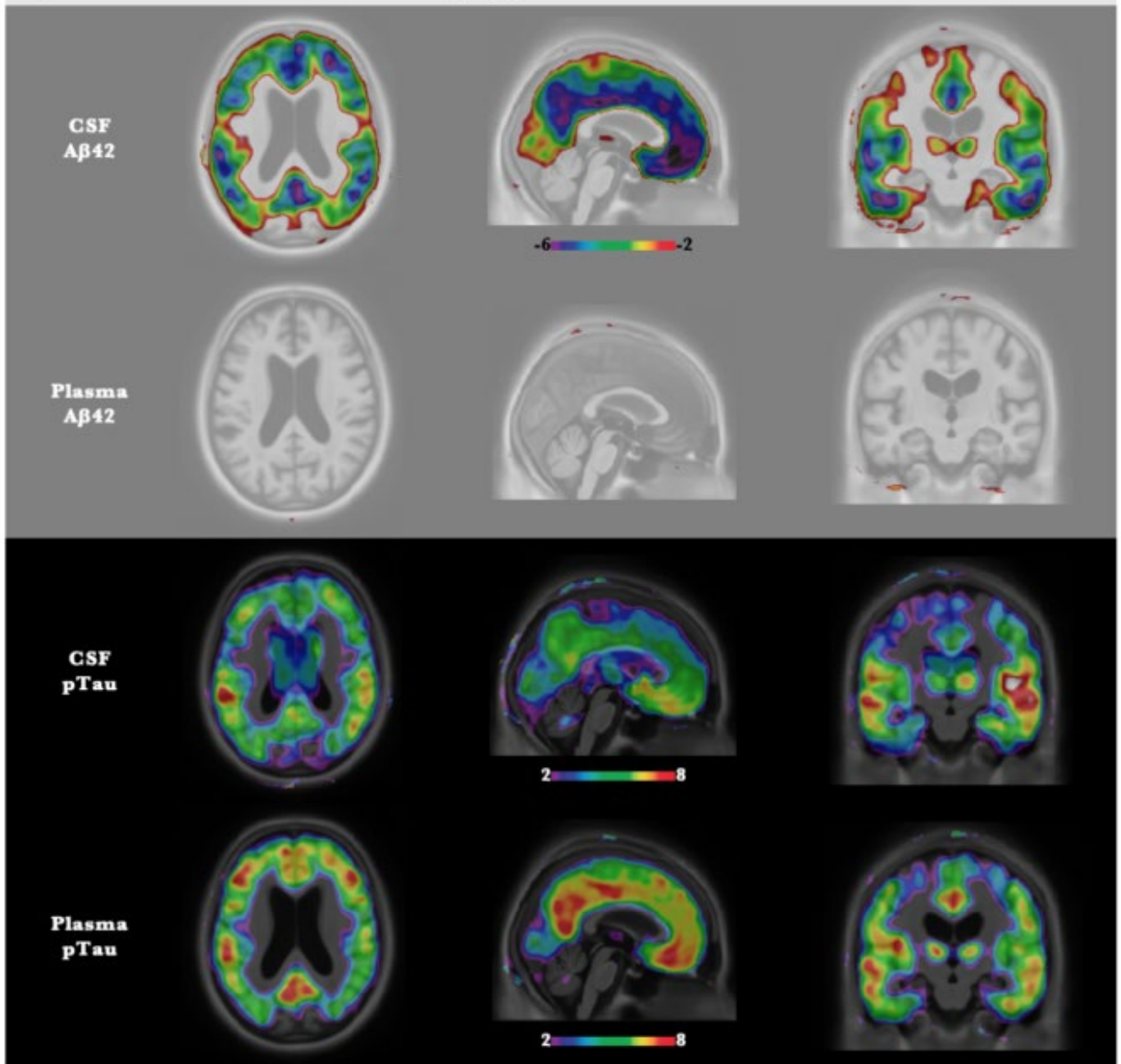
Conclusion: Our results support the high concordance between CSF biomarkers and [¹⁸F]NAV4694 PET SUVRs, especially when CSF A β 42/pTau ratio was used. Furthermore, these findings note that although CSF biomarkers generally correlate better with [¹⁸F]NAV4694 PET imaging biomarkers, when modelling properly, plasma pTau could be a promising biomarker for monitoring disease progression throughout the course of AD.

Figure 1. Correlation map of CSF, plasma biomarkers and NAV4694 SUVR



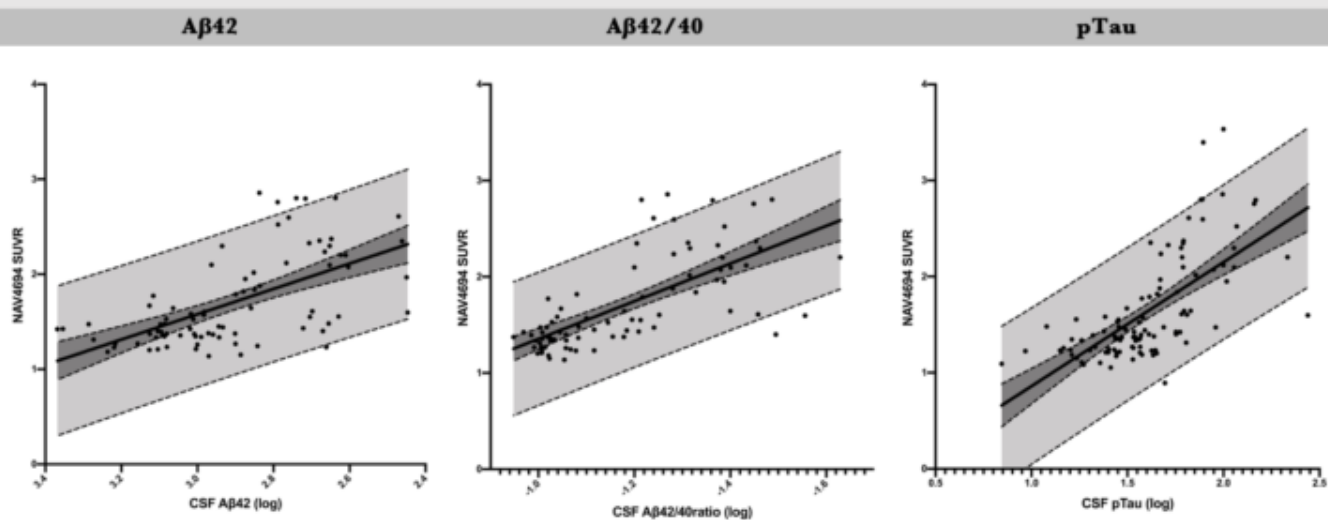
Associations between [¹⁸F]NAV4694 PET SUVR, CSF biomarkers and plasma biomarkers in the TRIAD cohort. [¹⁸F]NAV4694 PET SUVR showed the strongest correlation with CSF biomarkers Aβ42/pTau, while moderate correlation between NAV4694 SUVRs and CSF Aβ42/40, CSF pTau were also observed. Among plasma biomarkers, only pTau181 showed moderate correlation with [¹⁸F]NAV4694 PET SUVR. *Cerebellum GM* was used as the control region. *NAV4694 SUVR* indicated global Aβ PET measure, and different regions denoted the regional SUVR of [¹⁸F]NAV4694.

Figure 2. Voxelwise association between A β 42, pTau and NAV4694 SUVR



In voxel-wise analyses, significant negative correlation was found between NAV4694 global SUVR and CSF A β 42 level, no significant correlation was observed between NAV4694 global SUVR and plasma A β 42 concentration. On the other hand, significant positive correlations between NAV4694 SUVR and pTau in both CSF and plasma were identified in similar cortical regions. Colour bar indicates t-score.

Figure 3. Relationship between NAV4694 global SUVR and CSF A β 42, A β 42/40 and pTau



[¹⁸F]NAV4694 PET global SUVR showed linear relationship with A β 42 ($R^2=0.36$), A β 42/40 ($R^2=0.5$) and pTau ($R^2=0.45$). The values of A β 42 and A β 42/40 in x-axis were reversed for the illustration of AD disease progression. Dark grey indicated 95% confidence interval, light grey indicated 95% prediction interval.

Keywords: Alzheimer's disease, amyloid PET imaging, CSF biomarker, plasma biomarker

P52: PET beta-amyloid deposition in healthy older adults is associated with decreased lure discrimination on a spatial mnemonic similarity task

Christina Webb¹, Chris Foster¹, Marci Horn¹, Kristen Kennedy¹, Karen Rodrigue¹

¹*Center for Vital Longevity, The University of Texas at Dallas, 75235, TX, US*

Individuals with clinically significant beta-amyloid (A β) burden exhibit episodic memory impairment. There has been recent interest, however, in investigating associations between memory performance and subclinical A β deposition in cognitively normal older adults. Overall, the link between A β and memory performance in normal aging is typically weak; however, the majority of studies have utilized measures of general memory function. It remains to be determined whether performance on memory tests that tax hippocampal pattern separation specifically are sensitive to A β burden. Here we examine in 37 adults aged 55-98 years associations between Florbetapir uptake and performance on a spatial mnemonic similarity task that is highly sensitive to hippocampal pattern separation processes. During encoding, participants studied pictures of everyday items in various locations on a computer screen. At retrieval, they were presented with both studied and new items, as well as similar lure items that varied in the degree of similarity to the studied exemplar. Accurate lure discrimination involved identifying lures as being similar, but not exact, to that which was studied. Results of a linear mixed model showed independent effects of A β on the slope of lure discrimination across levels of lure similarity, beyond effects of age or APOE-e4 status. Specifically, greater A β deposition was associated with a reduced slope in lure discrimination across the three levels of lure similarity. Older adults with lower A β were better able to modulate accurate discrimination of old from similar lure items as a function of decreasing similarity. Older adults exhibiting higher A β , however, showed reduced mnemonic discrimination across levels of target-lure similarity, suggesting a diminished ability to separate memory representations even when they become increasingly distinct. Overall, results suggest that even subtle elevation in A β burden in cognitively normal adults negatively affects hippocampal pattern separation processes that support discrimination of highly similar memory representations.

Keywords: beta-amyloid, preclinical AD, subthreshold amyloid, pattern separation

P53: Socioeconomic status mediates racial differences seen using the A-T(N) Framework

Julie Wisch¹, Darrell Hudson¹, Dean Coble¹, Chengjie Xiong¹, Ganesh Babulal¹, Brian Gordon¹, Shaney Flores¹, Aylin Dincer¹, Tammie Benzinger¹, John Morris¹, Beau Ances¹

¹*Washington University, St. Louis, MO, US*

Background: Previous research shows African Americans are potentially at greater risk for developing Alzheimer's disease (AD). Genetic, social (psychosocial), environmental, and cardiovascular factors may increase the risk of AD.

The objectives of this project were to:

- 1) Assess neuroimaging biomarkers of amyloid (A), tau (T), and neurodegeneration (N) for potential racial differences.
- 2) Consider mediating effects of socioeconomic status and cardiovascular risk factors on observed race differences.

Methods: Biomarker measures of neurodegeneration (structural MRI and resting state functional connectivity (rs-fc)) and amyloid and tau PET data were collected from African American (n=169) and Caucasian (n=936) participants enrolled in studies at the Knight Alzheimer Disease Research Center (ADRC). Cardiovascular health (white matter hyperintensities on MRI, blood pressure, and body mass index (BMI)) and socioeconomic status (area-level socioeconomic status assessed by the area deprivation index (ADI)) were included in mediation analyses.

Results: Compared to Caucasian participants, African American participants had lower amyloid PET accumulation but greater neurodegeneration, as measured by decreased cortical volumes and decreased global intra-network rs-fc (Figure 1). African Americans also had lower socioeconomic status (SES), higher blood pressure, higher BMI, and greater WMH volumes. These proposed mediators (Figure 2) significantly influenced associations between race and cortical amyloid PET accumulation, AD cortical signature volume, and intra-network rs-fc signature. ADI in particular was a significant mediating factor (Figure 3).

Conclusions: Observed racial differences in AD are not primarily due to immutable, genetic differences, but rather by modifiable factors fueled by differences in social context and resources, especially area-level SES. Future studies should emphasize collection of relevant psychosocial factors (e.g. stress, discrimination, healthcare access, etc.) in addition to the development and implementation of intentional diversity and inclusion efforts to improve the racial/ethnic and socioeconomic representativeness of AD studies.

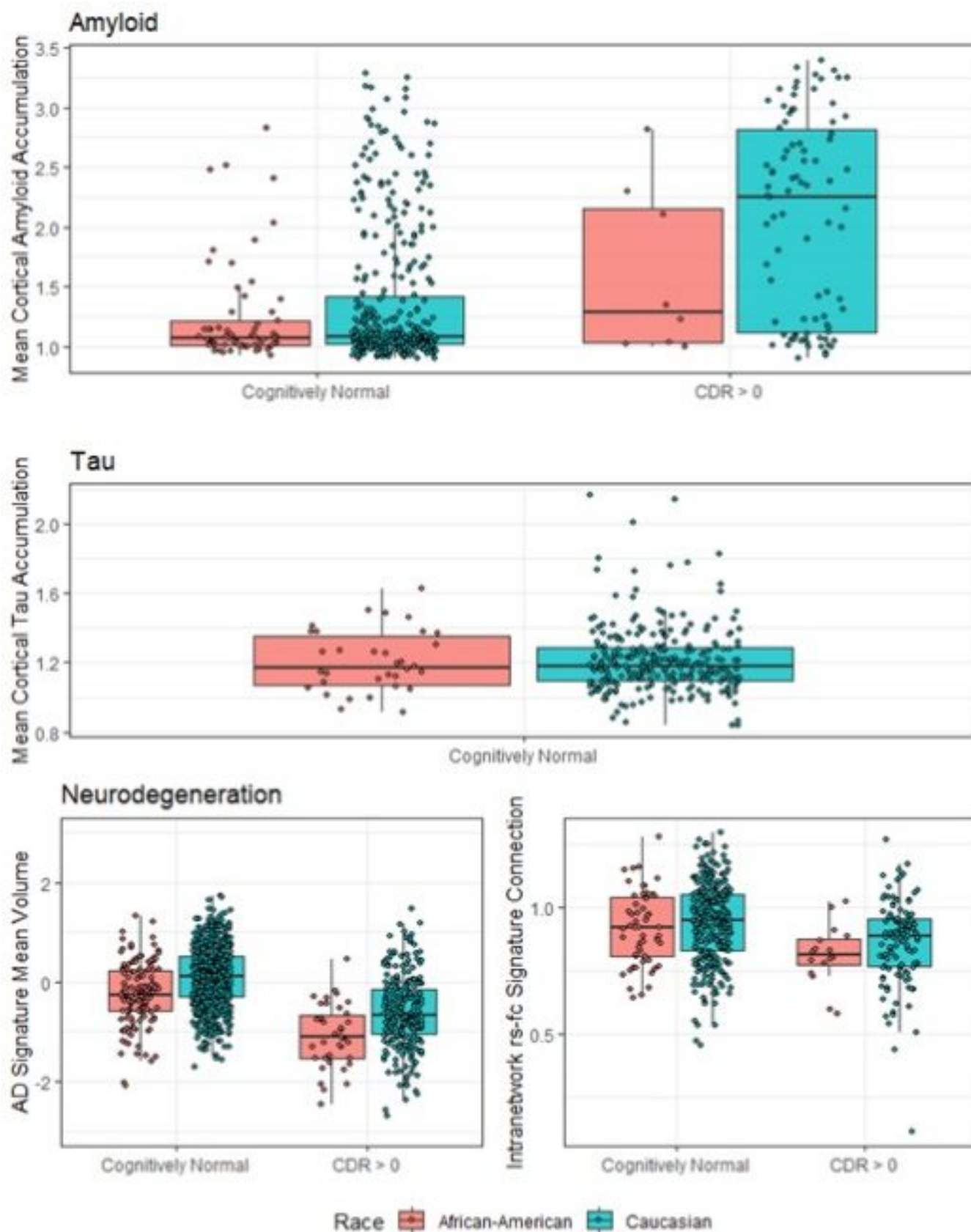


Figure 1. Racial differences are observable in amyloid accumulation (Caucasians have significantly greater amyloid accumulation), AD Signature volume, and rs-fc intranetwork connection strength. Differences by cognitive status are present for tau and neurodegeneration markers. We were unable to evaluate a race by cognitive status interaction for tauopathy due to insufficient sample size.

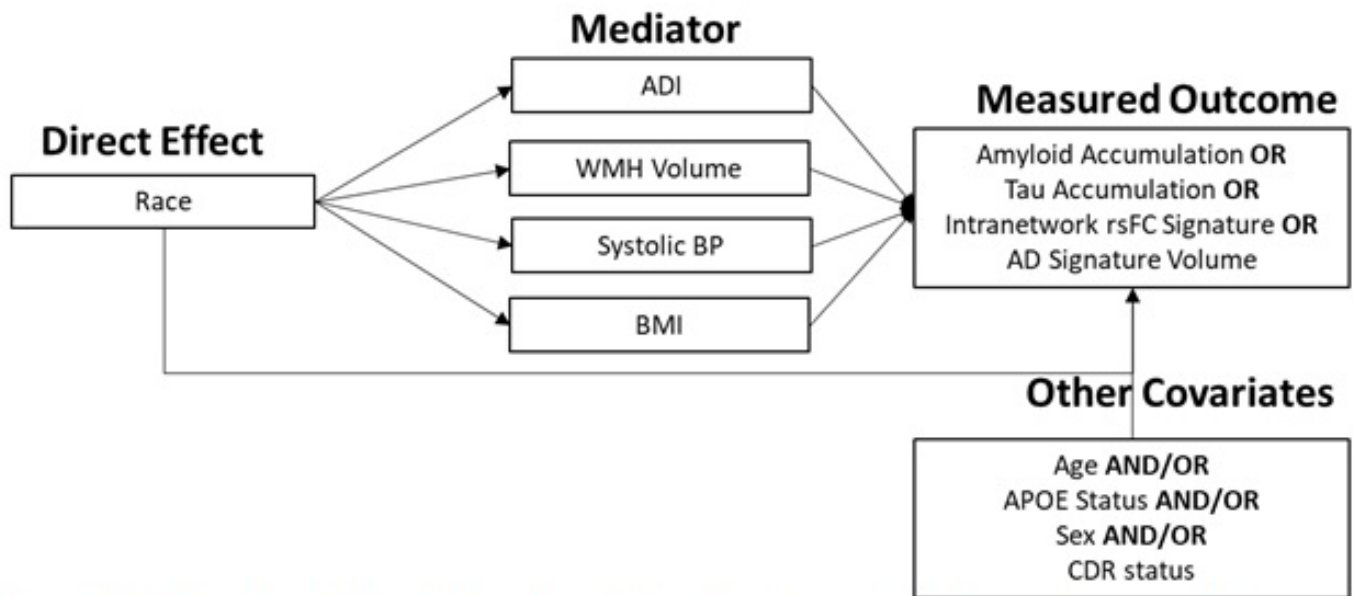


Figure 2. Our hypothesized mechanism of mediation. We aim to test whether socioeconomic status (ADI) or any of three cardiovascular-related factors have a mediating impact of the effect of race on the A-T(N) measures used throughout the analysis. In addition to forcing the hypothesized mediators into the model, we allow for the consideration of four other key covariates: age, APOE ϵ 4 status, sex, and cognitive status as possible mediators of the direct race effect.

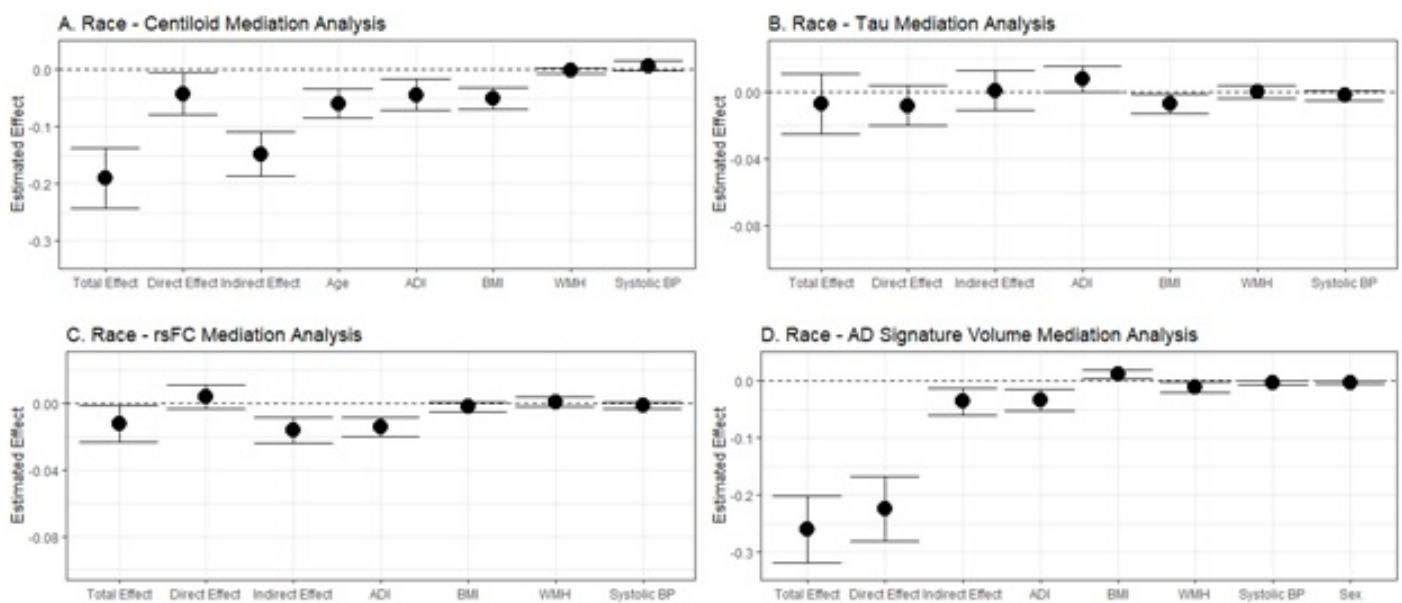


Figure 3. The effect of being African American, as opposed to Caucasian, on the A-T(N) measures considered is shown as the total race effect. The total effect is a sum of the direct and indirect effects. The direct effect indicates the size of the effect not explained by any of the mediating factors. The indirect effect indicates the size of the effect explained by the mediating factors. Age, ADI, and BMI explain nearly all of the race effect on amyloid accumulation (Fig. 3a). There is no significant race effect on tau (Fig. 3b). The indirect effect of race on intranetwork rs-fc signature is almost entirely explained by ADI (Fig. 3c). The majority of the racial effect on AD signature volume cannot be explained by any of the hypothesized parameters; however, ADI does make a significant contribution to the racial disparity, as does white matter hyperintensity volume (Fig. 3d).

Keywords: PET, fMRI, Race, Health Disparities

P54: Tau pathology and relative cerebral blood flow are independently associated with cognition in Alzheimer's disease

Emma Wolters^{1,2}, Denise Visser¹, Sander Verfaillie¹, Emma Coomans¹, Tessa Timmers^{1,2}, Hayel Tuncel¹, Ronald Boellaard¹, Albert Windhorst¹, Philip Scheltens², Wiesje van der Flier van der Flier^{2,4}, Rik Ossenkoppele^{2,3}, Bart van Berckel¹

¹*Department of Radiology & Nuclear Medicine, Amsterdam Neuroscience, Vrije Universiteit Amsterdam, Amsterdam UMC, Amsterdam, The Netherlands*

²*Alzheimer Center Amsterdam, Department of Neurology, Amsterdam Neuroscience, Vrije Universiteit Amsterdam, Amsterdam UMC, Amsterdam, The Netherlands*

³*Clinical Memory Research Unit, Lund University, Lund, Sweden*

⁴*Department of Epidemiology and Biostatistics, Vrije Universiteit Amsterdam, Amsterdam UMC, Amsterdam, The Netherlands*

Background: We aimed to investigate associations between tau pathology and relative cerebral blood flow (rCBF), and their relationship with cognitive impairment in Alzheimer's disease (AD) using a single dynamic [¹⁸F]flortaucipir PET scan.

Methods: Seventy-one amyloid positive patients with MCI/dementia (66±8 years, MMSE 23±4) underwent a dynamic 130-minute [¹⁸F]flortaucipir PET scan and extensive neuropsychological assessment covering memory, executive functioning, language and attention domains. Receptor parametric mapping (cerebellar gray matter reference region) was used to create non-displaceable binding potential (BP_{ND}) and R_l images, which reflect tau pathology and rCBF, respectively. We performed linear regression analyses between [¹⁸F]flortaucipir BP_{ND} and R_l and cognition in the following regions-of-interest (ROIs); medial and lateral temporal, parietal, occipital and frontal ROIs.

Results: Higher [¹⁸F]flortaucipir BP_{ND} was associated with lower R_l in the lateral temporal, parietal and occipital regions (table-1). Higher medial temporal BP_{ND} was associated with worse memory. Higher lateral temporal, parietal and frontal BP_{ND} were associated with worse executive functioning, language (except frontal BP_{ND}) and attention (except lateral temporal BP_{ND}). Higher occipital BP_{ND} was associated with lower cognitive scores across all domains (figure-1). For [¹⁸F]flortaucipir R_l , lower values in the lateral temporal and parietal ROIs were associated with worse executive functioning, language and attention, and lower occipital R_l with lower language and attention scores. When [¹⁸F]flortaucipir BP_{ND} and R_l were modelled simultaneously, associations between lower R_l in the lateral temporal and worse attention remained, as well as for lower parietal R_l and worse executive functioning and attention (table-2).

Conclusion: Tau pathology and low rCBF were both independently associated with worse cognitive performance. For tau pathology, these associations were found across the neocortex, while for rCBF independent associations were restricted to lateral temporal and parietal regions and the executive functioning and attention domains. These findings suggest that both biomarkers independently contribute to cognitive impairment in AD.

TABLE 1. Regional association between [¹⁸F]flortaucipir BP_{ND} (rows) and R₁ (columns).

[¹⁸ F]flortaucipir R ₁	Medial temporal	Lateral temporal	Parietal	Occipital	Frontal
[¹⁸F]flortaucipir BP_{ND}					
Medial temporal	-0.10 [-0.32 – 0.13]	-0.21 [-0.44 – 0.02]	-0.11 [-0.35 – 0.13]	0.03 [-0.21 – 0.27]	-0.18 [-0.41 – 0.05]
Lateral temporal	-0.15 [-0.38 – 0.08]	-0.32* [-0.56 – -0.08]	-0.24 [-0.49 – 0.01]	-0.10 [-0.35 – 0.16]	-0.19 [-0.43 – 0.06]
Parietal	0.10 [-0.18 – 0.38]	-0.14 [-0.44 – 0.16]	-0.43** [-0.72 – -0.14]	-0.29 [-0.59 – 0.00]	0.04 [-0.26 – 0.33]
Occipital	0.02 [-0.24 – 0.27]	-0.07 [-0.34 – 0.20]	-0.38** [-0.64 – -0.12]	-0.53** [-0.78 – -0.29]	0.13 [-0.13 – 0.40]
Frontal	0.12 [-0.12 – 0.36]	-0.18 [-0.43 – 0.08]	-0.23 [-0.49 – 0.03]	0.09 [-0.18 – 0.35]	-0.14 [-0.40 – 0.11]

Model is adjusted for age and sex. Standardized β's with 95% confidence intervals are reported. BP_{ND}

= non-displaceable binding potential. *p<0.01, †p<0.001, ‡p_{FDR}<0.05.

TABLE 2. Independent associations of [¹⁸F]flortaucipir BP_{ND} and R₁ with cognition.

	Memory (n=71)	Executive functioning (n=64)	Language (n=59)	Attention (n=64)
[¹⁸F]flortaucipir BP_{ND}				
Medial temporal	-0.44[§] [-0.67 – -0.20]	-0.08 [-0.34 – 0.17]	-0.17 [-0.48 – 0.12]	0.01 [-0.28 – 0.29]
Lateral temporal	-0.23 [-0.51 – 0.04]	-0.19 [-0.46 – 0.05]	-0.31* [-0.60 – -0.04]	-0.16 [-0.45 – 0.11]
Parietal	-0.23 [-0.55 – 0.09]	-0.36[§] [-0.70 – -0.11]	-0.27 [-0.68 – 0.05]	-0.36* [-0.72 – -0.10]
Occipital	-0.26 [-0.57 – 0.04]	-0.21 [-0.52 – 0.07]	-0.33* [-0.68 – -0.03]	-0.27 [-0.59 – 0.03]
Frontal	-0.16 [-0.42 – 0.11]	-0.33[§] [-0.64 – -0.11]	-0.20 [-0.56 – 0.10]	-0.31*[§] [-0.66 – -0.06]
[¹⁸F]flortaucipir R₁				
Medial temporal	-0.09 [-0.33 – 0.15]	0.03 [-0.23 – 0.28]	0.10 [0.19 – 0.38]	0.07 [-0.21 – 0.35]
Lateral temporal	-0.05 [-0.30 – 0.21]	0.21 [-0.02 – 0.46]	0.22 [-0.04 – 0.49]	0.28* [0.03 – 0.54]
Parietal	-0.00 [-0.26 – 0.25]	0.27* [0.06 – 0.50]	0.22 [-0.05 – 0.52]	0.39[§] [0.17 – 0.62]
Occipital	0.02 [-0.25 – 0.28]	0.09 [-0.17 – 0.37]	0.15 [-0.13 – 0.46]	0.20 [-0.07 – 0.50]
Frontal	-0.14 [-0.39 – 0.11]	0.11 [-0.12 – 0.34]	0.11 [-0.16 – 0.39]	0.09 [-0.17 – 0.35]

Model is adjusted for age, sex and education. [¹⁸F]Flortaucipir BP_{ND} and R₁ were simultaneously included in the model. Standardized β's with 95% confidence intervals are reported. BP_{ND} = non-displaceable binding potential. *p<0.05, †p<0.01, ‡p<0.001, §p_{FDR}<0.05.

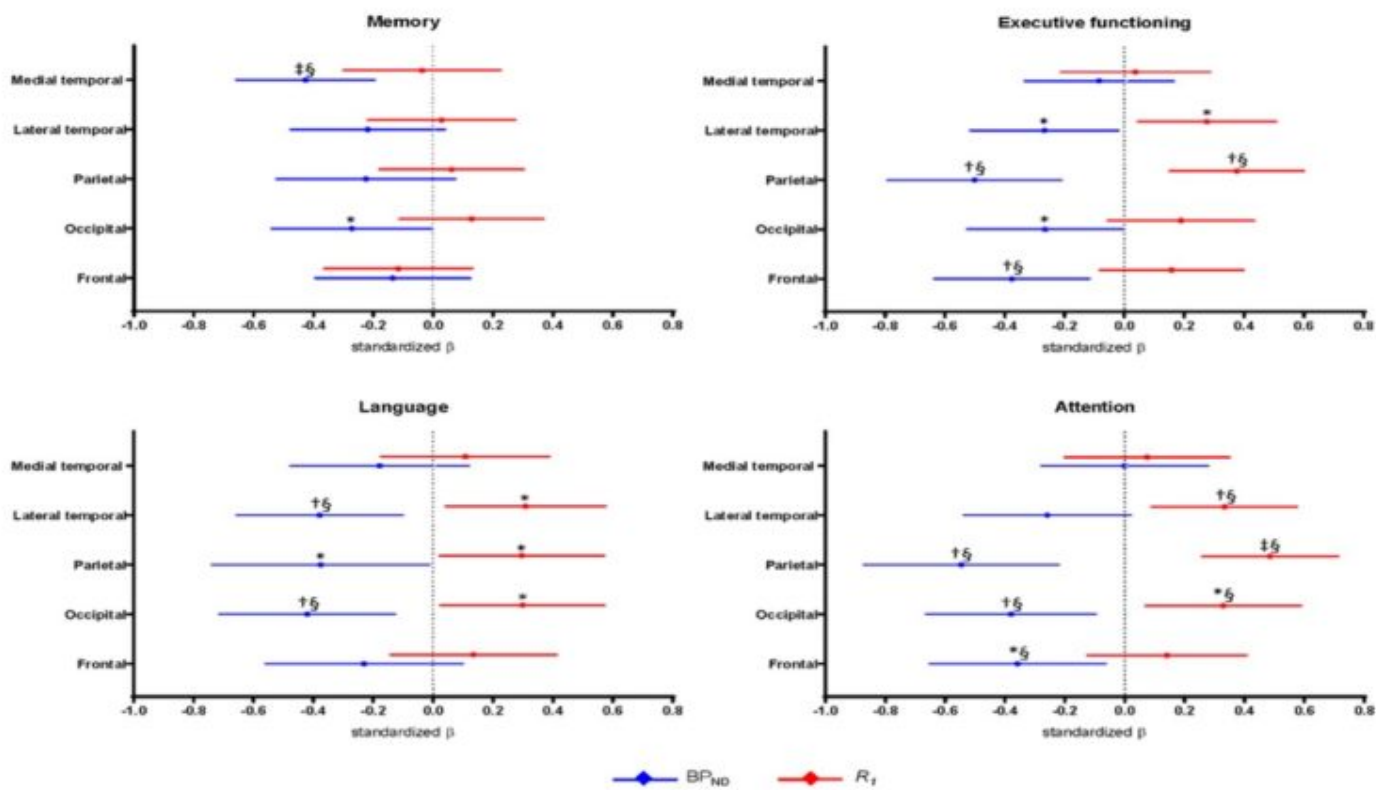


FIGURE 1. Regional associations between [¹⁸F]flortaucipir BP_{ND} or R₁ and cognition. Displayed are regression estimates (standardized β's) with 95% confidence intervals. All analyses are adjusted for age, sex and education. BP_{ND} = non-displaceable binding potential. *p<0.05, †p<0.01, ‡p<0.001, §p_{FDR}<0.05.

Keywords: Tau, cerebral blood flow, PET, Alzheimer's disease, cognition

P55: Amyloid Load trajectories and chronicity reveal groups of early amyloid accumulators in Down syndrome

Matt Zammit¹, Rebecca Kosci¹, Charles Laymon², Tobey Bethausen¹, Dana Tudorascu², Ann Cohen², Davneet Minhas², Sterling Johnson¹, Shahid Zaman³, Chester Mathis², William Klunk², Benjamin Handen², Bradley Christian¹

¹University of Wisconsin-Madison, Madison, WI, US

²University of Pittsburgh, Pittsburgh, PA, US

³University of Cambridge, Cambridge, UK

Background: Adults with Down syndrome (DS) are at increased risk to develop AD compared to the general population, with a sharp increase in prevalence after age 50. By modeling longitudinal A β , a measure of A β chronicity (estimated time to A β (+) onset) can be useful to investigate preclinical AD (Kosci et al. 2019, in review).

Methods: N=169 DS adults underwent [C-11]PiB scans. A subset (n=68) underwent longitudinal evaluation to date (3.0 \pm 0.7 scans; 2.4 \pm 0.6 years apart). In total, 301 PiB images were obtained. 50-70 minute SUVR images were created using cerebellar gray matter as a reference region. The Amyloid Load index ($A\beta_L$) was calculated from the SUVR images to determine global A β burden. Group-based trajectory modeling (GBTM) was applied across the $A\beta_L$ data to identify different patterns of A β accumulation (considering linear, quadratic, and cubic polynomials). The trajectories obtained from the model were solved to determine the estimated age of A β (+) onset ($A\beta_L$ cutoff: 21.5%). A β chronicity was determined by taking the difference between the estimated A β (+) age and the chronological age for each participant.

Results: GBTM identified two functions characterizing age-related A β accumulation patterns in our mostly non-demented DS sample (Figure 1). 93% of participants were assigned to the later A β (+) onset group and 7% to the earlier onset group. The estimated age of A β (+) for the earlier and later accumulating functions were 32.6 and 50.4 years, respectively. A β chronicity and $A\beta_L$ were highly correlated (Pearson's $r=0.85$, $p<0.0001$) with a quadratic model ($R^2=0.85$) indicating the best fit between these parameters (Figure 2).

Discussion: These findings illustrate the utility of A β chronicity to estimate the time to A β (+) onset that may be useful to compare the time course of AD biomarkers between DS and the general population. As this longitudinal study continues, additional A β scans will be included to inform the model.

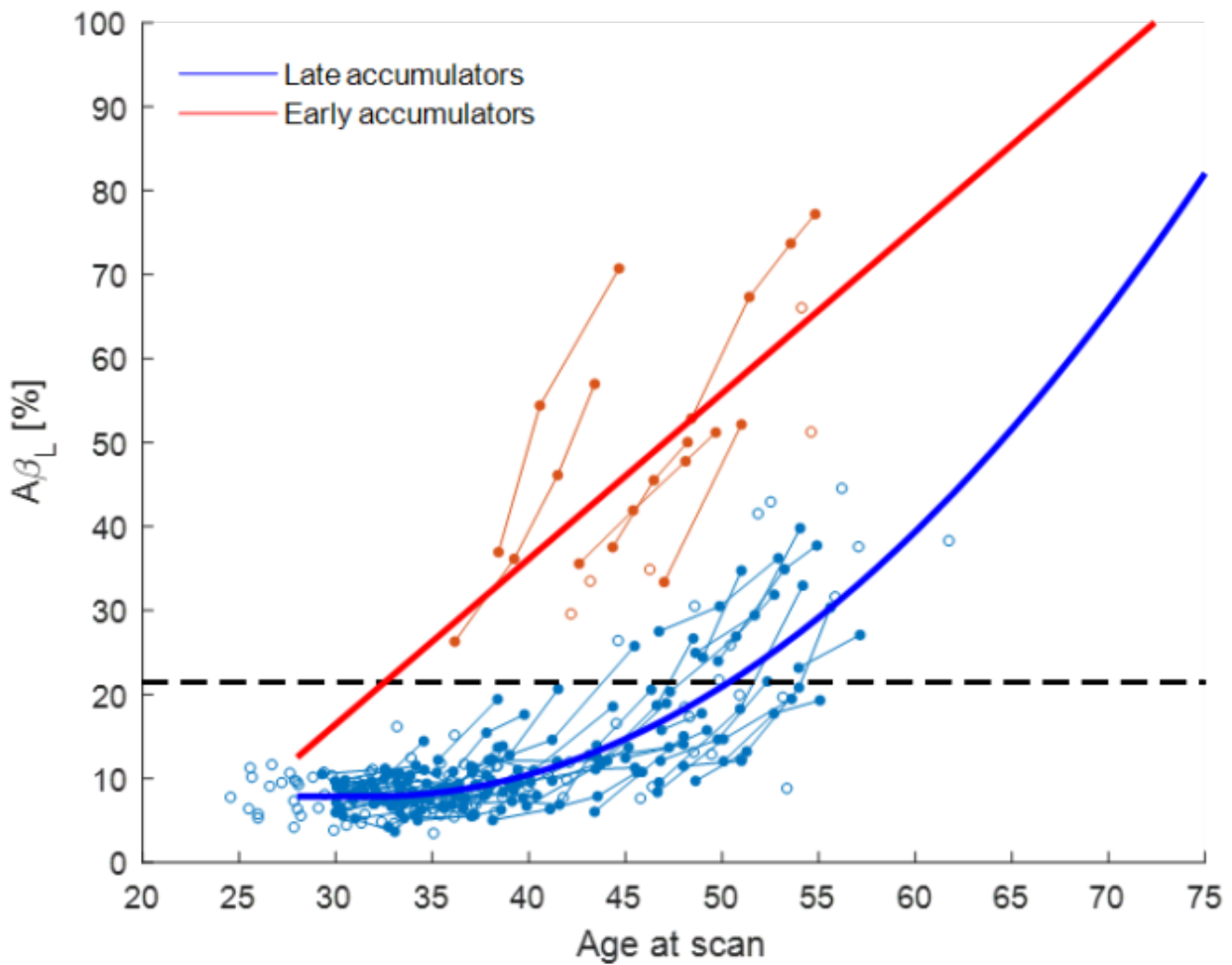


Figure 1. $A\beta_L$ trajectories determined from the group-based trajectory model. Connected points represent participants with longitudinal data. Open circles represent participants with only one time point. The dashed line represents the $A\beta_L$ cutoff for $A\beta(+)$.

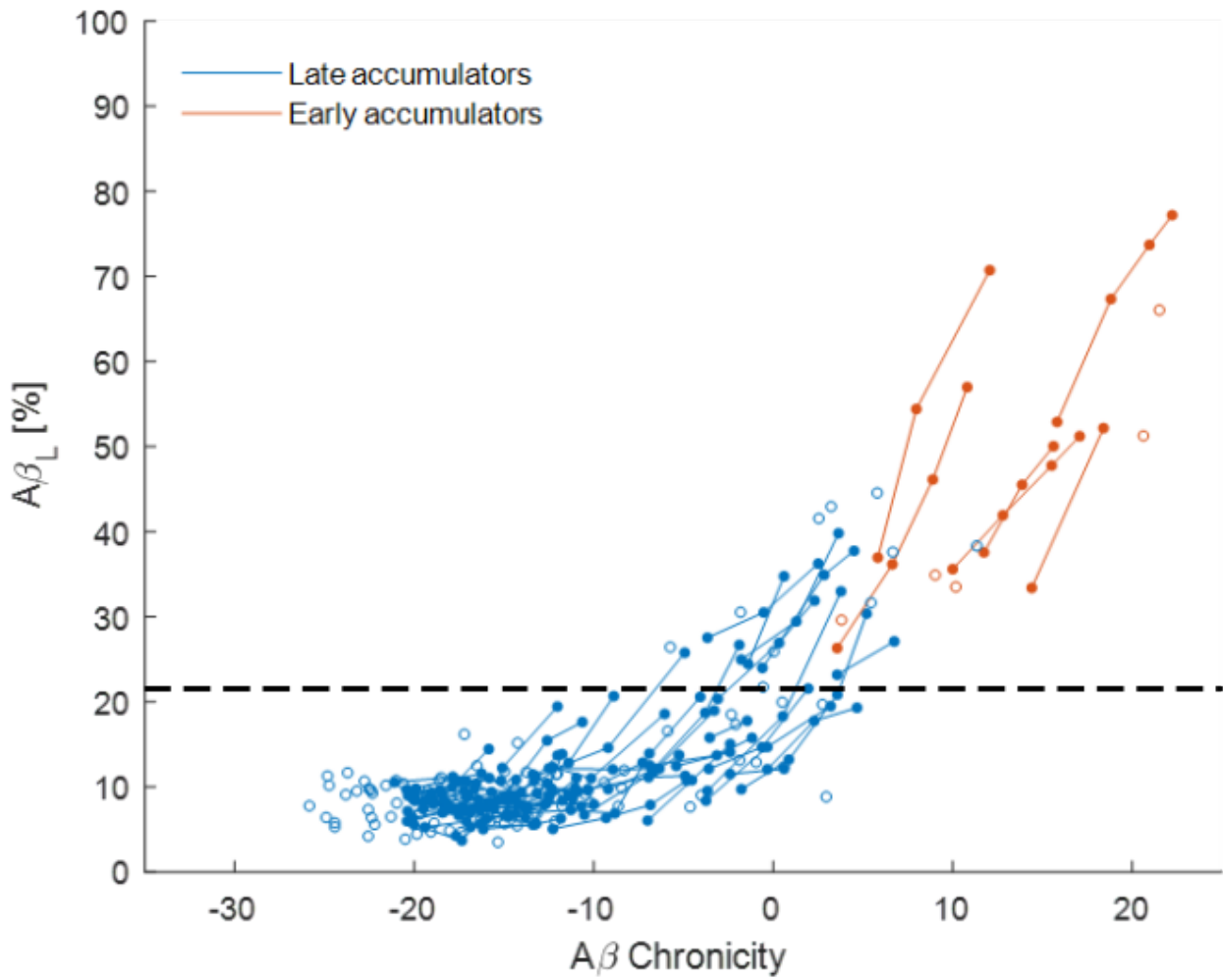


Figure 2. $A\beta_L$ represented as a function of $A\beta$ chronicity.

Keywords: Down syndrome, Amyloid Load, Amyloid Chronicity

P56: Hippocampal-retrosplenial cortex connectivity predicts tau accumulation in cognitively normal older adults

Jacob Ziontz¹, Jenna Adams¹, Suzanne Baker², William Jagust^{1,2}

¹Helen Wills Neuroscience Institute, University of California, Berkeley, Berkeley, CA, US

²Lawrence Berkeley National Laboratory, Berkeley, CA, US

Introduction: Tau is thought to spread transneuronally from medial temporal lobe (MTL) to medial parietal lobe (MPL) in cognitively normal older adults, but it is not known from which region(s) the pathology originates. We hypothesize that tau spreads to the MPL via connectivity with the hippocampus.

Methods: Ninety-seven cognitively normal older adults from the Berkeley Aging Cohort Study (76.4±6.1 years) received tau-PET with ¹⁸F-Flortaucipir, Ab-PET with ¹¹C-PiB, and resting state fMRI. We assessed unilateral resting state functional connectivity (FC) between retrosplenial cortex (RsC), an area of known connectivity with the MTL, and hippocampus (HC), anterolateral entorhinal cortex (alEC), and posteromedial entorhinal cortex (pmEC). We then used linear models to examine the association of FC strength (b-weight) between RsC and each MTL subregion with the proportion of suprathreshold voxels for tau accumulation (SUVR>1.4) in RsC, precuneus, and posterior cingulate cortex.

Results: Semipartial correlations revealed RsC FC with HC in the left [b=0.33, p<0.001] and right hemisphere [b=0.40, p<0.001], but not with alEC or pmEC in either hemisphere (Figure 1). Adjusting for age, sex, and amyloid status, strength of connectivity between RsC and HC predicted proportion of suprathreshold voxels for tau accumulation in the RsC [*Left*: b=0.11, p=0.06; *Right*: b=0.18, p=0.003] (Figure 2), precuneus [*Left*: b=0.18, p=0.001; *Right*: b=0.20, p=0.001], and posterior cingulate cortex [*Left*: b=0.12, p=0.04; *Right*: b=0.14, p=0.03]. Proportion of suprathreshold voxels was not associated with RsC-alEC or RsC-pmEC connectivity in any MPL region.

Discussion: We show that in cognitively normal older adults, RsC exhibits FC with the hippocampus but not alEC or pmEC. Further, only RsC-HC connectivity predicts tau accumulation in MPL structures, indicating that tau pathology may spread transneuronally from the MTL through the hippocampus. Future studies should investigate the role of amyloid in this process as well as associated cognitive changes.

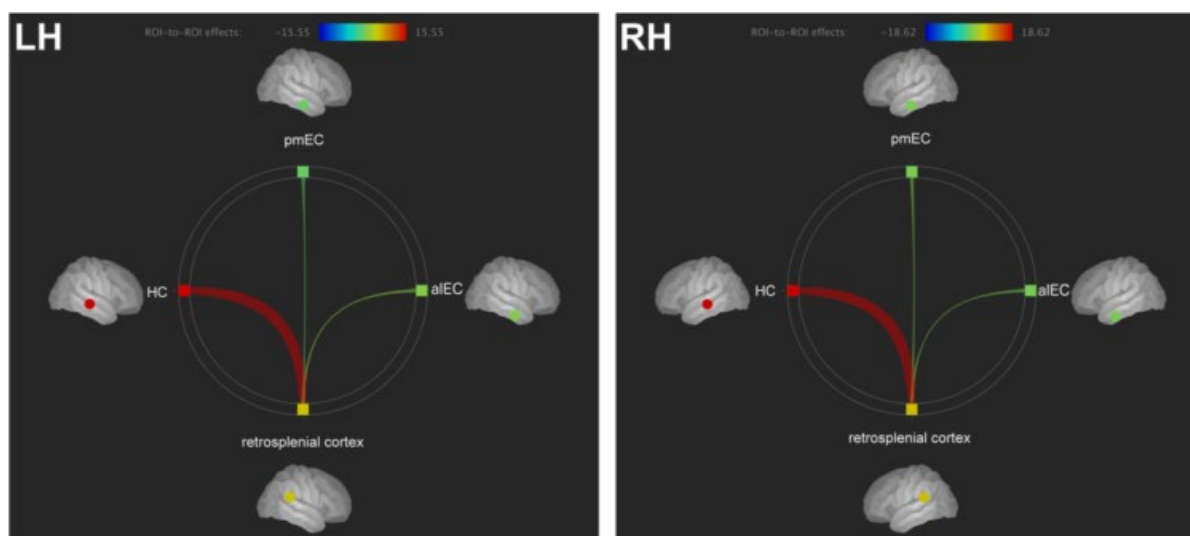


Figure 1. Retrosplenial cortex exhibits functional connectivity with hippocampus (HC) but not anterolateral (alEC) or posteromedial entorhinal cortex (pmEC) in *left* and *right* hemispheres. Line color and thickness correspond to T-value of semipartial correlations of resting state activity between regions.

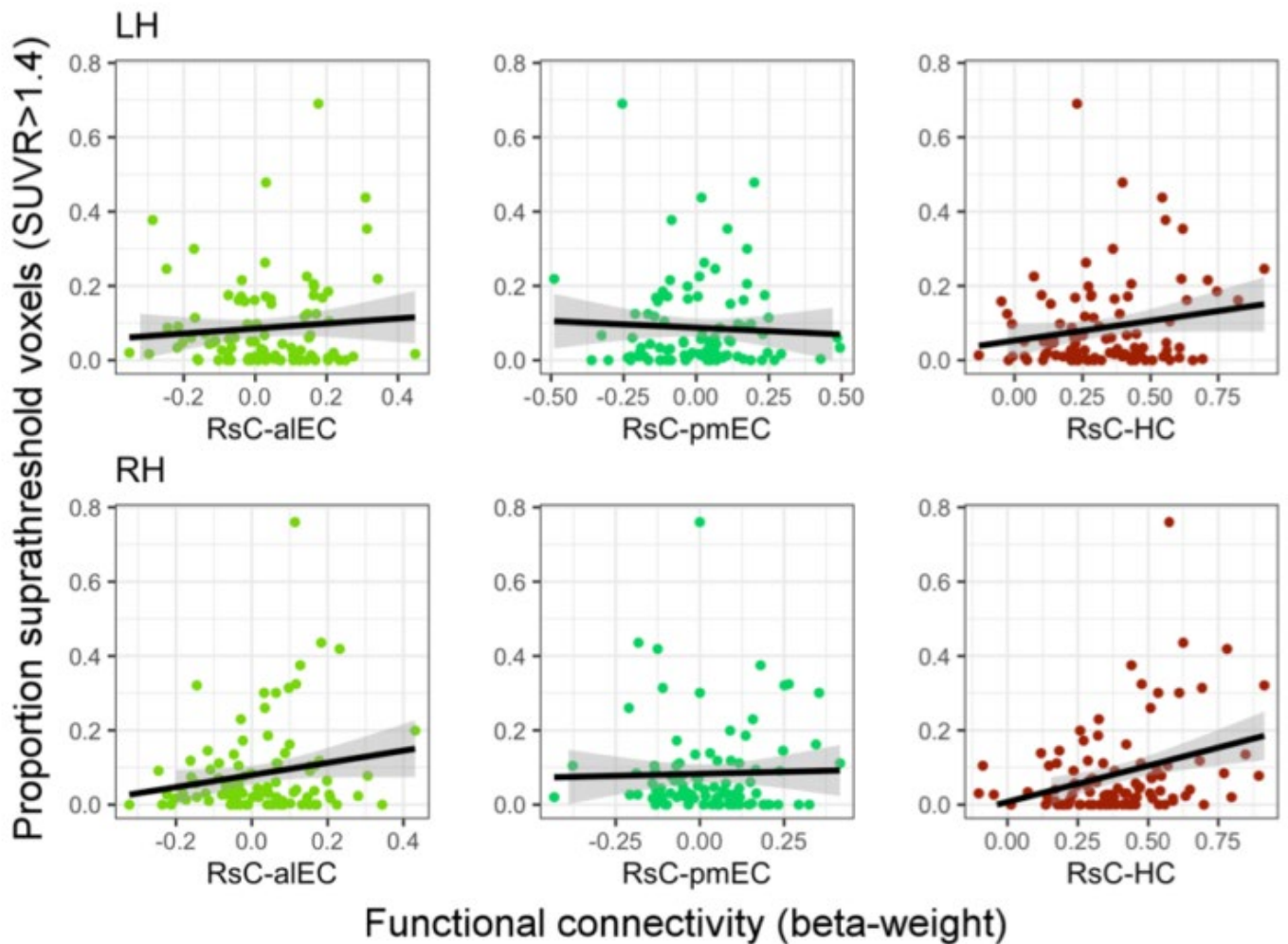


Figure 2. Proportion of voxels above threshold for tau accumulation (SUVR > 1.4) in retrosplenial cortex (RsC) as a function of connectivity between RsC and medial temporal lobe subregions. Suprathreshold voxel proportion is correlated with connectivity strength (beta-weights of semipartial correlations) between RsC and HC, but not with RsC-alEC or RsC-pmEC connectivity. *Top:* Left hemisphere. *Bottom:* Right hemisphere.

Keywords: Tau, connectivity, hippocampus, cognitively normal

Wednesday, January 15, 2020 - 1:45 - 3:15pm

SESSION 1: TECHNICAL I

Wednesday, January 15, 2020		
01:45 pm - 02:45	SESSION 1: TECHNICAL I	Brad Christian, PhD, <i>University of Wisconsin-Madison</i> Ansel Hillmer, PhD, <i>Yale University</i>
1:45 PM	Evaluation of 18F-JNJ-067 as a tau tracer	Suzanne Baker, PhD, <i>Lawrence Berkeley National Laboratory</i>
2:00 PM	A direct comparison of tau imaging agents [F-18]AV-1451 AND [F-18]MK-6240 in human subjects	Brian Lopresti, MS, <i>University of Pittsburgh</i>
2:15 PM	A multi-center comparison of [18F]flortaucipir, [18F]RO948 and [18F]MK6240 tau-PET tracers to detect optimal target ROIs for differential diagnosis	Rik Ossenkoppele, PhD, <i>VU University Medical Center</i>
2:30 PM	Capturing extra-cerebral MK-6240 signal with surface projections	Justin Sanchez, BA, <i>Massachusetts General Hospital</i>
2:45 PM	Discussion	

Evaluation of ¹⁸F-JNJ-067 as a tau tracer

Suzanne Baker¹, Karine Provost², Wesley Thomas³, AJ Whitman³, Mustafa Janabi¹, Mark Schmidt⁴, Maarten Timmers⁴, Hartmuth Kolb⁵, Gil Rabinovici², William Jagust^{1,3}

¹Lawrence Berkeley National Laboratory, Berkeley, CA, US

²University of California, San Francisco, San Francisco, CA, US

³University of California, Berkeley, Berkeley, CA, US

⁴Janssen Research and Development of Janssen Pharmaceutical, Beerse, Belgium

⁵Neuroscience Biomarker Research of Janssen Research and Development, La Jolla, CA, US

Introduction: Current tau PET tracers have obvious shortcomings. ¹⁸F-JNJ-067 is a new tau tracer that binds to aggregated tau in AD brain tissue with $K_i=2.4\text{nM}$. Our objective was to evaluate ¹⁸F-JNJ-067 in individuals with AD (N=3), MCI (N=3), PSP (N=2) and healthy controls (HC, N=3).

Methods: Following PIB and MRI scans, 11 subjects (see Figure 3) underwent 90 min dynamic scans after ¹⁸F-JNJ-067 injection on a Siemens Biograph PET/CT. Data were analyzed in native space with FreeSurfer ROIs. Time activity and SUVR curves and DVR were used to evaluate the tracer binding and pharmacokinetics.

Results: Subject ages ranged from 72-92. All AD and MCI subjects were PIB positive with MMSE scores from 18-30. All PSP and HCs were PIB negative. Steady state was not reached in ROIs with high levels of tracer retention within 90 minutes (Figure 1). Figure 2 shows the dynamic range for DVR (30-90, $k_{2\text{ref}}=0.05\text{min}^{-1}$ derived from SRTM) was 0.73-1.88 and figure 3 shows DVR images. Across all subjects binding was seen in the basal ganglia and thalamus and not appreciably higher in PSPs than HCs. Entorhinal cortex showed low binding in HCs, PSPs and MCIs. MCIs showed low cortical binding, one was indistinguishable from HCs, one showed very low binding and one showed focal binding in the right temporal lobe. All ADs showed high cortical binding, and MMSE and DVR in a meta-ROI were correlated (MCI/AD only $r^2=0.65$; all subjects $r^2=0.74$).

Conclusion: This tracer shows relatively slow pharmacokinetics with low levels of probable off-target binding in the basal ganglia and white matter but not elsewhere, and low entorhinal signal in HCs and MCIs. Binding in AD patients reflects a typical pattern of tau distribution seen with other tracers, and MCI patients are intermediate. These data suggest that ¹⁸F-JNJ-067 is suitable for investigation of the AD continuum.

Figure 1

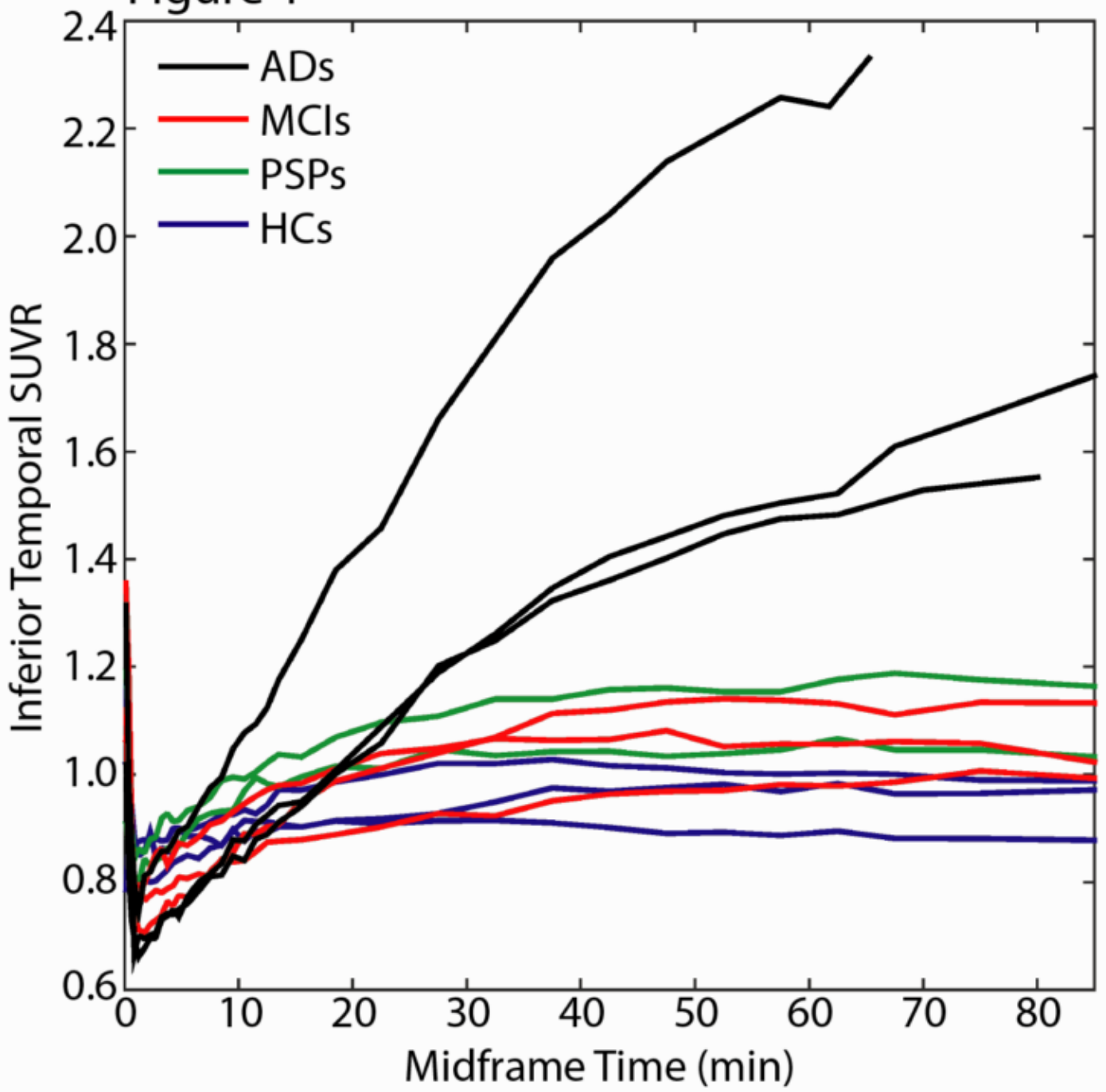


Figure 2

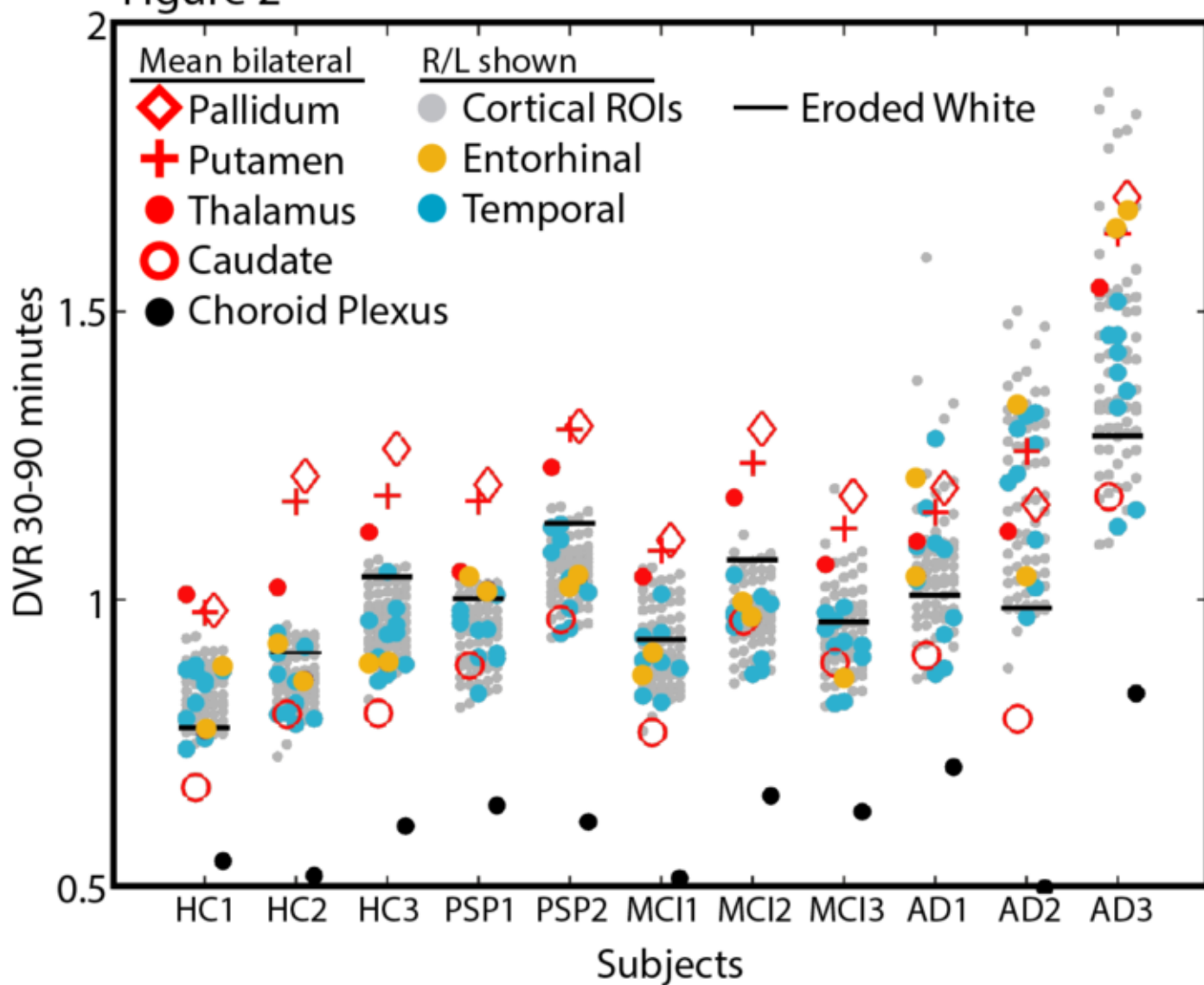
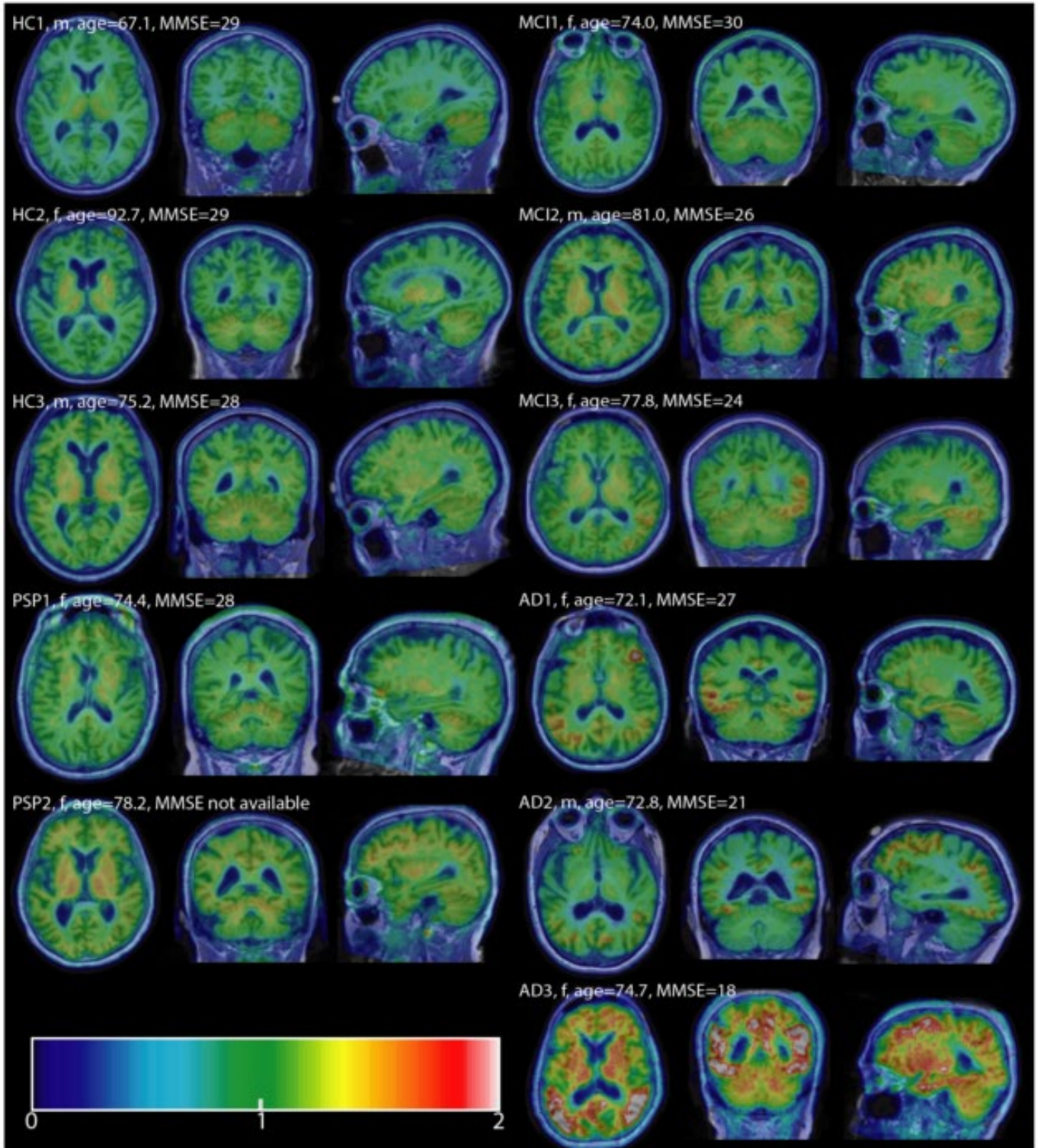


Figure 3



Keywords: 18F-JN-067 tau PET tracer

A direct comparison of tau imaging agents [F-18]AV-1451 AND [F-18]MK-6240 in human subjects

Brian Lopresti¹, Davneet Minhas¹, Alexandra Gogola¹, Charles Laymon¹, Ann Cohen², N. Scott Mason¹, Chester Mathis¹, William Klunk²

¹Department of Radiology, University of Pittsburgh School of Medicine, Pittsburgh, PA, US

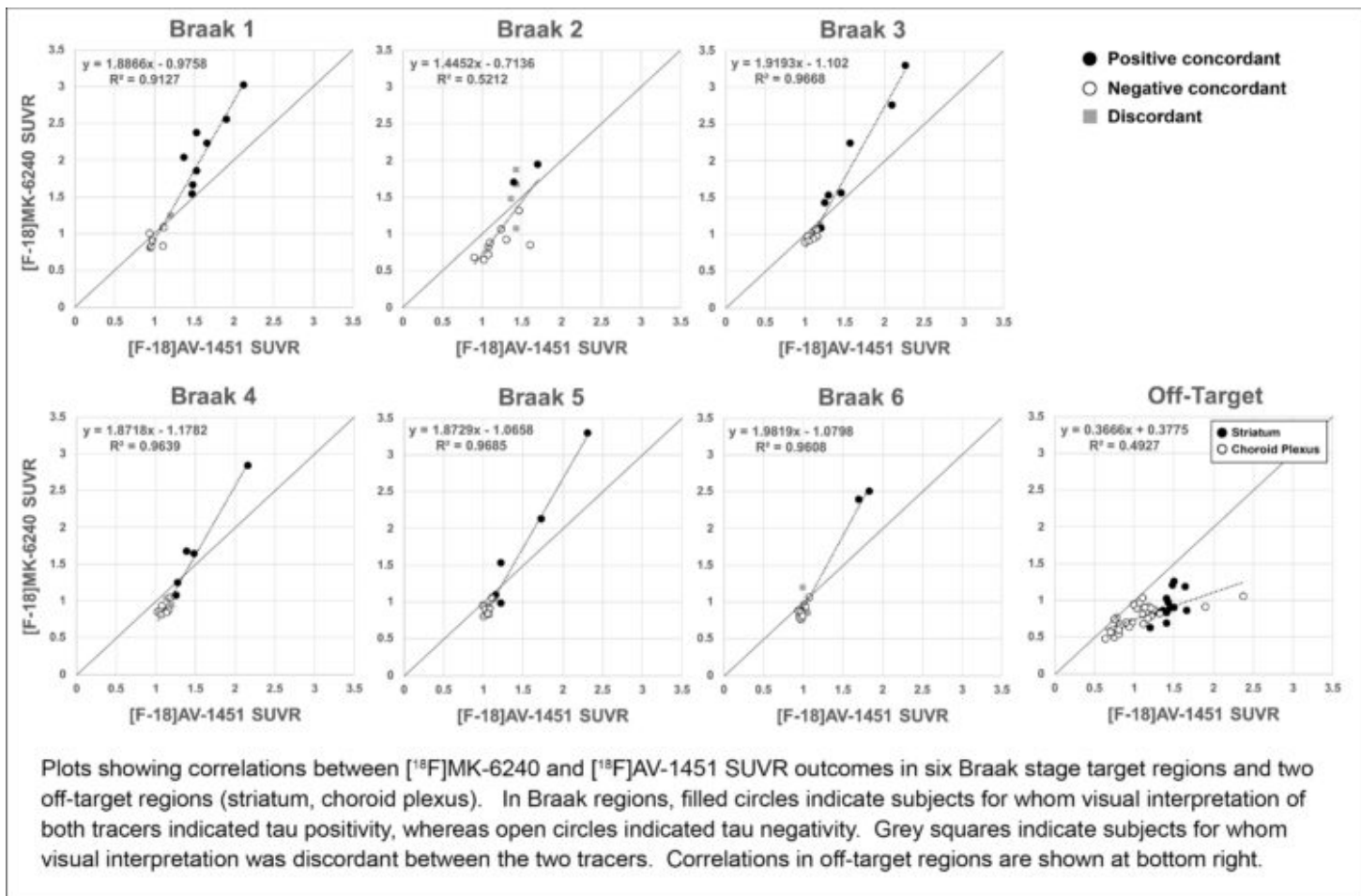
²Department of Psychiatry, University of Pittsburgh School of Medicine, Pittsburgh, PA, US

Background: Tau PET imaging agents exhibit varying levels of specific signal and distinct off-target binding patterns. This study compares the imaging properties of two frequently used tau imaging agents, [¹⁸F]AV-1451 and [¹⁸F]MK-6240, in the same subjects.

Methods: [¹⁸F]AV-1451 and [¹⁸F]MK-6240 scans were collected in 15 elderly subjects (6M, 9F, age 74±8) < 2 months apart, who varied in terms of clinical diagnosis (5 AD, 1 MCI, 9 NC) and cognition (MMSE 9-30). FreeSurfer v5.3 was used to define regions-of-interest (3T MPRAGE) corresponding to Braak pathologic stages (I-VI). Off-target binding was assessed in choroid plexus and a composite striatal region. SUVR outcomes were determined over 80-100 min ([¹⁸F]AV-1451) or 70-90 min ([¹⁸F]MK-6240) post-injection normalized to cerebellar grey matter. Blinded consensus visual interpretation of all images was performed by three expert readers, who scored each Braak region on a 4-point scale ranging from definitely negative (0) to definitely positive (3).

Results: Although the outcomes were highly correlated ($r^2 > 0.91$) for all Braak regions except Braak II (hippocampus, $r^2 = 0.52$), the dynamic range of SUVR values in target regions was ~2 fold higher for [¹⁸F]MK-6240 than [¹⁸F]AV-1451 (see figure). Cerebellar SUVs were similar for [¹⁸F]MK-6240 and [¹⁸F]AV-1451 (0.84 ± 0.16 vs 0.88 ± 0.19 , respectively), suggesting that differences in SUVR values are driven by specific signal. Off-target binding in striatum (STR) and choroid plexus was frequently observed with [¹⁸F]AV-1451, whereas off-target binding of [¹⁸F]MK-6240 was observed in the meninges of 9/15 subjects. Visual reads were highly concordant in 13/15 subjects.

Conclusion: Both [¹⁸F]MK-6240 and [¹⁸F]AV-1451 are capable of visualizing a spectrum of pathologic tau deposits. [¹⁸F]MK-6240 showed increased dynamic range and lower off-target binding in striatum and choroid plexus, but this resulted in no clear difference in the visual interpretation of PET scans.



Keywords: tau PET AV-1451 MK-6240

A multi-center comparison of [¹⁸F]flortaucipir, [¹⁸F]RO948 and [¹⁸F]MK6240 tau-PET tracers to detect optimal target ROIs for differential diagnosis

Antoine Leuzy¹, Rik Ossenkoppele^{1,2}, Ruben Smith^{1,3}, Philip Insel¹, Niklas Mattsson^{1,3,4}, Tharick Pascoal⁵, Andréa Benedet^{5,6}, Hannah Cho⁷, Chul H. Lyoo⁷, Renaud La Joie⁸, Gil Rabinovici⁸, Pedro Rosa-Neto^{5,9,10}, Oskar Hansson^{1,11}

¹Clinical Memory Research Unit, Department of Clinical Sciences, Malmö, Sweden

²VU University Medical Center, Neuroscience Campus Amsterdam, Amsterdam, The Netherlands

³Department of Neurology, Skåne University Hospital, Lund, Sweden

⁴Wallenberg Centre for Molecular Medicine, Lund University, Lund, Sweden

⁵Translational Neuroimaging Laboratory, McGill Centre for Studies in Aging, McGill University, Montreal, QC, Canada

⁶CAPES Foundation, Ministry of Education of Brazil, Brasilia, BR

⁷Department of Neurology, Gangnam Severance Hospital, Yonsei University College of Medicine, Seoul, Korea

⁸Department of Neurology, University of California San Francisco, Memory and Aging Center, San Francisco, CA, US

⁹Montreal Neurological Institute, Montreal, QC, Canada

¹⁰Department of Neurology and Neurosurgery, McGill University, Montreal, QC, Canada

¹¹Memory Clinic, Skåne University Hospital, Lund, Sweden

Objectives: To examine whether similar target-ROIs and cut-points can be used across [¹⁸F]flortaucipir, [¹⁸F]RO948 and [¹⁸F]MK6240 tau-PET tracers to differentiate AD dementia from i) cognitively unimpaired (CU) controls and ii) cases with non-AD neurodegenerative disorders.

Methods: Tau-PET data was collected across six-cohorts: ([¹⁸F]flortaucipir, BioFINDER [Sweden], ADNI [US]; UCSF [US], Gangnam Severance Hospital [South Korea]; [¹⁸F]RO948, BioFINDER-2 [Sweden]). Future analyses will also be performed with [¹⁸F]MK6240 (TRIAD, Canada). Diagnostic-groups were as follows: for [¹⁸F]flortaucipir, 179 AD dementia, 42 A β -CU and 247 non-AD; for [¹⁸F]RO948, 117 AD dementia, 201 A β -CU and 107 non-AD. A β -status was determined using CSF (A β ₄₂, A β ₄₂/A β ₄₀) or amyloid-PET, as available. SUVR values (inferior cerebellar reference) were calculated across FreeSurfer-ROIs ([¹⁸F]flortaucipir, 80-100 min; [¹⁸F]RO948 70-90 min). Diagnostic performance (area-under-the-ROC curve [AUC] for AD dementia vs CU and non-AD) was assessed across predefined (Braak I-II (entorhinal cortex), I-IV (meta-temporal ROI), V-VI (widespread neocortical areas) [Cho et al. *Neurology* 2016], and an early-Tau ROI [entorhinal cortex, inferior temporal, parahippocampus/fusiform-gyrus]) and data-driven target-ROIs (optimal classifiers were constructed using the least absolute shrinkage and selection operator [LASSO]). Cut-points were determined using the Youden-index (AD dementia vs A β -CU).

Results: LASSO based ROIs are shown for [¹⁸F]flortaucipir and [¹⁸F]RO948 in Figures 1 and 2. Diagnostic performance across ROIs and cut-points are shown in Table 1. For [¹⁸F]flortaucipir, the diagnostic performance (AUC) of the optimized LASSO-based ROIs was superior to that for Braak I-II/V-VI, but not for Braak I-IV/early-Tau regions. For [¹⁸F]RO948, the LASSO based ROIs were superior to the Braak V-VI/early-Tau ROIs, but not to Braak I-II and I-IV.

Conclusions: A common-ROI encompassing parts of the temporal lobe (i.e. Braak I-IV) can be used for differential diagnosis with both [¹⁸F]flortaucipir and [¹⁸F]RO948 tau-PET, and that using very similar cut-point of around 1.35 SUVR. Additional analyses will address whether this also holds true for [¹⁸F]MK6240.

Table 1. Summary of diagnostic performance and regional cut-points for [¹⁸F]flortaucipir and [¹⁸F]RO948 PET

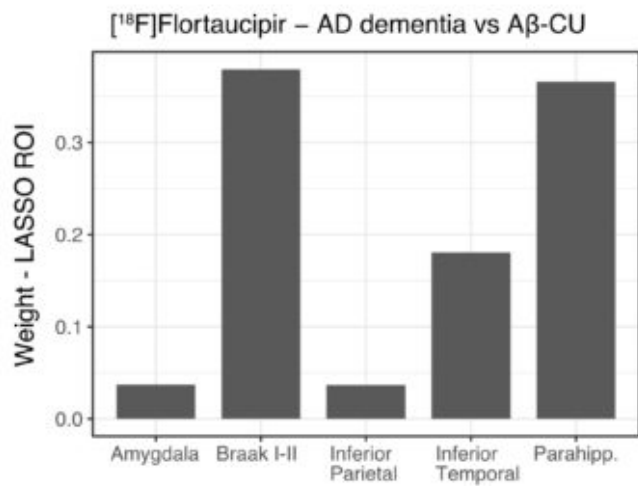
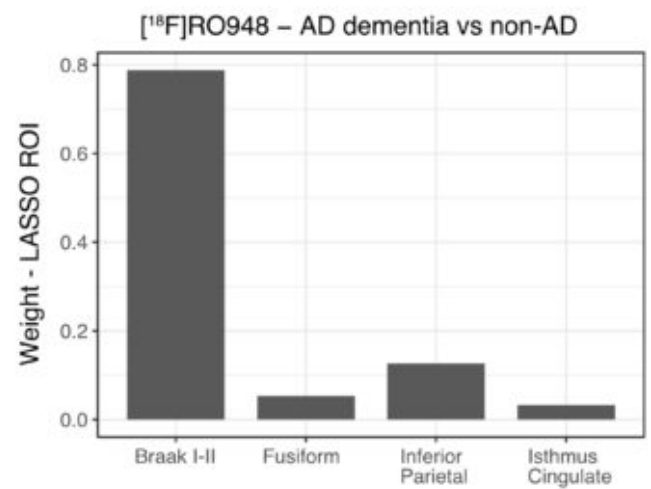
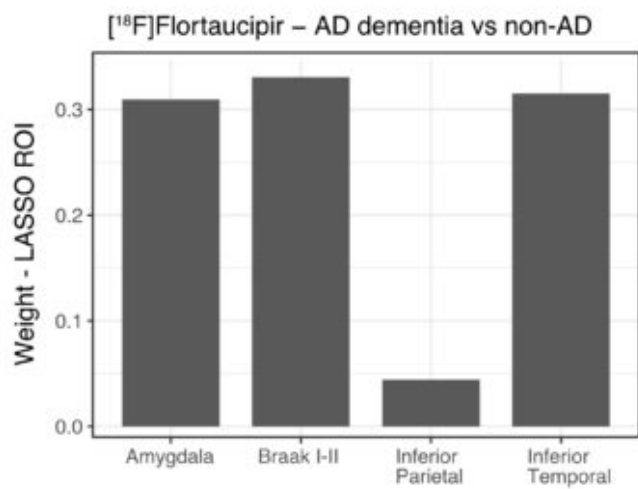
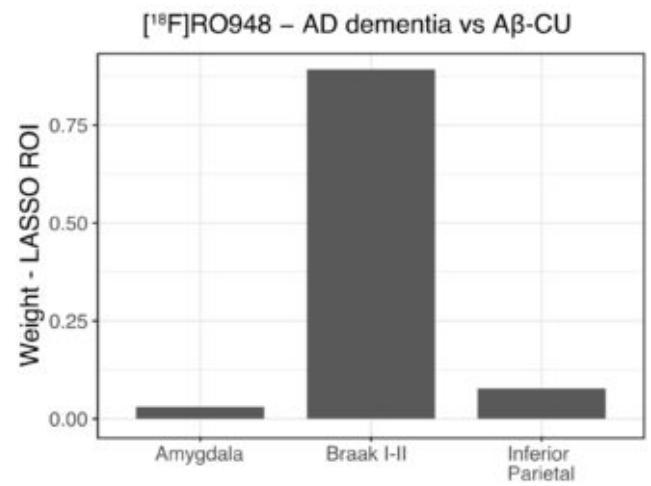
	AUC (95% CI)	Cut-point (Youden)	Sensitivity	Specificity
[¹⁸F]Flortaucipir				
AD vs controls				
Braak I-II (ERC)	0.915 (0.872-0.947)	1.414	85.0	83.3
Braak I-IV	0.956 (0.931-0.982)	1.367	89.4	92.3
Braak V-VI	0.892 (0.848-0.935)	1.266	85.0	85.7
Early-Tau (AVID)*	0.960 (0.936-0.984)	1.355	89.4	92.9
Optimised LASSO ROI**†	0.957 (0.931-0.983)	1.354	90.5	88.1
AD vs non-AD				
Braak I-II (ERC)	0.930 (0.904-0.958)	1.416	85.0	92.1
Braak I-IV	0.945 (0.923-0.970)	1.366	89.4	94.4
Braak V-VI	0.915 (0.884-0.947)	1.258	85.5	93.9
Early-Tau (AVID)*	0.947 (0.928-0.970)	1.348	90.5	91.9
Optimised LASSO ROI**†	0.954 (0.933-0.975)	1.364	93.9	89.3
[¹⁸F]RO948				
AD vs controls				
Braak I-II (ERC)	0.992 (0.983-1)	1.369	96.6	99.0
Braak I-IV	0.989 (0.982-0.998)	1.325	92.3	99.0
Braak V-VI	0.928 (0.895-0.961)	1.126	86.3	87.5
Early-Tau (AVID)*	0.989 (0.979-0.998)	1.350	92.3	99.5
Optimised LASSO ROI**†	0.993 (0.983-1)	1.367	96.9	99.5
AD vs non-AD				
Braak I-II (ERC)	0.980 (0.967-0.994)	1.474	93.2	92.2
Braak I-IV	0.969 (0.950-0.989)	1.343	91.5	93.2
Braak V-VI	0.922 (0.885-0.959)	1.133	85.6	88.3
Early-Tau (AVID)*	0.969 (0.949-0.988)	1.347	92.3	93.2
Optimised LASSO ROI**†	0.981 (0.967-0.996)	1.464	94.0	94.2

The Youden index is based on AD dementia vs A β -CU and A β -CU, respectively.

* The Early-Tau ROI (AVID) comprises regions expected to accumulate tau early on in the course of Alzheimer's disease (entorhinal cortex, fusiform, parahippocampal gyrus, and inferior temporal gyrus).

** Optimised LASSO based ROIs: [¹⁸F]flortaucipir, AD dementia vs A β -CU (amygdala, entorhinal cortex, inferior parietal cortex and parahippocampus) and AD dementia vs non-AD (amygdala, entorhinal cortex, inferior parietal and inferior temporal lobe); [¹⁸F]RO948, AD dementia vs A β -CU (amygdala, entorhinal cortex and inferior parietal cortex) and AD dementia vs non-AD (entorhinal cortex, fusiform gyrus, inferior parietal and isthmus cingulate).

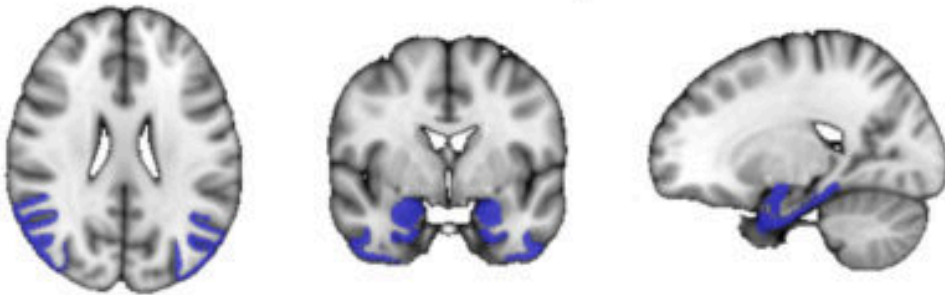
† Comparison of AUC values: [¹⁸F]flortaucipir, AD dementia vs A β -CU and non-AD (LASSO > Braak I-II and V-VI, P<0.001); [¹⁸F]RO948 PET: AD dementia vs A β -CU (LASSO > Early-Tau [P<0.05] and Braak V-VI [P<0001]).

A**B**

LASSO based ROIs

A. [18F]Flortaucipir PET

AD dementia vs A β -CU



AD dementia vs non-AD



B. [18F]RO948 PET

AD dementia vs A β -CU



AD dementia vs non-AD



Keywords: Tau, PET, Flortaucipir, RO948, MK6240

Capturing extra-cerebral MK-6240 signal with surface projections

Justin Sanchez¹, Alex Becker¹, Zoe Rubinstein¹, Danielle Mayblyum¹, Emma Thibault¹, Julie Price¹, Keith Johnson^{1,2}

¹Massachusetts General Hospital, Boston, MA, US

²Brigham and Women's Hospital, Boston, MA, US

Introduction: MK-6240 is a high-affinity tau PET ligand that occasionally shows high target-to-background cortical signal in high-binding cases, as well as off-target signal from extra-cerebral areas in the subarachnoid space, including meninges, which can conform to the convolutional anatomy of the cortical ribbon. We assessed whether surface projections of MK-6240 can be used to capture distinct cortical and extra-cerebral MK-6240 signal.

Methods: FreeSurfer surface projections of MK-6240 SUVr (90-110m post-injection) images were generated across various projection fractions (PF) to sample MK-6240 at the white-grey boundary (PF=0), grey matter midpoint (PF=0.5), pial surface boundary (PF=1) and beyond the pial surface (PF>1). Mean gyri SUVrs were computed to assess the effect of varying PF in several exemplary cases and a group of 29 low-a β clinically normal subjects (age 37-82, 64.7 \pm 11.6 years). Dynamic MK-6240 data projected with various PF was assessed in one subject with visually high extra-cerebral signal.

Results: Surface projection data were consistent with visually evident MK-6240 signal patterns: in cases with high cortical binding, SUVrs were highest inside the cortex (PF=0.5) and dropped off at higher PF (Fig.1A), while in cases with low cortical and high extra-cerebral signal, SUVr was highest outside the brain (PF=2.0, Fig.1B). In the low-a β group, SUVr difference between PF=2.0 and PF=0.5 was largest in frontal and lateral regions, and smaller in midline structures (cingulate) and areas with thinner meninges (insula, transverse temporal) (Fig.2). In dynamic data, cortical uptake was higher than extra-cerebral signal in early frames (0-40min), while extra-cerebral signal was higher than cortical in later frames (40-120min) (Fig.3).

Conclusions: Surface projections of MK-6240 using various PF may be used to capture extra-cerebral signal while preserving cortical ribbon signal. Cortical and extra-cerebral signal showed different trajectories over time post-injection, suggesting that extra-cerebral signal could be identified and corrected for using projections of dynamic MK-6240 data.

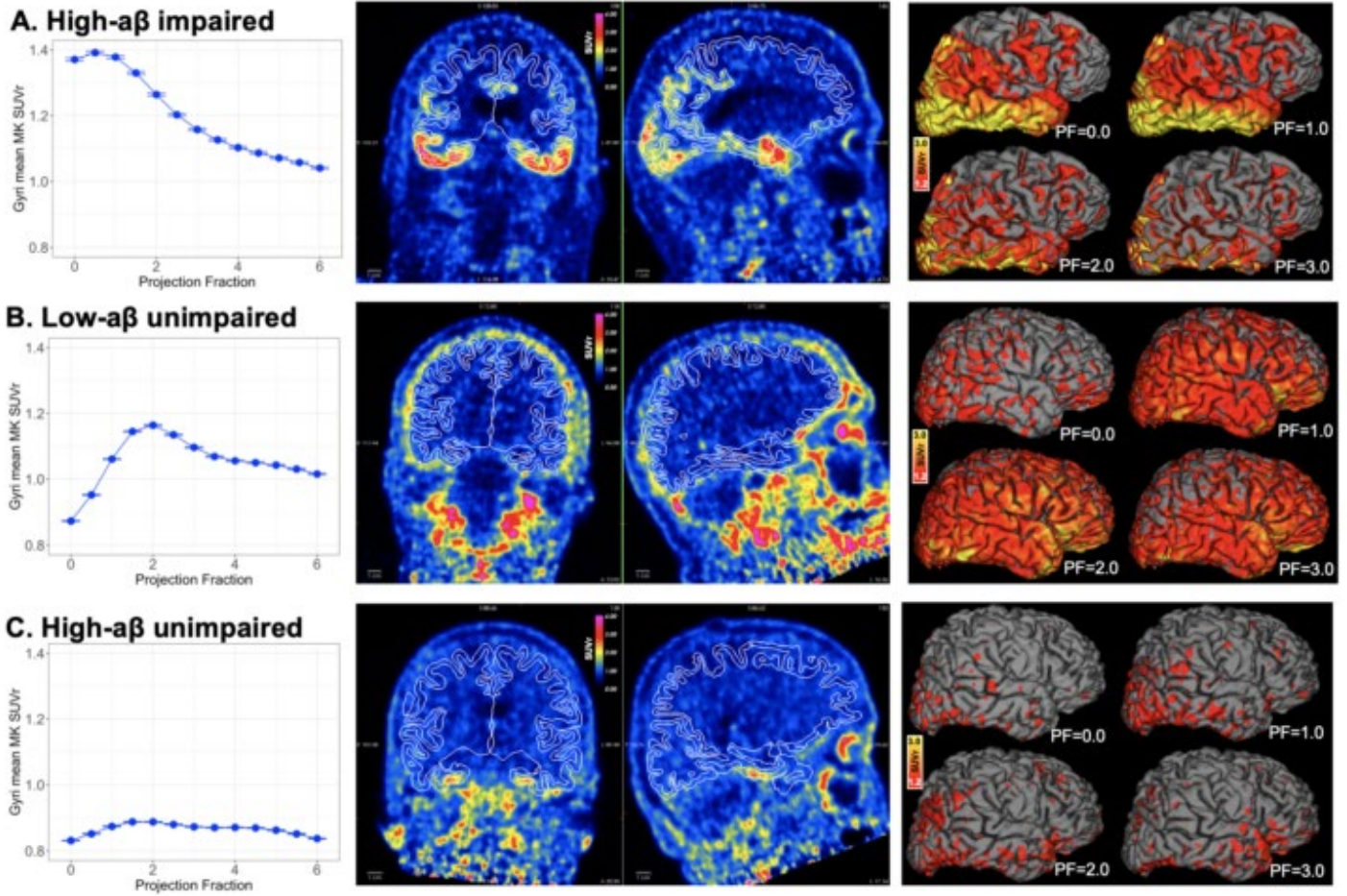


Figure 1. Three example cases showing (left to right) the change in mean MK6240 SUVr with change in projection fraction (PF), coronal and sagittal slices of MK6240 signal in relation to pial surface, and vertex-wise whole brain SUVr at various PF values. **A)** Impaired 59 year old male with high amyloid (Global PiB DVR=1.58); **B)** Cognitively normal 44 year old male with low amyloid (Global PiB DVR = 1.01); **C)** Cognitively normal 66 year old female with high amyloid (Global PiB DVR = 1.53)

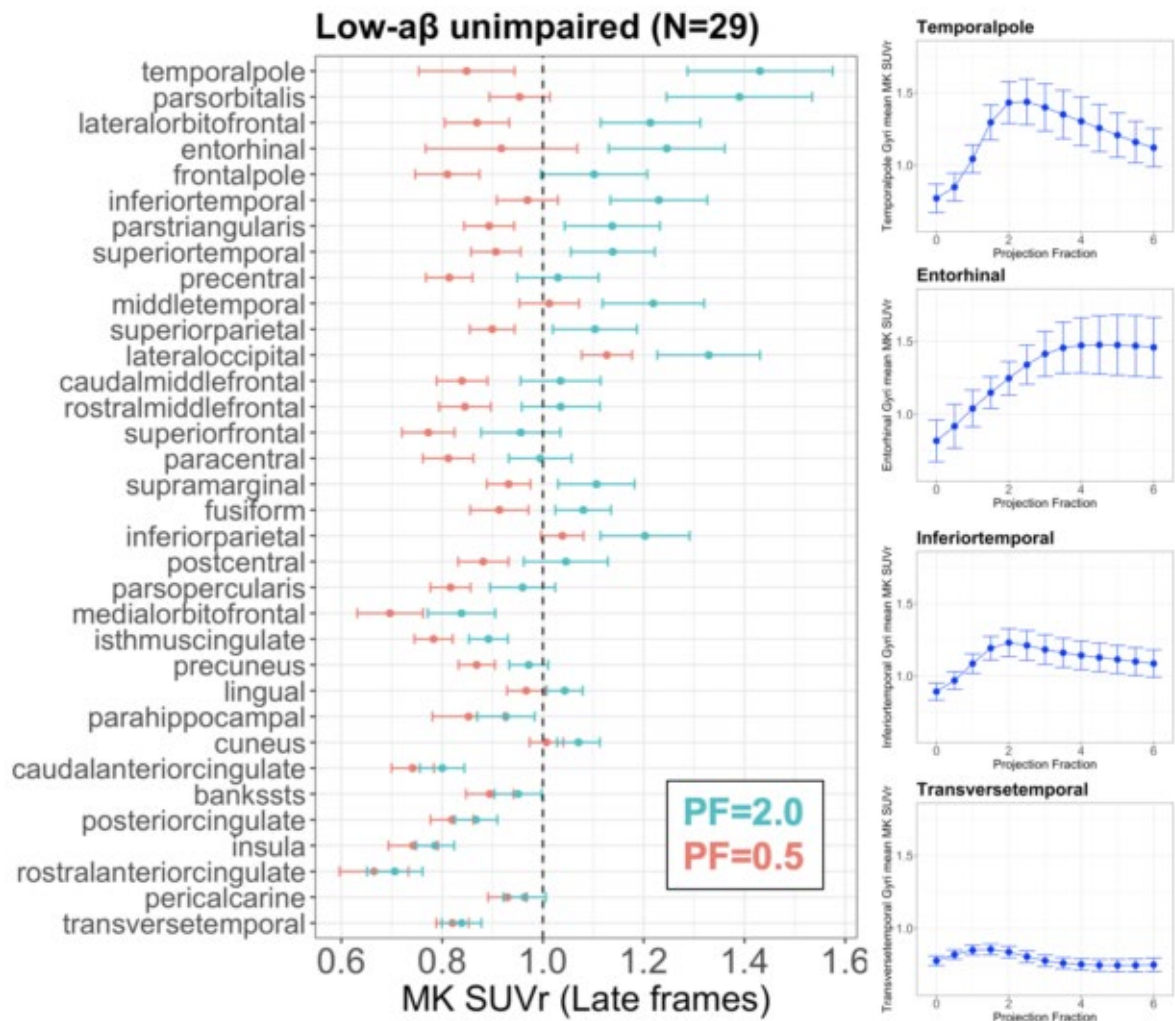


Figure 2. Forest plot of group mean MK6240 SUVR (90-110min post-injection) at the grey matter midpoint (PF=0.5, orange) and beyond the pial surface (PF=2.0, green) for cognitively normal individuals with low amyloid (Global PiB DVR < 1.16) in various cortical ROIs. Scatter plots (right) show group mean gyri SUVR for temporal pole, entorhinal cortex, inferior temporal gyrus, and transverse temporal ROIs at various PF; error bars indicate 95% confidence interval around mean.

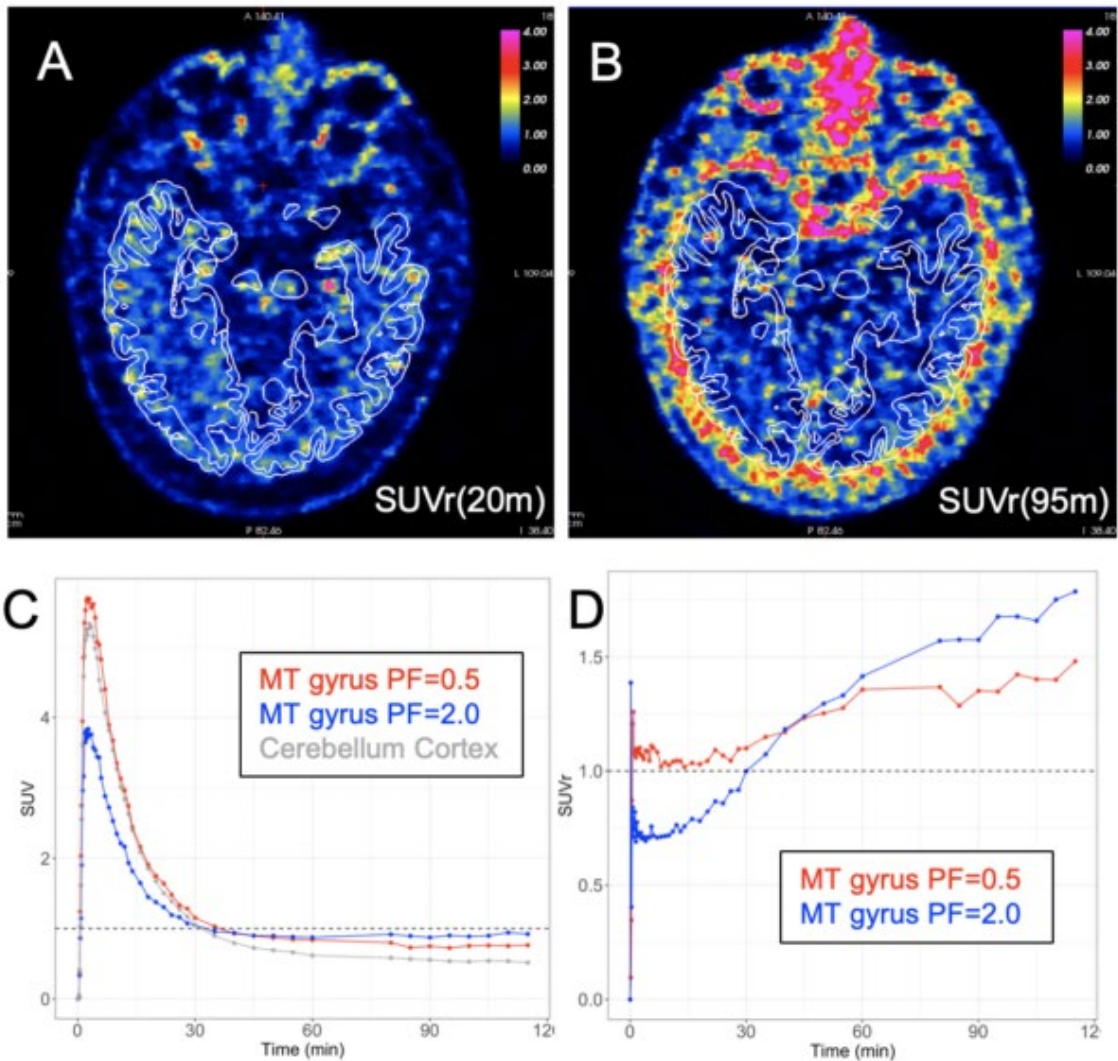


Figure 3. Cognitively normal 75 year-old female with low amyloid (PiB FLR=1.11) *Top*, axial view of MK-6240 SUVr at 20min (**A**, left) and 95min (**B**, right) post-injection; white lines indicate FreeSurfer-defined white and pial surface boundaries. *Bottom*, time activity curves for MK-6240 SUV (C) in middle temporal (MT) gyrus at PF=0.5 (red) and PF=2.0 (blue) in relation to cerebellum cortex (grey), MT SUVr normalized to cerebellum cortex (D).

Keywords: MK-6240, tau, meninges, cortex

KEYNOTE LECTURE 1

Pathology progression modelling in Alzheimer's disease

Alan Evans

Montreal Neurological Institute/McGill University, Montreal, QC, Canada

Although we lack a complete understanding of the specific cascade of pathological events that give rise to Alzheimer's disease (AD), the convergence of multiple threads in neuroscience give cause for optimism. Specifically, we see the emergence of (i) in vivo PET tracers that map the distribution of misfolded proteins, such as beta-amyloid and tau, complementing more routine imaging, genetics and behavioral measures, (ii) advanced multi-modal analytic strategies to identify disease sub-types and temporal stages as well as modelling of the progression of disease, and (iii) a culture of open neuroscience data-sharing that, supported by advanced neuroinformatics platforms, provides huge amounts of AD-relevant data freely to the global community. This talk will discuss our recent progress in these areas that reflect a shift away from clinical disease categorization towards a more mechanistic approach to disease characterization. This strategy should promote more informed design of biomarkers and therapeutic intervention, better patient stratification and, ultimately, personalized medicine.

SESSION 2: TECHNICAL II

Wednesday, January 15, 2020		
04:45 pm - 06:00	SESSION 2: TECHNICAL II	CHAIRS: Julie Price, PhD, <i>Harvard Medical School</i> Suzanne Baker, PhD, <i>Lawrence Berkeley National Laboratory</i>
4:45	Amyloid Load predicts elevated tau deposition in Down syndrome	Matt Zammit, MS, University of Wisconsin
5:00	TauIQ demonstrates increased power for cross-sectional and longitudinal analysis of Tau tracers as evidenced by [18F]Flortaucipir and [18F]GTP1	Roger Gunn, PhD, <i>Inivicro</i>
5:15	Spatiotemporal imaging phenotypes of tau pathology in Alzheimer's disease	Jacob Vogel, PhD (cand.), <i>McGill University</i>
5:30	Predicting structural, metabolic and pathologic disease progression in autosomal dominant Alzheimer's disease with machine learning	Patrick Lockett, PhD, <i>Washington University in St. Louis</i>
5:45	Correction of partial volume effects for tau PET imaging using the kernel method	Kuang Gong, PhD, <i>MGH/Harvard Medical School</i>
6:00	Discussion	

Amyloid Load predicts elevated tau deposition in Down syndrome

Matt Zammit¹, Charles Laymon², Dana Tudorascu², Ann Cohen², Davneet Minhas², Shahid Zaman³, Beau Ances⁴, Chester Mathis², William Klunk², Benjamin Handen², Bradley Christian¹

¹University of Wisconsin-Madison, Madison, WI, US

²University of Pittsburgh, Pittsburgh, PA, US

³University of Cambridge, Cambridge, UK

⁴Washington University in St. Louis, St. Louis, MO, US

Background: There is a high prevalence of AD in Down syndrome (DS) after age 50. Elevated A β deposition is detectable with PET imaging by their middle-to-late 30's, but the progression of tau in this population has yet to be characterized. This study aims to assess the associations between A β and tau while establishing preliminary tau(+) cutoffs in DS.

Methods: Adults with DS (N=140) underwent [C-11]PiB and [F-18]AV-1451 scans in addition to T1w-MRI. 50-70 minute PiB and 80-100 minute AV-1451 SUVR images were generated using gray matter cerebellum as the reference region. The Amyloid Load index ($A\beta_L$) was calculated from the PiB images to determine global A β burden. ROIs encompassing the Braak staging of tau pathology were parcellated from the MRI images using FreeSurfer v5.3.0. No methods (e.g. PVC) were used to minimize signal from off target binding. Using k-means clustering with resampling, preliminary tau(+) cutoffs were calculated for each Braak region – independent of $A\beta_L$. Linear regression models (considering up to cubic polynomials) were performed between Braak regional SUVR and $A\beta_L$. The functional form of the regression fit was solved to determine the threshold of $A\beta_L$ corresponding to tau(+) in each Braak region.

Results: Linear associations were observed between $A\beta_L$ and Braak regions 1-2, while Braak regions 3-6 displayed quadratic associations with $A\beta_L$ (Figure 1). The preliminary regional tau(+) cutoffs and estimated $A\beta_L$ corresponding to tau(+) in DS are displayed in Table 1. The estimated $A\beta_L$ thresholds for tau(+) increased as tau pathology progressed through the conventional Braak staging.

Discussion: These preliminary results suggest a method for determining tau(+) cutoffs in DS from AV-1451 images. Since A β is predominantly evident before tau in DS, these findings suggest that the $A\beta_L$ index may be a useful marker for the prediction of future tau deposition in a Braak region-dependent manner.

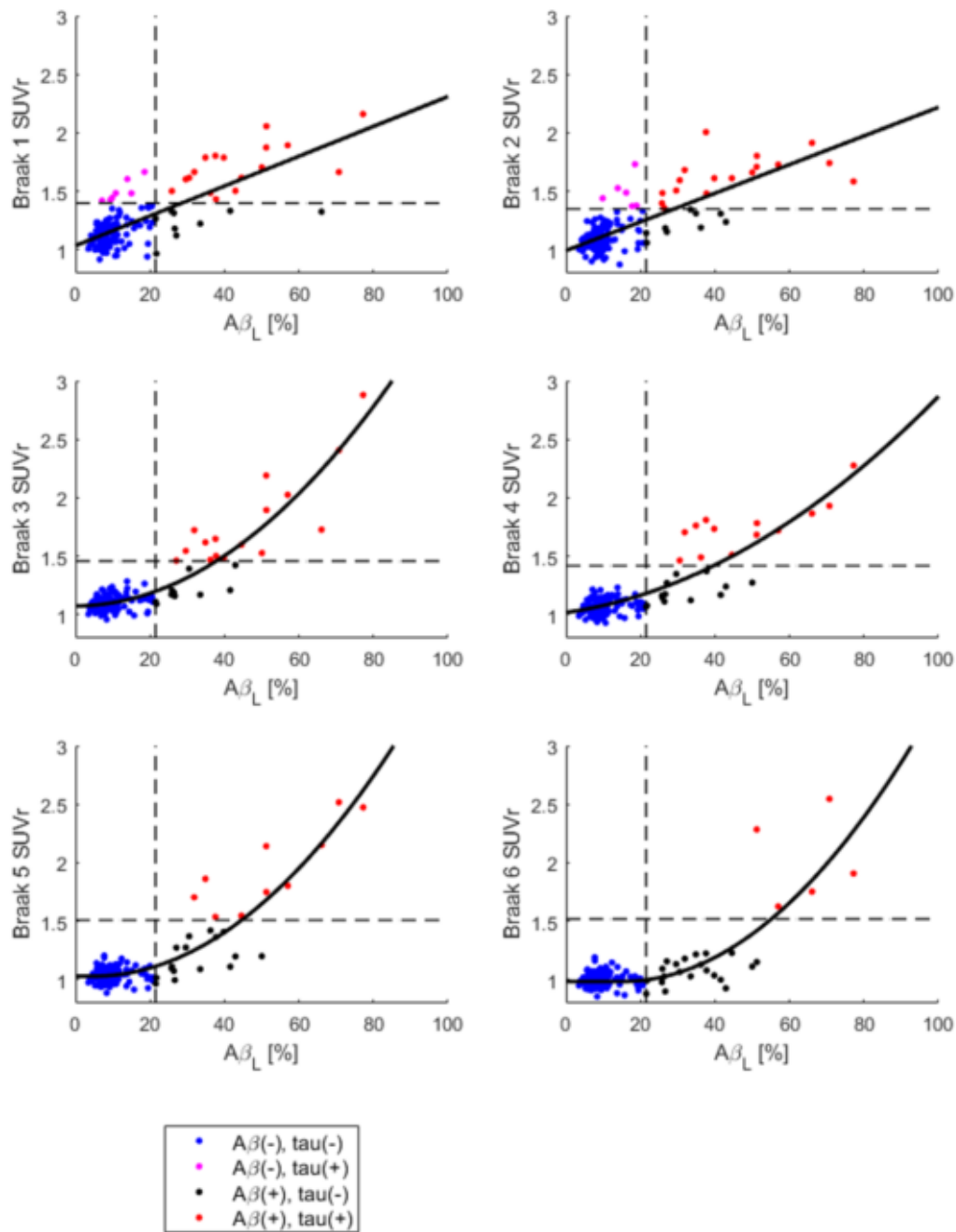


Figure 1. Fit of regression model between Braak regional tau SUVR and global $A\beta_L$. Dashed lines represent the cutoffs for $A\beta(+)$ and tau(+).

Table 1. Tau(+) cutoffs and their corresponding threshold of $A\beta_L$ for each Braak region. $A\beta(+)$ was defined as 21.5% $A\beta_L$.

Braak Region	Tau(+) cutoff (SUVR)	$A\beta_L$ threshold for tau(+)
Braak 1	1.40	28.6%
Braak 2	1.35	29.1%
Braak 3	1.46	37.8%
Braak 4	1.42	39.6%
Braak 5	1.51	44.6%
Braak 6	1.52	55.1%

Keywords: Down syndrome, Amyloid Load, Tau

TauIQ demonstrates increased power for cross-sectional and longitudinal analysis of Tau tracers as evidenced by [¹⁸F]Flortaucipir and [¹⁸F]GTP1

Alex Whittington¹, Jacob Hesterman¹, Sandra Sanabria², Paul Manser², Robby Weimer², John Seibyl¹, Roger N. Gunn^{1,3}

¹In vivo, Boston, MA, US

²Genentech, San Francisco, CA, US

³Imperial College London, London, UK

Introduction: Tau-PET has the potential to be an important biomarker for clinical trials of novel Alzheimer's Disease (AD) drugs. The Tau^{IQ} algorithm is applied to cross-sectional and longitudinal Tau-PET data to compare its performance against whole brain cortical SUVR.

Methods: Tau^{IQ} and SUVR analysis were applied to: [¹⁸F]Flortaucipir [Cross-sectional (N=675): 365 HC, 49 SMC, 82 EMCI, 113 MCI, 37 LMCI & 29 AD, Longitudinal (N= 60): 19 HC, 8 SMC, 15 EMCI, 5 MCI, 13 LMCI and [¹⁸F]GTP1 [Cross-Sectional & Longitudinal: N=61, 9 HC, 22 Prodromal-AD, 6 Mild-AD & 14 Moderate-AD]. Tau^{IQ} calculates a global tau load (Tau_L) and a local tau load using canonical image based regression (Figure 1).

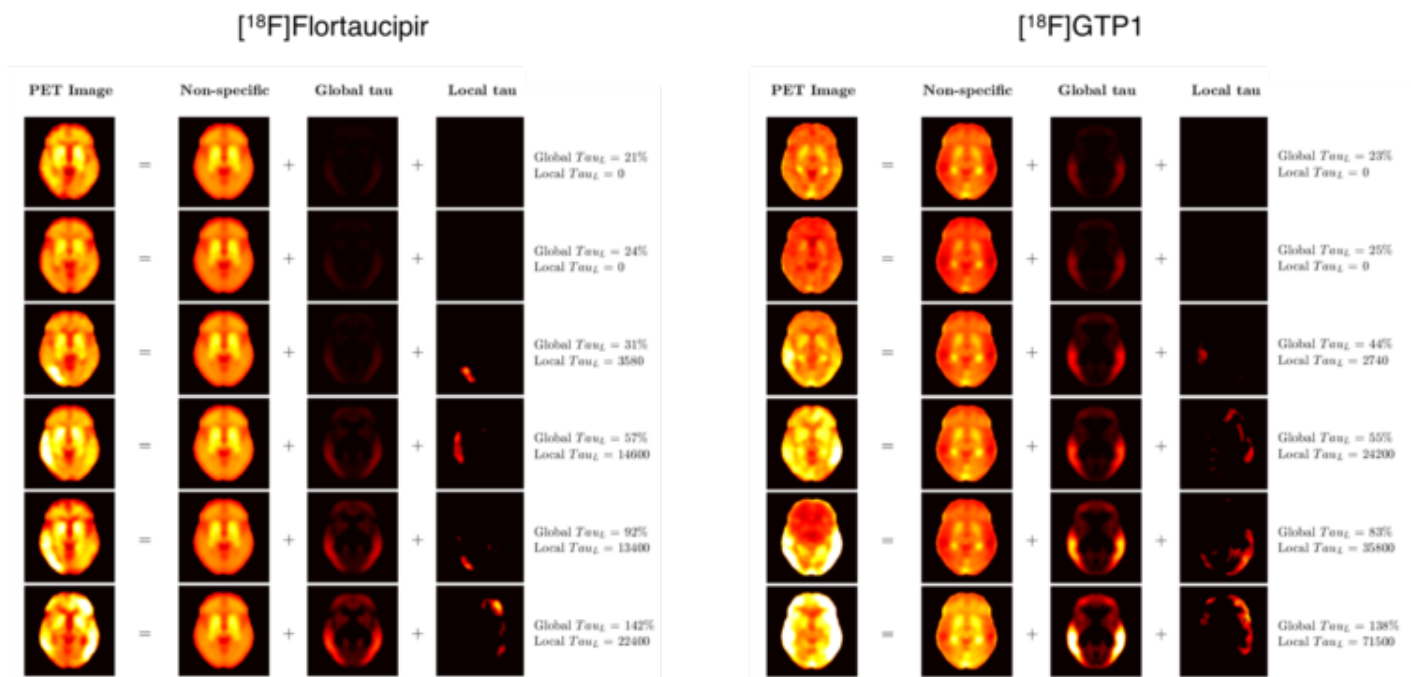


Figure 1: Application of Tau^{IQ} algorithm to [¹⁸F]Flortaucipir and [¹⁸F]GTP1 PET data. Illustrative examples from six different subjects for each tracer across the disease spectrum showing the decomposition into Non-specific, Global Tau Load and Local Tau Load.

SUVR was calculated using grey matter Cerebellum as the reference region and Tau_L and SUVR measures were compared. The cross-sectional comparison was performed by calculating effect sizes (Hedges' g) for each clinical group against the HC group. To facilitate longitudinal comparison, both outcome measures were converted to Z-scores (from the distribution of Aβ- HC at baseline) and the rates of accumulation of Aβ/Tau^{Low}, Aβ+/Tau^{Low} and Aβ+/Tau^{High} subjects were investigated.

Results: In cross-sectional analyses (Figure 2) there was an increase in effect size between HC and AD for Tau^{IQ} when compared to SUVR (17% increase for [¹⁸F]Flortaucipir and between 24%-49% for [¹⁸F]GTP1).

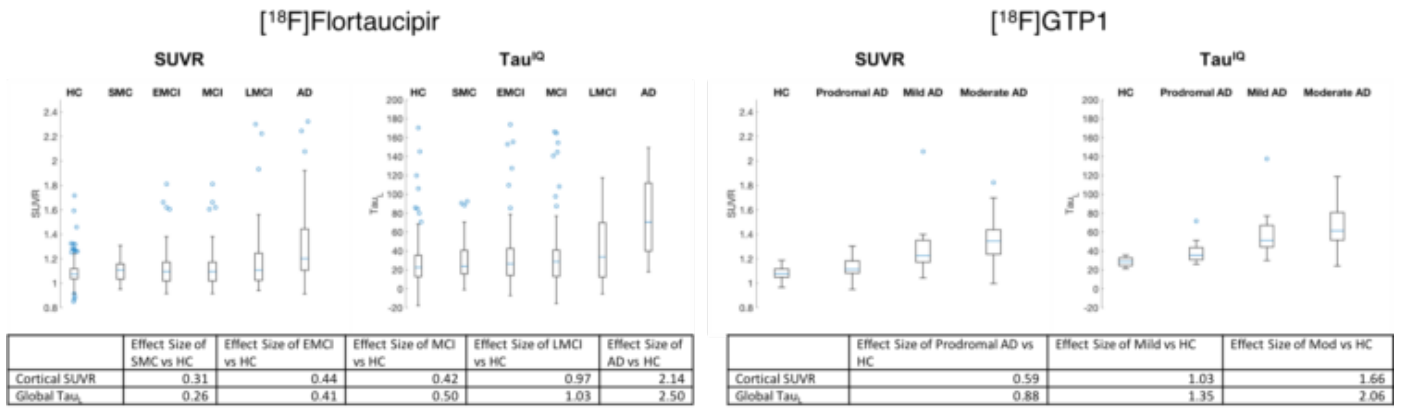


Figure 2: Comparison of SUVR and Tau^{IQ} outcome metrics in cross-sectional analysis of [¹⁸F]Flortaucipir and [¹⁸F]GTP1 PET data.

In the longitudinal analyses (Figure 3), Tau^{IQ} showed more significant accumulation in the Aβ⁺/Tau^{High} group ([¹⁸F]GTP1: Tau^{IQ} 0.70 STD/year, SUVR: 0.45 STD/year, [¹⁸F]Flortaucipir: Tau^{IQ} 0.53 STD/year, SUVR: 0.33 STD/year) and in the Aβ⁺/Tau^{Low} group ([¹⁸F]GTP1: Tau^{IQ} 0.18 STD/year, SUVR 0.09 STD/year, [¹⁸F]Flortaucipir: Tau^{IQ} 0.17 STD/year, SUVR 0.14 STD/year). Tau^{IQ} and SUVR showed no accumulation in the Aβ⁻/Tau^{Low} group for both tracers.

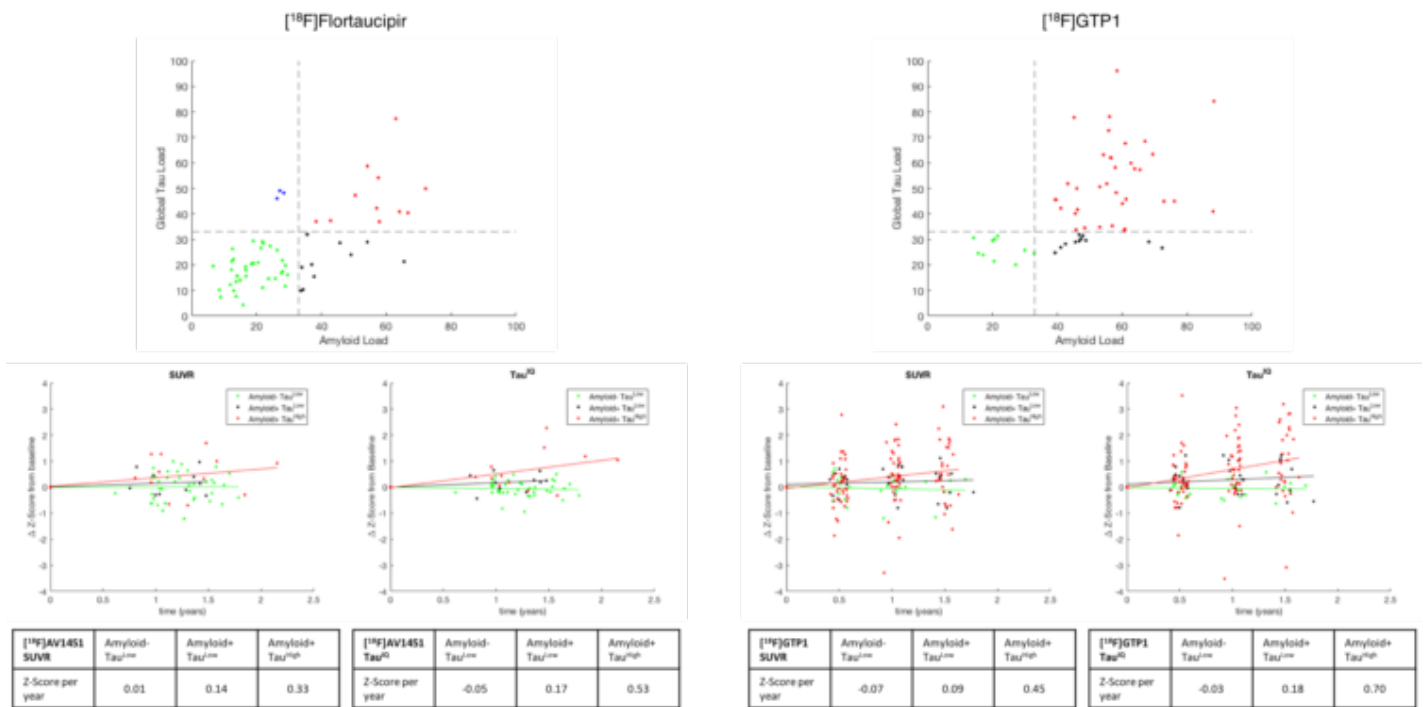


Figure 3: Comparison of SUVR and Tau^{IQ} outcome metrics in longitudinal analysis of [¹⁸F]Flortaucipir and [¹⁸F]GTP1 PET data. Top: Relationship between Amyloid Load and Tau Load derived from Amyloid^{IQ} and Tau^{IQ} with categorization into Aβ⁻/Tau^{Low}, Aβ⁺/Tau^{Low} and Aβ⁺/Tau^{High}. Bottom: Rates of accumulation of Tau for each category.

Conclusions: Tau^{IQ} showed increased power when evaluated in these [¹⁸F]Flortaucipir and [¹⁸F]GTP1 data sets and promises to be an important analytical tool for clinical trials in AD.

Keywords: Tau PET, TauIQ, Quantification, GTP1, Flortaucipir

Spatiotemporal imaging phenotypes of tau pathology in Alzheimer's disease

Jacob Vogel¹, Alexandra Young², Neil Oxtoby², Ruben Smith^{3,4}, Rik Ossenkoppele^{3,5}, Olof Strandberg³, Leon Aksman², Renaud La Joie⁶, Michel Grothe⁷, Chul Hyung Lyoo⁸, Gil Rabinovici⁶, Daniel Alexander², Alan Evans¹, Oskar Hansson^{3,4}

¹Montreal Neurological Institute, McGill University, Montreal, QC, Canada

²University College London, London, UK

³Lund University, Lund, Sweden

⁴Skane University Hospital, Lund, Sweden

⁵Alzheimer's Center, VU University Medical Center, Amsterdam, The Netherlands

⁶Memory and Aging Center, University of California, San Francisco, CA, US

⁷German Center for Neurodegenerative Diseases (DZNE), Rostock, Germany

⁸Gangnam Severance Hospital, Seoul, Korea

Introduction: The Braak staging scheme describes stereotypical spread of tau pathology in Alzheimer's disease. However, apparent subtypes described at autopsy and clinical variants of AD both suggest variation in tau patterning across the population. Previous imaging studies probing this variation have been limited by small samples, non-specific markers and difficulty disentangling global spatial pattern from temporal disease progression.

Methods: Subtype and Stage Inference (SuStaIn) is a data-driven algorithm that combines disease progression modeling with clustering to extract multiple spatiotemporal progressions (subtypes) from large cross-sectional datasets. SuStaIn infers membership of individuals to a subtype progression, whilst also assigning individuals to a stage along that progression. We apply SuStaIn to a multisite dataset (n=1474) of [¹⁸F]-flortaucipir tau-PET scans to characterize spatiotemporal subtypes of tau spreading events. We verify these subtypes in a second monocentric dataset (n=567) of [¹⁸F]-RO948 tau-PET scans. We selected 26 BraakStage x Lobe regions (13/hemisphere) for the SuStaIn model, converting these features to tau-positive probabilities using mixture modeling. We used convergence in the uncertainty of the model likelihood to determine the number of subtypes, discarding small subtypes (n<40). SuStaIn stage was compared to global cognitive measures and age.

Results: 881 subjects (59%) were unclassified by SuStaIn due to limited tau signal (Fig3), and 42 subjects (3%) fell into discarded subtypes. Of those classified, 56% demonstrated a typical Braak-like pattern (S1). The remaining subjects were classified into temporal predominant (S2), occipital-predominant (S3), hippocampal-sparing (S4) or right-hemisphere predominant (S5) subtypes (Fig1,2). Subtypes S1, S3 and S4 were replicated in the validation dataset. Increasing SuStaIn tau stage was associated with lower age and global cognition (Fig3).

Discussion: We observed substantial but consistent variation in tau patterning, indicating tau progression may deviate from prototypical Braak staging more often than previously described. Future work will characterize demographic, cognitive and genetic variation across spatiotemporal subtypes.

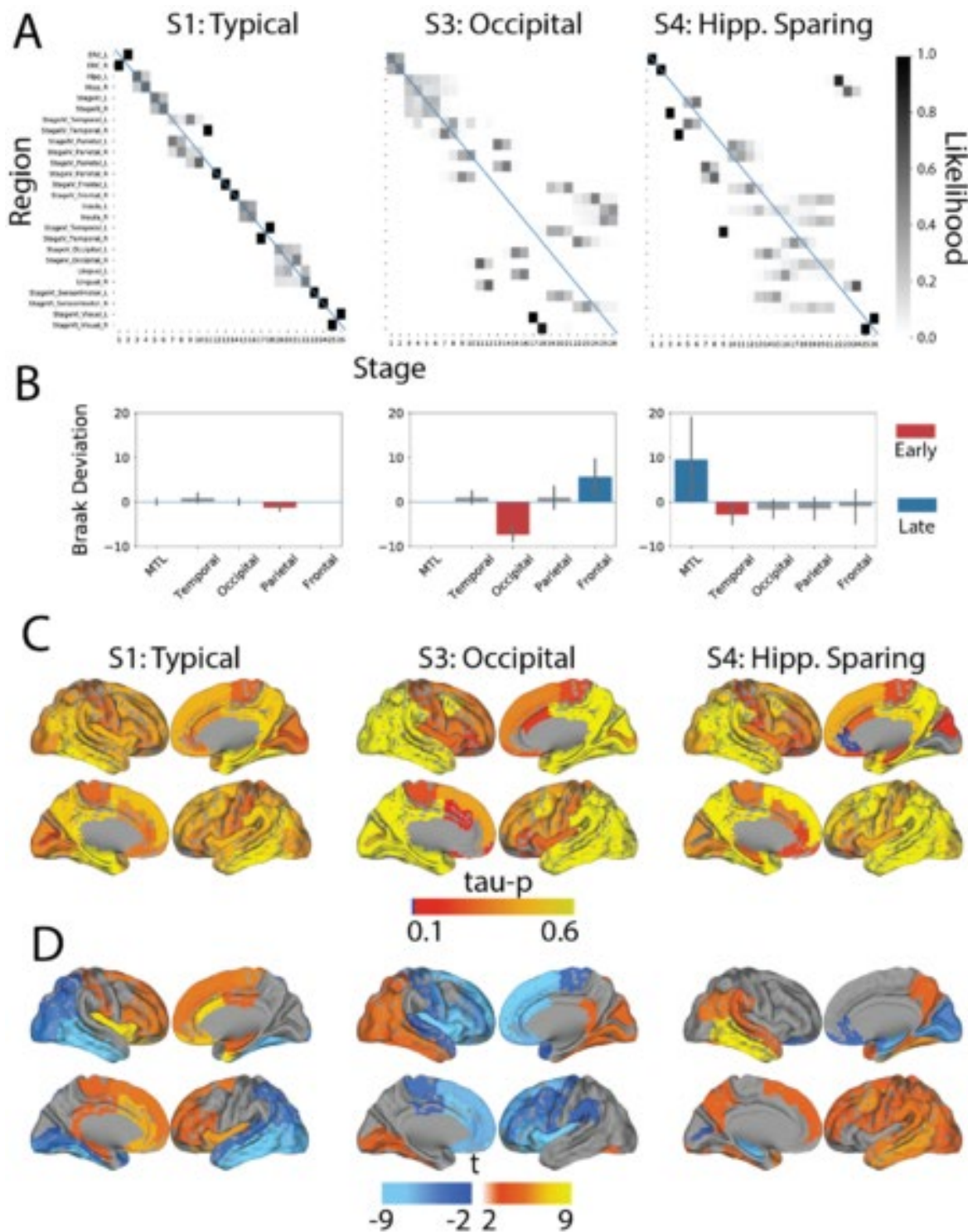


FIG1: Spatiotemporal subtypes of tau progression. A) Confusion matrices showing the archetypical sequence of events for each subtype (due to space limitations, only subtypes replicating in the validation cohort are included here). Colors represent the likelihood each region (y-axis) exhibits abnormal tau-PET binding at each stage (x-axis). Diagonal lines represent the expected order of events given Braak staging. **B)** For each subtype, the average deviation from expected sequence for regions in each lobe. Red regions become abnormal consistently earlier than expect, blue are abnormal consistently later. **C)** The average tau-positive probability of all subjects belonging to each subtype. A value of (say) 0.3 indicates 30% of subjects in a given subtype have abnormally high tau-PET signal in this region. **D)** For each subtype, regions showing significantly different tau compared to all other subtypes combined, adjusting for stage and multiple comparisons.

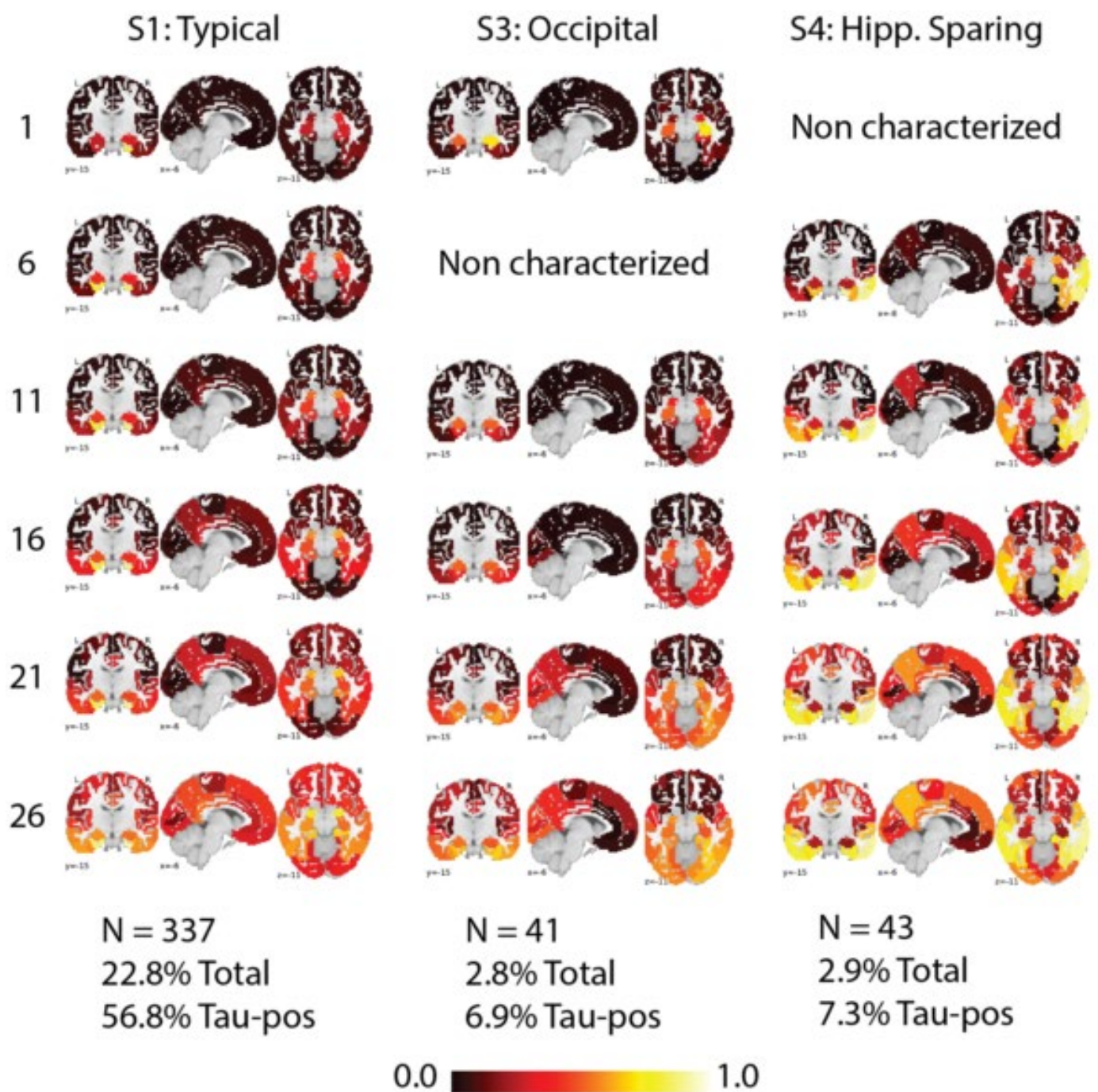


Fig2: Spatiotemporal evolution of each subtype. SuStaln identifies differentiable spatiotemporal progressions, assigns subjects to a progression, and to a stage along that progression. Each column is a subtype, and each row represents the mean tau-probability images of subjects falling into the indicated stage and the 4 stages before it (e.g. row 21 is the mean of subjects in stages 17-21). Row 1 is the mean of subjects only in stage 1. The overall number of individuals classified as each subtype is indicated, as well as the proportion of the overall, and tau-positive (i.e. classified) sample represented by the subtype.

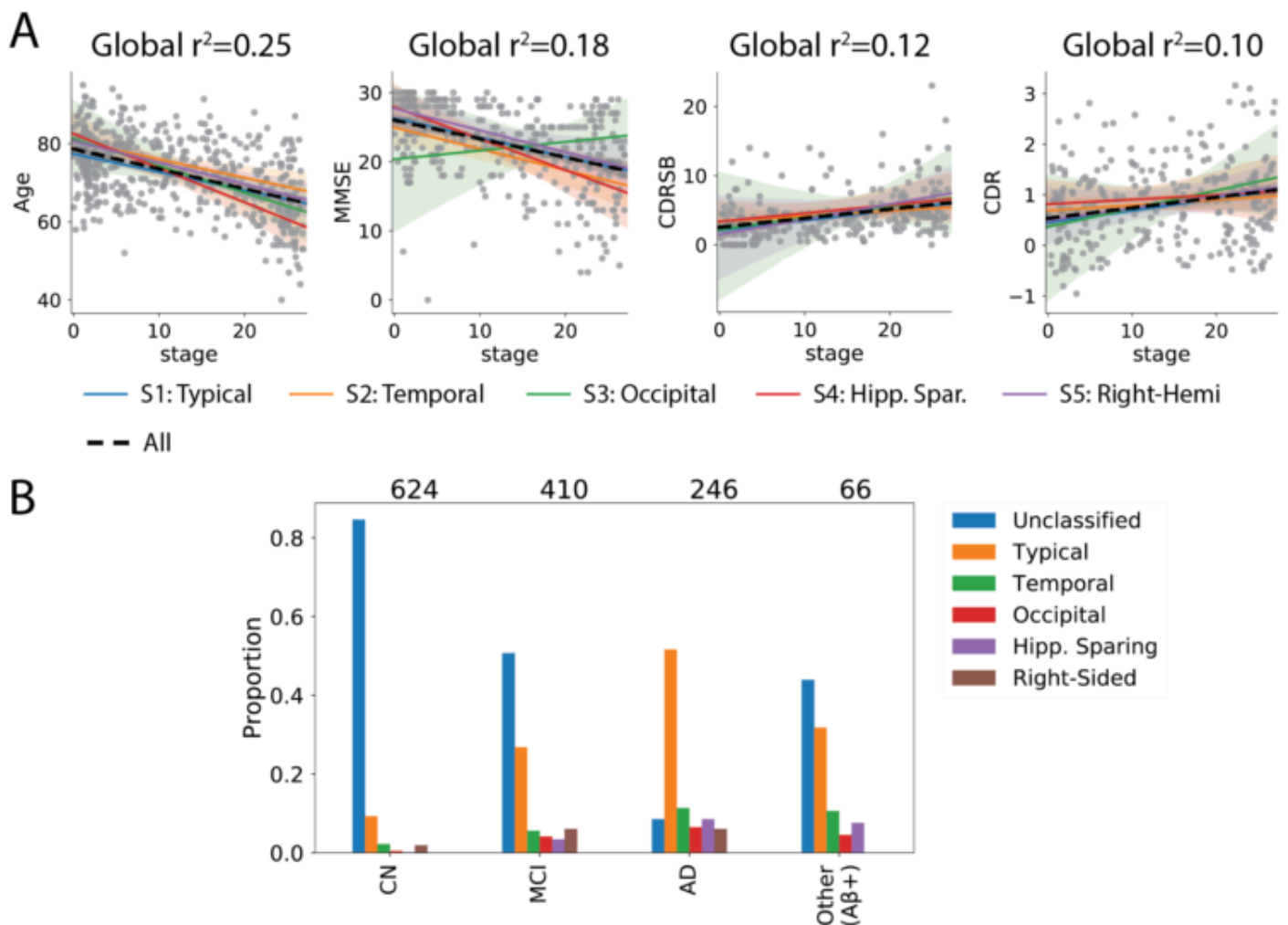


Fig3: (A) Associations between SuStaln stage, age and global cognition. Dotted lines represent the entire sample, whereas colored lines indicate trends for each subtype. Lower MMSE indicates worse cognition, whereas higher CDR and CDRSB indicate worse cognition. Across subtypes, individuals at higher SuStaln stages were younger and had lower cognition. Note: x-axis jittered for all plots, and y-axis jittered for CDR plot. **(B)** Proportion of subjects making up each subtype separated by diagnosis. MMSE = Mini mental state examination. CDR = Clinical dementia rating. CDRSB = Clinical dementia rating sum of boxes. CN = Cognitively normal. MCI = Mild cognitive impairment. AD = Alzheimer’s disease.

Keywords: tau, PET, subtype, method

Predicting structural, metabolic and pathologic disease progression in autosomal dominant Alzheimer's disease with machine learning

Patrick Luckett¹, Austin McCullough¹, Randall J. Bateman¹, Tammie Benzinger¹, Eric McDade¹, Beau Ances¹

¹Washington University School of Medicine in Saint Louis, Saint Louis, MO, US

Introduction: Predicting disease progression in autosomal dominant Alzheimer's disease (ADAD) would allow for targeted patient care and decision support models for evaluating the effects of specialized therapy. We propose a framework of machine learning algorithms to model disease progression in ADAD using multimodal neuroimaging, deep learning, and feature extraction algorithms. The data-driven approach represents an opportunity to discover novel mechanisms and disease trajectories of ADAD.

Methods: At least 2 separate imaging sessions were obtained from 131 mutation positive and 74 mutation negative participants from the Dominantly Inherited Alzheimer Network observational study. Participants were matched for age, education, and sex. Structural MRI, amyloid PET (PiB), and metabolic activity (FDG) was acquired at each time point for 44 Freesurfer brain regions of interest. Regional trajectories were calculated using rates of change normalized by the amount of time between scans. The imaging data was combined with familial expected year of onset, APOE e4 status, age, and sex. A deep feed forward neural network was trained to predict disease progression with respect to a given neuroimaging modality. Relief feature selection algorithms identified regions that were the strongest predictors of mutation status.

Results: The Relief algorithm identified the caudate, anterior cingulate, and precuneus as the strongest predictors among all modalities (Figure 1). The model yielded accurate results for predicting future values of PiB ($R^2=.95$, Mean Squared Error (MSE)=.2), FDG ($R^2=.93$, MSE=.1) (Figure 2), and volumes ($R^2=.95$). Simulations revealed a sigmoidal trajectory for PiB, a biphasic response for FDG, and a gradual decrease in volumetrics (Figure 3).

Conclusion: In order to provide targeted treatment to persons with ADAD, novel methods are needed to model disease trajectories. Our model is highly accurate and capable of reliably forecasting changes in amyloid, metabolism, and volumetrics. Model simulations suggest initial disease progression is primarily in subcortical and temporal regions.

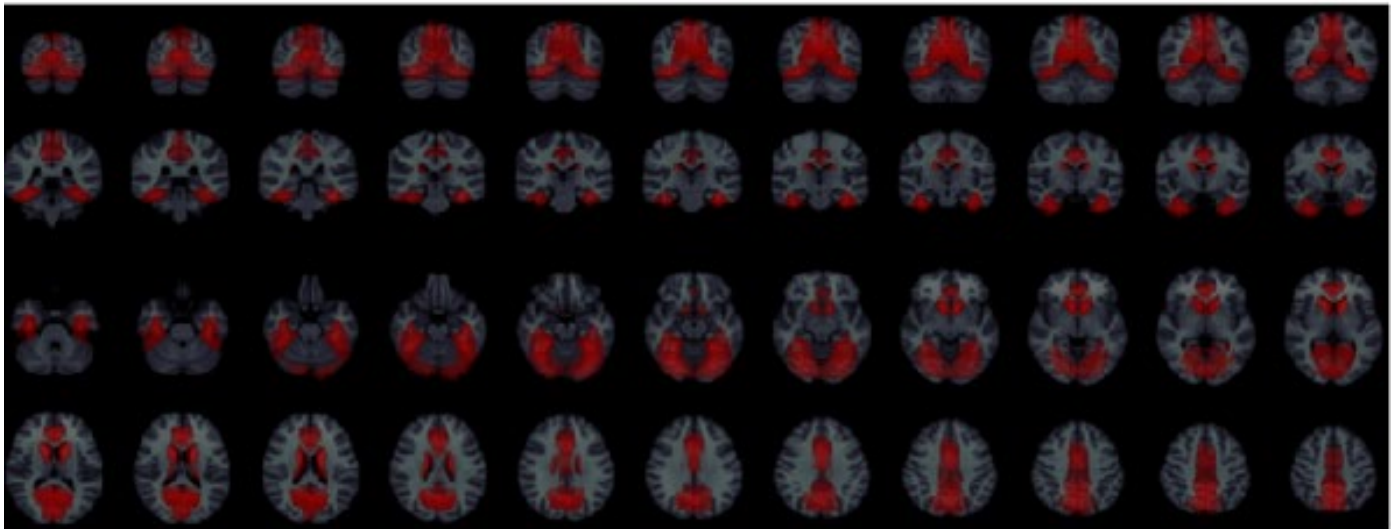
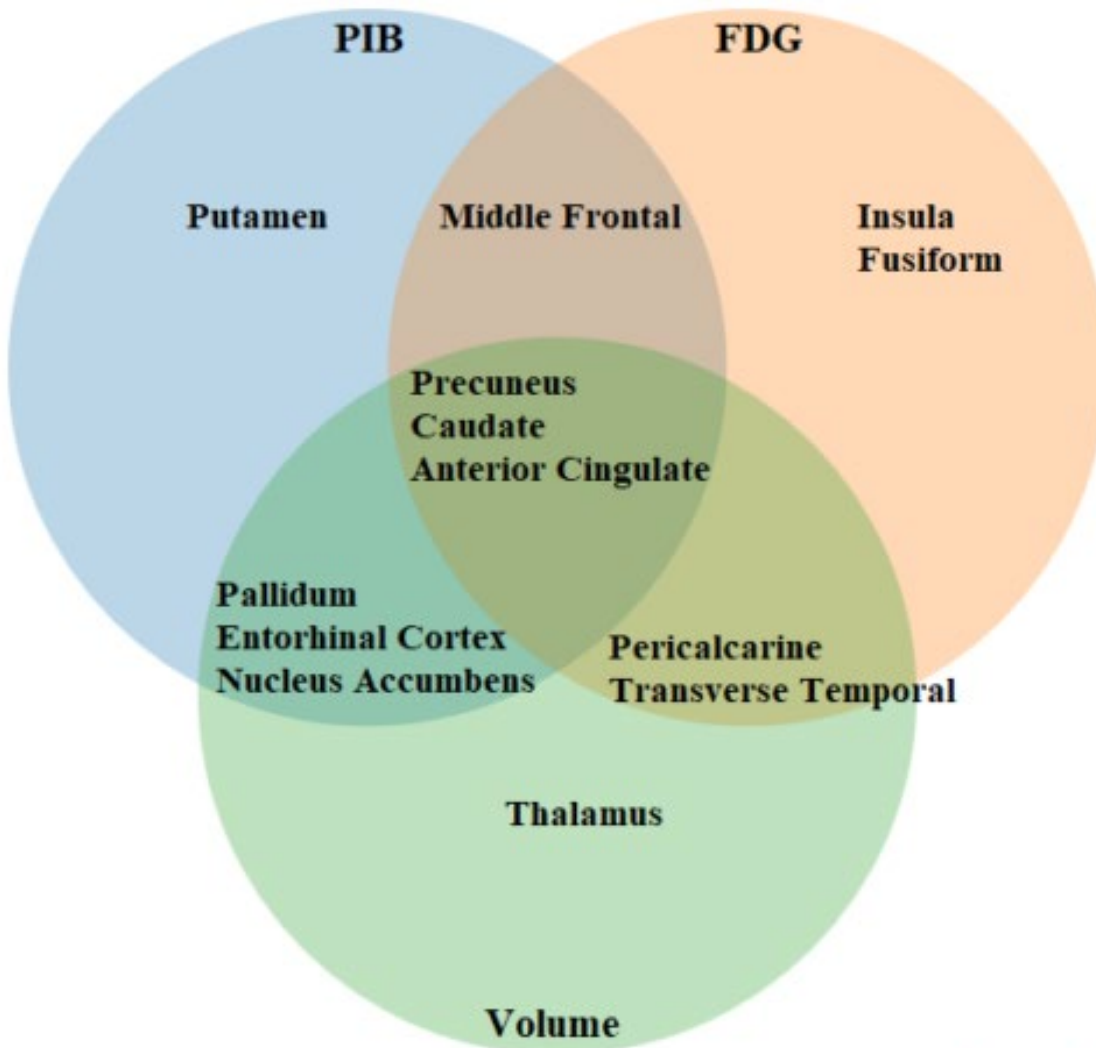


Figure 1: (Top) Strongest predictors of mutation status for each imaging modality. (Bottom) Regions most affected by ADAD

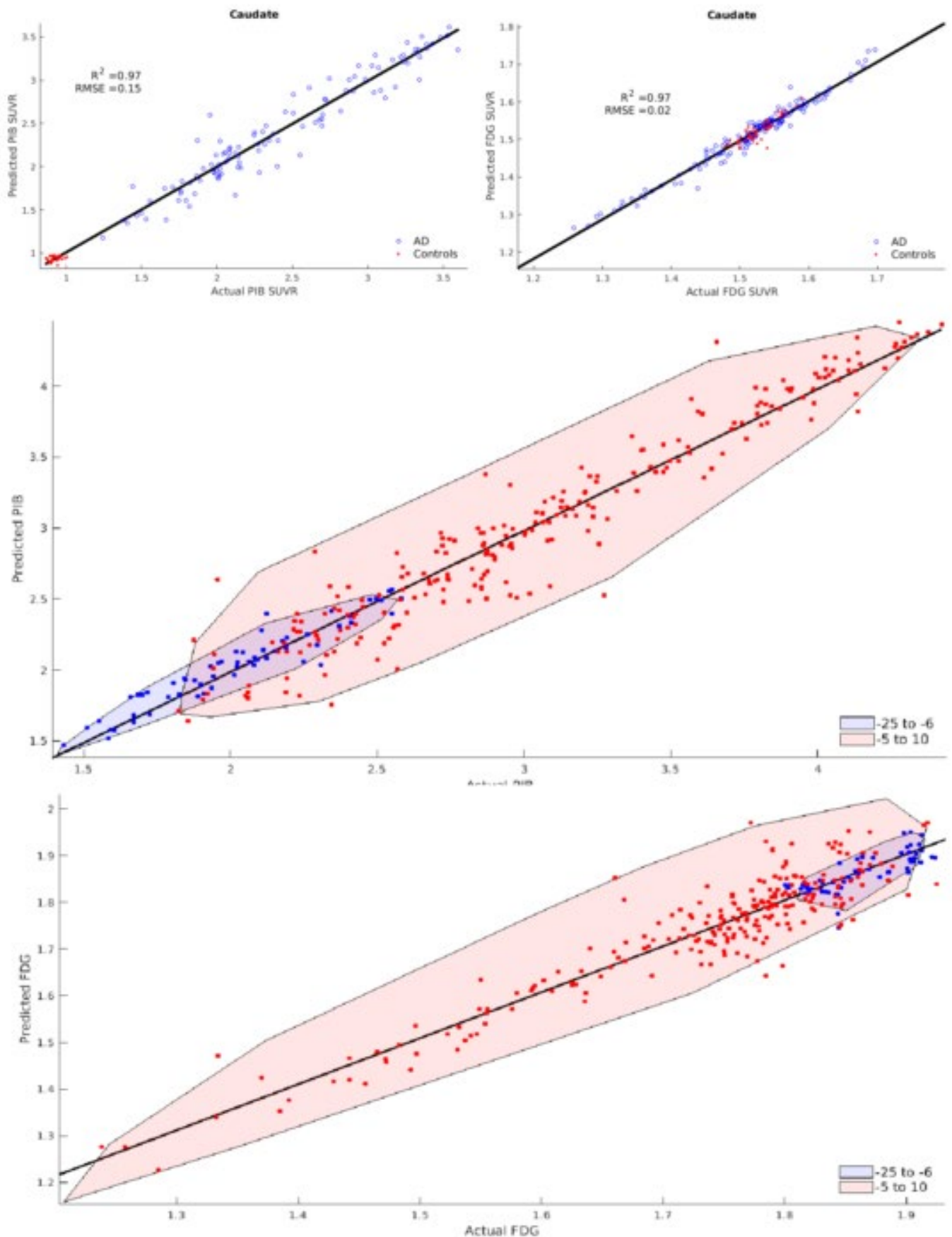


Figure 2: (Top) Predicted versus actual values for mutation positive participants and controls for PIB and FDG. **(Middle)** Predicted PIB values for mutation positive participants separated by distance to EYO. **(Bottom)** Predicted FDG values for mutation positive participants separated by distance to EYO.

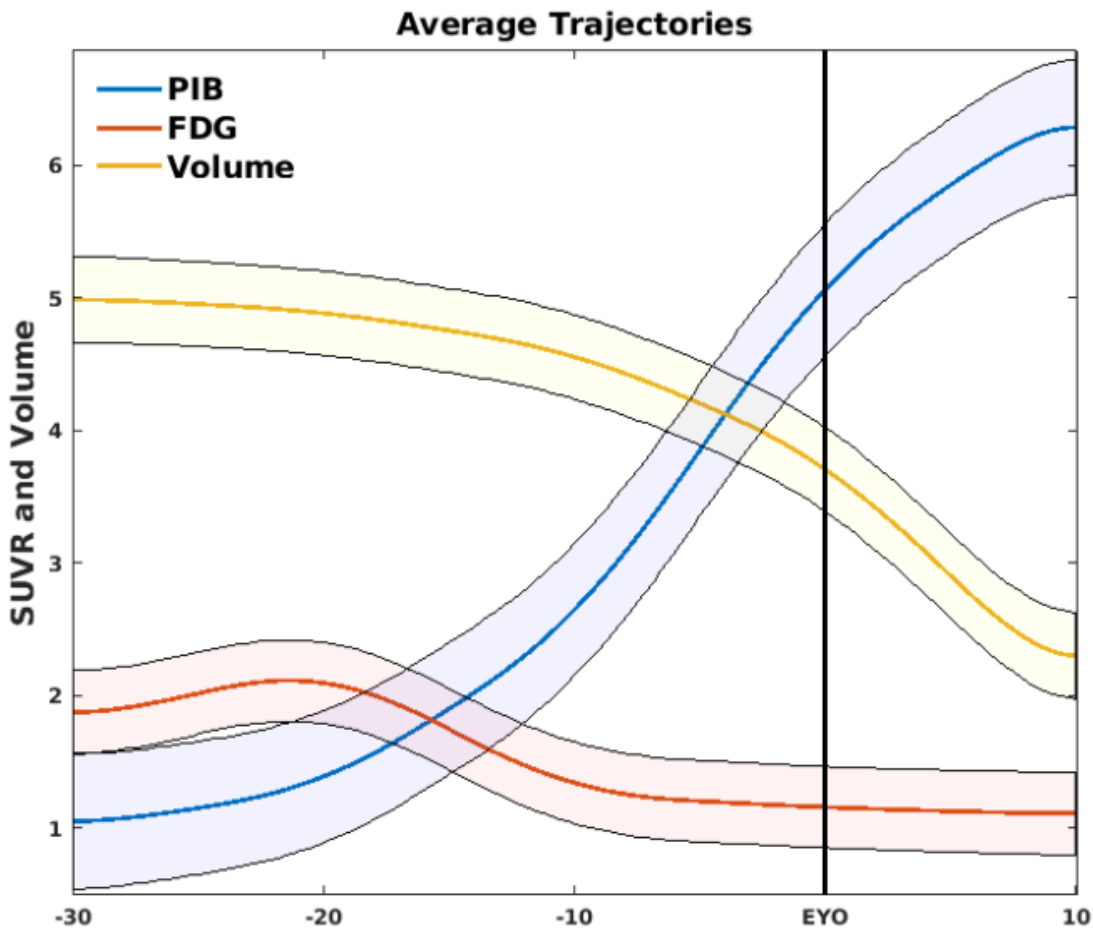


Figure 3: Simulated biomarker evolution for mean cortical PIB, mean cortical FDG, and total gray matter volume (scaled for display) from deep learning algorithm in mutation positive participants. Shaded regions indicate model variability.

Keywords: Alzheimer's Disease, Machine Learning, amyloid, PET

Correction of partial volume effects for tau PET imaging using the kernel method

Kuang Gong¹, Paul Han¹, Jianan Cui¹, Nicolas Guehl¹, Keith Johnson¹, Quanzheng Li¹, Georges El Fakhri¹

¹*Department of Radiology, Massachusetts General Hospital and Harvard Medical School, Boston, MA, US*

Introduction: The topographic patterns of tau retention in PET scans are consistent with Braak staging and correlate well with cognitive measurements. However, due to PET limited spatial resolution, quantitative accuracy of tau distribution is significantly compromised by the partial volume effect (PVE). Furthermore, PVE is a confounding factor when assessing tau distribution in the trans-entorhinal cortex due to uptake in the meninges. We have developed a novel PVE correction method, entitled the Kernel method, to fully extract the pathophysiological information present in a tau scan.

Methods: For the Kernel method, the main idea is to represent the PET unknown image intensity at each pixel as a linear combination of the basis vectors from other pixels. The basis vectors can be calculated from the patient's high-quality prior images, e.g. MPRAGE images. This kernel representation can be embedded into the traditional OSEM algorithm and is segmentation-free. To validate the effectiveness of the Kernel method for tau PET imaging, the ¹⁸F-MK-6240 datasets acquired from MCI subjects were processed using the proposed method and the traditional Gaussian post-processing method (4mm FWHM). The ¹⁸F-MK-6240 images (70-90 mins post-injection) were acquired from the DMI PET/CT (GE), and the MPRAGE images were acquired from the 3T Tim Trio (Siemens). Freesurfer was used to identify the Braak stage-related cortices for each subject.

Results and Conclusions: Figure 1 shows the coronal view in three MCI subjects with the Gaussian filtering and the Kernel method. Table 1 shows SUVR values for the Braak stage-related cortices. The proposed Kernel method yielded increased SUVR tau cortical uptake throughout the brain and significantly improved spatial resolution, while reducing ambiguity in tau activity due to meningeal uptake. In the future, we will perform more evaluations and analysis based on datasets from NC and MCI/AD groups.

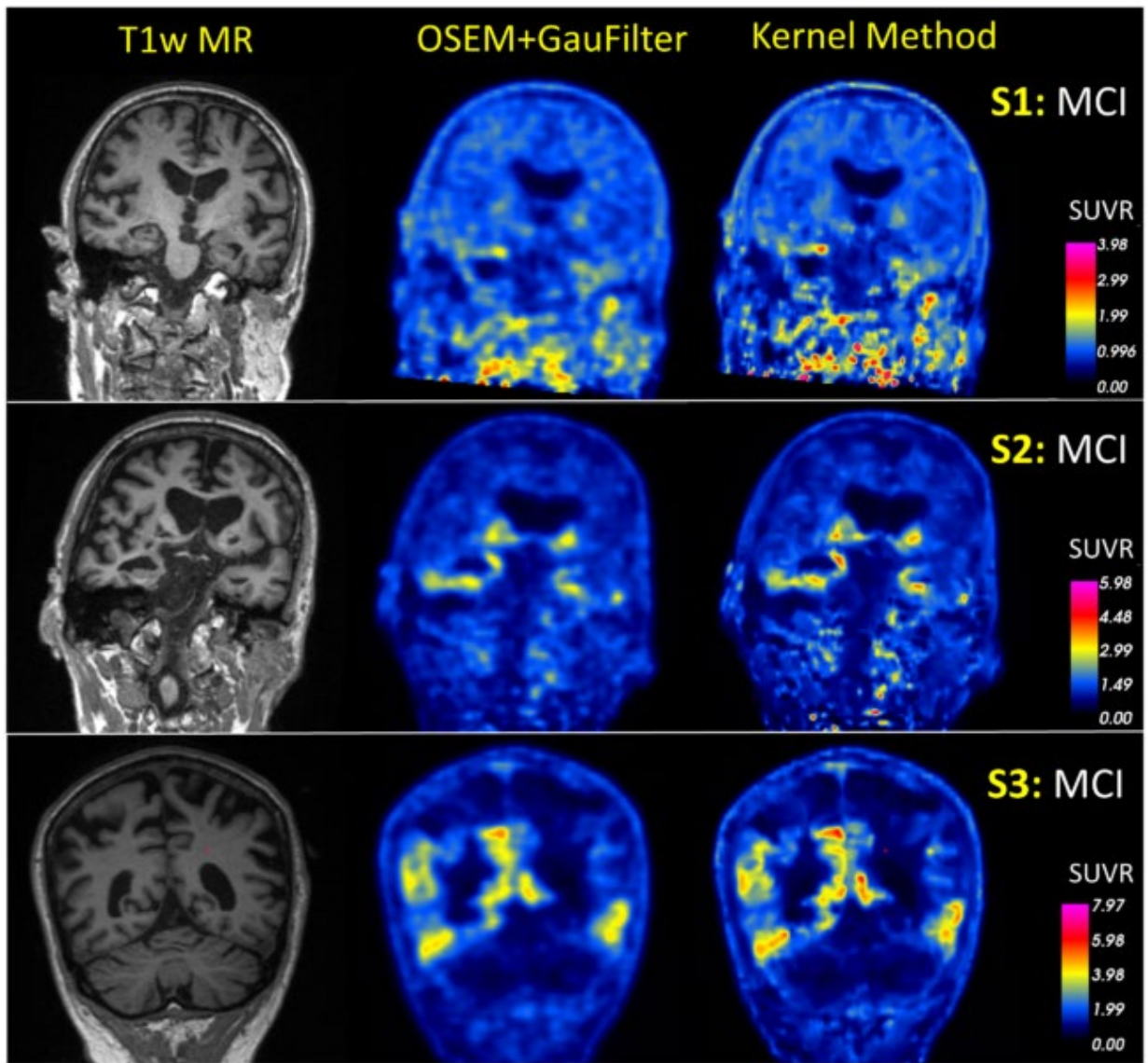


Figure 1. Coronal views of the SUVR images using the traditional Gaussian smoothing (4mm FWHM) and the proposed kernel method. The first column is the T1w MR image.

Table 1. The SUVR of Braak stage-related cortices for the three subjects using the Gaussian postprocessing and the proposed kernel method.

		Entorhinal	Para-hippocampal	Inferior temporal	Fusiform	Posterior cingulate
Subject 1	Gaussian	1.169	1.135	1.193	1.162	0.988
	Kernel method	1.172	1.169	1.203	1.159	0.992
	Improvement	0.25%	3.00%	0.84%	-0.26%	0.40%
Subject 2	Gaussian	2.136	1.637	1.439	1.458	1.083
	Kernel method	2.276	1.726	1.450	1.479	1.099
	Improvement	6.55%	5.44%	0.76%	1.44%	1.48%
Subject 3	Gaussian	2.148	2.722	2.848	2.299	2.100
	Kernel method	2.589	3.014	3.007	2.419	2.275
	Improvement	20.53%	10.72%	5.58%	5.22%	8.33%

Keywords: partial volume correction, tau imaging, kernel method, image reconstruction

SESSION 3: NEUROPATHOLOGY I

Thursday, January 16, 2020		
08:30 AM	SESSION 3: NEUROPATHOLOGY I	CHAIRS: Laetitia Lemoine, PhD, <i>Karolinska Institute</i> Teresa Gomez-Isla, MD <i>Massachusetts General Hospital</i>
8:30 AM	Flortaucipir PET often shows uptake greater in regions outside of the medial temporal lobe than in entorhinal cortex in low Braak tangle stage participants	Val Lowe, MD, <i>Mayo Clinic</i>
8:45 AM	Brain volume and [18F]flortaucipir PET analysis of progressive supranuclear palsy clinical variants	Jennifer Whitwell, PhD, <i>Mayo Clinic</i>
9:00 AM	Comparison of autoradiographic binding profiles of Flortaucipir, MK-6240 and PI-2620 in human postmortem tissue samples across the spectrum of neurodegenerative diseases	Cinthya Aguzo, MD, <i>Massachusetts General Hospital</i>
9:15 AM	Biochemical correlates of tau and amyloid PET imaging in four autopsy brains	Milos Ikonovic, MD, <i>University of Pittsburgh</i>
9:30 AM	Discussion	

Flortaucipir PET often shows uptake greater in regions outside of the medial temporal lobe than in entorhinal cortex in low Braak tangle stage participants

Val Lowe¹, Emily Lundt¹, Christopher Schwarz¹, Hugo Botha¹, Prashanthi Vemuri¹, Jeffrey Gunter¹, Ronald Petersen¹, Clifford Jack¹, Paul Min¹, Scott Przybelski¹, Matthew Senjem¹, Kejal Kantarci¹, Bradley Boeve¹, David Jones¹, Robert Reichard¹, Jessica Tranovich², Sydney Labuzan², Fadi Hanna Al-Shaikh², David Knopman¹, Dennis Dickson², Melissa Murray²

¹Mayo Clinic, Rochester, MN, US

²Mayo Clinic, Jacksonville, FL, US

Background: Flortaucipir PET (FTP) uptake in the entorhinal cortex (ERC) is an important predictor of memory impairment even in cognitively unimpaired individuals. Understanding the relationship of early uptake in the ERC vs other cortical regions can help improve the understanding of early tangle distribution in the brain. Therefore, we evaluated FTP ERC uptake relative to Braak tangle stage and other cortical regions in a group with autopsy verification.

Method: Participants (n=27) who had autopsy and FTP performed were evaluated. We assessed the frequency of having an ERC SUVr greater than any other cortical region. We also determined how many and the location of cortical regions that had an SUVr greater than ERC. Next, we categorized these findings relative to Braak tangle stage. An SUVr cutpoint for ERC of 1.27 was used. Off-target subcortical regions were excluded.

Results: There were 16 participants with Braak \geq IV and 11 with \leq Braak stage III. ERC SUVr had the highest correlation with Braak stages ($\rho=0.81$, $p<0.001$). There were 8 subjects with ERC SUVr greater than any other ROI. In Braak tangle stage I, II and III participants; 1 had a visual region; 1-2 had several extratemporal regions; and 2-6 had several extratemporal regions with SUVr's greater than ERC respectively (Table 1).

Table 1. Top ranked regions by # subjects having regional SUVr greater than ERC Tau SUVr listed by Braak tangle stage.

r	Braak	I	Braak	II	Braak	III	Braak	IV	Braak	V	Braak	VI
1	Primary_Visual	1	Cingulum	2	Insula	6	Cingulum	3	Insula	8	Insula	5
2	NA	NA	Insula	2	Paracentral_Lobule	6	Insula	3	Medial_Temporal	8	Medial_Temporal	5
3	NA	NA	Medial_Temporal	2	Postcentral	6	Medial_Temporal	3	Occipital	8	Paracentral_Lobule	4
4	NA	NA	Orbito_Frontal	2	Primary_Visual	6	Orbito_Frontal	3	Paracentral_Lobule	8	Postcentral	4
5	NA	NA	Paracentral_Lobule	2	Cingulum	5	Paracentral_Lobule	3	Postcentral	8	Precentral	4
6	NA	NA	Postcentral	2	Precentral	5	Postcentral	3	Precentral	8	Primary_Visual	4
7	NA	NA	Precentral	2	Rolandic_Oper	5	Precentral	3	Primary_Visual	8	Cingulum	3
8	NA	NA	Primary_Visual	2	PreFrontal	4	PreFrontal	3	Rolandic_Oper	8	Orbito_Frontal	3
9	NA	NA	Rolandic_Oper	2	Medial_Temporal	3	Rolandic_Oper	3	Supp_Motor_Area	8	PreFrontal	2
10	NA	NA	Supp_Motor_Area	2	Orbito_Frontal	3	Supp_Motor_Area	3	Cingulum	7	Rolandic_Oper	2
11	NA	NA	Parietal	1	Occipital	2	Parietal	2	Orbito_Frontal	7	Occipital	1
12	NA	NA	Precuneus	1	Parietal	2	Precuneus	2	Parietal	7	Supp_Motor_Area	1
13	NA	NA	PreFrontal	1	Precuneus	2	Primary_Visual	2	Precuneus	7	NA	NA
14	NA	NA	NA	NA	Supp_Motor_Area	2	Occipital	1	PreFrontal	7	NA	NA
15	NA	NA	NA	NA	Temporal	2	Temporal	1	Temporal	5	NA	NA

Conclusion: In early Braak tangle stage participants (I-III), FTP SUVr in regions outside the medial temporal lobe can often have SUVr's greater than ERC SUVr. This suggests the early presence of tau tangles outside of the medial temporal, which is discordant with other autopsy-based studies, and suggests a potential need for more widespread sampling to better characterize early stages of tangle accumulation. The relationship of non-specific FTP binding will also need to be investigated in these participants.

Keywords: Flortaucipir, PET, Autopsy, tau, Braak tangle stage.

Brain volume and [18F]flortaucipir PET analysis of progressive supranuclear palsy clinical variants

Jennifer Whitwell¹, Nirubol Tosakulwong¹, Hugo Botha¹, Farwa Ali¹, Heather Clark¹, Joseph Duffy¹, Rene Utianski¹, Chase Stevens¹, Stephen Weigand¹, Christopher Schwarz¹, Matthew Senjem¹, Clifford Jack¹, Val Lowe¹, J. Eric Ahlskog¹, Dennis Dickson², Keith Josephs¹

¹Mayo Clinic, Rochester, MN, US

²Mayo Clinic, Jacksonville, FL, US

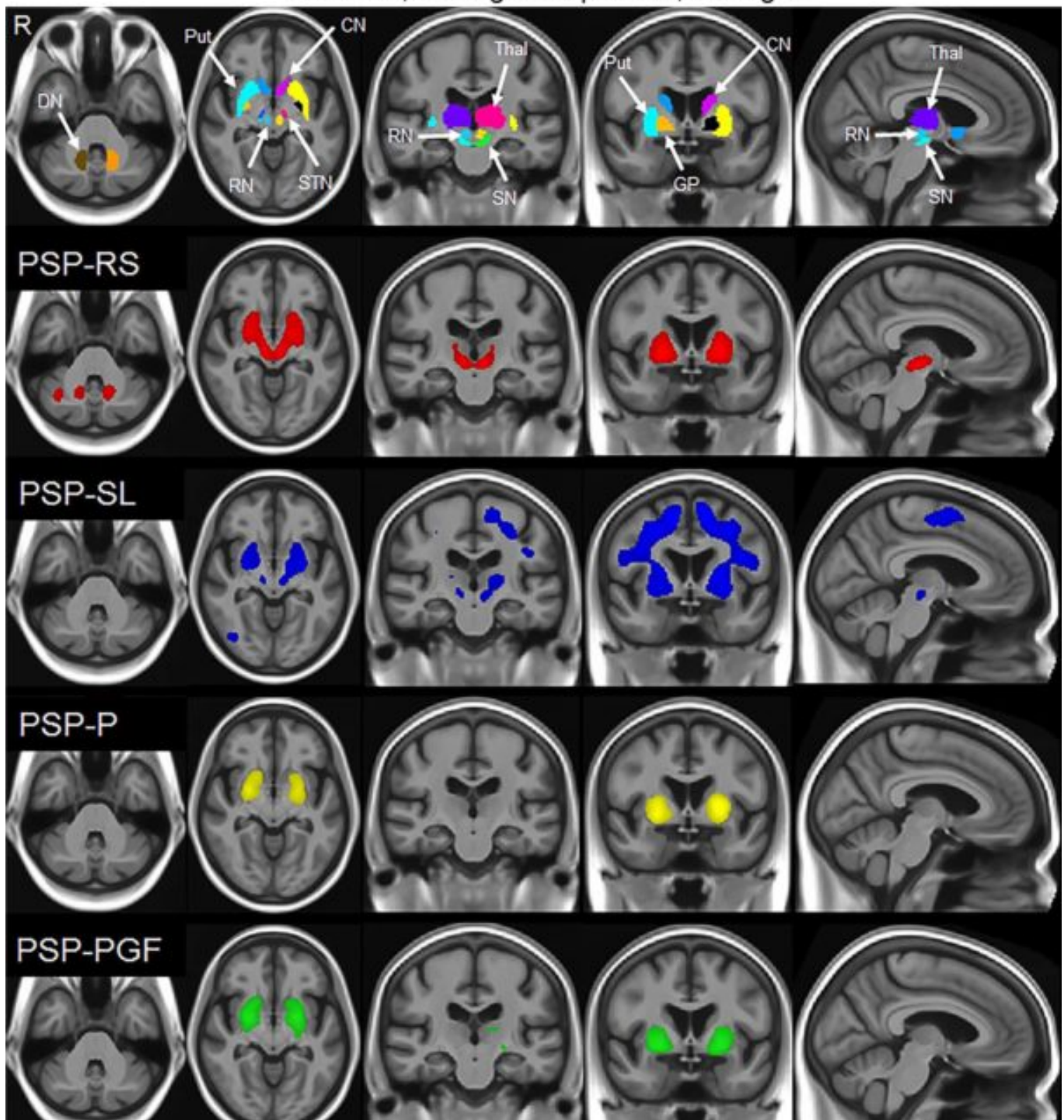
Background: Progressive supranuclear palsy (PSP) is a neurodegenerative tauopathy associated with the clinical variants of PSP-Richardson's syndrome (PSP-RS), PSP-parkinsonism (PSP-P), PSP-corticobasal syndrome (PSP-CBS), PSP-frontal (PSP-F), PSP-progressive gait freezing (PSP-PGF) and PSP-speech/language (PSP-SL). While PSP-RS has been well-characterized on neuroimaging, the characteristics of the other atypical variants are less well-defined and it is unknown how they compare to each other or relate to neuropathology. We aimed to assess and compare regional atrophy on MRI and [18F]flortaucipir uptake on PET across PSP variants.

Methods: 105 PSP patients (53 PSP-RS, 23 PSP-SL, 12 PSP-P, 8 PSP-CBS, 5 PSP-F and 4 PSP-PGF) underwent volumetric MRI, with 59 of these also undergoing flortaucipir PET. Voxel-level and region-level analyses were performed comparing PSP variants to 30 controls and to each other. Semi-quantitative tau burden measurements were also performed in 13 patients with autopsy-confirmed PSP.

Results: All variants showed evidence for atrophy or increased flortaucipir uptake in striatum, globus pallidus and thalamus (Figure). Lower superior cerebellar peduncle volume relative to controls was observed in PSP-RS, PSP-CBS and PSP-F. Lower volume in the frontal lobes was observed in PSP-SL, PSP-CBS and PSP-F, with these variants also showing highest cortical tau burden at autopsy. The PSP-P and PSP-PGF variants showed more restricted patterns of neurodegeneration predominantly involving striatum, globus pallidus, subthalamic nucleus and thalamus. The PSP-SL variant showed reduced volume and increased flortaucipir uptake in supplementary motor area and motor cortex compared to all other variants, but showed less involvement of subthalamic nucleus and midbrain. Compared to PSP-RS, PSP-P had larger midbrain volume and greater flortaucipir uptake in putamen.

Conclusion: The PSP variants have different patterns of involvement of subcortical circuitry, perhaps suggesting different patterns of disease spread through the brain. These findings will be important in the development of appropriate neuroimaging biomarkers for the different PSP variants.

Figure: Voxel-wise Flortaucipir findings in each PSP variant compared to controls. Top row illustrates the location of the subcortical nuclei from the atlases. DN = dentate nucleus of the cerebellum; Put = putamen; CN = caudate; RN = red nucleus; STN = subthalamic nucleus; SN = substantia nigra; Thal = thalamus; GP = globus pallidus; R = right



Keywords: flortaucipir, tau, PET, progressive supranuclear palsy

Comparison of autoradiographic binding profiles of Flortaucipir, MK-6240 and PI-2620 in human postmortem tissue samples across the spectrum of neurodegenerative diseases

Cinthya Aguero^{1,2}, Maeva Dhaynaut^{3,4}, Marta Marquie^{1,2}, Ana C Amaral^{1,2}, Ramesh Neelamegam^{3,4}, Sung-Hyun Moon^{3,4}, Patrick M. Dooley^{1,2,5}, Dominique Denbow^{1,2}, Georges El Fakhri^{3,4}, Matthew P Frosch⁵, Marc Normandin^{3,4}, Teresa Gómez-Isla^{1,2}

¹*Department of Neurology, Massachusetts General Hospital, Boston, MA, US*

²*MassGeneral Institute for Neurodegenerative Disease, Charlestown, MA, US*

³*Department of Radiology, Massachusetts General Hospital, Boston, MA, US*

⁴*Gordon Center for Medical Imaging, Division of Nuclear Medicine and Molecular Imaging, Massachusetts General Hospital, Boston, MA, US*

⁵*C.S. Kubik Laboratory for Neuropathology, Massachusetts General Hospital, Boston, MA, US*

Background: We and others have shown that [¹⁸F]-flortaucipir, the most validated tau PET tracer thus far, binds with strong affinity to tau aggregates in Alzheimer's (AD) but has relatively low affinity for tau aggregates in non-AD tauopathies, and exhibits off-target binding to neuromelanin- and melanin-containing cells, and to hemorrhages. Several second-generation tau tracers have recently been reported. [¹⁸F]-MK-6240 and [¹⁸F]-PI-2620 are the two that have garnered most attention. Our recent data indicate that the binding pattern of [¹⁸F]-MK-6240 closely parallels that exhibited by [¹⁸F]-flortaucipir. Comprehensive postmortem validations of [¹⁸F]-MK6240 and [¹⁸F]-PI-2620 are critical for determining their potential utility in diagnostic assessment and measurement of progression of AD and other tauopathies.

Goal: To directly compare autoradiographic binding properties and off-target profile of [¹⁸F]-flortaucipir, [¹⁸F]-MK-6240 and [¹⁸F]-PI-2620 in the same postmortem tissue specimens.

Methods: Phosphor screen and high resolution autoradiographic patterns of [¹⁸F]-flortaucipir, [¹⁸F]-MK-6240 and [¹⁸F]-PI-2620 were studied in the same tissue material from AD and non-AD tauopathies (Pick's disease, progressive supranuclear palsy, corticobasal degeneration, chronic traumatic encephalopathy and tau mutation carriers), cerebral amyloid angiopathy, synucleinopathies, transactive response DNA-binding protein-43-frontotemporal lobe degeneration (FTLD-TDP-43) and controls.

Results: [¹⁸F]-MK-6240 and [¹⁸F]-PI-2620 strongly bind to tangles in AD but do not seem to bind to a significant extent to tau aggregates in most non-AD tauopathies. [¹⁸F]-MK-6240 and [¹⁸F]-PI-2620 do not bind to lesions containing Beta-amyloid, Alpha-synuclein or TDP-43. [¹⁸F]-MK-6240 and [¹⁸F]-PI-2620, just like [¹⁸F]-flortaucipir, also exhibit strong off-target binding to neuromelanin and melanin-containing cells, and to areas of brain hemorrhage. Results from cross-blocking studies suggest that the three tracers have a common binding substrate.

Conclusion: The autoradiographic specificity and off-target binding patterns of [¹⁸F]-MK-6240 and [¹⁸F]-PI-2620 tracers closely parallel those exhibited by [¹⁸F]-flortaucipir. The correct identification of biological targets of tau imaging agents is an essential requirement for considering them as disease-specific and progression-specific biomarkers.

Keywords: [18F]-flortaucipir, [18F]-MK-6240, [18F]-AV-1451, [18F]-PI-2620, Autoradiography, PET.

Biochemical correlates of tau and amyloid PET imaging in four autopsy brains

Milos Ikonomovic¹, Eric Abrahamson¹, Julia Kofler¹, William Paljug¹, Carl Becker¹, Chester Mathis¹, Oscar Lopez¹, William Klunk¹

¹*University of Pittsburgh, Pittsburgh, PA, US*

Objectives: Correlation analyses of tau-PET and amyloid- β (A β)-PET with postmortem region-matched quantification of insoluble tau and A β concentrations.

Methods: [F-18]AV-1451 and [C-11]PiB PET scans were obtained from three subjects with probable Alzheimer's disease (AD; Cases #1,3,4; white males, 94, 91, and 62 y.o., respectively) and a cognitively normal 91 y.o. white female (Case#2). Imaging-to autopsy time intervals were on average 23.5 and 34.5 months (AV-1451 and PiB, respectively). Atrophy-corrected SUVR values were correlated with ELISA concentrations of guanidine-HCl extracted total tau and tau phosphorylated at Ser396, Ser199, and Thr231 or formic acid extracted A β 1-42 and A β 1-40 in 17 frozen gray matter samples from temporal, frontal, precuneus, and occipital cortex.

Results: AD neuropathology was intermediate in Case#1 and Case#2 (ABC scores A2,B3,C2 and A3,B2,C2, respectively), and high in Case#3 and Case#4 (both A3,B3,C3). Coexisting pathology included hippocampal sclerosis, TDP-43, ARTAG, remote infarcts, and CAA. All cases were Braak stage 5 except Case#2 (Braak stage 4). [C-11]PiB PET and A β 1-42 concentration correlated strongly in Case#1 and Case#2, weakly in Case#3, with a trend in Case#4. [C-11]PiB PET and A β 1-40 correlated only in Case#1. [F-18]AV-1451 PET correlated with pSer396/total tau ratio in Case#1 and Case#4, while a trend for correlation was observed in Case#3. [F-18]AV-1451 PET correlated with pSer199/total tau ratio in Case#4 and trends for correlations were observed in Case#1 and Case#3. [F-18]AV-1451 PET and pThr231/total tau ratio correlated in Case#4.

Conclusions: Data confirm insoluble A β 1-42 as the primary substrate for [C-11]PiB PET retention and support the use of [F-18]AV-1451 for detection of neocortical tau pathology in AD. Imaging-to-autopsy analyses of AV-1451 in additional cases with shorter imaging-to autopsy intervals are needed to better understand the relationship between the tracer's PET retention levels and tau pathology burden.

Acknowledgment: We thank Avid Radiopharmaceuticals for providing [F-18]AV-1451 precursor.

Keywords: tau, amyloid, PET, Alzheimer's, neuropathology

KEYNOTE LECTURE 2

Amyloid and tau: one of multiple pathways to tissue injury, degeneration, and Alzheimer's dementia

Julie Schneider

Rush University, Chicago, IL, US

Extracellular amyloid beta and intraneuronal phosphorylated tau are the central pathologies that define the diagnosis of Alzheimer's disease (AD). PET imaging has transformed research by allowing visualization of these proteins in the brain during life. Yet, amyloid and tau PET provide an incomplete picture of the brain in most persons living with Alzheimer's dementia, a heterogeneous clinical syndrome that is highlighted by prominent episodic memory loss. Other degenerative proteins including Lewy body and TDP-43 pathology are common in persons harboring AD pathology and with Alzheimer's dementia. Also extraordinarily common is brain vascular disease including small and large vessel diseases and macro and microinfarcts. The vast majority of older persons with Alzheimer's dementia have one or more of these other pathologies and each of these independently contributes to cognitive impairment and lower the threshold to dementia. Indeed, in some studies and cohorts, vascular pathologies alone contributes to about 1/3 of dementia and in other studies LATE (TDP/HS) is the primary driver of cognitive decline in AD. In addition to their additive effects, these pathologies may interact with amyloid and/or tau to accelerate tissue injury which may be difficult if not impossible to reverse. Preventing and treating cognitive impairment will requires an integrated understanding of amyloid, tangles, and these other pathologic processes that lead to tissue injury, neurodegeneration, and ultimately cognitive decline.

P2A: POSTER SESSION 2A

Board #	Poster Title	Authors	Presenter	Page
100	Entorhinal tau pathology is associated with medial temporal lobe hyperactivity in aging	Adams Maass Berron Harrison Baker Thomas Stanfill Jagust	Adams, Jenna	288
80	Sex differences in the rates of cognitive decline associated with temporal lobe FTP-PET signal: findings from the Harvard Aging Brain Study	Buckley Properzi Schultz Jacobs Kim Rentz Hanseeuw Johnson Sperling	Buckley, Rachel	246
73	Imaging synaptic and mitochondrial function in frontotemporal dementia using [11C]UCB-J, [18F]BCPP-EF and [11C]SA4503 PET	Clarke Mansur Passchier Lewis Evans Chen Schwarz Takano Gunn Cash Rabiner Rohrer	Clarke, Mica	236
105	Longitudinal associations between lifestyle risk, β -amyloid, and cognition in late-midlife	Cody Koscik Birdsill Berman Erickson Chin Clark Christian Betthausen Johnson	Cody, Karly	302
62	Correlation of QSM signal with Alzheimer's Disease biomarkers	Cogswell Wiste Senjem Therneau Lowe Knopman Botha Graff-Radford Jones Kantarci Vemuri Ferman Boeve Mielke Schwarz Gunter Petersen Jack	Cogswell, Petrice	214
71	Quantitative regional amyloid burden and white matter changes in preclinical AD	Collij Top Stickney Ingala Tomassen Lopes Alves Yaqub Wink Van 't Ent Scheltens Van Berckel Visser Barkhof Den Braber AMYPAD consortium	Collij, Lyduine	233
70	Individual variability in the cortical distribution of elevated 18F-AV1451 and 11C-PIB in a heterogeneous sample of AD patients	Collins Eckbo McGinnis Dickerson	Collins, Jessica	232
92	Amyloid deposition disrupts functional connectivity and graph properties within the default mode network	Ingala Wink Prent van 't Ent Tomassen ten Kate Konijnenberg Collij Yaqub Scheltens de Goes Teunissen Barkhof van Berckel Visser den Braber	den Braber, Anouk	273
93	Neuroinflammation in AD patients and correlates with amyloid and tau deposition	Edison Leng Dani Brooks	Edison, Paul	276
85	Sex differences in regional tau deposition in cognitively impaired patients with Alzheimer's disease	Edwards La Joie Iaccarino Kim Baker Casaletto Miller Jagust Rabinovici	Edwards, Lauren	260
69	Higher microglia biomarker levels are associated with slower rates of amyloid-beta accumulation in humans and in a transgenic mouse model of amyloid-beta	Ewers Brendel Suarez-Calvet Biechele Sacher Blume Haass Franzmeier	Ewers, Michael	229
99	Early declines in learning and executive function associated with accumulating A β not tau in low PIB adults	Farrell Papp Buckley Jacobs Schultz Properzi Hanseeuw Rentz Johnson Sperling	Farrell, Michelle	285
68	Association of tau tangle burden with depressive symptoms in community dwelling older adults: a longitudinal study	Gatchel Marshall Yang Donovan Buckley Properzi Quiroz Rabin Vannini Amariglio Chhatwal Rentz Blacker Sperling Johnson Hanseeuw	Gatchel, Jennifer	226
78	Amyloid deposition affects the topography of cortical thinning in Lewy Body Disease	Ye Touroutoglou Brickhouse Katz Growdon Johnson Dickerson Gomperts	Gomperts, Stephen	244
107	Data-driven approach to characterization of tau accumulation in Braak staging groups	Groh Svaldi Stage Sanjay Risacher Saykin Apostolova	Groh, Jenna	308
77	A sensitive composite model to determine subtle cognitive differences in preclinical Alzheimer's disease	Hahn Kim Kim Jang Kim Na Chin Seo	Hahn, Alice	243
61	Defining a Centiloid scale threshold predicting long-term progression to dementia in patients attending the Memory Clinic: an F18-Flutemetamol amyloid-PET study	Hanseeuw Malotau Dricot Quenon Cerman Buckley Farrar Ivanoiu Lhommel	Hanseeuw, Bernard	211
91	Prevalence of amyloid PET positivity in cognitively normal the East Asian populations	Kim Jung Na Kim Won Seo	Kim, Jaeho	270
74	First-in-human evaluations of [11C]PS13 for imaging COX-1 and [11C]MC1 for imaging COX-2	Kim Juarez Anaya Lee Hong Miller Telu Morse Singh Cortes-Salva Henry Ruiz-	Kim, Min-Jeong	238

Board #	Poster Title	Authors	Presenter	Page
		Perdomo Montero Santamaria Liow Zoghbi Fujita Katz Pike Innis		
64	Evaluating the relationships among odor identification, tau pathology and neuroinflammation in Alzheimer's disease	Klein Yan Johnson Tomljanovic Zou Polly Honig Brickman Stern Lee Kreisl	Klein, Julia	219
67	Distinct effects of APOE ε2 on Aβ in Alzheimer- and vascular-type cognitive impairment	Lee Lee Park Choe Park Cheon Hahn Ossenkoppele Kim Kim Yoo Jang Cho Kim Kim Jung Park DeCarli Weiner Yun Na Seo	Lee, Jin San	225
79	Longitudinal change in amyloid load over a 5-year period in cognitively healthy APOE4 carriers versus non-carriers: Effect of reference region	Luckett Adamczuk Schaevebeke Gabel Van Laere Dupont Vandenberghe	Luckett, Emma	245
113	Mild behavioral impairment is associated with tau pathology in cognitively impaired elderly individuals	Lussier Pascoal Therriault Tissot Savard Benedet Mathotaarachchi Stevenson Ismail Rosa-Neto Gauthier	Lussier, Firoza	317
114	Modeling the trajectory of tau deposition in autosomal-dominant AD using the high-affinity tau tracer [18F]MK6240	Lussier Therriault Pascoal Savard Mathotaarachchi Robb Stevenson Gauthier Rosa-Neto	Lussier, Firoza	319
101	Clinicopathological confirmation of 123I-FP-CIT SPECT (ioflupane) quantification methods in a spectrum of neurodegenerative syndromes and associated pathologies	Maltais Jordan Miyagawa Lesnick Przybelski Min Dickson Murray Kantarci Boeve Lowe	Maltais, Daniela	292
106	Exploring relationships between tau burden and naming in the aphasic variant of AD	Martersteck Sridhar Coventry Eldes Wood Kim Mesulam Rogalski	Martersteck, Adam	306
65	Elevated soluble phosphorylated tau is a marker of early amyloid PiB PET abnormalities and accumulation	McDade Li Joseph-Mathurin Benzinger Fagan Xiong Barthélemy Bateman	McDade, Eric	220
112	A clinically-relevant scheme for qualitatively rating tau PET, amyloid PET, and MRI in neurodegenerative cognitive presentations	McGinnis Collins Eckbo Brickhouse Dickerson	McGinnis, Scott	316
66	Cerebrospinal fluid and PET measures of tau pathology may indicate different stages of AD pathological progression	Meyer Pichet Binette Gonneau Breitner Villeneuve	Meyer, Pierre-Francois	222
96	Use of the plasma amyloid-beta 42/40 ratio for predicting amyloid PET in a community-based population	Mielke Algeciras-Schimmich Campbell Syrjanen Knopman Jack Jr. Peterson	Mielke, Michelle	280
111	Cerebrospinal fluid matrix metalloproteinases are associated with compromised white matter microstructure among older adults: the Vanderbilt memory & aging project	Moore Pechman Acosta Bell Anderson Landman Blennow Zetterberg Gifford Hohman Jefferson	Moore, Elizabeth	315
94	Development of new alpha7 nicotinic receptor ASEM analogs for PET imaging	Nordberg Lemoine Mohan Kuang Nag Jia Miranda Azpiazu Datta Arakawa Varnäs Ågren Långström Halldin	Nordberg, Agneta	277
108	Associations between AD biomarkers and cognition among cognitively normal older adults	Oh Correia Salloway	Oh, Hwamee	311
75	[11C]MK-6884 PET tracer for M4 muscarinic cholinergic receptors in AD: Comparison with [18F]FDG PET	Pascual Zanotti-Fregonara Yu Funk Arbones Wang Li Cheng Anderson Hostetler Basile Masdeu	Pascual, Belen	239
81	Amyloid and tau PET burden are associated with white matter bundle abnormalities in asymptomatic individuals at risk of AD	Pichet Binette Theaud Gonneau Poirier Descoteaux Villeneuve	Pichet Binette, Alexa	248
104	Increased risk of AD in alcohol use disorder is not mediated by amyloid-beta in a middle-aged cross-sectional cohort	Royse Himes Minhas Lopresti Flanigan Narendran	Royse, Sarah	300
86	Cross-sectional and longitudinal non-dichotomized CSF/PET Aβ data support existence of "CSF+ first" vs. "PET+ first" pathways of Aβ biomarkers changes	Sala Nordberg Rodriguez-Vieitez	Sala, Arianna	262
82	NeuroToolkit CSF biomarkers track the progression of AD at very early stages and show that inflammatory markers modulate cerebral amyloid accumulation	Salvadó Molinuevo Milà-Alomà Blennow Zetterberg Operto Falcón Batrla Battle Buckley Farrar Minguillon Fauria Sánchez-	Salvadó, Gemma	251

Board #	Poster Title	Authors	Presenter	Page
		Benavides Suárez-Calvet Gispert the ALFA study		
83	T1rho MRI measurement of amyloid plaque burden in cognitively unimpaired individuals: preliminary results in the ALFA+ cohort	Falcón Montesinos Grau-Rivera Suárez-Calvet Puig-Pijoan Cascales Navalpotro-Gomez Fernández-Lebrero Sánchez-Valle Gelpi Sanfeliu Rojas Perissinotti Niñerola-Baizán Salvadó Minguillon Fauria Molinuevo Sánchez-González Gispert the ALFA study	Salvadó, Gemma	254
84	Preliminary quantitative results of the AMYPAD prognostic and natural history study	Gispert Lopes-Alves Gray Buckley Collij Heeman Salvadó Scheltens Frisoni Ritchie Vellas Stephens Ford Molinuevo Farrar Barkhof the AMYPAD Consortium	Salvadó, Gemma	257
72	Effect of genetic risk, brain amyloid and hippocampal volume on normal variation in episodic memory performance in middle-aged and older adults	Schaefferbeke Gabel Adamczuk Van Laere Dupont Vandenberghe	Schaefferbeke, Jolien	235
103	White matter disruption is an early and progressive feature of pre-symptomatic Dutch-type hereditary cerebral amyloid angiopathy	Scott Schultz Sohrabi Gardener Taddei Bateman Benzinger Johnson Sperling Martins Greenberg Chhatwal Investigators	Scott, Matthew	296
88	Head-to-head comparison of F-Florbetaben and F-Flutemetamol uptakes in the cortex, striatum and white matter	Seo Cho Moon Choe Na	Seo, Sang Won	264
90	PI-2620 Tau PET is associated with amyloid-beta levels in scans from subjects of the elenbecestat MissionAD program	Stephens Bullich Mueller Berndt De Santi Scott Adamczuk Suh Kaplow Giroux Krause Chang Albala	Stephens, Andrew	268
110	Using famous faces to investigate the neural systems involved in name retrieval	Tennant Jagust La Joie Adams Winer	Tennant, Victoria	313
109	In vivo association of mitochondrial dysfunction with tau pathology in early AD	Terada Therriault Min Su Savard Ouchi Rosa-Neto	Terada, Tatsuhiro	312
102	Preliminary results: PiB and MK6240 regional PET measures associated with digitized clock drawing performance	Mayblyum Thibault Moody Farrell Jiang Jacobs Rubinstein Sanchez Katz Sperling Papp Rentz Johnson	Thibault, Emma	293
97	Associations between longitudinal cognitive measures and cross-sectional tau in adults with Down syndrome	Tudorascu Comer Zammit Laymon Minhas Ellison Zaman Ances Johnson Mathis Klunk Christian Handen Hartley Cohen	Tudorascu, Dana	281
60	Longitudinal flortaucipir ([18F]AV-1451) PET uptake in Semantic Dementia	Utianski Whitwell Martin Botha Schwarz Duffy Clark Spychalla Senjem Petersen Knopman Jack, Jr. Lowe Josephs	Utianski, Rene	207
76	Assessing A β , tau, and reactive astrocytosis in aging and AD	Villemagne Harada Doré Furumoto Mulligan Kudo Krishnadas Huang Yanai Rowe Okamura	Villemagne, Victor	240
63	Developing a novel alpha-synuclein (a-syn) positron emission tomography (PET) tracer for the diagnosis of Parkinson's disease (PD) and other a-synucleinopathies	Vokali Molette Tsika Ravache Rodriguez Jürgens Melo dos Santos Sandiego Russell Gunn Darmency Piorkowska Poli Kroth Capotosti Hliva Sol Marek Stöhr Lowe Pfeifer Kosco-Vilbois	Vokali, Efthymia	218
95	Biological underpinnings of typical and atypical Alzheimer's dementia phenotypes	Whitwell Tosakulwong Graff-Radford Weigand Schwarz Senjem Ertekin-Taner Jones Boeve Knopman Jack Petersen Lowe Josephs	Whitwell, Jennifer	278
89	Sleep impairment predicts longitudinal accumulation of β -amyloid	Winer Mander Jagust Walker	Winer, Joseph	265
87	Personality and amyloid accumulation in cognitively normal aging	Yoon Baker Korman Tennant Harrison Jagust	Yoon, Bora	263
98	Associations of amyloid deposition and FDG uptake in aging and cognitively impaired elders with and without moderate to severe periventricular white matter hyperintensities	Zukotynski Gaudet Kuo Adamo Goubran Scott Bocti Borrie Chertkow Frayne Hsiung Laforce Noseworthy Prato Sahlas Smith Sossi Thiel Soucy Tardif Black	Zukotynski, Katherine	284

P60: Longitudinal flortaucipir ([18F]AV-1451) PET uptake in Semantic Dementia

Rene Utianski¹, Jennifer Whitwell¹, Peter Martin¹, Hugo Botha¹, Christopher Schwarz¹, Joseph Duffy¹, Heather Clark¹, Anthony Spychalla¹, Matthew Senjem¹, Ronald Petersen¹, David Knopman¹, Cliff Jack, Jr.¹, Val Lowe¹, Keith Josephs¹

¹*Mayo Clinic, Rochester, MN, US*

Objective: To assess longitudinal volume loss and flortaucipir (FTP) uptake in patients with semantic dementia (SD).

Methods: Eight patients (3 female) with SD underwent neurological, neuropsychological, speech, and language assessments, FTP positron emission tomography (PET), and brain magnetic resonance imaging (MRI) imaging at two visits, approximately one year apart. Voxel-level comparisons of MRI gray and white matter volume loss and FTP-PET uptake were performed using SPM12, comparing SD patients to age and sex-matched controls at both baseline and follow-up visits. Individual annualized change in cortical thickness and FTP uptake were also calculated. Wilcoxon signed-rank tests were used to assess the annualized change in clinical measures in the SD group.

Results: There was statistically significant worsening on tests of general cognition and lexical access between visits. At the voxel level, the SD patients showed bilateral, left greater than right, gray volume loss in the temporal lobes at first visit, which extended posteriorly and more prominently in the right hemisphere at follow-up. However, white matter loss was noted only in the left temporal lobe at first visit. This extended posteriorly at follow-up, at which time additional mild white matter loss was noted in the right hemisphere. Increased FTP uptake was noted in the SD patients in the anterior portion of the temporal lobe at first visit, which again extended posteriorly at follow-up, without any uptake in the right hemisphere at either visit.

Conclusions: The biological mechanisms of FTP signal in suspected underlying TDP-43 pathology are unknown. The findings suggest that while FTP uptake may track with disease progression, MRI more robustly reflects the neurodegeneration underlying the clinical presentation.

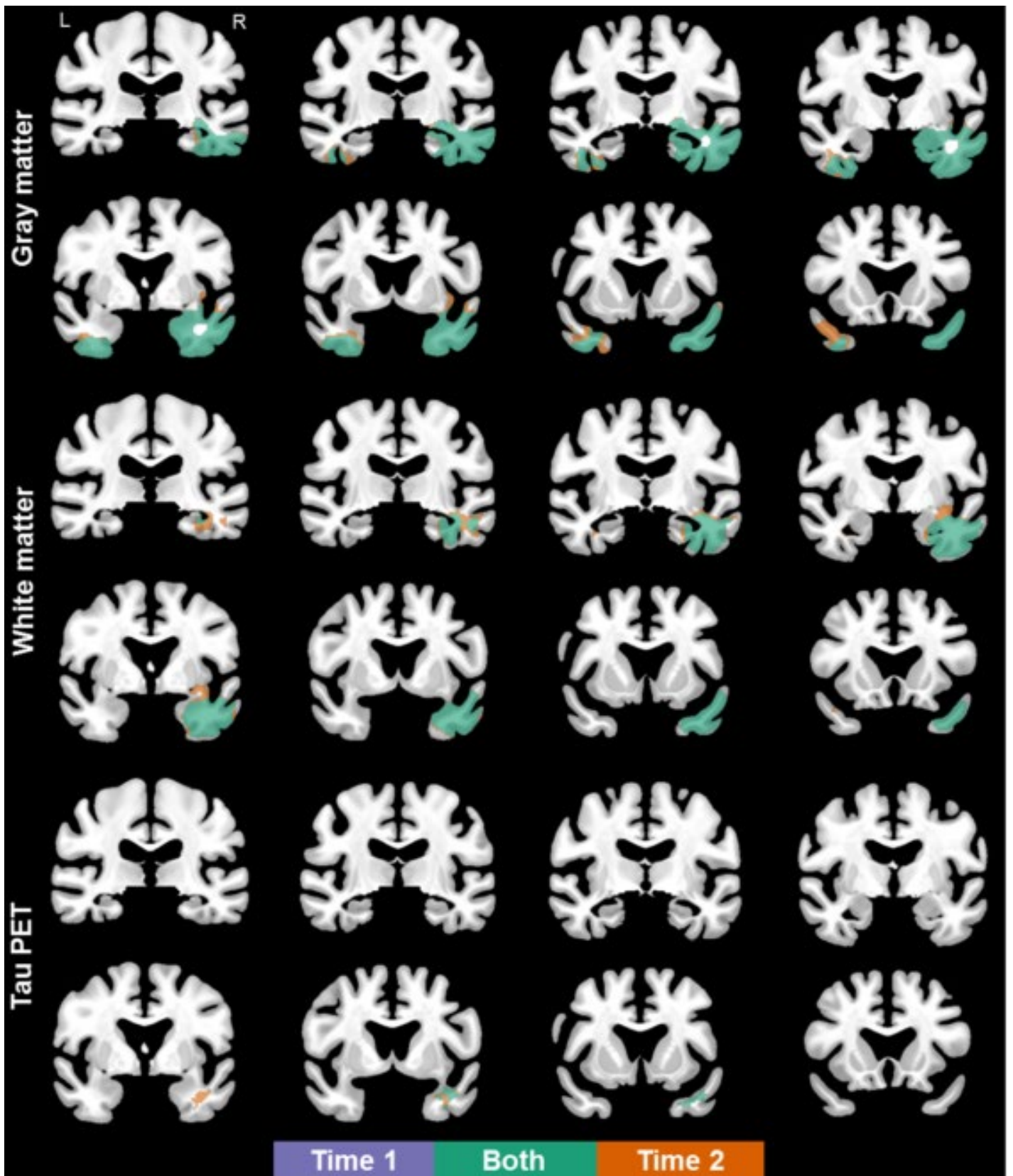


Figure 1. Coronal views of gray matter loss (top), white matter loss (middle), and FTP uptake (bottom) in semantic dementia patients, compared to age- and sex- matched controls (FDR, $p < .05$). Results shown in MCALT space.

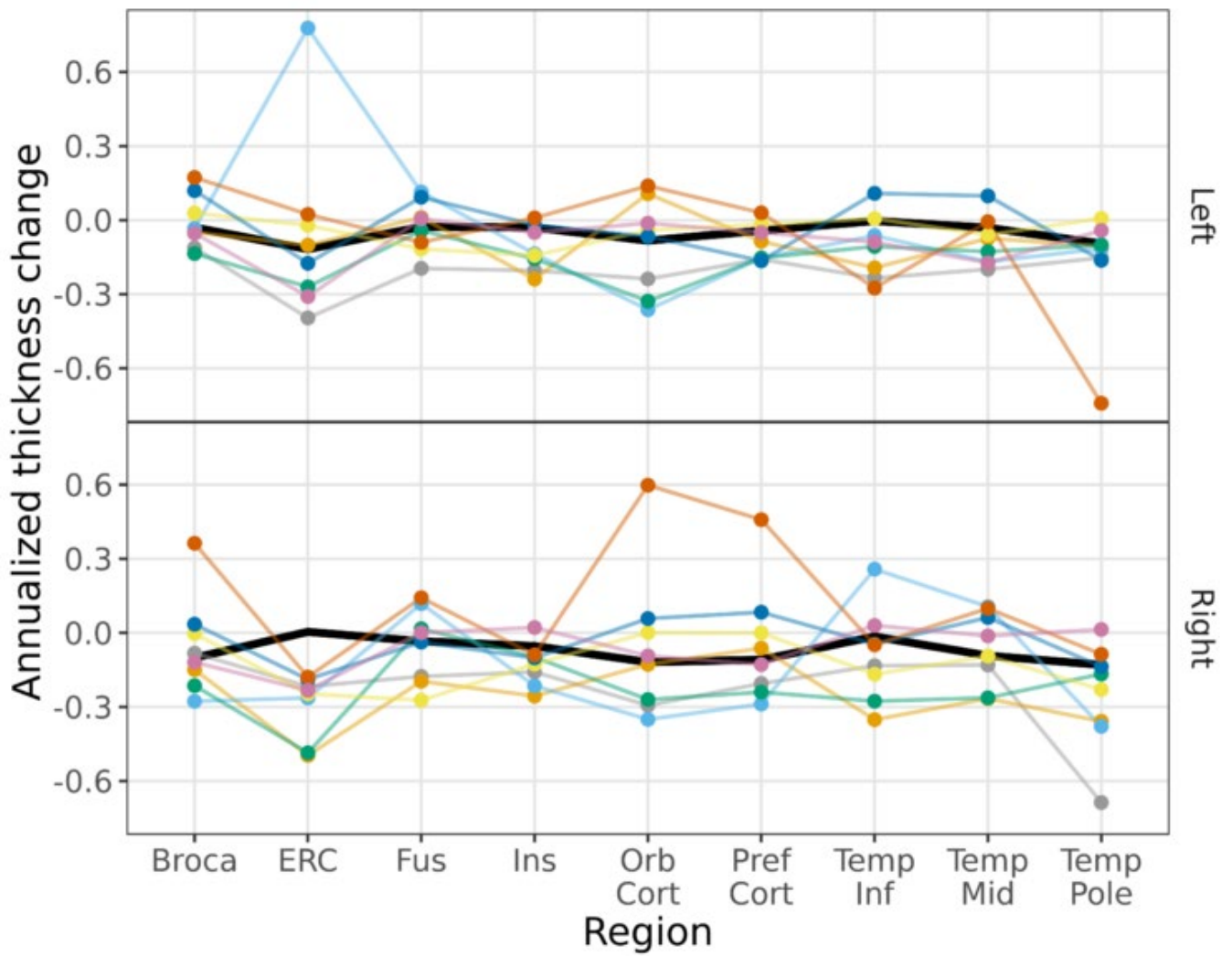


Figure 2. Plot of annualized change in cortical thicknesses by region and hemisphere. Dark underlaid black line represents the median change in the control cohort. Note: Broca's = Broca's area, ERC = entorhinal cortex, Fus = fusiform gyrus, Ins = insula, Orb Cort = orbitofrontal cortex, Pref Cort = prefrontal cortex, Temp Inf = inferior temporal gyrus, Temp Mid = middle temporal gyrus, and Temp Pole = temporal pole.

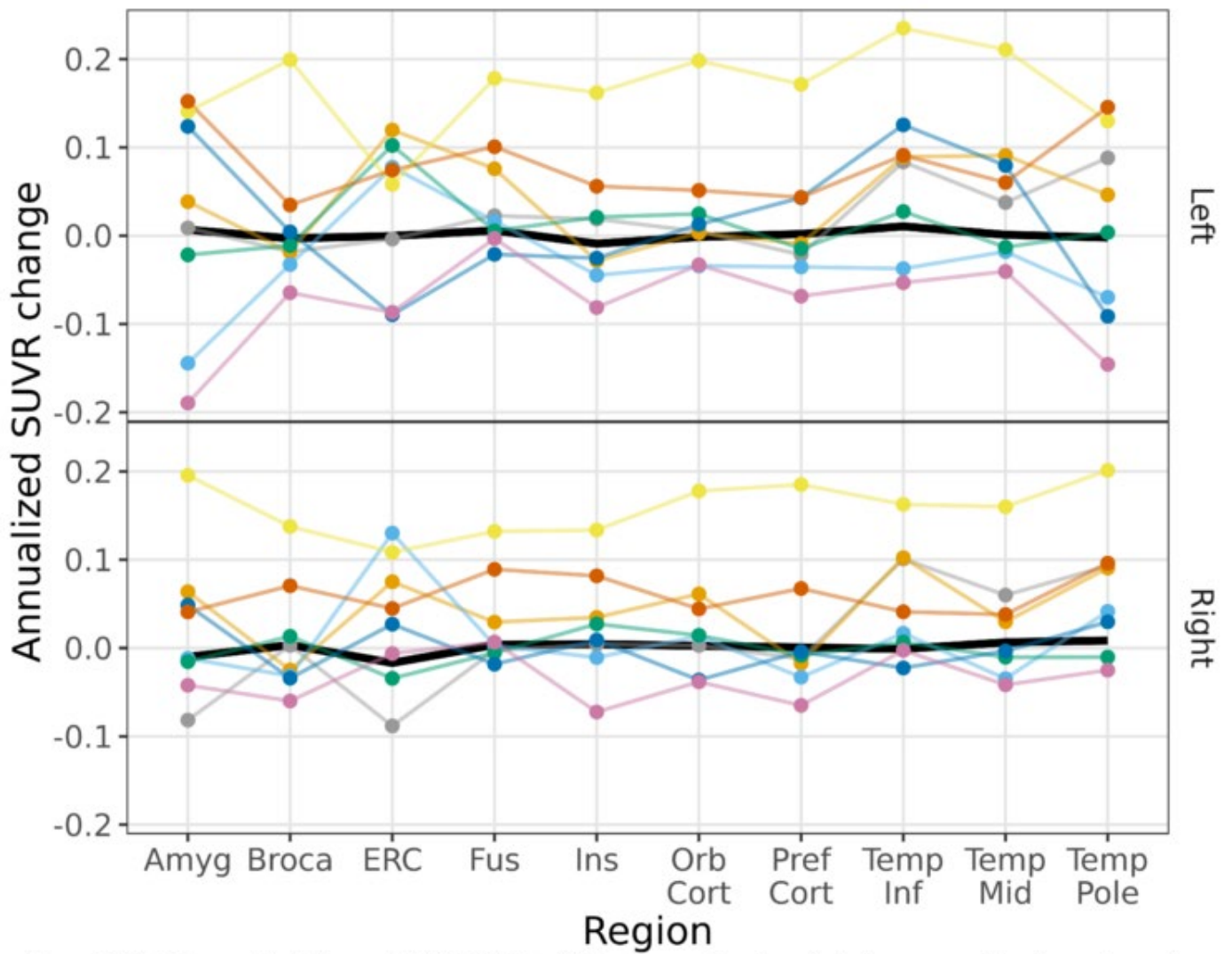


Figure 3. Plot of annualized change in FTP SUVR, with two-compartment partial volume correction, by region and hemisphere. Dark underlaid black line represents the median change in the control cohort. Note: Amyg = Amygdala, Broca's = Broca's area, ERC = entorhinal cortex, Fus = fusiform gyrus, Ins = insula, Orb Cort = orbitofrontal cortex, Pref Cort = prefrontal cortex, Temp Inf = inferior temporal gyrus, Temp Mid = middle temporal gyrus, and Temp Pole = temporal pole. Patients are represented as the same color as in Figure 2.

Keywords: semantic dementia; primary progressive aphasia; tau; PET; MRI

P61: Defining a Centiloid scale threshold predicting long-term progression to dementia in patients attending the memory clinic: An F18-Flutemetamol amyloid-PET study

Bernard Hanseeuw^{1,2}, Vincent Malotaux¹, Laurence Dricot¹, Lisa Quenon¹, Jiri Cerman³, Christopher Buckley⁴, Gill Farrar⁴, Adrian Ivanoiu¹, Renaud Lhommel¹

¹*Clinique Universitaires Saint-Luc, Brussels, Belgium*

²*Massachusetts General Hospital, Boston, MA, US*

³*Charles University, Second Faculty of Medicine, Prague, Czech Republic*

⁴*General Electrics Healthcare, Amersham, UK*

Background: Regulatory authorities have approved visual assessment of amyloid-PET images in older adults with cognitive complaints to assess the presence of amyloid- β (A β) pathology. In research studies, A β -PET quantitative measures are associated with greater risk of progression to dementia; but until recently, they lacked standardization. Therefore, the Centiloid scale, providing standardized A β -PET quantitation, was recently validated against autopsy data. We aimed to compare the predictive values of visual and quantitative assessment in a clinical cohort of non-demented patients, using progression to dementia after long follow-up as our standard of truth.

Methods: Ninety-eight non-demented patients, aged 54-86, were recruited at the Memory Clinic of Saint-Luc University Hospital (Belgium) to participate in an [¹⁸F]-Flutemetamol A β -PET study. Patients were followed until dementia diagnosis or were clinically stable for a median six years [4.0-7.9]. [¹⁸F]-Flutemetamol images were visually assessed following the manufacturer recommendations and classified as negative/positive by two independent experts. [¹⁸F]-Flutemetamol SUV_r values were converted on the Centiloid scale using GAAIN guidelines. We computed ROC curves predicting subsequent dementia with baseline PET data and calculated negative (NPV) and positive (PPV) predictive values at various thresholds.

Results: Centiloid=26 provided the highest overall predictive value=87% (NPV=85%, PPV=88%, Fig.1). Visual assessment as positive corresponded to Centiloid=42, excluding four cases (Centiloid=29-50) with conflicting visual assessments (Fig.2). Centiloid=42 predicted subsequent dementia with an overall predictive value=86% (NPV=81%, PPV=91%). Centiloid=12, suggested to detect incipient A β pathology in PET-autopsy studies, provided lower PPV=74% (NPV=85%). Including twenty-five additional patients who were only followed for a median two years [0.8-3.9] did not modify the best threshold (Centiloid=26), but also decreased the PPV=67% (NPV=88%), reflecting the many positive cases that did not progress to dementia after short follow-ups (Fig.3).

Conclusions: Centiloid-threshold=26 best predicts progression to dementia six years after PET. Visual assessment provides similar predictive value (86%), with higher specificity and lower sensitivity.

Fig.1 **Predicting dementia 6 years after Flutemetamol**

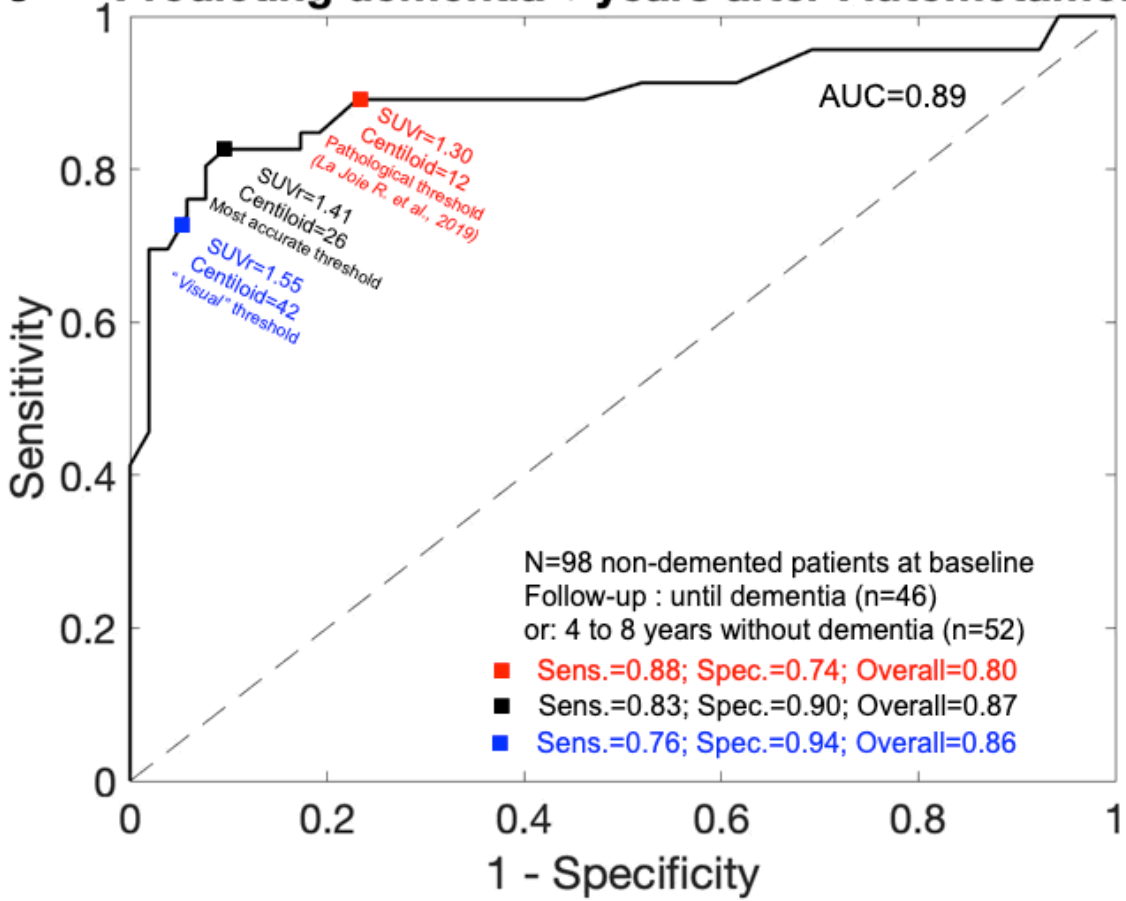


Fig.2

Centiloids = 120 * SUVr - 144

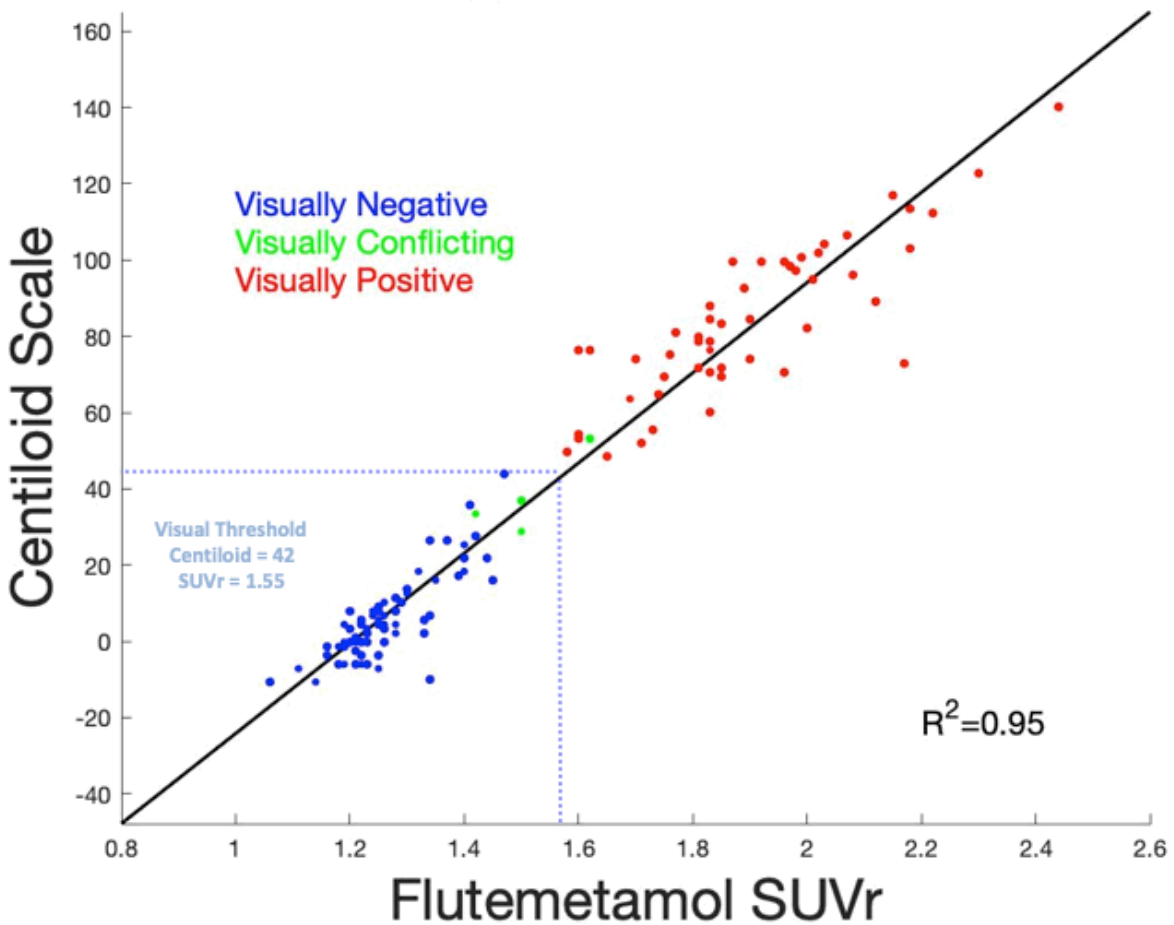
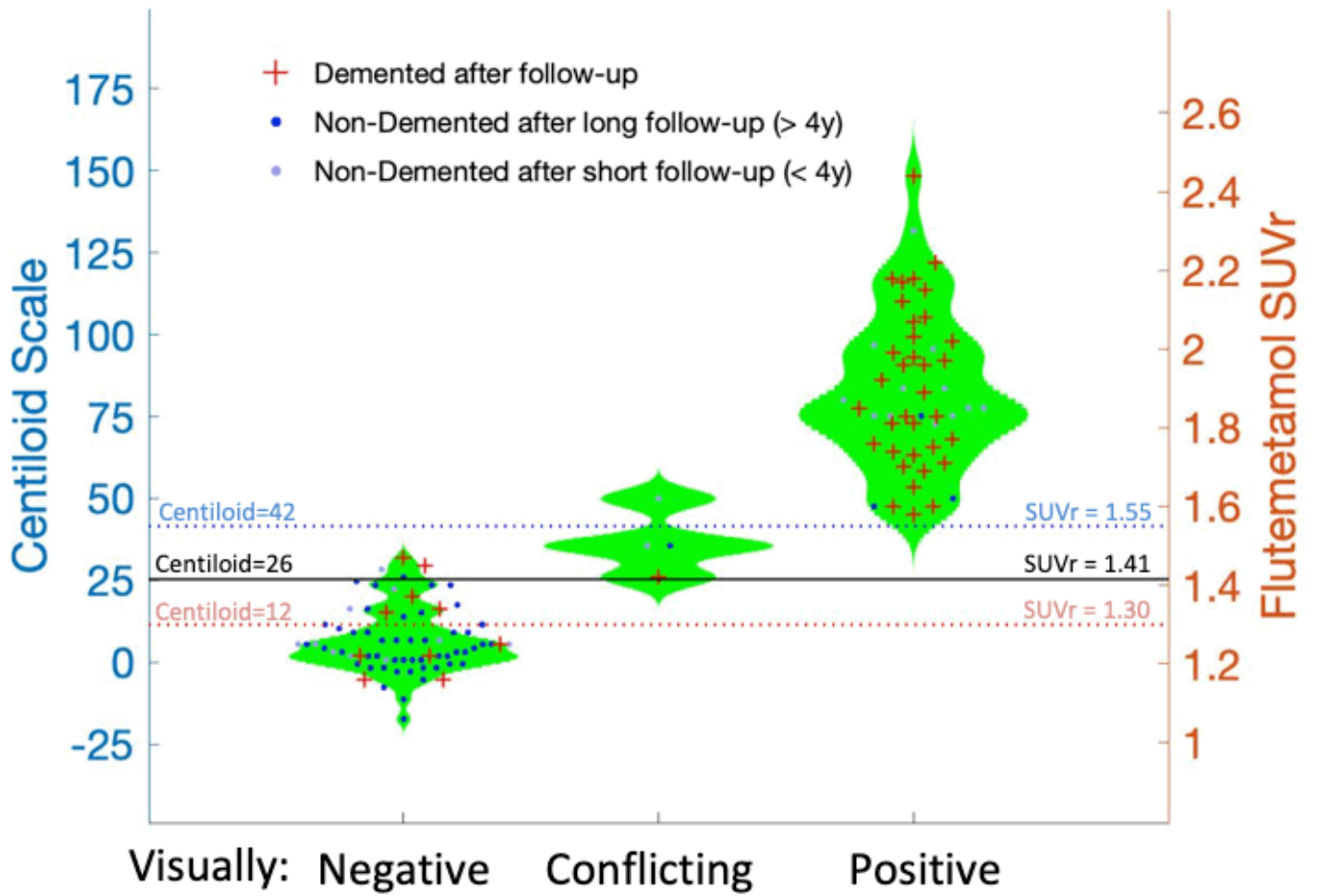


Fig.3



Keywords: Memory Clinic, Dementia prediction, Centiloid scale, visual assessment, Flutemetamol

P62: Correlation of QSM signal with Alzheimer's Disease biomarkers

Petrice Cogswell¹, Heather Wiste¹, Matthew Senjem¹, Terry Therneau¹, Val Lowe¹, David Knopman¹, Hugo Botha¹, Jonathan Graff-Radford¹, David Jones¹, Kejal Kantarci¹, Prashanthi Vemuri¹, Tanis Ferman¹, Bradley Boeve¹, Michelle Mielke¹, Christopher Schwarz¹, Jeffrey Gunter¹, Ronald Petersen¹, Clifford Jack¹

¹Mayo Clinic, Rochester, MN, MN, US

Objective: Altered iron metabolism has been hypothesized to be associated with Alzheimer's disease, supported by work showing the presence of iron in beta amyloid plaque. However, relationships between cerebral iron load and established Alzheimer's disease biomarkers remain unclear. Quantitative susceptibility mapping (QSM) is a recently popularized technique used to infer tissue iron concentration. Our objective was to assess the relationship of cerebral iron deposition based on QSM signal with age, amyloid PET, tau PET, and neurodegeneration.

Methods: Individuals from the Mayo Clinic Study of Aging (MCSA) and Alzheimer's Disease Research Center (ADRC) with multi-echo GRE imaging, amyloid PET (PiB), and tau PET (flortaucipir) were included. Spearman correlations were performed between regional QSM signal and age, amyloid PET standardized uptake value (SUVR), tau PET SUVR, and gray matter volumes (marker of neurodegeneration).

Results: The study included 488 participants (280 male, median age 70 years, range 34-97 years) with diagnoses of cognitively unimpaired 304(62%), mild cognitive impairment 81(17%), Alzheimer's clinical syndrome 51(10%), Lewy body dementia 25(5%), frontotemporal dementia 11(2), and other 16(3%). Spearman correlations (Figures 1, 2) were generally low to moderate and demonstrated no clinically meaningful pattern of correlation between QSM signal and amyloid PET or regional gray matter volume. Correlation between QSM signal and tau PET was greatest in the striatum (Figure 3) without meaningful correlations elsewhere. The striatum also showed a positive correlation between QSM signal and age.

Conclusions: Although iron has been found to be present in beta amyloid plaques, it does not appear to be of sufficient quantity for detection on QSM. Correlation of QSM signal with tau PET SUVR and age in the striatum is most likely due to the increase with age in both off-target binding of the tau ligand and physiologic iron deposition in the basal ganglia, although other explanations are possible.

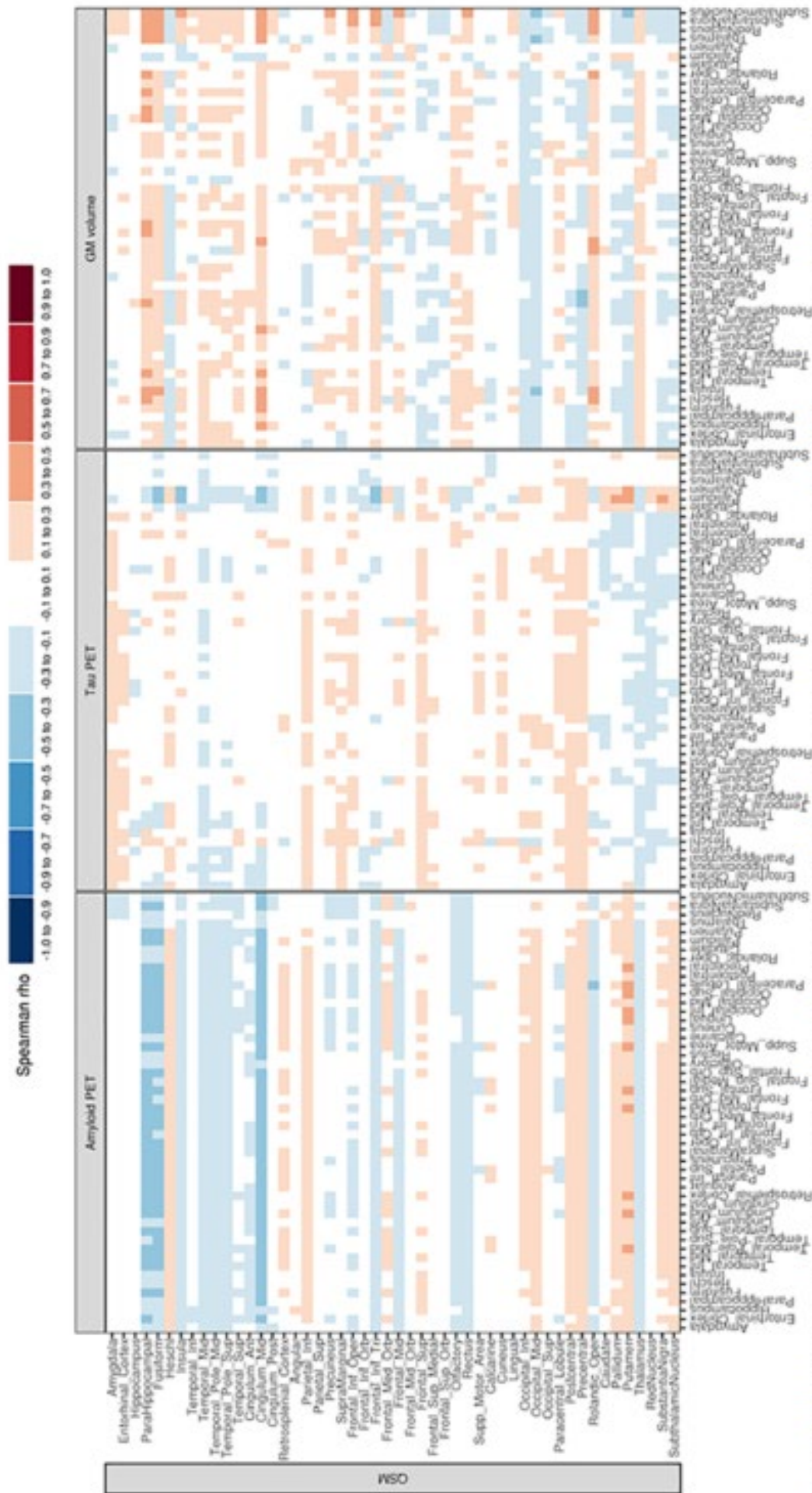


Figure 1: Heat maps of Spearman correlations between regional QSM signal and regional amyloid PET SUVR, regional tau PET SUVR, and regional gray-matter (GM) volume. The QSM signal was gray and white matter-sharpened and the mean QSM signal among voxels within regions was used for the QSM measure. Gray-matter volume was adjusted for the total intracranial volume. Tissue volume (gray matter and white matter) was used in the deep gray nuclei. Overall, regional correlations of QSM signal with amyloid PET, tau PET, and GM volume are low to moderate. The horizontal bands of signal indicate that QSM signal in a given region (e.g. putamen) has a similar correlation with amyloid PET SUVR across all regions.

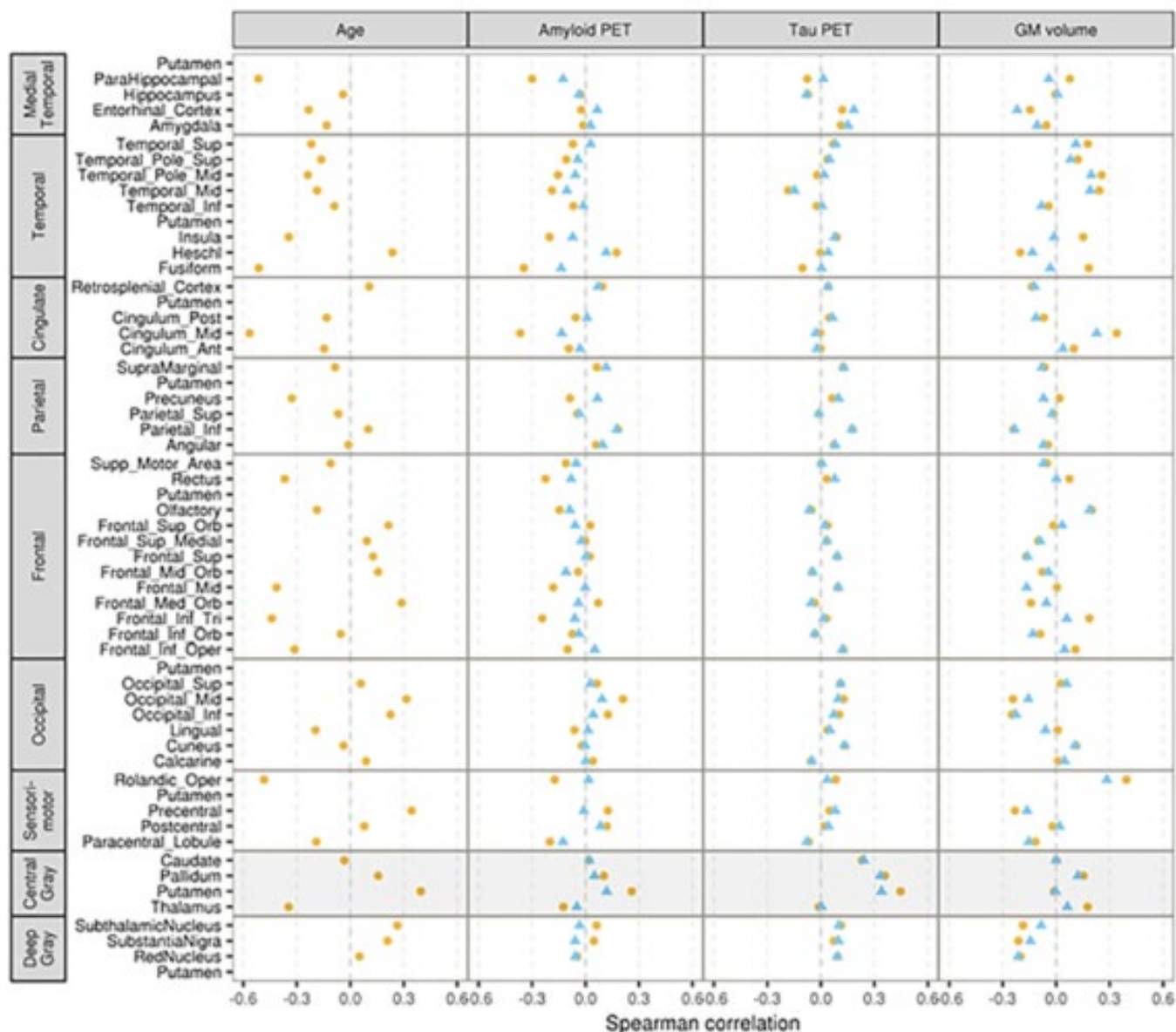


Figure 2: Spearman correlations between regional QSM and age and between QSM and amyloid PET SUVR, tau PET SUVR, and gray-matter volume within a given region, corresponding to the diagonal of the heat maps in Figure 1. Spearman correlations represented by gold points are not adjusted for age; correlations represented by blue triangles are adjusted for age. Correlations with age were performed only within the subset of MCSA participants due to differences in study populations. As highlighted in the grey shaded boxes, a positive correlation was seen between regional QSM signal and tau PET SUVR in the striatum ($\rho=0.36$ for pallidum and 0.45 for putamen; 0.33 and 0.34 respectively after correction for age) as well as between QSM signal and age in the striatum ($\rho=0.40$ for putamen). The putamen also showed a positive correlation between QSM signal and amyloid PET ($\rho=0.26$), which was attenuated by correction for age ($\rho=0.12$). Elsewhere correlations were variable among regions, with positive and negative correlations in adjacent ROIs that are likely not of clinical significance.

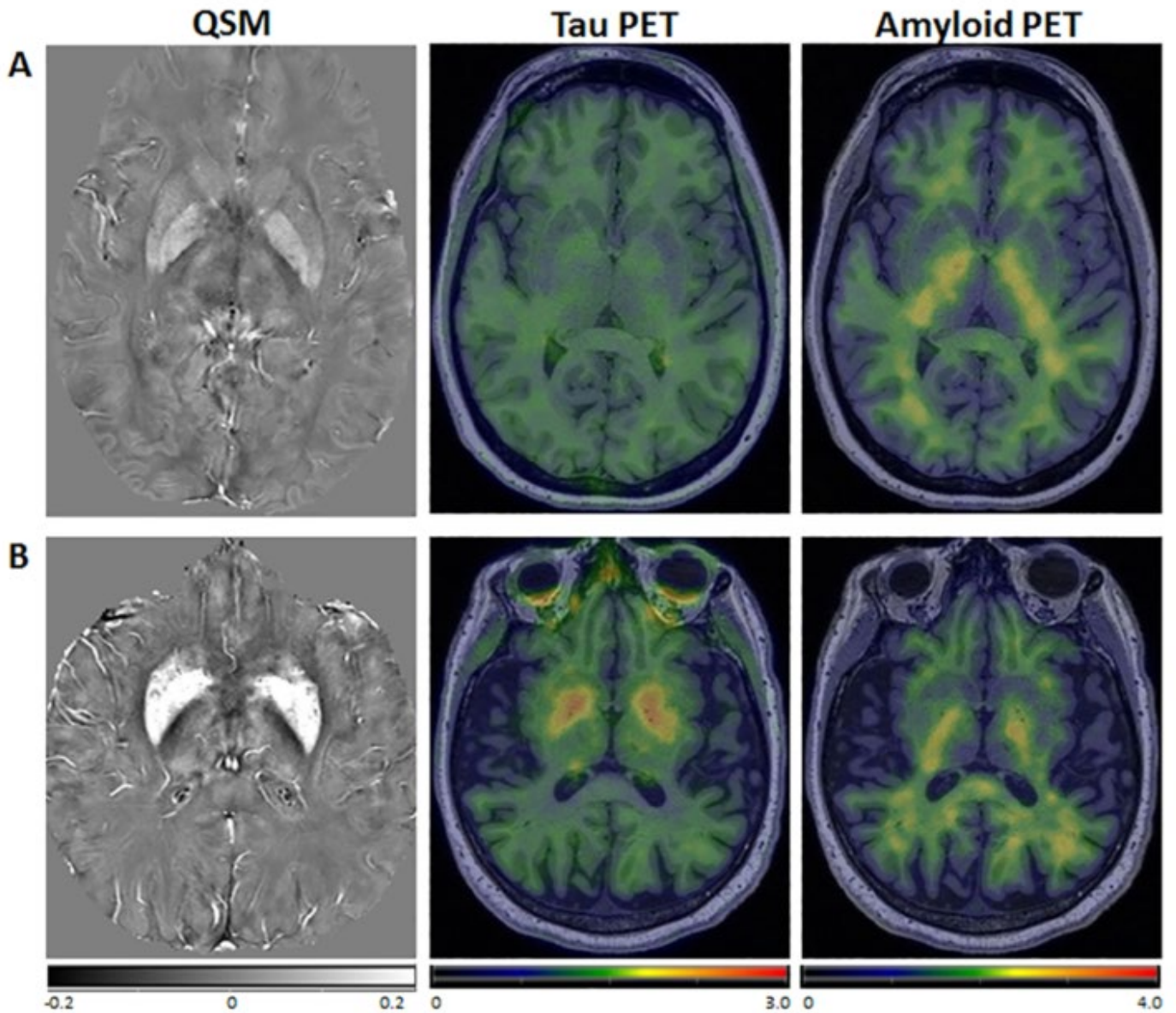


Figure 3: Images from representative participants. QSM, tau PET, and amyloid PET for (A) a 35-year-old participant and (B) an 80-year-old participant, both cognitively unimpaired. In the older participant, there was high signal in the pallidum and putamen on QSM with a similar distribution of elevated tau PET SUVR, which may be due to an increase with age in both off-target binding of the tau ligand and physiologic iron deposition in the basal ganglia. Amyloid PET SUVR was low throughout for both of the participants.

Keywords: Quantitative susceptibility mapping, amyloid PET, tau PET, Alzheimer's disease

P63: Developing a novel alpha-synuclein (a-syn) positron emission tomography (PET) tracer for the diagnosis of Parkinson's disease (PD) and other a-synucleinopathies

Efthymia Vokali¹, Jerome Molette¹, Elpida Tsika¹, Myriam Ravache¹, Patrick Rodriguez¹, Tanja Jürgens¹, Antonio Melo dos Santos¹, Christine Sandiego², David Russell^{2,3}, Roger Gunn², Vincent Darmency¹, Kasia Piorkowska¹, Sonia Poli¹, Heiko Kroth¹, Francesca Capotosti¹, Valérie Hliva¹, Olivier Sol¹, Kenneth Marek³, Jan Stöhr¹, David Lowe¹, Andrea Pfeifer¹, Marie Kosco-Vilbois¹

¹AC Immune SA, Lausanne, Switzerland

²Invicro, A Konica-Minolta Company, Boston, MA, US

³Institute of Neurodegenerative Disorders, New Haven, CT, US

Objective: To develop an a-syn aggregate-selective PET tracer for the diagnosis of synucleinopathies including PD.

Methods: [¹⁸F]-ACI-Cpd-AE dynamic PET imaging was conducted over 90 min in five PD subjects (four idiopathic PD, 69.4±7.4 years and MDS-UPDRS 'off' score 43.3±11.8, and one with a SNCA duplication, 49.7 years and MDS-UPDRS 'off' score 52) and five healthy volunteers (HV, 58.4±18.8 years). [¹²³I]DATscan screening in PD subjects showed abnormal striatal dopamine transporter uptake, compared with HV. Specific retention of [¹⁸F]-ACI-Cpd-AE was evaluated by calculating the distribution volume ratio (DVR) from kinetic analysis with an arterial input function and the standardized uptake value ratios (SUVr) from static analysis, using the middle frontal cortex as reference region. DVR and SUVr were evaluated across the amygdala, brainstem, cerebellum, hippocampus, pallidum, substantia nigra, thalamus and white matter.

Results: [¹⁸F]-ACI-Cpd-AE displayed fast brain uptake, very low non-specific retention, rapid metabolism and high free fraction. In this small cohort, no significant evidence of cross-sectional difference between healthy controls and PD subjects was observed. Averaged across target regions the SUVr (30-90min) range was 1.16-1.23 in PD subjects and 1.15-1.3 in HV. Mean SUVr was 1.32±0.15 in PD and 1.19±0.18 in HV in left substantia nigra.

Conclusions: In house medicinal chemistry efforts led to the discovery of ACI-Cpd-AE, a potential a-syn PET tracer that preclinically binds selectively and with high affinity to a-syn aggregates. In the first-in-human (FiH) study, ACI-Cpd-AE demonstrated fast brain uptake and low non-specific retention. Further analyses of the FiH data (e.g., kinetic modeling, population analysis) and evaluation in patients with expected higher levels of pathological brain a-syn aggregates are planned. In parallel, compounds with improved binding properties are being evaluated.

Keywords: alpha-synuclein, protein aggregation/misfolding, Biomarkers, PET Imaging

P64: Evaluating the relationships among odor identification, tau pathology and neuroinflammation in Alzheimer's disease

Julia Klein^{1,3}, Jack Yan², Aubrey Johnson¹, Zeljko Tomljanovic¹, James Zou¹, Krista Polly¹, Lawrence Honig¹, Adam Brickman¹, Yaakov Stern¹, Seonjoo Lee², William C. Kreisl¹

¹*Taub Institute, Columbia University Irving Medical Center, New York, NY, US*

²*Mailman School of Public Health, Columbia University Irving Medical Center, New York, NY, US*

³*Weill Cornell Medical College, New York, NY, US*

Background: Olfactory abilities are significantly impaired in Alzheimer's disease (AD) and can be measured with the University of Pennsylvania Smell Identification Test (UPSIT). Tau and neuroinflammation, two pathological contributors to AD, can be measured in vivo using PET imaging and CSF biomarkers. UPSIT performance is inversely related to the amount of tau pathology measured with PET. However, whether odor identification is related to neuroinflammation or CSF measures of tau pathology is unknown.

Methods: Participants were selected from an established research cohort of adults aged 50 and older who had neuropsychological testing, brain MRI, and amyloid PET. Fifty-four participants were administered the University of Pennsylvania Smell Identification Test (UPSIT) to measure odor identification ability. Fifty-three of these underwent 11C-PBR28 PET to measure the 18 kDa translocator protein (a biomarker of inflammation) and forty-one underwent 18F-MK-6240 PET to measure tau. Twenty-one participants had lumbar puncture to measure CSF concentrations of β -amyloid-42 (A β 42), total tau (t-tau), phosphorylated tau (p-tau), and inflammatory biomarkers sTREM2 and YKL-40.

Results: Analysis of variance, controlling for age and sex, showed that amyloid status and cognitive status exhibit independent effects on UPSIT performance ($p < .01$). Negative correlations between UPSIT performance and PET measures of neuroinflammation were seen in medial temporal cortex, hippocampus, middle/inferior temporal gyri, inferior parietal cortex and posterior cingulate cortex ($p < .05$). Similar inverse relationships were seen for tau. UPSIT performance negatively correlated with CSF concentrations of YKL-40, p-tau, and t-tau among amyloid-positive participants ($p < .05$).

Conclusions: Amyloid-positivity and cognitive impairment exhibit independent effects on odor identification, suggesting that 1) low UPSIT performance may signify risk of AD in cognitively normal individuals, and 2) impaired odor identification is associated with both AD- and non-AD-related neurodegeneration. Odor identification ability appears to decline with increasing tau pathology and neuroinflammation in those on the Alzheimer's continuum.

Keywords: MK6240, tau, neuroinflammation, odor identification, UPSIT

P65: Elevated soluble phosphorylated tau is a marker of early amyloid PiB PET abnormalities and accumulation

McDade¹, Yan Li¹, Nelly Joseph-Mathurin¹, Tammie Benzinger¹, Anne Fagan¹, Chengjie Xiong¹, Nicolas Barthélemy¹, Randall Bateman¹

¹Washington University School of Medicine, St. Louis, MO, US

Background: Soluble phosphorylated tau (p-tau) is an important biomarker of dysregulated tau in Alzheimer's disease. Currently, p-tau is considered a measure of neurofibrillary tau pathology. However, recent work from the Dominantly inherited Alzheimer Network study has demonstrated hyperphosphorylation of tau occurring 5-10 years prior to identification of tau-PET changes, more similar to the timing of amyloid deposition.

Objective: To evaluate CSF p-tau as a method of classifying carriers of dominantly inherited mutations as having abnormal levels of aggregated β -amyloid (PiB-PET)) and a predictor of regional PiB-PET accumulation.

Methods: A novel mass spectrometry based analysis of CSF p-tau quantified the ratio of phosphorylated:unphosphorylated tau at multiple positions (pT181, pS202, pT205, pT217) from 183 mutation carriers (63% CDR 0) and was used to classify participants as PiB-PET+ (SUVR >1.25) based on their Receiver Operating Characteristic (ROC) curves; in CDR 0 participants we further assessed the cross-sectional, bivariate correlations between each p-tau isoform and cortical PiB-PET SUVR and the ability of baseline p-tau measures to predict change in PiB-PET SUVR using linear mixed-effects models.

Results: Phosphorylation of tau at position 217 had a 97% AUC, followed by pT181 89%, pT205 74%, total tau 72% and pS202 69%, **figure 1**. We found a similar order in the strength of correlations with regional PiB-PET SUVR, with pT217 having the strongest correlations cross-sectionally, **figure 2**. However, only pT205 predicted longitudinal change in PiB-PET in the inferior temporal while pT217 did not predict longitudinal change in PiB-PET.

Conclusion: Although abnormal levels of CSF p-tau is considered a marker of NFT pathology we demonstrate that soluble p-tau is much more strongly linked to the initial development of amyloid beta plaques. These findings suggest important differences between soluble/insoluble tau in AD and that CSF p-tau could be an important measure of downstream response to amyloid specific therapies.

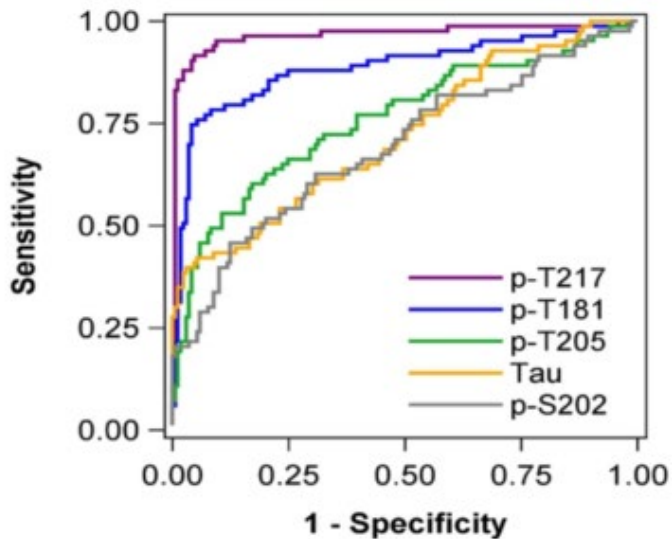


Figure 1. Receiver operating characteristics of tau phosphorylation with A β pathology based on A β PiB-PET (SUVR cutoff of 1.25), demonstrates a near perfect association with A β pathology for pT217/T217 (purple, AUC=0.97), with different associations with pT181/T181 (blue, AUC =0.89), pT205/T205 (green, AUC = 0.74), total tau (orange, AUC=0.72) and pS202/S202 (gray, AUC=0.69).

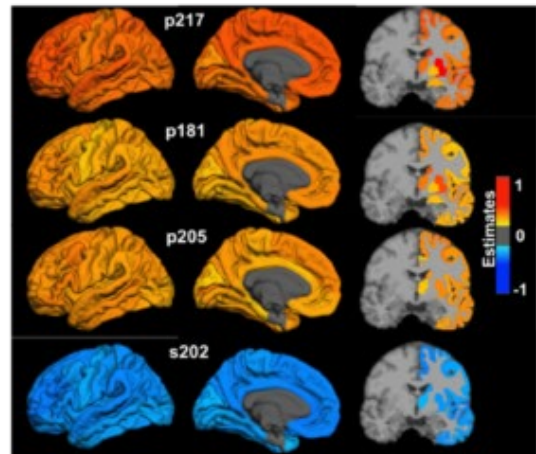


Figure 2. Cross-sectional, bivariate correlations between cortical and sub-cortical A β PiB-PET SUVR and site-specific phosphorylation for asymptomatic mutation carriers (n=152). The colors represent the correlation with positive correlations (yellow-red) and negative correlations (blue); all correlations represent statistically significant values surviving a false discovery rate ($p < 0.05$) and are arranged by the strength of the correlations from top to bottom.

Keywords: phosphorylated tau, PiB PET, Tau PET, AUC

P66: Cerebrospinal fluid and PET measures of tau pathology may indicate different stages of AD pathological progression

Pierre-Francois Meyer^{1,2,3}, Alexa Pichet Binette^{1,2,3}, Julie Gonneaud^{1,2}, John Breitner^{1,2,3}, Sylvia Villeneuve^{1,2,3,4}

¹Douglas Mental Health University Institute, Studies on Prevention of Alzheimer's Disease (StoP-AD) Centre, Montréal, QC, Canada

²Department of Psychiatry, McGill University, Montréal, QC, Canada

³McGill Centre for Integrative Neuroscience, McGill University, Montréal, QC, Canada

⁴Department of Neurology and Neurosurgery, McGill University, Montréal, QC, Canada

Background: Alzheimer's disease-(AD) pathological changes likely occur decades before cognitive impairment. It was recently suggested that discrepancy between CSF and PET measures of amyloid-beta (A β) reflects timing of disease processes. We sought to assess whether similar observations were true for measures *tau* pathology.

Methods: Three-hundred and twenty-two participants (213 cognitively unimpaired, 98 with Mild cognitive impairment and 11 with AD dementia) from the Alzheimer's Disease Neuroimaging Initiative had available CSF and PET (flortaucipir) measures of *tau* pathology within a 25-month interval. Using data-driven, clinically-relevant thresholds for CSF P-*tau* (≥ 26.64 pg/mL) and a flortaucipir-PET meta-ROI (SUVR ≥ 1.37), we categorized *tau* abnormality as CSF-/PET-, CSF+/PET-, CSF-/PET+, and CSF+/PET+. We compared these groups on demographic and clinical variables, A β -PET burden and flortaucipir-PET binding in Braak stage-related ROIs. We also compared these groups' five-year rates of CSF P-*tau* accumulation and cognitive decline prior to flortaucipir-PET scanning.

Table 1: Sample demographics. Sex F: number of participants of female sex; MCI: number of mild cognitive impairment patients, AD: number of Alzheimer disease dementia patients s.d: standard deviation.

	CSF-/PET-	CSF+/PET-	CSF-/PET+	CSF+/PET+	P-value
Number	210	63	15	34	
Age in years (s.d)	72.33 (7.06)	75.30 (7.58)	72.27 (7.34)	73.97 (8.30)	0.04 ^a
Sex F (%)	118 (56%)	35 (56%)	6 (40%)	21 (63%)	0.58
Diagnosis CU:MCI:AD	151 : 58 : 2	49 : 13 : 1	6 : 8 : 1	8 : 19 : 7	<0.01 ^{b,c,d,e}
Years of education (s.d)	16.81 (2.33)	16.21 (2.39)	17.87 (1.69)	15.53 (2.60)	<0.01 ^{c,d,f}
APOE $\epsilon 4$ carriers (%)	58 (27%)	28 (44%)	10 (67%)	23 (68%)	< 0.01 ^{a,b,c,e}
Memory composite (s.d)	0.93 (0.62)	0.79 (0.64)	0.22 (0.89)	-0.17 (1.00)	< 0.01 ^{b,c,d,e}
Executive function composite (s.d)	1.08 (0.82)	0.95 (0.86)	0.51 (1.07)	-0.29 (1.02)	< 0.01 ^{b,c,e,f}
CSF to PET months (median and range)	0.71 [0.00-24.61]	0.68 [0.00-24.39]	0.39 [0.00-22.58]	1.23 [0.00-24.90]	0.82

^a CSF-/PET- vs CSF+/PET- P<0.05; ^b CSF-/PET- vs CSF-/PET+ P<0.05; ^c CSF-/PET- vs CSF+/PET+ P<0.05; ^d CSF+/PET- vs CSF-/PET+ P<0.05; ^e CSF+/PET- vs CSF+/PET+ P<0.05; ^f CSF-/PET+ vs CSF+/PET+ P<0.05.

Results: Among all participants, 210 were CSF-/PET-, 63 were CSF+/PET-, 15 were CSF-/PET+ and 34 were CSF+/PET+ (Table 1, Figure 1). *Tau*-positive individuals by either measure showed an increase in $A\beta$ -PET burden. All CSF+/PET+ individuals were amyloid-positive and 76% were clinically diagnosed with MCI or AD (Figure 1). CSF+/PET- participants showed faster 5-year accrual of CSF P-*tau* and mildly increased Flortaucipir-PET binding in early Braak ROIs (Figure 1), but similar memory decline than CSF-/PET- participants.

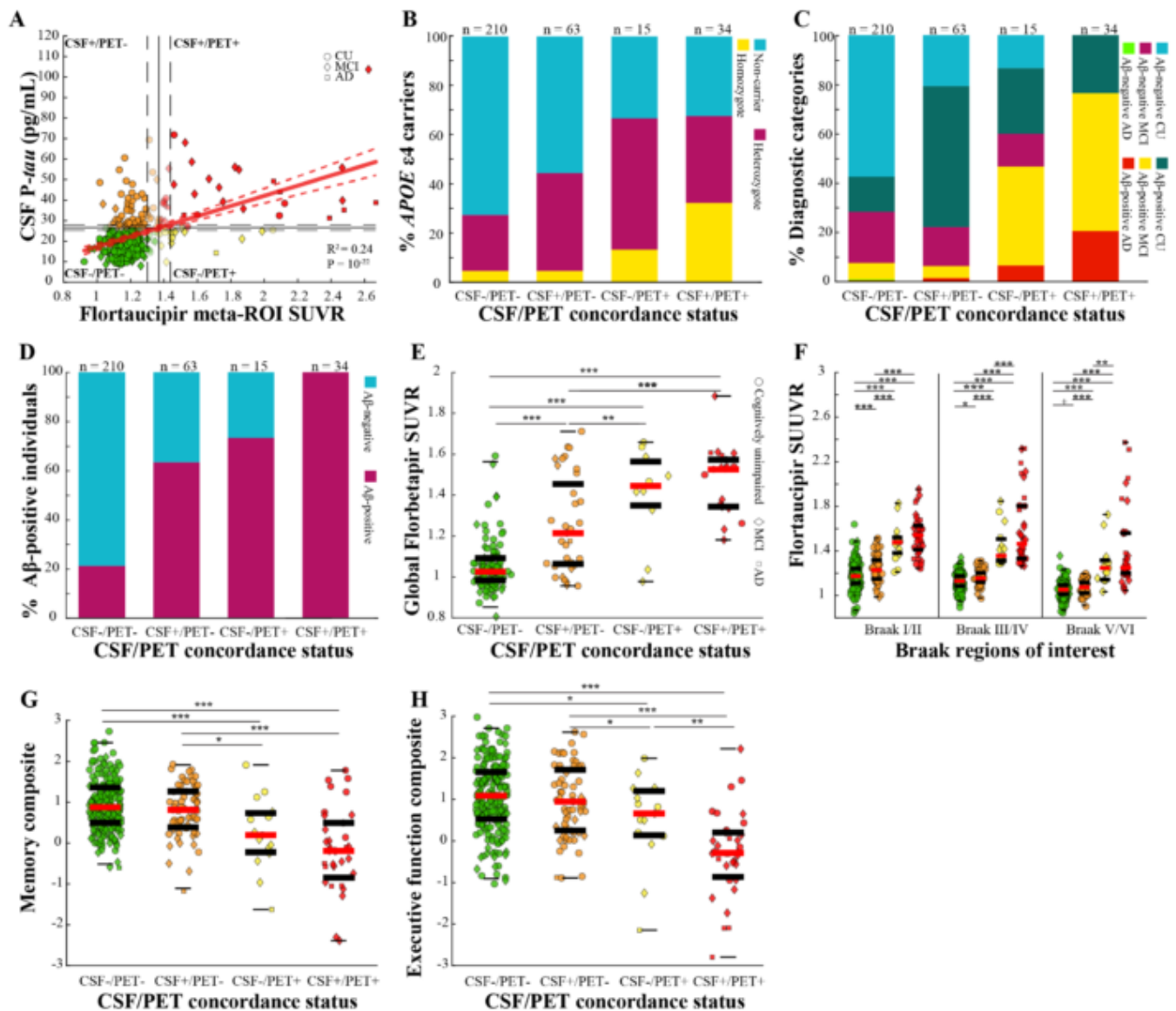


Figure 1: Cross-sectional results. (A) shows the linear association of CSF P- τ and metaROI flortaucipir SUVR. Color code represents the tau CSF/PET categories (P- τ positivity ≥ 26.64 pg/mL and flortaucipir-PET SUVR ≥ 1.37) and shape indicates clinical diagnosis. Dotted lines delineate a $\pm 5\%$ interval around thresholds and dots within this interval are faded. (B) shows proportions of APOE $\epsilon 4$ carriers and (C) the proportion of cognitively impaired participants. (D) shows the frequency of $A\beta$ -positivity and (E) the distribution of cortical florbetapir-PET uptake. (F) shows flortaucipir tracer retention in Braak-like ROIs. (G) Shows memory and (H) executive function performance.

When compared with the CSF-/PET- group, CSF+/PET+ individuals experienced faster 5-year accrual of CSF P- τ , had worse memory and executive functioning at flortaucipir-PET assessment and faster decline in the five years preceding it (Figure 2).

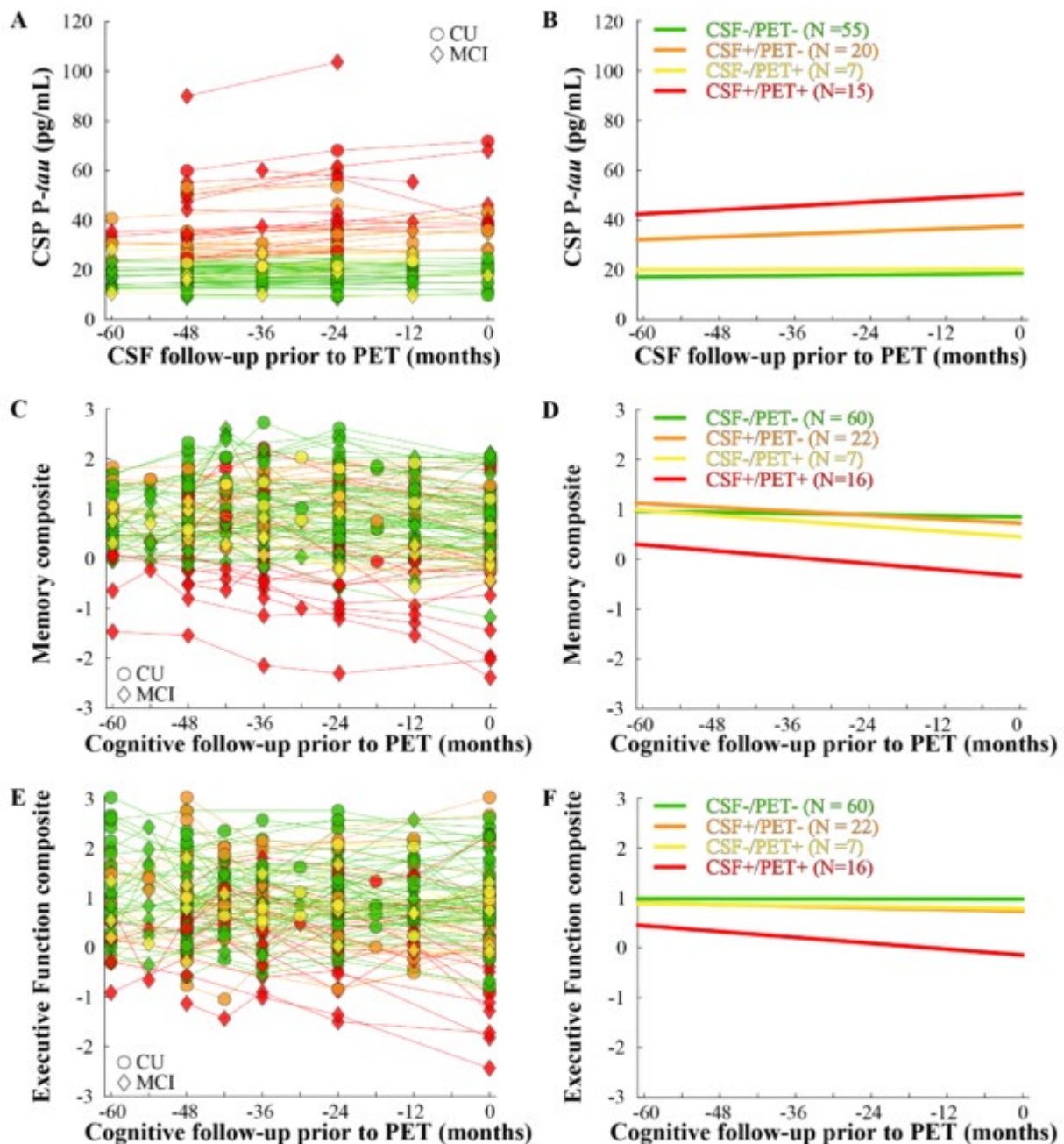


Figure 2: Retrospective trajectories of CSF P-tau, memory and executive function. (A) Individual trajectories and measures of CSF P-tau over the 5 years preceding the flortaucipir-PET scan. (B) Linear mixed-effects group-level 5-year change in CSF P-tau. (C) and (D) indicate the same information for the performance on the ADNI memory composite scale. (E) and (F) indicate the results of an identical analysis considering the ADNI executive function composite.

Conclusions: Supra-threshold CSF P-tau without flortaucipir abnormality may indicate an established AD-process without decline in cognitive functions and widespread tau pathology. Concordance of CSF/PET tau measures coincide with stronger cognitive decline. CSF P-tau abnormality may serve as an indicator of progressing AD processes prior to substantial cognitive impairment.

Keywords: Alzheimer's disease, Biomarkers, Cerebrospinal fluid, PET, tau

P67: Distinct effects of APOE ϵ 2 on A β in Alzheimer- and vascular-type cognitive impairment

Jin San Lee¹, Hyejoo Lee², Seongbeom Park², Yeongsim Choe², Yu Hyun Park², Bo Kyoung Cheon², Alice Hahn², Rik Ossenkoppele³, Hee Jin Kim², Seonwoo Kim², Heejin Yoo², Hyemin Jang², Soo Hyun Cho⁴, Seung Joo Kim⁵, Jun Pyo Kim², Young Hee Jung⁶, Key-Chung Park¹, Charles DeCarli⁷, Michael Weiner⁸, Gyihaon Yun¹, Duk L. Na², Sang Won Seo²

¹Kyung Hee University Hospital, Seoul, Korea

²Samsung Medical Center, Seoul, Korea

³VU University Medical Center, Amsterdam, Korea

⁴Chonnam National University Medical School, Gwangju, Korea

⁵Gyeongsang National University Changwon Hospital, Changwon, Korea

⁶Myungji Hospital, Goyang, Korea

⁷University of California, Davis, CA, US

⁸University of California, San Francisco, CA, US

Objective: To investigate the association between apolipoprotein E (*APOE*) genotype and amyloid- β (A β) burden measured with PET in patients with subcortical vascular cognitive impairment (SVCI) and in those with Alzheimer's disease-related cognitive impairment (ADCI).

Methods: A cross-sectional study was conducted in 310 patients with SVCI and in 999 with ADCI. To evaluate the effects of *APOE* genotype or diagnostic group on A β positivity, we performed multivariate logistic regression analyses. Further distinctive underlying features of the latent subgroups were examined by employing a latent class cluster analysis approach.

Results: In comparison with ϵ 3 homozygotes, in the ADCI group, ϵ 2 carriers showed a lower frequency of A β positivity (OR 0.43, 95% CI 0.23–0.79) while in the SVCI group, ϵ 2 carriers (OR 2.26, 95% CI 1.02–5.01) showed a higher frequency of A β positivity. In particular, there was an interaction of ϵ 2 carriers for A β positivity between the two groups (OR 5.12, 95% CI 1.93–13.56), suggesting that in comparison to the ADCI group, the SVCI group had a significantly higher frequency of A β positivity in ϵ 2 carriers than in ϵ 3 homozygotes. We also identified latent subgroups of A β -positive SVCI patients with *APOE* ϵ 2 carriers and A β -positive ADCI patients with *APOE* ϵ 4 carriers.

Conclusions: Our findings suggest that *APOE* ϵ 2 shows distinct effects on A β deposition in patients with SVCI and in those with ADCI. Our findings further suggest that there is a distinctive subgroup of A β -positive SVCI patients with *APOE* ϵ 2 carriers among patients with cognitive impairments.

Keywords: Subcortical vascular cognitive impairment, Alzheimer's disease, A β positivity, Apolipoprotein E, Latent class analysis

P68: Association of tau tangle burden with depressive symptoms in community dwelling older adults: a longitudinal study

Jennifer Gatchel^{1,2,4}, Gad A. Marshall^{1,3,4}, Hyun-Sik Yang^{1,3,4}, Nancy J. Donovan^{1,3,4}, Rachel F. Buckley^{1,3,7}, Michael Properzi^{1,4}, Yakeel T. Quiroz^{1,4}, Jennifer S. Rabin⁸, Patrizia Vannini^{1,3,4}, Rebecca E. Amariglio^{1,3,4}, Jasmeer Chhatwal^{1,3,4}, Dorene M. Rentz^{1,3,4}, Deborah Blacker^{1,4,6}, Reisa A. Sperling^{1,3,4}, Keith A. Johnson^{1,3,4}, Bernard J. Hanseeuw^{1,3,4}

¹Massachusetts General Hospital, Boston, MA, US

²McLean Hospital, Belmont, MA, US

³Brigham and Women's Hospital, Boston, MA, US

⁴Harvard Medical School, Boston, MA, US

⁵Cliniques Universitaires Saint-Luc, Brussels, Belgium

⁶Harvard T.H.Chan School of Public Health, Boston, MA, US

⁷The Florey Institute, The University of Melbourne, Victoria, Australia

⁸Hurvitz Brain Sciences Program, Sunnybrook Research Institute, Toronto, Canada

Background: Depressive symptoms are thought to be among the earliest behavioral changes in preclinical Alzheimer's disease (AD). However, the association between AD pathology and depressive symptoms in preclinical AD remains poorly understood. In the current study we examined the impact of pathology burden (amyloid and tau) on longitudinal change in depressive symptoms in cognitively unimpaired older adults.

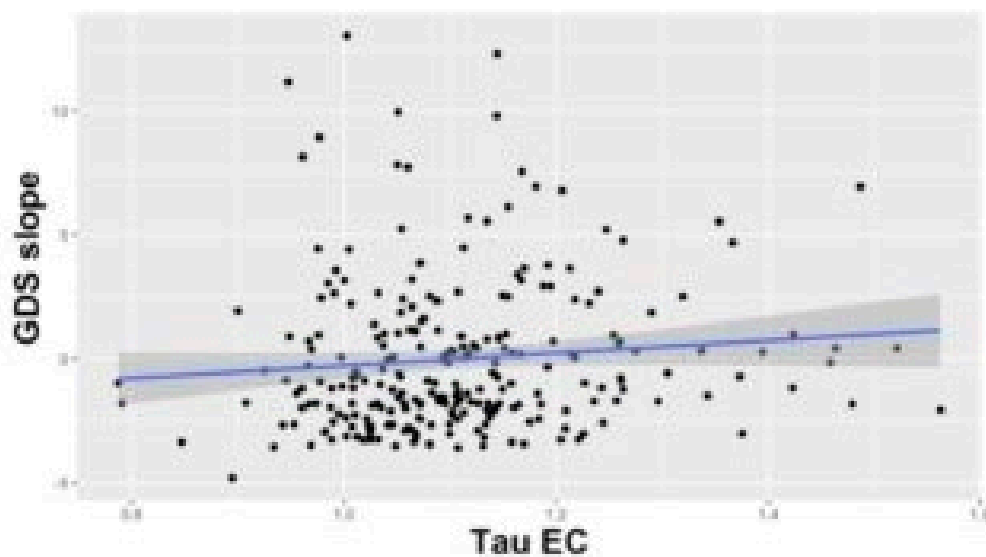
Methods: 252 adults (age: 70.8 ±8.2; 61% females) from the Harvard Aging Brain Study completed annual assessment with the 30-item Geriatric Depression Scale (GDS) (average follow-up=5.87 annual visits). All were cognitively normal, without clinically significant depression at study entry (mean GDS=3.19±3.12; range: (0-16)). All underwent tau (¹⁸F-Flortaucipir) and amyloid-β(¹¹C-Pittsburgh Compound B) PET at study year 3 or 4 to derive measures of inferior temporal (IT) and entorhinal cortex (EC) tau and cortical amyloid. A mixed model was employed with dependent variable GDS (for each annual study visit), a random intercept and slope for each participant, and fixed predictors: tau (IT or EC, at study year 3/4), cortical amyloid (at year closest to tau), time (time of tau PET), covariates: age, sex, education; and the interaction of predictors with time.

Results: Baseline tau burden was associated with increasing GDS over time. In the model with predictor EC tau, EC tau X time was a significant predictor of GDS ($\beta=0.48$; $t=3.80$; 95% CI (0.23, 0.73); $p=0.0002$). Findings were similar for IT tau:($\beta=0.71$; $t=3.67$; 95% CI (0.33, 1.1); $p=0.0002$). By contrast, amyloid was not a significant predictor of longitudinal GDS in tau models: ($\beta=-0.14$; $t=-1.58$; 95% CI(-0.23, -0.08); $p=0.11$).

Conclusions: Baseline tau, but not amyloid, is independently associated with increasing depressive symptoms over time. Future research incorporating longitudinal tau PET and individuals with more severe depressive symptoms is needed to delineate the temporal sequence of rising depressive symptoms and increasing tauopathy in preclinical AD.

Figure 1. Change in GDS (estimated random slopes of GDS) over all annual study visits vs. tau (^{18}F -Flortaucipir) SUVR in the entorhinal cortex (EC) (a) and inferior temporal lobe (IT)(b) (measured in study year 3 or 4). GDS= Geriatric Depression Scale; EC= entorhinal cortex; IT=inferior temporal cortex; SUVR=standard uptake volume ratio

a.



b.

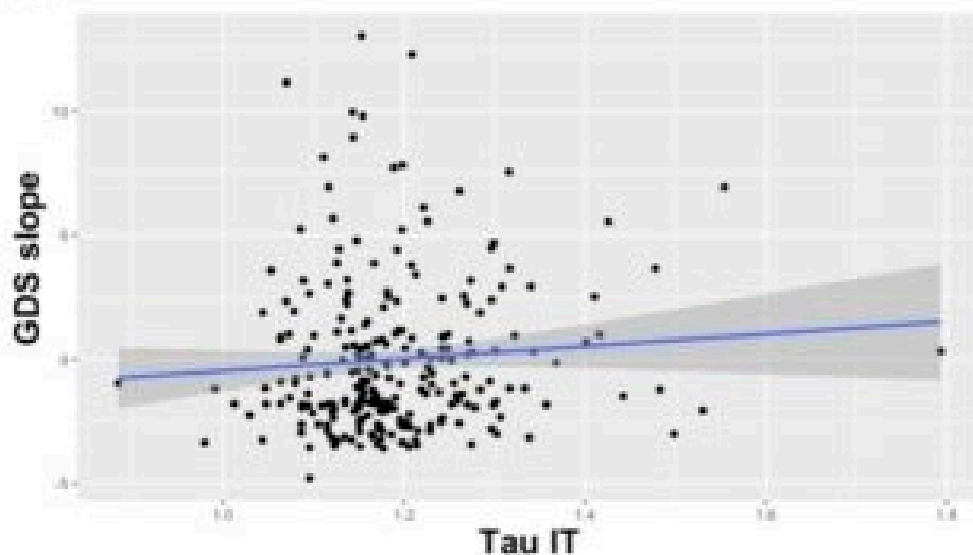
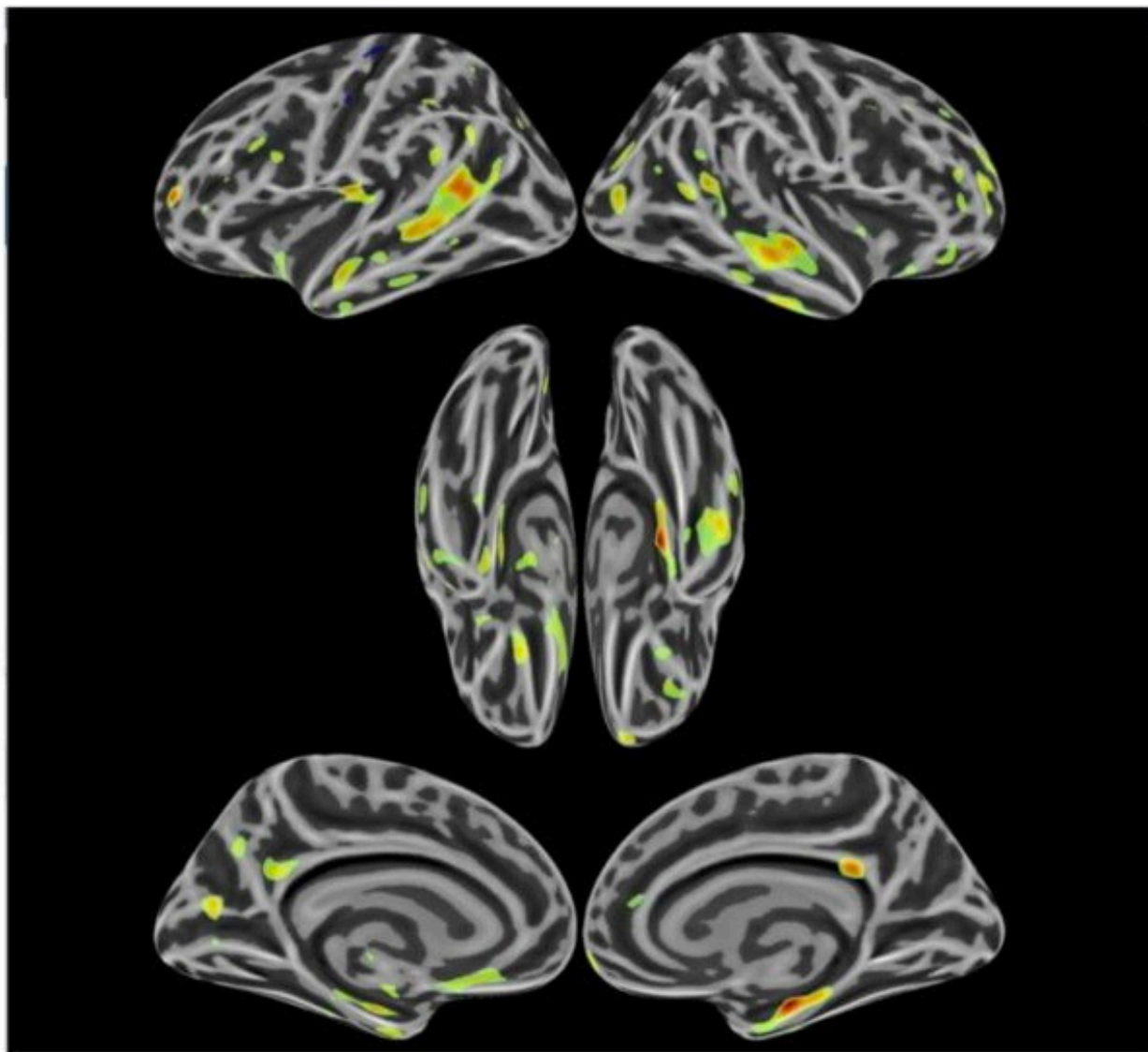


Figure 2. Vertex-wise map showing association between tau (^{18}F -Flortuacipir PET) and change in GDS (estimated random slopes of GDS) over all annual study visits, adjusted for age (age at tau PET), sex, and education. Data shown are partial volume corrected; color shading indicates the t statistic (maximum $t=4.08$, $p<0.0001$) for the association between tau and change in GDS. GDS=Geriatric Depression Scale.



Keywords: tau, amyloid, depression, Geriatric Depression Scale

P69: Higher microglia biomarker levels are associated with slower rates of amyloid-beta accumulation in humans and in a transgenic mouse model of amyloid-beta

Michael Ewers¹, Matthias Brendel², Marc Suarez-Calvet³, Gloria Biechele², Christian Sacher², Tanja Blume², Christian Haass⁴, Nicolai Franzmeier¹

¹*Institute for Stroke and Dementia Research, University Hospital, Ludwig Maximilian University (LMU) Munich, Munich, Germany*

²*Department of Nuclear Medicine, University Hospital, Ludwig Maximilian University (LMU) Munich, Munich, Germany*

³*Barcelonabeta, Brain Research Center, Barcelona, Spain*

⁴*German Center for Neurodegenerative Diseases (DZNE), Munich, Germany*

Background: Higher microglia activity, assessed by cerebrospinal fluid (CSF) biomarker levels of soluble TREM2 (sTREM2), showed protective effects associated with slower cognitive decline in patient with Alzheimer's disease (AD, Ewers et al. *Science Trans Med.*, 2019). However, whether microglia activity reduces the future accumulation of core AD-pathology remains unclear.

Aim: To test whether higher microglia activity is associated with lower rates of amyloid-beta (A β) accumulation in a) a transgenic mouse model of Ab and b) elderly non-demented and demented humans.

Methods: We assessed 206 A β -positive participants (global AV-45-PET SUVR > 0.79, Landau et al. 2015) encompassing 55 cognitively healthy subjects, 136 amnesic mild cognitive impairment (aMCI) and 15 AD dementia from ADNI. CSF sTREM2 and AV-45 PET were measured at baseline and AV-45 PET was repeated during follow-up (mean = 2 years, range = 1.71-6.1 years). In a translational approach, we assessed 15 *App*^{NL-G-F} knock-in mice and 43 C57BL/6 control mice with ¹⁸F-GE180 TSPO-PET and ¹⁸F-florbetaben amyloid-PET at ages 5 and 10 months.

Results: In subjects within the AD spectrum (n = 206), the rate of change in amyloid PET showed a quadratic curve as a function of baseline amyloid PET levels, peaking at SUVR = 0.95 (Fig. 1A). Linear mixed-effects regression showed that at higher baseline levels of CSF sTREM2, the rate of subsequent increase in A β was reduced, controlled for demographics, diagnosis, CSF p-tau₁₈₁, and ApoE e4 (Figure 1B). In the *App*^{NL-G-F} mice, higher microglia PET at baseline was associated with slower rate of increase in global amyloid PET during the 5-month follow-up, controlled for baseline amyloid PET (Figure 2).

Conclusions: Across mice and humans, higher microglia activation as measured by CSF sTREM2 or microglia PET show protective effects on subsequent amyloid accumulation, supporting the critical role of microglia activation in the evolution of AD.

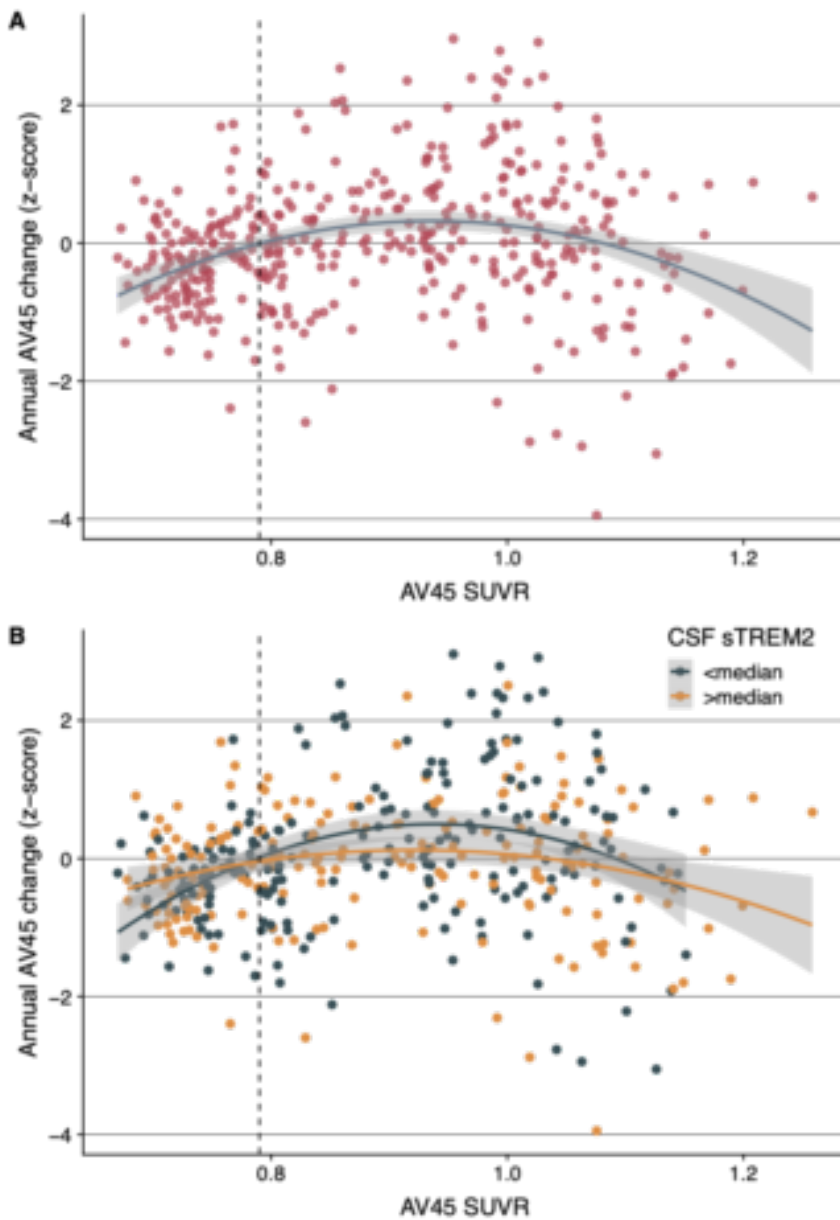


Figure 1. (A) Association between baseline AV45 (x-axis) and annual AV45 change (y-axis) across the entire sample. The vertical dashed line represents the Abeta-positivity threshold of 0.079.

(B) Association between baseline AV45 and annual AV45 change for groups of low and high CSF sTREM2 at baseline. The quadratic interaction between continuous measure of CSF sTREM2 and $(AV45 \text{ PET SUVR})^2$ was significant. The main effect of higher CSF sTREM2 on lower quadratic slope of AV45 PET change was also significant ($p = 0.01$).

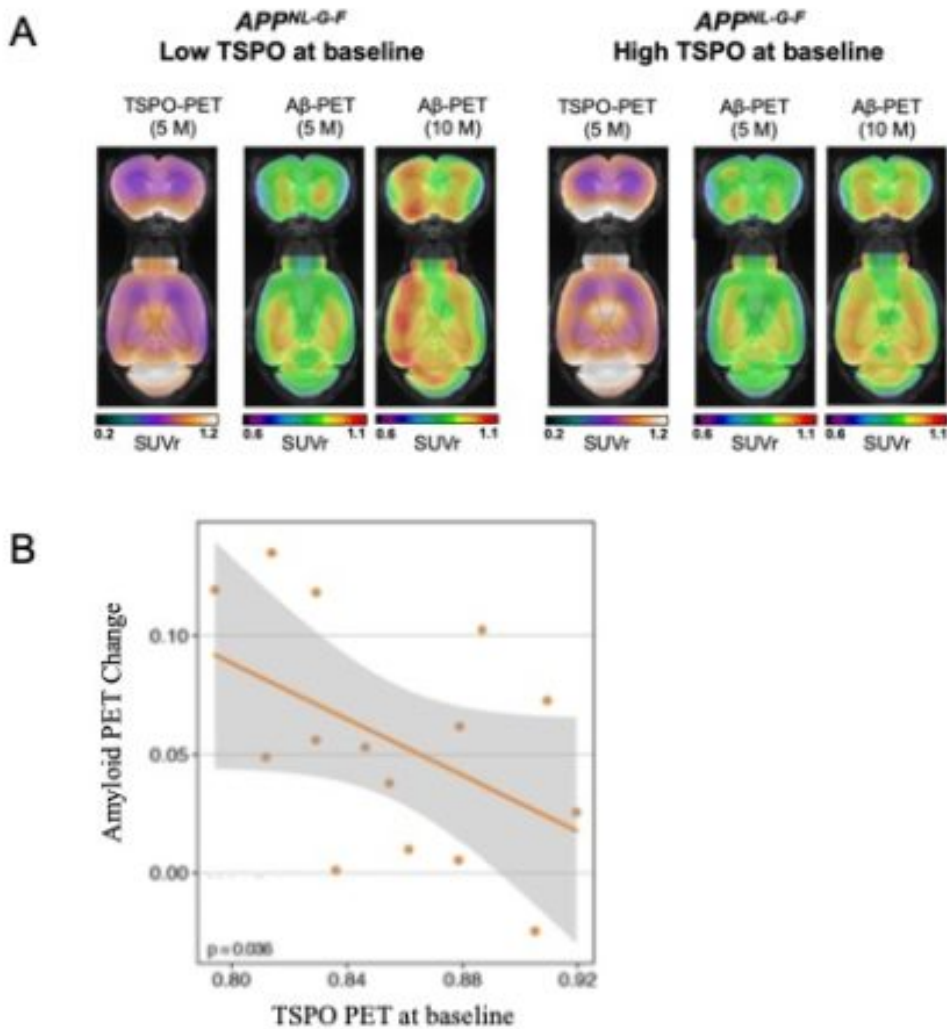


Figure 2. (A) Coronal (top row) axial (bottom row) slices of ¹⁸-F GE-180 TSPO (microglia) tracer and longitudinal ¹⁸F-florbetaben amyloid-PET in the *APP^{NL-G-F}* mice split by the mean level of global level GE-180 microglia PET, including low (left panel) and high (right panel) GE-180 TSPO PET. Mice with low baseline TSPO PET levels showed faster increase in amyloid PET between 5 and 10 months of age (left panel) compared to those at high baseline level of microglia PET

(B) Regression plot for the effect of TSPO at 5-months on subsequent amyloid-change from 5- to 10 months in the *APP*-ki mice.

Keywords: Microglia, immune system, *TREM2*, amyloid PET, longitudinal

P70: Individual variability in the cortical distribution of elevated 18F-AV1451 and 11C-PIB in a heterogeneous sample of AD patients

Jessica Collins¹, Ryan Eckbo¹, Scott McGinnis², Brad Dickerson¹

¹Massachusetts General Hospital, Boston, MA, US

²Brigham and Women's Hospital, Boston, MA, US

The goal of the present study was to investigate the degree to which the cortical distribution of elevated 18F-AV1451 and 11C-PIB varies across individual AD patients with heterogeneous clinical profiles, and to identify regions of common vulnerability to AB or tau pathology across the AD clinical spectrum. 25 AB+ patients with Alzheimer's disease (15 with PCA, 9 with PPA, 1 with amnesic AD presentations) underwent 18F-AV1451 and 11C-PIB imaging. 24 AB- age-matched older healthy controls (OCs) also underwent 18F-AV1451 and 11C-PIB imaging. Individual 11C-PIB and 18F-AV1451 SUVR maps were partial volume corrected and projected to a template cortical surface using FreeSurfer. Surface projected 11C-PIB and 18F-AV1451 SUVR maps for the 25 patients were converted to z-scores using data from the 24 OCs, and then binarized using a z-score threshold of 1.5. Percent overlap maps for each tracer were created by adding together the individual binarized z-score maps, and then converting to a percentage, both within the subsamples of patients with a PCA or PPA clinical phenotype, and across phenotypes for the AD sample as a whole. A cortical parcellation of the brain into 7 canonical intrinsic functional connectivity networks was used to estimate, across voxels, the average percent of patients with elevated uptake of each tracer within each network. Widespread cortical uptake of 11C-PIB was observed for 80-100% of all subjects across all intrinsic functional networks. The uptake of 18F-AV1451 was highly variable across patients, with the highest percentage of patients showing elevated uptake in the Dorsal Attention network (82%). 80-90% of PCA patients had elevated 18F-AV1451 uptake in bilateral Visual and Dorsal Attention networks. 70-80% of PPA patients had elevated 18F-AV1451 uptake in left Dorsal Attention, Salience, and Default Networks.

Keywords: Posterior Cortical Atrophy, Primary Progressive Aphasia, Amyloid, Tau

P71: Quantitative regional amyloid burden and white matter changes in preclinical Alzheimer's disease

Lyduine Collij¹, Herwin Top¹, Kristine Stickney², Silvia Ingala¹, Jori Tomassen³, Isadora Lopes Alves¹, Maqsood Yaqub¹, Alle Meije Wink¹, Dennis Van 't Ent², Philip Scheltens³, Bart N.M. Van Berckel¹, Pieter Jelle Visser³, Frederik Barkhof^{1,4}, Anouk Den Braber^{2,3}, On behalf of the AMYPAD consortium⁵

¹Department of Radiology and Nuclear Medicine, Amsterdam UMC, Location VUmc, Amsterdam, The Netherlands

²Department of Biological Psychology, VU University, Amsterdam, The Netherlands

³Alzheimer Center, Amsterdam UMC, Location VUmc, Amsterdam, The Netherlands

⁴Institute of Neurology and Healthcare Engineering, University College London, London, UK

⁵The project leading to this paper has received funding from the Innovative Medicines Initiative 2 Joint Undertaking under grant agreement No 115952, Brussel, Belgium

Background: Amyloid- β (A β) accumulation is the pathological hallmark of Alzheimer's disease (AD), suggested to be closely followed by white matter (WM) integrity alterations in preclinical subjects. However, reports on the relationship between the two measures have been conflicting. This study aimed to investigate the relationship between amyloid burden and WM integrity in preclinical AD on a regional level.

Methods: 179 subjects from the EMIF-AD preclinAD study who underwent Diffusion Weighted MRI (DWI) and dynamic [¹⁸F]flutemetamol PET imaging (Philips Ingenuity PET-MR) were included (**Table 1**).

Table 1. Demographics of the cohort

Continuous measures are shown as mean (SD) unless otherwise specified.

*Based on predefined cut-off using Gaussian mixture modelling (i.e. BP_{ND+1} > 1.15).

Cohort	N = 179
Gender F (%)	102 (57%)
Age	70.1 (7.14)
MMSE score	29.0 (1.15)
WMH load	5.41E ⁰³ (7.33E ⁰³)
APOE- ϵ 4 positivity (%)	74 (41.3%)
Global amyloid burden (BP _{ND+1})	1.03 (0.12)
Global amyloid positivity (%)*	20 (11.2%)
Cluster 1 amyloid (range)	1.31 (1.08 – 2.04)
Cluster 2 amyloid (range)	1.18 (0.90 – 1.74)
Cluster 3 amyloid (range)	1.03 (0.76 – 1.43)
Cluster 4 amyloid (range)	0.93 (0.70 – 1.26)

Global and tract-level Fractional anisotropy (FA) and mean diffusivity (MD) were determined using the JHU WM atlas. Amyloid burden was determined by the non-displaceable binding potential (BP_{ND+1}) with cerebellar grey matter as the reference region. The relationship between amyloid burden and WM integrity was tested using Generalized estimating equations, correcting for family relatedness. Linear and quadratic fits were tested using QIC. Analyses were corrected for age, sex, and white matter hyperintensity load. The strongest associations are shown (significance set at

$p < 0.05$, FWE-corrected).

Results: Low amyloid burden was associated with increased FA and decreased MD, followed by decreased FA and increased MD upon higher amyloid burden. This relationship was most robustly observed in the body of the corpus callosum (body CC), for which a quadratic fit was preferred according to QIC, and was mainly driven by amyloid accumulation in the precuneus (FA: $\beta_{linear}=0.352$, $\beta_{quadratic}=-0.103$, $\Delta QIC=6.7$,

Figure 1; MD: $\beta_{\text{linear}}=-0.434$, $\beta_{\text{quadratic}}=0.128$, $\Delta QIC=8.0$,

Figure 1. Association between amyloid burden and Fractional Anisotropy (FA)

Scatterplots show associations between standardized amyloid burden (x-axis) and standardized DTI FA measures (y-axis) corrected for age, sex, and WMH load. **A)** A significant but modest linear relationship was observed between global DVR and global WM FA. **B)** A linear relationship at trend level was observed between global DVR and FA in the body of the CC. **C)** The association between amyloid burden and FA in the body CC became quadratic and survived Bonferroni correction when only including amyloid burden in cluster 2 (i.e. lateral orbitofrontal, precuneal, insular and paracentral cortex). **D)** This association was mainly driven by the amyloid burden in the precuneus.

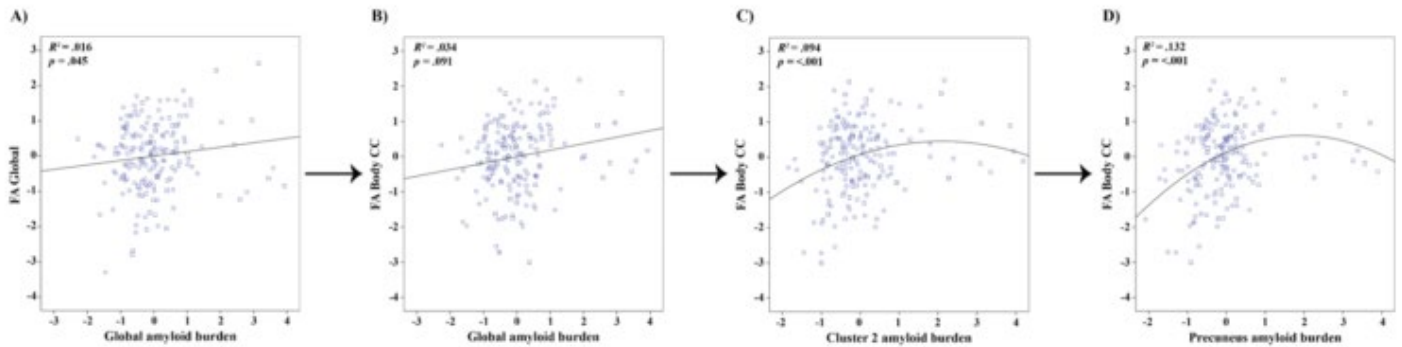
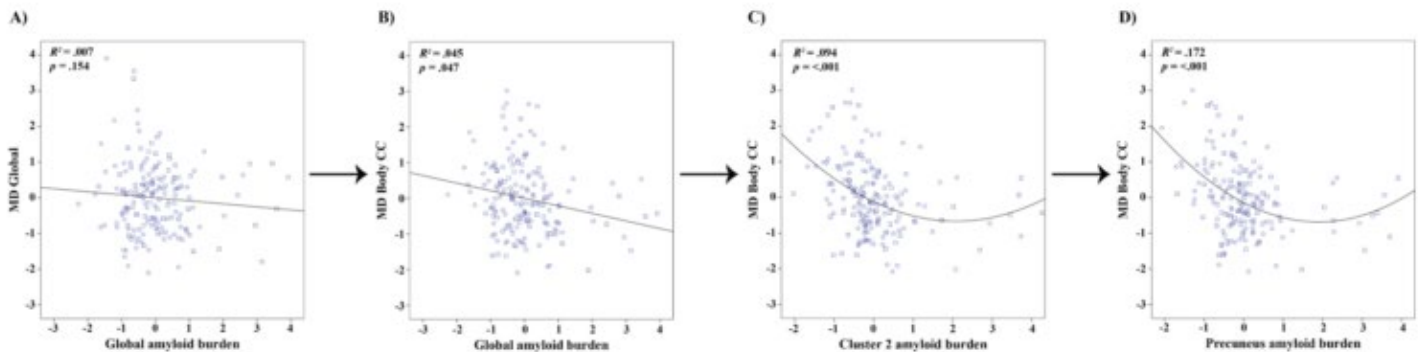


Figure 2), PCC (MD: $\beta_{\text{linear}}=-0.393$, $\beta_{\text{quadratic}}=0.101$, $\Delta QIC=4.0$), and to a lesser extent by the insula (MD: $\beta_{\text{linear}}=-0.256$, $\beta_{\text{quadratic}}=0.063$, $\Delta QIC=2.0$).

Figure 2. Association between amyloid burden and Mean Diffusivity (MD)

Scatterplots show the correlations between standardized amyloid burden (x-axis) and standardized DTI MD measures (y-axis) corrected for age, sex, and WMH load. **A)** No significant relationship was observed between global DVR and global WM MD. **B)** A significant but modest linear relationship was observed between global DVR and MD in the body of the CC. **C)** A quadratic association was observed between MD of the body CC and amyloid burden in cluster 2 (i.e. lateral orbitofrontal, precuneal, insular and paracentral cortex). **D)** This correlation with cluster 2 was mainly driven by the precuneus.



Conclusion: Early amyloid deposition is associated with WM changes, particularly evident in the body CC. Importantly, a quadratic fit was preferred by QIC, thus WM integrity in this tract could be considered as an indicator of early AD pathology in addition to amyloid burden in preclinical subjects.

Keywords: preclinical AD, amyloid PET, Diffusion Weighted Imaging, early biomarkers

P72: Effect of genetic risk, brain amyloid and hippocampal volume on normal variation in episodic memory performance in middle-aged and older adults

Jolien Schaefferbeke^{1,2}, Silvy Gabel^{1,2}, Katarzyna Adamczuk^{1,2,5}, Koen Van Laere³, Patrick Dupont^{1,2}, Rik Vandenberghe^{1,2,4}

¹Laboratory for Cognitive Neurology, Department of Neurosciences, KU Leuven, Leuven, Belgium

²Alzheimer Research Centre KU Leuven, Leuven Research Institute for Neuroscience & Disease, Leuven, Belgium

³Department of Nuclear Medicine & Molecular Imaging, University Hospitals Leuven, Leuven, Belgium

⁴Department of Neurology, University Hospitals Leuven, Leuven, Belgium

⁵Bioclinica LAB, Newark, CA, US

Background: A key characteristic of cognitive aging is episodic memory decline. Here we examined to which degree genetic risk, brain amyloid and hippocampal volume contribute to normal cognitive variation in subjects between 50 and 80 years old.

Methods: 180 community-recruited cognitively intact older adults belonging to the Flemish Prevent Alzheimer's Disease KU Leuven (F-PACK) cohort underwent detailed cognitive testing (within norms), genotyping, MRI and [¹⁸F]flutemetamol-PET. Factor analysis was applied on the neuropsychological dataset, yielding an episodic memory factor. Amyloid load was quantified in a composite neocortical volume on [¹⁸F]flutemetamol SUVR images with cerebellar grey matter reference. Structural T1-weighted MRI were processed using voxel-based morphometry and the Brainnetome atlas to obtain hippocampal volumes. Linear regressions investigated associations with episodic memory, which were further analyzed with bootstrapped mediation (R-package 'lavaan'), distinguishing indirect (*ab*) and direct (*c*) effects.

Results: *APOE* $\epsilon 4$ or *BDNF* *met* had no effect on episodic memory ($p > 0.68$). Higher amyloid load was associated with decreased episodic memory ($\beta = -0.766$, $p = 0.0496$). No significant association was observed between amyloid and hippocampal volume ($p = 0.249$). Linear regression also showed that lower hippocampal volume related to lower episodic memory ($\beta = 3.77$, $p = 0.0004$). In the mediation model, the association between amyloid and episodic memory was indirect ($ab = -0.389(0.174)$, $p = 0.025$) and mediated through a direct effect of age on both amyloid and episodic memory ($c = -0.377(0.355)$, $p = 0.29$). The association between hippocampal volume and episodic memory was also indirect ($ab = 2.73(0.645)$, $p < 0.001$) and mediated through a direct effect of age on both hippocampal volume and episodic memory ($c = 1.04(1.10)$, $p = 0.346$). There was no significant mediation effect of hippocampal volume or education ($p > 0.351$) on the relationship between age and episodic memory ($\beta = -0.066$, $p < 0.001$).

Conclusion: The well-established effect of age on normal episodic memory is not mediated by amyloid load or hippocampal volume. The underlying mechanism of age-related episodic memory decline remains an important research question.

Keywords: amyloid, hippocampus, path analysis, memory, aging

P73: Imaging synaptic and mitochondrial function in frontotemporal dementia using [¹¹C]UCB-J, [¹⁸F]BCPP-EF and [¹¹C]SA4503 PET

Mica Clarke¹, Ayla Mansur^{2,3}, Jan Passchier³, Yvonne Lewis³, Karleyton Evans⁴, Laigao Chen⁵, Adam Schwarz⁶, Akihiro Takano⁷, Roger Gunn^{2,3}, David Cash¹, Eugenio Rabiner^{3,8}, Jonathan Rohrer¹

¹Dementia Research Centre, UCL Queen Square Institute of Neurology, London, UK

²Division of Brain Sciences, Imperial College London, London, UK

³Invicro LLC., London, UK

⁴Biogen, Cambridge, MA, US

⁵Pfizer, Cambridge, MA, US

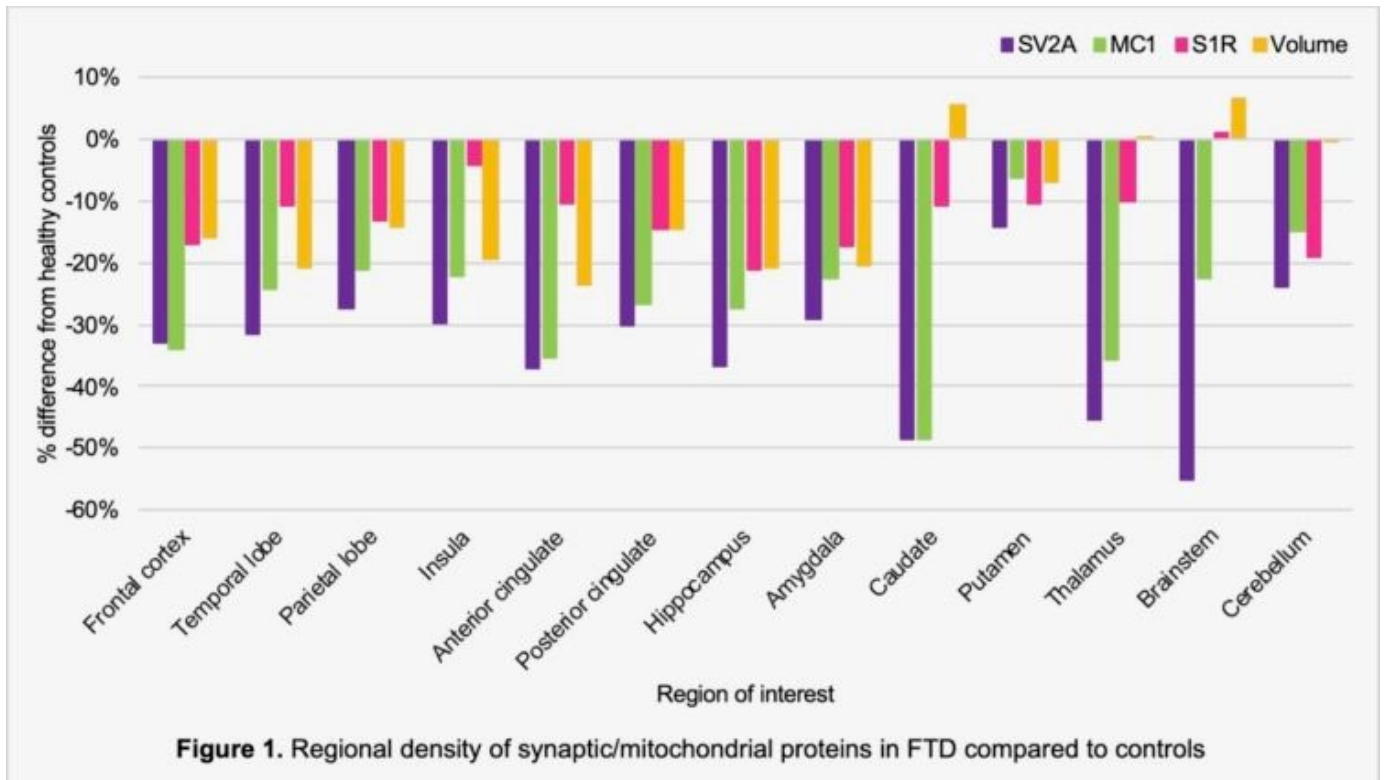
⁶Takeda Pharmaceuticals, Cambridge, MA, US

⁷Takeda Development Center Japan, Osaka, Japan

⁸King's College London, London, UK

⁹MINDMAPS Consortium, London, UK

It is hypothesized that a number of pathophysiological mechanisms are associated with neurodegeneration, including abnormalities in both mitochondrial and synaptic function. Novel radiotracers which enable the quantification of mitochondrial and synaptic proteins *in vivo* have not previously been explored in frontotemporal dementia (FTD). We used [¹¹C]UCB-J, [¹⁸F]BCPP-EF and [¹¹C]SA4503 to measure the density of synaptic vesicle protein 2A (SV2A), mitochondrial complex 1 (MC1) and the sigma 1 receptor (S1R) respectively. Five participants with behavioral variant FTD (mean age 63.6, SD 5.1) and 17 cognitively normal participants (63.7, 12.5) underwent 90-minute dynamic acquisition PET scans following injection of each of the three tracers, with metabolite corrected arterial input function. Regions of interest were defined on individual MR images using the CIC anatomical atlas. Regional density was evaluated using the V_T corrected for the plasma free fraction (f_p ; V_T/f_p) for the S1R, and the regional V_T normalised to the V_T in the centrum semiovale (DVR-1) for SV2A and MC1. Groups were compared using Mann-Whitney tests with Bonferroni correction for multiple comparisons. We found a significant reduction in regional density of SV2A in FTD compared to controls in multiple cortical and subcortical regions: frontal, temporal, parietal, insula, anterior cingulate and posterior cingulate cortices (all $p \leq 0.001$), as well as the hippocampus ($p=0.002$), thalamus ($p=0.001$) and cerebellum ($p=0.001$). Regional density of MC1 was also significantly reduced in frontal ($p=0.002$), insula ($p=0.002$), anterior cingulate ($p=0.001$) and posterior cingulate ($p=0.003$) cortices. Statistical comparisons were not performed for S1R as only two FTD scans were free from associated drug interactions at the S1R. Figure 1 illustrates the percentage differences in regional density of all proteins (and regional brain volumes) in FTD compared to controls. Evaluation of the full MINDMAPS-FTD cohort ($n=12$) will investigate the extent of molecular abnormalities in FTD and the relationship between regional densities and cognition.



Keywords: Frontotemporal dementia, synaptic, mitochondrial, biomarkers

P74: First-in-human evaluations of [¹¹C]PS13 for imaging COX-1 and [¹¹C]MC1 for imaging COX-2

Min-Jeong Kim¹, Fernanda Juarez Anaya¹, Jae-Hoon Lee¹, Jinsoo Hong¹, William Miller¹, Sanjay Telu¹, Cheryl Morse¹, Prachi Singh¹, Michelle Cortes-Salva¹, Katharine Henry¹, Yanira Ruiz-Perdomo², Jose Montero Santamaria¹, Jeih-San Liow¹, Sami Zoghbi¹, Masahiro Fujita¹, James Katz², Victor Pike¹, Robert Innis¹

¹Molecular Imaging Branch, National Institute of Mental Health, National Institutes of Health, Bethesda, MD, US

²National Institute of Arthritis and Musculoskeletal and Skin Diseases, National Institutes of Health, Bethesda, MD, US

Introduction: The cyclooxygenase (COX) system comprises two isoforms—COX-1 and COX-2—that are important targets for inflammatory biomarkers. We developed two PET radioligands: [¹¹C]PS13 for COX-1 and [¹¹C]MC1 for COX-2. This study sought to assess the distribution of binding and in vivo selectivity of [¹¹C]PS13 in healthy individuals and those of [¹¹C]MC1 in patients with rheumatoid arthritis.

Methods: Injection of radioligand was followed by dynamic PET scans. For [¹¹C]PS13, test-retest brain scans in 10 healthy individuals and whole-body scans in 24 healthy individuals were obtained. For [¹¹C]MC1, whole-body scans were obtained in two patients with rheumatoid arthritis and two healthy controls. Whole-body scans were repeated after administration of blocking drugs that preferentially target COX-1 (aspirin and ketoprofen) or COX-2 (celecoxib). Concurrent blood samples were obtained to measure concentrations of parent radioligand and radiometabolites.

Results: In baseline, substantial uptake of [¹¹C]PS13 was observed in most major organs, including the spleen, gastrointestinal tract, kidneys, and brain. This uptake was blocked by aspirin or ketoprofen but minimally blocked by celecoxib. In brain, [¹¹C]PS13 showed high uptake in the hippocampus and occipital cortices as well as pericentral cortices. When total distribution volume of [¹¹C]PS13 was calculated in brain, the overall test-retest variability was 6.0-8.5%. With [¹¹C]MC1, significantly higher uptake was observed in arthritic joints of the patients with rheumatoid arthritis compared to the corresponding joints of healthy controls. The increased uptake was blocked by celecoxib.

Conclusions: Our results suggest that COX-1 is constitutively expressed in major organs and that COX-2 is expressed in inflamed joints with rheumatoid arthritis. The in vivo selectivity of [¹¹C]PS13 and [¹¹C]MC1 was well demonstrated by pharmacological blockade. The test-retest reliability of brain [¹¹C]PS13 binding was also validated. Both [¹¹C]PS13 and [¹¹C]MC1 are potential probes for measuring brain and systemic inflammation in various conditions as well as target engagement by therapeutic drugs.

Keywords: Cyclooxygenase, PET, inflammation, neuroinflammation, rheumatoid arthritis

P75: [11C]MK-6884 PET tracer for M4 muscarinic cholinergic receptors in Alzheimer's disease: Comparison with [18F]FDG PET

Belen Pascual¹, Paolo Zanotti-Fregonara¹, Meixiang Yu¹, Quentin Funk¹, Victoria Arbones¹, Yuchuan Wang², Wenping Li², Amy Cheng², Matt Anderson², Eric D Hostetler², Anthony S Basile², Joseph C Masdeu¹

¹Houston Methodist Neurological Institute, Houston, TX, US

²Merck & Co. Inc., Kenilworth, NJ, US

Cholinergic neuron loss has long been known to be a hallmark of AD. The largest class of therapeutic agents targets acetylcholinesterase to increase acetylcholine availability. To evaluate regional cholinergic tone in individual patients and measure target engagement for potential therapies, it would be helpful to image muscarinic receptors *in vivo*. Several tracers have been developed over the years to image cholinergic receptors, but the findings have been either negative or too subtle to be useful. Recently, a M4 muscarinic cholinergic receptor PET tracer has been developed that shows good imaging characteristics. We report on the first group of AD patients to be studied with this tracer, [¹¹C]MK-6884.

Nine patients with Alzheimer's disease (MMSE=15.2±5.2), ages 60 to 76 years old (mean=68.9±5.5 years, five women), underwent [¹¹C]MK-6884 M4 receptor and [¹⁸F]FDG metabolism PET. After a bolus injection of approximately 370 MBq of [¹¹C]MK-6884, images were acquired over 90 minutes. Standardized uptake value ratios (SUVs) were calculated between 5 to 15 minutes using the cerebellum grey matter as the reference region. [¹⁸F]FDG SUVs were calculated following standard procedures, using the cerebellum grey matter as the reference region between 40 to 60 min.

As expected, [¹¹C]MK-6884 showed uptake in the basal ganglia, with low values in thalamus. Cortical uptake was reduced mostly in parieto-temporal association cortex, corresponding well with the clinical syndrome: patients with predominant language problems had greater loss in the left hemisphere and the opposite was true for those with visuospatial impairment. Frontal lobes were also affected, but not as much as the posterior structures. There was a concordance in cortical [¹¹C]MK-6884 and [¹⁸F]FDG PET values, indicating that the [¹¹C]MK-6884 binding was disease specific, but also discordant areas, highlighting the potential specificity of [¹¹C]MK-6884.

The initial experience with [¹¹C]MK-6884 suggests that this tracer may prove useful to image muscarinic receptors in AD.

Keywords: MK-6884 PET, FDG PET, M4 muscarinic cholinergic receptors, metabolism, Alzheimer's disease

P76: Assessing A β , tau, and reactive astrocytosis in aging and AD

Victor Villemagne^{1,7}, Ryuichi Harada^{2,3}, Vincent Doré^{1,4}, Shozo Furumoto², Rachel Mulligan¹, Yukitsuka Kudo³, Natasha Krishnadas¹, Kun Huang¹, Kazuhiko Yanai², Christopher Rowe^{1,6,7}, Nobuyuki Okamura^{2,5}

¹Department of Molecular Imaging & Therapy, Austin Health, Melbourne, Australia

²Department of Pharmacology, Tohoku University Graduate School of Medicine, Sendai, Japan

³Department of Geriatrics and Gerontology, Division of Brain Science, Institute of Development of Aging and Cancer, Tohoku University, Sendai, Japan

⁴CSIRO Health and Biosecurity Flagship: The Australian e-Health Research Centre, Melbourne, Australia

⁵Division of Pharmacology, Faculty of Medicine, Tohoku Medical and Pharmaceutical University, Sendai, Japan

⁶The Australian Dementia Network, Melbourne, Australia

⁷Department of Medicine, The University of Melbourne, Melbourne, Australia

Background: Alzheimer's disease (AD) is characterized by the accumulation of A β and tau along with an immune response. It has been proposed that reactive astrocytosis is an early event in the disease process. We aimed to characterize the regional distribution of A β and tau proteinopathies in relation to reactive astrocytosis as measured by a novel fluorinated MAO-B tracer, ¹⁸F-SMBT-1.

Methods: Nine participants, 5 healthy elderly controls (HC, 3F/2M, 78.5 \pm 6.0yrs) and 4 AD patients (3F/1M, 76.8 \pm 1.4yrs), underwent A β imaging with ¹⁸F-NAV4694, tau imaging with either ¹⁸F-MK6240 (n=7) or ¹⁸F-PI2620 (n=2), and MAO-B imaging with ¹⁸F-SMBT-1. A β burden was expressed in Centiloids. Tau tissue ratios were generated using the cerebellar cortex as reference region and expressed as z-scores. ¹⁸F-SMBT-1 studies were expressed as SUV or as tissue ratios using the cerebellar white matter as reference region. To ascertain ¹⁸F-SMBT-1 selective binding to MAO-B, participants underwent a second ¹⁸F-SMBT-1 scan after receiving 5mg selegiline twice daily for 5-days.

Results: As expected, A β and tau burdens were significantly higher in AD compared to controls (Fig. 1). ¹⁸F-SMBT-1 yielded high contrast images at 60-90 min post injection, with high tracer retention in basal ganglia, intermediate in neocortical regions, and lowest in cerebellum (Fig. 1). More than 85% of ¹⁸F-SMBT-1 signal was blocked by selegiline and no residual cortical activity was observed after the selegiline regimen (Fig. 2), indicating high selectivity for MAO-B. ¹⁸F-SMBT-1 retention was higher in AD patients in parahippocampus, fusiform and inferior temporal gyrus (Fig. 3). Despite the small number of HC (n=5) there were significant associations between rates of A β accumulation and ¹⁸F-SMBT-1 retention in several regions of the brain (Spearman's ρ 0.9, $p < 0.04$).

Conclusions: The confirmation of these preliminary findings with the highly selective MAO-B tracer ¹⁸F-SMBT-1 will require examination of a much larger series, also including participants with MCI.

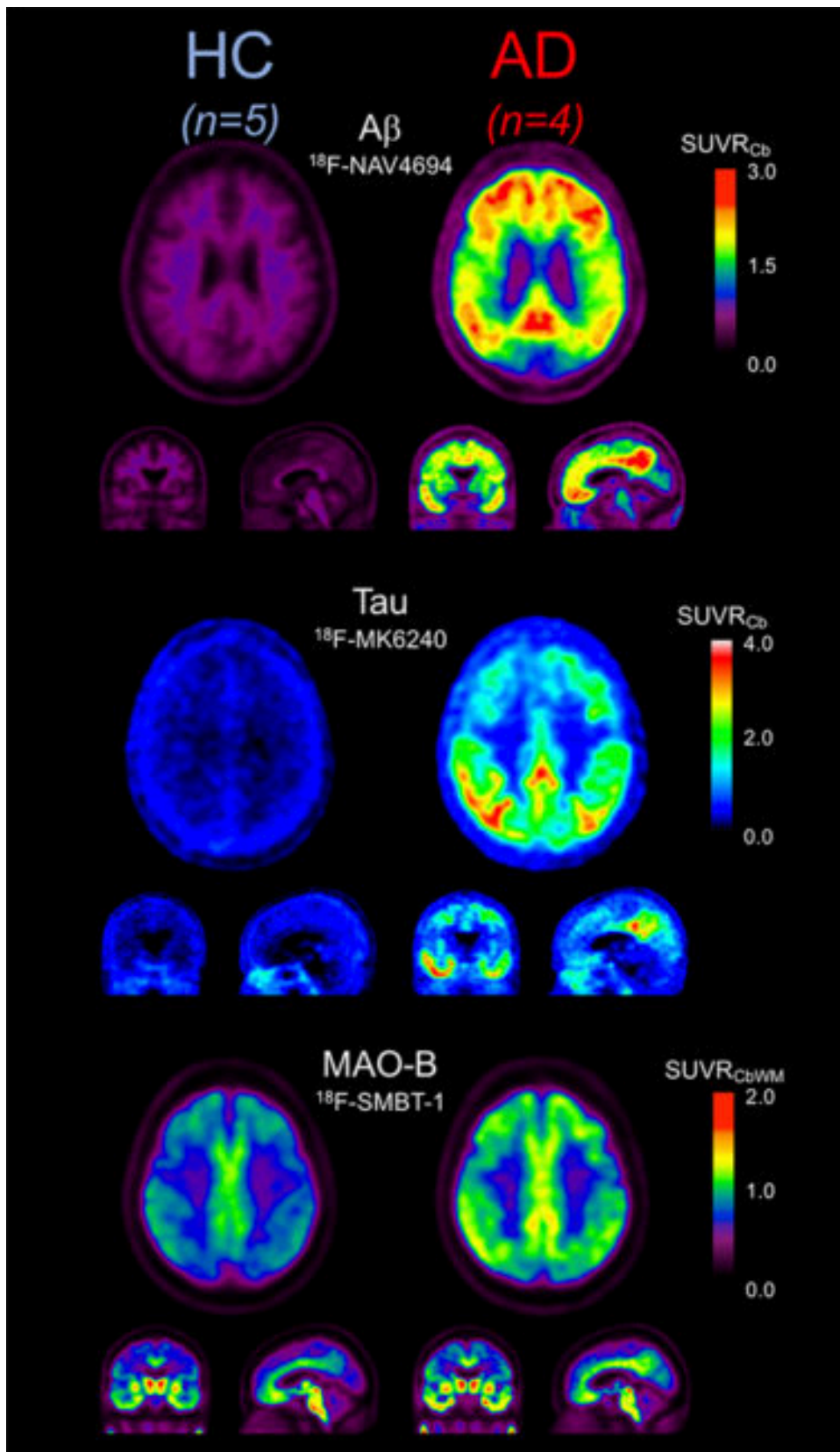


Figure 1. Average transaxial, coronal, and sagittal A β (^{18}F -NAV4694, top row), tau (^{18}F -MK6240, middle row) and MAO-B (^{18}F -SMBT-1, bottom row) PET images at 60-90 min post injection in HC (left column) and AD (right column). There was more widespread cortical and subcortical ^{18}F -SMBT-1 retention than the one observed with either ^{18}F -NAV4694 or ^{18}F -MK6240.

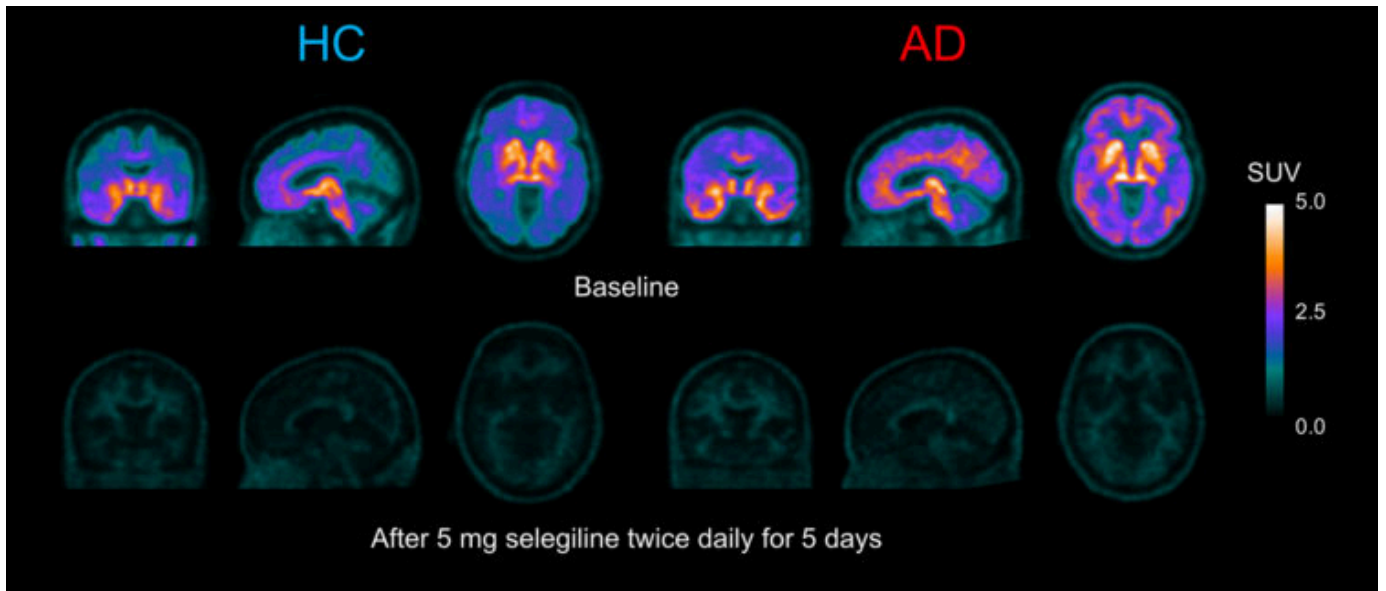


Figure 2. Representative coronal, sagittal and transaxial ^{18}F -SMBT-1 PET images at 60-90 min post injection in a HC (75 yo female, MMSE 28, on the left) and an AD patient (78 yo female, MMSE 21, on the right), before (top row) and after (bottom row) undergoing a twice daily 5 mg of selegiline for 5 consecutive days. More than 85% of the ^{18}F -SMBT-1 signal was blocked by selegiline, and no residual cortical activity was observed after the selegiline regimen.

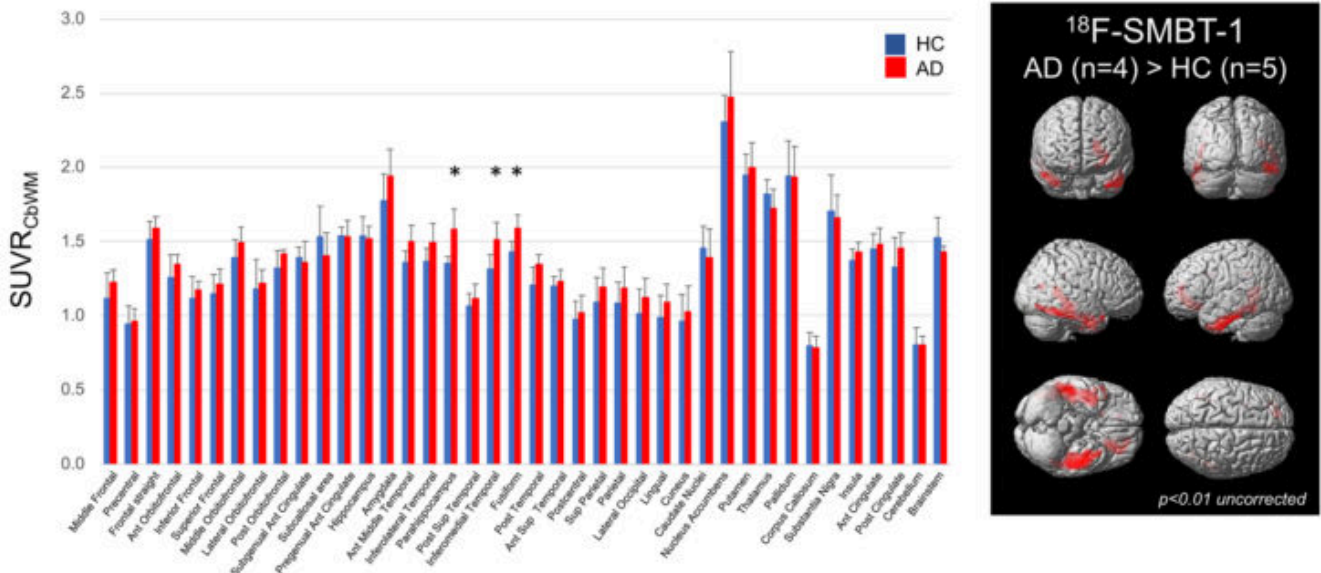


Figure 3. Bar graph (left) and SPM results (right) showing SMBT-1 regional brain retention at 60-90 min post injection in AD and HC. Highest SMBT-1 retention was observed in basal ganglia, intermediate in neocortical regions, and lowest in cerebellum. Despite the small sample size, SMBT-1 retention was higher in AD patients in parahippocampus, fusiform and inferior temporal gyri.

Keywords: Amyloid, tau, reactive astrocytosis, MAO-B

P77: A sensitive composite model to determine subtle cognitive differences in preclinical Alzheimer's disease

Alice Hahn^{1,2}, Young Ju Kim^{1,2}, Hee Jin Kim^{1,2}, Hyemin Jang^{1,2}, Soo Jong Kim^{1,2}, Duk L Na^{1,2,3}, Juhee Chin^{1,2,4}, Sang Won Seo^{1,2,4,5,6,7}

¹Department of Neurology, Samsung Medical Center, Sungkyunkwan University School of Medicine, Seoul, Korea

²Neuroscience Center, Samsung Medical Center, Seoul, Korea

³Stem Cell & Regenerative Medicine Institute, Samsung Medical Center, Seoul, Korea

⁴Samsung Alzheimer Research Center, Samsung Medical Center, Seoul, Korea

⁵Center for Clinical Epidemiology, Samsung Medical Center, Seoul, Korea

⁶Department of Health Sciences and Technology, SAIHST, Sungkyunkwan University, Seoul, Korea

⁷Clinical Research Design and Evaluation, SAIHST, Sungkyunkwan University, Seoul, Korea

Background: Recently, the focus of Alzheimer's disease (AD) research has shifted from the clinical stage to the preclinical stage. However, studies on the distinctive neuropsychological features of preclinical AD with adjusted measurement errors are insufficient. The present study aimed to investigate the distinctive cognitive features of preclinical AD and develop a cognitive composite model that can sensitively distinguish between the amyloid positive (A β +) and amyloid negative (A β -) status in cognitively normal (CN) elderly participants.

Methods: A total of 423 CN elderly participants with amyloid PET images were recruited. Using the multiple-indicator multiple-cause (MIMIC) model, sensitive cognitive domains to the A β + group were found. Then, several cognitive tests were selected to create the cognitive composite model as a result of the multivariate analysis of covariance (MANCOVA).

Results: The MIMIC model revealed that the domains of episodic memory and executive functions were significantly different between A β - and A β + ($p < 0.05$) participants. According to MANCOVA, the Seoul Verbal Learning Test-Elderly's version (SVLT-E) and the Rey-Osterrieth Complex Figure Test (RCFT) both distinguished between the A β + and the A β - groups on the delayed recall tests in terms of episodic memory ($p < 0.1$). On tests of executive functions, the A β + group performed worse than the A β - group in color reading of the Korean-Color Word Stroop test (K-CWST) and the animal naming of the Controlled Oral Word Association Test (COWAT) ($p < 0.1$). Consequently, the Preclinical Amyloid Sensitive Composite (PASC) model was comprised of SVLT-E delayed recall, RCFT delayed recall, K-CWST color reading, COWAT-animal, and the Korean Mini-Mental State Examination (K-MMSE) according to the results from our study and previous studies.

Conclusions: In the present study, we developed our own composite PASC model with the distinctive cognitive profiles of A β + CN individuals. Hence, this composite model can eventually contribute to not only early detection but also early interventions for AD.

Keywords: Preclinical Alzheimer's disease, cognitive composite, amyloid, neuropsychological test

P78: Amyloid deposition affects the topography of cortical thinning in Lewy Body Disease

Rong Ye¹, Alexandra Touroutoglou¹, Michael Brickhouse¹, Samantha Katz^{1,2}, John Growdon¹, Keith Johnson², Bradford Dickerson¹, Stephen Gomperts¹

¹Massachusetts General Hospital, Department of Neurology, Boston, MA, US

²Massachusetts General Hospital, Department of Radiology, Boston, MA, US

Background: Cortical atrophy in dementia with Lewy bodies (DLB) and Parkinson disease dementia (PDD) likely reflects extensive Lewy body pathology with alpha-synuclein deposits, as well as associated Alzheimer's disease co-pathologies, when present. Here we investigated the topographic distribution of cortical thinning in these Lewy body diseases compared to cognitively normal PD and healthy non-PD control subjects, explored the association of regional thinning with clinical features and evaluated the impact of amyloid deposition.

Methods: Twenty-one participants with dementia with Lewy bodies, 16 with Parkinson disease - associated cognitive impairment (PD-MCI and PDD), and 24 cognitively normal PD participants underwent MRI, PiB PET, and clinical evaluation. Cortical thickness across the brain and in regions of interest was compared across diagnostic groups to that of 115 age-matched healthy cognitively normal subjects acquired in previous studies and across subgroups stratified by amyloid status, and was related to clinical and cognitive measures.

Results: DLB and PD-impaired groups shared a similar distribution of cortical thinning that included regions characteristic of AD, as well as the fusiform, precentral, and paracentral gyri. Elevated PiB retention in DLB and PD-impaired but not in PD-normal participants was associated with more extensive and severe cortical thinning, in an overlapping topography that selectively affected the medial temporal lobe in DLB participants. In DLB, greater thinning in AD signature and fusiform regions was associated with greater cognitive impairment.

Conclusion: The pattern of cortical thinning is similar in DLB and PD-associated cognitive impairment, overlapping with and extending beyond AD signature regions to involve fusiform, precentral, and paracentral regions. Cortical thinning in AD signature and fusiform regions in these diseases reflects cognitive impairment and is markedly accentuated by amyloid co-pathology. The distinct topography of cortical thinning in DLB and PD-associated cognitive impairment might have value as a diagnostic and therapeutic biomarker in clinical trials.

Keywords: PiB, amyloid, cortical thinning, dementia with Lewy bodies, Parkinson disease dementia

P79: Longitudinal change in amyloid load over a 5-year period in cognitively healthy APOE4 carriers versus non-carriers: Effect of reference region

Emma Luckett^{1,2}, Katarzyna Adamczuk^{1,2,5}, Jolien Schaevebeke^{1,2}, Silvy Gabel^{1,2}, Koen Van Laere³, Patrick Dupont¹, Rik Vandenberghe^{1,2,4}

¹Laboratory for Cognitive Neurology, Department of Neurosciences, KU Leuven, Leuven, Belgium

²Alzheimer Research Centre KU Leuven, Leuven research Institute for Neuroscience & Disease, University of Leuven, Leuven, Belgium

³Department of Nuclear Medicine & Molecular Imaging, University Hospitals Leuven, Leuven, Belgium

⁴Neurology Department, University Hospitals Leuven, Leuven, Belgium

⁵Bioclinica LAB, 7707 Gateway Blvd, Newark, CA, US

Introduction: We aimed to elucidate the influence of APOE ε4 on changes in amyloid levels over time in the preclinical stage of Alzheimer's Disease (AD), using the Flemish Prevent AD Cohort KU Leuven (F-PACK cohort).

Methods: 53 cognitively intact healthy F-PACK participants (baseline age: 70 (56-80), 27 of which were APOE4 carriers, received a static [¹⁸F]flutemetamol-PET scan (acquisition window: 90-120 minutes), a structural MRI and neuropsychological test battery at recruitment (scores within norms) (2010-2015). They subsequently underwent a follow-up PET 4.8 years (3.4-6.28 years) after baseline. We calculated SUVRcomp in a neocortical volume of interest using cerebellar grey matter (CGM) or eroded subcortical white matter (ESWM) as a reference region at both timepoints. Spearman's correlation used to determine the influence of baseline SUVRcomp on follow-up SUVRcomp and t-tests to determine APOE4 effects. SUVRcomp cut-off: CGM=1.38; ESWM=0.68. Rate of change was defined as absolute change divided by time interval.

Results: There was a significant correlation between baseline and follow-up SUVRcomp when using either reference region (CGM: R=0.67, p=3.86e-08; ESWM: R=0.74, p=2.65e-10). There was a significant increase in SUVRcomp at follow-up (1.327±0.306) versus baseline (1.277±0.195) in APOE4 carriers, but only when using the CGM (CGM p=0.05; ESWM p=0.11). The rate of change observed in APOE4 carriers was higher than that in non-carriers (p = 0.04), however this was again not observed when using the ESWM (p=0.29). When above-threshold baseline participants were removed from the analyses, the difference in rate of change between APOE4 carriers versus non-carriers remained significant (CGM: p=0.03).

Conclusion: Amyloid rate of change is enhanced by APOE4. CGM is the more suited reference region to detect these longitudinal changes, compared to ESWM.

Keywords: Preclinical Alzheimer's Disease, APOE4, Amyloid

P80: Sex differences in the rates of cognitive decline associated with temporal lobe FTP-PET signal: findings from the Harvard Aging Brain Study

Rachel Buckley^{1,2,3}, Michael Properzi¹, Aaron Schultz¹, Heidi Jacobs¹, Dylan Kirm¹, Dorene Rentz^{1,2}, Bernard Hanseeuw^{1,4}, Keith Johnson¹, Reisa Sperling^{1,2}

¹Massachusetts General Hospital, Boston, MA, US

²Brigham and Women's Hospital, Boston, MA, US

³University of Melbourne, Melbourne, Australia

⁴Université Catholique de Louvain, Woluwe-Saint-Lambert, Belgium

Clinically-normal older women exhibit higher levels of ¹⁸F-Flortaucipir (FTP)-PET signal in temporal regions than men, however, an unanswered question is whether sex-divergent levels in tauopathy might influence cognitive trajectories.

We examined longitudinal cognitive trajectories in 251 clinically-normal participants with an FTP-PET scan (60% Female, Age=73(9.1)years). As FTP-PET was collected mid-study, cognitive time-points could occur prior (time=5.56(2.5)years) and post (time=2.41(1.8)years) FTP-PET scan. As sex-related survival biases may explain variance in our models, we ran boot-strapped joint-models of multivariate longitudinal and survival data, allowing for a linkage between random effects of both sub-models. For the longitudinal component we modeled the influence of sex and cross-sectional temporal FTP-PET SUVR (partial volume corrected [PVC]) on quadratic cognitive trajectories, adjusting for age, education and global Ab-PET DVR closest to FTP-PET. For the survival component, we modeled (1) attrition rates (definition: >18 months since last follow up; n=22), and (2) progression rates to MCI/dementia (n=18) between the sexes. For FTP-PET, a composite of bihemispheric regions of the temporal lobe (amygdala, fusiform gyrus, parahippocampal gyrus, inferior temporal lobe and entorhinal cortex) was created. For cognition, we used the Preclinical Alzheimer Cognitive Composite (PACC). We also examined non-PVC FTP-PET signal.

Women showed faster rates of PACC decline than men in higher levels of FTP-PET (B(SE)=-0.16(0.5),95%CI[-0.36,-0.006];Fig.1), after adjusting for baseline covariates and survival due to attrition (HR=1.17,95%CI[0.52,3.15]; Fig.2A). This effect disappeared (B(SE)=-0.01(0.01),95%CI[-0.03,0.002]) after adjusting for female-elevated risk for progression to a clinical diagnosis (HR=2.25,95%CI[0.47,8.4]; Fig.2B).

Sex moderated the association between temporal lobe tau deposition and global cognitive decline, and this effect was driven by women who were more likely to attain a clinical diagnosis. Notably, women tended to outperform men on this verbal-centric cognitive composite at lower levels of FTP-PET. These findings support sex-differentiated susceptibility to tau as a rationale for faster progression to a clinical diagnosis in women.

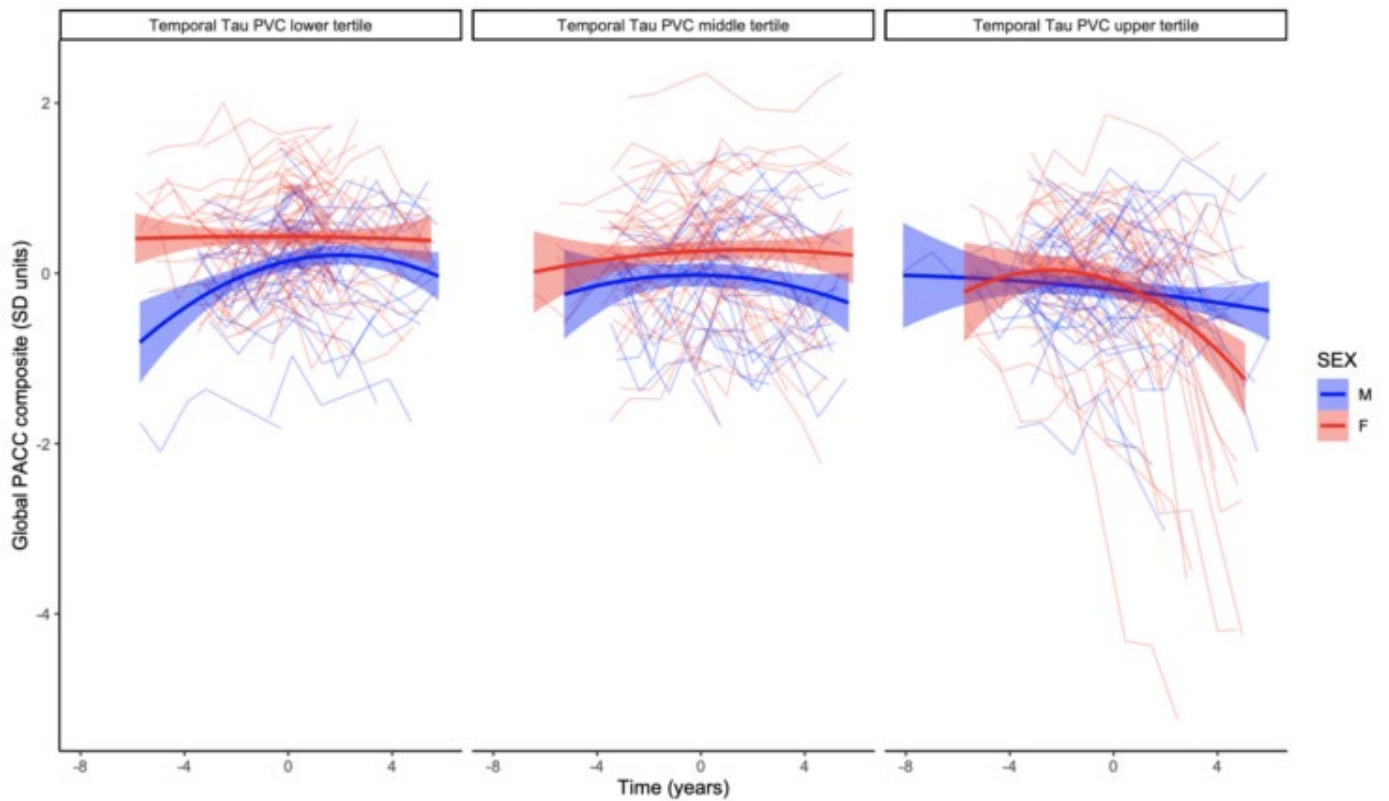


Figure 1. Spaghetti plot of cognitive trajectories over time (0th time represents the first FTP-PET scan) and faceted by a tertile split of temporal lobe FTP-PET signal with quadratic fit curves stratified by sex.

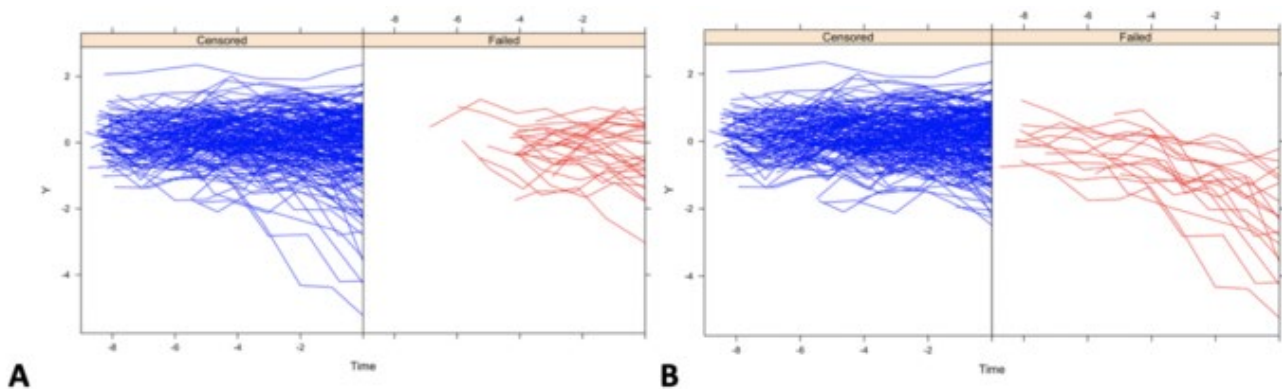


Figure 2. (A) PACC trajectories up to final time point prior to attrition (failed panel) or to the end of the study (censored) (B) PACC trajectories up to final time point prior to clinical diagnosis (failed panel) or to the end of the study (censored)

Keywords: sex differences; cognitive decline; tau-PET; clinical-progression; boot-strapped joint modelling

P81: Amyloid and tau PET burden are associated with white matter bundle abnormalities in asymptomatic individuals at risk of Alzheimer's disease

Alexa Pichet Binette¹, Guillaume Theaud², Julie Gonneaud¹, Judes Poirier¹, Maxime Descoteaux², Sylvia Villeneuve¹

¹*McGill University, Montreal, QC, Canada*

²*Université de Sherbrooke, Sherbrooke, QC, Canada*

Background: A β and *tau* proteins follow distinct patterns of regional accumulation in the brain. Regions preferentially affected by one protein or the other are connected with well-defined major white matter bundles. However, if pathology affects white matter fibers early in the course of Alzheimer's disease is still unclear. In asymptomatic older adults, we investigated relationships between A β and *tau* burden and diffusion metrics in bundles typically affected in Alzheimer's disease dementia.

Methods: We included 126 asymptomatic older adults (PREVENT-AD cohort, mean age=67 \pm 5). Diffusion-weighted MRI was used to reconstruct whole-brain tractogram from which white matter bundles of interest (anterior cingulum, posterior cingulum, uncinate fasciculus) were extracted (Fig.1). Free-water corrected diffusion metrics (fractional anisotropy; mean, radial and axial diffusivity) were extracted in each bundle. A β ([18F]NAV4694) and *tau* ([18F]AV-1451) SUVRs were extracted specifically at the cortical endpoints of each bundle. Using regression models, we tested for each bundle whether different diffusion metrics were associated with A β and *tau* at its endpoints.

Results: A β or *tau* were not associated with any diffusion metrics in the anterior or posterior cingulum. Higher free-water corrected fractional anisotropy and axial diffusivity in the left and right uncinate fasciculus was related to higher *tau* SUVR at the cortical endpoints of the uncinate fibers, especially in the temporal lobe (Fig.2). Results were independent of age, bundle volume and A β burden. Correlations in the opposite directions were observed with free-water corrected mean and radial diffusivity (Table 1). The same associations were observed with A β in the left uncinate fasciculus, when *tau* is not included in the model.

Conclusions: Diffusion metrics in the uncinate fasciculus, a bundle that connects the orbitofrontal cortex and anterior temporal lobe, were specifically related to *tau* burden at the endpoints of this bundle. We hypothesize that diffusion changes might be an early correlate of pathological insults.

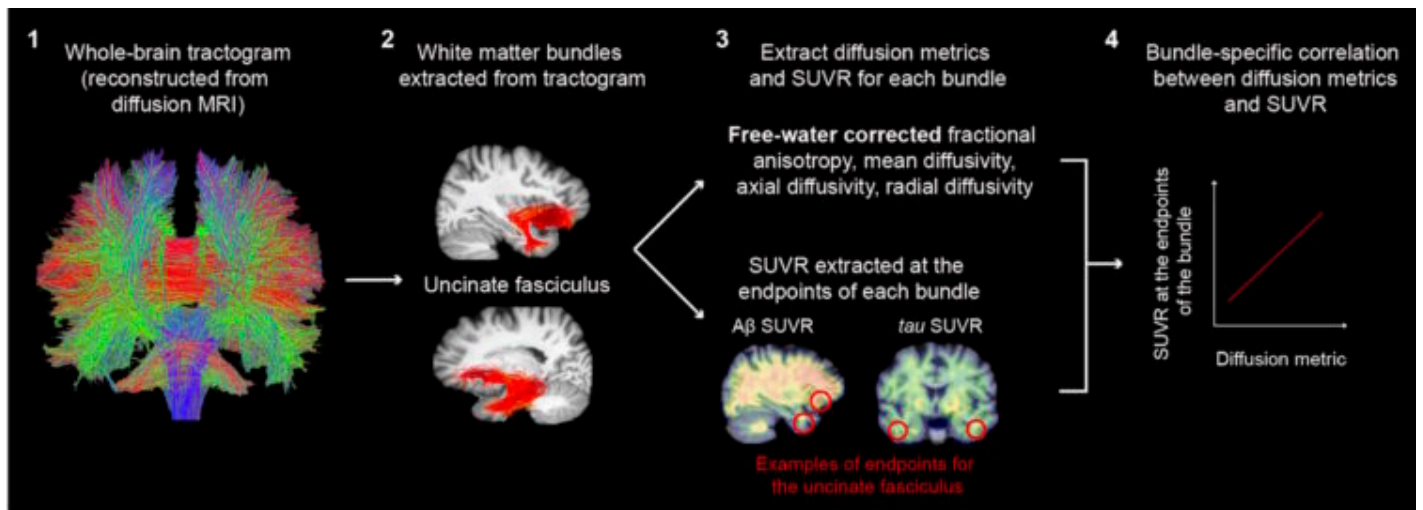


Figure 1. Overview of the processing pipeline. For each participant, a tractogram was reconstructed from the diffusion-weighted MRI using the pipeline *Tractoflow*. White matter bundles of interest (anterior cingulum, posterior cingulum and uncinatus fasciculus) were extracted using *Recobundle*. The uncinatus fasciculus is shown as an example. Free-water corrected diffusion metrics were calculated for each bundle. A β and tau SUVR was extracted at the cortical endpoints of each bundle. All computations were done in native-space of each participant.

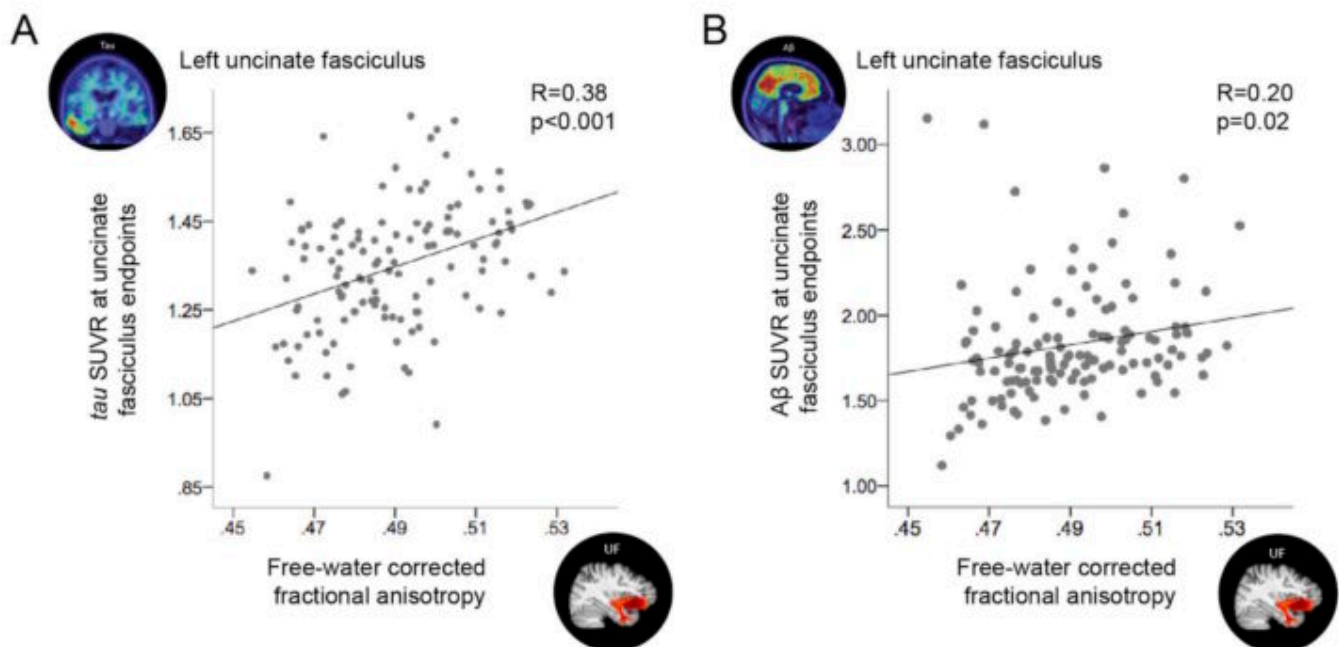


Figure 2. Correlations between free-water corrected fractional anisotropy and pathology in the left uncinatus fasciculus. Univariate correlations between free-water corrected fractional anisotropy in the left uncinatus fasciculus and tau SUVR at the cortical endpoints of the bundle (A) and A β SUVR at the cortical endpoints of the bundle (B).

Tau SUVR				
	Left uncinat fasciculus		Right uncinat fasciculus	
	Frontal endpoints SUVR	Temporal endpoints SUVR	Frontal endpoints SUVR	Temporal endpoints SUVR
Free-water corrected metrics				
Fractional anisotropy	0.23**	0.37***	0.17	0.23**
Axial diffusivity	0.19*	0.27***	0.12	0.19*
Mean diffusivity	-0.23**	-0.37***	-0.16	-0.23**
Radial diffusivity	-0.23**	-0.37***	-0.16	-0.23**
Aβ SUVR				
	Left uncinat fasciculus		Right uncinat fasciculus	
	Frontal endpoints SUVR	Temporal endpoints SUVR	Frontal endpoints SUVR	Temporal endpoints SUVR
Free-water corrected metrics				
Fractional anisotropy	0.17*	0.19*	0.11	0.13
Axial diffusivity	0.11	0.12	0.08	0.16
Mean diffusivity	-0.17*	-0.19*	-0.11	-0.13
Radial diffusivity	-0.17*	-0.19*	-0.11	-0.13

Table 1. Correlation coefficients between diffusion metrics in the uncinat fasciculus and Aβ and tau. Partial correlation coefficients between free-water corrected diffusion metrics in the left and right uncinat fasciculus and Aβ or tau SUVR at the cortical endpoints of the bundle (in the frontal and temporal lobe respectively). Correlations are adjusted for age and volume of the bundle. Relationships with tau hold when further adjusting for Aβ SUVR. Relationships with Aβ do not hold when further adjusting for tau SUVR. *2-sided p<0.05; ** p<0.01; *** p<0.001.

Keywords: amyloid, tau, white matter, preclinical

P82: NeuroToolkit CSF biomarkers track the progression of Alzheimer's disease at very early stages and show that inflammatory markers modulate cerebral amyloid accumulation

Gemma Salvadó^{1,2,3}, José Luis Molinuevo^{1,2,3,4}, Marta Milà-Alomà^{1,2,4}, Kaj Blennow^{5,6}, Henrik Zetterberg^{5,6,7,8}, Grégory Operto^{1,2,3,4}, Carles Falcón^{1,2,9}, Richard Batrla¹⁰, Mark Battle¹¹, Christopher Buckley¹¹, Gill Farrar¹¹, Carolina Minguillon^{1,2,4}, Karine Fauria^{1,2,4}, Gonzalo Sánchez-Benavides^{1,2,4}, Marc Suárez-Calvet^{1,2,4}, Juan Domingo Gispert^{1,2,3,9}, on behalf of the ALFA study¹

¹Barcelonabeta Brain Research Center, Pasqual Maragall Foundation, Barcelona, Spain

²IMIM (Hospital del Mar Medical Research Institute), Barcelona, Spain

³Universitat Pompeu Fabra, Barcelona, Spain

⁴CIBER Fragilidad y Envejecimiento Saludable (CIBERFES), Madrid, Spain

⁵Clinical Neurochemistry Laboratory, Sahlgrenska University Hospital, Mölndal, Sweden

⁶Department of Psychiatry and Neurochemistry, Institute of Neuroscience and Physiology, Sahlgrenska Academy at University of Gothenburg, Sahlgrenska University Hospital, Mölndal, Sweden

⁷Department of Neurodegenerative Disease, UCL Institute of Neurology, Queen Square, London, UK

⁸UK Dementia Research Institute at University College London, London, UK

⁹Centro de Investigación Biomédica en Red de Bioingeniería, Biomateriales y Nanomedicina (CIBER-BBN), Madrid, Spain

¹⁰Roche Diagnostics International Ltd, Roche Diagnostics, Rotkreuz, Switzerland

¹¹GE Healthcare Life Sciences, Amersham, UK

Introduction: The NeuroToolkit consists of a set of cerebrospinal fluid (CSF) biomarkers that have been developed to identify Alzheimer's disease (AD) co-pathologies, identify and characterize disease progression and monitor treatment response. In this work, we aimed at assessing the association between the NeuroToolkit biomarkers and cerebral amyloid deposition in a group of cognitively unimpaired individuals in the ALFA+ cohort.

Methods: A total of 326 cognitively unimpaired individuals from the ALFA+ cohort (mean age(SD): 61.5 (4.7) years) underwent a lumbar puncture and amyloid [¹⁸F]flutemetamol PET imaging. Biomarkers in the NeuroToolkit (see Figure 1) were determined using prototype Roche Elecsys® assays. In addition, CSF pTau levels were also measured in the same individuals using the commercially available Elecsys® CSF assay. PET images were scaled to SUV_r using the whole cerebellum as reference region and Centiloid values were derived. We calculated cross-correlation values between NeuroToolkit biomarkers and Centiloids. Voxel-wise associations between NeuroToolkit biomarkers and [¹⁸F]flutemetamol images were sought after accounting for the effect of age, sex, education and *APOE-ε4* status. Additional analyses were performed after correcting also for the Aβ₄₂/40 ratio or Centiloid values.

Results: Associations between NeuroToolkit biomarkers and Centiloids are shown in **Figure 1**. NeuroToolkit biomarkers were significantly associated with cerebral amyloid deposition as measured by [¹⁸F]flutemetamol (**Figure 2**). After correcting for global amyloid deposition, higher levels of the astroglial CSF marker YKL-40 were associated with increased amyloid deposition in the inferior and lateral temporal lobe, in parietal and orbitofrontal areas, as well as in the caudate heads (**Figure 3**).

Conclusions: Results show that the NeuroToolkit biomarkers track AD progression, as measured by [¹⁸F]flutemetamol PET, in cognitively unimpaired individuals. For the same global cerebral amyloid levels, higher YKL-40 levels were associated with regional increments of [¹⁸F]flutemetamol uptake, which supports for an early involvement of the astroglial response to cerebral amyloid deposition.

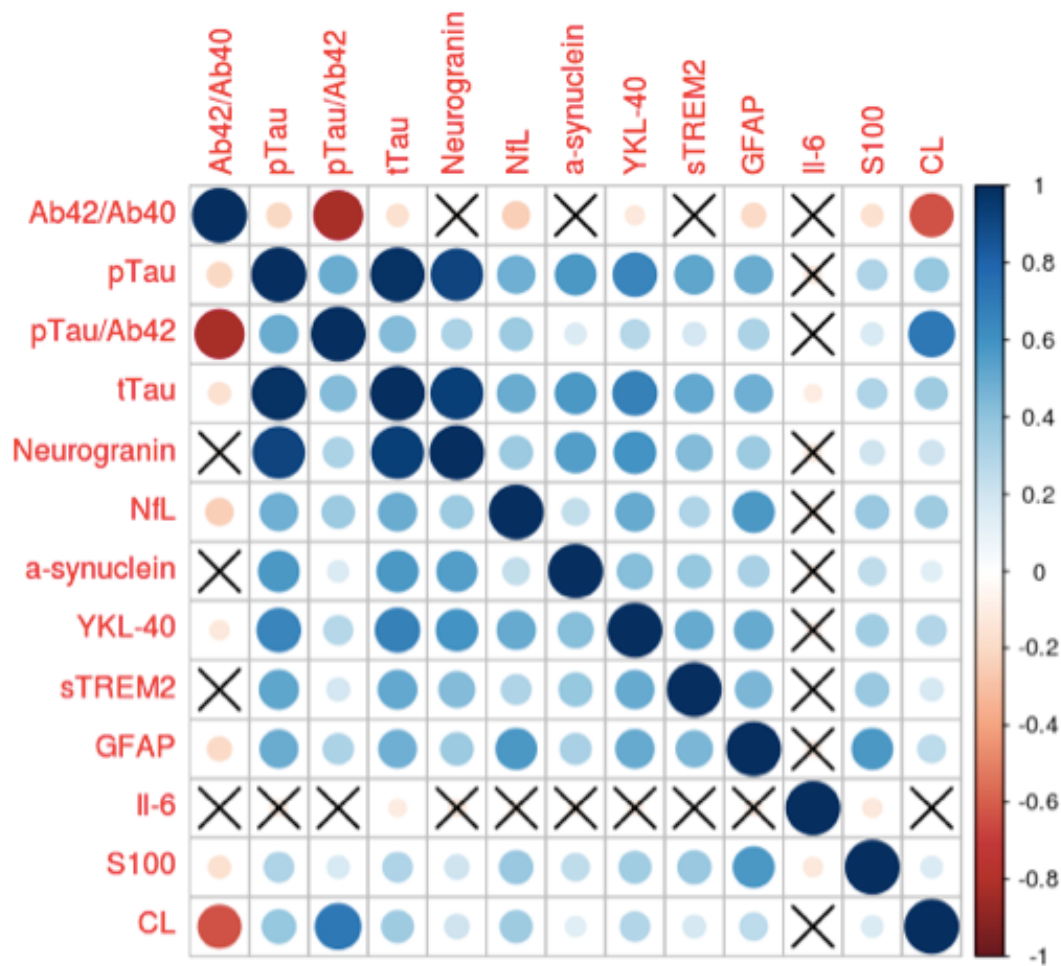


Figure 1: Cross-correlation between biomarkers measured using Elecsys® CSF assays and Centiloid values, as measured by Pearson's correlation. Crosses represent non-significant association ($p > 0.05$).

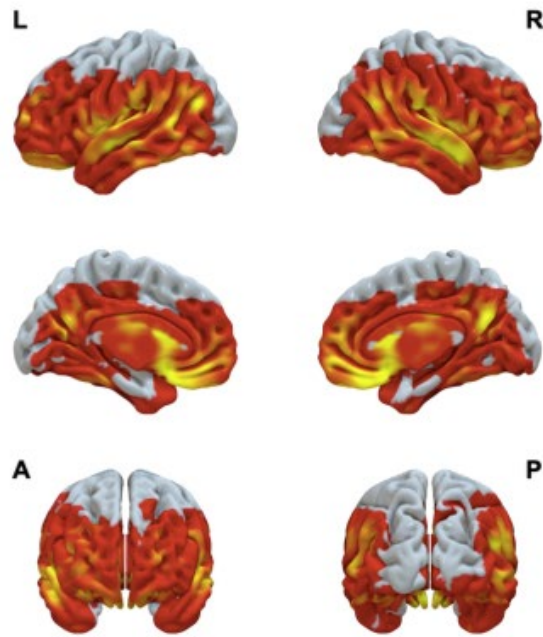


Figure 2: Areas of significant positive correlation between CSF pTau levels and [¹⁸F]flutemetamol PET uptake ($p < 0.001$, $k > 100$) once adjusted by age, sex, education, *APOE-ε4* status and Aβ_{42/40} CSF levels.

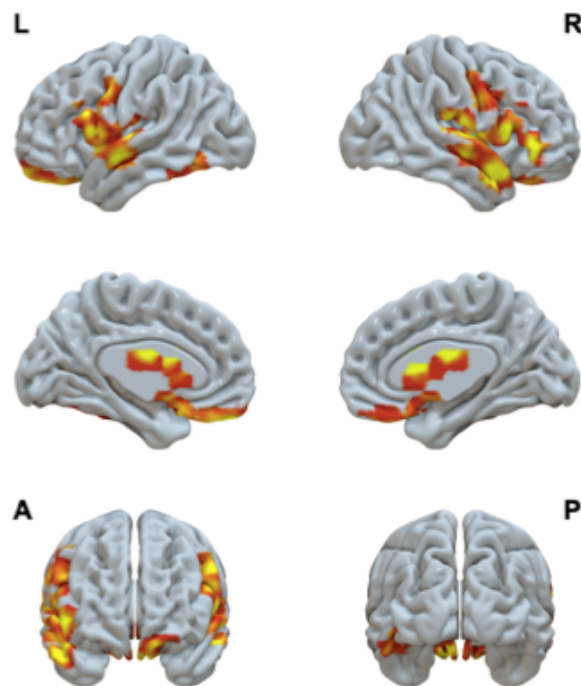


Figure 3: Areas of significant positive correlation between CSF YKL-40 levels and [¹⁸F]flutemetamol PET uptake ($p < 0.005$, $k > 100$) once adjusted by age, sex, education, *APOE-ε4* status and global amyloid deposition (Centiloids).

Keywords: amyloid PET, CSF, inflammation, early stages, cognitively unimpaired

P83: T1rho MRI measurement of amyloid plaque burden in cognitively unimpaired individuals: preliminary results in the ALFA+ cohort

Carles Falcón^{1,2,3}, Paula Montesinos⁴, Oriol Grau-Rivera^{1,3,5}, Marc Suárez-Calvet^{1,3,5}, Albert Puig-Pijoan^{6,7}, Diego Cascales^{1,6}, Irene Navalpotro-Gomez^{1,6}, Aida Fernández-Lebrero^{1,6}, Raquel Sánchez-Valle^{8,9}, Ellen Gelpi^{9,10}, Coral Sanfeliu^{11,12}, Santiago Rojas¹³, Andrés Perissinotti^{9,14}, Aida Niñerola-Baizán^{2,14}, Gemma Salvadó^{1,3,15}, Carolina Minguillon^{1,3,5}, Karine Fauria^{1,3,5}, José Luis Molinuevo^{1,3,5,15}, Javier Sánchez-González⁴, Juan Domingo Gispert^{1,2,3,15}, on behalf of the ALFA study¹

¹Barcelonabeta Brain Research Center, Pasqual Maragall Foundation, Barcelona, Spain

²Centro de Investigación Biomédica en Red de Bioingeniería, Biomateriales y Nanomedicina (CIBER-BBN), Madrid, Spain

³IMIM (Hospital del Mar Medical Research Institute), Barcelona, Spain

⁴Philips Healthcare, Madrid, Spain

⁵CIBER Fragilidad y Envejecimiento Saludable (CIBERFES), Madrid, Spain

⁶Department of Neurology, IMIM-Hospital del Mar, Barcelona, Spain

⁷Neurofunctionality and Language Group, Neurosciences Program, Hospital del Mar Research Institute (IMIM), Barcelona, Spain

⁸Alzheimer's Disease and Other Cognitive Disorders Unit, Hospital Clínic, Fundació Clínic per a la Recerca Biomèdica, Barcelona, Spain

⁹Institut d'Investigacions Biomèdiques August Pi i Sunyer (IDIBAPS), Universitat de Barcelona, Barcelona, Spain

¹⁰Neurological Tissue Bank and Neurology Department, Hospital Clínic de Barcelona, Universitat de Barcelona, Centres de Recerca de Catalunya (CERCA), Barcelona, Spain

¹¹Institut d'Investigacions Biomèdiques de Barcelona (IIBB), Consejo Superior de Investigaciones Científicas (CSIC), Barcelona, Spain

¹²CIBER de Epidemiología y Salud Pública (CIBERESP), Instituto de Salud Carlos III, Madrid, Spain

¹³Unit of Human Anatomy and Embryology, Department of Morphological Sciences, Faculty of Medicine, Universitat Autònoma de Barcelona, Bellaterra, Spain

¹⁴Nuclear Medicine Department, Hospital Clínic, Barcelona, Spain

¹⁵Universitat Pompeu Fabra, Barcelona, Spain

Background: Previous studies have demonstrated higher T1rho MRI in Alzheimer's Disease (AD) patients compared to control individuals. However, the extent to which T1rho is able to track the progression of core AD biomarkers in cognitively unimpaired individuals remains to be determined. In this study, we show preliminary results of the association between T1rho values and beta-amyloid (A β) deposition levels as measured by PET in cognitively unimpaired individuals.

Methods: Sixteen cognitively unimpaired individuals with a positive [¹⁸F]flutemetamol PET scan were selected from the ALFA+ cohort. T1-weighted (T1W) and T1rho sequences were acquired in a 3T Ingenia CX Philips scanner. The T1rho acquisition protocol consisted in 3D volumes weighed with five different spin-lock times of 0, 20, 40, 60 and 80 ms, respectively. All volumes were acquired with a 3D-View-FLAIR (TE/TI/TR = 21/1650/4800 ms, of 2x2x2 mm³ spatial resolution), with a scan time per volume of 130 s. T1rho maps were estimated according to a monoexponential decay and coregistered to T1W scans. [¹⁸F]flutemetamol PET scans of the same individuals were used to obtain Centiloid values using an in-house validated pipeline. T1rho values were averaged in the Centiloid cortical Volume of Interest (VOI) in the normalized space. Association between T1rho values and PET-derived Centiloids was assessed using correlation analysis.

Results: Of the 16 individuals scanned, 1 T1rho maps was discarded due to movement artifacts. In the

remaining 15 cases, there was a positive association between T1rho values and Centiloid values (Figure 2) which showed a tendency for significance (Spearman's rho = 0.499; p = 0.069).

Conclusion: Preliminary results indicate that T1rho MRI could potentially track cerebral amyloid accumulation in cognitively unimpaired individuals. Further research is underway to extend these results to amyloid-negative individuals and AD patients. In addition, associations with CSF core AD biomarkers (A β and p-tau) will also be sought.

Figure 1: Example of a T1rho MRI scan (top) and corresponding T1-weighted image (bottom).

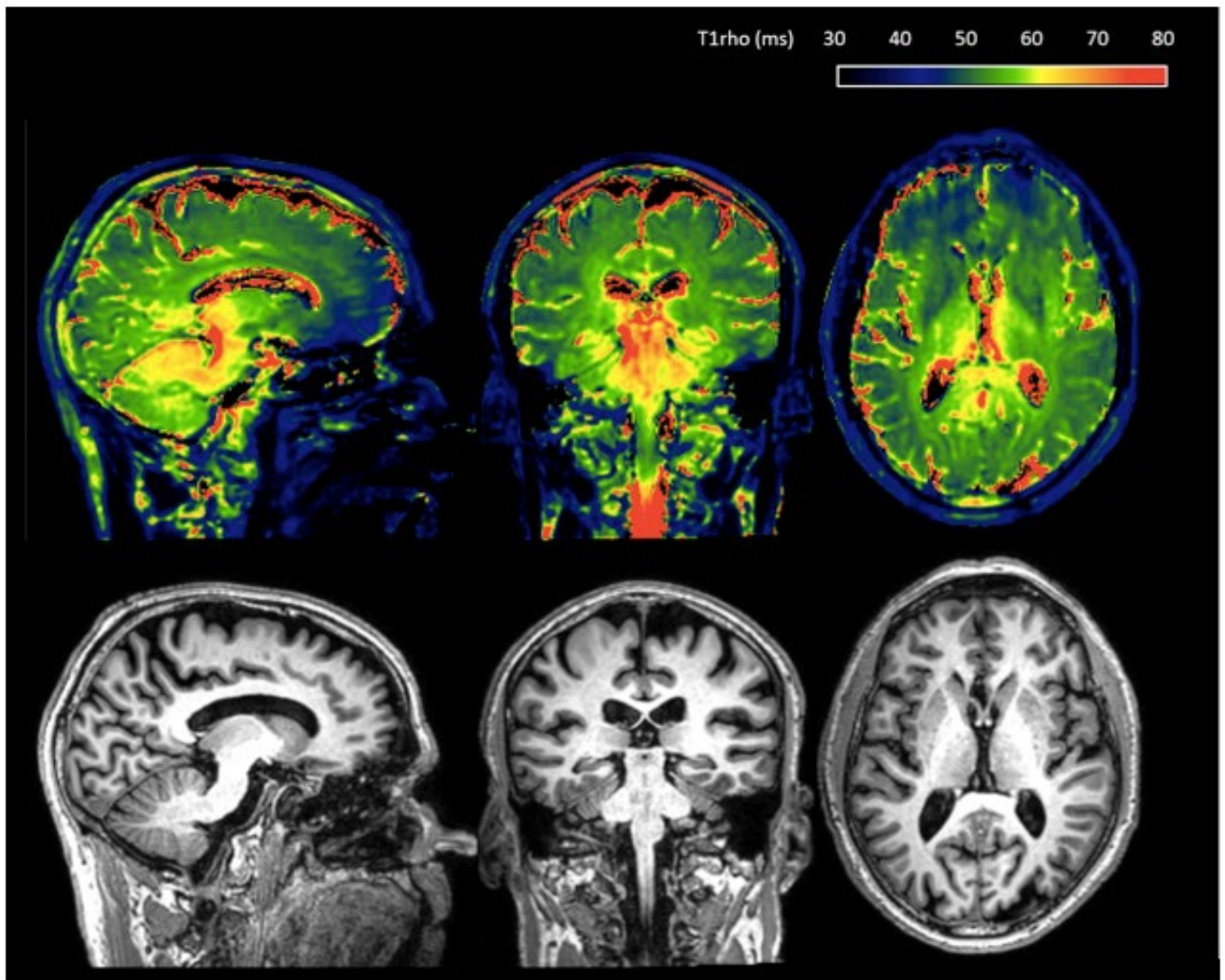
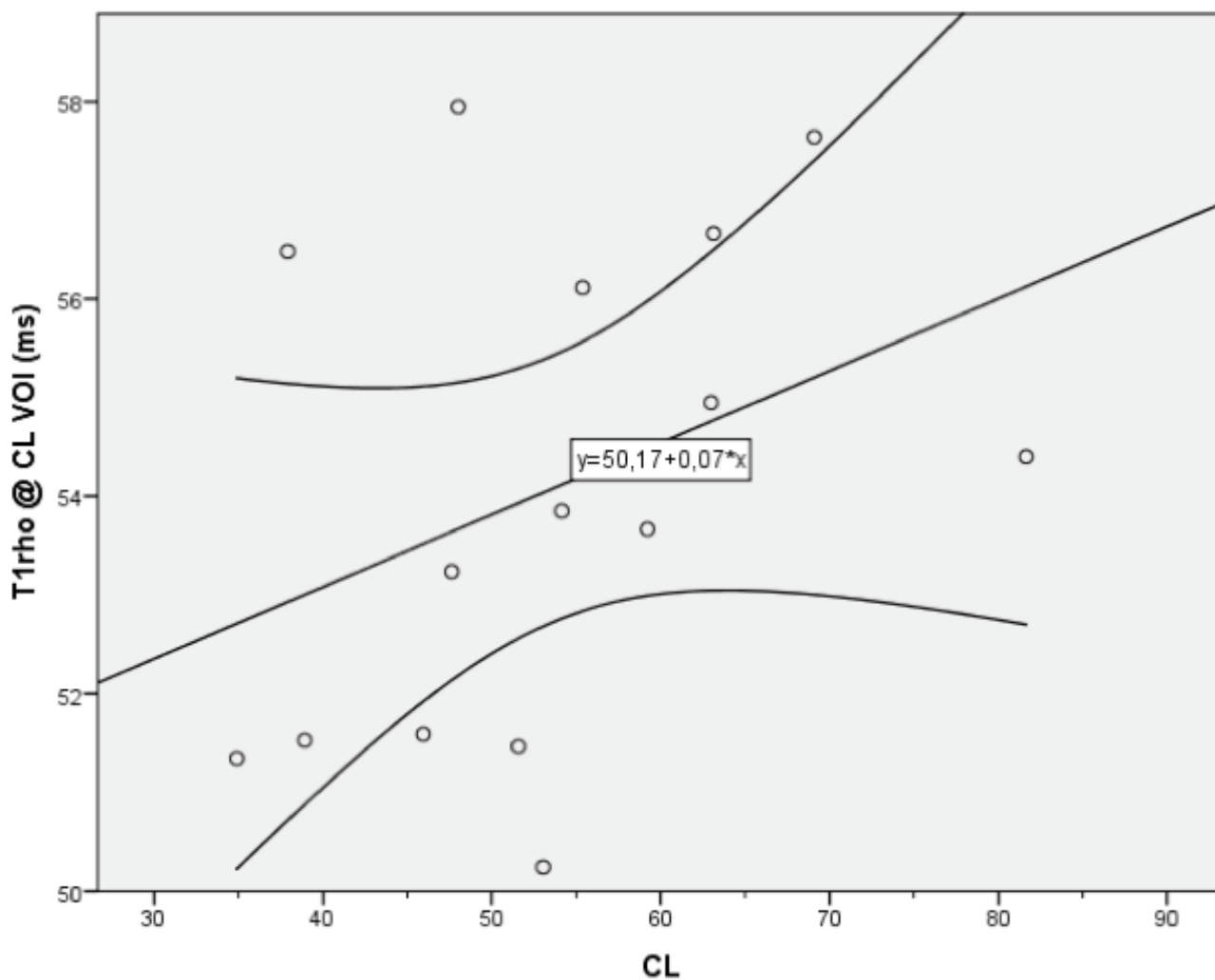


Figure 2: Scatterplot of the association between T1rho values in the standard Centiloid mask and Centiloid values derived from [¹⁸F]flutemetamol PET.



Keywords: T1rho, amyloid PET, cognitively unimpaired

P84: Preliminary quantitative results of the AMYPAD prognostic and natural history study

Juan Domingo Gispert^{1,2,3,4}, Isadora Lopes-Alves⁵, Katherine Gray⁶, Christopher Buckley⁷, Lyduine Collij⁵, Fiona Heeman⁵, Gemma Salvadó^{1,2,3}, Phillip Scheltens⁵, Giovanni Frisoni⁸, Craig W Ritchie⁹, Bruno Vellas¹⁰, Andrew W Stephens¹¹, Lisa Ford¹², José Luis Molinuevo^{1,2,3,13}, Gill Farrar⁷, Frederik Barkhof^{5,14}, on behalf of the AMYPAD Consortium¹⁵

¹Barcelonabeta Brain Research Center, Pasqual Maragall Foundation, Barcelona, Spain

²IMIM (Hospital del Mar Medical Research Institute), Barcelona, Spain

³Universitat Pompeu Fabra, Barcelona, Spain

⁴Centro de Investigación Biomédica en Red de Bioingeniería, Biomateriales y Nanomedicina (CIBER-BBN), Madrid, Spain

⁵Amsterdam UMC, Vrije Universiteit Amsterdam, Amsterdam, The Netherlands

⁶IXICO Plc, London, UK

⁷GE Healthcare Life Sciences, Amersham, UK

⁸University of Geneva, Geneva, Switzerland

⁹University of Edinburgh, Edinburgh, UK

¹⁰Centre Hospitalo-Universitaire de Toulouse, Toulouse, France

¹¹Life Molecular Imaging, GmbH, Berlin, Germany

¹²Janssen Research and Development, Titusville, NJ, US

¹³CIBER Fragilidad y Envejecimiento Saludable (CIBERFES), Madrid, Spain

¹⁴Institute of Neurology and Healthcare Engineering, University College London, London, UK

¹⁵This work has received support from the EU-EFPIA Innovative Medicines Initiatives 2 Joint Undertaking (grant No 115952), Amsterdam, The Netherlands

Background: The AMYPAD Prognostic and Natural History Study (PNHS) is an open-label, prospective, multi-centre cohort study (<http://amypad.eu/>) to evaluate the additional value of quantitative amyloid PET imaging in determining Alzheimer's Disease (AD) dementia risk. The AMYPAD PNHS aims at recruiting 2000 non-demented individuals with a particular focus on those with emerging amyloid pathology. Here, we provide preliminary results of AMYPAD PNHS.

Methods: As of September 30th 2019, 290 participants had consented to participate in the study. Of those, 215 had been scanned with either [¹⁸F]flutemetamol or [¹⁸F]florbetaben in 5 sites (VUmc Amsterdam, University of Edinburgh, Barcelonaβeta Brain Research Center; University of Geneva and Centre Hospitalier Universitaire de Toulouse). By that date, 108 PET scans and their corresponding T1-weighted MR images had been analyzed with IXICO's LEAP pipeline. The primary variable is the Centiloid value (CL) using the whole cerebellum as reference region, in order to enable quantitative comparability between the two tracers in the study. Subjects were categorized as negative (CL<12); in the gray-zone (12<CL<50) or positive (CL>50) and the association between continuous CL values and age was assessed.

Results: The first 108 consecutive participants in the AMYPAD PNHS had a mean age of 67.08 ± 7.71 years and 59% of them were female. Forty-five of them (42%) were negative, 40 (37%) in the gray-zone and 23 (21%) positive. The distribution of Centiloid values is shown in Figure 1 and ranged from -12.75 to 141.79 CL. As expected, CL values showed a positive association with age (p<0.001), with similar behavior for the two radiotracers in the study (Figure 2).

Conclusion: The AMYPAD Prognostic and Natural History Study is currently ongoing and 11 additional sites are expected to be actively recruiting by the end of 2019. Preliminary quantitative results indicate that the trial is effectively recruiting the intended target population.

Figure 1. Distribution of Centiloid values in the first consecutive 108 participants of AMYPAD PNHS

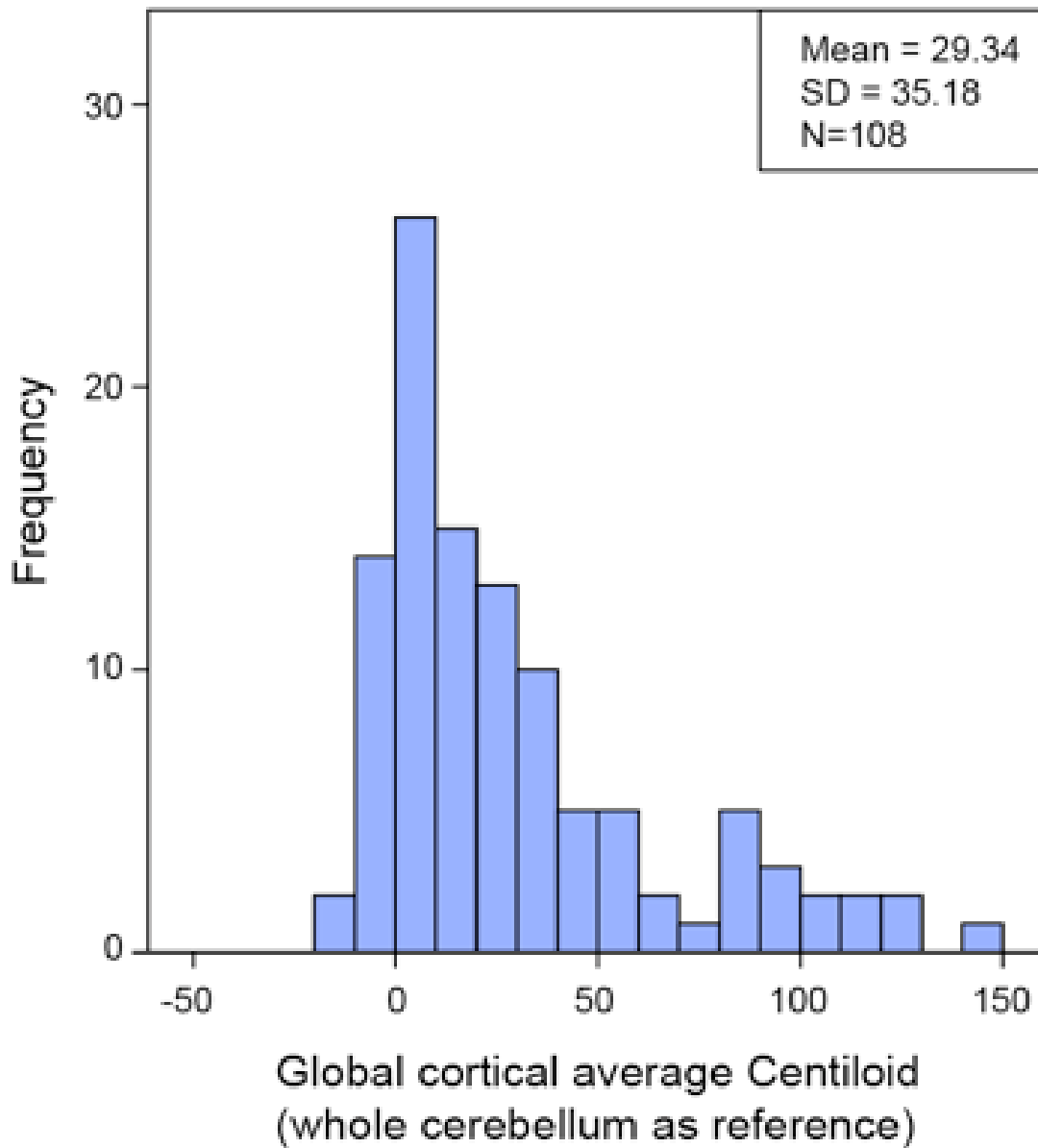
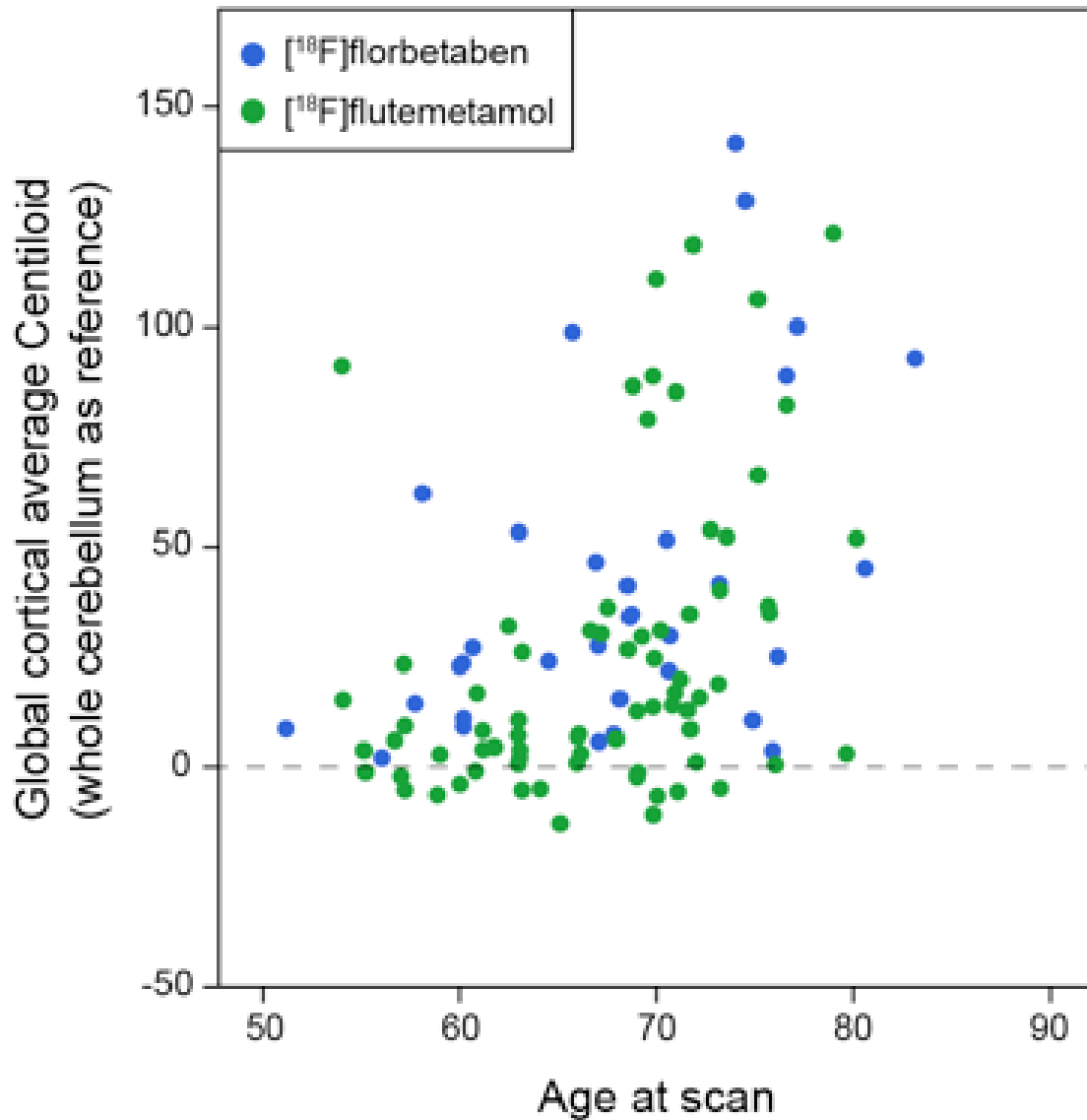


Figure 2. Scatter plot of Centiloid values and age. Colors indicate the radiotracer used (green: [^{18}F]flutemetamol; blue: [^{18}F]florbetaben)



Keywords: Amyloid PET, gray zone, early accumulation, multi-tracer, Centiloid

P85: Sex differences in regional tau deposition in cognitively impaired patients with Alzheimer's disease

Lauren Edwards¹, Renaud La Joie¹, Leonardo Iaccarino¹, Minseon Kim¹, Suzanne Baker², Kaitlin Casaletto¹, Bruce Miller¹, William Jagust^{2,3}, Gil Rabinovici^{1,2,3}

¹Memory and Aging Center, Department of Neurology, Weill Institute for Neurosciences, University of California, San Francisco, San Francisco, CA, US

²Life Sciences Division, Lawrence Berkeley National Laboratory, Berkeley, CA, US

³Helen Wills Neuroscience Institute, University of California, Berkeley, Berkeley, CA, US

Introduction: We assessed sex differences in the burden of amyloid and tau pathology quantified via PET in cognitively impaired patients with AD.

Methods: 118 patients with mild cognitive impairment or dementia due to AD underwent MRI, 18F-flortaucipir (FTP) tau-PET and 11C-PiB amyloid-PET. All were PiB-positive and received a neuropsychological evaluation that included the MMSE and episodic memory testing. We created SUVR images using tracer-specific reference regions (PiB: cerebellar grey matter, FTP: inferior cerebellar grey matter) and extracted cortical SUVR values using patient-specific native-space Freesurfer-derived masks. Regression models tested sex differences in 1) cognition, 2) regional FTP- and 3) global PiB-PET SUVR, adjusting for age and disease severity (Clinical Dementia Rating Sum of Boxes, CDR-SoB).

Results: Female patients were younger than males; no other demographic differences were observed (Table 1). MMSE, episodic memory and CDR-SoB did not differ adjusting for age (Table 1). Females had higher FTP SUVR than males in the entorhinal and inferior temporal cortices, as well as in the precuneus and superior parietal lobule (Figure 1). No sex effects were detected in the thalamus, putamen or choroid plexus, areas of known FTP off-target binding (Figure 1). Sex effects on FTP remained largely unchanged controlling additionally for PiB SUVR (Figure 2). Conversely, PiB SUVR was higher in females (2.14 ± 0.35 vs 2.00 ± 0.36 ; $p=0.047$, partial η^2 [η^2p]=0.03) but this effect was attenuated when adjusting for temporal FTP SUVR ($p=0.15$, $\eta^2p=0.02$). ApoE4 frequency did not differ by sex (Table 1) and sex effects on FTP were largely unchanged when controlling additionally for ApoE4 status. No ApoE4*sex interaction was observed ($p \geq 0.08$, $\eta^2p \leq 0.03$).

Conclusions: Women showed greater cortical tau burden than men with comparable cognitive and functional impairment, implying that women may have greater resilience to AD pathology. Characterization of sex differences will crucially inform AD pathogenesis and support development of personalized therapeutic strategies.

Table 1. Demographic, functional and cognitive comparisons of males and females in our sample of patients with AD

	Female (n=61)	Male (n=57)	p
Age, avg. [range]	64.0 [47-95]	67.4 [51-85]	0.047
Years of education, avg. [range]	16.9 [12-24]	17.0 [12-25]	0.893
Caucasian race reported, no. (%) (subgroup)	52 (91%) (n=57)	55 (98%) (n=56)	0.098
ApoE4 +, no. (%) (subgroup)	31 (57%) (n=54)	24 (51%) (n=47)	0.523
CDR-SoB, avg. [range]	3.76 [0-11]	4.25 [0.5-13]	0.203 ^a
MMSE, avg. [range]	21.9 [5-30]	21.8 [8-30]	0.587 ^a
Episodic memory composite z-score, avg. [range] (subgroup)	-0.04 [-1.36-2.28] (n=59)	0.06 [-1.22-2.04] (n=56)	0.437 ^a

^a Adjusted for age

Differences in demographic characteristics were assessed using student's t-test and χ^2 for continuous and categorical data, respectively. Differences in cognitive and functional scores were assessed using ANCOVA.

Figure 1. Sex differences in regional FTP SUVR, adjusting for age and CDR-SoB

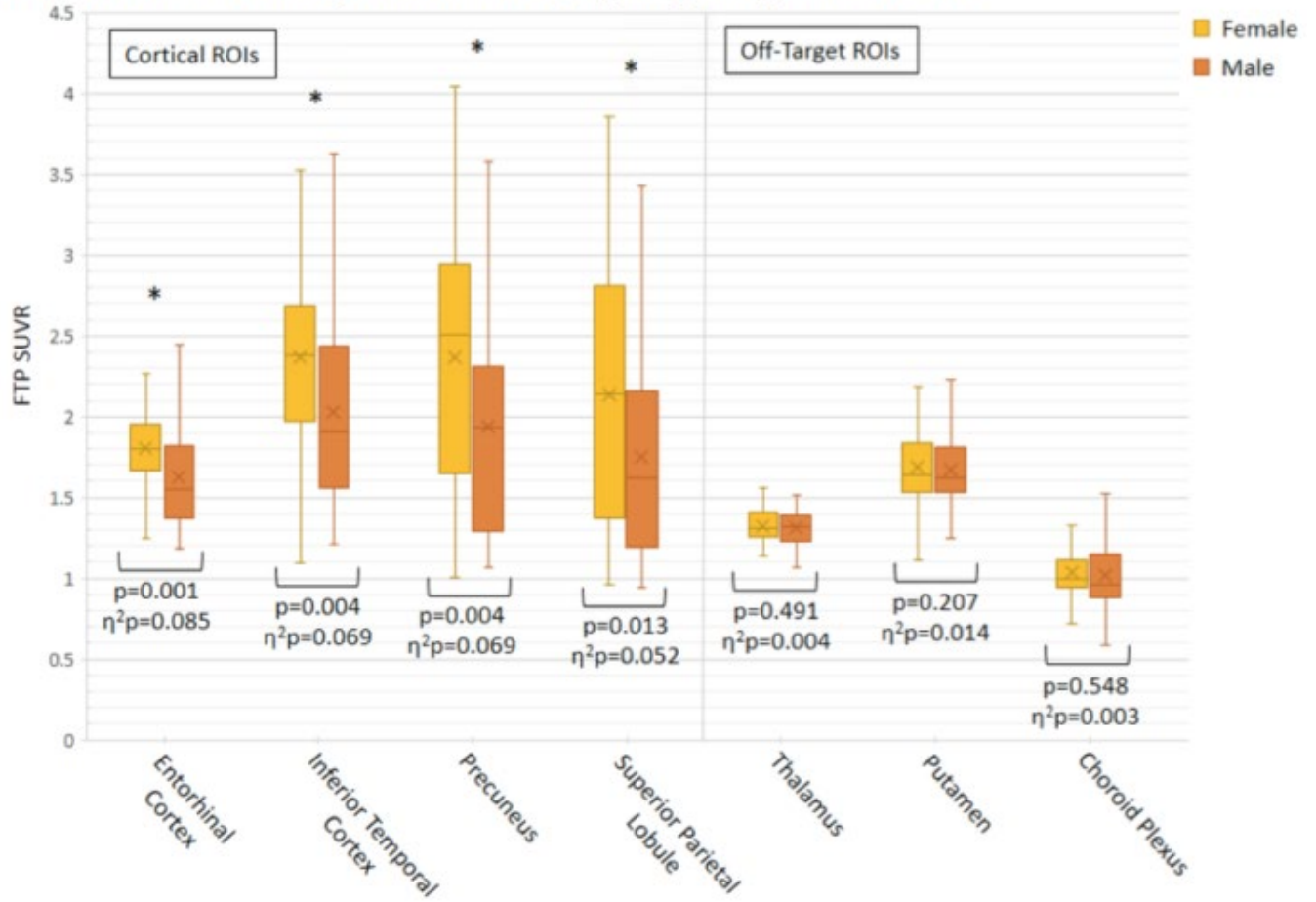
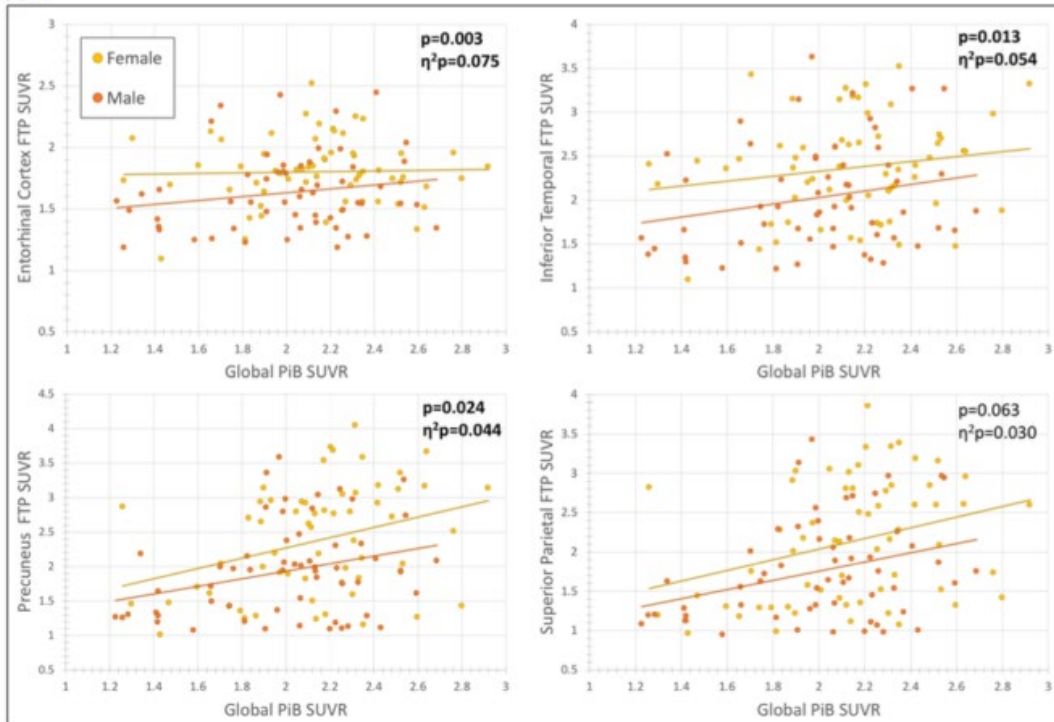


Figure 2. Sex differences in cortical FTP SUVR, adjusting for global amyloid burden in addition to age and CDR-SoB



Keywords: Alzheimer's disease, Flortaucipir, sex

P86: Cross-sectional and longitudinal non-dichotomized CSF/PET A β data support existence of “CSF+ first” vs. “PET+ first” pathways of A β biomarkers changes

Arianna Sala^{1,2,3}, Agneta Nordberg^{1,4}, Elena Rodriguez-Vieitez¹

¹*Division of Clinical Geriatrics, Department of Neurobiology, Care Sciences and Society, Karolinska Institutet, Stockholm, Sweden*

²*Vita-Salute San Raffaele University, Milan, Italy*

³*In vivo human molecular and structural neuroimaging Unit, Division of Neuroscience, IRCCS San Raffaele Scientific Institute, Milan, Italy*

⁴*Theme Aging, Karolinska University Hospital Huddinge, Stockholm, Sweden*

Recently, we provided evidence that discordance in results of CSF vs. PET A β -biomarkers represents a natural phase in the progression of A β -pathology, with either CSF *or* PET becoming abnormal first. Given the methodological limitations for defining cut-off values, in this study we aimed at testing whether existence of “CSF+ first” vs. “PET+ first” pathways of A β biomarkers changes is also supported by statistical modelling of non-dichotomized cross-sectional and longitudinal CSF/PET data.

We retrospectively selected N=867 cases from ADNI, ranging from cognitively normal to overtly demented, with CSF-A β 42 and [18F]Florbetapir-PET measurements obtained within three months. Additional CSF/PET measurements were available at 2-year follow-up in N=289 cases. “CSF+ first” vs. “PET+ first” pathways were identified by fitting of the whole CSF/PET cross-sectional and longitudinal data to a hyperbolic regression model ($R^2=0.62-0.63$), followed by an analysis of residuals in every individual subject.

The residual-based classification was very stable, with 83.7% of cases in each pathway being classified again likewise at 2-year follow-up. As expected, residuals analysis resulted in assignment of 100% of CSF+/pet- and csf-/PET+ discordant cases to the “CSF+ first” (residuals<0) and “PET+ first” (residuals>0) pathway, respectively. In contrast, the concordant groups (csf-/pet- and CSF+/PET+) had a mixed distribution of residuals, resulting in variable assignment to either “CSF+ first” or “PET+ first” pathways, consistently with longitudinal findings. Significant differences in sex, number of APOE- ϵ 4 alleles and polygenic hazard score were found between pathways. Increased levels of CSF A β 40 and A β 38 were consistently reported in subjects belonging to the “PET+ first” pathway.

In conclusion, cross-sectional and longitudinal non-dichotomized CSF/PET data support the existence of “CSF+ first” and “PET+ first” pathways of A β biomarkers changes, with genetic determinants leading each subject towards one pathway or the other. Differences in efficiency of removal of A β isoforms from brain to CSF might account for these observations.

Keywords: amyloid, Alzheimer’s disease, biomarker, CSF-A β 42, Florbetapir-PET

P87: Personality and amyloid accumulation in cognitively normal aging

Bora Yoon¹, Suzanne Baker², Deniz Korman², Victoria Tennant³, Theresa Harrison³, William Jagust^{2,3}

¹*Department of Neurology, Konyang University College of Medicine, Daejeon, Korea*

²*Molecular Biophysics and Integrated Bioimaging, Lawrence Berkeley National Lab, Berkeley, CA, US*

³*Helen Wills Neuroscience Institute, University of California, Berkeley, CA, US*

Backgrounds: Little is known about the association between personality and Alzheimer's disease (AD) biomarkers, and they have had inconsistent results yet. We aimed to determine whether personality was associated with amyloid accumulation in cognitively normal aging.

Methods: One hundred twenty-nine participants were included in this cross-sectional study. Personality was measured with the Big Five Inventory (BFI) and brain β amyloid deposition was assessed with mean distribution volume ratio (DVR) for [¹¹C] Pittsburgh compound B (PiB)-positron emission tomography (PET) imaging.

Results: ICC for agreeableness, conscientiousness, extraversion, neuroticism, and openness were 0.747, 0.824, 0.909, 0.790, 0.851, respectively, which meant BFI showed good reliability. Conscientiousness scores had a negative association with PiB_DVR in not only all participants (β [SE]=-0.19[0.08], $p=0.022$) but also PiB positive group only (β [SE]=-0.19[0.08], $p=0.034$).

Conclusions: This result indicates that conscientiousness is negatively associated with amyloid accumulation in cognitively normal aging. This suggests the possibility that conscientiousness plays a protective role in amyloid accumulation.

Keywords: personality, conscientiousness, amyloid, positron emission tomography

P88: Head-to-head comparison of F-Florbetaben and F-Flutemetamol uptakes in the cortex, striatum and white matter

Sang Won Seo¹, Soo Hyun Cho², Seung Hwan Moon, Yeong Sim Choe, Duk L. Na

¹*Department of Neurology, Samsung Medical Center, Sungkyunkwan University School of Medicine, Seoul, Korea*

²*Department of Neurology, Chonnam National University Hospital, Chonnam National University Medical School, Gwang-ju, Korea*

³*Department of Nuclear medicine, Samsung Medical Center, Sungkyunkwan University School of Medicine, Seoul, Korea*

Purpose: ¹⁸F-florbetaben (FBB) and ¹⁸F-flutemetamol (FMM) have been developed and approved for clinical use. It is important to understand the characteristics and differences of these ligands. We aimed to compare the imaging characteristics including a dynamic range of retention and the difference of quantitative measurement between FBB and FMM in the cortical, striatal and white matter (WM) regions.

Methods: Paired FBB and FMM PET images were acquired on two separate days in mean 4.0 ± 2.5 months interval times in 107 participants. We measured FBB and FMM SUVRs in the cortex, striatum, and WM using several reference regions (cerebellar gray matter (CG), whole cerebellum (WC), WC with brainstem (WC + B) and pons).

Results: The global cortical SUVR ($R^2 = 0.97$) and striatal SUVR ($R^2 = 0.95$) demonstrated excellent linear correlation between FBB and FMM. For amyloid- β ($A\beta$) deposition in global cortex and WM, FBB SUVR was significantly higher than FMM SUVR ($p < 0.001$). However, in the case of $A\beta$ deposition in striatum, FMM SUVR was significantly higher than FBB SUVR ($p < 0.001$). The effect size of differences in the cortical SUVR between $A\beta$ (+) AD and YC with FMM (3.01) was similar with that of FBB (2.92). However, the effect size of differences in the striatal SUVR seemed to be higher in FMM (2.61) than in FBB (2.34). Specifically, all reference regions consistently showed that there was no difference in the cortical SUVR ratio between two ligands but the striatal SUVR ratio was higher in FMM than in FBB.

Conclusions: Our findings suggested that FBB and FMM ligands are highly correlated each other and similar cortical retention with a little variance according to reference region, indicating these ligands are comparable for imaging amyloid pathology in vivo. However, FMM seems slightly superior to FBB in assessing striatal $A\beta$ burdens.

Keywords: Florbetaben, Flutemetamol, Amyloid imaging, Alzheimer's disease

P89: Sleep impairment predicts longitudinal accumulation of β -amyloid

Joseph Winer¹, Bryce Mander², William Jagust^{3,4}, Matthew Walker^{1,3}

¹*Department of Psychology, Center for Human Sleep Science, University of California, Berkeley, CA, US*

²*Department of Psychiatry and Human Behavior, University of California Irvine, Orange, CA, US*

³*Helen Wills Neuroscience Institute, University of California, Berkeley, CA, US*

⁴*Molecular Biophysics and Integrated Bioimaging, Lawrence Berkeley National Lab, Berkeley, CA, US*

Background: Sleep disturbance has been shown to predict β -amyloid ($A\beta$) burden in healthy older populations cross-sectionally. It remains untested whether objective measures of sleep quality predict the rate of $A\beta$ accumulation over time.

Methods: 32 healthy older adults (age 75.5 ± 4.3 at baseline, 23 female) received overnight sleep EEG recording to assess sleep architecture and slow wave activity (SWA). All subjects additionally received multiple ¹¹C-PIB PET scans to assess longitudinal change in $A\beta$ burden (2.5 ± 0.8 scans over 3.6 ± 2.3 years). A global cortical ¹¹C-PIB DVR (0-90 min, cerebellar gray reference) was calculated for every PET image, and a linear mixed-effects model was used to derive slopes of ¹¹C-PIB DVR change over time for every subject. All analyses were adjusted for age at baseline and gender, and longitudinal analyses were additionally adjusted for number of PET scans per subject.

Results: Lower <1Hz SWA at baseline predicted not only higher cross-sectional ¹¹C-PIB DVR, but further predicted an accelerated rate of ¹¹C-PIB DVR increase over time. This was similarly true for the measure of poor sleep efficiency, predicting both baseline and rate of ¹¹C-PIB DVR increase. The significance of these associations were attenuated when baseline ¹¹C-PIB DVR was included in the models, due to the strong correlation between ¹¹C-PIB DVR baseline and longitudinal change.

Conclusions: These findings demonstrate that impaired electrophysiological sleep quality (<1Hz SWA) and objective poor sleep quantity are not only sensitive to an individual's $A\beta$ burden at the time of measurement, but also predictive of subsequent accelerated $A\beta$ aggregation. Sleep may therefore serve as an informative, non-invasive and scalable biomarker for assessing pathological progression of Alzheimer's disease. If replicated in larger cohorts with high sensitivity, specificity, and accuracy, these objective sleep metrics may also provide a practical and cost-effective measure for tracking treatment intervention efficacy.

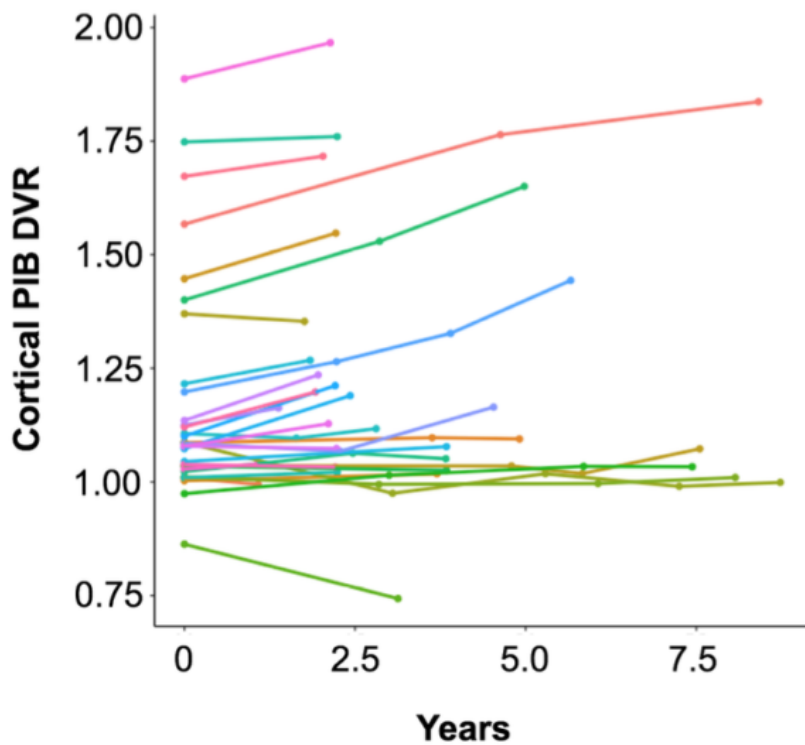


Figure 1. Spaghetti plots show individual trajectories of PIB DVR over time. Each point represents a PIB PET scan.

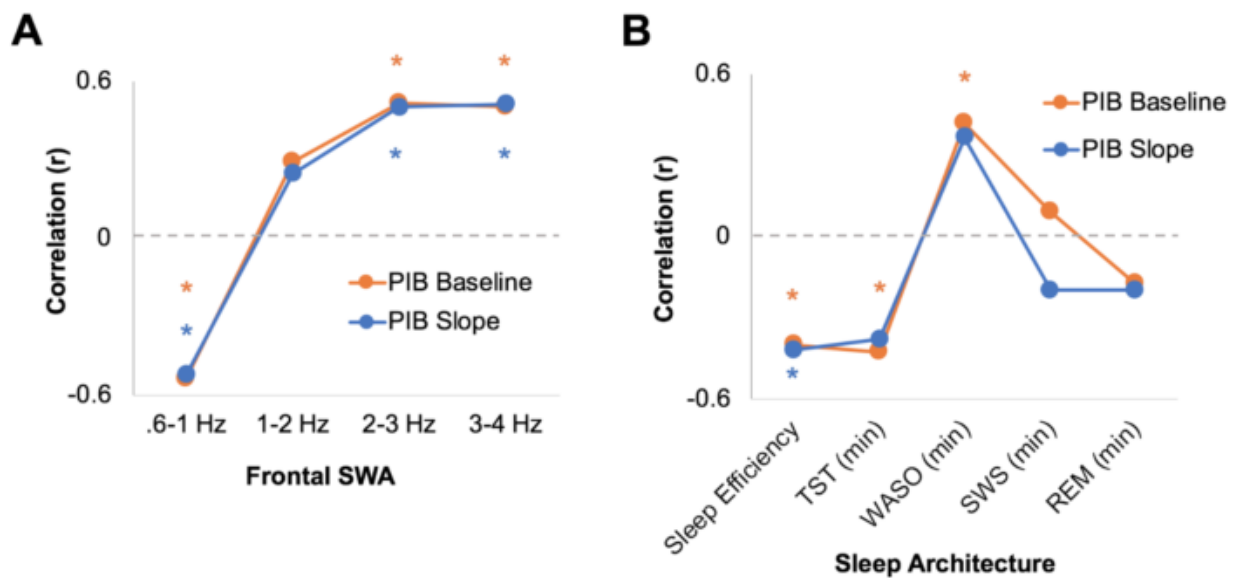


Figure 2. A) For both cross-sectional and longitudinal measures of PIB DVR, slow wave activity (SWA) below 1Hz is negatively associated with cortical PIB DVR, and SWA frequencies greater than 1Hz are positively associated with cortical PIB DVR. B) Greater sleep efficiency and more total sleep time predicted lower PIB DVR, and greater wake after sleep onset predicted greater PIB DVR. * notes $p < 0.05$, all analyses adjusted for age at baseline and gender, slope analyses additionally adjusted for number of PET scans per subject.

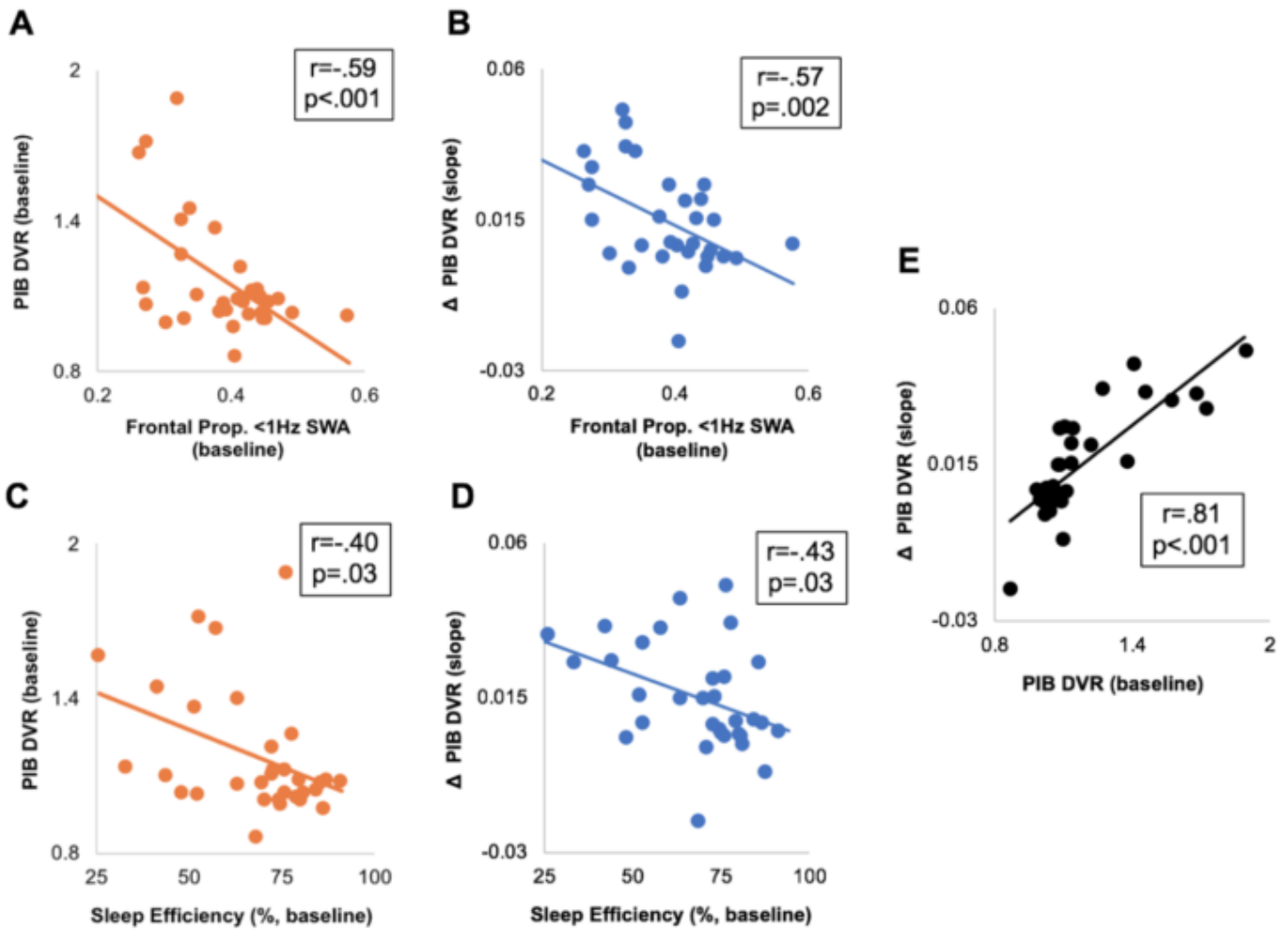


Figure 3. A) Lower proportion <1Hz slow wave activity at baseline is associated with greater cross-sectional PIB DVR burden. B) Lower proportion <1Hz slow wave activity at baseline predicts accelerated increase of PIB DVR longitudinally. C) Worse sleep efficiency at baseline is associated with greater cross-sectional PIB DVR burden. D) Worse sleep efficiency at baseline predicts accelerated increase of PIB DVR longitudinally. E) PIB DVR at baseline is strongly predictive of increased longitudinal PIB DVR. All analyses adjusted for age at baseline and gender, slope analyses additionally adjusted for number of PET scans per subject.

Keywords: sleep, β -amyloid, longitudinal, aging

P90: PI-2620 Tau PET is associated with amyloid-beta levels in scans from subjects of the elenbecostat MissionAD program

Andrew Stephens¹, Santiago Bullich¹, Andre Mueller¹, Mathias Berndt¹, Susan De Santi², David Scott³, Kate Adamczuk³, Joyce Suhy³, June Kaplow⁴, Monique Giroux⁴, Stephen Krause⁴, Julia Chang⁴, Bruce Albala⁴

¹*Life Molecular Imaging, Berlin, Germany*

²*Life Molecular Imaging Inc, Boston, MA, US*

³*Bioclinica, Newark, CA, US*

⁴*Eisai Inc, Woodcliff Lake, NJ, US*

Objectives: The study objective was to correlate regional tau deposition of [¹⁸F]PI-2620 PET to the amount of amyloid-beta as determined by Neuraceq PET in a sub-study of the elenbecostat MissionAD program.

Methods: Neuraceq visually PET-positive patients with MCI or mild AD (MMSE \geq 24, CDR global score 0.5, CDR Memory Box score \geq 0.5, and impaired episodic memory confirmed by a list-learning task) were included. Neuraceq cSUVR-levels were used to divide the study population into 4 groups: very low (cSUVR <1.25), low (1.25 \leq cSUVR \leq 1.48), intermediate (1.48 < cSUVR \leq 1.73) and high (cSUVR >1.73) amyloid-beta. The cSUVR-cutoff of 1.25 was determined as 2 SD above mean from an independent population of young healthy-controls (n=70; age=20-40yrs). The cSUVR cut-off of 1.48 was determined by ROC analysis of an independent histopathology study for amyloid-beta positivity. [¹⁸F]PI-2620 PET scans were obtained from 60-90min p.i.. SUVR in individual MRI-based subregions were investigated. Visual assessment of [¹⁸F]PI-2620 tau PET-scans was performed and subjects with uptake above cerebellar background in mesial-temporal, temporo-parietal and/or cortical regions were considered positive.

Results: The MMSE in the tau-PET group (n=77, mean age 75.9 \pm 6.5yrs) was 27.0 \pm 1.7; CDR-SB was 2.34 \pm 0.97. 38 subjects (49%) were tau-PET positive and 28 subjects (36%) were negative both visually and quantitatively, 9 subjects (12%) were only positive quantitatively and 2 subjects were visually positive only. There was a strong correlation between amyloid-beta load and [¹⁸F]PI-2620 accumulation. All subjects with very low amyloid-beta were visually tau PET negative. The lowest amyloid load with positive [¹⁸F]PI-2620 deposition in this population was cSUVR = 1.43. 19% of subjects with low amyloid were visually tau PET positive. 48% of subjects with intermediate amyloid-beta and 79% of subjects with high amyloid-beta were tau PET-positive.

Conclusions: The subjects recruited in the MissionAD tau PET substudy represents an early AD population and Tau positivity was associated with amyloid-beta load.

Figure 1

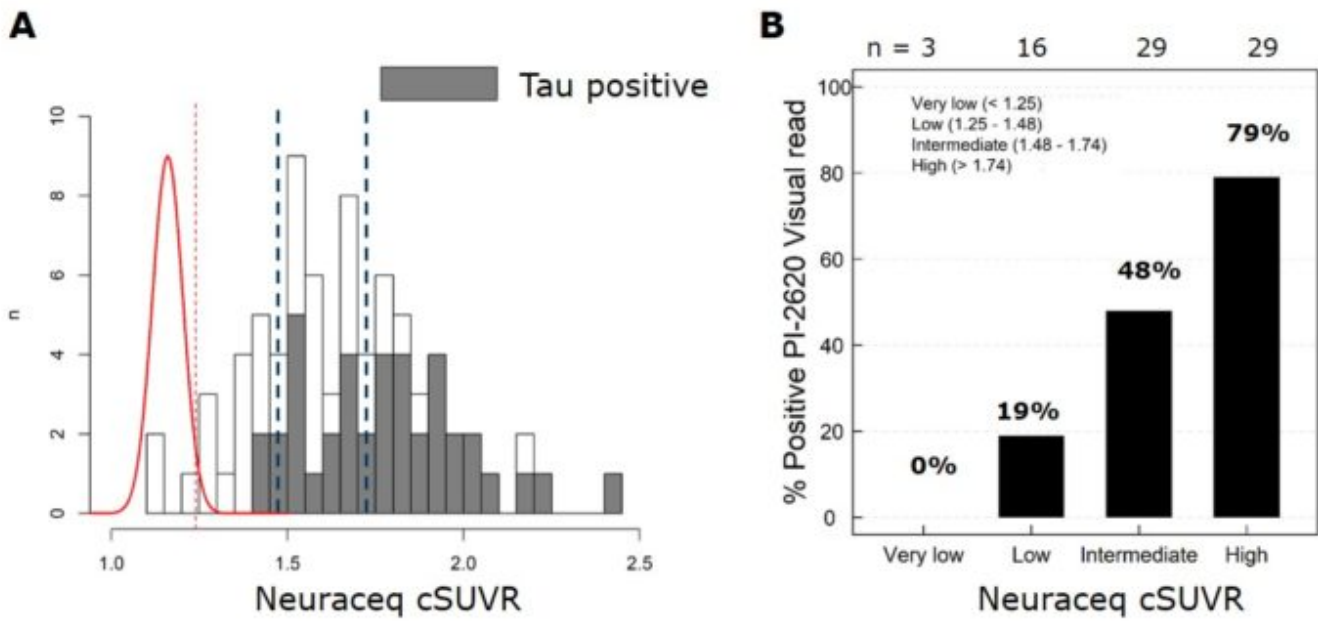


Figure 1. PI-2620 tau-positivity increases with degree of beta-amyloid load as measured by Neuraceq PET composite SUVR (cSUVR) using cerebellar grey as the reference region. **A)** distribution of subjects from the MissionAD tau-PET substudy according to Neuraceq cSUVR. **B)** PI-2620 visual tau-PET positivity correlated with beta-amyloid load.

Keywords: Tau, PET, PI-2620, Elenbecestat, amyloid-beta

P91: Prevalence of amyloid PET positivity in cognitively normal the East Asian populations

Jaeho Kim^{1,2,3}, Sang-Hyuk Jung^{7,8}, Duk L Na^{1,2,3,4,6}, Hee Jin Kim^{1,2,3}, Hong-Hee Won⁷, Sang Won Seo^{1,2,3,5,6}

¹Department of Neurology, Samsung Medical Center, Sungkyunkwan University School of Medicine, Seoul, Korea

²Neuroscience Center, Samsung Medical Center, Seoul, Korea

³Samsung Alzheimer Research Center, Samsung Medical Center, Seoul, Korea

⁴Stem Cell & Regenerative Medicine Institute, Samsung Medical Center, Seoul, Korea

⁵Department of Clinical Research Design & Evaluation, SAIHST, Sungkyunkwan University, Seoul, Korea

⁶Department of Health Sciences and Technology, SAIHST, Sungkyunkwan University, Seoul, Korea

⁷Department of Digital Health, SAIHST, Sungkyunkwan University, Seoul, Korea

⁸Department of Biostatistics, Epidemiology and Informatics, Perelman School of Medicine, University of Pennsylvania, Philadelphia, PA, US

Background: Cognitively normal (CN) individuals with increased amyloid- β (A β) are considered to be more vulnerable to AD progression. However, there may be a discrepancy in the frequency of A β (+) between the East Asian countries and the Western countries. Therefore, we compared the frequency of A β (+) in CN populations between the East Asian countries and the Western countries. We also investigated which factors, including genome-wide association study (GWAS) analysis, explain the difference.

Methods: A total of 423 Korean CN participants underwent ¹⁸F-labeled amyloid PET: 219 ¹⁸F-florbetaben PET; 203 ¹⁸F-flutemetamol PET; and 1 ¹⁸F-florbetapir PET scanning at the Samsung Medical Center. GWAS analysis for amyloid PET level was performed in 115 CN participants with ¹⁸F-florbetaben PET and in 89 with ¹⁸F-flutemetamol PET, respectively, with adjustment for sex, age, and four principal components (PCs). Finally, meta-analysis was conducted.

Results: We found approximately 18% A β positivity in our cohort, which was in line with the Asian population. However, it seemed to be lower than that of ADNI. The mean age was younger in our cohort (69.9 years), and the mean education years in our cohort was lower (11.8 years) than that of ADNI (16.4 years). Our cohort seemed to have a lower percentage of APOE ϵ 4 (23.9%). In our GWAS meta-analysis, we found a novel locus on chromosome 5 ($P=4.19\times 10^{-8}$) with the genome-wide significance level ($P<5\times 10^{-8}$) and two suggestive ($P<1\times 10^{-6}$) loci on chromosome 5 ($P=2.73\times 10^{-7}$) and chromosome 1 ($P=4.24\times 10^{-7}$). These candidate variants associated with brain amyloidosis did not overlap with previously reported GWAS loci for AD.

Conclusion: The discrepancy in amyloid positivity between different populations might be explained by the differences in the frequency of APOE ϵ 4, age, and education years of study participants. The comparison of GWAS results between Asian and European populations may further explain the discrepancy.

Table.1. Baseline characteristics of the participants with amyloid biomarker information

	Korea(SMC) (n=423)	J-ADNI (n=83)	ADNI (n=373)
Amyloid positivity prevalence	17.9%	23.0%	33.2%
APOE ε4 carrier	23.9%	25.0%	28.0%
Age (years)	69.9	67.9	73.7
Education (years)	11.8	13.9	16.4

Figure 1. A Manhattan plot of GWAS meta-analysis for amyloid PET level in Korean cognitively normal individuals

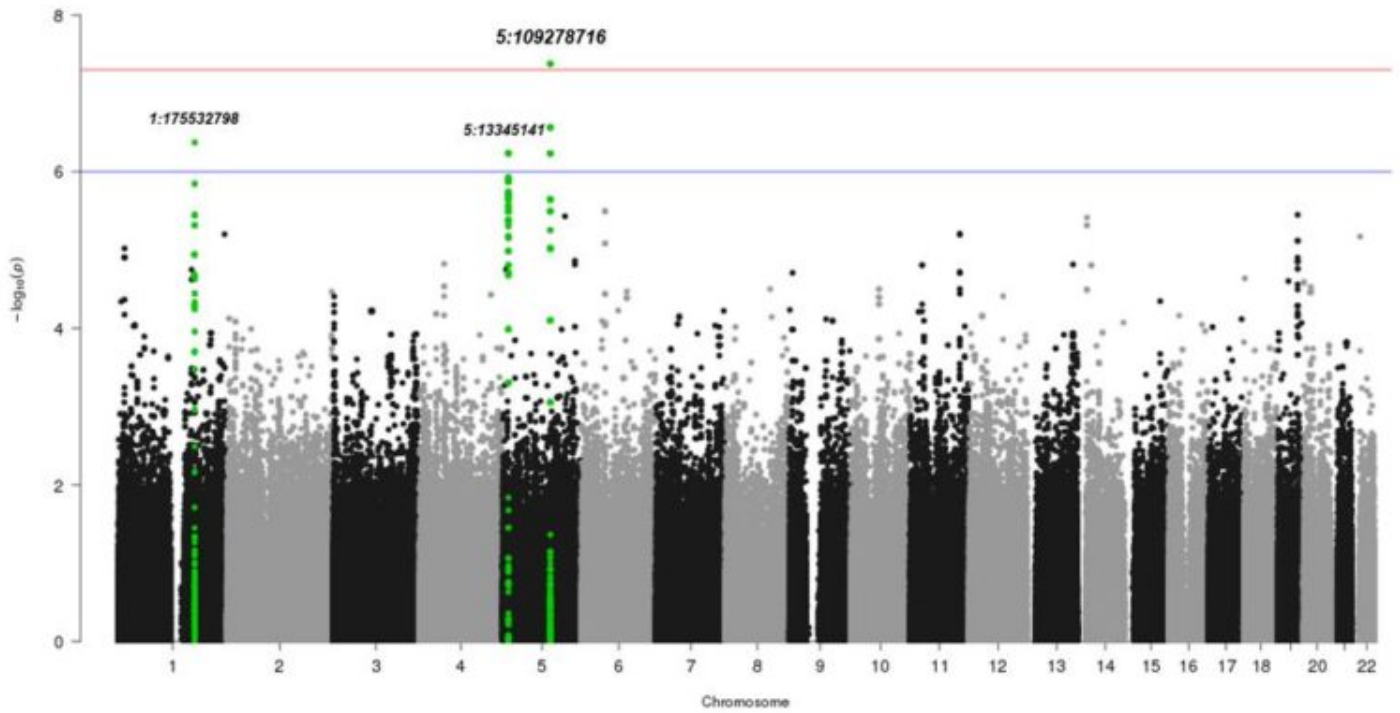
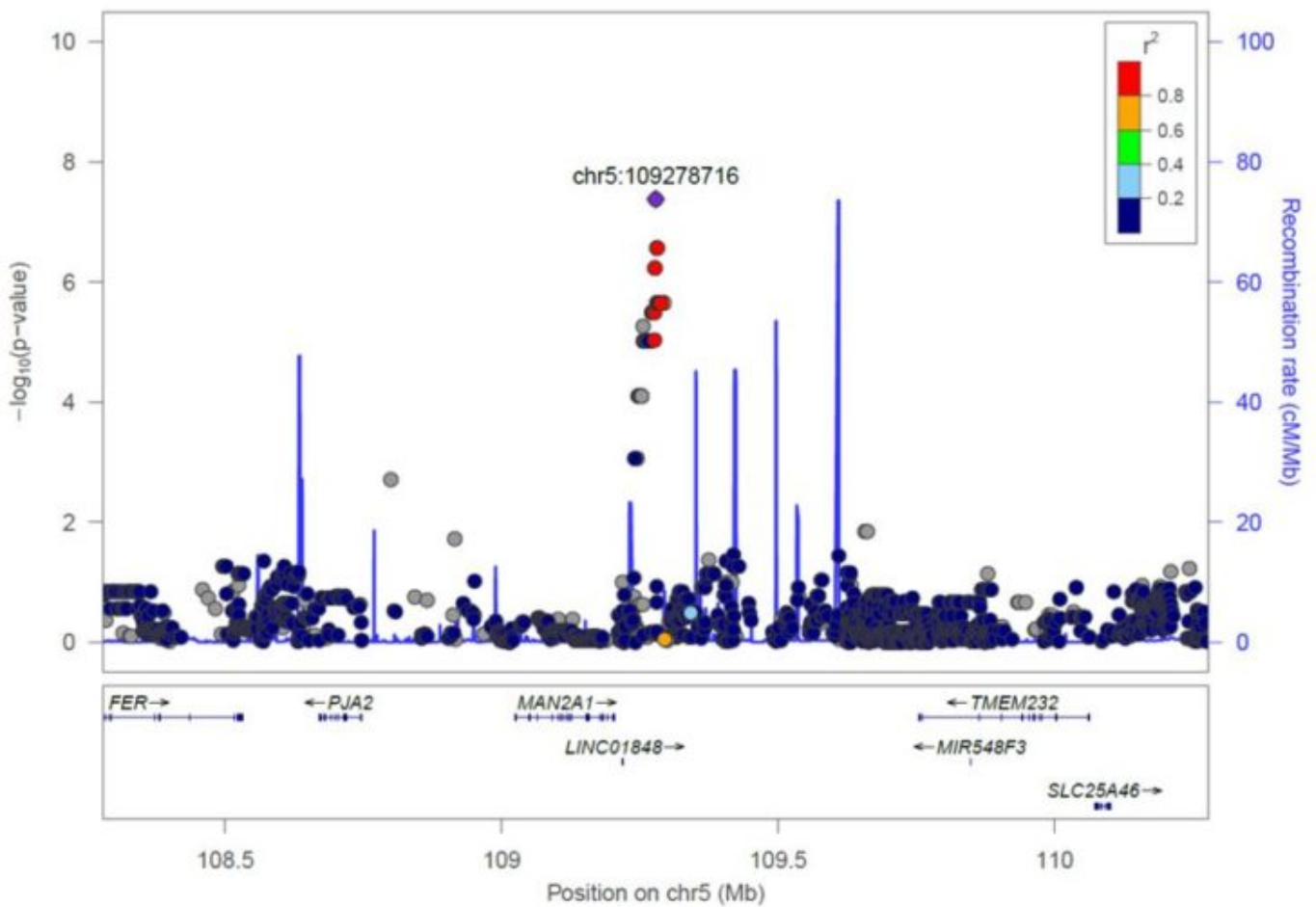


Figure 2. A regional plot of genome-wide significant locus associated with amyloid PET level



Keywords: amyloid PET, cognitively normal, GWAS, preclinical AD, East Asian countries

P92: Amyloid deposition disrupts functional connectivity and graph properties within the default mode network

Silvia Ingala¹, Alle Meije Wink¹, Naomi Prent², Dennis van 't Ent³, Jori Tomassen², Mara ten Kate^{1,2}, Ellen Konijnenberg², Lyduine E Collij¹, Maqsood M. Yaqub¹, Philip Scheltens², Eco JC de Goes³, Charlotte E Teunissen⁴, Frederik Barkhof^{1,5}, Bart NM van Berckel¹, Pieter Jelle Visser², Anouk den Braber^{2,3}

¹Department of Radiology and Nuclear Medicine, Amsterdam Neuroscience, VU University Amsterdam, Amsterdam UMC, Location VUmc, Amsterdam, The Netherlands

²Alzheimer Center Amsterdam, Department of Neurology, Amsterdam Neuroscience, VU University Amsterdam, Amsterdam UMC, Location VUmc, Amsterdam, The Netherlands

³Dept. of Biological Psychology, VU University Amsterdam, Neuroscience Amsterdam, Amsterdam, The Netherlands

⁴Department of Clinical Chemistry & Neurochemistry Laboratory, VU University Amsterdam, Amsterdam Neuroscience, Amsterdam UMC, Amsterdam, The Netherlands

⁵Institute of Neurology and Healthcare Engineering, University College London, London, UK

Background: Preclinical Alzheimer's disease (AD) stages can be detected through amyloid abnormalities in the cerebrospinal fluid (CSF) or PET regional deposition in the precuneus, medial orbitofrontal (MOF), and posterior cingulate (PCC) cortices.¹ These areas overlap with the default mode network (DMN), where changes in functional connectivity (FC) network structure occur early along AD course.²⁻⁴ We aimed at investigating the relation between amyloid burden and DMN properties in cognitively unimpaired older monozygotic twins.

Methods: 173 twins from EMIF-AD preclinAD study were included [Table 1].⁵ T1-weighted and resting-state functional MR and dynamic [18F]flutemetamol PET images were obtained. Amyloid burden was determined by CSF concentrations of A β 42 as measured with ADx Neurosciences/Euroimmun assay and PET non-displaceable binding potential (BP_{ND+1} = DVR) with cerebellar grey matter as the reference region. After DMN identification through independent component analysis, mean FC and voxelwise eigenvector centrality (EC) values within the DMN were calculated and served as outcomes for the generalized estimating equation models used to determine their relationship with amyloid burden (A β 42, global DVR, and DVR in precuneus, MOF and PCC).⁶ Analyses were adjusted for age, sex, cortical atrophy, and genetic relatedness.

Results: Decreased DMN FC was associated with increased CSF A β 42 (β =0.23, p-value=0.001) and amyloid burden in the PCC (β =-0.157, p-value=0.006). No relation with amyloid burden in the MOF cortex and precuneus was found [Table2]. Low EC values in voxels in the precuneus and PCC highly correlated with CSF A β 42 and DVR in the PCC [Figure1].

Conclusion: Early amyloid deposition as measured by A β 42 and DVR in the PCC is associated with disruption of FC and alterations of EC measures in the DMN. EC changes in the precuneus and PCC indicate that disruption of hierarchical organization of the network in these regions is associated with amyloid deposition in preclinical AD.

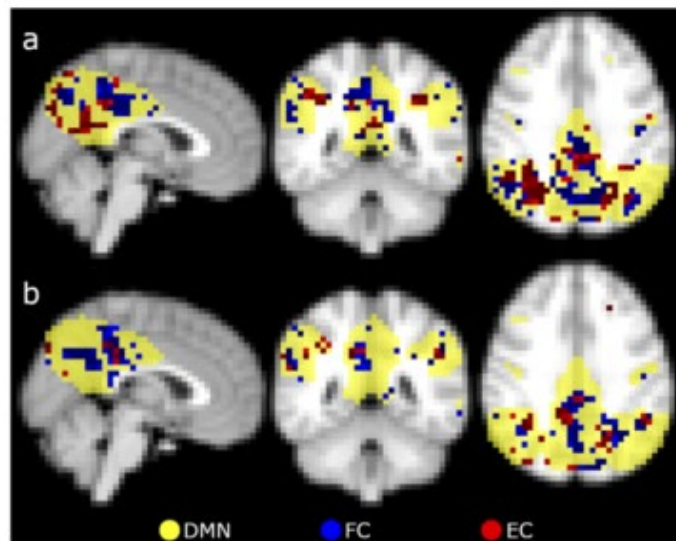
Table 1. Demographics and clinical characteristics of the cohort. *Acronyms.* CSF= cerebrospinal fluid; DMN= default mode network; DVR= distribution volume ratio; GM = gray matter; FC= functional connectivity.

	Mean	Standard Deviation
Age	70.29	7.40
CSF A β 42 (n=109)	882.20	317.24
Normalized GM volume (n=173)	72692.58	8573.68
Log FC in the DMN (n=173)	1.36	0.14
Global DVR (n=167)	1.03	0.13
Sex, n females (%)	100 (57.80%)	

Table 2. Association of mean FC in the DMN and amyloid burden. The z-score was used for both the outcome (FC in the DMN) and the predictors (amyloid). *Acronyms.* CSF= cerebrospinal fluid; DVR= distribution volume ratio; EC= eigenvector centrality; FC= functional connectivity; MOF= medio-orbitofrontal; PCC=posterior cingulate cortex. Significance was set at p-value<0.05 after Bonferroni correction.

	N	DMN FC z-score (n=173)	
		Regression Coefficient (β)	p-value
CSF A β 42 z-score	109	0.221	0.001
PET Global DVR	167	-0.055	0.415
PET DVR in Precuneus	167	-0.087	0.165
PET DVR in MOF cortex	167	-0.088	0.153
PET DVR in the PCC	167	-0.16	*0.006

Figure 1. Voxels with a p-value < 0.05 in voxelwise regression analyses between FC (blue) and EC (red) in the DMN (yellow) as predicted by CSF A β 42 (Fig. A) and amyloid deposition in the PCC (Fig. B). *Acronyms.* DMN= default mode network; EC= eigenvector centrality; FC= functional connectivity.



References

1. Palmqvist, S., Mattsson, N. & Hansson, O. Cerebrospinal fluid analysis detects cerebral amyloid- β accumulation earlier than positron emission tomography. *Brain* **139**, 1226–1236 (2016).
2. Palmqvist, S. *et al.* Earliest accumulation of β -amyloid occurs within the default-mode network and concurrently affects brain connectivity. *Nat. Commun.* **8**, (2017).
3. Binnewijzend, M. A. A. *et al.* Brain network alterations in Alzheimer's disease measured by Eigenvector centrality in fMRI are related to cognition and CSF biomarkers. *Hum. Brain Mapp.* **35**, 2383–2393 (2014).
4. Wink, A. M., de Munck, J. C., Van Der Werf, Y. D., Van Den Heuvel, O. A. & Barkhof, F. Fast Eigenvector Centrality Mapping of Voxel-Wise Connectivity in Functional Magnetic Resonance Imaging: Implementation, Validation, and Interpretation. *Brain Connect.* **2**, 265–274 (2012).
5. Konijnenberg, E. *et al.* The EMIF-AD PreclinAD study: Study design and baseline cohort overview. *Alzheimer's Res. Ther.* **10**, 1–12 (2018).
6. Carlin, J. B., Gurrin, L. C., Sterne, J. A. C., Morley, R. & Dwyer, T. Regression models for twin studies: A critical review. *Int. J. Epidemiol.* **34**, 1089–1099 (2005).

Keywords: Amyloid, functional connectivity (FC), eigenvector centrality (EC), default mode network (DMN), resting-state functional MRI

P93: Neuroinflammation in Alzheimer's disease patients and correlates with amyloid and tau deposition

Paul Edison¹, Fangda Leng¹, Melanie Dani¹, David Brooks²

¹Imperial College London, London, UK

²Newcastle University, Newcastle upon Tyne, UK

Background: 11C-PBR28 is a marker of microglial activation. Kinetic modelling of 11C-PBR28 has been challenging because of high inter-subject variability of 11C-PBR28 uptake even after accounting for 147 Ala/Thr polymorphism of TSPO gene. Moreover, splitting subjects in to high and medium affinity binders reduces statistical power 18F-AV1451 is a marker of tau deposition and 18F-Flutemetamol of amyloid deposition.

Aim: To explore a simplified method to evaluate neuroinflammation with 11C-PBR28 accounting for individual variability by using a pseudo-reference region, and to correlate with the levels of tau and amyloid deposition

Methods: We recruited 18AD, 30MCI and 16 healthy controls who underwent 11C-PBR28 scans. A subset were also scanned for 18F-Flutemetamol (n=58) and 18F-AV1451 (n=34). 90-120 minute summed 18F-Flutemetamol, 80-100 minute summed 18F-AV1451 and 60-90 minute summed 11C-PBR28 images were created. Tracer uptake in cerebellar grey matter was then sampled and individual image was divided by cerebellar uptake. 11C-PBR28 uptake ratio in major regions were compared using T-test at ROI level and at voxel level. Relationship between microglial activation and tau deposition was evaluated at ROI level.

Results: AD cohort showed increased 11C-PBR28 uptake ratio in medial temporal lobe (bilateral, p=0.04) while MCI group did not show significant increase compared to healthy controls in ROI analysis. Voxel-level analysis showed clusters of increased 11C-PBR28 uptake in bilateral temporal lobe in AD cohort (FWE-corrected cluster-level p<0.05). Significant correlation was present between 11C-PBR28 and 18F-AV1451 uptake in temporal (p=0.022), parietal (p=0.008) and occipital lobe (p=0.001) while 18F-Flutemetamol and 11C-PBR28 uptake correlated in temporal lobe (p=0.003) and occipital lobe (p=0.009).

Conclusion: Cortex-to-cerebellum uptake ratio using 60-90 minute frames may serve as a simple and reliable method in 11C-PBR28 analysis. Microglial activation correlated with tau deposition and amyloid load in established AD, indicating glial activation is associated with tau deposition in later stages of the disease.

Keywords: 11C-PBR28, 18F-AV1451, Neuroinflammation, reference region

P94: Development of new $\alpha 7$ nicotinic receptor ASEM analogs for PET imaging

Agneta Nordberg^{1,2}, Laetitia Lemoine¹, Sathya Mohan¹, Guanglin Kuang⁴, Sangram Nag³, Zhisheng Jia³, Patricia Miranda Azpiazu³, Prodip Datta³, Ryosuke Arakawa³, Katarina Varnäs³, Hans Ågren⁴, Bengt Långström⁵, Christer Halldin³

¹Karolinska Institutet, Department of Neurobiology, Care Sciences and Society, Stockholm, Sweden

²Karolinska University Hospital, Theme Aging, Stockholm, Sweden

³Karolinska Institutet, Department Clinical Neurosciences, Stockholm, Sweden

⁴Royal Institute of Technology (KTH), School of Biotechnology, Stockholm, Sweden

⁵Uppsala University, Department of Chemistry, Stockholm, Sweden

Background: Nicotinic acetylcholine receptors (nAChR) represent a family of ligand-gated ion channels widely distributed in the brain. The $\alpha 7$ -nAChR mainly expressed in hippocampus and cortical regions seems to play an important role in cognition and memory and is clinically assumed to be implicated in neurodegenerative disorders. The $\alpha 7$ -nAChR is present in astrocytes as well as in amyloid plaques and binds with high affinity to amyloid- β . It is therefore challenging to design PET tracers for in vivo brain imaging of $\alpha 7$ -nAChR. The aim of this study was to develop PET tracer candidates using ASEM ($\alpha 7$ -nAChR antagonist) as lead compound.

Methods: In silico methods including theoretical modelling and structure-based design of $\alpha 7$ -nAChR were performed. Compounds were synthesized and screened in transfected $\alpha 7$ -nAChR neuroblastoma cells and promising compounds labeled with [11C] or [3H]. Binding properties were evaluated using in vitro autoradiography (rodent and human tissue), homogenate binding studies (cells and human tissue) and in vivo PET studies in non-human primates (NHP).

Results: From in silico docking score and free energy calculations, in vitro cells screening and feasibility of radiolabelling five ASEM analogs have been characterized. All compounds showed high affinity binding in GH3-h $\alpha 7$ cells with IC50 in pmol range. KIn83 demonstrated two binding sites in human brain. Regional distribution was observed for [3H]-KIn83 using large hemisphere autoradiography and with high binding in AD temporal cortex, insula, hippocampus. In vivo PET in NHP showed similar regional distribution of [11C]KIn83 and [11C]KIn74 to [18F]ASEM, with relatively high uptake in thalamus, cortex, basal ganglia and low binding in the cerebellum and white matter. [11C]KIn74 showed higher brain uptake (2.4 SUV compared to [11C]KIn83 (1.6 SUV) in NHP but lower than [18F]ASEM (4.4 SUV).

Conclusions: Preliminary evaluation of two ASEM analogs KIn 83 and KIn74 showed favorable properties for imaging $\alpha 7$ -nAChR and further studies are ongoing.

Keywords: Alpha7 nicotinic receptor, PET, Human Brain, Autoradiography, ASEM analogs

P95: Biological underpinnings of typical and atypical Alzheimer's dementia phenotypes

Jennifer Whitwell¹, Nirubol Tosakulwong¹, Jonathan Graff-Radford¹, Stephen Weigand¹, Christopher Schwarz¹, Matthew Senjem¹, Nilufer Ertekin-Taner², David Jones¹, Bradley Boeve¹, David Knopman¹, Clifford Jack¹, Ronald Petersen¹, Val Lowe¹, Keith Josephs¹

¹Mayo Clinic, Rochester, MN, US

²Mayo Clinic, Jacksonville, FL, US

Background: Neuroimaging differences occur between typical and atypical clinical presentations of Alzheimer's disease (AD), the former showing greater medial temporal involvement, the latter greater cortical involvement. It is unclear, however, how these relationships differ between MRI volume and [¹⁸F]flortaucipir PET, according to age. We aim to investigate relationships between volume and [¹⁸F]flortaucipir uptake across different age tiers to better comprehend biological underpinnings of typical (Ty-AD) and atypical (Aty-AD) AD.

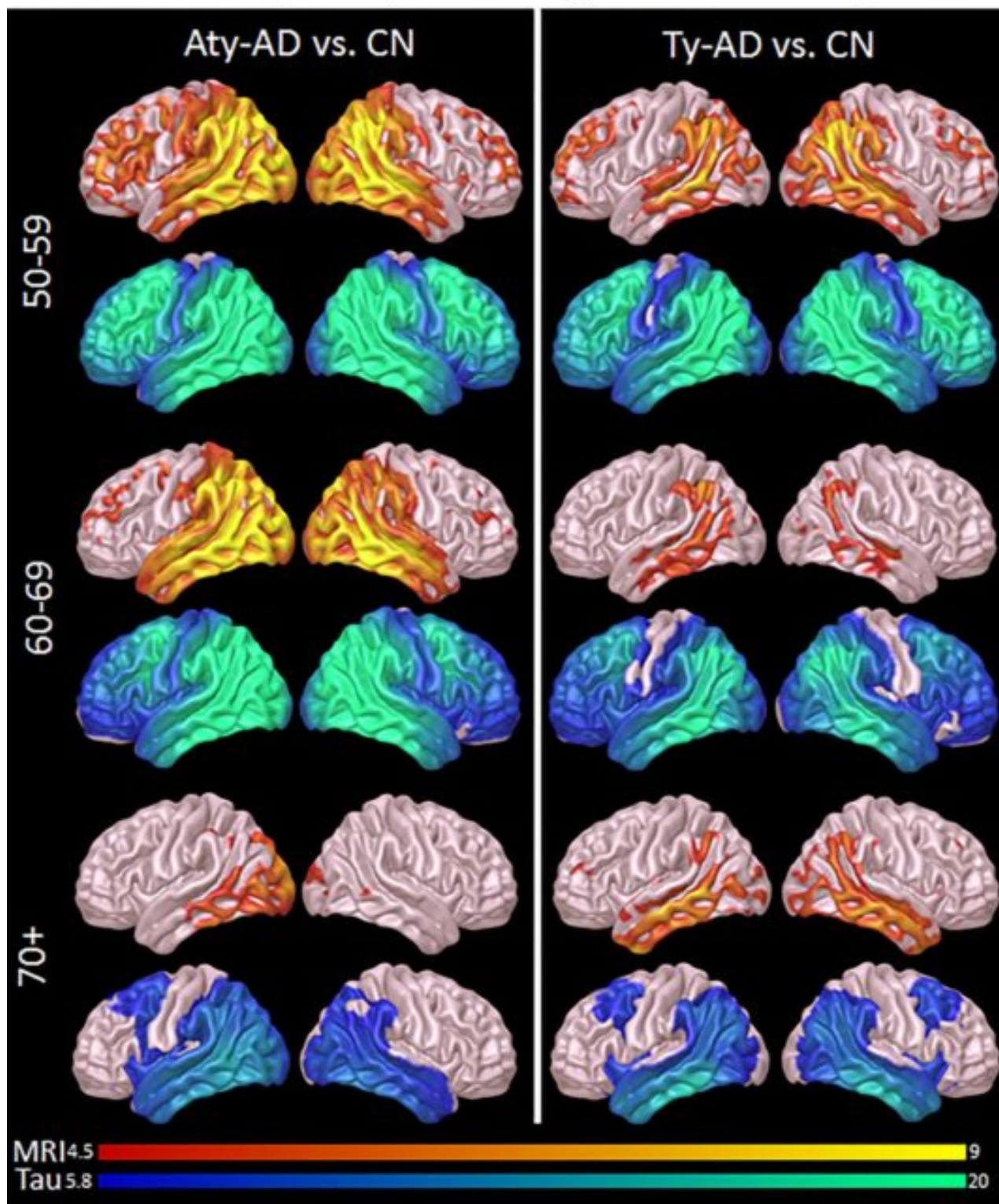
Methods: 148 patients with Ty-AD (n=75) or Aty-AD (n=73 [33 posterior cortical atrophy, 28 logopenic, 10 dysexecutive]) underwent apolipoprotein genotyping, MRI, flortaucipir and 11C-PiB; all were amyloid positive. Grey matter volume and flortaucipir standard uptake value ratios were calculated for hippocampus, entorhinal cortex and neocortex. Ratios of hippocampal-to-neocortical and entorhinal-to-neocortical volume and flortaucipir uptake were calculated. Linear regression models explored relationships between regional volume, flortaucipir uptake and ratios, between phenotypes, within three age at scan tiers (50-59, 60-69, 70+).

Results: In patients aged 50-59, no differences in imaging measures were observed between phenotypes. In 60-69, Ty-AD showed smaller volumes and greater flortaucipir uptake in the hippocampus than Aty-AD. In 70+, Ty-AD showed smaller hippocampal and entorhinal volumes, but no differences in flortaucipir uptake compared to Aty-AD. Higher neocortical flortaucipir uptake was associated with younger age, with regional patterns differing between phenotypes (Figure). The hippocampal-to-neocortical and entorhinal-to-neocortical ratios for volume and flortaucipir differed, but for different reasons, between phenotypes in the 60-69 and 70+ tiers. Apolipoprotein ε4 frequency was greater in Ty-AD in all tiers, with the highest frequencies occurring in the 60-69 tier.

Conclusion: Neuroimaging measures reveal different relationships to AD phenotypes across age tiers. Differences across phenotypes are driven predominantly by medial temporal regions in patients over age 60, although dissociation between volume and flortaucipir uptake in patients over 70 suggest additional contributions from other pathologies to volume loss.

Figure: Voxel-level cortical volume (red/yellow) and flortaucipir (blue/green) findings across phenotypes and age tiers.

Grey matter volume results are shown corrected for multiple comparisons using FWE at $p < 0.05$. Flortaucipir results are shown corrected for multiple comparisons using FWE correction at $p < 0.0001$.



Keywords: Alzheimer's disease, age, MRI, tau

P96: Use of the plasma amyloid-beta 42/40 ratio for predicting amyloid PET in a community-based population

Michelle Mielke¹, Alicia Algeciras-Schimmich¹, Michelle Campbell¹, Jeremy Syrjanen¹, David Knopman¹, Clifford Jack Jr.¹, Ronald Peterson¹

¹*Mayo Clinic, Rochester, MN, US*

Objective: Multiple platforms for measuring plasma amyloid-beta 40 and 42 are being investigated as a possible diagnostic screener for clinical trials. We measured plasma amyloid-beta 40, 42, and the ratio using a single molecular array (SiMoA) immunoassay and examined these markers or their ratio for prediction of elevated brain amyloid.

Methods: Participants from the Mayo Clinic Study of Aging (MCSA) with plasma amyloid-beta 40, 42, and the ratio, measured using the SiMoA immunoassay, and corresponding amyloid PiB-PET in an AD-signature region were included. A PiB-PET SUVR>1.48 was considered amyloid positive. Associations between plasma levels and amyloid PET were assessed using Spearman correlations and area under the receiver operating characteristic (AUROC) curve.

Results: The 196 participants were a median age of 79.6 (range 53.9-97.9) years, 50% were women, 173(88.3%) were cognitively unimpaired and 23 (11.7%) had a diagnosis of mild cognitive impairment. Spearman correlations with PiB-PET were 0.02 (p=0.79) for plasma amyloid-beta 40, -0.11 (p=0.17) for amyloid-beta 42, and -0.22 (p=0.005) for the amyloid-beta 42/40 ratio. There were 100 individuals (51.0%) with elevated brain amyloid by PiB. Using the the amyloid-beta 42/40 ratio to predict brain amyloid positivity, the AUROC was 0.64. Adding age and APOE to the amyloid-beta 42/40 ratio model increased the overall AUROC model to 0.75.

Conclusions: Although the predictive value for the plasma amyloid-beta 42/40 ratio alone was rather low, the combination of the ratio, age, and APOE has the potential to be used as a screener for elevated brain amyloid in the general population.

Keywords: plasma amyloid-beta; amyloid PET; prediction; screening

P97: Associations between longitudinal cognitive measures and cross-sectional tau in adults with Down syndrome

Dana Tudorascu¹, Diane Comer¹, Matthew Zammit², Charles Laymon¹, Davneet Minhas¹, Paul Ellison², Shahid Zaman³, Beau Ances⁴, Sterling Johnson², Chester Mathis¹, William Klunk¹, Bradley Christian², Benjamin Handen¹, Sigan Hartley², Ann Cohen¹

¹*University of Pittsburgh, Pittsburgh, PA, US*

²*University of Wisconsin-Madison, Madison, WI, US*

³*University of Cambridge, Cambridge, UK*

⁴*Washington University, St. Louis, MO, US*

Introduction: Adults with Down syndrome (DS) are uniformly affected by AD pathology by their 40's and have a 70-80% chance of clinical dementia by their 60's. The aim of the present study was to explore the relationship between cognitive decline and tau pathology using a regression model to explore the associations between longitudinal rates of cognitive decline and cross-sectional tau burden in adults with DS.

Methods: One hundred and twenty six participants (mean age: 39.19±8.44) with multiple cognitive assessments over a period of 9 years and one [F-18]AV-1451 scan were analyzed. Cognitive assessments included measures of overall function (DSMSE), episodic memory (cued recall), executive function (Stroop), and motor function (Purdue pegboard). FreeSurfer (v5.3.0) was used for the definition of ROIs. A two-stage analysis was performed: 1) a linear mixed model was applied to estimate the rates of change for cognitive outcomes over time and 2) the cognitive estimated rates from the trajectories were used as predictors of interest in a correlation analysis with [F-18]AV-1451 for each Braak-associated region (I-VI) as the outcome.

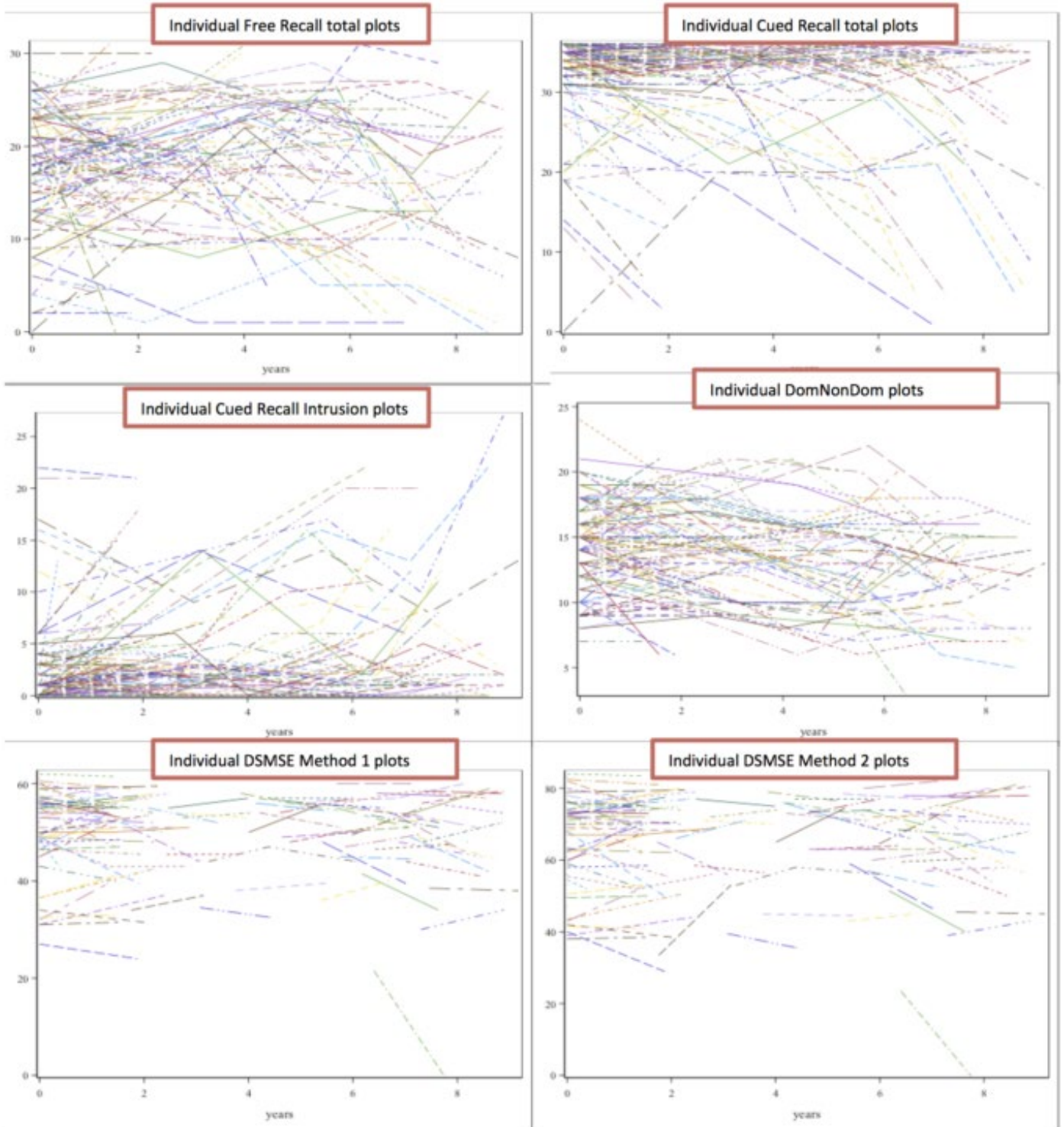
Results: Statistically significant associations ($\alpha=0.05$) were found between [F-18]AV-1451 retention in all Braak regions and 7 neuropsychological measures. All correlations are presented in Table 1 along with the corresponding 95% CI, with statistically significant associations for cued recall, DSMSE, and the Purdue pegboard task. Effect sizes were larger for higher Braak Regions.

Discussion: For this DS population, we found inverse associations between rates of neuropsychological decline and higher tau pathology in all Braak regions. In particular, decline in global cognition, verbal memory and motor function were all associated with higher tau pathology, but executive function was not. These correlations are in the expected direction with the effect sizes being larger for higher Braak Regions.

Table 1:Data is presented as Pearson's correlation estimates and 95% CI (SUVRs).

Estimate	Braak1	Braak2	Braak3	Braak4	Braak5	Braak6
Cued Recall Test - Free Recall Total						
Pred Mean (95% CI)	-0.45 (-0.58, -0.30)	-0.43 (-0.57, -0.28)	-0.56 (-0.67, -0.43)	-0.50 (-0.62, -0.36)	-0.52 (-0.63, -0.37)	-0.51 (-0.63, -0.37)
p	0.0000	0.0000	0.0000	0.0000	0.0000	0.0000
Cued Recall Test - Free and Cued Recall Total						
Pred Mean (95% CI)	-0.52 (-0.64, -0.38)	-0.44 (-0.57, -0.29)	-0.62 (-0.72, -0.50)	-0.62 (-0.72, 0.50)	-0.61 (-0.71, -0.49)	-0.50 (-0.62, -0.35)
p	0.0000	0.0000	0.0000	0.0000	0.0000	0.0000
Cued Recall Test - Cued Recall Intrusions						
Pred Mean (95% CI)	0.34 (0.18, 0.49)	0.34 (0.17, 0.49)	0.49 (0.35, 0.62)	0.43 (0.27, 0.56)	0.49 (0.34, 0.61)	0.48 (0.33, 0.60)
p	0.0001	0.0001	0.0000	0.0000	0.0000	0.0000
Stroop Cat Dog Switch - naming						
Pred Mean (95% CI)	0.03 (-0.15, 0.20)	0.11 (-0.06, 0.28)	0.02 (-0.15, 0.20)	0.03 (-0.14, 0.21)	0.004 (-0.17, 0.18)	-0.01 (-0.19, 0.16)
p	0.7427	0.2139	0.8056	0.7153	0.9685	0.9071
Purdue Pegboard - Dominant and Non-Dominant Hand						
Pred Mean (95% CI)	-0.31 (-0.46, -0.14)	-0.32 (-0.47, -0.15)	-0.45 (-0.58, -0.30)	-0.35 (-0.50, -0.19)	-0.41 (-0.54, -0.25)	-0.46 (-0.59, -0.31)
p	0.0004	0.0002	0.0000	0.0000	0.0000	0.0000
DSMSE - Total Score (Method 1)						
Pred Mean (95% CI)	-0.37 (-0.52, -0.21)	-0.26 (-0.42, -0.09)	-0.50 (-0.62, -0.36)	-0.48 (-0.60, -0.33)	-0.47 (-0.59, -0.32)	-0.37 (-0.51, -0.21)
p	0.0000	0.0028	0.0000	0.0000	0.0000	0.0000
DSMSE - Total Score (Method 2)						
Pred Mean (95% CI)	-0.39 (-0.53, -0.23)	-0.27 (-0.43, -0.10)	-0.47 (-0.60, -0.33)	-0.49 (-0.61, -0.34)	-0.45 (-0.58, -0.30)	-0.32 (-0.47, -0.15)
p	0.0000	0.0018	0.0000	0.0000	0.0000	0.0003

Figure 1: Individual trajectory plots for all 6 significant cognitive measures



Keywords: Down syndrome, Tau, cognition.

P98: Associations of amyloid deposition and FDG uptake in aging and cognitively impaired elders with and without moderate to severe periventricular white matter hyperintensities

Katherine Zukotynski^{1,2}, Vincent Gaudet⁵, Phillip Kuo³, Sabrina Adamo⁴, Maged Goubran⁴, Christopher Scott⁴, Christian Bocti⁶, Michael Borrie⁷, Howard Chertkow⁸, Richard Frayne⁹, Robin Hsiung¹⁰, Robert Jr. Laforce¹¹, Michael Noseworthy¹, Frank Prato⁷, Demetrios Sahlas¹, Eric Smith⁹, Vesna Sossi¹⁰, Alexander Thiel⁸, Jean-Paul Soucy¹², Jean-Claude Tardif¹³, Sandra Black^{2,4}

¹McMaster University, Hamilton, ON, Canada

²University of Toronto, Toronto, ON, Canada

³University of Arizona, Tucson, AZ, US

⁴Sunnybrook Research Institute, Toronto, ON, Canada

⁵University of Waterloo, Waterloo, ON, Canada

⁶Université de Sherbrooke, Sherbrooke, QC, Canada

⁷Western University, London, ON, Canada

⁸Jewish General Hospital, Montreal, QC, Canada

⁹Hotchkiss Brain Institute, Calgary, AB, Canada

¹⁰University of British Columbia, Vancouver, BC, Canada

¹¹Université Laval, Québec, QC, Canada

¹²Montreal Neurological Institute, Montréal, QC, Canada

¹³Montreal Heart Institute, Montréal, QC, Canada

Objective: To assess associations of amyloid deposition and FDG uptake in subjects with minimal versus moderate-severe periventricular white matter hyperintensity (pvWMH) using (18)F-Florbetapir and (18)F-FDG PET.

Materials and methods: A multi-center, observational, prospective clinical cohort study was designed to acquire data in subjects with moderate-severe pvWMH load and assess change over 2 years. Baseline data from the first 57 subjects recruited through either tertiary memory clinics or stroke prevention clinics formed the basis for this preliminary analysis. All subjects had 3T MRI, ¹⁸F-Florbetapir PET and neurological evaluation; ¹⁸F-FDG PET was available in 55. A matched cohort of 57 subjects with minimal pvWMH load was derived from ADNI. PETs were interpreted by 2 dual certified radiology/nuclear medicine physicians using MIM software (MIM Software Inc, Cleveland, Ohio) with final interpretation based on consensus. PETs were processed to obtain quantitative data in 59 regions of interest (ROIs) normalized to cerebellar grey matter. Two-year follow-up was available in 25 subjects. Machine learning (ML) including random forests (supervised) and K-means clustering (unsupervised) programmed in MATLAB and visual interpretation were used to study classification of (18)F-Florbetapir PET as positive and negative for amyloid deposition and associations of amyloid deposition, FDG uptake and pvWMH.

Results: Supervised and unsupervised ML had similar classification accuracy for ¹⁸F-Florbetapir PET with clinical interpretation as the gold standard. ROIs used for classification were, most commonly: the left posterior cingulate, left precuneus and left middle frontal gyrus; key default node network nodes, where amyloid deposition preferentially begins in the brain of subjects with Alzheimer's disease. While associations of FDG uptake with pvWMH were complex, amyloid deposition was higher in subjects with moderate-severe pvWMH at baseline and accumulated faster at 2-years in subjects with moderate-severe pvWMH than in matched ADNI controls.

Conclusions: Results suggest amyloid deposition and accumulation are associated with pvWMH load.

Keywords: periventricular white matter hyperintensity, (18)F-Florbetapir PET, (18)F-FDG PET, machine learning

P99: Early declines in learning and executive function associated with accumulating A β not tau in low PIB adults

Michelle Farrell¹, Kathryn Papp^{1,2}, Rachel Buckley^{1,2,3,4}, Heidi Jacobs^{1,5}, Aaron Schultz¹, Michael Properzi¹, Bernard Hanseeuw^{1,6}, Dorene M. Rentz^{1,2}, Keith Johnson^{1,2}, Reisa Sperling^{1,2}

¹Massachusetts General Hospital, Harvard Medical School, Charlestown, MA, US

²Brigham and Women's Hospital, Harvard Medical School, Boston, MA, US

³Florey institute of Neuroscience and Mental Health, Melbourne, Australia

⁴Melbourne School of Psychological Sciences, University of Melbourne, Melbourne, Australia

⁵Faculty of Health, Medicine and Life Sciences, School for Mental Health and Neuroscience, Alzheimer Centre Limburg, Maastricht University, Maastricht, The Netherlands

⁶Cliniques Universitaires Saint-Luc, Université Catholique de Louvain, Brussels, Belgium

Objective: Recent evidence supports the hypothesis that AD-related cognitive decline is primarily driven by neocortical tau accumulation in the presence of high A β . We assessed whether low levels of accumulating A β may be associated with subtle declines in different domains, independent of tau accumulation.

Methods: Participants included 91 clinically-normal adults from the Harvard Aging Brain Study with longitudinal PIB, FTP and cognitive data. The cognitive battery included measures of episodic and semantic memory, processing speed and executive function, including the Buschke Selective Reminding Test (SRT) and Digit Symbol Substitution Test (DSST). Since FTP was introduced at Year4 (Fig1 for timeline), slopes were extracted for neocortical PIB change Year1-4, neocortical PIB and inferior temporal (IT) FTP change Year4-6, and cognitive change Year4-6+. A series of linear regressions assessed the association of Year4 PIB and FTP level and change on cognitive change. To target early changes, analyses first focused on initially low PIB adults (n=67) before expanding into the full sample.

Results: In low PIB adults, PIB accumulation Year1-4 predicted subsequent decline on DSST and SRT learning (Fig2) Year4-6+, while FTP was unrelated to decline. In contrast to these early PIB-related changes, later FTP accumulation-related declines were detectable at higher PIB levels (PIB DVR*IT FTP change interaction) on multiple tasks, including SRT retention (Fig3).

Conclusion: Our findings support a model in which subtle decline in tasks that involve learning, executive function and processing speed are associated with the earliest increases in Ab rather than being driven by tau accumulation. Other cognitive processes, such as memory retention, only begin exhibiting decline in the presence of high Ab and accumulating neocortical tau. Continued research to clarify Ab's early effects on brain and behavior are needed to inform early intervention trials.

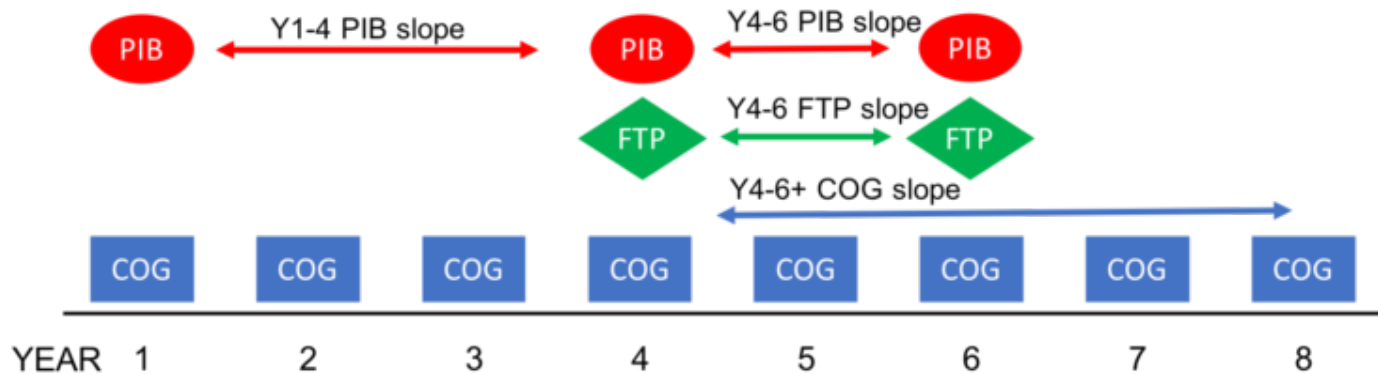


Figure 1. Timeline. Participants underwent annual cognitive testing and PIB scans at Year 1, 4 and 6. FTP was introduced later at Year 4 and repeated in Year 6. Slopes were extracted for PIB, FTP and cognition after Year 4, as well as earlier PIB accumulation Year1-4.

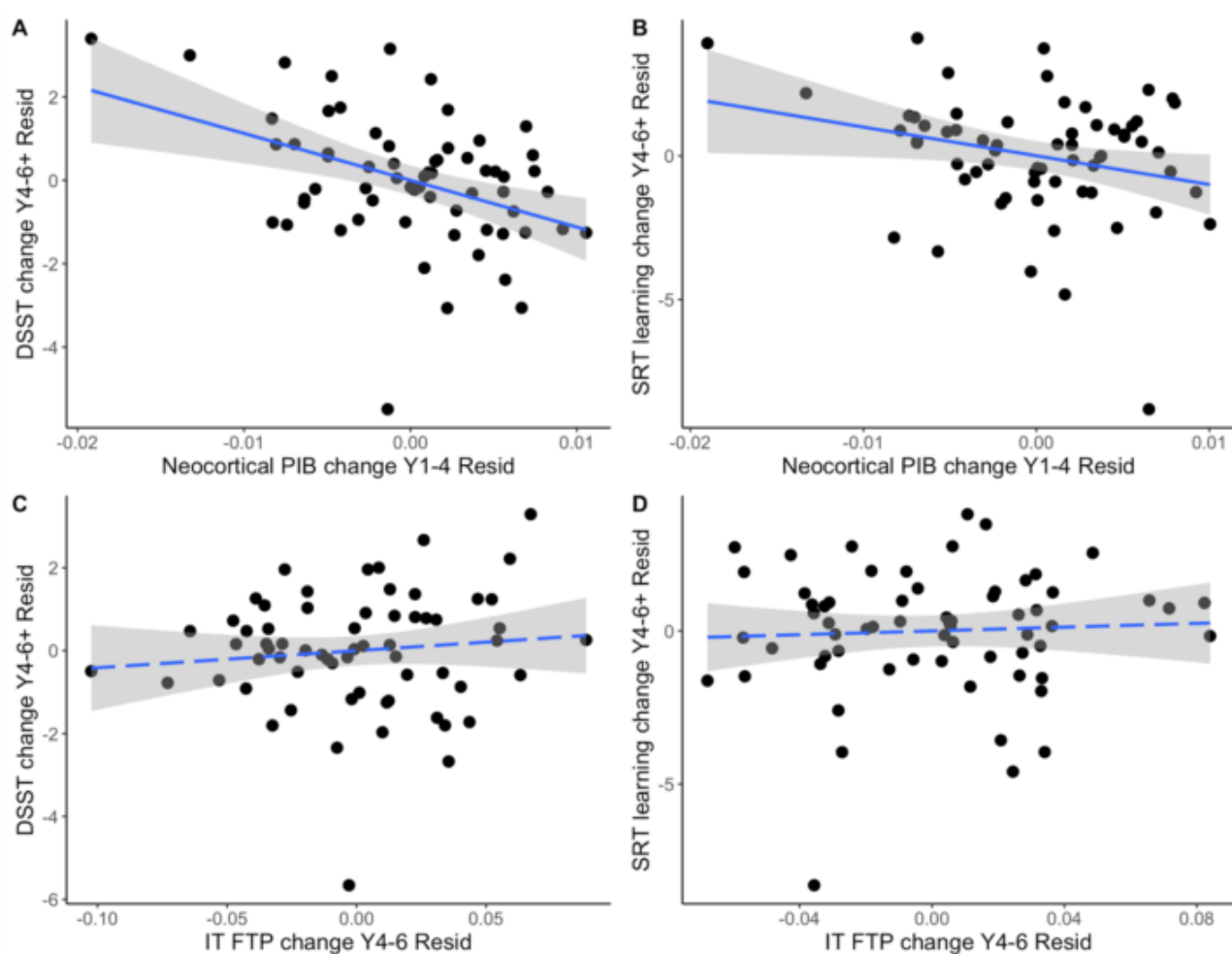


Figure 2. Effects of early PIB and FTP accumulation on DSST and SRT learning in low PIB adults. PIB accumulation from Year 1 to 4) predicted subsequent decline on (A) DSST ($\beta=-112.37$, $SE=33.88$, $p=.002$) and (B) SRT Learning ($\beta=-99.85$, $SE=49.16$, $p=.047$), while inferior temporal tau accumulation Year 4 to 6 were not associated with decline on (C) DSST ($\beta=-2.49$, $SE=5.68$, $p=.66$) or (D) SRT learning ($\beta=3.48$, $SE=8.43$, $p=.68$). Data shown were residualized for effects on Year 4 PIB and FTP, PIB change Year 4-6, Year 4 cognitive performance, age, sex, APOE and education.

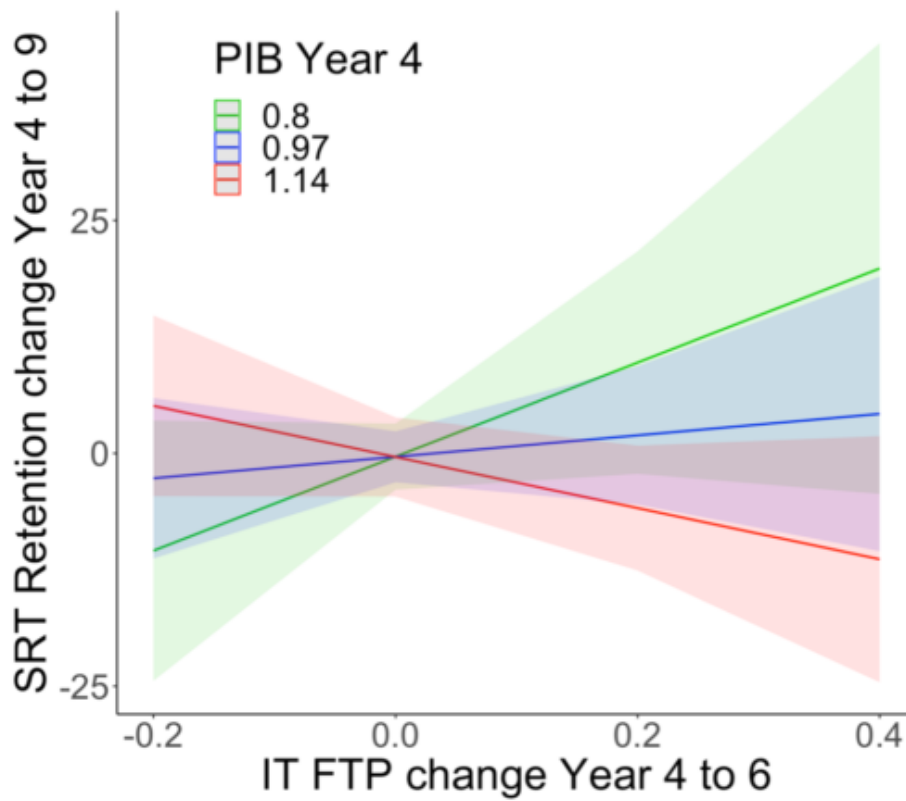


Figure 3. SRT retention declines with IT FTP accumulation in the presence of high PIB. In the full sample, SRT retention begins declining at high PIB levels (PIB Y4*IT FTP Change Y4-6: $\beta = -243.8$, $SE = 101.3$, $p = .02$), with the rate of decline accelerated by tau accumulation in the inferior temporal cortex. Data shown are simple slopes. Floodlight analysis revealed a significant effect of IT FTP change above 1.22 PIB DVR.

Keywords: amyloid, tau, cognition, subthreshold, early

P100: Entorhinal tau pathology is associated with medial temporal lobe hyperactivity in aging

Jenna Adams¹, Anne Maass^{1,2}, David Berron^{2,3,4}, Theresa Harrison¹, Suzanne Baker⁵, Wesley Thomas⁵, Morgan Stanfill¹, William Jagust^{1,5}

¹*Helen Wills Neuroscience Institute, University of California, Berkeley, Berkeley, CA, US*

²*German Center for Neurodegenerative Diseases, Magdeburg, Germany*

³*Institute of Cognitive Neurology and Dementia Research, Otto-von-Guericke University, Magdeburg, Germany*

⁴*Clinical Memory Research Unit, Department of Clinical Sciences Malmö, Lund University, Lund, Sweden*

⁵*Molecular Biophysics and Integrated Bioimaging, Lawrence Berkeley National Lab, Berkeley, CA, US*

Background: Aging is associated with functional changes in object and scene memory processing and tau deposition in the anterolateral and posteromedial entorhinal cortex (alEC/pmEC) and hippocampus. We hypothesized EC tau deposition would be related to activity reduction in alEC and increase in hippocampus during a memory task. We further predicted that tau would disrupt functional connectivity (FC) between EC and hippocampus.

Methods: 46 normal older adults (78±6 years, 29F) underwent high-resolution fMRI during an object and scene memory task (Fig-1A). Object or scene stimuli contrasted to baseline were used to measure functional activation. FC analyses were performed on residualized task data. MTL subregions were defined in native space on high-resolution T2 images using ASHS, with manual segmentation of alEC and pmEC subregions (Fig-1B). Tau-PET was performed with 18F-Flortaucipir (FTP), and mean FTP SUVR was extracted from native space EC ROIs (PVC corrected). All correlations controlled for age and sex.

Results: Activation of MTL ROIs was comparable to previous findings in aging, with alEC failing to show preference to object stimuli consistent with hypoactivation (Fig-2). EC tau was not associated with alEC activation to objects but was associated with increased activation in pmEC to both objects and scenes (Fig-3A/B). Increased EC tau was also associated with increased activation to both objects and scenes across most hippocampal subfields (DG/CA3/CA2, CA1, subiculum), demonstrating the strongest correlation with subiculum activation (Fig-3A/B). Finally, increased EC tau was associated with decreased FC between alEC and DG/CA3/CA2 in the left hemisphere ($r=-0.32$, $p=0.04$), but not between pmEC and DG/CA3/CA2 (p 's>0.05).

Conclusions: Dysfunction of alEC occurs in conjunction with tau-related increased and less differentiated (for scenes vs. objects) pmEC activation, as well as activation in multiple scene-specialized MTL subregions. EC tau also disrupted FC between alEC and the hippocampus, which may partly explain tau-related hyperactivity within the hippocampus.

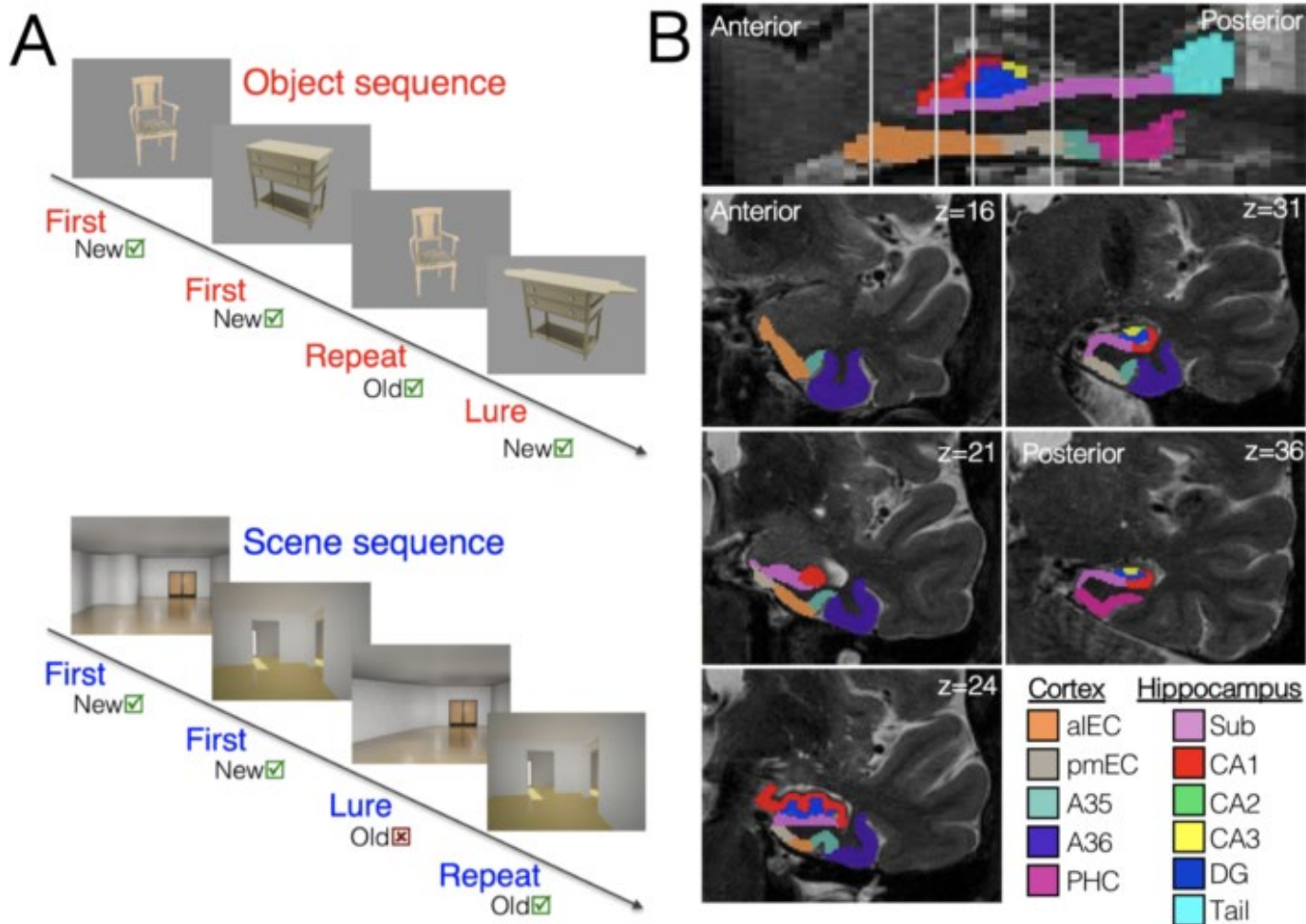
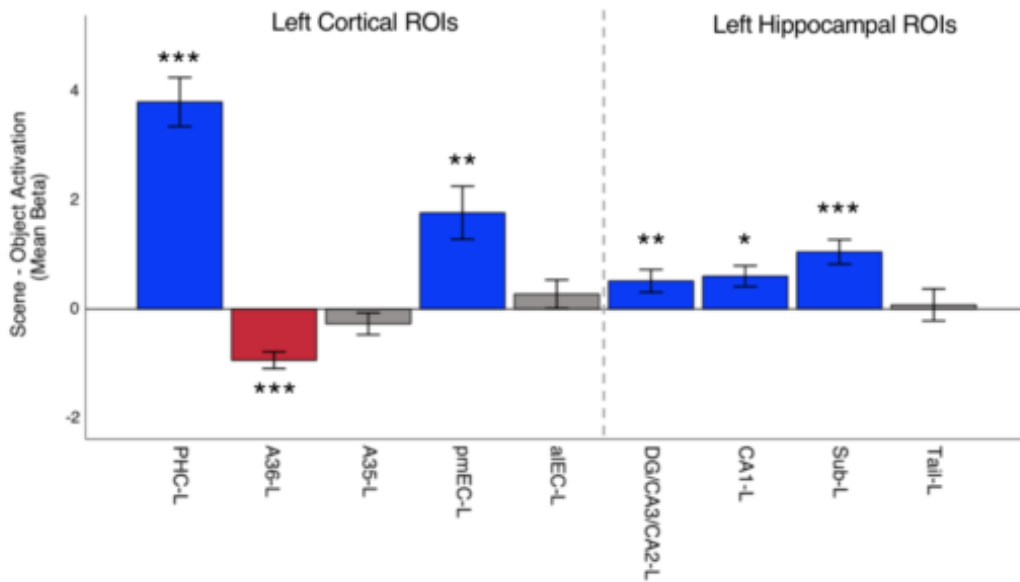


Figure 1. Visual representation of fMRI task and medial temporal lobe (MTL) segmentation. (A) Older adult subjects performed a memory task for object (top) and scene (bottom) stimuli during fMRI acquisition. The first two stimuli of each block are new stimuli, while the second two are either repeated stimuli or highly similar lure stimuli. Participants are instructed to respond “old” or “new” to each stimulus. We contrasted all object or scene stimuli to noise stimuli presented at the start and end of the task to derive object and scene activation. (B) High-resolution (0.5 x 0.5 x 1.5 mm) T2 images in native space were segmented with Automated Segmentation of Hippocampal Subfields (ASHS) to derive MTL ROIs for analysis. The full entorhinal cortex was manually subdivided into alEC and pmEC subregions using template ROIs inverse warped to native space as a visual guide. Cortical ROIs: anterolateral entorhinal cortex (alEC), posteromedial EC (pmEC), Area 35 of perirhinal cortex (A35), Area 36 of perirhinal cortex (A36), parahippocampal cortex (PHC); Hippocampal subfields: subiculum (Sub), CA1, CA2, CA3, dentate gyrus (DG), hippocampal tail (Tail). Due to fMRI resolution, subfields DG/CA3/CA2 were merged prior to analysis.

A



B

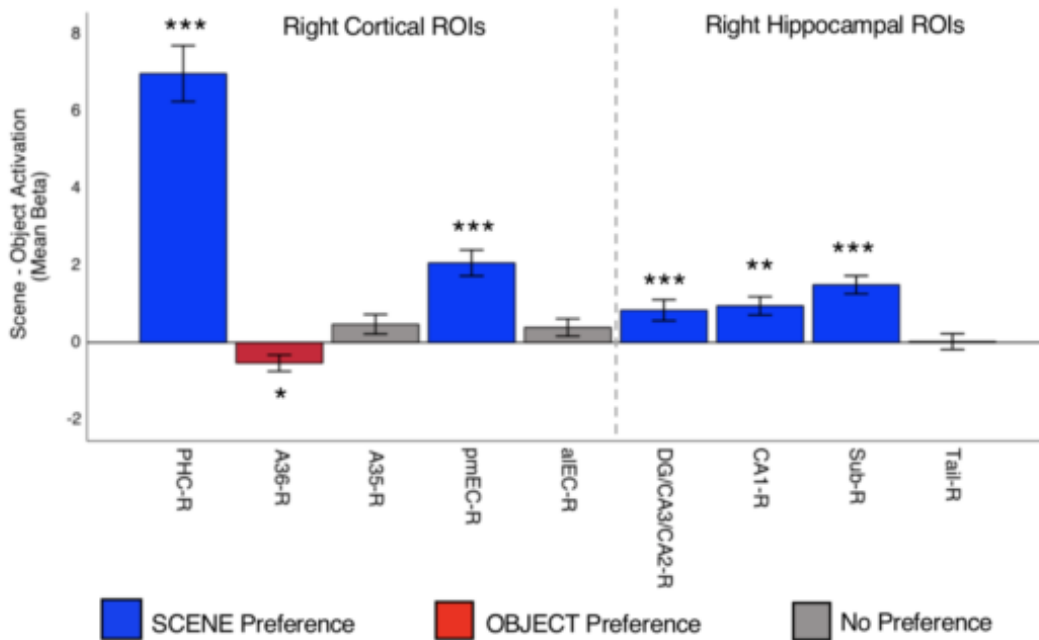


Figure 2. Domain specificity of medial temporal lobe ROIs to scenes versus objects. For each ROI, we calculated the domain specificity by contrasting activations to scenes compared to activation for objects, and extracted the mean beta value for each subject. One sample t-tests were performed for each ROI to determine if they had significantly more activation for scenes (blue, positive beta) or objects (red, negative beta) for the left (A) and right (B) hemispheres separately. Regions known to be involved in scene processing (PHC, pmEC, hippocampus) demonstrated scene preference, while only A36 (part of perirhinal cortex) demonstrated object preference. The aIEC, which normally exhibits object preference in healthy younger adults, did not show specificity for objects, suggesting age-related hypoactivation. * $p < 0.05$ ** $p < 0.01$ *** $p < 0.001$

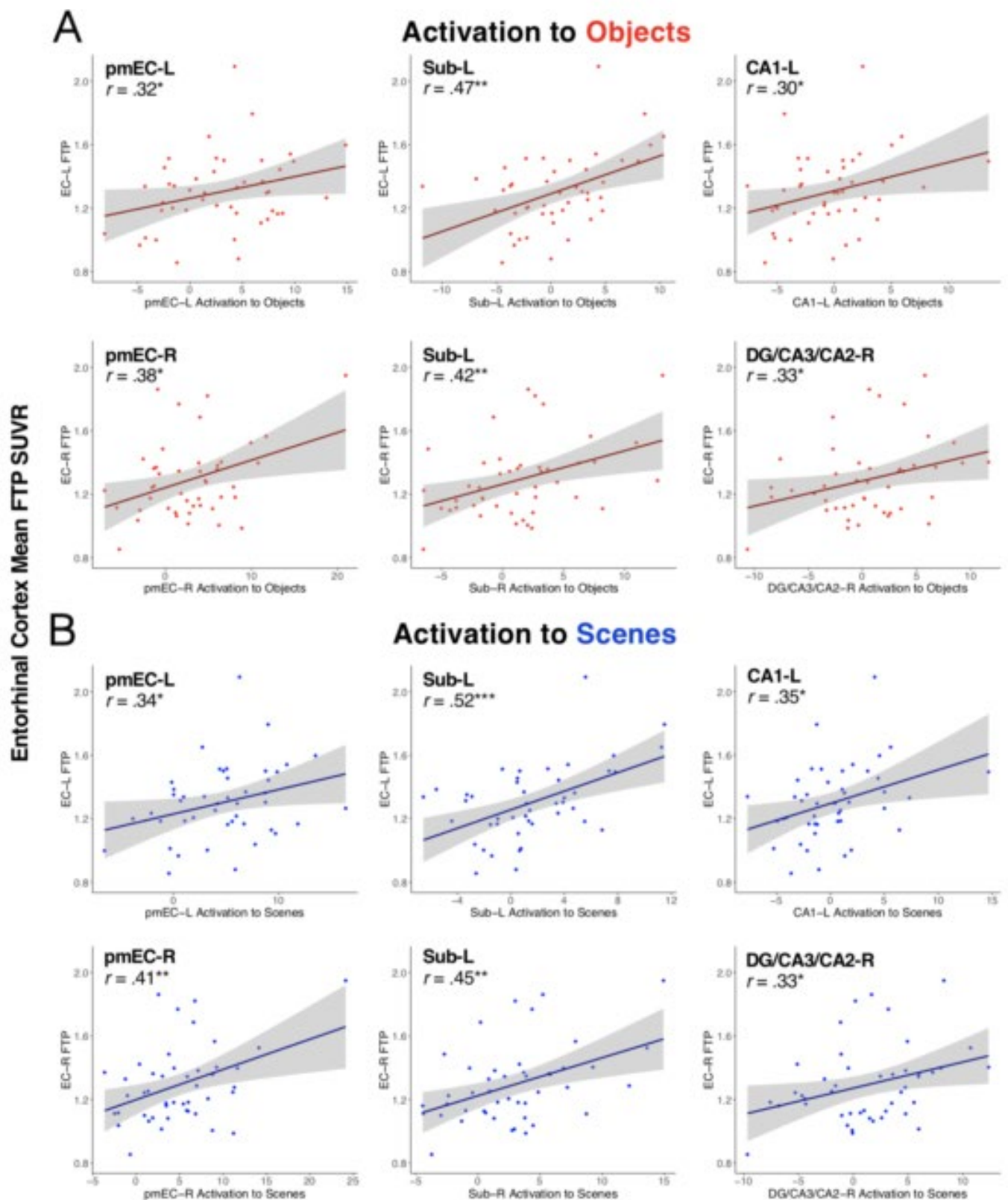


Figure 3. Associations between tau deposition and task activation to objects and scenes. We investigated relationships between tau deposition in the entorhinal cortex (EC) and task activation in specific EC subregions (anterolateral EC, alEC; posteromedial EC, pmEC) and hippocampal subfields (DG/CA3/CA2 [merged]; CA1; subiculum, Sub). Activation was defined as the contrast between either object or scene stimuli compared to baseline “noise” images, and the mean beta was extracted for each ROI. All correlations control for age and sex. The pmEC, subiculum, left CA1, and right DG/CA3/CA2 demonstrated positive correlations between EC tau and activation for both object (A) and scene (B) stimuli, indicating hyperactivity in response to tau deposition. * $p < 0.05$ ** $p < 0.01$ *** $p < 0.001$

Keywords: entorhinal cortex, hippocampus, tau, hyperactivity, aging

P101: Clinicopathological confirmation of ¹²³I-FP-CIT SPECT (ioflupane) quantification methods in a spectrum of neurodegenerative syndromes and associated pathologies

Daniela Maltais¹, Lennon Jordan¹, Toji Miyagawa¹, Timothy Lesnick¹, Scott Przybelski¹, Hoon-Ki Min¹, Dennis Dickson², Melissa Murray², Kejal Kantarci¹, Bradley Boeve¹, Val Lowe¹

¹*Mayo Clinic, Rochester, MN, US*

²*Mayo Clinic, Jacksonville, FL, US*

Rationale: To conduct a retrospective study comparing three ¹²³I-FP-CIT SPECT quantitative methods in patients with neurodegenerative syndromes as referenced to neuropathological findings.

Methods: ¹²³I-FP-CIT SPECT and neuropathological findings among patients with neurodegenerative syndromes from the Mayo Alzheimer's Disease Research Center (ADRC) and Mayo Clinic Study of Aging (MCSA) were examined. Three ¹²³I-FP-CIT SPECT quantitative assessment methods: MIMneuro (MIM Software Inc.), DaTQUANT (GE Healthcare), and manual region of interest (ROI) creation on an Advantage Workstation (GE Healthcare) were compared to neuropathological findings describing the presence or absence of Lewy body disease (LBD). Striatum to background ratios (SBRs) generated by DaTQUANT were compared to calculated SBRs using a manual method and MIMneuro. The left and right SBRs for caudate, putamen and striatum were evaluated with the manual method. For DaTQUANT and MIMneuro the left, right, total and average SBRs and z-scores for whole striatum, caudate, putamen, anterior putamen, and posterior putamen were calculated.

Results: The cohort included 24 patients [20 (83%) male, aged 75.4 +/- 10.0 at death]. The antemortem clinical diagnoses were Alzheimer's disease dementia (ADem, N=6), probable dementia with Lewy bodies (pDLB, N=12), mixed ADem/pDLB (N=1), Parkinson's disease with mild cognitive impairment (N=2), corticobasal syndrome (N=1), idiopathic REM sleep behavior disorder (N=1) and behavioral variant frontotemporal dementia (N=1). Seventeen (71%) had LBD pathology. All three ¹²³I-FP-CIT SPECT quantitative methods had AUROC values above 0.93 and up to 1.000 (p<0.001) and showed excellent discrimination between LBD and non-LBD patients in each region assessed, p<.001. There was no significant difference between the accuracy of the regions in discriminating the two groups, with good discrimination for both caudate and putamen.

Conclusions: All three ¹²³I-FP-CIT SPECT quantitative methods showed excellent discrimination between LBD and non-LBD patients in each region assessed, using both SBRs and z-scores.

Keywords: Dementia with Lewy Bodies; Lewy body disease; ¹²³I-FP-CIT SPECT; ¹²³I-ioflupane; neuropathology

P102: Preliminary results: PiB and MK6240 regional PET measures associated with digitized clock drawing performance

Danielle Mayblyum¹, Emma Thibault¹, Kirsten Moody¹, Michelle Farrell¹, Shu Jiang¹, Heidi IL Jacobs¹, Zoe Rubinstein¹, Justin Sanchez¹, Samantha Katz¹, Reisa Sperling^{1,2}, Kathryn Papp^{1,2}, Dorene Rentz^{1,2}, Keith Johnson^{1,2}

¹*Massachusetts General Hospital, Boston, MA, US*

²*Brigham and Women Hospital, Boston, MA, US*

Background: The clock-drawing test is a classic cognitive screening tool. Recently, use of a digital pen, featuring an embedded camera, has improved the quality of information gleaned from this task, increasing the sensitivity for early detection of subtle cognitive abnormalities. Here, we explore the relationships between digitized clock drawing performance (using DCTclock) and Alzheimer's disease molecular neuropathology measured with amyloid and tau PET in adults ranging from clinically normal (CN) to cognitively impaired (CI).

Methods: We studied 61 adults (52 CN and 9 CI, table 1) who completed a spontaneous drawing of a clock (COM-command). Participants underwent PIB and MK-6240 PET acquisition. Amyloid burden was assessed in terms of FLR (frontal, lateral temporal and retrosplenial cortices) DVR and tau SUVR (cerebellar reference) in entorhinal (EC), inferior temporal (IT), amygdala (AM), and hippocampus (HP).

Welch's two-sample t-tests were used to look at group mean differences in clock performance scores between low and high PiB CN and between all CN and CI were evaluated using Welch two-sample T-sample. We also correlated PET biomarkers and clock composite total score (DCT Score) as well as subcategory scores that included Drawing Efficiency, Information Processing, Simple Motor, and Spatial Reasoning.

Results: CI performed worse compared with CN on clock drawing (all $p < 0.05$), but there was no significant difference between high and low PIB groups (Fig.1). Across the entire sample, greater PiB FLR correlated with worse performance on all pen measures except the Simple Motor score (Fig.2). Greater MK-6240 signal across all regions was also associated with worse DCTclock performance across all measures.

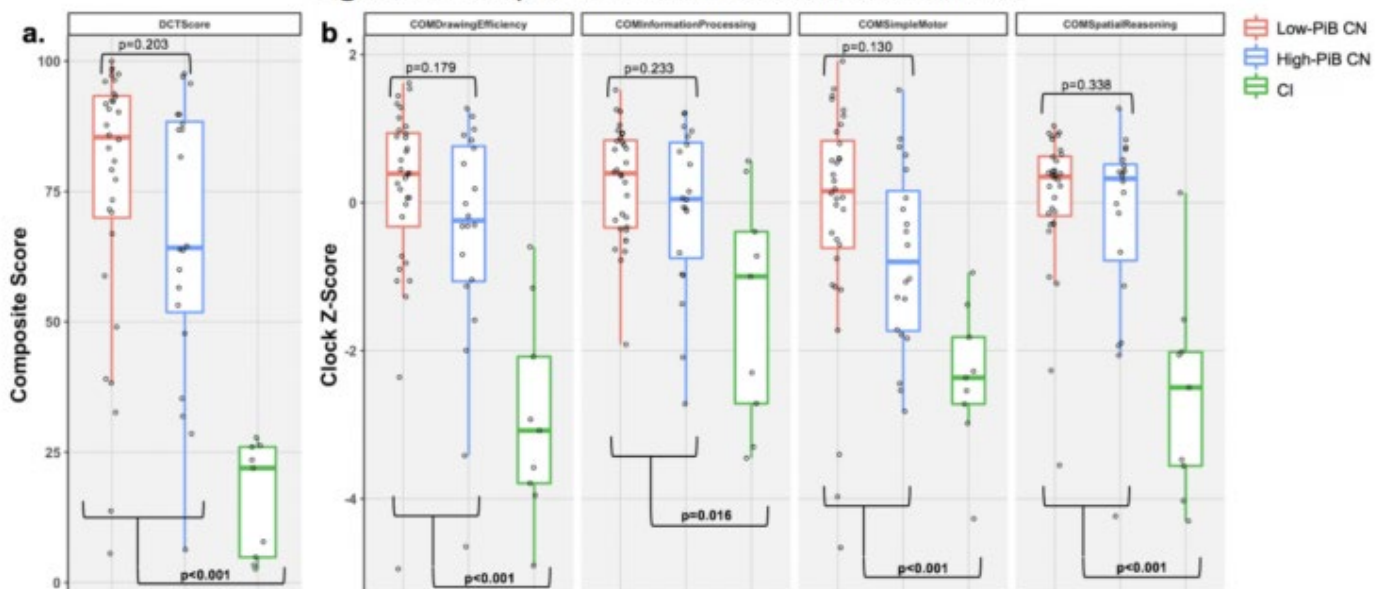
Conclusion: Preliminary findings show that DCTclock performance is negatively associated with PiB FLR and regional measures of MK-6240. Combining the digitized clock test with these imaging measurements could allow for better detection of subtle abnormalities that are not testable with normal cognitive measures.

Table 1. Subject demographic information

	All	Low-PiB CN	High-PiB CN	All CN	CI
N	61	32	20	52	9
Age	67.81 ± 11.01 (37.75-86.50)	64.02 ± 11.76 (37.75-82.5)	72.79 ± 8.33* (52.25-86.5)	67.46 ± 11.32 (37.75-86.50)	69.81 ± 10.12 (58.25-84.00)
Education	16.7 ± 2.59 (9-21)	16.5 ± 2.48 (9-21)	17.6 ± 2.41 (11-21)	16.92 ± 2.49 (9-21)	15.44 ± 2.96 (12-19)
Females N (%)	28 (45.9)	13 (40.6)	13 (65)	26 (50)	2 (22.2)
PiB FLR DVR	1.24 ± 0.27 (0.98-2.08)	1.04 ± 0.04 (0.98-1.14)	1.48 ± 0.25** (1.15-2.08)	1.21 ± 0.27 (0.98-2.08)	1.4 ± 0.26~ (1.10-1.82)
Entorhinal MK SUVR	1.26 ± 0.72 (0.64-4.25)	0.9 ± 0.20 (0.64-1.66)	1.49 ± 0.69* (0.71-3.58)	1.13 ± 0.54 (0.64-3.58)	2.03 ± 1.11* (1.00-4.25)
Inferior temporal MK SUVR	1.34 ± 0.99 (0.69-6.06)	0.97 ± 0.13 (0.69-1.28)	1.31 ± 0.76~ (0.85-3.98)	1.10 ± 0.5 (0.69-3.98)	2.7 ± 1.82* (0.98-6.06)
Amygdala MK SUVR	0.88 ± 0.63 (0.44-4.04)	0.58 ± 0.1 (0.44-0.88)	0.99 ± 0.51* (0.5-2.67)	0.74 ± 0.38 (0.44-2.67)	1.68 ± 1.12* (0.59-4.04)
Hippocampus MK SUVR	0.85 ± 0.35 (0.52-2.77)	0.69 ± 0.12 (0.52-1.06)	0.92 ± 0.27* (0.56-1.69)	0.78 ± 0.22 (0.52-1.69)	1.25 ± 0.64~ (0.76-2.77)
DCT Score	63.87 ± 31.56 (2.61-100)	75.86 ± 25.53 (5.56-100)	66.23 ± 26.43 (6.32-97.6)	72.15 ± 26.05 (5.56-100)	16.02 ± 11.00** (2.61-27.81)
COM Drawing Efficiency	-0.51 ± 1.72 (-4.95-1.62)	0.12 ± 1.32 (-4.95-1.62)	-0.45 ± 1.54 (-4.65-1.27)	-0.10 ± 1.42 (-4.95-1.62)	-2.9 ± 1.39** (-4.9-0.6)
COM Information Processing	-0.10 ± 1.16 (-3.45-1.52)	0.27 ± 0.76 (-1.92-1.52)	-0.08 ± 1.10 (-2.72-1.21)	0.13 ± 0.91 (-2.72-1.52)	-1.43 ± 1.55* (-3.45-0.56)
COM Simple Motor	-0.67 ± 1.56 (-4.66-1.91)	-0.14 ± 1.54 (-4.66-1.91)	-0.74 ± 1.24 (-2.82-1.52)	-0.37 ± 1.45 (-4.66-1.91)	-2.37 ± 0.97** (-4.27-0.94)
COM Spatial Reasoning	-0.44 ± 1.47 (-4.30-1.28)	0.07 ± 0.96 (-3.55-1.04)	-0.27 ± 1.35 (-4.24-1.28)	-0.06 ± 1.12 (-4.24-1.28)	-2.60 ± 1.40** (-4.30-0.13)

Legend: Welch's two-sample t-tests were done between low and high PiB CN and between all CN and CI. There was a group mean difference between CN and CI clock performance scores. mean ± SD (min-max), ~p<0.10, *p<0.05, **p<0.001

Figure 1. Group differences in clock measurements

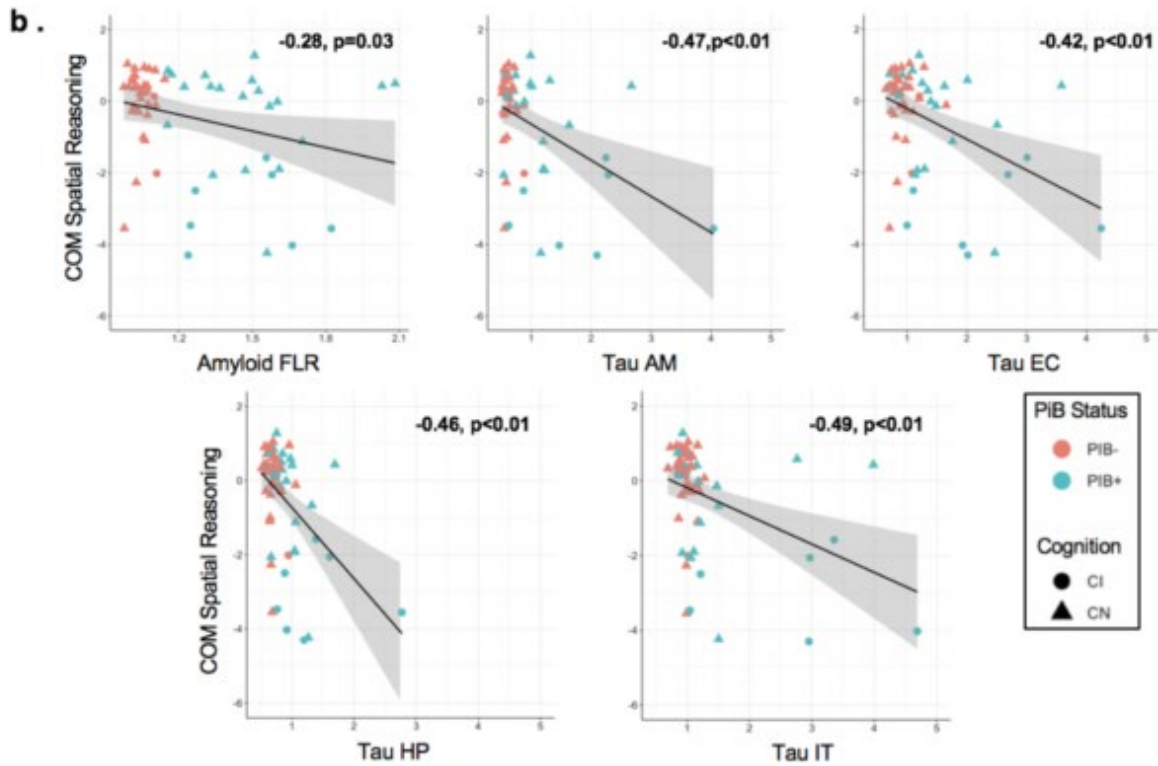


Legend: Boxplots showing the distribution of DCT scores (a) and subcategory scores (b) in the low and high-PiB CN groups, as well as in the CI group. There were no group mean differences in DCTclock performance between low and high-PiB individuals, but there were differences in performance between CN and CI individuals. Significant p-values < 0.05 are in bold.

Figure 2. Cross-Sectional regional amyloid and tau correlations with DCT clock scores

a.

	Amyloid FLR		Tau AM		Tau HP		Tau EC		Tau IT	
	r	p	r	p	r	p	r	p	r	p
DCT Score	-0.28	0.03	-0.34	<0.01	-0.34	<0.01	-0.34	<0.01	-0.43	<0.01
COM Drawing Efficiency	-0.23	0.08	-0.32	0.01	-0.31	0.01	-0.28	0.03	-0.37	<0.01
COM Information Processing	-0.33	0.01	-0.46	<0.01	-0.46	<0.01	-0.44	<0.01	-0.52	<0.01
COM Simple Motor	-0.15	0.25	-0.26	0.04	-0.25	0.05	-0.22	0.09	-0.25	0.05
COM Spatial Reasoning	-0.28	0.03	-0.47	<0.01	-0.46	<0.01	-0.42	<0.01	-0.49	<0.01



Legend: (a) In the entire sample, PiB FLR was negatively correlated with all of the DCTclock scores except COM simple motor performance. MK-6240 signal in all four ROIs was also associated with the clock composite and all the COM subcategory scores. (b) Scatterplots are shown displaying the relationship between PiB FLR and regional MK-6240 with the COM spatial reasoning subcategory. Significant p-values < 0.05 are in bold.

CN = cognitively normal; CI = cognitively impaired; AM = amygdala; HP = hippocampus; EC = entorhinal; IT = inferior temporal

Keywords: DCTclock, amyloid, tau, MK-6240-PET, PiB-PET

P103: White matter disruption is an early and progressive feature of pre-symptomatic Dutch-type hereditary cerebral amyloid angiopathy

Matthew Scott¹, Aaron Schultz¹, Hamid Sohrabi^{2,3}, Samantha Gardener², Kevin Taddei², Randall Bateman⁴, Tammie Benzinger⁴, Keith Johnson¹, Reisa Sperling¹, Ralph Martins^{2,3}, Steven Greenberg¹, Jasmeer Chhatwal¹, DIAN Investigators⁴

¹*Departments of Neurology and Radiology, Massachusetts General Hospital/Harvard Medical School, Boston, MA, US*

²*School of Medical and Health Sciences, Edith Cowan University, Joondalup, Australia*

³*Department of Biomedical Sciences, Macquarie University, North Ryde, Australia*

⁴*Departments of Neurology and Radiology, Washington University School of Medicine, St. Louis, MO, US*

Introduction: Dutch-type autosomal dominant cerebral amyloid angiopathy (D-CAA), caused by a point mutation in the Amyloid Precursor Protein (APP E693Q), offers a unique window into early CAA pathophysiology as mutation carriers can be studied during pre-symptomatic stages of disease, prior to intracranial hemorrhage or even susceptibility MRI-evident microhemorrhages. As part of an effort to develop clinical trials in D-CAA and sporadic CAA, a variety of biomarkers of CAA pathobiology have been examined, including 11C-Pittsburgh Compound B PET (PiB) PET. Recent work suggests that white matter changes in CAA occur early and may be particularly useful in tracking disease progression. In this context, we examined longitudinal white matter hyperintensity (WMH) volume and peak width of skeletonized mean diffusivity (PSMD; a diffusion tensor marker) changes in D-CAA carriers.

Methods: 21 asymptomatic participants from the Dominantly Inherited Alzheimer Network (DIAN; age: mean[SD]=42.7[7.3]; follow-up visits: mean[SD]=3.2[1.3]; mutation carriers: n[%]=10[47.7]; **Table 1**) underwent longitudinal MRI, including both diffusion tensor (DTI) and fluid-loss attenuated recovery (FLAIR) imaging. Linear mixed-effect models correcting for age were used to estimate both the cross-sectional and the longitudinal effects of mutation carriage on each biomarker.

Results: APP E693Q carriers exhibited higher PSMD than non-carriers cross-sectionally ($t(16)=2.83$, $\beta=6.2 \times 10^{-6}$, $p=0.01$) and greater rates of increased PSMD longitudinally ($t(58)=2.34$, $\beta=3.4 \times 10^{-6}$, $p=0.02$) as compared to non-carriers. Longitudinal change in FLAIR WMH was also strikingly different between mutation carriers and non-carriers ($t(62)=5.58$, $\beta=1004.3$, $p<0.00001$).

Discussion: Longitudinal changes in both PSMD and WMH were both significantly different in D-CAA mutation carriers vs non-carriers. Differential rates of longitudinal change in PSMD and WMH between APP E693Q carriers and non-carriers were of greater magnitude than the rates of change in longitudinal PiB PET in this sample and suggest that markers of white matter disruption may provide a useful compliment to amyloid PET and other biomarkers in CAA clinical research.

	Non-carriers	Carriers	All
Number of subjects	11	10	21
N (%)			
<i>APOE</i> ε4+	3 (27.3)	2 (20.0)	5 (23.8)
Sex(F)	7 (63.6)	7 (70.0)	14 (66.7)
Mean (SD)			
Age	40.3 (8.0)	45.4 (5.6)	42.7 (7.3)
Years of education	14.4 (3.0)	13.8 (2.6)	14.1 (2.8)
MMSE	28.3 (1.8)	28.6 (1.3)	28.4 (1.6)
Logical Memory (DR)	15.4 (5.3)	16.3 (4.1)	15.8 (4.7)
Follow-up sessions	2.7 (1.2)	3.7 (1.3)	3.2 (1.3) [#]
Follow-up range (years)	3.3 (2.2)	4.5 (1.6)	3.8 (2.0)
WMH volume (mm ³)	1.7x10 ³ (8.5x10 ²)	1.2x10 ⁴ (1.3x10 ⁴)	6.7x10 ³ (1.0x10 ⁴) [*]
PSMD (mm ² /s)	2.3x10 ⁻⁴ (2.2x10 ⁻⁵)	3.0x10 ⁻⁴ (6.9x10 ⁻⁵)	2.6x10 ⁻⁴ (6.2x10 ⁻⁵) ^{**}

Table 1. Demographic Information

Sample characteristics at baseline are presented within both carrier and non-carrier subgroups, as well as across all participants. Two sample t-tests and chi-squared tests were used for group comparison. All subjects had a global CDR of 0 at baseline except one non-mutation carrier (0.5). Moreover, two subjects had a global CDR of 0.5 at one follow-up visit. However, each of these participants subsequently scored 0 for the remainder of their visits. No participants in either group had a symptomatic intracranial hemorrhage.

Key: [#]*p*<0.01; ^{*}*p*<0.05; ^{**}*p*<0.01; ^{***}*p*<0.001 for comparison of mutation carriers and non-carriers; SD = standard deviation; *APOE* ε4 = Apolipoprotein E4 genotype; DR = delayed recall; CDR = Clinical Dementia Rating; MMSE = Mini-Mental State Examination; WMH = white matter hyperintensity; PSMD = peak width of skeletonized mean diffusivity (Diffusion Tensor Imaging).

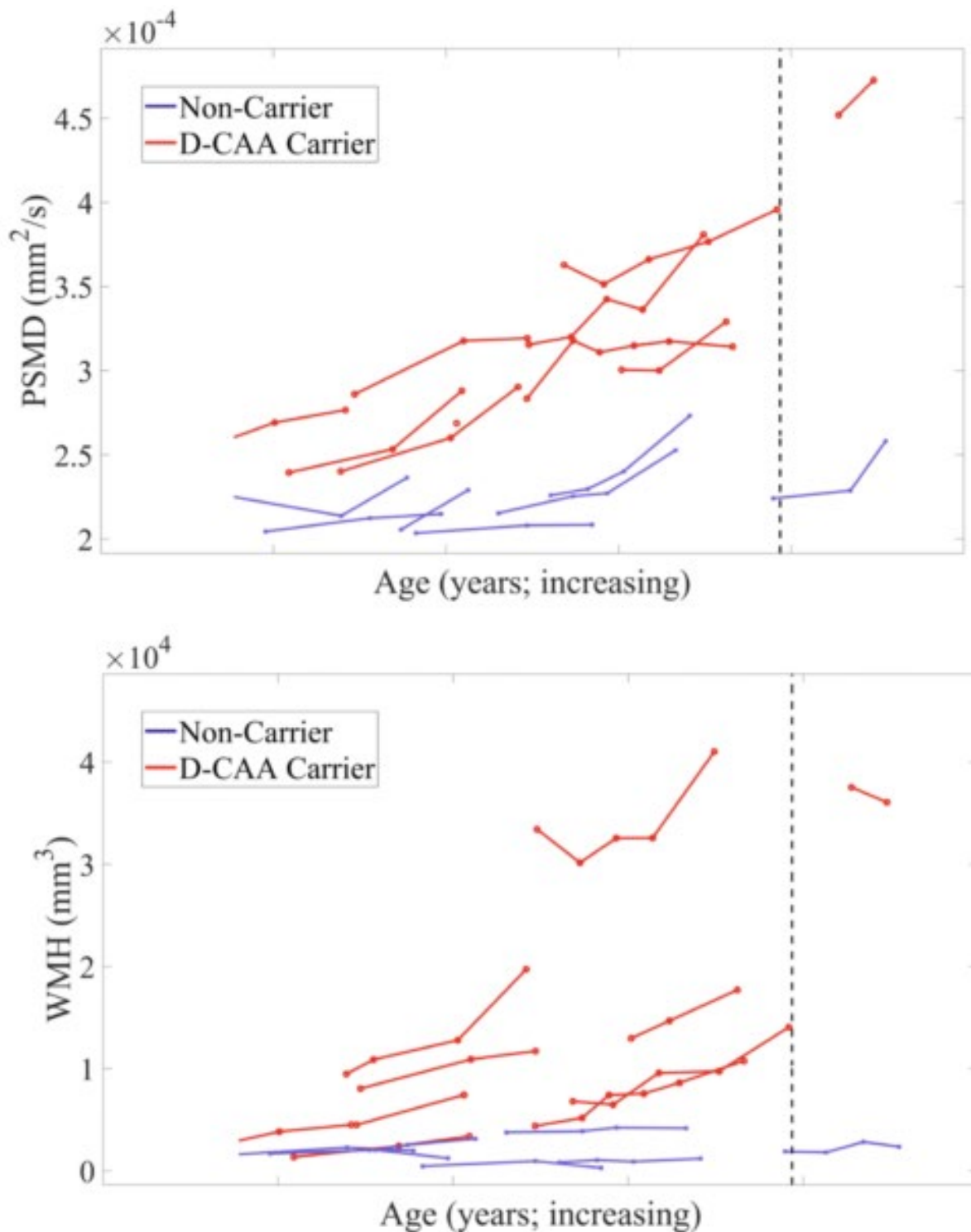


Figure 1. Longitudinal PSMD and WMH of mutation carriers and non-carriers

Unadjusted WMH and PSMD imaging data of Dutch-type CAA mutation carriers and non-carriers are plotted over time, using age as a temporal reference. Lines shown connect measurements from an individual participant during longitudinal follow-up. Dashed lines indicate median age of first hemorrhage in D-CAA. The lower end of the age range has been censored and age is not shown to reduce the chances of a participant surmising their mutation status.

Key: APP E693Q Carrier = red; Non-carrier = purple; WMH = white matter hyperintensity; PSMD = peak width of skeletonized mean diffusivity; CAA = cerebral amyloid angiopathy.

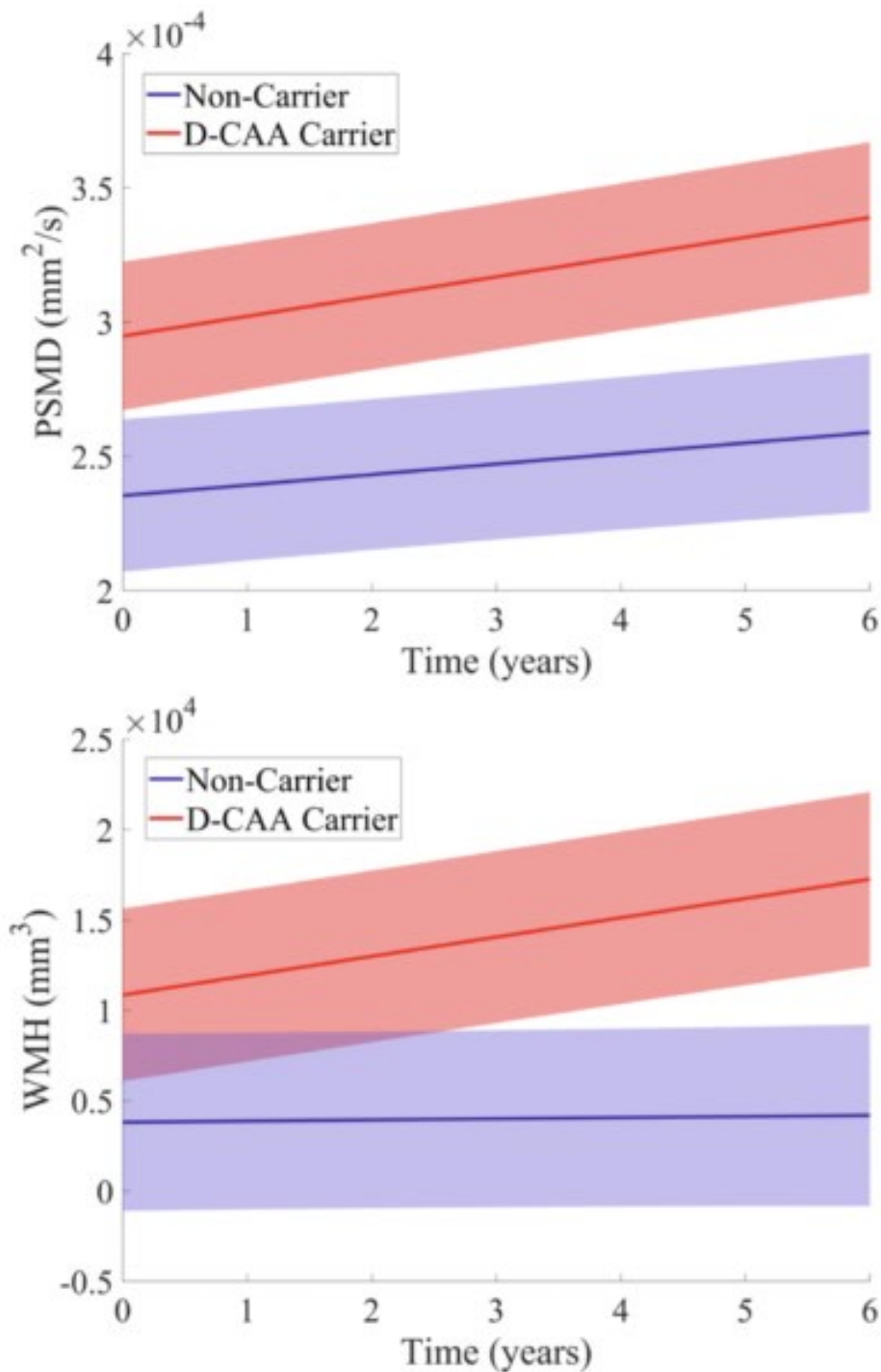


Figure 2. Simulation of mutation × time effect on longitudinal PSMD and WMH

Using linear mixed-effect models with baseline age as a covariate and random subject intercepts, we estimated the effect of mutation carriage × time on each imaging biomarker longitudinally. Significant effects were observed with both PSMD and WMH, however more noticeable rates differentials between carriers and non-carriers were observed with WMH.

Key: APP E693Q Carrier = red; Non-carrier = purple; WMH = white matter hyperintensity; PSMD = peak width of skeletonized mean diffusivity.

Keywords: D-CAA, DTI, MRI, White Matter

P104: Increased risk of Alzheimer's disease in alcohol use disorder is not mediated by amyloid-beta in a middle-aged cross-sectional cohort

Sarah Royse¹, Michael Himes², Davneet Minhas¹, Brian Lopresti¹, Margaret Flanigan², Rajesh Narendran²

¹University of Pittsburgh Department of Radiology, Pittsburgh, PA, US

²University of Pittsburgh Department of Psychiatry, Pittsburgh, PA, US

Introduction: Alcohol use disorder (AUD) is associated with cognitive impairment and dementia. Recent epidemiological studies suggest that AUD increases and shifts the risk of developing Alzheimer's disease (AD) from late-life to middle-age (Schwarzinger, 2018). This work examines in vivo amyloid-beta (A β) burden, cortical thickness, and gray matter volumes in a middle-aged AUD cohort relative to healthy controls (HC).

Methods: [¹¹C]PiB PET scans and corresponding T1 MPRAGE MRI scans were collected in 19 AUD (55.0 \pm 6.2 years, 4F/15M) and 20 HC (55.0 \pm 6.9 years, 6F/14M) subjects. AUD subjects met DSM-5 criteria for AUD and SAMHSA criteria for heavy drinking. MRI scans were processed using FreeSurfer v5.3 to define regions-of-interest (ROIs) for PET sampling, cortical thickness measures, and gray matter (GM) volumes. [¹¹C]PiB SUVR values (cerebellar GM reference) were determined for 9 target regions, which were combined into a global index of A β load. Cortical thickness values were combined into a single composite surface area-weighted average of entorhinal, inferior temporal, middle temporal, and fusiform regions. Regional GM volumes were normalized to the estimated total intracranial volume. Group differences between [¹¹C]PiB SUVRs, cortical thickness, and GM volumes were assessed using two-sample t-tests.

Results: No significant group differences were observed for regional ($p \geq 0.10$) or global PiB SUVR values ($p=0.99$). Compared to healthy controls, AUD subjects displayed a 6.1% reduction in mean cortical thickness ($p=0.0003$). Subjects with AUD also showed 9.7% reduction in hippocampal volume ($p=0.002$) and a 7.5% reduction in amygdala volume ($p=0.02$) compared to controls.

Conclusion: These results, which are consistent with previous post-mortem findings (Aho, 2009), suggest cortical thinning and gray matter atrophy precede typical AD A β pathology in AUD subjects. Individuals with AUD may have less brain reserve and as a result, exhibit signs of clinical AD earlier and more frequently compared to the rest of the population.

Table 1. Mean SUVR, cortical thickness, and GM volumes

Measure	Mean (SD)		p-value
	Healthy Controls (n = 20)	Patients with Alcohol Use Disorder (n = 19)	
SUVR			
Global	1.10 (0.04)	1.10 (0.06)	0.99
Anterior cingulate	1.17 (0.08)	1.17 (0.10)	0.95
Anterior ventral striatum	1.11 (0.08)	1.09 (0.12)	0.59
Superior frontal	1.09 (0.07)	1.10 (1.0)	0.71
Orbitofrontal	1.13 (0.05)	1.14 (0.08)	0.64
Insula	1.12 (0.05)	1.13 (0.06)	0.70
Lateral temporal	1.07 (0.03)	1.07 (0.04)	0.80
Parietal	1.08 (0.04)	1.07 (0.05)	0.62
Posterior cingulate	1.19 (0.06)	1.16 (0.06)	0.10
Precuneus	1.18 (0.06)	1.16 (0.07)	0.42
Cortical Thickness			
Composite	2.81 (0.11)	2.63 (0.15)	0.0003
Entorhinal	3.68 (0.36)	3.49 (0.39)	0.12
Inferior temporal	2.76 (0.14)	2.62 (0.17)	0.01
Middle temporal	2.83 (0.13)	2.63 (0.15)	0.0001
Fusiform	2.72 (0.12)	2.56 (0.17)	0.002
GM Volumes			
Hippocampus	29.31 (2.18)	26.46 (3.08)	0.002
Amygdala	11.48 (0.87)	10.62 (1.30)	0.02

Keywords: Alzheimer's disease, alcohol use disorder, amyloid-beta, cortical thickness, gray matter volume

P105: Longitudinal associations between lifestyle risk, β -amyloid, and cognition in late-midlife

Karly Cody¹, Rebecca Kosciak², Alex Birdsill¹, Sara Berman¹, Claire Erickson¹, Nathaniel Chin¹, Lindsay Clark^{1,2}, Brad Christian^{1,3}, Tobey Betthausen^{1,2}, Sterling Johnson^{1,2}

¹*Wisconsin Alzheimer's Disease Research Center, University of Wisconsin School of Medicine and Public Health, Madison, WI, US*

²*Wisconsin Alzheimer's Institute, University of Wisconsin School of Medicine and Public Health, Madison, WI, US*

³*Waisman Center, University of Wisconsin, Madison, WI, US*

Background: Recent studies suggest that duration of β -amyloid positivity is associated with cognitive decline. Lifestyle risk has been associated with cognitive impairment, but it is unknown whether lifestyle risk is associated with β -amyloid duration or if lifestyle risk is associated with longitudinal cognitive decline after accounting for β -amyloid duration. We utilized the Lifestyle for BRAin health (LIBRA) index (1) to investigate whether baseline lifestyle risk predicts incident cognitive decline and/or β -amyloid onset; (2) to examine the effect of longitudinal lifestyle risk on cognitive decline in the presence of β -amyloid.

Methods: Participants (n=1244, Table 1) from the Wisconsin Registry for Alzheimer's Prevention, a cohort enriched for AD risk, completed serial health and neuropsychological assessments with a subset (n=236) undergoing [¹¹C]PiB PET imaging. Cox regressions assessed the predictive utility of baseline LIBRA for incident cognitive decline (1.5 SD below covariate adjusted 3-test Preclinical Alzheimer's Cognitive Composite, PACC-3) and β -amyloid duration (i.e. age at assessment – estimated age PiB(+)). Linear mixed models examined the main effects and age interactions of LIBRA and β -amyloid duration on longitudinal cognitive performance.

Results: In the survival analysis, baseline LIBRA predicted risk for incident cognitive decline of subjects unimpaired at baseline (HR=1.18; Figure 1). In the imaging subset, baseline LIBRA did not predict β -amyloid onset (HR=0.85; Figure 1). Linear mixed effects models indicated a significant main effect of LIBRA (higher LIBRA risk = worse PACC-3) and a significant interaction of β -amyloid duration \times age on PACC-3 (longer β -amyloid duration = faster PACC-3 decline; Figure 2).

Conclusions: These findings suggest that a healthy lifestyle is associated with overall cognitive performance but not the rate of cognitive decline. Our data also suggest that lifestyle risk may not influence the onset of β -amyloid accumulation or hasten AD-related cognitive decline. Future studies with larger sample sizes, more AD biomarkers, and alternative risk indices are needed.

Table 1. Characteristics of the WRAP population				
Variable	Total study sample	Incident cognitive impairment	Cognitively unimpaired	Group p-value^a
N, cognitively unimpaired at baseline ^b	1244	156 (12.5%)	1088 (87.5%)	--
Age at baseline	59.3 (6.8)	59.6 (6.7)	59.2 (6.8)	.604
Years of follow-up	5.5 (3.6)	5.5 (3.6)	5.5 (3.5)	.245
Number of study visits	3 (1 to 6)	3 (1 to 5)	3 (1 to 6)	.587
PiB PET Imaging, n	236	38	198	--
PiB PET positive at last visit	49 (20.8%)	9 (23.7%)	40 (20.7%)	.628
Estimated age PiB positive, years	60.2 (8.2)	56.7 (7.5)	60.9 (8.3)	.167
APOE e4 positive ^c	472 (38.7%)	75 (50.3%)	397 (37.1%)	.002
Female sex	871 (70.0%)	108 (69.2%)	763 (70.1%)	.819
Less than 16 yrs of education	467 (37.5%)	61(39.1%)	406 (37.3%)	.667
LIBRA index components:				
Low/moderate alcohol consumption	1069 (85.9%)	132 (84.6%)	937 (86.1%)	.613
Cardiovascular disease	28 (2.3%)	5 (3.2%)	23 (2.1%)	.390
Physical inactivity	411 (33.0%)	56 (35.9%)	355 (32.6%)	.417
Renal dysfunction	22 (1.8%)	5 (3.2%)	17 (1.6%)	.145
Diabetes	91 (7.3%)	13 (8.3%)	78 (7.2%)	.601
High cholesterol	198 (15.9%)	23 (14.7%)	175 (16.1%)	.669
Smoking	76 (6.1%)	18 (11.5%)	58 (5.3%)	.002
Obesity	452 (36.3%)	60 (38.5%)	392 (36.0%)	.555
Hypertension	662 (53.2%)	86 (55.1%)	576 (52.9%)	.609
Depression	153 (12.3%)	31 (19.9%)	122 (11.2 %)	.002
High Cognitive Activity	276 (22.2%)	22 (14.1%)	254 (23.3%)	.009
LIBRA1 ^d Risk score	0.6 (-4.2 to 8.1)	1.5 (-4.2 to 6.8)	0.6 (-4.2 to 8.1)	.000
LIBRA2 ^e Risk score	1.0 (-4.2 to 8.3)	1.6 (-3.6 to 7.1)	0.7 (-4.2 to 8.3)	.000
Note: Values are present as n(%), mean (SD), or median (range). Incident cognitive impairment was defined as 1.5 SD below mean performance on covariate-adjusted three-test preclinical Alzheimer's cognitive composite (PACC-3).				
^a p-value for difference between groups of cognitively unimpaired participants and those with incident cognitive impairment				
^b Excluding 12 subjects with Mild Cognitive Impairment at baseline				
^c APOE e4 status (n=1219), missing for 25 subjects				
^d LIBRA1 index (modifiable risk factors only)				
^e LIBRA2 index + scores for age, sex, and education				

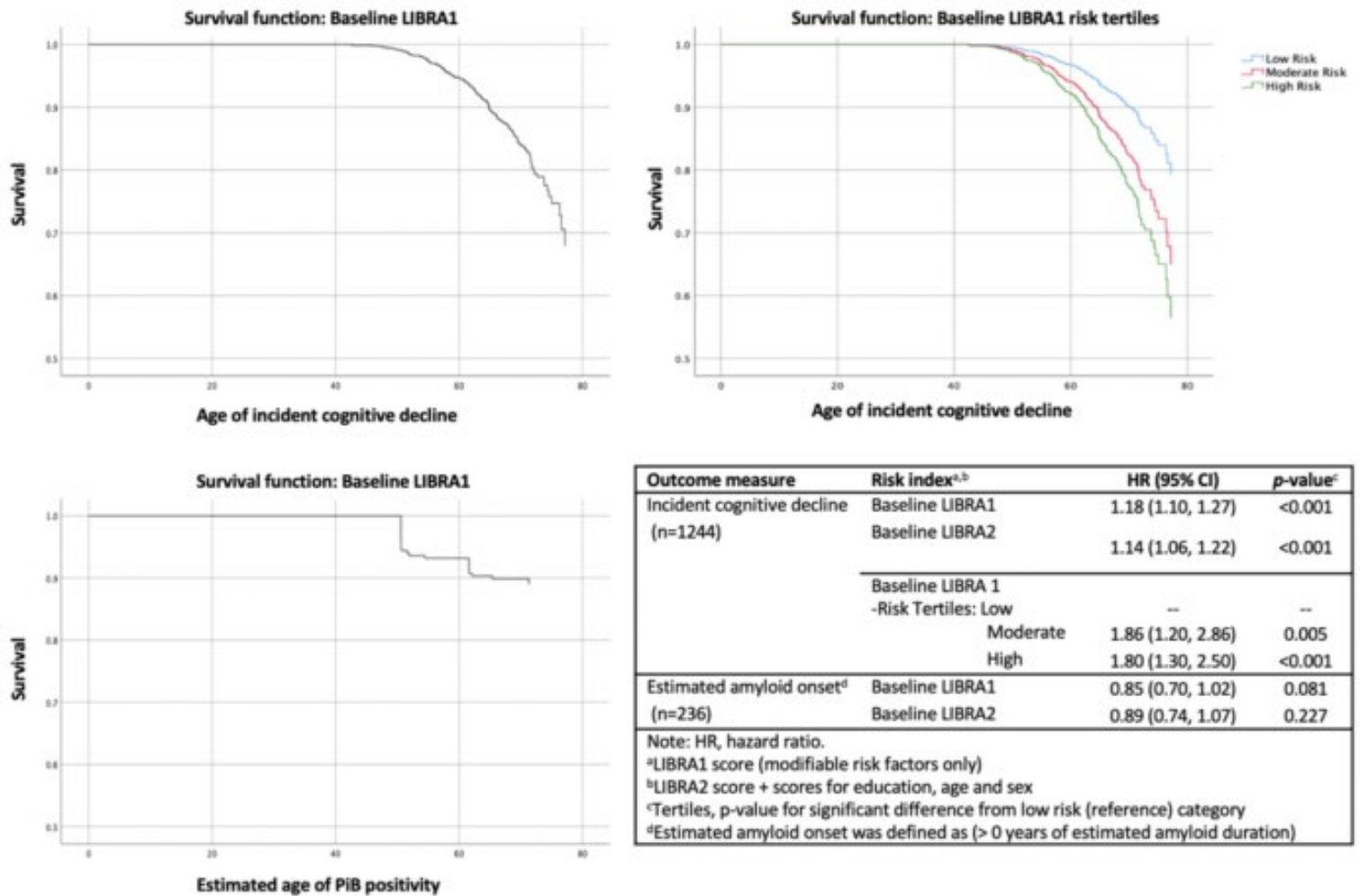


Figure 1. Survival probability for incident cognitive decline and amyloid duration. The predictive value of baseline LIBRA scores (also depicted in tertiles) for cognitive decline and amyloid duration as assessed by means of Cox proportional hazard models.

Primary Model of Interest Statistics			
Variable	β	95% CI	p
Covariates			
Intercept	-0.5717	-0.80, -0.34	<0.0001
Female	0.4720	0.31, 0.64	<0.0001
Education	0.2717	0.09, 0.45	0.0034
WRAT III	0.0217	0.01, 0.03	<0.0001
Practice	0.0709	0.03, 0.10	0.0020
Predictors of Interest			
Age	-0.0475	-0.0615, -0.0336	<0.0001
Amyloid Duration	-0.0028	-0.0088, 0.0032	0.3647
Age×Amyloid Duration	-0.0011	-0.0016, -0.0005	0.0002
LIBRA1	-0.0290	-0.0444, -0.0136	0.0002
PACC-3 ~ Covariates + Age + Amyloid duration + Amyloid duration×Age + LIBRA1 + random slope + random intercept			

Figure 2. Model of best fit. A total of 248 subjects (including 12 subjects who had mild cognitive impairment at baseline) with up to 5 visits were included in the model. A stepwise model-building approach was used to determine the best model for predicting longitudinal PACC-3 decline. Akaike information criterion (AIC; smaller = better model fit) was used to assess model quality. Model building steps included:

- 1) PACC-3 ~ Cov + Age + Amyloid duration+ random slope + random intercept (AIC=1267)
- 2) PACC-3 ~ Cov + Age + Amyloid duration + Amyloid duration×Age + random slope + random intercept (AIC=1255)
- 3) **PACC-3 ~ Cov + Age + Amyloid duration + Amyloid duration×Age + LIBRA1 + random slope + random intercept (AIC=1083)**
- 4) PACC-3 ~ Cov + Age + Amyloid duration + LIBRA + Amyloid duration×Age + LIBRA1×Age + random slope + random intercept (AIC=1084; Fixed effect of LIBRA1×Age, p=.3302)

Keywords: Amyloid, cognitive decline, lifestyle

P106: Exploring relationships between tau burden and naming in the aphasic variant of Alzheimer's disease

Adam Martersteck^{1,2}, Jaiashre Sridhar¹, Christina Coventry¹, Fatima Eldes¹, Jessica Wood¹, Iktae Kim¹, M.-Marsel Mesulam^{1,3}, Emily Rogalski^{1,4}

¹Mesulam Center for Cognitive Neurology and Alzheimer's Disease, Northwestern University Feinberg School of Medicine, Chicago, IL, US

²Department of Radiology, Northwestern University Feinberg School of Medicine, Chicago, IL, US

³Department of Neurology, Northwestern University Feinberg School of Medicine, Chicago, IL, US

⁴Department of Psychiatry and Behavioral Sciences, Northwestern University Feinberg School of Medicine, Chicago, IL, US

Background: Primary progressive aphasia (PPA) is a clinical dementia syndrome characterized by asymmetric atrophy of the language-dominant hemisphere. Alzheimer's disease neuropathology (AD) is present in ~40% of PPA cases. Previous cross-sectional studies examining the relationship between cognitive function and tau PET have reported a close relationship. However, most studies have been in amnesic AD.

Objective: Examine flortaucipir PET burden and cortical thickness relationships with naming in aphasic AD.

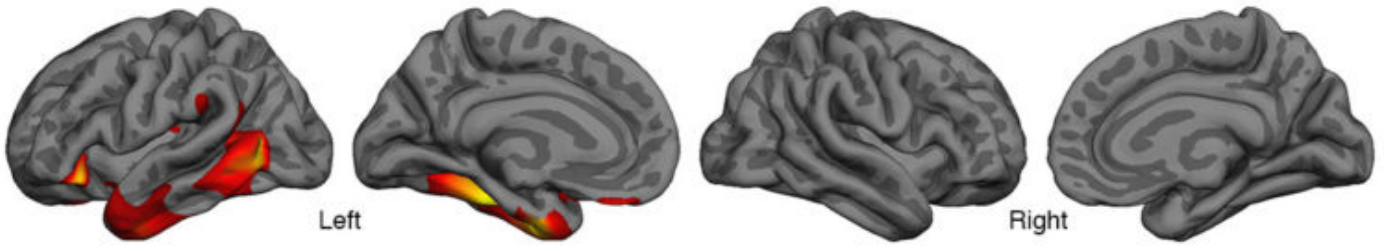
Methods: Seventeen PPA participants with suspected underlying Alzheimer's disease pathology (¹⁸F-florbetapir cortex to whole-cerebellar SUVR > 1.17) underwent ¹⁸F-flortaucipir PET, structural MR imaging, and neuropsychological testing. Eight participants received follow-up neuropsychological testing one year later. T₁-weighted Freesurfer v6.0.0 reconstructions provided Desikan-Killiany segmentations and surfaces for Rousset (Baker, et al. 2017) and Müller-Gärtner partial volume correction (PVC). The hotspot-removed inferior cerebellar grey from Baker et al. was used as a reference region in all analyses. A general linear model at every surface vertex was used to determine significant associations between tau PET, cortical thickness, and Boston Naming Test (BNT). Baseline tau burden and cortical thickness were used to predict the decline in naming over the following year. All analyses were corrected for multiple comparisons with FDR q=0.05 criterion.

Results: There was a significant relationship between BNT and cortical thinning in the left middle and anterior temporal regions at baseline (Figure 1A). The association between BNT and tau burden was more widespread (Figure 1B). Eight participants with follow-up testing revealed no significant relationship with change in BNT and baseline cortical thickness (Figure 2A). Conversely, tau burden across distributed regions significantly predicted the decline in the BNT (Figure 2B). Regional analyses with Rousset PVC replicated all findings.

Conclusions: In the aphasic variant of AD, focal atrophy is more closely linked to clinical symptoms while distributed tau burden is correlated with current naming ability and decline.

Figure 1. Relationship between baseline BNT and baseline imaging (n=17)

A. BNT and cortical thickness



B. BNT and tau burden

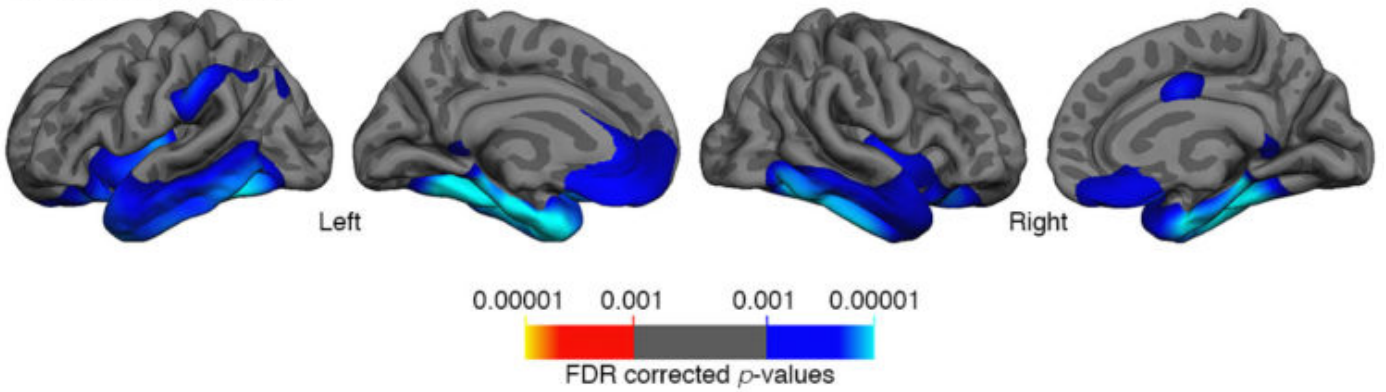
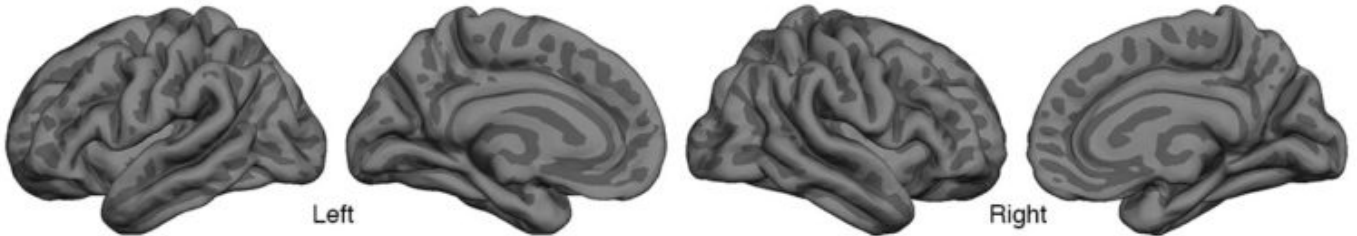
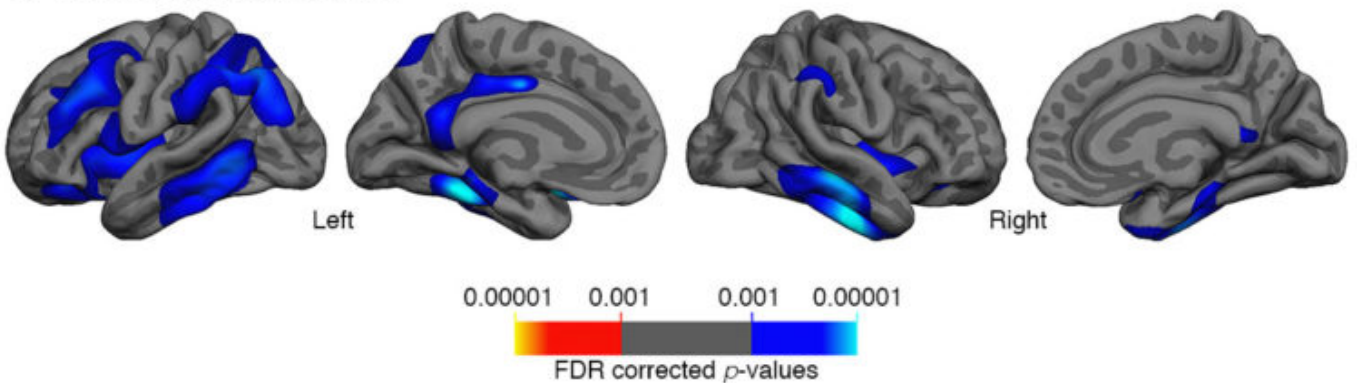


Figure 2. Relationship between 1-year change in Boston Naming Test (BNT) and baseline imaging (n=8)

A. BNT % change and cortical thickness



B. BNT % change and tau burden



Keywords: atypical dementia, primary progressive aphasia, tau, atrophy

P107: Data-driven approach to characterization of tau accumulation in Braak staging groups

Jenna Groh¹, Diana O. Svaldi¹, Edwin Stage¹, Apoorva Sanjay¹, Shannon Risacher¹, Andrew Saykin¹, Liana G. Apostolova¹

¹Indiana University School of Medicine, Indianapolis, IN, US

Background: While tau imaging is showing promise as a prognostic biomarker in Alzheimer's disease, additional work is needed to fully characterize its clinical usefulness. Using a data-driven approach, we classified individuals based on tau deposition in Braak regions and assessed how demographic, cognitive, and imaging biomarkers behaved in relation to tau deposition in the brain.

Methods: We included 317 participants [126 cognitively normal, 152 MCI, 39 dementia] with available: AV1451 -PET, FDG PET, AV45 PET, and MPRAGE MRI. We used k-means clustering to derive a two-group solution for each Braak stage (Figure A) and the 75th percentile + interquartile range of the negative group from each clustering solution to define tau-positivity. Subjects were grouped depending on tau positivity in each Braak region (see Table 1). We used ANOVA with Bonferroni correction for multiple comparisons to compare demographic, cognitive, and imaging biomarker measures across the groups.

Results: Tau positive Braak 1&2 individuals (group 211) were significantly older compared to individuals with diffuse tau positivity.

Mean cortical AV45 SUVR, percent amyloid-positive and cortical hypometabolism increased with increase in tau burden (group 111<211<221<222, Figure 1B). Absence of significant tau binding did not indicate lack of amyloid deposition or hypometabolism (Figure 1B). In contrast, global tau deposition (group 222) associated with global amyloid deposition and hypometabolism.

Cognitive performance was highly variable in individuals with no tau (group 111), while individuals with global tau deposition were globally impaired. There was a significant effect of tau Braak stage on Animal Fluency and Trails B (group 111<211<221<222).

Conclusions: The severity of tau deposition makes individuals more likely to exhibit cognitive deficits. Absence of tau did not correlate with absence of cognitive impairment. Greater prevalence of limbic-predominant AD pathology in older individuals and diffuse tau pathology in those who are younger is in line with previous observations.

Table 1

Group	Braak 1&2	Braak 3&4	Braak 5&6
111 (n=245)	Negative	Negative	Negative
211 (n=41)	Positive	Negative	Negative
221 (n=17)	Positive	Positive	Negative
222 (n=11)	Positive	Positive	Positive

*Groups 112, 121, 122, and 212 each had 1 or less group members and were excluded from analysis

Table 2

Total N = 314	111 (n=245)	211 (n=41)	221 (n=17)	222 (n=11)	P values
Age, Mean (SD)	76.2 (7.7)	80.3 (6.6)	79.6 (8.1)	73.8 (7.1)	0.003
Years of Education, Mean (SD)	16.4 (2.7)	16.3 (2.7)	15.4 (2.9)	16.8 (1.8)	0.415
AV45 Whole Cortex SUVR, Mean (SD)	1.07 (0.15)	1.25 (0.24)	1.35 (0.13)	1.42 (0.19)	<0.0001
Percentage Amyloid Positive	14.7%	55.6%	93.3%	100%	<0.0001
Diagnosis (%DEM)	4.3%	33.3%	38.8%	63.6%	<0.0001
FDG Whole Cortex SUVR, Mean (SD)	1.311 (0.12)	1.19 (0.13)	1.19 (0.1)	1.084 (0.09)	<0.0001
Hippo. Volume Mean (SD)	3170 (1139)	3097 (1401)	3153 (1069)	3314 (595)	.955
AV1451 PET SUVR Mean (SD)	1.44 (0.12)	1.60 (0.17)	1.93 (0.14)	2.89 (0.65)	<0.0001
Global CDR, Mean (SD)	0.23 (0.27)	0.71 (0.52)	0.79 (0.53)	1.18 (0.56)	<0.0001
MMSE, Mean (SD)	28.6 (1.8)	25.8 (3.7)	23.8 (5.3)	20.6 (6.5)	<0.0001
Fluency: Animals, Mean (SD)	19.3 (5.3)	15.2 (6.7)	12.3 (6.5)	10.2 (4.0)	<0.0001
Trails B sec, Mean (SD)	95.0 (59.6)	137.5 (86.7)	162.7 (89.5)	246.4 (94.0)	<0.0001
AVLT Immediate Recall, Mean (SD)	7.6 (4.2)	3.2 (3.3)	2.3 (3.7)	1.6 (1.6)	<0.0001
AVLT 30 min Delayed Recall, Mean (SD)	6.4 (4.5)	2.8 (6.14)	1.3 (3.6)	0.7 (1.3)	<0.0001

Figure 1A

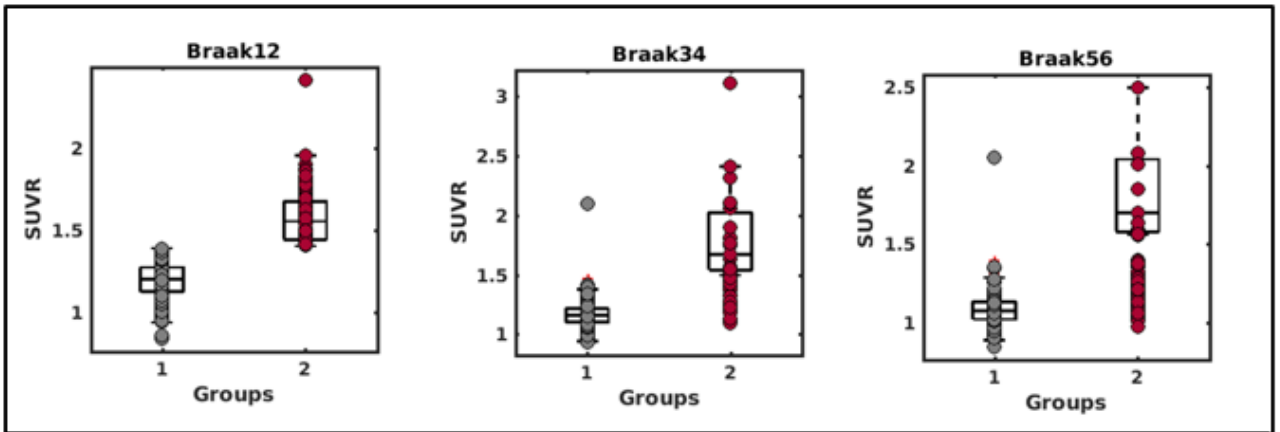
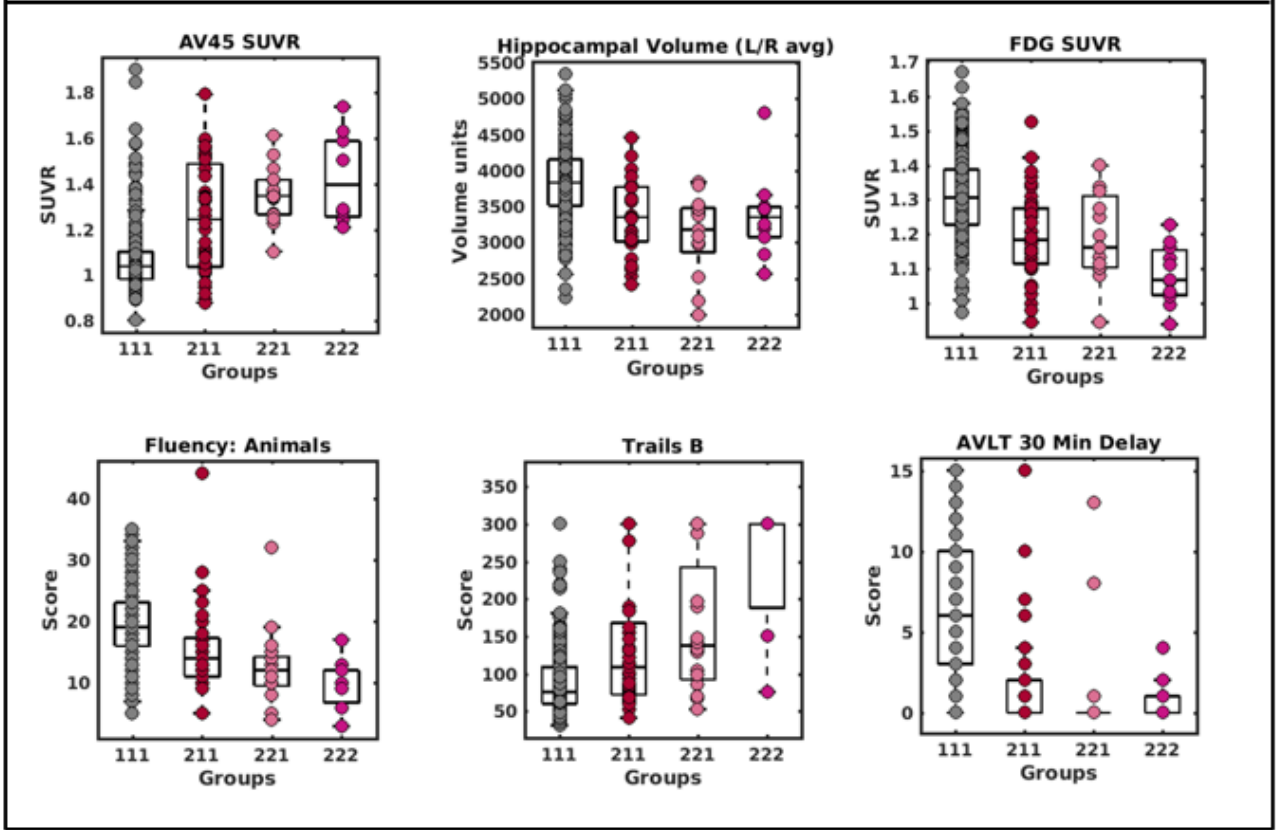


Figure 1B



Keywords: Tau cut-off, data-driven approach, Braak regions

P108: Associations between Alzheimer's disease biomarkers and cognition among cognitively normal older adults

Hwamee Oh^{1,2,3}, Stephen Correia^{1,2,3}, Stephen Salloway^{1,2,3}

¹*Department of Psychiatry and Human Behavior, Warren Alpert Medical School, Brown University, Providence, RI, US*

²*Carney Institute of Brain Science, Brown University, Providence, RI, US*

³*Memory and Aging Program, Butler Hospital, Providence, RI, US*

Background: Although the presence of brain A β plaques has been related to steeper cognitive decline over time and an increased risk of developing AD, a co-presence of tau pathology in these individuals makes it challenging to link AD pathologies to specific cognitive function and brain structure. We examined how A β and tau pathologies differentially affect cognition and brain structure among clinically intact older adults.

Methods: We assessed the relationship between A β and tau pathology, gray matter atrophy, and cognition among 78 cognitively normal older adults in the Alzheimer's Disease Neuroimaging Initiative whose brain A β deposition and tau-protein neurofibrillary tangles were detected by 18F-Florbetapir and 18F-Flortaucipir, respectively. Within a subset of the sample, CSF measures of amyloid (A β ₄₀ and A β ₄₂) and tau (t-tau and p-tau) pathologies were assessed in relation to cognition and cortical thickness. Multiple regression models were applied to assess the relationships between AD pathologies, gray matter atrophy, and cognition using region-of-interest and whole-brain surface-based approaches.

Results: Higher entorhinal tau PET counts corresponded to greater gray matter atrophy in the entorhinal cortex and hippocampus and poorer executive function performance, controlling for age, sex, and whole-brain amyloid load. In the subset of the sample, whole-brain amyloid load related to poorer memory and executive function performance, controlling for age, sex, and CSF total tau. Age was associated with memory and executive function performance, independent of entorhinal tau PET counts, CSF total tau, and whole-brain amyloid load. Entorhinal tau PET counts did not correlate with CSF total tau or p-tau among cognitively normal older adults.

Conclusions: Amyloid and tau pathologies differentially influence cognition and brain structure. A low correlation between tau PET and CSF total tau measures in cognitively normal older adults may warrant further investigation on the source of discordance in these measures.

Keywords: amyloid PET, tau PET, cortical atrophy, cognition, cognitively normal older adults

P109: In vivo association of mitochondrial dysfunction with tau pathology in early Alzheimer's disease

Tatsuhiko Terada^{1,2,3}, Joseph Therriault¹, Peter Kang Min Su¹, Melissa Savard¹, Yasuomi Ouchi², Pedro Rosa-Neto¹

¹The McGill University Research Centre for Studies in Aging, Verdun, QC, Canada

²Hamamatsu University School of Medicine, Department of Biofunctional Imaging, Hamamatsu, Japan

³Shizuoka Institute of Epilepsy and Neurological Disorders, Department of Neurology, Shizuoka, Japan

Background: In addition to the amyloid and tau, mitochondrial dysfunction is important event in the Alzheimer's disease (AD). However, it remains unclear how these abnormal proteins associated with mitochondrial dysfunction in vivo. The purpose of this study is to clarify the mutual relationship among mitochondrial dysfunction and AD pathologies in the patients with early stage AD by using positron emission tomography (PET).

Methods: Sixteen amyloid positive AD patients at the CDR 0.5 or 1 (mean age \pm SD: 73.2 \pm 6.3 years) underwent series of PET measurements with [¹¹C]PiB for amyloid deposition, [¹¹C]PBB3 for tau deposition, [¹⁸F]FDG for glucose metabolism, and [¹⁸F]BCPP for mitochondrial function. Association among these four PET parameters were evaluated by using voxel-based regression model and region of interest methods.

Results: The medial and lateral temporal area and front-parietal area were identified as the region in which [¹⁸F]BCPP SUVR was negatively correlated with [¹¹C]PBB3 BP_{ND}. There was significant negative correlation of [¹⁸F]BCPP SUVR with [¹¹C]PBB3 BP_{ND} in the Braak stage 2 area, but not with [¹¹C]PiB SUVR and [¹⁸F]FDG SUVR.

Conclusion: Our results suggested that mitochondrial dysfunction is closely associated with tau pathology. The negative correlation between mitochondrial dysfunction and tau deposition in the entorhinal region suggested that tau pathology might precede mitochondria-related energy failure in the early neurodegenerated region in AD. Mitochondrial dysfunction in this area is considered an early pathophysiological feature of AD.

Keywords: Alzheimer's disease (AD), mitochondria, tau, [¹⁸F]BCPP, [¹¹C]PBB3

P110: Using famous faces to investigate the neural systems involved in name retrieval

Victoria Tennant^{1,2}, William Jagust^{1,2}, Renaud La Joie³, Jenna Adams¹, Joseph Winer⁴

¹*Helen Wills Neuroscience Institute, University of California, Berkeley, Berkeley, CA, US*

²*Lawrence Berkeley National Laboratory, Berkeley, CA, US*

³*University of California, San Francisco, San Francisco, CA, US*

⁴*Department of Psychology, University of California, Berkeley, Berkeley, CA, US*

Objective: The inability to retrieve names from long term memory is a common complaint in older adults. We aimed to investigate if the ability to name famous faces was associated with neuroimaging biomarkers; including measures of cortical thickness, amyloid- β , and regional tau pathology.

Methods: 85 cognitively normal older adults (mean age 81; range 66-92) from the Berkeley Aging Cohort Study who had available structural MRI, PIB-PET and Flortaucipir-PET were tested using the Northwestern Famous Faces (NUFFACE) test. This test distinguishes the ability to freely retrieve the names of famous faces after being shown their picture (“naming”) versus generally recognizing the person (“recognition”). Neuroimaging measures affected in aging and early Alzheimer’s were selected, including cortical thickness in bilateral temporal areas, a global amyloid- β value (i.e. cortical PiB-DVR) and Flortaucipir in temporo-parietal regions (partial volume corrected SUVR).

Results: Participants did significantly worse on the naming (mean 30/40; range 10-40), compared to the recognition task (mean score 36/40; range 20-40). Bivariate correlations between neuroimaging measures, demographics, and NUFFACE scores are shown in Table1. All 6 significant variables from Table1 were entered into a backwards stepwise model, dropping variables until reaching minimal Akaike information criterion (AIC). The final model indicated that lower fusiform thickness and greater entorhinal tau independently predicted worse naming scores (Table2). Complementary analyses were conducted on R/L fusiform separately and were significant on both sides but stronger on the right (Figure 1). The fusiform thickness and entorhinal tau model did not predict recognition scores ($p > .82$ and $p > .06$).

Conclusions: Fusiform thickness and entorhinal tau pathology were the best predictors of performance on the NUFFACE naming task after controlling for other temporo-parietal regions and memory ability. These findings implicate effects of tau and neurodegeneration on neural systems involved in facial identification and memory in a common complaint of aging.

Table 1. Results from bivariate analyses predicting NUFFACE naming score

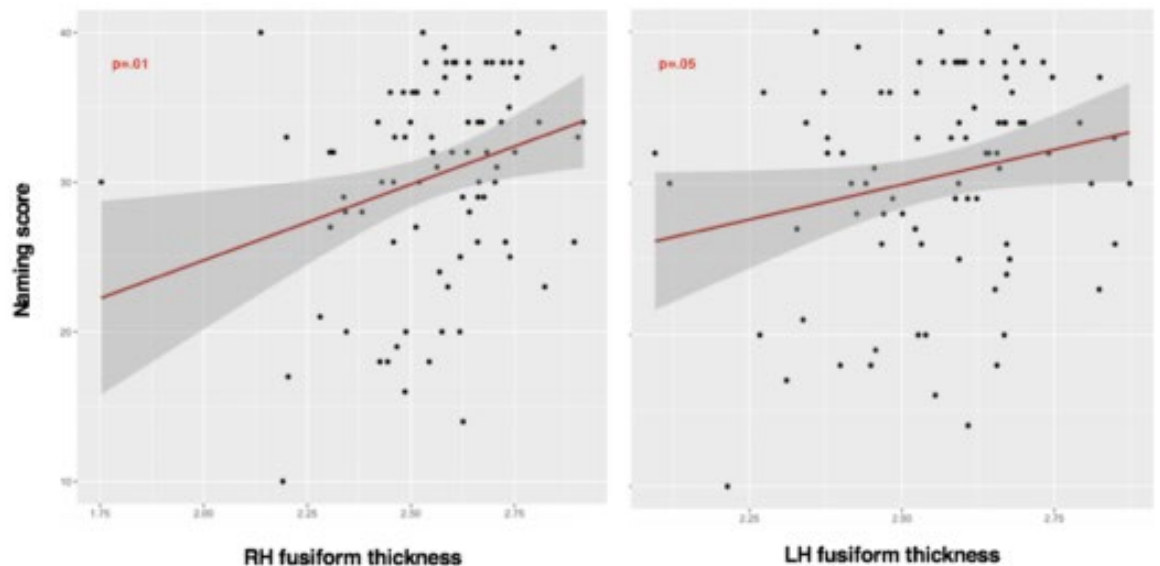
Predictor	t	p	Stand. Estimate
Age*	-2.29	0.025	-0.244
Sex	-1.57	0.120	-0.169
Education yrs.	0.41	0.681	-0.045
Episodic memory*	2.84	0.006	0.298
Entorhinal thickness*	2.74	0.008	0.288
Fusiform thickness*	2.46	0.016	0.261
Precuneus thickness	1.23	0.222	0.134
Fusiform tau (SUVR _{PVC}) *	-3.01	0.003	-0.314
Entorhinal tau (SUVR _{PVC}) *	-4.16	<.001	-0.415
Cortical A β (PiB-DVR)	-4.94	0.113	-0.173

*Based on the significant correlation with NUFFACE naming scores, all these variables were entered into a stepwise regression (see Table 2)

Table 2. Results from final model selected through backwards stepwise linear regression $R^2 = 0.26$

Predictor	t	p	Stand. Estimate
Fusiform thickness	2.63	0.010	0.251
Entorhinal tau (SUVR _{PVC})	-4.36	<.001	-0.416

This 2-variable model was selected by stepwise regression in which the AIC of the models is computed and the model that yields the lowest AIC is retained for the next iteration. Based on the 6 variables originally selected from bivariate correlations (Table 1).

Fig 1. Unilateral fusiform thickness and performance on NUFFACE naming task

Keywords: tau, amyloid, fusiform thickness, aging

P111: Cerebrospinal fluid matrix metalloproteinases are associated with compromised white matter microstructure among older adults: the Vanderbilt Memory & Aging Project

Elizabeth Moore¹, Kimberly Pechman¹, Lealani Mae Acosta¹, Susan Bell^{1,2}, Adam Anderson³, Bennett Landman³, Kaj Blennow⁴, Henrik Zetterberg^{4,5}, Katherine Gifford¹, Timothy Hohman¹, Angela Jefferson^{1,2}

¹Vanderbilt Memory & Alzheimer's Center, Department of Neurology, Vanderbilt University Medical Center, Nashville, TN, US

²Division of Cardiovascular Medicine, Department of Medicine, Vanderbilt University Medical Center, Nashville, TN, US

³Department of Biomedical Engineering, Vanderbilt University, Nashville, TN, US

⁴Department of Psychiatry and Neurochemistry, Institute of Neuroscience and Physiology, The Sahlgrenska Academy at University of Gothenburg, Gothenburg, Sweden

⁵United Kingdom Dementia Research Institute at University College London, London, UK

Background: Matrix metalloproteinases (MMPs) regulate extracellular matrix remodeling, blood-brain barrier permeability, and cell growth. While they have been implicated in vascular cognitive impairment and Alzheimer's disease (AD), associations with white matter integrity remain poorly understood. This study relates cerebrospinal fluid (CSF) biomarkers of MMP-2, MMP-3, and MMP-9 to white matter microstructure, assessed on diffusion tensor imaging (DTI).

Methods: Vanderbilt Memory & Aging Project participants (n=152, 72±6 years, 38% mild cognitive impairment (MCI)) underwent fasting lumbar puncture to obtain CSF and 3T brain MRI to obtain DTI. Voxel-wise analyses were completed using non-parametric permutation analyses correcting for multiple comparisons. CSF MMP-2, MMP-3, and MMP-9 were cross-sectionally related to DTI metrics, adjusting for age, sex, education, race/ethnicity, Framingham Stroke Risk Profile, diagnosis, and apolipoprotein E (*APOE*)-ε4 status. Follow-up models tested *CSF biomarker x diagnosis*, *APOE-ε4 status*, and *amyloid-β* (Aβ) interactions.

Results: In main models, lower MMP-2 was associated with compromised white matter microstructure (corrected p-values<0.05). MMP-2 interacted with diagnosis, *APOE*-ε4 status, and Aβ, such that associations were driven by MCI (corrected p-values<0.05), *APOE*-ε4 carriers (corrected p-values<0.05), and Aβ positive groups (corrected p-values<0.05). In main models, higher MMP-3 was associated with compromised white matter microstructure (corrected p-values<0.024). MMP-3 interacted with *APOE*-ε4 status and Aβ, such that associations were driven by *APOE*-ε4 non-carriers (corrected p-values<0.05) and Aβ negative groups (corrected p-values<0.05). MMP-9 was not associated with any DTI metric (corrected p-values>0.12).

Conclusions: Among older adults, lower CSF concentrations of MMP-2 and higher CSF concentrations of MMP-3 related to compromised white matter microstructure. MMP-2 associations were driven by MCI, *APOE*-ε4 carriers, and Aβ positive groups, suggesting MMP-2 modulation may be one pathway to white matter damage in AD. MMP-3 associations were driven by *APOE*-ε4 non-carriers and Aβ negative groups, suggesting MMP-3 may represent a non-AD pathway to white matter injury in older adults.

Keywords: Matrix metalloproteinases; cerebrospinal fluid; white matter microstructure; diffusion tensor imaging

P112: A clinically-relevant scheme for qualitatively rating tau PET, amyloid PET, and MRI in neurodegenerative cognitive presentations

Scott McGinnis^{1,2,3,4}, Jessica Collins^{1,4}, Ryan Eckbo^{1,4}, Michael Brickhouse^{1,4}, Brad Dickerson^{1,2,4}

¹*Frontotemporal Disorders Unit, Department of Neurology, Massachusetts General Hospital, Boston, MA, US*

²*Massachusetts Alzheimer's Disease Research Center, Boston, MA, US*

³*Department of Neurology, Brigham and Women's Hospital, Boston, MA, US*

⁴*Harvard Medical School, Boston, MA, US*

A comprehensive diagnostic formulation for neurodegenerative cognitive presentations incorporates syndrome, severity, and predicted underlying neuropathology. While there are recognized advantages to characterizing clinical syndrome and predicted neuropathology independently, to our knowledge there are no validated methodological schemes for predicting neuropathology from qualitative ratings of biomarker data across a range of neurodegenerative cognitive phenotypes in the spectrum of Alzheimer's disease (AD), frontotemporal lobar degeneration (FTLD), and Lewy body diseases (LBD). We developed a novel scale for rating tau PET scans by characterizing overall uptake (substantially elevated, mild/moderately elevated, not elevated), distribution, and symmetry of uptake, lastly indicating the suspected most likely primary underlying neuropathology suggested by the findings in aggregate. MRI scans were rated in analogous fashion with a scale characterizing the magnitude, distribution, and symmetry of atrophy. Amyloid PET scans were rated using previously-validated methods for binary classification of amyloid status as "elevated" or "not-elevated," and further identification of regions with elevated amyloid. Ratings from all three scales were synthesized to yield a prediction regarding most likely primary neuropathology in cases with independent syndromic classifications including amnesic mild cognitive impairment/dementia, posterior cortical atrophy, logopenic primary progressive aphasia (PPA), nonfluent/agrammatic PPA, semantic PPA, behavioral variant frontotemporal dementia, corticobasal syndrome, progressive supranuclear palsy, dementia with Lewy bodies, Parkinson disease dementia, and cognitively normal aging. Preliminary results suggest that our methods have high intra- and inter-rater reliability and that biomarker-derived neuropathological predictions agree well with syndrome/neuropathology relationships established from autopsy studies.

Keywords: tau PET, amyloid PET, clinical/biomarker correlations, Alzheimer's disease, frontotemporal lobar degeneration, Lewy body disease

P113: Mild behavioral impairment is associated with tau pathology in cognitively impaired elderly individuals

Firoza Lussier^{1,2}, Tharick A. Pascoal^{1,2}, Joseph Therriault^{1,2}, Cécile Tissot^{1,2}, Mélissa Savard^{1,2}, Andrea Lessa Benedet^{1,2}, Sulantha Mathotaarachchi^{1,2}, Jenna Stevenson², Zahinoor Ismail⁴, Pedro Rosa-Neto^{1,2}, Serge Gauthier³

¹*Translational Neuroimaging Laboratory, McGill University, Verdun, QC, Canada*

²*McGill University Research Centre for Studies in Aging, Verdun, QC, Canada*

³*Douglas Hospital Research Centre, Verdun, QC, Canada*

⁴*Hotchkiss Brain Institute and O'Brien Institute for Public Health, University of Calgary, Calgary, AL, Canada*

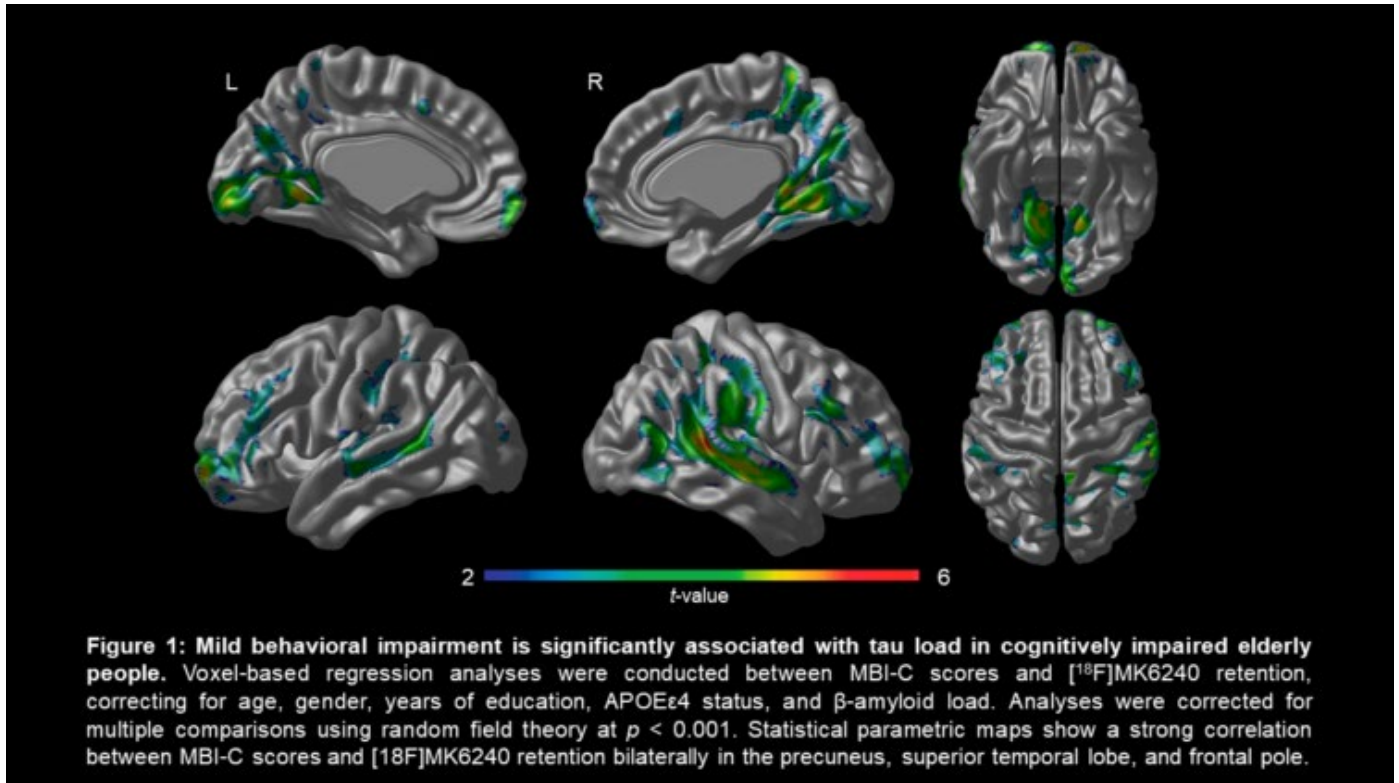
Background: Mild behavioral impairment (MBI) is a neurobehavioral syndrome characterized by the emergence of sustained non-cognitive neuropsychiatric symptoms in elderly persons, representing an at-risk state for dementia and a potential marker of Alzheimer's disease (AD). However, there is currently no published literature examining the association between MBI and imaging biomarkers of AD.

Objective: To investigate whether MBI is associated with the pathological accumulation of tau in cognitively impaired older adults.

Methods: Eighty-seven older adults underwent neuropsychological evaluation, MRI, [¹⁸F]AZD4694 β -amyloid-PET, and [¹⁸F]MK6240 tau-PET. [¹⁸F]MK6240 and [¹⁸F]AZD4694 standardized uptake value ratios (SUVRs) were calculated between 90-110 min and 40-70 min post-injection, respectively, using cerebellum grey matter as the reference region. All participants were cognitively impaired, as determined by Clinical Dementia Rating score ≥ 0.5 . MBI was assessed with the MBI Checklist (MBI-C), a rating scale designed to evaluate neuropsychiatric symptoms according to MBI criteria. Voxel-based regression analyses were used to evaluate the relationship between [¹⁸F]MK6240 retention and MBI-C score, adjusting for age, gender, education, APOE ϵ 4 status, and β -amyloid load. Analyses were corrected for multiple comparisons using random field theory at $p < 0.001$.

Results: Positive correlations were found between MBI-C total score and retention of the tau tracer [¹⁸F]MK6240 bilaterally in the precuneus, superior temporal lobe, and frontal pole. Furthermore, [¹⁸F]MK6240 SUVR values extracted for these regions (1.99 ± 1.29) were significantly higher ($p < 0.001$) than values in an age-matched cognitively unimpaired control group (1.06 ± 0.11), corroborating that the correlation observed is due to accumulation of pathological tau.

Conclusion: This is the first analysis to reveal an association between mild behavioral impairment and brain deposition of tau in a cognitively impaired population. Our results provide strong evidence for MBI as a clinical manifestation of AD pathology and support the use of the MBI-C as a tool for clinical trial enrollment and therapeutic intervention.



Keywords: Mild behavioral impairment, neuropsychiatric symptoms, tau

P114: Modeling the trajectory of tau deposition in autosomal-dominant Alzheimer's disease using the high-affinity tau tracer [18F]MK6240

Firoza Lussier^{1,2}, Joseph Therriault^{1,2}, Tharick A. Pascoal^{1,2}, Mélissa Savard^{1,2}, Sulantha Mathotaarachchi^{1,2}, Laura Robb², Jenna Stevenson², Serge Gauthier³, Pedro Rosa-Neto^{1,2}

¹*Translational Neuroimaging Laboratory, McGill University, Verdun, QC, Canada*

²*McGill Research Centre for Studies in Aging, Verdun, QC, Canada*

³*Douglas Hospital Research Centre, Verdun, QC, Canada*

Background: Changes in Alzheimer's disease biomarkers begin many years before the appearance of clinical symptoms. The study of autosomal-dominant Alzheimer's disease (ADAD) provides a unique means to model the progression of AD pathology during this preclinical stage due to the quasi-100% penetrance of mutations and the consistency of age at symptom onset. Here, we examine tau deposition across the course of ADAD using the second-generation tau PET tracer [¹⁸F]MK6240.

Objective: To investigate tau deposition as a function of proximity to the expected onset of symptoms in mutation carriers and noncarriers.

Methods: Cross-sectional data was acquired for 12 mutation carriers (MC), 6 of whom were symptomatic, and 11 asymptomatic noncarriers (NC). Most participants (91%) were from families with PSEN1 mutations. Estimated years from symptom onset (EYO) was obtained by subtracting the parent's age at symptom onset from the participant's age at the time of assessment. [¹⁸F]MK6240 SUVR was calculated 90-110 minutes post-injection using inferior cerebellar grey matter as the reference region. Statistical analyses performed included ROI-based and voxel-based linear regression analyses to examine the association between tau load and EYO in MC and NC.

Results: ROI-based analyses of [¹⁸F]MK6240 SUVR as a function of EYO revealed a strong positive correlation in Braak stages 1-2, 3-4, and 5-6 in MC. None of these associations were significant in NC. Voxel-based analyses showed significant correlations between [¹⁸F]MK6240 retention and EYO bilaterally in the entorhinal cortex and in the right posterior cingulate and precuneus in MC, while no associations survived correction for multiple comparisons in NC.

Conclusion: Our study corroborates the framework in which tau pathology appears up to 10 years before the onset of clinical symptoms. Similarly to sporadic AD, tau aggregation appears to follow Braak stages in ADAD. These results support the applications of disease-modifying therapeutic interventions in the preclinical stage of AD.

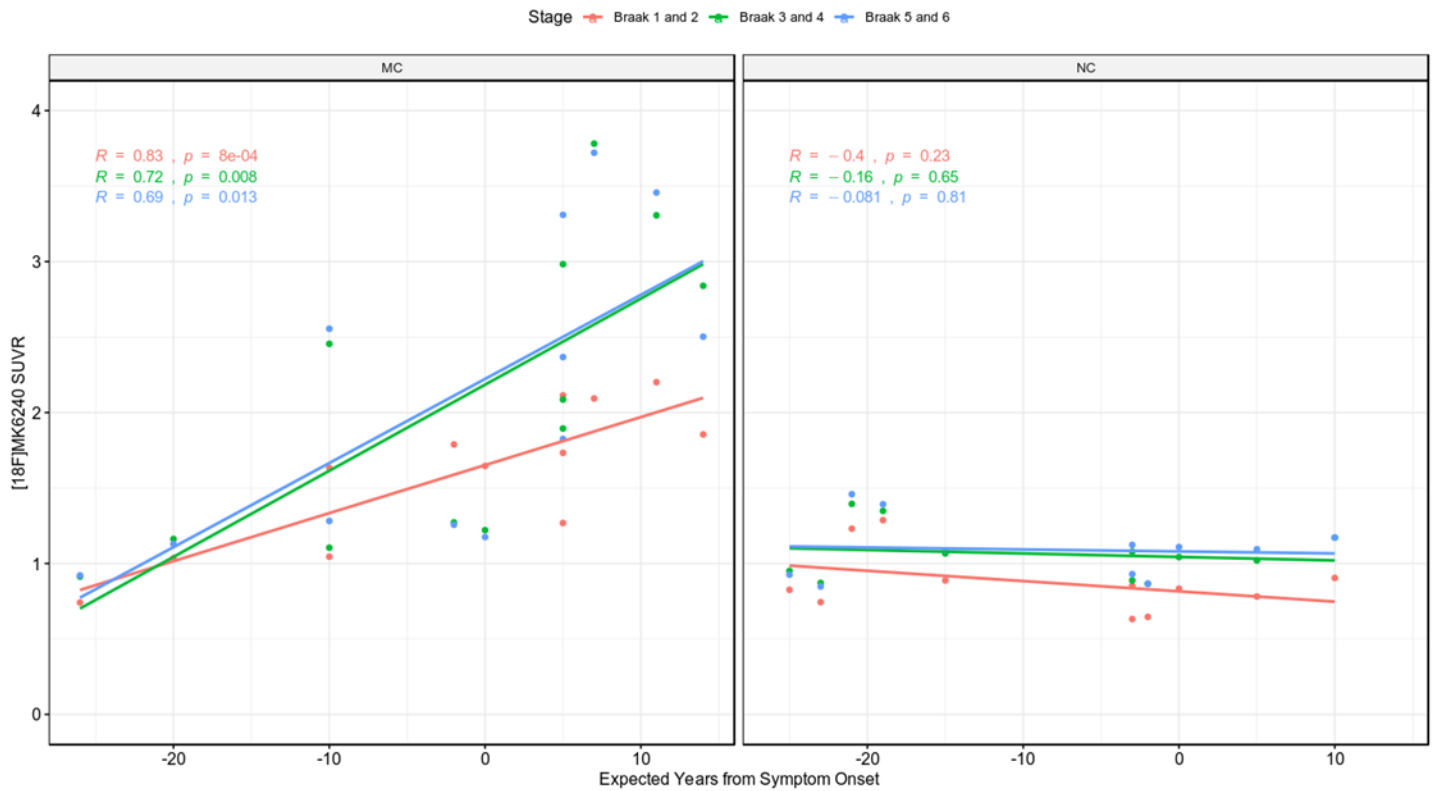
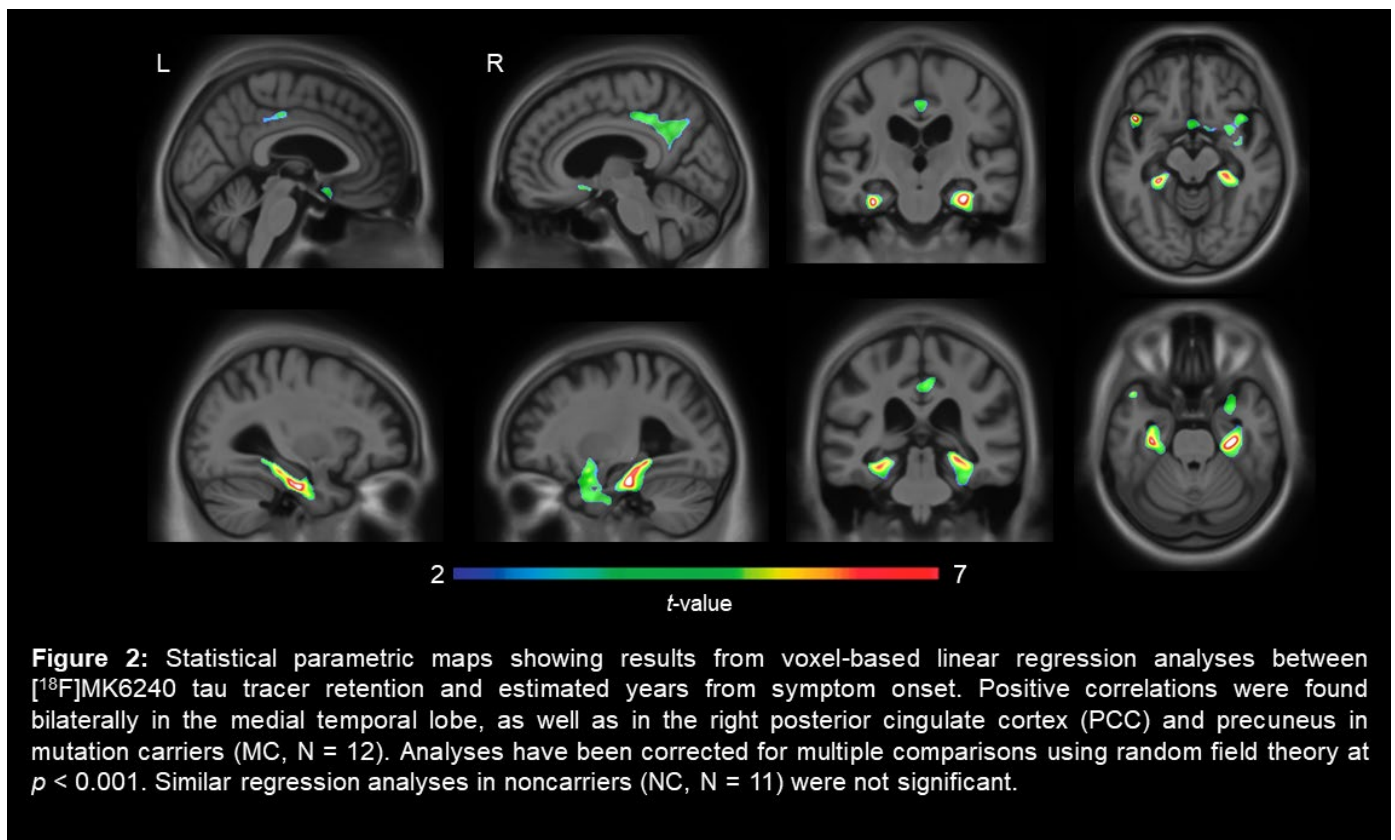


Figure 1: ROI-based linear regression analyses reveal significant positive correlations between estimated years from symptom onset and [¹⁸F]MK6240 SUVR for stages Braak 1-2, Braak 3-4, and Braak 5-6 in mutation carriers (MC, N = 12). None of these associations were significant in noncarriers (NC, N = 11).



Keywords: Autosomal-dominant Alzheimer's disease, tau, PSEN1

SESSION 4: NEUROPATHOLOGY II

Thursday, January 16, 2020		
11:30 AM	SESSION 4: NEUROPATHOLOGY II	CHAIRS: Melissa Murray, PhD, <i>Mayo Clinic</i> Julie Schneider, MD, MS, <i>Rush University</i>
11:30 AM	Derivation and potential utility of an Abeta-PET based pathology accumulation index for estimation of brain Abeta load	Ruben Smith, MD, PhD, <i>Lund University</i>
11:45 AM	In vitro study of the evidence of tauopathy in Parkinson's disease (PD) brains using a tau PET tracer, [³ H]MK-6240, by autoradiography	Zhizhen Zeng, MD, PhD, <i>Merck & Co. Inc.</i>
12:00 PM	In vitro characterization of second-generation tau pet tracers in human autopsy brain tissue	Mona-Lisa Malarte, PhD (cand.), <i>Karolinska Institute</i>
12:15 PM	Neurofibrillary tangle maturity: a comprehensive review	Christina Moloney, PhD, <i>Mayo Clinic</i>
12:30 PM	Discussion	

Derivation and potential utility of an A β -PET based pathology accumulation index for estimation of brain A β load

Antoine Leuzy¹, Johan Lilja^{1,2,3}, Christopher J. Buckley⁴, Rik Ossenkoppele^{1,5}, Mark Battle⁴, Gill Farrar⁴, Dietmar R. Thal^{6,7}, Shorena Janelidze¹, Erik Stomrud^{1,8}, Olof Strandberg¹, Ruben Smith^{1,9}, Oskar Hansson^{1,8}

¹Clinical Memory Research Unit, Department of Clinical Sciences, Lund University, Malmö, Sweden

²Department of Surgical Sciences, Nuclear Medicine and PET, Uppsala University, Uppsala, Sweden

³Hermes Medical Solutions, Stockholm, Sweden

⁴GE Healthcare Life Sciences, Amersham, UK

⁵VU University Medical Center, Neuroscience Campus Amsterdam, Amsterdam, The Netherlands

⁶Department of Imaging and Pathology, Laboratory of Neuropathology, and Leuven Brain Institute, Campus Gasthuisberg, Leuven, Belgium

⁷Department of Pathology, UZ-Leuven, Leuven, Belgium

⁸Memory Clinic, Skåne University Hospital, Lund, Sweden

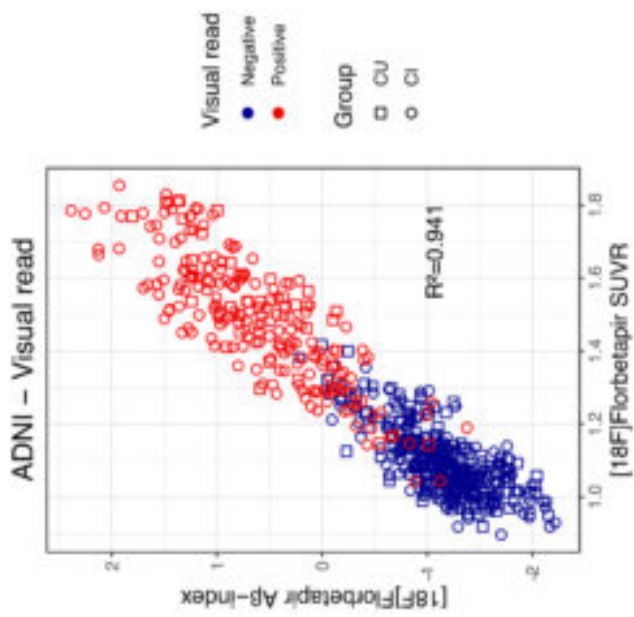
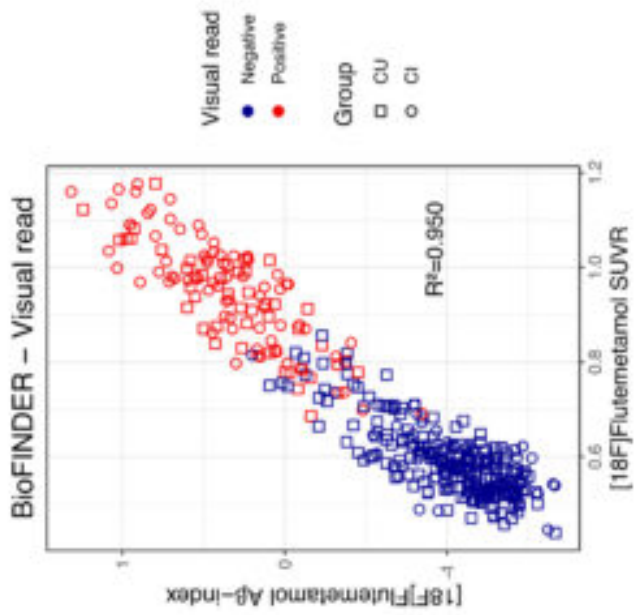
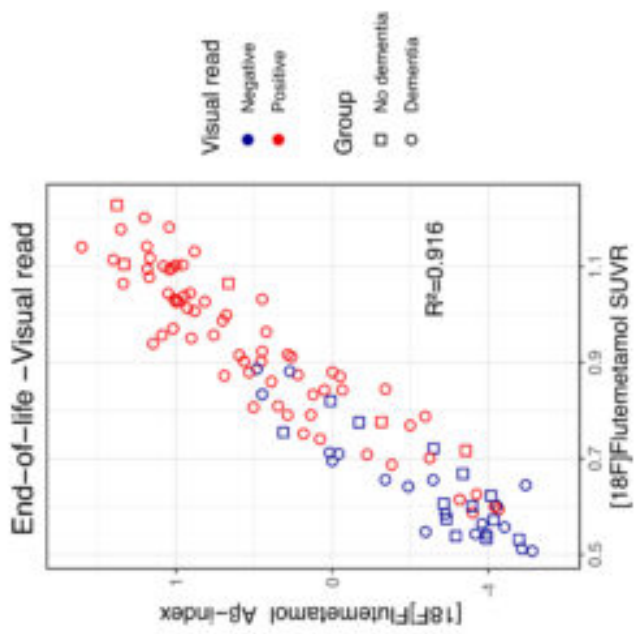
⁹Department of Neurology, Skåne University Hospital, Lund, Sweden

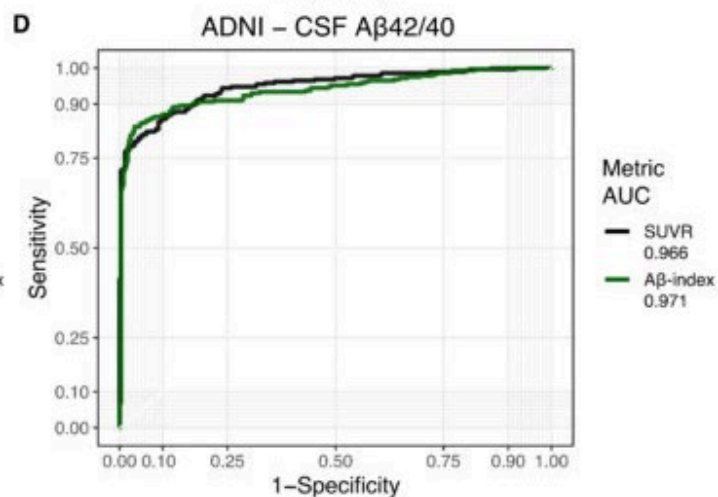
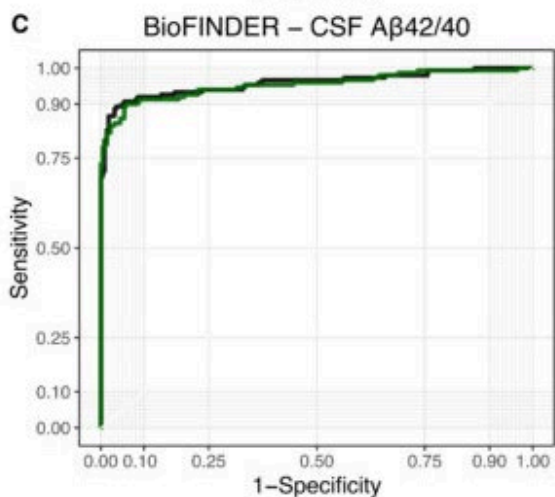
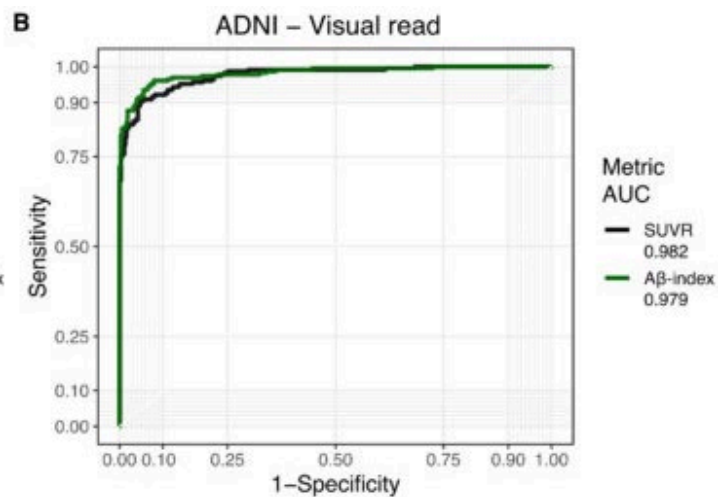
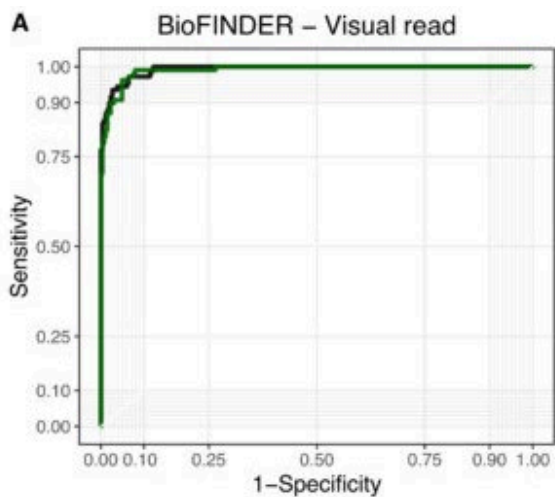
Objectives: To compare a novel A β -PET derived measure of A β pathology (A β accumulation index [A β -index]) and SUVR in three independent cohorts, including the assessment of their ability to discriminate subjects based on their A β -status using visual read, CSF A β ₄₂/A β ₄₀ and *post-mortem* neuritic plaque burden as standards of truth.

Methods: 1121 subjects (with and without cognitive impairment) with A β -PET: Swedish BioFINDER, n=392, [¹⁸F]flutemetamol; ADNI, n=629, [¹⁸F]florbetapir; phase-3 end-of-life study, n=100, [¹⁸F]flutemetamol). The A β -index was generated as part of an automated PET-only method for spatial normalization of A β -PET images. As part of this method, a principal component (PC) based adaptive template (spanning range from A β -negative to A β -positive) is adapted to the input image (i.e. optimal template = PC image-1 + A β -index*PC image-2; a positive A β -index yields a template with a more A β -positive appearance and a negative value yields a template with a more A β -negative appearance). SUVR was calculated using a composite cortical ROI, using the pons and cerebellum as reference for [¹⁸F]flutemetamol and [¹⁸F]florbetapir, respectively. Two *post-mortem* based neuritic plaque assessment methods were included: Bielschowsky silver stain (applied to paraffin-embedded cortical sections, as per CERAD) and the anti-A β 4G8 based Thal staging system. Diagnostic performance (area under the receiver operating characteristic curve) of A β -index and SUVR were compared using visual-read, CSF A β ₄₂/A β ₄₀ and *post-mortem* A β -histopathology as standards.

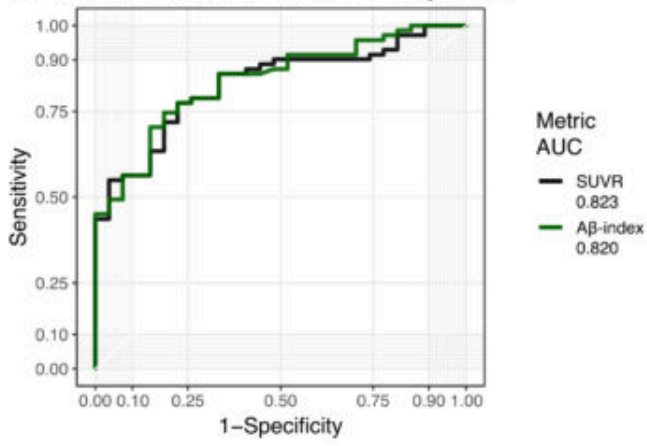
Results: Strong associations were observed between A β -index and SUVR (R², BioFINDER, 0.950; ADNI, 0.941, end-of-life, 0.916) (Figure 1). Both measures performed equally well in differentiating A β -positive from A β -negative subjects (Figure 2,3A-B) and showed a similar distribution across histopathology based A β -phases (Figure 3C-D).

Conclusions: The proposed A β -index carries an advantage over SUVR in that it is MRI-free and does not require the definition of ROIs. The A β -index may therefore be simpler to implement in clinical settings and may also facilitate the comparison of A β -PET findings.

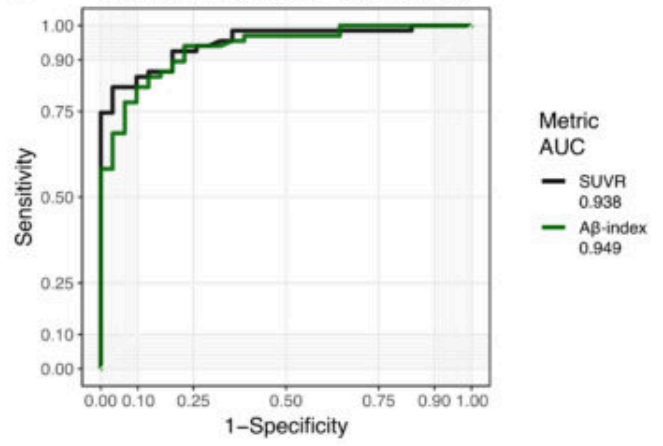




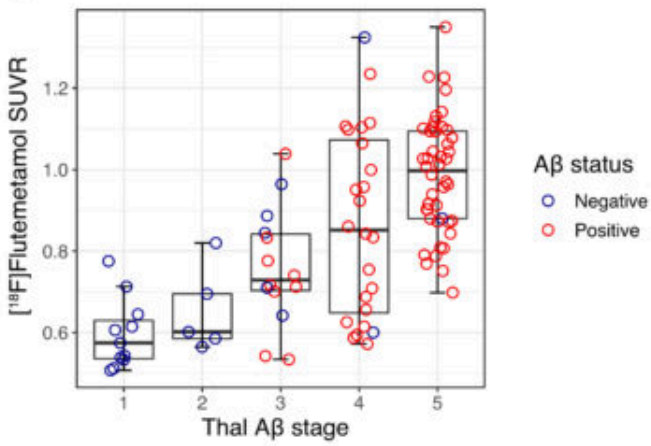
A End-of-life cohort – Bielschowsky score



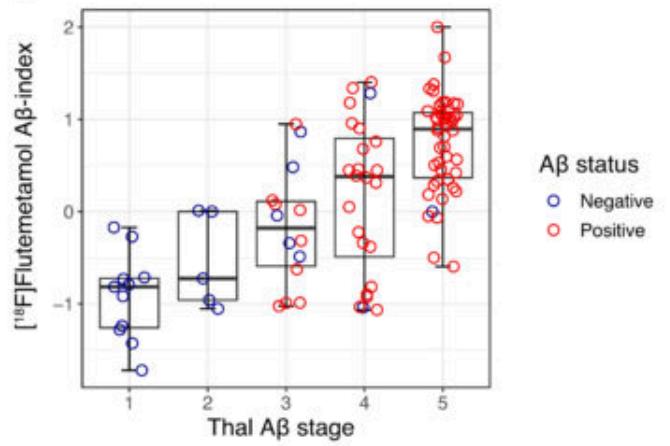
B End-of-life cohort – Visual read



C



D



Keywords: Amyloid, PET, quantification

In vitro study of the evidence of tauopathy in Parkinson's disease (PD) brains using a tau PET tracer, [³H]MK-6240, by autoradiography

Zhizhen Zeng¹, Stacey O'Malley¹, Patricia Dockery¹, Mallory Stenslik¹, Wenping Li¹, Eric Hostetler¹

¹Merck & Co. Inc., West Point, PA, US

Objectives: Tauopathies are neurodegenerative disorders, characterized by intracellular accumulation of abnormally aggregated tau protein. In Parkinson's disease, the primary neuropathological hallmark is alpha-synuclein aggregates, Lewy Bodies. However, there is emerging evidence of concomitant abnormal tau aggregation in PD brain¹. MK-6240 has been developed as a clinical PET tracer with high specific binding to neurofibrillary tangle pathology. The study is to investigate the evidence of tauopathy in postmortem brains of Parkinson's Disease using immunostaining for phospho-tau and autoradiography with the tau radioligand [³H]MK-6240².

Methods: Fresh frozen postmortem PD brains (22 SN, 13 CPu, 1 Ctx), AD and non-AD brain (1 Ctx each) were included. Frozen tissue sections (14 μm) were soaked in assay buffer (PBS, pH 7.4, 0.1% BSA with no ligand) for 15 min, and followed by 90 min incubation at RT with 0.5 nM [³H]MK-6240 (SA: 26.98 Ci/mmol). Tissue sections were washed in ice cold wash buffer (PBS, pH 7.4) for 3 times, 3 minutes/each, followed by 10 seconds rinse in ice cold diH₂O, and dried by air blower. Once tissue sections were completely dried, they were placed in cassette and exposed to new BAS-IP TR 2040 storage phosphor screens for 21 days at RT. Screens were scanned on GE Typhoon Phosphorimager and the images were analyzed using MCID 7.1 software.

Results: [³H]MK-6240 binding in PD SN and CPu was completely correlated to AT8 Immunoreactivity (IR) from the adjacent sections. 18 of 22 PD SN and 9 of 13 PD CPu showed positive [³H]MK-6240 binding. [³H]MK-6240 Off-target binding in PD brain was minimal but observed in the neuromelanin-containing cells and possible melanocytes of choroid plexus.

Conclusions: [³H]MK-6240 binding reveals the presence of NFT pathology in the substantia nigra, striatum, and cerebral cortex of PD brains. The potential of [¹⁸F]MK-6240 to image tau pathology in PD patients warrants further consideration.

Keywords: MK-6240, tauopathy, Parkinson's Disease, autoradiography, Immunohistochemistry

In vitro characterization of second-generation tau pet tracers in human autopsy brain tissue

Mona-Lisa Malarte¹, Agneta Nordberg^{1,2}, Laetitia Lemoine¹

¹*Center of Alzheimer Research, Department of Neurobiology, Care Sciences and Society, Karolinska Institutet, Stockholm, Sweden*

²*Theme Aging, Karolinska University hospital Stockholm, Stockholm, Sweden*

Background: Tauopathies are all characterised by an abnormal accumulation of tau protein which can result in an imbalance of 3R and/or 4R tau isoforms. Tau PET tracers have been designed to measure in vivo, the distribution of tau protein, and more particularly neurofibrillary tangles (NFT). Characterization of the first generation Tau tracers such as THK5117 and T-807 have provided important knowledge to understand tau pathology in AD brains but they displayed some MAO-B off-target binding. Second generation of tau tracers does not seem to have MAO-B off target and have better binding affinity to AD. From the second generation tau tracers, MK6240 seems to be more specific to AD, when PI2620 has been shown to bind to AD as well as progressive supranuclear palsy (PSP). The aim of this study was to characterise MK6240 and PI2620 in AD and PSP as well as comparing their binding properties with THK5351.

Methods: 3H-M6240 and 3H-PI2620 were used for all the set of experiments. Saturation and competition binding assays were performed on cortical brain homogenates from AD cases. Single concentration regional distributions were carried out on human brain homogenates of AD cases from several regions. Finally, large frozen hemisphere autoradiography will be carried out on AD and PSP cases.

Results: Regional distribution of 3H-MK6240 showed high binding in cortical regions on brain homogenates as well as in autoradiography. No-off target binding in control cases as well as in the thalamus, caudate nucleus and cerebellum was observed. Unlabeled PI2620 as well as unlabeled MK6240 did not compete with 3H-THK5351. Preliminary results, both saturation and competition suggest high binding affinity in AD brain for 3H-PI2620.

Conclusion: Further studies are ongoing to fully understand the binding characteristics of second generation tracers in AD and PSP. These preliminary results already highlight the complexity of tau PET tracers.

Keywords: Tauopathies, Tau, AD, PSP, MK6240, PI2620,

Neurofibrillary tangle maturity: A comprehensive review

Christina M. Moloney¹, Val J. Lowe², Melissa E. Murray¹

¹Department of Neuroscience, Mayo Clinic, Jacksonville, FL, US

²Department of Radiology, Mayo Clinic, Rochester, MN, US

Background: The accumulation of tau inside a neuron is a dynamic process that occurs over the lifespan of a neurofibrillary tangle. Our goal was to perform a comprehensive literature review of tangle morphology, tau isoforms, post-translational modifications, and staining techniques to provide a deeper understanding of tau neurobiology for interpretation of tau PET radioligand binding.

Methods: We performed a comprehensive review to summarize neuropathologic evidence of neurofibrillary tangle maturity in Alzheimer's disease (AD). To provide an overview, we detailed a historical timeline of neurofibrillary tangles, from the development of H&E staining in 1875 up until the development of modern tau PET radioligands. Additionally, we created a detailed tau antibody map to better understand structural relevance and how each antibody relates to maturity levels of tau.

Results: We use the term “neurofibrillary tangle” to encompass the lifespan of maturity from pre-tangles, to mature tangles, and to ghost tangles. Pre-tangles are the earliest level of neurofibrillary tangle maturity developing in morphologically normal neurons. Next, mature tangles accumulate in neurons with a displaced nucleus. Finally, extracellular ghost tangles are the remaining bundles of fibers after the neuron has died. Mature tangles and ghost tangles are both argyrophilic and ubiquitin-positive, but not pre-tangles. Hyperphosphorylated tau antibodies differentially label across the lifespan of neurofibrillary tangles. Tau isoforms also differ with pre-tangles composed of more 4R tau, mature tangles composed of both 3R and 4R tau, and ghost tangles composed of more 3R tau.

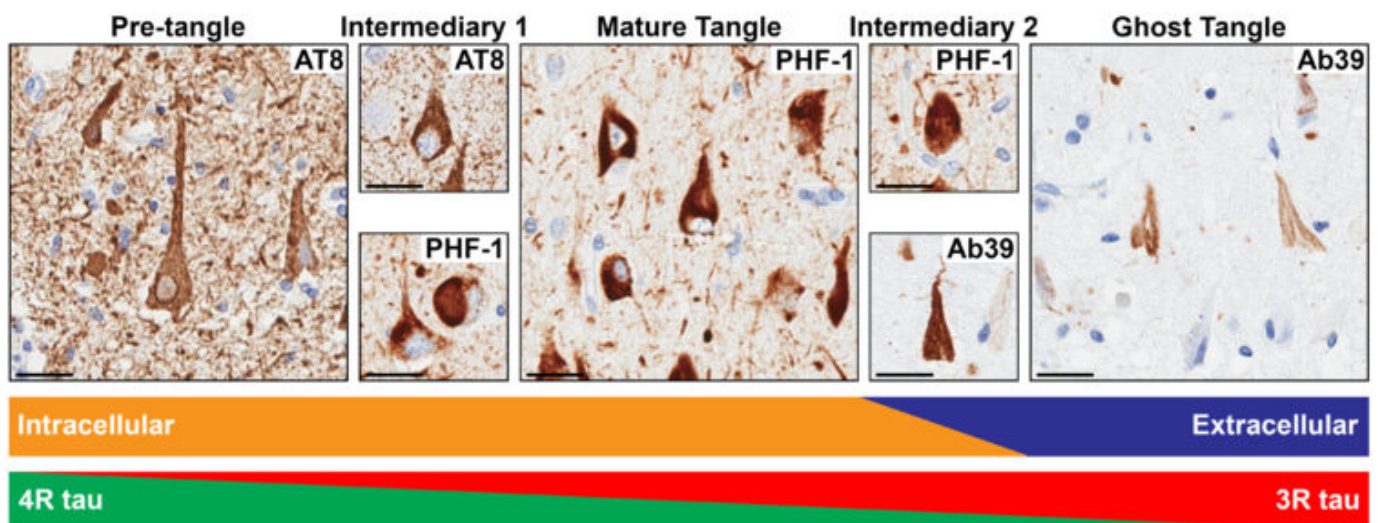


Figure 1. Neurofibrillary tangle lifespan summary. Neurofibrillary tangle maturity is a dynamic process progressing from pre-tangles, to mature tangles, and to ghost tangles, with intermediaries between these levels. Scale bar measures 25µm.

Conclusion: The dynamic aspect of neurofibrillary tangle maturity raises intriguing possibilities for biomarker labeling and therapeutic intervention. A deep review of the relevant neuropathologic and biochemical literature may greatly benefit our knowledge and interpretation of tau PET radioligands. Biomarkers that reveal earlier aspects of neurofibrillary tangle maturity may identify individuals with pre-clinical AD earlier in their disease course thereby increasing treatment efficacy.

Keywords: Neuropathology, neurofibrillary tangle maturity, tau, 3R/4R tau isoforms

Thursday, January 16, 2020 - 2:30 - 4:00pm

SESSION 5: CLINICAL I

Thursday, January 16, 2020		
2:30 PM	SESSION 5: CLINICAL I	CHAIRS: Keith Johnson, MD, <i>Massachusetts General Hospital</i> Pedro Rosa-Neto MD, PhD, <i>McGill University</i>
2:30 PM	History of Head Injury is Associated with Greater Tau Deposition on [18F]Flortaucipir PET in MCI and AD Patients	Shannon Risacher, PhD, <i>Indiana University School of Medicine</i>
2:45 PM	In vivo measurement of widespread synaptic loss in early Alzheimer's disease with SV2A PET	Adam Mecca, MD, PhD, <i>Yale University</i>
3:00 PM	Amyloid PET is more than just positive or negative: A β -amyloid level impacts risk of clinical progression in non-demented individuals	Christopher Rowe, MD, <i>Austin Health</i>
3:15 PM	18F-PI2620 tau-PET in Progressive Supranuclear Palsy – A multi-center evaluation	Matthias Brendel, MD, <i>University Hospital of Munich</i>
3:30 PM	Discussion	

History of head injury is associated with greater tau deposition on [18F]Flortaucipir PET in MCI and AD patients

Shannon Risacher¹, John West¹, Rachael Deardorff¹, Sujuan Gao¹, Liana Apostolova¹, Andrew Saykin¹

¹Indiana University School of Medicine, Indianapolis, IN, US

Introduction: A history of head injury is linked an increased future risk of dementia. In addition, chronic traumatic encephalopathy (CTE) is characterized by cerebral deposition of hyperphosphorylated tau. Thus, we sought to determine whether a history of head injury was associated with increased [¹⁸F]flortaucipir binding in two aging cohorts (Indiana Memory and Aging Study (IMAS) and Alzheimer's Disease Neuroimaging Initiative (ADNI)).

Methods: 760 individuals were included. Medical history reports were evaluated to determine the presence of self-report of head injury with or without loss of consciousness (LOC). [¹⁸F]flortaucipir scans were downloaded for ADNI and collected in IMAS as previously described [Risacher et al. 2017 *Alz&Dem:DADM*]. Scans were processed using standard techniques and normalized to the cerebellar crus to create SUVR images. Mean SUVR was extracted from the medial and lateral temporal lobe (MTL; LTL) and parietal lobe. Two-way ANCOVA were used to assess the effect of diagnosis (cognitively normal (CN) or impaired (early/late MCI, AD)) and head injury. The initial analysis was conducted with head injury regardless of LOC, but was repeated looking at only head injury with LOC.

Results: A significant effect of head injury history on [¹⁸F]flortaucipir was observed, such that those with a history of head injury and cognitive impairment had increased tau in the MTL, LTL, and parietal lobe (Figure 1). This effect was stronger when limited to individuals with head injury with LOC (Figure 2).

Discussion: These findings suggest that individuals with a history of head injury have an increased risk for tau deposition during the clinical stages of AD. This finding may provide a biological basis for the increased risk of dementia in those with a history of head injury. Future studies in larger samples are needed to fully understand this relationship.

Figure 1.

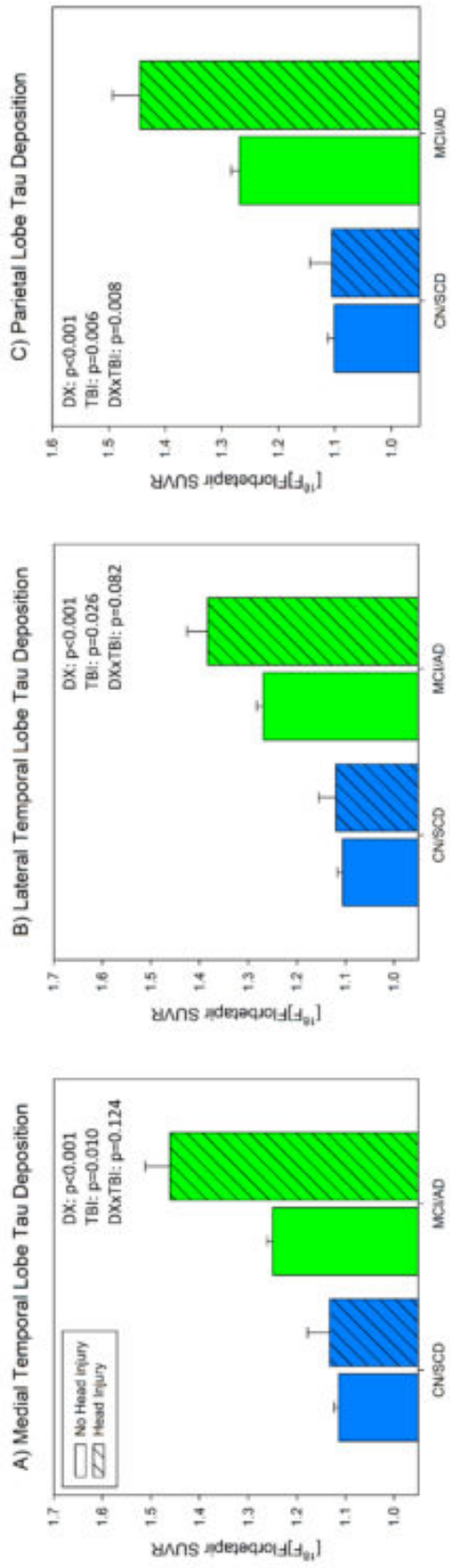
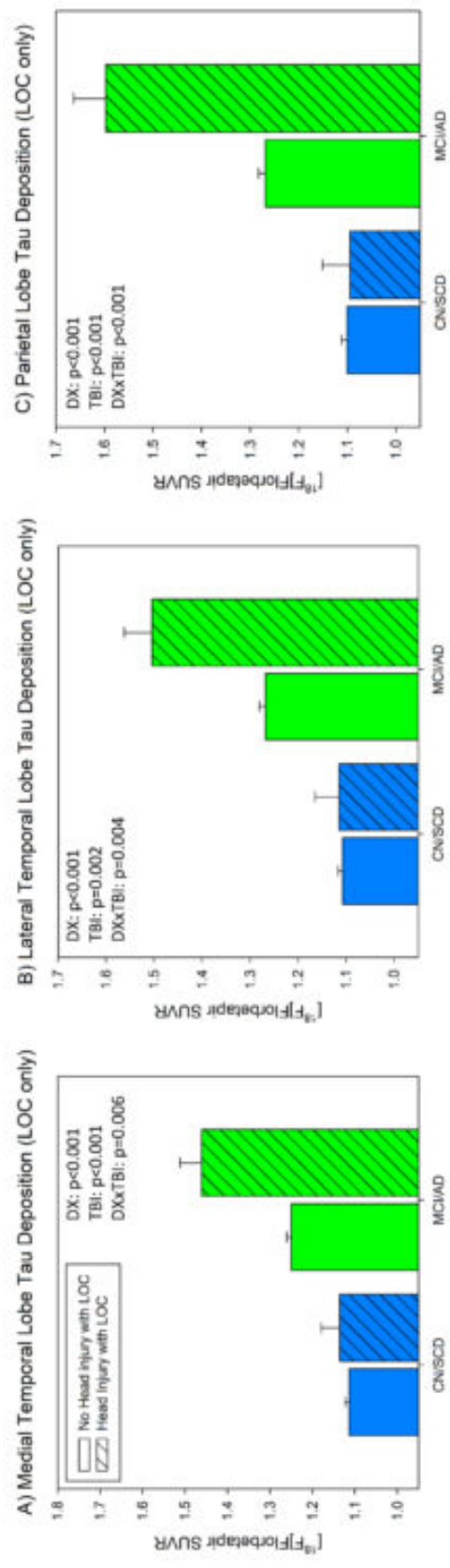


Figure 2.



Keywords: traumatic brain injury, tau PET, Alzheimer's

In vivo measurement of widespread synaptic loss in early Alzheimer's disease with SV2A PET

Adam Mecca¹, Ming-Kai Chen¹, Ryan O'Dell¹, Mika Naganawa¹, Tyler Godek¹, Joanna Harris¹, Hugh Bartlett¹, Wenzhen Zhao¹, Nabeel Nabulsi¹, Brent Vander Wyk¹, Pradeep Varma¹, Amy Arnsten¹, Yiyun Huang¹, Richard Carson¹, Christopher van Dyck¹

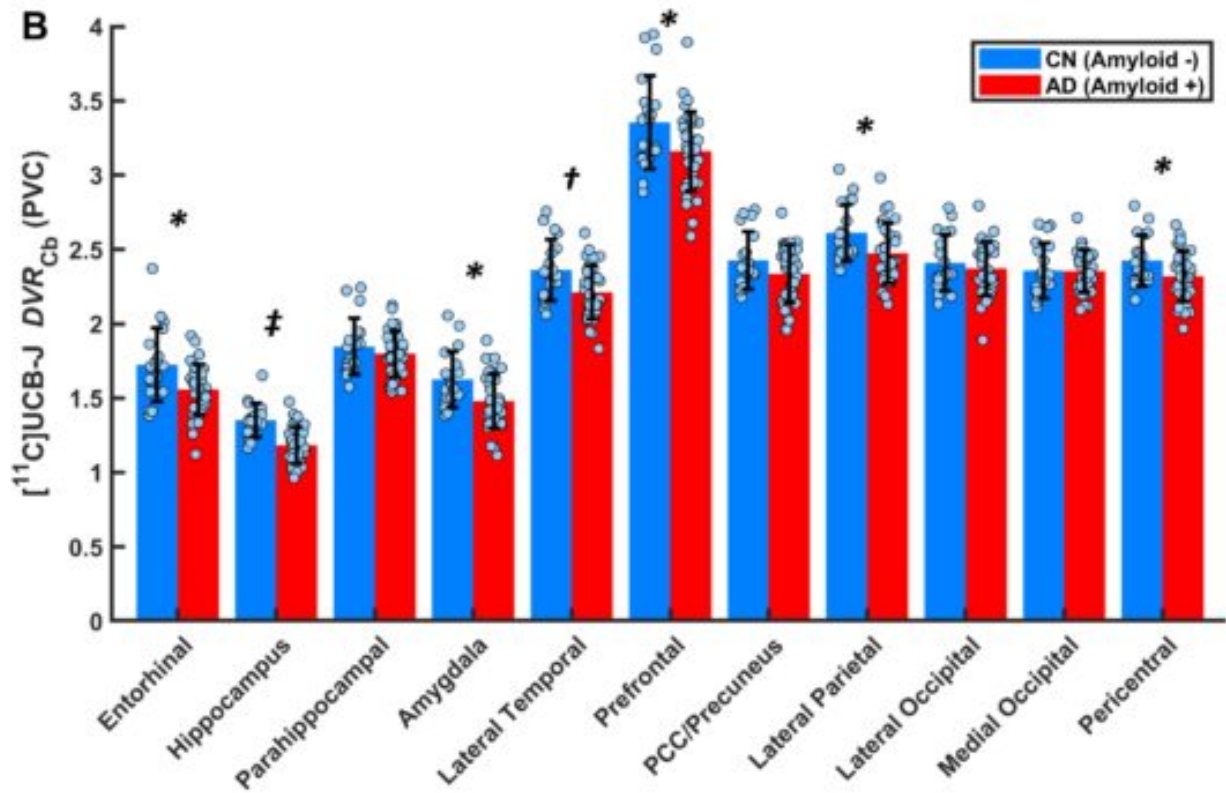
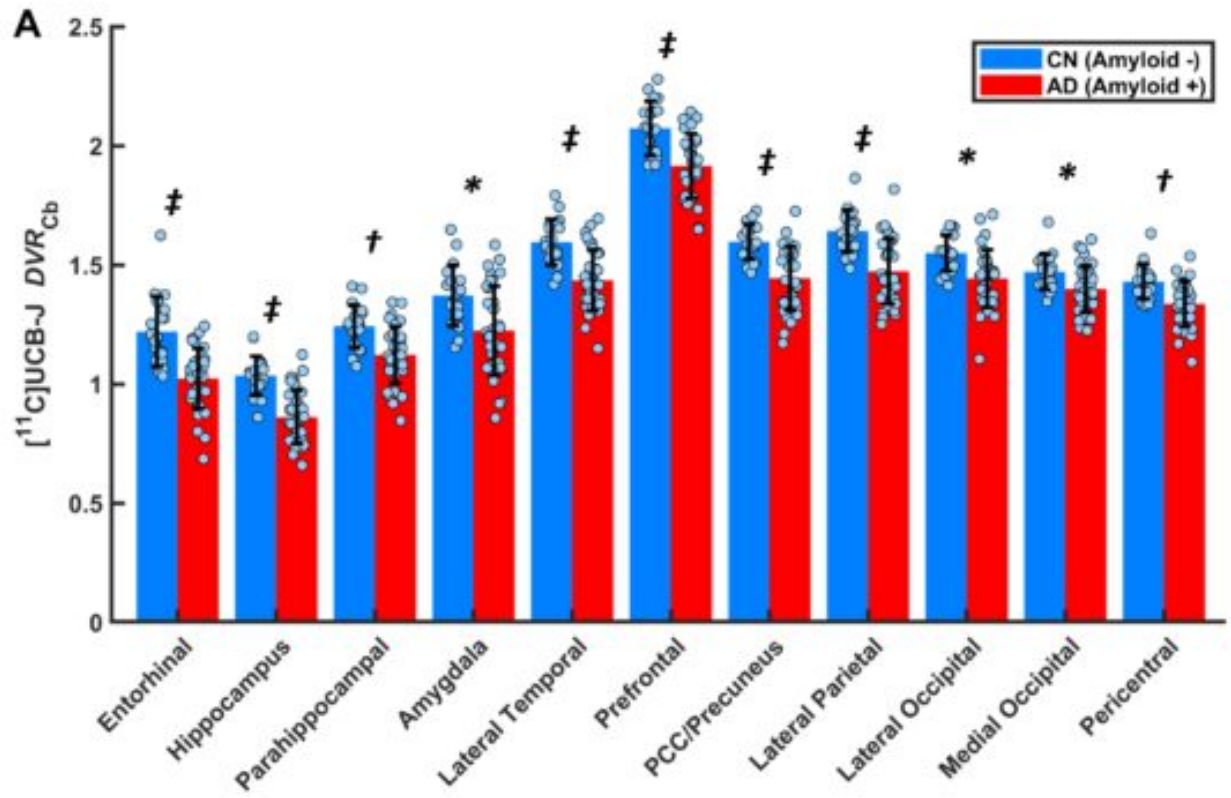
¹Yale University School of Medicine, New Haven, CT, US

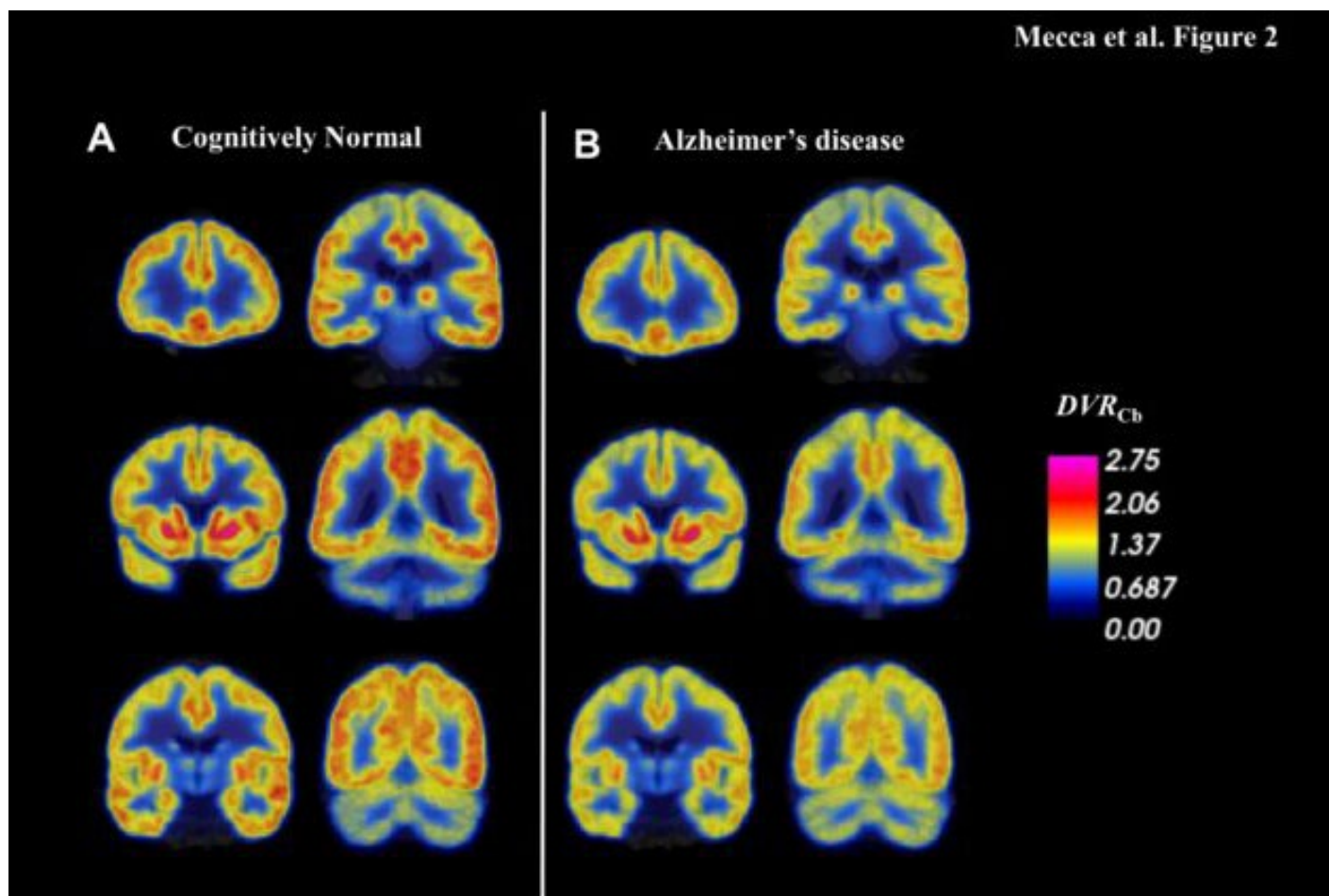
Background: Using [¹¹C]UCB-J-PET we have shown significant reductions in hippocampal SV2A specific binding as a marker of synaptic density in participants with early AD. However, postmortem studies have suggested more widespread neocortical reductions in synaptic density.

Methods: We measured SV2A binding with [¹¹C]UCB-J-PET in 34 participants with early AD (MMSE=23.1±4.1, CDR=0.5-1.0, Aβ+) and 19 cognitively normal (CN) participants (MMSE=29.3±1.1, CDR=0, Aβ-). We re-examined the suitability of reference regions: centrum semiovale (CS) versus cerebellum (Cb) in a subset of participants with arterial blood sampling to estimate the distribution volume V_T . We then calculated the distribution volume ratio for regions of interest (ROIs) using both reference regions (DVR_{CS} , DVR_{Cb}).

Results: Values of V_T were very similar between groups for CS and Cb, supporting the validity of both reference regions. However, DVR_{Cb} showed significantly lower variability than DVR_{CS} across ROIs, suggesting it has practical superiority in AD studies. Our primary analysis of group differences in SV2A binding demonstrated a significant effect of group ($F(1,51) = 33.4$, $P < 0.00001$) and group*region ($F(10,510) = 2.4$, $P = 0.01$) as predictors of SV2A binding (DVR_{Cb}). Post-hoc comparisons revealed significant group differences in all medial temporal regions and more broadly in neocortical regions (Figures 1 and 2). SV2A reductions in AD were most pronounced in the hippocampus (DVR_{Cb} -17.3%, $P < 0.00001$; BP_{ND} -19.8%) and entorhinal cortex (DVR_{Cb} -15.7%, $P < 0.00001$; BP_{ND} -17.6%) but were also present in the parahippocampal, amygdala, lateral temporal, prefrontal, posterior cingulate/precuneus, lateral parietal, and pericentral ROIs. These reductions were largely maintained after correction for volume loss and were more extensive than decreases in gray matter volume.

Conclusion: We observed widespread reductions of synaptic density with [¹¹C]UCB-J-PET in medial temporal and neocortical regions in early AD. Future studies will evaluate the utility of SV2A PET for monitoring AD progression and therapeutic interventions.





Keywords: synaptic imaging, PET, $[^{11}C]UCB-J$, Alzheimer's disease

Amyloid PET is more than just positive or negative: A β -amyloid level impacts risk of clinical progression in non-demented individuals

Laura M van der Kall¹, Thanh Truong¹, Samantha Burnham², Vincent Doré^{1,2}, Rachel Mulligan¹, Svetlana Bozinovski¹, Pierrick Bourgeat³, Regan Tyrrell¹, Jürgen Fripp³, Colin L Masters⁴, Victor L Villemagne^{1,6}, Christopher C Rowe^{1,5,6}

¹Dept of Molecular Imaging & Therapy, Austin Health, Melbourne, Australia

²CSIRO Health and Biosecurity Flagship: The Australian e-Health Research Centre, Melbourne, Australia

³CSIRO Health and Biosecurity Flagship: The Australian e-Health Research Centre, Brisbane, Australia

⁴The Florey Institute of Neuroscience and Mental Health, Melbourne, Australia

⁵The Australian Dementia Network, Melbourne, Australia

⁶Department of Medicine, The University of Melbourne, Melbourne, Australia

Background: A β -amyloid (A β) PET positivity is an important predictor of clinical progression. However, the level of A β deposition likely provides additional prognostic information over a binary report. We determined the effect of A β burden on the progression risk to MCI or dementia in cognitively normal (CN) individuals and to dementia in persons with MCI from the AIBL study.

Methods: We included 534 CN (age 72 \pm 6 yrs; mean follow-up 5.3 \pm 1.7 yrs) and 125 MCI with >3 years follow-up. A β burden was expressed in Centiloids (CL) and divided into five categories: <15 CL negative, 15-25 uncertain, 26-50 moderate, 51-100 high, >100 very high. Cox proportional hazards analysis and linear mixed effect models were used to assess risk of clinical progression to MCI or dementia and to examine association between A β burden and change in cognition.

Results: At baseline, 63% of CN were negative, 10% uncertain, 10% moderate, 14% high and 3% very high A β . Fifty-seven CN (11%) progressed to MCI during follow-up. Risk of progression to MCI and decline on AIBL PACC score were proportional to A β level (negative or uncertain n.s.; moderate: HR 3.2, PACC -0.07 SD/yr, p=0.05; high: HR 7.0, PACC -0.32, p<0.001; very high: HR 11.4, PACC -1.38, p<0.001). At baseline, 29% of MCI were negative, 2% uncertain, 14% moderate, 34% high and 20% very high. Sixty MCI (48%) progressed to dementia at 3 years, 65% of persons with high or very high A β , 30% with moderate A β and 5% with a negative scan. Decline in CVLT-II delayed recall was -0.1 SD/year in moderate and -0.2 SD/year in high and very high A β groups, all p < 0.01.

Conclusions: Three categories of increasing A β burden based of CL improves prognostic accuracy. Greater than 50 CL of A β substantially increases risk of clinical progression and rate of cognitive decline.

Keywords: A β , prognostic value, Centiloids, MCI, AD

18F-PI2620 tau-PET in Progressive Supranuclear Palsy – A multi-center evaluation

Matthias Brendel¹, Henryk Barthel², Thilo van Eimeren^{3,4,5,6}, Ken Marek^{7,8}, Leonie Beyer¹, Mengmeng Song¹, Carla Palleis⁹, Gesine Respondek^{6,10}, Julia Sauerbeck¹, Christian Zach¹, Jochen Hammes⁴, Michael Barbe⁵, Özgür Onur⁵, Frank Jessen^{6,11,12}, Dorothee Saur¹³, Matthias L. Schroeter^{14,15,16}, Jost-Julian Rumpf¹³, Michael Rullmann², Andreas Schildan², Marianne Patt², Bernd Neumaier^{3,4}, Oliver Barret^{7,8}, Jennifer Madonia^{7,8}, David S. Russel^{7,8}, Andrew Stephens¹⁷, Sigrun Roeber¹⁸, Jochen Herms^{6,18}, Kai Bötzel⁹, Johannes Levin^{6,9}, Joseph Classen¹³, Guenter Hoeglinger^{6,10,19}, Peter Bartenstein^{1,20}, Victor Villemagne^{21,22,23}, Alexander Drzezga^{4,6}, John Seibyl^{7,8}, Osama Sabri²

¹Department of Nuclear Medicine, University Hospital of Munich, LMU Munich, Munich, Germany

²Department of Nuclear Medicine, University of Leipzig, Leipzig, Germany

³Cognitive Neuroscience, Institute for Neuroscience and Medicine (INM-3), Research Centre Juelich, Juelich, Germany

⁴Department of Nuclear Medicine, University Hospital Cologne, Cologne, Germany

⁵Department of Neurology, University Hospital Cologne, Cologne, Germany

⁶German Center for Neurodegenerative Diseases (DZNE), Bonn, Germany

⁷InviCRO, LLC, Boston, MA, US

⁸Molecular Neuroimaging, A Division of inviCRO, New Haven, CT, US

⁹Department of Neurology, University Hospital of Munich, LMU Munich, Munich, Germany

¹⁰Department of Neurology, Technical University Munich, Munich, Germany

¹¹Center for Memory Disorders, University Hospital Cologne, Cologne, Germany

¹²Department of Psychiatry, University Hospital Cologne, Cologne, Germany

¹³Department of Neurology, University of Leipzig, Leipzig, Germany

¹⁴Clinic for Cognitive Neurology, University of Leipzig, Leipzig, Germany

¹⁵LIFE - Leipzig Research Center for Civilization Diseases, University of Leipzig, Leipzig, Germany

¹⁶Max-Planck-Institute of Human Cognitive and Brain Sciences, Leipzig, Germany

¹⁷Life Molecular Imaging GmbH, Berlin, Germany

¹⁸Center for Neuropathology and Prion Research, University Hospital of Munich, LMU Munich, Munich, Germany

¹⁹Department of Neurology, Medizinische Hochschule Hannover, Hannover, Germany

²⁰Munich Cluster for Systems Neurology (SyNergy), Munich, Germany

²¹Department of Molecular Imaging & Therapy, Austin Health, Heidelberg, Australia

²²The Florey Institute of Neuroscience and Mental Health, The University of Melbourne, Melbourne, Australia

²³Department of Medicine, Austin Health, The University of Melbourne, Melbourne, Australia

Background: Progressive supranuclear palsy (PSP) is a 4-repeat (4R) tauopathy and region-specific tau deposits establish the neuropathological diagnosis of “definite PSP” *post mortem*. Future interventional trials against tau in PSP would strongly benefit from biomarkers to validate the specific presence of the target before therapy initiation. The novel second generation tau-PET ligand ¹⁸F-PI2620 proved absent off-target binding to monoamine oxidases and high affinity to 3/4R tau in Alzheimer’s disease (AD). The aim of this multicenter-evaluation was to investigate ¹⁸F-PI2620 in patients with suspected 4R tau pathology in clinically diagnosed PSP.

Methods: 56 patients (70±7y, n=31 female) with probable or possible PSP [n=38 Richardson syndrome (PSP-RS)] according to MDS-PSP criteria underwent ¹⁸F-PI2620 PET at four different centers together with 10 healthy controls (HC) and 18 disease controls (n=8 α-synucleinopathy, n=10 AD). Multilinear reference tissue modeling with cerebellar reference served for calculation of 0-60 min distribution volume

ratios (DVR). DVR data in PSP target regions were compared between PSP, HC, and disease controls, controlled for center, age and gender. Regions with $DVR \geq 2$ standard deviations above HC were binary judged as elevated.

Results: Strongest elevation of ^{18}F -PI2620 DVR was observed in the globus pallidus of PSP-RS patients (PSP rating scale: 38 ± 15 ; range 13-71) when compared to all controls (1.16 ± 0.09 vs. HC: 0.99 ± 0.06 , α -syn.: 1.02 ± 0.03 , AD: 1.05 ± 0.06). PSP-non-RS patients (PSP rating scale: 26 ± 10 ; range 11-41) also indicated elevated binding in the globus pallidus (DVR: 1.10 ± 0.11). Binarized quantification revealed at least one positive region for 82% of PSP-RS and 50% of PSP-non-RS whereas no positive region was observed for 100% α -synucleinopathies and 80% of AD disease controls.

Conclusions: This multi-center evaluation indicates a value of ^{18}F -PI2620 to diagnose and differentiate suspected PSP patients, may facilitating earlier and more reliable diagnosis of PSP.

Keywords: tau, PET, PSP, PI-2620

Thursday, January 16, 2020 - 4:45 - 6:00pm

SESSION 6: CLINICAL II

Thursday, January 16, 2020		
4:45 PM	SESSION 6: CLINICAL II	CHAIRS William Jagust, MD, <i>University of California, Berkeley</i> David Wolk, MD, <i>University of Pennsylvania</i>
4:45 PM	Tau-PET associations with amyloid positivity and cognitive impairment	Susan Landau, PhD, <i>University of California, Berkeley</i>
5:00 PM	Locus coeruleus integrity tracks with initial Alzheimer's disease-related pathology and cognitive decline	Heidi Jacobs, PhD, <i>Massachusetts General Hospital</i>
5:15 PM	Area 35 is the earliest subregion in the medial temporal lobe affected by tau pathology	David Berron, PhD, <i>Lund University</i>
5:30 PM	Discussion	

Tau-PET associations with amyloid positivity and cognitive impairment

Susan Landau¹, Deniz Korman¹, Robert Koeppe², William Jagust¹

¹University of California, Berkeley, Berkeley, CA, US

²University of Michigan, Ann Arbor, MI, US

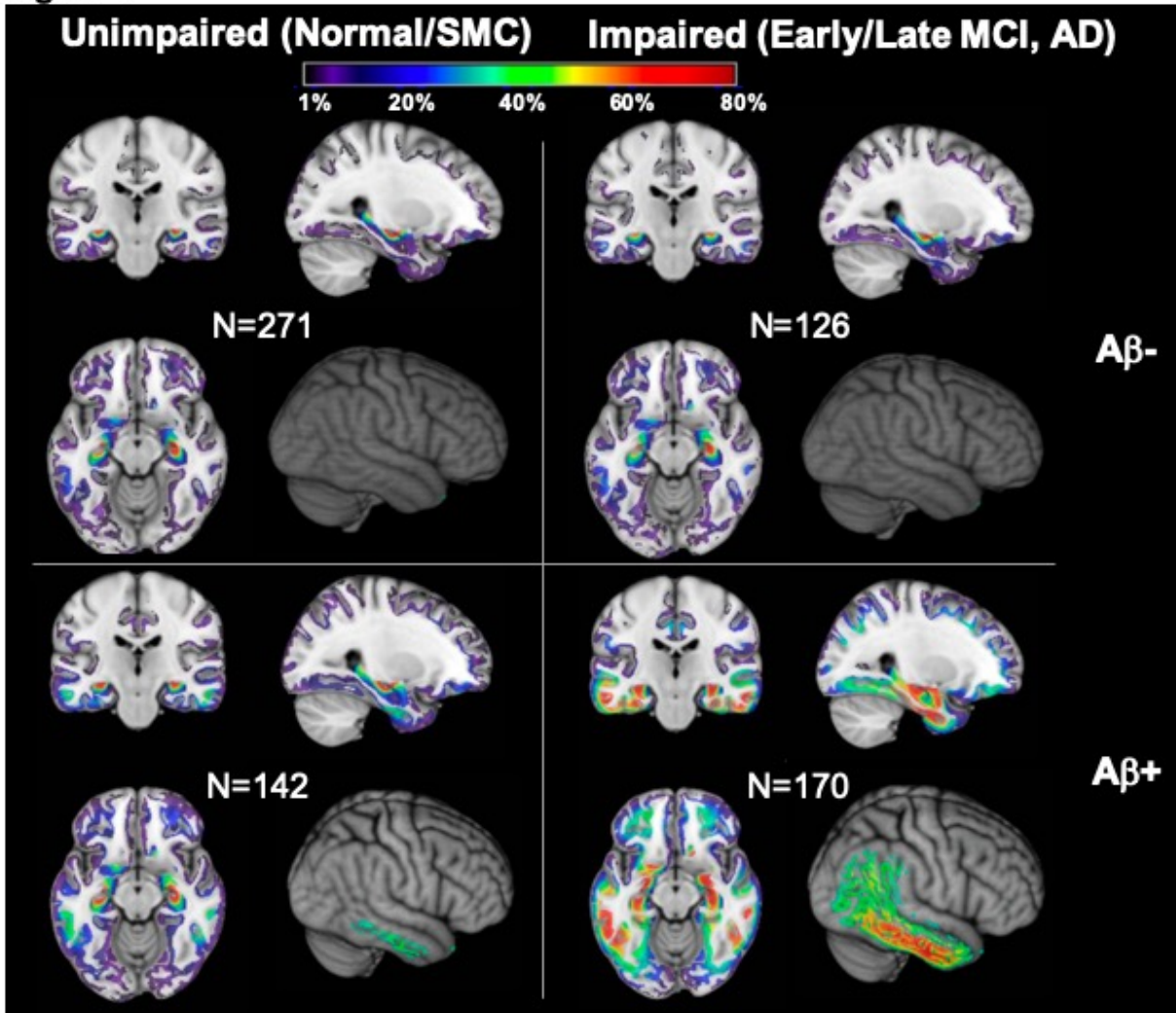
Objectives: We examined dichotomous and continuous measurements of flortaucipir in relation to amyloid and cognitive impairment in order to understand how these factors contribute to elevations in regional tau.

Methods: In 709 ADNI participants scanned with flortaucipir-PET, we examined the regional distribution of suprathreshold (SUVR>1.4) abnormal cortical voxels measured dichotomously as a function of cognitive impairment (MCI/AD vs Normal) and Abeta +/- status. We also examined tau SUVRs measured continuously in native space using FreeSurfer-defined Braak stage ROIs (1, 3/4, 5/6) with inferior cerebellar normalization and without partial volume correction. We carried out separate regression models predicting each Braak stage ROI SUVR, with Abeta status, impairment status, Abeta X impairment, age, sex, and education as independent variables.

Results: In our voxelwise suprathreshold analysis, only regions adjacent to the hippocampus (parahippocampal gyrus, amygdala, entorhinal cortex) were consistently abnormal (>40% of individuals) across unimpaired/impaired and Abeta +/- groups (**Fig1**). The proportion of abnormal voxels increased with Abeta positivity and impaired status, but tau outside the medial temporal lobe (e.g. lateral temporal) only occurred consistently in Abeta+ groups, regardless of impairment. In our Braak stage ROI analysis of tau measured continuously (**Fig2**), however, Abeta and impairment status were similar to one another in the amount of variance they explained for each Braak stage ROI. In all three Braak stage ROIs, Abeta and impairment each accounted for 11-18% variance. Abeta X Impairment accounted for additional variance that was also similar across Braak stage ROIs (5-8%).

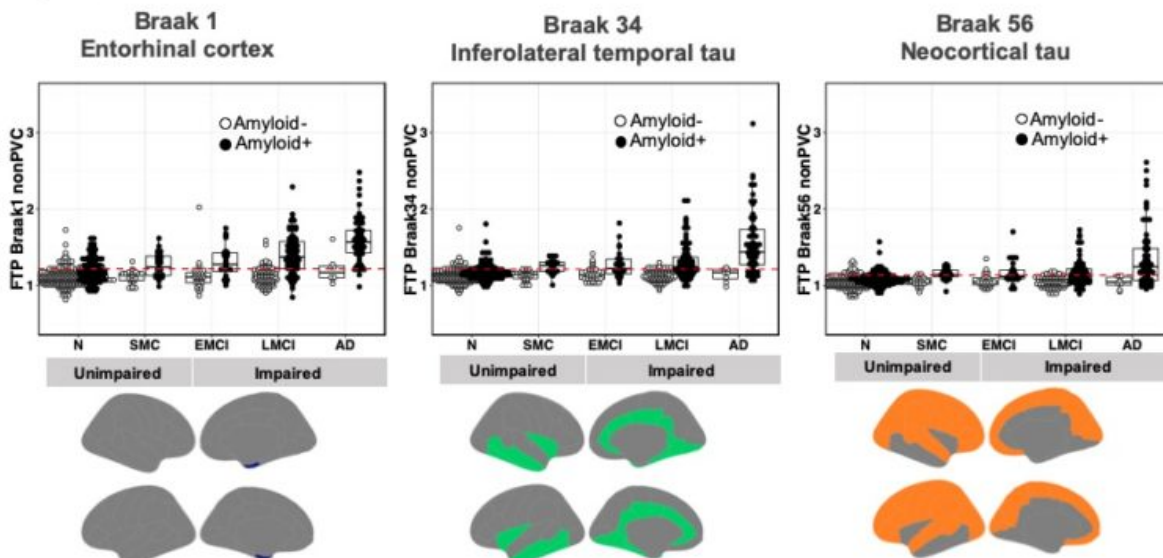
Conclusion: Spread of suprathreshold tau outside the medial temporal lobe was linked to amyloid positivity more than impairment. However, tau measured continuously was associated similarly with amyloid and impairment across all ROIs. Together, these findings suggest that Abeta drives abnormal extratemporal tau, and further accumulation of tau across all regions beyond an SUVR of 1.4 drives clinically-relevant impairment.

Figure 1



Spatially- and intensity-normalized flortaucipir (grey matter only) maps in 709 ADNI participants. Color scale represents the percent of participants with abnormal flortaucipir (>1.4; Maass et al. NeuroImage 2018) at each voxel.

Figure 2



Flortaucipir SUVRs (inferior cerebellar grey matter normalization, no partial volume correction) are shown for each Braak stage by amyloid status and diagnosis. The red dashed lines indicate suggested positivity thresholds based on the upper 90th percentile of amyloid-negative normals.

Keywords: amyloid, tau, cognitive impairment

Locus coeruleus integrity tracks with initial Alzheimer's disease-related pathology and cognitive decline

Heidi Jacobs^{1,2}, John Alex Becker¹, Kenneth Kwong¹, Fred D'Oleire Uquillas¹, Kathryn Papp^{1,3}, Michael Properzi¹, Reisa Sperling^{1,3}, Keith Johnson¹

¹Massachusetts General Hospital / Harvard Medical School, Boston, MA, US

²Maastricht University, Maastricht, The Netherlands

³Brigham and Women's Hospital / Harvard Medical School, Boston, MA, US

Background: Autopsy studies report that the locus coeruleus (LC) is the first site to accumulate tau lesions. Current PET-tracers do not allow us to measure tau burden directly in the LC, however MRI-measures of LC integrity provide a proxy for neuronal density of the LC. We examined whether LC integrity is associated with cortical amyloid and tau deposition and whether LC integrity predicts retrospective Alzheimer's Disease (AD)-related cognitive decline.

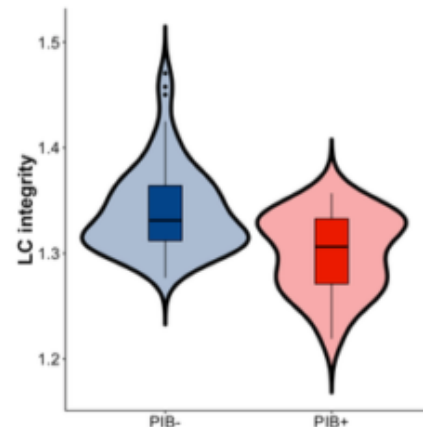
Methods: One-hundred-and-five individuals (Table 1) from the Harvard Aging Brain Study underwent 3T-MRI (including LC imaging), Amyloid and tau-PET imaging and neuropsychological assessments. Assessments up to 8 years prior to LC-imaging were included (median:5.02 years, IQR[4.38-5.36 years]). LC integrity (intensity referenced to pontine region) was regressed onto each vertex of the cortical mantle of the PET data. We used robust regressions and mediation analyses to relate LC integrity to regional tau and amyloid burden and cognition (several cognitive composites and their subtests). Linear mixed effects models examined interactive effects of LC integrity and AD pathology on retrospective cognitive changes. Covariates were age, sex and education.

Results: LC integrity correlated with age ($r=-0.25$, $p=0.011$) and was lower in elevated amyloid compared to low amyloid participants ($p<0.001$). LC integrity was associated with medial and lateral temporal (peak: entorhinal cortex ($t=4.69$)) and medial prefrontal tau, and showed widespread negative associations with amyloid (Figure 1, $p<0.005$). LC integrity was positively associated with cross-sectional memory performance ($p=0.024$), but not with other cognitive domains (Figure 2A-B). This relationship between LC integrity and memory was mediated specifically by entorhinal tau (mediation effect: $p=0.007$). Finally, lower LC integrity predicted amyloid-associated retrospective memory decline (Figure 2C, $p=0.0009$).

Conclusion: MRI-measures of LC integrity are associated with initial cortical AD pathology, and closely track with AD-related cognitive decline. LC integrity may foreshadow AD-related memory decline in clinically normal older individuals.

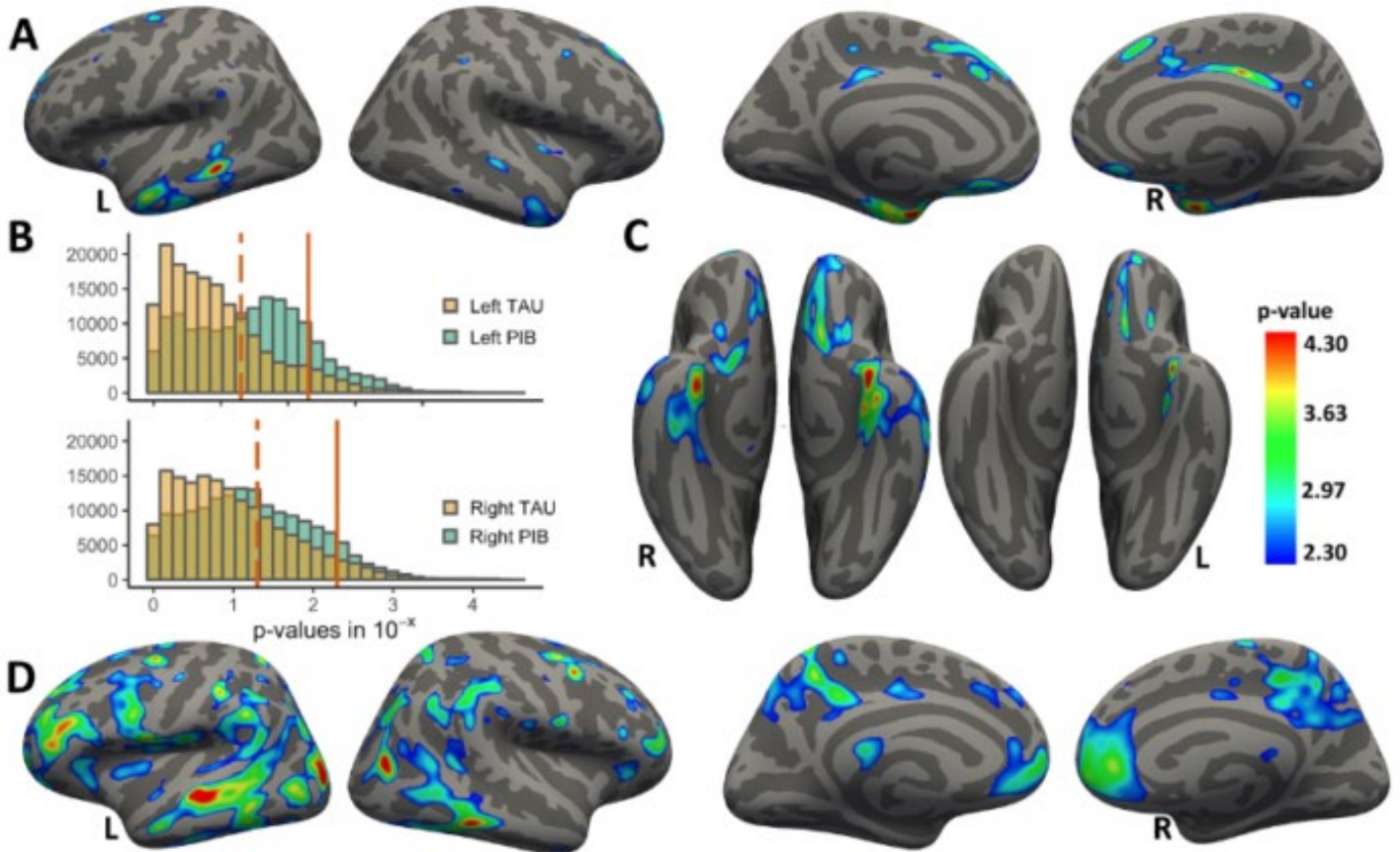
Table 1

N=105	Mean (sd), n (%)
Age (years)	72.77 (10.40)
Sex (females)	62 (59%)
Education	16.25 (2.74)
Neocortical PIB DVR PVC	1.383 (0.378)
Elevated PIB	29 (27.62%)
Entorhinal tau SUVR PVC	1.344 (0.383)
LC integrity	1.329 (0.043)
MMSE	28.72 (1.60)



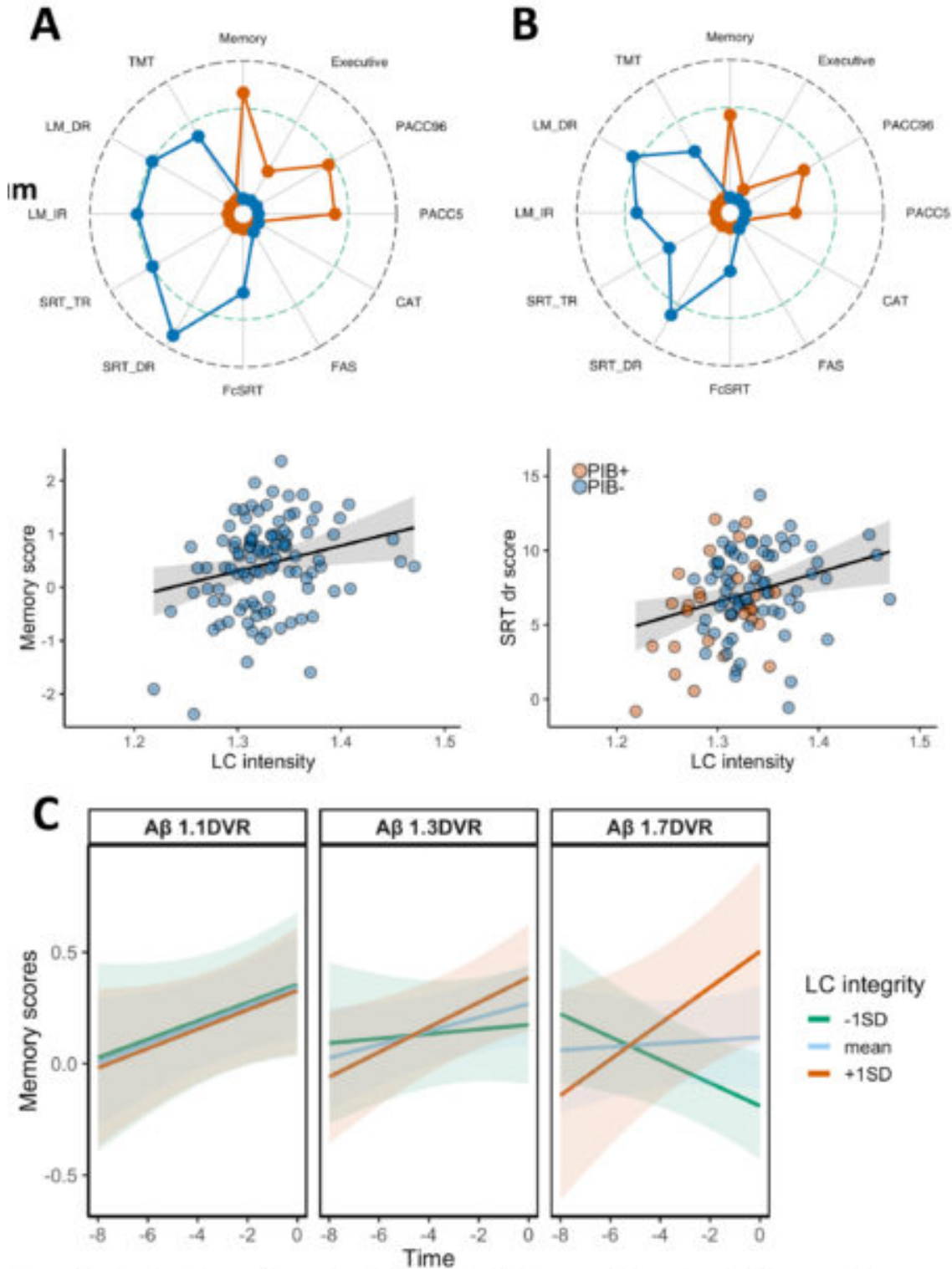
Note: The table provides the descriptives of the sample. LC integrity was significantly lower in individuals with elevated A β compared to those with lower A β .

Figure 1



Note: A) vertex-wise tau analyses associated with LC intensity (adjusted for age and sex). Only negative associations were observed. B) Distribution p-values (expressed as 10^{-x}) of the entire cortical mantle, left and right, for tau (yellow) and A β (green). The first dashed vertical line indicates the threshold at 1.3 ($p=0.05$), the second solid line at 2.3 ($p=0.005$). C) left (part of A): vertex-wise tau associations with LC intensity (adjusted for age and sex), right: additionally adjusted for A β . (D) vertex-wise A β associations with LC intensity (adjusted for age and sex). Only negative associations were observed. Threshold was set at $p<0.005$ (expressed as 10^{-x}). The scale bars reflect the magnitude of the associations (red: greater effect size; blue: smaller effect size). Abbreviations: L=left; R=right

Figure 2



Note: A) radar chart showing the magnitude of the relationship between LC intensity and different cognitive measures (adjusted for age, sex, education and number of previous test exposures). The red outline indicates the effect size for the composites (memory, executive function, PACC5 and PACC96), while the blue outline indicates the effect size for the subtests. The radar chart and scatter plot in B is adjusted for A β . The magnitude of effect is expressed in t-values and the green dotted line indicates t-value=1.96 (p<0.05). TMT scores were inverted to facilitate comparisons across effect sizes. Middle row shows the association between LC intensity and memory composite scores or SRT delayed recall (shown are predicted values adjusted for covariates). C) Linear mixed effects model showing the synergistic association between LC integrity and A β predicting retrospective memory decline. Abbreviations: PACC=Preclinical Alzheimer's disease Cognitive Composite; CAT: Categorical Fluency; FAS: phonological fluency; FcSRT: free and cued selective reminding test; SRT: selective reminding test (dr=delayed recall and tr=total recall); LM: Logical memory (TR=total recall; IR=immediate recall); TMT: Trail Making Test.

Keywords: Locus coeruleus, tau, amyloid, cognition, PET

Area 35 is the earliest subregion in the medial temporal lobe affected by tau pathology

David Berron¹, Olof Strandberg¹, Jacob Vogel³, Philip Insel¹, Erik Stomrud^{1,2}, Niklas Mattsson^{1,4,5}, Ruben Smith¹, Oskar Hansson^{1,2}

¹Clinical Memory Research Unit, Department of Clinical Sciences Malmö, Lund University, Lund, Sweden

²Memory Clinic, Skåne University Hospital, Malmö, Sweden

³Montreal Neurological Institute, McGill University, Montreal, QC, Canada

⁴Department of Neurology, Skåne University Hospital, Lund, Sweden

⁵Wallenberg Center for Molecular Medicine, Lund University, Lund, Sweden

Background: Neurofibrillary tangles (NFT) have been described to appear first in the transentorhinal region, a subregion within the medial temporal lobe (MTL) that largely overlaps with area 35 and represents the medial perirhinal cortex. From there NFT spread towards the entorhinal cortex (ERC) and hippocampal CA1 before they extend outside of the MTL. However, it remains unclear when NFT spread along the anterior-posterior axis of the parahippocampal gyrus and the hippocampus.

Methods: 294 cognitively unimpaired (CU) (72 b-amyloid positive), 90 b-amyloid positive individuals with mild cognitive impairment (MCI) and 117 b-amyloid positive patients with Alzheimer's dementia (AD) underwent [18]F-RO948 Tau PET and structural T1-weighted MRI scans. MTL subregions were defined on T1 images and individual volume and thickness estimates were derived using ASHS-T1 (Xie et al., 2019). Mean SUVR was extracted from individual MTL subregions (PVE corrected). Linear regression models and event-based modelling (Young et al., 2014) were used to determine the sequence of MTL subregions affected by tau deposition.

Results: We found that A35 was the only region showing a significant difference in cortical thickness between Ab- and Ab+ CU (Fig1A). Furthermore, linear regression showed that MTL tau deposition in Ab+ CU was significantly associated with A35 cortical thickness only (Fig1B). Event-based modelling predicted ERC and A35 showing tau deposition in the earliest stages. In later stages, ERC and A35 are followed by the anterior hippocampus, A36, parahippocampal cortex and the posterior hippocampus (Fig1C-D). Similarly, A35 and ERC are the earliest subregions affected by atrophy (Fig1E).

Conclusion: Our findings highlight the potential of A35 thickness as a marker of early tau related atrophy. Furthermore, the sequence of tau deposition and atrophy across subregions within the MTL might have important implications for memory functions that are represented by specific MTL subregions such as object and scene memory.

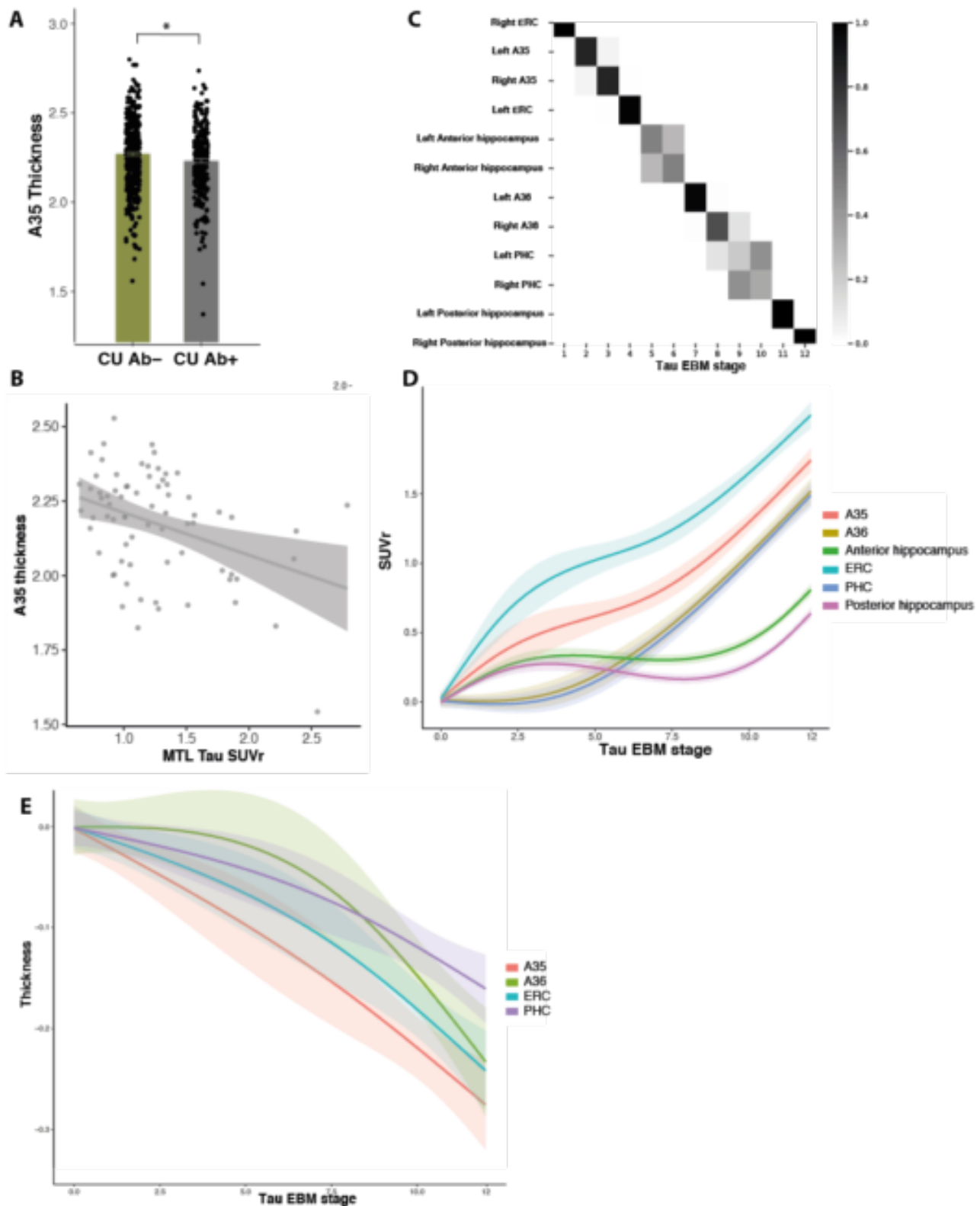


Figure 1A: Only A35 thickness showed a significant difference when thickness/volume of all MTL subregions was compared between Ab+ and Ab- CU. **B:** Furthermore, only A35 thickness was significantly related to MTL tau signal in Ab+ CU. **C:** The event-based model, that assigned a different tau stage to each individual in the sample based on estimates from individual MTL subregions predicted ERC and A35 to become abnormal in the earliest stages followed by the anterior hippocampus, A36, parahippocampal cortex and the posterior hippocampus. **D:** Linear regression models show tau deposition in individual MTL subregions across EBM stages. **E:** Linear regression models show cortical thickness of individual extrahippocampal MTL subregions across EBM stages. Abbreviations: A35, are 35; ERC, entorhinal cortex; PHC, parahippocampal cortex; CU, cognitively unimpaired; MCI, mild cognitive impairment; AD, Alzheimer's dementia; EBM, event-based model.

Keywords: Tau PET, medial temporal lobe subregions, transentorhinal region, cortical thickness, preclinical AD

Friday, January 17, 2020 - 8:30am - 9:15am

SESSION 7A: TAU I

Friday, January 17, 2020		
8:30 AM	SESSION 7A: TAU I	CHAIRS: Tobey Betthausser, PhD, <i>University of Wisconsin</i> Sylvia Villeneuve, PhD, <i>McGill University</i>
8:30 AM	The implications of different approaches to define AT(N) in Alzheimer's disease	Antoine Leuzy, PhD, <i>Lund University</i>
8:45 AM	Towards a CenTauR cortical mask	Vincent Dore, PhD, <i>CSIRO</i>
9:00 AM	Tau Positivity: Comparing Flortaucipir Meta-ROI vs. Maximum of Regional Z-Scores	Christopher Schwarz, MD, <i>Mayo Clinic</i>

The implications of different approaches to define AT(N) in Alzheimer's disease

Antoine Leuzy¹, Niklas Mattsson^{1,2,3}, Shorena Janelidze¹, Sebastian Palmqvist^{1,2}, Erik Stomrud^{1,4}, Olof Strandberg¹, Ruben Smith^{1,2}, Oskar Hansson^{1,4}

¹Clinical Memory Research Unit, Department of Clinical Sciences, Lund University, Malmö, Sweden

²Department of Neurology, Skåne University Hospital, Lund, Sweden

³Wallenberg Centre for Molecular Medicine, Lund University, Lund, Sweden

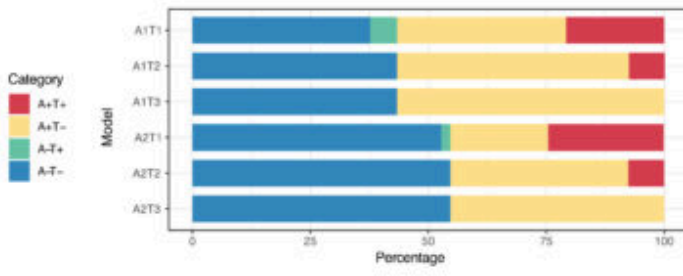
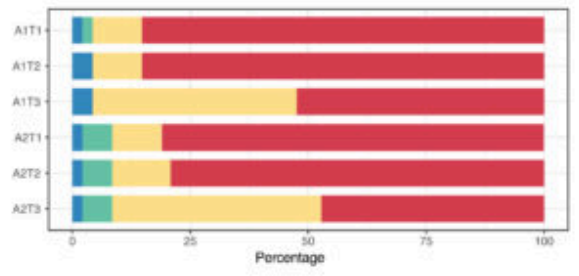
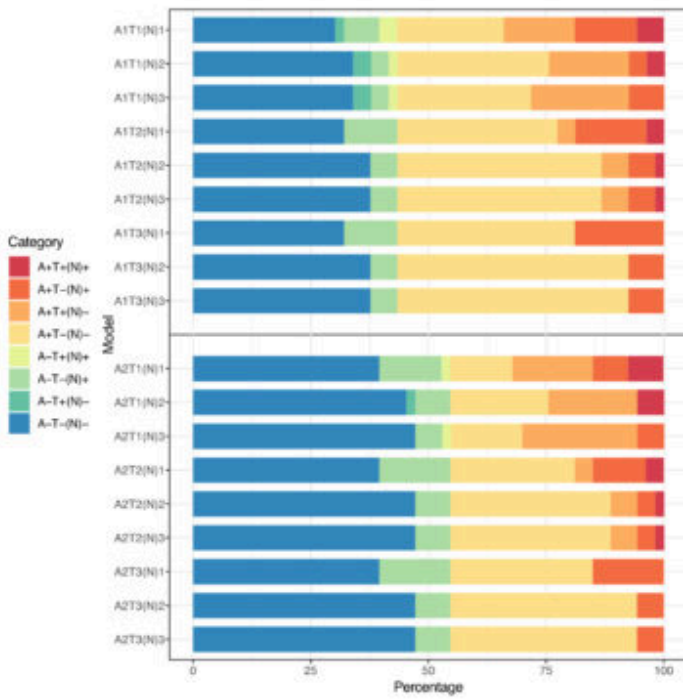
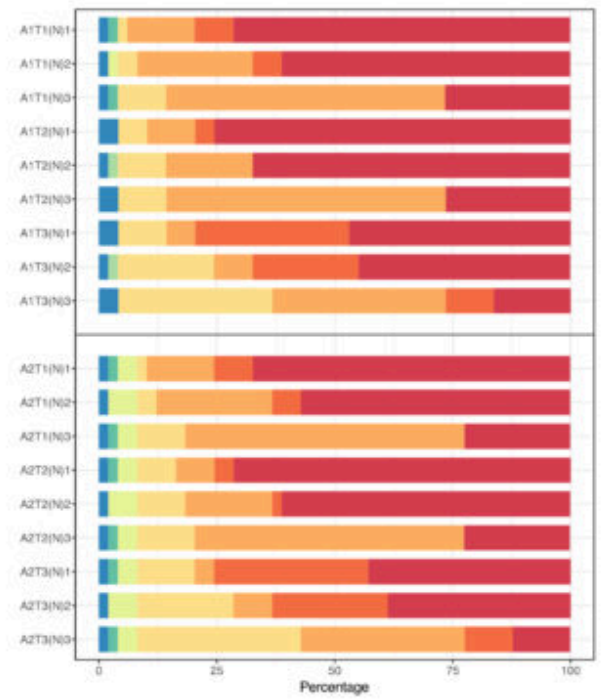
⁴Memory Clinic, Skåne University Hospital, Lund, Sweden

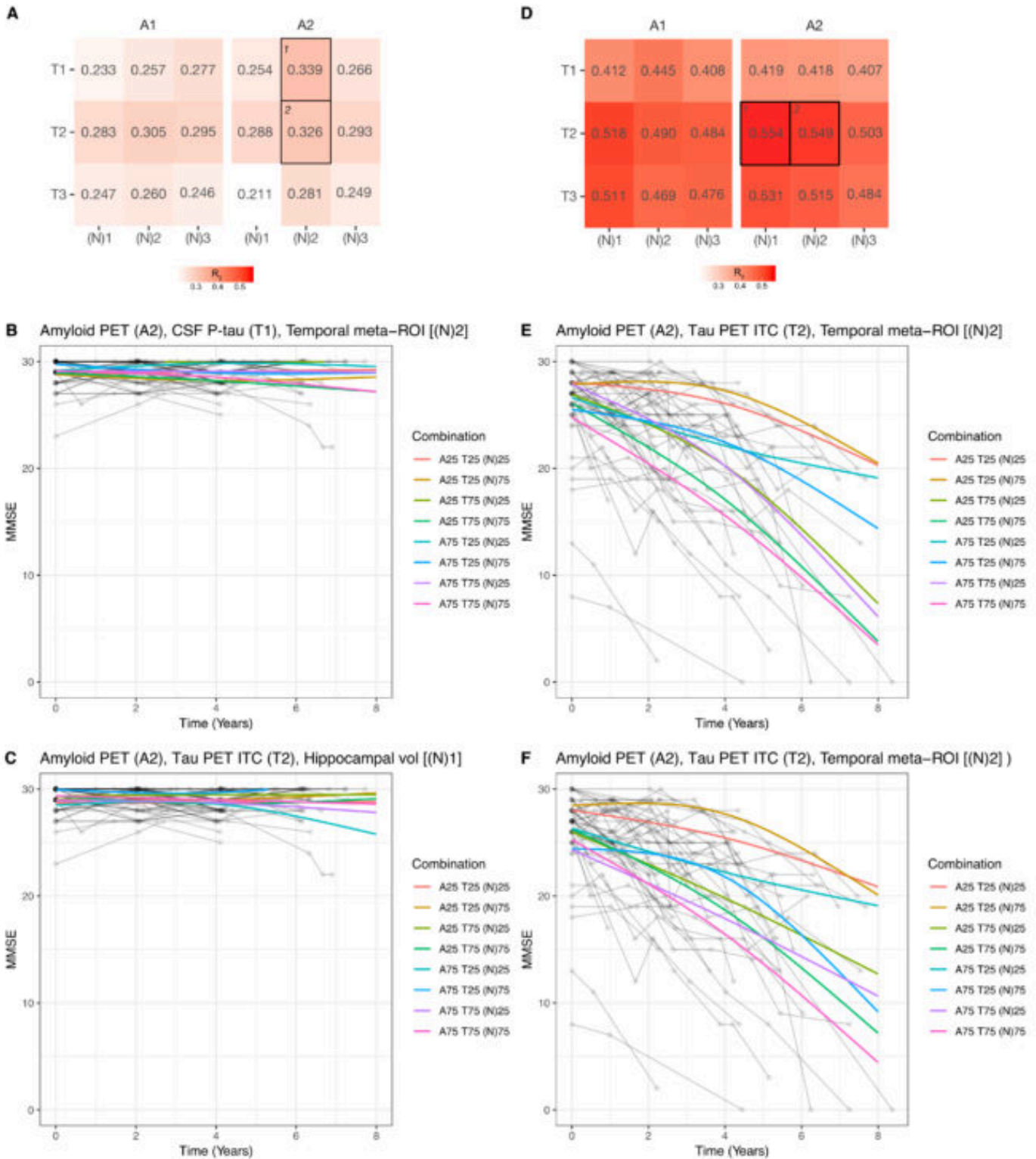
Objectives: To compare different amyloid- β (A), tau (T) and neurodegeneration (N) [AT(N)] variants within the Swedish BioFINDER-1 and 2 studies.

Methods: A total of 490 participants were classified into AT(N) groups. These included 53 cognitively unimpaired (CU) and 48 cognitively impaired (CI) participants (14 mild cognitive impairment [MCI] and 34 AD dementia) from BioFINDER-1 and 389 participants from BioFINDER-2 (245 CU and 144 CI subjects [138 MCI and six AD dementia]). Biomarkers for “A” were CSF A β_{42} and Amyloid-PET ([¹⁸F]flutemetamol); for “T” CSF P-tau and Tau-PET ([¹⁸F]flortaucipir); and for “(N)” hippocampal volume, temporal cortical thickness and CSF neurofilament light (NfL). Binarization of biomarkers was achieved using cut-offs defined in other cohorts. The relationship between different AT(N) combinations and cognitive trajectories (longitudinal Mini-Mental State Examination (MMSE) scores) was examined using linear mixed modelling and coefficient of variation.

Results: Among CU subjects, A-T-(N)- or A+T-(N)- variants were most common (Figure 1). However, more T+ cases were seen using P-tau than Tau-PET. Among CI subjects, A+T+(N)+ was more common; however, more (N)+ cases were seen for MRI-measures relative to CSF NfL. Tau-PET best predicted longitudinal cognitive decline in CI subjects and P-tau in CU subjects (Figure 2). Among CI subjects, continuous T (especially Tau-PET) and (N) measures improved the prediction of cognitive decline compared to binary measures.

Conclusions: Our findings suggest that different AT(N) variants are not interchangeable, and that optimal variants may differ by clinical stage. In some cases, dichotomizing biomarkers may result in loss of important prognostic information.

A A and T in CU**C A and T in CI****B A, T and (N) in CU****D A, T and (N) in CI**



Panels A and D show R^2 for different AT(N) variants in CU and CI subjects, respectively (divided by A biomarkers). Panels B-C and E-F are the top two best models for CU and CI, respectively; 25 and 75 refer to 25th and 75th quartiles, respectively, where higher indicates a more abnormal biomarker).

Keywords: Alzheimer's disease, Cognitive aging, MRI, CSF, PET

Towards a CenTauR cortical mask

Vincent Dore^{1,2}, Christopher Rowe², Pierrick Bourgeat¹, Samantha Burnham¹, Kun Huang², Natasha Kirshnadas², Colin Masters³, Jurgen Fripp¹, Victor Villemagne²

¹CSIRO, Parkville, Australia

²Department of Nuclear Medicine, Austin Hospital, Heidelberg, Australia

³Florey institute, Parkville, Australia

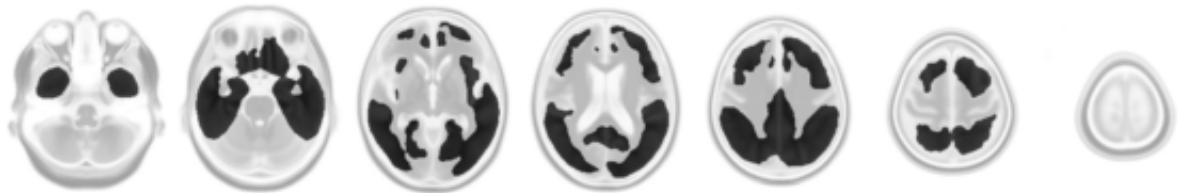
Background: In recent years, an increasing number of tau imaging tracers have become available. Among them, ¹⁸F-AV1451, ¹⁸F-MK6240 and ¹⁸F-PI2620. Each of these tracers present different dynamic ranges, tracer kinetics, off-target binding, etc. In a similar way as was done for A β -imaging (Centiloids), there is a need to standardize quantitative tau measures across tracers, supporting a universal scale (CenTauR) for tau imaging studies. In this work we developed a new cortical tau mask derived from three major tau ligands.

Methods: 288 participants underwent tau scans with either ¹⁸F-AV1451 (HC=54/AD=24), ¹⁸F-MK6240 (HC=157/AD=22) or ¹⁸F-PI2620 (HC=10/AD=21). SUVR images for each tracer were generated using the cerebellar cortex as reference. In order to construct a “universal” tau mask, a difference image between the means of the A β -HC and A β +AD patients was then generated for each tracer. The three resulting masks were subsequently intersected to generate a tau composite mask. To further refine the mask, a MRI-derived grey matter mask was applied to the composite mask. In order to minimize the asymmetry in the mask reflecting the distribution of tau deposits in the assessed participants, a mirrored mask was generated by merging L and R. Agreement between masks was assessed by dice-scores.

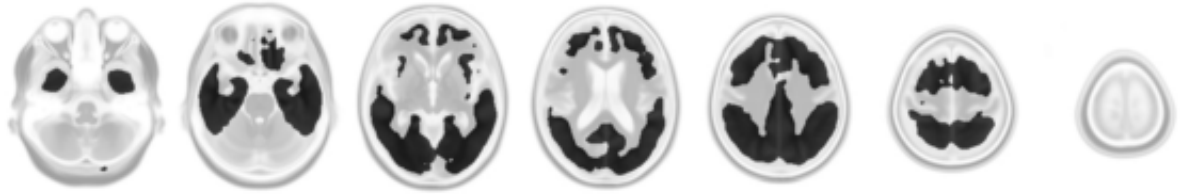
Results: Visually, the three tracer-specific masks appeared very similar (Fig 1, rows 1-3). None of the known off-target binding regions was discernible in the resulting masks. There was good agreement between all masks, with dice-scores of 0.60 and 0.66 for cortical regions.

Conclusion: We constructed a “universal” cortical tau mask based on three commonly used tau tracers. This mask can be used to standardize tau quantification across tracers and across centres. It can also be segmented into smaller regions to focus on specific areas or to construct a subset of composite masks that might better capture early tau deposition and spreading.

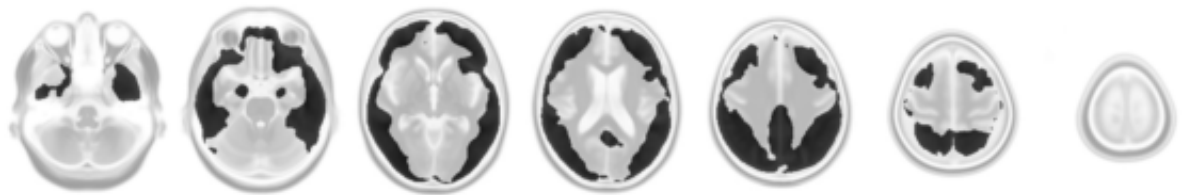
MK6240
NC=157
AD=22



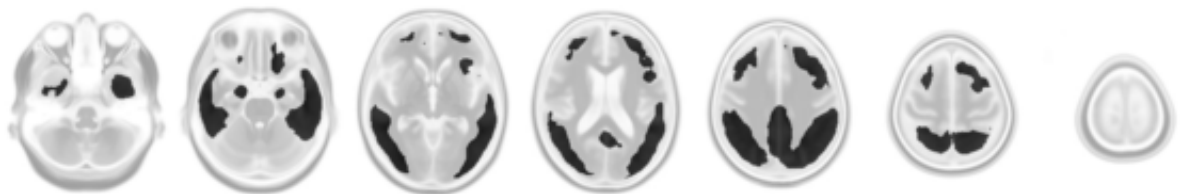
AV1451
NC=54
AD=24



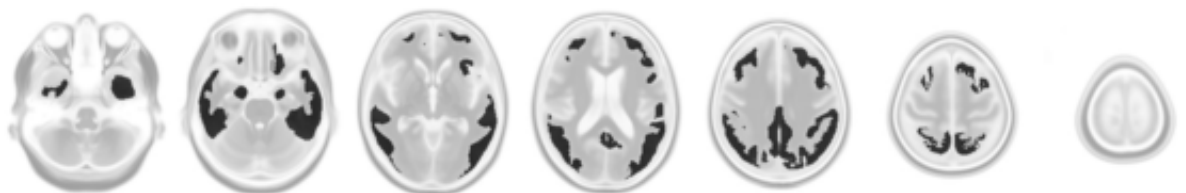
PI2620
NC=10
AD=21



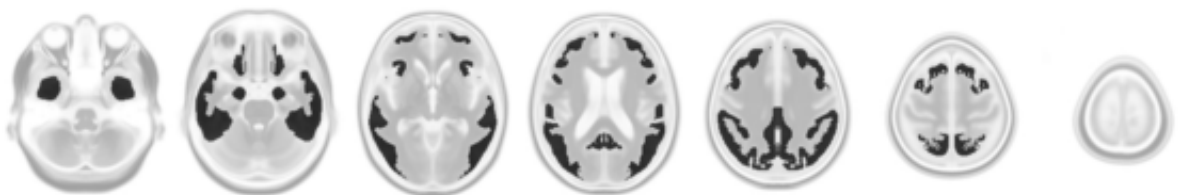
composite
mask



composite
cortical
mask



composite
cortical &
mirrored
mask



Keywords: tau MK6240 PI2620 AV1451

Tau positivity: comparing flortaucipir meta-ROI vs. maximum of regional Z-scores

Christopher Schwarz¹, Terry Therneau¹, Scott Przybelski¹, Heather Wiste¹, Jeffrey Gunter¹, Matthew Senjem¹, Val Lowe¹, Kejal Kantarci¹, Ronald Petersen¹, David Knopman¹, Clifford Jack¹

¹Mayo Clinic, Rochester, MN, US

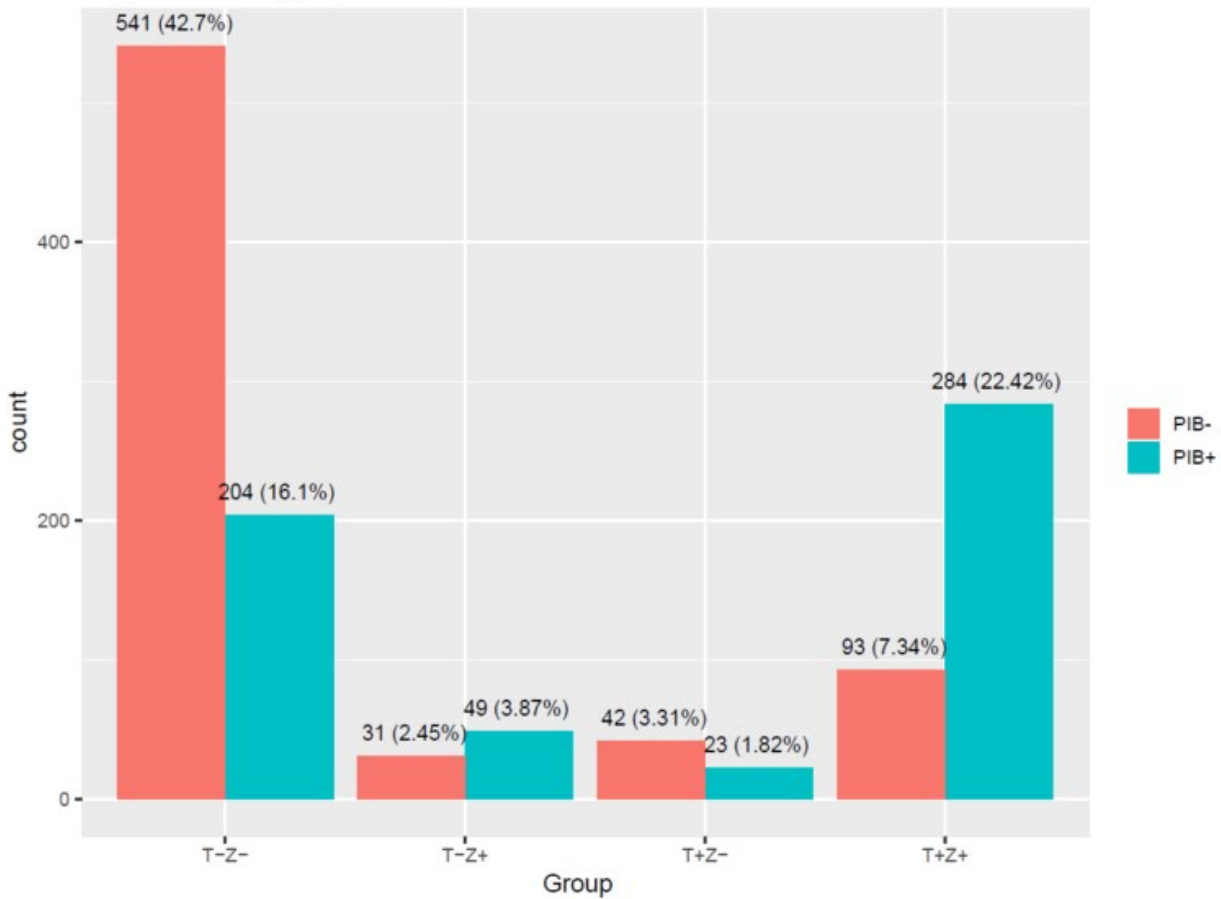
Background: Meta-ROI or reporter ROI approaches are commonly used to determine abnormal tau biomarker status, but these approaches may not detect elevated signal in focal or atypical cortical regions.

Methods: We computed regional flortaucipir (18F-AV-1451) PET SUVR for Mayo Clinic MCSA and ADRC participants. Cognitively unimpaired participants ages 30-50 (n=144) were defined as a normative population, and per-region mean (SD) were calculated across scans (SD included only SUVRs>median). We Z-transformed all regional SUVRs and computed the within-person maximum across cortical ROIs ("ZMax"). We used the 97.5th percentile of ZMax among the normative group to define abnormality (Z+: ZMax>5.16) and compared this with our existing temporal meta-ROI (GlobalTau: entorhinal, amygdala, parahippocampal, fusiform, inferior temporal, middle temporal) and cut-point (T+: GlobalTau SUVR >= 1.25). Using the remaining (n=1267) baseline scans, we compared the populations identified as T+ (abnormal meta-ROI) vs. Z+ (abnormal in any ROI).

Results: 457 (36%) scans were Z+, while 442 (35%) were T+. T-Z+ individuals were older (median=75y), 61% were PiB+, and 44% were clinically impaired. T+Z- individuals were younger (median=69y), 35% were PiB+, and 19% were clinically impaired. ZMax was more correlated (Spearman -0.24 vs. -0.16) with annualized change in auditory verbal learning test (AVLT). Among T-Z+ scans (n=80), 54% had the largest signal in a medial-temporal region; 15% in another (non-medial) temporal region; and 31% elsewhere. Across all 1267 scans, these were 36%, 30%, and 34% respectively.

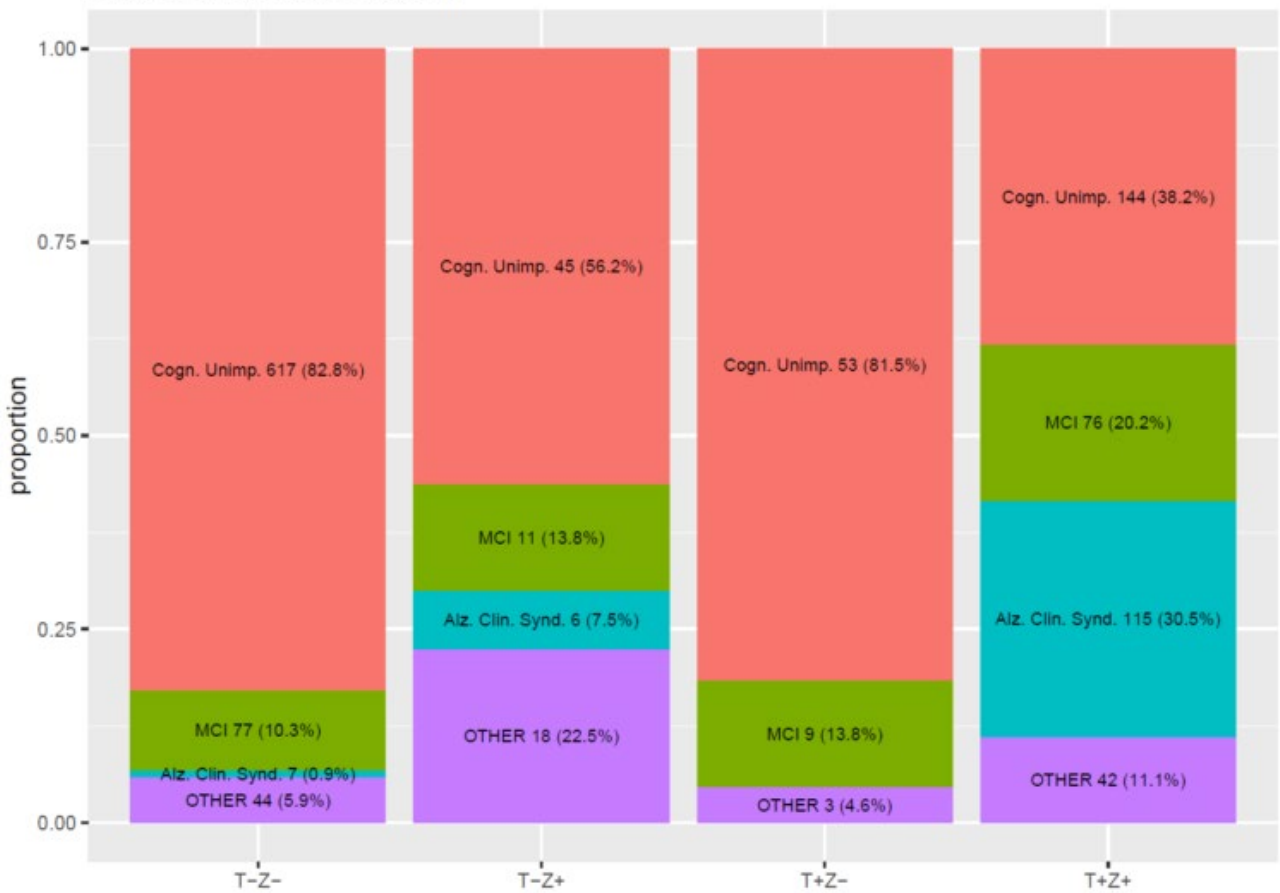
Discussion: Replacing our meta-ROI approach with ZMax may capture a more pathologic set of individuals as tau-positive. The largest Z-scores typically occurred in relatively small temporal lobe regions whose contributions to meta-ROIs may be weakened when using a mean, rather than a maximum, across regions. Our major findings were consistent across several variants of ZMax threshold, replacing maximum with mean-of-top-n-regions, and replacing per-region median-across-voxels with 95th percentile.

Amyloid status by group



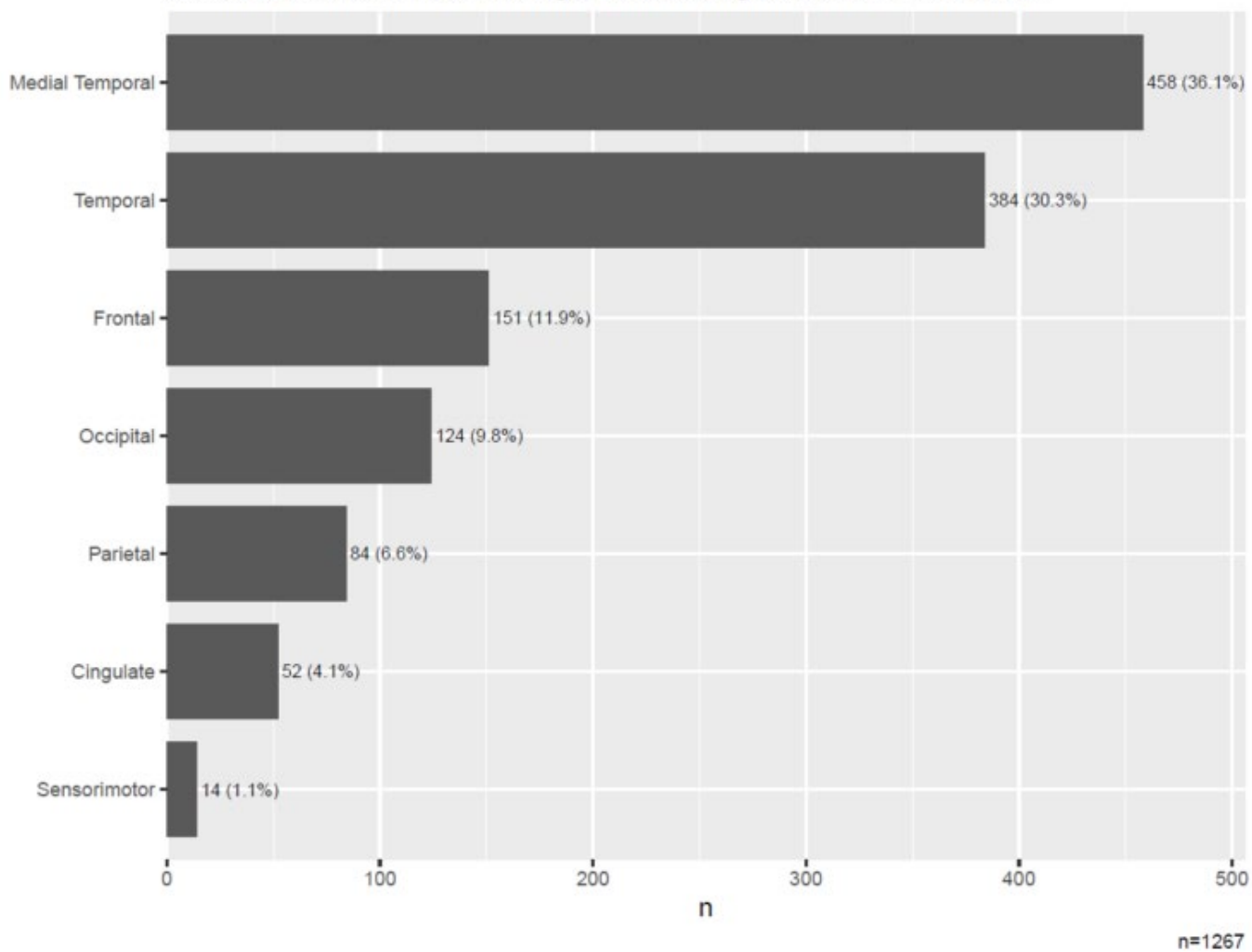
n=1267

Diagnosis proportions per group



n=1267

Across all scans, where did the region with the largest SUVR Z-Score occur?



Keywords: flortaucipir, tau, cutoff, positivity, cutpoint

P3A: POSTER SESSION 3A

Board #	Poster Title	Authors	Presenter	Page
120	Depression is predicted by tau imaging biomarker among cognitively normal adults	Babulal Roe Stout Rajasekar Wisch Benzinger Morris Ances	Ances, Beau	359
172	Temporal evaluation for maximum CSF pTau181 – [18F]Flortaucipir concordance	Wisch Gordon Schindler Flores Dincer Fagan Benzinger Morris Ances	Ances, Beau	479
144	Cerebrospinal fluid tau phosphorylated at amino acid 181 or 231: a biomarker comparison in the detection of neurofibrillary tangle pathology in the AD spectrum	Benedet J. Ashton A. Pascoal Stoops Francois Vanmechelen K. Karikari Mathotaarachchi Savard Therriault Chamoun Zetterberg Blennow Rosa-Neto	Benedet, Andrea	412
121	Local associations between tau and neurodegeneration among non-demented older adults	Bilgel Wong Resnick	Bilgel, Murat	360
122	Perfusion-phase 18F-PI-2620 tau-PET imaging as a surrogate marker of neuronal injury	Brendel Beyer Nitschmann Barthel van Eimeren Marek Song Palleis Respondek Sauerbeck Hammes Barbe Onur Jessen Saur Schroeter Rumpf Rullmann Schildan Patt Neumaier Barret Madonia Russel Stephens Roeber Herms Bötzel Levin Classen Hoeglinger Bartenstein Villemagne Drzezga Seibyl Sabri	Brendel, Matthias	363
123	Binding characteristics of 18F-PI-2620 differentiate the clinically predicted tau isoform in suspected 3/4-repeat and 4-repeat tauopathies	Brendel Song Beyer Barthel van Eimeren Marek Palleis Kaiser Respondek Sauerbeck Hammes Barbe Onur Jessen Saur Schroeter Rumpf Rullmann Schildan Patt Neumaier Barret Madonia Russel Stephens Roeber Herms Bötzel Levin Classen Hoeglinger Bartenstein Villemagne Drzezga Seibyl Sabri	Brendel, Matthias	365
124	18F-PI2620 tau-PET for assessment of heterogeneous neuropathology in corticobasal syndrome	Brendel Palleis Prix Gehmeyr Bötzel Danek Höllerhage Sauerbeck Beyer Nitschmann Song Stephens Barthel Patt Sabri Drzezga van Eimeren Villemagne Bartenstein Perneckzy Haass Levin Hoeglinger	Brendel, Matthias	367
125	Optimal reference region for the quantification of tau load in the brain using 18F-PI-2620 PET	Bullich Müller Roé-Vellvé Jovalekic Perrotin De Santi Koglin Stephens	Bullich Roig, Santiago	369
126	Quantifying tau PET imaging reliably in the presence of off-target binding	Chen Gordon McCullough Zaza Mejias Dincer Flores Keefe Paulick Jackson Koudelis Su Morris Benzinger	Chen, Charles	370
127	[18F]THK5317 imaging as a predictive tool of prospective cognitive decline in prodromal and dementia-stage AD	Chiotis Savitcheva Poulakis Saint-Aubert Wall Antoni Nordberg	Chiotis, Konstantinos	372
128	Comparison of quantitative cutoff methods for [18F]AV-1451	Minhas Laymon Lopresti Snitz Tudorascu Aizenstein Lopez Mathis Klunk Cohen	Cohen, Ann	374
129	Pilot study on the relationship between 18F-MK-6240 and VBM in early and late stages of AD	Fernandez Arias Pascoal Benedet Thierrault Su Kang Savard Ottoy Mathotaarachchi Lussier Tissot Thomas Stevenson Rahmouni Wang Massarweh Soucy Gauthier Rosa-Neto	Fernandez Arias, Jaime	375
130	Functional connectivity brain architecture predicts the rate of tau accumulation in AD	Franzmeier Neitzel Rubinski Smith Strandberg Ossenkoppele Hansson Ewers	Franzmeier, Nicolai	377
131	How innocent is PART?: Mesial temporal tau is associated with worse cognitive performance in A β -negative cognitively normal individuals	Groot	Groot, Colin	381
132	CSF P-tau detects cerebral tau accumulation earlier than tau PET in amyloid positive elderly adults	Guo Jagust Landau	Guo, Tengfei	384

Board #	Poster Title	Authors	Presenter	Page
133	Amyloid, tau, and atrophy in preclinical AD: A longitudinal study	Hanseuw Jacobs Schultz Buckley Properzi Farrell Scott Hampton Sanchez Sperling Johnson	Hanseuw, Bernard	388
134	Increased levels and phosphorylation of soluble tau proteins occur earlier than changes in Tau PET in AD	Hansson Andersson Janelidze Ossenkoppele Insel Strandberg Zetterberg Blennow Chai Dage Stomrud Smith Palmqvist Mattsson	Hansson, Oskar	391
135	Preclinical characterization of [18F]THK-5562, a novel tau PET tracer with little off-target binding	Harada Lerdisiruk Yiqing Ezura Shimizu Morito Arai Yanai Kudo Furumoto Okamura	Harada, Ryuichi	392
136	Comparison of tau PET imaging using 18F-APN-1607 and 18F-THK5351 in Alzheimer disease patients and normal controls	Hsiao Lin Huang Huang	Hsiao, Ing-Tsung	393
137	In vivo amyloid-PET and tau-PET evidence in early-onset AD: taking the LEADS	Iaccarino La Joie Lesman-Segev Soleimani-Meigooni Provost Collins Aisen Borowski Eloyan Fagan Foroud Gatsonis Jack Jr. Kramer Saykin Toga Vemuri Day Graff-Radford Honig Jones Masdeu Mendez Onyike Rogalski Salloway Wolk Wingo Koeppe Dickerson Apostolova Carrillo Rabinovici	Iaccarino, Leonardo	395
138	Multimodal in vivo investigation of amyloid and tau biomarkers associations with cerebrospinal fluid NfL and YKL40 levels	Iaccarino La Joie Edwards Lesman-Segev Strom Pham Chaudhary Fenton Jerome Janabi Baker Miller Jagust Fagan Rabinovici	Iaccarino, Leonardo	399
139	Activated microglia and amyloid load potentiate tau deposition leading to cognitive dysfunction in AD	Kang Otto Savard Pascoal Mathotaarachchi Benedet Chamoun Therriault Lussier Tissot Thomas Stevenson Rahmouni Arias Wang Massarweh Soucy Gauthier Rosa-Neto	Kang, Min Su	403
140	Tauopathy in females is more vulnerable to amyloid or neuroinflammation in AD	Kang Otto Chamoun Mathotaarachchi Savard Benedet Pascoal Therriault Lussier Tissot Thomas Stevenson Rahmouni Fernandez-Arias Wang Massarweh Soucy Gauthier Rosa-Neto	Kang, Min Su	404
141	Prediction of brain tau accumulation in amyloid positive cognitive impairment patients using multimodal biomarkers with machine learning approach	Kim Park Park Kang Kim Jang Kim Na Lee Seo	Kim, Jaeho	406
142	Comparison of longitudinal change metrics for 18F-RO948 PET among cognitively unimpaired and patients with MCI or AD dementia in the BioFINDER2 study	Klein Sanabria Leuzy Borroni Mattsson Palmqvist Stomrud Smith Hansson	Klein, Gregory	408
145	Diagnostic performance of [18F]RO948 tau positron emission tomography in the differentiation of AD from other neurodegenerative disorders	Leuzy Smith Ossenkoppele Santillo Borroni Klein Olsson Jögi Palmqvist Mattsson Strandberg Stomrud Hansson	Leuzy, Antoine	415
146	Longitudinal changes in tau pathology measured by [18F]RO948 tau-PET are associated with elevated CSF P-tau: Preliminary findings from the Swedish BioFINDER-2 study	Leuzy Klein Ossenkoppele Mattsson Janelidze Palmqvist Strandberg Coloma Borroni Stomrud Smith Hansson	Leuzy, Antoine	418
147	A comparison of ischemic stroke-induced changes on 18F-APN-1607 (18F-PMPBB3) and 18F-THK-5351 uptake patterns	Lin Hsiao Huang Huang	Lin, Kun-Ju	420
148	Longitudinal change in [18F]GTP1 SUVR over 18 months depends on baseline SUVR intensity and spatial distribution and shows trends with cognitive decline	Manser Sanabria Bohorquez Teng Baker Toth Marik Weimer	Manser, Paul	421
149	18F-APN-1607: a promising PET tracer for multiple tauopathies	Margolin Lin Tempest Chen Marek Russell Sandiego Huang Hsiao Tamagnan Alagille Guan Lu Zuo Higuchi Jang	Margolin, Richard	423
150	Entorhinal cortical tau accumulation is inversely associated with hippocampal synaptic density in older individuals with normal cognition and early AD	Mecca Chen Naganawa Toyonaga Godek Harris Bartlett Zhao Gallezot Nabulsi Huang Arnsten Carson van Dyck	Mecca, Adam	425

Board #	Poster Title	Authors	Presenter	Page
151	Mental and physical activity during the uptake period affects off-target binding in extra- and within-brain Tau PET (18F-FTP)	Min Apgar Scott Hol Lundt Albertson Schwarz Botha Vemuri Gunter Petersen Jack Lowe	Min, Hoon-Ki	427
143	Validation of clinical protocols for clinicians analyzing 18F-PI-2620 tau PET/MRI images	Koran Shams Adams Cazevedo Toueg Corso Hunt Castillo Hall Sha Fredericks Greicius Wagner Zaharchuk Davidzon Chin Mormino	Mormino, Elizabeth	410
152	In vivo uptake of 18F-PM-PBB3 (18F-APN-1607) in patients with corticobasal syndrome	Nakano Shimada Tagai Matsuoka Kubota Takahata Takado Shinotoh Yamamoto Sano Seki Hirano Ono Tempest Jang Sahara Kawamura Zhang Kuwabara Higuchi	Nakano, Yoshikazu	430
153	Factors predicting tau PET status in cognitively unimpaired and impaired individuals	Ossenkoppele Leuzy Cho La Joie Strandberg Mattsson Palmqvist Lyoo Rabinovici Smith Hansson	Ossenkoppele, Rik	431
154	Widespread amyloid is necessary to detect tau-PET signal beyond the entorhinal cortex and cognitive decline	Ozlen Binette Köbe Meyer Villeneuve	Ozlen, Hazal	433
155	Using 18F-Flortaucipir visual assessment to define T-status in the AT(N) framework: evaluation of intra- and inter-rater reliability	Provost Iaccarino Soleimani-Meigooni Lesman-Segev La Joie Edwards Strom Pham Mellinger Janabi Baker Jagust Rabinovici	Provost, Karine	436
156	Defining T-status in the AT(N) framework: comparison of 18F-Flortaucipir visual assessment, SUVR quantification and CSF pTau	Provost Iaccarino Soleimani-Meigooni Lesman-Segev La Joie Mattsson Hansson Eichenlaub Edwards Strom Pham Mellinger Janabi Baker Jagust Rabinovici	Provost, Karine	440
157	Plasma neurofilament light is associated with regional tau tangle burden in autosomal dominant AD: findings from the COLBOS Project	Quiroz Zetterberg Reiman Sanchez Guzman-Velez Fox-Fuller Arboleda-Velasquez Baena Gatchel Sperling Johnson Blennow Lopera	Quiroz, Yakeel	443
158	Application of tau PET as a biomarker of AD in therapeutic trials: A pharmaceutical industry perspective	Salinas Lohith Guo Wooten Tulip Sanjeewa Comley Sur Hostetler Beaver Martarello	Salinas, Cristian	444
159	Measuring increases of tau pathology in AD using [18F]GTP1 (Genentech tau probe 1) PET imaging	Sanabria Bohorquez Baker Manser Toth Teng Marik Weimer	Sanabria Bohorquez, Sandra	446
160	Evaluation of tau PET staging in the A4/LEARN study	Sanchez Becker Jacobs Hanseeuw Mayblyum Rubinstein Thibault Schultz Seshadri Quiroz Rentz Price Sperling Johnson the A4 Study Team	Sanchez, Justin	449
161	Clinical evaluation of [18F]-JNJ-64326067, a candidate PET tracer for the detection of tau pathology in AD	Schmidt Janssens Moechars Rombouts Timmers Barret Constantinescu Madonia Russell San Diego Kolb	Schmidt, Mark	453
162	Association between cerebrospinal fluid neurofilament light chain and markers of neurofibrillary pathophysiology: findings from the Knight Alzheimer Disease Research Center	Schultz Schindler Chen Sutphen Morris Fagan Gordon Benzinger	Schultz, Stephanie	454
163	18F-PM-PBB3 (18F-APN-1607) uptake associates with plasma NfL level and motor disability in patients with progressive supranuclear palsy	Shimada Tagai Tatebe Matsuoka Kubota Takahata Takado Shinotoh Yamamoto Sano Seki Nakano Ono Hirano Tempest Jang Sahara Kawamura Zhang Tokuda Higuchi	Shimada, Hitoshi	457
164	The rate of accumulation of tau aggregates is higher in females and younger individuals	Smith Mattsson Pontecorvo Devous Strandberg Ossenkoppele Hansson	Smith, Ruben	458
165	Resting state functional connectivity associations with F18-Florbetapir PET versus F18-Flortaucipir PET	Svaldi Goñi Stage Abbas Dziedzic West Risacher Saykin Apostolova	Svaldi, Diana	462
166	Tau positivity: Comparing flortaucipir meta-ROI vs maximal single region	Therneau Schwarz Wiste Gunter Senjem Lowe Kantarci Petersen Knopman Mielke Jones Jack	Therneau, Terry	466
167	Intrinsic connectivity of the human brain provides scaffold for tau aggregation in AD	Therriault Pascoal Savard Mathotaarachchi Benedet Chamoun Gauthier Saha-Chaudhuri Massarweh Rosa-Neto	Therriault, Joseph	469
168	Changes in volumetric MRI measures at 12 months significantly correlate	Toth Sanabria Bohorquez Manser Baker Teng Marik Weimer	Toth, Balasz	473

Board #	Poster Title	Authors	Presenter	Page
	with baseline [18F]GTP1 SUVR, but not [18F]GTP1 change			
169	Elevated medial temporal lobe Tau PET with 18F-PI2620 in normal controls with “borderline” neuropsychological testing profiles	Toueg Deutsch Castillo Hunt Corso Trelle Harrison Azevedo Shen Anders Hall Fredericks Sha Davidzon Chin Khalighi Wagner Mormino	Toueg, Tyler	475
170	Hippocampal tau accumulation predicts individual differences in episodic memory in cognitively normal older adults	Trelle Toueg Castillo Channappa Corso Hunt Jayakumar Nadiadwala Guo Azevedo Shin Davidson Deutsch Hall Sha Fredericks Kerchner Carr Chin Wagner Mormino	Trelle, Alexandra	476
171	Temporo-limbic tau burden, as measured by 18F-AV1451, is a correlate of hippocampal volume loss over time	Fischer Ahnen Dissertori Lustermann Weber Buck Kagerer Gietl Hock Unschuld	Unschuld, Paul	477
173	[18F]flortaucipir PET is more closely associated with disease severity than CSF p-tau in AD	Wolters Ossenkuppele Verfaillie Coomans Timmers Visser Tuncel Golla Windhorst Boellaard van der Flier Teunissen Scheltens van Berckel	Wolters, Emma	481
174	Associations of tau pathology and functional connectivity with retrospective cognitive change among cognitively normal older adults	Shafer Bilgel Ziontz Wong Resnick	Ziontz, Jacob	485

P120: Depression is predicted by tau imaging biomarker among cognitively normal adults

Ganesh Babulal¹, Catherine Roe¹, Sarah Stout¹, Ganesh Rajasekar¹, Julie Wisch¹, Tammie Benzinger¹, John Morris¹, Beau Ances¹

¹Washington University School of Medicine, St. Louis, MO, US

Objective: Depression is both a risk factor and consequence of Alzheimer's disease (AD). Biomarker studies using cerebrospinal fluid and amyloid Positron Emission Tomography (PET) have found elevated levels of AD biomarkers are associated with the development of depressive symptoms over time. This study examines whether tau and amyloid imaging, predicts a depression diagnosis among cognitively normal adults. Secondary analysis assesses how antidepressant modifies this relationship.

Methods: Cognitively normal participants (Clinical Dementia Rating = 0) were enrolled from the Knight Alzheimer's Disease Research Center at Washington University. Logistic regression models evaluated whether, *in vivo* tau PET (Flortaucipir), predicted depression diagnosis, after adjusting for covariates including age, sex, education, race, and apolipoprotein $\epsilon 4$. Similarly, a second model tested the statistical interaction between tau PET and antidepressant use in predicting depression, while adjusting for the same covariates. A second set of models were conducted substituting tau PET with amyloid PET imaging (Florbetapir). We also examined group differences on depressive symptoms, neuropsychiatric symptoms, and a neuropsychological composite score.

Results: Data were available from 301 cognitively normal participants (46.2 to 91.3 years old and mean of 69.5 (SD=8.0)). Participants with elevated tau PET were twice more likely to be depressed. The interaction between tau and antidepressant use was also significant suggesting those with elevated tau and taking antidepressants had a greater risk of depression. Relatedly, amyloid was not statistically significant in predicting depression. There were no differences between groups on depressive symptoms, neuropsychiatric symptoms, and a neuropsychological composite score.

Conclusions: Our results demonstrate that tau, not amyloid PET predicts a depression diagnosis, however, there was no relationship with depressive symptoms. Additionally, antidepressant use interacts with tau to increase the risk of depression among cognitively normal adults.

Keywords: Tau PET, Amyloid PET, Depression, Antidepressants

P121: Local associations between tau and neurodegeneration among non-demented older adults

Murat Bilgel¹, Dean Wong², Susan Resnick¹

¹*Laboratory of Behavioral Neuroscience, National Institute on Aging, Baltimore, MD, US*

²*Department of Radiology and Radiological Science, Johns Hopkins University School of Medicine, Baltimore, MD, US*

Introduction: We propose a framework for studying individual-level local associations between tau and neurodegeneration, as measured by cerebral blood flow (CBF) and gray matter (GM) volume.

Methods: We used cross-sectional data for 50 non-demented participants from the Baltimore Longitudinal Study of Aging. For each participant, we quantified the local associations of tau (FTP-SUVR) with CBF (PiB- R_1) within the cerebral cortex using geographically weighted regressions (Figure 1). We also separately assessed the local associations of tau and GM volume (measured by RAVENS). All models were adjusted for local amyloid burden (PiB-DVR). Using the resulting association maps for each participant, we performed a t-test at each voxel of the tau-CBF and tau-GM association maps.

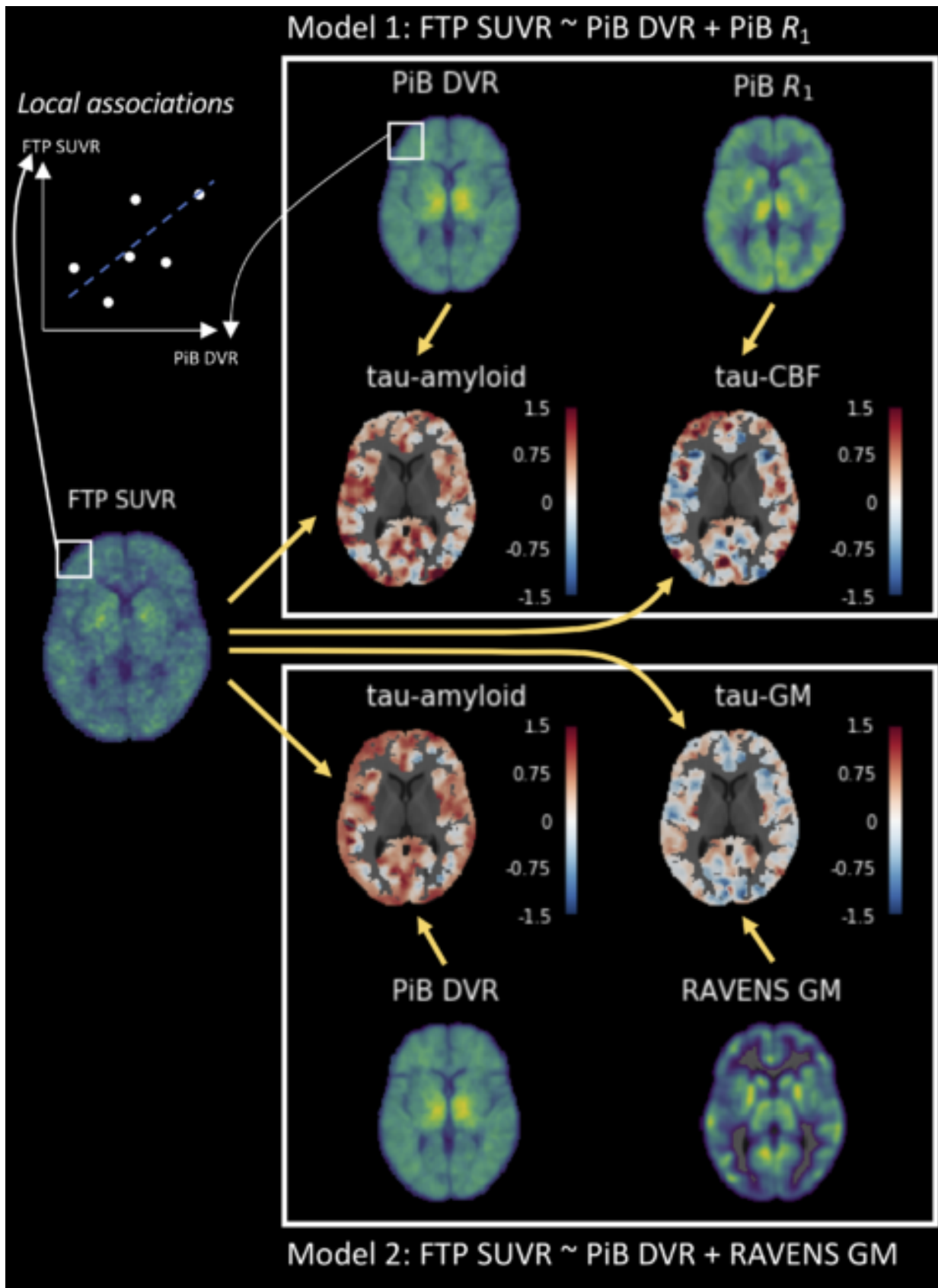


Figure 1. Method overview. For each participant, we carried out two separate geographically weighted regressions to quantify the local associations of tau with cerebral blood flow (CBF) and with gray matter (GM) volume in the cerebral cortex, adjusting for amyloid burden. The resulting association maps were then analyzed across participants.

Results: Higher FTP-SUVR was associated with higher PiB-DVR throughout the cerebral cortex. These

widespread associations remained in analyses stratified by PiB status.

Adjusting for PiB-DVR, higher FTP-SUVR was associated with higher PiB- R_1 bilaterally in the superior frontal gyrus, inferior and middle temporal gyri, fusiform, posterior cingulate, precuneus, and lingual gyrus. There were negative associations in the left central operculum and insula (Figure 2).

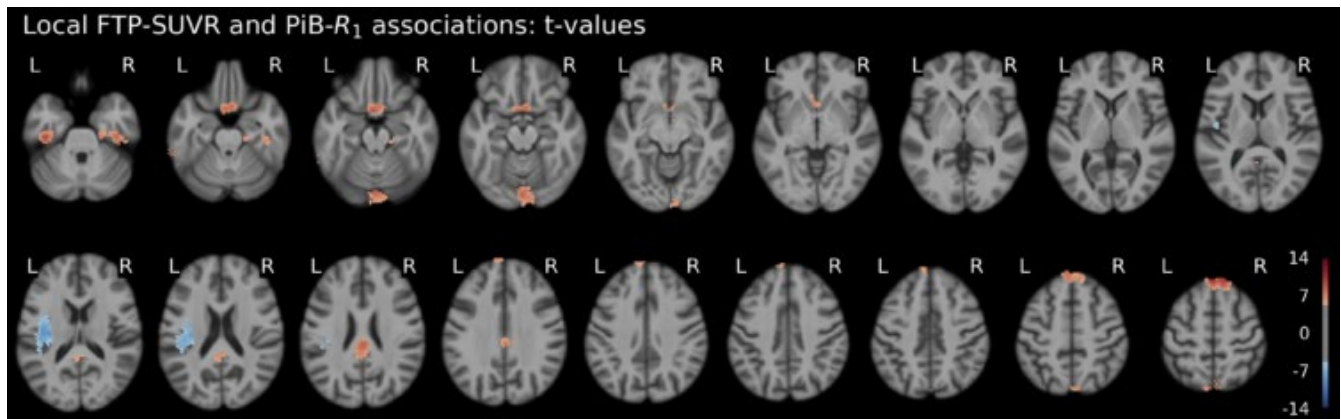


Figure 2. Local associations between FTP-SUVR and PiB- R_1 (a surrogate measure of cerebral blood flow), adjusted for local PiB-DVR. Red and blue indicate where the mean association across participants was positive or negative (permutation test multiple comparison corrected $p < 0.05$), respectively.

Adjusting for local PiB-DVR, higher FTP-SUVR was associated with lower GM volume in the right planum temporale, transverse and superior temporal gyri, and bilaterally in the insula and operculum. There were positive associations in the right inferior occipital gyrus (Figure 3).

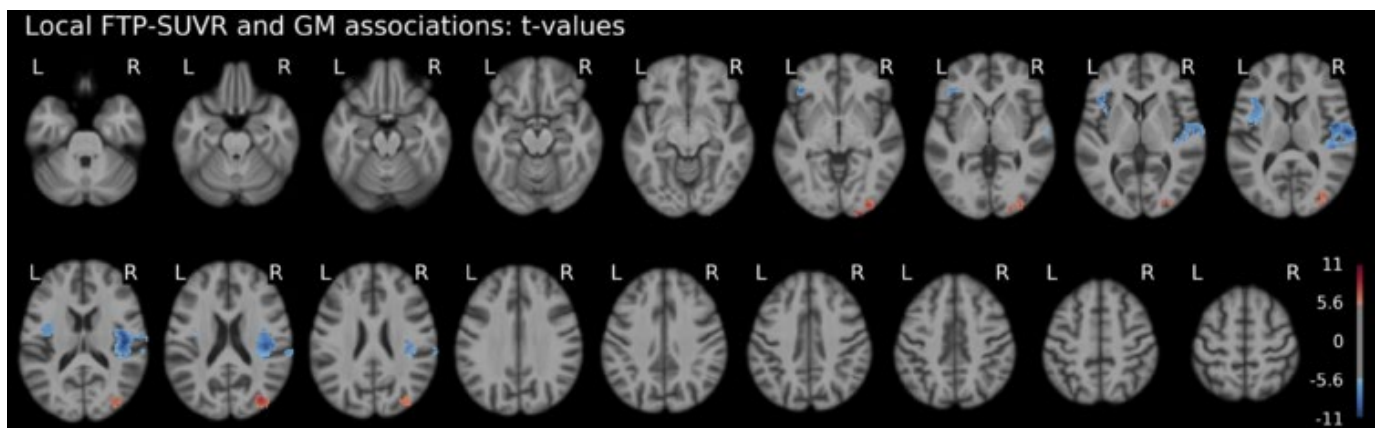


Figure 3. Local associations between FTP-SUVR and GM volume, adjusted for local PiB-DVR. Red and blue indicate where the mean association across participants was positive or negative (permutation test multiple comparison corrected $p < 0.05$), respectively.

Discussion: The widespread association between FTP-SUVR and PiB-DVR, regardless of PiB status, suggests that there is a common source of signal in the FTP and PiB scans. The positive associations between FTP-SUVR and PiB- R_1 support the notion of a period of hyperactivity associated with initial tau accumulation. The negative associations between FTP-SUVR and GM volume suggest that greater tau is associated with greater insular atrophy in non-demented individuals.

This research was supported by the Intramural Research Program of the NIH, National Institute on Aging.

Keywords: FTP, PiB, CBF, neurodegeneration, tau

P122: Perfusion-phase ^{18}F -PI-2620 tau-PET imaging as a surrogate marker of neuronal injury

Matthias Brendel¹, Leonie Beyer¹, Alexander Nitschmann¹, Henryk Barthel², Thilo van Eimeren^{3,4,5,6}, Ken Marek^{7,8}, Mengmeng Song¹, Carla Palleis⁹, Gesine Respondek^{6,10}, Julia Sauerbeck¹, Jochen Hammes⁴, Michael Barbe⁵, Özgür Onur⁵, Frank Jessen^{6,11,12}, Dorothee Saur¹³, Matthias L. Schroeter^{14,15,16}, Jost-Julian Rumpf¹³, Michael Rullmann², Andreas Schildan², Marianne Patt², Bernd Neumaier^{3,4}, Oliver Barret^{7,8}, Jennifer Madonia^{7,8}, David S. Russel^{7,8}, Andrew Stephens¹⁷, Sigrun Roeber¹⁸, Jochen Herms^{6,18}, Kai Bötzel⁹, Johannes Levin^{6,9}, Joseph Classen¹³, Guenter Hoeglinger^{6,10,19}, Peter Bartenstein^{1,20}, Victor Villemagne^{21,22,23}, Alexander Drzezga^{4,6}, John Seibyl^{7,8}, Osama Sabri²

¹*Department of Nuclear Medicine, University Hospital of Munich, LMU Munich, Munich, Germany*

²*Department of Nuclear Medicine, University of Leipzig, Leipzig, Germany*

³*Cognitive Neuroscience, Institute for Neuroscience and Medicine (INM-3), Research Centre Juelich, Juelich, Germany*

⁴*Department of Nuclear Medicine, University Hospital Cologne, Cologne, Germany*

⁵*Department of Neurology, University Hospital Cologne, Cologne, Germany*

⁶*German Center for Neurodegenerative Diseases (DZNE), Bonn, Germany*

⁷*InviCRO, LLC, Boston, MA, US*

⁸*Molecular Neuroimaging, A Division of inviCRO, New Haven, CT, US*

⁹*Department of Neurology, University Hospital of Munich, LMU Munich, Munich, Germany*

¹⁰*Department of Neurology, Technical University Munich, Munich, Germany*

¹¹*Center for Memory Disorders, University Hospital Cologne, Cologne, Germany*

¹²*Department of Psychiatry, University Hospital Cologne, Cologne, Germany*

¹³*Department of Neurology, University of Leipzig, Leipzig, Germany*

¹⁴*Clinic for Cognitive Neurology, University of Leipzig, Leipzig, Germany*

¹⁵*LIFE - Leipzig Research Center for Civilization Diseases, University of Leipzig, Leipzig, Germany*

¹⁶*Max-Planck-Institute of Human Cognitive and Brain Sciences, Leipzig, Germany*

¹⁷*Life Molecular Imaging GmbH, Berlin, Germany*

¹⁸*Center for Neuropathology and Prion Research, University Hospital of Munich, LMU Munich, Munich, Germany*

¹⁹*Department of Neurology, Medizinische Hochschule Hannover, Hannover, Germany*

²⁰*Munich Cluster for Systems Neurology (SyNergy), Munich, Germany*

²¹*Department of Molecular Imaging & Therapy, Austin Health, Heidelberg, Australia*

²²*The Florey Institute of Neuroscience and Mental Health, The University of Melbourne, Melbourne, Australia*

²³*Department of Medicine, Austin Health, The University of Melbourne, Melbourne, Australia*

Aim: Second generation tau radioligands for use with positron emission tomography (PET) have been developed for visualization of tau deposits in vivo. For several β -amyloid and first generation tau radioligands, it has been shown that reduced early-phase perfusion can be used as a surrogate of neuronal injury. Therefore, we investigated the performance of early acquisitions of the novel tau radioligand ^{18}F -PI-2620 for the assessment of neuronal injury.

Methods: Twenty-six subjects were referred with suspected tauopathies and received a dynamic ^{18}F -PI-2620 tau-PET (0-60 min p.i.) and ^{18}F -fluorodeoxyglucose (FDG)-PET (30-50 min p.i.). Regional standard-uptake-value-ratios of early-phase perfusion images (single frame SUV_r) and the blood flow estimate (R_1) of ^{18}F -PI-2620 were correlated with corresponding quantification of FDG-PET (global mean/ cerebellar normalization). Reduced tracer uptake in cortical target regions was interpreted visually using 3-dimensional stereotactic surface projections by three experienced and three expert readers and intraclass

correlation coefficients (ICC) were calculated between tau-PET perfusion and FDG-PET.

Results: Highest agreement with FDG quantification was reached for ^{18}F -PI-2620 acquisition from 0.5 to 2.5 min p.i. for global mean ($R > 0.69$) and cerebellar scaling ($R > 0.63$). Correlation coefficients (summed 0.5-2.5 min SUV_T & R_1) displayed excellent agreement in all cortical target regions for global mean ($R_{\text{SUV}_T} 0.75 \pm 0.10$, $R_{R_1} = 0.75 \pm 0.10$) and cerebellar normalization ($R_{\text{SUV}_T} 0.67 \pm 0.10$, $R_{R_1} = 0.67 \pm 0.12$). Visual interpretation revealed high regional ICC between tau-PET perfusion and FDG-PET independent of the reader experience ($\text{ICC}_{\text{SUV}_T} = 0.62 \pm 0.07$, $\text{ICC}_{R_1} = 0.66 \pm 0.07$).

Conclusion: Perfusion phase imaging of ^{18}F -PI-2620 can serve as a surrogate biomarker for neuronal injury. Dynamic imaging or a dual time point protocol for tau-PET imaging could replace additional FDG-PET imaging by indexing both the distribution of tau and the amount of neuronal injury.

Keywords: tau, PET, perfusion, neuronal injury, PI-2620

P123: Binding characteristics of 18F-PI-2620 differentiate the clinically predicted tau isoform in suspected 3/4-repeat and 4-repeat tauopathies

Matthias Brendel¹, Mengmeng Song¹, Leonie Beyer¹, Henryk Barthel², Thilo van Eimeren^{3,4,5,6}, Ken Marek^{7,8}, Carla Palleis⁹, Lena Kaiser¹, Gesine Respondek^{6,10}, Julia Sauerbeck¹, Jochen Hammes⁴, Michael Barbe⁵, Özgür Onur⁵, Frank Jessen^{6,11,12}, Dorothee Saur¹³, Matthias L. Schroeter^{14,15,16}, Jost-Julian Rumpf¹³, Michael Rullmann², Andreas Schildan², Marianne Patt², Bernd Neumaier^{3,4}, Oliver Barret^{7,8}, Jennifer Madonia^{7,8}, David S. Russel^{7,8}, Andrew Stephens¹⁷, Sigrun Roeber¹⁸, Jochen Herms^{6,18}, Kai Bötzel⁹, Johannes Levin^{6,9}, Joseph Classen¹³, Guenter Hoeglinger^{6,10,19}, Peter Bartenstein^{1,20}, Victor Villemagne^{21,22,23}, Alexander Drzezga^{4,6}, John Seibyl^{7,8}, Osama Sabri²

¹Department of Nuclear Medicine, University Hospital of Munich, LMU Munich, Munich, Germany

²Department of Nuclear Medicine, University of Leipzig, Leipzig, Germany

³Cognitive Neuroscience, Institute for Neuroscience and Medicine (INM-3), Research Centre Juelich, Juelich, Germany

⁴Department of Nuclear Medicine, University Hospital Cologne, Cologne, Germany

⁵Department of Neurology, University Hospital Cologne, Cologne, Germany

⁶German Center for Neurodegenerative Diseases (DZNE), Bonn, Germany

⁷InviCRO, LLC, Boston, MA, US

⁸Molecular Neuroimaging, A Division of inviCRO, New Haven, CT, US

⁹Department of Neurology, University Hospital of Munich, LMU Munich, Munich, Germany

¹⁰Department of Neurology, Technical University Munich, Munich, Germany

¹¹Center for Memory Disorders, University Hospital Cologne, Cologne, Germany

¹²Department of Psychiatry, University Hospital Cologne, Cologne, Germany

¹³Department of Neurology, University of Leipzig, Leipzig, Germany

¹⁴Clinic for Cognitive Neurology, University of Leipzig, Leipzig, Germany

¹⁵LIFE - Leipzig Research Center for Civilization Diseases, University of Leipzig, Leipzig, Germany

¹⁶Max-Planck-Institute of Human Cognitive and Brain Sciences, Leipzig, Germany

¹⁷Life Molecular Imaging GmbH, Berlin, Germany

¹⁸Center for Neuropathology and Prion Research, University Hospital of Munich, LMU Munich, Munich, Germany

¹⁹Department of Neurology, Medizinische Hochschule Hannover, Hannover, Germany

²⁰Munich Cluster for Systems Neurology (SyNergy), Munich, Germany

²¹Department of Molecular Imaging & Therapy, Austin Health, Heidelberg, Australia

²²The Florey Institute of Neuroscience and Mental Health, The University of Melbourne, Melbourne, Australia

²³Department of Medicine, Austin Health, The University of Melbourne, Melbourne, Australia

Aim: Tau proteins consist of different isoforms, characterized by the number of repeats (R) of their microtubule binding sites. Preliminary evidence suggests that the novel second-generation tau PET tracer ¹⁸F-PI-2620 is able to visualize the predominantly 3/4R-tauopathy Alzheimer's disease (AD) and the 4R-tauopathies Corticobasal syndrome (CBS) and Progressive supranuclear palsy (PSP) by PET, but - apart from the obvious topographical differences - likely with different kinetics and magnitude of affinity among them. The aim of this study was to determine whether binding characteristics of ¹⁸F-PI-2620 are different between 3/4R- and 4R-tauopathies.

Methods: We evaluated 14 patients with suspected 3/4R tauopathy and 29 patients with suspected 4R tauopathy (14 CBS, 15 PSP) at two different centers according to current diagnosis criteria. ¹⁸F-PI-2620 PET scans were acquired 0-60min p.i. and distribution volume ratios (DVR, cerebellar reference) were calculated. Cortical and subcortical clusters exceeding 20 voxels of elevated DVR (≥ 2.5 SD vs. 10 healthy

controls) per region were evaluated by non-invasive kinetic modelling. R1 (perfusion), k2 (clearance), DVR, 30-60 min standard-uptake-value-ratios (SUV_{r30-60}) and the linear slope of SUV_r between 10 and 60 min p.i. were compared between 3/4R- and 4R-tauopathies.

Results: Cortical tau-positive clusters in 4R-tau cases had equal R1 but higher k2 values when compared to 3/4R-tau cases ($p<0.001$). Higher mean DVR (1.35 ± 0.19 vs. 1.17 ± 0.60 , $p<0.01$), higher mean SUV_{r30-60} (1.67 ± 0.33 vs. 1.31 ± 0.22 , $p<0.001$) and steeper slopes (0.85 ± 0.51 vs. 0.43 ± 0.49 , $p<0.001$) were observed in cortical clusters of 3/4R-tau cases when compared to 4R-tau cases. Subcortical clusters did not show significant differences.

Conclusion: ¹⁸F-PI-2620 binding characteristics in tau-positive cortical regions differentiate clinically suspected 3/4R-tauopathies from 4R-tauopathies. Higher tracer clearance indicates less stable binding in 4R tauopathies when compared to 3/4R-tau cases.

Keywords: tau, PET, isoforms, binding parameter, PI-2620

P124: 18F-PI2620 tau-PET for assessment of heterogeneous neuropathology in corticobasal syndrome

Matthias Brendel¹, Carla Palleis², Catharina Prix², Mona Gehmeyr², Kai Bötzel², Adrian Danek², Matthias Höllerhage³, Julia Sauerbeck¹, Leonie Beyer¹, Alexander Nitschmann¹, Mengmeng Song¹, Andrew Stephens⁴, Henryk Barthel⁵, Marianne Patt⁵, Osama Sabri⁵, Alexander Drzezga^{6,7}, Thilo van Eimeren^{6,7,8,9}, Victor Villemagne^{10,11,12}, Peter Bartenstein^{1,13}, Robert Perneczky^{7,14,15,16}, Christian Haass^{7,13,17}, Johannes Levin^{2,7}, Guenter Hoeglinger^{3,7,18}

¹Department of Nuclear Medicine, University Hospital of Munich, LMU Munich, Munich, Germany

²Department of Neurology, University Hospital of Munich, LMU Munich, Munich, Germany

³Department of Neurology, Technical University Munich, Munich, Germany

⁴Life Molecular Imaging GmbH, Berlin, Germany

⁵Department of Nuclear Medicine, University of Leipzig, Leipzig, Germany

⁶Department of Nuclear Medicine, University Hospital Cologne, Cologne, Germany

⁷German Center for Neurodegenerative Diseases (DZNE), Bonn, Germany

⁸Cognitive Neuroscience, Institute for Neuroscience and Medicine (INM-3), Research Centre Juelich, Juelich, Germany

⁹Department of Neurology, University Hospital Cologne, Cologne, Germany

¹⁰Department of Molecular Imaging & Therapy, Austin Health, Heidelberg, Australia

¹¹The Florey Institute of Neuroscience and Mental Health, The University of Melbourne, Melbourne, Australia

¹²Department of Medicine, Austin Health, The University of Melbourne, Melbourne, Australia

¹³Munich Cluster for Systems Neurology (SyNergy), Munich, Germany

¹⁴Department of Psychiatry, University Hospital of Munich, LMU Munich, Munich, Germany

¹⁵Neuroepidemiology and Ageing Research Unit, School of Public Health, Imperial College, Charing Cross Hospital, London, UK

¹⁶West London Mental Health NHS Trust, Southhall, UK

¹⁷Chair of Metabolic Biochemistry, Biomedical Center (BMC), University Hospital of Munich, LMU Munich, Munich, Germany

¹⁸Department of Neurology, Medizinische Hochschule Hannover, Munich, Germany

Aim: The phenotype of corticobasal syndrome (CBS) is characterized by 4-repeat (4R)-tau in ~50% and by (3/4R)-tau in ~25% of histopathologically evaluated patients. The next generation tau-PET ligand ¹⁸F-PI2620 showed high affinity to 3/4R tau in Alzheimer's disease (AD) and also revealed affinity to 4R-tau pathology. The aim of this study was to investigate ¹⁸F-PI2620 in patients with clinical CBS.

Methods: Twenty-two patients (69±8y) with probable or possible CBS according to MDS-PSP or Armstrong-criteria underwent ¹⁸F-PI2620 PET together with ten age-matched healthy-controls. Distribution volume ratios (DVR, 0-60min) of subcortical and cortical brain-regions were generated using cerebellar reference tissue. DVR-data were quantitatively and visually compared between CBS and healthy-controls. Regional ¹⁸F-PI2620 binding was compared with clinical severity (PSPRS), and disease duration. Amyloid-PET served for assessment of β-amyloid status.

Results: 23% (5/22) of CBS patients (PSPRS: 24±14) were amyloid-positive. Significantly elevated ¹⁸F-PI2620 DVR was observed in the whole group of CBS patients versus healthy controls in the putamen, globus pallidus and subthalamic nucleus while a trend was observed in frontal cortex. Overall, a visually discernible ¹⁸F-PI2620 signal was observed in 14 subjects (64%) of the total cohort [9/17 (53%) of the amyloid negative, 5/5 (100%) of amyloid-positive CBS patients]. Cortical binding in CBS was heterogeneous with involvement of motor and/or parieto-temporal regions (positive in 41%; 9/22). ¹⁸F-PI2620 binding was not associated with disease severity but showed a correlation with disease duration in

frontal cortex (R=0.48, p=0.039).

Conclusion: Our data indicate a value of ^{18}F -PI2620 for evaluation of CBS, facilitating detection of heterogeneous neuropathology and variable cortical and subcortical deposition sites, which could serve for target engagement.

Keywords: tau, PET, CBS, heterogeneity, PI-2620

P125: Optimal reference region for the quantification of tau load in the brain using 18F-PI-2620 PET

Santiago Bullich¹, Andre Müller¹, Núria Roé-Vellvé¹, Aleksandar Jovalekic¹, Audrey Perrotin¹, Susan De Santi², Norman Koglin¹, Andrew W. Stephens¹

¹*Life Molecular Imaging GmbH, Berlin, Germany*

²*Life Molecular Imaging Inc, Boston, MA, US*

Introduction: Definition of a suitable reference region (RR) is essential for accurate quantification of static tau PET. Cerebellar cortex is widely used as RR to quantify tau PET by means of the standardized uptake value ratio (SUVR). However, this RR is not free of potential drawbacks. Cerebellar gray matter (CGM) is a small region, close to the edge of the field of view and with the risk of activity spill-over from nearby regions with tau deposition (e.g. inferior temporal-lobe). Additionally, tau tracers quite often show uptake in the vermis. The objective of this study was to determine the optimal way to delineate cerebellar RR for quantification of the tau load using ¹⁸F-PI-2620 PET.

Methods: Three healthy controls and three Alzheimer's disease subjects (58-75 years) underwent two ¹⁸F-PI-2620 PET scans. SUVRs were calculated using regions of interest derived from the intersection between the standard Automated Anatomic Labeling template and the normalized gray matter segmentation from the MRI. Several cerebellar reference regions were used to derive SUVRs: CGM (RR₁), CGM removing vermis (RR₂), CGM removing vermis and anterior lobe surrounding the vermis (RR₃), CGM removing cerebellar superior lobe (RR₄). All the reference regions were tested without and with the cerebellar white matter (CWM).

Results: Whole CGM (RR₁) provided the lowest test-retest variability (TRTV) (3.52% (median)). TRTV increased in smaller RRs (3.70% (RR₂), 4.3% (RR₃) and 4.44% (RR₄)). SUVR obtained using RR₁ and RR₂ were lower in comparison to RR₃ and RR₄ due to the bias induced by tracer retention in the vermis. CWM kinetics and activity at pseudo-equilibrium was similar to the activity in the CGM. However, including CWM in any RR did not provide significant improvement in terms of TRTV.

Conclusion: CGM excluding vermis and anterior lobe surrounding the vermis (RR₃) provided the optimal balance between accuracy and TRTV.

Keywords: tau, PI-2620, reference region

P126: Quantifying tau PET imaging reliably in the presence of off-target binding

Charles Chen¹, Brian Gordon¹, Austin McCullough¹, Aiad Zaza¹, Christopher Mejias¹, Aylin Dincer¹, Shaney Flores¹, Sarah Keefe¹, Angela Paulick¹, Kelley Jackson¹, Deborah Koudelis¹, Yi Su², John Morris¹, Tammie Benzinger¹

¹Washington University in St. Louis, St. Louis, MO, US

²Banner Health, Phoenix, AZ, US

Introduction: Tau PET imaging is a powerful tool for studying the *in vivo* pattern of neurofibrillary tangles across the brain, but off-target binding raises questions about *where* and *what degree* of tracer uptake indicates a positive scan for tau pathology in Alzheimer's disease. One common approach focuses on *the distribution* of elevated tracer uptake across the brain by using a modified Braak staging, which is based on the pattern of neurofibrillary lesions at autopsy. Other approaches focus more on *the degree* of tracer uptake in temporal lobe regions. While both types of approaches have been pivotal in establishing tau PET biomarkers for Alzheimer's disease, they rely on heuristic thresholds for tracer uptake in individuals grouped by amyloid PET imaging and cognitive testing results; while these groupings may be instrumental in avoiding complications from off-target binding, their *a priori* assumptions could raise new complications when translating tau PET imaging into future clinical use.

Methods: To avoid these complications, we propose a probabilistic model that learns regions of interest and a threshold for tracer uptake solely from the tau PET imaging data of a cohort spanning the spectrum from normal aging to Alzheimer's disease ($n = 388$).

Results: We evaluate model performance by testing how well the model agrees with visual reads (error rate = 4.58%, $n = 131$), how well the model separates clinical groups (controls versus preclinical Alzheimer's disease, Cliff's $d = 0.49$, preclinical versus symptomatic Alzheimer's disease, Cliff's $d = 0.63$, $n = 330$), and how well the model compares to previous approaches for quantifying tau positivity.

Discussion: Our results suggest a tau PET biomarker learned solely from tau PET imaging data performs reliably in the presence of off-target binding.

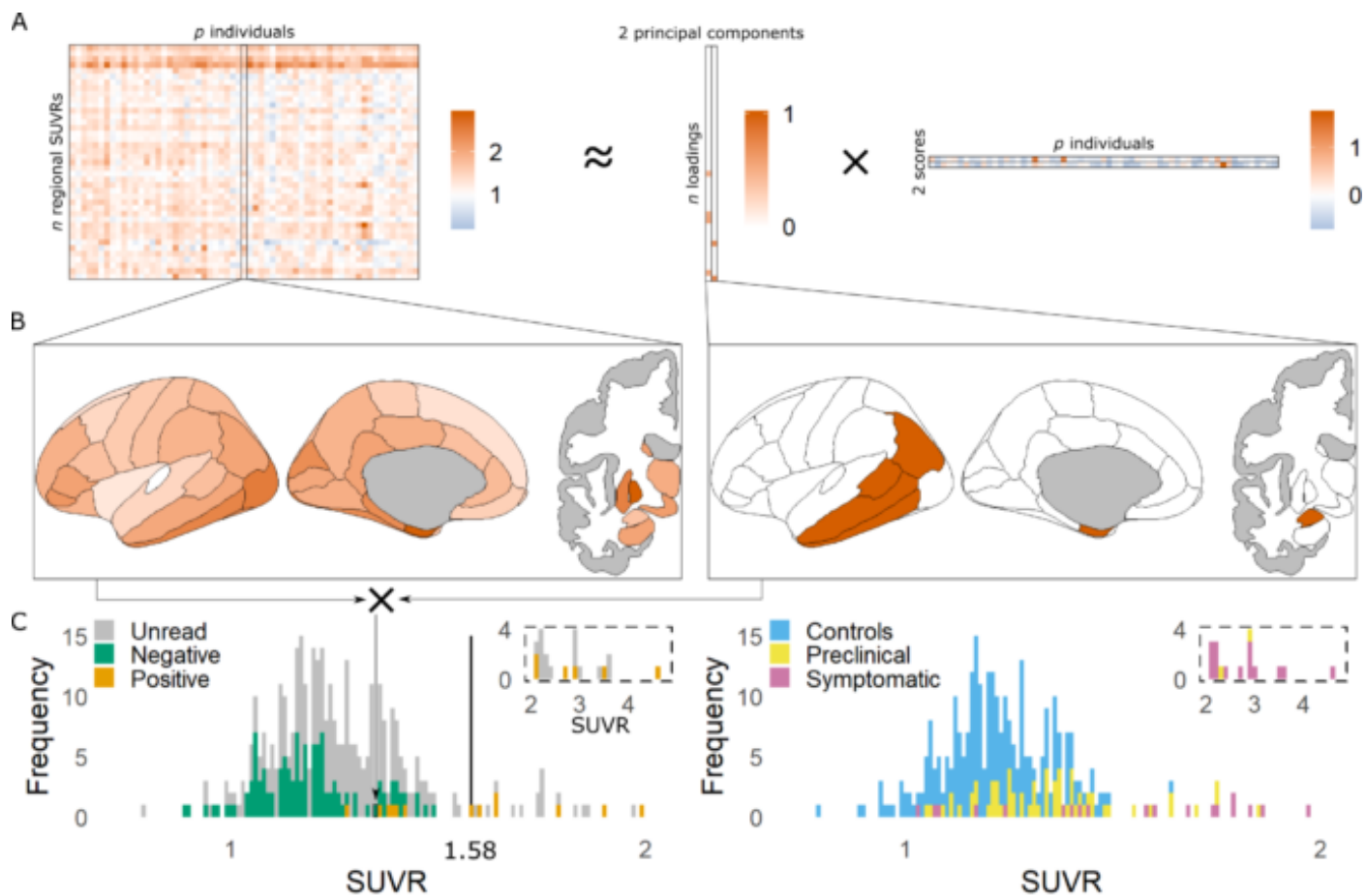


Fig 1: An illustration of our model for quantifying tau positivity. (A) A PCA-based method is used to transform a $n \times p$ data matrix containing $n = 41$ regional SUVRs for $p = 388$ individuals (left) into a $n \times 2$ linear map containing $n = 41$ loadings for two principal components (middle) and a $2 \times p$ scores matrix containing two scores for p individuals (right). (B) The linear map is sparsity constrained to have $k = 6$ non-zero loadings overall; these indicate the k regions of interest learned by the model (right). Regional SUVRs within the k regions of interest are averaged to define a summary SUVR for each individual (left). (C) Summary SUVRs are fitted by hard assignment to a Gaussian mixture model with a tau negative and tau positive component, and this model is used to infer a SUVR threshold at 1.58. Model performance is evaluated by how well its classifications agree with visual reads (left) and how well it separates controls, preclinical Alzheimer's disease, and symptomatic Alzheimer's disease (right).

Keywords: Tau PET, Alzheimer's disease, probabilistic modeling, off-target binding, visual reads

P127: [18F]THK5317 imaging as a predictive tool of prospective cognitive decline in prodromal and dementia-stage Alzheimer's disease

Konstantinos Chiotis^{1,2}, Irina Savitcheva³, Konstantinos Poulakis⁴, Laure Saint-Aubert^{1,5}, Anders Wall^{6,7}, Gunnar Antoni⁷, Agneta Nordberg^{1,8}

¹*Nordberg Translational Molecular Imaging Lab, Division of Clinical Geriatrics, Center for Alzheimer Research, Department of Neurobiology, Care Sciences and Society, Karolinska Institutet, Stockholm, Sweden*

²*Theme Neurology, Karolinska University Hospital, Stockholm, Sweden*

³*Medical Radiation Physics and Nuclear Medicine, Karolinska University Hospital, Stockholm, Sweden*

⁴*Westman neuroimaging group, Division of Clinical Geriatrics, Center for Alzheimer Research, Department of Neurobiology, Care Sciences and Society, Karolinska Institutet, Stockholm, Sweden*

⁵*Toulouse NeuroImaging Center, University of Toulouse, Inserm, UPS, Toulouse, France*

⁶*Department of Surgical Sciences, Uppsala University, Uppsala, Sweden*

⁷*Department of Medicinal Chemistry, Uppsala University, Uppsala, Sweden*

⁸*Theme Aging, Karolinska University Hospital, Stockholm, Sweden*

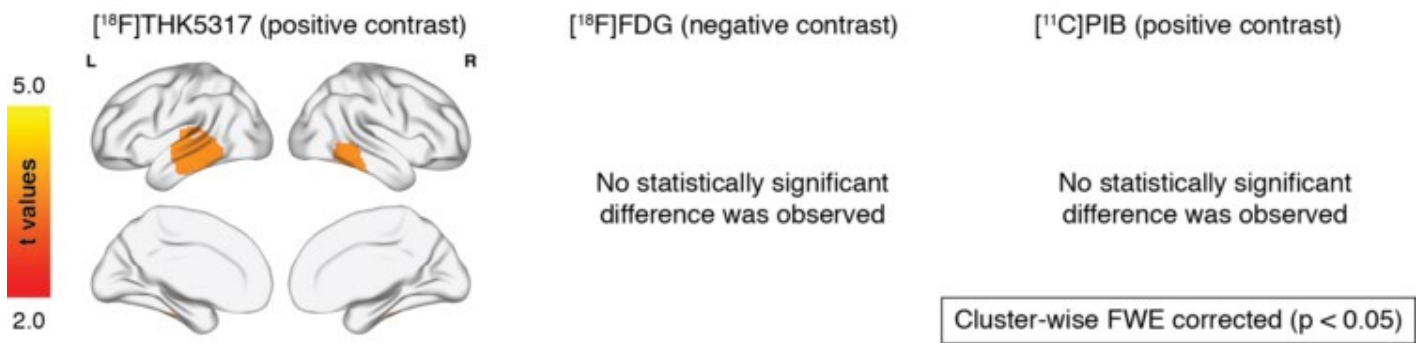
Background: Tau-PET imaging has proved promising in following neurodegeneration and cognitive impairment in Alzheimer's disease (AD) in cross-sectional designs. This study assessed the accuracy of baseline [18F]THK5317 binding to predict prospective cognitive decline in patients with AD and compared the tracer's accuracy with that of [18F]FDG PET, CSF, neuropsychological and atrophy markers.

Methods: Twenty patients with clinical biomarker-based diagnosis in the AD-spectrum (cognitive impairment and a positive amyloid-beta [11CPIB] PET scan; prodromal and dementia-stage AD) underwent at baseline neuropsychological assessment, PET with [18F]THK5317 for tau, [18F]FDG for glucose metabolism, CSF-sampling, and structural MRI. After a median of 35.62 (interquartile range=24.88:43.70) months, the patients underwent follow-up assessment for evaluating clinically evident cognitive decline (cognitively stable vs cognitive deterioration groups), including MMSE rating.

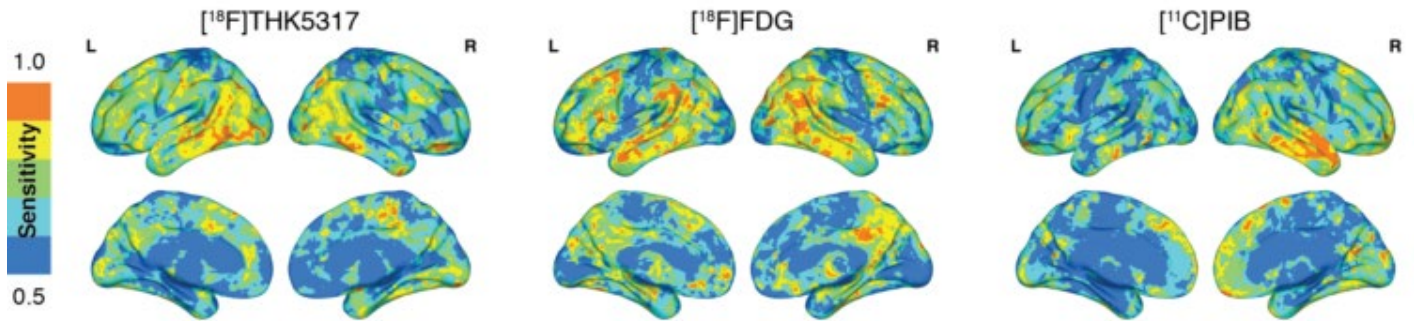
Results: Eleven patients deteriorated further cognitively, while nine remained cognitively stable at follow-up. Baseline [18F]THK5317 binding load showed excellent accuracy at predicting cognitive decline (area under the curve (AUC) 0.96-1.00) and related strongly with the pace of decline. Conversely, the levels of the other baseline biomarkers showed fair/poor accuracy to predict cognitive decline (AUC 0.58-0.77) and did not associate with the pace of decline. Baseline [18F]THK5317 binding and CSF tau associated stronger with MMSE at follow-up than at baseline.

Conclusions: These findings support the temporal offset between tau deposition and cognitive impairment, and highlight that tau-PET performs better than other biomarkers in predicting prospective cognitive decline. Our results question the deterministic role of a single amyloid-beta biomarker positivity for classifying patients in the AD-continuum of cognitive decline at clinically-relevant follow-up intervals. Tau-PET could prove pertinent for accurate diagnostics and as a screening tool in clinical trials.

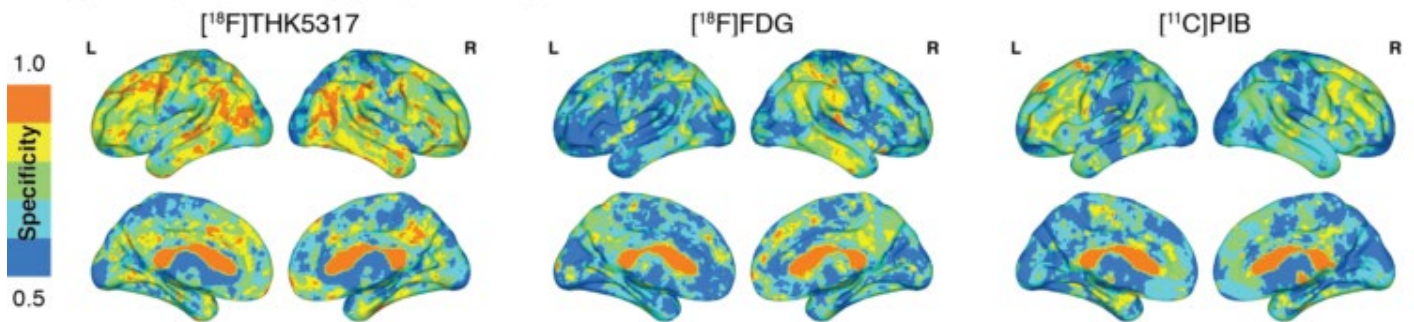
A. Cognitively stable vs cognitive deterioration groups after adjusting for age and baseline diagnosis.



B. Sensitivity at predicting prospective cognitive deterioration.



C. Specificity at predicting prospective cognitive deterioration.



(A) Voxel-wise comparisons,
(B) sensitivity and
(C) specificity in discriminating between patients exhibiting cognitive stability and patients that deteriorated cognitively over time, based on baseline [¹⁸F]THK5317, [¹⁸F]FDG and [¹¹C]PIB binding/uptake.

Keywords: Tau PET, amyloid PET, CSF, follow-up, cognition

P128: Comparison of quantitative cutoff methods for [18F]AV-1451

Davneet Minhas¹, Charles Laymon¹, Brian Lopresti¹, Beth Snitz², Dana Tudorascu³, Howard Aizenstein⁴, Oscar Lopez², Chester Mathis¹, Wiliam Klunk⁴, Ann Cohen⁴

¹University of Pittsburgh, School of Medicine, Department of Radiology, Pittsburgh, PA, US

²University of Pittsburgh, School of Medicine, Department of Neurology, Pittsburgh, PA, US

³University of Pittsburgh, School of Medicine, Department of Medicine, Pittsburgh, PA, US

⁴University of Pittsburgh, School of Medicine, Department of Psychiatry, Pittsburgh, PA, US

Background: [18F]AV-1451 has allowed for assessment of brain tau pathology across the AD spectrum. However, a gap exists in classification of [18F]AV-1451 into tau-positive and -negative groups. The goal here is to evaluate quantitative methods of [18F]AV-1451 classification and compare these methods to consensus visual reads of [18F]AV-1451 images.

Methods: [18F]AV-1451 scans were collected in 211 elderly subjects (78M, 133F, 75.7±6.3) across clinical diagnoses (5AD, 37MCI, 169NC). Braak stage (I,III-VI) regions-of-interest (ROIs) were defined using FreeSurfer, and regional SUVR measures and images were created using cerebellar gray as reference. We applied two quantitative methods for determining [18F]AV-1451 Braak ROI cutoffs to the entire cohort, the iterative outlier (IO) approach and k-means (KM) cluster approach. We then performed consensus visual reads of [18F]AV-1451 SUVR images for 76 subjects (34M, 42F, 76.1±7.1), and assessed overall agreement between visual reads and the two cutoff methods.

Results: Overall, IO demonstrated higher, more conservative cutoffs across Braak stages. For both methods, there was relatively good agreement between visual reads and the cutoffs for Braak 1. This agreement decreased for KM with increasing Braak stage while IO showed better agreement in higher Braak stages (Table 1).

Discussion: The KM and IO approaches generally agreed with visual reads. IO cutoffs were higher than KM, particularly in higher Braak regions. Additionally, KM cutoffs in higher Braak regions were unreasonably low, an explanation for this phenomenon may be because of the small number of AD patients used here, KM may have failed to find suitable midpoints in higher Braak regions. Additionally, lower agreement between visual reads and quantitative approaches may be because Braak ROIs are large composite regions and smaller positive hotspots within higher Braak ROIs may be diluted. Ongoing studies will explore the performance of these methods across all FreeSurfer regions, to further evaluate their performance.

Keywords: AV-1451, cutoffs

P129: Pilot study on the relationship between 18F-MK-6240 and VBM in early and late stages of AD

Jaime Fernandez Arias^{1,4}, Tharick Pascoal^{1,4}, Andrea Benedet^{1,4}, Joseph Thierrault^{1,4}, Min Su Kang^{1,3,4}, Melissa Savard^{1,4}, Julie Ottoy², Sulantha Mathotaarachchi¹, Firoza Lussier^{1,4}, Cécile Tissot^{1,4}, Emilie Thomas¹, Jenna Stevenson^{1,4}, Nesrine Rahmouni^{1,4}, Tina Wang^{1,4}, Gassan Massarweh³, Jean-Paul Soucy³, Serge Gauthier^{1,3,4}, Pedro Rosa-Neto^{1,3,4}

¹*Translational Neuroimaging Laboratory, The McGill University Research Centre for Studies in Aging, Montreal, QC, Canada*

²*Molecular Imaging Center Antwerp, University of Antwerp, Antwerp, Belgium*

³*Montreal Neurological Institute, Montreal, QC, Canada*

⁴*Douglas Mental Health Research Institute, Verdun, QC, Canada*

Introduction: multiple studies have linked the development of tau tangles to neuronal loss or neurodegeneration in AD. A few studies have previously examined the association between Voxel based morphometry (VBM) and PET using first-generation tracers, mostly 18F-AV-1451. However, to the best of our knowledge, no study has reported this association using 18F-MK-6240, which is a second-generation tracer with higher sensitivity to tau tangles as compared to 18F-AV-1451.

Objective: we aimed at exploring the relationship between tau PET, indexed here by 18F-MK-6240, and VBM in the Translational Biomarkers in Aging and Dementia (TRIAD) cohort.

Methods: Structural MRI and tau PET (18F-MK-6240) were acquired for 34 AD, 47 mild cognitive impairment (MCI) and 19 young control participants. MRI were segmented into probabilistic grey (GM) and white (WM) maps, non-linearly registered to the ADNI template using Dartel and smoothed with an 8mm FWHM gaussian kernel. Voxel-wise linear models were applied, using VoxelStats, to test for the association between VBM and tau PET adjusting for age and gender. Analyses were performed in the whole sample and within diagnostic groups.

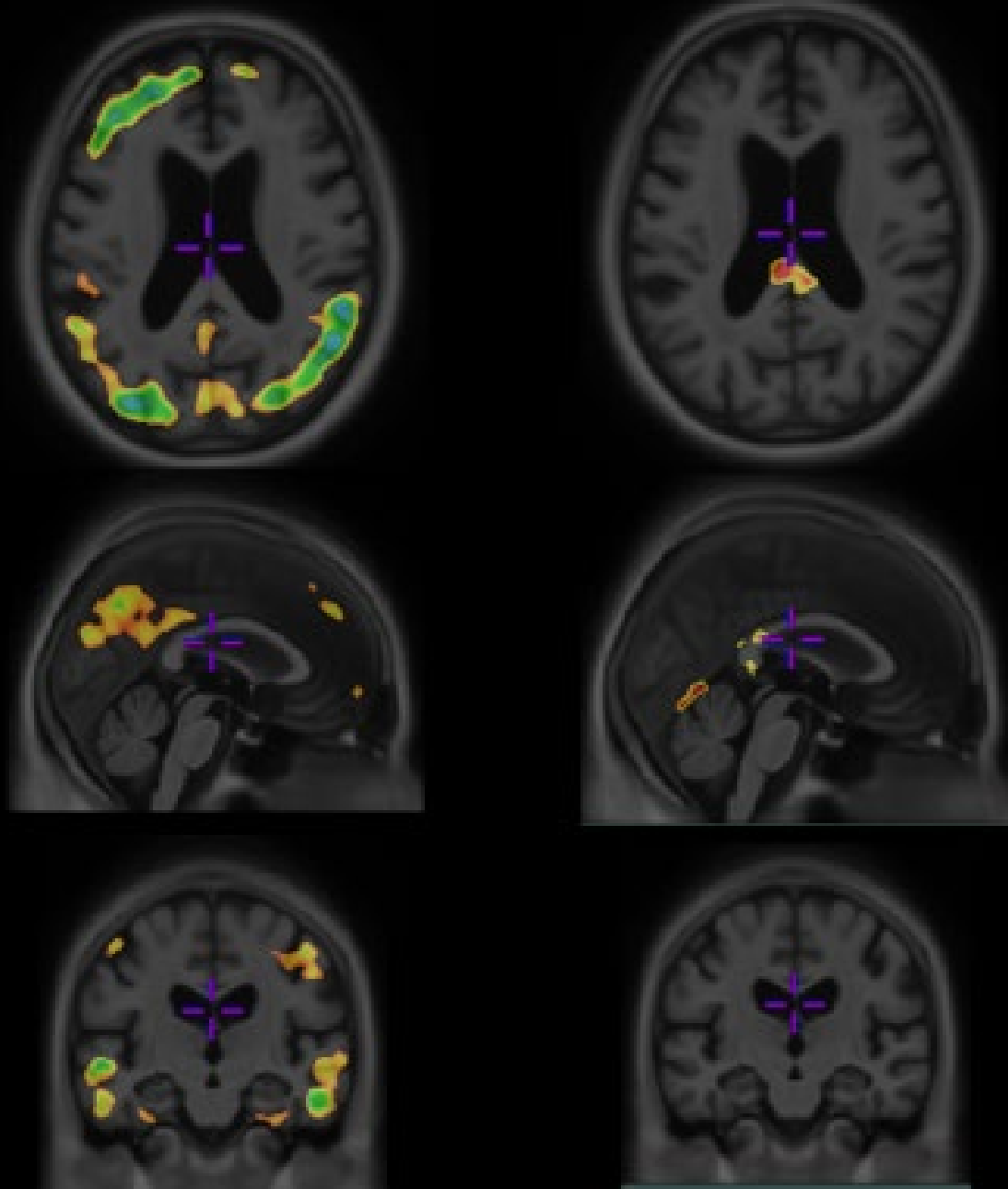
Results: we found a negative association between VBM and tau uptake in participants with a diagnose of MCI or AD in the medial temporal lobe (MTL), the temporoparietal cortices, the occipital cortex, the parietal cortex and the left prefrontal cortex (PFC). We did not find any association in young controls.

Conclusions: the pilot study further confirms previous findings on the association between tau pathology and neurodegeneration in brain areas susceptible to AD pathology. In addition, our study supports 18F-MK-6240 as a promising biomarker for tau pathology.

VBM ~ MK+age+sex

CI

Young controls



-6 |  | -2.5
t-stats

Keywords: tau, PET, VBM, 18F-MK-6240

P130: Functional connectivity brain architecture predicts the rate of tau accumulation in Alzheimer's disease

Nicolai Franzmeier¹, Julia Neitzel¹, Anna Rubinski¹, Ruben Smith^{2,3}, Olof Strandberg³, Rik Ossenkoppele^{3,4}, Oskar Hansson^{3,5}, Michael Ewers¹

¹*Institute for Stroke and Dementia Research, Klinikum der Universität München, Ludwig-Maximilians-Universität LMU, Munich, Germany*

²*Department of Neurology, Skåne University Hospital, Lund, Sweden*

³*Clinical Memory Research Unit, Department of Clinical Sciences Malmö, Lund University, Lund, Sweden*

⁴*Alzheimer Center Amsterdam, Department of Neurology, Amsterdam Neuroscience, Vrije Universiteit Amsterdam, Amsterdam UMC, Amsterdam, The Netherlands*

⁵*Memory Clinic, Skåne University Hospital, Lund, Sweden*

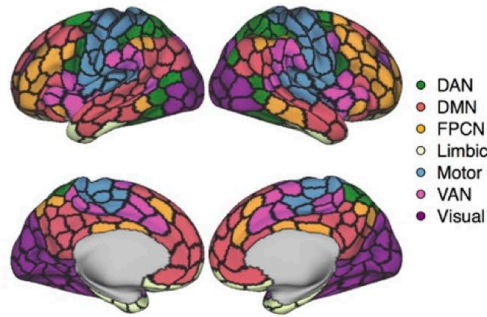
Background: In Alzheimer's disease (AD), tau pathology is a key driver of cognitive decline. Preclinical evidence suggests that tau spreads in a connectivity-based manner. Supporting this, cross-sectional tau-PET patterns resemble functional brain networks in AD. However, whether inter-regional functional connectivity (FC) predicts faster tau accumulation is unclear. Here, we assessed in two independent AD samples whether fMRI-assessed FC predicts correlated longitudinal tau-PET accumulation and whether future tau-PET accumulation can be modeled by combining baseline tau-PET with FC.

Methods: We assessed baseline resting-state fMRI and longitudinal AV1451 tau-PET in two independent samples (ADNI/BioFINDER: ~1.3/1.9yrs follow-up), including amyloid-positive (Ab+) preclinical to AD dementia patients (ADNI/BioFINDER: n=53/41) and Ab- controls (ADNI/BioFINDER: n=28/16). For 400 neocortical ROIs (Fig.1A), we estimated longitudinal tau-PET changes. In Ab+, we computed ROI-to-ROI correlations of longitudinal tau-PET changes (Fig.1B), yielding a 400x400 covariance in tau-PET change matrix for each sample (Fig.1C). Additionally, we computed fMRI-based group-average 400x400 FC matrices. To test whether FC predicts correlated tau-PET accumulation, we computed the association between group-average FC and tau-PET covariance matrices in Ab+. Next, we assessed whether ROIs with strongest tau-accumulation (i.e. "hotspots") were preferentially connected to other tau-accumulating hotspots. Lastly, we determined whether a spreading model combining baseline FC and tau-PET predicted future tau accumulation.

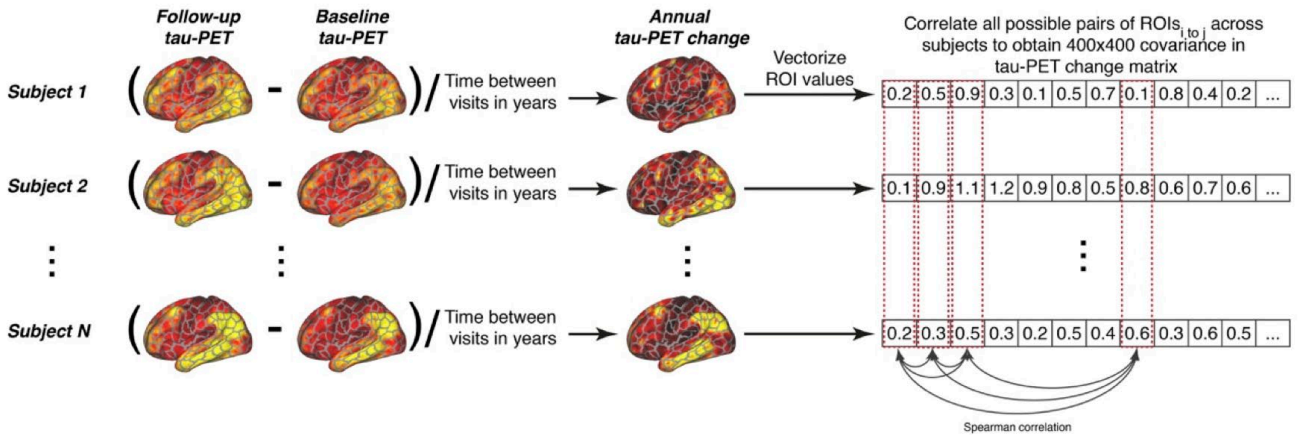
Results: Longitudinal temporo-parietal tau-PET increase was found in Ab+ but not in Ab- (p<0.005). In Ab+, higher inter-regional FC predicted stronger covariance in tau-PET accumulation (ADNI: b=0.38,p<0.001; BioFINDER: b=0.30,p<0.001, Fig.2A&B), which was consistent across functional brain networks (Fig.2C&D). In Ab+, FC of inferiotemporal tau-hotspots predicted tau accumulation in connected ROIs (ADNI: b=0.524,p<0.001; BioFINDER: b=0.398,p<0.001, Fig.3A&B). Our spreading model combining baseline tau with FC predicted future tau accumulation in Ab+ (ADNI: b=0.471,p<0.001; BioFINDER: b=0.400,p<0.001, Fig.3C&D).

Conclusions: Connectivity predicts tau spread in AD, supporting the view of transneuronal tau-spreading. Limiting tau-spreading may be a promising approach to slow AD progression.

A: 400 ROI brain parcellation



B: Assess covariance in tau-PET change in A β +



C: Covariance in tau-PET change matrix

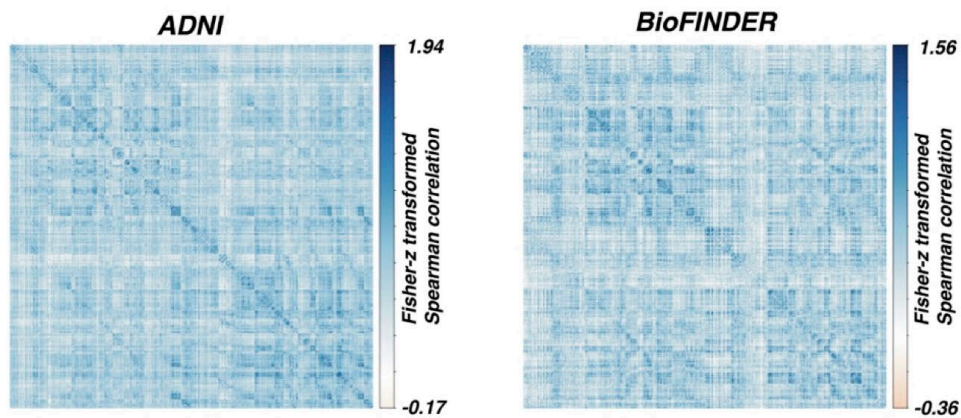


Figure 1: (A) Surface rendering of the 400 ROI brain parcellation that was applied to tau-PET and resting-state fMRI data for ROI based analyses. (B) Assessment of covariance in tau-PET change. In a first step, annual change in tau-PET was determined as the ROI-wise difference in tau-PET between baseline and follow-up divided by the time between both tau-PET assessments in years. ROI specific annual tau-PET change scores were vectorized for each of the A β subjects within each sample, yielding subject specific 400-element vectors. Within the A β groups of the ADNI (N=53) and BioFINDER (N=41) samples, the subject specific 400-element vectors were concatenated across subjects to a 53x400 (ADNI) and 41x400 (BioFINDER) matrix, where we assessed the Fisher-z transformed Spearman correlation in tau-PET change between ROIs across subjects, yielding a (C) 400x400 covariance in tau-PET change matrix for each sample.

Association between functional connectivity and covariance in tau-PET change in A β ⁺

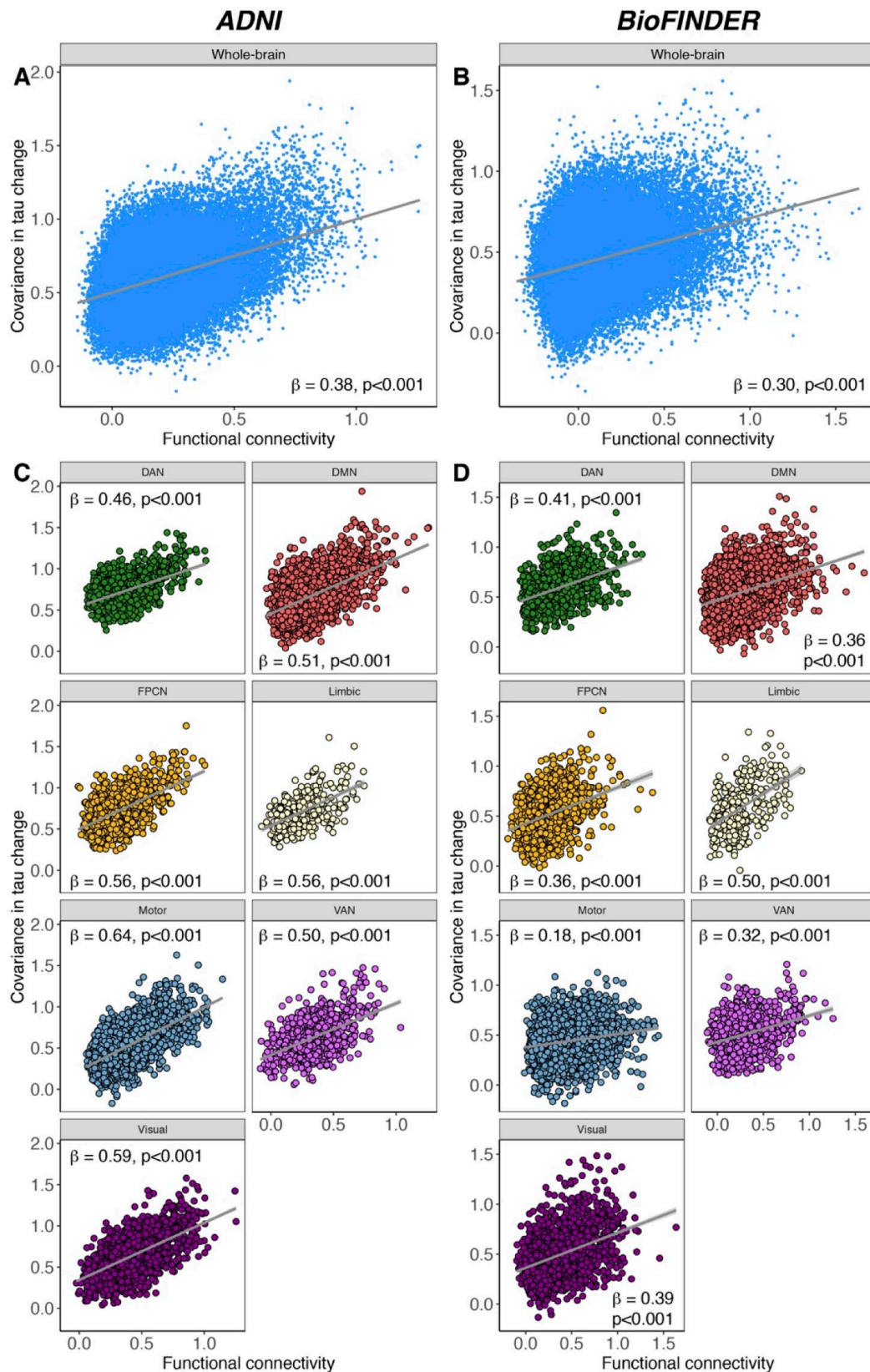


Figure 2: Scatterplots illustrating the association between group-average functional connectivity and covariance in tau-PET change in the A β ⁺ groups of the ADNI (N=53) and BioFINDER (N=41) samples, for the whole brain (A&B) or for the 7 canonical brain networks (C&D). Standardized β - and p-values were derived from linear regression.

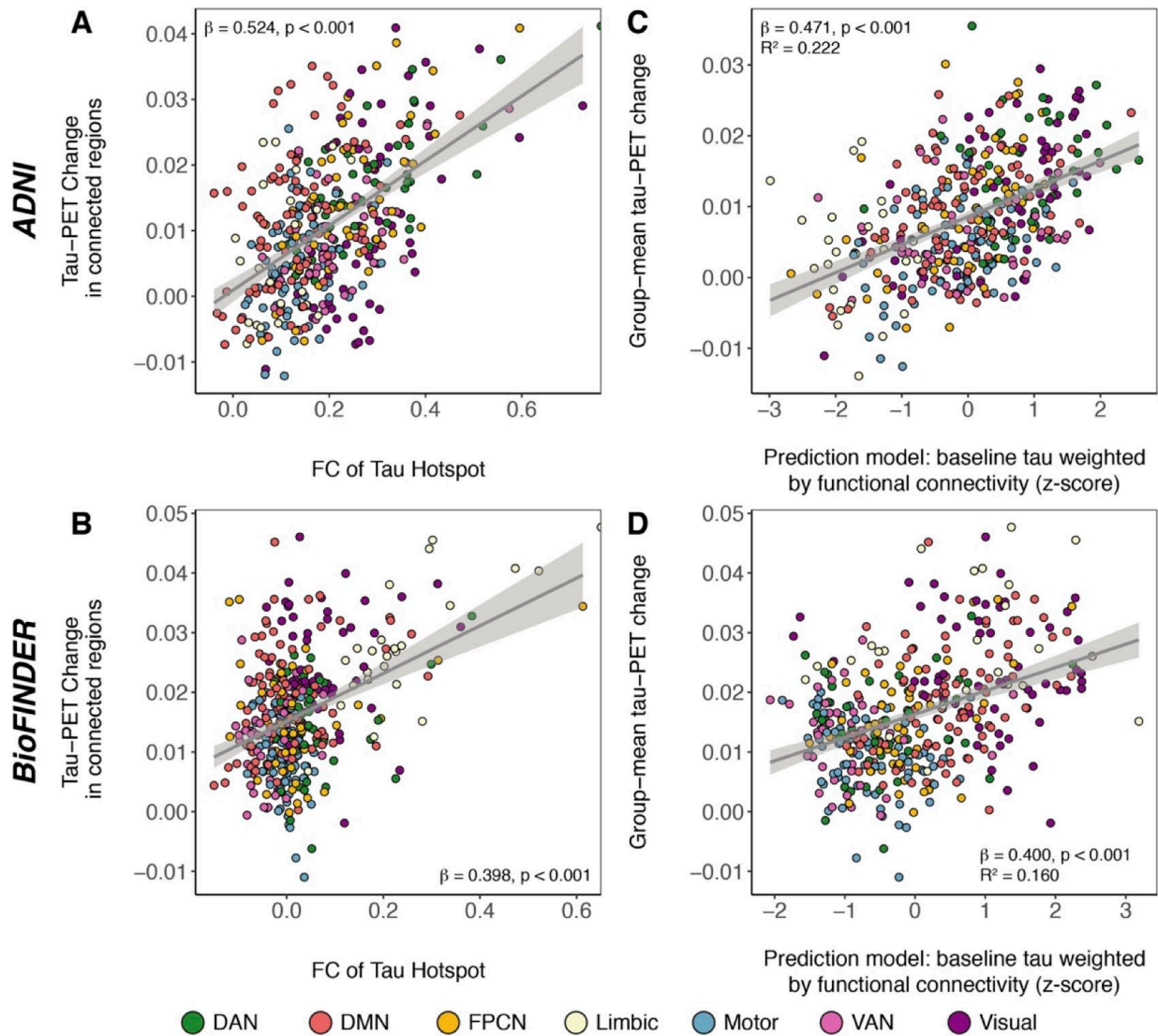


Figure 3: Scatterplot of the association between seed-based functional connectivity (FC, *x*-axis) and annual tau-PET change in connected regions (*y*-axis) for ROIs with maximum annual tau-PET change in AD subjects of the ADNI (A) and BioFINDER (B) sample. Scatterplots illustrating the performance of baseline tau-PET and connectivity-based spreading models as predictors of group-mean ROI-specific tau-PET change in AD subjects of the ADNI (C) and BioFINDER (D) sample.

Keywords: Tau-PET imaging, Tau spreading, Alzheimer's disease, functional connectivity

P131: How innocent is PART?: Mesial temporal tau is associated with worse cognitive performance in A β -negative cognitively normal individuals

Colin Groot

¹*VU University Medical Center, Amsterdam UMC, Amsterdam, The Netherlands*

Background: It has been postulated that tau aggregation is present in many individuals and is part of the aging process. Here we assess the effects of mesial temporal tau on cognitive performance and neocortical tau in A β -negative, cognitively normal individuals.

Methods: We assessed 47 cognitively normal subjects with negative A β -PET from the Australian Imaging Biomarkers and Lifestyle (AIBL) cohort who underwent [¹⁸F]flortaucipir-PET imaging to assess tau. The MeTeR template was used to map regional tau and to determine mesial temporal (Mecomprising entorhinal cortex, hippocampus, parahippocampus, and amygdala) tau-positivity (SUVR>1.2; n=10/47 [21.3%]). We assessed the effects of Me-tau (categorical [Me+/Me-] and continuous) on cognition (i.e. MMSE, composite memory, composite non-memory and the pre-Alzheimer's cognitive composite (AIBL version) and on voxelwise tau-burden. Additionally, we assessed the effect of age and continuous A β -burden on tau.

Results: Voxelwise analyses revealed that Me+ subjects had worse cognition compared to Me- subjects and greater neocortical tau burden, which was corroborated by our observation that continuous Me-tau was negatively associated with cognition and positively associated with neocortical tau. Furthermore, Me-tau was marginally associated with higher age (p=0.08), but there was no association with A β burden.

Conclusion: Our findings show that, in A β -negative individuals performing within the normal range of cognitive functioning, mesial temporal tau is associated with worse cognitive performance and higher neocortical tau burden, indicating that tau in these subjects is starting to spread from mesial temporal areas to cortical areas. While this tau-pathology is likely age-related (PART) it might not be as benign as the term "aging" implies.

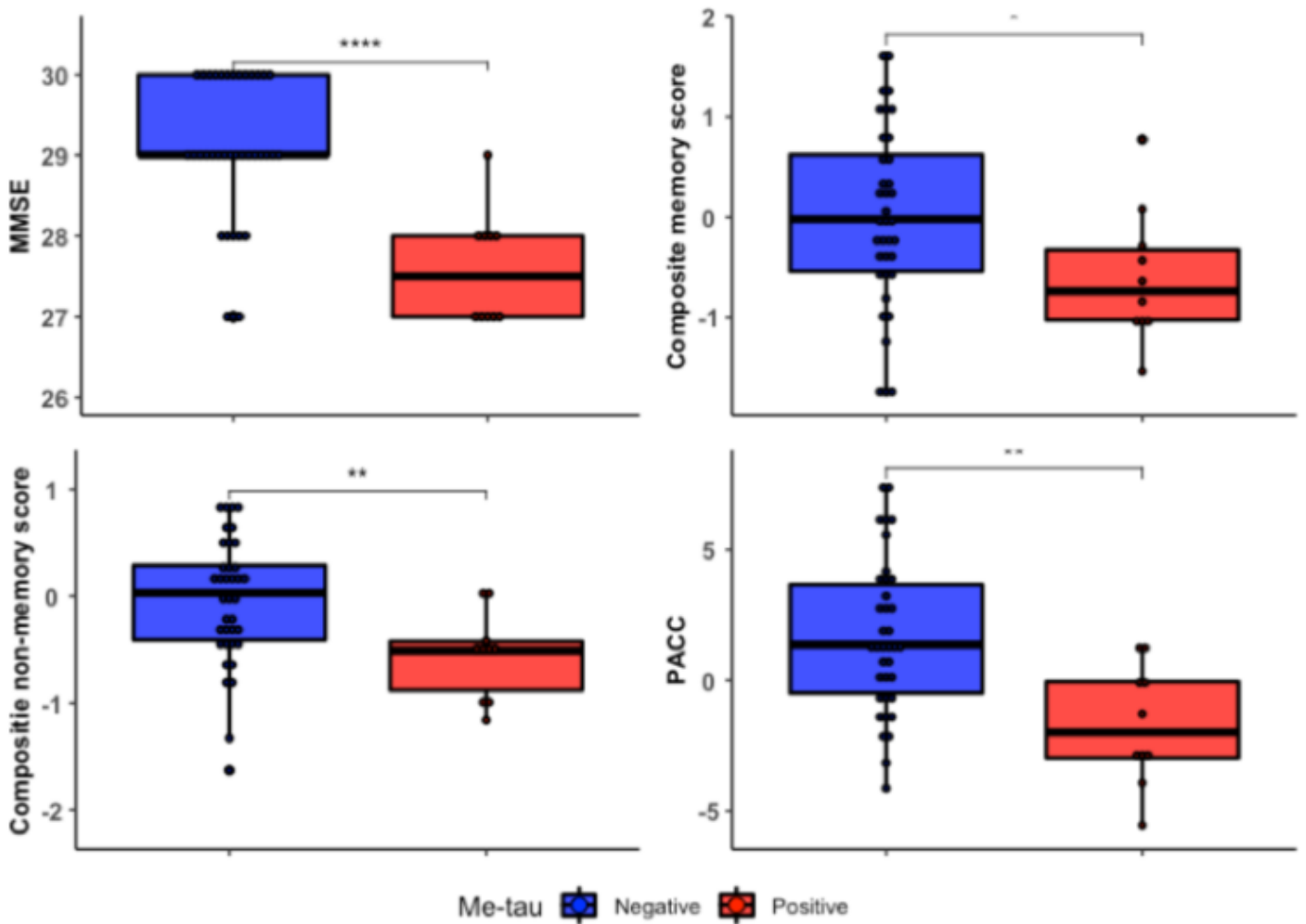


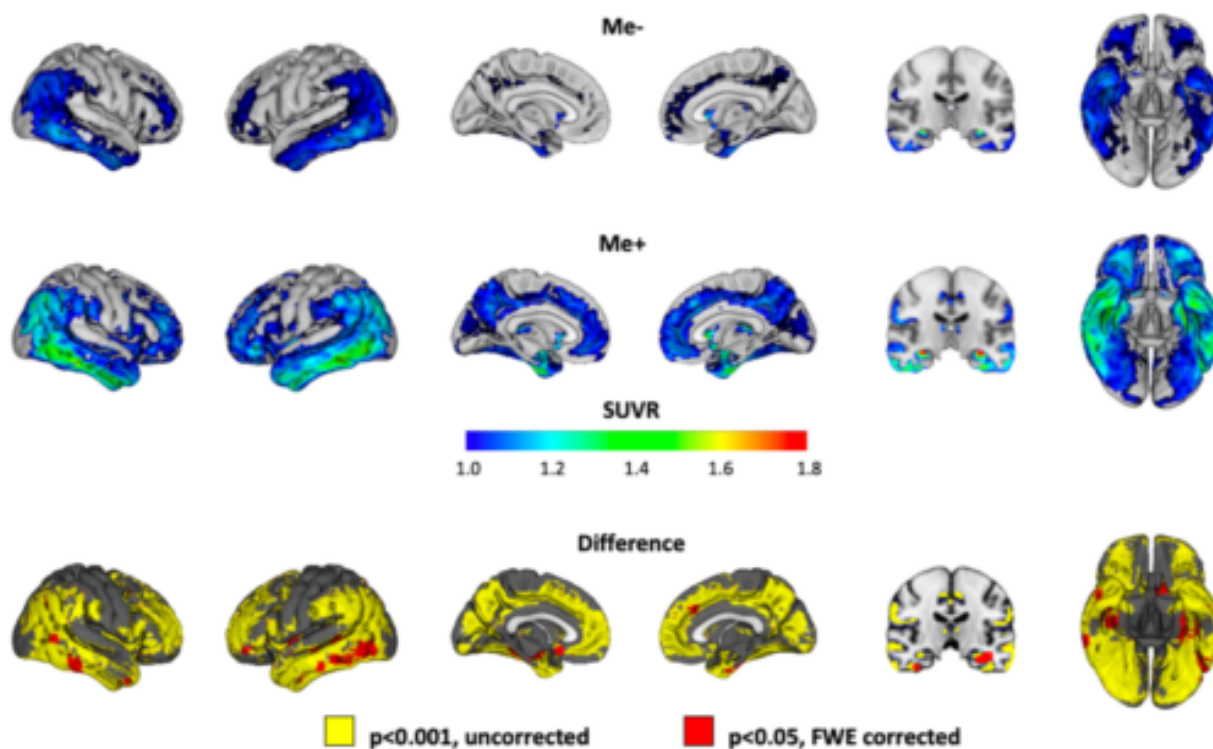
Figure 1. Difference in cognitive performance between Me+ and Me- subjects

Boxplot of scores across cognitive tests, stratified according to Me+ vs Me- subjects.

Differences between groups were assessed by univariate general linear models.

MMSE – mini-mental state examination, PACC - pre-Alzheimer's cognitive composite.

* significant effect at $p < 0.05$, **significant effect at $p < 0.01$



	Total	Me-	Me+	p
Me-tau, SUVR	1.09 (0.12)	1.04 (0.08)	1.26 (0.08)	<0.001
Te-tau, SUVR	1.10 (0.10)	1.07 (0.07)	1.22 (0.11)	<0.001
R-tau, SUVR	1.05 (0.10)	1.02 (0.08)	1.15 (0.12)	<0.001
NC-tau, SUVR ^a	1.08 (0.10)	1.05 (0.07)	1.19 (0.11)	<0.001

Figure 2. Difference in [¹⁸F]flortaucipir SUVR between Me+ and Me- subjects

The top two rows display the average [¹⁸F]flortaucipir SUVR in subgroups of Me- and Me+ subjects and the bottom row displays significant voxels from independent samples t-tests assessing the difference between the groups, adjusted for age and gender. Threshold for tau-positivity (Me+/Me-) SUVR > 1.2. Reference region: cerebellar cortex. The table displays differences in tau burden across the MeTeR template ROIs between Me+ and Me- subjects. Me – mesial temporal, Te – temporal, R – rest of the neocortex, NC – neocortical tau, SUVR – standardized uptake value ratio.

a – average of Te-tau and R-tau.

Keywords: PET, Flortaucipir, cognition, older adults, tau

P132: CSF P-tau detects cerebral tau accumulation earlier than tau PET in amyloid positive elderly adults

Tengfei Guo^{1,2}, William Jagust^{1,2}, Susan Landau^{1,2}

¹*Helen Wills Neuroscience Institute, University of California, Berkeley, Berkeley, CA, US*

²*Molecular Biophysics and Integrated Bioimaging, Lawrence Berkeley National Laboratory, Berkeley, CA, US*

Objective: To investigate the relationship between CSF P-tau and flortaucipir (FTP) PET in cognitively unimpaired (CU) and impaired elderly adults.

Methods: We analyzed amyloid PET, CSF P-tau and FTP PET data from 356 CU, MCI and AD ADNI participants. We examined the correlations between P-tau and FTP SUVRs in 34 Freesurfer-defined cortical ROIs and amygdala controlling for amyloid, diagnosis, gender and age (Fig 1, FDR<0.05), and because the strongest correlations were within the Temporal-metaROI (entorhinal, amygdala, parahippocampal, fusiform, inferior-temporal, and middle-temporal) (Jack *et al.* 2017), it was selected for further analyses. P-tau and Temporal-metaROI FTP were associated in A β + participants only. 153 A β + participants were classified as normal/abnormal on P-tau and Temporal-metaROI FTP (using thresholds of 23 and 1.27 respectively) and we compared baseline FTP, hippocampal volume (HCV), Preclinical Alzheimer's Cognitive Composite (PACC) and annual FTP change between these groups. Finally, we examined prediction of annual FTP change using baseline amyloid, P-tau and FTP controlling for diagnosis, gender and age.

Results: Among A β + participants, contemporaneous P-tau and FTP were concordant for the majority (45.1% PTAU+/FTP+; 25.5% PTAU-/FTP-); 24.2% were PTAU+/FTP- (76% of which were CU), and 5.2% were PTAU-/FTP+ (Fig.2). Compared to the PTAU-/FTP- group, PTAU+/FTP+ but not PTAU+/FTP- individuals had significantly higher FTP, lower HCV and PACC; whereas the PTAU+/FTP- and PTAU+/FTP+ groups both showed faster annual FTP increase (Fig.2C). Both amyloid and P-tau but not contemporaneous FTP predicted subsequent temporal FTP increases in the whole cohort, whereas only P-tau was predictive in A β + participants and none of them was predictive in A β - participants (Fig.3).

Conclusions: CSF P-tau is moderately associated with tau PET across ROIs predominately in Braak stages I-IV in A β + individuals. Among A β + individuals, abnormal CSF P-tau may reflect cerebral tau accumulation that occurs prior to abnormal FTP in medial and lateral temporal regions.

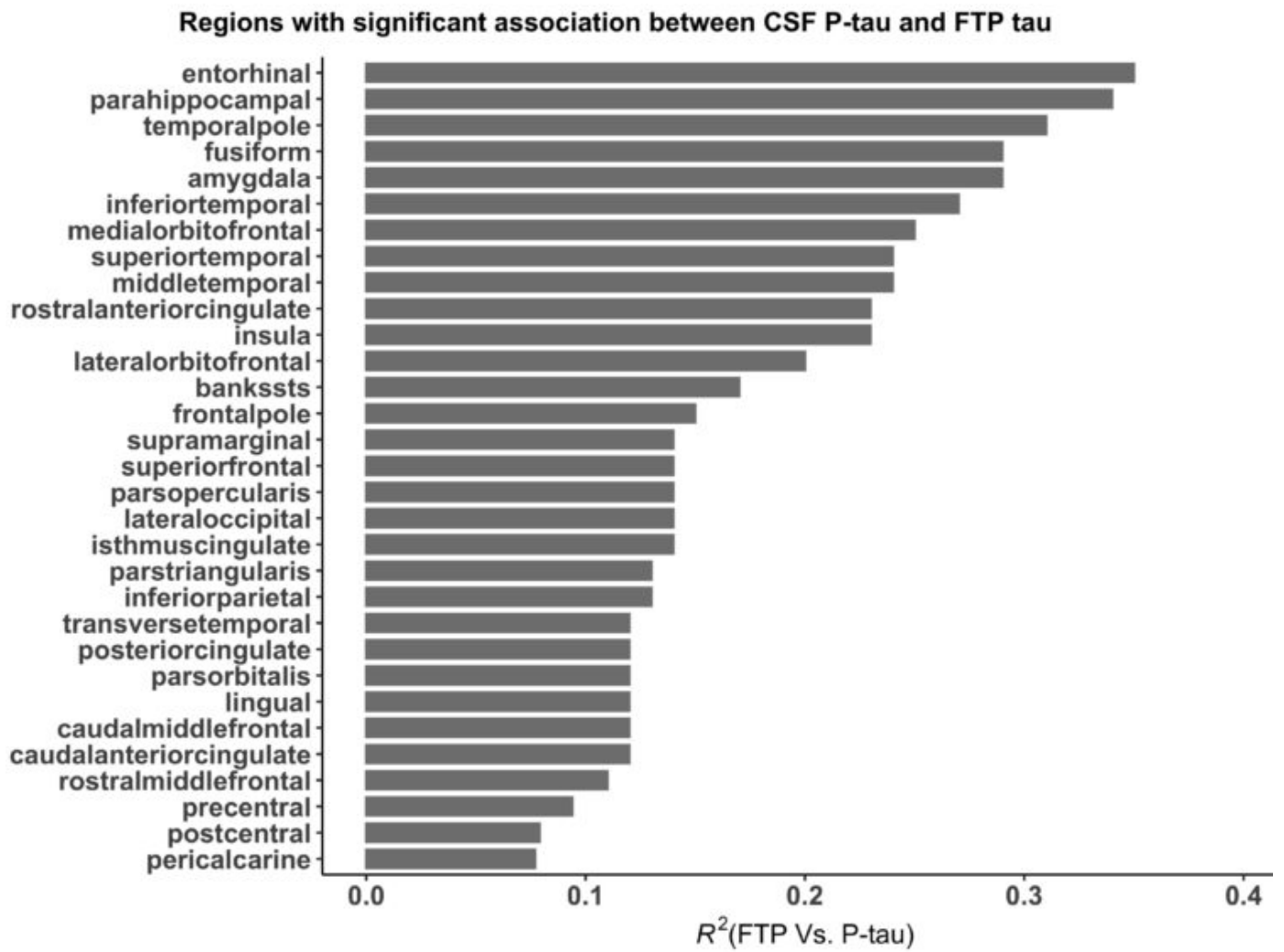


Fig.1. Regions with significant association between CSF P-tau and tau PET in 356 ADNI participants (CU: 234, MCI: 92 and AD: 30).

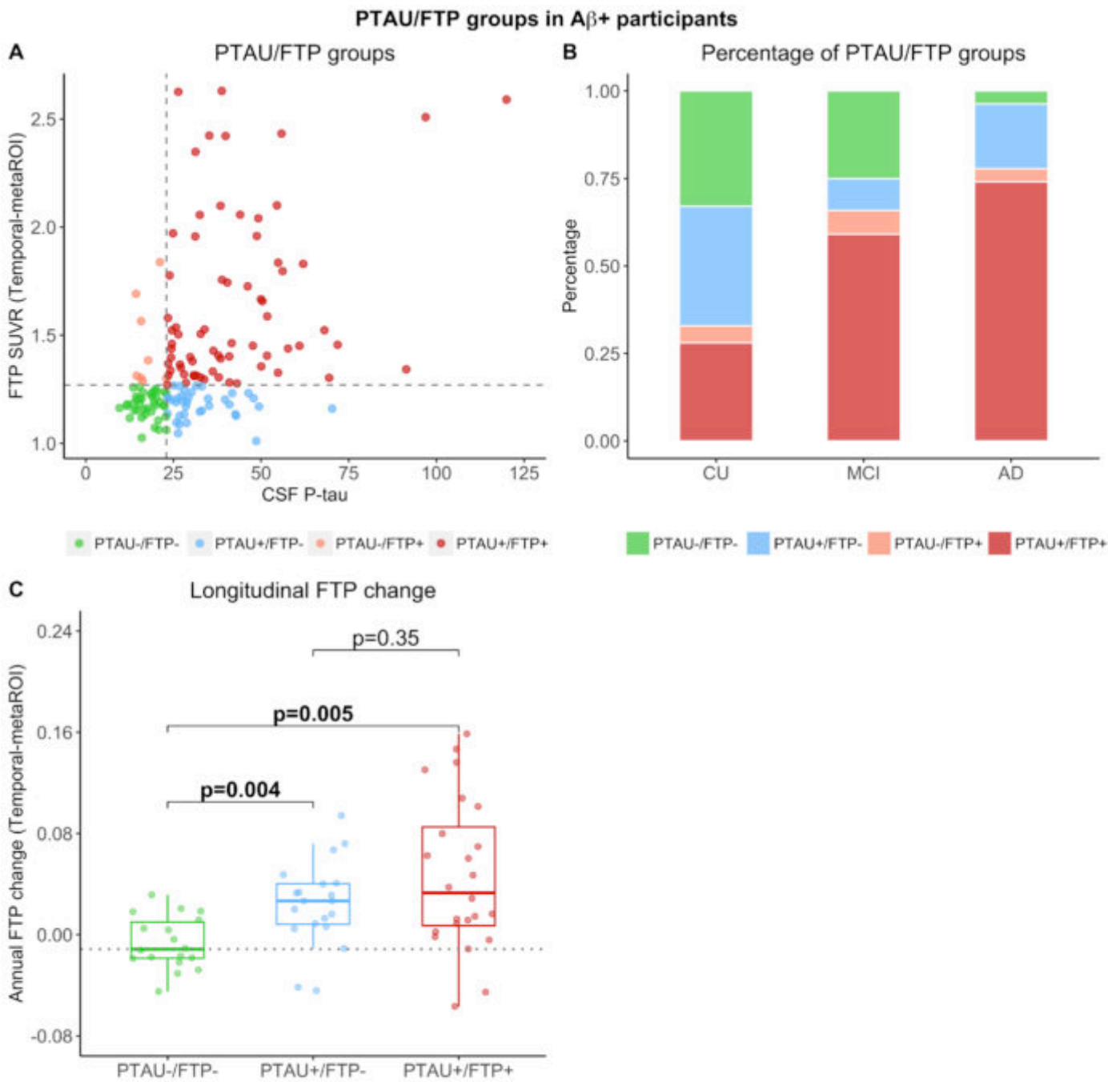


Fig.2. Scatter plot of CSF P-tau and FTP tau in A β + participants at baseline (A), percentages of PTAU/FTP +/- status in different diagnosis groups (B), and comparison of annual FTP change by PTAU/FTP +/- status.

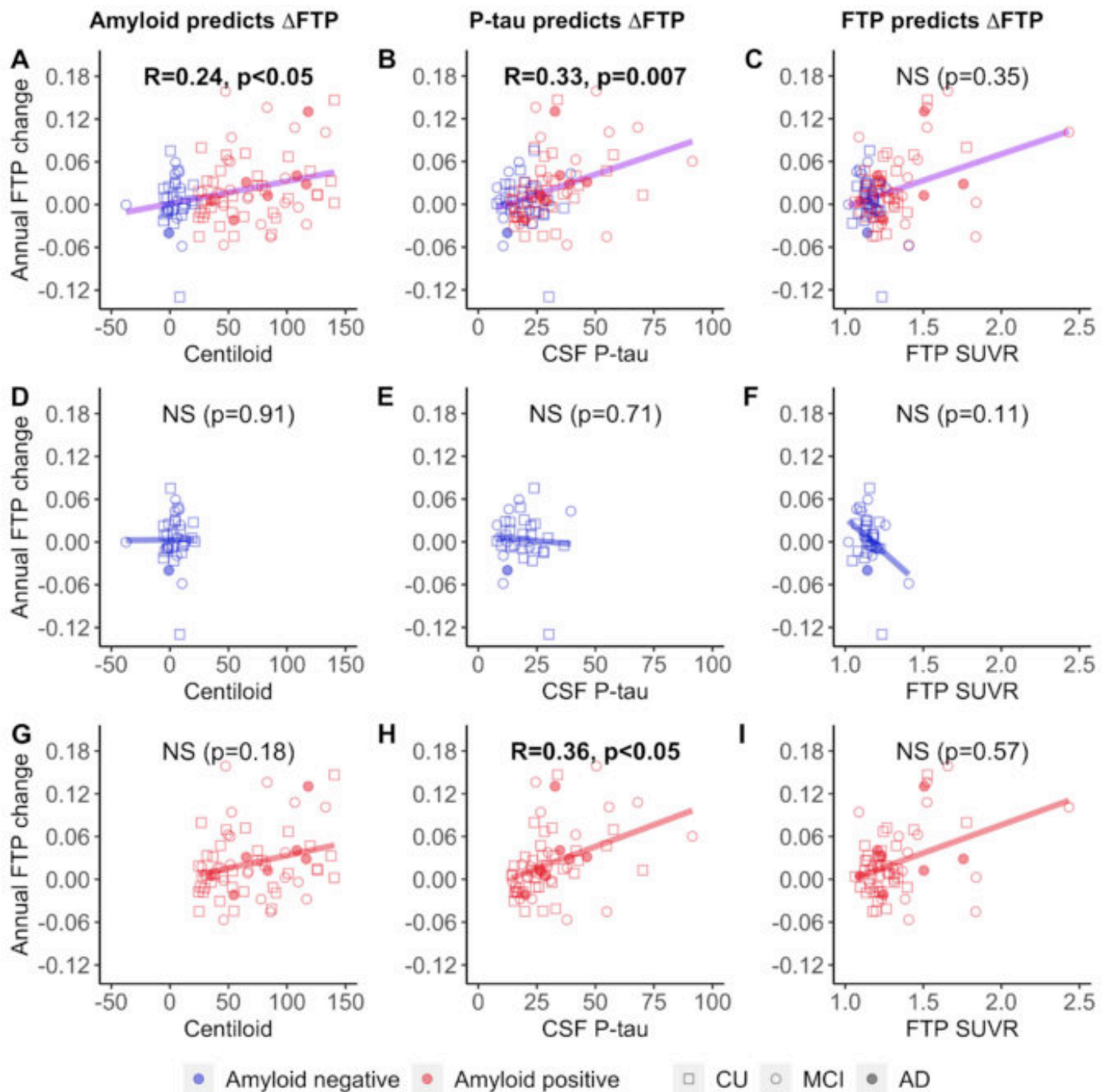


Fig.3. Associations between annual FTP tau change (Temporal-metaROI) and baseline Centiloid, CSF P-tau, and FTP SUVR (Temporal-metaROI) in (A-C) all participants with longitudinal FTP, (D-F) 35 $A\beta^-$ participants, and (G-I) 66 $A\beta^+$ participants.

Keywords: CSF P-tau, 18F-flortaucipir, tau PET, longitudinal, Alzheimer's disease

P133: Amyloid, tau, and atrophy in preclinical Alzheimer's disease: A longitudinal study

Bernard Hanseeuw^{1,2}, Heidi Jacobs¹, Aaron Schultz¹, Rachel Buckley¹, Michael Properzi¹, Michelle Farrell¹, Matthew Scott¹, Olivia Hampton¹, Justin Sanchez¹, Reisa Sperling¹, Keith Johnson¹

¹Massachusetts General Hospital, Boston, MA, US

²Cliniques Universitaires Saint-Luc, Brussels, Belgium

Background: Amyloid- β (A β), tau, and atrophy are pathological hallmarks of Alzheimer's disease. We investigated their longitudinal associations in clinically normal (CN) participants from the Harvard Aging Brain Study, testing the hypothesis that tau changes mediate the effect of A β on hippocampal volume (HV).

Methods: Serial PiB-PET (A β , [1.9-8.5y]), Flortaucipir-PET (tau, [0.8-6.0y]), and MRI (HV [1.3-7.0y]) measures were obtained from 128 CN participants followed over a median of 5.1 years (y). Participants had a median of 3PiB-PET [2-5], 2 Flortaucipir-PET [2-4], and 3MRIs [2-5]. All PET data were expressed as PVC-SUVr scaled on subcortical white matter. PiB was measured in a neocortical aggregate, Flortaucipir in inferior temporal (IT) and entorhinal (EC) cortices. Longitudinal HVs were processed using Freesurfer v.6 and adjusted for intracranial volume. We predicted imaging data over time with random intercept and slope in linear mixed-models and extracted PiB, tau, and HV slopes for each subject. Baseline and slope data were entered in age-adjusted correlation and mediation models to assess their associations.

Results: HV slope correlated with tau slope (Fig.1-2, IT: age-adjusted $R^2=0.12$, EC: $R^2=0.15$, $p<0.0001$) more strongly than with PiB slope (Fig.3, $R^2=0.05$, $p=0.011$). Adjusting for baseline data, HV slope correlated with tau slope ($R^2>0.04$, $p<0.019$), but not with PiB slope ($R^2=0.006$, $p=0.392$). PiB levels increased the effect of IT-tau slope on HV slope (PiB-by-Tau slope interaction: $p=0.03$). However, the effect of EC-tau slope on HV slope was not PiB-dependent ($p=0.29$). Sequential mediations demonstrated that PiB slope and IT-tau slope successively mediated the effect of baseline PiB on final HV, adjusting for baseline HV and age (Sobel-test=2.3, $p=0.02$). The mediation was not observed using EC-tau slope, because it was not associated with PiB, adjusting for baseline data.

Conclusions: In preclinical AD, longitudinal hippocampal atrophy is associated with an A β -independent entorhinal tau accumulation and an A β -dependent neocortical tau accumulation.

Fig.1

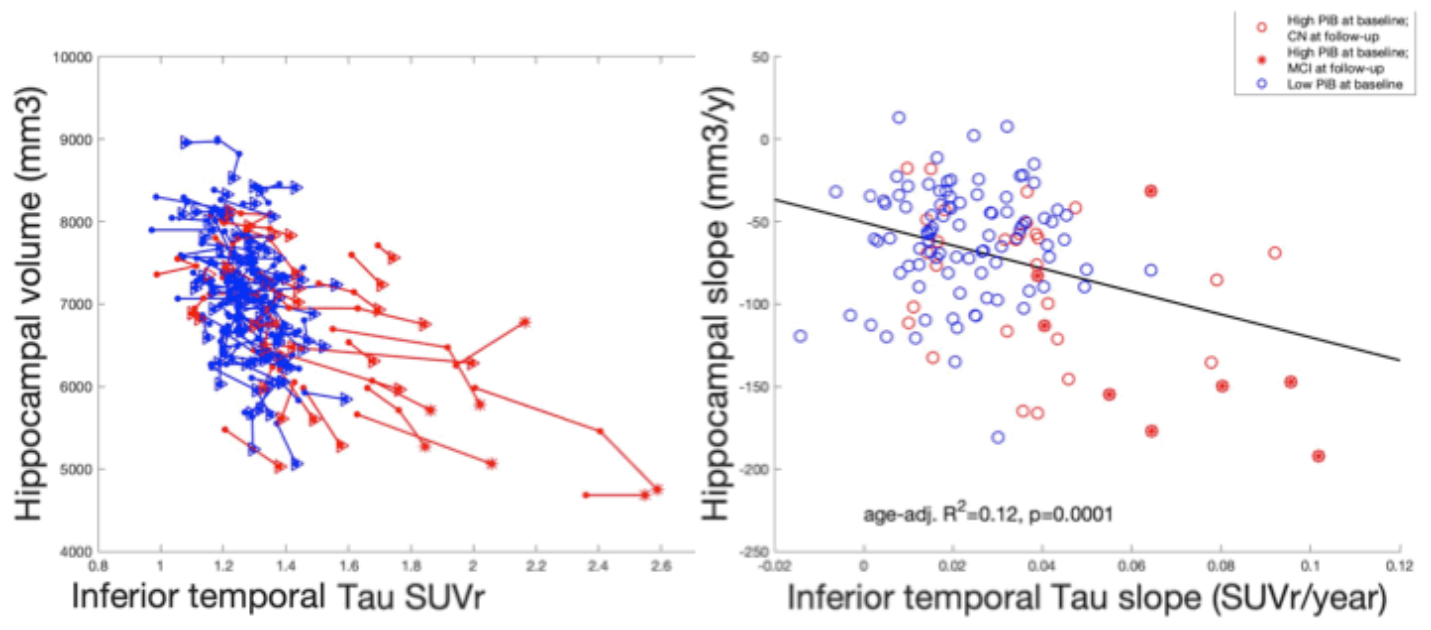


Fig.2

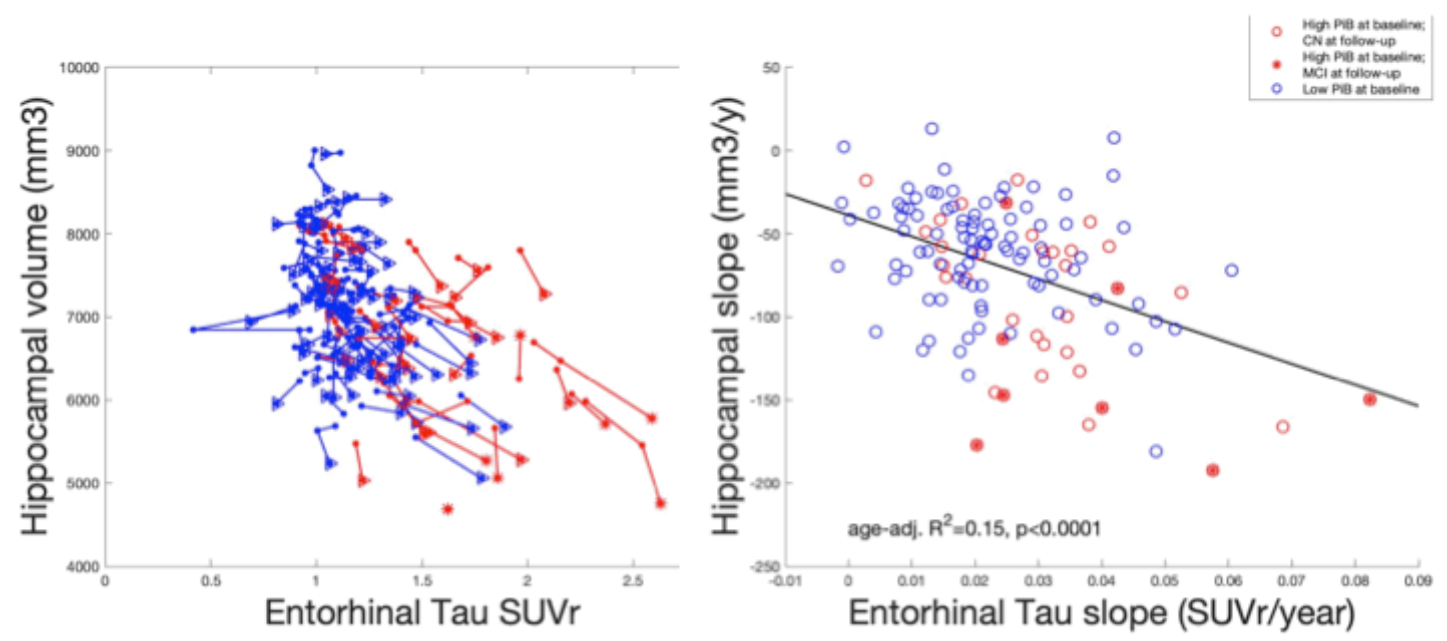
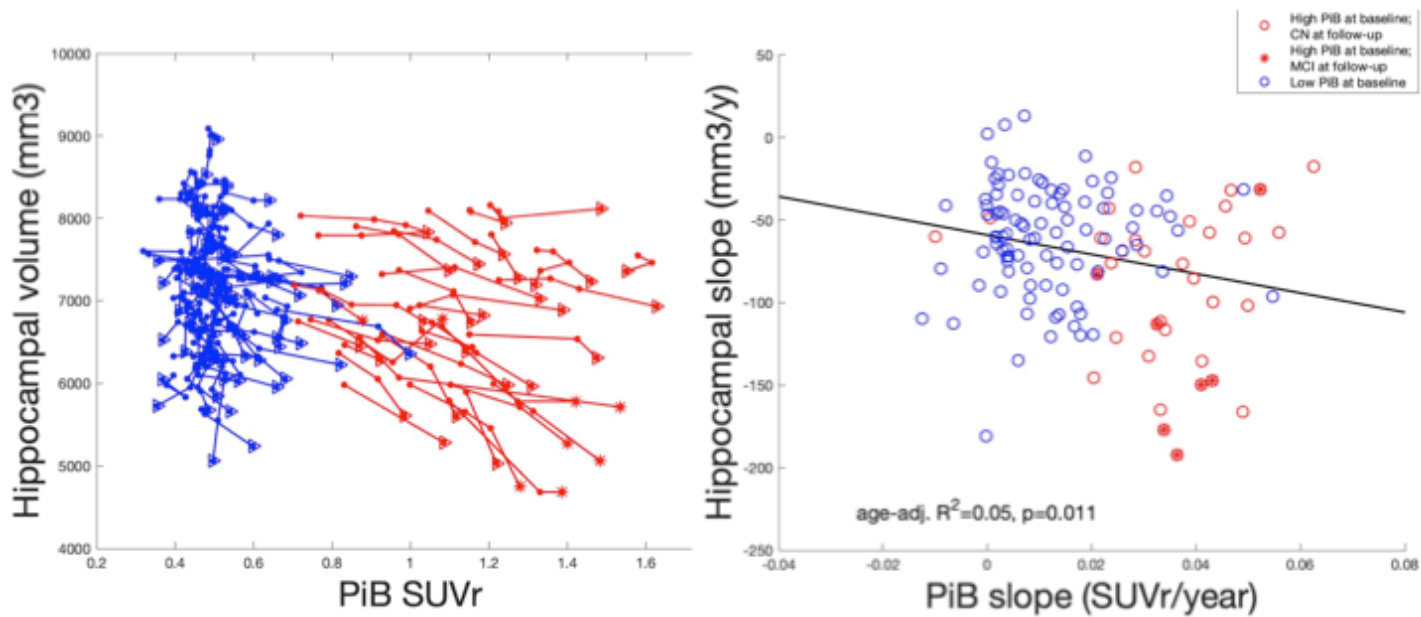


Fig.3



Keywords: Longitudinal study; Tau-PET; Amyloid-PET; Hippocampal Volume; temporal sequence of biomarkers

P134: Increased levels and phosphorylation of soluble tau proteins occur earlier than changes in Tau PET in Alzheimer's disease

Oskar Hansson¹, Emelie Andersson¹, Shorena Janelidze¹, Rik Ossenkoppele¹, Philip Insel¹, Olof Strandberg¹, Henrik Zetterberg², Kaj Blennow², Xiyun Chai³, Jeffrey Dage³, Erik Stomrud¹, Ruben Smith¹, Sebastian Palmqvist¹, Niklas Mattsson¹

¹*Clinical Memory Research Unit, Lund University, Lund, Sweden*

²*Department of Psychiatry and Neurochemistry, Institute of Neuroscience and Physiology, the Sahlgrenska Academy at the University of Gothenburg, Gothenburg, Sweden*

³*Eli Lilly and Company, Indianapolis, IN, US*

The links between aggregation of β -amyloid ($A\beta$) and tau in Alzheimer's disease are unclear. Cognitively unimpaired persons with $A\beta$ plaques (abnormal Amyloid positron emission tomography, PET) had increased cerebrospinal fluid (CSF) total-tau (T-tau) and phosphorylated tau (P-tau181 and P-tau217), which increased over time, despite lack of insoluble tau aggregates (normal Tau PET). CSF T-tau and P-tau increased prior to the threshold for Amyloid PET positivity, while Tau PET started to increase after Amyloid PET positivity. Further, Tau PET was only abnormal in $A\beta$ + individuals with already increased CSF P-tau. Effects of Amyloid PET on Tau PET were mediated by CSF P-tau (and partly by T-tau), and high CSF tau predicted increased Tau PET rates. In 5xFAD mice, CSF tau increased when Ab aggregation started. These results show that $A\beta$ pathology may induce changes in soluble tau secretion and phosphorylation (measured in CSF), which is followed by tau aggregation (measured with Tau PET) several years later in humans.

Keywords: CSF, PET, tau pathology, early diagnosis

P135: Preclinical characterization of [¹⁸F]THK-5562, a novel tau PET tracer with little off-target binding

Ryuichi Harada^{1,2}, Pradith Lerdsirisuk³, Du Yiqing¹, Michinori Ezura⁴, Yuki Shimizu³, Takahiro Morito¹, Hiroyuki Arai², Kazuhiko Yanai¹, Yukitsuka Kudo², Shozo Furumoto³, Nobuyuki Okamura^{2,3,5}

¹Department of Pharmacology, Tohoku University Graduate School of Medicine, Sendai, Japan

²Department of Geriatrics and Gerontology, Division of Brain Science, Institute of Development, Aging and Cancer, Tohoku University, Sendai, Japan

³Cyclotron and Radioisotope Center, Tohoku University, Sendai, Japan

⁴Department of Neurology, Tohoku University Graduate School of Medicine, Sendai, Japan

⁵Division of Pharmacology, Faculty of Medicine, Tohoku Medical and Pharmaceutical University, Sendai, Japan

Background: Recent validation studies have revealed that [¹⁸F]THK-5351, which was originally designed to detect tau aggregates, bound to monoamine oxidase B (MAO-B) with high affinity. Further efforts to develop highly selective tau tracers identified a novel tau PET tracer named [¹⁸F]THK-5562. The aim of this study was to evaluate the binding property of [¹⁸F]THK-5562 as a PET tracer for imaging tau aggregates in vivo.

Methods: [¹⁸F]fluoroethyl harmine and [³H]THK-5351 were used for competitive binding assay to recombinant MAO-A and MAO-B, respectively. In vitro autoradiography of the human brain sections was performed using [¹⁸F]THK-5562, [¹⁸F]SMBT-1 (a novel MAO-B tracer), [¹⁸F]THK-5351, [¹⁸F]AV-1451, [¹⁸F]PI-2620, [³H]MK-6240, and [¹⁸F]florbetaben. Pharmacokinetics and metabolism were additionally assessed in normal mice after intravenous injection of [¹⁸F]THK-5562.

Results: THK-5562 was highly selective to tau aggregates over other proteins including amyloid- β , α -synuclein, TDP-43, MAO-A and MAO-B. In vitro autoradiography of the human brain demonstrated the intense laminar binding of [¹⁸F]THK-5562 to the neocortex of AD, in contrast with no significant binding to the basal ganglia of AD and PSP. [¹⁸F]THK-5351 and [¹⁸F]AV-1451 showed the binding to the basal ganglia of PSP, which was not matched with tau immunohistochemistry. [¹⁸F]THK-5562 showed high initial brain uptake and rapid washout after intravenous administration and the radiolabeled metabolites of [¹⁸F]THK-5562 did not penetrate the blood-brain barrier in mice.

Conclusions: [¹⁸F]THK-5562 is a promising candidate for selective tau PET tracer in AD, which will enable accurate monitoring of tau aggregates in the human brain.

Keywords: radiopharmaceuticals, tau, autoradiography

P136: Comparison of tau PET imaging using ^{18}F -APN-1607 and ^{18}F -THK5351 in Alzheimer's disease patients and normal controls

Ing-Tsung Hsiao^{1,2}, Kun-Ju Lin^{1,2}, Chin-Chang Huang³, Kuo-Lun Huang³

¹Dept MIRS and Healthy Aging Center, Chang Gung University, Taoyuan, Taiwan

²Dept Nuclear Medicine, Chang Gung Memorial Hospital, Taoyuan, Taiwan

³Dept Neurology, Chang Gung Memorial Hospital, Taoyuan, Taiwan

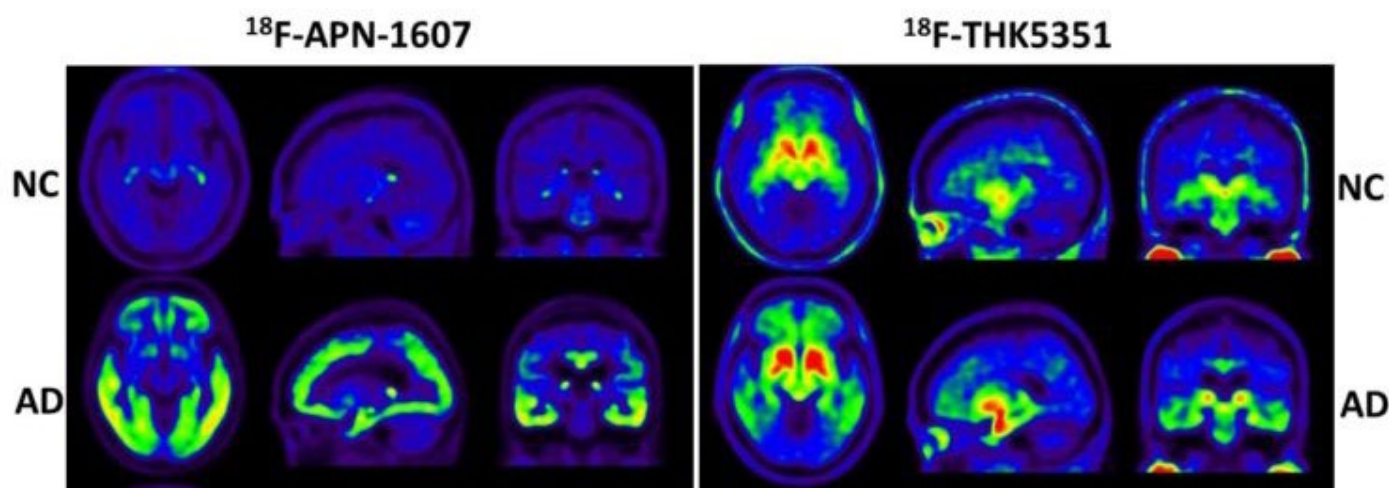


Figure 1: The mean SUVR images of NC (upper row) and AD (lower row) for both ^{18}F -APN1607 (left) and ^{18}F -THK5351 (right) imaging.

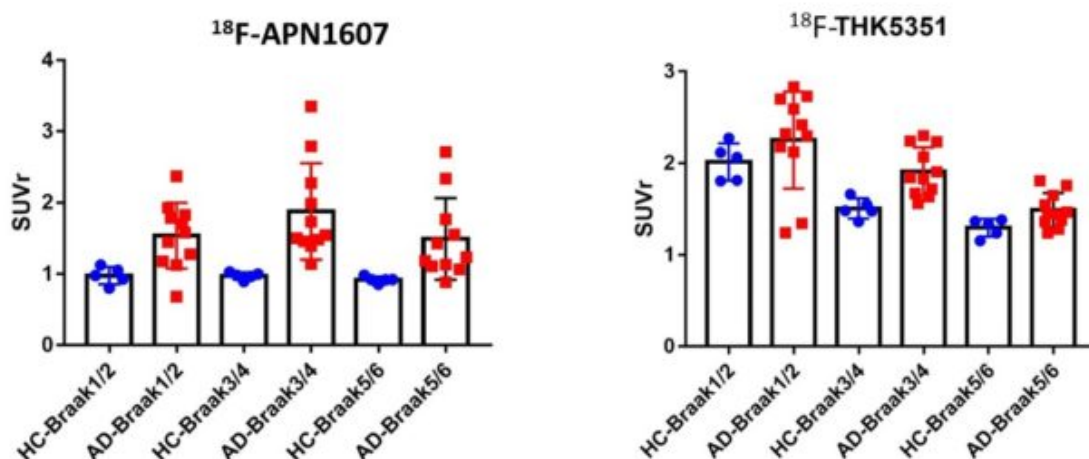


Figure 2: The regional SUVR plots for both ^{18}F -APN1607 (left) and ^{18}F -THK5351 (right) imaging of NC and AD in the VOIs of Braak stages 1/2, 3/4 and 5/6.

Aim: To compare the brain uptake pattern of the tau tracers ^{18}F -APN-1607 and ^{18}F -THK-5351 in Alzheimer's diseases (AD) patients and normal controls (NC)

Methods: A total of 5 NC subjects and 10 AD patients underwent both ^{18}F -APN-1607 and ^{18}F -THK-5351

PET scans. MRI was performed to enable image registration. PET images were acquired 90-110min and 50-60min post-injection for ^{18}F -APN-1607 and ^{18}F -THK-5351, respectively. Each image was spatially normalized to MNI space. Frontal, temporal, parietal and occipital lobe volumes of interest (VOIs) and Braak-like VOIs for stages 1/2, 3/4 and 5/6 were delineated from corresponding individual MRI scans. SUVr for VOIs were computed using inferior cerebellar cortex as reference region for both tracers.

Results: For the mean images of both tracers (Figure 1), higher background uptake in basal ganglia and thalamus was observed, as expected in NC for ^{18}F -THK-5351, while no background signal was seen in NC for ^{18}F -APN-1607. The same pattern was observed in the SUVr plots (Figure 2), and almost the same SUVr was seen across different regions in NC for ^{18}F -APN-1607, while the regional SUVr level varied across different regions for ^{18}F -THK-5351. For AD, ^{18}F -APN-1607 displayed no off-target binding in basal ganglia, and relatively more dynamic SUVr ranges than ^{18}F -THK-5351, particularly in the Braak stage 3/4 and 5/6 VOIs.

Conclusion: In this preliminary study of two tau tracers, different distribution patterns were observed, and notably, no off-target uptake was seen for ^{18}F -APN-1607 as compared to ^{18}F -THK-5351 in the basal ganglia and thalamus. Regional quantitation indicates better differential diagnostic power between AD and NC for ^{18}F -APN-1607 than for ^{18}F -THK-5351. Future work will include longitudinal study and identification of an optimal reference region for ^{18}F -APN-1607 imaging.

Keywords: Tau PET imaging, ^{18}F -APN-1607, ^{18}F -THK5351, Alzheimer's disease

P137: In vivo amyloid-PET and tau-PET evidence in early-onset Alzheimer's Disease: taking the LEADS

Leonardo Iaccarino¹, Renaud La Joie¹, Orit Lesman-Segev¹, David Soleimani-Meigooni¹, Karine Provost¹, Jessica A. Collins², Paul S. Aisen³, Bret J. Borowski⁴, Ani Eloyan⁵, Anne M. Fagan⁶, Tatiana M. Foroud⁷, Constantine Gatsonis⁸, Clifford R. Jack Jr.⁴, Joel H. Kramer⁹, Andrew J. Saykin⁷, Arthur W. Toga¹¹, Prashanti Vemuri⁴, Gregory S. Day¹², Neill R. Graff-Radford¹³, Lawrence S. Honig¹⁴, David T. Jones⁴, Joseph C. Masdeu¹⁵, Mario Mendez¹⁶, Chiadi U. Onyike¹⁷, Emily J. Rogalski¹⁸, Stephen Salloway¹⁹, David A. Wolk²⁰, Thomas S. Wingo²¹, Robert Koeppe¹⁰, Brad C. Dickerson²², Liana G. Apostolova²⁴, Maria C. Carrillo²³, Gil D. Rabinovici¹

¹Memory and Aging Center, Department of Neurology, Weill Institute for Neurosciences, University of California, San Francisco, CA, USA, San Francisco, CA, US

²Massachusetts General Hospital, Boston, MA, USA, Boston, MA, US

³Alzheimer's Therapeutic Research Institute, San Diego, CA, USA, San Diego, CA, US

⁴Mayo Clinic, Rochester, MN, USA, Rochester, MN, US

⁵Brown University, Providence, RI, USA, Providence, RI, US

⁶Department of Neurology, Washington University School of Medicine, St. Louis, MO, USA, St. Louis, MO, US

⁷Indiana University, Indianapolis, IN, US

⁸Department of Biostatistics, Brown University, Providence, RI, USA, Providence, RI, US

⁹University of California, San Francisco, San Francisco, CA, USA, San Francisco, CA, US

¹⁰University of Michigan, Ann Arbor, MI, USA, Ann Arbor, MI, US

¹¹Laboratory of Neuro Imaging, Stevens Neuroimaging and Informatics Institute, Keck School of Medicine, University of Southern California, Los Angeles, CA, USA, Los Angeles, CA, US

¹²Washington University School of Medicine, St. Louis, MO, USA, St. Louis, MO, US

¹³Mayo Clinic, Jacksonville, FL, USA, Jacksonville, FL, US

¹⁴Columbia University Medical Center, New York, NY, USA, New York, NY, US

¹⁵Houston Methodist Neurological Institute, Houston, TX, USA, Houston, TX, US

¹⁶David Geffen School of Medicine at University of California, Los Angeles, Los Angeles, CA, USA, Los Angeles, CA, US

¹⁷Johns Hopkins University, Baltimore, MD, USA, Baltimore, MD, US

¹⁸Northwestern University, Chicago, IL, US

¹⁹Butler Hospital, Providence, RI, USA, Providence, RI, US

²⁰University of Pennsylvania, Philadelphia, PA, USA, Philadelphia, PA, US

²¹Emory University School of Medicine, Atlanta, GA, USA, Atlanta, GA, US

²²Massachusetts General Hospital/Harvard Medical School, Boston, MA, USA, Boston, MA, US

²³Alzheimer's Association, Chicago, IL, US

²⁴Department of Radiology and Imaging Sciences, Indiana University School of Medicine, Indianapolis, IN, US

Background: Patients with sporadic early-Onset Alzheimer's Disease (EOAD) (aged 65 or younger) are less likely to harbor age-related co-pathologies and thus provide a framework to study the interplay of amyloid and tau pathology in AD. We here present preliminary results from the ongoing Longitudinal Early-Onset Alzheimer's Disease Study (LEADS). This report is based on data collected between August 2018 and October 2019.

Methods: Ninety-eight patients (aged 59±4 years, see Tab.1) meeting clinical criteria for probable AD or Mild Cognitive Impairment due to AD were included from 12 US centers. At screening, ¹⁸F-Florbetaben amyloid-PET (FBB-PET) was used to assign patients to EOAD (amyloid-positive) or EOnonAD (amyloid-

negative) subgroups based on visual rating and semi-quantification. Eighty-six participants had ¹⁸F-Flortaucipir tau-PET (FTP-PET) available. FBB-PET neocortical composite and FTP-PET regional analysis in meta/Braak regions were performed using structural 3T-MRI acquired concurrently. Thirty-eight cognitively-normal controls (aged 55±6 years) were included.

Results: Out of the 98 patients, 77 were amyloid-positive (EOAD) and 21 were amyloid-negative (EOnonAD). Compared to EOAD, EOnonAD patients had higher MMSE scores and were more frequently male (Tab.1). EOAD patients showed elevated FTP-PET SUVR compared to EOnonAD and controls in all regions of interest (Fig.1). EOAD showed elevated FTP-PET binding in temporoparietal, frontal and occipital regions (Fig.2). Some EOAD cases showed mild temporoparietal FTP-PET binding or patterns suggestive of AD focal subtypes, including posterior-dominant and asymmetric patterns (Fig. 2). Patients with EOnonAD did not differ from controls in any PET-based amyloid- or tau-PET measurement. Few EOnonAD patients showed abnormal FTP-PET patterns, possibly suggestive of other neurodegenerative conditions, e.g. asymmetric mild temporoparietal binding (Fig. 2).

Conclusions: Preliminary LEADS findings show very elevated FTP-PET binding in a multicentric cohort of early-onset AD patients. Our evidence suggests that amyloid screening in young symptomatic patients is needed given the relatively high rate of negative FBB-PET scans.

Table 1. Demographics, clinical and biomarker summary split by group and cognitively-impaired subgroups

	CN	PT*	EOnonAD*	EOAD*	PT vs CN	EOAD vs CN	EOAD vs EOnonAD
N	38	98	21	77	-	-	-
Age	55±6	59±4	58.8±6.2	58.5±3.9	<0.001	0.001	0.2
Sex (%F)	68%	52%	24%	60%	0.12	0.42	0.006
MMSE	29±1	23±5	26.1±2.4	21.9±4.8	<0.001	<0.001	0.0001
FBB-PET Composite Score	1±0.1	1.4±0.3	1±0.1	1.5±0.2	<0.001	<0.001	<0.001
FTP-PET Available (N, %)	38 (100%)	86 (88%)	19 (90%)	67 (87%)	-	-	-

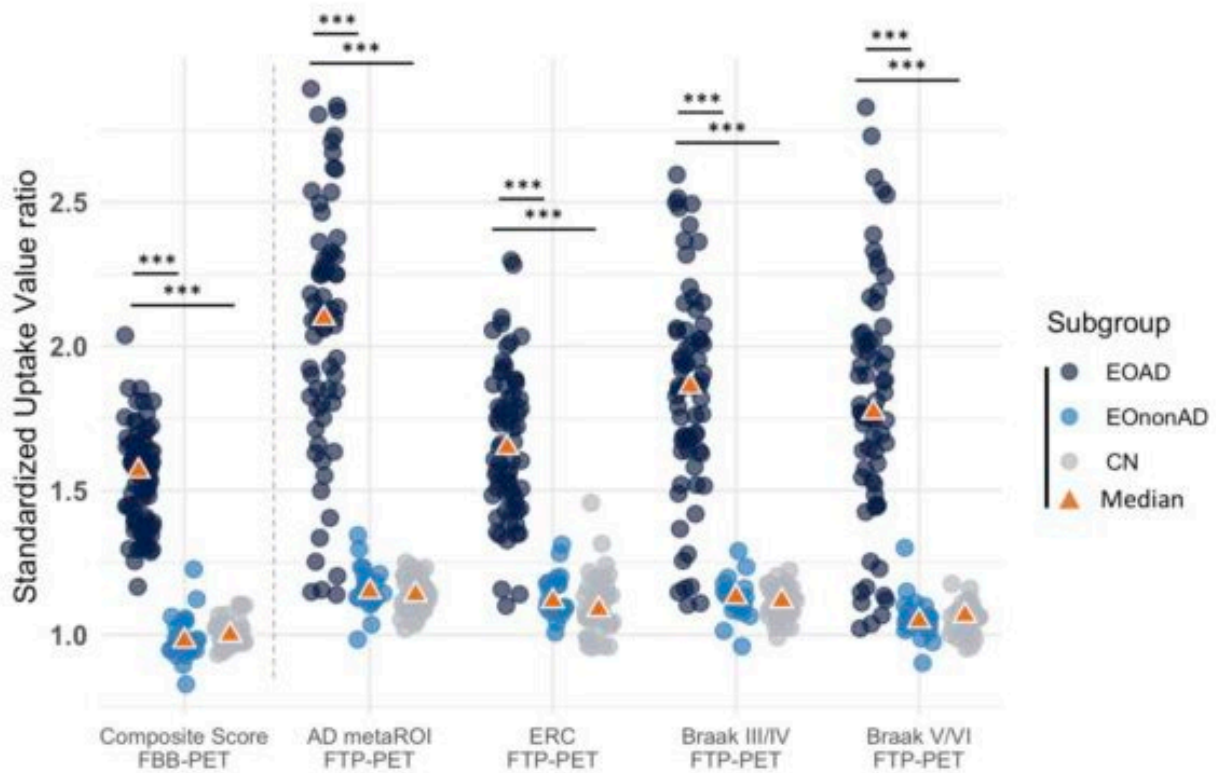
*: Patients were split into EOAD and EOnonAD based on the results of the FBB-PET.

P-values indicate Wilcoxon Rank Sum test for continuous variables and Fisher's Exact test for discrete variables.

FTP-PET metaROI represents a weighted mean of entorhinal, amygdala, parahippocampal, fusiform, inferior temporal, and middle temporal regions of interest scaled to the inferior cerebellar gray matter.

Legend: CN: Cognitively-Normal; PT: Patient; EOnonAD: Early-Onset non-Alzheimer's Disease; EOAD: Early Onset Alzheimer's Disease; MMSE: MiniMental State Examination; FBB: ¹⁸F-Florbetaben; ROI: region of interest; FTP: ¹⁸F-Flortaucipir; ERC: Entorhinal Cortex.

Figure 1. PET regional analysis split by Subgroups

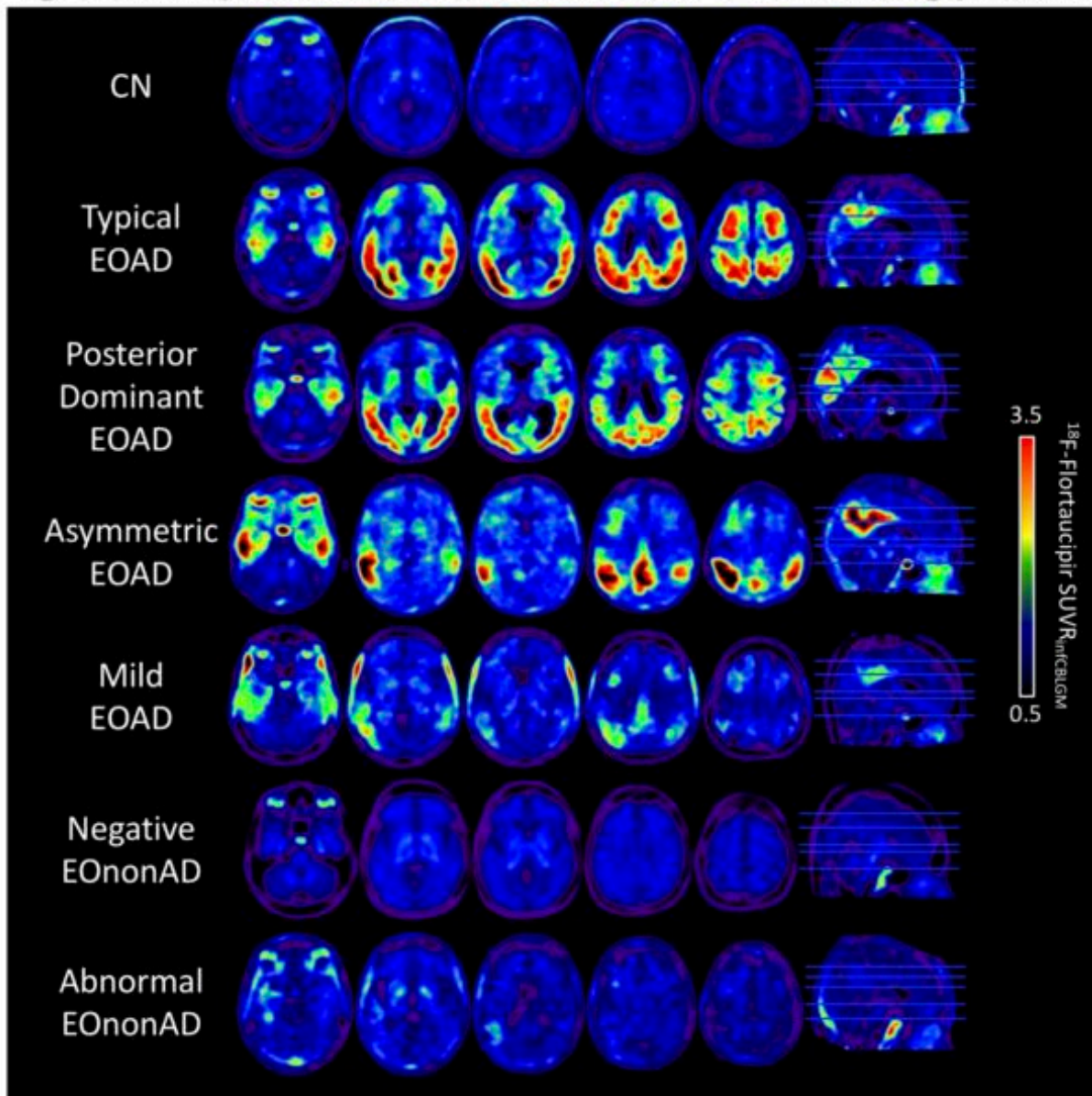


*** indicate Wilcoxon Rank Sum test results at $p < 0.001$

FTP-PET metaROI represents a weighted mean of entorhinal, amygdala, parahippocampal, fusiform, inferior temporal, and middle temporal regions of interest scaled to the inferior cerebellar gray matter.

Legend: CN: Cognitively-Normal; EOnonAD: Early-Onset non-Alzheimer's Disease; EOAD: Early Onset Alzheimer's Disease; FBB: ^{18}F -Florbetaben; ROI: region of interest; FTP: ^{18}F -Flortaucipir; ERC: Entorhinal Cortex.

Figure 2. Representative individual FTP-PET binding patterns



FTP-PET SUVR images were created with inferior cerebellar gray matter as reference region. Images were affine-transformed to the Montreal Neurological Institute (MNI) space for the sake of visualization. Each image comes from a different LEADS participating institution.

Legend: FTP: ^{18}F -Flortaucipir; CN: Cognitively-Normal; EOnonAD: Early-Onset non-Alzheimer's Disease; EOAD: Early Onset Alzheimer's Disease; SUVR: Standardized Uptake Value Ratio

Keywords: Early-Onset AD, tau-PET, amyloid-PET, LEADS

P138: Multimodal in vivo investigation of amyloid and tau biomarkers associations with cerebrospinal fluid NfL and YKL40 levels

Leonardo Iaccarino¹, Renaud La Joie¹, Lauren Edwards¹, Orit Lesman-Segev¹, Amelia Strom¹, Julie Pham¹, Kiran Chaudhary¹, Laura Fenton², Gina Jerome³, Mustafa Janabi⁴, Suzanne Baker⁴, Bruce Miller¹, William Jagust^{2,4}, Anne Fagan³, Gil Rabinovici^{1,2,4,5}

¹Memory and Aging Center, Department of Neurology, Weill Institute for Neurosciences, University of California, San Francisco, San Francisco, CA, US

²Helen Wills Neuroscience Institute, University of California, Berkeley, Berkeley, CA, US

³Knight Alzheimer Disease Research Center, Department of Neurology, Washington University, St. Louis, MO, US

⁴Lawrence Berkeley National Laboratory, Berkeley, CA, US

⁵Department of Radiology and Biomedical Imaging; University of California, San Francisco, San Francisco, CA, US

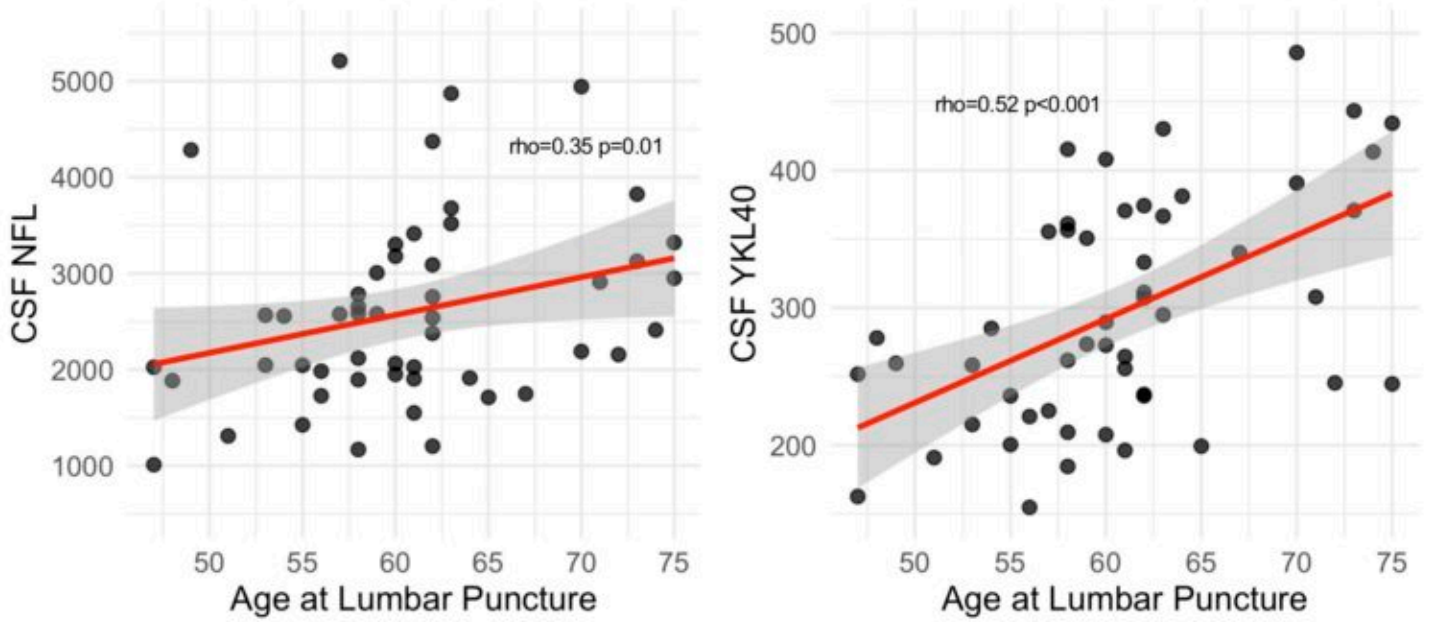
Background: CSF Neurofilament Light (NfL) chain and YKL40 proteins reflect axonal injury and inflammatory processes, respectively, and have been proposed to be novel candidate biomarkers for Alzheimer's Disease (AD) course. Their relationship with AD amyloid and tau markers has yet to be fully elucidated.

Methods: Fifty-one amyloid-positive patients (aged 61±7 years, N=29/51 females, MMSE 22±6, CDR-sb 4.2±2.3) with a clinical diagnosis of AD dementia or Mild Cognitive Impairment due to AD were included. Imaging markers included PET with ¹⁸F-Flortaucipir (FTP), ¹¹C-PiB (PiB), and ¹⁸F-FDG (neurodegeneration/hypometabolism), whereas fluid-based markers included cerebrospinal fluid (CSF) markers of Aβ₁₋₄₂, total-tau (T-tau), phosphorylated-tau181 (P-tau), NfL and YKL40 proteins. Correlations covarying for age and sex were tested between all fluid and imaging biomarkers. All analyses were repeated in subgroups split by median age (60 years).

Results: CSF NfL and YKL40 correlated significantly with age (partial Spearman rho=.35, p=0.01 and r=.52, p<0.001, respectively, Figure 1). NfL, not YKL40, correlated significantly with T-tau (r=0.6, p<0.001 and r=0.39, p=0.09). Neither marker correlated with P-tau (r=0.24, p=1 and r=0.26, p=0.82) or Aβ₁₋₄₂ (r=0.03, p=1 and r=-0.07, p=1) (see Figure 2). Relationships between NfL and T-tau were confirmed in age subgroups, with a stronger effect observed in younger patients (r=0.72, p=0.007 vs. r=0.58, p=0.03 in older patients). YKL40 and T-tau levels, conversely, were significantly associated in older (r=0.64, p=0.007) but not younger (r=0.23, p=1) patients. NfL levels correlated significantly with medial frontal, anterior temporal, and insular ¹⁸F-FTP binding, partially overlapping with regions in which FTP-PET correlated with CSF T-tau (Figure 3). YKL40 levels correlated with left temporoparietal ¹⁸F-FTP binding in older patients, although at lower statistical thresholds (p<0.01 uncorrected). There were no significant CSF-to-¹⁸F-FDG correlations.

Conclusions: Our findings suggest that the degree of neuroinflammation (YKL40) and neurodegeneration (NfL) associate more with tau rather than amyloid pathology.

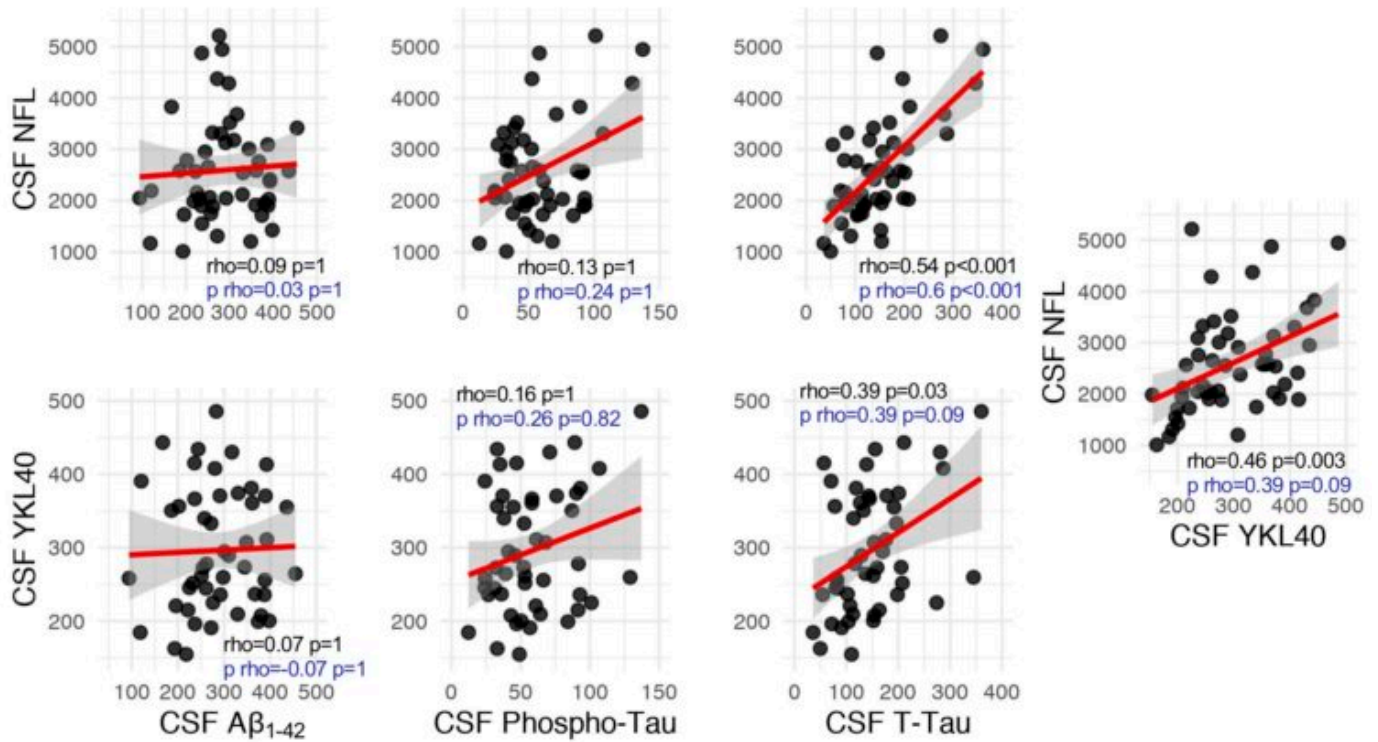
Figure 1. Relationships between CSF NfL and YKL40 and age at lumbar puncture



Scatterplots showing relationships between CSF NfL (left) and CSF YKL40 (right) with age at lumbar puncture. Red lines show linear fit with grey area showing confidence interval. Each scatterplot shows respective simple Spearman rho and p-value.

Legend: CSF: Cerebrospinal Fluid; NfL: Neurofilament Light Chain;

Figure 2. Relationships between CSF-based biomarkers



Scatterplots showing relationships between CSF NfL (top row) and CSF YKL40 (bottom row) with CSF Aβ₁₋₄₂, CSF phospho-tau and CSF total-tau. The single plot in the right panel shows the relationship between CSF NfL and YKL40. Red lines show linear fit with grey area showing confidence intervals. Each scatterplot shows respective simple Spearman rho (black) and partial Spearman rho (blue), corrected for age and sex. All the shown p-values are Holm-Bonferroni corrected for multiple comparisons.

Legend: CSF: Cerebrospinal Fluid; Aβ₁₋₄₂: β-amyloid₁₋₄₂; NfL: Neurofilament Light Chain; P-tau: Phospho-tau 181; T-tau: Total tau

P139: Activated microglia and amyloid load potentiate tau deposition leading to cognitive dysfunction in Alzheimer's disease

Min Su Kang^{1,3,4}, Julie Ottoy², Melissa Savard^{1,4}, Tharick Pascoal^{1,4}, Sulantha Mathotaarachchi¹, Andréa Benedet^{1,4}, Mira Chamoun^{1,4}, Joseph Therriault^{1,4}, Firoza Lussier^{1,4}, Cécile Tissot^{1,4}, Emilie Thomas¹, Jenna Stevenson^{1,4}, Nesrine Rahmouni^{1,4}, Jaime Arias^{1,4}, Tina Wang^{1,4}, Gassan Massarweh³, Jean-Paul Soucy³, Serge Gauthier^{1,3,4}, Pedro Rosa-Neto^{1,3,4}

¹*Translational Neuroimaging Laboratory, The McGill University Research Centre for Studies in Aging, Montréal, QC, Canada*

²*Molecular Imaging Center Antwerp, University of Antwerp, Antwerp, Belgium*

³*Montreal Neurological Institute, Montréal, QC, Canada*

⁴*Douglas Mental Health Research Institute, Verdun, QC, Canada*

Background: Growing evidence from *in vitro* studies suggest that the interaction between amyloid-beta (A β) and neuroinflammation leads to neurofibrillary tangles (NFT) in Alzheimer's disease (AD). In this multimodal PET study, we aimed to reveal that the A β ([¹⁸F]NAV4694) and activated microglia ([¹¹C]PBR28) converges to potentiate the NFTs ([¹⁸F]MK6240) deposition in AD. We hypothesized that the NFTs deposition driven by A β and neuroinflammation leads to cognitive dysfunction in A β + individuals.

Methods: A total of 95 participants (67 CN, 18 MCI, and 10 AD; 60 A β - and 35 A β +) with high-affinity binding for TSPO from the TRIAD cohort underwent 3 PET scans and MMSE, CDR-SoB, and MOCA. Static 40–60min [¹⁸F]NAV4694, 90-110min [¹⁸F]MK6240, and 60-90min [¹¹C]PBR28 SUVR images were generated. All PET images were normalized to the ADNI template, used cerebellar grey as a reference region, and adjusted for age, sex, education, and APOE.

Results: We showed a significant synergistic effect between A β and neuroinflammation on NFTs in Precuneus/PCC, entorhinal cortex, basolateral temporal cortex, and medial frontal cortex (Figure). This was mainly driven by the A β + group as there was no significant interaction in A β - group. Consequently, the greater NFTs driven by the interactive effect in A β + group was associated with significantly greater cognitive dysfunction based on MOCA (F(1)=7.04, p=0.0097) and MMSE(F(1)=3.86, p=0.053) and a trend with CDR-SoB (F(1)=3.09, p=0.084).

Conclusion: Our study demonstrated that the A β and neuroinflammation converge to greater NFTs deposition in AD vulnerable regions. Consequently, NFTs load in these regions was associated with greater cognitive dysfunction in AD. This supports the idea that targeting A β and neuroinflammation as a combination therapy may have greater therapeutic efficacy in AD.

Keywords: Alzheimer's pathophysiology, cognitive dysfunction, amyloid, tau, activated microglia

P140: Tauopathy in females is more vulnerable to amyloid or neuroinflammation in Alzheimer's disease

Min Su Kang^{1,3}, Julie Ottoy², Mira Chamoun¹, Sulantha Mathotaarachchi¹, Melissa Savard¹, Andréa Benedet¹, Tharick Pascoal¹, Joseph Therriault¹, Firoza Lussier¹, Cécile Tissot¹, Emilie Thomas¹, Jenna Stevenson¹, Nesrine Rahmouni¹, Jaime Fernandez-Arias¹, Tina Wang¹, Gassan Massarweh³, Jean-Paul Soucy³, Serge Gauthier¹, Pedro Rosa-Neto¹

¹*Translational Neuroimaging Laboratory, The McGill University Research Centre for Studies in Aging, Montréal, QC, Canada*

²*Molecular Imaging Center Antwerp, University of Antwerp, Antwerp, Belgium*

³*Montreal Neurological Institute, Montréal, QC, Canada*

Background: Understanding sex dimorphism in neurodevelopment and neurodegeneration is imperative for clinical trial enrichment and personalized medicine. However, the manifestation of sex dimorphism in Alzheimer's disease (AD) pathophysiology is still poorly understood. Here, we aimed to investigate how sex modulates the association among the major targets of AD clinical trials – amyloid ([¹⁸F]NAV4694), tau ([¹⁸F]MK6240), and neuroinflammation ([¹¹C]PBR28) – through a multimodal PET study. We hypothesized that amyloid or neuroinflammation show a greater positive effect on tau in females compared to males.

Methods: A total of 95 participants (67 CN, 18 MCI, and 10 AD) with a high-affinity binder for TSPO from the TRIAD cohort underwent 3 PET scans. Static 40–60min [¹⁸F]NAV4694, 90-110min [¹⁸F]MK6240, and 60-90min [¹¹C]PBR28 SUVR images were generated. All PET images were normalized to the ADNI template, used cerebellar grey as a reference region, and adjusted for age, sex, education, and APOE.

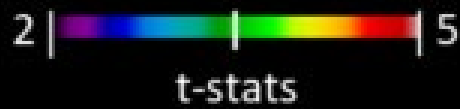
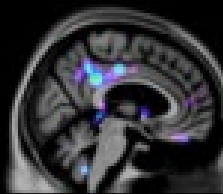
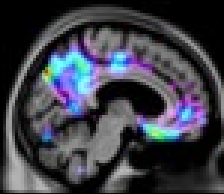
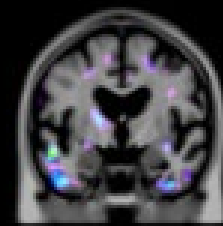
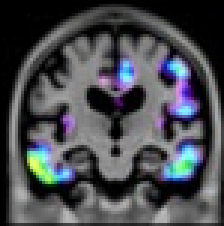
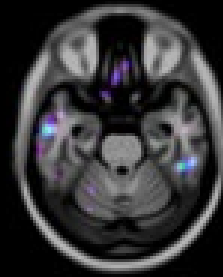
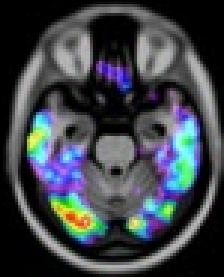
Results: Our results showed that the females had a greater positive association between tau and amyloid in Precuneus/PCC, basolateral temporal cortex, and medial frontal cortex (Figure). In addition, our results demonstrated that the females had a greater positive association between tau and neuroinflammation in Precuneus/PCC and basolateral temporal cortex compared to males (Figure).

Conclusion: Our study demonstrated that the sex intersects amidst the complex AD pathophysiology where the greater positive association between tau and amyloid or neuroinflammation was observed in females compared to males. This study supports the framework that females are more vulnerable compared to males in the AD pathophysiology.

Female > Male

Tau ~ A β *Sex

Tau ~ Neuroinflammation*Sex



Keywords: Sex, amyloid, tau, neuroinflammation, cognitive dysfunction

P141: Prediction of brain tau accumulation in amyloid positive cognitive impairment patients using multimodal biomarkers with machine learning approach

Jaeho Kim^{1,2,3}, Seongbeom Park¹, Yuhyun Park^{1,5}, Sung Hoon Kang^{1,2,3}, Soo Jong Kim¹, Hyemin Jang^{1,2,3}, Hee Jin Kim^{1,2,3}, Duk L. Na^{1,2,3,4,6}, Hyejoo Lee^{1,2,3}, Sang Won Seo^{1,2,3,5,6}

¹Department of Neurology, Samsung Medical Center, Sungkyunkwan University School of Medicine, Seoul, Korea

²Neuroscience Center, Samsung Medical Center, Seoul, Korea

³Samsung Alzheimer Research Center, Samsung Medical Center, Seoul, Korea

⁴Stem Cell & Regenerative Medicine Institute, Samsung Medical Center, Seoul, Korea

⁵Department of Clinical Research Design & Evaluation, SAIHST, Sungkyunkwan University, Seoul, Korea

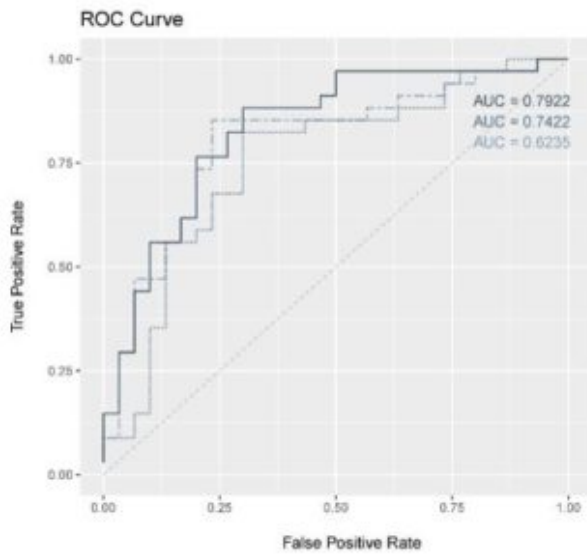
⁶Department of Health Sciences and Technology, SAIHST, Sungkyunkwan University, Seoul, Korea

Background: Brain tau accumulation is an important marker to predict cognitive function and decline. In prodromal Alzheimer's disease (AD), brain tau burden appears in various spectrum. However, brain tau PET imaging is costly, and access is restricted to specialized centers. Therefore, there is a need to develop a prediction model to detect prodromal AD who are liable to be tau positive prior to tau PET imaging. We aimed to develop a classifier of tau positivity in prodromal AD using statistical learning algorithms.

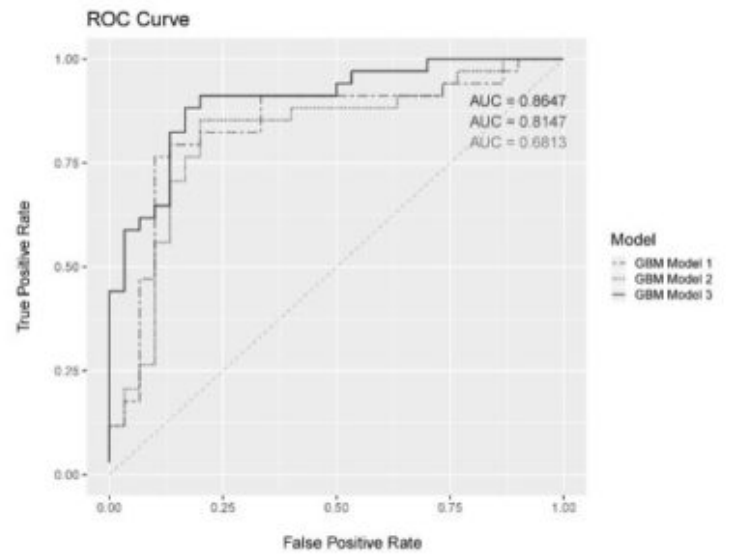
Methods: We used the Alzheimer's Disease Neuroimaging Initiative (ADNI) dataset, and included MCI patients who underwent 3.0T MRI scanning, 18F-AV45(flortbetapir) PET, and AV1451(flortaucipir) PET at baseline. We defined participants as having abnormal "Tau" (T+) if their in-vivo Braak stage was \geq III/IV by a conditional inference tree approach. Then, we performed machine learning algorithms to develop a statistical classifier to classify tau positivity.

Results: Our machine learning algorithm of GBM and RF predicted tau positivity in prodromal AD patients with the AUC of 0.865 for GBM and 0.792 for RF. We found that additional information of neuropsychological test to baseline patient information (age, gender, education) increased the AUC value from 0.681 to 0.815 in the GBM model and further increased to 0.865 when the brain MRI information was added. Through analysis of impact order of variables in each classifier, cortical thickness of parietal, occipital lobe, neuropsychological tests of memory domain, and sex were found to be more important features for each classifier.

Conclusion: We have developed a novel algorithm for predicting the brain tau burden in prodromal AD using baseline information, neuropsychological test results, and brain structural changes. Since our novel algorithm showed fair to good accuracy to predict brain tau burden, it can be useful to screen study population targeting tau and predict disease severity and prognosis.

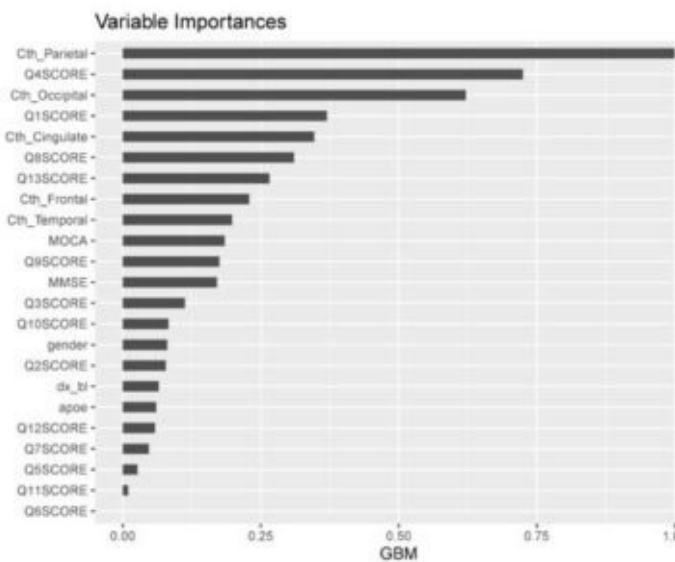


(a)

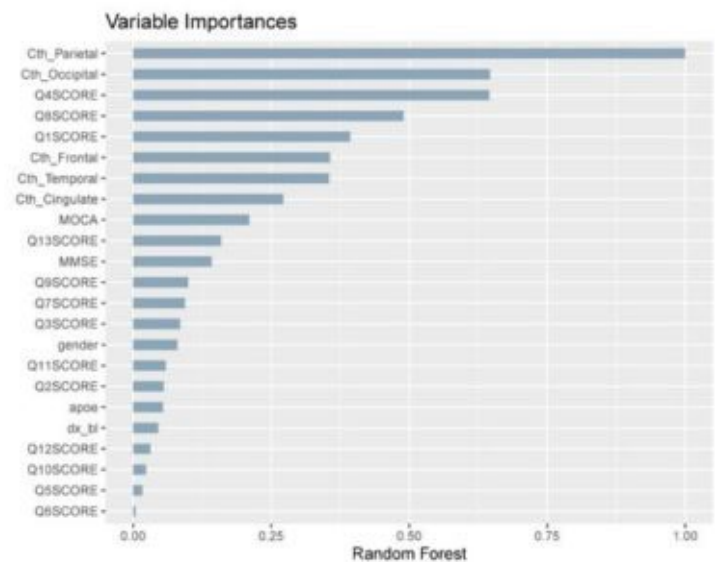


(b)

Model	Model Description	GBM			RF		
		AUC	Loggloss	Class error mean	AUC	Loggloss	Class error mean
model 1	Baseline(Age, Gender, Education) + MCI stage	0.681373	0.705760	0.364706	0.623529	0.653322	0.364706
model 2	Baseline + MCI stage + NP test	0.814706	0.559130	0.206863	0.742157	0.598142	0.219608
model 3	Baseline+ MCI stage + NP test + APOE4 + cortical thickness	0.864706	0.486635	0.175490	0.792157	0.548046	0.296078



(a)



(b)

Keywords: brain tau, machine learning, prodromal AD, classifier, tau PET

P142: Comparison of longitudinal change metrics for 18F-RO948 PET among cognitively unimpaired and patients with MCI or AD dementia in the BioFINDER2 study

Gregory Klein¹, Sandra Sanabria⁴, Antoine Leuzy², Edilio Borroni¹, Niklas Mattsson², Sebastian Palmqvist^{2,3}, Erik Stomrud^{2,3}, Ruben Smith^{2,3}, Oskar Hansson^{2,3}

¹*Roche Pharma Research and Early Development, Basel, Switzerland*

²*Clinical Memory Research Unit, Department of Clinical Sciences, Malmö, Sweden*

³*Memory Clinic, Skåne University Hospital, Malmö, Sweden*

⁴*Genentech, Inc., San Francisco, CA, US*

Objectives: Compare tau PET metrics of longitudinal change using 18F-RO948 PET in a population of cognitively unimpaired (CU) individuals, patients with mild cognitive impairment (MCI) or Alzheimer's disease (AD) dementia, recruited to date in the Swedish BioFINDER2 study.

Methods: Study participants (N=51) are scanned at baseline and 12 months with 18F-RO948 tau PET, obtained for 20 minutes, 70 min post injection. A MPRAGE T1-MRI sequence is used for PET processing. Two processing pipelines are compared: 1) FreeSurfer SUVR [1], and 2) A Hammer's atlas-based method computing SUVR, tau extent and tau load [2]. Both pipelines used a Braak staging model, defining ROIs approximating the anatomical definitions of entorhinal/hippocampal (stage I/II), temporal/limbic (III/IV), and neocortical (V/VI) stages. Subjects were analysed separately based on CSF A β 42/A β 40 amyloid status (A β ⁺ or A β ⁻) and baseline clinical diagnosis: cognitively unimpaired (CU), MCI and dementia due to AD. Cohen's effect size of annualized longitudinal change is used to compare processing pipelines.

Results: Both pipelines showed highest effect size in Braak I/II for CU_A β ⁺, Braak III/IV for MCI_A β ⁺ and Braak V/VI for AD_A β ⁺ groups respectively. Freesurfer methods showed higher effect size compared to the Hammer's atlas method for SUVR-based comparisons. Highest effect size overall in the CU and MCI groups was obtained with the Hammers tau load metric.

Conclusions: Tau burden change seen with 18F-RO948 replicates the post-mortem spreading pattern of tau, with the highest effect size and percent change seen in Braak regions I/II for A β ⁺ CU subjects, and Braak regions III/IV and V/VI for A β ⁺ MCI and AD subjects, respectively. A tau extent and load metric may offer superior effect size in detecting change for early AD.

References

[1] Cho et al., *Ann Neurol* ; 2016 ; 80 :247-258

[2] Sanabria Bohorquez, et al *Eur J Nucl Med Mol Imaging*. 2019

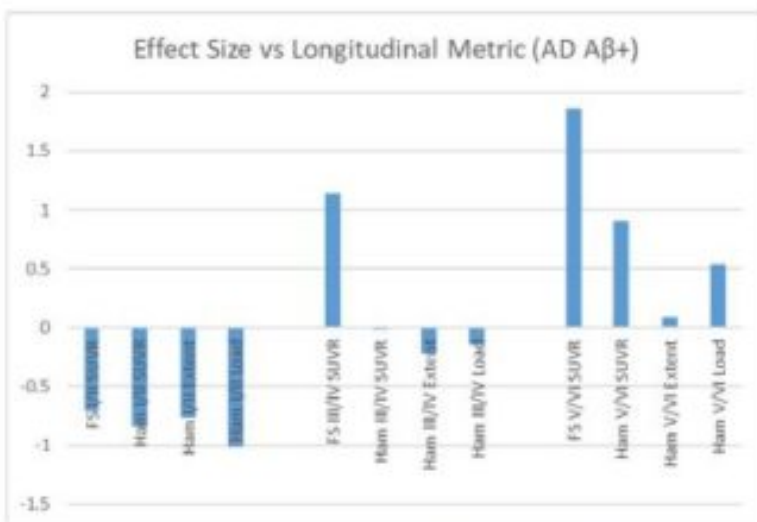
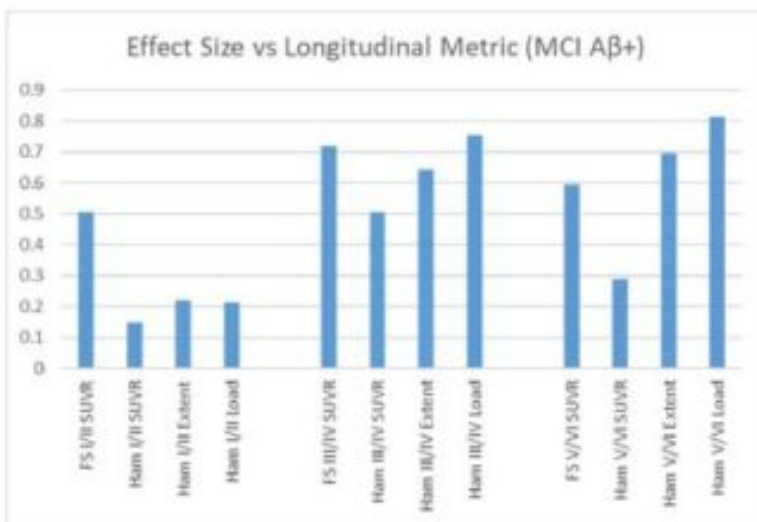
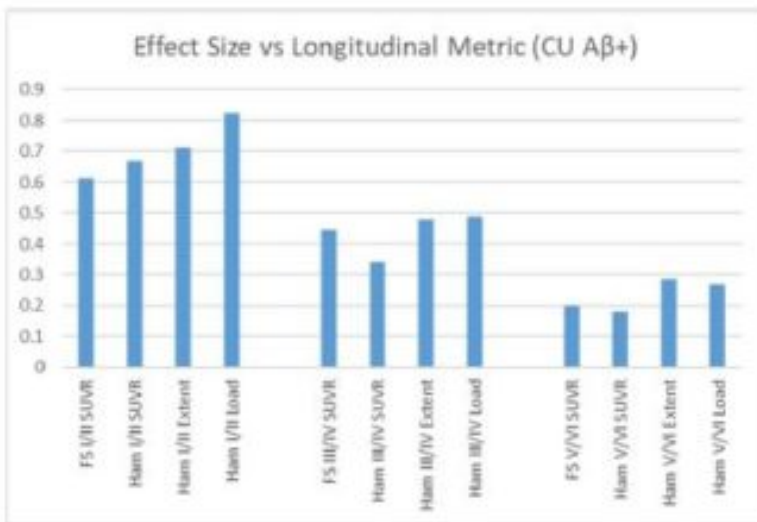


Figure 1. Effect size for Aβ+ CU, MCI and AD groups for each longitudinal metric. Highest effect size for the CU group is seen in Braak I/II, for the MCI's in Braak III/IV, and for AD's Braak V/VI. The Freesurfer (FS) method results with higher effect size than the Hammers atlas (Hamm) method when measuring only SUVR, however for the CU and MCI groups, slightly higher effect size is obtained using the tau extent and tau load measures.

Keywords: Tau PET, RO948, Image analysis

P143: Validation of clinical protocols for clinicians analyzing 18F-PI-2620 tau PET/MRI images

Mary Ellen Koran¹, Sara Shams¹, Patrick Adams¹, Emily Cazevedo¹, Tyler N. Toueg¹, Nicole Corso¹, Madison Hunt¹, Jessa Castillo¹, Jacob Hall¹, Sharon Sha¹, Carolyn Fredericks¹, Michael Greicius¹, Anthony Wagner¹, Greg Zaharchuk¹, Guido Davidzon¹, Frederick Chin¹, Elizabeth Mormino¹

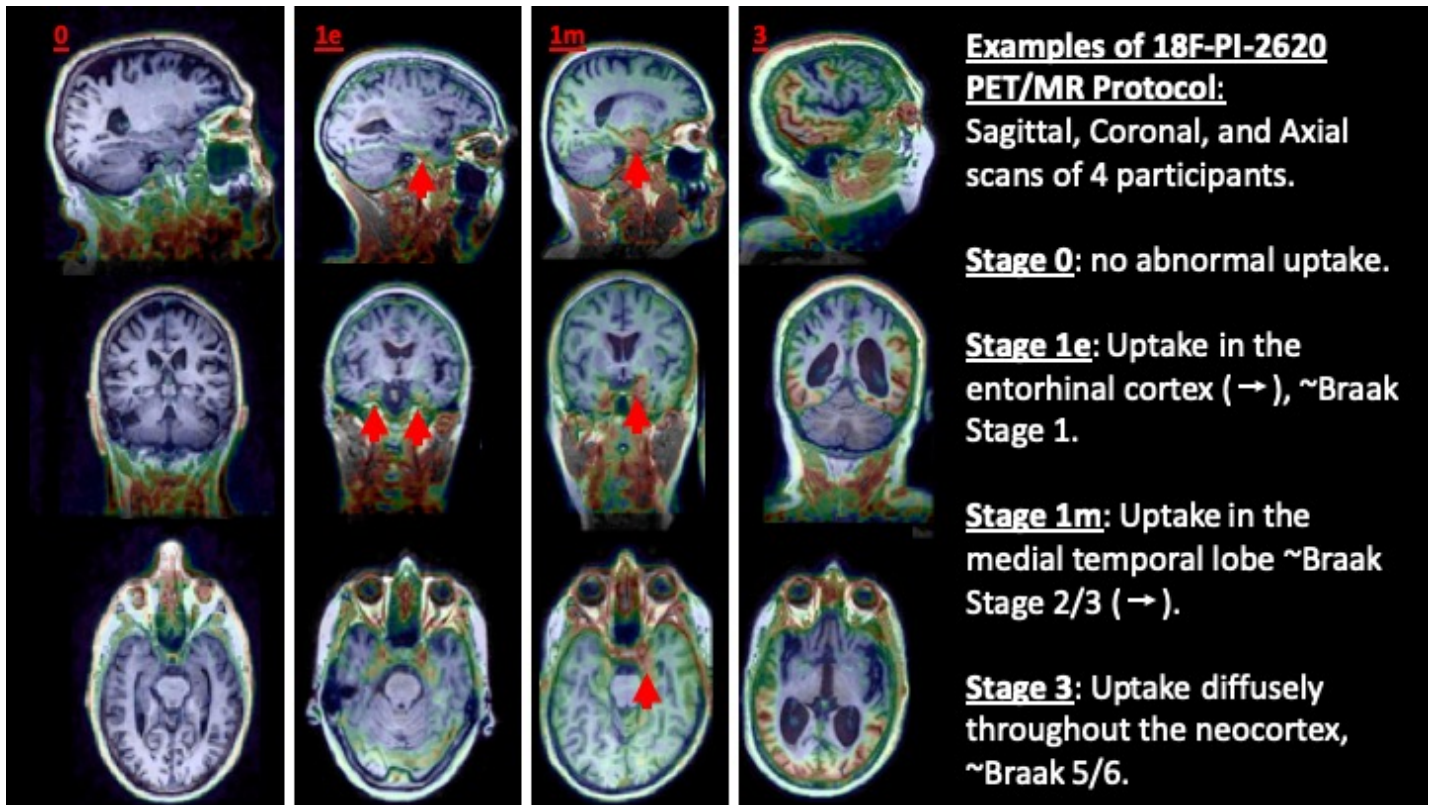
¹Stanford University, Stanford, CA, US

Diagnosing tau pathology *in vivo* is crucial in disease diagnosis and therapy development. The goal of this study was to create and validate a clinical visual rating protocol for ¹⁸F-PI2620 PET/MRI and correlate with regional values and disease.

A protocol was created following Braak staging of tau accumulation with the following scoring system of tracer uptake greater than inferior cerebellum--0: none, 1e: entorhinal cortex, 1h: hippocampus, 1m: medial temporal lobe (MTL), 2: inferior/lateral temporal lobe, 3: in neocortex beyond the temporal lobe. Two radiologists were blinded to clinical data such as diagnosis and age, and independently evaluated fused PET/MRI for 48 subjects along the non-AD and AD spectrum (normal controls, mild cognitive impairment and AD dementia, as well as semantic variant primary progressive aphasia, corticobasal syndrome, progressive supranuclear palsy, and dementia with Lewy bodies. Data were collected on a GE Signa PET-MRI system at Stanford.

Using this protocol, there was significant agreement for cases with cortical binding, such that all cases with a score of 2 and higher were consistently rated this way across readers. Overall, there was interrater reliability for the protocol that reflected disagreement within the medial temporal lobe (stages 1e, 1h, and 1m scores; K = 0.67; p < 0.0001). Despite differences in qualitative reads for individuals with focal medial temporal lobe uptake, group level differences were observed for medial temporal lobe standardized uptake value ratios (SUVRs, inferior cerebellum normalized) between normal controls and patients with mild cognitive impairment and AD dementia (p < 0.0001). Cortical SUVRs correlated with radiologist rating (F = 12.7, p < 0.0001).

As tau tracers are being implemented in clinical trials, clinical evaluation is necessary. ¹⁸F-PI2620 PET/MRI is promising for characterizing disease burden *in vivo* clinically, using modified Braak staging protocols and quantitative SUVRs.



Keywords: tau PET, PI2620, clinical, visual

P144: Cerebrospinal fluid tau phosphorylated at amino acid 181 or 231: a biomarker comparison in the detection of neurofibrillary tangle pathology in the Alzheimer's disease spectrum

Andrea Benedet¹, Nicholas Ashton^{2,3,4,5}, Tharick Pascoal¹, Erik Stoops⁶, Cindy Francois⁶, Eugene Vanmechelen⁶, Thomas Karikari², Sulantha Mathotaarachchi¹, Melissa Savard¹, Joseph Therriault¹, Mira Chamoun¹, Henrik Zetterberg^{2,7,8,9}, Kaj Blennow^{2,7}, Pedro Rosa-Neto^{1,10,11}

¹*Translational Neuroimaging Laboratory, McGill Centre for Studies in Aging, McGill University, Montreal, QC, Canada*

²*Department of Psychiatry and Neurochemistry, Institute of Neuroscience & Physiology, the Sahlgrenska Academy at the University of Gothenburg, Möndal, Sweden*

³*Wallenberg Centre for Molecular and Translational Medicine, University of Gothenburg, Gothenburg, Sweden*

⁴*King's College London, Institute of Psychiatry, Psychology & Neuroscience, Maurice Wohl Clinical Neuroscience Institute, London, UK*

⁵*NIHR Biomedical Research Centre for Mental Health & Biomedical Research Unit for Dementia at South London & Maudsley NHS Foundation, London, UK*

⁶*ADx NeuroSciences, Ghent, Belgium*

⁷*Clinical Neurochemistry Laboratory, Sahlgrenska University Hospital, Möndal, Sweden*

⁸*Department of Neurodegenerative Disease, UCL Institute of Neurology, London, UK*

⁹*UK Dementia Research Institute at UCL, London, UK*

¹⁰*Montreal Neurological Institute, Montreal, QC, Canada*

¹¹*Department of Neurology and Neurosurgery, McGill University, Montreal, QC, Canada*

Introduction: Neurofibrillary tangles (NFT) are key hallmarks of the Alzheimer's disease (AD) pathology and they are constituted of paired helical filaments. These are promoted by the abnormal phosphorylation of tau protein (p-tau), which can occur on several amino acids. P-tau phosphorylated at threonine residue 181 (p-tau181) is an established and specific biomarker for AD. However, alternative phosphorylation sites merit further evaluation as they can potentially better index NFT pathology and track disease progression in AD.

Aims: To compare the cross-sectional association between CSF p-tau231 and p-tau181 with tau and amyloid PET in the AD spectrum using data from the Translational Biomarkers of Aging and Dementia (TRIAD) cohort.

Methods: Were evaluated 111 participants (17 young controls, 57 normal controls (CN), 25 mild cognitive impairment (MCI) and 12 AD) with cross-sectional CSF p-tau181 and 231, t-Tau/p-Tau181 ratio and [¹⁸F]MK6240 and [¹⁸F]AZD4694 PET. For PET, standard uptake value ratios (SUVR) were determined using the cerebellar cortex as reference tissue. LUMIPULSE® G1200 (Fujirebio) was used to measure CSF p-tau181 whereas CSF p-tau231 was quantified using a custom ELISA assay (ADx Neuroscience). Linear regression was implemented at the voxel level, in order to examine the association between CSF and PET-based measures.

Results: Overall, as compared to p-tau181 and t-Tau/p-Tau181 ratio, p-tau231 was better correlated with MMSE, global amyloid and tau load (Figure 1). ROC curves revealed p-tau231 as the best predictor of diagnosis (Figure 2). The voxel-wise analysis demonstrated an association between CSF p-tau and tau PET in the temporal, posterior cingulate and medial prefrontal cortices, in which p-tau231 seemed to be more strongly associated with tau PET than p-tau181 (Figure 3). Similar findings were observed in the associations with amyloid PET, with p-tau231 showing high correlations with amyloid load.

Conclusion: These findings suggest that CSF p-tau231 may be a superior fluid biomarker that reflects NFT

pathology in the AD spectrum.

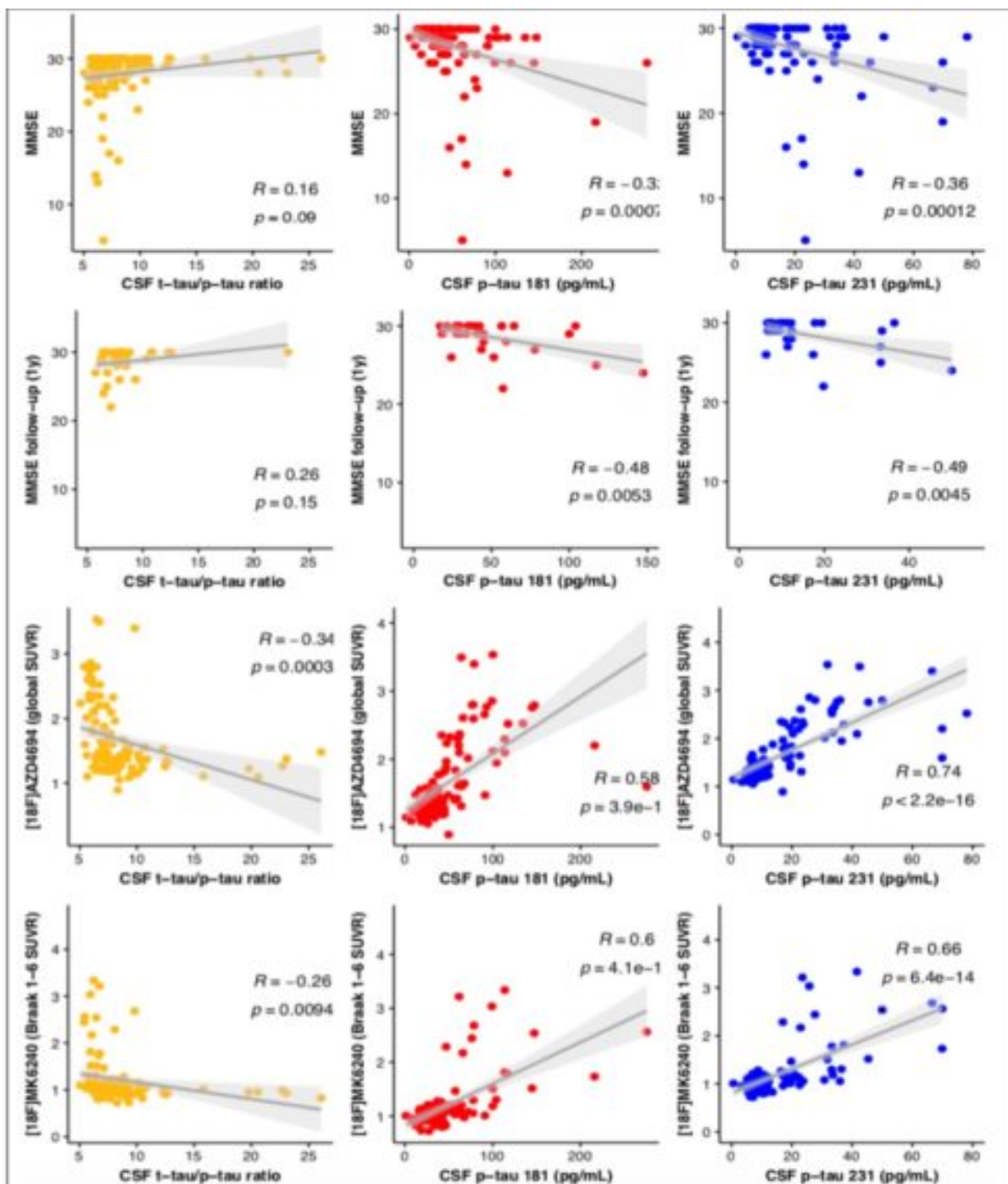


Figure 1. Correlations between CSF biomarkers and MMSE, tau and amyloid PET

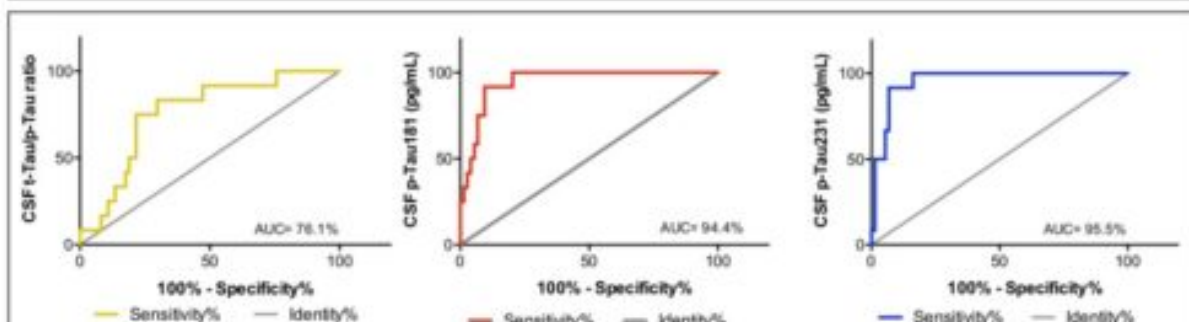
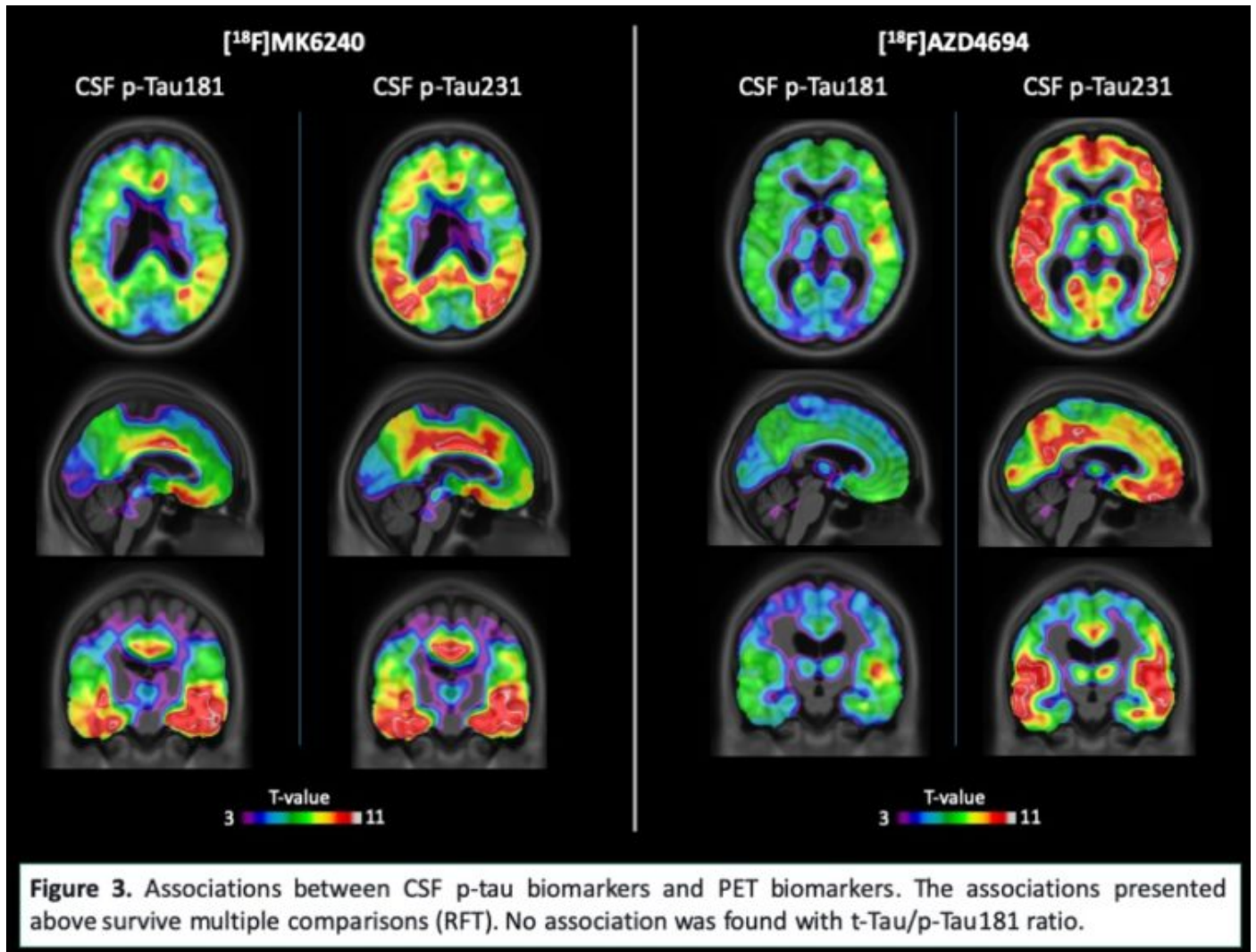


Figure 2. Receiver operating characteristic (ROC) curves: CN vs AD



Keywords: phosphorylated tau, MK6240, NFT, PET, Alzheimer's disease,

P145: Diagnostic performance of [¹⁸F]RO948 tau positron emission tomography in the differentiation of AD from other neurodegenerative disorders

Antoine Leuzy¹, Ruben Smith^{1,2}, Rik Ossenkoppele^{1,3}, Alexander Santillo¹, Edilio Borroni⁴, Gregory Klein⁴, Tomas Olsson⁵, Jonas Jögi⁶, Sebastian Palmqvist^{1,2}, Niklas Mattsson^{1,2,7}, Olof Strandberg¹, Erik Stomrud^{1,8}, Oskar Hansson^{1,8}

¹*Clinical Memory Research Unit, Department of Clinical Sciences, Lund University, Malmö, Sweden*

²*Department of Neurology, Skåne University Hospital, Lund, Sweden*

³*VU University Medical Center, Neuroscience Campus Amsterdam, Amsterdam, Sweden*

⁴*Roche Pharma Research and Early Development, Basel, Switzerland*

⁵*Department of Radiation Physics, Skåne University Hospital, Lund, Sweden*

⁶*Skåne University Hospital, Department of Clinical Physiology and Nuclear Medicine, Lund, Sweden*

⁷*Wallenberg Centre for Molecular Medicine, Lund University, Lund, Sweden*

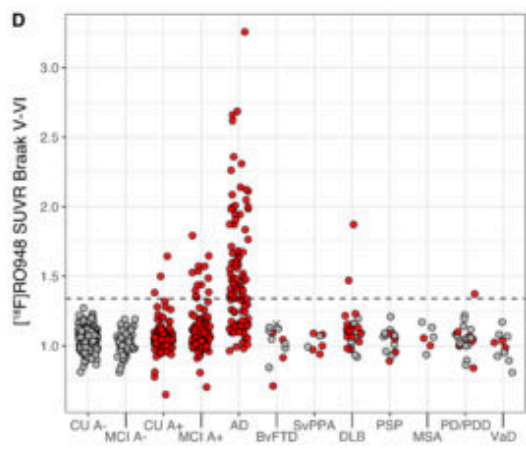
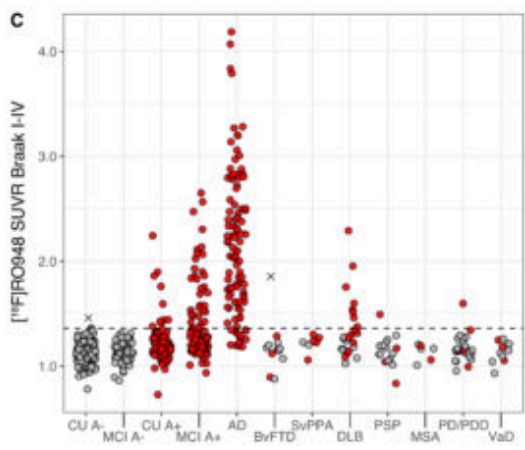
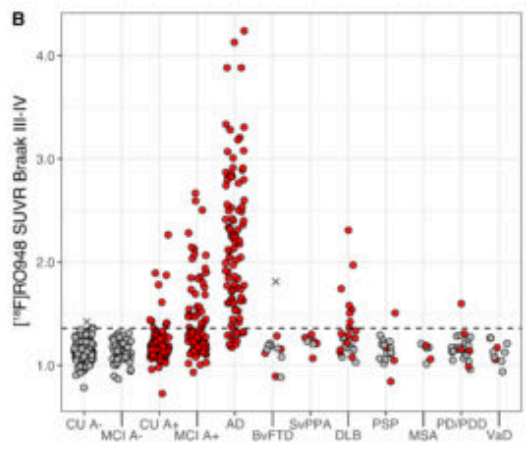
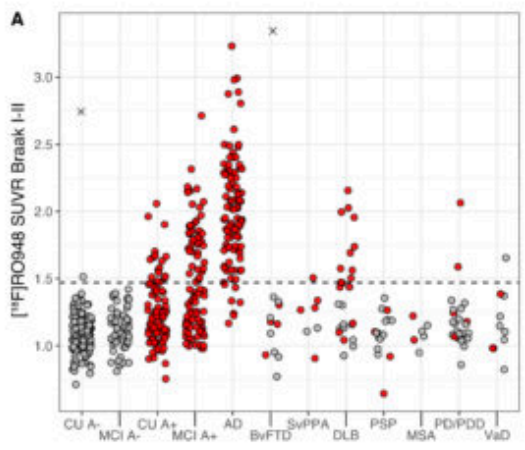
⁸*Memory Clinic, Skåne University Hospital, Lund, Sweden*

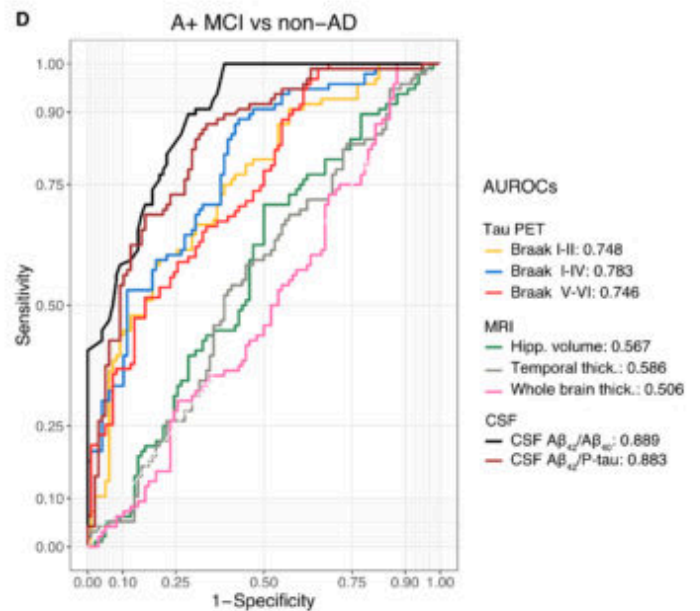
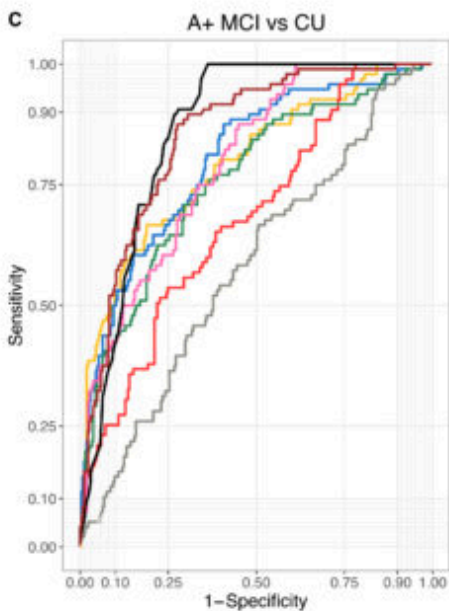
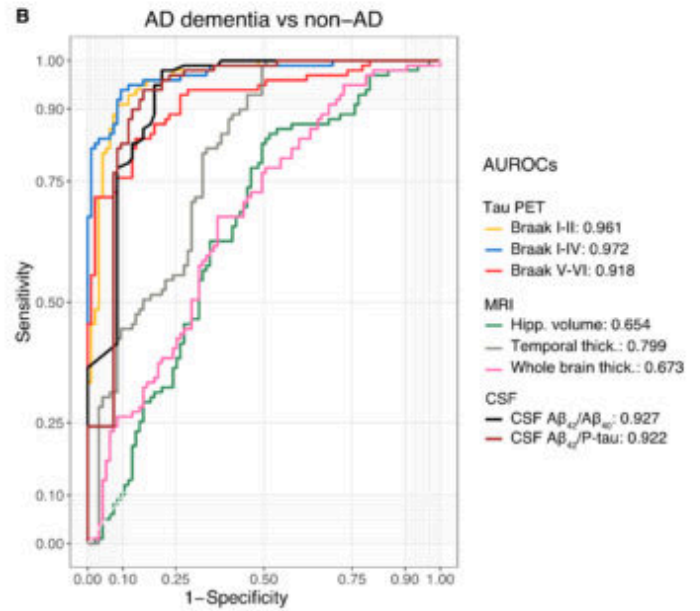
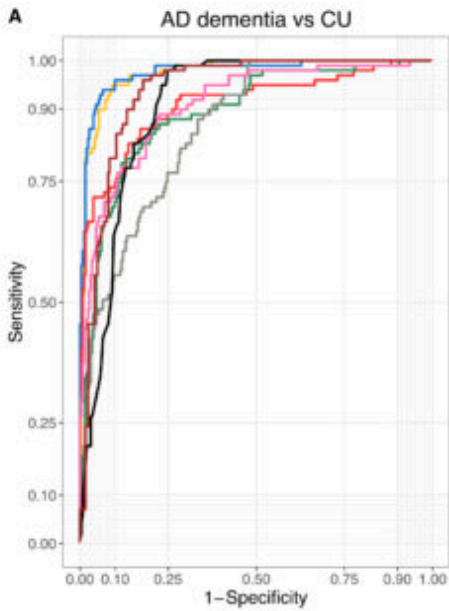
Objectives: To examine the diagnostic performance of the novel tau-PET tracer [¹⁸F]RO948 in discriminating AD from other neurodegenerative disorders.

Methods: We included 613 subjects with [¹⁸F]RO948 PET from the Swedish BioFINDER-2 study, including 257 cognitively unimpaired (CU) controls, 154 patients with MCI, 100 with AD dementia, and 102 with various non-AD disorders. [¹⁸F]RO948 PET was performed 70-90 min post-injection. Three svPPA patients underwent an additional [¹⁸F]flortaucipir scan (80-100 min post-injection). For tau-PET, FreeSurfer-based ROIs were created: Braak I-II (entorhinal), III-IV (temporal/limbic), I-IV (temporal meta-ROI) and V-VI (widespread neocortical areas). For the head-to-head [¹⁸F]RO948/[¹⁸F]flortaucipir comparison in svPPA, subject-specific ROIs were drawn (temporal voxels showing elevated SUVR values, including subcortical WM). The diagnostic performance of [¹⁸F]RO948 SUVR was compared against MRI (hippocampal volume, temporal meta-ROI and whole-brain cortical-thickness) and CSF (A β ₄₂/A β ₄₀, A β ₄₂/P-tau) biomarkers. Area-under-the-curve (AUC) values from receiver operating characteristic analyses were compared using bootstrap (n=1000) procedures.

Results: [¹⁸F]RO948 SUVR within Braak-stages were higher in AD dementia compared to other diagnostic groups (Figure 1). [¹⁸F]RO948 showed high accuracy for distinguishing AD dementia from CU and non-AD subjects, with the highest AUC seen when using Braak I-IV (0.977, versus CU, and 0.972 non-AD disorders), which outperformed MRI (highest AUC versus CU, whole-brain thickness, 0.910; non-AD disorders, temporal thickness, 0.798) and CSF (highest AUC versus CU, A β ₄₂/P-tau, 0.931; non-AD disorders, A β ₄₂/A β ₄₀, 0.927) (Figure 2). Generally, [¹⁸F]RO948 cortical positivity was only observed in A β ⁺ cases/*MAPT* R406W mutation-carriers. [¹⁸F]RO948 retention was not increased in svPPA, and showed lower temporal lobe uptake compared to [¹⁸F]flortaucipir.

Conclusions: [¹⁸F]RO948 Tau-PET positivity was only found among A β -positive cases and the retention was lower compared to [¹⁸F]flortaucipir in svPPA (predominantly caused by TDP-43 type-C pathology). This supports that [¹⁸F]RO948 has high specificity for AD-type tau and highlight its potential as a diagnostic marker in the differential diagnosis of AD.





Keywords: Tau, PET, RO948, Flortaucipir, Alzheimer

P146: Longitudinal changes in tau pathology measured by [18F]RO948 tau-PET are associated with elevated CSF P-tau: preliminary findings from the Swedish BioFINDER-2 study

Antoine Leuzy¹, Gregory Klein², Rik Ossenkoppele^{1,3}, Niklas Mattsson^{1,4,5}, Shorena Janelidze¹, Sebastian Palmqvist^{1,4}, Olof Strandberg¹, Preciosa Coloma², Edilio Borroni², Erik Stomrud^{1,6}, Ruben Smith^{1,4}, Oskar Hansson^{1,6}

¹*Clinical Memory Research Unit, Department of Clinical Sciences, Lund University, Malmö, Sweden*

²*Roche Pharma Research and Early Development, Basel, Switzerland*

³*VU University Medical Center, Neuroscience Campus Amsterdam, Amsterdam, The Netherlands*

⁴*Department of Neurology, Skåne University Hospital, Lund, Sweden*

⁵*Wallenberg Centre for Molecular Medicine, Lund, Sweden*

⁶*Memory Clinic, Skåne University Hospital, Lund, Sweden*

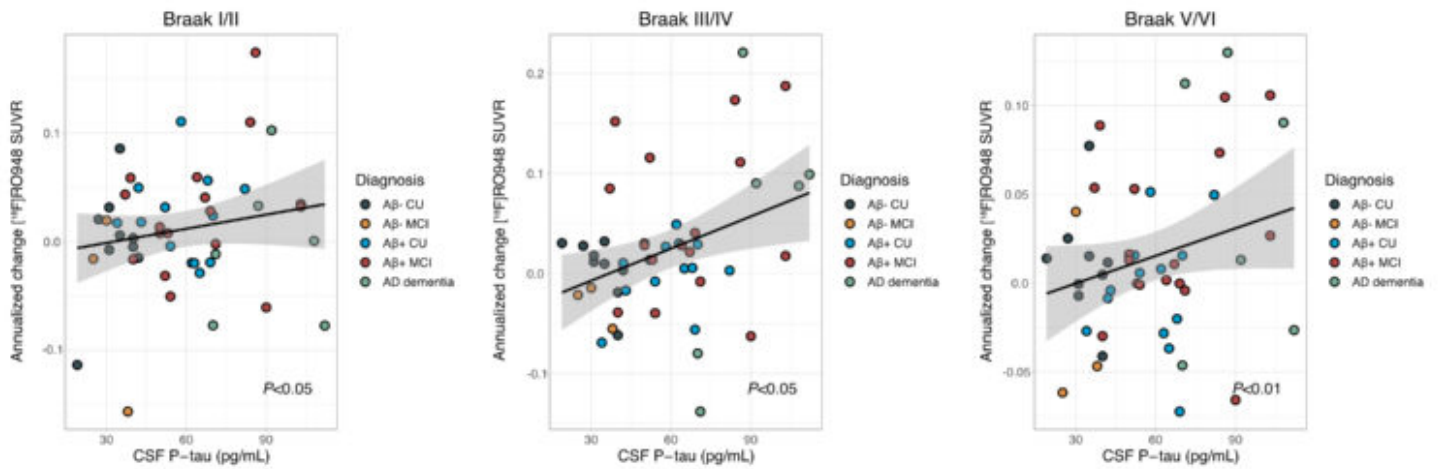
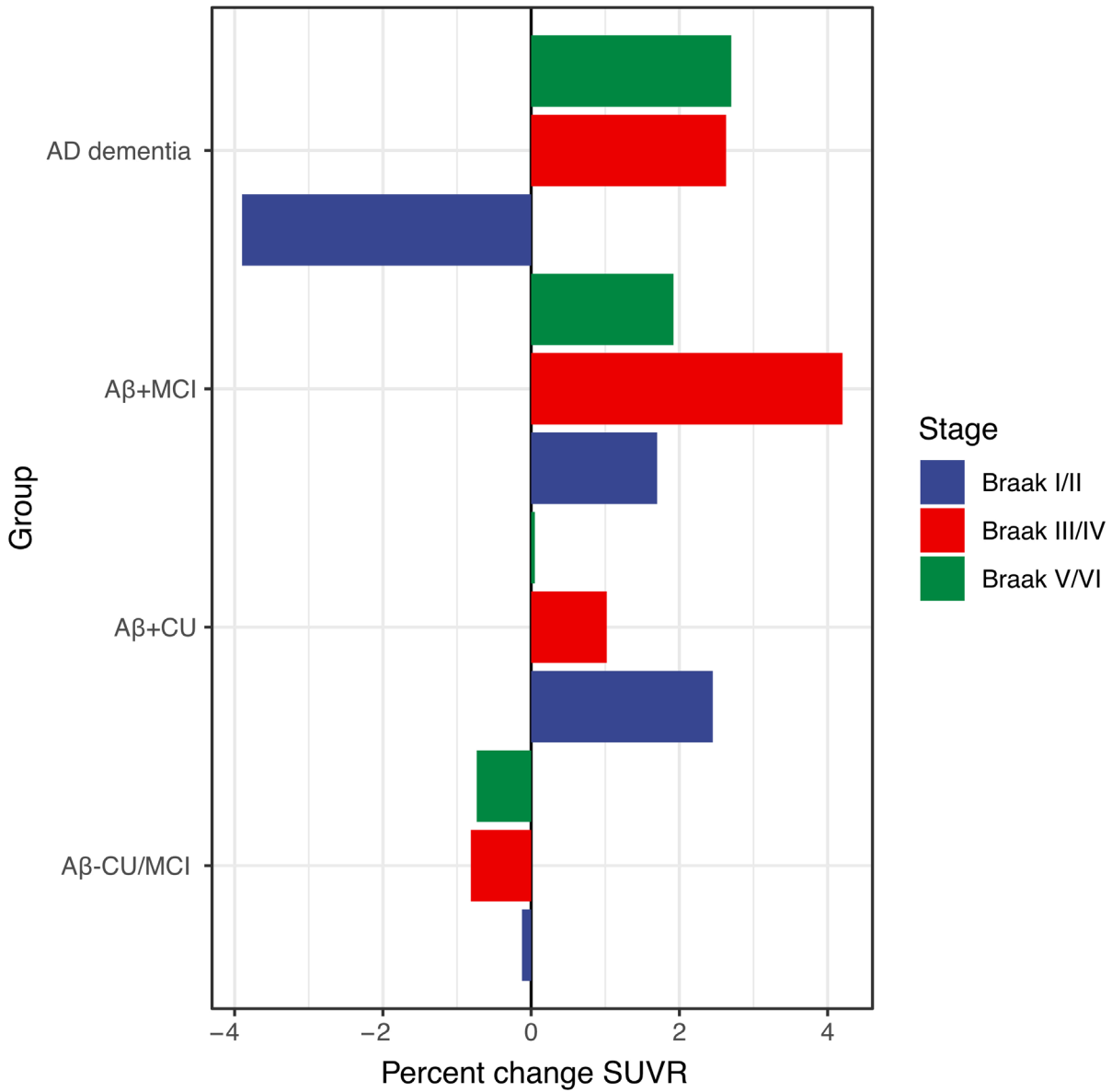
Objectives: 1) To describe the longitudinal change in tau pathology seen after approximately one-year using [18F]RO948-PET in a cohort of cognitively unimpaired (CU), MCI, and AD dementia subjects from the Swedish BioFINDER-2 study; 2) To examine the association between longitudinal increases in [18F]RO948 SUVR and CSF phosphorylated-tau (P-tau).

Methods: 51 subjects from the ongoing BioFINDER-2 longitudinal sub-study were included: 23 CU (9 A β -, 14 A β +), 21 MCI (3 A β -, 18 A β +) and 7 AD dementia (all A β +), with A β -status determined using CSF A β ₄₂/A β ₄₀. All participants underwent [18F]RO948-PET (list-mode, 70-90 min post-injection) at baseline and at a targeted follow-up of approximately 12-months (mean=13.2;SD=2.6). FreeSurfer (v.6.0) was used to calculate mean-SUVR values (inferior cerebellar grey reference) across Braak-stages (I/II, entorhinal/hippocampus; III/IV, temporal/limbic; V/VI, neocortical). Longitudinal measures included annualized percentage-change and effect-size (Cohen's d). CSF P-tau was measured using a commercial assay (INNOTEST, Fujirebio). The relationship between P-tau and change in [18F]RO948 SUVR was examined ROI-wise using linear-regression, adjusting for age, baseline-SUVR, diagnostic-group and interscan-interval.

Results: The largest longitudinal change and effect-size (Figure 1) for A β +CU subjects was seen in the Braak I/II region (+3.14%, effect-size 0.72). For A β +MCI and AD dementia subjects, the largest changes and effect-sizes were seen in the Braak III/IV (+3.62%, effect-size 0.61) and V/VI regions (+3.98%, effect-size 0.58), respectively. No significant increases were seen across A β - subjects (average-change across stages, -0.65%; CU and MCI combined due small sample-size). CSF P-tau was significantly associated with increases in [18F]RO948 SUVR across Braak-stages (Figure 2).

Conclusions: Initial longitudinal results with the novel tau-PET tracer [18F]RO948 indicate that it is able to capture the progression of early tau pathology in A β +CU subjects, as well as cortical increases in subjects with cognitive impairment. Importantly, increases in [18F]RO948 SUVR were significantly associated to baseline P-tau, supporting its use as a biomarker predictive of tau PET.

Change [¹⁸F]RO948 SUVR by Group/Braak stage



Keywords: Tau, PET, RO948, CSF, P-tau

P147: A comparison of ischemic stroke-induced changes on ¹⁸F-APN-1607 (¹⁸F-PMPBB3) and ¹⁸F-THK-5351 uptake patterns

Kun-Ju Lin^{1,3}, Ing-Tsung Hsiao^{1,3}, Kuo-Lun Huang², Chin-Chang Huang²

¹*Department of Nuclear Medicine and Molecular Imaging Center, Linkou Chang Gung Memorial Hospital, Taoyuan, Taiwan*

²*Department of Neurology, Chang Gung Memorial Hospital Linkou Medical Center and College of Medicine, Taoyuan, Taiwan*

³*Department of Medical Imaging and Radiological Sciences and Healthy Aging Research Center, Taoyuan, Taiwan*

Background: Post-stroke cognitive impairment (PSCI) may affect up to one third of stroke survivors, however, the mechanism underlying it remains unknown. Several novel radiotracers, such as ¹⁸F-APN-1607 (¹⁸F-PM-PBB3) and ¹⁸F-THK-5351, are available for visualization of in vivo tau protein distribution in patients with tauopathy. However, alternative targeting to MAO-B was reported for ¹⁸F-THK-5351. To explore differences, we compared the ¹⁸F-APN-1607 and ¹⁸F-THK-5351 imaging presentations in patients with chronic ischemic stroke.

Method: Three patients with PSCI were recruited for ¹⁸F-APN-1607 and ¹⁸F-THK-5351 imaging studies. The cerebellum cortex was used as the reference region for standardized uptake value ratio (SUVR) calculation. Another 12 healthy controls were recruited for ¹⁸F-APN-1607 PET studies to determine the extent of ¹⁸F-APN-1607 uptake in ischemic stroke patients.

Results: ¹⁸F-APN-1607 and ¹⁸F-THK-5351 were performed in two patients with PCA territorial infarction and one patient with MCA infarction. Increased ¹⁸F-THK-5351 uptake was not only observed prominently in the areas around ischemic lesions but also in basal ganglia, thalamus and midbrain. On the other hand, off-target binding in basal ganglia, thalamus and midbrain was not observed on ¹⁸F-APN-1607 imaging. Conversely, ¹⁸F-APN-1607 uptake was not significantly increased in the peri-lesional areas as compared to the background values of healthy controls.

Conclusion: Different binding patterns between ¹⁸F-APN-1607 and ¹⁸F-THK-5351 on PET scans may suggest that the increased uptake of ¹⁸F-THK-5351 in the peri-lesional area may result from off target binding such as MAO-B rather than tau. However, the pathogenesis is complex and changes with time. Longitudinal observation, e.g., by pathological and clinical correlation is warranted.

Keywords: Post-stroke cognitive impairment, Tau, Amyloid, ¹⁸F-APN-1607, ¹⁸F-THK-5351

P148: Longitudinal change in [18F]GTP1 SUVR over 18 months depends on baseline SUVR intensity and spatial distribution and shows trends with cognitive decline

Paul Manser¹, Sandra Sanabria Bohorquez¹, Edmond Teng¹, Suzanne Baker¹, Balazs Toth¹, Jan Marik¹, Robby Weimer¹

¹Genentech, South San Francisco, CA, US

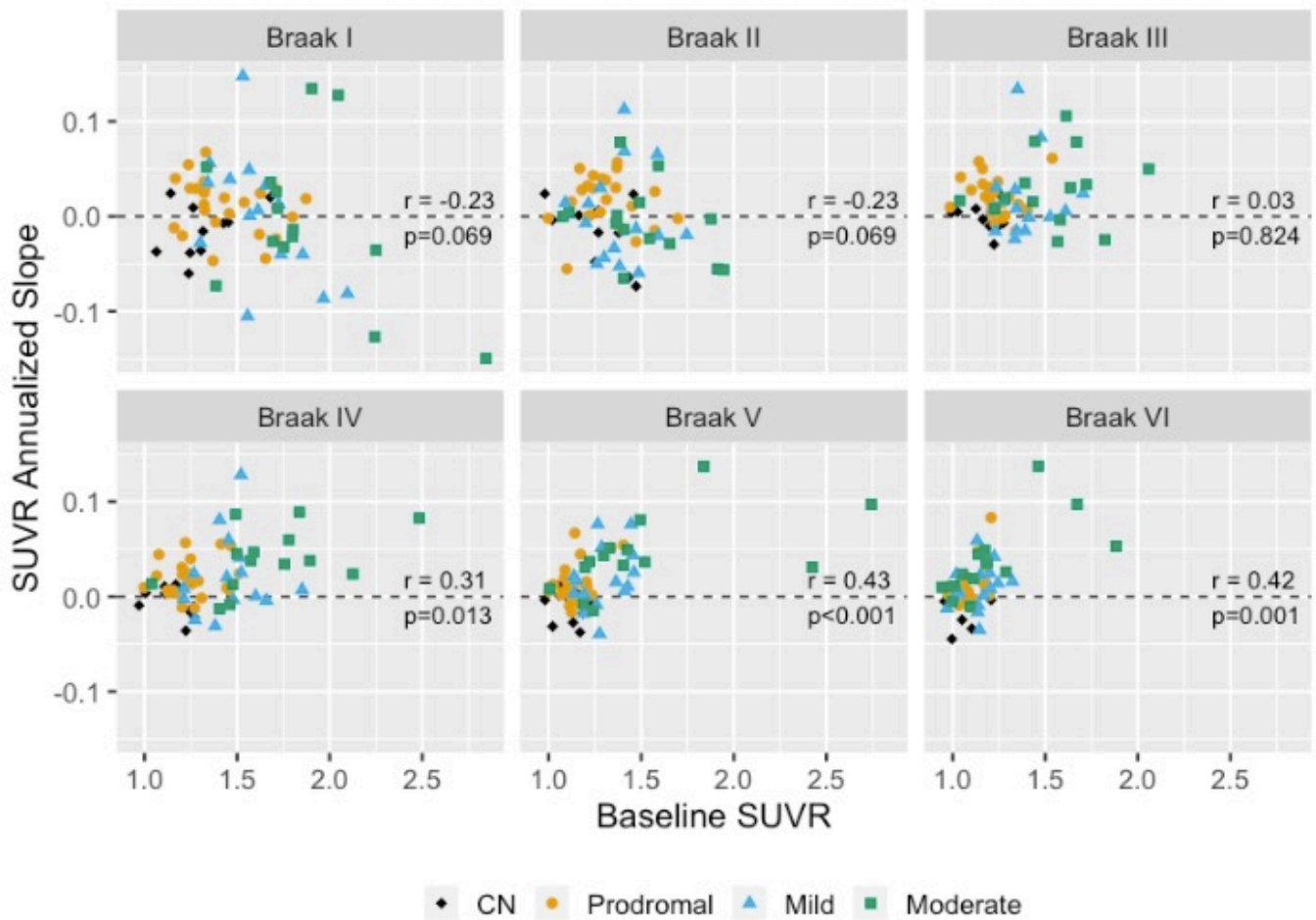
Objective: To characterize the longitudinal change in tau burden measured by [18F]GTP1 and its relationship with cognitive decline and baseline [18F]GTP1 signal.

Methods: [18F]GTP1 PET scans were performed at baseline 6, 12 and 18 months in amyloid PET negative and positive cognitive normal subjects (CN; n=2 and 7, respectively), and amyloid PET positive prodromal (Prod; n=24; MMSE 24-30, CDR = 0.5) and mild/moderate (MM; n=30; MMSE 22-30, CDR = 0.5-2) AD subjects. Measurements were made within whole cortical gray matter (WCG), at the regional level, within *in vivo* Braak ROIs (Schöll et al., Neuron 2016). Relationships between change in SUVR and change in cognitive scores were summarized by timepoint with Spearman correlations. Annualized rates of SUVR change for each subject were calculated using simple linear regression and compared against baseline SUVR using Spearman correlations.

Results: Local baseline [18F]GTP1 was prognostic of annualized rate of local SUVR change in AD subjects: baseline SUVR in Braak 1&2 had a negative correlation with its annualized SUVR change ($r_s = -0.23$, $p=0.069$; $r_s = -0.23$, $p=0.069$), while later Braak ROIs (4, 5, and 6) had positive correlations ($r_s = 0.31$, $p=0.013$; $r_s = 0.43$, $p<0.001$, $r_s = 0.42$, $p=0.001$). Change in [18F]GTP1 WCG SUVR showed weak positive correlations with change in ADAS-Cog13 and CDR-SB at 18 months that did not meet statistical significance ($r_s = 0.14$, $p=0.323$; $r_s = 0.18$, $p=0.210$).

Conclusions: We observed that baseline [18F]GTP1 SUVR was prognostic of 18 month SUVR change in an *in vivo* Braak ROI-dependent manner. We observed weak positive correlations between changes in [18F]GTP1 SUVR and CDR-SB and ADAS-Cog13. These results support the clinical utility of [18F]GTP1 and its use in AD clinical trials.

Figure 1: Annualized [¹⁸F]GTP1 slope vs baseline SUVR by Braak Stage. Cognitive Normal: black; Prodromal AD: orange; Mild AD: blue; Moderate AD: Green



Keywords: [¹⁸F]GTP1, tau PET, cognitive decline

P149: 18F-APN-1607: a promising PET tracer for multiple tauopathies

Richard Margolin^{1,2}, Kun-ju Lin^{1,3,4}, Paul Tempest¹, Poe-Jou Chen¹, Kenneth Marek⁵, David Russell⁵, Christine Sandiego⁵, Chin-Chang Huang^{4,6}, Ing-Tsung Hsiao^{3,4}, Gilles Tamagnan⁷, David Alagille⁷, Yihui Guan⁸, Jiaying Lu⁸, Chuantao Zuo⁸, Makoto Higuchi⁹, Ming-Kuei Jang¹

¹*APRINOIA Therapeutics, Taipei, Taiwan*

²*CNS Research Solutions LLC, Cambridge, MA, US*

³*Department of Nuclear Medicine and Molecular Medicine Center, Chang Gung Memorial Hospital Linkou, Taoyuan City, Taiwan*

⁴*Department of Medical Imaging and Radiological Sciences, and Healthy Aging Research Center, College of Medicine, Chang-Gung University, Taoyuan City, Taiwan*

⁵*Invicro, LLC, New Haven, CT, US*

⁶*Department of Neurology, Chang Gung Memorial Hospital Linkou, Taoyuan City, Taiwan*

⁷*Xingimaging LLC, Beijing, China*

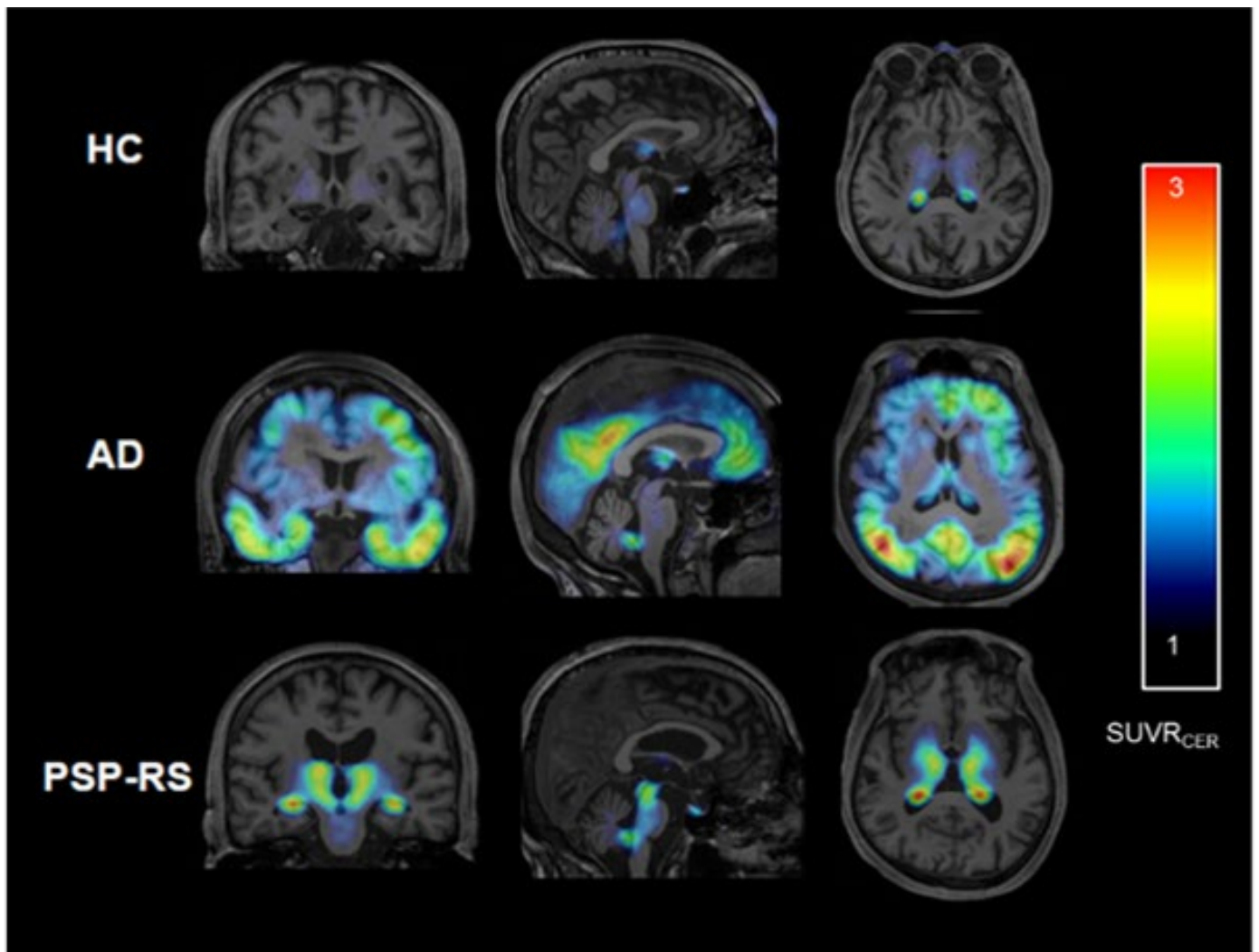
⁸*Huashan Hospital/Fudan University, Shanghai, China*

⁹*Quantum Sciences and Technology Institute, Chiba, Japan*

Background: Tau aggregation/deposition is a key feature of AD and non-AD tauopathies (NADTs), including PSP, CBD, and MAPT mutation-induced FTD. Tauopathies differ by repeat type: 3R-predominant (PiD), 4R-predominant (PSP, CBD), and mixed (AD). PET tracers are enabling tau burden characterization in-vivo; one PET tracer for all tauopathies could illuminate pathology and be clinically useful. While several tracers perform well in AD, their 4R-predominant tauopathy performance is unclear. An initial PBB-class tracer, [11]C-PBB3, demonstrated appropriate signal but had problematic radiopharmaceutical properties. A second-generation PBB, [18F]APN-1607 (originally [18]F-PM-PBB3), lacked off-target binding on in-vitro screen; competition showed no MAO A/B binding. In a 4R mouse model (rTg4510) signal increased over time, mirroring histopathology. NHP imaging revealed good brain uptake; initial human scans supported further evaluation.

Methods: APN-1607 has been evaluated in investigator-initiated studies, 2 sponsored proof-of-concept studies and 2 Phase 1 studies investigating dosimetry, kinetics, and test/retest. Dynamic DVR and static SUVR analyses were performed, referencing cerebellar cortex.

Results: APN-1607 has favorable dosimetry (6.4 mSv/185 mBq), excellent SUVR/DVR agreement between 60-150 min post-injection in HC and AD ($R^2 > 0.95$), and test/retest DVR/SUVR %CVs consistently <5%. Approximately 265 individuals have been scanned in Taiwan, Japan, US, and China, including 75 HC, 40 AD, 45 PSP, 17 MAPT FTD, and 9 CBS. No meningeal binding was noted; choroid plexus uptake unrelated to known biochemical/clinical factors is sometimes seen. Little uptake occurs in HC; aMCI/AD patterns match known tau pathology distribution, with uptake and clinical severity generally correlated. In PSP, retention is observed in relevant subcortical regions and brainstem, often prominent in the latter (Figure). Importantly, signal intensity correlates with clinical severity (PSPRS), a previously unreported finding. Uptake in a CBS case correlated with biopsy-confirmed tau.



Representative HC, AD and PSP (Richardson's Syndrome) scans.

Conclusion: APN-1607 merits clinical development; preliminary NADT findings extend 4R-tau model results. Further study in diverse tauopathies/clinical settings is planned.

Keywords: APN-1607, PET, PSP, tau, tauopathy

P150: Entorhinal cortical tau accumulation is inversely associated with hippocampal synaptic density in older individuals with normal cognition and early Alzheimer's disease

Adam Mecca¹, Ming-Kai Chen¹, Mika Naganawa¹, Takuya Toyonaga¹, Tyler Godek¹, Joanna Harris¹, Hugh Bartlett¹, Wenzhen Zhao¹, Jean-Dominique Gallezot¹, Nabeel Nabulsi¹, Yiyun Huang¹, Amy Arnsten¹, Richard Carson¹, Christopher van Dyck¹

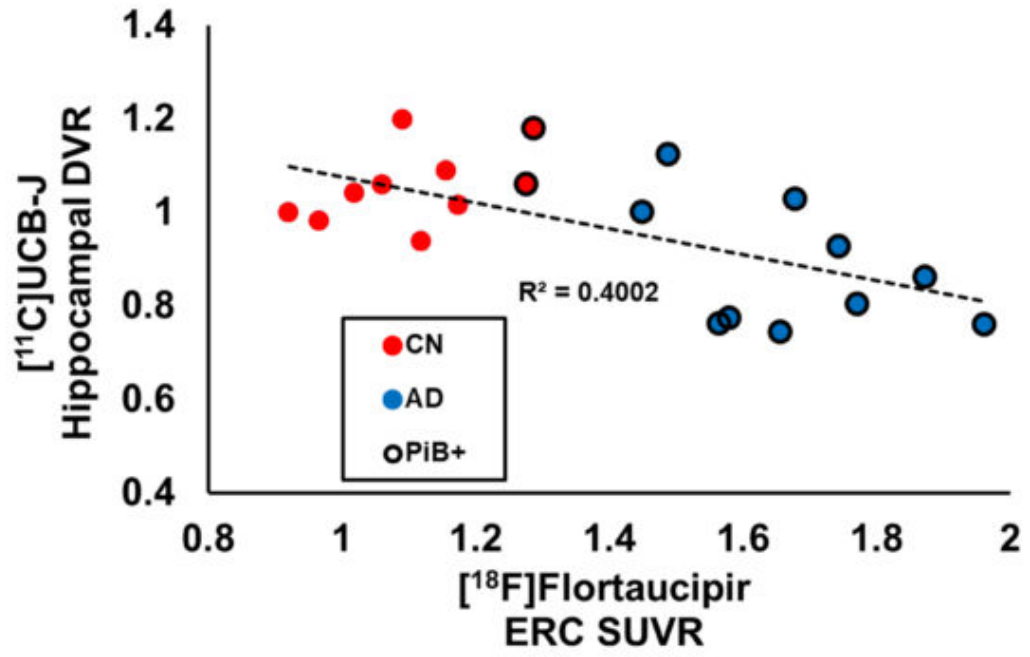
¹*Yale University School of Medicine, New Haven, CT, US*

Background: Synaptic loss is the major structural correlate of cognitive impairment in Alzheimer's disease (AD). Using [¹¹C]UCB-J-PET we have shown significant reductions in hippocampal SV2A specific binding as a marker of synaptic density in participants with AD, consistent with the early degeneration of entorhinal cortical (ERC) cells that project to hippocampus via the perforant path. We performed PET imaging with [¹⁸F]flortaucipir and [¹¹C]UCB-J and hypothesized that tau deposition in ERC would be inversely associated with synaptic density in hippocampus.

Methods: [¹¹C]UCB-J binding to SV2A and [¹⁸F]flortaucipir binding to tau were measured in 10 AD and 10 cognitively normal (CN) participants. [¹¹C]UCB-J distribution volume ratios (DVRs) were calculated using SRTM2 and a whole cerebellum reference region. [¹⁸F]Flortaucipir standardized uptake value ratios (SUVRs) were calculated using an inferior cerebellum reference region.

Results: AD participants (68.8±6.6 years, CDR=0.5-1.0) were all Aβ+ by [¹¹C]Pittsburgh Compound B ([¹¹C]PiB) PET and spanned the disease stages from amnesic Mild Cognitive Impairment (aMCI, n=5) to mild dementia (n=5). CN participants (72.1±7.9 years) were free of clinical symptoms (CDR=0); 8 were found to be Aβ- by [¹¹C]PiB PET, but 2 were Aβ+. AD compared to CN participants demonstrated significant reductions in hippocampal [¹¹C]UCB-J binding (AD DVR=0.88±0.13, CN DVR=1.06±0.08, p=0.002) and significant increases in ERC [¹⁸F]flortaucipir binding (CN SUVR=1.11±0.12, AD SUVR=1.68±0.16, p<0.00001). In the overall sample, ERC-tau was inversely associated with hippocampal synaptic density (r=-0.63, p=0.005, Figure 1).

Conclusions: Our results revealed higher ERC tau and lower hippocampal synaptic density in AD compared to CN participants. Consistent with our hypothesis, in the overall sample ERC tau accumulation was associated with lower hippocampal synaptic density. This inverse association may reflect synaptic failure due to tau pathology in ERC neurons projecting to the hippocampus. Further studies are needed to elucidate the relationship between tau accumulation and synaptic loss in AD.



Keywords: synaptic imaging, $[^{11}\text{C}]$ UCB-J, Alzheimer's disease, SV2A, PET

P151: Mental and physical activity during the uptake period affects off-target binding in extra- and within-brain Tau PET (18F-FTP)

Hoon-Ki (Paul) Min¹, Christopher Apgar¹, Nancy Scott¹, Haakon Hol¹, Emily Lundt¹, Sabrina Albertson¹, Christopher Schwarz¹, Hugo Botha¹, Prashanthi Vemuri¹, Jeffrey Gunter¹, Ronald Petersen¹, Clifford Jack¹, Val Lowe¹

¹Mayo Clinic, Rochester, MN, US

With tau PET imaging now available, there has been growing interest to accurately trace longitudinal tau changes in Alzheimer's Disease. Thus, identifying factors that cause unwanted PET signal variability is critical. Off-target tau PET(18F-FTP) signals both within and external to the brain have been observed, which might bleed into on-target tau regions. At the 2019 HAI, we presented preliminary results showing that walking and sleeping activity during the uptake period affects the extra-brain off-target tau signal(n=136). The current study of n=330 subjects confirms our initial results and reviews effects in within-brain areas. In our standard tau PET procedure, following ligand infusion, we release the participant during the uptake period. They may engage in various activities prior to scanning. We administered a questionnaire on uptake activities following their PET scan. The tau values of off-target extra- and within-brain areas were measured in SUV and SUVR units. Linear regression models were used to assess the relationship between the participant's activities and ligand distribution in brain and non-brain areas. Participants who reported 'sleep' during the uptake period had higher SUV values in oculomotor muscles and cortical bone/meninges, while participants who reported 'walking' had a lower uptake value in those areas (p<0.05). The effects of 'sleep' were related to time; the more sleep, the greater the off-target signal (p<0.05). For within-brain regions, only 'walking' was associated with decreased SUVR in the basal ganglia. Meta-ROI of on-target tau regions, WM reference regions and internal carotid artery (control area) was not affected by uptake activities. We have observed that certain activities during uptake: (1) affect extra-brain off-target tau signals; (2) affect within-brain off-target tau signals; and (3) do not affect within-brain on-target tau signals. Our results suggest implementing an uptake activity restriction protocol during tau PET that would help reduce extra- and within-brain off-target signal variability.

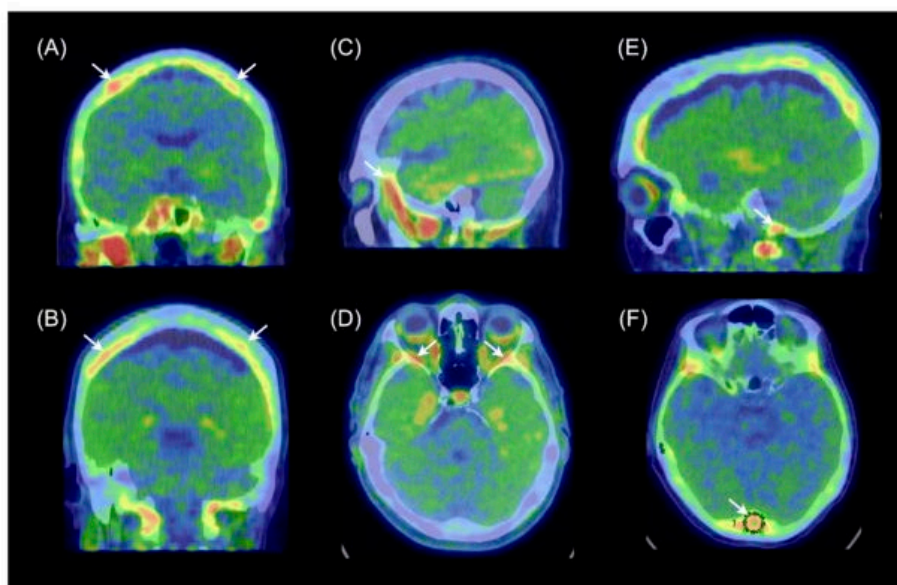


Figure 1. Examples of off-target tau PET signal outside of the brain, but close enough for possible bleed-in effects. (A,B) Upper Skull/Meninges, (C) Temporalis muscle, (D) Oculomotor muscles, (E) Base of Skull, (F) Occipital bone.

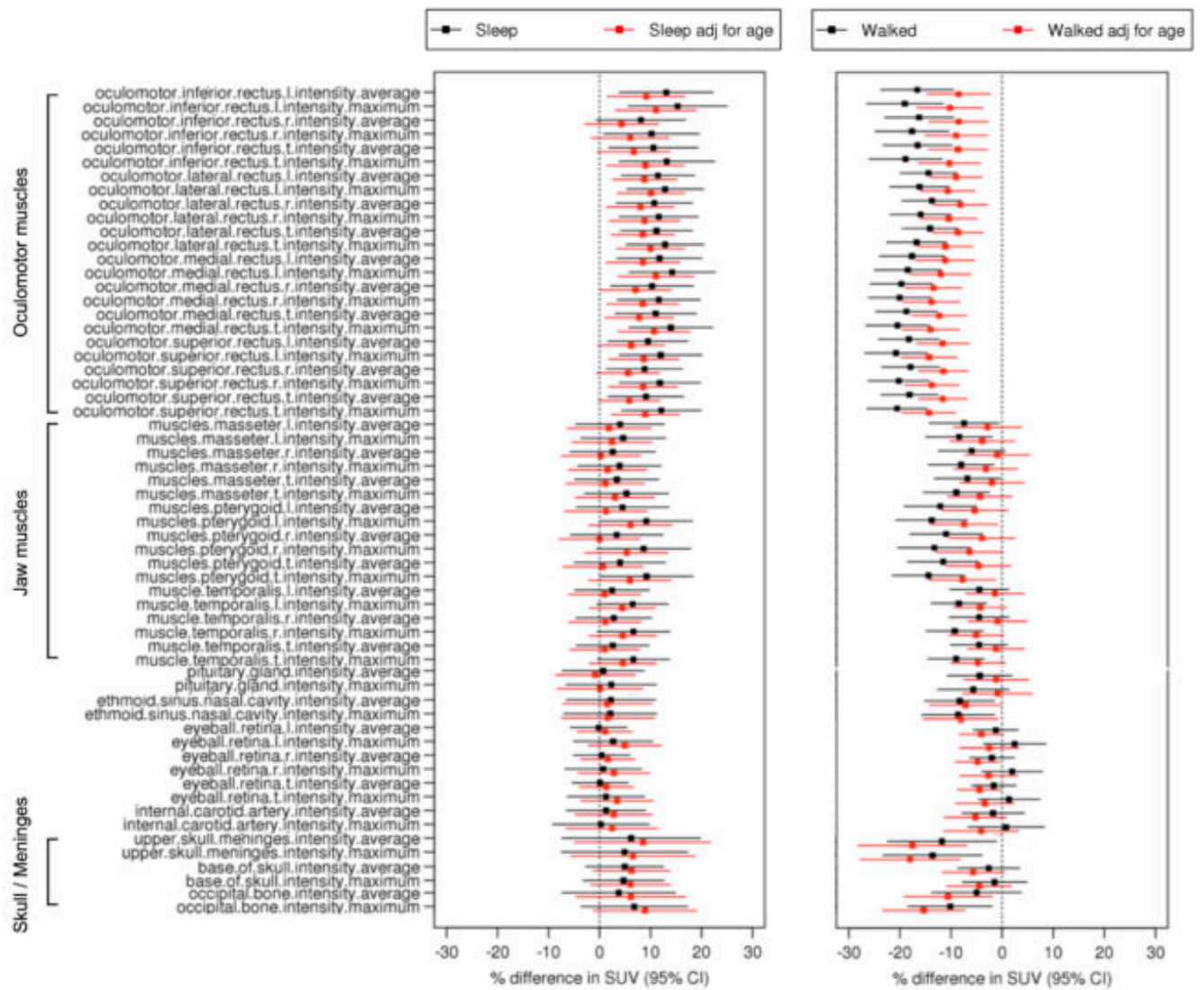


Figure 2. Extra-brain regions: Linear regression models (black) between extra-brain off-target tau SUVs and sleeping (yes/no) or walking (yes/no). Red lines show effects with age adjustment.

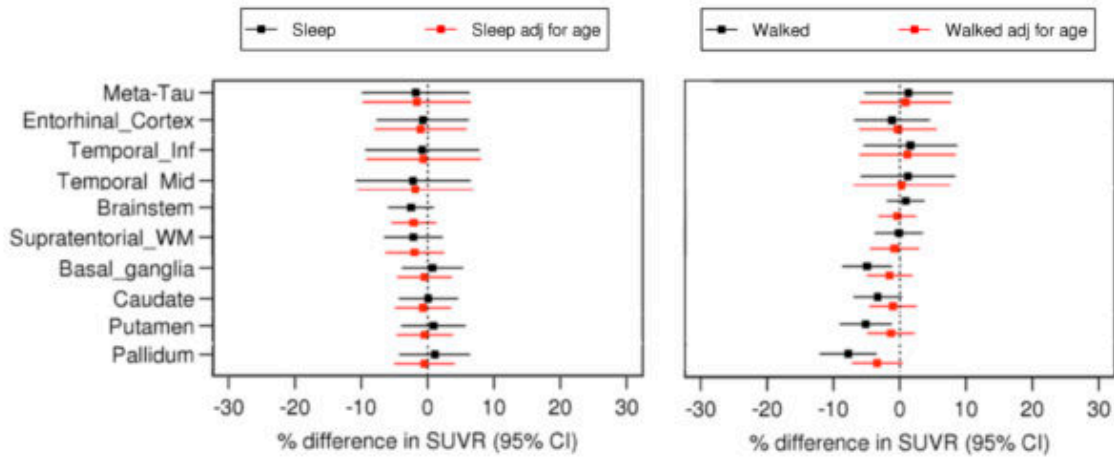


Figure 3. Within-brain regions: Linear regression models (black) between within-brain tau SUVRs and sleeping (yes/no) or walking (yes/no). Red lines show the effect with age adjustment.

Keywords: Tau, PET, Off-target, Sleep, Walk

P152: In vivo uptake of 18F-PM-PBB3 (18F-APN-1607) in patients with corticobasal syndrome

Yoshikazu Nakano¹, Hitoshi Shimada¹, Kenji Tagai¹, Kiwamu Matsuoka¹, Manabu Kubota¹, Keisuke Takahata¹, Yuhei Takado¹, Hitoshi Shinotoh^{1,2}, Yasuharu Yamamoto¹, Yasunori Sano¹, Chie Seki¹, Shigeki Hirano^{1,3}, Maiko Ono¹, Paul Tempest⁴, Ming-Kuei Jang⁴, Naruhiko Sahara¹, Kazunori Kawamura¹, Ming-Rong Zhang¹, Satoshi Kuwabara³, Makoto Higuchi¹

¹National Institute of Radiological Sciences, National Institutes for Quantum and Radiological Science and Technology, Chiba, Japan

²Neurology Clinic Chiba, Chiba, Japan

³Department of Neurology, Chiba University Graduate School of Medicine, Chiba, Japan

⁴APRINOIA Therapeutics Inc, Taipei, Taiwan

Objectives: Corticobasal syndrome (CBS) is a clinical syndrome based on diverse pathological backgrounds chiefly consisting of Alzheimer's disease (AD) and 4-repeat tauopathies such as corticobasal degeneration and progressive supranuclear palsy. Aims of the present study are 1) to estimate pathological background in CBS by PET scan with ¹⁸F-PM-PBB3 (¹⁸F-APN-1607), 2) to characterize the distribution of tau aggregates, and 3) to assess its correlation with clinical features in patients with CBS based on suspected non-AD tauopathy.

Methods: Seven patients diagnosed as CBS by Cambridge's criteria, and nine cognitively healthy controls (HCs) were recruited. The age and years of education matched between two groups. All participants underwent PET scans with ¹⁸F-PM-PBB3 and ¹¹C-PiB for estimating regional tau and A β deposition. Parametric PET images were generated by voxel-based calculation of standard uptake value ratio (SUVR) using the cerebellar cortex as a reference region. ¹⁸F-PM-PBB3 and ¹¹C-PiB uptake were judged positive or negative with visual assessment. Participants were classified as amyloid positive or negative ((A(-) or A(+)) by ¹¹C-PiB PET and tau positive or negative ((T(+)) or T(-)) by ¹⁸F-PM-PBB3 PET. As for A(-)T(+) CBS cases, ¹⁸F-PM-PBB3 SUVR were compared with HCs by voxel-base analysis.

Results: One of the seven CBS cases was amyloid positive, and another case was tau negative. ¹⁸F-PM-PBB3 accumulation in A(+) case was obviously higher than the other A(-)T(+) CBS cases. Five A(-)T(+) CBS cases had predominant symptoms in their right side limbs, and the voxel-base analysis showed higher accumulation in left globus pallidum and precentral gyrus, which are pathologically reported as areas of predilection for tau pathologies in CBD.

Conclusions: ¹⁸F-PM-PBB3 was able to track tau lesions in patients with CBS. Visual assessment of this ligand may be applicable to diagnose tauopathy one by one.

Keywords: CBS, CBD, 18F-PM-PBB3 (18F-APN-1670)

P153: Factors predicting tau PET status in cognitively unimpaired and impaired individuals

Rik Ossenkoppele¹, Antoine Leuzy¹, Hannah Cho³, Renaud La Joie², Olof Strandberg¹, Niklas Matsson¹, Sebastian Palmqvist¹, Chul Lyoo³, Gil Rabinovici², Ruben Smith¹, Oskar Hansson¹

¹Lund University, Lund, Sweden

²UCSF, San Francisco, CA, US

³Gangnam Severance Hospital, Seoul, Korea

Background: A substantial proportion of A β + patients with AD dementia and mild cognitive impairment (MCI) are tau PET-negative, while several individuals with normal cognition or a non-AD neurodegenerative disorder are tau PET-positive. We aimed to investigate which factors contribute to tau PET status in early to late Braak regions-of-interest (ROIs).

Methods: We included 1312 participants (457 cognitively normal, 189 A β + MCI, 296 A β + AD dementia and 370 non-AD neurodegenerative disorder) who underwent tau PET with either [¹⁸F]flortaucipir (n=676) or [¹⁸F]RO948 (n=702) at research centers in Sweden, South Korea and the USA. Cut-offs for tau-positivity were previously determined in Braak I-II, Braak I-IV and Braak V-VI ROIs using the mean+2*SD in older healthy controls for [¹⁸F]flortaucipir and the mean+2.5*SD in young healthy controls for [¹⁸F]RO948. To identify factors predicting tau status, we performed bivariate binary logistic regression models with tau-status in the Braak regions (+/-) as dependent variable and age, sex, apolipoprotein (APOE) ϵ 4 status, A β -status (only in analyses including controls and non-AD participants), MMSE and cortical thickness in an AD-signature region as predictors. Additionally, we performed multivariable binary logistic regression models to account for all other predictors in the same model.

Results: Participant characteristics are presented in Table-1.

Table 1. Participant characteristics

	A β -positive AD dementia	A β -positive MCI	Non-AD disorders	Cognitively unimpaired
N	296	189	370	457
Age	70.8 \pm 8.9	71.2 \pm 8.6	69.3 \pm 8.3	65.8 \pm 13.2
Sex, %male	42.9	52.3	58.1	43.3
MMSE	20.2 \pm 5.0	26.4 \pm 2.6	24.1 \pm 5.7	28.8 \pm 1.3
APOE ϵ 4+, %	57.8	59.3	22.4	39.4
A β +, %	100	100	25.4	30.2
[¹⁸ F]FTP/[¹⁸ F]RO948, n	179/117	83/106	254/116	160/297
Tau PET + Braak I/II, %	86.8	47.1	18.4	10.1
Tau PET + Braak I/IV, %	89.5	47.1	9.7	4.4
Tau PET + Braak V/VI, %	70.9	26.5	4.9	2.1
AD-signature thickness, mm ³	2.35 \pm 0.17	2.51 \pm 0.19	2.50 \pm 0.20	2.67 \pm 0.16

In A β + AD dementia, age (younger in Braak I-II and older in Braak I-IV and V-VI regions) and higher MMSE scores were associated with tau-negativity (Table-2). In A β + MCI, APOE ϵ 4 non-carriership and higher cortical thickness were associated with tau-negativity in Braak I-IV and V-VI regions (Table-2). In individuals with normal cognition and non-AD neurodegenerative disorders, presence of A β pathology, lower MMSE scores and reduced cortical thickness were the main predictors of tau-positivity across ROIs (Table-3).

Table 2. Factors contributing to T(au) status in A β + AD dementia and in A β + Mild cognitive impairment

A β + AD dementia						
	Braak I-II (T+ = 1, T- = 0)		Braak I-IV (T+ = 1, T- = 0)		Braak V-VI (T+ = 1, T- = 0)	
	OR (95% CI)	P	OR (95% CI)	P	OR (95% CI)	P
A. UNIVARIATE MODEL						
Age	1.04(1.01-1.07)	<0.001	0.90(0.85-0.95)	<0.001	0.88(0.85-0.95)	<0.001
Sex, % male	0.72(0.44-1.18)	0.188	0.90(0.43-1.93)	0.789	0.71(0.43-1.18)	0.188
APOE ϵ 4+, %	1.85(1.09-3.13)	0.023	2.57(1.14-5.97)	0.025	1.24(0.72-2.12)	0.430
MMSE	0.96(0.91-1.01)	0.169	0.80(0.72-0.89)	<0.001	0.90(0.85-0.95)	<0.001
Thickness	0.67(0.16-2.73)	0.577	0.67(0.16-2.73)	0.577	0.12(0.02-0.54)	0.007
B. MULTIVARIABLE MODEL						
Age	1.04(1.01-1.08)	0.006	0.88(0.82-0.94)	<0.001	0.87(0.83-0.91)	<0.001
Sex, % male	0.95(0.54-1.66)	0.845	1.32(0.53-3.40)	0.553	0.69(0.37-1.26)	0.227
APOE ϵ 4+, %	2.04(1.17-3.57)	0.012	2.44(1.00-6.10)	0.051	1.20(0.63-2.24)	0.579
MMSE	0.96(0.90-1.02)	0.212	0.79(0.68-0.91)	0.001	0.92(0.85-0.99)	0.033
Thickness	0.96(0.17-5.33)	0.964	0.18(0.00-3.43)	0.266	0.05(0.00-0.33)	0.003
Aβ+ Mild cognitive impairment						
	OR (95% CI)	P	OR (95% CI)	P	OR (95% CI)	P
A. UNIVARIATE MODEL						
Age	1.04(1.01-1.08)	0.028	1.01(0.97-1.04)	0.770	0.95(0.92-0.99)	0.013
Sex, % male	1.03(0.58-1.83)	0.911	0.67(0.38-1.20)	0.178	0.79(0.41-1.51)	0.470
APOE ϵ 4+, %	1.88(1.00-3.55)	0.050	1.86(0.99-3.56)	0.054	1.81(0.86-4.05)	0.132
MMSE	0.96(0.86-1.08)	0.525	0.87(0.78-0.98)	0.025	0.91(0.80-1.04)	0.153
Thickness	0.31(0.06-1.39)	0.131	0.31(0.07-1.39)	0.131	0.02(0.01-0.03)	<0.001
B. MULTIVARIABLE MODEL						
Age	1.03(0.99-1.07)	0.199	1.03(0.99-1.07)	0.051	0.88(0.83-0.93)	<0.001
Sex, % male	0.88(0.48-1.63)	0.693	0.88(0.48-1.63)	0.248	0.79(0.34-1.78)	0.571
APOE ϵ 4+, %	1.94(1.02-3.76)	0.047	1.94(1.02-3.76)	0.002	4.83(1.84-10.5)	0.002
MMSE	0.97(0.86-1.10)	0.634	0.97(0.86-1.10)	0.021	0.87(0.74-1.01)	0.077
Thickness	0.41(0.07-2.42)	0.331	0.41(0.072-4.2)	<0.001	0.09(0.00-0.38)	<0.001

Table 3. Factors contributing to T(au) status in non-AD neurodegenerative disorders and in cognitively normal individuals

Non-AD neurodegenerative disorders						
	Braak I-II (T+ = 1, T- = 0)		Braak I-IV (T+ = 1, T- = 0)		Braak V-VI (T+ = 1, T- = 0)	
	OR (95% CI)	P	OR (95% CI)	P	OR (95% CI)	P
A. UNIVARIATE MODEL						
Age	0.99(0.96-1.02)	0.481	1.09(1.04-1.14)	<0.001	1.07(1.00-1.14)	0.040
Sex, % male	1.38(0.81-2.42)	0.246	1.01(0.51-2.06)	0.977	1.47(0.56-4.30)	0.453
APOE ϵ 4+, %	0.97(0.48-1.89)	0.935	2.55(1.19-5.50)	0.016	1.92(0.65-5.55)	0.222
A β +, %	1.64(0.90-2.92)	0.099	18.3(7.34-55.6)	<0.001	21.8(5.99-140.5)	<0.001
MMSE	0.95(0.91-0.99)	0.026	0.89(0.85-0.94)	<0.001	0.91(0.85-0.98)	0.006
Thickness	0.19(0.05-0.68)	0.011	0.03(0.01-0.05)	<0.001	0.03(0.00-0.06)	<0.001
B. MULTIVARIABLE MODEL						
Age	0.95(0.91-0.97)	0.039	1.03(0.96-1.11)	0.413	0.95(0.86-1.04)	0.274
Sex, % male	2.08(1.01-4.50)	0.051	1.13(0.43-3.07)	0.813	1.28(0.36-4.93)	0.705
APOE ϵ 4+, %	0.68(0.30-1.47)	0.339	1.36(0.51-3.64)	0.542	0.75(0.20-2.68)	0.658
A β +, %	3.14(1.43-7.01)	0.004	17.5(5.34-80.2)	<0.001	36.3(5.80-700.3)	0.001
MMSE	0.93(0.87-0.99)	0.025	0.91(0.83-0.98)	0.018	0.95(0.86-1.06)	0.383
Thickness	0.14(0.03-0.78)	0.024	0.24(0.02-2.60)	0.235	0.06(0.00-1.10)	0.059
Cognitively normal individuals						
	OR (95% CI)	P	OR (95% CI)	P	OR (95% CI)	P
A. UNIVARIATE MODEL						
Age	1.06(1.03-1.09)	<0.001	1.06(1.02-1.12)	0.009	1.05(0.99-1.12)	0.117
Sex, % male	0.67(0.35-1.125)	0.220	0.55(0.19-1.39)	0.225	0.55(0.12-2.02)	0.396
APOE ϵ 4+, %	2.26(1.20-4.33)	0.012	4.81(1.83-15.0)	0.003	6.23(1.54-41.2)	0.022
A β +, %	5.87(3.10-11.6)	<0.001	14.80(4.86-64.2)	<0.001	9.75(2.41-65.2)	0.004
MMSE	0.87(0.71-1.08)	0.189	0.76(0.58-1.02)	0.051	0.63(0.44-0.92)	0.011
Thickness	0.01(0.00-0.02)	<0.001	0.01(0.00-0.02)	<0.001	0.03(0.02-0.04)	0.001
B. MULTIVARIABLE MODEL						
Age	1.01(0.98-1.05)	0.520	1.00(0.93-1.06)	0.938	0.98(0.54-1.08)	0.551
Sex, % male	0.66(0.32-1.33)	0.258	0.44(0.13-1.25)	0.141	0.44(0.08-1.91)	0.307
APOE ϵ 4+, %	1.53(0.74-3.21)	0.256	3.10(1.03-10.8)	0.055	4.20(0.88-3.10)	0.098
A β +, %	4.53(2.12-10.0)	<0.001	9.71(2.75-47.1)	0.001	7.14(1.33-5.94)	0.017
MMSE	0.98(0.77-1.28)	0.891	0.74(0.53-1.06)	0.088	0.58(0.37-0.92)	0.036
Thickness	0.02(0.00-1.34)	<0.001	0.03(0.00-0.09)	0.002	0.02(0.00-0.14)	0.007

Conclusion: We identified several demographic, clinical and neurobiological factors that are important to explain the variance seen in tau PET retention in MCI and AD.

Keywords: Tau status, flortaucipir, RO948, AD, non-AD

P154: Widespread amyloid is necessary to detect tau-PET signal beyond the entorhinal cortex and cognitive decline

Hazal Ozlen^{1,2}, Alexa Pichet Binette^{1,2,4}, Theresa Köbe^{1,2}, Pierre-Francois Meyer^{1,2,4}, Sylvia Villeneuve^{1,2,3,4}

¹Douglas Mental Health University Institute, Centre for Studies on the Prevention of Alzheimer's Disease (StoP-AD), Montréal, QC, Canada

²Department of Psychiatry, McGill University, Montréal, QC, Canada

³Department of Neurology and Neurosurgery, McGill University, Montréal, QC, Canada

⁴McGill Centre for Integrative Neuroscience, McGill University, Montréal, QC, Canada

Objective: The amount and the spatial distribution of A β -pathology necessary to detect elevated tau-PET signals are unknown. Given increasing evidence suggesting that subthreshold A β accumulation in older adults is biologically relevant, we sought to assess the amount and spread of A β burden needed to measure increased tau-PET signal and cognitive decline in asymptomatic individuals at risk of AD.

Methods: One hundred and twenty-nine cognitively unimpaired individuals with a family history of AD (PREVENT-AD cohort) underwent A β ([¹⁸F]NAV4694) and tau ([¹⁸F]AV1451) PET scans. We used Gaussian-mixture models to create region-specific thresholds of A β positivity in seven regions identified previously to be sensitive to early A β accumulation (Villeneuve et al, Brain, 2015). Individuals who were A β -positive in all regions were classified as the Widespread A β group; those who were positive in one or more regions were included in the Regional A β group, while the others were considered A β -negative. We compared the three groups' demographics, tau-PET binding (in five regions corresponding to Braak I to IV, Ossenkoppele et al., JAMA 2018), subjective memory complaint and baseline cognitive performance. Linear mixed-effects models also compared cognitive trajectories over up to seven years of assessments (Table 1).

Results: The Regional A β group had elevated tau-PET binding in the entorhinal cortex and middle temporal gyrus when compared with the A β -negative group (Fig. 1). The Widespread A β group had elevated tau PET signal compared with the two other groups across all five regions investigated. Only individuals with Widespread A β (and associated tau) showed a faster cognitive decline over time, while the other two groups did not decline or differed at baseline (Fig. 2).

Conclusions: Elevated tau-PET signal outside of the entorhinal cortex and measurable cognitive decline are detected when A β deposition is widespread across the cortex.

Table 1. Sample Demographics.

	Aβ Negative Group (n = 81)	Regional Aβ Group (n = 28)	Widespread Aβ Group (n = 20)	P<0.05
Age (Mean(SD))	63 (± 4.6)	63 (±3.8)	66 (±5.6)	b
Education (Mean(SD))	15.6 (±3.56)	14.7 (±2.75)	13.75 (±2.4)	
Gender (Female %)	74% (60/21)	82% (23/5)	65% (13/7)	
ApoE	27.16% (22/59)	64.29% (18/10)	65% (13/7)	a,b
Tau – Entorhinal (Mean(SD))	1.035(±0.10)	1.09(±0.13)	1.21(±0.17)	a,b,c
Tau – Inferior Temporal (Mean(SD))	1.13(±0.07)	1.18(±0.13)	1.29(±0.22)	b,c
ECoG Total Score (Mean(SD))	1.22(±0.23)	1.21(±0.18)	1.39(±0.30)	b,c
BL RBANS Total Score (Mean(SD))	105 (±12)	104.7 (±10.5)	99.35 (±10.7)	
BL RBANS Immediate Memory (Mean(SD))	105.2(±11.15)	109.1(±11.1)	103.9(±10.3)	
BL RBANS Delayed Memory (Mean(SD))	107.4(±9)	106.9(±7.9)	100.9(±12.6)	b
BL RBANS Attention (Mean(SD))	106(±14.7)	108.2(±16.6)	103.9(±14.6)	

Individuals were separated in three groups based on their amyloid status in seven regions: rostral anterior cingulate, precuneus, medial orbitofrontal, rostral middle frontal, inferior parietal, superior frontal, and posterior cingulate. APOE: Apolipoproteinε4; BL: Baseline; RBANS: Repeatable Battery for the Assessment of Neuropsychological Status; ECoG: Score on Everyday Cognition questionnaire assessing subjective cognitive complaint. a = p<0.05 between Aβ Negative and Regional Aβ Groups; b = sig. p<0.05 between Aβ Negative and Widespread Aβ Groups; c = sig. p<0.05 between Regional Aβ and Widespread Aβ Groups.

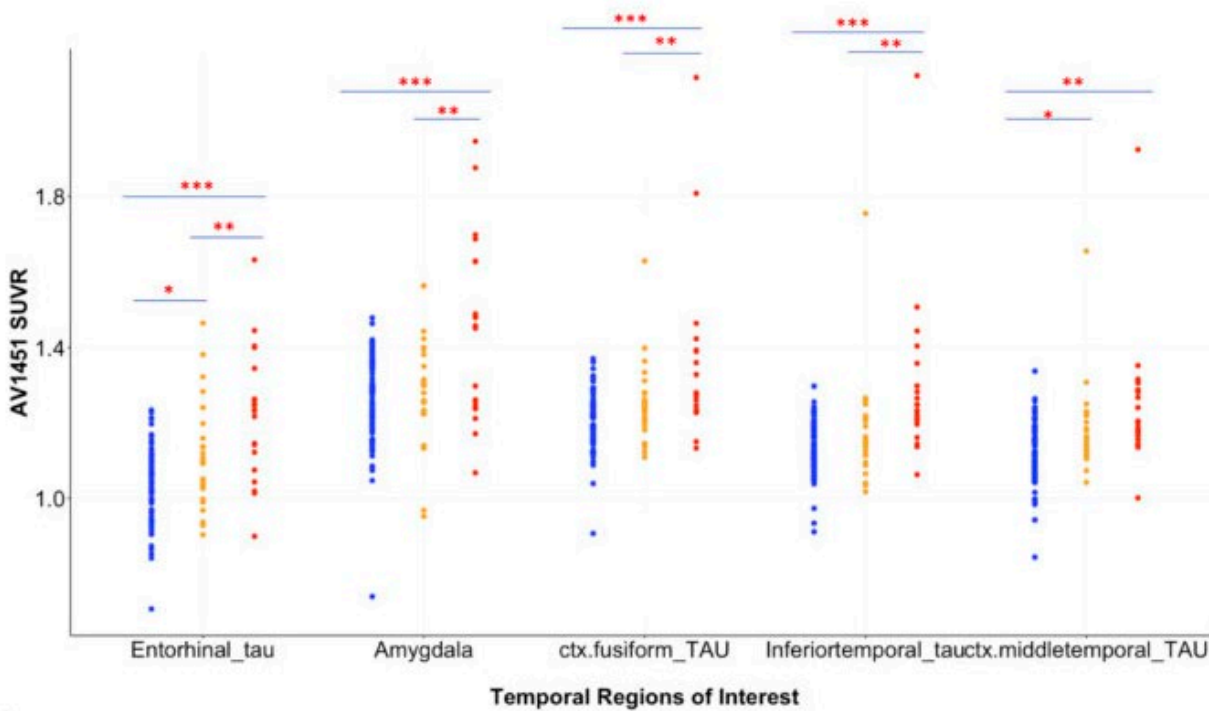


Figure 1. Regional tau-PET signal between the 3 Aβ groups

Five regions were chosen to represent Braak I to IV, Ossenkoppele et al., JAMA 2018. * p<0.05; ** p<0.01; ***p<0.001; etc. The Widespread Aβ group showed an increased uptake in all regions when compared with the two other groups.

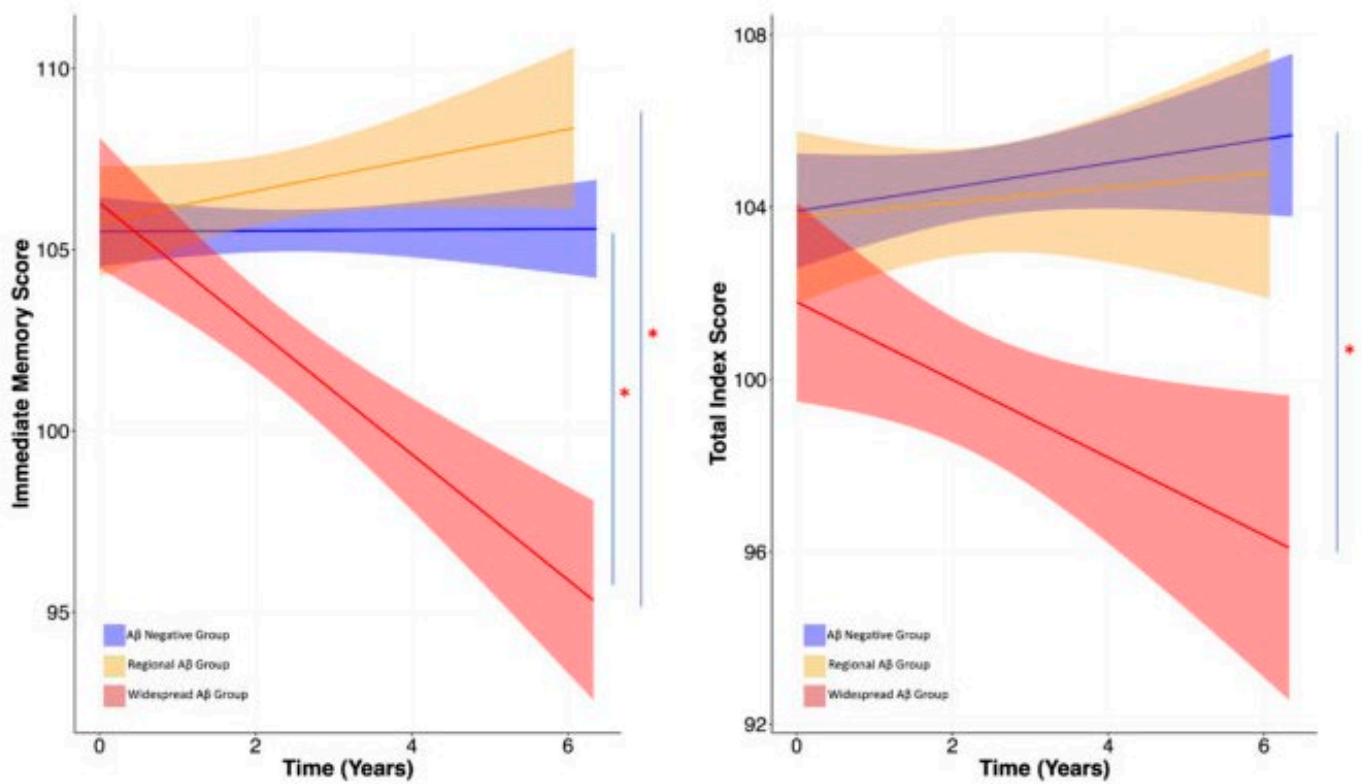


Figure 2. Change in Cognition Over Time Between the three A β Groups.

Cognitive test scores of “Total Score” and “Immediate Memory Score” on the RBANS over time in the three different groups. Statistics were obtained from linear mixed-effect models corrected for sex, education and apolipoprotein ϵ 4 status. * $p < 0.05$

Keywords: Preclinical AD, amyloid, tau, PET, Cognitive decline

P155: Using 18F-Flortaucipir visual assessment to define T-status in the AT(N) framework: evaluation of intra- and inter-rater reliability

Karine Provost¹, Leonardo Iaccarino¹, David Soleimani-Meigooni¹, Orit Lesman-Segev¹, Renaud La Joie¹, Lauren Edwards¹, Amelia Strom¹, Julie Pham¹, Taylor Mellinger¹, Mustafa Janabi², Suzanne Baker², William Jagust^{2,3}, Gil D. Rabinovici^{1,2,3,4}

¹Memory and Aging Center, Department of Neurology, University of California San Francisco, San Francisco, CA, US

²Lawrence Berkeley National Laboratory, Berkeley, CA, US

³Helen Wills Neuroscience Institute, University of California Berkeley, Berkeley, CA, US

⁴Department of Radiology and Biomedical Imaging, University of California San Francisco, San Francisco, CA, US

Objective: The amount and the spatial distribution of A β -pathology necessary to detect elevated tau-PET signals are unknown. Given increasing evidence suggesting that subthreshold A β accumulation in older adults is biologically relevant, we sought to assess the amount and spread of A β burden needed to measure increased tau-PET signal and cognitive decline in asymptomatic individuals at risk of AD.

Methods: One hundred and twenty-nine cognitively unimpaired individuals with a family history of AD (PREVENT-AD cohort) underwent A β ([¹⁸F]NAV4694) and tau ([¹⁸F]AV1451) PET scans. We used Gaussian-mixture models to create region-specific thresholds of A β positivity in seven regions identified previously to be sensitive to early A β accumulation (Villeneuve et al, Brain, 2015). Individuals who were A β -positive in all regions were classified as the Widespread A β group; those who were positive in one or more regions were included in the Regional A β group, while the others were considered A β -negative. We compared the three groups' demographics, tau-PET binding (in five regions corresponding to Braak I to IV, Ossenkoppele et al., JAMA 2018), subjective memory complaint and baseline cognitive performance. Linear mixed-effects models also compared cognitive trajectories over up to seven years of assessments (Table 1).

Results: The Regional A β group had elevated tau-PET binding in the entorhinal cortex and middle temporal gyrus when compared with the A β -negative group (Fig. 1). The Widespread A β group had elevated tau PET signal compared with the two other groups across all five regions investigated. Only individuals with Widespread A β (and associated tau) showed a faster cognitive decline over time, while the other two groups did not decline or differed at baseline (Fig. 2).

Conclusions: Elevated tau-PET signal outside of the entorhinal cortex and measurable cognitive decline are detected when A β deposition is widespread across the cortex.

	UCSF (n=99)	ADNI (n=180)
Age (mean)	62.8 y	72.6 y
Sex	49 M / 50 F	76 M / 104 F
Education (mean)	16.9 y	16.3 y
MMSE (mean)	22.8	27.7
Amyloid status	64 A β + / 35 A β -	85 A β + / 95 A β -
Clinical diagnosis		
CN	0	80
MCI	11	84
AD	50	16
Non-AD	38	0

Table 1. Patient characteristics

AD: Alzheimer's disease dementia, MCI: mild cognitive impairment, non-AD: non-AD dementia, CN: cognitively normal


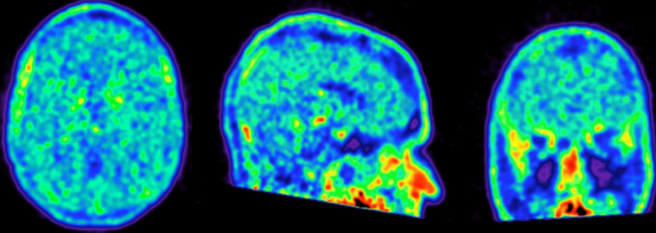
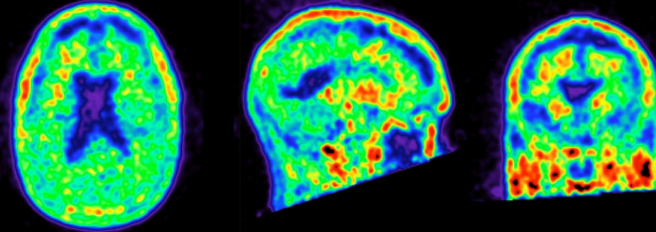
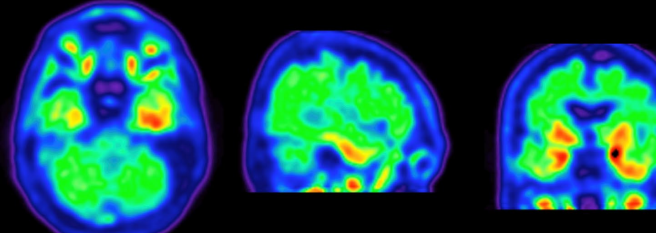
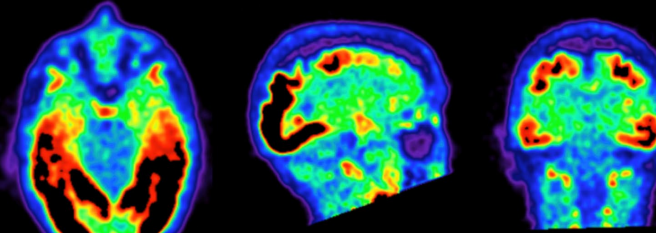
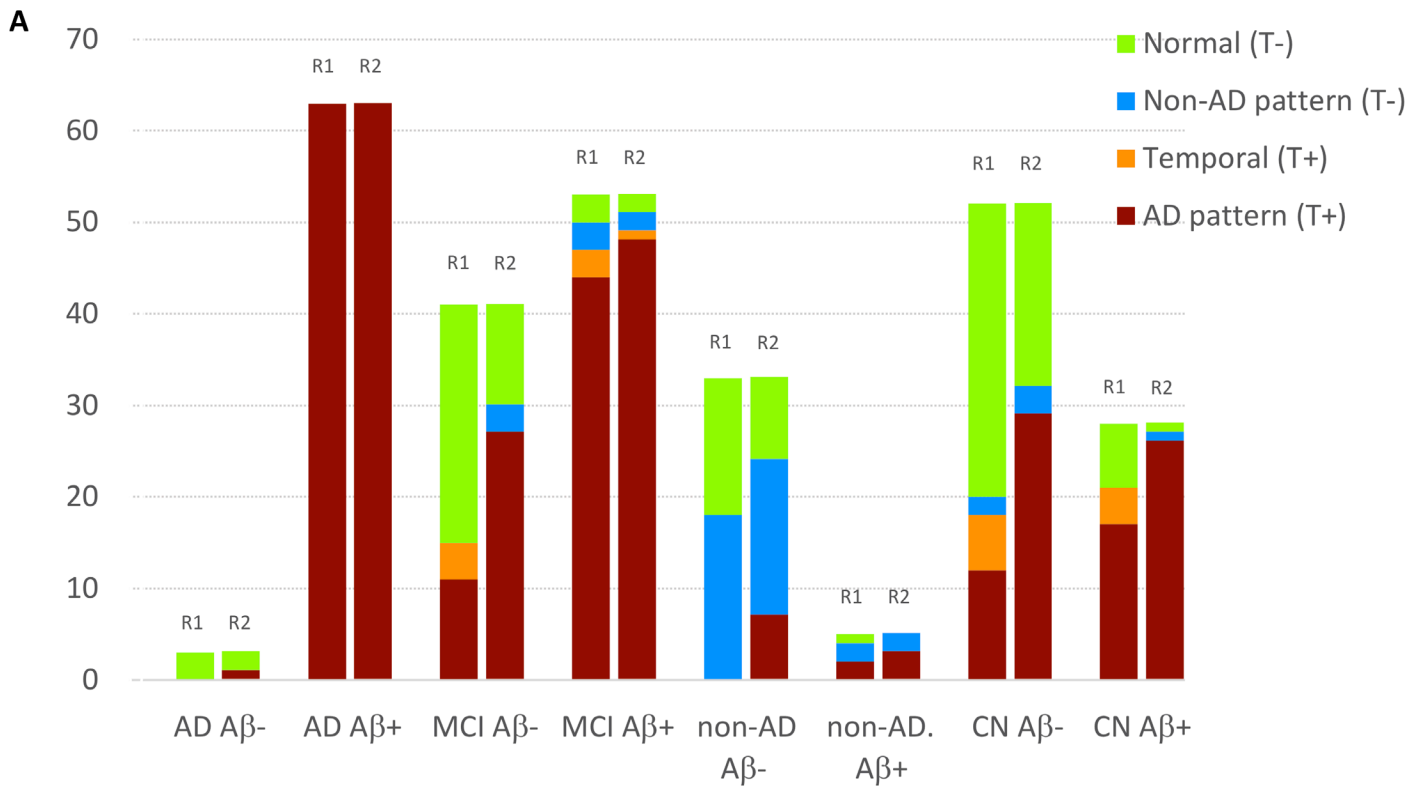
Patterns	Example 	T-status
Normal Scan		T -
Non-AD-like pattern (abnormal scan, but distribution inconsistent with AD pathology)		
Mild Temporal Binding		T +
AD-like pattern (extending beyond temporal lobes)		

Figure 1. ¹⁸F-Flortaucipir pattern of binding to define T-status

Raters assigned one of four patterns to each ¹⁸F-Flortaucipir Tau PET after blinded visual assessment. The four patterns are based on previous work from our group (Sonni et al. *in preparation*). Images were scaled manually based on cerebellar gray matter. Normal and non-AD like patterns were defined as T-negative, while mild temporal binding and AD-like patterns were defined as T-positive.



B

	UCSF κ (95%CI)	ADNI κ (95%CI)
All	0.82 (0.71-0.94)	0.59 (0.48-0.71)
CN		0.55 (0.39-0.72)
MCI	1.00 (1.00-1.00)	0.61 (0.43-0.78)
AD	1.00 (1.00-1.00)	0.94*
Non-AD	0.27 (0.11-0.43)	
A β +	0.85 (0.56-1.00)	0.55 (0.27-0.84)
A β -	0.80*	0.49 (0.34-0.63)

Figure 2. A Assigned pattern of binding by clinical diagnosis and amyloid status (reader 1, R1 and reader 2, R2). **B** Inter-rater reliability by clinical diagnosis and amyloid status. *Absolute percent agreement is shown (constant, kappa cannot be computed). AD: Alzheimer's disease dementia, MCI: mild cognitive impairment, non-AD: non-AD dementia, CN: cognitively normal

Keywords: Tau PET, Tau imaging, Flortaucipir, Alzheimer's disease, biomarkers

P156: Defining T-status in the AT(N) framework: comparison of ¹⁸F-Flortaucipir visual assessment, SUVR quantification and CSF pTau

Karine Provost¹, Leonardo Iaccarino¹, David Soleimani-Meigooni¹, Orit Lesman-Segev¹, Renaud La Joie¹, Niklas Mattsson², Oskar Hansson², Udo Eichenlaub³, Lauren Edwards¹, Amelia Strom¹, Julie Pham¹, Taylor Mellinger¹, Mustafa Janabi⁴, Suzanne Baker⁴, William Jagust^{4,5}, Gil Rabinovici^{1,4,5,6}

¹*Memory and Aging Center, Department of Neurology, University of California San Francisco, San Francisco, CA, US*

²*Clinical Memory Research Unit, Lund University, Lund, Sweden*

³*Roche Diagnostics GmbH, Penzberg, Germany*

⁴*Lawrence Berkeley National Laboratory, Berkeley, CA, US*

⁵*Helen Wills Neuroscience Institute, University of California Berkeley, Berkeley, CA, US*

⁶*Department of Radiology and Biomedical Imaging, University of California San Francisco, San Francisco, CA, US*

Objectives: To compare T-status derived from ¹⁸F-Flortaucipir PET visual assessment, ¹⁸F-Flortaucipir SUVR quantification, and CSF pTau.

Methods: We included participants from two cohorts (UCSF n=99, ADNI n=179, Table 1) with clinical diagnoses of MCI (n=94, 53 Aβ+), Alzheimer's disease (AD) dementia (n=66, 63 Aβ+), non-AD disorders (n=38, 5 Aβ+), and cognitively normal controls (n= 80, 28 Aβ+) who underwent ¹⁸F-Flortaucipir PET (80-100 minutes post injection) and CSF analysis within 1 year. Amyloid-PET was used to define amyloid status. T-status was derived from ¹⁸F-Flortaucipir consensus blinded visual assessment based on *a priori* criteria and from a temporal meta-ROI SUVR using previously validated thresholds (SUVR 1.27, SUVR 1.20). T-status for CSF pTau (Roche Elecsys) was derived using ROC-based thresholds, obtained comparing amyloid-positive AD/MCI vs. amyloid-negative healthy controls (pTau>22.0, pTau>22.2).

Results: Overall agreement between the 3 classification criteria ranged from 63% to 95% (Figure 1). T+ was assigned in 96%, 92% and 79% of AD patients using ¹⁸F-Flortaucipir visual assessment, SUVR quantification and CSF pTau respectively; vs. 68%, 49% and 61% in MCI; 11%, 11% and 21% in non-AD; and 54%, 33% and 36% in CN. Using amyloid-positive AD/MCI as gold standard, sensitivity was highest with ¹⁸F-Flortaucipir visual assessment, while specificity was highest applying SUVR thresholds (Figure 2). In a subset of patients with autopsy (n=11), T-status derived from ¹⁸F-Flortaucipir visual assessment had an accuracy of 100% for intermediate-to-high ADNC, compared to 82% for SUVR quantification and 64% for CSF pTau. Patients with concordant T-status across modalities were significantly younger, had higher CSF pTau values, higher ¹⁸F-Flortaucipir SUVR values, and were more likely to be amyloid positive.

Conclusions: Concordance of T-status derived from CSF pTau, ¹⁸F-Flortaucipir visual assessment and SUVR quantification is stage dependent. ¹⁸F-Flortaucipir visual assessment increases sensitivity, while SUVR thresholds maximize specificity.

	UCSF (n=99)	ADNI (n=179)			
Age (y; mean, SD)	62.8 (8.4)	72.7 (8.1)			
Sex	49 M / 50 F	76 M / 103 F			
Education (y; mean, SD)	16.9 (3.7)	16.3 (2.5)			
MMSE (mean, SD)	22.8 (6.2)	27.7 (2.7)			
Amyloid status	64 A β + / 35 A β -	85 A β + / 94 A β -	T+ <i>¹⁸F-FTP visual</i>	T+ <i>¹⁸F-FTP SUVR</i>	T+ <i>CSF pTau</i>
Clinical diagnosis					
CN	0	80	54%	33%	36%
CN, A β -	0	52	38%	17%	25%
CN, A β +	0	28	82%	61%	57%
MCI	11	83	68%	49%	61%
AD	50	16	96%	92%	79%
Non-AD	38	0	11%	11%	21%

Table 1. Patient characteristics and T-status by modality and diagnosis

AD: Alzheimer’s disease dementia, MCI: mild cognitive impairment, non-AD: non-AD dementia, CN: cognitively normal

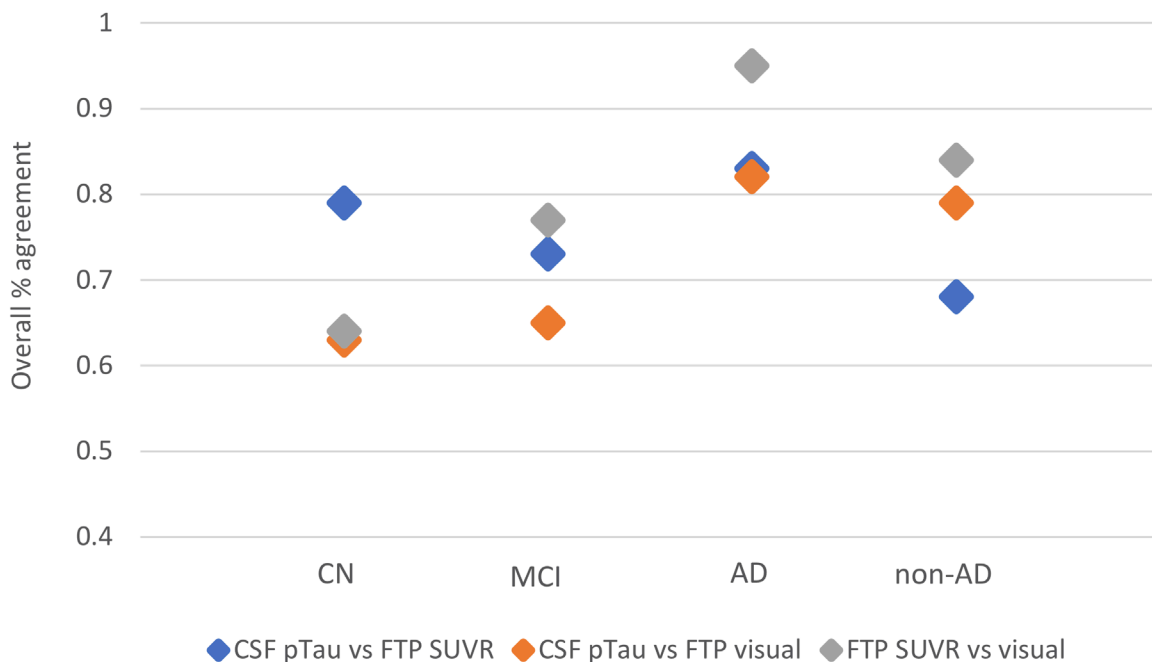
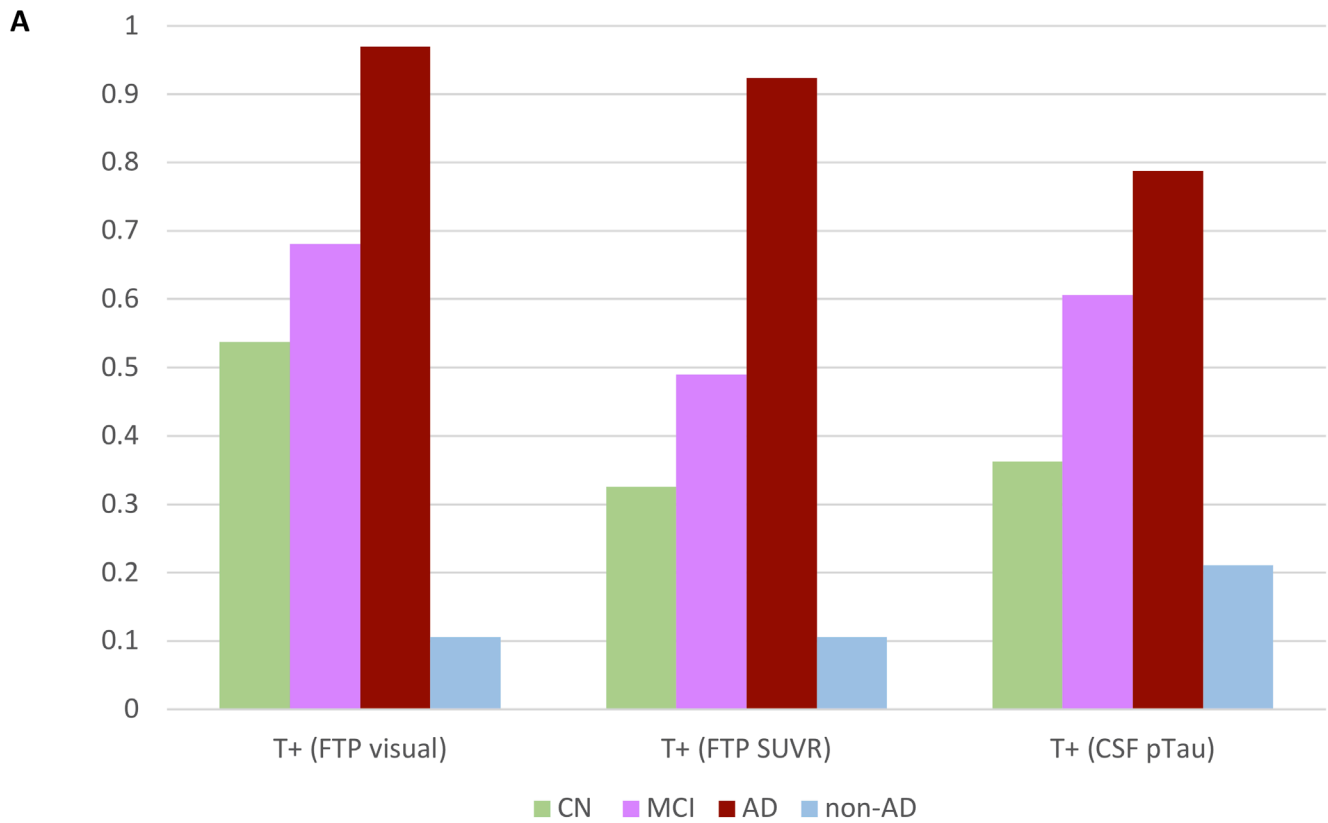


Figure 1. Inter-modality overall percent agreement between modalities by cohort and clinical diagnosis

CN: cognitively normal controls, MCI: mild cognitive impairment, AD: Alzheimer’s disease dementia, non-AD: non-AD dementia, FTP: Flortaucipir



B

	FTP visual assessment	FTP SUVR quantification	CSF pTau
Sensitivity (95%CI)	0.95 (0.89-0.98)	0.89 (0.82-0.94)	0.82 (0.74-0.88)
Specificity (95%CI)	0.60 (0.52-0.68)	0.79 (0.72-0.85)	0.69 (0.61-0.76)

Figure 2. A Proportion of assigned T-status by clinical diagnosis and modality.

B Sensitivity and specificity by modality (using amyloid-positive AD/MCI as gold standard)

AD: Alzheimer's disease dementia, MCI: mild cognitive impairment, non-AD: non-AD dementia, CN: cognitively normal controls, FTP: Flortaucipir

Keywords: Tau PET, Flortaucipir, Alzheimer's disease, biomarkers, CSF

P157: Plasma neurofilament light is associated with regional tau tangle burden in autosomal dominant Alzheimer's disease: findings from the COLBOS Project

Yakeel T. Quiroz¹, Henrik Zetterberg², Eric Reiman³, Justin Sanchez¹, Edmarie Guzman-Velez¹, Josh Fox-Fuller¹, Joseph Arboleda-Velasquez⁵, Ana Baena⁴, Jennifer Gatchel¹, Reisa Sperling⁶, Keith Johnson¹, Kaj Blennow², Francisco Lopera⁴

¹Massachusetts General Hospital, Charlestown, MA, US

²Clinical Neurochemistry Laboratory, Sahlgrenska University Hospital, Mölndal, Sweden, Mölndal, Sweden

³Banner Alzheimer's Institute, Phoenix, AZ, US

⁴Universidad de Antioquia, Medellin, CO

⁵Schepens Eye Research Institute, Boston, MA, US

⁶Brigham and Women's Hospital, Boston, MA, US

Background: Neurofilament light (NfL) is a promising biomarker of neuronal degeneration. We recently characterized the associations among plasma NfL, age and cognitive decline in over 2,000 members of the Colombian kindred with autosomal dominant Alzheimer's disease, and reported that NfL distinguished carriers from non-carriers 22 years before their median age at clinical onset of 44. Here we investigated the associations among NfL, hippocampal volume, brain pathology and memory in individuals from the same kindred.

Methods: We examined cross-sectional (n = 45, 24 carriers) and longitudinal (n = 19, 9 carriers) measures in non-demented PSEN1 mutation carriers and non-carriers (mean age: 38 years). Participants underwent tau (18F-Flortaucipir) and amyloid (PiB) PET imaging, MRI, blood sampling and cognitive testing. We measured associations among baseline NfL and hippocampal volume, brain pathology and memory; and longitudinal change in brain pathology over 2 years.

Results: Compared to non-carriers, carriers had higher baseline plasma NfL concentrations (carriers: 9.01 +/- 3.98; non-carriers: 4.79 +/- 2.13 pg/ml), and greater levels of baseline brain pathology (p<0.001). Higher baseline NfL concentrations were associated with lower hippocampal volume (r=-0.35, p=0.01), greater amyloid (r=0.58, p<0.001) and regional tau burden (entorhinal: r=0.44, p=0.02; inferior temporal: r=0.35, p=0.01; precuneus: r=0.53, p=0.001), and lower cognitive scores (e.g. MMSE: r=-0.49, p<0.001; CERAD Word List Recall: r=-0.59, p<0.001). Longitudinally, higher baseline NfL was associated with greater annual tau burden in inferior temporal lobe (r=0.57, p=0.01). Associations between NfL and tau pathology did not remain significant after adjusting by baseline amyloid or age. Associations between NfL and cognitive measures remained significant, even after those adjustments.

Conclusion: These findings provide support of the value of NfL as a blood biomarker for AD-related neurodegeneration, pathology and cognitive decline in individuals at risk to develop Alzheimer's disease. They also further support plasma NfL as a useful method for tracking disease progression.

Keywords: NfL, tau PET, PiB, cognition, autosomal-dominant Alzheimer's disease

P158: Application of tau PET as a biomarker of Alzheimer's disease in therapeutic trials: A pharmaceutical industry perspective

Cristian Salinas¹, Talakad Lohith², Qi Guo³, Dustin Wooten³, Thom Tulip⁴, Sulantha Sanjeeva⁴, Robert Comley³, Cyrille Sur², Eric Hostetler², John Beaver¹, Laurent Martarello¹

¹*Biogen Inc., Cambridge, MA, US*

²*Merck & Co., Inc., West Point, PA, US*

³*AbbVie Inc., North Chicago, IL, US*

⁴*Cerveau Technologies Inc., Knoxville, TN, US*

The success of tau PET as a biomarker of Alzheimer's disease (AD) in the context of a therapeutic trial entitles addressing specific objectives by using quantitative endpoints that can be applied with a sense of practicality and have a strong connection to the relevant biological pathways and mechanism of action. Patient selection, stratification (e.g. to predict disease progression) and response to treatment as it relates to drug-target engagement and therapeutic effect are critical elements supporting the design and decision-making process of therapeutic AD trials. Tau PET is expected to play a fundamental role in these objectives and alignment within the pharmaceutical industry is desirable. In 2018, Biogen, Merck, AbbVie and Cerveau Technologies started a pre-competitive collaboration to explore analytical methodologies that effectively make use of [¹⁸F]MK-6240, a second-generation tau PET tracer, in AD clinical trials. Specifically, assessment of tau positivity, tau burden (signal intensity), and tau spread are being investigated. Additionally, formation and harmonization of a collaborative imaging database with contributions from pharma and academia has played an important role and provided an indispensable resource in the ability to explore, develop and apply fit-for-purpose methodologies.

Herein, we share an initial perspective from a sub-set of pharma partners on tau PET analysis seeking feedback to refine our views and align our approaches with the wider tau imaging community in the hope that it will produce a significant and valuable impact in the development of therapies that are intended to change the course of AD.

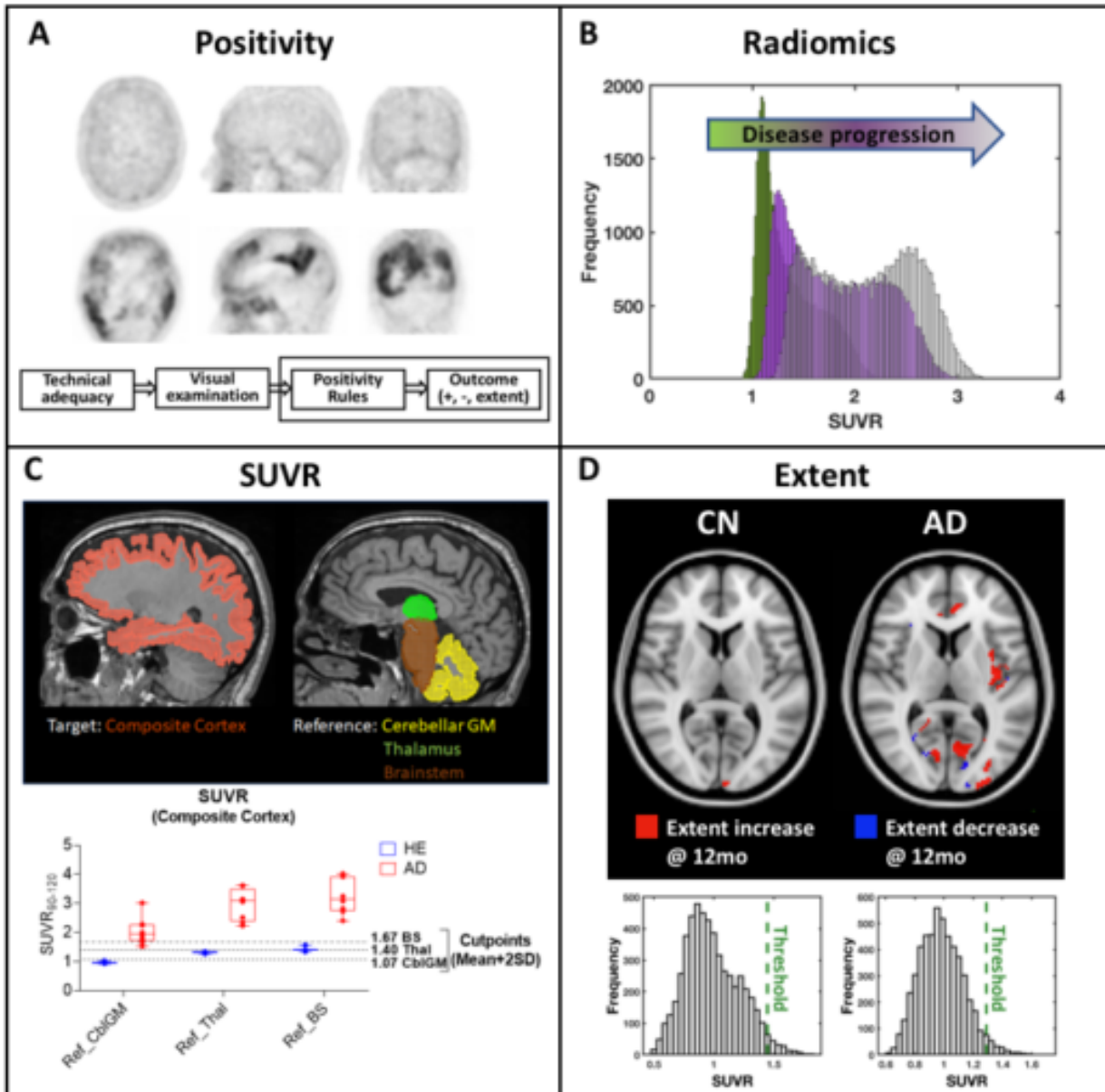


Figure : **A)** Determination of tau PET positivity will play a fundamental role in the design of future AD clinical trials. **B)** Changes in the histogram derived from an AD signature region in a patient as disease progresses. Histogram based radiomic features have the potential to be used to measure spread of tau. **C)** Target and reference region considerations for quantifying SUVR. Composite cortical SUVR magnitude in AD and cutoffs based on healthy amyloid negative (HE) individuals highest in brainstem among 3 chosen reference regions. Impact of different reference regions on AD signal change in longitudinal scans needs further exploration. **D)** Extent, defined as the fraction of voxels above a threshold, is an exploratory metric intended to assess the spread of tau pathology. In the example, the extent difference between baseline and 12 months is highlighted for a cognitively normal (CN) subject and one with AD.

Keywords: Tau PET, Alzheimer's Disease, MK-6240, Quantification, Pharmaceutical Industry

P159: Measuring increases of tau pathology in Alzheimer's disease using [18F]GTP1 (Genentech tau probe 1) PET imaging

Sandra Sanabria Bohorquez¹, Suzanne Baker^{1,2}, Paul Manser¹, Balazs Toth¹, Edmond Teng¹, Jan Marik¹, Robby Weimer¹

¹*Genentech, Inc., South San Francisco, CA, US*

²*Molecular Biophysics and Integrated Bioimaging, Lawrence Berkeley National Laboratory, Berkeley, CA, US*

Objective: To quantify tau burden change using [18F]GTP1 SUVR and Extent in Alzheimer's disease (AD).

Methods: [18F]GTP1 imaging was performed at baseline, 6, 12 and 18 months in amyloid negative and positive cognitive normal subjects (CN; n=2 and 7, respectively), and amyloid positive prodromal (Prod; n=24; MMSE 24-30, CDR = 0.5) and mild/moderate (MM; n=30; MMSE 22-30, CDR = 0.5-2) AD subjects. SUVR and Extent were calculated using the cerebellum gray. For each scan, a voxelwise tau positivity threshold was defined as the average uptake in the cerebellum plus 2 standard deviations. Global measurements were performed in the whole cortical gray matter (CG), and regionally, in the *in vivo* Braak regions. SUVR and Extent vs. time were assumed to be linear and the annualized percentage change (APC) was calculated using simple linear regression.

Results: Figures shows baseline measurements, the average APC ($\pm 95\%$ CI) and example images of tau burden change. Tau burden increased globally and regionally in prodromal and MM groups but not in CN. In AD, the average GM SUVR and Extent APC ($\pm 95\%$ CI) were $2.8 \pm 1.2\%$ and $6.2 \pm 2.4\%$, respectively. Prodromal subjects displayed similar increases in SUVR and Extent across Braak regions (1.9-3.0% and 5.7-7.9%, respectively). In MM subjects, no SUVR and Extent increases were observed in Braak 1/2, but increases of $2.9 \pm 2.1\%$ and $3.2 \pm 2.1\%$ in the SUVR APR, and of $4.6 \pm 3.4\%$ and $6.9 \pm 3.8\%$ in the Extent APR were observed in Braak 3/4 and 5/6, respectively. Overall, the APC variance relative to the mean rates were similar for SUVR and Extent.

Conclusion: Similar global tau burden increases were observed in the AD groups but there were regional differences between prodromal and MM subjects. Results support further investigation of Extent to assess AD tau pathology change in observational and interventional studies.

Figure 1. [^{18}F]GTP1 SUVR and Extent in GM and Braak ROIs. MM: red; Prod: blue; CN: black.

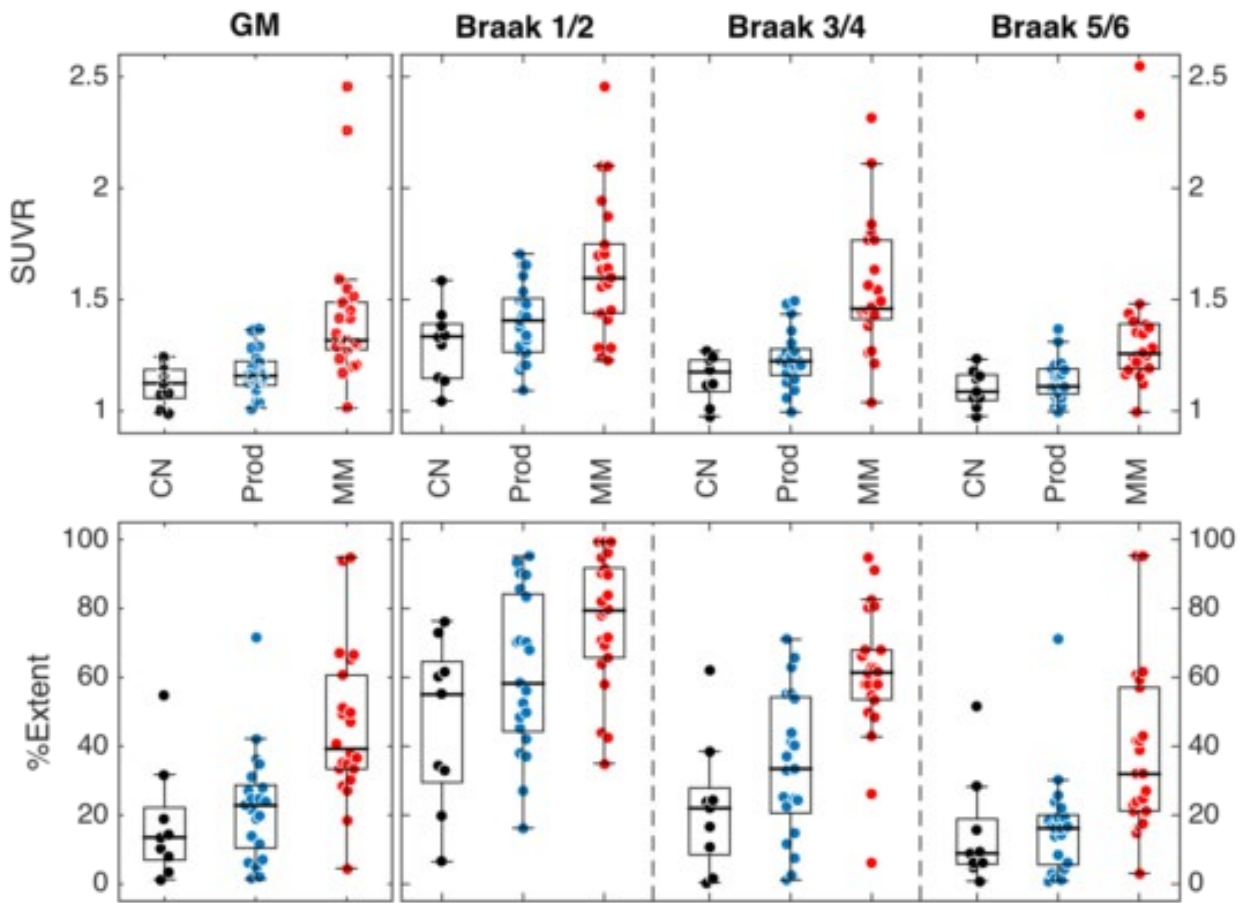


Figure 2. Measured average SUVR (top) and Extent (bottom) annualized percentage change and their corresponding 95% confidence intervals in GM and Braak ROIs. MM: red; Prod: blue; CN: black.

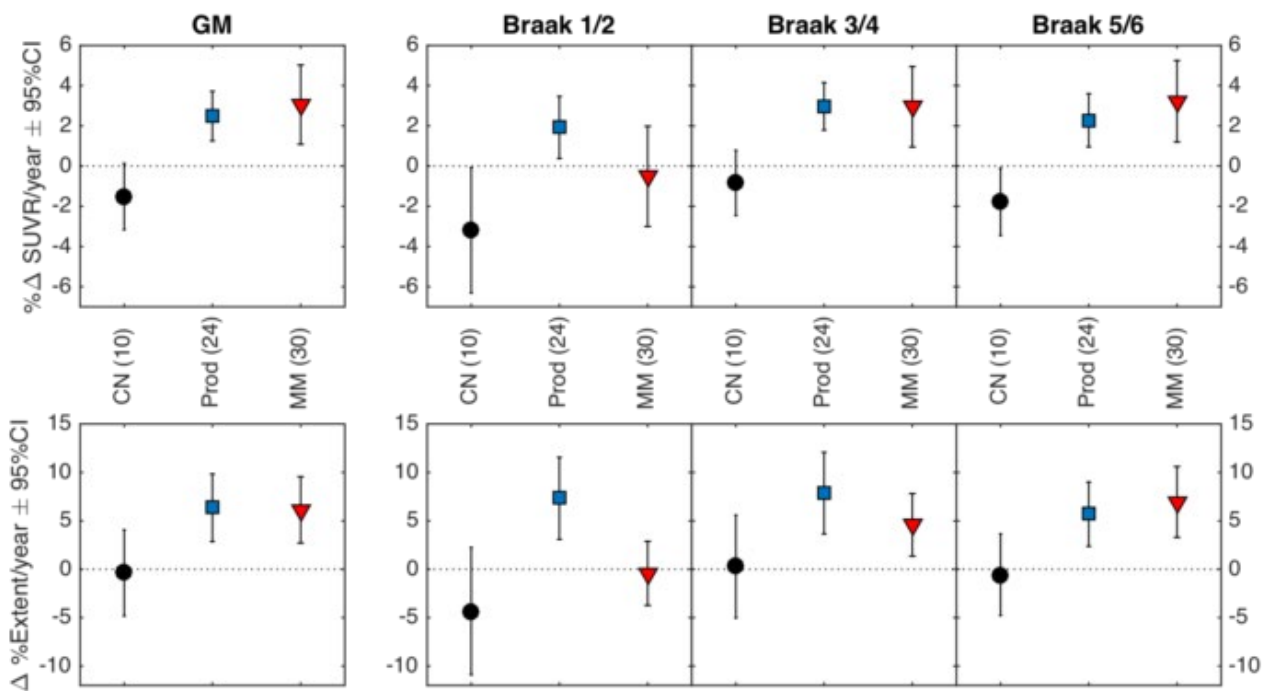
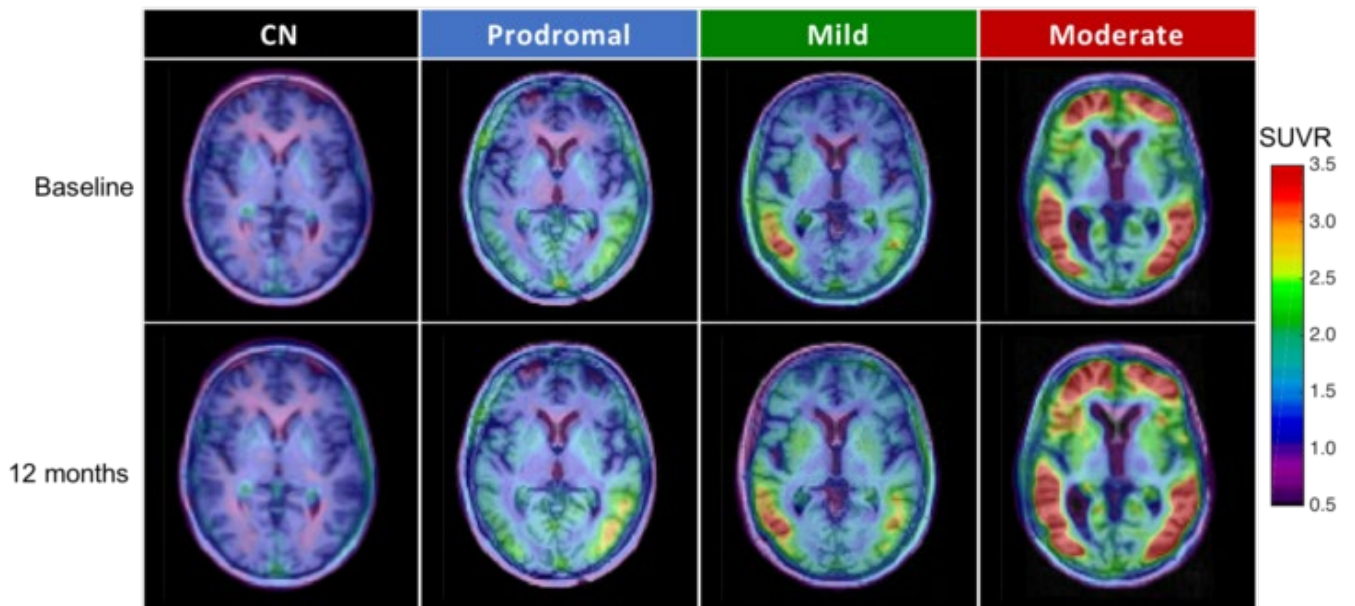


Figure 3. Individual examples of longitudinal tau burden change over 12 months



Keywords: Tau PET, [18F]GTP1, longitudinal study, SUVR, Extent

P160: Evaluation of tau PET staging in the A4/LEARN study

Justin Sanchez¹, Alex Becker¹, Heidi Jacobs^{1,3}, Bernard Hanseeuw^{1,4}, Danielle Mayblyum¹, Zoe Rubinstein¹, Emma Thibault¹, Aaron Schultz¹, Sudha Seshadri^{5,6}, Yakeel Quiroz¹, Dorene Rentz^{1,2}, Julie Price¹, Reisa Sperling^{1,2}, Keith Johnson^{1,2}, on behalf of the A4 Study Team²

¹Massachusetts General Hospital, Boston, MA, US

²Brigham and Women's Hospital, Boston, MA, US

³Maastricht University, Maastricht, The Netherlands

⁴Université Catholique de Louvain, Brussels, Belgium

⁵Boston University School of Medicine, Boston, MA, US

⁶The Framingham Heart Study, Framingham, MA, US

⁷University of Texas, San Antonio, San Antonio, TX, US

⁸Grupo de Neurociencias, Universidad de Antioquia, Antioquia, CO

Introduction: The spatiotemporal progression of cortical tauopathy, as implied by autopsy studies, proceeds from medial temporal lobe (MTL) to temporal neocortex and then to extra-temporal neocortex, in association with rising levels of amyloid-beta ($\text{a}\beta$). We previously identified successive, region-specific tau PET elevation thresholds in a sample of clinically normal adults and validated these thresholds with longitudinal PET measures (Sanchez, HAI 2019). Here we derive thresholds in an independent data set and validate them in the cross-sectional A4/LEARN data set (N=441).

Methods: In order to maximize expected between-group difference, the reference sample used for threshold derivation consisted of 47 high- $\text{a}\beta$, cognitively-impaired participants and 71 low- $\text{a}\beta$, cognitively-unimpaired participants aged 21-49years (Fig.1). Applying Gaussian mixture models to reference sample Flortaucipir (FTP) SUVR data, proxy ROIs defined 3 staging thresholds: Tp1, rhinal cortex (RC), the typical area of initial cortical deposition, Tp2, inferior temporal (IT), representing temporal neocortex, and Tp3, precuneus (PC), representing extra-temporal neocortex. A4/LEARN participants (age mean/sd=71.8/4.8) underwent FTP and Florbetapir PET. $\text{A}\beta$ burden range was approximately -20 to 190CL. We assessed concordance of the staging scheme using binomial tests as well as the proportion of high-tau participants in each region by age, $\text{a}\beta$, and APOE genotype.

Results: Elevated FTP in A4/LEARN was observed most commonly in RC (40.4%), followed by IT (24.7%), followed by PC (7.9%) (Fig.2). 95% of participants showed FTP tau elevations concordant with the Tp staging scheme (binomial test vs discordant, $p < 0.0001$, Fig.2). As expected, higher Tp stage was associated with greater $\text{a}\beta$ burden and APOEe4 carrier frequency (Fig 2,3).

Conclusions: Tau PET staging in A4/LEARN using GMM thresholds from an independent sample accorded with the spatiotemporal progression scheme implied by autopsy studies. These results suggest the generalizability of a regional threshold based Tp staging system, and the utility of MTL ROIs like RC for detecting early tau pathology.

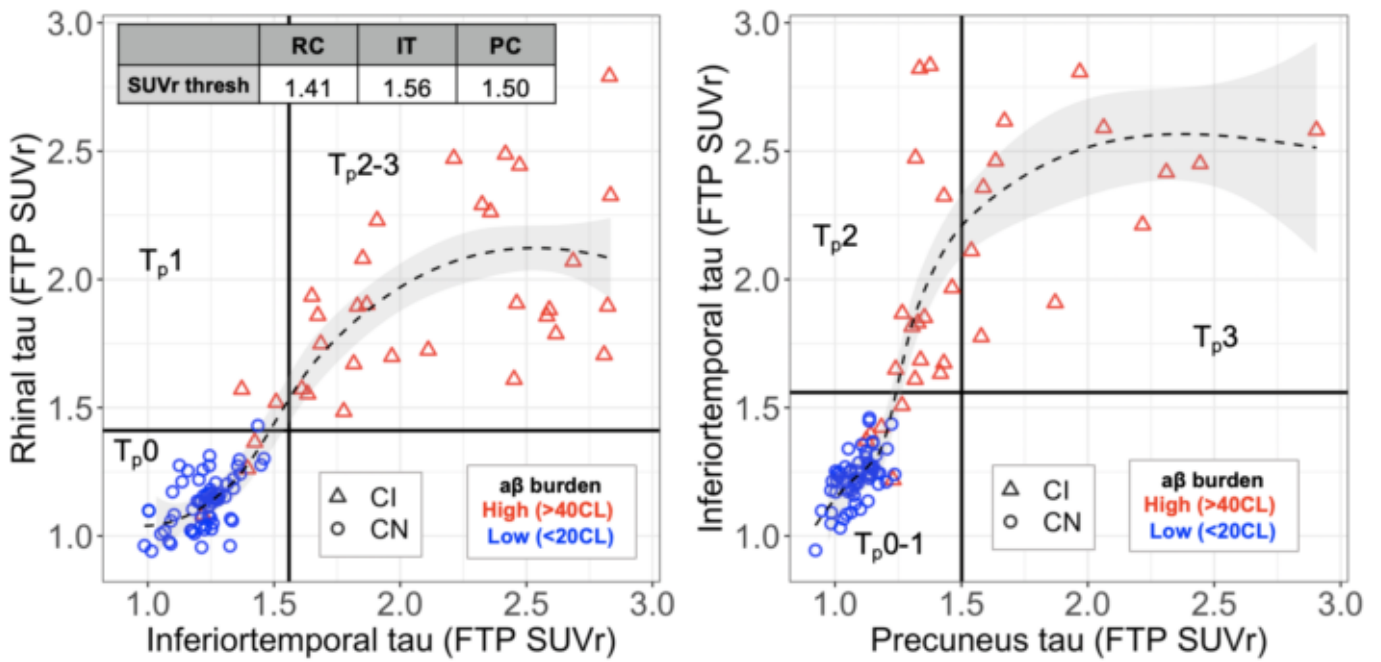


Figure 1. Derivation of tau PET thresholds in a reference sample.

SUVr thresholds for each proxy region were derived in a reference sample consisting of 47 high- $a\beta$ cognitively impaired (CI) participants referred from memory disorders clinics (triangles) and 71 low- $a\beta$ clinically normal (CN) adults aged 21-49. Thresholds were derived from 2-component Gaussian mixture models (GMM), allowing for unequal variance between components, and are shown on scatter plots as solid black lines, with values indicated in the table inset at top left.

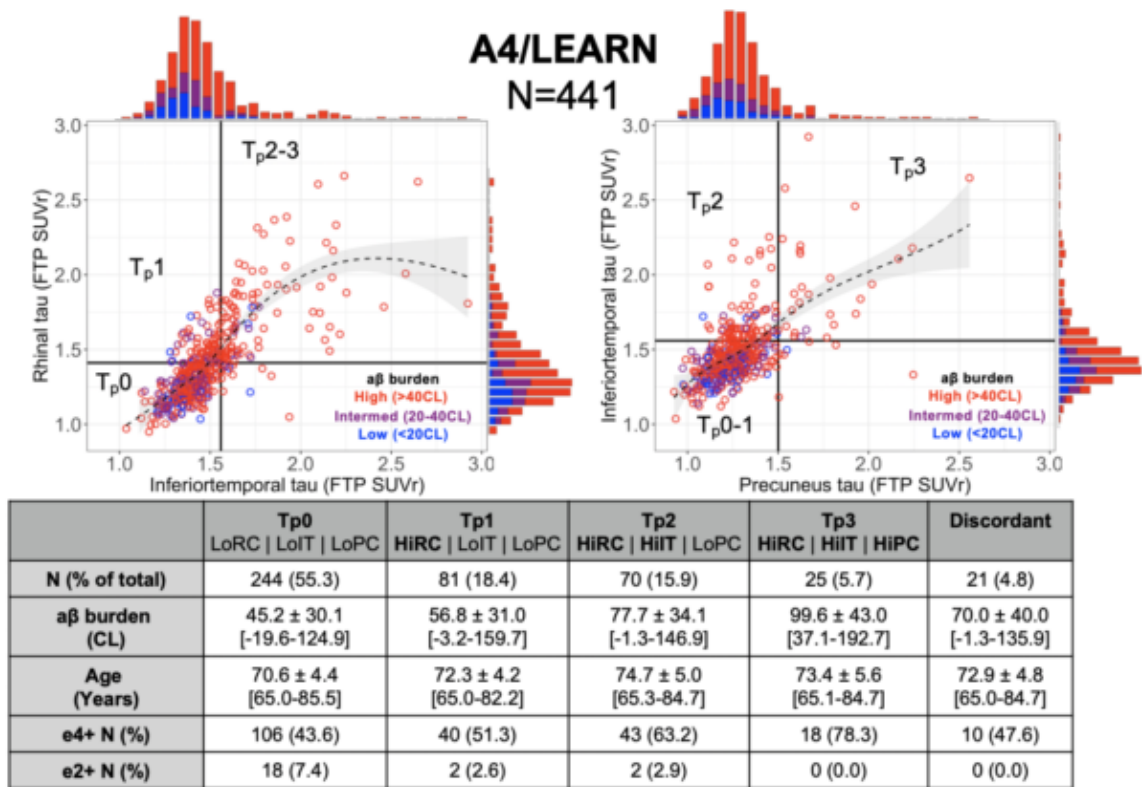


Figure 2. Evaluation of tau PET (Tp) staging in A4/LEARN.

Tp stages are defined by three proxy regions: rhinal cortex (RC) for medial temporal lobe (Tp1), inferior temporal (IT) for temporal neocortex (Tp2), and precuneus (PC) for extra-temporal neocortex (Tp3).

Scatter plots and histograms show the distributions of and relationships between RC, IT (*left*) and PC (*right*) tau; color of dots and bars indicates participants' amyloid-beta (aβ) burden as measured with PET (Florbetapir) and normalized to the Centiloid (CL) scale.

All participants' tau levels were dichotomized on the basis of these SUVR thresholds derived from reference sample (Fig. 1) to determine Tp stage; Frequencies and demographics of each Tp stage are shown for each sample in tables below scatter plots. "Discordant" refers to participants who showed elevated tau in a pattern that did not conform to the Tp staging scheme (e.g., LoRC-HiIT-LoPC). e4+ includes APOEε34 and APOEε44; e2+ includes APOEε23 and APOEε22 (APOEε24 were excluded).

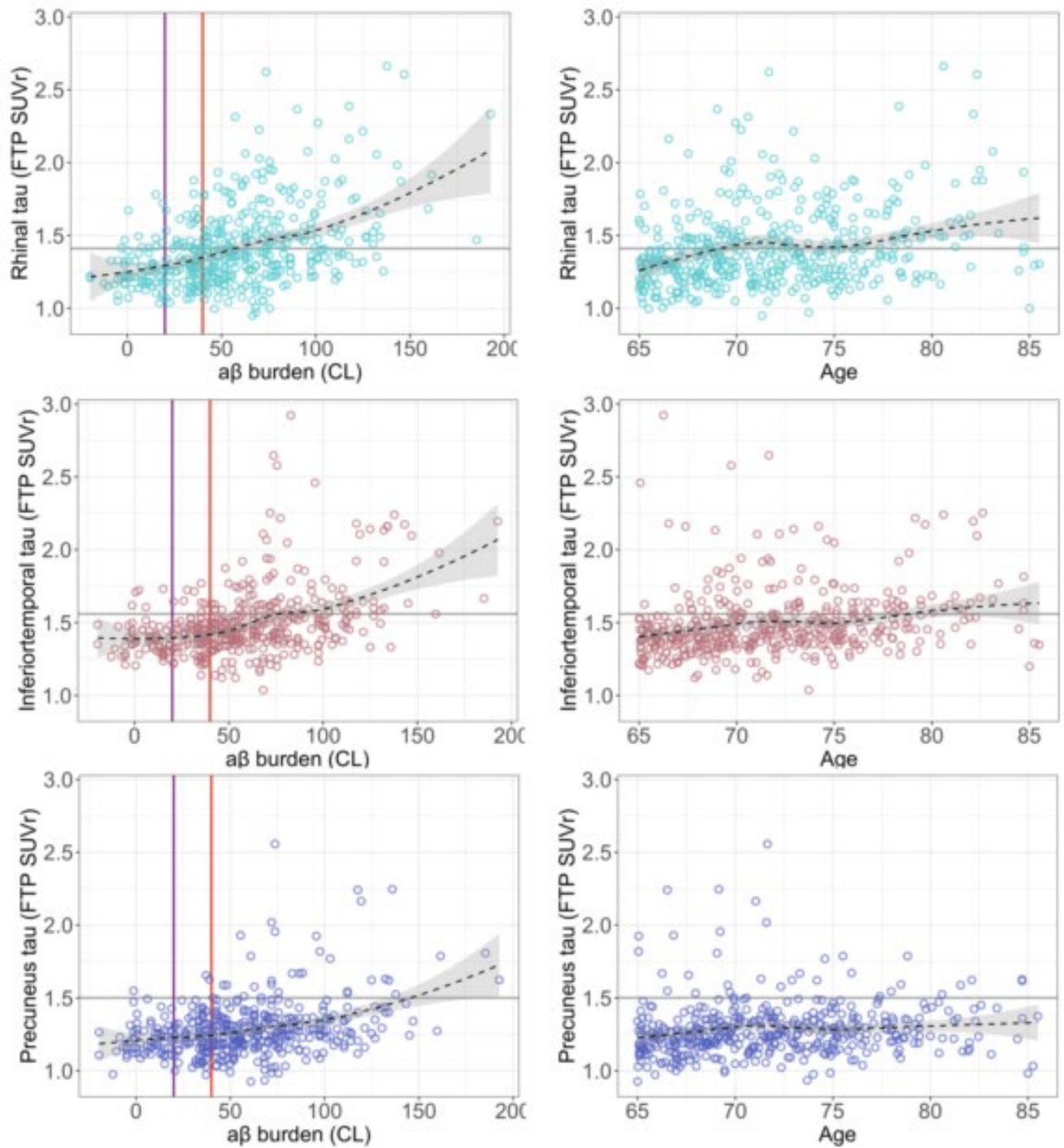


Figure 3. Relationships between regional tau and age, $a\beta$.

Scatter plots show relationships between regional tau PET and $a\beta$ (*left*) and age (*right*), with LOESS fit as dashed line with 95% CI in grey, and SUVr thresholds derived from GMM in reference sample indicated by horizontal grey lines.

Vertical lines on $a\beta$ plots indicate the CL cut-points between low and intermediate (20CL, dark magenta) and between intermediate and high (40CL, red).

Keywords: Tau, Staging, MTL

P161: Clinical evaluation of [18F]-JNJ-64326067, a candidate PET tracer for the detection of tau pathology in Alzheimer's disease

Mark Schmidt¹, Luc Janssens¹, Diederik Moechars¹, Frederik Rombouts¹, Maarten Timmers¹, Olivier Barret², Christian Constantinescu², Jennifer Madonia², David Russell², Christine Sandiego², Hartmuth Kolb³

¹Janssen Research & Development, a division of Janssen Pharmaceutica NV, Beerse, Belgium

²Invicro, a Konica Minolta company, New Haven, CT, US

³Janssen Research & Development, La Jolla, CA, US

Introduction: The accumulation of misfolded tau is a feature of several neurodegenerative disorders. Earlier we identified [18F]-JNJ-64326067, a novel isoquinoline derivative with high affinity and selectivity for tau aggregates from human Alzheimer's disease (AD) brain with a favorable preclinical profile. Here, we report the dosimetry of [18F]-JNJ-64326067 and results of a proof-of-concept study comparing subjects with probable AD to age matched controls.

Methods: [18F]-JNJ-64326067 PET scans were acquired continuously for 90 minutes and then from 120-180 minutes in 5 probable AD (4M, 1F; age 63-85) and 5 healthy controls (3M, 2F; age 60-78). [18F]-florbetapir PET was positive in all probable AD subjects and negative in all healthy controls. Whole body [18F]-JNJ-64326067 PET CT scans were acquired in six healthy subjects (3M/3F; age 54-75). Brain PET scans were visually reviewed. Regional (Hammers atlas) quantification of [18F]-JNJ-64326067 included kinetic analysis of distribution volume ratio (DVR), estimated by non-invasive Logan graphical analysis, and static analysis of SUVR averaged over 120-180 min; both methods used the ventral cerebellar cortex as a reference region.

Results: One healthy control had focal areas of [18F]-JNJ-64326067 signal in occipital and parietal cortex underlying the site of a gunshot injury as an adolescent. Four healthy controls had no retention of brain signal. Four of the 5 AD subjects had [18F]-JNJ-64326067 retention in relevant cortical regions: three in temporal cortex and one in frontal cortex. Cortical SUVR in visually positive subjects approached steady state by 120 minutes. Temporal and frontal cortical SUVR/DVR in visually positive AD subjects ranged from 1.21-3.09/1.20-2.18 and from 0.92-1.28/0.91-1.16 in healthy controls. SUVR correlated well with DVR in AD subjects with signal ($R^2=0.94$). Whole-body effective dose was estimated to be 2.71 E-02 mSv/MBq for females and 2.10 E-02 mSv/MBq for males.

Conclusions: [18F]-JNJ-64326067 could be a useful PET ligand for detection and quantitation of tau aggregates.

Keywords: tau, Alzheimer's, PET, isoquinoline

P162: Association between cerebrospinal fluid neurofilament light chain and markers of neurofibrillary pathophysiology: findings from the Knight Alzheimer Disease Research Center

Stephanie Schultz¹, Suzanne Schindler¹, Charlie Chen¹, Courtney Sutphen¹, John Morris¹, Anne Fagan¹, Brian Gordon¹, Tammie Benzinger¹

¹Washington University in St. Louis, St. Louis, MO, US

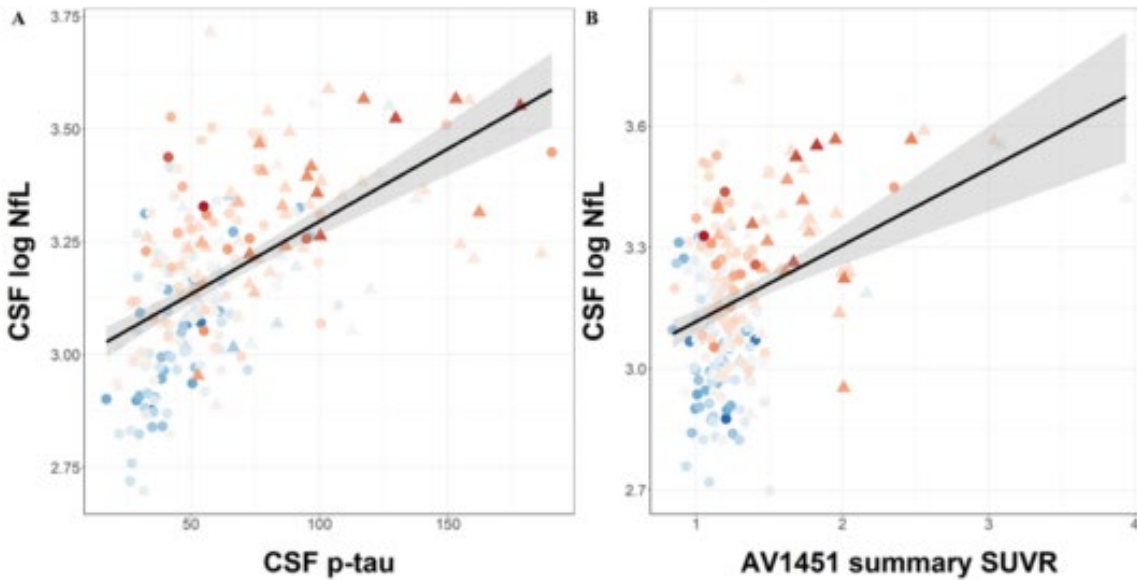
Objective: To examine the relationship between cerebrospinal fluid (CSF) neurofilament light (NfL) chain levels and established biomarkers of neurofibrillary tangle (NFT) pathophysiology. Secondly, we assessed the discordance of beta-amyloid, NFT, and neurodegeneration markers.

Methods: 236 individuals (207 cognitively normal and 29 cognitively impaired) were selected based on completion of CSF collection and AV1451 and AV45 PET imaging within 1 year, and measurement of CSF NfL, beta-amyloid-42, total-tau, and phosphorylated-tau181 (p-tau). Using covariate-adjusted linear regressions we compared log-transformed CSF NfL to AV1451 summary SUVRs and CSF p-tau. Using Gaussian mixture models, we determined positivity thresholds in markers of beta-amyloid (CSF beta-amyloid-42 and AV45), NFT (CSF p-tau and AV1451), and neurodegeneration (CSF total-tau and CSF NfL) and assessed discordant results between related biomarkers.

Results: CSF NfL was highly associated with CSF p-tau (B[SE]=0.002[.0003], p=9.83e-10; Figure 1A), whereas CSF NfL was marginally associated with AV1451 (B[SE]=0.083[.03], p=0.006; Figure 1B). CSF p-tau and AV1451 were only moderately correlated (r=0.457; Figure 2B). The differences in relationship between tau and NfL markers may be due to effects of age on these three biomarkers of interest. Age was minimally correlated with AV1451 (r=0.326; Figure 3A) and moderately correlated with CSF p-tau and NfL (r=0.410 and 0.512, respectively; Figure 3B-C). Secondly, we found that our sample was 18.1% discordant between beta-amyloid markers, 18.6% discordant between NFT markers, and 17.8% discordant between neurodegeneration markers (Figure 2A-C).

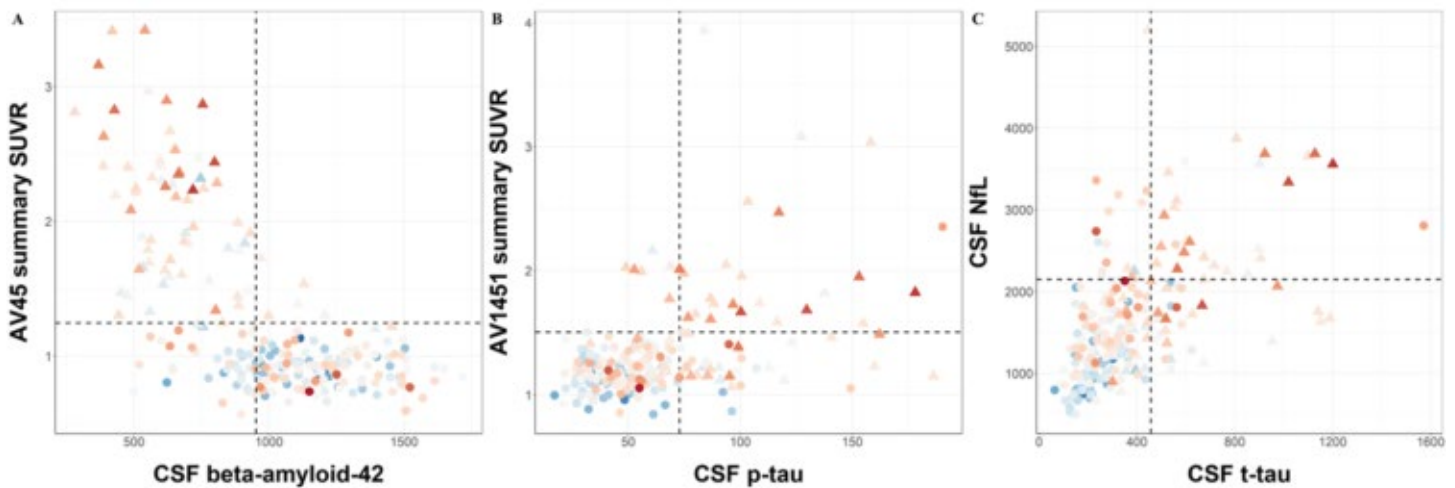
Conclusions: The relationship between CSF NfL and NFT pathophysiology differed depending on the NFT biomarker that was considered and may be related to elevations in certain CSF biomarkers as a function of age. Currently, CSF p-tau and AV1451 are often considered interchangeable measures of NFT pathophysiology. These results suggest more careful consideration and assessment of biomarkers should be taken when choosing markers of beta-amyloid, NFT, and neurodegeneration.

Figure 1.



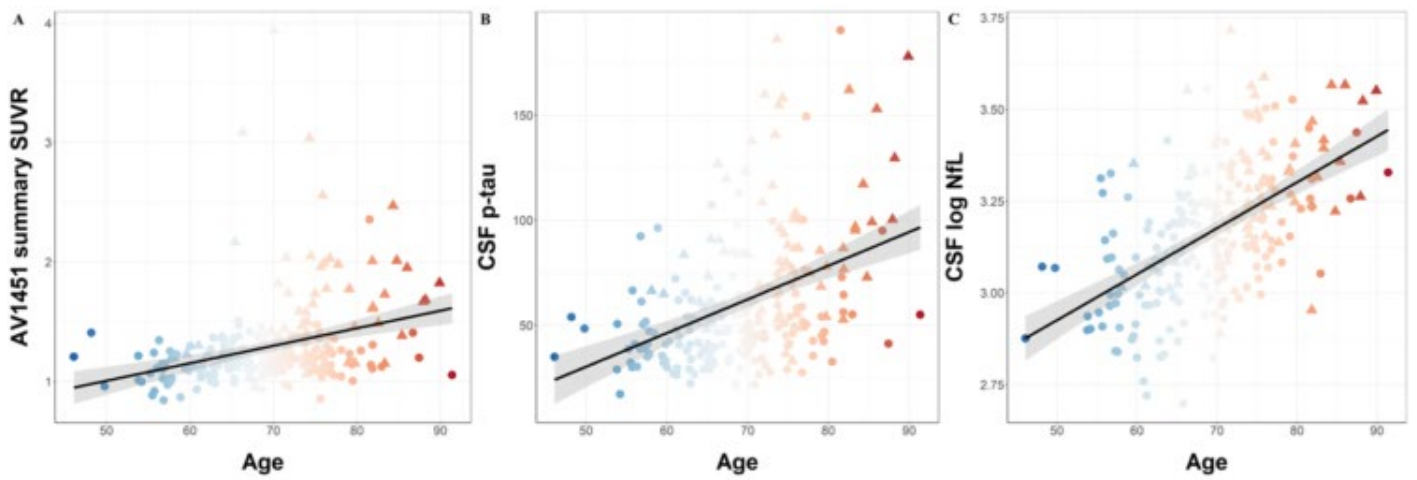
The association between log-transformed CSF NfL and (A) CSF p-tau and (B) AV1451 summary SUVRs. Individual points are color-coded by age. Circle= beta-amyloid negative; triangle= beta-amyloid positive. Beta-amyloid positivity was defined as a Summary AV45 SUVR >1.19.

Figure 2.



Association between markers of (A) beta-amyloid, (B) NFT, and (C) neurodegeneration. Dotted lines represent threshold for abnormality, for each biomarker, determined with a Gaussian mixture model. Individual points are color-coded by age. Circle= beta-amyloid negative; triangle= beta-amyloid positive. Beta-amyloid positivity was defined as a Summary AV45 SUVR >1.19.

Figure 3.



The association between age and (A) AV1451 summary SUVRs, (B) CSF p-tau, and (C) log-transformed CSF NfL. Individual points are color-coded by age. Circle= beta-amyloid negative; triangle= beta-amyloid positive. Beta-amyloid positivity was defined as a Summary AV45 SUVR >1.19.

Keywords: Biomarkers, tau, beta-amyloid, neurodegeneration, neurofilament light chain

P163: 18F-PM-PBB3 (18F-APN-1607) uptake associates with plasma NfL level and motor disability in patients with progressive supranuclear palsy

Hitoshi Shimada¹, Kenji Tagai¹, Harutsugu Tatebe², Kiwamu Matsuoka¹, Manabu Kubota¹, Keisuke Takahata¹, Yuhei Takado¹, Hitoshi Shinotoh^{1,4}, Yasuharu Yamamoto¹, Yasunori Sano¹, Chie Seki¹, Yoshikazu Nakano¹, Maiko Ono¹, Shigeki Hirano⁴, Paul Tempest⁵, Ming-Kuei Jang⁵, Naruhiko Sahara¹, Kazunori Kawamura¹, Ming-Rong Zhang¹, Takahiko Tokuda², Makoto Higuchi¹

¹National Institute of Radiological Sciences, National Institutes for Quantum and Radiological Science and Technology, Chiba, Japan

²Kyoto Prefectural University of Medicine, Kyoto, Japan

³Neurology Clinic Chiba, Chiba, Japan

⁴Department of Neurology, Chiba University Graduate School of Medicine, Chiba, Japan

⁵APRINOIA Therapeutics Inc, Taipei, Taiwan

Objectives: Our previous studies demonstrated that ¹⁸F-PM-PBB3 (¹⁸F-APN-1607) uptake may reflect characteristic distributions of tau pathologies in 4-repeat tauopathies including progressive supranuclear palsy (PSP). The present study aimed to investigate the association among ¹⁸F-PM-PBB3 uptake, neurodegenerative biomarker level, and clinical symptoms in PSP with Richardson syndrome (PSP-RS) patients.

Methods: 21 patients with probable PSP-RS underwent PET scans with ¹⁸F-PM-PBB3 and ¹¹C-PiB for estimating regional tau and A β deposition. Plasma neurofilament light chain (NfL) levels were also checked as a neurodegenerative biomarker. Parametric ¹⁸F-PM-PBB3- and ¹¹C-PiB- images were generated by voxel-based calculation of the standardized uptake value ratio (SUVR) to the cerebellar cortex. Three patients, who were diagnosed as amyloid-positive by visual assessment of ¹¹C-PiB SUVR image, were excluded. Finally, the other 18 PiB-negative PSP-RS patients were included for further analyses. Regional ¹⁸F-PM-PBB3 SUVR was estimated in dentate, midbrain, subthalamus, striatum, pre- and post-central gyri in addition to PSP tau PET meta-ROI. We assessed Pearson's correlation of regional ¹⁸F-PM-PBB3 SUVR with plasma NfL levels and motor severity assessed by PSP rating scale.

Results: Plasma NfL levels showed positive correlation with ¹⁸F-PM-PBB3 SUVR in striatum, pre- and post-central gyri as well as PSP tau PET meta-ROI ($r = 0.77, 0.98, 0.95,$ and $0.78; p < 0.05$, followed by Bonferroni correction), and a trend toward significance in midbrain and dentate ($r = 0.68$ and $0.51; p = 0.008$ and 0.043 , without multiple comparison). PSP rating scale score positively correlated with plasma NfL ($r = 0.73; p < 0.01$, followed by Bonferroni correction), and there were trends towards significance between PSP rating scale and ¹⁸F-PM-PBB3 SUVR in midbrain and PSP tau PET meta-ROI ($r = 0.66$ and $0.65; p = 0.01$ and 0.03 , without multiple comparison).

Conclusions: Accumulations of PM-PBB3 may reflect neurotoxic tau pathologies in PSP-RS, in tight association with clinical symptoms.

Keywords: Tau PET, 18F-PM-PBB3 (18F-APN-1607), PSP, NfL, Parkinsonism

P164: The rate of accumulation of tau aggregates is higher in females and younger individuals

Ruben Smith^{1,2}, Niklas Mattsson^{1,2,3}, Michael Pontecorvo⁴, Michael Devous⁴, Olof Strandberg¹, Rik Ossenkoppele^{1,5}, Oskar Hansson^{1,6}

¹Clinical Memory Research Unit, Department of Clinical Sciences, Lund University, Malmö, Sweden

²Department of Neurology, Skåne University Hospital, Lund, Sweden

³Wallenberg Centre for Molecular Medicine, Lund University, Lund, Sweden

⁴Avid Radiopharmaceuticals, Philadelphia, PA, US

⁵VU University Medical Center, Neuroscience Campus Amsterdam, Amsterdam, The Netherlands

⁶Memory Clinic, Skåne University Hospital, Malmö, Sweden

Background: Development of tau PET tracers allow tau pathology to be visualized *in vivo*. Despite this, factors modifying the rate of tau accumulation are still largely unknown.

Methods: We included 338 participants who underwent two to four ¹⁸F-Flortaucipir PET scans within the Swedish BioFINDER (n=57), AVID05 (n=158) and ADNI-studies (n=123). Amyloid-beta (Ab) status was determined using ¹⁸F-Florbetapir or ¹⁸F-Flutemetamol PET. Clinical data of the participants are presented in Table 1. ¹⁸F-Flortaucipir images were centrally and uniformly analyzed at Lund University. ROI parcellations were performed on midpoint longitudinal MRI images created from baseline and follow-up MRI scans that were then warped back onto the individual MRI scans to decrease variation. To determine the accumulation rate of tau in each subject, slopes were derived from linear regression models for each subject and each ROI based on all available PET scans.

Results: The Ab+ CU were older than the other groups (Table 1). Longitudinal tau-PET retention by age is depicted in Figure 1. Slopes of tau-PET increase were significantly steeper in Ab+ MCI and AD compared to Ab- CU and Ab- MCI in Braak regions I-IV and III-IV, and in AD compared to Ab- CU and Ab- MCI in Braak V-VI (Figure 2). We tested for interactions with rate of change of tau-PET using a generalized linear model of tau slope, adjusting for Ab-status, ApoE-e4-positivity, age, sex, study and baseline ¹⁸F-Flortaucipir. We found interactions with sex (t=3.99, p<0.001), age (t=-2.66, p<0.01) and baseline ¹⁸F-Flortaucipir (t=12.74, p<0.001), indicating faster progression in younger individuals, females, and individuals with higher baseline tau.

Conclusions: Using a large, multicenter, longitudinal ¹⁸F-Flortaucipir dataset we found that tau pathology progresses faster in females, younger individuals and subjects with higher baseline tau. There was no effect of the ApoE e4 genotype on rate of tau deposition.

Table 1. Clinical characteristics

	A β - CU	A β - MCI	A β + CU	A β + MCI	AD	p-value
Number	88	58	65	82	45	
Age	71.1 \pm 9.4	71.5 \pm 9.1	77.8 \pm 6.9	73.4 \pm 7.7	72.4 \pm 10.7	b ^{***} , e ^{***} , h [*] , i [*]
Sex (F/M)	40/48	27/31	37/28	38/44	22/23	<u>n.s.</u>
Education	15.3 \pm 2.8	15.7 \pm 3.0	15.2 \pm 3.6	15.8 \pm 3.1	14.5 \pm 3.1	<u>n.s.</u>
MMSE	29.4 \pm 0.8	28.2 \pm 2.3	28.4 \pm 2.2	27.1 \pm 2.6	21.8 \pm 4.4	a [*] , c ^{***} , d ^{***} , g ^{***} , h [*] , i ^{***} , j ^{***}
ApoE ϵ4-alleles (0/1/2)	73/14/1	44/13/1	33/28/4	35/33/14	15/20/10	b ^{***} , c ^{***} , d ^{***} , e ^{**} , f ^{***} , g ^{***} , i [*]
Tau slopes						
Braak I-II (SUVR/year)	0.005 \pm 0.047	0.001 \pm 0.052	0.014 \pm 0.039	0.023 \pm 0.086	0.021 \pm 0.12	<u>n.s.</u>
Braak I-IV (SUVR/year)	0.004 \pm 0.031	-0.005 \pm 0.027	0.016 \pm 0.036	0.049 \pm 0.101	0.058 \pm 0.148	c ^{**} , d ^{**} , f ^{***} , g ^{***} , i [*]
Braak III-IV (SUVR/year)	0.004 \pm 0.031	-0.005 \pm 0.026	0.016 \pm 0.037	0.050 \pm 0.104	0.060 \pm 0.150	c ^{**} , d ^{**} , f ^{***} , g ^{***} , i [*]
Braak V-VI (SUVR/year)	0.005 \pm 0.030	-0.003 \pm 0.029	0.009 \pm 0.029	0.029 \pm 0.079	0.048 \pm 0.110	d ^{**} , f [*] , g ^{***}

Table legend. Statistical comparisons between ^a A β - CU and A β - MCI; ^b A β - CU and A β + CU; ^c A β - CU and A β + MCI; ^d A β - CU and A β + AD; ^e A β - MCI and A β + CU; ^f A β - MCI and A β + MCI; ^g A β - MCI and A β + AD; ^h A β + CU and A β + MCI; ⁱ A β + CU and A β + AD; ^j A β + MCI and A β + AD. * p < 0.05; ** p < 0.01; *** p < 0.001.

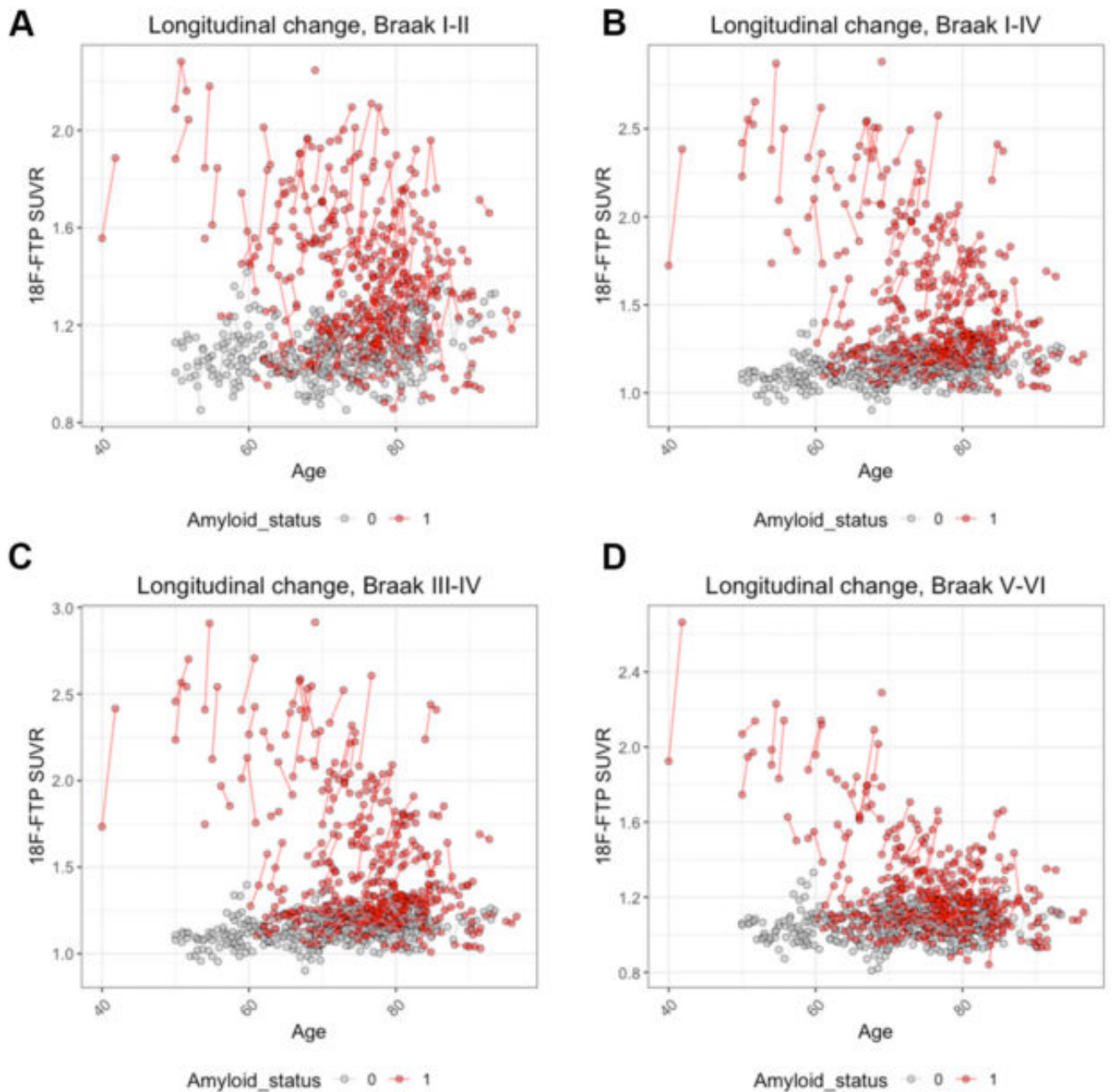


Figure 1: Longitudinal change in tau

Change in ^{18}F -Florbetapir SUVR with age in (A) Medial temporal lobe (Braak I-II), (B) Temporal lobe (Braak I-IV), (C) Lateral temporal lobe (Braak III-IV), and (D) Neocortex (Braak V-VI). Dots from the same subject are connected by lines. Red dots indicate $\text{A}\beta^+$ subjects and grey $\text{A}\beta^-$ subjects.

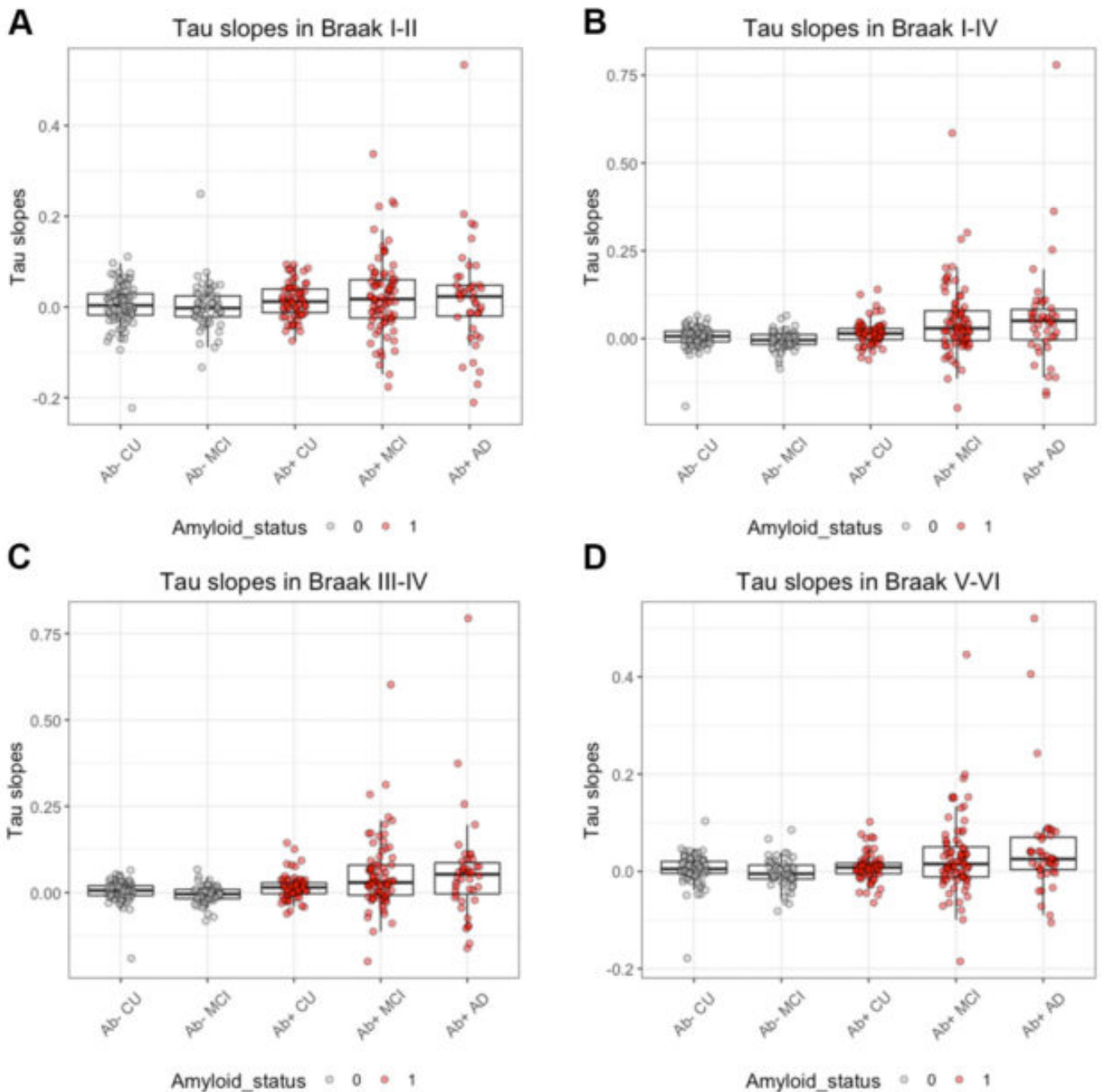


Figure 2: Rate of tau accumulation.

The rate of tau accumulation was estimated within each individual subject by extracting slopes of linear regressions of the tau scans (change in SUVR/year) in (A) Medial temporal lobe (Braak I-II), (B) Temporal lobe (Braak I-IV), (C) Lateral temporal lobe (Braak III-IV), and (D) Neocortex (Braak V-VI). Data is shown over diagnostic groups with A β + subjects in red and A β - subjects in grey.

Keywords: Tau, longitudinal, PET, AD, disease progression

P165: Resting state functional connectivity associations with F18-Florbetapir PET versus F18-Flortaucipir PET

Diana Svaldi¹, Joaquin Goñi², Edwin Stage¹, Kausar Abbas², Mario Dziedzic¹, John West¹, Shannon Risacher¹, Andrew Saykin¹, Liana Apostolova¹

¹*Indiana University School of Medicine, Indianapolis, IN, US*

²*Purdue University, West Laffayette, IN, US*

Objective: Alzheimer's disease (AD) pathology results in dysfunctional signaling that drives further propagation of pathology. We assess the relationship of functional connectivity (FC) with AV45 PET, and AV1451 PET.

Methods: Resting-state-fMRI, F18-Flortaucipir-PET(AV1451), and F18-Florbetapir-PET(AV45) scans from ADNI3 (Table1) were assessed. Average cortical-AV45-SUVR and average-AV1451-SUVR (Braak1-2, Braak3-4, and Braak5-6 regions) were determined. Whole brain functional connectomes (FCs) were estimated using 286 ROIs. ROIs were assigned to resting state networks (RSNs)--visual (VIS), somatomotor (SM), dorsal-attention (DA), ventral-attention (VA), limbic (L), default-mode (DMN), frontoparietal (FP), subcortical (SB), and cerebellar (CER)-- with hippocampus assigned to SUB. RSN-strengths, or sum of connections between every pair of RSNs were calculated, resulting in 45 FC-strength measurements.

Two steps were used to filter RSNs significantly associated to SUVR outcomes. First, partial correlation ($r > 0.15$) was used, controlling for age and other relevant covariates. For AV45, we controlled for mean AV1451-SUVR (Braak regions). For AV1451, we controlled for mean cortical AV45-SUVR. RSNs selected were then used as predictors in a stepwise regression predicting SUVR ($\alpha_{inclusion}=0.05$).

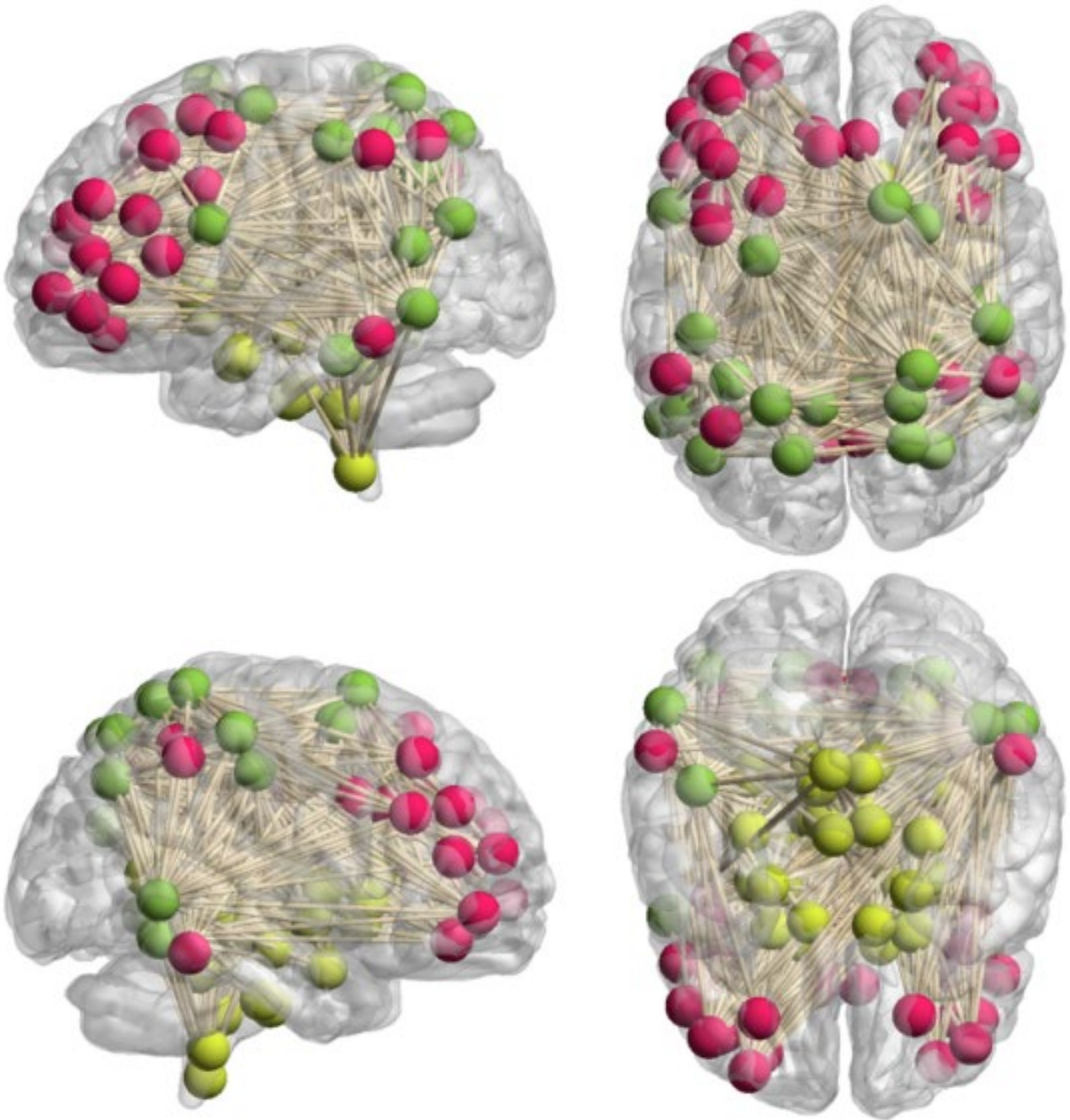
Results: The first step selected 10 RSNs for AV45 SUVR, 9 RSNs for AV1451-Braak12 SUVR, 4 RSNs for AV1451-Braak34 SUVR, and 3 RSNs for AV1451-Braak56 SUVR. The final step selected DA-DA, DA-FP, and DA-SUB for AV45 (Figure1). SUB-CER and VIS-DA were selected for Braak12 AV1451 SUVR (Figure2). FP-SUB was selected for Braak34 and Braak56 AV1451 SUVR (Figure2), while FP-FP strength was selected only for Braak56 AV1451.

Conclusions: Although Amyloid and Tau associations with FC are independent, they occur in overlapping RSNs. Amyloid association with FC is more widespread than Tau. Deposition of Tau in Braak34 and Braak56 regions is similarly associated to FC, while deposition in Braak12 regions appears to be independently associated. Furthermore, Tau and Amyloid are associated to FC independently of aging and independently of one another.

Table 1 Demographics Information

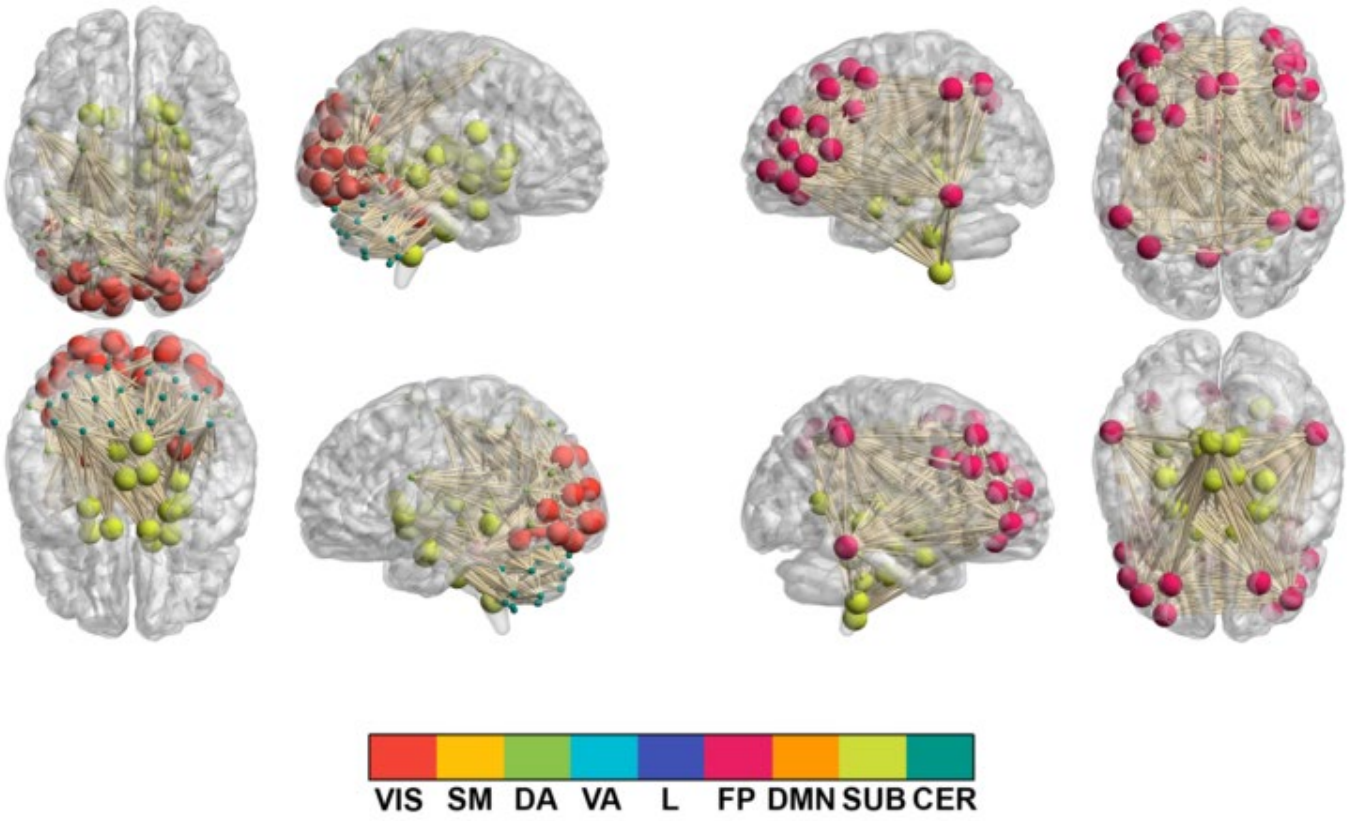
	Cognitively Normal (CN, n = 75)	Early Mild Cognitive Impairment (EMCI, n = 20)	Cognitive Impairment (CI, n = 16)	p-value
Age years mean (SD)	74.6 (7.3)	73.5 (6.6)	74.8 (10.4)	N.S.
# Female N (%)	45 (60.0%)	7 (35.0%)	7 (43.75%)	N.S.
AV 45 SUVR Mean (SD)	1.12 (0.17)	1.20 (0.30)	1.27 (0.28)	N.S.
AV 1451 BRAAK12 SUVR Mean (SD)	1.15 (0.12)	1.27 (0.24)	1.39 (0.34)	< 0.001
AV 1451 BRAAK34 SUVR Mean (SD)	1.12 (0.09)	1.22 (0.24)	1.4 (0.52)	< 0.001
AV 1451 BRAAK56 SUVR Mean (SD)	1.08 (0.09)	1.05 (0.12)	1.17 (0.30)	< 0.001

AV45 Associated RSNs



**AV1451 Braak12
Associated RSNs**

**AV1451 Braak34 & 56
Associated RSNs**



Keywords: Amyloid, Tau, resting state fMRI, connectivity, PET

P166: Tau positivity: Comparing flortaucipir meta-ROI vs maximal single region

Terry Therneau¹, Christopher Schwarz¹, Heather Wiste¹, Jeffrey Gunter¹, Matthew Senjem¹, Val Lowe¹, Kejal Kantarci¹, Ronald Petersen¹, David Knopman¹, Michelle Mielke¹, David Jones¹, Clifford Jack¹

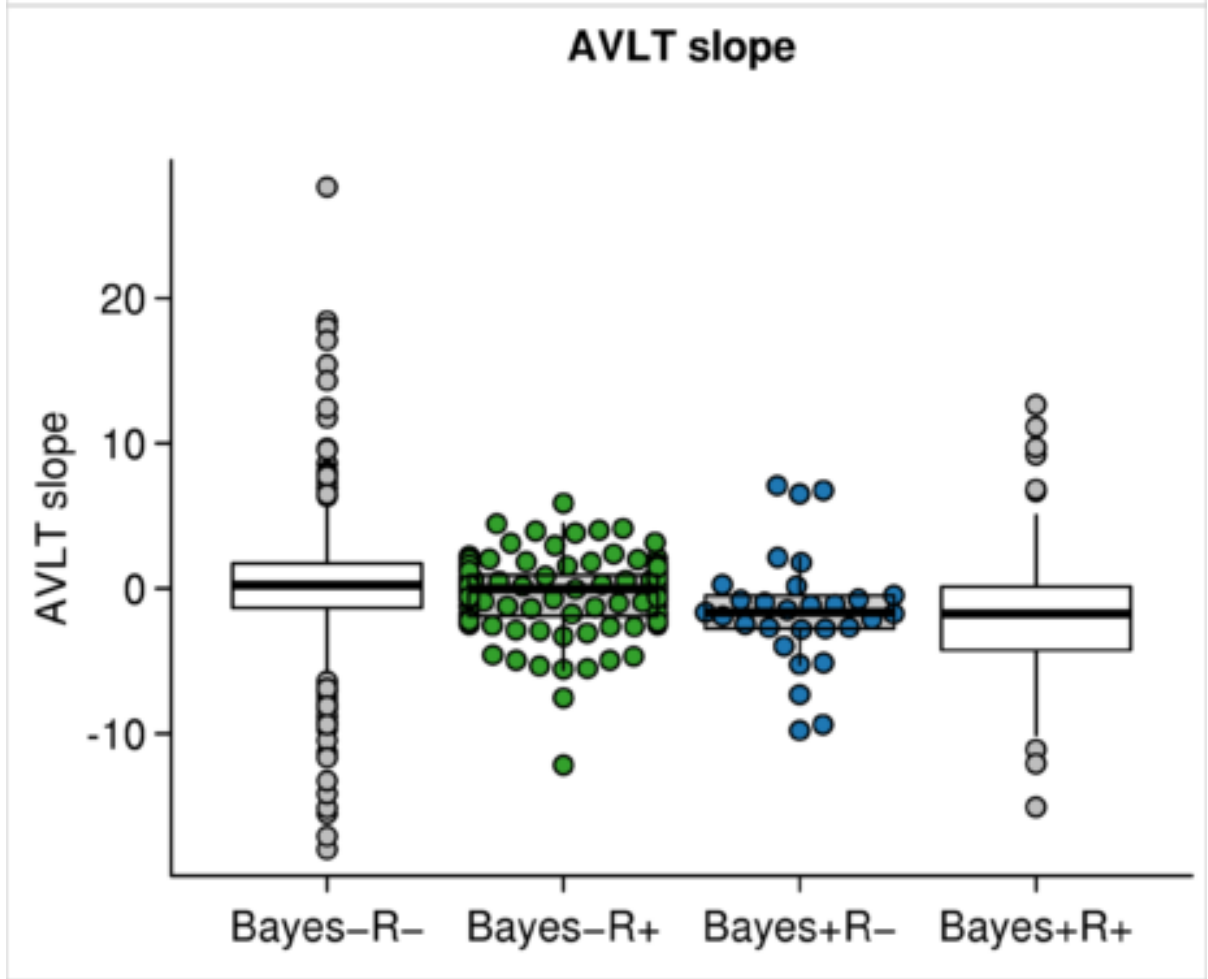
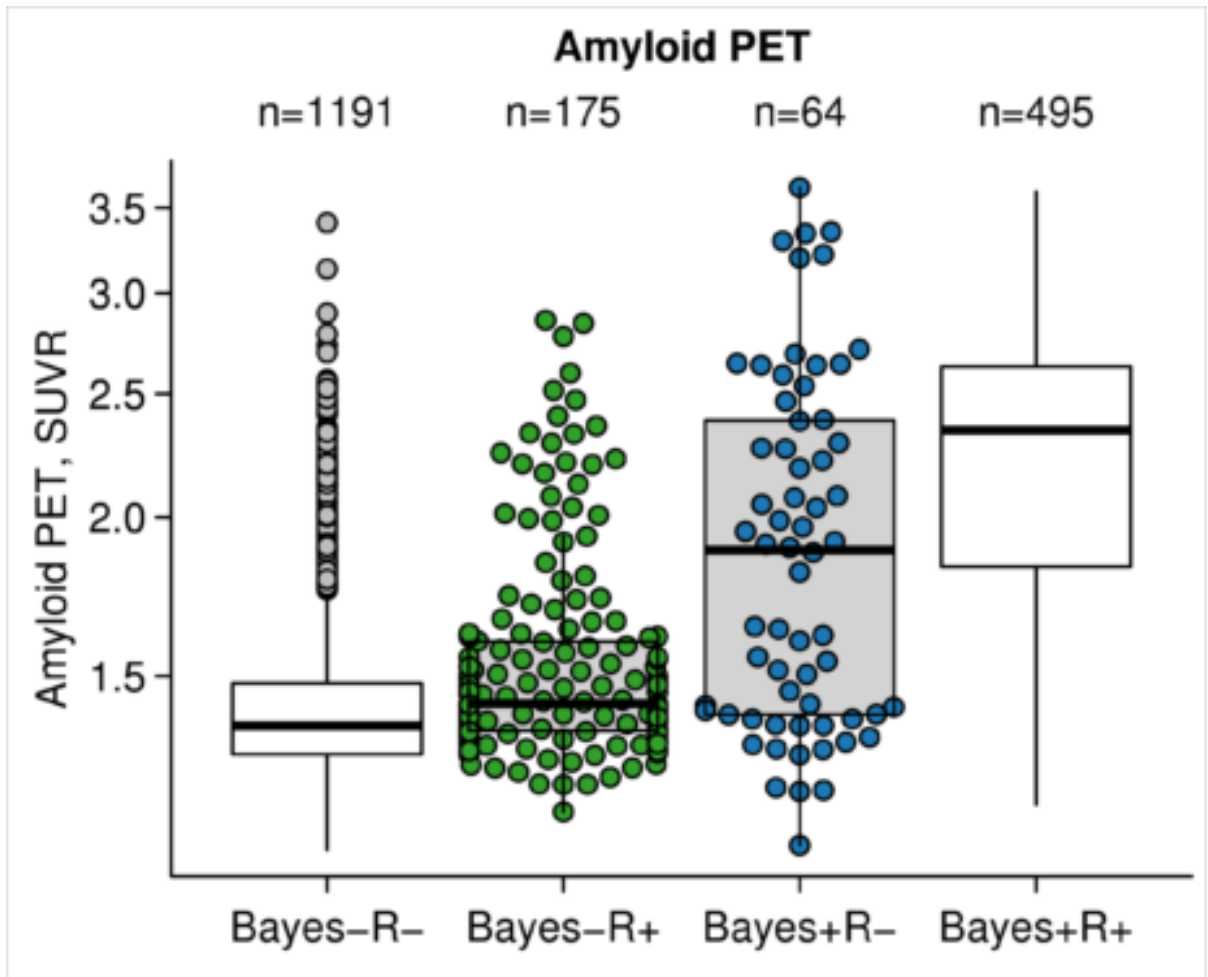
¹*Mayo Clinic, Rochester, MN, US*

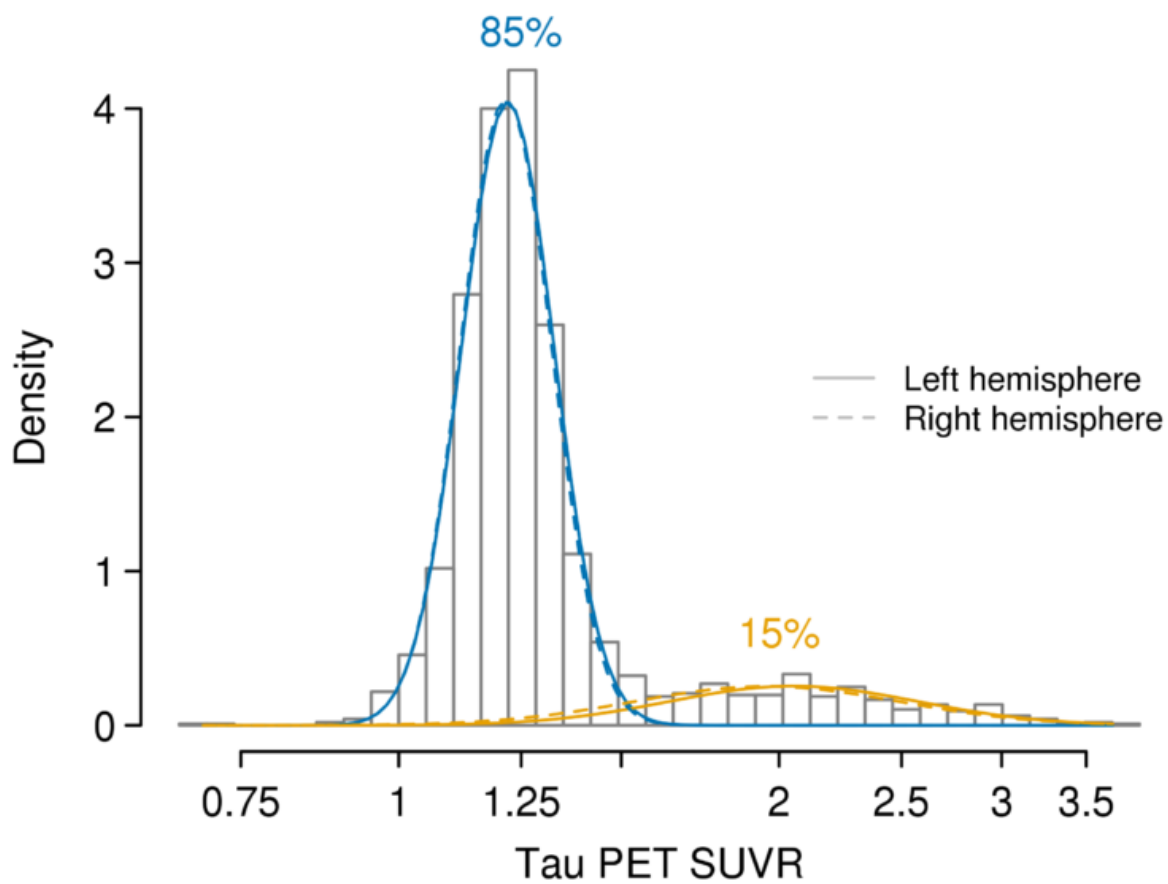
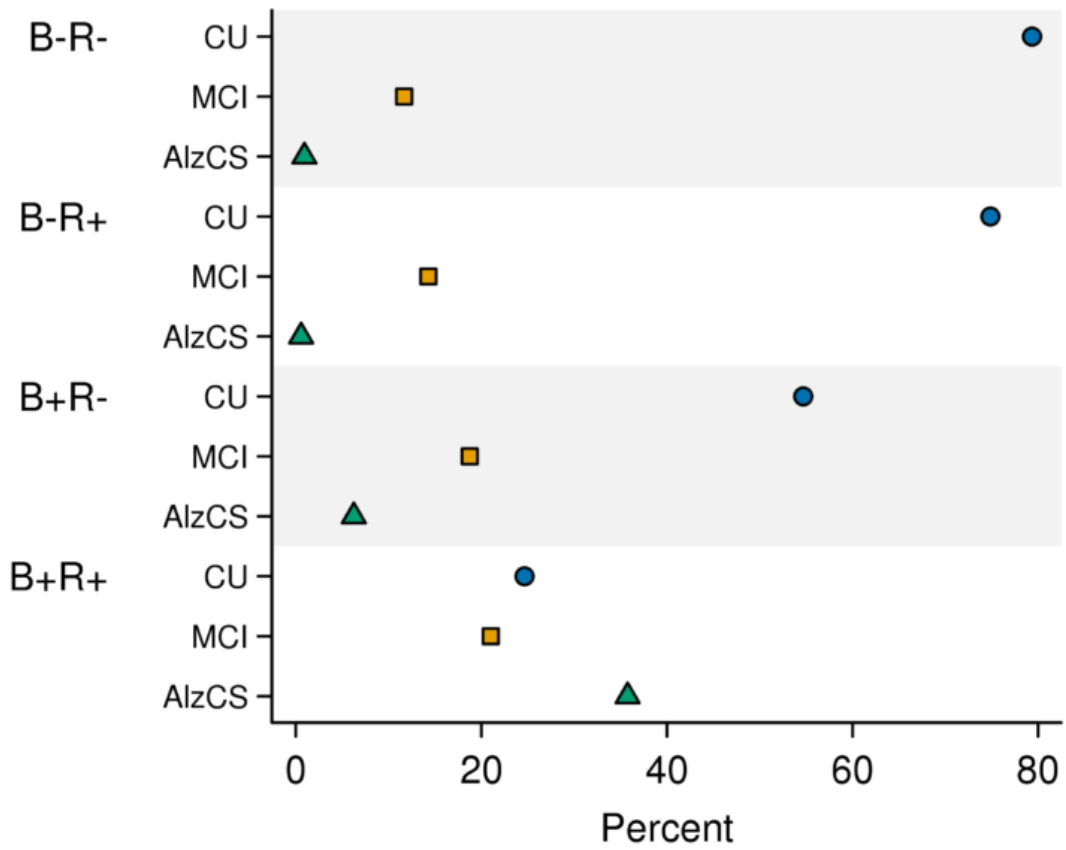
Background: Meta-ROI or reporter ROI approaches are commonly used to determine abnormal tau biomarker status, but these may not detect elevated signal in other brain locations.

Methods: Using data from 1925 flortaucipir scans from the Mayo Clinic Study of Aging and ADRC, we fit separate 2 component mixture models for each of 86 left and right brain regions, yielding a normal and abnormal peak for each. For each participant we then computed the Bayes posterior probability, for each region, that it arose from the ‘abnormal’ distribution. Any participant who had even one positive region is labeled as Bayes+. This classification was compared with our existing temporal meta-ROI (entorhinal, amygdala, parahippocampal, fusiform, inferior temporal, middle temporal) and abnormal cut-point which is denoted as R+ (mean SUVR ≥ 1.25).

Results: Figure 1 shows a typical region; 15% of the 1925 left inferior temporal scans are estimated to be in the abnormal peak. The estimated mixtures were essentially identical for left/right in all but one region (olfactory). Overall, 559 scans were estimated to be Bayes+ (29%) while 670 were R+ (35%). Figures 2 and 3 show that in comparison to Bayes–R+, Bayes+R– participant have higher PIB burden, a greater rate of AVLT loss, and were more often clinically symptomatic; they were also slightly older (mean 73, 76). Of the 64 Bayes+R– subjects, 58 were positive in only 1-3 of the 43 regions, either left or right; 42/64 were positive in either the entorhinal cortex (39) or amygdala (11).

Conclusions: For the majority of participant (88%) a “maximal region” and “mean reference region” approach gave identical classifications. For the 12% where Bayes and R were discordant, the Bayes+ criteria appears to choose participant who were more likely to have tau pathology – i.e. were older, more often amyloid positive and more often clinically symptomatic.





Keywords: biomarkers, tau PET, Gaussian mixture modeling

P167: Intrinsic connectivity of the human brain provides scaffold for tau aggregation in Alzheimer's disease

Joseph Therriault¹, Tharick Pascoal¹, Melissa Savard¹, Sulantha Mathotaarachchi¹, Andrea Benedet¹, Mira Chamoun¹, Serge Gauthier¹, Paramita Saha-Chaudhuri¹, Gassan Massarweh¹, Pedro Rosa-Neto¹

¹McGill Center for Studies in Aging, Montreal, QC, Canada

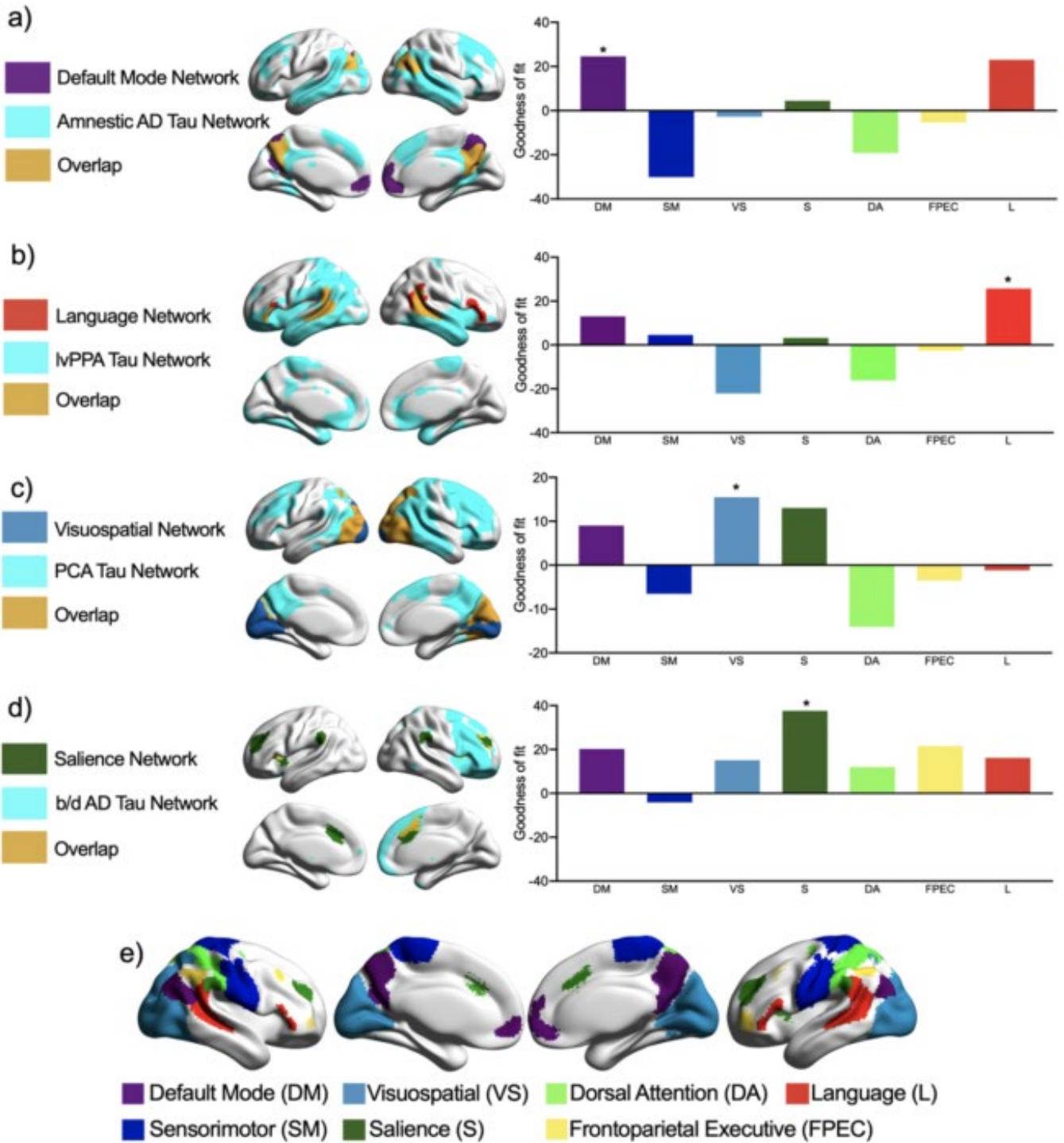
Introduction: Preclinical animal models suggest that tau pathology spreads intracellularly, thought to explain the topographical distribution of tau observed in Alzheimer's disease (AD). However, these findings have yet to be extended to humans.

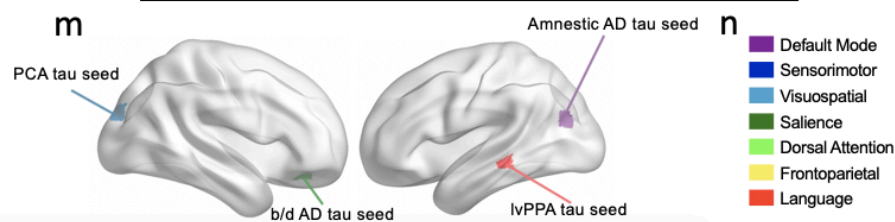
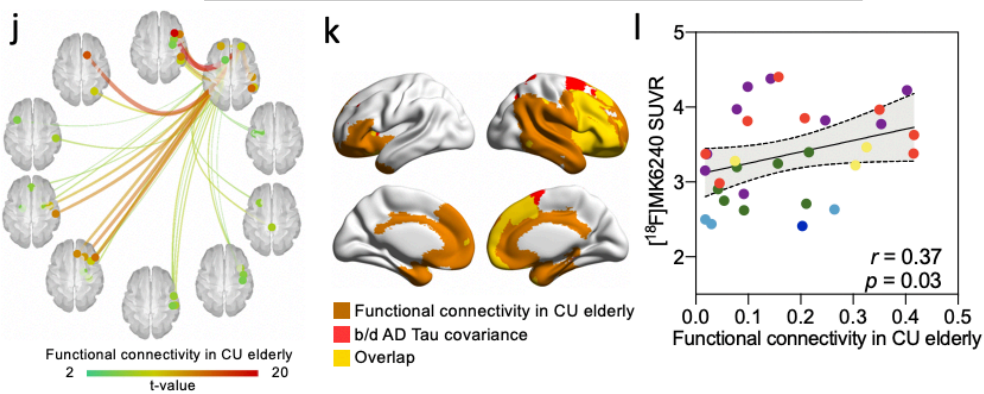
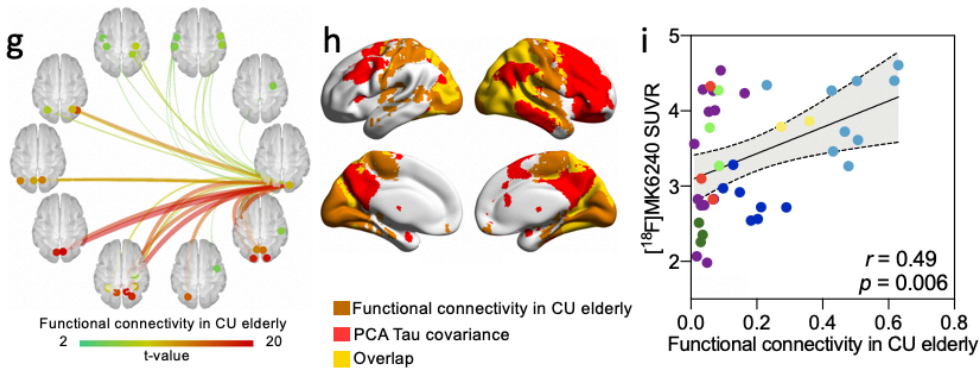
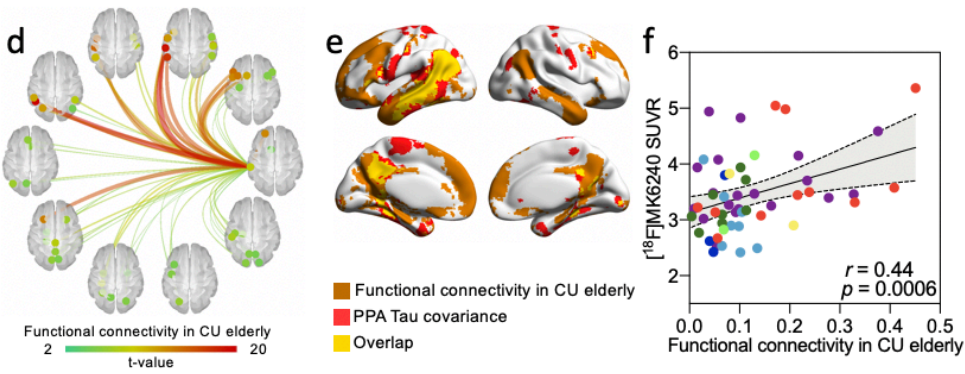
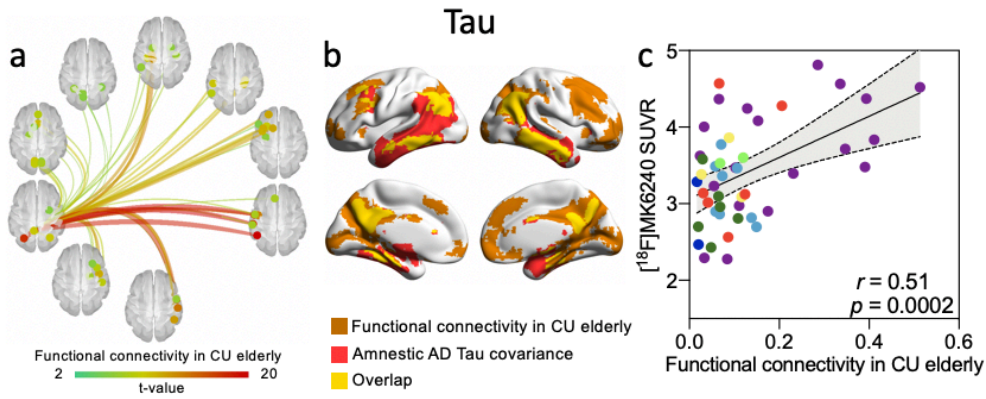
Methods: We assessed 131 cognitively unimpaired elderly and 63 AD individuals who underwent amyloid-PET with [¹⁸F]AZD4694, tau-PET with [¹⁸F]MK6240, structural MRI, fMRI and diffusion-weighted MRI. Of the subjects with AD, 11 had behavioural/dysexecutive AD, 18 had PCA and 11 had Logopenic variant PPA, while 23 subjects had an amnesic presentation (all were Ab+/Tau+). A voxelwise multivariate regression model was employed to determine the peak difference in [¹⁸F]MK6240 SUVR between each AD variant and CU elderly, with each clinical diagnosis entered as a different categorical variable and correcting for age, gender and MMSE score. Within each AD variant, the peak voxels derived from the regression model were used to compute the correlation between [¹⁸F]MK6240 SUVR in the seed voxel and [¹⁸F]MK6240 SUVR in every voxel, thus generating an [¹⁸F]MK6240 covariance network for each AD group. The same seeds were also employed in functional connectivity and diffusion tractography analyses in the CU elderly group. To determine whether the topographical distribution of tau pathology is related to connectivity properties of the human brain, we applied regression models to assess the relationship between functional/structural connectivity values from the CU population and [¹⁸F]MK6240 SUVR in each variant of AD.

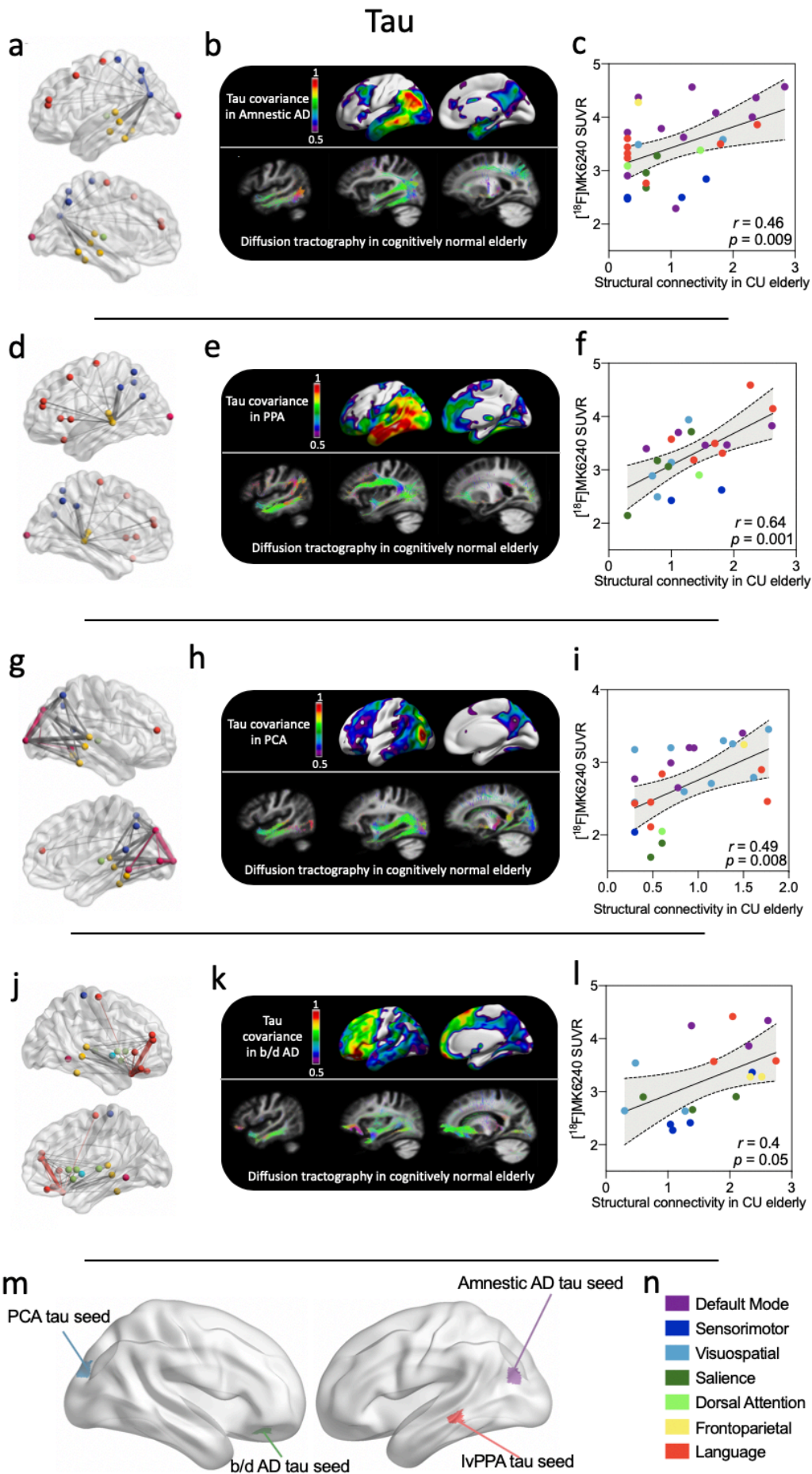
Results: Tau organization differed between AD groups, reflecting clinical phenotypes and organizing within distinct brain networks (Fig.1). Furthermore, functional (Fig.2) and structural (Fig.3) connectivity patterns of the human brain predicted *in vivo* [¹⁸F]MK6240 SUVR across the cerebral cortex in each variant of AD.

Conclusion: These results support a framework in which the intrinsic connectivity of the human brain provides a scaffold for tau pathology to spread to anatomically distant regions.

Tau







Keywords: Amyloid, Tau, fMRI, DWI, Networks

P168: Changes in volumetric MRI measures at 12 months significantly correlate with baseline [¹⁸F]GTP1 SUVR, but not [¹⁸F]GTP1 change

Balasz Toth¹, Sandra Sanabria Bohorquez¹, Paul Manser¹, Suzanne Baker¹, Edmond Teng¹, Jan Marik¹, Robby Weimer¹

¹Genentech, South San Francisco, CA, US

Objective: To characterize the longitudinal change in volumetric MRI and its relationship with tau burden as measured by [¹⁸F]GTP1.

Methods: [¹⁸F]GTP1 PET and T1-weighted MRI scans were performed at baseline and 12 months in amyloid negative and positive cognitive normal subjects (CN; n=2 and 7, respectively), and amyloid positive prodromal (Prod; n=20; MMSE 24-30, CDR = 0.5) and mild/moderate (MM; n=28; MMSE 22-30, CDR = 0.5-2) AD subjects. [¹⁸F]GTP1 SUVR measurements were made within whole cortical gray matter (WCG) and a temporal meta-ROI (Jack et al., Brain 2017) using cerebellum as reference. MRI volumes and cortical thickness measurements were made using FreeSurfer version 6.0. Relationships between MRI and [¹⁸F]GTP1 were summarized with Spearman correlations.

Results: Percentage change from baseline at month 12 for multiple volumetric MRI measures is shown in figure 1. Decreases in cortical volume were observed in all four cohorts across 12 months. Figure 2 plots percentage change from baseline of both temporal meta-ROI volume and thickness against baseline [¹⁸F]GTP1 temporal meta-ROI SUVR. Baseline [¹⁸F]GTP1 SUVR was significantly related to subsequent atrophy as measured by changes in both volume and thickness ($r = -0.43$ $p = 0.003$; $r = -0.48$, $p < 0.001$, respectively). Changes in [¹⁸F]GTP1 SUVR at month 12 were not significantly correlated with changes in volume or thickness ($r = -0.02$ $p = 0.897$; $r = -0.10$, $p = 0.527$, respectively).

Conclusion: Changes in volumetric MRI measures significantly correlated with baseline [¹⁸F]GTP1 SUVR, but not with changes in [¹⁸F]GTP1 SUVR. These results support the use of tau PET to identify patients who may be more prone to atrophy. A relationship between change in tau PET and atrophy was not observed but may exist over a longer period of time than 12 months.

Figure 1: Percentage change from baseline in cortical volume, ventricular volume, and temporal meta-ROI volume and thickness by cohort.

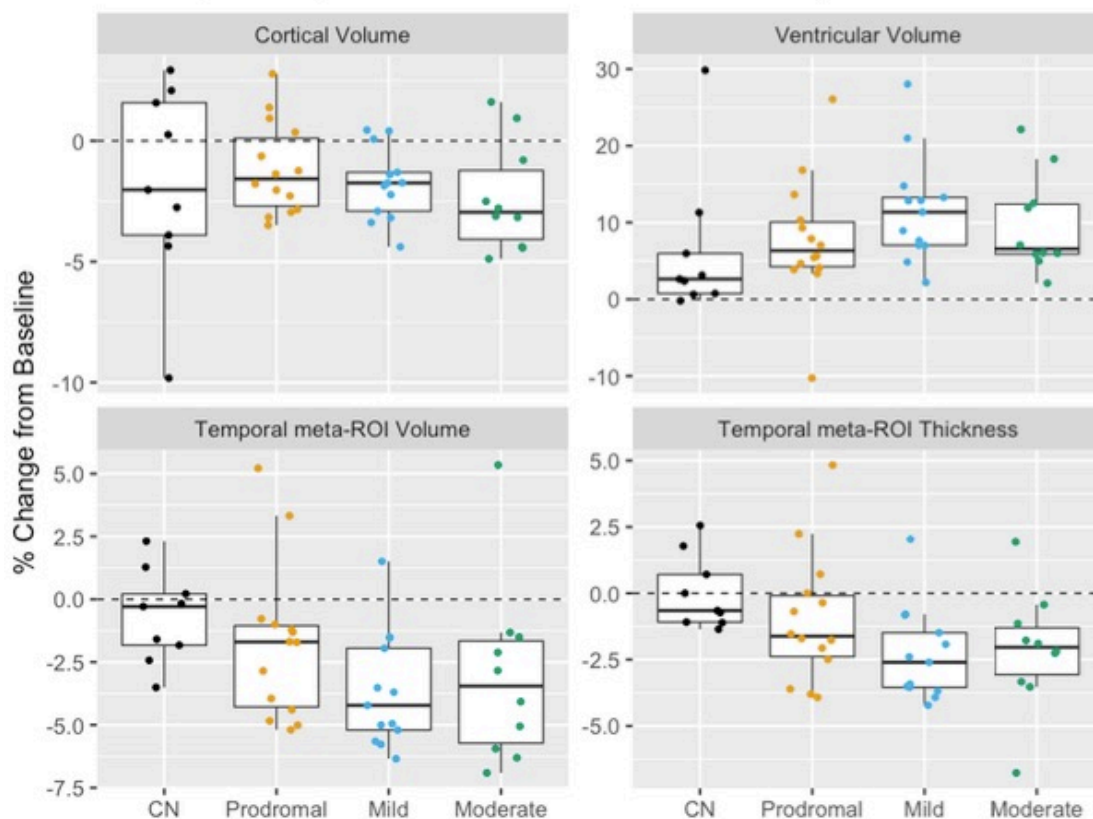
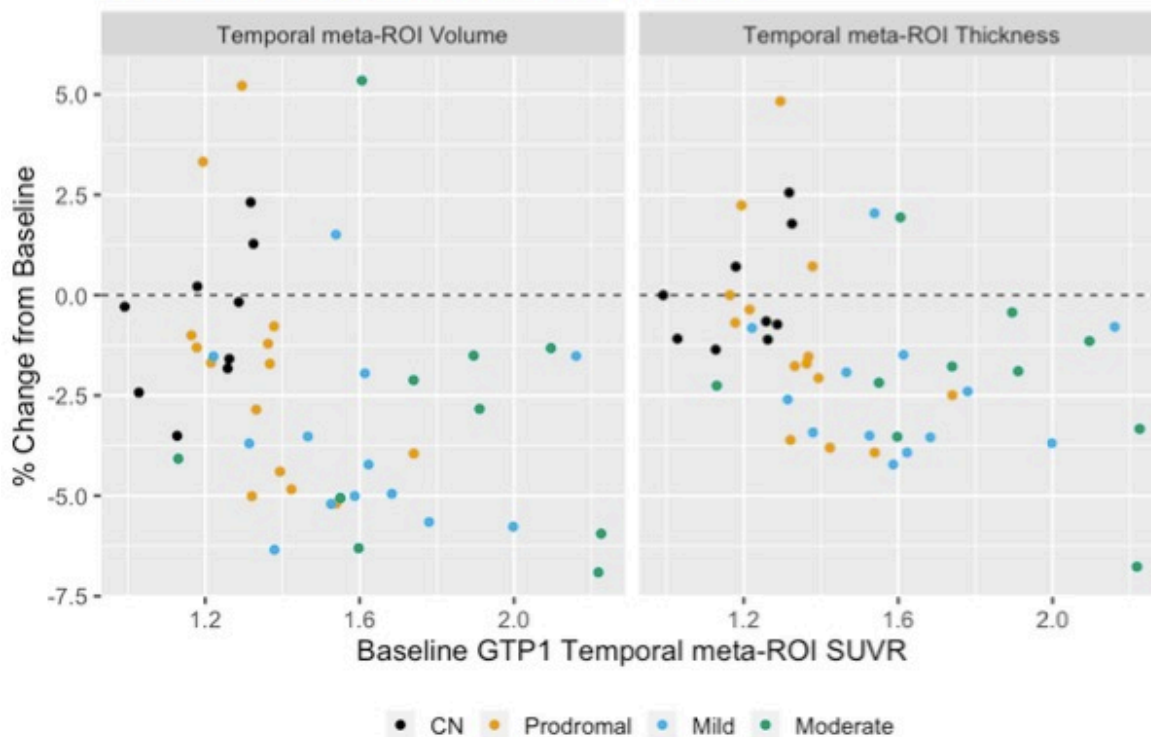


Figure 2: Percentage change from baseline in temporal meta-ROI volume and thickness plotted against baseline $[^{18}\text{F}]\text{GTP1}$ SUVR. Cognitive Normal: black; Prodromal: orange; Mild: blue; Moderate: green.



Keywords: GTP1, tau PET, MRI

P169: Elevated medial temporal lobe Tau PET with 18F-PI2620 in normal controls with “borderline” neuropsychological testing profiles

Tyler Toueg¹, Gayle Deutsch¹, Jessa Castillo², Madison Hunt³, Nicole Corso³, Alexandra Trelle³, Marc Harrison³, Carmen Azevedo², Bin Shen², David Anders², Jacob Hall¹, Carolyn Fredericks⁴, Sharon Sha¹, Guido Davidzon², Frederick Chin², Mehdi Khalighi², Anthony Wagner³, Elizabeth Mormino¹

¹Stanford University School of Medicine, Department of Neurology and Neurological Sciences, Stanford, CA, US

²Stanford University, Department of Radiology, Stanford, CA, US

³Stanford University, Department of Psychology, Stanford, CA, US

⁴Yale University School of Medicine, Department of Neurology, New Haven, CT, US

Objective: Early detection of Alzheimer’s disease (AD) pathology is critical for prevention strategies and understanding the transition between normal aging and disease. We explored early medial temporal lobe (MTL) Tau PET using ¹⁸F-PI2620 in cognitively normal older adults (CN) and neuropsych-defined “borderline” cognitively normal older adults (CN-B), and compared these groups to participants diagnosed with cognitive impairment.

Methods: Participants were recruited from the Stanford Aging and Memory Study (SAMS), a biomarker study of normal aging. Participants (N=241) completed neuropsychological evaluation and were enrolled into SAMS if classified as CN by a consensus panel comprised of neuropsychologists and neurologists. Individuals were classified as CN-B (N=35) with either a global CDR of 0.5 (indicative of informant concerns while within 1.5 SD on neuropsych), performance below 1.5 SD on one or more individual tests, or within 1-1.5 SD below population norms on a majority of tests. CN-B are similar to “Stage 2” described in the recent NIA-AA recommendations for categorizing AD on clinical and biomarker dimensions (Jack et al., 2018). A subset of 34 CN and 9 CN-B underwent Tau PET. Additionally, we examined Amyloid+ patients with amnesic MCI or AD dementia from the Stanford Memory Disorders Clinic (N=7).

Results: MTL Tau was elevated in CN-B compared to CN ($W = 81, p = 0.031$), whereas Amyloid+ patients had elevated MTL Tau compared to both CN-B ($W=9, p= 0.016$) and CN groups ($W=2, p<0.0001$). Entorhinal ($W=205, p=0.13$) and hippocampal ($W=210, p=0.09$) volume showed trend level differences across CN and CN-B.

Discussion: Although not meeting criteria for MCI, CN-B may have higher risk of early focal Tau pathology in the MTL compared to CN. Early signal within the MTL using ¹⁸F-PI2620 may emerge during the transition between CN and initial subtle cognitive changes.

Keywords: Tau PET, preclinical AD, aging, cognition

P170: Hippocampal tau accumulation predicts individual differences in episodic memory in cognitively normal older adults

Alexandra N. Trelle¹, Tyler N. Toueg¹, Jessa B. Castillo¹, Divya Channappa¹, Nicole Corso¹, Madison Hunt¹, Manasi Jayakumar³, Ayesha Nadiadwala², Wanjia Guo⁴, Carmen Azevedo¹, Bin Shin¹, Guido A. Davidson¹, Gayle Deutsch¹, Jacob N. Hall¹, Sharon J. Sha¹, Carolyn Fredericks⁵, Geoffrey Kerchner¹, Valerie Carr⁶, Frederick Chin¹, Anthony D. Wagner¹, Elizabeth C. Mormino¹

¹Stanford University, Stanford, CA, US

²University of Texas at Austin, Austin, TX, US

³Columbia University, New York, NY, US

⁴University of Oregon, Eugene, OR, US

⁵Yale University, New Haven, CT, US

⁶San Jose State University, San Jose, CA, US

Objective: To investigate the impact of early tau accumulation in the entorhinal cortex (ERC) and hippocampus (HC) on episodic memory in cognitively normal older adults using novel tau PET ligand ¹⁸F-PI2620.

Methods: Participants were cognitively normal (CN) older adults (ages 60-88 years) enrolled in the Stanford Aging and Memory Study (SAMS). Ninety-seven had CSF amyloid and phospho-tau data available, whereas 36 were scanned with ¹⁸F-PI2620 PET to measure focal tau accumulation in ERC and HC using standardized uptake value ratios (SUVRs, inferior cerebellum reference). Seven amyloid+ patients with cognitive impairment (ages 59-86) were also scanned with ¹⁸F-PI2620 PET. Episodic memory was assayed using two measures: 1) associative memory for word-image pairs (associative d'), and 2) mnemonic discrimination of studied objects from perceptually similar lure objects (lure discrimination d').

Results: HC tau and ERC tau was significantly lower in CN compared to amyloid+ patients with cognitive impairment. Within CN, HC tau was related to CSF AB₄₂, but not CSF phospho-tau. In contrast, ERC tau was marginally related to CSF phospho-tau, but not CSF AB₄₂. HC tau SUVR exhibited a significant negative relationship with both associative d' and lure discrimination d' . In contrast, ERC tau SUVR and global measures of CSF phospho-tau and CSF AB₄₂ did not explain significant variance in either measure of episodic memory.

Conclusions: Despite lower values of ¹⁸F-PI2620 medial temporal lobe tau in cognitively normal older adults compared to impaired patients, HC tau variability within this range contributes to individual differences in episodic memory and is associated with abnormal CSF amyloid. The use of novel ligand ¹⁸F-PI2620 to measure regional tau accumulation may offer increased sensitivity relative to global (i.e., CSF) measures of tau burden for detecting the earliest effects of tau pathology on episodic memory in cognitively normal older adults.

Keywords: Tau PET, CSF Amyloid, Hippocampus, Normal Aging, Episodic Memory

P171: Temporolimbic tau burden, as measured by 18F-AV1451, is a correlate of hippocampal volume loss over time

Jannis Fischer¹, Max Ahnen¹, Günther Dissertori¹, Werner Lustermann¹, Bruno Weber², Alfred Buck², Sonja Kagerer^{3,4}, Anton Gietl^{3,4}, Christoph Hock³, Paul Unschuld^{3,4}

¹*Institute for Particle Physics and Astrophysics, ETH Zurich, Zurich, Switzerland*

²*Institute of Pharmacology and Toxicology, University of Zurich (UZH) and ETH Zurich, Zurich, Switzerland*

³*Institute for Regenerative Medicine (IREM), University of Zurich (UZH), Zurich, Switzerland*

⁴*Psychiatric University Hospital Zurich (PUK), Zurich, Switzerland*

⁵*Data used in preparation of this study were obtained from the Alzheimer's Disease Neuroimaging Initiative (ADNI) database (adni.loni.usc.edu). A complete listing of ADNI investigators can be found at: http://adni.loni.usc.edu/wp-content/uploads/how_to_apply/ADNI_Acknowledgement_List.pdf, San Francisco, CA, US*

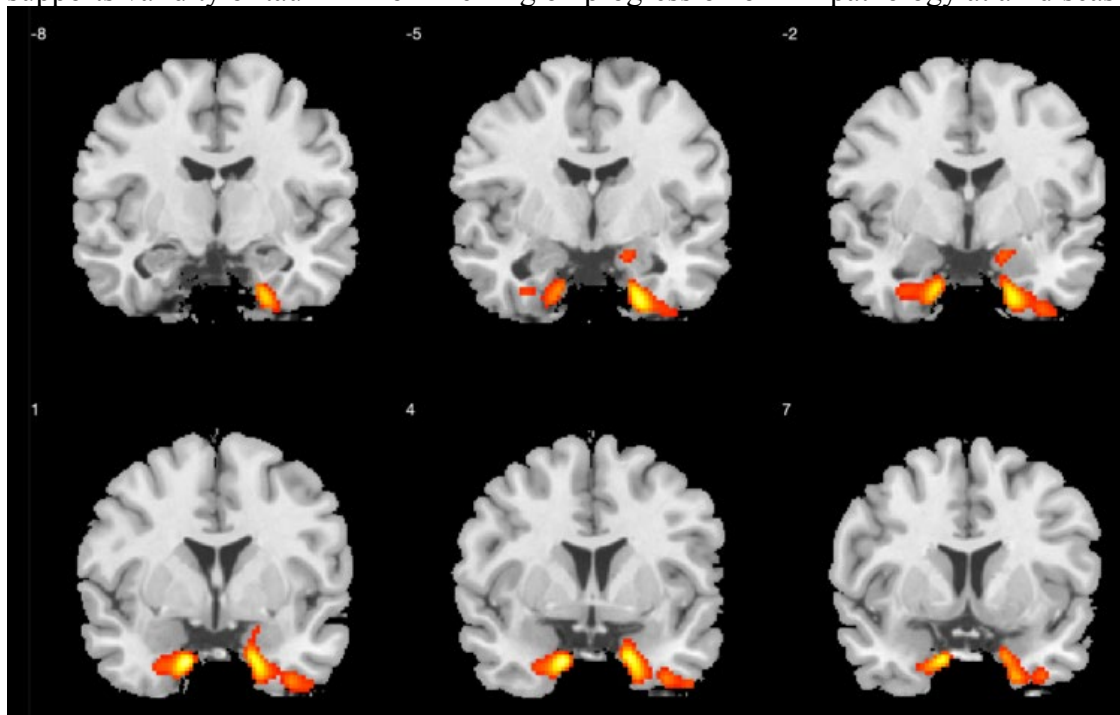
The positron emission tomography (PET) tracer 18F AV1451 is a valid measure for tau pathology in Alzheimer's disease (AD). The current study was aimed at characterizing predictive validity of regional 18F AV1451 SUVR for hippocampal volume loss over time, irrespective of present cognitive performance levels.

Data were obtained from the Alzheimer's Disease Neuroimaging Initiative database (adni.loni.usc.edu). For the current study 102 participants with 18F AV1451 PET and at least three longitudinal T1 weighted Magnetic Resonance Imaging (MRI) scans were included (mean age: 76.02 ± 6.44 years). Cognitive performance levels ranged from normal to severe cognitive dysfunction (mean MMSE 27.85, ± 2.85, min. 14, max. 30). Mean time between first and last MRI was 1664.1 ± 546.5 days. Hippocampal volume, and change over time was obtained by FreeSurfer subcortical segmentation. SPM12 was used to determine regional 18F AV1451 SUVR with strongest regression effects for hippocampal atrophy per year. No partial volume correction was applied.

The average slope of all annual hippocampal volume trajectories was -0.047 (± 0.056) ml/year. Strongest effects of AV1451 SUVR on annual hippocampal atrophy resulted for two clusters (extent threshold k=300 voxels) located in: 1.) Right Temporal Lobe, Superior Temporal Gyrus, kE=573 voxels, peaks (MNI): -16/2/-32 (T=11.49), -6/16/-16 (T=9.6), -30/0/-34 (T=9.47); 2.) Left Limbic Lobe, ParaHippocampal Gyrus, kE=741 voxels, peaks (MNI): 34/16/-38 (T=11.19), 16/4/-30 (T=11.16), 20/-4/-38 (T=11.11).

Our data demonstrate a strong relationship between temporal and limbic lobe AV1451 SUVR, and annual hippocampal atrophy in old aged adults. Our findings are consistent with earlier reports on regional brain volume loss in old age and corroborate an association between temporolimbic tau burden and neurodegenerative brain damage, as reflected by trajectories of hippocampal atrophy. Moreover, our study

supports validity of tau-PET for inferring on progression of AD pathology at all disease stages.



Peak AV-1451 SUVR with strongest effects on annual hippocampal atrophy trajectories.

Keywords: AV1451, tau, hippocampal atrophy

P172: Temporal evaluation for maximum CSF pTau181 – [18F]Flortaucipir concordance

Julie Wisch¹, Brian Gordon¹, Suzanne Schindler¹, Shaney Flores¹, Aylin Dincer¹, Anne Fagan¹, Tammie Benzinger¹, John Morris¹, Beau Ances¹

¹Washington University, St. Louis, MO, US

Background: Alzheimer’s disease (AD) is characterized by mis-aggregation of amyloid and tau proteins. Clinical trials for AD have historically emphasized amyloid reduction/prevention, but have generally demonstrated poor efficacy in preventing cognitive change. Tau is now a therapeutic target of interest. The Amyloid-Tau(Neurodegeneration) (A-T(N)) framework includes cerebrospinal fluid (CSF) pTau₁₈₁ and positron emission tomography (PET) tau imaging as appropriate measures of tau.

This analysis aims to identify the time window for which CSF pTau₁₈₁ and tau PET have greatest concordance and specify the optimal CSF pTau₁₈₁ threshold for tau positivity.

Methods: PET for amyloid and tau were obtained for 161 participants enrolled at the Knight Alzheimer Disease Research Center (Table 1). CSF pTau₁₈₁ was assayed (using an Elecsys platform) for these participants. We used two-year bins to calculate the Spearman correlation of CSF pTau₁₈₁ with tauopathy (Figure 1) and regional tau as measured by [¹⁸F]flortaucipir (Figure 2). Finally, we performed receiver operating characteristic analysis to identify the optimal CSF pTau₁₈₁ threshold (and the appropriate time window for data collection) associated with tau PET positivity.

Results: The greatest concordance occurs when lumbar puncture is performed 4 to 6 years prior to PET imaging in a mixed cohort (R = 0.541) and 6 to 8 years prior to PET in a cohort of individuals with AD pathologic change (R = 0.602). CSF pTau₁₈₁ is a reasonably good predictor of tau PET positivity (AUC = 0.749).

Conclusions: Understanding the temporal relationship between CSF and PET could be a powerful tool in clinical trial outcome development. If a drug targeting tau can reduce mature tangle development, this could be evaluated by comparing earlier CSF pTau₁₈₁ measurements with current tau PET. Further, care should be taken when classifying individuals as “Tau Positive” in the A-T(N) framework and utilizing CSF and PET measures interchangeably.

Table 1. Participant demographics do not differ on the bases of sex, years of education, APOE status, race, cognitive status, or amyloid status. Individuals with a PET scan and LP within 2 years of each other are older than individuals with PET and LP obtained 6 or more years apart.

	(-13,-10]	(-10,-8]	(-8,-6]	(-6,-4]	(-4,-2]	(-2,0]	(0,2]	p
n	17	51	66	51	114	75	28	
Age at LP (mean (sd))	62.55 (7.93)	63.48 (8.43)	64.88 (7.31)	67.92 (6.77)	66.38 (7.67)	69.86 (7.90)	71.62 (8.87)	<0.001
Age at PET scan (mean (sd))	73.70 (8.05)	72.51 (8.35)	71.63 (7.41)	73.05 (6.70)	69.48 (7.60)	70.48 (8.02)	71.20 (8.86)	0.053
Sex: Number of males (%)	5 (29.4)	10 (19.6)	24 (36.4)	21 (41.2)	46 (40.4)	36 (48.0)	15 (53.6)	0.028
Years of Education (mean (sd))	16.82 (2.38)	15.75 (2.37)	16.08 (2.31)	16.14 (2.38)	16.25 (2.23)	16.25 (2.40)	16.46 (2.41)	0.700
APOE4+ (%)	5 (31.2)	19 (37.3)	20 (30.8)	19 (38.0)	33 (28.9)	24 (32.0)	8 (29.6)	0.913
Race (%)								0.830
Asian	0 (0.0)	1 (2.0)	1 (1.5)	0 (0.0)	1 (0.9)	1 (1.3)	0 (0.0)	
Black	0 (0.0)	1 (2.0)	1 (1.5)	1 (2.0)	7 (6.1)	5 (6.7)	1 (3.6)	
White	17 (100.0)	49 (96.1)	64 (97.0)	50 (98.0)	106 (93.0)	69 (92.0)	27 (96.4)	
CDR (%)								0.778
0	17 (100.0)	46 (90.2)	60 (90.9)	48 (94.1)	110 (96.5)	69 (92.0)	26 (92.9)	
0.5	0 (0.0)	5 (9.8)	5 (7.6)	2 (3.9)	4 (3.5)	5 (6.7)	2 (7.1)	
1	0 (0.0)	0 (0.0)	1 (1.5)	1 (2.0)	0 (0.0)	1 (1.3)	0 (0.0)	
Amyloid Positive (%)	3 (17.6)	12 (23.5)	16 (24.2)	12 (23.5)	28 (24.6)	19 (25.3)	8 (28.6)	0.993

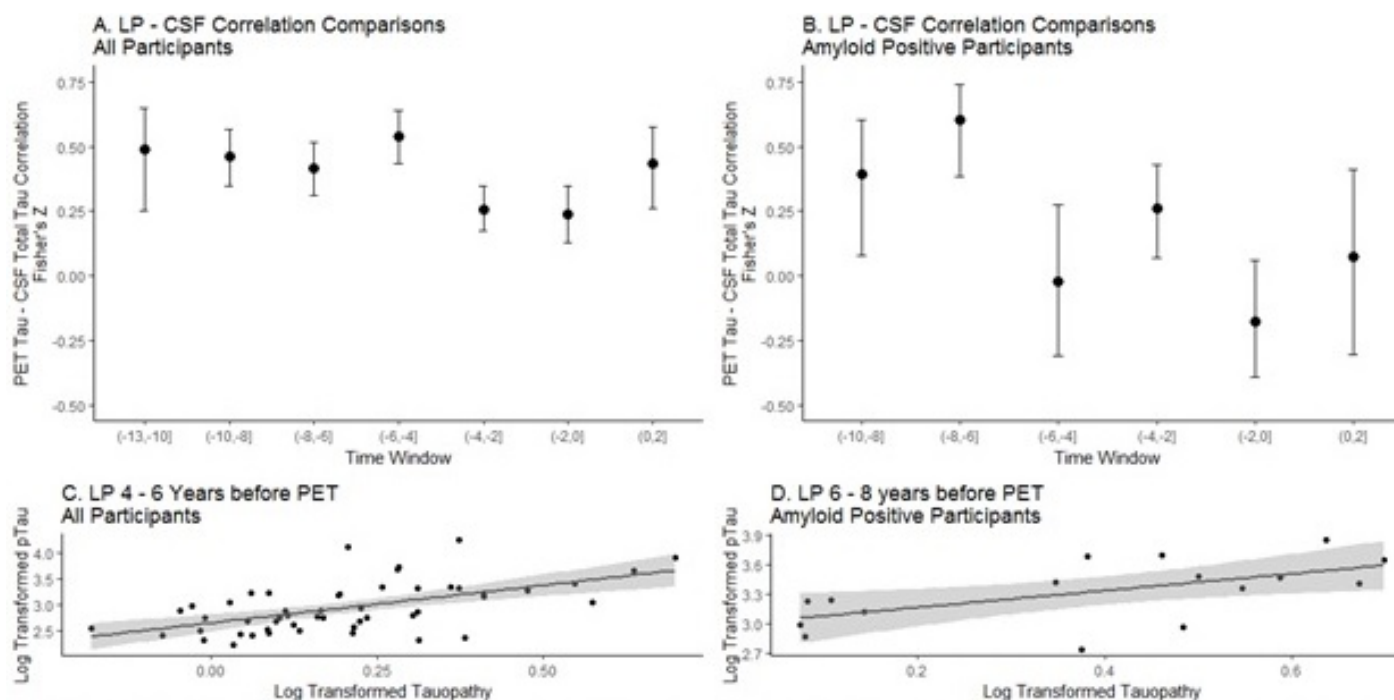


Figure 1. Overall, participants who underwent LP 4 – 6 years before PET scan had the highest correlation between PET tau and CSF pTau. For individuals exhibiting early signs of Alzheimer Disease pathology, the strongest correlation between PET tau and CSF pTau occurred when the measurements were taken 6 – 8 years apart.

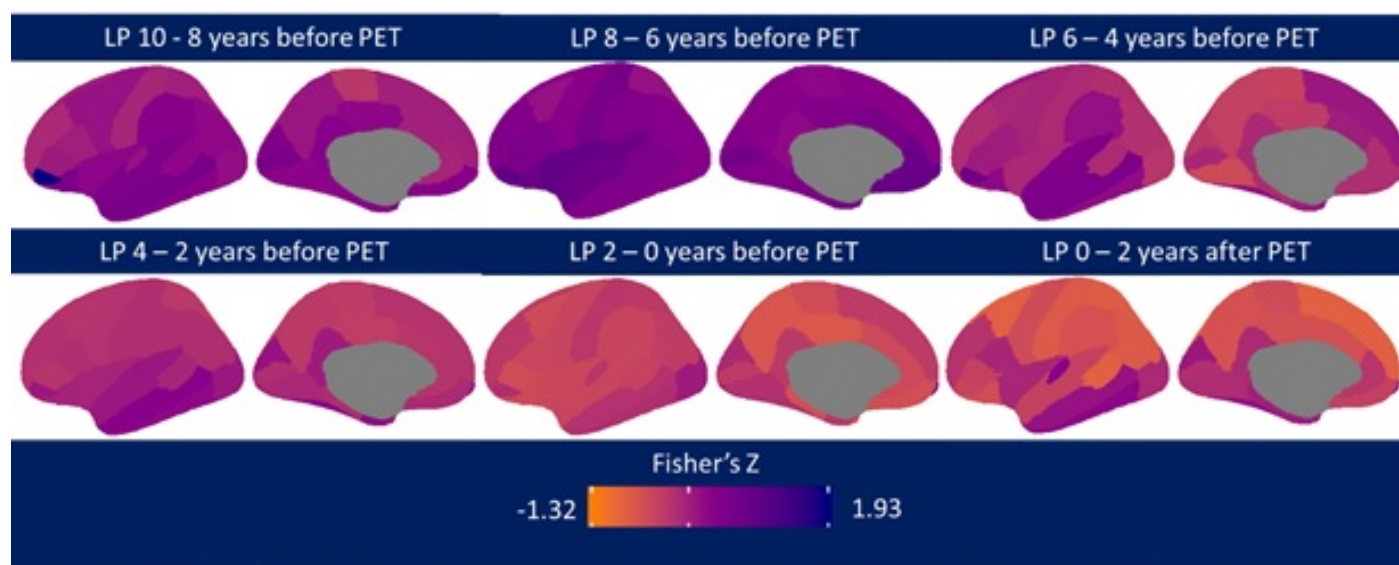


Figure 2. We found the highest regional correlations with CSF pTau₁₈₁ to have occurred during the 4 to 6 year time window. Specifically, the fusiform gyrus ($R = 0.732$), inferior temporal ($R = 0.625$), and entorhinal cortex ($R = 0.550$) all had very high correlations with CSF pTau₁₈₁. Notably, these three regions are in Braak stages I/II and III/IV, suggesting that the earlier stages of tau deposition may occur 4 to 6 years after levels of pTau₁₈₁ start to elevate in the CSF.

Keywords: PET, CSF, Alzheimer's disease, flortaucipir

P173: [¹⁸F]flortaucipir PET is more closely associated with disease severity than CSF p-tau in Alzheimer's disease

Emma Wolters^{1,2}, Rik Ossenkoppele^{2,3}, Sander Verfaillie¹, Emma Coomans¹, Tessa Timmers^{1,2}, Denise Visser¹, Hayel Tuncel¹, Sandeep Golla¹, Albert Windhorst¹, Ronald Boellaard¹, Wiesje van der Flier^{2,4}, Charlotte Teunissen⁵, Philip Scheltens², Bart van Berckel¹

¹Department of Radiology & Nuclear Medicine, Amsterdam Neuroscience, Vrije Universiteit Amsterdam, Amsterdam UMC, Amsterdam, The Netherlands

²Alzheimer Center Amsterdam, Department of Neurology, Amsterdam Neuroscience, Vrije Universiteit Amsterdam, Amsterdam UMC, Amsterdam, The Netherlands

³Clinical Memory Research Unit, Lund University, Lund, Sweden

⁴Department of Epidemiology and Biostatistics, Vrije Universiteit Amsterdam, Amsterdam UMC, Amsterdam, The Netherlands

⁵Neurochemistry Laboratory, Department of Clinical Chemistry, Vrije Universiteit Amsterdam, Amsterdam UMC, Amsterdam, The Netherlands

Background: *In vivo* Alzheimer's disease (AD) biomarkers for tau pathology are cerebrospinal fluid (CSF) phosphorylated tau (p-tau) and [¹⁸F]flortaucipir PET. Our aim was to assess i) associations between CSF p-tau with [¹⁸F]flortaucipir PET, and ii) associations of both tau biomarkers with cognition and atrophy.

Methods: We included 78 amyloid positive cognitively impaired patients (MCI (n=8) and AD dementia (n=45)) and 25 cognitively normal subjects (40% amyloid-positive). Dynamic 130 minute [¹⁸F]flortaucipir PET scans were acquired to generate binding potential (BP_{ND}) images using receptor parametric mapping. We obtained regional BP_{ND} from regions-of-interest (ROIs) closely aligning to the Braak stages. Cognition was assessed using MMSE and composite scores of four cognitive domains, while atrophy was measured using the using gray matter volumes covering the major brain lobes. We performed linear regression models to investigate associations between CSF p-tau and tau PET and between CSF p-tau, tau PET and cognition or atrophy (model 1). We then assessed the independent effects of CSF p-tau and tau PET on cognition or atrophy by simultaneously adding the other tau biomarker as a predictor (model 2). Models were adjusted for age, sex, time lag between assessments, education (cognition only) and total intracranial volume (atrophy only).

Results: Higher [¹⁸F]flortaucipir BP_{ND} across all ROIs were associated with higher CSF p-tau (range of standardized betas, $s\beta = 0.43-0.46$, all $p < 0.01$, figure 1). When [¹⁸F]flortaucipir BP_{ND} and CSF p-tau were entered simultaneously, [¹⁸F]flortaucipir BP_{ND} (range $s\beta = -0.20 - -0.57$, all $p < 0.05$) was strongly associated with multiple cognitive domains and atrophy regions, while CSF p-tau was exclusively associated with MMSE ($s\beta = -0.21$, $p < 0.05$), particularly for MCI/AD patients (table-1, 2).

Conclusion: [¹⁸F]flortaucipir BP_{ND} showed stronger associations with cognition and neurodegeneration than CSF p-tau. As such, tau PET may more accurately reflect disease severity in AD than CSF p-tau.

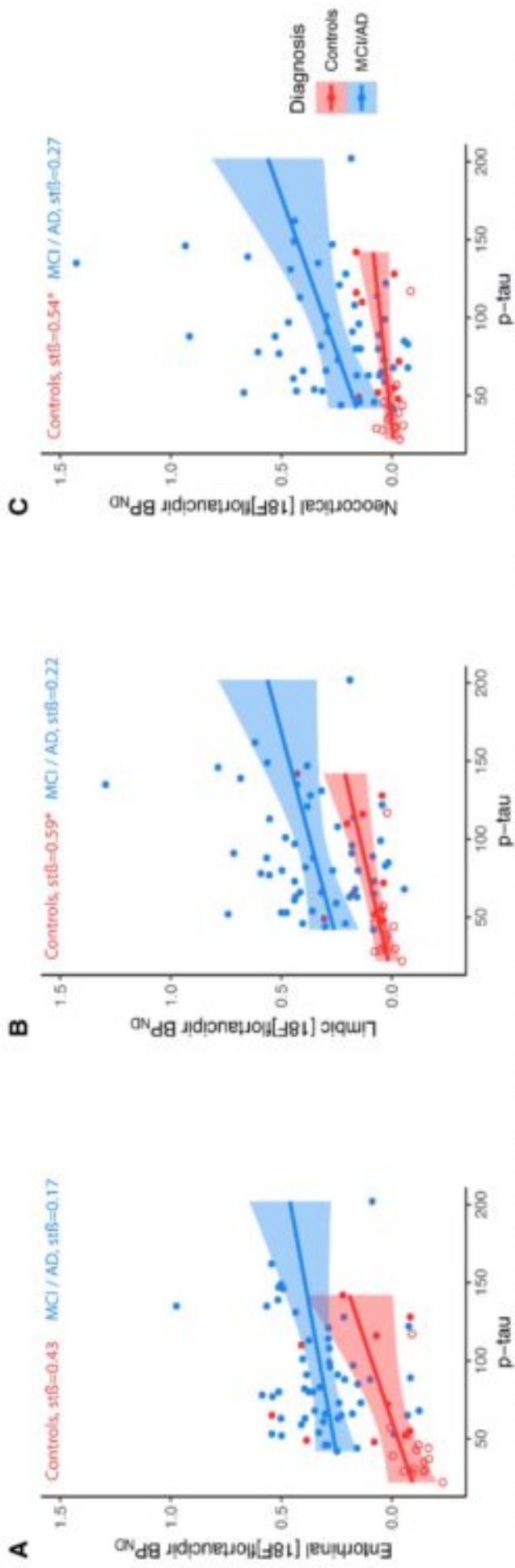


Figure 1 Scatterplots of the observed relationship between CSF p-tau with entorhinal, limbic and neocortical [^{18}F]flortaucipir BP_{ND} . Each symbol represents one subject. The fitted lines are stratified over AD (blue) and controls (red); closed circles are $\text{A}\beta$ positive, open circles are $\text{A}\beta$ negative. Correlations were adjusted for age, sex and time lag between LP and [^{18}F]flortaucipir PET scan.

	Total Sample (n=78)		Controls (n=25)		MCI/AD (n=53)	
	Model 1	Model 2	Model 1	Model 2	Model 1	Model 2
CSF						
p-tau						
MMSE	-0.44^b	-0.21^a	0.07	0.20	-0.29^a	-0.17
Memory	-0.26^a	-0.12	-0.10	0.10	-0.05	-0.04
Attention	-0.18	-0.01	-0.16	0.08	-0.05	0.03
Executive	-0.14	0.06	0.28	0.48^a	-0.03	0.07
Language	-0.10	-0.00	0.11	0.32	-0.00	0.01
[¹⁸F]flortaucipir PET						
Entorhinal region						
MMSE	-0.41^b	-0.25^a	-0.23	-0.21	-0.01	-0.04
Memory	-0.54^b	-0.52^b	-0.50^b	-0.50^a	-0.27	-0.27
Attention	-0.14	-0.35	-0.17	-0.14	0.43^b	0.45^b
Executive	-0.29^b	0.25 ^a	0.07	-0.01	0.13	0.14
Language	-0.23^a	-0.22	-0.18	-0.41	0.20	0.21
Limbic region						
MMSE	-0.64^b	-0.54^b	-0.22	-0.20	-0.50^b	-0.45^b
Memory	-0.46^b	-0.41^b	-0.24	-0.22	-0.10	-0.09
Attention	-0.45^b	-0.41^b	-0.29	-0.32	-0.22	-0.21
Executive	-0.52^b	-0.52^b	-0.06	-0.23	-0.34^a	-0.34^a
Language	-0.33^b	-0.33^a	-0.10	-0.24	-0.11	-0.11
Neocortical region						
MMSE	-0.64^b	-0.53^b	-0.17	-0.13	-0.50^b	-0.43^b
Memory	-0.38^b	-0.29^a	-0.32	-0.29	0.04	0.07
Attention	-0.55^b	-0.52^b	-0.40^a	-0.42	-0.38^a	-0.39^a
Executive	-0.56^b	-0.57^b	-0.16	-0.31	-0.39^a	-0.41^a
Language	-0.27^a	-0.25	-0.25	-0.39	0.00	0.02

Standardized β coefficients (significant in bold) from multiple regression analysis with cognitive measures as the dependent variables and either CSF p-tau or [¹⁸F]flortaucipir BP_{ND} as predictors using separate analyses.

Model 1 = Effects adjusted for age, sex, education, and time lag between cognitive testing and LP or [¹⁸F]flortaucipir PET

Model 2 = Effects adjusted for age, sex, education, time lag between cognitive testing and LP or [¹⁸F]flortaucipir PET, and neocortical [¹⁸F]flortaucipir (for CSF p-tau) or CSF p-tau (for [¹⁸F]flortaucipir analysis).

^a Significant standardized β coefficient at $p < 0.05$.

^b Significant standardized β coefficient at $p < 0.01$.

Table 1 Standardized β coefficients for the relationship between cognitive outcome and CSF p-tau or entorhinal, limbic and neocortical [¹⁸F]flortaucipir BP_{ND} over the total sample and stratified per disease group

	Total Sample (n=78)		Controls (n=25)		MCI/AD (n=53)	
	Model 1	Model 2	Model 1	Model 2	Model 1	Model 2
CSF p-tau						
Medial temporal	-0.15	-0.01	0.18	0.25	0.03	0.08
Lateral temporal	-0.21^a	-0.00	0.15	-0.01	-0.13	-0.01
Medial parietal	-0.17	0.04	0.17	0.29	-0.09	0.04
Lateral parietal	-0.20^a	0.02	0.25	0.33	-0.13	-0.00
Temporoparietal	-0.20^a	0.02	0.18	0.27	-0.12	0.01
Frontal	-0.10	0.09	0.21	0.33	-0.07	0.04
Occipital	-0.22^a	-0.15	0.15	0.30	-0.18	-0.07
[¹⁸F]flortaucipir PET						
Entorhinal region						
Medial temporal	-0.42^b	-0.45^b	-0.14	-0.22	-0.26^a	-0.27^a
Lateral temporal	-0.33^b	-0.31^b	-0.09	-0.16	-0.23	-0.20
Medial parietal	-0.27^b	-0.27^b	-0.08	-0.16	0.18	-0.15
Lateral parietal	-0.31^b	-0.29^b	-0.10	-0.21	-0.16	-0.12
Temporoparietal	-0.32^b	-0.31^b	-0.09	-0.17	-0.22	-0.19
Frontal	-0.23^a	-0.25^a	-0.19	-0.32	-0.11	-0.09
Occipital	-0.27^b	-0.20^a	-0.21	-0.32	-0.14	-0.09
Limbic region						
Medial temporal	-0.38^b	-0.40^b	-0.14	-0.20	-0.26^a	-0.23
Lateral temporal	-0.48^b	-0.46^b	-0.07	-0.18	-0.50^b	-0.49^b
Medial parietal	-0.41^b	-0.43^b	-0.11	-0.26	-0.41^b	-0.40^b
Lateral parietal	-0.40^b	-0.41^b	-0.01	-0.26	-0.37^b	-0.35^b
Temporoparietal	-0.46^b	-0.48^b	-0.07	-0.21	-0.47^b	-0.47^b
Frontal	-0.31^b	-0.34^b	-0.08	-0.26	-0.29^a	-0.28^a
Occipital	-0.38^b	-0.37^b	-0.16	-0.32	-0.37^b	-0.34^b
Neocortical region						
Medial temporal	-0.32^b	-0.33^b	-0.01	-0.08	-0.18	-0.20
Lateral temporal	-0.47^b	-0.48^b	-0.06	-0.13	-0.48^b	-0.47^b
Medial parietal	-0.45^b	-0.48^b	-0.09	-0.18	-0.49^b	-0.49^b
Lateral parietal	-0.49^b	-0.51^b	-0.00	-0.12	-0.50^b	-0.49^b
Temporoparietal	-0.48^b	-0.49^b	-0.06	-0.15	-0.49^b	-0.48^b
Frontal	-0.39^b	-0.44^b	-0.11	-0.24	-0.41^b	-0.40^b
Occipital	-0.47^b	-0.47^b	-0.18	-0.28	-0.50^b	-0.42^b

Standardized β coefficients (significant in bold) from multiple regression analysis with grey matter density as the dependent variable and either CSF p-tau or [¹⁸F]flortaucipir BP_{ND} as predictors using separate analyses.

Model 1 = Effects adjusted for age, sex, intracranial volume and time lag between MRI and LP or [¹⁸F]flortaucipir PET

Model 2 = Effects adjusted for age, sex, intracranial volume, time lag between MRI and LP or [¹⁸F]flortaucipir PET, and neocortical [¹⁸F]flortaucipir (for CSF p-tau) or CSF p-tau (for [¹⁸F]flortaucipir analysis).

^a Significant standardized β coefficient at $p < 0.05$. ^b Significant standardized β coefficient at $p < 0.01$.

Table 2 Standardized β coefficients for the relationship between regional grey matter atrophy and CSF p-tau or [¹⁸F]flortaucipir BP_{ND} over the total sample and stratified per disease group

Keywords: Tau, CSF, PET, cognition, atrophy

P174: Associations of tau pathology and functional connectivity with retrospective cognitive change among cognitively normal older adults

Andrea Shafer¹, Murat Bilgel¹, Jacob Ziontz^{1,2}, Dean Wong³, Susan Resnick¹

¹Laboratory of Behavioral Neuroscience, National Institute on Aging, Baltimore, MD, US

²Helen Wills Neuroscience Institute, University of California Berkeley, Berkeley, CA, US

³Department of Radiology and Radiological Science, Johns Hopkins University School of Medicine, Baltimore, MD, US

Introduction: Tau pathology in cognitively normal (CN) older adults is associated with hyper-connectivity. Tau and functional connectivity are individually related to cognition, but how they interact to influence cognitive change in CN individuals remains unclear.

Methods: We used data for 59 individuals (mean age at tau PET 77.9, SD 8.6) in the Baltimore Longitudinal Study of Aging to investigate the cross-sectional association between hippocampal tau (measured as FTP SUVR) and intra-regional connectivity (measured using resting state fMRI) for the default mode network (DMN) and DMN subregions important for memory (hippocampus) and visuospatial ability (precuneus). We then investigated the associations of hippocampal tau and connectivity with retrospective rates of change in memory (California Verbal Learning Test composite of immediate and delayed recall, n=393 longitudinal observations) and visuospatial ability (Card Rotation Test, n=376). We repeated analyses using parahippocampal instead of hippocampal tau due to potential choroid plexus signal spillover.

Results: Controlling for age, sex, PiB status, and fMRI motion, higher hippocampal tau was associated with greater hippocampal connectivity [b=0.63, p=0.049]. Longitudinally, after controlling for age, sex, and PiB status, higher hippocampal tau at last visit was related to steeper retrospective memory decline [b=-0.086, p=0.0001], while higher hippocampal connectivity at last visit was related to a less severe decline in memory over time [b=0.267, p=0.001] (Figure 1). Higher precuneus connectivity was linked to steeper decline in visuospatial ability [b=-0.165, p=0.043], and this association was exacerbated in individuals with more hippocampal tau (time*hippocampal tau*precuneus connectivity interaction: [b=-0.872, p=0.005]) (Figure 2). All results were replicated in models with parahippocampal tau.

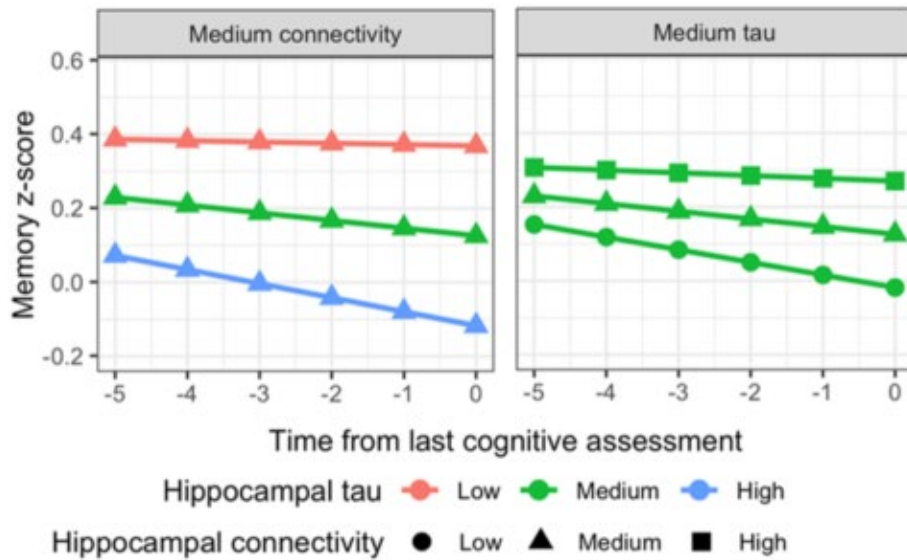


Figure 1. *Left:* Higher hippocampal tau is associated with steeper retrospective memory decline. Predicted memory z-scores over a 5-year period are shown, given a medium level of hippocampal connectivity. *Right:* Higher hippocampal connectivity is associated with attenuated retrospective memory decline. Predicted memory z-scores over a 5-year period are shown, given a medium level of hippocampal tau.

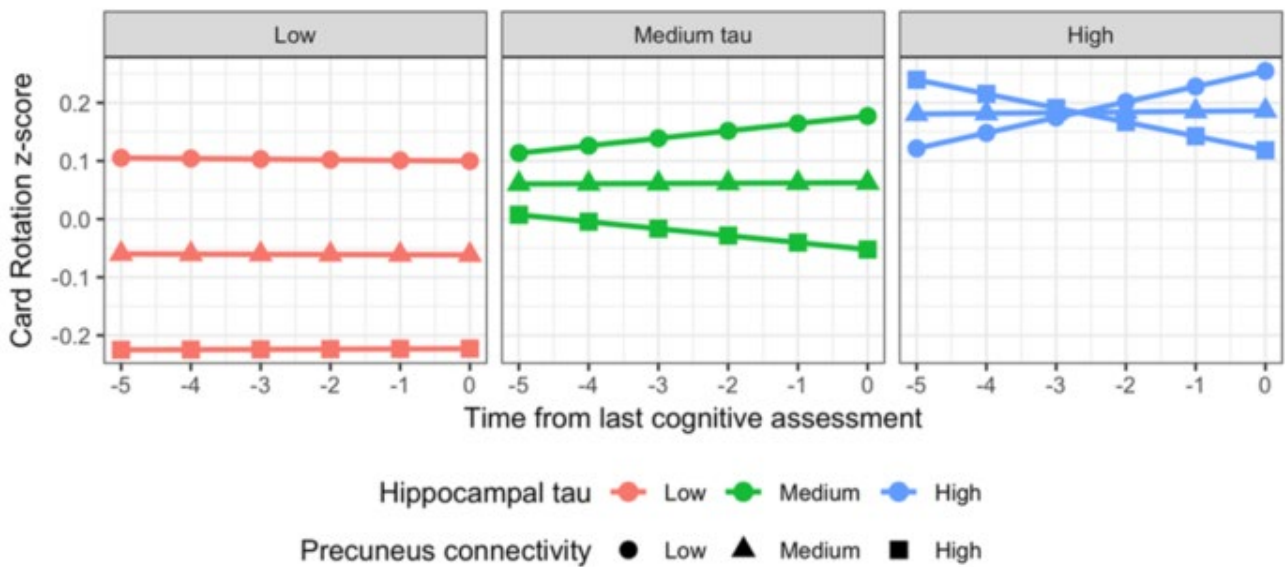


Figure 2. Steepest declines in visuospatial ability, measured by the Card Rotation Test, are observed among individuals with high hippocampal tau and high precuneus connectivity. The direction of the association between precuneus connectivity and rate of change in visuospatial ability is dependent on the level of hippocampal tau.

Discussion: Our results show regionally dependent relationships between PET markers of pathological protein accumulation, connectivity, and cognition. Consistent with previous findings, we show tau is related to intra-regional functional connectivity. Extending previous work, we show cognitive change is modified by hippocampal tau and intra-regional connectivity.

Keywords: FTP, resting state, fMRI, memory, visuospatial

Friday, January 17, 2020 - 10:00 - 11:00am

SESSION 7B: TAU II

Friday, January 17, 2020		
10:00 AM	SESSION 7B: TAU II	CHAIRS: Clifford Jack, MD, <i>Mayo Clinic</i> Reisa Sperling, MD, <i>Brigham and Women's Hospital</i> Victor Villemagne, MD, <i>Austin Health</i>
10:00 AM	Critical threshold of elevated amyloid associated with rapid tau accumulation: a ca-tau-strophe in the making	Keith Johnson, MD, <i>Massachusetts General Hospital</i>
10:15 AM	The Meaning of Tau Positivity with Respect to Clinical Progression	Michael Devous, PhD, <i>Avid Pharmaceuticals</i>
10:30 AM	Longitudinal tau PET changes in cognitively unimpaired persons with different β -amyloid levels	David Knopman, MD, <i>Mayo Clinic</i>
10:45 AM	Defining a tau positive flortaucipir PET signal relative to AD neuropathology	Michael Pontecorvo, PhD, <i>Avid Pharmaceuticals</i>
11:00 AM	Discussion (7A and 7B)	

Critical threshold of elevated amyloid associated with rapid tau accumulation: a ca-tau-strophe in the making

Keith Johnson¹, Heidi Jacobs¹, Bernard Hanseeuw^{1,2}, Justin Sanchez¹, John Alex Becker¹, Aaron Schultz¹, Kathryn Papp^{1,3}, Julie Price¹, Dorene Rentz^{1,3}, Reisa Sperling^{1,3}

¹Massachusetts General Hospital / Harvard Medical School, Boston, MA, US

²Cliniques Universitaires Saint-Luc, Brussels, Belgium

³Brigham and Women's Hospital / Harvard Medical School, Boston, MA, US

Introduction: Amyloid-beta ($A\beta$) and PHF tau proteinopathies define Alzheimer's disease and follow a spatiotemporal sequence by which tau accumulation is rapidly accelerated with $A\beta$, transforming a seemingly benign medial temporal lobe tauopathy into a cascade of injurious events that leads to dementia. Therapeutic strategies to interrupt the disease process may be more advantageously applied at specific critical points in the interacting trajectories of $A\beta$ and tau.

Methods: We characterized concurrent change in $A\beta$ and tau in HABS participants (N=131 with mean age=75.18 years, SD=6.96 years; 78 females; n=123 with CDR=0 and n=8 with CDR \geq 0.5) using cortical PiB DVR and Flortaucipir (FTP, composite of entorhinal and inferior temporal cortex) SUVR. Longitudinal PET imaging of up to four time points (299 observations, median 29.65 months [IQR, 22.36 – 39.53 months] was included (Figure 1). Subject-specific slopes in FTP and PiB were associated using linear regressions, covarying for baseline PiB and baseline age. Nonlinear relationships between both biomarkers were assessed in a model-free manner using Generalized Additive Models (GAM).

Results: We found a positive relationship between PiB change (y-axis) and FTP change (Figure 1 & 2 scale bar SUVR, $t=3.72$, $p<0.001$, adjusted for baseline PiB), such that FTP accumulation accelerated once a critical baseline $A\beta$ -level was reached (approximate PiB DVR= 1.1 - 1.2, with quadratic effect of the interaction baseline PiB by PIB change $t=-1.98$, $p=0.050$). Higher levels of baseline PiB (x-axis) were associated with faster rates of both PiB and FTP accumulation (GAM, $p<0.005$; Figure 2). Rapid $A\beta$ and tau accumulation coincided with cognitive decline, with the majority of these participants progressing to mild cognitive impairment (Figure 3).

Conclusion: Reaching a critical threshold of amyloidosis appears necessary to precipitate rapid accumulation of both $A\beta$ and tau in a subset of clinically normal older individuals and is associated with imminent clinical decline.

Figure 1

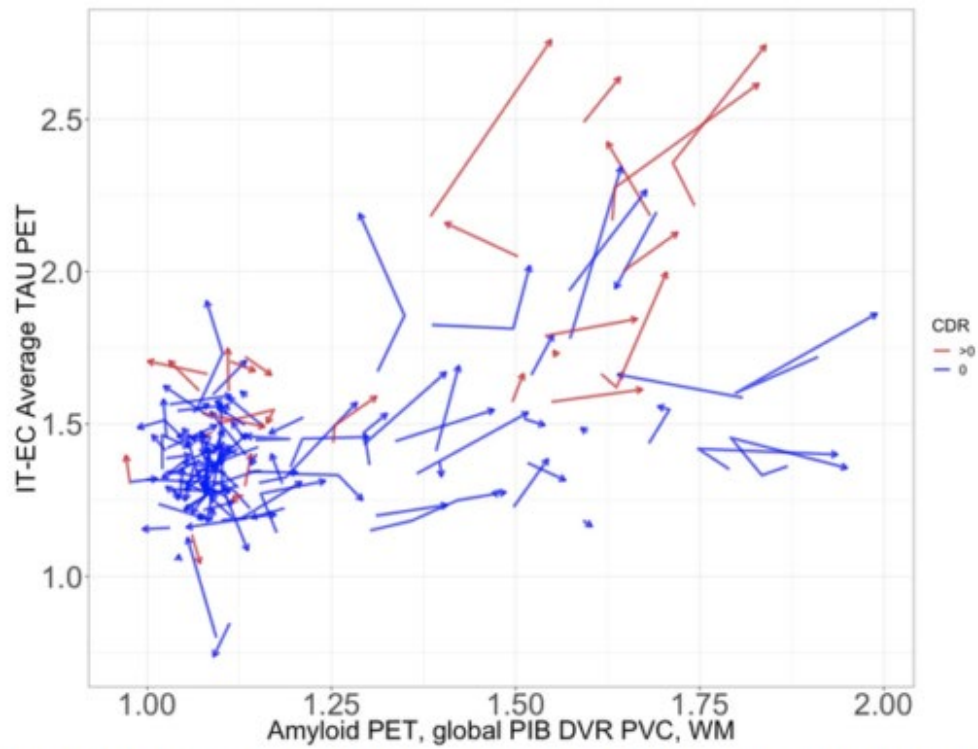


Figure 1: Spaghetti plot showing individual HABS participants' relationship between changes in PiB and changes in FTP (N=131) over a median of 29 months. Blue lines show the clinically normal individuals and red lines the individuals who progressed to MCI. Arrowheads indicate the follow-up time point.

Figure 2

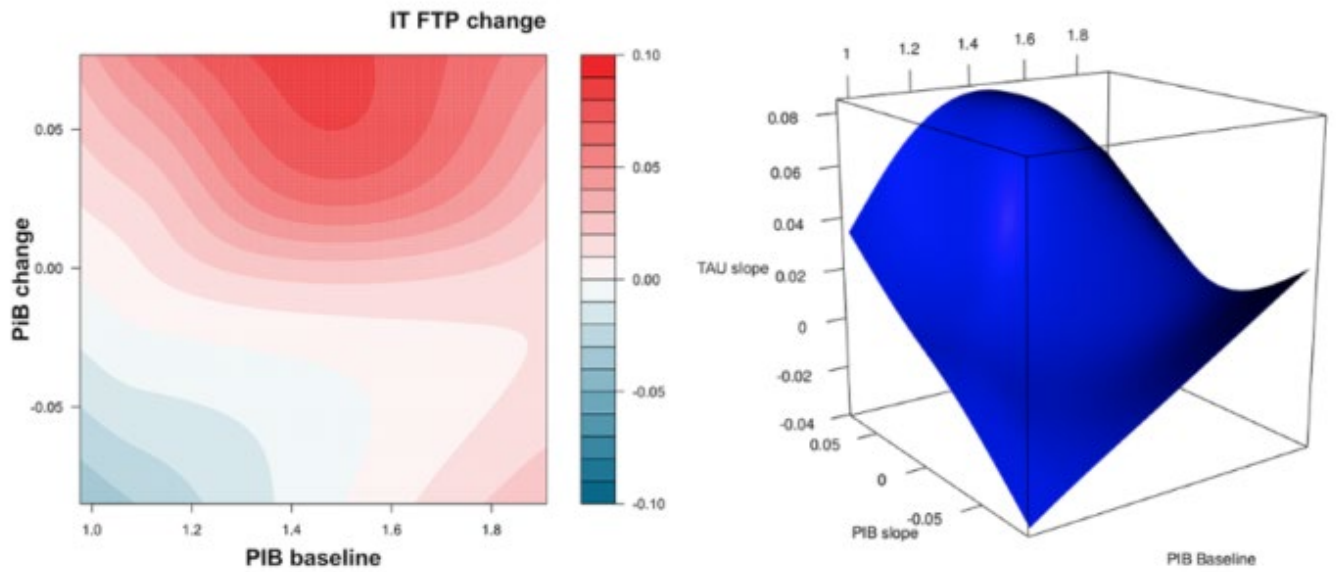


Figure 2. 2D and 3D- Visualization of a generalized additive model (GAM, $n=131$), indicating a positive relationship between PiB change (y-axis) and FTP IT tau change (scale bar, SUVR), which accelerates at higher levels of baseline PiB (x-axis)(~ 1.1 DVR, $p=0.005$). This visualization suggest that exceeding a critical baseline $a\beta$ level (approximate PiB DVR= 1.1 - 1.2) is associated with accelerated rise in accumulation of tau. At these levels of $a\beta$ and tau pathology, decline on the PACC is prominent (see Hanseeuw et al., 2019).

Figure 3

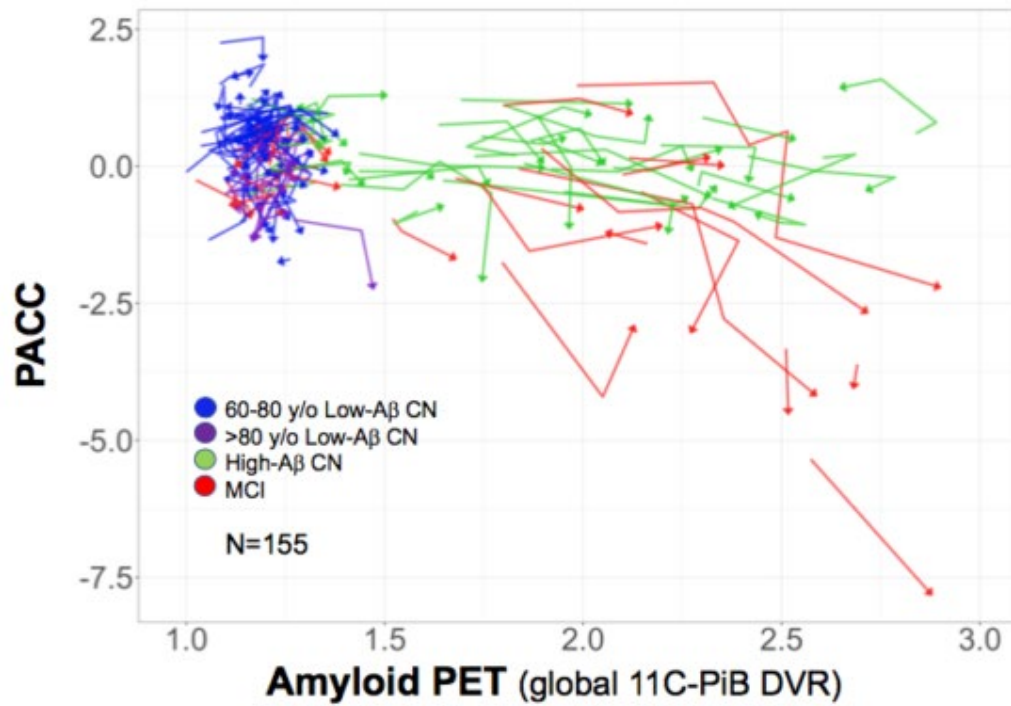


Figure 3. Spaghetti plot showing individual HABS participants' relationship between changes in PiB and changes in PACC (N=155) over a median of 24 months. Arrowheads indicate the follow-up time point.

Keywords: Amyloid, tau, cognitive decline, trajectories, PET

The meaning of tau positivity with respect to clinical progression

Michael Devous¹, Adam Fleisher¹, Michael Pontecorvo¹, Ming Lu¹, Vikas Kotari¹, Nicholas Galante¹, Sudeepti Southeikal¹, Anupa Arora¹, Mark Mintun¹

¹Avid Radiopharmaceuticals, Philadelphia, PA, US

Objective: Identify characteristics of flortaucipir scans associated with significant risk of progression.

Methods: The relationship of baseline flortaucipir to 18-month cognitive decline was investigated in two pivotal registration trials, A05C (159 MCI/AD; MMSE 20-27) and PX01 (205 A β + MCI/AD, MMSE 20-30), and by studies A05E (149 MCI/AD) and the tau addendum of LZAX (TZAX; 204 A β + AD). A05C and PX01 evaluated relationships between flortaucipir visual image reads and risk of subjects' cognitive and functional deterioration. Visual reads were dichotomized into: an Advanced tau AD pattern (increased parietal uptake, or frontal uptake with posterolateral temporal, parietal, or occipital uptake) or no evidence of an Advanced tau AD pattern.

Quantitative analyses used a weighted neocortical VOI (MUBADA) and an "early tau" VOI (E τ) incorporating mesial and inferior temporal regions (Figure 1A). SUVr positivity was set as \geq mean+2.5*SD of young controls. Multivariate stepwise regression analyses were conducted using subjects from the pooled longitudinal sample, with CDR-SB, MMSE, ADAS, and FAQ change from baseline as dependent variables and predefined independent risk factors (Table 1B).

Results: The primary aim for the two pivotal trials (CDR-SB \geq 1-pt change) was missed in A05C (p=.067) but met in PX01 (p=.0313). All progression endpoints were significant in pooled analyses showing elevated risk for Advanced vs. non-Advanced pattern subjects (Table 1A, Figure 2). MUBADA SUVr was significant (p<0.0001) for each test in multivariate models (Table 1B). Subjects with E τ SUVr above but MUBADA below threshold (Figure 1B) showed intermediate progression in MUBADA and E τ SUVr, cortical thickness, and MMSE compared to subjects below threshold (least progression) or above threshold (most progression) on both measures.

Conclusions: Visual read patterns and quantitative measures were associated with 18 month progression in pooled analyses. E τ SUVr was associated with progression midway between tau negative and MUBADA tau positive subjects for MMSE.

Table 1. A. Hazard ratio or risk ratio for clinically meaningful progression in studies A05E, A05C, TZAX and PX01 individually and pooled for an Advanced tau AD pattern vs a non-Advanced tau AD pattern. **B.** Regression models of the relationship between MUBADA SUV_r and cognitive change with adjustment for covariates.

A.

	A05E		A05C		TZAX		PX01		Pooled	
	RR ¹	p	HR ²	p	RR/HR ³	p	RR ⁴	p	RR	p
CDR-SB 1-pt change			1.581	.067	1.762	.0034	1.355	.0313	1.535	<.0001
CDR-G change >0			2.371	.0039	3.33	.0016	1.283	.2814	1.92	<.0001
MMSE 3-pt change	2.891	.0006	2.506	.007	2.907	.0001	1.347	.0833	1.974	<.0001
ADAS 4-pt change	1.486	.0726	1.359	.2934	2.554	.0003	1.771	.0141	1.907	<.0001
FAQ 3-pt change	2.110	.0007	2.785	<.0001	2.339	.0006	1.322	.0639	1.851	<.0001

¹Calculated in A05E as crude (no cofactors) relative risk (PPV/1-NPV). CDR not available at baseline in A05E.

²Cox proportional HR adjusted for baseline age, ANART, and baseline score.

³In the TZAX study, CDR was only performed at baseline and endpoint so RRs were calculated, whereas HRs were calculated for MMSE, ADAS and FAQ. RR and HR were adjusted for treatment arm, age, years of education, and baseline test score.

⁴PX01 RRs were adjusted for treatment arm, age, years of education, and baseline test score.

B.

	CDR-SB		MMSE		ADAS		FAQ	
	r square	p	r square	p	r square	p	r square	p
MUBADA	0.1264	<.0001	0.2322	<.0001	0.2013	<.0001	0.0773	<.0001
Study	---	ns	0.0214	.0010	0.0079	.0879	---	ns
Age	0.0495	<.0001	0.0226	.0003	0.0164	.0014	0.0385	<.0001
Baseline Score	0.0039	.1467	0.0034	.1099	0.0031	.1440	0.0417	<.0001
Sex	---	ns	0.0031	.1003	---	ns	---	ns
Amyloid	---	ns	---	ns	---	ns	0.0096	.0128
ApoE	---	ns	---	ns	---	ns	---	ns
Total	0.1797		0.2827		0.2286		0.1671	

Figure 1. Panel A: MUBADA and Et τ VOI in MNI space. **Panel B:** Change from baseline SUVr, cognition, function, or cortical thickness in subjects with SUVr above threshold on both MUBADA and Et τ ROI (Q1), only the Et τ ROI (Q2) or neither ROI (Q3) in the A05E and TZAX pooled data.

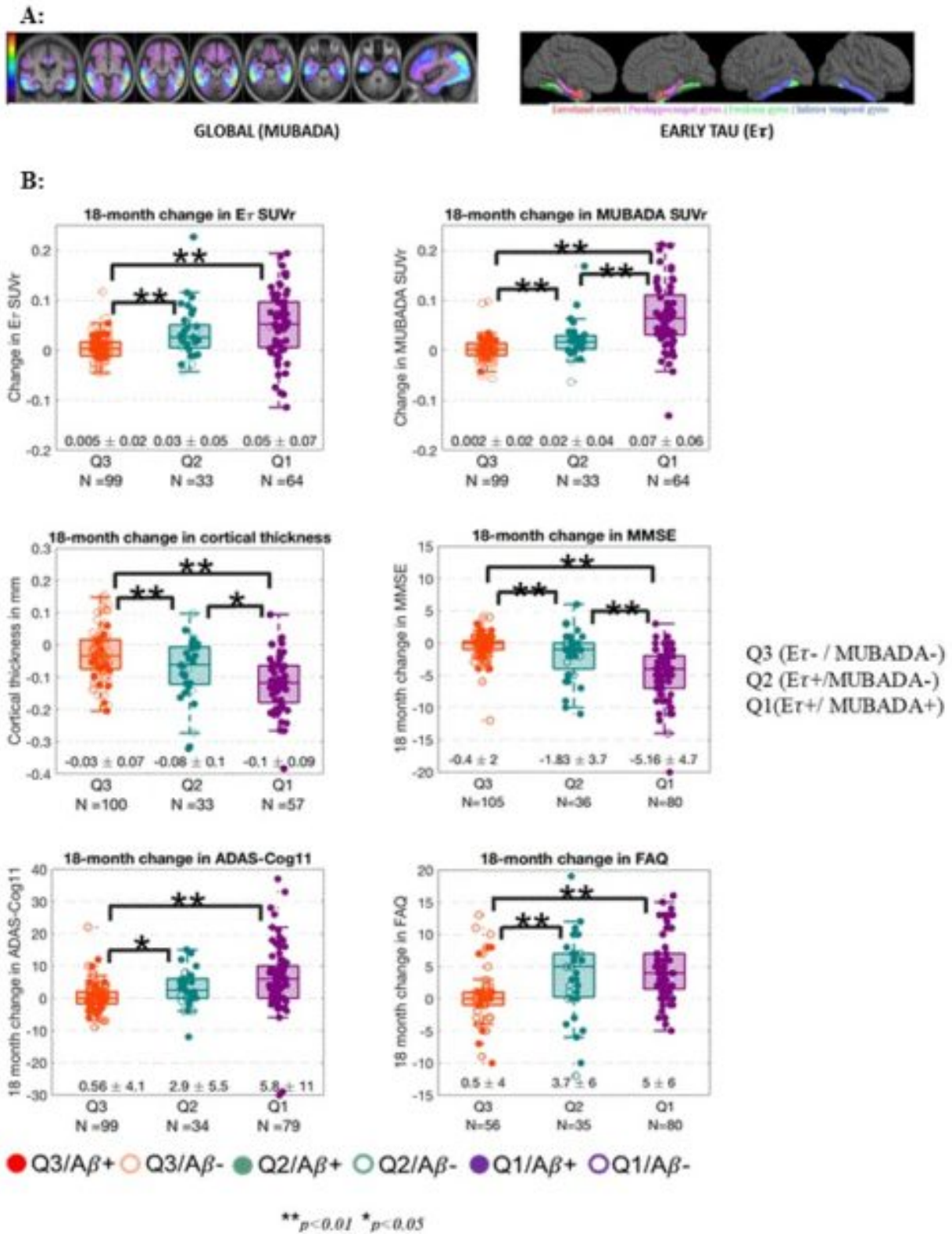
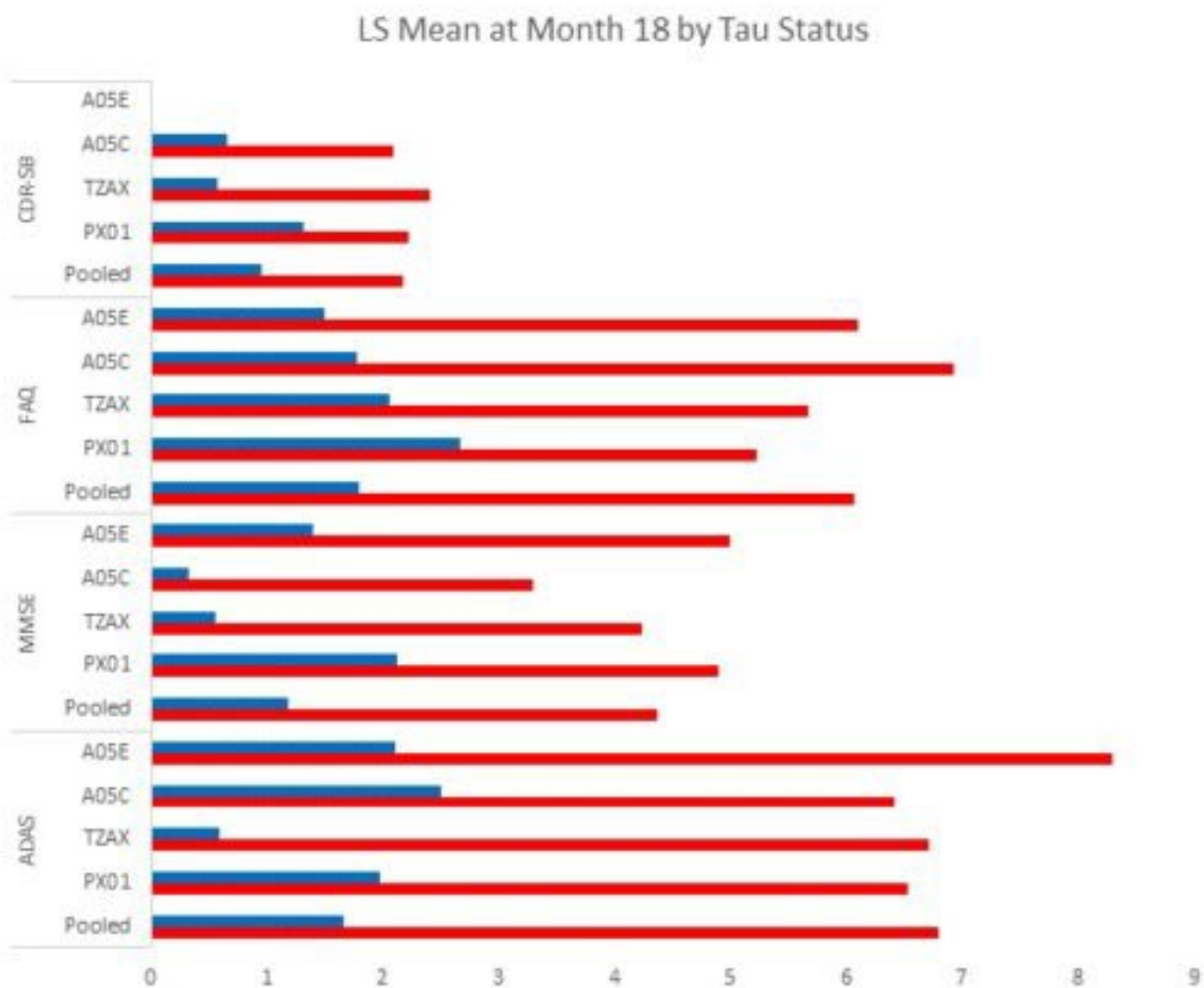


Figure 2. LS mean change by trial for Advanced tau AD pattern or non-Advanced tau AD pattern (for CDR-SB, MMSE, FAQ and ADAS-cog).



LS mean change in Advanced tau AD pattern (red bars) vs non-Advanced tau AD pattern (blue bars) subjects for each major outcome variable and for the pooled analysis. LS mean change is calculated adjusting for age and baseline value as analyzed in the original study using either MMRM (MMSE, ADAS, FAQ) or ANCOVA (CDR-SB in TZAX and pooled analysis, since TZAX measured CDR-SB only at baseline and 18 months). Note CDR-SB was not collected at baseline in A05E, so no change value is shown.

Keywords: Progression, Tau, Flortaucipir, Positive Scan

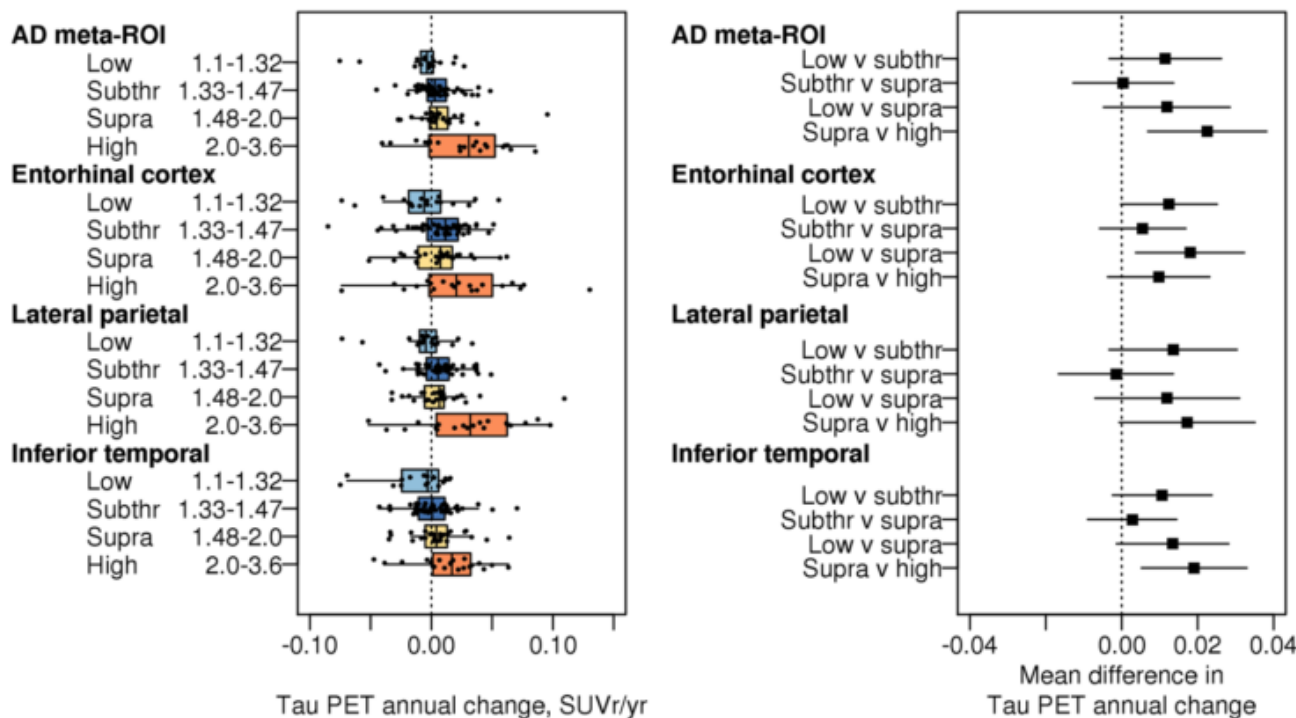
Longitudinal tau PET changes in cognitively unimpaired persons with different β -amyloid levels

David Knopman¹, Emily Lundt¹, Terry Therneau¹, Michelle Mielke¹, Val Lowe¹, Sabrina Albertson¹, David Jones¹, Jon Graff-Radford¹, Ronald Petersen¹, Cliff Jack¹

¹Mayo Clinic, Rochester, MN, US

Tau PET imaging is a candidate outcome measure for clinical trials for AD. We studied cognitively unimpaired (CU) individuals > 50 years in the Mayo Clinic Study of Aging who had serial cognitive assessments, MR scans and 11C Pittsburgh compound B ($A\beta$) and 18F-AV1451 (tau) PET scans. We stratified participants by $A\beta$ PET scan into 1) low $A\beta$, 2) above-background-but-still-subthreshold (threshold=22 centiloid) $A\beta$, 3) low-suprathreshold $A\beta$ and 4) high $A\beta$. We examined change over ~15 months in tau PET signal in 4 regions – entorhinal, inferior temporal, lateral parietal and an AD meta-ROI. Few 50-65 yo participants had suprathreshold $A\beta$ levels, and none had high $A\beta$ levels. In 65-85 yos, index $A\beta$ levels were distributed across the full range. Mean baseline tau signal was elevated in $A\beta$ ranges compared to low $A\beta$. The high $A\beta$ group had significantly higher tau signal compared to the other $A\beta$ groups only in the entorhinal ROI. Tau accumulation rates (Figure) in the subthreshold $A\beta$ and low-suprathreshold $A\beta$ groups in all regions were very low with no differences in tau accumulation between these two $A\beta$ groups. Tau accumulation rates in inferior temporal and AD meta-ROI in the high $A\beta$ group were greater than in the other $A\beta$ groups. Rate of entorhinal cortex tau accumulation in the high $A\beta$ group was attenuated. Sample size estimates (25% reduction in tau accumulation rate, 80% power) for subthreshold $A\beta$ and low-suprathreshold $A\beta$ groups were in the multi-thousands, while estimates for the high $A\beta$ group were 6X smaller.

Suprathreshold $A\beta$ and substantial acceleration of tau accumulation are related, but the latter takes years to evolve. The use of changes in tau signal as an outcome measure in clinical trials of CU persons becomes feasible only in older individuals with high $A\beta$, representing about half of CU persons with nominally suprathreshold $A\beta$.



Keywords: Amyloid PET, tau PET, clinical trials, normal cognition, longitudinal

Defining a tau positive Flortaucipir PET signal relative to AD neuropathology

Michael Pontecorvo¹, Adam Fleisher¹, Michael Devous¹, Ming Lu¹, Vikas Kotari¹, Nicholas Galante¹, Edwin Lu¹, Sudeepti Southekal¹, Mark Mintun¹

¹*Avid Radiopharmaceuticals, Philadelphia, PA, US*

Objective: To evaluate characteristics of the flortaucipir PET signal that could define tau positivity relative to Braak NFT staging at autopsy.

Methods: 83 participants who underwent flortaucipir PET were evaluated for NFT stage and amyloid status at autopsy (Figure 1). Flortaucipir images were visually interpreted by 10 imaging physicians across 2 pivotal studies as consistent with AD (moderate: posterior lateral temporal/occipital signal; or advanced: signal extended to parietal lobe, or frontal + parietal/temporal) or not consistent (Not AD: no uptake/restricted to anterior temporal or frontal lobes). Quantitative analyses used weighted neocortical (MUBADA) and “early tau” (E τ) VOIs. SUVrs \geq mean+2.5*SD of young controls were considered positive. Groupwise average z-score surface maps were generated regionally and Freesurfer vertex-wise.

Results: Moderate/advanced visual interpretation was associated with B3 (Braak V/VI) NFT scores, positive amyloid status and high ADNC, with both studies meeting the primary endpoint (95% LCL>0.50 for both sensitivity and specificity in \geq 3/5 readers). Majority read sensitivity/specificity were 89.1%/86.1% and 89.4%/80.0% for B3 NFT and 95.1%/82.9% and 95.1%/75.6% for high ADNC in Studies 1 and 2, respectively. Visual reads of the anterior and medial temporal regions did not improve accuracy for detecting B3 or B2 level NFT. MUBADA SUVr was more specific (100%) but less sensitive than visual interpretation (Figure 2A) for B3 NFT. Although MUBADA and visual interpretation did not appear to detect B2 NFT, 12/15 B2 NFT cases (including 10/11 Braak IV cases) had elevated Et SUVr, (Figure 2B). Thus, an Et VOI, potentially in combination with MUBADA or visual reads, might help identify subjects with intermediate stage tauopathy. Regional and vertex-wise analyses revealed flortaucipir signal as a function of NFT stage (Figure 3).

Conclusions: In two studies, moderate to advanced flortaucipir visual read was associated with B3/high ADNC pathology. Detection of earlier NFT stages may require quantitative methods.

Figure 1. Flortaucipir PET majority visual interpretation as a function of neuropathological assessment of tau NFT (Braak stage) and amyloid status (CERAD score) in Pivotal Study 1. Note symbols randomly placed within grid squares to minimize overlap.

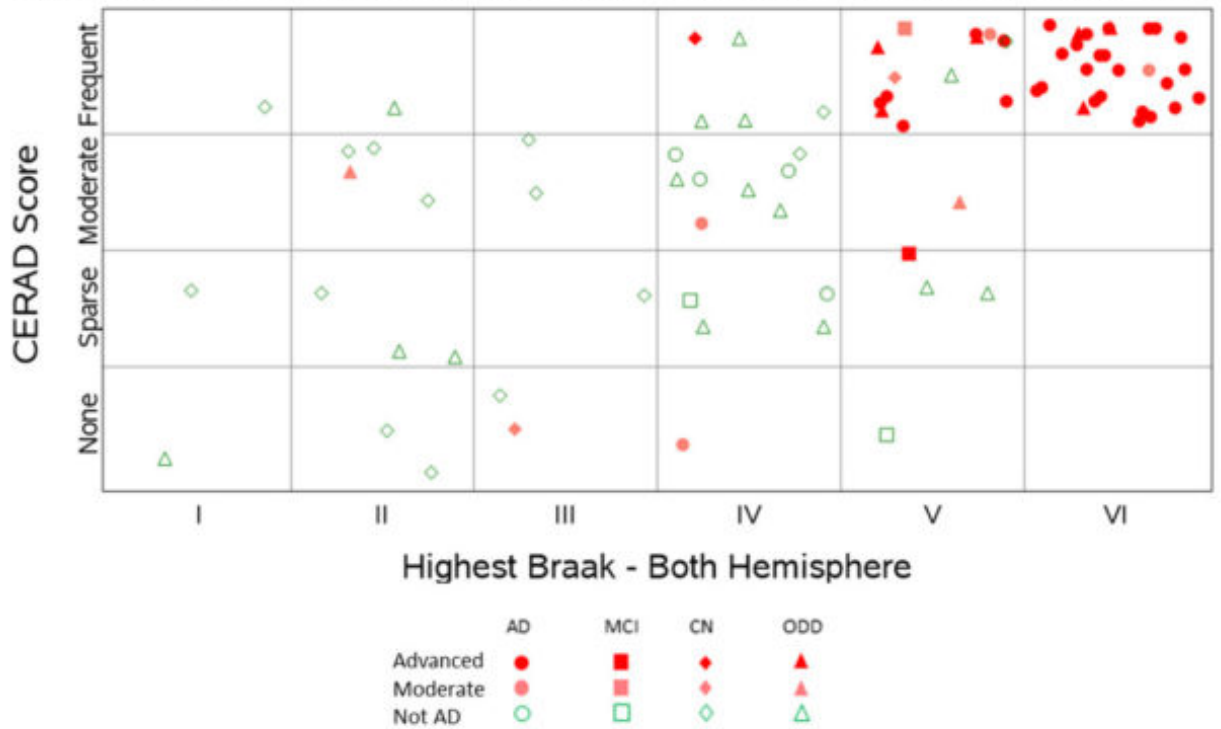


Figure 2. Relationship between neuropathological assessment of tau NFT (B score/Braak stage) and flortaucipir PET SUVR in a global ROI weighted to discriminate AD vs clinically normal controls (Panel A) and flortaucipir SUVR in an early tau ROI focused on inferior temporal regions (Panel B). For each case CERAD amyloid status is represented by open vs closed symbols (none/sparse: A β -; moderate/frequent: A β +), and flortaucipir PET majority visual read is represented by color (advanced: red; moderate: blue; not AD: green).

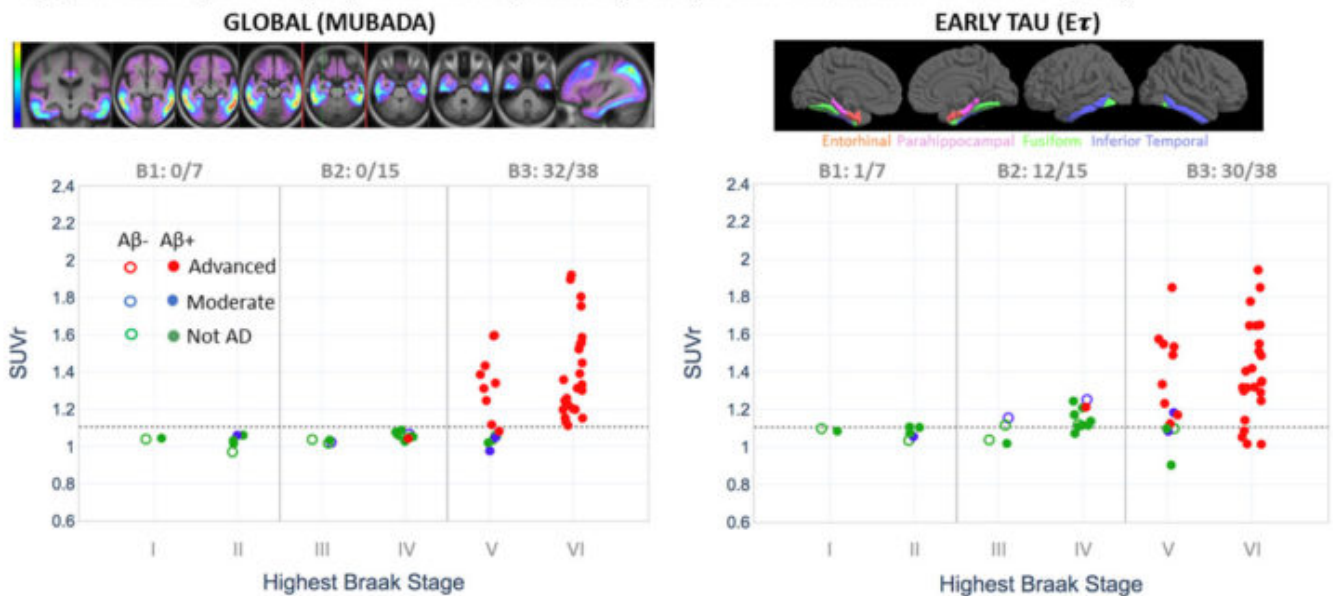
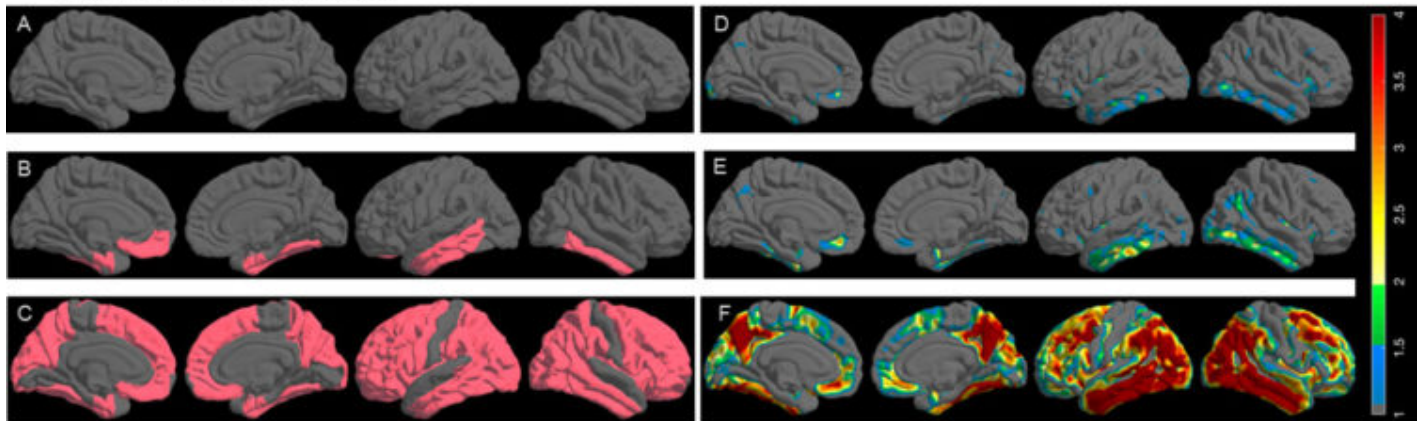


Figure 3. FreeSurfer regions (left) and voxels (right) with flortaucipir SUVr > 2.5 SD beyond young cognitively normal controls as a function of NFT score/Braak stage.



A. Average tau positivity surface map of B1 NFT score subjects showing lack of elevated flortaucipir signal in the entire cortex.
B. Average tau positivity surface map of B2 NFT score subjects. There is elevated flortaucipir signal primarily in the regions of Et VOI region with the exception of left middle temporal gyrus and left medial orbitofrontal gyrus. Bilateral parahippocampal gyrus and left fusiform appear to lack signal potentially due to extensive atrophy.
C. Average tau positivity surface map of B3 NFT score subjects. Widespread elevation in flortaucipir signal across the entire cortex with the exception of postcentral and paracentral gyri, bilateral superior temporal gyrus, bilateral lingual gyrus and isthmus, posterior, and anterior cingulate.
D, E, and F are voxel-wise version of figures A, B and C respectively.

Keywords: Tau, Flortaucipir, Braak stage, Positive Scan

KEYNOTE LECTURE 3

Tsai, Li-Huei

Leveraging brain rhythms as a therapeutic intervention for Alzheimer's disease

Li-Huei Tsai

Picower Institute for Learning and Memory, Department of Brain and Cognitive Sciences, Massachusetts Institute of Technology, Cambridge, MA, US

Rhythmic neural activity in the gamma range (30-80 Hz) is modulated during various aspects of cognitive function and has been shown to be disrupted in several neurological conditions, including Alzheimer's disease (AD). Impaired gamma oscillations have also been reported in several AD mouse models, even before the onset of A β accumulation and major cognitive impairment. It is well established that local network oscillations at specific frequencies can be induced in cortical areas using sensory stimuli. Recently, we applied this approach, which we term Gamma ENtrainment Using Sensory stimuli (GENUS), using a light programmed to flicker at 40 Hz to induce gamma oscillations in the visual cortex of AD model mice. We found a profound reduction in amyloid load in visual cortex after 1 hr of visual GENUS that appears to involve the concerted actions of many different cell types, including neurons and microglia to reduce the production and enhance clearance of A β , respectively. Chronic exposure to GENUS reduced amyloid plaque and phosphorylated Tau pathology in multiple brain regions in 5XFAD and P301S transgenic mice, respectively, and improved learning and memory. Therefore, GENUS represents a novel and powerful non-invasive approach to combat AD related pathology and symptoms. We are currently testing GENUS in human subjects to determine it's utility in tackling human neurological disorder.

Friday, January 17, 2020 - 2:00 - 3:15pm

SESSION 8: Clinical III

Friday, January 17, 2020		
2:00 PM	SESSION 8: CLINICAL III	CHAIRS: Elizabeth Mormino, PhD, <i>Stanford University</i> Susan Landau, PhD, <i>University of California, Berkeley</i>
2:00 PM	Glucose metabolism reflects local atrophy and tau pathology at symptomatic stages of Alzheimer's disease	Amelia Strom, BS, <i>University of California San Francisco</i>
2:15 PM	Plasma FLT1 predicts amyloid- β related cognitive decline in cognitively normal older adults	Hyun-Sik Yang, MD, <i>Brigham and Women's Hospital</i>
2:30 PM	Reducing sample sizes to detect longitudinal amyloid accumulation	Isadora Lopes Alves, PhD, <i>VUmc</i>
2:45 PM	Discussion	

Glucose metabolism reflects local atrophy and tau pathology at symptomatic stages of Alzheimer's disease

Amelia Strom¹, Leonardo Iaccarino¹, Lauren Edwards¹, Orit Lesman Segev¹, David Soleimani-Meigooni¹, William Jagust^{2,3}, Bruce Miller¹, Gil D. Rabinovici^{1,3}, Renaud La Joie¹

¹*University of California, San Francisco, San Francisco, CA, US*

²*University of California, Berkeley, Berkeley, CA, US*

³*Lawrence Berkeley National Laboratory, Berkeley, CA, US*

Background. We assessed the relative contributions of three potential mechanisms associated with FDG-PET hypometabolism in posterior cingulate cortex (PCC) and inferior parietal (IP) regions, two primary regions of hypometabolism in AD: local (amyloid and tau) pathology and atrophy, pathology in distant but connected regions, and deafferentation from the degenerating medial temporal lobe (MTL).

Methods. Eighty-five patients with MCI or AD dementia underwent MRI and PET with FDG, PIB (all positive by visual read) and FTP within one year (Table 1). SUVR were calculated using tracer-specific reference regions: FDG-SUVR_{30-60min} (pons), PIB-SUVR₅₀₋₇₀ (cerebellar cortex) and FTP-SUVR₈₀₋₁₀₀ (inferior cerebellar cortex). PCC and IP were defined in native space using FreeSurfer. Regions with high or low connectivity to PCC/IP were defined based on task-free fMRI data from neurosynth.org (Fig1a). Imaging variables were transformed into age-adjusted z-scores using demographic-matched modality-specific control groups (Table 1). Multiple regression analyses were run to identify variables associated with FDG-SUVR.

Results. Local gray matter volume (GMV) and FTP-SUVR, but not PIB-SUVR, were independently associated with FDG-SUVR in PCC ($R^2=.461$, $\beta_{GMV}=0.425$, $\beta_{FTP}=-0.479$) and IP ($R^2=.652$, $\beta_{GMV}=0.476$, $\beta_{FTP}=-0.416$, Fig1). Models including PIB/FTP in connected regions did not outperform models with local GMV/FTP alone (Fig1b). Results were similar when including measures of pathology in non-connected regions (Fig1c). MTL volume was weakly associated with PCC-FDG but not IP-FDG (Fig2a). When analyses were repeated in subgroups split by median age (62 yo), the detrimental effect of MTL atrophy on PCC-FDG was only seen in the older patient group (Fig2b).

Conclusion. Hypometabolism reflected local atrophy and tau pathology. A distant effect of MTL atrophy on PCC hypometabolism was seen primarily in older patients, suggesting that drivers of hypometabolism might be region- and group-dependent. Our data did not support hypotheses of a detrimental effect of pathology in connected regions in the symptomatic stage of AD.

	Patients	Cognitively Normal Controls			F or X^2	p
		FDG	FTP/PIB	MRI		
N	85	78	80	80	0.33	0.95
Age (years)	64.6 (9.5)	66.8 (17.8)	68.8 (14.7)	66.8 (17.9)	0.94	0.44
Sex (% female)	51	55	54	56	0.60	0.90
Education (years)	16.8 (2.9)	16.8 (2.1)	17.1 (1.8)	16.7 (3.3)	0.29	0.83
MMSE	21.4* (6.1)	28.8 (1.2)	28.9 (1.0)	28.9 (1.2)	42.6	<.001
MCI/Dementia	45/40	--	--	--	--	--

Table 1. Demographics of patients and cognitively normal controls for w-scoring. Continuous variables are presented as mean (standard deviation). Group comparisons were conducted using ANOVA for continuous variables and Chi-square for categorical variables. *Post-hoc analyses showed significant differences between patients and all control groups; there were no differences between control groups.

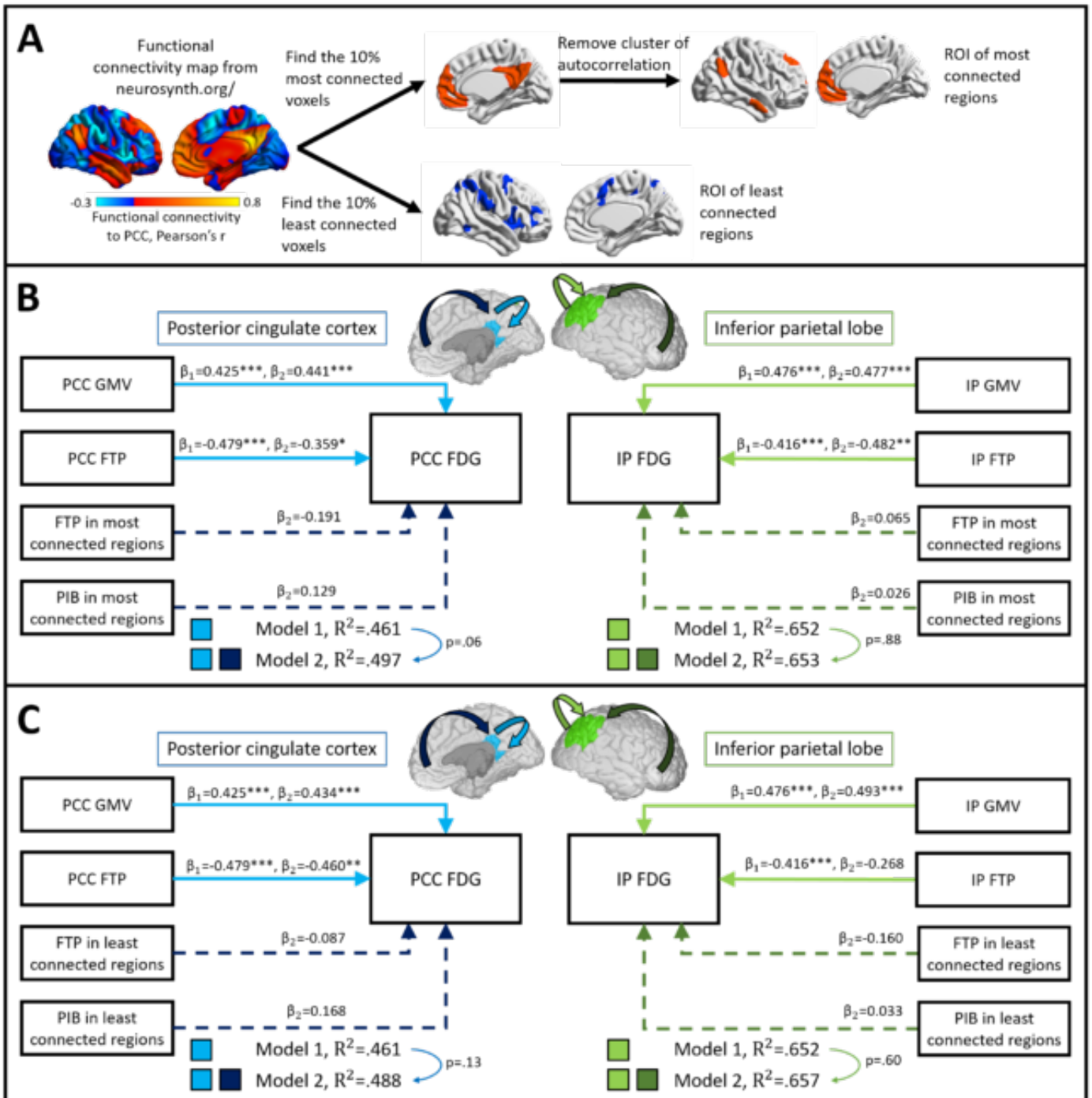


Figure 1. Multiple regression analyses evaluating effects of local pathology and GMV and pathology in distant regions.

(A) Schematic describing the creation of ROIs of most and least connected regions, using PCC as an example. FTP and PIB values were extracted from these ROIs as measures of pathology in connected and non-connected areas. (B-C) Regression models begin with local predictors only, where regional FDG in either PCC or IP is the singular dependent variable. Then, measures of pathology in (B) most connected regions and (C) least connected regions are added to evaluate if they improve the model independently of local factors. * $p<.05$, ** $p<.01$, *** $p<.001$. Additionally, $p<.05$ is represented by a solid arrow line and $p>.05$ by a dashed line.

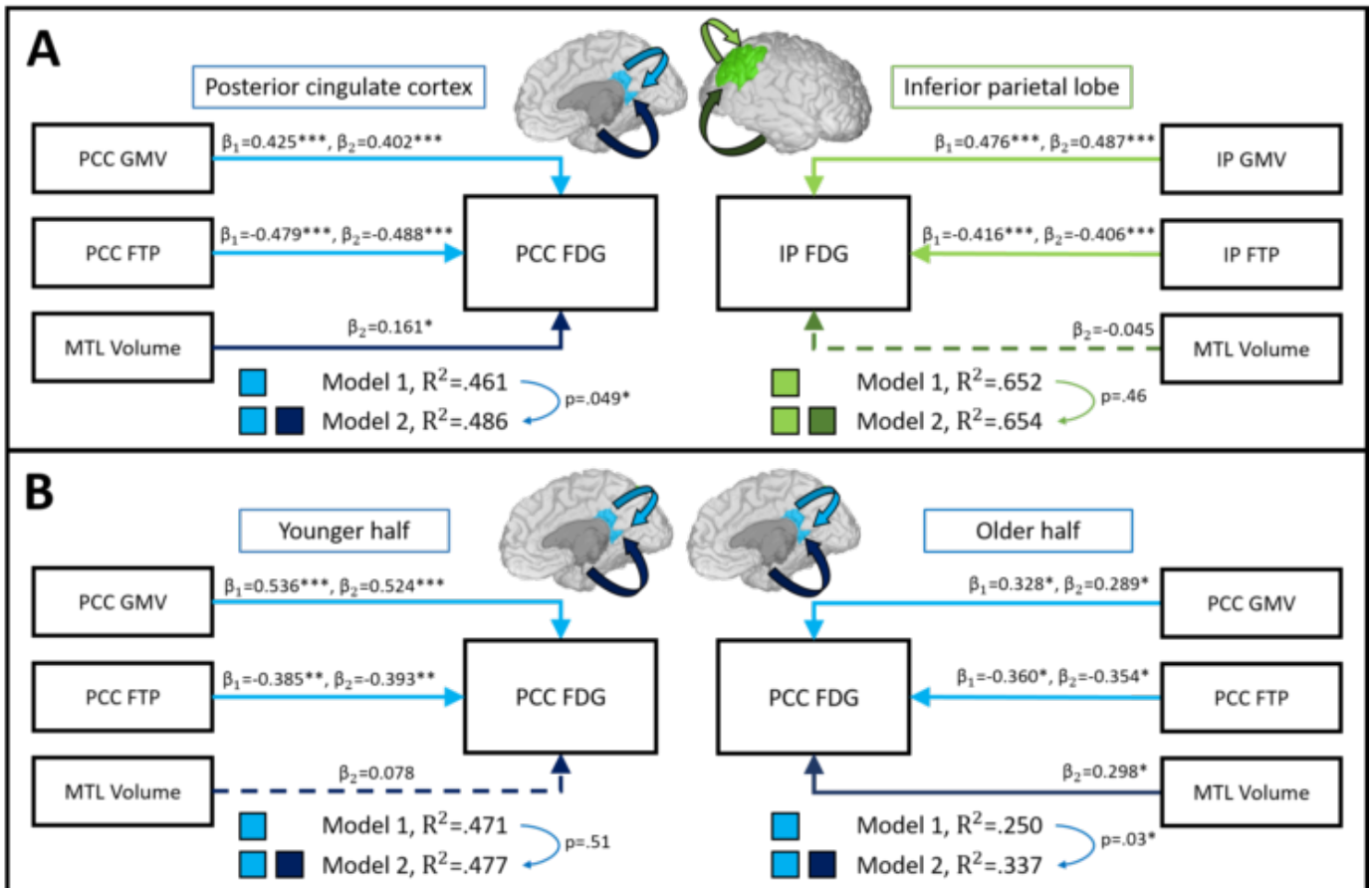


Figure 2. Multiple regression analyses evaluating effects of MTL volume.

Regression models begin with local predictors only, where regional FDG is the singular dependent variable. Then, MTL volume is added to evaluate if it improves the model independently of local factors in (A) the whole group for PCC-FDG and IP-FDG separately, and (B) in subgroups split by the median age of 62 years for PCC-FDG only. * $p<.05$, ** $p<.01$, *** $p<.001$. Additionally, $p<.05$ is represented by a solid arrow line and $p>.05$ by a dashed line.

Keywords: metabolism, connectivity, Flortaucipir

Plasma FLT1 predicts amyloid- β related cognitive decline in cognitively normal older adults

Hyun-Sik Yang¹, Becky Carlyle^{1,3}, Bianca Trombetta¹, Can Zhang^{1,3}, Aaron Schultz^{1,3}, Jeremy Pruzin^{1,2,3}, Colleen Fitzpatrick¹, Dylan Kirn^{1,2}, Dorene Rentz^{1,2,3}, Rudolph Tanzi^{1,3}, Keith Johnson^{1,2,3}, Reisa Sperling^{1,2,3}, Steven Arnold^{1,3}, Jasmeer Chhatwal^{1,3}

¹Massachusetts General Hospital, Boston, MA, US

²Brigham and Women's Hospital, Boston, MA, US

³Harvard Medical School, Boston, MA, US

Background: Vascular endothelial growth factor (VEGF) pathway dysregulation has been implicated in Alzheimer's disease (AD) pathophysiology through cerebrospinal fluid and *post-mortem* brain studies. However, *in vivo* relationships between plasma VEGF pathway biomarkers and prospective cognitive trajectories remain unclear. Here, we examined plasma VEGF pathway measures in the Harvard Aging Brain Study (HABS) and their relationship to individual cognitive trajectories, amyloid- β (A β) pathology, and systemic inflammatory state.

Methods: Data came from 298 cognitively normal (CN) HABS participants with baseline A β measure (Pittsburgh Compound B PET), baseline plasma collection, and longitudinal Preclinical Alzheimer's Cognitive Composite 5 (PACC5). First, we screened five plasma VEGF pathway measures, VEGF-A, VEGF-C, VEGF-D, PIGF, and FLT1 (also known as soluble VEGFR1), measured on the Meso-Scale Discovery V-PLEX platform, to identify plasma markers that predict cognitive decline on the PACC5. Second, we tested the association of the identified plasma marker with baseline demographic and imaging characteristics. Finally, using linear mixed effect models, we tested the interactive association of the identified marker with A β in predicting longitudinal cognitive decline.

Results: Baseline plasma FLT1 predicted PACC5 decline in CN older adults (adjusted for age, sex and education; $\beta=-0.025$, nominal $p=9.0\times 10^{-3}$, FDR=0.045), while VEGF-A, VEGF-C, VEGF-D, and PIGF did not (FDR>0.05). FLT1 was associated with age ($\beta=0.042$, $p=3.2\times 10^{-8}$), but not sex, *APOE* $\epsilon 4$, baseline A β , or baseline hippocampal volume. FLT1 was not associated with baseline Framingham Heart Study Cardiovascular Risk, but was strongly associated with baseline C-reactive Protein (CRP, marker of systemic inflammation; Figure 1A; $p=6.8\times 10^{-4}$) and baseline FLAIR white matter hyperintensity volume (WMH; Figure 1B; $p=0.013$). FLT1 robustly interacted with A β to predict PACC5 decline (Figure 1C), even after adjusting for WMH and CRP ($\beta=-0.12$, $p=3.7\times 10^{-3}$).

Conclusion: Plasma FLT1 (soluble VEGFR1) is associated with markers of systemic inflammation, vascular brain injury, and with A β -related cognitive decline in CN older adults.

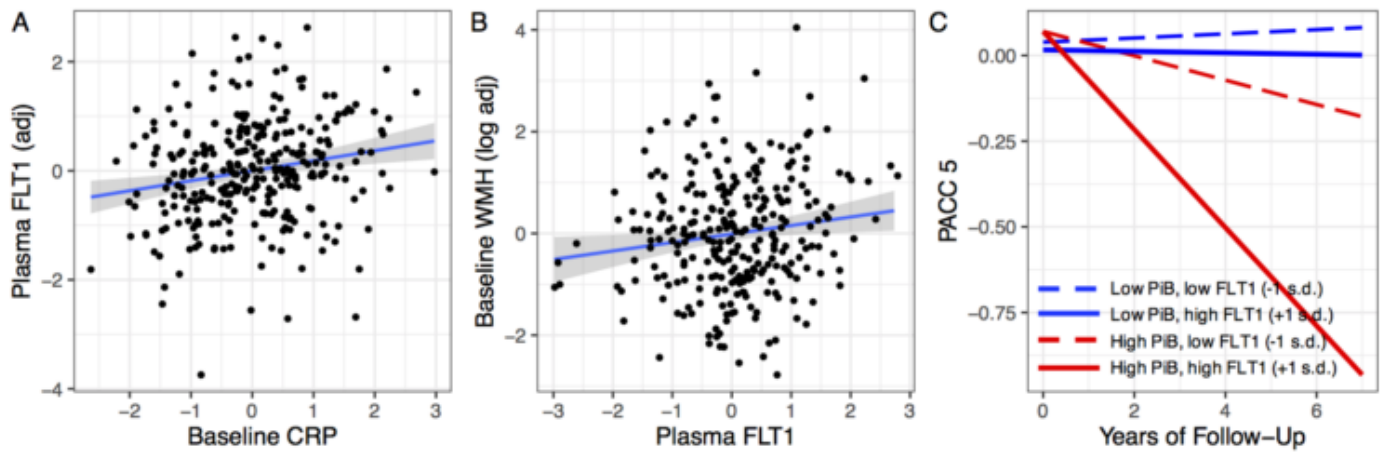


Figure 1. Cross-sectional and longitudinal correlates of baseline plasma FLT1. (A) Baseline FLT1 is associated with baseline CRP, after controlling age and sex ($\beta=0.19$, 95% CI 0.08 to 0.30, $p=6.8 \times 10^{-4}$). (B) Baseline FLT1 is associated with baseline log₂-transformed FLAIR white matter hyperintensity (WMH), after controlling age, sex, and intracranial volume ($\beta=0.19$, 95% CI 0.04 to 0.33, $p=0.013$). (C) Predicted PACC5 trajectory according to baseline A β (measured by PiB DVR) and baseline plasma FLT1, from a linear mixed model. Modeled value for the mean baseline age (72.0) was plotted. Blue dashed line: PiB DVR=1.08, FLT1 -1 s.d.; blue solid line: PiB DVR=1.08, FLT1 +1 s.d.; red dashed line: PiB DVR=1.46, FLT1 -1 s.d.; red solid line: PiB DVR=1.46, FLT1 +1 s.d. PiB DVR=PiB neocortical composite distributed volume ratio at baseline.

Keywords: plasma biomarker; amyloid- β ; VEGF; FLT1; cognitive decline

Reducing sample sizes to detect longitudinal amyloid accumulation

Isadora Lopes Alves¹, Lyduine Collij¹, Fiona Heeman¹, José Luis Molinuevo², Mark Schmidt³, Adriaan Lammertsma¹, Frederik Barkhof^{1,4}, Juan Domingo Gispert², On behalf of the AMYPAD Consortium⁵

¹Department of Radiology and Nuclear Medicine, Amsterdam UMC, location VUmc, Amsterdam, The Netherlands

²BarcelonaBeta Brain Research Center, Barcelona, Spain

³Janssen Pharmaceutica NV, Beerse, Belgium

⁴Institute of Neurology and Healthcare Engineering, University College London, London, UK

⁵This work has received support from the EU-EFPIA Innovative Medicines Initiatives 2 Joint Undertaking (grant No 115952), Brussels, Belgium

Background: Detecting amyloid- β plaque accumulation in initially amyloid negative subjects can help understanding the earliest stages of Alzheimer's disease (AD). This study aimed to determine sample sizes that would be needed to detect statistically significant longitudinal changes using semi- (standard uptake value ratios; SUVR) and quantitative (distribution volume ratios; DVR) PET measures at global and regional levels.

Methods: [¹¹C]PIB scans of 239 cognitively normal (CN) subjects in the OASIS-3 data-set, who underwent at least two PET scans, were included. Regional SUVR and DVR were extracted using cerebellar gray matter as reference region. PET positivity was defined by Gaussian Mixture Modelling of the global SUVR (SUVR>1.16). Annual accumulation rates were calculated using linear regression, and sample sizes to detect a significant longitudinal change ($\alpha=0.05$; $1-\beta=0.80$) were determined with the *sampsizewr* function in Matlab. The percentage of accumulators (rates of change >2SD of negative group) was also computed.

Results: As expected, rates of change were higher in subjects with positive PET at baseline, and APOE- $\epsilon 4$ carriership increased accumulation rates in both negative and positive groups (**Table 1**). Using either metric, orbitofrontal and precuneus displayed the highest rates of change in the negative group. SUVR rendered higher accumulation rates than DVR, but also displayed higher variability. As a consequence, to detect 0.22% early accumulation (mean of negative group), global DVR required $N=584$ compared with $N=917$ for global SUVR (**Figure 1**). In addition, DVR classified 13% of subjects as accumulators compared with 9% for SUVR. Finally, precuneus and orbitofrontal regions classify more subjects as accumulators than global SUVR, i.e. 17 and 25%, respectively.

Table 1. Observed annual rates of change in CNs from OASIS-3 data-set

	amyloid negative			amyloid positive		
	Total	NC	C	Total	NC	C
Number of subjects	186	143	43	53	18	35
Baseline Global SUVR	1.06 (0.046)	1.06 (0.44)	1.06 (0.05)	1.48 (0.25)	1.48 (0.28)	1.48 (0.24)
% annual change	0.45 (1.68)	0.33 (1.57)	0.84 (1.96)	2.06 (2.06)	1.39 (2.06)	2.40 (2.00)
Baseline Global DVR	1.02 (0.04)	1.02 (0.04)	1.03 (0.01)	1.34 (0.19)	1.34 (0.22)	1.34 (0.18)
% annual change	0.22 (1.34)	0.14 (1.25)	0.48 (1.61)	1.80 (1.61)	1.29 (1.67)	2.07 (1.54)

*NC = non-carrier; C = carrier

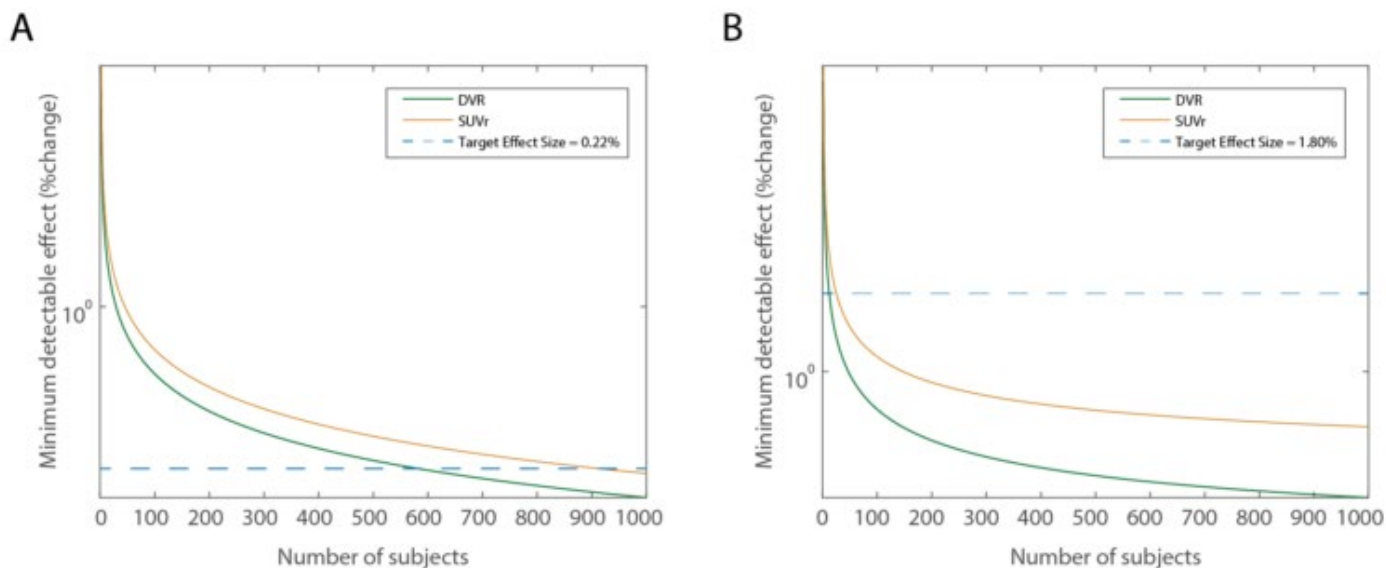


Figure 1. Detectable effects as a function of sample size. **(A)** Assuming no accumulation as the null hypothesis, DVR requires 60% of the sample size required by SUVR to detect a 0.22% annual amyloid accumulation rate, which corresponds to the average observed in initially amyloid PET negative subjects measured with DVR. **(B)** Assuming the observed annual amyloid accumulation rates in the negative group as the null hypothesis, DVR requires 50% of the sample size required by SUVR to detect a 1.80% annual amyloid accumulation rate, which corresponds to the average observed in amyloid PET positive subjects measured with DVR.

Conclusion: As compared to SUVR, DVR can reduce the sample size needed to detect longitudinal amyloid changes by approximately 40% in amyloid negative populations. Additional improvements in statistical power can be achieved by focusing on precuneus and orbitofrontal regions.

Keywords: sample sizes, amyloid PET, accumulation, trial design

SESSION 9: PLASMA

Friday, January 17, 2020		
4:15 PM	SESSION 9: PLASMA	CHAIR Gil Rabinovici, MD, <i>UCSF</i>
4:15 PM	Plasma P-tau181 as a marker of tau pathology in Alzheimer's disease: relationship to Tau PET, differential diagnosis, neuropathology and longitudinal progression	Oskar Hansson, PhD, <i>Lund University</i>
4:30 PM	Plasma levels of an N-terminal tau fragment are highly associated with future cognitive decline and neurodegeneration in clinically normal elderly: findings from the Harvard Aging Brain Study	Jasmeer Chhatwal, MD, <i>MGH/Harvard University</i>
4:45 PM	Plasma biomarkers associate with amyloid and tau PET binding in cognitively unimpaired older adults with a parental history of AD	Pierre-Francois Meyer, PhD, <i>McGill University</i>
5:00 PM	High-performance plasma phospho-tau181 biomarker for Alzheimer's disease	Tharick Pascoal, PhD, <i>McGill University</i>
5:15 PM	Discussion	

Plasma P-tau181 as a marker of tau pathology in Alzheimer's disease: relationship to Tau PET, differential diagnosis, neuropathology and longitudinal progression

Oskar Hansson¹, Shorena Janelidze¹, Niklas Mattsson¹, Sebastian Palmqvist¹, Ruben Smith¹, Thomas Beach², Geidy Serrano², Xiyun Chai³, Nicholas Proctor³, Henrik Zetterberg⁴, Kaj Blennow⁴, Eric Reiman⁵, Jeffrey Dage³

¹*Clinical Memory Research Unit, Lund University, Lund, Sweden*

²*Banner Sun Health Research Institute, Sun City, AZ, US*

³*Eli Lilly and Company, Indianapolis, IN, US*

⁴*Department of Psychiatry and Neurochemistry, the Sahlgrenska Academy at the University of Gothenburg, Gothenburg, Sweden*

⁵*Banner Alzheimer's Institute, Phoenix, AZ, US*

Plasma phosphorylated tau181 (P-tau181) might be increased in Alzheimer's disease (AD), but it is unclear if it can be used for differential diagnosis and prognosis. We studied plasma P-tau181 in three cohorts, with a total of 589 individuals, including cognitively unimpaired participants and patients with mild cognitive impairment (MCI), AD dementia, and non-AD neurodegenerative diseases. Plasma P-tau181 was increased in preclinical AD and further increased at the MCI and dementia stages. It correlated with CSF P-tau181 and predicted positive Tau PET scans (AUC=0.87-0.91) (Figures 1 and 2a-c). Plasma P-tau181 differentiated AD dementia from non-AD neurodegenerative diseases with an accuracy similar to Tau PET and CSF P-tau181 (AUC=0.94-0.98) (Figure 2d-f), and it could also detect AD neuropathology in individuals with neuropathological confirmation. High plasma P-tau181 was associated with subsequent development of AD dementia in cognitively unimpaired and MCI subjects with a hazard ratio of 3.8 (per SD unit increment) (Figure 3). In conclusion, plasma P-tau181 is a non-invasive diagnostic and prognostic biomarker of AD, which may be useful in clinical practice. Further, in clinical trials plasma P-tau181 might be used to screen for individuals with high risk of AD-like tau pathology where Tau PET could be used to subsequently confirm presence of tau pathology.

Figure 1

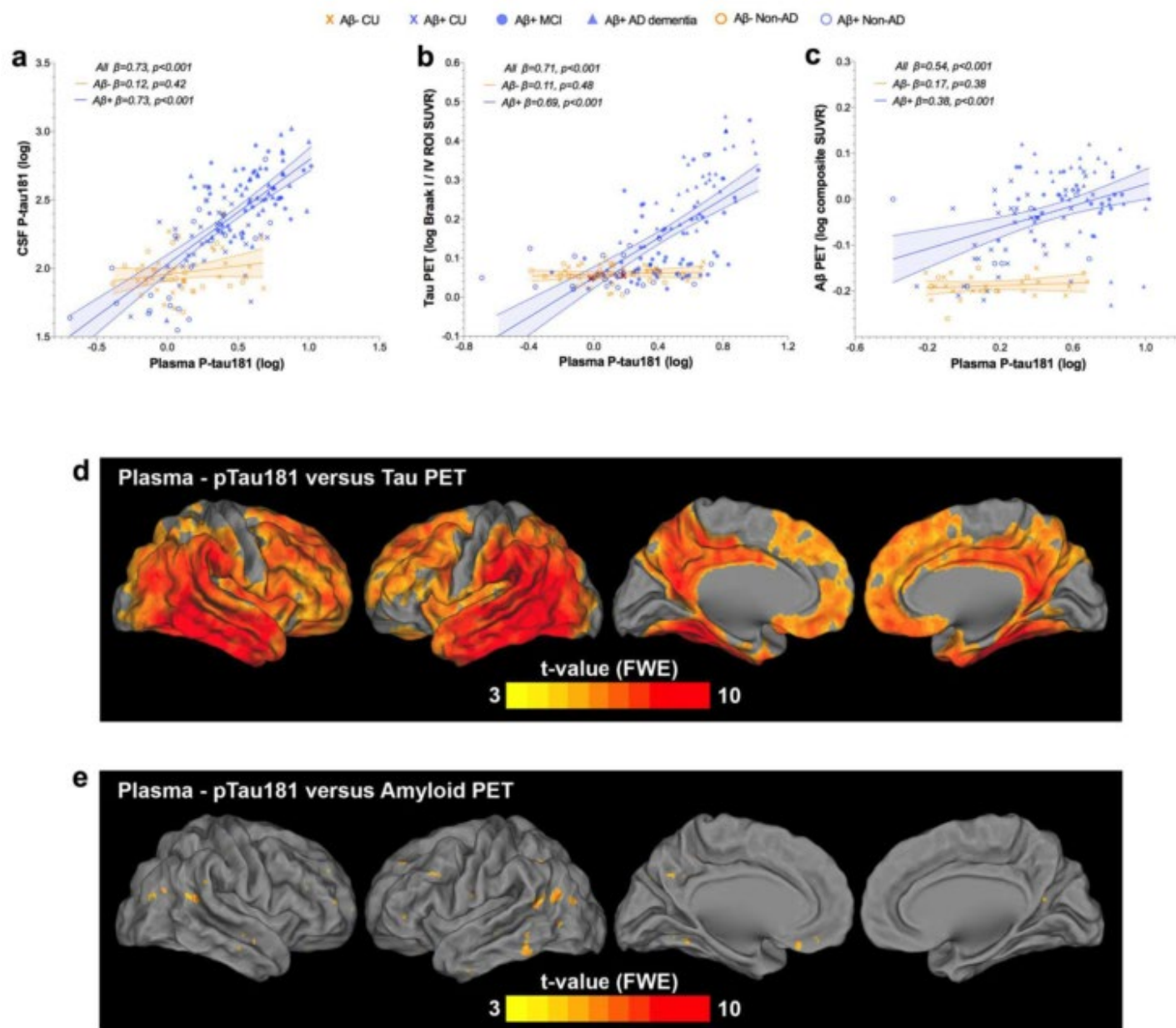
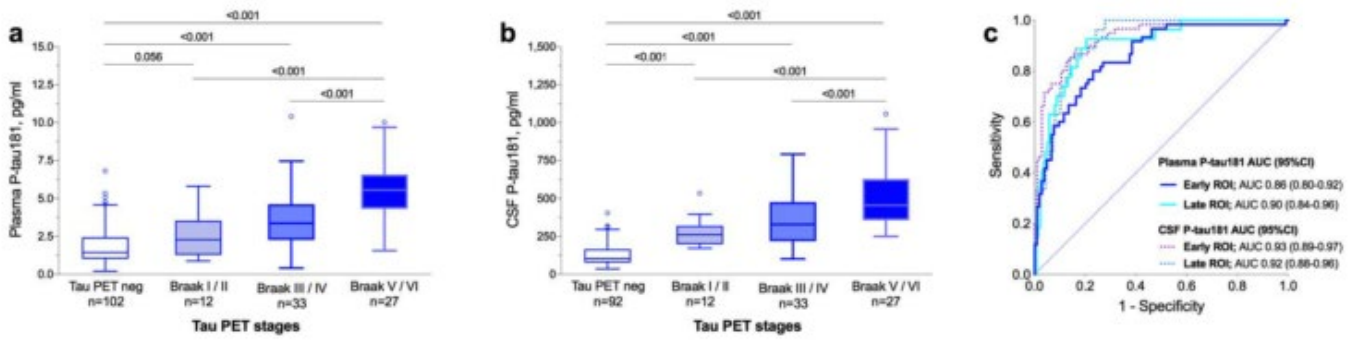


Figure 2

Plasma P-tau181 vs Tau PET, cohort 1



Plasma P-tau181 in diagnostic groups, cohorts 1 and 2

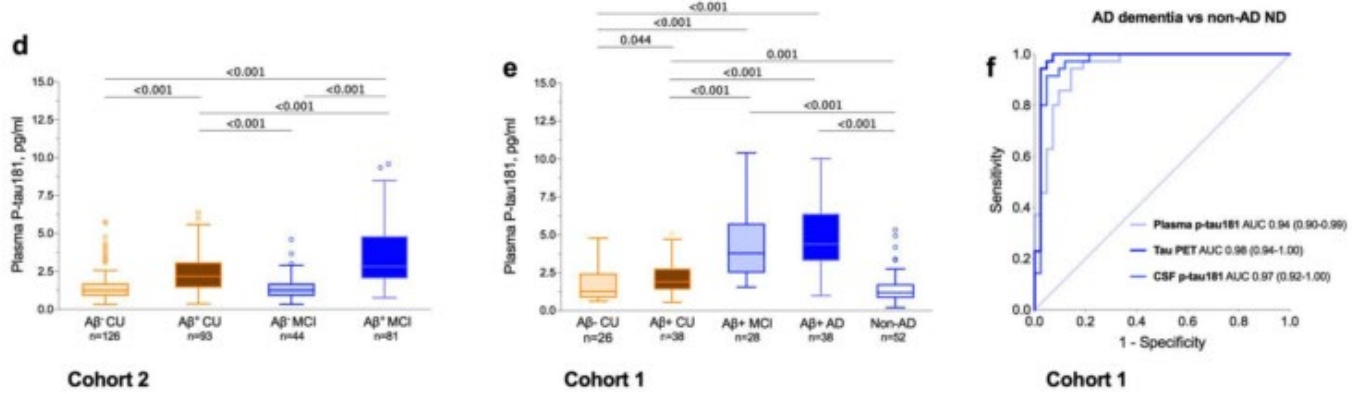
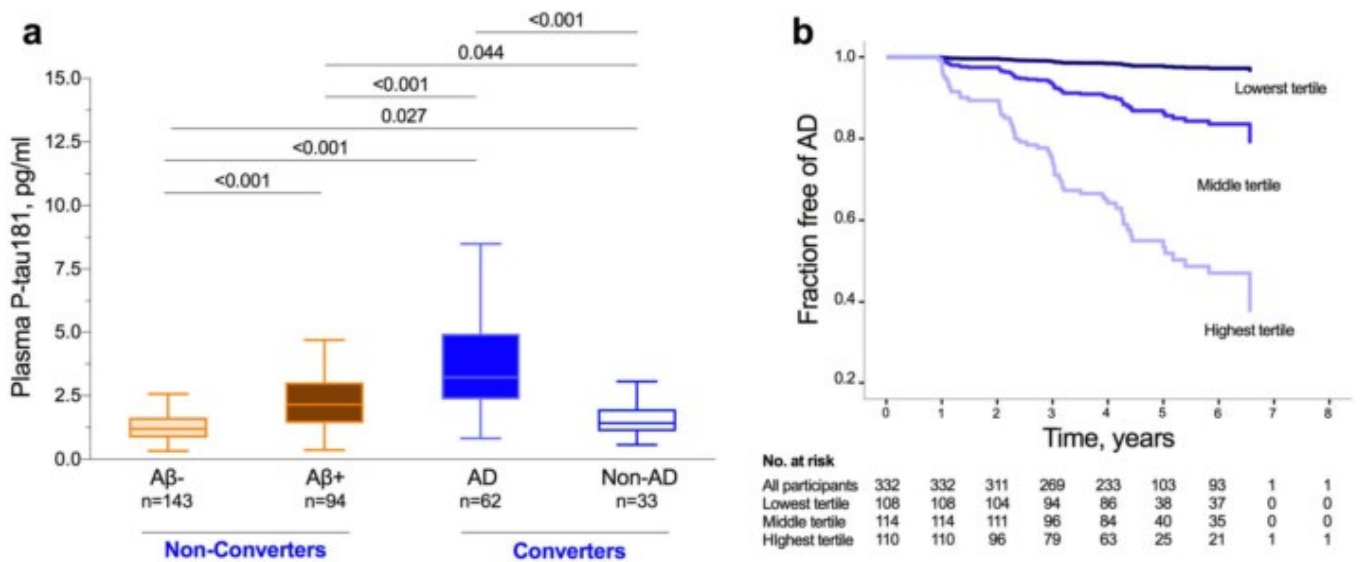


Figure 3



Keywords: Plasma P-tau, blood-based biomarker, Tau PET, early diagnosis, prognosis

Plasma levels of an N-terminal tau fragment are highly associated with future cognitive decline and neurodegeneration in clinically normal elderly: findings from the Harvard Aging Brain Study

Jasmeer Chhatwal^{1,2,3}, Aaron Schultz^{1,3}, Yifan Dang², Beth Ostaszewski², Lei Liu², Hyun-Sik Yang^{1,2,3}, Keith Johnson^{1,2,3}, Reisa Sperling^{1,2,3}, Dennis Selkoe^{2,3}

¹Massachusetts General Hospital, Boston, MA, US

²Brigham & Women's Hospital, Boston, MA, US

³Harvard Medical School, Boston, MA, US

Introduction: High sensitivity biofluid assays have accelerated biomarker development for neurodegenerative disease, including for Alzheimer's disease (AD). Building on recent work demonstrating that levels of an N-terminal fragment of the tau protein (NT1) in cerebrospinal fluid and plasma can differentiate clinically-normal people from those with mild cognitive impairment and dementia due to AD, we asked whether plasma levels of NT1 in clinically-normal elderly are predictive of prospective cognitive decline and neurodegeneration.

Methods: Baseline plasma samples from participants in the Harvard Aging Brain Study (n=236) were assayed for NT1 and neurofilament light (NfL) using single-molecule array technology (Quanterix Simoa). Baseline NT1 and NfL were assessed alone or interactively with β -amyloid (11C-Pittsburgh Compound-B PET; PiB-PET) as predictors of longitudinal cognitive decline (Preclinical Alzheimer's Cognitive Composite; PACC) and neurodegeneration using linear mixed effects models. In participants with plasma NT1 measured within 1 year of 18F-Flortaucipir PET (FTP-PET), we assessed cross-sectional associations between NT1 and regional tau pathology.

Results: Greater plasma NT1 at baseline was highly predictive of greater cognitive decline during longitudinal follow-up (median 5.04 \pm 0.99y; $p < 0.0001$; Figure 1). This effect was synergistic with baseline β -amyloid burden ($p < 0.005$). Greater NT1 was also associated with greater decreases in cortical gray matter and hippocampal volumes measured by longitudinal structural MRI (Figure 2). We observed a significant association between NT1 and FTP-PET signal in the entorhinal cortex ($p = 0.002$) but not in the inferior temporal cortex. Baseline plasma NfL also interacted with β -amyloid to predict PACC decline ($p = 0.0327$). However, NT1 remained a strong predictor of PACC decline after correcting for NfL and its interaction with β -amyloid (NT1*PiB: $p < 0.0001$; NfL*PiB: $p = 0.234$).

Discussion: Plasma NT1 levels may reflect ongoing neurodegenerative and tau-related pathobiologic processes. Plasma NT1 has the potential to be a useful, non-invasive biomarker in clinical and translational AD research, particularly when combined with measures of β -amyloid.

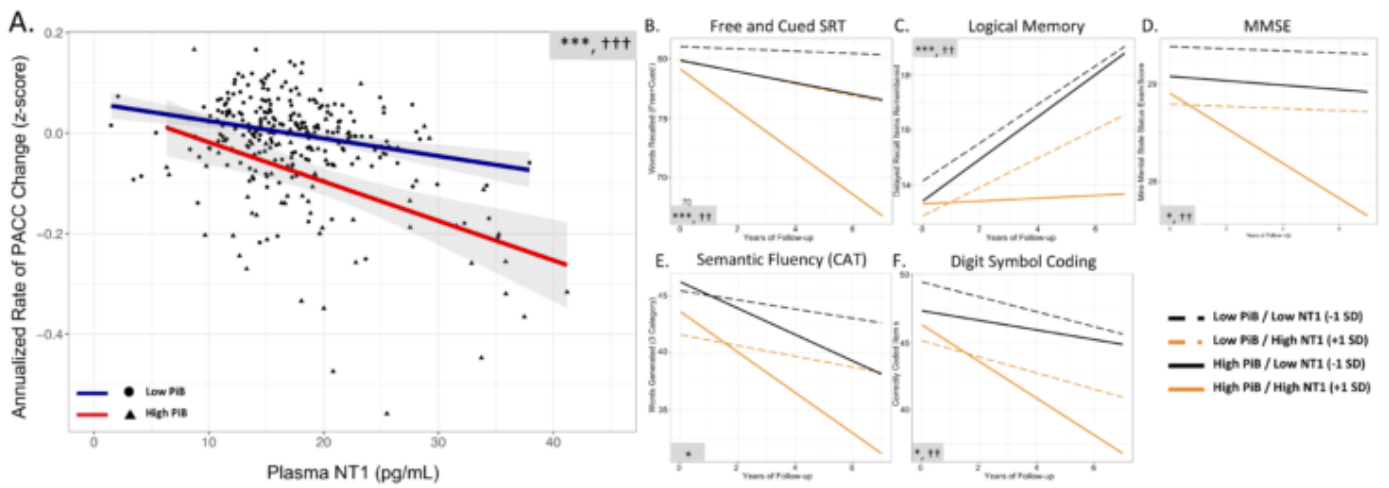


Figure 1: Higher baseline NT1 is associated with greater cognitive decline, alone and synergistically with elevated A β . Greater levels of plasma NT1 were associated with greater performance declines on the preclinical Alzheimer’s cognitive composite (PACC; Panel A). This association was present in individuals with both elevated (triangles; red line) and non-elevated levels of β -amyloid (circles, blue line) at study baseline (assessed by PiB PET), but was significantly stronger in individuals with elevated amyloid burden. A similar pattern was seen across all of the constituent measures that comprise the PACC. Individuals with both high NT1 (1 SD above the group mean; orange lines) and high PiB (mean value for the high A β group; solid lines) showed the greatest decreases in cognitive performance - especially in measures of episodic memory (B, C), but also in measures of language function (E) and executive function. ***, **, * corresponds to $p \leq 0.0005$, ≤ 0.005 , and ≤ 0.05 , respectively, for the association of baseline NT1 to each longitudinal cognitive measure after correction for age, sex, ApoE $\epsilon 4$ status, years of education; +++, ++, + corresponds to $p \leq 0.0005$, ≤ 0.005 , and ≤ 0.05 , respectively, for the interaction of baseline NT1 and PiB PET to each longitudinal cognitive measure after correction for age, sex, ApoE $\epsilon 4$ status, years of education.

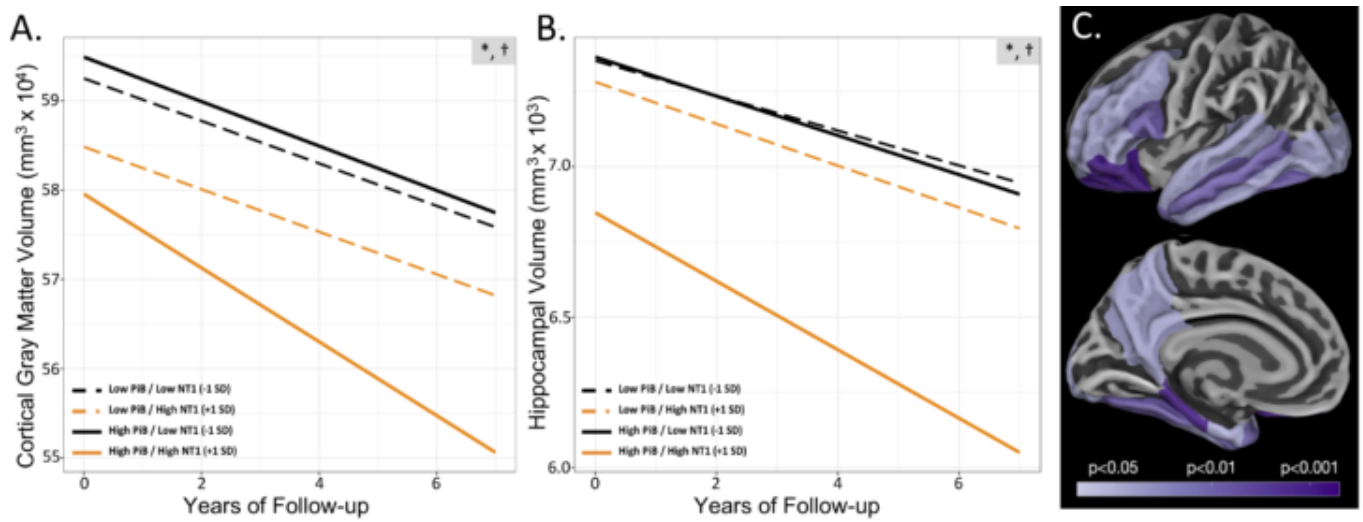


Figure 2: Higher baseline NT1 is associated with greater longitudinal neurodegeneration as measured by longitudinal structural MRI, particularly in those with high β -amyloid at baseline. Greater levels of plasma NT1 were associated with greater longitudinal decreases in total gray matter volume (A), hippocampal volume (B). These associations were present in individuals with both elevated (orange lines) and non-elevated levels of β -amyloid (black lines) assessed by PiB PET at study baseline, but the relationship of higher NT1 to neurodegeneration measures was particularly strong in individuals with higher amyloid burden (orange solid line). High (orange lines) and low NT1 (black lines) corresponds to 1 SD above and below the group mean. High (solid lines) and low PiB (dashed lines) corresponds to the mean value for A β ⁺ and A β ⁻ individuals based on previously published cutoff values for PiB PET. An exploratory analysis of regions where the interaction of baseline NT1 and baseline PiB PET was significantly associated with regional cortical thickness is shown in panel C, with p-values indicated on the color scale. * corresponds to $p < 0.05$ for the association of NT1 with neurodegeneration; † to $p < 0.05$ for the interaction of NT1 and PiB group with respect to neurodegeneration.

Keywords: plasma, biomarker, tau, neurodegeneration, amyloid

Plasma biomarkers associate with amyloid and tau PET binding in cognitively unimpaired older adults with a parental history of AD

Pierre-Francois Meyer^{1,2,4}, Nicholas Ashton⁵, Thomas Karikari⁵, Theresa Köbe¹, Julie Gonneaud¹, Alexa Pichet Binette^{1,2,4}, Hazal Ozlen¹, Anne Labonté¹, Josef Pannee⁵, Joel Simrén⁵, Anne Labonté¹, Pedro Rosa-Neto^{1,2,3,4}, John Breitner^{1,2,4}, Judes Poirier^{1,2}, Henrik Zetterberg^{5,6}, Kaj Blennow⁵, Sylvia Villeneuve^{1,2,3,4}

¹Douglas Mental Health University Institute, Centre for Studies on the Prevention of Alzheimer's Disease (StoP-AD), Montréal, QC, Canada

²Department of Psychiatry, McGill University, Montréal, QC, Canada

³Department of Neurology and Neurosurgery, McGill University, Montréal, QC, Canada

⁴McGill Centre for Integrative Neuroscience, McGill University, Montréal, QC, Canada

⁵Department of Psychiatry and Neurochemistry, Institute of Neuroscience and Physiology, The Sahlgrenska Academy, University of Gothenburg, Gothenburg, Sweden

⁶Department of Neurodegenerative Disease, UCL Queen Square Institute of Neurology, University College London, London, UK

Objective: Plasma biomarkers may facilitate or accelerate the detection of amyloid-beta (A β) and tau pathology in early AD pathogenesis. We therefore investigated the relation of plasma biomarkers with Ab and tau PET-binding in pre-symptomatic AD.

Methods: A β -[¹⁸F-NAV-4694] and tau-PET [¹⁸F-AV-1451] were obtained from 129 cognitively unimpaired older individuals with a parental history of AD from the PREVENT-AD cohort (Table 1). Plasma A β (A β ₄₀ and A β ₄₂) biomarkers were measured with with Single Molecule Array technology (SiMoA, Quanterix, Billerica, MA, USA) and immunoprecipitation coupled with mass spectrometry (IP-MS). Plasma tau (¹⁸¹P-tau and total-tau) biomarkers were measured with SiMoA only. Linear regression analyses investigated associations of plasma and PET measures using region of interest (global cortical ROI for A β and temporal metaROI for tau) and voxel-wise approaches. ROC analyses further determined plasma biomarker performance for detection of A β -PET positivity.

Table 1: Sample demographics.

	All OA	A β -negative OA	A β -positive OA	P for difference
Sample size	129	103	26	
Age	68.50 (5.49)	67.13 (4.72)	68.50 (5.49)	0.21
Sex %F (N)	74 (85)	75 (77)	73 (19)	1
APOE carriers % (N)	41 (53)	35 (36)	65 (17)	0.007
Education years	15.15 (3.28)	15.47 (3.40)	13.88 (2.41)	0.03
Global Aβ SUVR	1.34 (0.34)	1.20 (0.08)	1.90 (0.39)	< 0.001
metaROI AV1451 SUVR	1.18 (0.12)	1.16 (0.08)	1.28 (0.18)	< 0.001

Sex F: Number of participants of female sex, OA: Older adults, SUVR: Standard Uptake Value Ratio. All data, unless otherwise specified are given as mean (standard deviation).

Results: Plasma A β_{42} /A β_{40} ratio measured by either method and ¹⁸¹P-tau were associated with ¹⁸F-NAV-4694 SUVRs (R^2 range=0.07-0.12 and R^2 =0.07, all P <0.001). Only plasma ¹⁸¹P-tau was associated with increased ¹⁸F-AV1451 binding (R^2 =0.11, P <0.001, Figure 1A-C). Voxel-wise analyses indicated that both plasma A β_{42} /A β_{40} measures were associated with Ab-PET binding in ‘typical’ Ab-regions (*e.g.* precuneus and medial pre-frontal cortex, Figure 2D-E). Only plasma ¹⁸¹P-tau correlated with ¹⁸F-AV-1451 binding in regions recognized for ‘early’ tau accumulation (Figure 1F).

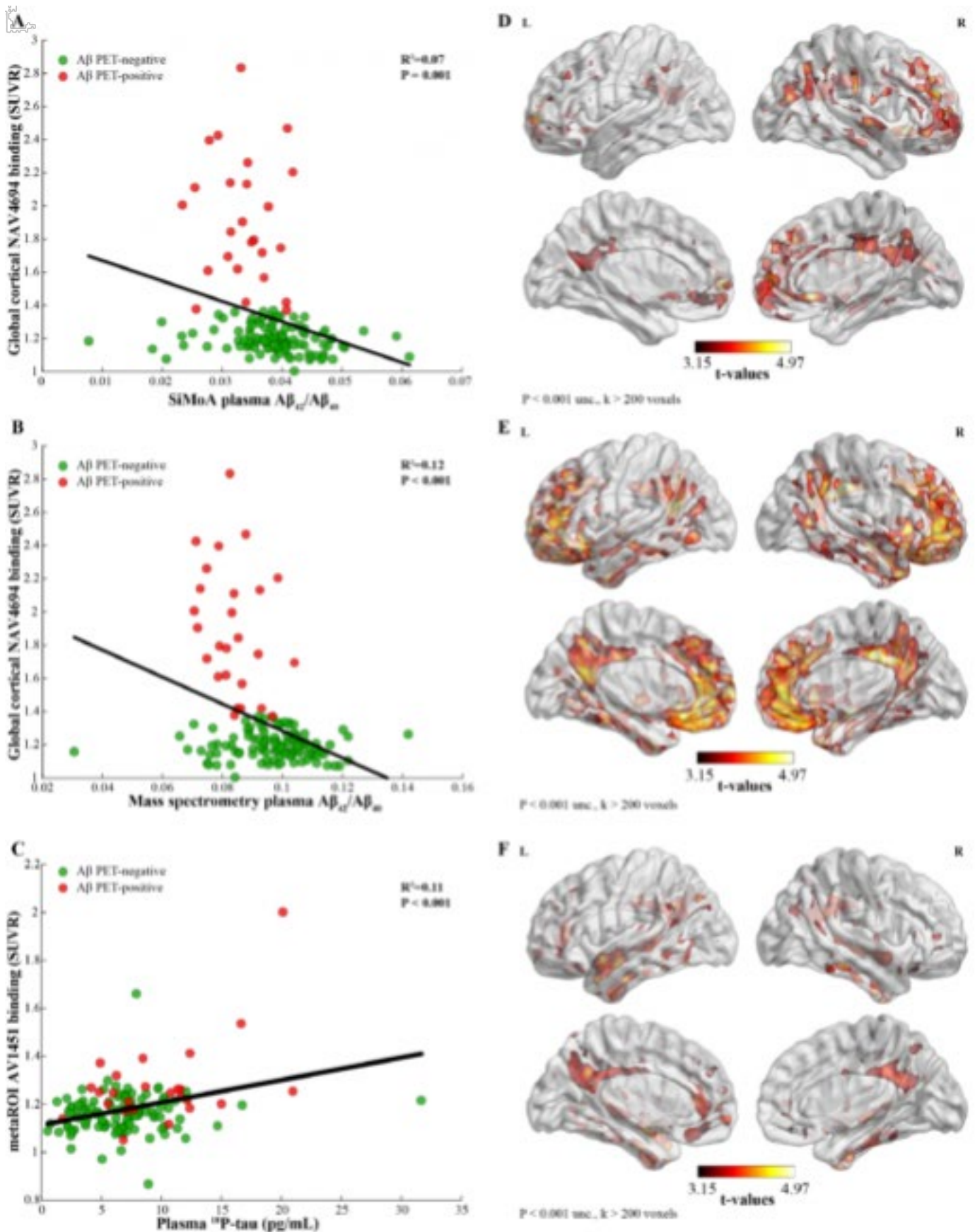


Figure 1: Plasma biomarkers correlate with PET measures of AD pathology. Linear regression analyses investigated the association of imaging and plasma biomarkers of A β and tau pathologies. SiMoA (A) and mass spectrometry (B) measures of the A $\beta_{42}/A\beta_{40}$ correlated weakly with ^{18}F -NAV4694 retention in a global cortical region of interest. (C) Plasma ^{181}P -tau correlated to a similar degree with AV1451 retention in the metaROI region of interest. Voxelwise analyses also suggested that there was stronger associations between mass spectrometry measures of the A $\beta_{42}/A\beta_{40}$ and A β -PET (E) than SiMoA measures of A $\beta_{42}/A\beta_{40}$ (D). In both instances, however, the associations were strongest in regions expected to display amyloid accumulation. (F) Plasma ^{181}P -tau levels correlated more strongly with AV1451 binding in 'early' tau regions.

In ROC analyses, combining $A\beta_{42}/A\beta_{40}$ and ^{181}P -tau yielded highest accuracy to detect PET $A\beta$ -positivity status (area under the curve range=0.808-0.836; Figure 2). In all analyses, mass spectrometry measures of $A\beta_{42}/A\beta_{40}$ were more sensitive than SiMoA to $A\beta$ -PET binding.

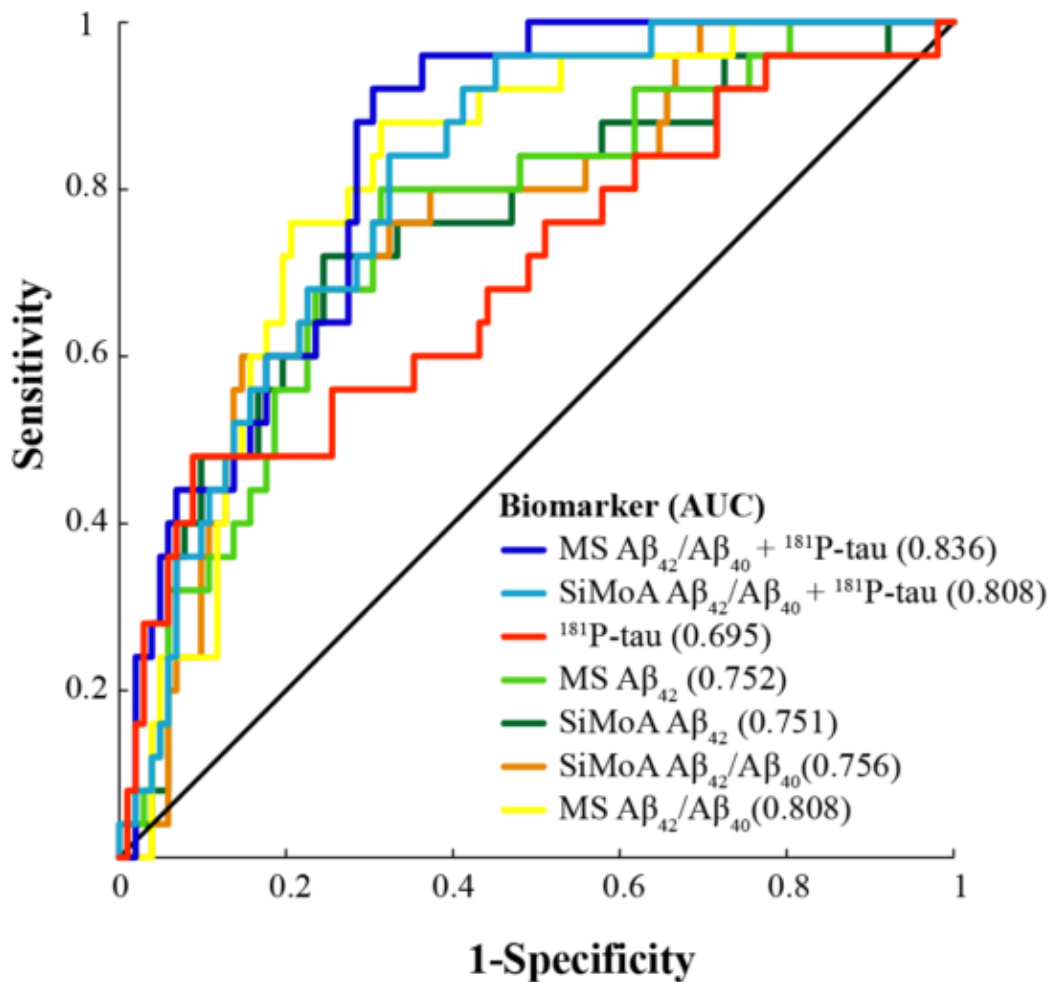


Figure 2: Blood biomarker performance for detection of $A\beta$ -PET status. Receiver operating curve (ROC) analyses investigated the ability of plasma biomarkers to discriminate PET $A\beta$ -positive from $A\beta$ -negative individuals. Combining plasma measures of ^{181}P -tau with mass spectrometry measures of $A\beta_{42}/A\beta_{40}$ yielded the highest predictive performance with an AUC of 0.836

Conclusions: In cognitively unimpaired older adults at risk for AD dementia owing to a family history of the disease, plasma biomarkers capture PET evidence of established $A\beta$ pathology and nascent tau pathology. Thus, plasma biomarkers show promise for the detection of AD pathology even at the earliest stage of AD pathological progression.

Keywords: Plasma, PET, biomarkers, amyloid, tau

High-performance plasma phospho-tau181 biomarker for Alzheimer's disease

Tharick Pascoal², Thomas Karikari¹, Nicholas Ashton¹, Andréa Benedet², Melissa Savard², Min Su Kang², Joseph Therriault², Michael Schöll¹, Gassan Massarweh², Jean-Paul Soucy², Serge Gauthier², Henrik Zetterberg¹, Pedro Rosa-Neto², Kaj Blennow¹

¹University of Gothenburg, Gothenburg, Sweden

²McGill University, Montreal, Canada

Objective: To present the discovery and validation of a novel high-performance plasma phospho-tau181 biomarker to depict brain neurofibrillary tangles accumulation in Alzheimer's disease (AD).

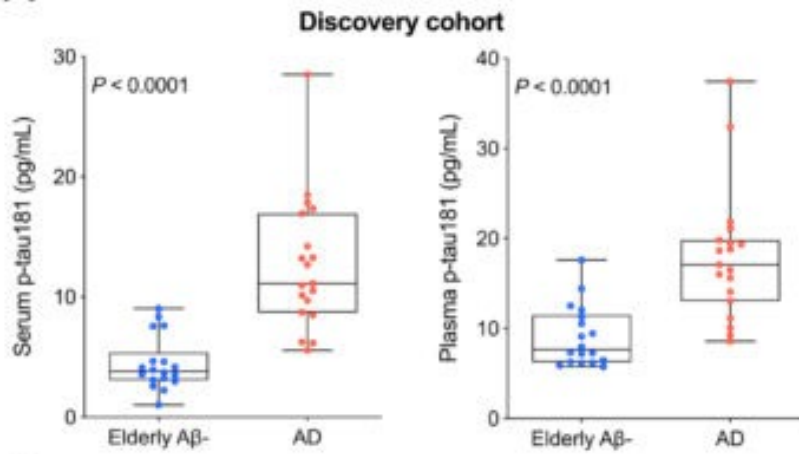
Methods: We developed and validated an automated ultrasensitive Single Molecule Array assay for quantifying phospho-tau181 in plasma and serum. Discovery and validation of the novel assay were performed in three independent cohorts in Sweden and Canada using positron emission tomography (PET) tau and amyloid- β (A β), cerebrospinal fluid, and both cross-sectional and longitudinal cognitive and structural brain imaging measurements.

Results: Serum and plasma p-tau181 accurately discriminated AD from age-matched controls in the discovery sample (AUCs \geq 90%) (Fig. 1A, B). In the validation sample ($n=226$), plasma phospho-tau181 showed a progressive increase from young adults to cognitively unimpaired (CU) elderly A β negative, cognitively unimpaired (CU) elderly A β positive, MCI A β positive, and AD dementia ($P<0.0001$) (Fig. 1C). Plasma phospho-tau181 discriminated AD dementia from CU elderly (AUC=98.24%), frontotemporal dementia patients (AUC=100%), and young adults (AUC=99.44%) (Fig. 1D). Plasma phospho-tau181 was highly correlated (Fig. 2) and predicted brain tau (AUC=93%) and A β (AUC=88%) pathologies measured by PET (Fig. 3). Plasma phospho-tau181 differentiated individuals tau PET negative A β positive from A β negative (Fig. 3D). Remarkably, plasma phospho-tau181 was highly associated with 1-year cognitive impairment and reduction in hippocampal volume ($P<0.0001$). In the second validation cohort that consisted of individuals assessed in a clinical setting ($n = 105$), plasma phospho-tau181 accurately discriminated AD from young adults (AUC=100%) and CU elderly (AUC=84.44%).

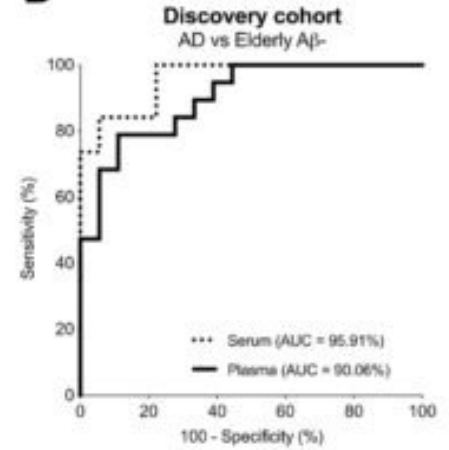
Conclusions: To conclude, we have presented a high-performance blood p-tau181 assay that may represent a simple, cost-effective, and scalable test for the diagnosis of AD. This technology has immediate applications for diagnosis and recruitment for disease-modifying trials. This assay has the potential to be incorporated in clinical practice as a rapid screening test to rule out AD pathophysiology and guide therapy and clinical management of dementia patients.

Figure 1

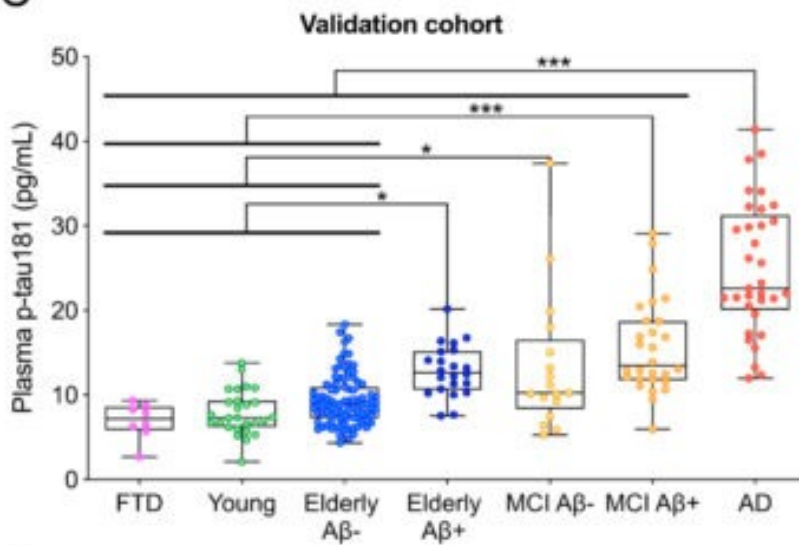
A



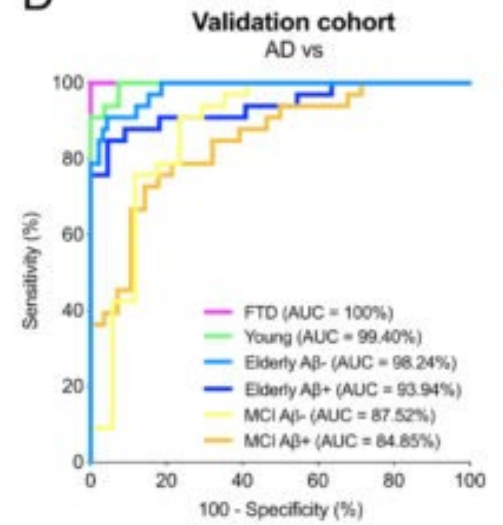
B



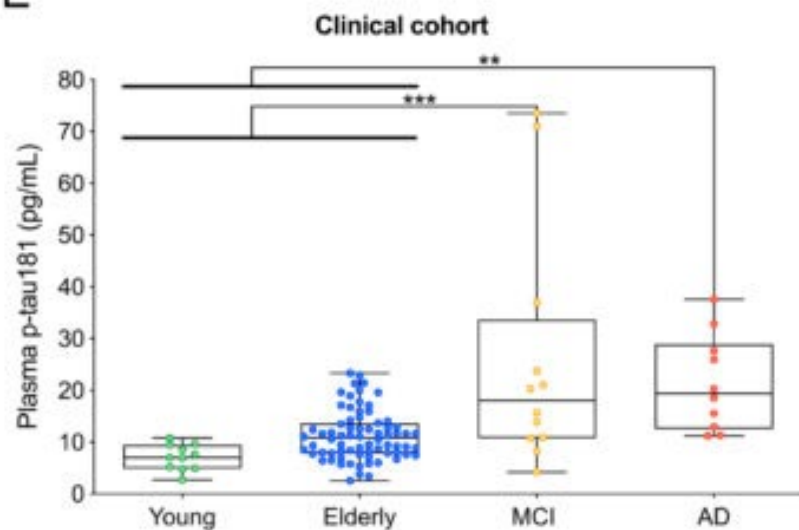
C



D



E



F

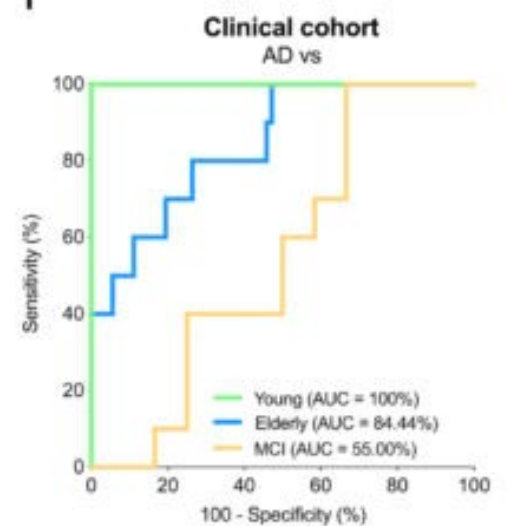
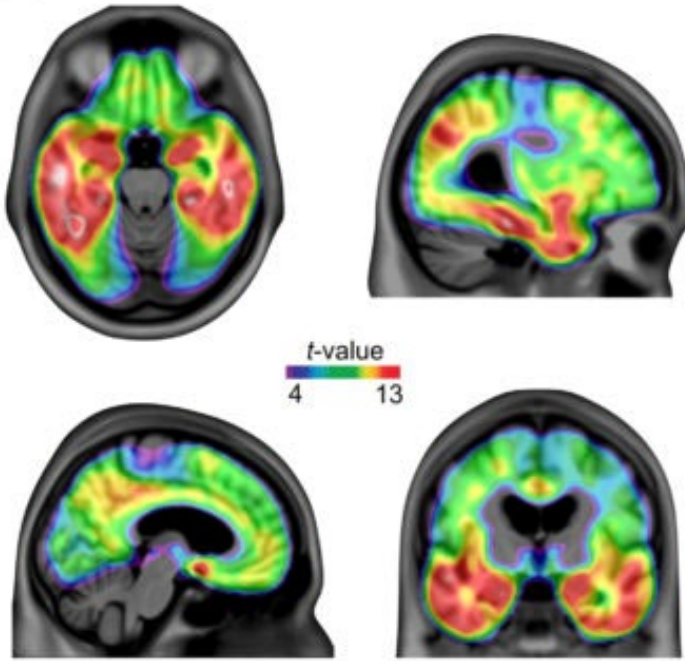
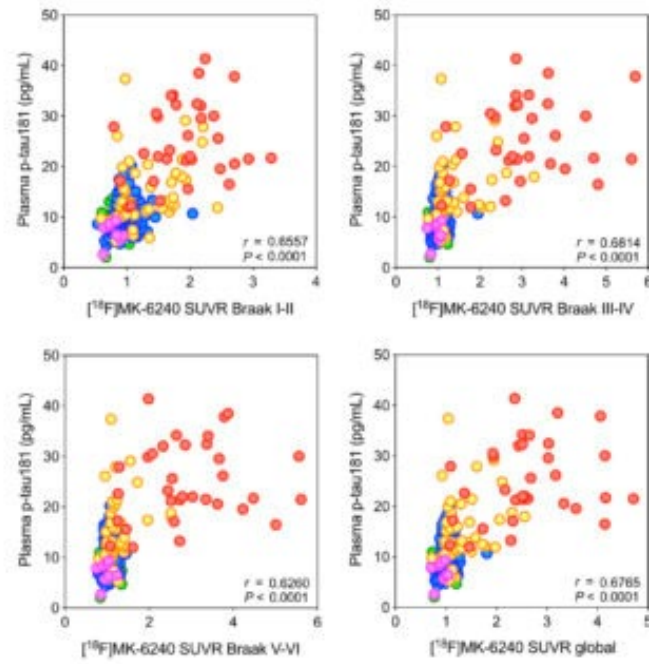


Figure 2

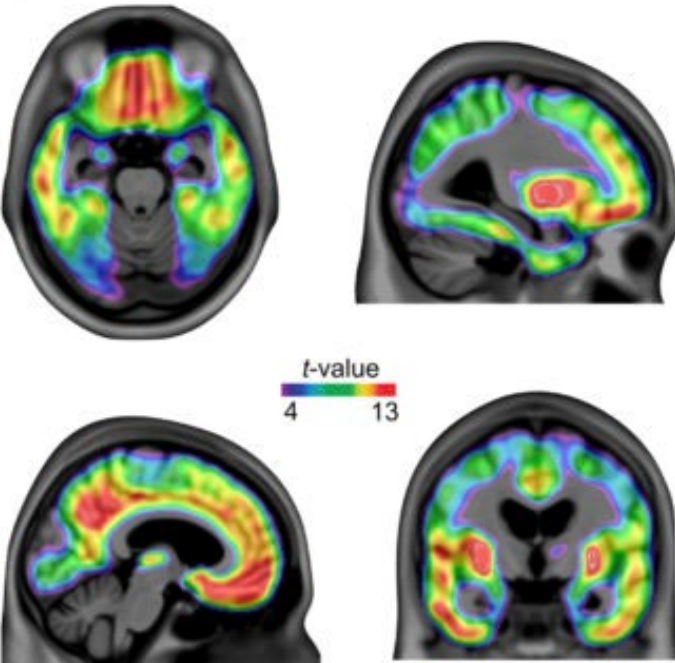
A Plasma p-tau181 vs tau [¹⁸F]MK-6240



B



C Plasma p-tau181 vs A β [¹⁸F]AZD4694



D

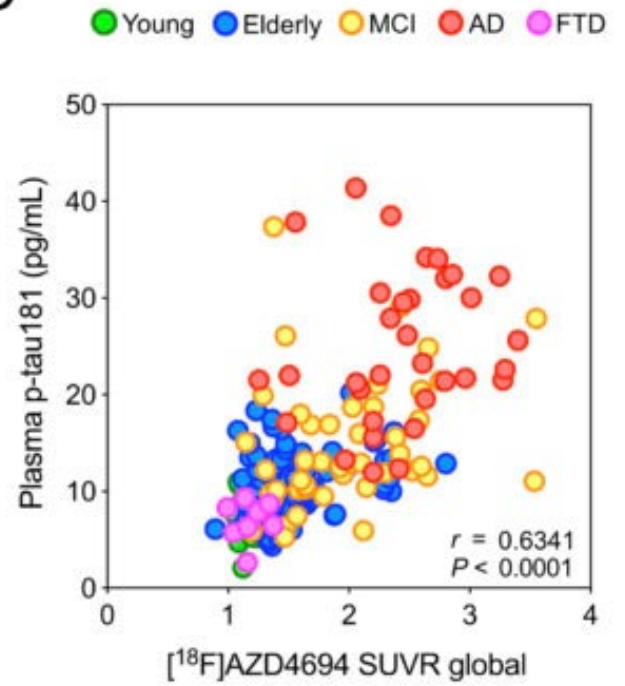
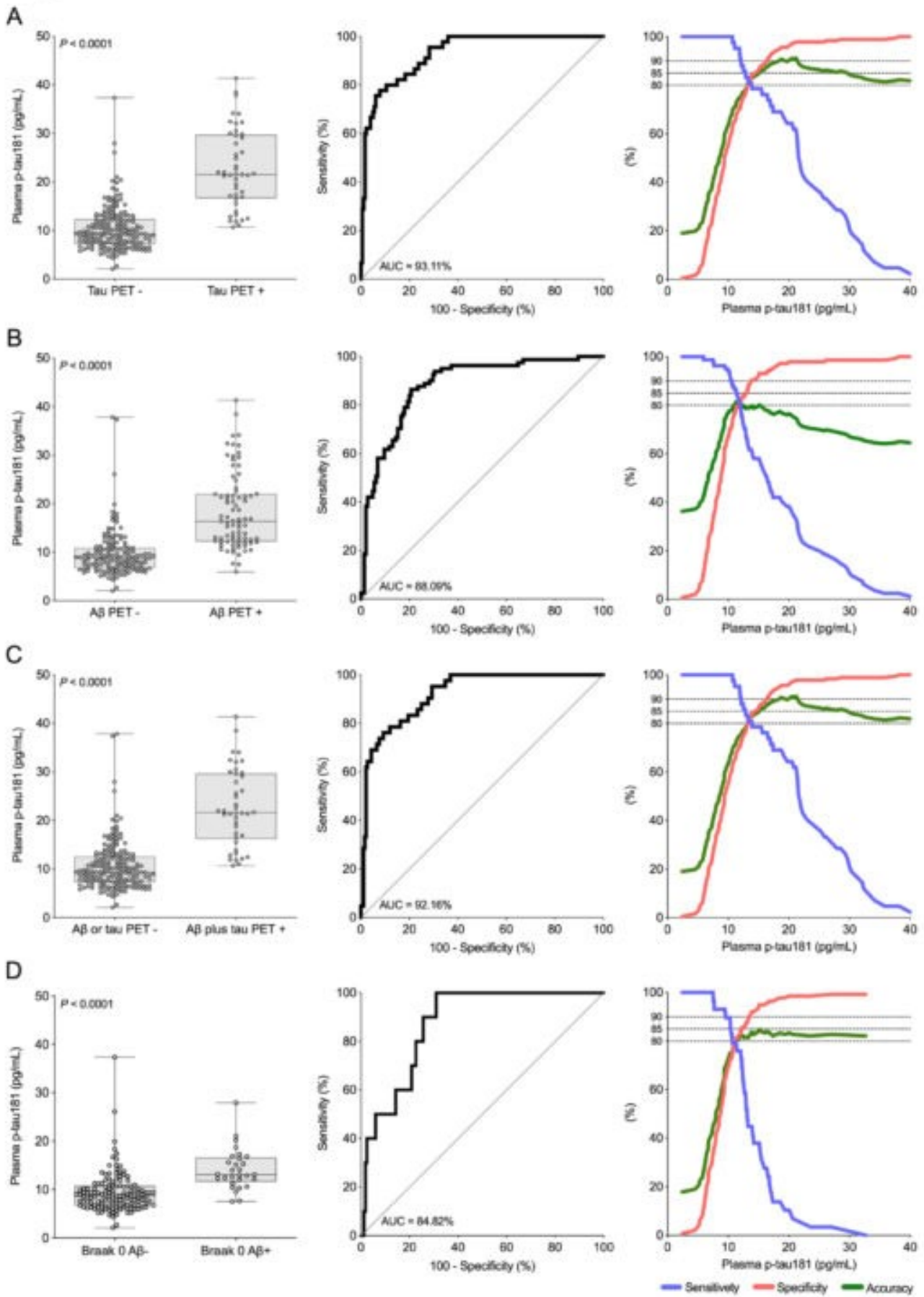


Figure 3



Keywords: p-tau, neurofibrillary tangle, blood biomarker, Alzheimer's disease, amyloid



National Institutes of Health

Funding for this conference was made possible in part by grant R13 AG042201 from the National Institute on Aging.

The views expressed in written conference materials or publications and by speakers and moderators do not necessarily reflect the official policies of the Department of Health and Human Services; nor does mention by trade names, commercial practices, or organizations imply endorsement by the U.S. Government.

The 14th Human Amyloid Imaging Conference is supported through educational grants and sponsorships from:

ASSOCIATE ORGANIZER



PLATINUM



SILVER



BRONZE

